

EXPLORATION FOR PLATINUM-GROUP ELEMENTS DEPOSITS

Mineralogical Association of Canada
Short Course Series Volume 35

Edited by

James E. Mungall
University of Toronto



Short Course delivered on behalf of the Mineralogical Association of Canada in Oulu, Finland,
6-7 August 2005.

AEROQUEST LIMITED



TABLE OF CONTENTS

Introduction	xvi
GEOCHEMISTRY OF PLATINUM-GROUP ELEMENTS	
1. Magmatic Geochemistry of the PGE J.E. Mungall	1-34
2. The Aqueous Geochemistry of the Platinum Group Elements (PGE) in Surficial, Low-T Hydrothermal and High-T Magmatic-Hydrothermal Environments J.J. Hanley	35-56
DESCRIPTIVE PLATINUM-GROUP ELEMENT ORE DEPOSIT MODELS – PRECIOUS-METAL-DOMINANT	
3. Stratiform PGE Deposits in Layered Intrusions R.G. Cawthorn	57-73
4. PGE Deposits in the Marginal Series of Layered Intrusions M.J. Iljina, C.A. Lee	75-96
5. Behavior of PGE and PGM in the Supergene Environment: A Case Study of Persistence and Redistribution in the Main Sulfide Zone of The Great Dyke, Zimbabwe T. Oberthür, F. Melcher	97-111
6. Placers Associated with Ural-Alaska-type Complexes N.D. Tolstikh, E.G. Sidorov, A.P. Krivenko	113-143
7. Descriptive Ore Deposit Models: Hydrothermal and Supergene Pt & Pd Deposits A. Wilde	145-161
DESCRIPTIVE PLATINUM-GROUP ELEMENT ORE DEPOSIT MODELS – BASE-METAL-DOMINANT	
8. Sudbury Cu-(Ni)-PGE Systems: Refining the Classification Using McCreedy West Mine and Podolsky Project Case Studies C.E.G. Farrow, J.O. Everest, D.M. King, C. Jolette	163-180
9. The Conduits of Magmatic Ore Deposits N.T. Arndt	181-201
10. PGE Potential of Porphyry Deposits M. Economou-Eliopoulos	203-246
EXPLORATION METHODS	
11. PGE Exploration: Economic Considerations and Geological Criteria A. Green, D. Peck	247-274
12. The Geophysical Signatures of PGE Deposits S. Balch	275-285
13. PGE in Geochemical Exploration E.M. Cameron, K.H. Hattori	287-307

14. Lithogeochemical Prospecting W.D. Maier, S.-J. Barnes	309-341
CASE HISTORIES	
15. Fedorov-Pana layered mafic intrusion, (Kola Peninsula, Russia): approaches, methods, and criteria for prospecting PGEs F.P. Mitrofanov, A.U. Korghagin, K.O. Dudkin, T.V. Rundkvist	343-358
16. The Discovery and Characterization of the Nickel Rim South Deposit; Sudbury Ontario S.A. McLean, K.H. Straub, K.M. Stevens	359-368
17. Discovery and Geology of the Lac Des Iles Palladium Deposits M.J. Lavigne, M.J. Michaud, J. Rickard	369-390
18. Discovery of the J-M Reef, Stillwater Complex, Montana: the role of soil and silt platinum and palladium geochemical surveys M.L. Zientek, S.R. Corson, R.D. West	391-407
19. Exploration and Mining Perspective of the Main Sulfide Zone of the Great Dyke, Zimbabwe - Case Study of the Hartley Platinum Mine A.H. Wilson, R.T. Brown	409-429
20. The Platinova Reef of the Skaergaard intrusion T.F.D. Nielsen, J.C.O. Andersen, C.K. Brooks	431-455
21. Polymetallic PGE-Au Mineralization of the Sukhoi Log Deposit, Russia V.V. Distler, M.A. Yudovskaya	457-485
22. Ni-Cu-Cr-PGE Mineralization Types: Distribution and Classification R. Eckstrand	487-494
Index	495

DETAILED LIST OF CONTENTS

GEOCHEMISTRY OF PLATINUM-GROUP ELEMENTS

1. MAGMATIC GEOCHEMISTRY OF THE PLATINUM-GROUP ELEMENTS

J.E. Mungall

INTRODUCTION	1
PLATINUM-GROUP ELEMENTS	1
GEOLOGICAL CONTROLS – GENESIS OF PARENTAL MAGMAS	3
Origins of Basaltic Magmas	3
Physical Environments for PGE Deposits	7
GEOCHEMICAL CONTROLS – PARTITIONING OF CHALCOPHILE ELEMENTS	8
Direct Precipitation	8
PGE Alloy Solubility	8
Partition Coefficients	9
Mineral – Silicate Melt Partitioning	10
Sulfide Melt – Silicate Melt Partitioning	11
Solubility of Sulfide in Basaltic Melts	12
Mass Balance in Sulfide Melt – Silicate Melt Partitioning	14
Monosulfide Solid Solution – Sulfide Melt Partitioning	17
Fluid – Silicate Melt Partitioning	20
MANTLE MELTING AND MAGMA FERTILITY	20
SYNTHESIS AND CONCLUSIONS	24
FINAL COMMENTS	25
Appendix: Partitioning in magmatic systems	32

2. THE AQUEOUS GEOCHEMISTRY OF THE PLATINUM-GROUP ELEMENTS (PGE) IN SURFICIAL, LOW-T HYDROTHERMAL AND HIGH-T MAGMATIC-HYDROTHERMAL ENVIRONMENTS

J.J. Hanley

INTRODUCTION	35
Concentration, Activity and Fugacity	35
Complexation	37
PGE Chemistry in Aqueous Fluids	38
Surficial Environments (~25°C, 1 atm)	38
Low Temperature Hydrothermal Fluids (<500°C)	39
Experimental Studies in Chloride-bearing Systems at low T	42
Experimental Studies in Bisulfide-bearing Systems at Low T	42
Chloride or Bisulfide?	42
The Role of Other Ligands	45
High Temperature, Magmatic Volatiles and Post-cumulus Magmatic Fluids (> 500°C)	46
Experimental Evidence for Significant PGE Solubility at High Temperature (800–900°C)	47
Additional Factors Limiting the Solubility of the PGE in Aqueous Fluids	48
The Importance of Field-based Observations	49
Estimating Fluid Salinity, Fluid Composition and Temperature	49
Estimating $f(\text{O}_2)$	50
Major Conclusions to Take from this Chapter	50

DESCRIPTIVE PLATINUM-GROUP ELEMENT ORE DEPOSIT MODELS – PRECIOUS-METAL-DOMINANT

3. STRATIFORM PLATINUM-GROUP ELEMENT DEPOSITS IN LAYERED INTRUSIONS

R. G. Cawthorn

INTRODUCTION	57
BUSHVELD COMPLEX	57
UG2 Chromitite	57
Merensky Reef	59
STILLWATER COMPLEX	64
GREAT DYKE	65
MUNNI MUNNI INTRUSION	66
SKAERGAARD INTRUSION	66
CONTRASTS AND COMPARISONS	67
Stratigraphic Association	67
Mineral Compositions	68
Within-Reef Fractionation of the PGE	68
Cu/Pd values	70
SUMMARY	70

4. PGE DEPOSITS IN THE MARGINAL SERIES OF LAYERED INTRUSIONS

M.J. Iljina, C.A. Lee

INTRODUCTION	75
PORTIMO AND KOILLISMAA MARGINAL SERIES DEPOSITS	75
Portimo Stratigraphy and Structure	75
Diverse Portimo sulfide-PGE Mineralizations	79
Disseminated Suhanko and Konttijärvi Marginal Series Sulfides	81
Massive Suhanko Marginal Series Sulfides	81
Correlation of Portimo and Penikat Complexes	84
Haukiahö and Murtolampi Sulfide–PGE Deposits, Koillismaa	84
BUSHVELD COMPLEX	84
Platreef, Northern Bushveld	84
Platreef Stratigraphy	87
Platinum-group Minerals	88
Inter-relationship of Metals	88
Isotope Studies on the Platreef	88
SHEBA'S RIDGE, EASTERN BUSHVELD COMPLEX	89
EAST BULL LAKE INTRUSIVE SUITE	90
Se/S RATIO	92
CONCLUSIONS	94
ACKNOWLEDGEMENTS	95
REFERENCES	95

5. BEHAVIOR OF PGE AND PGM IN THE SUPERGENE ENVIRONMENT: A CASE STUDY OF PERSISTENCE AND REDISTRIBUTION IN THE MAIN SULFIDE ZONE OF THE GREAT DYKE, ZIMBABWE

T. Oberthür, F. Melcher

INTRODUCTION	97
GEOLOGICAL SETTING	97
SAMPLES AND METHODS	98
PRISTINE MAIN SULFIDE ZONE	98
Geochemistry	98
PGM and PGE-Carriers	99

Trace PGE Contents in Sulfides	100
OXIDIZED MAIN SULFIDE ZONE	100
Geochemistry	100
PGM and PGE-Carriers	102
(1) Relict PGM, and gold	104
(2) (Pt,Pd)-oxides and/or Hydroxides	106
(3) Secondary PGM (neoformations)	106
(4) PGE in Iron- and Manganese-hydroxides	106
(5) PGE in Smectites and Chlorites	108
DISCUSSION AND CONCLUSIONS	108
METALLURGICAL IMPLICATIONS	109
<hr/>	
6. PLATINUM-GROUP ELEMENT PLACERS ASSOCIATED WITH URAL-ALASKA TYPE COMPLEXES	
N.D. Tolstykh, E.G. Sidorov, A.P. Krivenko	
INTRODUCTION	113
CLASSIFICATION OF PGM PLACERS AND THEIR LODE SOURCES	113
URAL-ALASKA TYPE COMPLEXES	116
Historical Geological Concepts for Ural-Alaska Type Zoned, Igneous Complexes	116
Geodynamic Conditions of Formation of the Ural-Alaska type complexes	116
PGE-BEARING PLACERS CONNECTED WITH URAL-ALASKA TYPE COMPLEXES	117
The commercial significance of the platinum placers	117
Features of PGM Placer Deposits	118
Morphology of PGM grains	119
Composition of Pt-Fe alloys in Placers	120
Composition of Os-Ir-Ru alloys in placers	125
Equilibrium Mineral Paragenesis in PGE-Bearing Placers	129
1. Pt-Fe Alloy-Osmium Paragenesis	129
2. Isoferroplatinum-Iridium Paragenesis	129
DISCUSSION	136
Typomorphic Features of Placers Related to Ural-Alaska Complexes as Compared to Placers Associated with Ophiolites	136
Evolution of the Ore-Forming System of Ural-Alaska Complexes	137
CONCLUSIONS	138
<hr/>	
7. DESCRIPTIVE ORE DEPOSIT MODELS: HYDROTHERMAL AND SUPERGENE Pt & Pd DEPOSITS	
A. Wilde	
INTRODUCTION	145
DEPOSITS OF REDUCED PASSIVE MARGINS	148
Orogenic Au-Pt-Pd Deposits in Carbonaceous Metasedimentary Rocks	148
Sediment-Hosted Ni-Mo-Zn Deposits	149
DEPOSITS OF OXIDIZED INTRACRATONIC BASINS	153
Unconformity Type U-Au-Pt-Pd Deposits	153
Sediment-Hosted Cu Deposits	154
Jacutinga Au-Pd Deposits	155
NEAR-SURFACE (SUPERGENE) DEPOSITS	155
Listwaenite-hosted	155
Lateritic Deposits	156
DISCUSSION	156
CONCLUSIONS	158

DESCRIPTIVE PLATINUM-GROUP ELEMENT ORE DEPOSIT MODELS – BASE-METAL-DOMINANT

8. SUDBURY Cu-(Ni)-PGE SYSTEMS: REFINING THE CLASSIFICATION: USING McCREEDY WEST MINE, AND PODOLSKY PROJECT CASE STUDIES	
C.E.G. Farrow, J.O. Everest, D.M. King, C. Jolette	
INTRODUCTION	163
SUDBURY AREA GEOLOGY	163
STYLES OF Ni-Cu-PGE SULFIDE DEPOSITS AT SUDBURY	164
GEOLOGY OF THE Cu-(Ni)-PGE DEPOSITS AT SUDBURY	165
Geological Characteristics	165
‘Sharp-Walled’ Vein Systems: McCreedy West 700 Complex	166
‘Low-Sulfide’ Mineralization: The McCreedy West PM Deposit	167
‘Hybrid’ Systems: Podolsky North & 2000 Zones	169
Geochemical Characteristics	171
DISCUSSION	175
Genetic Interpretation of Cu(-Ni)-PGE Systems: Towards a Unifying Hypothesis	175
CONCLUSIONS	177

9. THE CONDUITS OF MAGMATIC ORE DEPOSITS	
N.T. Arndt	
INTRODUCTION	181
MAGMA DYNAMICS: THE PASSAGE OF MAGMA THROUGH THE CRUST	181
NORIL’SK-TALNAKH CU-NI-PGE SULFIDE DEPOSITS	183
Models for the Formation of Noril’sk-Talnakh Deposits	188
Differences between the compositions of lavas and intrusive rocks	189
Phase Equilibria Constraints	192
S Isotope Ratios	192
Differences in Trace Element Ratios and Isotopic Compositions	193
Magmatic Plumbing of the Noril’sk-Talnakh System	193
ORE DEPOSITS OF THE BUSHVELD COMPLEX	195
The Role of Crustal Structure in Ore Formation and a New Classification of Deposits	197
CONCLUSIONS	198

10. PLATINUM-GROUP ELEMENT POTENTIAL OF PORPHYRY DEPOSITS	
M. Economou-Eliopoulos	
INTRODUCTION	203
DISTRIBUTION OF PORPHYRY Cu DEPOSITS ALONG CONVERGENT PLATE MARGINS	204
CHARACTERISTICS OF ALKALINE INTRUSIONS	205
ALTERATION TYPES OF PORPHYRY INTRUSIONS	205
MINERALIZATION OF PORPHYRY Cu SYSTEMS	206
TRANSPORT OF PGE IN HYDROTHERMAL SYSTEMS	206
Experimental Data	206
Field Observations	210
Applications to Porphyry Systems	211
PGE MINERALIZATION IN PORPHYRY SYSTEMS	211
Distribution of Au in Cu-minerals, Gold and Electrum	211
Pd-Pt-Minerals	214
Tetrahedrite-tennantite	216
Galena-Clausthalite	216
Linnaeite-siegenite-carrollite	216
SIGNIFICANT Pd AND Pt CONTENTS IN ONLY CERTAIN PORPHYRY COPPER DEPOSITS WORLDWIDE	216

TYPICAL CHARACTERISTICS OF PORPHYRY Cu–Au–Pd±Pt DEPOSITS	216
CRITICAL FACTORS FOR THE FORMATION OF PORPHYRY Cu+Au+Pd ±Pt DEPOSITS	217
Sources of Metals and Sulfur in Porphyry Copper Deposits	217
Evolution of Mineralized Systems	221
Importance of Vapor Phase in the Transport of Ore Elements	221
Exploration – Key Characteristics of Cu+Au+Pd ±Pt Deposits	222
EVALUATION OF Pd AND Pt AS AN ECONOMIC FACTOR FOR PORPHYRY Cu–Au SYSTEMS	223
PALLADIUM AND PLATINUM RECOVERY	224
ACKNOWLEDGEMENTS	224
APPENDIX	235

EXPLORATION METHODS

11. PLATINUM-GROUP ELEMENTS EXPLORATION: ECONOMIC CONSIDERATIONS AND GEOLOGICAL CRITERIA	
A. Green, D. Peck	
INTRODUCTION	247
PGE DEMAND	247
PGE SUPPLY, RESOURCES AND EXPLORATION PROGRESS	249
ECONOMIC CONSIDERATIONS FOR EXPLORATION	251
PGE DEPOSIT CLASSIFICATION	252
MAGMATIC DEPOSITS – GENERAL CHARACTERISTICS	252
Age	252
Size and shape	254
Setting	257
LOW S MAGMATIC DEPOSITS	257
Overview	257
General Geology	257
Stratabound Reefs	257
Non-Stratabound and Contact Types	258
Mineralization	258
Stratabound Reefs	258
Non-Stratabound and Contact Types	258
Exploration Models	258
Stratabound Reefs	258
Exploration Methods	259
HIGH S MAGMATIC DEPOSITS	260
Overview	260
Setting of the Noril'sk-Talnakh Deposits	260
General Geology – Noril'sk-Talnakh Deposits	260
Mineralization	260
Exploration Model	261
Exploration Methods	261
BLACK SHALE-HOSTED PGE DEPOSITS	262
Classification	262
General Geology	262
Mineralization	262
Exploration Models	264
PGE as Bisulfide Complexes	264
PGE as Chloride Complexes	264
Exploration Methods	265
Examples	265

DISCUSSION: EXPLORATION STRATEGIES FOR PGE	265
Getting Started	265
Source-Transport-Trap Theory	265
Source	266
Transport	268
Trap	268
Recommended Strategies	269
SUMMARY	270

12. THE GEOPHYSICAL SIGNATURES OF PLATINUM-GROUP ELEMENT DEPOSITS	
S. Balch	
INTRODUCTION	275
GEOPHYSICAL METHODS	275
NI-CU SULFIDE DEPOSITS	277
Ultramafic Flows	281
Large Layered Intrusions	282
Magmatic Intrusions	283
DISCUSSION	283

13. PLATINUM-GROUP ELEMENTS IN GEOCHEMICAL EXPLORATION	
E.M. Cameron, K.H. Hattori	
INTRODUCTION	287
BEHAVIOR OF PGE IN WEATHERING ENVIRONMENTS	287
MOBILITY OF PGE IN SURFACE ENVIRONMENTS	290
GEOCHEMICAL EXPLORATION METHODS	291
Based on Clastic Dispersion	291
Stream Sediments	291
Glacial Till and Derived Soils	292
Based on Hydromorphic Dispersion	293
Organic Trapping of Pd along Drainage Courses	293
Biogeochemistry	294
Palladium and Platinum in Waters	296
Based on both Clastic and Hydromorphic Dispersion	296
Lake Sediments	296
Based on Residual Accumulations	298
Laterite Soils and Gossans	298
Use of Other Indicator Elements for PGE-Bearing Mineralization	301
ANALYTICAL CONSIDERATIONS AND QUALITY CONTROL	302
CONCLUSIONS	303

14. APPLICATION OF LITHOGEOCHEMISTRY TO EXPLORATION FOR PGE DEPOSITS	
W.D. Maier, S.-J. Barnes	
INTRODUCTION	309
LITHOGEOCHEMICAL INDICATORS USED IN THE EXPLORATION FOR PGE	
REEF-TYPE DEPOSITS	310
Introduction	310
Evaluation of Chalcophile Metal Depletion	310
Methods Applied to Whole Rocks	310
Methods Applied to Minerals	311
Contamination of Magma with Crust	313
Lithophile Incompatible Trace Elements	313
Strontium and Neodymium Isotopes	314
Osmium Isotopes	316

Lead Isotopes	316
Sulfur Isotopes	317
Oxygen Isotopes	318
LITHOGEOCHEMICAL INDICATORS USED IN THE EXPLORATION FOR MASSIVE	
Ni–Cu SULFIDE DEPOSITS	319
Introduction	319
Evaluation of Chalcophile Metal Depletion	319
Methods Applied to Whole Rocks	319
Methods Applied to Minerals: Ni Contents of Olivine and Pyroxenes	322
Compatible Elements as Indicators for Prospective Volcanological Environments	325
Contamination of Magma with Crust	326
Lithophile-incompatible Trace Elements	326
Strontium and Neodymium Isotopes	328
Osmium Isotopes	330
Sulfur Isotopes	330
Oxygen Isotopes	331
SUMMARY	332

CASE HISTORIES

15. FEDOROV-PANA LAYERED MAFIC INTRUSION (KOLA PENINSULA, RUSSIA):	
APPROACHES, METHODS, AND CRITERIA FOR PROSPECTING PGEs	
F.P. Mitrofanov, A.U. Korghagin, K.O. Dudkin, T.V. Rundkvist	
FEDOROV-PANA INTRUSION: GEOLOGY AND PGE-MINERALIZATION	343
History of PGE prospecting	343
General Description	344
Fedorov Massif	345
West Pana Massif	346
Northern PGE-bearing Reef	347
Southern PGE-bearing Reef	349
East Pana Massif	349
PGE-mineralization	349
PROSPECTING FOR PGE IN THE FEDOROV-PANA LAYERED INTRUSION OF THE	
KOLA PENINSULA: APPROACH AND EXPERIENCE	351
Prospecting Methodology	351
Geological Mapping and Prospecting Using Eluvial Boulders	351
Magnetic Survey	352
Electrical IP Survey	354
Inductive EM Survey	354
Geochemical Survey	355
Drilling	356
Key criteria for PGE-localization within the Fedorov-Pana intrusion	356
Criteria for the identification of PGE-bearing layered intrusions in the Kola platinum belt	357
CONCLUSIONS	357

16. THE DISCOVERY AND CHARACTERIZATION OF THE NICKEL RIM SOUTH DEPOSIT,	
SUDBURY, ONTARIO	
S.A. McLean, K.H. Straub, K.M. Stevens	
INTRODUCTION	359
General Geology	359
Discovery	360
Nickel Rim South Deposits	362
Contact Mineralization	362

Transitional Mineralization	364
Footwall Mineralization	364
Metal Zonation and Distribution	367
SUMMARY	367
<hr/>	
17. DISCOVERY AND GEOLOGY OF THE LAC DES ILES PALLADIUM DEPOSITS	
M.J. Lavigne, M.J. Michaud, J. Rickard	
EXPLORATION AND DEVELOPMENT HISTORY	369
REGIONAL GEOLOGY	376
Geology of the Lac des Iles Intrusive Complex (LDI-IC)	377
Geology of the Roby Zone	379
High-Grade Ore	380
North Roby Ore	383
Breccia Ore	383
Geology of the Twilight Zone	386
Baker Zone	387
DISCUSSION	387
<hr/>	
18. GEOCHEMICAL SURVEYS OF SOIL AND TALUS FINES AND THE DISCOVERY OF THE J-M REEF, STILLWATER COMPLEX, MONTANA	
M.L. Zientek, S.R. Corson, R.D. West	
INTRODUCTION	391
Surficial Geology of the Study Area	391
Igneous Stratigraphy of the Stillwater Complex	392
Discovery of the J-M Reef	394
Soil and Talus Fines Sampling Program	395
Johns-Manville Anomalous Samples	395
Population Statistics	395
Interpolated Surfaces	397
Platinum and Palladium Soil and Talus Fines Geochemistry in Relation to the Outcrop Trace of the J-M Reef	398
East Side of Boulder River Canyon	398
East Boulder Plateau and headwaters of East Boulder River	398
Iron Creek drainage and cliffs along the West Fork of the Stillwater River	398
West Fork Stillwater River to Stillwater River	404
Stillwater River to Black Butte	404
DISCUSSION AND SUMMARY	404
<hr/>	
19. EXPLORATION AND MINING OF THE MAIN SULPHIDE ZONE OF THE GREAT DYKE, ZIMBABWE – CASE STUDY OF THE HARTLEY PLATINUM MINE	
A.H. Wilson, R.T. Brown	
INTRODUCTION	409
EXPLORATION HISTORY	409
GEOLOGICAL SETTING, STRUCTURE AND STRATIGRAPHY	411
The Host Rocks to the MSZ and the Enclosing Rock Types	411
Distribution of Sulfide in the MSZ	414
PGE and Base Metal Mineralization in the MSZ	414
Platinum Group Mineralogy of the MSZ	416
Nature of the MSZ at Hartley Platinum Mine	416
PGE Distribution in the Ore Zone	417
Stratigraphic PGE Distributions in a Single Borehole	417
Inter-element Variations for the Data Set	417
Regional Controls on PGE distribution in the MSZ	418

Cumulative PGE Contents	419
MINING GEOLOGY AT HARTLEY PLATINUM MINE	422
Grade Control	422
Marking the BMSZ	423
Chip Sampling	424
Channel Sampling	424
Grade History	424
INTEGRATION OF EXPLORATION DATA, MINE EVALUATION AND GRADE CONTROL	426
SUMMARY AND CONCLUDING COMMENTS	427
<hr/>	
20. THE PLATINOVA REEF OF THE SKAERGAARD INTRUSION	
T.F.D. Nielsen, J.C.O. Andersen, C.K. Brooks	
INTRODUCTION	431
REGIONAL MAGMATIC AND GEOCHEMICAL CONTEXT	432
Precambrian Basement and Mesozoic to Paleogene Sedimentary Rocks	432
Paleogene Volcanic Rocks	432
THE SKAERGAARD INTRUSION	433
Access	433
Geological Introduction	435
Shape of the Intrusion	435
Zone and Sub-zones	437
Internal Structure	438
Line of Liquid Descent	438
EXPLORATION HISTORY	438
Pre-exploration Geochemical and Mineralogical Studies	439
Discovery Stage (1986–1988)	439
Early Exploration Stage (1989–1991)	440
Preliminary Resource Estimates	440
POST-EXPLORATION STUDIES (1991–2004)	441
Structure of the Platinova Reef	441
Stratigraphic Control	442
Mineralogy of the Platinova Reef	442
Sulfides, Magnetite and Ilmenite	442
PGE and Au phases	446
Metallurgic investigations	448
RE-JUVENATED EXPLORATION (2000– 2004)	449
TOWARD A MODEL FOR THE SKAERGAARD-TYPE MINERALIZATION	449
LESSONS LEARNED FROM THE PLATINOVA REEF	450
<hr/>	
21. POLYMETALLIC PLATINUM-GROUP ELEMENT (PGE)-Au MINERALIZATION OF THE	
SUKHOI LOG DEPOSIT, RUSSIA	
V.V. Distler, M.A. Yudovskaya	
INTRODUCTION	457
HISTORY OF EXPLORATION	457
REGIONAL GEOLOGICAL SETTING	458
Deposit-scale Geologic Setting	460
Types of Ore	461
Ore Composition	462
Age of Mineralization	463
Carbonaceous Matter in the Ore-hosting Black Shale	465
Carbonaceous Matter and Noble Metals	467
Mineralogy of the Ores	468
Native Gold	468

Minerals of the Fe–Ni–S System	468
Minerals of the Ni–Co–Fe–As–S System	471
Minor and Rare Minerals	472
Native metals and alloys	473
PLATINUM MINERALIZATION	474
Analytical Procedures	474
Direct Determination of the Mode of Occurrence of PGE	474
Ultra Heavy Concentrates	475
Carbon-rich Concentrates	475
General Features of PGE Mineralization	476
PGE Mineralogy	477
Some Important Results on Mineral and Concentrate Studies	480
Geochemical Characteristics of Mineralization REE Fractionation	480
Stable Isotopes	481
Thermochemical Characteristics of Ore-forming Fluids	481
Genetic Model	482
Searching Criteria for the Sukhoi Log-type Ore Mineralization	483

22. Ni–Cu–Cr–PGE MINERALIZATION TYPES: DISTRIBUTION AND CLASSIFICATION

R. Eckstrand	
A MAGMATIC DEPOSITS	487
A1 Basal Sulfide Concentrations	487
A1a Sills/chonoliths	487
A1b Impact melt	487
A1c Komatiites	487
A2 Reefs	487
A2a Sulfide Reefs	488
A2b Chromitite Reefs	488
A2c Magnetitite Reefs	488
A3 Internal Zones of Sulfide Dissemination	488
A4 Magmatic Breccia	488
A5 Stock-like Intrusions	488
A6 Sulfides in Ophiolites	488
A7 Tectonically Remobilized Sulfides	488
A8 Podiform Chromite	489
A9 Chromite-arsenide	489
B SEDIMENTARY DEPOSITS	489
B1 Placer deposits	489
B2 Black Shale	489
C HYDROTHERMAL DEPOSITS	489
C1 Polymetallic Veins	489
C2 Hydrothermally Remobilized Sulfide	489
C3 Unconformity U–Au–PGE	489
C4 Clastic sediment-hosted	489
C5 Iron formation	489
C6 Cu Porphyry	489
C7 Kupferschiefer	489
D LATERITE	490

MINERALOGICAL ASSOCIATION OF CANADA SHORT COURSE 35

EXPLORATION FOR PLATINUM-GROUP ELEMENT DEPOSITS

INTRODUCTION

The principal aim of this book and the short course is to bridge a gap between exploration geologists and academics. In keeping with the educational mandate of UNESCO, which has generously sponsored the activities of IGCP Project 479, our goal is to disseminate current knowledge of platinum group element ore genesis and exploration techniques to as wide an audience as possible worldwide. To further promote global dissemination of knowledge, the book will be available for free download from the MAC on the Internet after a one-year moratorium.

This book is designed to give a progression from the general to the specific, while focussing on factual information and avoiding unnecessary attention to some of the more contentious issues surrounding petrogenesis of PGE deposits. Introductory chapters by J.E. Mungall and J.J. Hanley provide an overview of the geochemical controls on the distribution of PGE in the Earth's crust. An attentive reader should be able to apply the contents of these first two chapters to make critical appraisals of the enormous range of petrogenetic models they will encounter in the published literature on PGE deposits.

In the next section, R.G. Cawthorn gives an overview of the geology, structure, and geochemistry of stratiform PGE deposits hosted by layered intrusions. These deposits account for the lion's share of known PGE reserves globally. The following article by M.J. Iljina and C.A. Lee describes PGE mineralization hosted by marginal facies of several major layered intrusions, which are increasingly dominating the tally of newly-discovered deposits worldwide. The fate of precious metal mineralization in the weathering environment is discussed next by T. Oberthür and F. Melcher, who focus on the deeply weathered profile over the Main Sulfide Zone of the Great Dike of Zimbabwe. The following article, by N.D. Tolstykh, E.G. Sidorov, and A.P. Krivenko, deals with the characteristics of placer deposits of PGE derived from deeply eroded Ural-Alaskan-type mafic-ultramafic complexes. Historically these deposits were the primary source of PGE. This section of the book concludes with an

overview by A. Wilde of the geology of PGE deposits formed by hydrothermal or meteoric fluids, an extremely varied group of deposits that promises to grow to major importance in future despite their historical lack of economic importance.

In the following section of the book, attention swings from PGE-dominated deposits to those which are primarily deposits of the base metals, but which also provide economically-significant PGE credits. The two largest such systems worldwide, the Sudbury mining camp and the Noril'sk-Talnakh deposits, are discussed first. C.E.G Farrow, J.O. Everest, D.M. King and C. Jollette provide a revised classification and petrogenetic scheme for the PGE-rich facies of the Sudbury ore deposits. N.T. Arndt then discusses the structure and petrogenesis of the enormous magmatic sulfide deposits at Noril'sk in the conduit system that fed the Siberian Traps volcanic succession, as part of his description of the importance of magma conduits in the generation of PGE-rich deposits. The vast and currently virtually unknown potential for PGE mineralization associated with Cu and Au-Cu porphyry deposits is discussed next by M. Economou-Eliopoulos, who provides a thorough summary of current knowledge of the distribution of PGE in these enormous deposits worldwide.

The third section of the book gives the reader a view of the principles and techniques presently used to direct and assist in the actual search for new deposits of the PGE. All of the articles in this section were written by people with extensive applied experience in the methods they describe. A. Green and D. Peck share their views on the fundamental economic and geological considerations that must inform the explorationist in his or her search for a prospective region in which to explore. An overview of the geophysical tools available to help in the detection of PGE deposits is given by S. Balch. E.M. Cameron and K. Hattori describe a variety of methods of detection of PGE deposits based on sampling of surficial materials, after which W.D. Maier and S.-J. Barnes show how to use systematic studies of whole rock

geochemistry to infer the presence of invisible or buried PGE mineralization in large magmatic systems.

The fourth, and final, section of the book is a series of case studies outlining how several major deposits of the PGE were discovered or brought into a state of feasibility for exploitation. F.P. Mitrofanov and others describe the discovery of mineralization in the Fedorov-Pana intrusion in the Kola Peninsula, giving valuable insights into the approaches necessary for exploration in areas of low topographic relief and deep permafrost. S.A. McLean, K.H. Straub, and K.M. Stevens then show how a well-conceived exploration program in the shadow of a head-frame turned up an important new discovery at the Nickel Rim deposit, in a mining camp that has already seen over a century of determined exploration. The discovery and development of the Lac Des Iles palladium deposit is described by M.J. Lavigne, M.J. Michaud and J. Rickard, who give a frank assessment of the relative utility of the various exploration methods available in areas of thin but persistent recent glacial overburden in the boreal forest. The importance of soil geochemical surveys in the discovery of the J-M reef of the mountainous Stillwater intrusion is then discussed by M.L. Zientek, S.R. Corson, and R.D. West. One of the eternal problems facing miners of PGE is grade control, due to the commonly invisible nature of the ore minerals. This important topic is addressed in detail by A.H. Wilson and R.T. Brown, in their account of the development of the Hartley Platinum Mine in the Main Sulfide Zone of the Great Dike of Zimbabwe. A fascinating account of serendipity and perseverance in the discovery of the extremely well-hidden Platinoval Reef of the Skaergaard intrusion is given by T.F.D. Nielsen, J.C.O. Andersen, and C.K. Brooks. There is a lesson well taken, in the ease with which major deposits of the PGE can be

overlooked even in the most-intensively studied rocks in the world. The concluding case study is that of the Sukhoi Log orogenic Au-Pt deposit in central Asia, written by V.V. Distler and M. Yudovskaya. Their study shows how the application of unconventional ore deposit models to apparently conventional deposits can pay off in the discovery of PGE mineralization.

The book concludes with a PGE ore deposit classification and accompanying thematic maps of PGE deposit distribution worldwide, prepared by R. Eckstrand and L. Chorlton from data contained in the database of the World Minerals Project of the Geological Survey of Canada.

With contributors originating or working in countries including Canada, the USA, the United Kingdom, Germany, Greece, Finland, Denmark, Russia, Japan, South Africa, Zimbabwe, and Australia, this book is the fruit of a truly international effort by dozens of people representing the best of academic and industrial experts on PGE deposits. As Editor, I am indebted to them and to a small army of reviewers who gave generously of their time to keep the book balanced, accurate, and topical.

This book is published by the Mineralogical Association of Canada as the handbook to accompany Short Course "Exploration for Platinum Group Element Deposits". The course is also sponsored by International Geological Correlation Project 479 "Sustainable Use of PGE in the 21st Century: Risks and Opportunities", the United States Geological Survey, and The Society of Economic Geologists. Financial support permitting presentations of chapters at the short course by employees of Falconbridge Ltd, FNX Mining Company Inc, Aeroquest Limited, and Ridge Mining has been instrumental in the success of the short course.

James E. Mungall
University of Toronto,
20 June 2005

CHAPTER 1: MAGMATIC GEOCHEMISTRY OF THE PLATINUM-GROUP ELEMENTS

James E. Mungall
Dept of Geology, University of Toronto
22 Russell St, Toronto, ON, M5S 3B1, Canada
E-mail: mungall@geology.utoronto.ca

INTRODUCTION

This chapter has been written with the aim of providing readers with a series of simple conceptual tools to guide their choice of exploration targets in the search for PGE. Upon a first reading it might appear rather dense, and indeed, the rest of the book can probably be understood without consulting this chapter at all. My hope is that those readers who are interested enough in the nuts and bolts of igneous petrology will be able to use this chapter to create their own set of tools with which they can test ideas as they develop exploration databases. Armed with complete exploration assays for Cu, Ni, Pt, Pd, Au, and S in their mineralized samples, and possibly with a few major-element whole-rock analyses of basalts, chilled margins, and mineralized cumulate rocks, a reader can use the equations and concepts explained here and elsewhere in this book to understand how their rocks fit into the spectrum of recognized PGE deposits, and to refine the search in their own area for more mineralization.

The vast majority of the world supply of platinum group elements (PGE) is produced from magmatic ores derived from basaltic magmas. The study of the origins of PGE deposits is therefore intricately linked to the more general study of petrogenesis of basaltic magmas. The formation of magmatic PGE ore deposits depends on the successful operation of several processes. During melting, elements present throughout the upper mantle at subeconomic concentrations must find their way into the magma at sufficient concentration to make it fertile. As the magma travels from the asthenosphere to a place in the lithosphere that will eventually be accessible to mining, it undergoes cooling and crystallization. At some point, before crystallizing phases have removed the elements of interest, the magma must become saturated with a phase that concentrates the PGE to high tenors and this phase must be collected from a large volume of magma into a small enough volume of rock to provide attractive bulk rock metal grades. The final

requirement for the generation of an orebody is for all of the preceding processes to act on a large enough volume of magma to produce sufficient tonnage to justify the capital costs of opening a mine. The principal phases that can participate in the deposition of ores of the PGE are platinum group minerals (PGM) directly precipitated from silicate melt, immiscible sulfide liquids, and magmatic volatile phases. In this article, I briefly review the origins of basaltic magmas, the geochemical controls on the compartment of the PGE in igneous systems, and the petrogenetic consequences of these controls with reference to the deposition of PGE ores. I make passing reference to the role of fluids in transporting and concentrating the PGE in igneous systems, but that subject is treated in greater depth in the following chapter. The emphasis in this chapter is on the fundamental geochemical controls on PGE in igneous systems; descriptions of actual occurrences appear throughout the remainder of this book. The appendix to this chapter includes derivations of some equations that are useful in numerical modeling to test simple petrogenetic hypotheses. Throughout this article I make passing reference to various deposits without providing any details. I have tried in such cases to refer to other chapters in this volume in which the deposits in question are discussed at greater length.

PLATINUM-GROUP ELEMENTS

The platinum-group elements (Ru, Rh, Pd, Os, Ir, and Pt) are Group VIII and VIIIA transition metals with positions in the fifth and sixth rows of the periodic table under Fe, Co, and Ni. All six of the PGE share with Fe and Ni the tendency to prefer the formation of metallic bonds over ionic bonds, behavior which places them in the siderophile (*i.e.*, iron-loving) group of elements (*e.g.*, Barnes & Maier 1999). The PGE also share with Cu, Ag and Au a tendency to favor the formation of covalent bonds with sulfur in preference to ionized bonds with oxygen, behavior which places them in the

group of chalcophile (*i.e.*, copper-loving) elements. The fundamental controls on the behavior and distribution of the PGE in the Earth are therefore posed by the presence or absence metallic or sulfide phases. The degree to which the PGE are concentrated by various phases is summarized in Table

1-1; these partition coefficients are discussed in detail later in this article. Due to their siderophile nature the PGE were strongly depleted from the silicate Earth during the segregation of its molten iron-nickel core, leaving average PGE concentrations in the bulk silicate Earth of between 1 and 7

TABLE 1-1A. PARAMETERIZATIONS OF PARTITION COEFFICIENTS AND SOLUBILITIES OF PGE IN COMMON MAGMATIC PHASES.

Solubilities (ppm) of pure metals in silicate melts, at 1200°C and $\log f(O_2)$ within two units of QFM.	
Parameterization	Reference
$\log([Ir]) = 0.23\log f(O_2) + 2.46$	Borisov <i>et al.</i> (1994)
$\log([Rh]) = -5440/T(K) + 3.9 + 0.5(2.5 + \log f(O_2))$	Fortenant <i>et al.</i> (2003)
$\log([Pt]) = -2830/T(K) + 2.9 + 0.5\log f(O_2)$	Fortenant <i>et al.</i> (2003)
$\log([Pd]) = 0.17\log f(O_2) - 3730/T(K) + 4.145 (<QFM)$	Borisov <i>et al.</i> (1994)
Partition coefficients $D_M^{sul/sil}$ (sulfide melt/silicate melt) for base and precious metals.	
Parameterization	Reference
$\log(D_{Cu}^{sul/sil}) = 0.38 \frac{\log f(S_2)^{1/2}}{\log f(O_2)^{1/2}} + 1.27$	Gaetani & Grove (1997)
$\log(D_{Ni}^{sul/sil}) = 0.60 \frac{\log f(S_2)^{1/2}}{\log f(O_2)^{1/2}} + 1.40$	Peach & Mathez (1993)
$\log(D_{Co}^{sul/sil}) = 0.69 \frac{\log(fS_2)^{1/2}}{\log(fO_2)^{1/2}} - 0.88$	Gaetani & Grove (1997)
$\log(D_{Cu}^{sul/sil}) = 0.2548 \frac{\log(fS_2)^{1/2}}{\log(fO_2)^{1/2}} + 1.9501$	Ripley <i>et al.</i> (2002)
Partition coefficients $D_M^{mss/liq}$ for PGE. Regressions are from Figure 1-13; data are from Fleet & Stone (1991), Fleet <i>et al.</i> (1999b), Ballhaus <i>et al.</i> (2001), Barnes <i>et al.</i> (2001), Mungall <i>et al.</i> (2005)). S+O in the sulfide liquid is expressed in mole%.	
Parameterization	Reference
$\log(D_{Au}) = 0.0021(S+O) - 2.2551$	this study
$\log(D_{Ir}) = 0.0201(S+O) - 0.2658$	this study
$\log(D_{Ru}) = -0.0758(S+O) + 4.644$	this study
$\log(D_{Rh}) = 0.0390(S+O) - 1.449$	this study
$\log(D_{Pt}) = 0.1523(S+O) - 8.6063$	this study
$\log(D_{Pd}) = 0.0837(S+O) - 5.0498$	this study
Solubility of sulfur at sulfide saturation in basaltic magma, as function of P, T (Mavrogenes & O'Neill 1999)	
$\ln S_{Scss} = \frac{-6684}{T(K)} + 11.52 - \frac{0.047P(Kbar)}{T(K)} + \ln a_{FeS}^{sulfide}$	
To a first approximation, it might be appropriate to assume ideal mixing of NiS, CuS, FeO and FeS in the sulfide liquid, permitting a_{FeS} to be estimated simply as the mole fraction of FeS.	

TABLE 1-1B. PREFERRED VALUES OF PARTITION COEFFICIENTS FOR MAGMAS NEAR 1200°C AND OXYGEN FUGACITY NEAR THE QFM.

	Cu	Ni	Co	Os	Ir	Ru	Rh	Pt	Pd	Au	Reference
Cpx/silicate liquid								1.5			Gaetani & Grove (1997)
Olivine/silicate liquid					2						Brenan <i>et al.</i> (sub.)
Spinel/silicate liquid					5–132	1000	75		0.01		Brenan <i>et al.</i> (2003)
Sulfide/silicate liquid	1383	800			14000				23000	15000	Peach <i>et al.</i> (1990)
Mss/sulfide liquid	0.2	0.6–1.5			5	10	4	0.05	0.1	0.005	Fleet <i>et al.</i> (1999a)
				4							Mungall <i>et al.</i> (2005)
											Brenan (2002)

ppb. In the time since core formation, the distribution of PGE has been most strongly affected by their sequestration in sulfide liquids in the mantle and crust. The concentrations of the PGE in the bulk Earth and bulk silicate Earth are listed in Table 1-2.

A high-grade PGE ore deposit typically contains several ppm (equivalent to grams per tonne) of Pt and Pd combined, with cutoff grades around 2 ppm being normal, reflecting a concentration of 1,000 to 10,000 times that of the bulk silicate Earth.

It is convenient to present geochemical data for the PGE on plots similar to the familiar 'spider' diagrams used for lithophile trace elements, with their abundances expressed as ratios of sample concentration to concentration in a widely recognized reservoir such as the primitive mantle or average CI chondritic meteorites. The order in which elements are plotted on the abscissa of ratio plots is generally chosen to reflect increasing tendency to partition into silicate melts toward the left side of the diagram, but in the case of the PGE it is sulfide – silicate or metal – silicate partitioning that is important, and unfortunately the relevant partition coefficients have been extremely difficult to measure precisely. The convention that has been adopted is to plot the PGE in decreasing order of melting point of the pure metal, with the sequence Os, Ir, Ru, Rh, Pt, Pd. The other commonly analyzed chalcophile elements are often added to the plot, in the sequence (Ni, Co), PGE, (Au, Ag, Cu). Examples of ratio plots appear near the end of this article, where the PGE contents of various magma types are discussed.

It is conventional to refer to the subgroup Os, Ir, Ru as the IPGE, and Pt, Pd and sometimes

Rh as the PPGE, in recognition of the tendency for these two subgroups to behave coherently during magmatic processes.

GEOLOGICAL CONTROLS – GENESIS OF PARENTAL MAGMAS

Origins of Basaltic Magmas

In order to be able to relate the geochemistry of the PGE to the tectonic and magmatic processes that give rise to magmatic suites which may form the targets of exploration programs, it is necessary to understand the basic controls on basaltic magmatism on the Earth. I therefore begin with an overview of the principal types of magmatism before discussing PGE geochemistry. This preliminary discussion combines many concepts which are in general circulation; for excellent discussions of the processes involved and for numerous citations to primary literature the reader is referred to Schubert *et al.* (2001).

Basaltic magmas originate in the upper mantle and travel to the crust or the surface due to their buoyancy relative to solid rock of the lithosphere. There are four principal mechanisms for the generation of basaltic magmas. At mid-ocean spreading centers, extension of the lithosphere permits normal asthenospheric mantle to rise to very shallow depths, causing decompression melting at low pressures to form mid-ocean ridge basalt (MORB; Fig. 1-1). The basaltic melt is able to separate from its peridotite source at very low melt fractions, percolating upward. As a given parcel of mantle rises under the ridge, it undergoes progressively greater degrees of partial melting. Fractional removal of melt throughout this rising melt region results in a complex process of re-

TABLE 1-2. CHALCOPHILE ELEMENT CONTENTS OF TERRESTRIAL RESERVOIRS AND COMMON ROCK TYPES (Cu, Ni, Co IN PPM, PGE AND AU IN PPB).

	Cu	Ni	Co	Os	Ir	Ru	Rh	Pt	Pd	Au	Reference
Bulk Earth (CI chondrite)	120	10500	500	490	455	710	130	1010	550	140	McDonough & Sun (1995)
Bulk silicate Earth (primitive mantle)	30	1960	105	3.4	3.2	5.0	0.9	7.1	3.9	1.0	McDonough & Sun (1995)
average continental crust	25	56	24	0.05	0.05	0.1	0.06	0.4	0.4	2.5	Wedepohl (1995)
average komatiite	64	1246		1.5	1.7	4.4	1.4	10.5	10.5	2.9	Crockett (2002)
CFB picrite Tk	69	295			0.190		0.29	10.5	9.0	1.5	Brüggemann <i>et al.</i> (1993)
CFB tholeiite Mr	109	97			0.070		0.23	4.7	4.0	1.61	Brüggemann <i>et al.</i> (1993)
CFB tholeiite Nd	50	16						0.12	0.13		Lightfoot & Keays (2005)
MORB	61	106		0.021	0.009			0.304	0.265		Peucker-Ehrenbrink <i>et al.</i> (2003)
	88	144		0.022	0.030	0.067	0.008	0.41	0.46	1.2	Crockett (2002)
boninite	27	522			0.07	1.2		5.4	5.5	0.44	Peck & Keays (1990)
boninite				0.03	0.08	0.18		6.02	3.49		Woodland <i>et al.</i> (2002)
arc picrite				0.055	0.073	0.19		3.0	2.4		Pearson & Woodland (2000)
arc andesite				0.018	0.002	0.13		0.95	0.38		Pearson & Woodland (2000)
alkali OIB	47	148		0.061	0.22			0.95	0.75	1.3	Crockett (2002)
tholeiitic OIB	125	186		0.38	0.38	0.69	0.11	3.6	2.4	1.8	Crockett (2002)
picritic OIB	103			0.863	1.32	1.48		5.94	7.32		Bennet <i>et al.</i> (2000)

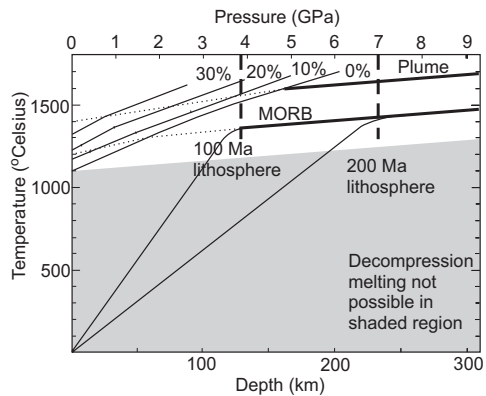


FIG. 1-1. P-T diagram showing the origins of MORB and plume magmas. Diagonal lines from the origin are conductive geotherms for ancient (>200 Ma) and young (100 Ma) continental lithosphere. The adiabatic geotherm of the convecting mantle is shown as a heavy line joining the two conductive geotherms, labeled 'MORB'. The dotted extension of this curve to the surface shows the path it would follow during adiabatic ascent, and is slightly deflected downward from the potential temperature of 1280°C due to the cooling effects of the heat of fusion consumed during melting. The mantle beneath continental crust is brittle and cold to the base of the conductive portion of the geotherm, at the indicated depths of about 125 km to 225 km for lithosphere that was cratonized 100 to 200 Ma previously. Older subcontinental lithosphere is probably not much thicker. Extensional thinning of continental lithosphere may allow asthenospheric mantle to rise along the adiabat (MORB dotted line) until partial melting begins at about 2 GPa. Continued rifting to the point of opening of a new ocean basin allows up to about 15% partial melting to form MORB-type magmas, as indicated by the melting contours labeled 0% to 30%. Plumes may carry much hotter peridotite up below the subcontinental lithosphere, following an adiabat with a potential temperature of about 1500°C as shown.

equilibration of deep-seated small-degree partial melts with shallower, larger-degree partial melts, all of which pool in the axial magma system before being erupted as MORB. The pooling of melts from throughout the melting column lends a monotonous similarity to the MORB, and allows their genesis to be modeled to a first approximation as a batch equilibrium melting process. The MORB magma is focused into the axis of the spreading center and leaves the mantle to form ophiolitic crustal sequences of ultramafic cumulates, gabbroic plutons, sheeted gabbro dikes, and overlying pillow basalts. By the time a particular volume of mantle peridotite has risen through the melting zone and

spread to the side under the newly formed oceanic crust, it will probably have had about 15% of its mass removed as basaltic melt, to leave a strongly melt-depleted harzburgitic residue.

When similar processes cause extension of the much thicker continental lithosphere, decompression melting also occurs, but at much higher pressure than in the case of MORB (Fig. 1-1). The resulting magmas are generally alkaline in character, rich in volatile components such as H₂O and CO₂, and commonly have compositions reflecting large contributions from ancient continental lithosphere that has undergone a long history of metasomatic addition of incompatible elements. Extension may continue until the continent has been completely rifted apart to form a new ocean basin. In this case extensional melts will show a progression in composition reflecting greater degrees of partial melting at shallower depths until normal MORB begins to erupt as the new oceanic crust forms between the rifted continental segments. Melt volumes remain small, and the stratigraphic sequence of the resulting continental margin is dominated by the deposition of clastic sediments over the block-faulted former continental crust. If rifting is aborted before a new ocean basin has opened, then the rift-related volcanic sequence will be restricted to small-volume, deep-sourced alkaline magmas.

A third mechanism for the generation of basaltic melts in the mantle is related to the upwelling of abnormally hot peridotitic mantle from either the core-mantle boundary or the transition zone between the lower and upper mantle. These masses of hot mantle rock are referred to as plumes, and it is generally assumed that they arrive at the base of the lithosphere as mushroom-shaped blobs whose heads have diameters of up to 2500 km (Fig. 1-2). The center of a plume (the tail) is thought to be an axial domain along which abnormally hot mantle rock will continue to rise diapirically for many millions of years after the initial plume head has arrived, spread, and cooled beneath the lithosphere. Hotspots such as the one which has formed the Hawaiian island chain are regarded as the physical manifestations of plume tails. As illustrated in Figure 1-1, the amount of melt that can be generated from a plume head as it rises to the base of the lithosphere can be much greater than the 15% melting that occurs at mid-ocean spreading centres. The degree of partial melting achieved by the hottest plume heads probably has reached 40% or more, to form komatiite melts. Smaller degrees

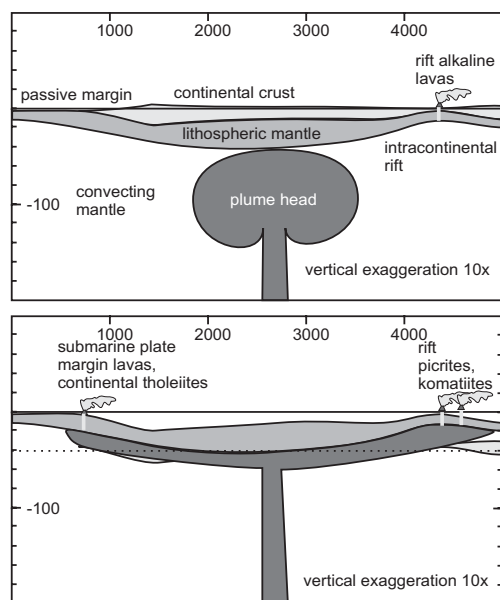


FIG. 1-2. Cartoon of a plume head arriving and spreading under thick continental lithosphere. If a plume impinges on lithosphere much older than 100 Ma, no melting will ensue (compare with Figure 1-1). The buoyant plume will migrate laterally under the continental root until it rises under younger, shallower lithosphere with a geotherm like that shown for 100 Ma. If the plume simply rises to the base of 100 Ma lithosphere then it will undergo about 20% partial melting, to produce picrite or high-Mg basalt. If the plume rises into a rift or ancient passive margin, the extent of melting might reach the indicated maximum possible extent of > 30%, to produce komatiite.

the hottest plume heads probably has reached 40% of partial melting will generate less magnesian magmas ranging from komatiite through picrite at melt fractions on the order of 25% to high-Mg basalts between 20 and 15% partial melting. Ascent and melting of plume heads occurs quickly, leading to the eruption of millions of km^3 of picrite and basalt during times commonly less than 1 Ma.

Under old, thick, continental lithosphere a moderately hot plume head may not reach sufficiently shallow depth to begin to melt. In such cases it will spread laterally under the lithosphere and rise under the shallowest, thinnest portions of the lithosphere where it has been rifted or along its continental margins (*e.g.*, Johnston & Thorkelson 2000). As the hot plume material approaches the thinner edges of the continental lithosphere it will begin to melt, leading to the preferential emplacement of plume-derived picritic magmas on continental margins or within pre-existing rift structures.

This process has been shown to have occurred in the North Atlantic Volcanic Province (NAVP) when picrite emerged in widely spaced localities such as Scotland and west Greenland before rifting of the Laurasian continent permitted the formation of the main volcanic sequences in East Greenland. A similar process probably accounts for the existence of widespread komatiitic to picritic magmatism around the entire Superior Province margin circa 1919 to 1880 Ma. These magmas were emplaced onto or through passive margin sequences that recorded continental rifting at least 100 Ma prior to the arrival of the picritic suites.

If a plume head spreads into a continental rift environment it may promote further rifting and the formation of a new oceanic spreading center (Courtillot *et al.* 1999). In this case the final rifting event will occur during the eruption of very large quantities of picritic and basaltic magmas derived by decompression melting of the plume head. The stratigraphic column of the continental margin succession will be dominated by basaltic lavas and comagmatic intrusions, followed at later times by clastic sediments. The resulting passive margin sequence is referred to as a volcanic rifted margin (White & McKenzie 1989), in contradistinction to the non-volcanic type described above. Volcanic and non-volcanic rifted margins can be distinguished from one another by the relative timing of volcanism and sedimentation.

The previously described mechanisms cause melting to occur by perturbing the thermal structure of the mantle, bringing hot material into shallow depths where it will spontaneously begin to melt. A fourth common mechanism for the generation of important volumes of basaltic magmas involves the transfer of volatiles (dominated by H_2O) from subducting lithospheric slabs into the overlying wedge of normal asthenospheric mantle, without substantially changing its temperature. The addition of volatiles sharply decreases the solidus temperature of peridotite, permitting the removal of large fractions of partial melt without heating or decompression (Fig. 1-3). The resulting basaltic magmas rise to form linear chains of intrusions and volcanoes called island arcs when they form on oceanic lithosphere or magmatic arcs if they are situated on continental margins. Arc magmas are volatile-rich and moderately to extremely oxidized compared to MORB or plume-related magmas, and have distinctive and easily recognizable patterns of trace element abundance.

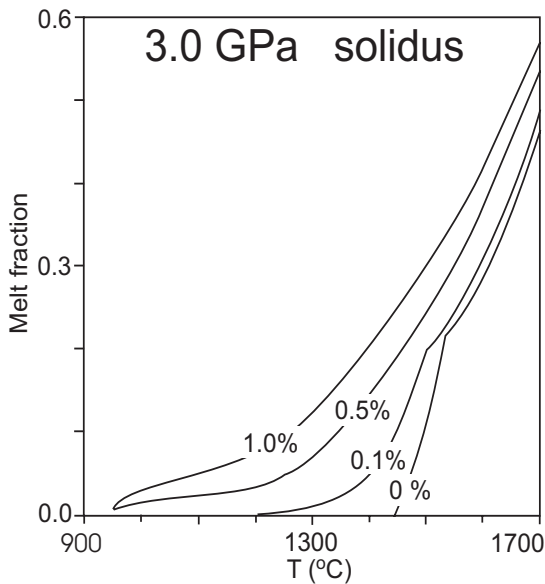


FIG. 1-3. P-T diagram showing the effects of addition of volatiles to the mantle solidus, calculated using the parameterization of Katz (2003). Addition of just 0.1 wt% H₂O to dry mantle peridotite lowers the temperature at which melting first occurs by about 250°C. Continued addition of small quantities of H₂O permits melting at very low temperatures and greatly increases the degree of partial melting at a given temperature. The effects of carbonic fluids (e.g., CO₂, CH₄) and K₂O are similar to those of H₂O.

Physical Environments for PGE Deposits

To form PGE deposits, magmas must initially be PGE-rich, and a process must operate by which phases rich in the PGE become highly concentrated out of a large volume of magma into a small volume of rock. The two principal collector phases are sulfide liquid and chromite. The optimal physical setting for mechanical collection of either sulfide liquid or chromite is a conduit through which a large volume of magma passes (Fig. 1-4). If the magma reaches saturation in the collector phase always at the same point in the conduit, then that phase will tend to collect in one place from the entire volume of magma that passes that point. Alternatively, if the magma was already saturated with a collector phase that was carried along in suspension, the collector phase may be preferentially deposited at a single site due to fluid dynamic controls like a lowering of velocity at a widening of the conduit.

Conduits come in many shapes and sizes. Examples include dikes (the Great Dyke, Zimbabwe), sills (e.g., Noril'sk, Russia), large layered intrusions which are in essence just

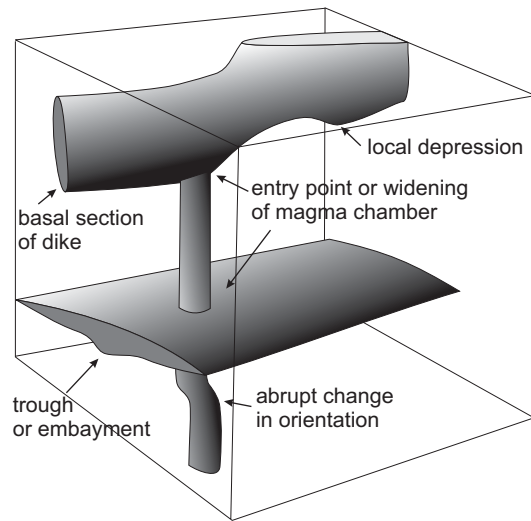


FIG. 1-4. Cartoon of conduits showing common geometries of structural traps in which sulfide liquid may accumulate. Sulfide melt may form due to assimilation of wallrocks at any point along the margins of the intrusion, but can be entrained in flowing magma or settle through crystal mushes and will only accumulate to significant extents where either a level surface or concavity arrests its motion, or where sudden changes in flow regime allow suspended droplets to be dumped together.

enormous sills (Bushveld Intrusion, South Africa, Stillwater Intrusion, USA), and cylindrical bodies of ultramafic cumulates such as Alaskan-Uralian type complexes. The mineralized zones formed by concentrations of the collector phase may be zones of disseminated or massive sulfide which form as pools along the bases of magmatic conduits or chambers, stratiform bodies enriched in sulfide or chromite, or they may be wispy, layered, or tubular concentrations of chromite hosted by ultramafic cumulate rocks.

A signal characteristic of a conduit system is that it typically contains excessive quantities of cumulus phases (which may include the collector phase itself), such that the bulk composition of the rocks preserved within the conduit differs markedly from the bulk composition of the original magma that passed through it. Conduits can therefore commonly be recognized as bodies of ultramafic rock lacking complementary mafic or felsic fractionates. A secondary characteristic of conduits for basaltic magmas is the common presence of a thermal aureole much wider than would be expected considering the size of the intrusion. This can result from the continuous passage of hot magma through the conduit, depositing heat in its host rocks much

more efficiently than could be accomplished by simple injection and cooling of a single pulse of liquid.

GEOCHEMICAL CONTROLS – PARTITIONING OF CHALCOPHILE ELEMENTS

The key to understanding how igneous processes affect the distribution of the PGE is knowledge of how the PGE are distributed between coexisting phases. This knowledge can then be combined with field-based observations of the mechanical sorting of these phases (*e.g.*, accumulation of sulfide, volatile migration) to infer the overall controls on the deposition of the PGE. The principal phases of interest are silicate minerals, silicate melt, oxide minerals, alloys and other PGM, Fe–S–O (*i.e.*, sulfide) liquids, and aqueous fluids. A given magmatic system may contain at least six such phases at once. In the following sections, I review what is currently known about partitioning of the PGE, Cu and Ni between various common pairs of phases, beginning with the possible precipitation of PGM directly from the silicate magma. Preferred values of key geochemical parameters or simple equations which can be used to predict them are provided in Table 1-1.

Direct Precipitation

Despite their exceedingly low natural abundances, considerable evidence exists to show that the PGM are able to precipitate directly from silicate magmas as phenocryst phases. The most common examples, and the only ones for which there is direct field and experimental evidence, are laurite (RuS₂) and alloys. Brenan & Andrews (2001), and Bockrath *et al.* (2004) have demonstrated that under appropriate conditions of T, P, *f*O₂ and *f*S₂, it is possible for laurite and PGE alloys to precipitate from basaltic liquids. The common occurrence of laurite and alloys as inclusions within natural chromite crystals in layered intrusions and ophiolites has been cited as field evidence for this process (Peck *et al.* 1992, Cabri 1992). Apart from alloys, discussed in the following paragraphs, there is little evidence for the natural occurrence of any other PGM as phenocrysts. Most natural PGM are probably formed during cooling and recrystallization of primary minerals within which the PGE were originally dissolved in solid solution (*e.g.*, Peregoedova & Ohnenstetter 2002, Peregoedova *et al.* 2004).

PGE Alloy Solubility

The PGE are all able to exist as alloys or pure metals in equilibrium with silicate melts, and natural alloys are known of all of the members of the group. Several experimental studies have shown that pure metals dissolve in silicate melts as oxide species, through the following type of dissolution reaction (Borisov & Palme 2000; and references to Table 1-1):



The valence state of the metal once it has dissolved is equal to $2n$; for example, Pt combines with $\frac{1}{2} O_2$ and dissolves as PtO, by acquiring a +2 valence. The O₂ in reaction 1 is of critical importance, because it means that in the absence of other concentrating phases, PGE solubilities with respect to alloy phases each depend sensitively on the free oxygen content of the system, represented by oxygen fugacity *f*O₂ in equation 2;

$$X_{\text{PtO}}^{\text{sil}} = \frac{K_1 \cdot a_{\text{Pt}}^{\text{alloy}} \cdot fO_2^{n/2}}{\gamma_{\text{PtO}}^{\text{sil}}} \quad (2)$$

If activity coefficients do not depend on composition, a graph of $X_{\text{PtO}}^{\text{sil}}$ versus log *f*O₂ at alloy saturation should give a straight line, whose slope can be used to determine the valence state of the dissolved metal. A complicating factor stems from the fact that natural magmas all contain Fe. Because Fe forms alloys with all of the PGE to varying degrees, and similarly several of the PGE alloy readily together, the activity of PGE in the alloy is below unity in natural systems, reducing the PGE concentration at saturation (*i.e.*, the solubility). By considering the activity–composition relations for Fe-PGE alloy systems, one can use the measured solubilities of native PGE in Fe-free systems to calculate the concentrations expected in natural magmas (Fig. 1-5; Borisov & Palme 2000). Comparison with the concentrations of the PGE in various natural magma types listed in Table 1-1 indicates that many basaltic magmas are at or near to saturation with respect to alloys of Os, Ir, Ru and Pt. We should therefore anticipate that under some circumstances direct precipitation of these alloys will exert an important control on the distribution of these elements.

A peculiar attribute of the PGE is that they are able to form minute crystals of alloy called micronuggets, apparently in equilibrium with enclosing silicate melts or aqueous fluids (*e.g.*,

Borisov & Palme 1997). Micronuggets are too small to detect by optical or even scanning electron microscopy, but are detectable by microanalytical tools like laser ablation – inductively coupled plasma – mass spectrometry (LA–ICP–MS) (Sylvester 2001).

Bulk analysis of synthetic glass or crystals containing micronuggets gives an apparent concentration far above the true equilibrium concentration, because the analyte is actually a mechanical mixture of glass and alloy particles. During LA–ICP–MS analysis the micronuggets appear as transient peaks in PGE count rates as the laser burns through them (Fig. 1-6). An adequate thermodynamic description of micronuggets or clusters, as they may be called if they are of colloidal size (Tredoux *et al.* 1995), has not yet been devised and their relevance to natural systems remains an open question. Their importance to

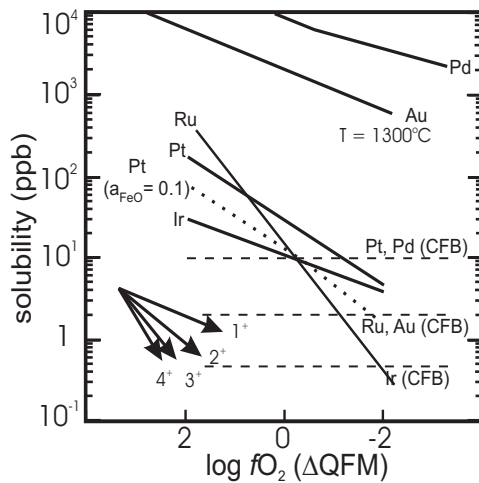


FIG. 1-5. PGE concentration vs fO_2 at alloy saturation, with and without adjustment for a_{FeO} . Arrows show the slopes of the alloy solubility curves expected if they are dissolved as cations with the indicated valence states. Typical concentrations of Pt, Pd, Au, Ru and Ir in natural continental flood basalt (CFB) are shown as horizontal dashed lines. In CFB near to the QFM oxygen buffer, the observed concentrations of Pt is near to alloy saturation. Alloys of Ir, Ru and Os will have solubilities lower than the pure metal solubilities shown, so that Ru and Ir are also probably at or near to saturation with alloy in the natural compositions shown. Minor reduction in fO_2 , such as can be locally induced by the crystallization of chromite, will lead to the growth of alloy crystals. Pd and Au are not close to alloy saturation and are therefore not expected to crystallize directly from basaltic magmas. After Borisov & Palme (2000).

experimental studies has only recently been appreciated, with the result that many early attempts to measure partition coefficients for PGE were bedeviled by incorrect measurements of PGE concentrations in bulk materials (Ertel *et al.* 1999).

Partition Coefficients

The most convenient way to discuss the distribution of elements between coexisting phases is through the use of the Nernst partition coefficient $D_M^{a/b}$, which is defined as the concentration of an element M in one phase a divided by its concentration in another, b . For example, we can consider the distribution of Pt between sulfide melt and monosulfide solid solution (mss, *i.e.*, magmatic pyrrhotite). The exchange can be treated as a heterogeneous chemical reaction between components of the solid and liquid solutions, as follows:



The equilibrium constant for reaction 3 is defined as

$$K_1 = \frac{a_{PtS}^{mss} \cdot a_{FeS}^{sul}}{a_{PtS}^{sul} \cdot a_{FeS}^{mss}} \quad (4)$$

where a denotes the activity of the subscripted component in the superscripted phase. By introducing activity coefficients γ and solving for the weight fractions X of Pt in the two phases we find that

$$\frac{X_{PtS}^{mss}}{X_{PtS}^{sul}} = \frac{K_1 \cdot \gamma_{PtS}^{sul} \cdot X_{FeS}^{mss} \cdot \gamma_{FeS}^{mss}}{\gamma_{PtS}^{mss} \cdot X_{FeS}^{sul} \cdot \gamma_{FeS}^{sul}} \quad (5)$$

If the mole fractions of FeS and the activity coefficients of the Pt species do not change significantly in the sulfide melt and mss as Pt is exchanged between them (*i.e.*, Pt is behaving as a trace constituent) then these terms and the activity coefficients can be treated as constants. The stoichiometric term to change PtS to Pt can be incorporated, and all these terms can be rolled into a single constant. If this constant shows little dependence on Pt content of either phase, in other words the element obeys Henry's Law:

$$D_{Pt}^{mss/sul} \equiv \frac{X_{Pt}^{mss}}{X_{Pt}^{sul}} \approx constant \quad (6)$$

If D is larger than 1 it is preferentially retained by the upper phase (mss in this example), and the element is considered to be a compatible element. On the other hand, incompatible elements.

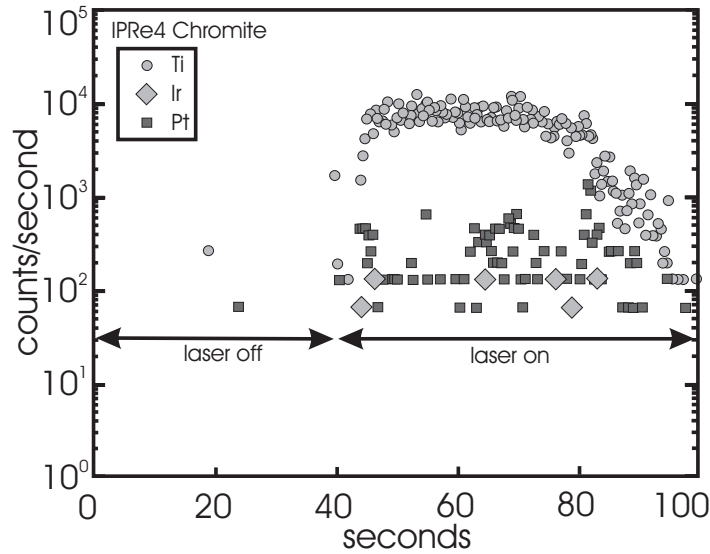


FIG. 1-6. Time-resolved LA-ICP-MS spectrum for synthetic chromite crystal. The left-hand part of the diagram shows the number of counts received by the detectors before the laser was turned on. The count rates climb rapidly upon illumination of the sample with the laser. Ti shows a smooth, flat profile for about 30 seconds, indicating a homogeneous major element composition. The spectrum for Pt contains at least three spikes in which count rates temporarily increase ten-fold. These spikes are common in spectra for glasses and chromite crystals, and are interpreted to result as the laser ablates through micronuggets of Pt minerals that are too small to detect by optical or electron microscopy. Bulk analysis of materials containing micronuggets will lead to erroneous interpretation of equilibrium phase compositions.

are defined as those whose D is smaller than 1.

In practice, D is determined experimentally by measurement of the concentrations of the element in question in each of the two coexisting phases. If more than two phases are present in a system at equilibrium, for example, melt, solid, and vapor, then the partition coefficient for a given pair of phases must be the same as it would be if only those two phases were present. Therefore, if we know, for example, the partition coefficients for solid/melt and for solid/vapor, then we can infer the vapor/melt coefficient without actually measuring it. Often, when several phases are present, we are interested only in the partitioning of an element between just one of those phases (*e.g.*, silicate melt) and the rest of the system. In such cases it is convenient to define a bulk partition coefficient D_M^* as:

$$D_M^* = \sum_{j=1}^n X^j D_M^j \quad (7)$$

where the D_M^j are the partition coefficients for each of the n other phases relative to silicate melt.

As is shown in the appendix, if we can assume that D_M is a constant, we can use simple one-line equations to predict the concentrations of an element in various phases as a magmatic process

takes place. Later in this chapter I use examples of numerical models of melting, crystallization and sulfide liquation to demonstrate the probable controls on PGE behavior in magmas.

Mineral – Silicate Melt Partitioning

Although no common rock-forming minerals are known to host economically significant proportions of the PGE, the crystallization of these phases from basaltic magmas can exert significant controls on the PGE distribution in evolving magmas. Many individual mineral/melt partition coefficients for PGE have not yet been measured since the advent of precise microanalytical tools with the very low detection limits required to make such measurements, such as LA-ICP-MS. The data that are available at time of writing are summarized in Table 1-1. The principal observations that can be made from Table 1-2 are that all of the IPGE are retained in solid mantle assemblages (*i.e.*, olivine, pyroxene, spinel) during melting to produce basalts, and are again partitioned into crystals that form early in the evolution of basaltic magmas as they cool in the crust. On the other hand, the PPGE remain incompatible with silicate and oxide minerals under all circumstances, with the possible exception of Pt in clinopyroxene.

The PPGE will achieve high concentrations in silicate liquids during mantle melting in the absence of phases other than oxides and silicates, and will increase in concentration as the magmas evolve through crystallization. We should anticipate therefore that basaltic magmas will show strong enrichments in PPGE relative to IPGE, and that this relative enrichment will be intensified as the magmas evolve.

The partitioning of PGE into chromite presents a special case. Natural chromite commonly contains minute grains of alloys of Os, Ir, Ru and Pt, despite the virtual absence of these phases from any coexisting silicate minerals deposited from the same magmas (*e.g.*, Merkle 1992, Ballhaus & Sylvester 2000). The concentrations of PGE alloys included in chromite can reach economic levels. The association may be accounted for by considering the importance of oxygen fugacity as a control on alloy solubility. Since chromite crystals grow by disproportionate addition of Fe^{+3} and Cr^{+3} relative to Fe^{+2} and Cr^{+2} in the enclosing melt, the compositional boundary layer surrounding growing chromite crystals will be impoverished in these constituents relative to the ambient melt. Because it is the homogeneous equilibrium between Fe^{+3} and Fe^{+2} , and to a lesser degree Cr^{+3} and Cr^{+2} , that controls $f\text{O}_2$ in basalts, the result of chromite crystal growth is a local reduction in $f\text{O}_2$ along the crystal–melt interface. This depression in $f\text{O}_2$ is apparently sufficient to

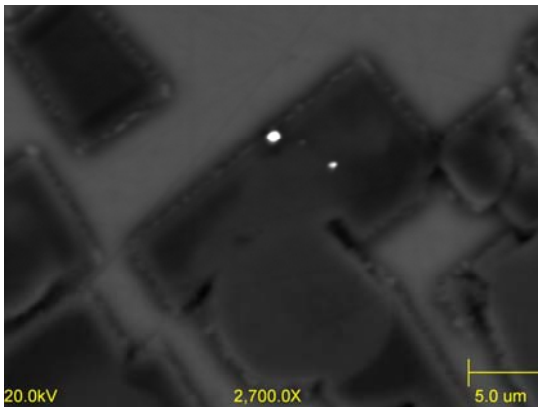


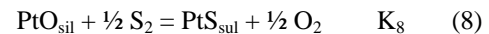
FIG. 1-7. Back-scattered electron micrograph of alloy micronuggets in synthetic chromite. Chromite (dark grey) has crystallized from basaltic liquid, now quenched to glass (light grey). Bright specks are grains of Ru alloy that grew from the silicate melt in the diffusive boundary layer surrounding the growing chromite crystals and were then overgrown by the crystal (C. Finnigan, personal communication).

induce alloy saturation. The growing chromite crystals overgrow alloy grains formed in this manner, leading to bulk enrichment of alloy-forming elements in the chromite grains even if they are not actually present in solid solution within the chromite crystal structure (Mungall 2002a, Finnigan *et al.*, 2005a,b). The extent to which this process has contributed to previous determinations of spinel–melt partition coefficients is not clear, since much previous work was done using bulk analytical methods to determine the compositions of the spinel crystals (Capobianco & Drake 1990, Capobianco *et al.* 1994, Righter *et al.* 2004). In any case, due either to true compatibility of the PGE or to coprecipitation of PGM, chromite is a major collector phase for the IPGE and Pt in magmas.

Sulfide Melt – Silicate Melt Partitioning

The phase most commonly implicated in the generation of PGE deposits is sulfide liquid, which commonly forms as immiscible droplets suspended within the silicate melt. All of the chalcophile elements Cu, Ni, Co, Au, and the PGE, are extremely compatible with sulfide liquid relative to silicate melt (see partition coefficients in Table 1-1). The separation of sulfide liquid from basaltic magma will sequester virtually all of the chalcophile elements present unless the modal proportion of sulfide is very small.

The partitioning of elements between silicate and sulfide melt can be considered in a context similar to that of equation 1, except that there is a concomitant exchange of sulfur and oxygen implicit in the reaction:



Solving for the partition coefficient as before, we find that

$$D_{\text{Pt}}^{\text{sul/sil}} \approx \frac{X_{\text{PtS}}^{\text{sul}}}{X_{\text{PtO}}^{\text{sil}}} = K_8 \frac{\gamma_{\text{PtO}}^{\text{sil}}}{\gamma_{\text{PtS}}^{\text{sul}}} \cdot \frac{f\text{O}_2^{1/2}}{f\text{S}_2^{1/2}} \quad (9)$$

There is an explicit dependence of $D_{\text{Pt}}^{\text{sul/sil}}$ upon both $f\text{O}_2$ and $f\text{S}_2$. As will be seen in the discussion on solubility of sulfide in silicate magmas, the relation between $f\text{O}_2$ and $f\text{S}_2$ is narrowly prescribed by the equilibrium between FeS_{sul} and FeO_{sil} , so that they cannot vary independently if the system is cosaturated with silicate melt and sulfide liquid. Nevertheless, this dependence on the intensive parameters is thought to cause greater than 10-fold variations in $D_{\text{PGE}}^{\text{sul/sil}}$ as measured experimentally (*e.g.*, Fleet *et al.*

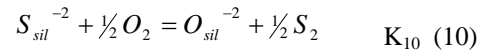
1999a). $D_{PGE}^{sul/sil}$ have also been inferred by direct measurement of the compositions of naturally occurring coexisting globules of sulfide minerals and silicate glass thought to represent quenched immiscible liquids (Peach *et al.* 1990). Experimentally determined and natural values of $D_{PGE}^{sul/sil}$ are presented in Table 1-1, which shows that they increase dramatically with increasing fO_2 of equilibration. Basaltic magmas commonly evolve along liquid lines of descent internally buffered close to the quartz–fayalite–magnetite (QFM) solid oxygen buffer (*i.e.*, the fO_2 at which these three phases can coexist; Carmichael & Ghiorso 1986, Carmichael 1991). The $D_{PGE}^{sul/sil}$ in Table 1-1 were determined at the magnetite–wüstite oxygen buffer, well below QFM. If the positive dependance on fO_2 continues to QFM, then in typical basaltic systems $D_{PGE}^{sul/sil}$ are probably all somewhat larger, perhaps as high as 50,000. The extremely high values of $D_{PGE}^{sul/sil}$ account for the overwhelming importance of sulfide as a collector phase for PGE in the formation of ore deposits.

As is illustrated in Figure 1-8, there remain serious discrepancies between the partition coefficients that have been measured experimentally for sulfide–silicate melt equilibrium, compared with those which can be inferred from alloy–sulfide melt and sulfur-free alloy–silicate melt equilibrium. This discrepancy might result from the formation of MS complexes like dissolved PtS_{sil} in addition to oxide species like PtO_{sil} . The homogeneous equilibrium

between dissolved PtO_{sil} and PtS_{sil} would permit much higher bulk Pt solubilities than that of PtO_{sil} alone. Alternatively, it could be that all of the silicate glass compositions used to calculate $D_M^{sul/sil}$ were compromised by the presence of alloy micronuggets. As will be seen below, for most practical purposes it does not really matter much whether $D_M^{sul/sil}$ is 10^4 or 10^6 , due to the overwhelming importance of the sulfide/silicate mass ratio in determining the distribution of PGE in natural systems.

Solubility of Sulfide in Basaltic Melts

The ability of basaltic magmas to transport PGE and the conditions under which the PGE are finally concentrated are profoundly affected by the solubility of sulfide in basaltic liquids. It is important to distinguish between the solubility of S in a melt as a response to an externally imposed sulfur fugacity, and the solubility of S at the point of sulfide liquid saturation. In systems lacking a free sulfide phase, the amount of sulfur dissolved in the silicate melt obeys the following mass action expression:



Assuming that the concentration of O^{-2} does not change appreciably in the silicate melt, the concentration of S^{-2} can be related to a constant similar to an equilibrium constant and referred to as

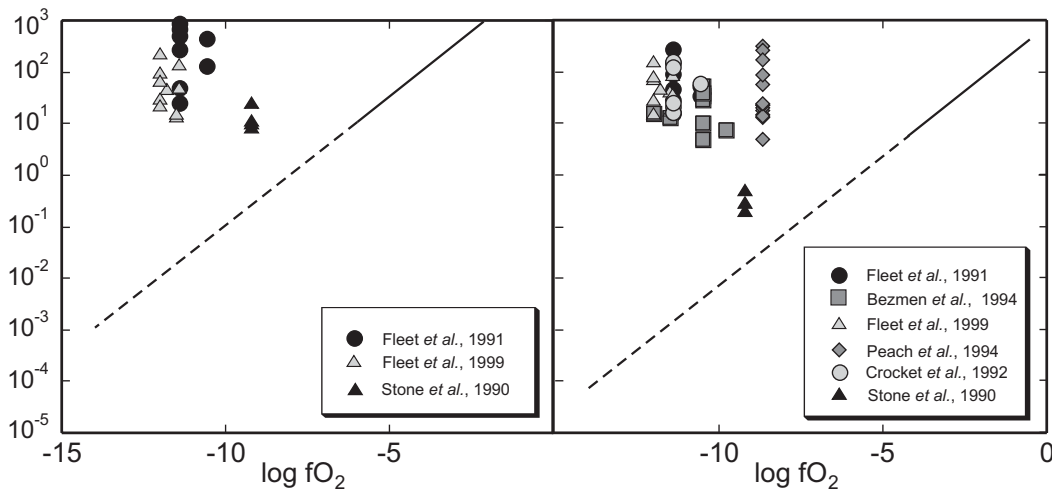


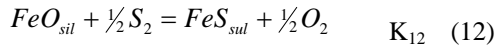
FIG. 1-8. Comparison of PGE solubility predicted from S-free pure metal solubility experiments with measured PGE contents of glasses in equilibrium with sulfide. Measured concentrations greatly exceed predicted values, possibly either due to the presence of micronuggets in the experimental glasses, or due to large increases in solubility in the presence of PGE–S complexes in the melt (J. Brennan, personal communication).

the sulfide capacity C_s (Fincham & Richardson 1954):

$$C_s \equiv X_{S^{-2}} \cdot \frac{fO_2^{1/2}}{fS_2^{1/2}} = \frac{K_{10}}{X_{O^{-2}}} = \text{constant} \quad (11)$$

At a given temperature, the sulfide capacity is a constant for a given melt composition, making the prediction of sulfide solubility possible over wide ranges of fO_2 and fS_2 once C_s is known. On the other hand, C_s is a strong function of the composition of the silicate melt, being greatly increased by increases in FeO and TiO_2 content, and decreased significantly by increases in SiO_2 or Al_2O_3 content (O'Neill & Mavrogenes 2002). The experimental data show that the bulk of S dissolved in basaltic liquids is present as a FeS_{sil} complex.

The quantity of interest to economic geologists is the sulfide solubility when a separate sulfide phase is present, commonly referred to as sulfide saturation at sulfide saturation (SCSS). If a magma contains less S than SCSS, it will be sulfide-undersaturated. When the bulk system contains more S than SCSS, a separate sulfide liquid phase will nucleate and grow into droplets suspended in the silicate melt. The transfer of Fe and S into the sulfide melt proceeds according to



Following thermodynamic convention we can write

$$K_{12} = \frac{a_{FeS}^{sul} \cdot fO_2^{1/2}}{a_{FeO}^{sil} \cdot fS_2^{1/2}} = \exp\left\{\frac{-\Delta G_{R12}}{RT}\right\} \quad (13)$$

If we convert $X_{S^{-2}}$ to X_{FeS} , combine equations 13 and 11, and take logarithms, we arrive at a useful expression for the solubility of sulfide in the silicate melt when it coexists with sulfide liquid:

$$\ln X_{S(SCSS)} = \frac{\Delta G}{RT} + \ln C_s + \ln a_{FeS}^{sul} - \ln a_{FeO}^{sil} \quad (14)$$

Equation 14 can be implemented by assuming that a_{FeS}^{sul} is unity, and calculating a_{FeO}^{sil} and C_s as functions of melt composition, pressure, and temperature using published empirical relationships (Snyder & Carmichael 1992, O'Neill & Mavrogenes 2001). It is worth noting that SCSS does not depend explicitly on fO_2 or fS_2 . However, the converse is not true; a system in which sulfide melt coexists with silicate melt must still obey equation 13. The sulfur fugacity of a sulfide-saturated magma is therefore completely prescribed by fO_2 , which was imposed by melting conditions in the mantle and is usually near to QFM (Carmichael

1991), and the sulfide capacity of the magma. Fe-rich magmas with high sulfide capacities will equilibrate with sulfide at high fS_2 , whereas Fe-poor magmas will have lower fS_2 at sulfide saturation.

The upshot of all of this is that the solubility of sulfide liquid is seen to show some fairly simple relations to composition, temperature and pressure. As noted above, SCSS depends strongly upon FeO content of the magma; Fe-rich magmas like ferropicrite will have much greater carrying capacity for sulfide than Fe-poor MORB or strongly fractionated intermediate magmas. The addition of SiO_2 and Al_2O_3 to a magma through assimilation of crustal rocks will lead to substantial decreases in sulfide solubility.

SCSS has been found to decrease with decreasing temperature but increases with decreasing pressure (Mavrogenes & O'Neill 1999). A simple empirical equation for SCSS as a function of temperature and pressure for a typical basalt is given in Table 1-1; another useful parameterization which is more general but unfortunately based upon a less reliable database was presented by Wallace & Carmichael (1992). Even a primary magma extracted from the mantle initially in a state of sulfide-saturation (that is, it equilibrates with and leaves behind a sulfide liquid phase in the residue) will become strongly sulfide-undersaturated during its ascent toward the surface of the Earth (Figure 1-9). Countervailing this tendency for all mantle-derived magmas to sulfide-undersaturation are the effects of cooling and assimilation of Si- and Al-rich wall-rocks, both of which decrease SCSS. Also at play is the crystallization of S-free silicate minerals such as olivine, which causes the actual sulfide concentration in the melt to increase as the volume of melt in which it is dissolved is diminishing.

There are two paths to saturation with sulfide liquid for fresh batches of mantle-derived basaltic magmas. One is to carry forward with cooling, assimilation, and crystallization until the point at which decreasing sulfide solubility matches the increasing sulfide concentration and the magma moves passively into a state of sulfide saturation. In this scenario, the first sulfide liquid to appear in the system will do so at extremely small modal proportions. The other way to reach sulfide saturation is for the magma to assimilate large quantities of S from external sources like S-rich metasedimentary rocks or H_2S gas. In such cases it is exceedingly unlikely that the amount of sulfide

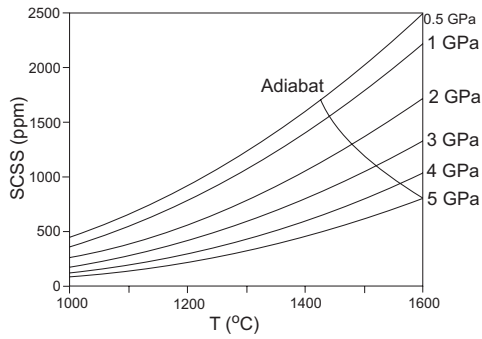


FIG. 1-9. Solubility S as a function of P , T after Mavrogenes & O'Neill (1999). Note that the solubility of S increases markedly with decreasing pressure but decreases only slightly with decreasing temperature. Since adiabatic ascent of magmas from the mantle results in simultaneous loss of pressure and lowering of temperature, the solubility of sulfide increases during extraction of melt from the mantle. Even magmas which left residual sulfide in their source regions will be sulfide-undersaturated upon reaching the lithosphere or being erupted at the surface.

added will be precisely the amount required just to reach sulfide saturation; the more probable result will be gross oversaturation of the magma in sulfide liquid, and the consequent equilibration of sulfide and silicate liquids at relatively high modal proportions of sulfide. The modal proportion of sulfide is a matter of some importance as will be discussed in the following paragraphs.

Mass Balance in Sulfide Melt – Silicate Melt Partitioning

Because the chalcophile elements show very large partition coefficients $D^{sul/sil}$, their concentrations in sulfide liquid at equilibrium with silicate magmas are relatively very high. The sulfide phase may commonly contain virtually all of the PGE in the entire magmatic system despite being present at very low modal abundance. The relationship between the modal abundance of sulfide melt, the concentrations of the PGE in the bulk system, and the partition coefficients, is worth some careful scrutiny. Campbell & Naldrett (1979) showed that the ratio of the mass of silicate melt to sulfide melt R could be related to the partition coefficient $D^{sul/sil}$ and the initial concentration C^o of the element in question, to predict the concentration of the element in the sulfide melt at equilibrium with the silicate magma, as follows:

$$C_{sul} = C^o D^{sul/sil} \frac{R+1}{R + D^{sul/sil}} \quad (15)$$

This equation is a restatement of the equilibrium crystallization equation, because it essentially describes a batch equilibration of the coexisting sulfide and silicate melt phases, as discussed in the Appendix to this chapter. The consequences of equation 15 are illustrated in Figures 1-10c and 1-11.

Inspection of equation 15 shows that as long as R is greater than or equal to D , the metal concentration in the silicate melt will show little dependence on R but will remain near to C^o , and its concentration in the sulfide melt will be close to $C^o D$. If R is substantially less than D , the concentrations of metals in the two phases depend more upon R than D . Thus, for R not greater than a few thousand (*i.e.*, the modal abundance of sulfide exceeds 0.01%), it does not matter if D is 10^4 or 10^6 ; the compositions of the phases are almost insensible to the difference.

In systems characterized by very high values of R , the concentration of base and precious metals in the sulfide liquid will all be very high. As a consequence of the very high concentrations in the sulfide melt, there will be only very subtle decreases in the concentrations of the PGE in the coexisting silicate melt upon extraction of the sulfide phase. In systems with lower values of R , the PGE tenors in the sulfide liquid will be much lower, and the silicate melt will become correspondingly strongly impoverished in the PGE. The hallmark of a magmatic system containing a small quantity of sulfide melt with very high PGE tenors will be the retention of high PGE concentrations in the silicate melt. Due to their relatively small partition coefficients, the concentrations of the base metals Cu and Ni in the sulfide melt do not show such extreme dependence on R . Over a wide range of values of R , both Cu and Ni remain at high concentrations in the sulfide. Their concentrations only begin to drop to discouragingly low values when R drops toward 100.

A consequence of the different partitioning behavior of the base and precious metals is that the PGE are much more sensitive to a history of sulfide segregation than are the base metals (Barnes & Maier 1999). The ratio of Cu/Pd in the silicate melt rises sharply as soon as the first depletion of PGE is felt. This issue is described in more detail by Barnes & Maier (this volume), and can be used to identify magmas which have equilibrated with sulfide liquid at some point during their evolution.

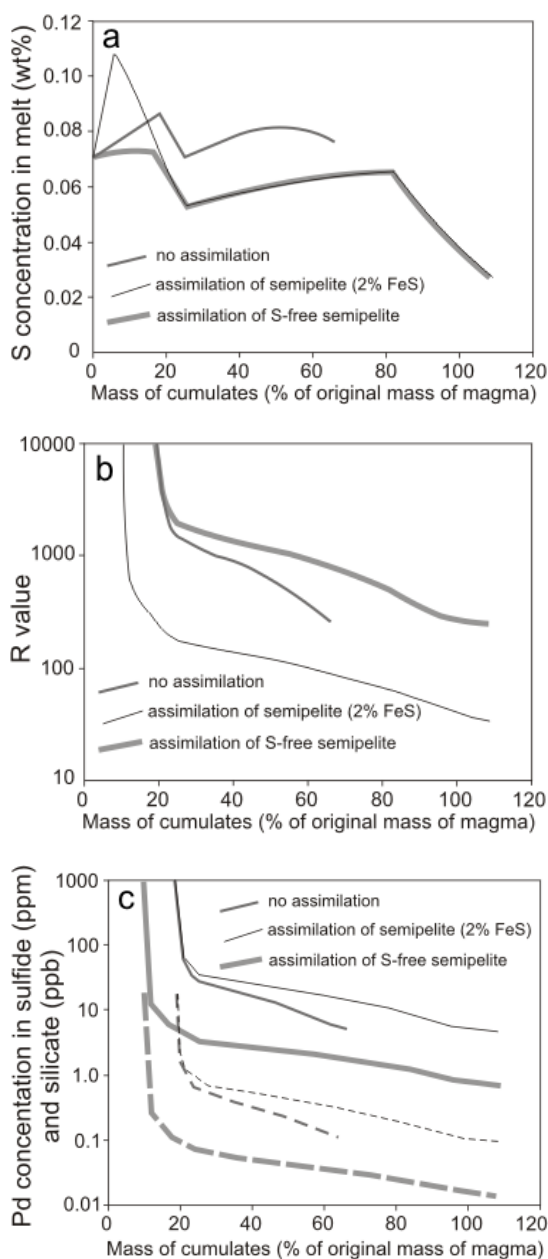


FIG. 1-10a. S concentration in komatiitic basalt magma (Expo Intrusive Suite, Cape Smith fold belt; Mungall unpublished data) undergoing cooling and equilibrium crystallization or assimilation of semipelitic sedimentary rocks. Modeling was done using IRIDIUM (Boudreau 2003 and a magma containing 700 ppm S. The abscissa records wt% of cumulates relative to the original mass of magma before assimilation and crystallization began. Note that the amount crystallized can exceed 100% because material is being added during assimilation. If no assimilation takes place, S concentration rises passively as the magma crystallizes olivine until sulfide saturation is

reached (maximum S concentration, at ~ 20% crystallized). If the same magma assimilates semipelite isenthalpically, sulfide saturation is reached at a lower concentration due to the effects of added SiO_2 and Al_2O_3 on S solubility. Continued cooling and assimilation causes S solubility to drop until plagioclase begins to crystallize, whereupon S solubility increases again due to the increase in FeO content of the melt until it reaches a second maximum as magnetite appears on the liquidus. If the same magma assimilates a semipelite identical to the first except for the presence of 2 wt% pyrrhotite, the concentration of S in the magma rises much faster, reaching sulfide saturation at less than 10% crystallized, after which the S solubility follows a nearly identical path as before.

FIG. 1-10b. Silicate/sulfide mass ratio (R) for the three examples shown in part a (note logarithmic scale for R). R always begins at infinity as the first droplet of sulfide appears, but drops rapidly as the amount of sulfide liquid increases. The rapid addition of S to the magma during assimilation of S-rich sediment causes R to drop to much lower values than in the cases of assimilation of sediment lacking S or crystallization without assimilation. Very high R values persist through >20% crystallization of the system in these latter cases.

FIG. 1-10c. Concentrations of Pd in coexisting silicate melt and sulfide melt in the same magmas shown in parts a and b. Sulfide melt compositions are shown as before (scale to be read in ppm), whereas the corresponding coexisting silicate melts are shown as dashed lines with the same line weights and shadings (scale to be read in ppb). The sulfide produced during assimilation of S-rich sediment has potential to form PGE-rich deposits only during a brief interval from about 10% to 15% crystallized. Sulfide produced during assimilation of sediment lacking S or during simple cooling and closed system crystallization has high potential for PGE deposit formation at any time during the evolution of the system. Note however that without assimilation, the high-tenor sulfide comprises only 0.134% of the total mass of the system when it is 60% solidified, whereas 1.2% of the system is sulfide liquid after 100% of the original mass of the system is solidified when S-rich sediment is being assimilated. The latter case thus produces 10 times as much sulfide as the former. Recognition that the silicate melt has interacted with sulfide is straightforward because in all cases the Pd content of the silicate melt drops to less than 1 ppb within the first few percent of crystallization following sulfide saturation. If a silicate magma is depleted from 10 ppb to any value greater than 1 ppb, this is a sign that sulfide liquid has been removed at a very high R value and is going to be correspondingly rich in Pd.

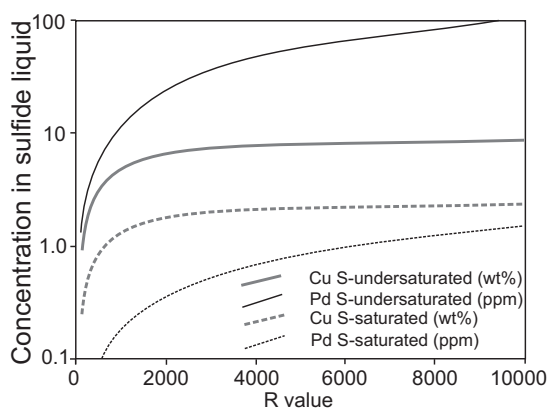


FIG. 1-11. Metal concentrations in sulfide melt as functions of R during sulfide segregation (ppm for Cu, ppb for Pd). As R increases the concentrations of Cu and Pd increase in both the sulfide melt and the silicate melt. The increase in Cu levels off at relatively low R values, so that Cu is little affected by R when R exceeds about 1000, whereas Pd shows continued enrichment as R increases to beyond 10000. Two examples are shown. The solid curves correspond to the sulfide that could equilibrate with a silicate magma removed from the mantle in a state of sulfide-undersaturation (calculated in Figure 15, below). The dashed curves show the sulfide compositions that could equilibrate with magmas that left residual sulfide in the mantle. Magmas previously saturated with sulfide cannot later form sulfide liquids with economically attractive PGE tenors, though the Cu and Ni contents may be of some interest.

Recognition of silicate magmas strongly depleted in PGE relative to their primary compositions is evidence of the existence of *low-grade* sulfide mineralization somewhere in the system. The key indication that *high-grade* mineralization may exist is that PGE concentrations in the silicate magmas are only slightly reduced from their primary values. Failure to make this distinction may lead to disappointing results.

The basalts associated with the fabulous deposits of the Noril'sk camp (Naldrett *et al.* 1992, 1994; see also article by Arndt in this volume) offer a good example of this. One group of lavas, of the Nadezhdinsky Formation, is strongly PGE-depleted, with Pt and Pd concentrations generally below detection limits (Naldrett *et al.* 1992, Lightfoot *et al.* 1990, in press). These lavas have been shown to correlate geochemically with underlying intrusions of the lower Talnakh group (Arndt *et al.* 2003), which contain subeconomic low-tenor disseminated sulfide mineralization of a composition that matches that which must have equilibrated with the

Nadezhdinsky lavas according to equation 15. The overlying lavas of the Morongovsky Formation show a rather subtle depletion in the PGE, and correlate geochemically with the upper Talnakh intrusion, which hosts important high-PGE-tenor sulfide deposits. One is led to conclude that the extreme Nadezhdinsky-type PGE depletions are indications of poor-quality magmatic sulfide mineralization at depth, whereas the weak Morongovsky-type PGE depletions are the signature of valuable high-grade mineralization at depth. This is true whether one suggests that the low-quality sulfides that first equilibrated with the Nadezhdinsky magmas were later upgraded to high metal tenor by continued re-equilibration with the younger Morongovsky magmas (*e.g.*, Naldrett *et al.* 1996), or proposes that the later high-tenor Morongovsky-type sulfides never combined with the earlier, low-tenor Nadezhdinsky-type sulfides (Arndt *et al.* 2003, this volume). Either way, it is the Morongovsky-type, weakly depleted basalt that points to the existence of the high PGE grades in sulfides below the volcanic pile.

It is important to recognize that the parameter R monitors the extent to which the system is oversaturated with sulfide. In other words, as a magma first becomes sulfide-saturated, R will initially have an extremely high value. Continued cooling or assimilation leading to further formation of sulfide liquid without physical separation of the sulfide will lead to lower values of R . Although one commonly hears about the need for magmas to attain high values of R to achieve high metal tenors in the sulfide phase, it is perhaps more appropriate to think of avoiding the unwanted dilution of those metals through the addition of excessive quantities of sulfide above the amount required to achieve sulfide saturation.

These relations become evident in the two cases shown in Figure 1-10c. When the silicate magma becomes sulfide-saturated passively by crystallizing sulfide-free mineral phases, it does so relatively slowly, compared to the rate at which new mineral phases are forming. In this case, the magma will initially separate very small quantities of sulfide liquid, leading to very high values of R and high PGE tenors in the resulting sulfide. On the other hand, assimilation of sulfide-rich sediment by a silicate magma will tend to lead to rapid and extreme sulfide oversaturation, resulting in the separation of sulfide liquid with relatively low PGE tenors but still appreciable base-metal contents. The passive route to sulfide saturation, in quiescent

slowly cooled magma chambers, has been invoked for the formation of stratiform PGE-rich sulfide horizons in such localities as the Munni Munni intrusion of Australia (Barnes *et al.* 1990, Barnes 1993; Mungall 2002b), the Great Dyke of Zimbabwe (Wilson & Tredoux 1990), and Skaergaard Intrusion of east Greenland (Nielsen *et al.*, this volume). The more precipitous and hasty route to sulfide saturation, by assimilation of S-rich crustal rocks, has generally been held to account for the generation of base-metal sulfide deposits like those at Noril'sk (Naldrett *et al.* 1994, 1996), Kambalda, or Raglan.

In general, for a given size of magmatic system, high R values lead to comparatively small tonnages of high-grade mineralization, whereas low R values produce large tonnages of lower grade mineralization. Therefore, in order to attain the crucial combination of high PGE grade and large tonnage required for profitable mining, a PGE deposit must have formed from a large body of magma.

There is a natural tendency for geologists to categorize deposits, and the relations described here for magmatic sulfide deposits have led to a distinction in most geologists' minds between PGE-dominant (high R -value) deposits hosted by large layered intrusions, and base-metal dominant (low R -value) magmatic sulfide deposits hosted by magma conduits or channelized lava flows. The PGE-dominant group includes examples such as the J-M Reef, Great Dyke, and Merensky Reef deposits, whereas the base-metal dominant group includes Kambalda, Voisey's Bay, and other relatively PGE-poor deposits. Although some deposits can easily be classified in this way, over-reliance on this type of classification obscures the essential continuity in grade and tonnage between the two groups. With bulk Pd grades of several 10's of g/t in the massive sulfides, the deposits of the Noril'sk camp are the prime examples of extremely PGE-rich 'base-metal' sulfide deposits (Naldrett *et al.* 1994, 1996). At Noril'sk the effective R at which sulfides separated from their parental silicate magma approached the values typically associated with 'PGE-dominant' deposits. Exploration geologists should remain conscious of the fact that each deposit is unique and will tend to defy simple categorization. Not all PGE-rich deposits will be found in layered intrusions, and not all base-metal sulfide deposits will be found in conduits. The Ruby Zone of the Lac des Iles complex is a good

example of a disseminated sulfide accumulation combining attributes of both PGE- and base-metal-dominant systems (see also Lavigne, this volume).

Monosulfide Solid Solution – Sulfide Melt Partitioning

When sulfide liquid has formed in a magma, it may collect into pools at the base of the magma chamber or conduit because it is denser than the host silicate magma. Although sulfide liquid is superheated under its usual conditions of formation at the liquidus temperature of basaltic magma, it will eventually cool to its liquidus temperature and begin to solidify. As illustrated in Figure 1-12, the first phase to crystallize is usually monosulfide solid solution (mss; *i.e.*, magmatic pyrrhotite), often followed shortly afterward by magnetite (Naldrett 1969; Ballhaus *et al.* 2001; Mungall *et al.* 2005). Most sulfide magmas appear to have crystallized along the magnetite–mss cotectic over the temperature range from about 1100°C to about 850°C, although in rare cases a more copper-rich solid called intermediate solid solution (iss; *i.e.*, magmatic chalcopyrite) can be inferred to have joined mss on the liquidus (*e.g.*, Naldrett *et al.* 1994, 1999).

The example of a partition coefficient in Equation 6 was written to describe PGE partitioning between mss and sulfide liquid. Following the assumptions used to arrive at Equation 6, we have calculated $D_{PGE}^{mss/sul}$ from a number of experimental studies (Figure 1-5). $D_{PGE}^{mss/sul}$ is a strong function of the composition of the sulfide liquid. At high sulfur fugacities the sulfide melt has a low ratio of metal cations to anions (*i.e.*, sulfur + oxygen), calculated as molar proportion (Fe+Ni+Cu)/(S+O) (abbreviated as M/S), and the partition coefficients of all of the PGE are considerably smaller than they are at low values of M/S. There are insufficient data currently available to determine the temperature dependence of $D_{PGE}^{mss/sul}$. Figure 1-13 illustrates the way that K_D depends on temperature and M/S of the sulfide liquid for the PGE and Au.

Although Cu and Ni are not PGE, they are important components of magmatic sulfides so I digress a bit here to discuss their partitioning between mss and sulfide liquid. Using Ni as an example, the distribution of the base metals at equilibrium will be governed by the following exchange reaction:



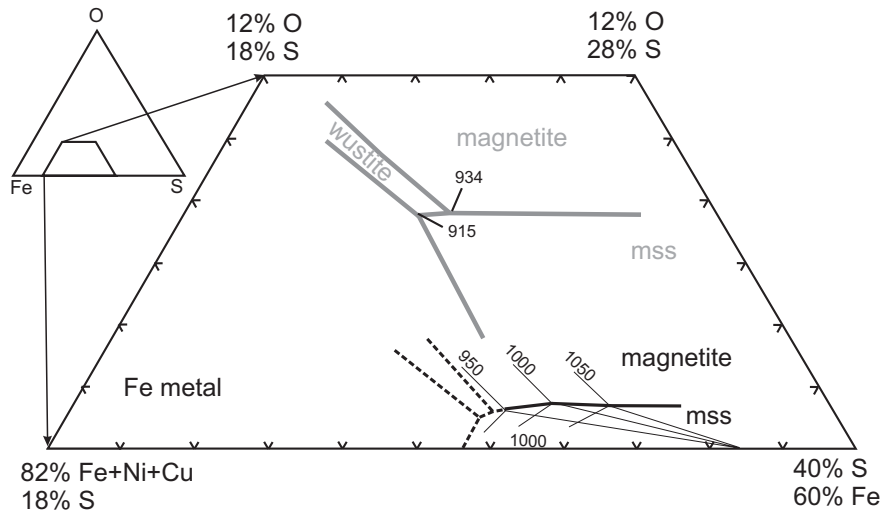


FIG. 1-12. Fe–Ni–Cu–S–O system with typical magmatic compositions (wt%). Under normal conditions of sulfide segregation from basaltic magmas, the sulfide magma will have a composition close to the magnetite–mss cotectic. The magnetite–mss cotectics shown correspond to the Ni- and Cu- free subsystem Fe–S–O (grey line; Naldrett, 1969) or to the five-component system containing about 5 wt% each of Ni and Cu (black line; Mungall *et al.* 2005). Isothermal liquidus surfaces shown schematically for 950, 1000, and 1100°C.

Whereas the assumptions behind simplifying Equation 5 to arrive at the convenient partition coefficient in Equation 6 appear to have been valid for PGE at trace concentrations, these assumptions cannot hold for Cu and Ni because they are major components of mss and sulfide melt. Instead, it is appropriate to define a distribution coefficient

$$K_D = \frac{\frac{X_{NiS}^{mss}}{X_{NiS}^{sul}}}{\frac{X_{FeS}^{mss}}{X_{FeS}^{sul}}} = \frac{K_{15} \cdot \gamma_{NiS}^{sul} \cdot \gamma_{FeS}^{mss}}{\gamma_{NiS}^{mss} \cdot \gamma_{FeS}^{sul}} \quad (17)$$

K_D can be calculated from experimental data (Ebel & Naldrett 1996, Fleet *et al.* 1993, Fleet & Pan 1994, Li *et al.* 1996) for NiS, CuS and \square S, where \square S is a fictive component created to account for the presence of vacancies in the cation sites of naturally-occurring mss.

Pt, Pd, Au and Cu are invariably incompatible in mss as it crystallizes from cooling sulfide melts. Ni is incompatible at high temperatures but becomes mildly compatible at temperatures near to the solidus of common sulfide magmas. Ir, Ru, and Rh are highly compatible in sulfide magmas equilibrated with silicate melt at oxygen fugacities close to QFM, which is typical of ordinary basaltic magmas, but these elements could become incompatible in sulfide melts equilibrated at unusually low fS_2 and fO_2 , such as at the conditions of formation of FeNi alloy at Disko Island in

Greenland.

As sulfide magmas crystallize, the residual sulfide liquid is expected to become highly enriched in Cu, Pt, Pt, and Au, while suffering strong depletion in the elements Ir, Ru, and Rh. Sulfide liquids separated from their mss cumulates at low temperatures will be depleted in Ni, whereas those separated at high temperatures will show Ni enrichment. Effects of this sort have been documented in detail at Sudbury and Noril'sk (Li *et al.* 1992, Naldrett *et al.* 1994, 1999, Czamanske *et al.* 1995, 2002). The operation of sulfide fractionation by equilibrium or fractional crystallization of the sulfide magma may be substantially aided in the most extreme cases by the lowering of the sulfide solidus by trace impurities such as Cl (Li *et al.* 1992, Mungall & Brenan 2003), low-melting point components including Ag, Te, Sb, As (Frost *et al.* 2002) or H₂O (Wykes & Mavrogenes in press).

The consequences of the partitioning behavior described here are illustrated in Figure 1-14, which shows the concentrations of Cu, Ni, Pt and Ir in sulfides from the Lindsley deposit at Sudbury (Mungall *et al.* 2005, data from Naldrett, pers. comm. 2000). Superimposed on the data are model trends for sulfide liquids and mss during crystallization of the sulfide magma at equilibrium. The most Cu-rich sulfide samples represent residual sulfide liquid that has been extracted and separated

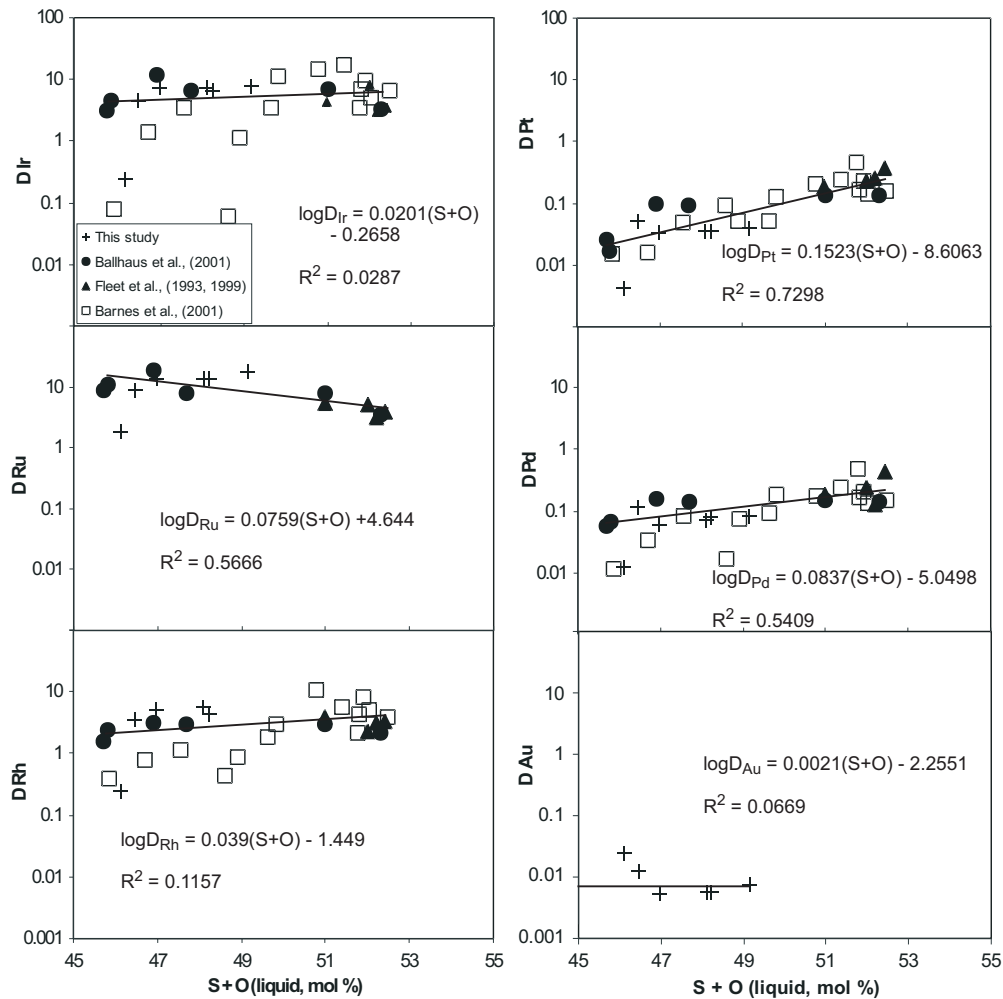


FIG. 1-13. Variation of $D^{mss/liq}$ with the cation content of the melt (after Mungall *et al.* 2005). Partition coefficients generally increase with increasing molar $S+O$ in the liquid. At typical conditions of fS_2 and fO_2 at which natural basaltic magmas precipitate sulfide liquids, Ir, Ru and Rh are compatible in mss whereas Pt, Pd and Au are strongly incompatible. Data sources: Fleet & Stone (1991), Fleet *et al.* (1999b), Ballhaus *et al.* (2001), Barnes *et al.* (2001), Mungall *et al.* (2005).

from its mss cumulates at a late stage in the cooling history of the sulfide magma. The more Ni-rich samples are slightly melt-depleted mixtures of mss and liquid. Late migration of Cu-rich residual sulfide liquid is a common phenomenon in magmatic sulfide deposits, particularly where large pools of sulfide liquid have formed to generate massive sulfides. However this kind of migration has also been evident in large volumes of disseminated sulfide mineralization at Sudbury (*e.g.*, Mungall 2002c).

The result of the separation of the Cu- and PGE-rich sulfide melt is the formation of veins or disseminations of sulfide mineralization abnormally rich in chalcopyrite, and commonly also containing

significant amounts of rarer minerals including cubanite, bornite, mooihookite and talnakhite (*e.g.*, Naldrett *et al.* 1994, Zientek *et al.* 1994). In some instances the primary exploration target is the fractionated Cu- and PGE-rich vein system, because of the extraordinarily high value of such material. For example, the relative economic importance of fractionated sulfide veins increases with depth of mining at Sudbury, to the extent that continued deep mine development in some deposits now depends entirely on the discovery of the veins rather than the much larger, lower-tenor deposits from which they originated (see also articles by McLean and by Farrow, this volume).

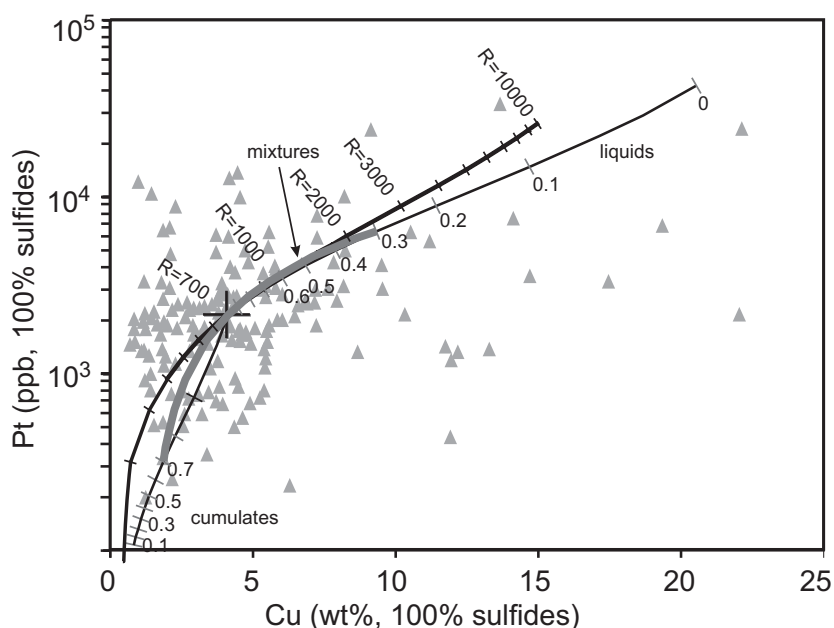


FIG. 1-14. Equilibrium crystallization of sulfide magmas at Lindsley (from Mungall *et al.* 2005). A sulfide liquid formed by liquation from the original silicate magma of the SIC would have compositions along the trend shown by the curve labeled with various R values. The liquid at $R = 700$ is a plausible initial sulfide magma, which will form extremely Pt-poor cumulus mss upon first reaching its liquidus temperature. No samples with such depleted compositions are observed. Continued equilibration of mss with the residual melt until at least 70% of the original melt has solidified will allow the cumulates to approach the most Pt-depleted compositions actually observed. The majority of sulfide ore samples at Lindsley can be interpreted as mixtures of Pt-poor mss and Pt-enriched residual liquid after 70% solidification. A small number of samples scatter along the trend toward extreme Cu and Pt enrichment, and are probably examples of fractionated liquid that has migrated away from the mss cumulates, preventing further re-equilibration.

Fluid – Silicate Melt Partitioning

All natural magmas contain some volatile components, and as magmas cool they will inevitably become saturated with a fluid phase. The role of fluids in the deposition or redistribution of PGE in large layered intrusions has been contentious for decades. Hanley *et al.* (2005a) have demonstrated that hypersaline aqueous fluids coexisting with silicate melts similar to those that form the interstitial residuum of crystallization of mafic magmas can carry PGE at concentrations similar to the grades of PGE ore deposits themselves (*i.e.*, several ppm). Despite the demonstrated importance of sulfide melt as a collector for the PGE in magmatic systems, it is evident that fluids in equilibrium with PGE-rich sulfides could themselves be efficient and far-reaching carriers of PGE due to their great mobility in cooling igneous bodies. Since even relatively dry mafic magmas containing ~1 wt% H_2O will eventually reach water saturation in the last stages of crystallization of intercumulus melt throughout the cumulate pile, it is inevitable that deuteric fluids

will stream upward through partially solidified cumulate rocks, modifying or possibly even creating new PGE deposits along the way. Hydrothermal fluids are, in fact, magmatic phases. The commonly held distinction between hydrothermal and magmatic processes is a false one, and leads to a great deal of disagreement over what is in reality undoubtedly a complex series of processes driven by mass transfer in all phases present within cooling magmas, which are known to include silicate melts, sulfide melts, halide melts, aqueous fluids, carbonic fluids, and solids (*e.g.*, Hanley *et al.*, 2005b). The role of hydrothermal fluids in the transport and deposition of PGE is discussed in greater detail by Hanley (this volume).

MANTLE MELTING AND MAGMA FERTILITY

Mantle peridotite is assumed to contain approximately 250 ppm of S, in the reduced form as S^{2-} (McDonough & Sun 1995). At the conditions of temperature and pressure at which MORB, most arc magmas, and most plume-related picrites are

formed by partial melting of peridotite, sulfide is present within the mantle in the form of Fe–Ni–Cu–S–O sulfide liquid. Melting at higher pressure but low temperature to form small-volume alkaline magmas may occur in the presence of both solid mss and sulfide liquid (*cf.* Bockrath *et al.*, 2004b). In this chapter I consider only melting processes where mss is not stable during mantle melting, since there are no significant PGE deposits yet known to occur in rocks related to deep-seated alkaline magmas.

Due to the nearly ubiquitous presence of sulfide liquid during mantle melting, the same constraints apply to the compositions of coexisting silicate and sulfide melts as were discussed above in the discussion of segregation of ore-forming sulfide liquids. As long as sulfide liquid is present, the concentrations of PGE in the coexisting silicate melt will tend to remain low (MacLean 1969; Hamlyn & Keays 1985a, b). Since sulfide dissolves in silicate melt with SCSS on the order of 1000 ppm, the progressive formation of greater amounts of silicate melt will permit progressively greater amounts of the total amount of S present to be dissolved in the silicate rather than remaining as sulfide liquid. When 25% of the original mantle peridotite has melted, the silicate melt phase will contain all of the sulfide originally present. In other words, the melting process consumes sulfide by transferring it from sulfide melt into silicate melt. Once sulfide melt has been entirely consumed, the PGE are no longer sequestered in the mantle residue to melting, and the basaltic melt will become highly enriched in PGE. It has recently been suggested that sulfide liquid can be entrained in rising silicate melt during partial melting of the mantle, permitting basaltic magmas to rise into the lithosphere carrying high PGE concentrations even when the magma remains saturated with sulfide liquid in the source region (Bockrath & Ballhaus 2004b). There remain serious objections to this hypothesis (Mungall & Su, 2005) and here I maintain the assumption that sulfide liquid and its load of PGE will remain trapped in the solid residual mantle.

Using the assumption of equilibrium batch melting of peridotite containing 250 ppm S as sulfide, solubility of S in silicate melt of 1000 ppm, and partition coefficients for PGE as listed in Table 1-1, I have calculated the PGE contents of basaltic magmas as a function of the degree of partial melting. This calculation ignores the possible effects of partitioning of PGE between mss and

sulfide liquid in the source region. The results are shown in Figure 1-15 (see also Barnes & Maier 1999).

There are several different types of behavior, depending on the relative magnitudes of the partitioning coefficients between sulfide melt, silicate melt, and the solid residue. The concentration of Ni rises steadily with increasing degree of partial melting. The dominant control on Ni concentration in the basaltic liquid is olivine–melt partitioning. Since Ni is compatible with olivine, the Ni concentration in the melt will be highest at the highest degree of partial melting. The presence or absence of sulfide liquid has little effect on Ni. As a result, even magmas generated by melting in the presence of sulfide can contain substantial amounts of Ni, and therefore nearly any mantle-derived magma has the potential to generate economic Ni deposits if it has not undergone extensive removal of olivine after being emplaced in the crust.

The concentration of Cu rises slowly at first, but increasingly fast with increasing degree of melting until it reaches its peak at the melt fraction at which all of the sulfide has been consumed. From this point onward the concentration of Cu in the melt diminishes with continued increase in the degree of partial melting because all of the Cu is already in the melt, and continued addition of new melt merely dilutes Cu. Pd and Au show very similar behavior to that of Cu, except that they begin at much more depleted concentrations at the earliest stages of melting because they partition so strongly into the sulfide melt. As with Cu, they reach their maximum possible concentrations in the melt at the point at which sulfide has been consumed, decreasing thereafter. The behavior of Ir combines the characteristics of Ni and Cu. At the early stages of melting the concentration of Ir is suppressed in the basaltic melt because most of the Ir is sequestered in sulfide melt. However, once sulfide melt has been entirely dissolved in the silicate melt, the concentration of Ir will be controlled by olivine–melt partitioning instead. Since Ir, like Ni, is compatible with olivine, its concentration continues to rise with increasing degree of partial melting.

The scenario outlined in Figure 1-15 is appropriate to the genesis of MORB and plume-related magmas at low to intermediate pressures. MORB is generated by low-pressure melting at melt fractions too low to consume sulfide in the source

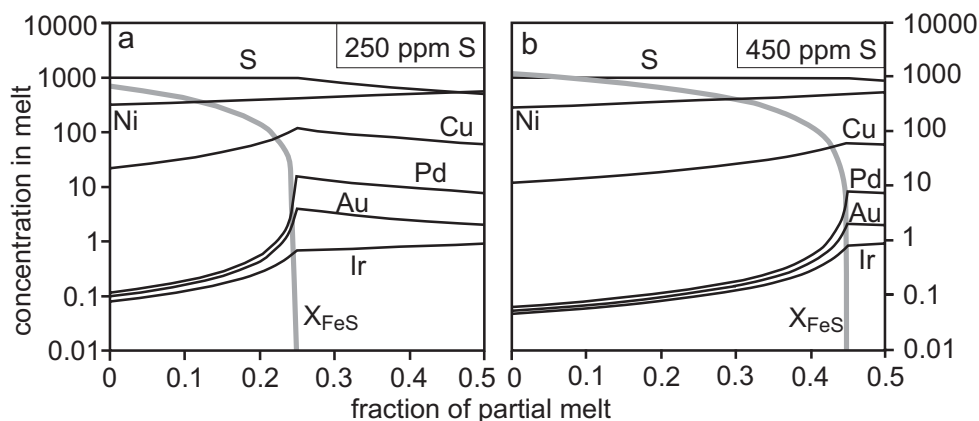


FIG. 1-15a, b. Chalcophile element concentrations in equilibrium partial melts of the mantle. As partial melting proceeds, the amount of sulfide melt in the residual mantle (X_{FeS}) decreases until all sulfide has been dissolved in the basaltic liquid at about 25% partial melting. As this point is approached, those elements which were strongly sequestered into sulfide melt begin to rise in concentration, until they reach their maxima at the exact point where X_{FeS} has dropped to zero. Concentrations of chalcophile elements that are incompatible with silicate minerals drop slowly thereafter, due to dilution by the continued addition of melt, whereas the concentrations of compatible elements (Ni, Ir) increase steadily with continued melting. Mantle containing 450 ppm S, as might result from the metasomatic addition of S above subduction zone, will not melt in a state of sulfide-undersaturation until the degree of partial melting exceeds 45%, which is very unlikely. The magmas in these two figures at 30% partial melting were used to construct Figure 1-11.

mantle, leading to the eruption of lavas extremely depleted in the PGE. The higher degrees of partial melting required to form picrite and komatiite in plume heads or tails are sufficient to permit extraction of sulfide-undersaturated melts, with high PGE abundances (*e.g.*, Hamlyn & Keays 1985a, b).

It is also interesting to consider what happens if melting occurs in mantle that has been metasomatized by the addition of fluids carrying sulfur, as is thought to occur in the mantle wedge above subduction zones (*e.g.*, Mungall 2002d). The addition of sulfur to the mantle wedge increases the quantity of sulfide melt and effectively prohibits sulfide-undersaturated melting, as shown in Figure 1-16. Because nearly all arc magmas are sulfide-saturated in their source regions, there are no known examples of PGE-rich magmatic sulfide deposits related to arc magmatism. Nevertheless, there are a number of low-grade Ni deposits such as Montcalm in Ontario (Barrie *et al.* 1990), Giant Mascot in British Columbia (formerly Pacific Nickel; Aho 1956) and St Stephens, New Brunswick (Paktunc 1989) which are hosted by probable arc-related plutons. The presence in these examples of moderate Ni grades in Cu- and PGE-poor magmatic sulfides is consistent with the compositions predicted by Figure 1-16.

A special problem which has received a lot of attention is posed by the existence of magmas rich

in PGE, MgO and SiO₂. Such magmas are considered to have been the parental liquids to the Stillwater and Bushveld layered intrusions (Harmer & Sharpe 1985), which host the world's principal PGE-sulfide deposits (see also article by Cawthorn, this volume). There are two possible origins for magmas of this type. They may be highly contaminated komatiite (Barnes 1989), or they may be boninite (Hamlyn & Keays 1985a, b). A komatiite magma can assimilate more than half of its own weight in continental crust, simultaneously crystallizing a mass of ultramafic cumulates similar to that of the assimilant, and becoming in the process a siliceous, high-Mg basalt (Huppert *et al.* 1984; see also model results in Figure 1-10). Boninite is the product of very low-pressure, low-temperature partial melting of mantle harzburgite that has already undergone significant partial melting, due to the fluxing effects of slab-derived H₂O in the shallowest parts of subduction zones. In either case, the parental liquid is the eventual product of >> 30% partial melting of fertile mantle peridotite and is therefore expected to be strongly sulfide-undersaturated at the source. Both processes will be expected to produce magmas very similar to the magma type of the large layered intrusions. The occurrence of the large intrusions in question at mid-crustal levels in stable continental interiors would seem to argue in favor of the

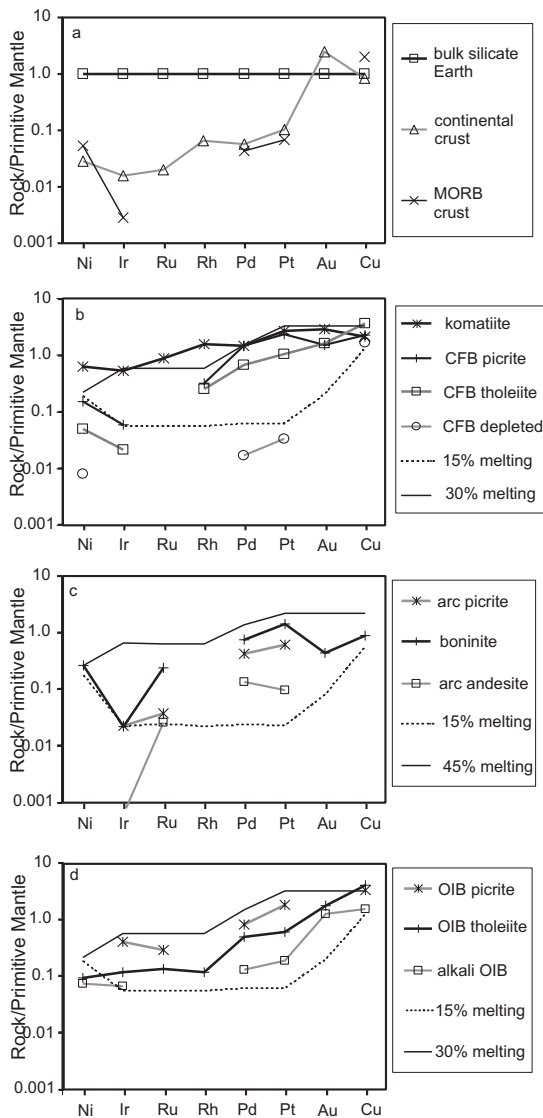


FIG. 1-16a. Chalcophile element abundances in major Earth reservoirs. Crustal rocks are strongly depleted in the PGE but not Au and Cu, which show little fractionation between the mantle and the crust.

FIG. 1-16b. Chalcophile element abundances in magmas thought to be generated by mantle plumes. Lines without symbols show the compositions of model melts from the same calculations shown in Figure 1-15a. Komatiites and continental flood basalt (CFB) picrites share high PGE contents because they left no sulfide in their mantle residue. CFB tholeiites shown are weakly depleted by interaction with sulfide melt during the formation of the Noril'sk ore deposits; the composition listed as CFB depleted is for a lava from the strongly depleted Nadezhdinsky Fm (discussed in the text). The signatures of sulfide depletion due to sulfide-saturated melting and due to sulfide

segregation in the crust are indistinguishable, as evidenced by the close correspondance of the 15% melting model curve (sulfide retained in source) and the CFB depleted curve (sulfide segregated in the crust).

FIG. 1-16c. Chalcophile element abundances in arc magmas. Lines without symbols show the compositions of model melts from the same calculations shown in Figure 1-15b. Boninites appear to result from very high degrees of partial melting, andesites reflect loss of PGE to residual sulfide in the mantle, whereas the arc picrites show intermediate values consistent with high degrees of partial melting.

FIG. 1-16d. Chalcophile element abundances in ocean island basalt suites (OIB). All data are for samples from Hawaii. Lines without symbols show the compositions of melts from the same calculations shown in Figure 1-15a. OIB picrite closely resembles the 30% melting curve, whereas the tholeiites and alkali basalts fall closer to the 15% melting (sulfide-saturated) model curve.

contaminated komatiite hypothesis, but given the current state of knowledge of Archean and Paleoproterozoic tectonics it is hard to be sure. In any case, since the products of both proposed melting processes are so similar, and since the magmas would be PGE-rich in either case, the differences between these two petrogenetic hypotheses are moot in the present context.

Highly oxidized Au-rich arc magmas present a final case worth some speculative discussion (*e.g.*, Mungall 2002d). The preceding discussion has been based on the assumption that all or most of the S in the mantle source region of basaltic magmas is in the form of S⁻². An important exception to this rule occurs when a major flux of oxidizing potential from subducting lithospheric slabs into the asthenospheric mantle wedge causes complete oxidation of S⁻² to S⁺⁶, as sulfate. If complete sulfide oxidation occurs, then even at the lowest degrees of partial melting, the basaltic magma will be extracted from its mantle source in a state of sulfide undersaturation. This process has been implicated in the genesis of anomalously Au-rich alkaline magmas at very low degrees of partial melting (Mungall 2002d), and should similarly affect the PGE. Whereas the solubility of Pd is quite high in basaltic liquid in the absence of a sulfide phase, Pt and the IPGE are known to be close to alloy saturation at typical concentrations in basaltic magmas (Fig. 1-5). It is therefore likely that Au-rich alkaline arc magmas are also rich in Pd

whereas the IPGE and Pt will have concentrations dictated by alloy saturation and therefore highly sensitive to variations in oxygen fugacity. There are as yet no economic PGE deposits known to be associated with this magma type, although very interesting PGE grades have been reported in hydrothermal deposits related to such magmas (*e.g.*, average Pd grade of 0.1 ppm in approximately 1 Mt in the Afton deposit, British Columbia, Canada; Behre-Dolbear & Company 2004).

The major chromite-hosted Pt deposits that have given rise to the world's principal placer Pt alloy deposits are all hosted by Alaskan-Uralian type mafic ultramafic complexes. These complexes are the cumulate roots of arc volcanoes (Murray 1972) and are known for the exceptionally high oxygen fugacities recorded by their mineral assemblages (Garuti *et al.* 2003), and for an association between Pt-rich ultramafic rocks with potassic syenogabbro (*e.g.*, Nixon & Hammack 1991). I suggest that the Pt-mineralized complexes represent the plumbing systems of volcanoes erupting Au-rich oxidized potassic alkaline arc magmas similar to those that generate major Au-Cu porphyry and epithermal Au deposits (Mungall 2002d). Pt alloys hosted by these deposits have been deposited from magma (Peck *et al.* 1992) as it rose through the conduit, in response to variations in oxygen fugacity induced by chromite crystallization or contamination.

SYNTHESIS AND CONCLUSIONS

The foregoing discussions of the igneous geochemistry of the PGE can be used to state some general rules about the magma types and physical or tectonic settings most favorable for the generation of economic PGE mineralization. I will focus on the items identified in the introduction, *i.e.*, fertility of the magma, nucleation of a collector phase, and collection of the collector.

MORB and normal arc magmas (Table 1-2, Figure 1-16) are not prospective parental magmas for the generation of PGE deposits, because of the profound importance of residual sulfide on the distribution of PGE during melting of the upper mantle. The magma types most prospective for PGE deposits are those with plume-related picritic to komatiitic parental liquids, which combine extraordinarily large volumes with the essential characteristic of being sulfide-undersaturated at source. A second, less-understood group consists of those deep-seated alkaline magmas that have not equilibrated with sulfide in sufficient quantity to be

PGE-depleted. These include highly oxidized potassic arc magmas and adakites, as well as the rare extremely alkaline magmas that are produced by partial melting of peridotite at high pressure below the sulfide solidus. Since the alkaline magmas tend to form in relatively small volumes, it is unlikely that very large deposits can form from them, but they should be kept in view as possible targets nonetheless. Finally, the boninite clan of magmas derived by large degrees of melting at low pressure in the presence of excess H₂O is prospective for the same reasons as the plume-related magmas. Since it may be difficult to distinguish between boninite and contaminated komatiite in ancient rocks this latter distinction may be difficult or impossible to apply in practice until a considerable amount of data have been acquired in a given magmatic suite.

Leaving aside chromitite-hosted magmatic PGE deposits, it can be said that a magma must become saturated with sulfide liquid if a PGE deposit is to be formed, even if the eventual ore deposit is formed by the action of fluids on that sulfide (*cf.* Boudreau & McCallum 1992). The two routes I have described to sulfide saturation are (a): passive saturation due to the concurrent increase in S concentration as silicate minerals crystallize and the decrease in SCSS with falling temperature and iron content and increasing silica and alumina content, or (b): dynamic saturation by the assimilation of S-rich country rock. Passive saturation lends itself to the separation of small volumes of very PGE-rich sulfide at extremely high *R* values. Dynamic saturation lends itself to the formation of large volumes of PGE-poor sulfides that may be either rich or poor in the base metals Cu and Ni.

Recognition of magmas that have had sulfide removed from them is potentially a powerful prospecting tool, but it must not be done superficially. Correct interpretation of the compositions of igneous rocks inferred to have been liquids (*e.g.*, lavas or chilled margins of intrusions) requires the collection of a number of samples whose conditions of formation can be clearly understood not to have involved collection or depletion of magmatic sulfide on the hand specimen scale. In this way, a primitive, PGE-undepleted magma type might be identified and contrasted with PGE-depleted members of the same suite to support the inference that PGE-rich sulfide mineralization exists somewhere within the system.

The final physical form taken by an accumulation of PGE-bearing sulfides depends on

the dynamics of the magma system. Questions related to this issue remain the most contentious aspects of the economic geology of PGE deposits. For example, although most workers agree that the PGE presently found as stratiform bodies in large layered intrusions was initially stripped from the magma within sulfide droplets, there remain deep disagreements over the manner of segregation of these sulfides into discrete layers. Whereas one group would argue that the sulfides rained into their present locations directly from the overlying magma (Campbell *et al.* 1983), others argue that the sulfides were initially dispersed throughout the cumulate pile as trace disseminations, and were later collected into metasomatic alteration fronts at the sites of the deposits by migrating aqueous or carbonic fluids (Boudreau & McCallum 1992). I would suggest that some deposits have formed in the former, 'downer' mode (*e.g.*, offset PGE horizons at the Munni Munni intrusion (Mungall 2002b), the Skaergaard Intrusion, and the Great Dyke of Zimbabwe) and that others have formed in the latter, 'upper' mode (*e.g.*, unconformity-hosted stratiform deposits like the J-M reef of the Stillwater Intrusion, Montana, and the Merensky and UG2 reefs of the Bushveld Intrusion, SA), but will avoid dwelling on contentious genetic models in this article.

There is less disagreement regarding the mechanism of formation of the large base-metal-rich sulfide deposits. All workers in the field agree upon the fundamentally magmatic nature of the massive and disseminated base-metal sulfides, and agree that some physical process must sort small amounts of sulfide from large volumes of silicate magma, collecting the sulfide in structural traps where it can achieve economic modal abundance.

A great array of structural traps has been recognized within conduits. Geologists should consider the characteristics of magma flow in the system they are interested in, to identify those places where contamination might locally have provoked sulfide saturation, or where suspended sulfide might have been dropped due to a sudden drop in the flow velocity of the magma. Typical environments of this sort include embayments in the margins of dikes or sills, hollows in the bases of ultramafic lava channels, sharp bends or sudden widenings of dikes or sills, magmatic breccias, or the entry points of dikes into larger magma chambers.

Once sulfide magma has segregated into a mass or dissemination within a larger igneous body,

it may become internally differentiated into a cumulate body rich in IPGE and Ni, and a residual sulfide liquid rich in Cu, PGE and possibly also Ni.

Although it is normal for residual sulfide liquids to migrate downward through host silicate rocks due to their high relative density, it is possible for the migration to be lateral or even upward if the local pressure gradient is not purely hydrostatic. The possible existence of fractionated sulfide veins or disseminations can be inferred by calculating mass balances between a postulated parental silicate magma and the average composition of the mineralized rocks. Deficiencies in Cu, Pt, Pd and Au may point to the existence of a migrated PGE-rich zone outside of known limits to the mineralization. In some instances the only parts of a deposit worth mining are the fractionated Cu- and PGE-rich vein systems, so their recognition is of prime importance in exploration.

FINAL COMMENTS

My aim in this chapter has been to supply readers with a toolkit of methods and ideas that can be applied to the understanding of the behavior of the PGE in igneous environments, using nothing more sophisticated than a spreadsheet. It is worth the effort required to learn to apply simple petrogenetic models to the genesis of magmatic PGE deposits. A relatively small investment in the methods described in this article might prevent large expenditures of exploration dollars on inappropriate targets, or might point the way to the best targets when too many targets exist. It is important to recognize that each magmatic suite is unique, and blind application of simple generalizations will usually lead to incorrect conclusions. Application of the underlying concepts is much more likely to lead to success.

REFERENCES

- AHO, A.E. (1956): Geology and genesis of ultrabasic nickel-copper-pyrrhotite deposits at the Pacific Nickel property, Southwestern British Columbia. *Econ. Geol.* **51**, 444-481.
- ARNDT, N.T., CZAMANSKE, G.K., WALKER, R.J., CHAUVEL, C. & FEDORENKO, V.A. (2003): Geochemistry and origin of the intrusive hosts of the Noril'sk-Talnakh Cu-Ni-PGE sulfide deposits. *Econ. Geol.* **98**, 495-515.
- BALLHAUS, C. & SYLVESTER, P.J. (2000): Noble metal enrichment processes in the Merensky

- Reef, Bushveld Complex. *Jour. Petrol.* **41**, 545-561.
- BALLHAUS, C., TREDoux, M. & SPÄTH, A. (2001): Phase relations in the Fe–Ni–Cu–PGE–S system at magmatic temperature and application to the massive sulphide ores of the Sudbury Igneous Complex. *J. Petrol.* **42**, 1911-1926.
- BARNES, S.J. (1989): Are bushveld U-type parent magmas boninites or contaminated komatiites. *Contrib. Mineral. Petrol.* **101**, 447-457.
- BARNES, S.J. (1993): Partitioning of the platinum group elements and gold between silicate and sulphide magmas in the Munni Munni Complex, Western Australia. *Geochim. Cosmochim. Acta* **57**, 1277-1290.
- BARNES, S. J., MCINTYRE, J. R., NISBET, B. W. & WILLIAMS, C. R. (1990): Platinum-group element mineralization in the Munni Munni Complex, Western Australia. *Mineral. Petrol.* **42**, 141-164.
- BARNES, S.-J. & MAIER W. (1999): The fractionation of Ni, Cu and the noble metals in silicate and sulphide liquids. In *Dynamic Processes in Magmatic Ore Deposits and their Application in Mineral Exploration* (R.R. Keays, C.M. Leshner, P.C. Lightfoot & C.E.G. Farrow, eds.) *Geol. Assoc. Can. Short Course Notes* **13**, 69-106.
- BARNES, S.-J., VAN ACHTERBERGH, E., MAKOVICKY, E. & LI, C. (2001): Proton microprobe results for the partitioning of platinum-group elements between monosulfide solid solution and sulphide liquid. *S. African J. Geol.* **104**, 275-286.
- BARRIE, C.T., NALDRETT, A.J. & DAVIS, D.W. (1990): Geochemical constraints on the genesis of the Montcalm gabbroic complex and Ni–Cu deposit, western Abitibi subprovince, Ontario. *Can. Mineral.* **28**, 451-474.
- BEHRE DOLBEAR & COMPANY (2004): Mineral Resource Estimate for the Afton Cu/Au project, Kamloops, BC. Unpublished report to DRC Resources Corporation.
- BENNET, V.C., NORMAN, M.D. & GARCIA, M.O. (2000): Rhenium and platinum-group element abundances correlated with mantle source components in Hawaiian picrites: sulfides in the plume. *Earth Planet. Sci. Lett.* **183**, 513-526.
- BEZMEN, N.I., ASIF, M., BRUGMANN, G.E., ROMANENKO, I.M. & NALDRETT, A.J. (1994): Distribution of Pd, Rh, Ru, Ir, Os, and Au between sulfide and silicate melts. *Geochim. Cosmochim. Acta* **58**, 1251-1260.
- BOCKRATH, C., BALLHAUS, C. & HOLZHEID, A. (2004a): Stabilities of laurite RuS₂ and monosulfide liquid solution at magmatic temperature. *Chem. Geol.* **208**, 265-271.
- BOCKRATH, C., BALLHAUS, C. & HOLZHEID, A. (2004b): Fractionation of the platinum-group elements during mantle melting. *Science* **305**, 1951-1953.
- BORISOV, A. & PALME, H. (1997): Experimental determination of the solubility of platinum in silicate melts. *Geochim. Cosmochim. Acta* **61**, 4349-4357.
- BORISOV, A. & PALME, H. (2000): Solubilities of noble metals in Fe-containing silicate melts as derived from experiments in Fe-free systems. *Amer. Mineral.* **85**, 1665-1673.
- BORISOV, A., PALME, H. & SPETTEL, B. (1994): Solubility of Pd in silicate melts: Implications for core formation in the Earth. *Geochim. Cosmochim. Acta* **58**, 705-716.
- BOUDREAU, A.E. (2003): IRIDIUM - a program to model reaction of silicate liquid infiltrating a porous solid assemblage. *Comp. Geosci.* **29**, 423-429.
- BOUDREAU, A.E. & MCCALLUM, I.S. (1992): Concentration of platinum-group elements by magmatic fluids in layered intrusions. *Econ. Geol.* **87**, 1830-1848.
- BRENAN, J.M. & ANDREWS, D. (2001): High-temperature stability of laurite and Ru–Os–Ir alloy and their role in PGE fractionation in mafic magmas. *Can. Mineral.* **39**, 341-360.
- BRENAN, J.M. (2002): Re–Os fractionation in magmatic sulfide melt by monosulfide solid solution. *Earth Planet. Sci. Lett.* **199**, 257-268.
- BRENAN, J.M., MCDONOUGH, W.F. & ASH, R. (submitted): An experimental study of the solubility and partitioning of iridium and osmium between olivine and silicate melt.
- BRENAN, J.M., MCDONOUGH, W.F. & DALPÉ, C. (2003): Experimental constraints on the partitioning of rhenium and some platinum-group

- elements between olivine and silicate melt. *Earth Planet. Sci. Lett.* **212**, 135-150.
- BRÜGMANN, G.E., NALDRETT, A.J., ASIF, M., LIGHTFOOT, P.C., GORBACHEV, N.S. & FEDORENKO, V.A. (1993): Siderophile and chalcophile metals as tracers of the evolution of the Siberian Trap in the Noril'sk region, Russia. *Geochim. Cosmochim. Acta* **57**, 2001-2018.
- CABRI, L.J. (1992): The distribution of trace precious metals in minerals and mineral products. *Mineral. Mag.* **56**, 289-308.
- CAMPBELL, I.H. & NALDRETT, A.J. (1979): The influence of silicate:sulfide ratios on the geochemistry of magmatic sulfides. *Econ. Geol.* **74**, 1503-1505.
- CAMPBELL, I.H., NALDRETT, A.J. & BARNES, S.J. (1983): A model for the origin of the platinum-rich sulfide horizons in the Bushveld and Stillwater Complexes. *Jour. Petrol.* **24**, 133-165.
- CAPOBIANCO, C.H. & DRAKE, M. (1990): Partitioning of ruthenium, rhodium, and palladium between spinel and silicate melt and implications for platinum-group element fractionation trends. *Geochim. Cosmochim. Acta* **54**, 869-874.
- CAPOBIANCO, C.H., HERVIG, R.L. & DRAKE, M. (1994): Experiments on crystal/liquid partitioning of Ru, Rh and Pd for magnetite and hematite solid solutions crystallised from silicate melt. *Chem. Geol.* **113**, 23-43.
- CARMICHAEL, I.S.E. (1991): The redox states of basic and silicic magmas: a reflection of their source regions? *Contrib. Mineral. Petrol.* **106**, 106-129.
- CARMICHAEL, I.S.E. & GHIORSO, M.S. (1986): Oxidation-reduction relations in basic magma: a case for homogeneous equilibrium. *Earth Planet. Sci. Lett.* **78**, 200-210.
- COURTILLOT, V., JAUPART, C., MANIGHETTI, I., TAPPONNIER, P. & BESSE, J. (1999): On causal links between flood basalts and continental breakup. *Earth Planet. Sci. Lett.* **166**, 177-195.
- CROCKET, J.H. (2002): Platinum group element geochemistry of mafic and ultramafic rocks. In *The Geology, Geochemistry, Mineralogy and Beneficiation of PGE* (L.J. Cabri, ed.), *CIM Spec. Vol.* **54**, 177-210.
- CROCKET, J.H., FLEET, M.E. & STONE, W.E. (1992): Experimental partitioning of osmium, iridium and gold between basalt melt and sulphide liquid at 1300 °C. *Aust. J. Earth Sci.* **39**, 427-432.
- CZAMANSKE, G.K., ZEN'KO, T.E., FEDORENKO, V.A., CALK, L.C., BUDAHN, J.R., BULLOCK, J.H., JR., FRIES, T.L., KING, B.S., & SIEMS, D.F. (1995): Petrography and geochemical characterization of ore-bearing intrusions of the Noril'sk type, Siberia; with discussion of their origin. *Res. Geol. Spec. Iss.* **18**, 1-48.
- CZAMANSKE, G.K., ZEN'KO, T.E., FEDORENKO, V.A., CALK, L.C., BUDAHN, J.R., BULLOCK, J.H., JR., FRIES, T.L., KING, B.S., & SIEMS, D.F. (2002): Petrography and geochemical characterization of ore-bearing intrusions of the Noril'sk type, Siberia; with discussion of their origin. <http://geopubs.wr.usgs.gov/open-file/of02-074/>.
- EBEL, D.S. & NALDRETT, A.J. (1996): Fractional crystallization of sulfide ore liquids at high temperature. *Econ. Geol.* **91**, 607-621.
- ERTEL, W., O'NEILL, H.St.C., SYLVESTER, P.J. & DINGWELL, D.B. (1999): Solubilities of Pt and Rh in a haplobasaltic silicate melt at 1300 °C. *Geochim. Cosmochim. Acta* **63**, 2439-2449.
- FINCHAM, C.J.B. & RICHARDSON, F.D. (1954): The behavior of sulphur in silicate and aluminate melts. *Proc. Royal Soc. London* **A223**, 40-62.
- FINNIGAN, C., BRENNAN, J.M. & MUNGALL, J.E. (2005a): Reduction-precipitation: A mechanism for platinum-group element fractionation and enrichment. Submitted to *Jour. Petrol.*
- FINNIGAN, C., BRENNAN, J.M. & MUNGALL, J.E. (2005b): Experimental evidence for the co-precipitation of platinum-group minerals and chromite by local reduction. Submitted to *Nature*.
- FLEET, M.E. & PAN, Y. (1994): Fractional crystallization of anhydrous sulfide liquid in the system Fe-Ni-Cu-S, with application to magmatic sulfide deposits. *Geochim. Cosmochim. Acta* **58**, 3369-3377.
- FLEET, M.E. & STONE, W.E. (1991): Partitioning of platinum-group elements in the Fe-Ni-S system and their fractionation in nature. *Geochim. Cosmochim. Acta* **55**, 245-253.

- FLEET, M.E., CHRYSOULIS, S.L., STONE, W.E. & WEISNER, C.G. (1993): Partitioning of platinum-group elements and Au in the Fe–Ni–Cu–S system: experiments on the fractional crystallization of sulfide melt. *Contrib. Mineral. Petrol.* **115**, 36–44.
- FLEET, M.E., CROCKET, J.H., LIU, M. & STONE, W.E. (1999a): Laboratory partitioning of platinum-group elements (PGE) and gold with application to magmatic sulfide-PGE deposits. *Lithos* **47**, 127–142.
- FLEET, M.E., LIU, M. & CROCKET, J.H. (1999b): Partitioning of trace amounts of highly siderophile elements in the Fe–Ni–S system and their fractionation in nature. *Geochim. Cosmochim. Acta* **63**, 2611–2622.
- FORTENANT, S.S., GÜNTER, D., DINGWELL, D.B. & RUBIE, D.C. (2003): Temperature dependence of Pt and Rh solubilities in a haplobasaltic melt. *Geochim. Cosmochim. Acta* **67**, 123–131.
- FROST, B.R., MAVROGENES, J.A. & TOMKINS, A.G. (2002): Partial melting of sulfide ore deposits during medium- and high-grade metamorphism. *Can. Mineral.* **40**, 1–18.
- GAETANI, G.A. & GROVE, T.L. (1997): Partitioning of moderately siderophile elements among olivine, silicate melt, and sulfide melt: Constraints on core formation in the Earth and Mars. *Geochim. Cosmochim. Acta* **61**, 1829–1846.
- GARUTI, G., PUSHKAREV, E.V., ZACCARINI, F., CABELLA, R. & ANIKINA, E. (2003): Chromite composition and platinum-group mineral assemblage in the Uktus Uralian-Alaskan-type complex (Central Urals, Russia). *Mineralium Deposita* **38**, 312–326.
- HAMLIN, P.R. & KEAYS, R.R. (1985a): Precious metals in magnesian low-Ti lavas – implications for metallogenesis and sulfur saturation in primary magmas. *Geochim. Cosmochim. Acta* **49**, 1797–1811.
- HAMLIN, P.R. & KEAYS, R.R. (1985b): Sulfur saturation and 2nd stage melts – application to the Bushveld platinum metal deposits. *Econ. Geol.* **81**, 1431–1445.
- HANLEY, J.J., MUNGALL, J.E., PETTKE, T. & SPOONER, E.T.C. (2005a): Solubility of Au and Pt in NaCl brines at 1.5 kbar, 600 to 800°C: a laser ablation–ICP–MS pilot study of synthetic fluid inclusions. *Geochim. Cosmochim. Acta* in press.
- HANLEY, J.J., MUNGALL, J.E., PETTKE, T. & SPOONER, E.T.C. (2005b): Ore metal redistribution by hydrocarbon–brine and hydrocarbon–halide melt mixtures, North Range footwall of the Sudbury Igneous Complex, Ontario, Canada. Submitted to *Mineralium Deposita*.
- HARMER, R.E. & SHARPE, M.R. (1985): Field relations and strontium isotope systematics of the marginal rocks of the Eastern Bushveld Complex. *Econ. Geol.* **80**, 813–837.
- HUPPERT, H.E., SPARKS, R.S.J., TURNER, J.S. & ARNDT, N.T. (1984): Emplacement and cooling of komatiite lavas. *Nature* **309**, 19–22.
- JOHNSTON, S.T. & THORKELSON, D.J. (2000): Continental flood basalts: episodic magmatism above long-lived hotspots. *Earth Planet. Sci. Lett.* **175**, 247–256.
- KATZ, R.F., SPIEGELMAN, M. & LANGMUIR, C.H. (2003): A new parameterization of hydrous mantle melting. *Geochem. Geophys. Geosystems* **4**, 9/1073 DOI 10.1029/2002GC000433.
- LI, C., BARNES, S.-J., MAKOVICKY, E., ROSE-HANSEN, J. & MAKOVICKY, M. (1996): Partitioning of nickel, copper, iridium, rhenium, platinum, and palladium between monosulfide solid solution and sulfide liquid: Effects of composition and temperature. *Geochim. Cosmochim. Acta* **60**, 1231–1238.
- LI, C., NALDRETT, A.J., COATS, C.J.A. & JOHANNESSEN, P. (1992): Platinum, palladium, gold and copper-rich stringers at Strathcona Mine, Sudbury: Their enrichment by fractionation of a sulfide liquid. *Econ. Geol.* **87**, 1584–1596.
- LIGHTFOOT, P.C. & KEAYS, R.R. (2005): submitted to *Econ. Geol.*
- LIGHTFOOT, P.C., NALDRETT, A.J., GORBACHEV, N.S., DOHERTY, W. & FEDORENKO, V.A. (1990): Geochemistry of the Siberian Trap of the Noril'sk area, USSR, with implications for the relative contributions of crust and mantle to flood basalt magmatism. *Contrib. Mineral. Petrol.* **104**, 631–644.

- MACLEAN W.H. (1969): Liquidus phase relations in FeS–FeO–Fe₃O₄–SiO₂ system, and their application in geology. *Econ. Geol.* **64**, 865-884.
- MAVROGENES, J.A. & O'NEILL, H.ST.C. (1999): The relative effects of pressure, temperature and oxygen fugacity on the solubility of sulfide in natural magmas. *Geochim. Cosmochim. Acta* **63**, 1173-1180.
- MCDONOUGH, W.F. & SUN, S.-S. (1995): The composition of the Earth. *Chem. Geol.* **120**, 223-253.
- MERKLE, R.K.W. (1992): Platinum-group elements in the middle group of chromitite layers at Marikana, western Bushveld Complex: indications for collection mechanisms and postmagmatic modification. *Can. Jour. Earth Sci.* **29**, 209-21.
- MUNGALL, J.E. (2002a): A model for co-precipitation of platinum-group minerals with chromite from silicate melts. *Proc. 9th Ann. Pt Symp.*, Billings, Montana, July 21-25, 2002.
- MUNGALL, J.E. (2002b): Kinetic controls on the partitioning of trace elements between silicate and sulphide liquids. *Jour. Petrol.* **43**, 749-768.
- MUNGALL, J.E. (2002c): Late-stage sulfide liquid mobility in the Main Mass of the Sudbury Igneous Complex; examples from the Victor Deep, McCreedy East and Trillabelle deposits. *Econ. Geol.* **97**, 1563-1576.
- MUNGALL, J.E. (2002d): Roasting the mantle: slab melting and the genesis of major Au and Au-rich Cu deposits. *Geology* **30**, 915-918.
- MUNGALL, J.E. & BRENNAN, J.M. (2003): Experimental evidence for the chalcophile behaviour of the halogens. *Can. Mineral.* **41**, 207-220.
- MUNGALL, J.E., ANDREWS, D.R.A., CABRI, L.J., SYLVESTER, P.J. & TUBRETT, M. (2005): Partitioning of Cu, Ni, Au, and platinum-group elements between monosulfide solid solution and sulfide melt under controlled oxygen and sulfur fugacities. *Geochim. Cosmochim. Acta* in press.
- MUNGALL, J.E. & SU, S. (2005): Interfacial tension between magmatic sulfide and silicate liquids. *Earth Planet. Sci. Lett.* in press.
- MURRAY, C.G. (1972): Zoned ultramafic complexes of the Alaskan type: feeder pipes of andesitic volcanoes. *Geol. Soc. Amer. Mem.* **132**, 313-333.
- NALDRETT, A.J. (1969): A portion of the system Fe–S–O between 900 and 1080°C and its application to sulfide ore magmas. *J. Petrol.* **10**, 171-202.
- NALDRETT, A.J., LIGHTFOOT, P.C., FEDORENKO, V., DOHERTY, W. & GORBACHEV, N.S. (1992): Geology and geochemistry of intrusions and flood basalts of the Noril'sk region, USSR, with implications for the origin of the Ni–Cu ores. *Econ. Geol.* **87**, 975-1004.
- NALDRETT, A.J., ASIF, M., GORBACHEV, N.S., KUNILOV, V.YE., STEKHIN, A.I., FEDORENKO, V.A. & LIGHTFOOT, P.C. (1994): The composition of the Ni–Cu ores of the Oktyabr'sky Deposit, Noril'sk Region. in Proceedings of the Sudbury–Noril'sk Symposium (P.C. Lightfoot and A.J. Naldrett, eds), *Ont. Geol. Surv. Spec. Vol.* **5**, 357-371.
- NALDRETT, A.J., FEDORENKO, V.A., ASIF, M., SHUSHEN, L., KUNILOV, V.E., STEKHIN, A.I., LIGHTFOOT, P.C. & GORBACHEV, N.S. (1996): Controls on the composition of Ni–Cu sulfide deposits as illustrated by those at Noril'sk, Siberia. *Econ. Geol.* **91**, 751-773.
- NALDRETT, A.J., ASIF, M., SCHANDL, E., SEARCY, T., MORRISON, G.G., BINNEY, W.P. & MOORE, C. (1999): Platinum-group elements in the Sudbury ores: significance with respect to the origin of different ore zones and to the exploration for footwall ore bodies. *Econ. Geol.* **94**, 185-210.
- NIXON, G.T. & HAMMACK, J.L. (1991): Metallogeny of mafic–ultramafic rocks in British Columbia with emphasis on platinum-group elements. In *Ore Deposits, Tectonics and Metallogeny in the Canadian Cordillera*, B.C. Ministry of Energy, Mines and Petroleum Resources, *Paper* **1991-4**, 125-161.
- O'NEILL, H.ST.C. & MAVROGENES, J.A. (2002): The sulfide capacity and the sulfur content at sulfide saturation of silicate melts at 1400 °C and 1 bar. *Jour. Petrol.* **43**, 1049-1087.
- PAKTUNC, A.D. (1989): Petrology of the St. Stephen intrusion and the genesis of related nickel–copper sulfide deposits. *Econ. Geol.* **84**, 817-840.
- PEACH, C.L. & MATHEZ, E.A. (1993): Sulfide

- melt–silicate melt distribution coefficients for nickel and iron and implications for the distribution of other chalcophile elements. *Geochim. Cosmochim. Acta* **57**, 3013-3021.
- PEACH, C.L., MATHEZ, E.A. & KEAYS, R.R. (1990): Sulfide melt–silicate melt distribution coefficients for noble metals and other chalcophile elements as deduced from MORB: Implications for partial melting. *Geochim. Cosmochim. Acta* **54**, 3379-3389.
- PEACH, C.L., MATHEZ, E.A., KEAYS, R.R. & REEVES, S.J. (1994): Experimentally determined sulfide melt–silicate melt partition coefficients for iridium and platinum. *Chem. Geol.* **117**, 361-377.
- PEARSON, D.G. & WOODLAND, S.J. (2000): Solvent extraction/anion exchange separation and determination of PGEs (Os, Ir, Pt, Pd, Ru) and Re–Os isotopes in geological samples by isotope dilution ICP–MS. *Chem. Geol.* **165**, 87-107.
- PECK, D. C. & KEAYS, R. R. (1990): Geology, geochemistry and origin of platinum-group element-chromitite occurrences in the Heazlewood River Complex, Tasmania. *Econ. Geol.* **85**, 765-793.
- PECK, D.C., KEAYS, R.R. & FORD, R.J. (1992): Direct crystallization of refractory platinum-group element alloys from boninitic magmas: Evidence from western Tasmania. *Austral. Jour. Earth Sci.* **39**, 373-387.
- PEREGOEDOVA, A. & OHNENSTETTER, M. (2002): Collectors of Pt, Pd and Rh in a S-poor Fe–Ni–Cu sulfide system at 760 degrees C: Experimental data and application to ore deposits. *Can. Mineral.* **40**, 527-561.
- PEREGOEDOVA, A., BARNES, S.-J. & BAKER, D.R. (2004): The formation of Pt–Ir alloys and Cu–Pd-rich sulfide melts by partial desulfurization of Fe–Ni–Cu sulfides: results of experiments and implications for natural systems. *Chem. Geol.* **208**, 247-264.
- PEUCKER-EHRENBRINK, B., BACH, W., HART, S.R., BLUSZTYAJN, J.S. & ABBRUZZESE, T. (2003): Rhenium–osmium isotope systematics and platinum-group element concentrations in oceanic crust from DSDP/ODP Sites 504 and 417/418. *Geochem. Geophys. Geosys.* **4**, 10.1029/2002GC000414.
- RIGHTER K., CAMPBELL, A.J., HUMAYUN, M. & HERVIG, R.L. (2004): Partitioning of Ru, Rh, Pd, Re, Ir, and Au between Cr-bearing spinel, olivine, pyroxene and silicate melts. *Geochim. Cosmochim. Acta* **68**, 867-880.
- RIPLEY, E.M., BROPHY, J.G. & LI, C. (2002): Copper solubility in a basaltic melt and sulfide liquid/silicate melt partition coefficients of Cu and Fe. *Geochim. Cosmochim. Acta* **66**, 2791-2800.
- SCHUBERT, G., TURCOTTE, D.L. & OLSON, P. (2001): *Mantle Convection in the Earth and Planets*. Cambridge University Press, Cambridge, 940 pp.
- SNYDER, D.A. & CARMICHAEL, I.S.E. (1992): Olivine–liquid equilibria and the chemical activities of FeO, NiO, Fe₂O₃, and MgO in natural basic melts. *Geochim. Cosmochim. Acta* **56**, 303-318.
- STONE, W.E., CROCKETT, J.H. & FLEET, M.E. (1990): Partitioning of palladium, iridium, platinum, and gold between sulfide liquid and basalt at 1200°C. *Geochim. Cosmochim. Acta*, **54**, 2341-2344.
- SYLVESTER P.J. (2001): A practical guide to platinum-group element analysis of sulfides by laser ablation ICPMS. *In Laser–Ablation–ICP–MS in the Earth Sciences, Principles and Applications* (P. Sylvester, Ed.), Min. Assoc. Canada, *Short Course* **29**, Chapter 13, 203-211.
- TREDOUX, M., LINDSAY, N.M., DAVIES, G. & MCDONALD, I. (1995): The fractionation of platinum-group elements in magmatic systems, with the suggestion of a novel causal mechanism. *S. Afr. Jour. Geol.* **98**, 157-167.
- WALLACE, P. & CARMICHAEL, I.S.E. (1992): Sulfur in basaltic magmas. *Geochim. Cosmochim. Acta* **56**, 1863-1874.
- WEDEPOHL, K.H. (1995): The composition of the continental crust. *Geochim. Cosmochim. Acta* **59**, 1217-1232.
- WHITE, R. & MCKENZIE, D. (1989): Magmatism at rift zones: the generation of volcanic continental margins and flood basalts. *Jour. Geophys. Res.* **94B**, 7685-7729.
- WILSON, A. H. & TREDOUX, M. (1990): Lateral and vertical distribution of platinum-group elements and petrogenetic controls on the sulfide mineralization in the P1 pyroxenite layer of the

Darwendale subchamber of the Great Dyke, Zimbabwe. *Econ. Geol.* **85**, 556-584.

WOODLAND, S.J., PEARSON, D.G. & THIRLWALL, M.F. (2002): A platinum-group element and Re-Os isotope investigation of siderophile element recycling in subduction zones: comparison of Grenada, Lesser Antilles arc, and the Izu-Bonin arc. *Jour. Petrol.* **43**, 171-198.

ZIENTEK, M.L., LIKHACHEV, A.P., KUNILOV, V.E., BARNES, S.-J., MEIER, A.L., CARLSON, R.R., BRIGGS, P.H., FRIES, T.L. & ADRIAN, B.M. (1994): Cumulus processes and the composition of magmatic ore deposits: Examples from the Talnakh District, Russia. *in* Proceedings of the Sudbury–Noril'sk Symposium (P.C.Lightfoot and A.J. Naldrett, eds), *Ont. Geol. Surv. Spec. Vol. 5*, 373-392.

Appendix: Partitioning in magmatic systems.

Preamble: the Nernst partitioning coefficient. Consider the following reaction (as an example; we could use any similar reaction)



$$K = \frac{a_{\text{NiS}}^{\text{sul}} \cdot a_{\text{FeO}}^{\text{sil}}}{a_{\text{NiO}}^{\text{sil}} \cdot a_{\text{FeS}}^{\text{sul}}} \quad \text{equilibrium constant} \quad 2$$

$$K = \frac{X_{\text{NiS}}^{\text{sul}} \cdot \gamma_{\text{NiS}}^{\text{sul}} \cdot X_{\text{FeO}}^{\text{sil}} \cdot \gamma_{\text{FeO}}^{\text{sil}}}{X_{\text{NiO}}^{\text{sil}} \cdot \gamma_{\text{NiO}}^{\text{sil}} \cdot X_{\text{FeS}}^{\text{sul}} \cdot \gamma_{\text{FeS}}^{\text{sul}}} \quad \text{introduce activity coefficients} \quad 3$$

$$\frac{X_{\text{NiS}}^{\text{sul}}}{X_{\text{NiO}}^{\text{sil}}} = \frac{K \cdot \gamma_{\text{NiO}}^{\text{sil}} \cdot X_{\text{FeS}}^{\text{sul}} \cdot \gamma_{\text{FeS}}^{\text{sul}}}{\gamma_{\text{NiS}}^{\text{sul}} \cdot X_{\text{FeO}}^{\text{sil}} \cdot \gamma_{\text{FeO}}^{\text{sil}}} \quad \text{solve for NiS/NiO} \quad 4$$

If the mole fractions of FeO and FeS do not change significantly in the silicate and sulfide melts as Ni is exchanged between them (*i.e.*, Ni is behaving as a trace constituent) then these terms and the activity coefficients can be treated as constants. The stoichiometric terms to change NiO and NiS to Ni can be incorporated, and all these terms can be rolled into a single constant.

$$\frac{X_{\text{Ni}}^{\text{sul}}}{X_{\text{Ni}}^{\text{sil}}} \approx D \quad 5a$$

In the presence of a number j of phases, the weighted average of the individual phase D^j 's can be used as a bulk D ; if the phase assemblage does not change then the bulk D is approximately constant.

$$D = \sum_j X_i^j D^j \quad \text{mass action equation} \quad 5b$$

notation:

X_i^o	concentration of i in bulk system	6
X_i^α	concentration of i in phase α	7
X_i^β	concentration of i in phase β	8
Y	total mass of element i in system	9
N	total mass of system	10
y^α	total mass of element i present in phase α	11
y^β	total mass of element i present in phase β	12
n^α	mass of phase α in system	13
n^β	mass of phase β in system	14

Some equations:

Concentrations $X_i^o = \frac{Y}{N}$, $X_i^\alpha = \frac{y^\alpha}{n^\alpha}$, $X_i^\beta = \frac{y^\beta}{n^\beta}$ 15 a,b,c

mass balance $F = \frac{n^\alpha}{N}$ mass fraction of phase α in system 16

$n^\alpha + n^\beta = N$ 17

$y^\alpha + y^\beta = Y$ 18

$D = \frac{X_i^\beta}{X_i^\alpha}$ mass action 19

(D here is assumed to be a bulk partition coefficient, representing the weighted average of the individual partitioning coefficients.)

substitute concentration expressions 15a,b,c into 18

$$X_i^\beta n^\beta + X_i^\alpha n^\alpha = X_i^o N \quad 20$$

express n^α in terms of NF , n^β in terms of N and X_i^β in terms of D (using equ'ns 16-19 in equ'n 20)

$$X_i^\alpha D(N - NF) + X_i^\alpha NF = X_i^o N \quad 21$$

simplify

$$\frac{X_i^\alpha}{X_i^o} = \frac{1}{D(1 - F) + F} \quad 22$$

Note that if we define α as the melt phase and β as the mineral, then D is a mineral/melt partitioning coefficient, and this is the batch melting equation.

If we reverse the phase definitions, so that α is the mineral phase and β is the melt, then by convention the partitioning coefficient is the inverse of the partitioning coefficient defined above so that the new mineral/melt D will be

$$D = \frac{X_i^\alpha}{X_i^\beta} \quad 23$$

leading to

$$\frac{X_i^\alpha}{X_i^o} = \frac{D}{(1 - F) + FK_d} \quad 24$$

which is the equation describing the composition of crystals as they form during an equilibrium crystallization process.

This equation can also be used to describe the separation of a sulfide melt α at equilibrium with the silicate melt β . Campbell & Naldrett (1979) used the same equation except that in the place of F they used R , defined as

$$R = \frac{n^\beta}{n^\alpha} = \frac{1}{F} - 1 \quad 25$$

Rewriting the equilibrium crystallization equation in terms of their R factor gives

$$\frac{X_i^\alpha}{X_i^o} = \frac{D(R+1)}{R + K_d} \quad 26$$

Returning to the equilibrium crystallization of a mineral or mineral assemblage β from a melt α , consider what happens if the solids are continuously removed as they form. This situation is referred to as fractional crystallization, and can be described with the Rayleigh distillation equation.

In an infinitesimally small period of time,

$$N \rightarrow N - dN \quad 27$$

$$Y \rightarrow Y - dY \quad 28$$

and therefore the composition of phase β is

$$X_i^\beta = \frac{dY}{dN} \quad 29$$

$$X_i^\alpha = \frac{Y - dY}{N - dN} \quad 30$$

mass action as before

$$X_i^\beta = \frac{dY}{dN} = DX_i^\alpha \quad 31$$

In equation 30, taking the limit as $dY, dN \rightarrow 0$

$$X_i^\alpha \cong \frac{Y}{N} \quad \text{so} \quad Y \cong NX_i^\alpha \quad 32$$

differentiate both sides of 32 wrt N

$$\frac{dY}{dN} = N \frac{dX_i^\alpha}{dN} + X_i^\alpha \frac{dN}{dN} \quad 33$$

combine equations 31 and 33, rearrange

$$\frac{X_i^\alpha (D-1)}{dX_i^\alpha} = \frac{N}{dN} \quad 34$$

invert

$$\frac{1}{(D-1)} \frac{dX_i^\alpha}{X_i^\alpha} = \frac{dN}{N} \quad 35$$

integrate between N^o and N^F on lhs ; between X_i^o and X_i^F on rhs

$$\frac{1}{(D-1)} \ln \left(\frac{X_i^\alpha}{X_i^o} \right) = \ln \left(\frac{N^F}{N^o} \right) \quad 36$$

and

$$\frac{X_i^\alpha}{X_i^o} = \left(\frac{N^F}{N^o} \right)^{(D-1)} \quad 37$$

Since

$$F = \frac{N^F}{N^o} \quad (F \text{ is the melt fraction remaining, so that } N^F = N^o F) \quad 38$$

we have derived

$$X_i^\alpha = X_i^o F^{(D-1)} \quad 39$$

which is the fractional crystallization (distillation) equation.

CHAPTER 2: THE AQUEOUS GEOCHEMISTRY OF THE PLATINUM-GROUP ELEMENTS (PGE) IN SURFICIAL, LOW-T HYDROTHERMAL AND HIGH-T MAGMATIC-HYDROTHERMAL ENVIRONMENTS

Jacob J. Hanley
Department of Geology, University of Toronto
22 Russell Street, Toronto, Ontario, M5S 3B1, Canada
E-mail: hanley@geology.utoronto.ca

INTRODUCTION

In order to understand the behavior of the platinum-group elements (PGE) in *aqueous* fluids, some important thermodynamic and geochemical terminology needs to be defined to the interested reader. Table 2-1 summarizes some of the terminology used in this article. There are several excellent references that serve as an introduction to the fundamentals of aqueous solutions and hydrothermal geochemistry with specific application to ore-forming systems. G.M. Anderson's book "Thermodynamics of Natural Systems" (Anderson 1996) is a good starting point for understanding the basics of chemical thermodynamics. Applications of the basic concepts described by Anderson (1996) to ore-forming environments are described by, for example, Wood and Samson (1998) and Wood (1998). In summary, there are a few major concepts that the reader needs to be familiar with in order to be able to understand and calculate PGE solubility in fluids over a range of conditions:

Concentration, activity and fugacity

In aqueous and gaseous solutions, the *molality* of a dissolved species (m_i) or the *partial pressure* of a dissolved species (P_i in bars) are the most commonly used units of *concentration*. The *activity* of a dissolved species (a_i) may be described as the "effective" or "reactive" concentration of the species, that is, the molality or partial pressure multiplied by a factor that accounts for the difference between an *ideal solution* and a real solution. For gaseous species, activity is interchangeable with *fugacity* (f_i). The factor that accounts for the degree of ideality in the solution is known as the *activity coefficient* (γ_i). Molality and partial pressure are related to the activity and activity coefficient of a dissolved species by the following expressions:

(in aqueous solutions)

$$a_i = \gamma_i m_i \quad (1)$$

(in gaseous solutions)

$$f_i = a_i = \gamma_i P_i \quad (2)$$

(Note that activity or fugacity is a dimensionless term because it is actually a ratio with the denominator equal to 1 molal concentration or 1 bar fugacity reference state). Ideal solutions are those that obey idealized solution models such as *Henry's Law* that states that the activity of a dissolved species is directly proportional to its concentration, as stated in eq'n (1). Unfortunately, because the constant of proportionality, the activity coefficient, is not equal to 1 for many naturally occurring aqueous solutions, Henry's Law is not strictly followed and activity coefficients can be calculated to express accurately the true equilibrium activity of a dissolved species. This is the case for concentrated solutions, for example, that contain a high concentration of dissolved salts (a case commonly encountered in ore-forming systems). Henryan activity coefficients can be calculated in aqueous solutions using relationships known as *Debye-Hückel equations* that relate the value of γ_i to the ionic strength of the solution (I) and a number of constants (A, B, \hat{a}_i) that are related to P- and T-specific properties of the solvent (H₂O) and the size of dissolved ions in solution. For our purposes, it is important to understand that solubility will be defined in terms of the concentration of a dissolved metal or metal complex, not activity; that is, in dilute (ideal) solutions, the activity coefficients for dissolved species are close to ~1 and therefore, the concentration of a dissolved species is equal to the activity of a dissolved species.

TABLE 2-1. GLOSSARY OF IMPORTANT TERMINOLOGY USED IN THIS ARTICLE

Term	Definition
aqueous	describing a solution in which the solvent phase is water
molality (m_i)	moles of solute “i” per kilogram of solvent; a unit of aqueous concentration
partial pressure (P_i)	the mole fraction of a dissolved gas species in a gaseous solution multiplied by the total pressure (in bars) of the system
concentration	quantity of solute per unit quantity of solvent; measure of solubility
ideal solution	a solution that behaves ideally as governed by Henry’s Law
fugacity (f_i)	the partial pressure (P_i) of dissolved species “i” in a gaseous solution multiplied by an activity coefficient (γ_i); accounts for the non-ideal behavior of the dissolved species due to solute–solute interaction; for example oxygen fugacity, $f(O_2)$
activity (a_i)	the molality (m_i) of dissolved species “i” in an aqueous solution multiplied by an activity coefficient (γ_i); accounts for the non-ideal behavior of the dissolved species due to solute–solute interaction
Henry’s Law	the activity of a dissolved species in a solution is directly proportional to its concentration; concentration of a dissolved species equals its activity
Debye-Hückel equation	an equation to calculate an activity coefficient (γ_i) which takes into account the ionic strength of the solution (I), the size of the ions involved, and properties of the solvent that change as a function of pressure and temperature
complexation	the coordinated bonding of metal ions (<i>e.g.</i> , Pt^{2+}) to one or more negatively charged or molecular ligands (<i>e.g.</i> , Cl^- , H_2O)
ligand	a negatively charged ion or molecule that binds to a metal ion to form a coordination complex (<i>e.g.</i> , Cl^- , H_2O)
stability constant (β)	in a simple example, for the reaction $xi + yj \rightarrow i_xj_y$, the stability constant is calculated by the following: $\beta_{ij} = m_{i_xj_y} / (m_i)^x(m_j)^y$, where β_{ij} is the stability constant for complex i_xj_y , composed of metal ion “i” bound to ligand “j”, m_i is the concentration of metal ion “i”, x is the number of metal ions “i” in the complex, m_j is the concentration of ligand “j”, and y is the number of ligands “j” in the complex; a high value of β indicates that the complex is easily formed and relatively stable; a type of equilibrium constant
pH	a measurement of the acidity of an aqueous solution; equal to the negative log of the concentration of the hydrogen ion (H^+); solutions with $pH < 7$ are acidic; > 7 are alkaline (relative to pure H_2O at room T)
anion	a negatively charged ion
soft Lewis acid or base	an electron pair acceptor (acid) or donor (base); soft, in the Lewis sense, refers to ions that have a low charge-to-radius ratio and are easily polarizable, whereas hard ions are those with a high charge-to-radius ratio, are dominated by electrostatic interactions, and are not easily polarized; importantly, a soft Lewis acid will bind to a soft Lewis base
electrolyte	a solution that conducts electricity due to the presence of negatively or positively charged dissolved ions
electrostriction	a decrease in the “space” available for solutes to dissolve into an aqueous solution due to increasing electrostatic interaction of the solvent molecules with one another
dielectric constant	a measure of the ability of water to store a charge when an electric field is applied; decreases with increasing T, thereby changing the properties of an electrolytic solution
amorphous	a solid that is not crystalline; lacking crystalline structure
buffer	a solid (mineral) assemblage that will maintain constant pH or $f(O_2)$ in a solution

hydroxysilicate	a silicate mineral containing hydroxyl groups (OH ⁻ , <i>i.e.</i> , biotite)
hydration	the complexation of a metal ion or neutrally charged species by water molecules
wt.% eq. NaCl	a measure of the salinity of a fluid, expressed as the amount of equivalent NaCl dissolved in the fluid
exsolution	the separation of a fluid phase from a silicate liquid due to saturation being reached; occurs, for example, due to a decrease in confining pressure on a fluid-rich magma (“second boiling”)
homogenize	the transition from a multiphase system (<i>e.g.</i> , liquid+vapor) to a single phase system (<i>e.g.</i> , liquid only); used in fluid inclusion studies to describe the temperature at which a trapped fluid enters the single phase field upon heating; the homogenization temperature is a minimum estimate of the fluid’s trapping temperature in a rock
daughter phase	a crystal of a compound that is oversaturated in a fluid phase; form during cooling of a trapped fluid in a fluid inclusion (<i>e.g.</i> , halite)
ΔNNO	the log unit difference in oxygen fugacity ($f(O_2)$) of a system relative to the nickel-nickel oxide buffer; <i>e.g.</i> , ΔNNO = -1 represents an $f(O_2)$ one log unit below NNO.

Complexation

Complexation is an important process by which metal ions bind to one or more negatively charged ionic or molecular *ligands* (*e.g.*, Cl⁻, H₂O). In the absence of complexing species, most geochemists agree that the concentrations of simple metal ions (*e.g.*, Pt²⁺) in aqueous solutions in equilibrium with ore minerals cannot reach levels high enough to allow significant (economic) transport of metals in the aqueous fluid (*e.g.*, Barnes 1979). However, ore metal ions complexed in solution can reach very high concentrations. To exemplify the importance of complexation, consider the formation of the Pt²⁺ ion in an aqueous solution by the oxidation of Pd metal:



The *solubility constant* (K) expression for this reaction, assuming that the activities of pure species are ~1 and activity coefficients for dissolved species are ~1 (for a dilute solution) will be:

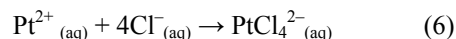
$$K = \frac{(m_{\text{Pt}^{2+}})}{(m_{\text{H}^+})^2 (f_{\text{O}_2})^{0.5}} \quad (4)$$

Reaction (3) and expression (4) show that the concentration of the Pt²⁺ ion is dependent on the *oxygen fugacity* ($f(O_2)$) and *pH* imposed on the solution by the mineral assemblages the solution is in contact with or reacting with. Recalling that the solubility is always defined in terms of concentration, not activity, the solubility of Pt in solution will be equal to the concentration of only the dissolved Pt²⁺ ion and the solubility of that ion

is fixed by the reaction above. Rearranging expression (4), the total amount of Pt in solution will be:

$$\sum \text{Pt}_{\text{dissolved}} = K(m_{\text{H}^+})^2 (f_{\text{O}_2})^{0.5} \quad (5)$$

Now consider the formation of the Pt (2⁺) tetrachloride complex by the reaction of the Pt²⁺ ion with Cl⁻ anions:



And the *stability constant* (β) expression for this reaction:

$$\beta = \frac{(m_{\text{PtCl}_4^{2-}})}{(m_{\text{Pt}^{2+}})(m_{\text{Cl}^-})^4} \quad (7)$$

In reaction (6) and expression (7), it can be seen that the concentration of the PtCl₄²⁻ complex shows some dependence on the concentrations of the dissolved Pt²⁺ and Cl⁻ ions, but of these two it is far more sensitive to changes in Cl⁻ concentration. For example, if the concentration of the Cl⁻ ion increases 1 order of magnitude, then the concentration of the PtCl₄²⁻ complex increases 4 orders of magnitude! As Pt²⁺ is consumed by complexation, reaction (3) must progress to the right to replace Pt²⁺ lost due to reaction (6). By both reactions (3) and (6), the total amount of Pt in solution is now equal to the sum of the concentrations of the PtCl₄²⁻ and Pt²⁺ ion. Rearranging and combining expressions (4) and (7), the total amount of Pt dissolved in solution will be:

$$\begin{aligned}
\Sigma Pt_{dissolved} &= (m_{Pt^{2+}}) + (m_{PtCl_4^{2-}}) \\
&= K(m_{H^+})^2 (f_{O_2})^{0.5} + \beta(m_{Pt^{2+}})(m_{Cl^-})^4 \\
&= K(m_{H^+})^2 (f_{O_2})^{0.5} + \beta[K(m_{H^+})^2 (f_{O_2})^{0.5}](m_{Cl^-})^4 \\
&= K(m_{H^+})^2 (f_{O_2})^{0.5} [1 + \beta(m_{Cl^-})^4] \quad (8)
\end{aligned}$$

Considering that the value of β is likely to be $\gg K$ (e.g., at 25°C, an estimated $\log \beta = 13.99$ whereas $\log K = -0.2$, calculated using data from Barner & Scheuerman 1978), it is immediately apparent, comparing eq'n (5) and (8), that eq'n (8) will yield a higher dissolved Pt concentration than eq'n (5). High PGE solubilities require either large solubility constants (K) for the source mineral phase, or large stability constants (β) for the complexes being formed, or both. An additional benefit of complexation is that, collectively, the various complexes of Pt^{2+} and Cl^- are stable over a much wider range of pH and Cl^- concentrations than the uncomplexed metal ion (Mountain & Wood 1988).

PGE Chemistry in Aqueous Fluids

At geologically relevant $f(O_2)$, the predicted oxidation states for all of the PGE in solution are 2^+ (Wood 2002, Sassani & Shock 1998, Xiong & Wood 2000). Additionally, at very oxidizing conditions (e.g., supergene environments, oxidized surface waters, oxidized porphyry systems), the oxidation state 4^+ is predicted for Pt (Gammons 1996), and 3^+ , 6^+ and 8^+ are predicted for Os (Mountain & Wood 1988). In most hydrothermal environments (<500°C), PGE (2^+) ions will behave as *soft Lewis acids* and should form the strongest complexes with *soft Lewis bases* such as bisulfide (HS^-). With increasing temperature (above 500°C) changes in the structure of aqueous *electrolyte* solutions (increasing *electrostriction*, decreasing *dielectric constant* of H_2O , decreasing degree of ionic dissociation) may allow the PGE to form strong complexes with (i) hard (in the Lewis sense) ligands such as hydroxide (OH^-), (ii) intermediate hardness ligands such as (Cl^-) whose interactions with the PGE ions become harder with increasing temperature, and (iii) neutrally charged species such as hydrogen chloride (HCl^0 , Frank *et al.* 2002, Hanley *et al.* 2005a). Similarly, with increasing oxidation state at low T (e.g., in some surficial environments), strong complexation between the PGE and hard ligands such as hydroxide, organic carboxylic acids (acetate, oxalate), humic substances (humic and fulvic acid) and amino acids may result in

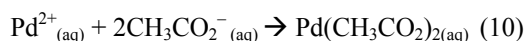
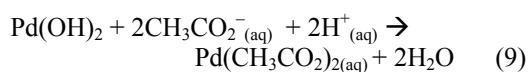
significant PGE mobility (Wood 2002). Below, I review (briefly!) the most important results of experimental and theoretical studies that investigated PGE dissolution in aqueous fluids by way of the complexes listed above. A more detailed discussion of the topics covered in this review paper was given by Wood (2002) and is recommended to the reader.

Surficial Environments (~25°C, 1 atm)

Understanding the conditions required for the PGE to be mobile in surface environments has important implications for mineral exploration and understanding the mass transfer of the PGE as toxins in the living environment. In surface environments (tills, soils, shallow aquifers, surface waters) the PGE may be derived from natural sources (e.g., exposed or near-surface ore deposits) or industrial sources (e.g., catalytic converters, smelting and refining, sewage sludge). In the context of mineral exploration, exploration methods rely on the ability to detect elevated concentrations of PGE in drill core or rock outcrops, or by geophysical prospecting methods. However, in cases where PGE ore deposits are sulfide-poor, undetectable using conventional geophysics, or not exposed on surface, biogeochemical analyses of surface media (plant matter, soil, humus, till) for the PGE may be useful during regional exploration (Hattori & Cameron 2004).

An important requirement to predict quantitatively the mass transfer of PGE in surface environments is an understanding of the nature and solubility of the PGE as aqueous organic or hydroxide complexes. There are limited thermodynamic data available for such complexes involving the PGE, despite mounting field evidence showing they may be important in redistributing the PGE in laterite (Bowles 1986, Bowles *et al.* 1994, 1995) and B horizon soils (e.g., Wood & Vlassopoulos 1990, Hattori & Cameron 2004) in proximity to PGE deposits in mafic rocks. Experimental and theoretical studies provide the following major conclusions about PGE solubility in aqueous solutions containing organic compounds: (i) humic substances (fulvic acid, humic acid) increase the solubility of *amorphous* $Pt(OH)_2$ or $Pd(OH)_2$ (Wood 1990, Wood *et al.* 1994); (ii) amino acids (comprising up to 50% of soil-hosted nitrogen) form strong complexes with both Pt^{2+} and Pd^{2+} and may account for a significant amount of the Pt and Pd in seawater (Li & Byrne 1990, Wood 1990, Wood & Van Middlesworth 2004); (iii) carboxylic acids

(*e.g.*, oxalate, acetate, malonate, citrate) increase the solubility of amorphous Pd(OH)₂ and may bind strongly to Pd²⁺; notably, Pd-oxalate complexes could account for a significant % of the organic-bound Pd in acidic soils, even at very low oxalate concentrations (Wood 2002). Pd solubility by acetate complexation has been shown to be highly sensitive to acetate concentration and pH at 25°C (Nabivanets & Kalabina 1972, Pickrell 1997, Wood & Van Middlesworth 2004); conditional equilibrium/ stability constants for the formation of the Pd-diacetate complex have been derived at 25°C and 1 bar (Table 2-2, Wood & Van Middlesworth 2004) for the reactions:



(iv) siderophores (naturally occurring organic ligands secreted by microbes to metabolize Fe) increase the solubility of amorphous Pd(OH)₂ and of metallic Pt, Pd, Rh and Ir (Normand & Wood 2005). It is unlikely that amorphous PGE hydroxides are solubility-controlling phases in nature, but the results of these studies demonstrate that their solubility (as an analog to more stable, less soluble phases in nature) are enhanced by the presence of organic ligands and formation of PGE-organic ligand complexes.

The formation of Pd hydroxide species and mixed hydroxy-chloride species with the general formula PdCl_n(OH)_m^{2-n-m} in oxidized, near neutral to alkaline (pH > 8) surface waters may be more important in environments where the amount of available organic matter is extremely low. However, accurate prediction of the amount of PGE soluble as these complexes is limited by large discrepancies in the theoretical estimates of stability constants for PGE hydroxide complexes such as Pd(OH)⁺ (see the review by Wood 2002). Mountain & Wood (1988) proposed that the species Pd(OH)₄²⁻ (Table 2-2) predominates (at ppb levels) over a wide range in pH in dilute surface waters. However, in a recent experimental study conducted at 25–85°C and 1 bar, Van Middlesworth & Wood (1999) determined conditional stability constants (Table 2-2) for a number of Pd-hydroxide species and a mixed Pd hydroxychloride species, PdCl₃(OH)⁻², and suggested that mixed hydroxychloride species may be equally important as simple Pd-hydroxides in

transporting Pd in surface waters and that the mixed complex may be the dominant Pd species in seawater.

Low Temperature Hydrothermal Fluids (<500°C)

Post-magmatic hydrothermal alteration involving low-temperature (<500°C) aqueous fluids has been well-documented in most conventional Ni–Cu–PGE deposits and sites of sub-economic mineralization at, for example, the Sudbury Igneous Complex, Canada (Springer 1989, Farrow & Watkinson 1992, Li 1992, Li & Naldrett 1993, Jago *et al.* 1994, Farrow 1994, Farrow & Watkinson 1996, 1997, McCormick & McDonald 1999, Marshall *et al.* 1999, Molnar *et al.* 2001, Magyarosi *et al.* 2002, Hanley 2002, Hanley & Mungall 2003, Hanley *et al.* 2005b), the Stillwater Complex, Montana, U.S.A (Polovina *et al.* 2004), Rathbun Lake, Ontario (gabbro-hosted disseminated sulfides; Rowell & Edgar 1986, Edgar *et al.* 1989), New Rambler, Wyoming (metagabbro-hosted sulfide veins, McCallum *et al.* 1976, Nyman *et al.* 1990), Salt Chuck, Alaska (pyroxenite and gabbro-hosted disseminated sulfides, Watkinson & Melling 1992) and others (see review by Wood 2002). A strong spatial association between PGE occurrences and Cl-rich hydrothermal fluids has been shown in the deposits listed. Host rocks exhibiting the greatest alteration intensity appear commonly to be negatively or positively correlated with PGE content (Polovina *et al.* 2004, J. Rickard, personal communication).

In alteration assemblages, the occurrence of high salinity fluid inclusions containing Cl⁻ as the principal anion (Fig. 2-1a, b, *e.g.*, Farrow 1994, Nyman *et al.* 1990, Molnar *et al.* 2001), Cl-rich hydroxysilicate minerals containing biotite, amphibole and pyrosmalite (Fig. 2-1c, d, Li 1992, Farrow 1994) and PGE-halide minerals such as Pd–Bi–Cl (Li 1992) within sulfide-bearing, PGE-rich assemblages has led many researchers to suggest that transport and redistribution of PGE in fluids occurred by chloride complexation during the cooling and alteration of magmatic Ni–Cu–PGE deposits. Recent microanalytical data from Sudbury, for example, provide evidence that high salinity fluids trapped in saline fluid inclusions were PGE- and Au-bearing at lower T (150–300°C) (Hanley *et al.* 2005b). However, much of the evidence put forth suggesting the importance of chloride for PGE

TABLE 2-2. SELECTED LOG EQUILIBRIUM AND STABILITY CONSTANTS FOR SOLUBILITY REACTIONS INVOLVING PT AND PD

Reaction	Log K or β value	Ref.
$Pd_{(s)} + 2H^+ + 4Cl^- + \frac{1}{2}O_{2(g)} = PdCl_4^{2-} + H_2O$	log K=12.65±0.5 (300°C, P _{sat})	1
	log K=12.81±0.18 (300°C, P _{sat})	2
	log K=22.533-7.3977(10 ² T)+1.4329(10 ⁻⁴ T ²)-1.0344(10 ⁻⁸)T ³ (from 25 to 300°C, P _{sat})	1
$PdS_{(s)} + 4Cl^- + H^+ + 2O_{2(g)} = PdCl_4^{2-} + HSO_4^-$	log K=44.04±0.5 (300°C, P _{sat})	1
$PdS_{(s)} + 4Cl^- + 2H^+ = PdCl_4^{2-} + H_2S$	log K=-9.41±0.5 (300°C, P _{sat})	1
$Pt_{(s)} + 2H^+ + 3Cl^- + \frac{1}{2}O_{2(g)} = PtCl_3^- + H_2O$	log K=14.84±0.3 (300°C, P _{sat})	1
$PtS_{(s)} + 3Cl^- + H^+ + 2O_{2(g)} = PtCl_3^- + HSO_4^-$	log K=47.02±0.3 (300°C, P _{sat})	1
$PtS_{(s)} + 3Cl^- + 2H^+ = PtCl_3^- + H_2S$	log K=-6.43±0.3 (300°C, P _{sat})	1
$Pd(OH)_{2(s)} + 2CH_3CO_2^- + 2H^+ = Pd(CH_3CO_2)_2 + 2H_2O$	log K=6.3±0.1 (25°C, 1 bar)	3
$Pd^{2+} + 2CH_3CO_2^- = Pd(CH_3CO_2)_2$	log β = 9.3±0.3 (25°C, 1 bar)	3
$Pd^{2+} + 3Cl^- + OH^- = PdCl_3(OH)^{2-}$	log β = 20.21 (25°C, 1 bar)	4
	log β = 20.21 (25°C, 1 bar, 0.1m)	
	log β = 19.36 (25°C, 1 bar, 0.5m)	
	log β = 18.23 (25°C, 1 bar, 1.0m)	
$Pt^{2+} + 2OH^- = Pt(OH)_2$	log β = 29.0±0.1 (25°C, 1 bar)	5
$Pd^{2+} + OH^- = Pd(OH)^+$	log β = 11.95 (25°C, 1 bar, 0.5m)	4
$Pd^{2+} + 2OH^- = Pd(OH)_2$	log β = 18.9 (25°C, 1 bar, 0.1m)	5
$Pd^{2+} + 2OH^- = Pd(OH)_2$	log β = 23.8 (25 °C, 1 bar, 0.1m)	4
	log β = 23.2 (25 °C, 1 bar, 0.5m)	
	log β = 23.4 (25 °C, 1 bar, 1m)	
$Pd^{2+} + 3OH^- = Pd(OH)_3^-$	log β = 20.9 (25 °C, 1 bar)	5
	log β = 26.2 (25 °C, 1 bar, 1m)	4
$Pt_{(s)} + 3H_2O + \frac{1}{2}O_{2(g)} = PtOH_4^{2-} + 2H^+$	log K = 5.8 (25 °C, 1 bar)	6
	log K = -6.1 (300 °C, P _{sat})	
$Pd_{(s)} + 3H_2O + \frac{1}{2}O_{2(g)} = PdOH_4^{2-} + 2H^+$	log K = 5.4 (25 °C, 1 bar)	6
	log K = -6.1 (300 °C, P _{sat})	
$Pt_{(s)} + 4HS^- + 2H^+ + \frac{1}{2}O_{2(g)} = Pt(HS)_4^{2-} + H_2O$	log K = 51 (25 °C, 1 bar)	6
	log K = 31 (300 °C, P _{sat})	
$Pd_{(s)} + 4HS^- + 2H^+ + \frac{1}{2}O_{2(g)} = Pd(HS)_4^{2-} + H_2O$	log K = 52 (25 °C, 1 bar)	6
	log K = 30 (300 °C, P _{sat})	
$PtS_{(s)} + HS^- + H^+ = Pt(HS)_2^0$	log K = 2.77±0.48 (300°C, P _{sat})	7
$PdS_{(s)} + HS^- + H^+ = Pd(HS)_2^0$	log K = 2.60±0.34 (300°C, P _{sat})	7

Notes: P_{sat} = saturated water vapor pressure. References: 1 Gammons *et al.* (1992); 2 Gammons *et al.* (1993); 3 Wood & Van Middlesworth (2004); 4 Van Middlesworth & Wood (1999); 5 Wood (1991); 6 Mountain & Wood (1988); 7 Pan & Wood (1994). Unless indicated, equilibrium (solubility) and stability constants apply at infinite dilution (ionic strength = 0 m). The author makes no claims as to the accuracy of the constants listed above or as to consistency between those constants listed and those determined in other studies not listed above.

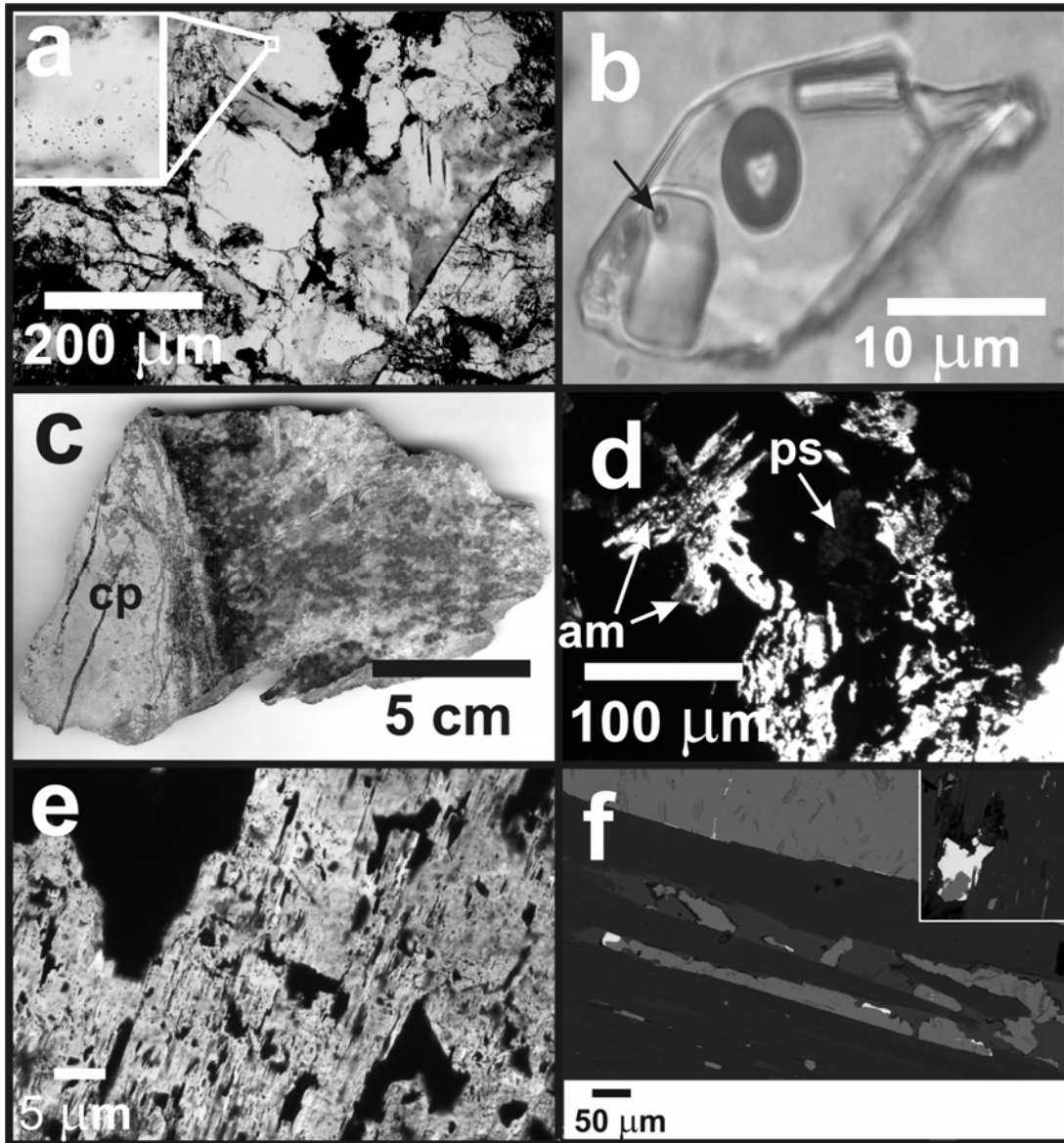


FIG. 2-1. Textural and petrographic evidence for low temperature (<500°C) hydrothermal processes in conventional magmatic Ni-Cu-PGE deposits. **a.** Photomicrograph of chlorite-epidote-actinolite alteration in formerly gabbroic cumulates, Lac des Iles, Ontario, Canada. Inset shows saline fluid inclusions containing a 20 wt.% NaCl eq. aqueous fluid. **b.** Photomicrograph of a high-salinity (38 wt.% eq. NaCl) brine inclusion in quartz from a footwall-style Cu-Ni-PGE ore body, Sudbury, Ontario, Canada. Note the presence of multiple daughter crystals including halite (cubic), calcium chloride (rod-like prism), and Fe-Mn-chloride (small, red ball, arrowed). **c.** Massive sulfide (chalcopyrite, cp) vein margin from a footwall-style Cu-Ni-PGE ore body showing a dark rind of Cl-rich hydroxysilicate minerals. **d.** Photomicrograph of the vein margin in (c) showing crystals of Cl-rich amphibole (am) and pyrosmalite $[(\text{Fe}^{2+}, \text{Mn})_8\text{Si}_6\text{O}_{15}(\text{OH}, \text{Cl})_{10}]$; ps] included in sulfide. **e.** Photomicrograph showing elongate sulfide grains occurring along parting planes in secondary amphibole, Stillwater Complex, Montana. Were the sulfides deposited with the amphibole during alteration or is the amphibole replacing massive sulfide? **f.** Back-scattered electron images of PGE minerals (bright white phases) occurring in altered reef rocks. The PGE mineral grains are attached to sulfide grains (medium grey) which appear to have been partially replaced by amphibole and psilomelane (darkest phases). Are the sulfides being selectively dissolved, leaving PGE minerals hosted in hydroxysilicate minerals? In the inset image, a large kotulskite (PdTe) grain is attached to a minor amount of sulfide and hosted in amphibole. Was this kotulskite grain formerly hosted entirely in sulfide?

redistribution in those deposits may be circumstantial. Equally ambiguous is the generally low temperature of crystallization (<500°C, Makovicky 2002) of many of the PGE minerals identified in the deposits (*e.g.*, tellurides, bismuthides); this does not necessarily imply that the PGE minerals were deposited by aqueous fluids (Molnar *et al.* 2001) since down-temperature re-equilibration of sulfide ores in the absence of a fluid phase can produce PGE-bearing mineral assemblages that are very different from those at the original magmatic temperatures of formation (Makovicky 2002, C. Farrow, pers. comm.).

Experimental Studies in Chloride-bearing Systems at low T

Whereas chloride complexation of the PGE has been studied extensively at standard conditions (see Wood 2002 for a complete listing of those studies), only a few experimental studies have attempted to quantify the solubility of the PGE in aqueous chloride solutions at elevated T (>25°C, <500°C) under controlled conditions (*i.e.*, pH, $f(\text{O}_2)$), Gammons *et al.* 1992, 1993, Gammons 1995, 1996, Xiong & Wood 2000). In general, experimental studies have confirmed that the complexes PtCl_4^{2-} and PdCl_4^{2-} predominate between 25 and 300°C and that these complexes are the predominant species at the total Cl^- concentrations observed in most hydrothermal solutions. The studies by Gammons and co-workers, conducted at T=300°C, provide the most reliable equilibrium constants (Table 2-2) for the formation of Pd (2⁺) tetrachloride and Pt (2⁺) trichloride complexes in solutions containing up to 3 m NaCl. Additionally, Gammons *et al.* 1992 derived a relationship between the equilibrium constant for the formation of the Pd (2⁺) chloride complex and temperature (Table 2-2). The experimentally based equilibrium constant for the Pd (2⁺) chloride complex from Gammons *et al.* (1992) agrees well with predicted equilibrium constants estimated from thermodynamic data (Wood *et al.* 1992) and was later confirmed by Gammons *et al.* (1993) using a completely different method. There are no experimentally derived equilibrium constants for the solubility of other PGE as chlorides at elevated temperatures. Some well-constrained solubility measurements for Os and Pd at 400–500°C (not permitting equilibrium constant derivation) were recently collected by Xiong & Wood (2000). Over this temperature range, they determined that the solubility of Os and Pd in moderately to strongly oxidizing (nickel–

nickel oxide to magnetite-hematite *buffer*), acidic (pH = 4.5–5) and weakly saline fluids (0.1 to 1.5 m KCl) is in the order of 10–1000 ppb! The experiments of Gammons and co-workers and Xiong & Wood (2000) demonstrated PGE solubilities many orders of magnitude higher than those predicted theoretically using Helgeson-Kirkham-Flowers equation parameters from Sassani & Shock (1990, 1998).

Experimental Studies in Bisulfide-bearing Systems at Low T

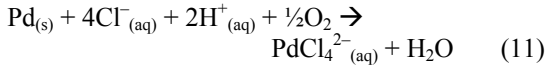
In reduced, neutral pH, low-T hydrothermal systems, the bisulfide ion (HS^-) is potentially a very important ligand for PGE transport (Mountain & Wood 1988). Experimental studies of PtS (cooperite) and PdS (braggite) solubility in bisulfide solutions were conducted by Gammons & Bloom (1993), Pan & Wood (1994) and Wood *et al.* (1994). Those experiments demonstrated that Pt and Pd solubilities by bisulfide complexation (i) are comparable and in the ppb to low-ppm range over the range of experimental conditions imposed, (ii) are at a maximum within the stability field of the minerals PtS or PdS, (iii) are at a maximum at ~150°C and (iv) are only sensitive to pH at pH values > 7. Additionally, Pan & Wood (1994) determined that the complex $\text{Pd}(\text{HS})_2^0_{(\text{aq})}$ prevailed over the entire range of conditions in their experiments (200–350°C, pH = 5.9–9.4, $\Sigma\text{S} = 0.3\text{--}2.2$ m). Wood (2002) admitted that there are uncertainties in the exact speciation mechanism involving HS^- , which requires additional experiments to confirm. Although bisulfide complexes of other PGE (Os, Ru, Ir) have been suggested (Pittwell 1965) but confirmation of their occurrence and stability regime await experimentation. Selected equilibrium constants for complexes of Pt and Pd with the bisulfide ion can be found in Table 2-2.

Chloride or Bisulfide?

The experiments described above confirm that PGE solubility at low temperatures in hydrothermal systems is highly sensitive to changes in fluid pH, $f(\text{O}_2)$, and the concentration of the predominant ligand in solution. How then, at least semi-quantitatively, can we determine (i) the solubility of the PGE, and (ii) the relative importance of the Cl^- vs. the HS^- ligand in mobilizing the PGE in a conventional magmatic Ni–Cu–PGE deposit? As an example, consider an ore-forming system at a T ~300°C in which the alteration assemblages and

mineral chemistry as indicators of pH and $f(\text{O}_2)$ in the hydrothermal system are used in conjunction with the available solubility data:

As a first estimate of PGE solubility in an ore-forming system, consider the following expression for the formation of the Pd (2⁺) tetrachloride complex (Gammons *et al.* 1992):



The equilibrium constant expression for this reaction is:

$$K_{P,T} = \frac{(a_{\text{PdCl}_4^{2-}})(a_{\text{H}_2\text{O}})}{(a_{\text{Pd}})(a_{\text{Cl}^-})^4(a_{\text{H}^+})^2(f_{\text{O}_2})^{0.5}} \quad (12)$$

where $\log K$ at 300°C and water vapor-saturated conditions = 12.65 ± 0.5 (Table 2-2, Gammons *et al.* 1992). From the above expression, it can be seen that the concentration of the Pd (2⁺) tetrachloride complex will increase 4 orders of magnitude for every order of magnitude increase in the concentration of the Cl⁻ ion, and 2 orders of magnitude for every unit decrease in pH. A 2 order of magnitude increase in $f(\text{O}_2)$ is required to increase the metal complex concentration by 1 log unit. As discussed, this expression may be further simplified by assuming activities of pure species are ~ 1 and that activity coefficients are ~ 1 for charged species if the hydrothermal solution is a dilute solution:

$$K'_{P,T} = \frac{(m_{\text{PdCl}_4^{2-}})}{(m_{\text{Cl}^-})^4(m_{\text{H}^+})^2(f_{\text{O}_2})^{0.5}} \quad (13)$$

An estimate of the concentration of the Cl⁻ ion (m_{Cl^-}) in solution can be obtained from fluid inclusion studies (see discussion in a later section). Let us assume that, from microthermometric measurements, the salinity of the fluid in question is 5.9 wt.% eq. NaCl and that NaCl is the major ionic compound dissolved in the fluid. At low temperature, where ionic species should be highly dissociated, the Cl⁻ concentration will be:

$$\begin{aligned} \sim 35,790 \text{ ppm} &= 35.8 \text{ g of Cl}^- \text{ per kg of solvent} \\ &\quad (\text{H}_2\text{O}) \\ &= 35.8 \text{ g} \times (1 \text{ mol Cl}^- / 35.5 \text{ g Cl}^-) \\ &\approx 1 \text{ mol Cl}^- \text{ per kg of solvent} \\ &= 1 \text{ molal Cl}^- \end{aligned}$$

Using the calculated Cl⁻ concentration and the

equilibrium constant of Gammons *et al.* (1992) in Table 2-2, eq'n (13) can be rearranged to a new expression that relates Pd solubility as the Pd(2⁺) tetrachloride complex to $f(\text{O}_2)$ and pH:

$$\log(m_{\text{PdCl}_4^{2-}}) = 12.65 + 4 \log(1 \text{ mol}) - 2 \text{pH} + 0.5 \log f_{\text{O}_2} \quad (14)$$

$$\log(m_{\text{PdCl}_4^{2-}}) = 12.65 - 2 \text{pH} + 0.5 \log f_{\text{O}_2} \quad (15)$$

An estimate of the $f(\text{O}_2)$ and pH of the fluid involves a careful examination of the mineral assemblages present, which is not always possible because it requires unambiguous textural evidence for the stable coexistence of specific mineral assemblages that buffer $f(\text{O}_2)$ or pH. In the absence of stable buffer assemblages, these parameters can only be loosely constrained by mineral species present in contact with the fluid. This is demonstrated in Figure 2-2, in which contours of constant Pd concentration [as the dissolved complexes Pd(Cl)₄²⁻ and Pd(HS)₂⁰] calculated at varying pH and $f(\text{O}_2)$ using equilibrium constants from Gammons *et al.* (1992) and Pan & Wood (1994) are plotted on a $\log f(\text{O}_2)$ -pH diagram. The diagram summarizes the Pd-PdS-buffered, Pd-S-Cl-H₂O fluid system at a chloride activity = 1 (comparable to our measured fluid inclusion salinity) and total sulfur content = 0.001 m. Mineral stability fields for sulfide and oxide minerals found in PGE ore-forming systems (conventional and unconventional) are shown. The mineral stability fields help to constrain pH and $f(\text{O}_2)$. For example, a fluid in equilibrium with the assemblage pyrrhotite-pyrite-magnetite in Figure 2-2 has a fixed pH and $\log f(\text{O}_2)$ of ~8.1 and ~-34 bars, respectively. Inserting these values into eq'n (15) gives:

$$\log(m_{\text{PdCl}_4^{2-}}) = 12.56 - 2(8.1) + 0.5(-34) = -20.64$$

Therefore,

$$\begin{aligned} m_{\text{PdCl}_4^{2-}} &= 2.3 \times 10^{-21} \text{ molal} \\ \Sigma \text{Pd}_{(aq)} &= 2.45 \times 10^{-19} \text{ g / kg} \\ &= 2.45 \times 10^{-16} \text{ ppt} \end{aligned}$$

From this calculation, we see that the solubility of Pd as the predicted Pd(2⁺) tetrachloride complex is extremely low. A sharp decrease in PdCl₄²⁻_(aq) concentration is shown by the concentration contours (1 ppm and 1 ppt) moving from the upper left (low pH, high $f(\text{O}_2)$) to lower right side of

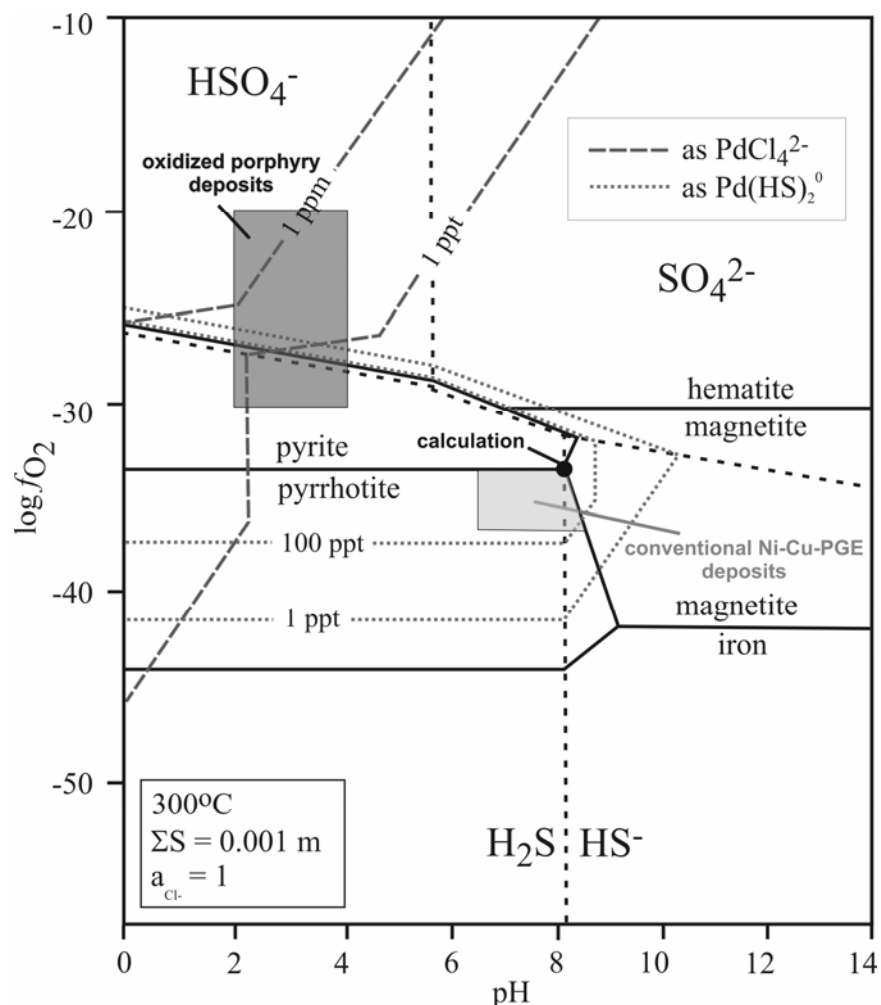


FIG. 2-2. Log $f(\text{O}_2)$ -pH diagram for the Pd-S-Cl-H₂O system at 300°C modified from Wood (2002; originally modified from Pan & Wood 1994). Fluid has a total S content = 0.001 m and a chloride activity (\sim molality) = 1, and is in equilibrium with solid Pd and PdS. Solid lines separate stability fields for common Fe-bearing minerals in the ore assemblages which may control or indicate $f(\text{O}_2)$ and pH. Dotted black lines separate field of stability for dominant sulfur species in solution. The dashed grey lines correspond to lines of constant Pd concentration as the dissolved complex PdCl_4^{2-} (from Gammons *et al.* 1992). The dotted grey lines correspond to lines of constant Pd concentration as the dissolved complex $\text{Pd}(\text{HS})_2^0$ (from Pan & Wood 1994). The range of pH and $f(\text{O}_2)$ conditions applicable to hydrothermal alteration in conventional magmatic Ni-Cu-PGE deposits is represented by the light grey area (near-neutral to slightly alkaline pH, coexistence of pyrrhotite, pyrite, magnetite). Our calculated Pd solubility as a Pd (2⁺) tetrachloride complex is plotted as a solid black circle. Significant Pd solubility in this area by chloride complexation is impossible because the fluids (at 300°C) are not sufficiently acidic or oxidizing; in this compositional field, HS⁻ complexing is more likely. For comparison, conditions for oxidized Cu-Au porphyry hydrothermal processes are shown in dark grey; in such deposits, hydrothermal solutions are sufficiently oxidizing and acidic to dissolve significant amounts of Pd as chloride complexes.

Figure 2-2. In general, it can be seen from Figure 2-2 that in low-T hydrothermal fluids, significant concentrations of Pt and Pd (> 10 ppt to ppm levels) will dissolve into solution as chloride complexes

only under highly oxidizing ($\log f(\text{O}_2) > -25$ atm) or highly acidic ($\text{pH} < \sim 2$) conditions (Gammons & Bloom 1993, Wood 2002). Such conditions are typical of oxidized porphyry systems (dark grey

boxed area in Figure 2-2). In conventional magmatic Ni–Cu–PGE deposit (light grey boxed area in Figure 2-2), conditions appear to be inappropriate for any significant PGE solubility as a chloride complex. Pt and Pd solubility by bisulfide complexation appeared to be many, many orders of magnitude higher than by chloride complexation at near-neutral, reducing conditions. At the conditions where pyrite-pyrrhotite-magnetite coexist, the solubility of the complex $\text{Pd}(\text{HS})_2^0$ (aq) is > 100 ppt according to Figure 2-2.

Consequently, the presence of chloride-rich fluids during the development of many Ni–Cu–PGE systems may be coincidental and unrelated to PGE transport during post-cumulus hydrothermal activity and metamorphism. A lack of low pH, high $f(\text{O}_2)$ alteration assemblages in magmatic Ni–Cu–PGE deposits such as those listed above makes it unlikely that chloride complexation played any significant role in the remobilization of precious metals at temperatures less than 300°C. The low-T alteration assemblage that coexists with the PGE minerals observed in many conventional magmatic Ni–Cu–PGE deposits is typically chlorite-actinolite-epidote-calcite-dominated with albite as the stable Na-silicate phase, indicating a near-neutral pH. At the acidic conditions required for significant Pt or Pd transport by chloride complexation, the stable assemblage would have to contain a hydroxysilicate mineral such as paragonite (or muscovite in the equivalent K-bearing system) at geologically realistic salinities (*i.e.*, for a 20–50 wt.% NaCl eq. brine). Furthermore, the $f(\text{O}_2)$ in such deposits could not have exceeded the sulfide-sulfate buffer ($\log f(\text{O}_2) \sim -28$ at a pH of ~ 6) which is several orders of magnitude below the $f(\text{O}_2)$ and pH required for significant Pt or Pd solubility (Figure 2-2).

Although chloride may not be important for PGE transport in many of the deposits where it has been identified as a major anion in fluid inclusions, recent studies show that chloride-rich fluids may play a role in selectively removing base-metal sulfides from magmatic deposits, thereby modifying the original metal tenor (*e.g.*, Cu:Pd ratio) of the deposit. At the conditions where PGE solubility by chloride complexation may be insignificant, the solubility of Cu, Fe and S can be still be substantial (~ 10 – 100 ppm in chloride fluids buffered by pyrrhotite-bearing sulfide assemblages, Hemley *et al.* 1992). Textural evidence for significant S and base metal dissolution can be found in most magmatic Ni–Cu–PGE deposits that have undergone any degree of alteration or

metamorphism. For example, Li *et al.* 2004 observed this phenomenon *locally* in the Merensky Reef where sulfide minerals hosting PGM have been replaced by amphiboles (actinolite-tremolite), epidote, magnetite, and calcite. At the Stillwater Complex, Polovina *et al.* (2004) observed a similar but more pervasive alteration of the olivine-bearing unit containing the J-M reef. Consequently, the common textural association of relatively low-T PGM hosted in hydroxysilicate mineral assemblages may be an artifact of the removal of primary (magmatic) base metal sulfides (hosting the PGM) by chloride-rich fluids and may not indicate that PGM have a hydrothermal origin; Figures 2-1 e-f exemplify this process at the Stillwater Complex.

It is important to note that there are several unconventional (in a magmatic sense) styles of PGE mineralization in which PGE transport by chloride was more likely (oxidized porphyry systems, unconformity-related U–Au–PGE deposits, Lake Superior-type iron formation, stratiform-hosted Cu “Kupferschiefer” systems) and may have been responsible for the economic concentration of PGE in those systems. More detailed description of atypical hydrothermal PGE deposits can be found in this short course volume (see chapters by Wilde, by Distler and Yudovskaya, and by Economou-Eliopoulos). PGE transport by chloride was more likely in such settings because one or both of the chemical requirements for significant PGE transport by chloride at low temperature was met (*i.e.*, high $f(\text{O}_2)$, low pH, or both; Figure 2-2).

The Role of Other Ligands

Other ligands which have been suggested to complex with the PGE in hydrothermal systems include hydroxide, mixed hydroxychloride, ammonia, bromide, iodide, cyanide, bitelluride, biselenide, and thioarsenite (see review by Wood, 2002). Limited experimental and theoretical data are available for PGE complexes involving these ligands. Aside from hydroxide or hydroxychloride, which may be important at very high T, or at low T in oxidizing, alkaline- to neutral-pH fluids, significant PGE transport by the species listed is unlikely. Although the stability of $\text{Pt}(2^+)$ and $\text{Pd}(2^+)$ complexes with ligands such as Br^- , I^- , CN^- are much higher than for Cl^- or HS^- at 25°C and 1 bar (Wood 2002), the very low abundance in natural fluids of the ligands suggested makes them unlikely to be important metal complexing agents in hydrothermal fluids.

Hydroxide or mixed hydroxy-chloride

PGE complexes may be important under certain chemical conditions in low T hydrothermal solutions (*e.g.*, in alkaline solutions, as discussed above) or at very high T where neutral complexes might predominate (see below, Hanley *et al.* 2005a). In low T solutions, there are essentially no thermodynamic data available that have been confirmed through experimentation, and order of magnitude discrepancies exist in stability constants measured or calculated at standard conditions (see review by Wood 2002).

High Temperature, Magmatic Volatiles and Post-cumulus Magmatic Fluids (> 500°C)

Substantial evidence exists from studies of mineral chemistry and igneous petrology, and from very limited work on fluid inclusions, that high temperature aqueous fluids (“deuteric” or exsolved magmatic volatile phases) interacted with PGE-bearing sulfide liquids, silicate melts, and partially crystallized rocks in a variety of mafic–intermediate igneous systems, notably layered complexes such as the Bushveld Complex, South Africa (Schiffries 1982, Ballhaus & Stumpfl 1986, Boudreau *et al.* 1986, Rudashevsky *et al.* 1992, Willmore *et al.* 2000 and others therein), the Stillwater Complex, Montana, U.S.A. (Boudreau *et al.* 1986, Boudreau & McCallum 1986, Meurer *et al.* 1998, Boudreau 1999, Hanley *et al.* 2005c) and the Lac des Iles Complex, Ontario, Canada (Talkington and Watkinson 1984, Brugmann *et al.* 1989, Tellier *et al.* 1991, Lavigne, pers. comm. 2001). Recent experimental work by Mathez & Webster (2005) confirmed that hydrosaline brines were present during the late stages of crystallization of the layered intrusions. Although the evidence demonstrates unambiguously that volatiles modified the composition and texture of the igneous host rocks in the deposits, models which hypothesize that high temperature fluids alone were responsible for the economic concentration of the base and precious metals are not widely accepted. Moreover, owing to a complete lack of fluid inclusion data in the majority of deposits, the exact source and composition of the proposed volatile phases has not been identified, and the relative importance of fluid enrichment processes in generating the economic grade of the deposits is therefore unclear. Strictly magmatic models for the PGE mineralization in layered intrusions involving sulfide precipitation augmented by kinetic controls (*e.g.*, Campbell *et al.*

1983, Mungall 2002) have considerable merit because they predict the observed cumulate and ore compositions (*i.e.*, metal ratios, metal concentrations) with reasonable accuracy.

Major points of evidence put forth for the involvement of a chloride-rich volatile phase in the evolution of layered intrusions hosting PGE deposits include: (i) the presence of intercumulus halogen-bearing minerals, such as apatite and micas, that exhibit high Cl/F ratios below the platiniferous horizons but then drop sharply to very low values above the platiniferous horizons (*e.g.*, Boudreau *et al.* 1986, Willmore *et al.* 2000) (ii) extremely high salinity, PGE-bearing fluid inclusions (Figure 2-3a) hosted in the pegmatitic lithologies and intercumulus quartz below or within the platiniferous horizons (Figure 2-3a, Ballhaus & Stumpfl 1986, Hanley *et al.* 2005c); (iii) the presence of pegmatitic lithologies (Figure 2-3b-d, occasionally cored with PGE-rich sulfide assemblages and commonly showing evolved rock compositions relative to normal host cumulates) within, immediately below, or transgressing platiniferous horizons (*e.g.*, Meurer *et al.* 1998, Boudreau 1999) and (iv) the presence of pothole structures interpreted to represent (possibly) “fumarolic” structures, and discordant ultramafic pipes (occasionally mineralized) and breccia bodies cross-cutting igneous stratigraphy (Schiffries 1982, Reid *et al.* 1993, Boorman *et al.* 2001).

Models which propose a high-T, hydrothermal origin for PGE concentrations in layered intrusions have been described by Boudreau & Meurer (1999) and Willmore *et al.* (2000). The computer program PALLADIUM (Boudreau 2004) illustrates the phenomena thought to drive the concentration of precious metals to a single horizon in a fluid-rich cumulate pile. These researchers point out that the stratigraphic distribution of S, Cu and the PGE in layered intrusions cannot be explained solely by the precipitation of sulfide as a cotectic phase. In the model of Boudreau & co-workers, a Cl-rich volatile phase exsolves from the intercumulus (interstitial to crystals) liquid and dissolved PGE, S, and base metals from sulfide minerals in the cumulate pile. The metal and S-bearing fluid rises upward, driven by fluid oversaturation and crystal compaction. When the metal-bearing fluid reaches the top of the cumulate pile, the fluid component dissolves into a fluid-undersaturated magma and the PGE, base metals, and S precipitate out of solution as PGM and base

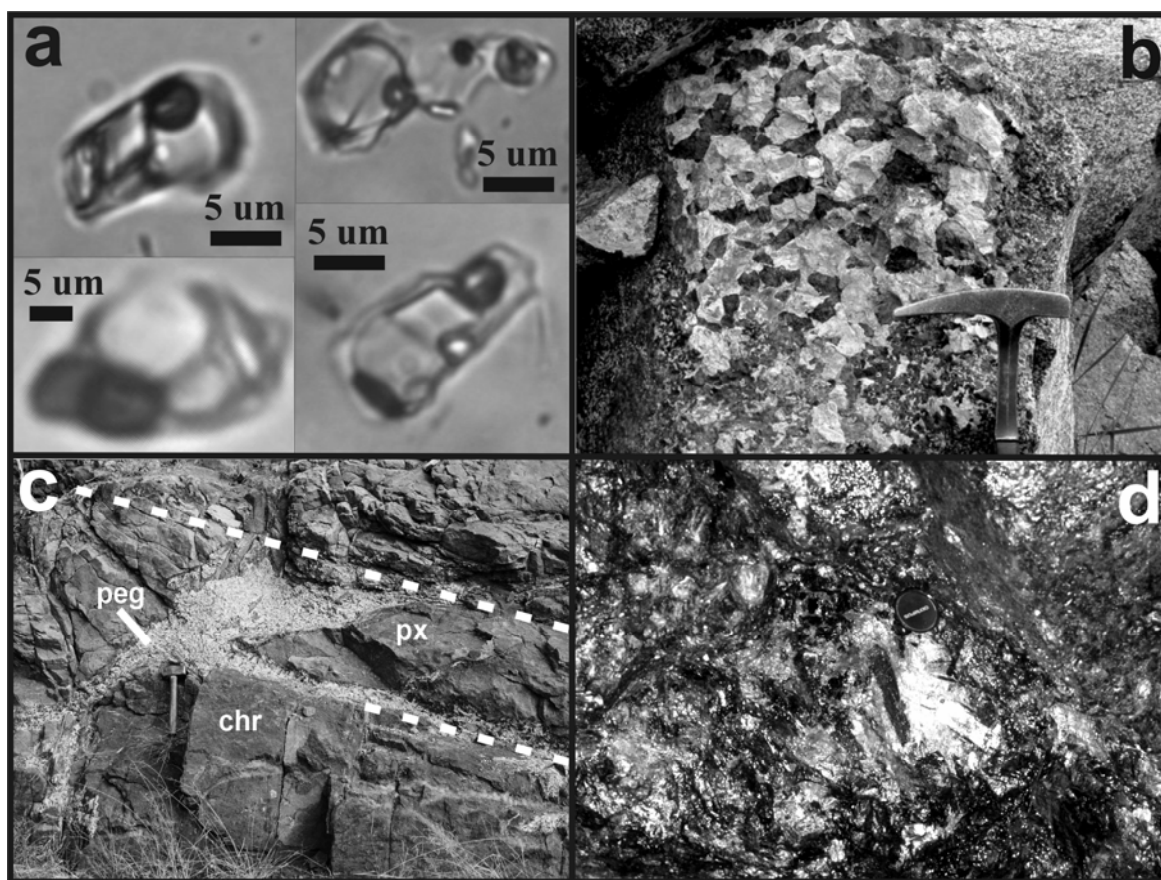


FIG. 2-3. Textural and petrographic evidence for high temperature (>500°C) volatiles in conventional magmatic Ni-Cu-PGE deposits. **a.** Photomicrographs showing extremely high salinity (50–60 wt.% eq. NaCl), PGE-bearing brines in quartz from a pegmatite below the J-M reef, Stillwater Complex, Montana, U.S.A. Note the abundance and diversity of daughter minerals, suggesting many mutually soluble salts present in the trapped fluid. **b.** Patch of pegmatitic gabbro within a gabbro-norite cumulate, Stillwater Complex. **c.** Gabbroic pegmatoid body (peg) cutting across layered cumulates (dotted lines indicate stratiform contacts) composed of chromitite (chr) and pyroxenite (px), Bushveld Complex, South Africa. **d.** Troctolitic pegmatite body containing massive PGE-rich sulfide at its core (as a vug infilling), Stillwater Complex, Montana, U.S.A.

metal sulfides at a mineralized “front” (or “reef”), analogous to an oxidation/reduction roll front in sandstone-hosted uranium deposits (Rackley & Johnson 1971).

Experimental Evidence for Significant PGE Solubility at High Temperature (800–900°C)

As for the lower temperature studies, chloride has been suggested as the major ligand for the PGE at higher T. At very high temperatures, strict pH and $f(\text{O}_2)$ requirements are suggested to be not as critical for significant PGE transport by chloride (Wood *et al.* 1992). Neutral dichloride species are expected to dominate at higher temperatures; however, theoretical calculations (Wood 1987, Sassani & Shock 1990, 1998) and

earlier experiments in H_2O -free vapors (Fleet & Wu 1993, 1995) demonstrated that (i) significant (>10 ppt) PGE transport as a chloride vapor species is only possible above 1000°C and (ii) the volatility of the PGE is enhanced by the presence of both Cl and S in the vapor phase, but not S alone. Wood (1987) pointed out that under the conditions at which the PGE are expected to be most soluble in high temperature Cl-rich fluids, the base metals Fe, Ni, and Cu are more soluble by several orders of magnitude. Therefore, the enrichment of PGE over Fe, Ni and Cu, that is characteristic of platinumiferous reefs such as the Merensky or J-M reefs, cannot be explained by high-T fluids processes alone. As suggested earlier, the observation that some reef deposits (*e.g.*, portions of the J-M reef) are enriched

in PGE over base metals may partly be an artifact of the post-cumulus removal of base metal sulfides by lower-temperature fluids. [Hydrogen isotope data (Mathez *et al.* 1994) from the Bushveld Complex argues against this by demonstrating that sufficient permeability for pervasive fluid migration within the intrusion was not available after the intrusion solidified].

There are no studies of PGE solubility in aqueous fluids at magmatic temperatures. However, in recent years, a few researchers have investigated PGE solubility in saline fluids at 500–900°C as analogues for the “post-cumulus” interaction of fluids with crystallized silicate rocks (Orlova *et al.* 1987, Hsu *et al.* 1991, Ballhaus *et al.* 1994, Plyusina *et al.* 1997, Hanley *et al.* 2005a). Of these studies, we are aware of only two in which PGE solubility was investigated at adequately controlled $f(\text{O}_2)$, salinity, pH, T and P.

Ballhaus *et al.* (1994) reacted a NaCl-saturated, C–S–Cl–O–H fluid with Au and Pt metal, Fe–Cu–Ni-sulfide and silicate melt at 800–900°C. Fluids trapped in inclusions in quartz were analyzed for Cu, Fe, Ni, Au and Pt by PIXE. The trapped fluids showed very complex compositions and, unlike the other metals, Pt contents measured in the trapped fluids varied from below detection limits to wt.% levels within a single inclusion population. The extreme variability in Pt concentration was attributed to either (i) the occurrence of soluble polyatomic complexes (Pt with Ni and Fe), (ii) the presence of tiny particles of Pt in the fluid, or (iii) the entrapment of disequilibrium fluid compositions.

Recently, Hanley *et al.* (2005a) reacted Pt with a simple NaCl-brine while controlling HCl concentration and $f(\text{O}_2)$ in brines of 20–70 wt.% eq. NaCl at 800°C. Platinum-bearing brines were trapped in synthetic fluid inclusions in quartz and vesicles in a felsic glass and analyzed by laser ablation ICP–MS. Measured metal concentrations were very high (1–1000 ppm Pt) over the range of experimental conditions imposed, and Pt concentration in the inclusions showed a strong inverse correlation with salinity. Hanley *et al.* (2005a) interpreted this trend to be the result of the “salting out” (reduction of available water for complex hydration) of neutrally charged hydroxide complexes (*e.g.*, $\text{Pt}_{(s)} + 0.5\text{O}_2 + n\text{H}_2\text{O}_{(l)} = \text{Pt}(\text{OH})_2 \cdot (\text{H}_2\text{O})_{n-1(\text{aq})}$) or hydrogen chloride complexes (*e.g.*, $\text{Pt}_{(s)} + 0.5\text{O}_2 + 3\text{HCl}_{(\text{aq})} = \text{PtCl}_3\text{H}_{(\text{aq})} + \text{H}_2\text{O}_{(l)}$). The results of the study by Hanley and co-workers, like those of Ballhaus *et al.* (1994), are difficult to

interpret because Pt concentrations within fluid inclusions varied by 2–3 orders of magnitude within single experiments. Similar variability in metal concentration was observed in studies of Au solubility at high salinity (Frank *et al.* 2002). Therefore, the results must be interpreted with extreme caution until future experiments can confirm the concentrations of Pt measured and solubility mechanisms proposed. At least qualitatively, the limited amount of experimental work conducted to date suggests that PGE solubility in S-free fluids may be economically significant at near-magmatic temperatures.

Additional Factors Limiting the Solubility of the PGE in Aqueous Fluids

Although the thermochemical conditions in the fluid phase may be ideal for PGE transport under certain conditions, it is important to note that in natural systems, additional factors will limit the solubility of the PGE in a way that has not been adequately addressed in the experimental studies.

In the first case, rarely do the PGE occur as native elements. Rather, they occur as alloys, solid solutions, or mineral phases containing (most commonly) S, Fe, Te, Se, As, Sn, Sb, Cu, Bi, Ag, and other PGE. Such phases have been shown to be far more stable than native PGE (Mountain & Wood 1988). Similarly, at conditions where the PGE minerals have not yet stabilized, the PGE content of a fluid phase would depend partly on the concentration of the PGE dissolved in the coexisting melt that is undersaturated with respect to the PGE in question. Consequently, any estimates of the solubility of the PGE based on experiments which used pure metals as source materials probably significantly overestimate the true solubility because the sources of the PGE in nature will *not* be native elements. In fact, the low solubility of PGE minerals such as arsenides or tellurides implies the reaction between the PGE in solution and elements listed above will cause the precipitation of PGE minerals (Wood 2002). Competition between the PGE and other cations (Cu, Fe, Mn, Ca, K) for available ligands in a hydrothermal solution will also significantly limit the solubility of the PGE. This is particularly relevant to systems in which very high salinity, multi-cation fluids have been identified in fluid inclusions (*e.g.*, Farrow 1994). The availability of Cl^- or HS^- to the PGE will be greatly diminished in complex fluids containing abundant additional cations.

In addition to the problems described above, Hanley *et al.* (2005a) showed that Pt solubility at very high temperature and salinity may be severely affected by the availability of free H₂O in the fluid phase. As NaCl (or other salt phases) become major components of an aqueous solution, the activity of H₂O will no longer be equal to unity. Furthermore, a significant amount of the H₂O present may be tied up in *hydrating* the large numbers of Na⁺ and Cl⁻ ions (or other ions), thereby limiting the amount of H₂O available to hydrate PGE complexes in solution.

The Importance of Field-based Observations

Unfortunately, our knowledge of the hydrothermal geochemistry of the PGE is so limited at present that quantitative estimation of the mass transfer of the PGE in the deposits is impossible. The results of well-constrained experimental studies dealing with PGE solubility (*e.g.*, Gammons *et al.* 1992) cast doubt on the validity of using the available theoretical data for calculating PGE solubility (Sassani & Shock 1990, 1998). However, it is possible to make some preliminary guesses about the importance of aqueous fluid phases in any deposit. With the aid of the limited experimental data available to us, the role of aqueous fluids in transporting some of the PGE (Pt, Pd) may be assessed at least semi-quantitatively or qualitatively by (i) demonstrating through careful textural and paragenetic studies that aqueous fluids interacted with sulfide liquids, crystallized host rocks or sulfide ores, (ii) estimating the thermochemical characteristics of the fluid phase (pH, concentration of Cl⁻ and HS⁻, *f*(O₂)) at the time of its interaction with PGE-bearing phases (in host rocks or sulfides), (iii) implementing those thermochemical parameters in the limited number of experimentally derived solubility product expressions available from Gammons *et al.* (1992) and Wood *et al.* (1992) and with major uncertainties, thermodynamic data from Sassani & Shock (1990, 1998). An example of a solubility calculation was presented earlier in this article.

Estimating Fluid Salinity, Fluid Composition and Temperature

Provided that a reasonably well-preserved fluid inclusion assemblage is present, the salinity and trapping temperature of the fluids present should be determined by microthermometric methods. Microthermometric studies of high salinity fluid inclusions of primary origin in several

of the deposits listed above indicate that the highest temperature fluids were NaCl brines containing significant concentrations of other positively charged ions, notably the transition metals (Fe, Mn, Ba, K, Ca, Zn and Pb). In the Bushveld Complex, Ballhaus & Stumpfl (1986) reported hypersaline (~60–95 wt.% *eq. NaCl*) inclusions in postcumulus and intercumulus quartz in the Merensky Reef. These inclusions are absent from quartz in the rock units above the PGE-enriched horizon. Pressure and temperature estimates for the formation of the fluids, possibly by *exsolution* from a melt phase, are ~3 kbar and 750°C. Molnar *et al.* (2001) found similar inclusions containing a 33–60 wt.% *eq. NaCl* fluid in pegmatites within the footwall of the Sudbury Igneous Complex, which are spatially associated with Cu–Ni–PGE sulfide ore bodies. The inclusions *homogenized* between 400 and 650°C by the dissolution of halite or an unidentified anisotropic *daughter phase*. The temperature and pressure of exsolution of the magmatic parental fluid for these inclusions was estimated at ~750–800°C and 1.1–1.6 kbar. Similar inclusions have been found in pegmatites below the J-M reef by Hanley *et al.* (2005c) (Figure 2-3a).

Boudreau & McCallum (1986) estimated compositions of fluids in equilibrium with a typical cumulate solid assemblage composed of low-Ca pyroxene, anorthitic plagioclase (~Ab₁₅) and quartz. This assemblage is equivalent to the least evolved pegmatites observed in the Stillwater Complex below the PGE-bearing J-M reef. More evolved pegmatites have been shown to contain more albitic plagioclase (up to Ab₄₂), less pyroxene, and more quartz (Braun *et al.* 1994). Pegmatites in the footwall of the Sudbury Igneous Complex have a similar composition but contain minor hornblende instead of pyroxene (Molnar *et al.* 2001). Boudreau & McCallum (1986) estimated that the HCl concentration of a fluid in equilibrium with these assemblages would increase from 180 ppm HCl at 500°C to 1100 ppm at 800°C at a low bulk salinity ($\Sigma\text{Cl} = 2 \text{ m}$). This range in HCl concentration is well within the range of values in experimental studies of Pt solubility at high T (Hanley *et al.* 2005a). Rough estimation of the HCl concentration in a fluid, which has direct bearing on the solubility of the PGE if HCl complexes (*e.g.*, PtCl₃H) are involved, can be made by modeling fluid compositions in equilibrium with silicate mineral assemblages. This can be accomplished using various programs available for geochemical modeling (EQ/3; EQBRM) provided that accurate

equilibrium constants and activity models for mineral-forming reactions and HCl dissociation are available. Although methods of predicting HCl concentration in magmatic volatile phases using melt composition are available for felsic igneous systems (*e.g.*, Williams *et al.* 1997), none have been developed for more complex, mafic to intermediate rock forming systems.

At lower T, where ionic compounds such as NaCl and HCl are highly dissociated in solution, estimates of the Cl⁻ content of hydrothermal fluids may be taken directly from the salinity of fluid inclusions, provided that the fluid generation can be proven to be coeval with the ore assemblages. The presence of HS⁻ may be confirmed using laser Raman spectroscopy on individual fluid inclusions, although estimation of the concentration of HS⁻ in solution may require chemical modeling similar to that required to calculate the HCl concentration in a high-T brine.

Estimating $f(\text{O}_2)$

At low T, alteration mineral assemblages may provide a reasonable estimate of the $f(\text{O}_2)$ imposed on the system during post-cumulus fluid-rock or fluid-sulfide interaction. Relatively common assemblages in cumulus, post-cumulus and sulfide assemblages can provide constraints on $f(\text{O}_2)$ if stable coexistence of the mineral phases within the assemblage can be demonstrated (*e.g.*, pyrrhotite-magnetite, magnetite-hematite, bornite-chalcocopyrite). Determination of the Fe³⁺/Fe²⁺ ratio of certain silicate minerals (*e.g.*, epidote, amphibole, Farrow 1994) or the composition of mineral end-members in exsolution textures (*e.g.*, two spinel pairs) allow estimates of $f(\text{O}_2)$ and have been used previously to predict the $f(\text{O}_2)$ during post-cumulus hydrothermal activity (Rudashevsky *et al.* 1992, Farrow 1994).

There are few well-constrained estimates of the $f(\text{O}_2)$ imposed on PGE–Au-bearing magmatic systems during higher T hydrothermal processes (cumulus and postcumulus). Estimates of $f(\text{O}_2)$ at high temperatures are problematic because of mineral re-equilibration with falling temperature and must be used with extreme caution. In general, however, it has been observed that T– $f(\text{O}_2)$ paths followed by cooling, crystallizing silicate melts are parallel or subparallel to solid oxygen buffer assemblages such as nickel–nickel oxide (NNO) (*e.g.* Sato and Valenza 1980, Mathez *et al.* 1989). Boudreau & McCallum (1986) estimated $f(\text{O}_2)$ values associated with mineralizing processes at the

Picket Pin Deposit located stratigraphically above the J-M reef using the composition of Ca-pyroxene from magnetite-bearing assemblages. They reported $f(\text{O}_2)$ values as high as $\Delta\text{NNO} = -1$ to -2 (quartz-fayalite-magnetite to wustite-magnetite) buffered by partially crystallized silicate rocks at T = 900 to 1200°C. In the Bushveld complex, Ballhaus (1988) estimated $f(\text{O}_2)$ values for the Bushveld parent magma as high as $\Delta\text{NNO} = -1$ prior to sulfide precipitation. Rudashevsky *et al.* (1992) used spinel mineral compositions to estimate $f(\text{O}_2)$ values of $\Delta\text{NNO} = -2$ to -3 for the formation of PGE-rich dunite-hortonolite (magnesian fayalite) pipes which transect the Bushveld stratigraphy. The pipe structures have been suggested to be the product of modification of primary cumulate rocks by focused aqueous fluid flow involving a Cl-rich fluid at T ~ 700°C and P ~ 5 kbar (Schiffries 1982). These estimates of $f(\text{O}_2)$ are consistent with the observation of igneous graphite in the Critical Zone of the Bushveld Complex and J-M reef of the Stillwater Complex; this graphite is thought to have started to crystallize from initially H₂O-poor fluids at supersolidus conditions (*i.e.* T = 1050°C) which then cooled down towards the solidus temperature along a T– $f(\text{O}_2)$ path parallel to and approximately 2–3 log units below the NNO buffer, as their water content increased (Mathez *et al.* 1989).

Major Conclusions to Take from this Chapter

The ability for an aqueous fluid phase to dissolve, transport and reprecipitate the PGE will depend on the solubility of the PGE in the fluid phase, and amount of PGE made available to the fluid (*e.g.*, in a coexisting silicate liquid), the possible presence of saturated phases (*e.g.*, platinum-group minerals), and the mass flux and efficiency of the final precipitation mechanism in the hydrothermal system. The thermochemical conditions imposed on the fluid (pH, $f(\text{O}_2)$, T, salinity, S content) will not only determine the amount of PGE metal which may dissolve in the fluid phase, but also the nature of the PGE metal complexes in solution. Despite convincing field evidence for the importance of aqueous fluids in deposit development in both conventional and unconventional Ni–Cu–PGE settings, few well-constrained experimental data are available over a wide enough range of conditions to allow accurate determination of the solubility of the PGE in aqueous fluids. However, the data available suggest that PGE solubility in surficial, low-T hydrothermal (<500°C) and high-T post-cumulus aqueous fluids

can be significant at geologically realistic conditions.

In surficial environments, PGE may be complexed by organic ligands (carboxylic acids, humic substances, amino acids) or by hydroxide in neutral to alkaline systems containing little organic matter. Additionally, the presence of organic compounds such as humic substances prevents the precipitation of the PGE where they occur as dissolved hydroxides species.

In low-T hydrothermal environments, the occurrence of Cl-rich hydroxysilicate minerals and high salinity fluid inclusions do not imply that Cl⁻ was the ligand responsible for any significant PGE transport during post-ore alteration and metamorphism. Rather, it is more likely that under these conditions, the bisulfide ion (HS⁻) is responsible for PGE transport (if any); significant transport of the PGE by bisulfide, however, is unlikely at any conditions. If bisulfide is responsible for PGE remobilization in hydrothermal systems within conventional Ni-Cu-PGE environments, then fluid:rock ratios would have had to be very high and depositional mechanisms would have had to be highly efficient to redistribute any significant amount of PGE. Chloride may still play a role in most low-T hydrothermal solutions in redistributing S, base metals such as Cu and Fe, and other precious metals (*e.g.*, Ag), thereby modifying primary metal ratios in the ores. PGE minerals hosted in hydroxysilicate-dominated alteration assemblages should not be interpreted as evidence for hydrothermal origin because base metal sulfides may have been removed from the rocks (replaced by hydroxysilicates).

In high-T, magmatic-hydrothermal environments, Cl-rich magmatic volatiles (either aqueous or H₂O-free) may be responsible for the primary concentration and redistribution of the PGE, although models which invoke an entirely magmatic model (independent of fluids) have considerable merit because they predict the observed cumulate and ore compositions with reasonable accuracy. Experimental data are lacking, but indicate that (i) Pt solubility may be very high (ppm-level) in high-T (800–900°C), high salinity brines; (ii) theoretical predictions of PGE solubility at elevated temperatures and salinities significantly underestimate PGE solubility, (iii) PGE solubility in aqueous solutions at elevated T (800–900°C) and salinities (20–70 wt.% NaCl) may be controlled by HCl complexing (*e.g.*, PtCl₃H), hydroxide complexing (*e.g.*, PtOH₂), or the formation of

heterogeneously distributed colloidal particles (hydrated Pt oxides or hydroxides) or clusters and (iii) in the absence of H₂O, vapor transport of the PGE is only significant above 1000°C and enhanced by the presence of both Cl and S in the vapor phase (but not S alone).

ACKNOWLEDGEMENTS

This article has benefited from careful reviews by S. Wood and E. Mathez. Thanks to S. Wood for supplying the original log $f(\text{O}_2)$ -pH diagram for Figure 2-2 which was modified for use in this article.

REFERENCES

- ANDERSON, G. (1996): *Thermodynamics of Natural Systems*. Wiley and Sons, New York, 382 p.
- BALLHAUS, C.G. (1988): Potholes of the Merensky Reef at Brakspruit Shaft, Rustenburg platinum mines; primary disturbances in the magmatic stratigraphy. *Econ. Geol.* **83**, 1140-1158.
- BALLHAUS, C.G. & STUMPFL, E.F. (1986): Sulfide and platinum mineralization in the Merensky Reef: Evidence from hydrous silicates and fluid inclusions. *Contrib. Mineral. Petrol.* **94**, 193-204.
- BALLHAUS, C.G., RYAN, C.G., MERNAGH, T.P. & GREEN, D.H. (1994) The partitioning of Fe, Ni, Cu, Pt, and Au between sulphide, metal, and fluid phases: A pilot study. *Geochim. Cosmochim. Acta* **58**, 811-826.
- BARNER, H.E. & SCHEUERMAN, R. (1978): *Handbook of Thermochemical Data for Compounds and Aqueous Species*. John Wiley, New York, 861 pp.
- BARNES, H.L. (1979): Solubilities of ore minerals. In *Geochemistry of hydrothermal ore deposits*, 2nd ed. (ed. H.L. Barnes). Wiley-Interscience, New York, 404-460.
- BOORMAN, S.L., MCGUIRE, J.B., BOUDREAU, A.E. & KRUGER, F.J. (2003): Fluid overpressure in layered intrusions; formation of a breccia pipe in the eastern Bushveld Complex, Republic of South Africa. *Mineral. Dep.* **38**, 356-369.
- BOUDREAU, A.E. (1999): Fluid fluxing of cumulates: the J-M Reef and associated rocks of Stillwater Complex, Montana. *J. Petrol.* **40**, 755-772.
- BOUDREAU, A.E. (2004): PALLADIUM, a program

- to model the chromatographic separation of the platinum-group elements, base metals and sulfur in a solidifying pile of igneous crystals. *Can. Min.* **42**, 393-404.
- BOUDREAU, A.E. & MCCALLUM, I.S. (1986): Investigations of the Stillwater Complex: III. The Picket Pin Pt/Pd Deposit. *Econ. Geol.* **81**, 1953-1975.
- BOUDREAU, A.E. & MEURER, W.P. (1999): Chromatographic separation of the platinum-group elements, base metals, gold and sulfur during degassing of a compacting and solidifying igneous crystal pile. *Contrib. Mineral. Petrol.* **134**, 174-185.
- BOUDREAU, A.E., MATHEZ, E.A. & MCCALLUM, I.S. (1986): Halogen geochemistry of the Stillwater and Bushveld Complexes: evidence for transport of the platinum-group elements by Cl-rich fluids. *J. Petrol.* **27**, 967-986.
- BOWLES, J.F.W. (1986): The development of platinum-group minerals in laterites. *Econ. Geol.* **81**, 1278-1285.
- BOWLES, J.F.W., GIZE, A.P. & COWDEN, A. (1994): The mobility of the platinum-group elements in the soils of the Freetown Peninsula, Sierra Leone. *Can. Min.* **32**, 957-967.
- BOWLES, J.F.W., GIZE, A.P., VAUGHAN, D.J. & NORRIS, S.J. (1995): Organic controls on platinum-group element (PGE) solubility in soils: Initial data. *Chron. Rech. Min.* **520**, 65-73.
- BRAUN, K., MEURER, W., BOUDREAU, A.E. & MCCALLUM, I.S. (1994): Compositions of pegmatoids beneath the J-M Reef of the Stillwater Complex, Montana, U.S.A. *Chem. Geol.* **113**, 245-257.
- BRUGMANN, G.E., NALDRETTE, A.J. & McDONALD, A.J. (1989): Magma mixing and constitutional zone refining in the Lac Des Iles Complex, Ontario: Genesis of platinum-group element mineralization. *Econ. Geol.* **84**, 1557-1573.
- CAMPBELL, I. H., NALDRETT, A. J. & BARNES, S. J. (1983): A model for the origin of the platinum-rich sulfide horizons in the Bushveld and Stillwater Complexes. *J. Petrol.* **24**, 33-165.
- DISTLER, V.V. & YUDOVSKAYA, M.A. (2005): Polymetallic platinum-group element (PGE)-Au mineralization of the Sukhoi Log deposit, Russia. *In* Exploration for Platinum-group Element Deposits (J.E. Mungall, ed.). *Mineral. Assoc. Canada, Short Course 35*, 459-489.
- ECONOMOU-ELIOPOULOS, M. (2005): Platinum-group element potential of porphyry deposits. *In* Exploration for Platinum-group Element Deposits (J.E. Mungall, ed.). *Mineral. Assoc. Canada, Short Course 35*, 203-246.
- EDGAR, A.D., CHARBONNEAU, H.E. & MCHARDY, D.C. (1989): Pd-bismutho-telluride minerals at Rathbun Lake, Ontario: Significance to post-magmatic evolution of PGE deposits. *Neues Jahrbuch für Mineralogie, Monatshefte*, 461-475.
- FARROW, C.E.G. (1994): *Geology, alteration, and the role of fluids in Cu-Ni-PGE mineralization of the footwall rocks to the Sudbury Igneous Complex, Levack and Morgan Townships, Sudbury District, Ontario*. Ph.D. thesis, Carleton University, Ottawa, Ontario.
- FARROW, C.E.G. & WATKINSON, D.H. (1992): Alteration and the role of fluids in Ni,Cu, and platinum-group element deposition, Sudbury Igneous Complex contact, Onaping-Levack area, Ontario. *Mineral. Petrol.* **46**, 67-83.
- FARROW, C.E.G. & WATKINSON, D.H. (1996): Geochemical evolution of the epidote zone, Fraser Mine, Sudbury, Ontario: Ni-Cu-PGE remobilization by saline fluids. *Explor. Min. Geol.* **5**, 17-31.
- FARROW, C.E.G. & WATKINSON, D.H. (1997): Diversity of precious-metal mineralization in footwall Cu-Ni-PGE deposits, Sudbury, Ontario; implications for hydrothermal models of formation: *Can. Mineral.* **35**, 817-839.
- FLEET, M.E. & WU, T (1993) Volatile transport of platinum-group elements in sulphide-chloride assemblages at 1000°C. *Geochim. Cosmochim. Acta* **57**, 3519-3531.
- FLEET, M.E. & WU, T (1995): Volatile transport of precious metals at 1000°C: Speciation, fractionation and the effect of base-metal sulphide. *Geochim. Cosmochim. Acta* **59**, 487-495.
- FRANK, M.R., CANDELA, P.A., PICCOLI, P.M. & GLASCOCK, M.D. (2002): Gold solubility, speciation, and partitioning as a function of HCl in the brine-silicate melt-metallic gold system at 800°C and 100 MPa. *Geochim. Cosmochim. Acta* **66**, 3719-3732.

- GAMMONS, C.H. (1995): Experimental investigations of the hydrothermal geochemistry of platinum and palladium: IV. The stoichiometry of Pt(IV) and Pd(II) chloride complexes at 100 to 300°C. *Geochim. Cosmochim. Acta* **59**, 1655-1667.
- GAMMONS, C.H. (1996): Experimental investigations of the hydrothermal geochemistry of platinum and palladium: V. Equilibria between Pt metal, Pt(II) and Pt(IV) chloride complexes at 25° to 300°C. *Geochim. Cosmochim. Acta* **60**, 1683-1694.
- GAMMONS, C.H. & BLOOM, M.S. (1993) Experimental investigations of the hydrothermal geochemistry of platinum and palladium: II. The solubility of PtS and PdS in aqueous sulphide solutions. *Geochim. Cosmochim. Acta* **57**, 2451-2467.
- GAMMONS, C.H., BLOOM, M.S & YU, Y. (1992): Experimental investigation of the hydrothermal geochemistry of platinum and palladium: I. Solubility of platinum and palladium sulphide minerals in NaCl/H₂SO₄ solutions at 300°C. *Geochim. Cosmochim. Acta* **56**, 3881-3894.
- GAMMONS, C.H., YU, Y. & BLOOM, M.S (1993): Experimental investigation of the hydrothermal geochemistry of platinum and palladium: III. The solubility of Ag-Pd alloy + AgCl in NaCl/HCl solutions at 300°C. *Geochim. Cosmochim. Acta* **57**, 2469-2479.
- GAMMONS, C.H. & WILLIAMS-JONES, A.E. (1995): The solubility of Au-Ag alloy + AgCl in HCl/NaCl solutions at 300°C: New data on the stability of Au(I) chloride complexes in hydrothermal fluids. *Geochim. Cosmochim. Acta* **59**, 3453-3468.
- HANLEY, J.J. (2002): The distribution of the halogens in Sudbury Breccia matrix as pathfinder elements for footwall Cu-PGE mineralization at the Fraser Cu Zone, Barnet Main Copper Zone, and surrounding margin of the Sudbury Igneous Complex, Onaping-Levack Area, Ontario, Canada. *M.Sc. thesis, University of Toronto*.
- HANLEY, J.J. & MUNGALL, J.E. (2003): Chlorine enrichment and hydrous alteration of the Sudbury Breccia hosting footwall Cu-Ni-PGE mineralization at the Fraser mine, Sudbury, Ontario, Canada. *Can. Mineral.* **41**, 857-881.
- HANLEY, J.J., PETTKE, T., MUNGALL, J.E., & SPOONER, E.T.C. (2005a): The solubility of platinum and gold in NaCl brines at 1.5 kbar, 600 to 800°C: A laser ablation ICP-MS pilot study of synthetic fluid inclusions. *Geochim. Cosmochim. Acta* **69**, 2593-2611.
- HANLEY, J.J., MUNGALL, J.E., PETTKE, T., SPOONER, E.T.C., & BRAY, C.J. (2005b): Ore metal redistribution by hydrocarbon-brine and hydrocarbon-halide melt phases, North Range footwall of the Sudbury Igneous Complex, Ontario, Canada. *Mineral. Deposita, in press*.
- HANLEY, J.J., MUNGALL, J.E., PETTKE, T., & SPOONER, E.T.C. (2005c): Fluid and melt inclusion evidence for platinum-group element transport by high salinity fluids and halide melts below the J-M reef, Stillwater Complex, Montana, U.S.A. *10th Platinum Symposium Abstracts (Oulu, Finland)*.
- HATTORI, K.H. & CAMERON, E.M. (2004): Using the High Mobility of Palladium in Surface Media in Exploration for Platinum Group Element Deposits: Evidence from the Lac des Iles Region, Northwestern Ontario. *Econ. Geol.* **99**, 157-171.
- HEMLEY, J.J, CYGAN, G.L., FEIN, J.B., ROBINSON, G.R, JR., & D'ANGELO, W.M. (1992): Hydrothermal ore-forming processes in light of studies in rock-buffered systems; I, Iron-copper-zinc-lead sulfide solubility relations. *Econ. Geol.* **87**, 1-22.
- HSU, L.C., LECHLER, P.J. & NELSON, J.H. (1991): Hydrothermal solubility of palladium in chloride solutions from 300° to 700°C: Preliminary experimental results. *Econ. Geol.* **86**, 422-427.
- JAGO, B.C., MORRISON, G.G. & LITTLE, T.L. (1994): Metal zonation patterns and microtextural and micromineralogical evidence for alkali- and halogen-rich fluids in the genesis of the Victor Deep and McCreedy East footwall copper ore bodies, Sudbury Igneous Complex. *In Proc. Sudbury-Noril'sk Symposium (P.C. Lightfoot & A.J. Naldrett, eds.)*. *Ontario Geol. Surv., Spec. Vol.* **5**, 65-75.
- LI, C. (1992): A quantitative model for the formation of sulfide ores at Sudbury and a study on the distributions of platinum-group elements in the Strathcona copper-rich zones, Sudbury, Ontario. *Ph.D. thesis, University of Toronto*.
- LI, C. & NALDRETT, A.J. (1993): High chlorine alteration minerals and calcium-rich brines in

- fluid inclusions from the Strathcona deep copper zone, Sudbury, Ontario. *Econ. Geol.* **88**, 1780-1796.
- LI, C., RIPLEY, E.M. & MERINO, E. (2004): Replacement of base metal sulfides by actinolite, epidote, calcite, and magnetite in the UG2 and Merensky Reef of the Bushveld Complex, South Africa. *Econ. Geol.* **99**, 173-184.
- LI, J.-H. & BYRNE, R.H. (1990): Amino acid complexation of palladium in seawater. *Environ. Sci. Tech.* **24**, 1038-1041.
- MAGYAROSI, Z., WATKINSON, D.H. AND JONES, P.C. (2002): Mineralogy of Ni-Cu-Platinum-Group Element Sulfide Ore in the 800 and 810 Orebodies, Copper Cliff South Mine, and P-T-X Conditions during the Formation of Platinum-Group Minerals. *Econ. Geol.* **97**, 1471-1486.
- MAKOVICKY, E. (2002): Ternary and Quaternary Phase Systems with PGE. In *The Geology, Geochemistry, Mineralogy and Mineral Beneficiation of Platinum-Group Elements* (ed. L.J. Cabri). Canadian Institute of Mining, Metallurgy and Petroleum, Montreal. pp. 131-175.
- MARSHALL, D., WATKINSON, D., FARROW, C., MOLNÁR, F. & FOUILLAC, A.-M. (1999): Multiple fluid generations in the Sudbury Igneous Complex: fluid inclusion, Ar, O, H, Rb and Sr evidence. *Chem. Geol.* **154**, 1-19.
- MATHEZ, E.A. & WEBSTER, J.D. (2005): Partitioning behaviour of chlorine and fluorine in the system apatite-silicate melt-fluid. *Geochim. Cosmochim. Acta* **69**, 1275-1286.
- MATHEZ, E.A., DEITRICH, V.J., HOLLOWAY, J.R. & BOUDREAU, A.E. (1989): Carbon distribution in the Stillwater Complex and evolution of vapor during crystallization of Stillwater and Bushveld magmas. *J. Petrol.* **30**, 153-173.
- MATHEZ, E.A., AGRINIER, P., & HUTCHINSON, R. (1994): Hydrogen isotope composition of the Merensky Reef and related rocks, Atok section, Bushveld Complex. *Econ. Geol.* **89**, 791-802.
- MCCALLUM, M.E., LOUCKS, R.R., CARLSON, R.R., COOLEY, E.F. & DOERGE, T.A. (1976): Platinum metals associated with hydrothermal copper ores of the New Rambler Mine, Medicine Bow Mountains, Wyoming. *Econ. Geol.* **71**, 1429-1450.
- MCCORMICK, K.A. & McDONALD, A.M. (1999): Chlorine-bearing amphiboles from the Fraser mine, Sudbury, Ontario, Canada: description and crystal chemistry. *Can. Mineral.* **37**, 1385-1403.
- MEURER, W. P., WILLMORE, C.C., & BOUDREAU, A. E. (1998): Metal redistribution during fluid exsolution and migration in the Middle Banded series of the Stillwater Complex, Montana. *Lithos* **47**, 143-156.
- MOLNÁR, F., WATKINSON, D.H. & JONES, P.C. (2001): Multiple hydrothermal processes in footwall units of the North Range, Sudbury Igneous Complex, Canada, and implications for the genesis of vein-type Cu-Ni-PGE deposits. *Econ. Geol.* **96**, 1645-1670.
- MOUNTAIN, B.W. & WOOD, S.A. (1988): Chemical controls on the solubility, transport, and deposition of platinum and palladium in hydrothermal solutions: A thermodynamic approach. *Econ. Geol.* **83**, 492-510.
- MUNGALL, J.E. (2002): Kinetic controls on the partitioning of trace elements between silicate and sulfide liquids. *J. Petrol.* **43**, 749-768.
- NABIVANETS, B.I. & KALABINA, L.V. (1972): Oxalate complexes of palladium and their application in analysis. *Zhurnal Analiticheskoy Khimiy* **27**, 1134-1139.
- NORMAND, C. & WOOD, S.D. (2005): Effect of the trihydroxamate siderophores desferrioxamine-B and ferrichrome on the mobility of Pd, Pt, Rh and Ir. 15th Annual Goldschmidt Conference Abstracts, p. A329.
- NYMAN, M.W., SHEETS, R.W. & BODNAR, R.J. (1990): Fluid inclusion evidence for the physical and chemical conditions associated with intermediate-temperature PGE mineralization at the New Rambler deposit, southeastern Wyoming. *Can. Mineral.* **28**, 629-638.
- ORLOVA, G.P., RYABCHIKOV, I.D., DISTLER, V.V. & GLADYSHEV, G.D. (1987): Platinum migration in fluids during the formation of magmatic sulfides. *Int. Geol. Rev.* **29**, 360-362.
- PAN, P. & WOOD, S.A. (1994): Solubility of Pt and Pd sulfides and Au metal in aqueous bisulfide solutions; II, Results at 200°C to 350°C and saturated vapor pressure. *Mineral. Deposita* **29**, 373-390.
- PICKRELL, J.M. (1997): Stability Constants of Pd²⁺

- Complexes from 25° to 85°C. Unpublished M.S. thesis, University of Idaho, Moscow, Idaho, 120 p.
- PITTWELL, L.R. (1965): Thiometallates of the group-eight metals. *Nature* **207**, 1181-1182.
- PLYUSINA, L.P., LIKHOIDOV, G.G., NEKRASOV, I.YA. & SHEKA, ZH.A. (1997): Solubility of platinum in aqueous chloride media in the presence of manganese oxides at 300-500°C, 1 kbar. *Doklady Akadememii Nauk* **333**, 631-633.
- POLOVINA, J.S., HUDSON, D.M. & JONES, R.E. (2004): Petrographic and geochemical characteristics of postmagmatic hydrothermal alteration and mineralization in the J-M Reef, Stillwater Complex, Montana. *Can. Mineral.* **42**, 261-278.
- RACKLEY, R.I. & JOHNSON, R.L. (1971): The geochemistry of uranium roll-front deposits with a case history from the Powder River Basin. *Econ. Geol.* **66**, 202-203.
- REID, D.L., CAWTHORN, R.G., KRUGER, F.J. & TREDOUX, M. (1993): Isotope and trace-element patterns below the Merensky Reef, Bushveld Complex, South Africa; evidence for fluids? *Chem. Geol.* **106**, 171-186.
- ROWELL, W.F. & EDGAR, A.D. (1986): Platinum-group element mineralization in a Hydrothermal Cu-Ni sulfide occurrence, Rathbun Lake, northeastern Ontario. *Econ. Geol.* **81**, 1272-1277.
- RUDASHEVSKY, N.S., AVDONTSEV, S.N. & DNEPROVSKAYA, M.B. (1992): Evolution of PGE mineralization in hortonolitic dunites of the Mooihoek and Onverwacht Pipes, Bushveld Complex. *Mineral. Petrol.* **47**, 37-54.
- SASSANI, D.C. & SHOCK, E.L. (1990): Speciation and solubility of palladium in aqueous magmatic-hydrothermal solutions. *Geology*, **18**, 925-928.
- SASSANI, D.C. & SHOCK, E.L. (1998): Solubility and transport of platinum-group elements in supercritical fluids: Summary and estimates of thermodynamic properties for Ru, Rh, Pd, and Pt solids, aqueous ions and aqueous complexes. *Geochim. Cosmochim. Acta* **62**, 2643-2671.
- SATO, M., & VALENZA, M. (1980): Oxygen fugacity of the layered series of the Skaergaard Intrusion, East Greenland. *Amer. J. Sci.* **280A**, 134-158.
- SCHIFFRIES, C.M. (1982): The platiferous dunite pipe in the Bushveld complex: Infiltration metasomatism by a chloride solution. *Econ. Geol.* **77**, 1439-1453.
- SPRINGER, G. (1989): Chlorine-bearing and other uncommon minerals in the Strathcona Deep Copper Zone, Sudbury District, Ontario. *Can. Mineral.* **27**, 311-313.
- TALKINGTON, R.W. & WATKINSON, D.H. (1984): Trends in the distribution of the precious metals in the Lac des Iles Complex, northwestern Ontario. *Can. Min.* **22**, 125-136.
- TELLIER, M.L., BRUGMANN, G.E. & NALDRETT, A.J. (1991): Gabbro-hosted PGE mineralization in the Lac des Iles Complex: a geochemistry and fluid inclusion study. *Mineral. Ass. Canada - Geol. Ass. Canada, Prog. Abst.* **16**, 123.
- VAN MIDDLESWORTH J. & WOOD, S.A. (1999) The stability of palladium(II) hydroxide and hydroxychloride complexes: An experimental solubility study at 25-85°C and 1 bar. *Geochim. Cosmochim. Acta* **63**, 1751-1765.
- WATKINSON, D.H. & MELLING, D.R. (1992): Hydrothermal origin of platinum-group mineralization in low-temperature copper sulfide-rich assemblages, Salt Chuck intrusion, Alaska. *Econ. Geol.* **87**, 175-184.
- WILDE, A. (2005): Descriptive ore deposit models: Hydrothermal and supergene Pt & Pd deposits. In Exploration for Platinum-group Element Deposits (J.E. Mungall, ed.). *Mineral. Assoc. Canada, Short Course* 35, 145-161.
- WILLIAMS, T.J., CANDELA, P.A., & PICCOLI, P.M. (1997) Hydrogen-alkali exchange between silicate melts and two-phase aqueous mixtures; an experimental investigation. *Contrib. Min. Pet.* **128**, 114-126.
- WILLMORE, C.C., BOUDREAU, A.E. & KRUGER, F.J. (2000): The halogen geochemistry of the Bushveld Complex, Republic of South Africa: Implications for chalcophile element distribution in the Lower and Critical zones. *J. Petrol.* **41**, 1517-1539.
- WOOD, S.A. (1987): Thermodynamic calculations of the volatility of the platinum group elements (PGE): The PGE content of fluids at magmatic temperatures. *Geochim. Cosmochim. Acta*, **51**, 3041-3050.

- WOOD, S.A. (1990): The interaction of dissolved platinum with fulvic acid and simple organic acid analogues in aqueous solutions. *Can. Min.* **28**, 665-673.
- WOOD, S.A. (1991): Experimental determination of the hydrolysis constants of Pt^{2+} and Pd^{2+} at 25°C from the solubility of Pt and Pd in aqueous hydroxide solutions. *Geochim. Cosmochim. Acta* **55**, 1759-1767.
- WOOD, S.A. (1998): Calculation of activity-activity and $\log f(O_2)$ -pH diagrams. In *Techniques in hydrothermal ore deposits geology* (eds. J.P. Richards & P.B. Larson). Reviews in Economic Geology, **10**, 81-96.
- WOOD, S.A. (2002): The Aqueous Geochemistry of the Platinum-Group Elements with Applications to Ore Deposits. In *The Geology, Geochemistry, Mineralogy and Mineral Beneficiation of Platinum-Group Elements* (ed. L.J. Cabri). Canadian Institute of Mining, Metallurgy and Petroleum, Montreal. pp. 211-249.
- WOOD, S.A. & VAN MIDDLESWORTH, J. (2004): The influence of acetate and oxalate as simple organic ligands on the behavior of palladium in surface environments. *Can. Min.* **42**, 411-421.
- WOOD, S.A. & VLASSOPOULOS, D. (1990): The dispersion of Pt, Pd and Au in surficial media about two PGE-CU-Ni prospects in Quebec. *Can. Min.* **28**, 649-663.
- WOOD, S.A. & SAMSON, I.M. (1998): Solubility of Ore Minerals and Complexation of Ore Metals in Hydrothermal Solutions. In *Techniques in Hydrothermal Ore Deposits Geology* (eds. J.P. Richards & P.B. Larson). Reviews in Economic Geology, **10**, 33-80.
- WOOD, S.A. & VAN MIDDLESWORTH, J. (2004): The influence of acetate and oxalate as simple organic ligands on the behavior of palladium in surface environments. *Can. Min.* **42**, 411-422.
- WOOD, S.A., MOUNTAIN, B.W. & PAN, P. (1992): The aqueous geochemistry of platinum, palladium and gold: Recent experimental constraints and a re-evaluation of theoretical predictions. *Can. Min.* **30**, 955-982.
- WOOD, S. A., PAN, P., ZHANG, Y., & MUCCI, A. (1994): The solubility of Pt and Pd sulfides and Au in bisulfide solutions; I, Results at 25°-90°C and 1 bar pressure. *Mineral. Deposita* **29**, 309-317.
- XIONG, Y. & WOOD, S.A. (2000): Experimental quantification of hydrothermal solubility of platinum-group elements with special reference to porphyry copper environments. *Mineral. Petrol.* **68**, 1-28.

CHAPTER 3: STRATIFORM PLATINUM-GROUP ELEMENT DEPOSITS IN LAYERED INTRUSIONS

R. Grant Cawthorn
School of Geosciences, University of the Witwatersrand,
P O Wits, 2050, South Africa.
E-mail address: cawthorn@geosciences.wits.ac.za

INTRODUCTION

Four of the five largest platinum-group element (PGE) deposits occur near the stratigraphic middle of large layered intrusions, namely the Merensky and UG2 Chromitite Reefs of the Bushveld Complex, South Africa (Vermaak 1976, Lee 1996, Barnes & Maier 2002a, Cawthorn *et al.* 2002a), the Main Sulfide Zone of the Great Dyke, Zimbabwe (Wilson 2001, Oberthür 2002) and the Johns-Manville (JM) Reef of the Stillwater Complex, USA (Bow *et al.* 1982, Todd *et al.* 1982, Raedeke & Vian 1985, Zientek *et al.* 2002). The fifth deposit, the Noril'sk-Talnakh deposits in Russia occur at several different levels within and below thick sills, which show variable differentiation, but not with the distinct layering of the previous three examples. The Russian occurrences will not be discussed further. Other layered intrusions have been identified that contain PGE-enriched horizons near their centres, but are not currently economic. Most intrusions with central mineralization have a large area:thickness ratio, especially the Bushveld and Stillwater Complexes, and also Munni Munni, Australia (Barnes 1993), Fox River, Canada (Peck *et al.* 2002) and Penikat, Finland (Alapieti & Lahtinen 1986), but exceptions exist, *e.g.*, the Skaergaard intrusion, Greenland (Andersen *et al.* 1998). Less commonly PGE mineralization may occur at the bases of such layered intrusions, *e.g.*, Narkau, Finland (Alapieti & Lahtinen 2002, Iljina & Lee 2005) and Muskox, Canada (Barnes & Francis 1995), but only in the case of the Platreef in the Bushveld Complex is it currently economic (White 1994, Iljina & Lee 2005). The remarkable concentration of PGE within relatively thin vertical successions, compared to the overall thickness of the layered intrusions, and their extreme lateral continuity make them excellent examples of stratiform ore deposits. Several of these examples are described here, and common and distinctive features are compared and contrasted.

BUSHVELD COMPLEX

Since the discovery of the Merensky Reef in 1924, the deposits of the Bushveld Complex have increased in importance in terms of PGE production, paralleled by the influence that hypotheses derived from this deposit have had on geological thought and exploration. The Bushveld Complex (Fig. 3-1) is a remarkably well preserved, extremely large mid-Proterozoic intrusion that has escaped regional metamorphism and extensive deformation. It shows a complete differentiation sequence from magnesian ultrabasic rocks to apatite ferrodiorites (Eales and Cawthorn 1996 and references therein). The PGE-mineralized Upper Group 2 (UG2) chromitite and Merensky Reef occur at the top of a strongly layered succession of chromitite, pyroxenite, norite and anorthosite called the Critical Zone. Individual layers, including the Merensky Reef and UG2 Chromitite, have great lateral continuity (over 100 km in both the eastern and western limbs), but in detail can be quite variable.

Detailed descriptions of the mineralization are presented in Barnes & Maier (2002a) and Cawthorn *et al.* (2002a). The locations of the platinum mines are shown in Fig. 3-1. Every layer of chromitite is anomalously enriched in PGE (Fig. 3-2), typically 1–3 g.t⁻¹ (von Gruenewaldt *et al.* 1986, Lee & Parry 1988, Scoon & Teigler 1994). However, economic grades occur only in the UG2 Chromitite and the Merensky Reef in the eastern and western limbs, and also in a thick layer close to the basal contact in the northern limb, called the Platreef (Iljina & Lee 2005).

UG2 Chromitite

Mineralization in the UG2 Chromitite is simpler to document in terms of its geology and PGE content than the Merensky Reef. The UG2 Chromitite layer ranges from 40 to 120 cm thick, and has sharp basal and upper contacts (Fig. 3-3), and contains 60–90% chromite. Two or three thin

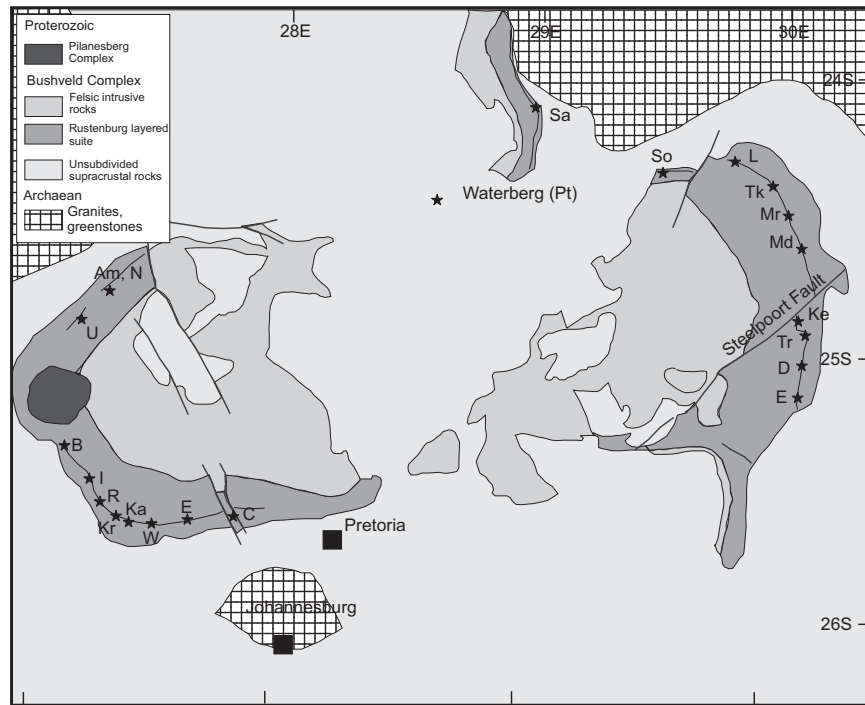


FIG. 3-1. Outcrop map of the Bushveld Complex, South Africa (after Eales & Cawthorn 1996). The following PGE mines and prospects are indicated (clockwise). Eastern limb: So – Southern Era, L – Lebowa, Tk – Twickenham, Mr – Marula, Md – Modikwa, Ke – Kennedy's Vale, Tr – Two Rivers, D – De Brochen, E – Everest. Western limb: C Crocodile River/Barplats, E – Eastern, W – Western, Ka – Karee, Kr – Kroondal (Aquarius), R – Rustenburg, I – Impala, B – Bafokeng Rasimone, U – Union, Am – Amandelbult, N – Northam. Potgietersrus limb: Sa – Sandsloot.

chromitite layers exist above the main UG2 layer in a feldspathic (often olivine-bearing) pyroxenite. The UG2 is usually underlain by a coarse-grained feldspathic (olivine) pyroxenite that may contain schlieren of chromitite. In such situations the basal contact may be irregular on scales from centimetres upward, although always sharp, with disrupted fragments of chromitite in this pegmatitic facies. Less frequently, the layer may be underlain by anorthosite, in which case the contact is relatively planar.

PGE grade is always strictly contained in chromitite. Where mineralization is reported in the pegmatitic footwall it is within the chromitite schlieren. The distribution of mineralization within the UG2 is summarized by Lee (1996). Grades for the complete layer can range up to 10 g.t^{-1} , but typically are about 5 g.t^{-1} , with some suggestion that the thinner the layer the higher the grade. The first of the hanging wall chromitite layers may also contain moderate PGE content, but only where the UG2 thins or the top of the UG2 itself appears to have split (Fig. 3-4). The distribution of grade within the layer is not uniform. It is generally

bottom loaded, with another peak near the middle or top (Lee 1996). In the western limb there may be three high PGE zones, as shown in Figure 3-5, taken from a very detailed geochemical study of the UG2 (Hiemstra 1985, 1986), using a sample spacing of 2 cm. Most reported grades in the reef use samples 10 to 20 cm thick, and so cannot reveal this kind of detailed chemical structure.

Within the layer, a significant increase in absolute content and Pt/Pd value occur at the level where there is a distinct change in the texture of the rock (Fig. 3-3). In the northern part of the eastern limb, the lower half contains granular silicate phases and the upper half is poikilitic, which Lee (1996) suggested might indicate the juxtaposition of two chemically distinct successive chromitite layers without any intervening silicate layer, or frequently with only very thin lenses of pyroxenite as a parting between these two textural types.

The value of Pt/Pd averaged through the entire UG2 layer is significantly lower in the eastern (1.2) than the western (2.0) limbs. In the northern part of the eastern limb there is a UG3 chromitite layer overlying the UG2 cyclic unit, and it has a

STRATIFORM PLATINUM-GROUP ELEMENT DEPOSITS IN LAYERED INTRUSIONS

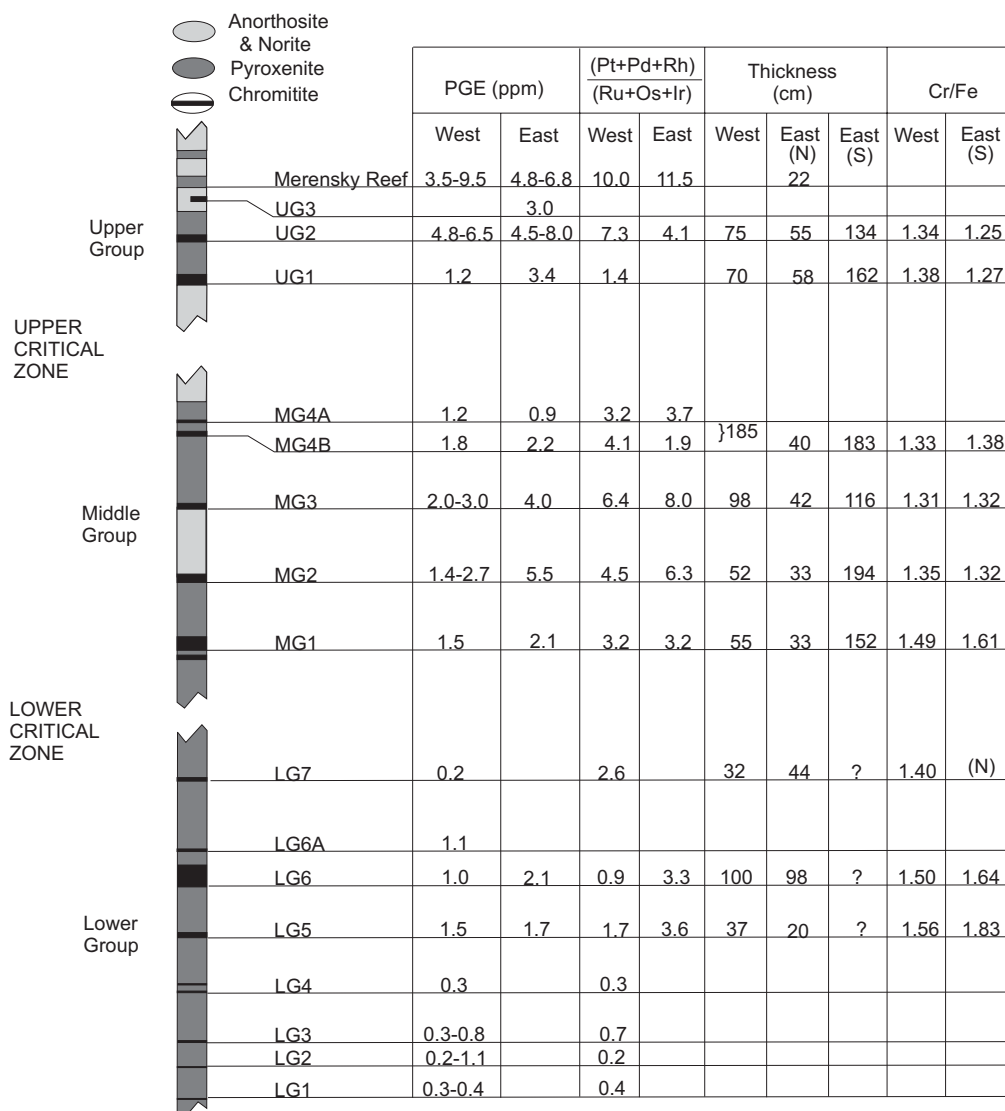


FIG. 3-2. Stratigraphic section of the Critical Zone of the Bushveld Complex showing the PGE content in the east and west limbs (Lee & Parry 1988, Scoon & Teigler 1994)

very high Pt/Pd value (Gain 1985). In the western limb, there is no UG3, and it is possible that the UG2 and UG3 have coalesced, as shown in Figure 3-6, as a result of non-deposition of the intervening silicate package. The combined effect of the high Pt/Pd in the UG3 superposed on the UG2 is to increase the thickness and Pt/Pd value of the combined unit (and as a consequence, the UG2 in the west could be considered to be made of three discrete layers).

In the UG2, Cu, Ni and S values are extremely low (average 0.01, 0.024 and 0.023% respectively, Hiemstra 1986). Platinum, Pd, Cu, Ni and S all correlate quite closely in the detailed

sampling reported by Hiemstra (1985, 1986). At the Southern Era Mine (Fig. 3-1), the UG2 contains a much higher base-metal sulfide component than elsewhere, but still has a PGE grade of 5.7 g.t^{-1} , and so is no different from the typical sulfide-poor facies (von Gruenewaldt *et al.* 1990).

Merensky Reef

The PGE-rich Merensky Reef and an overlying PGE-poor Bastard pyroxenite lie at the bases of cyclic units that contain a trivially thin basal chromitite layer, overlain by pyroxenite, norite and anorthosite (Vermaak 1976). The Merensky cyclic unit is the thinnest of all cycles,



FIG. 3-3. Photograph of UG2 Chromitite, eastern Bushveld Complex, showing the underlying pegmatitic pyroxenite with an irregular basal contact to the UG2 (in line with hammer head), showing downward protruding chromitite (to right of hammer tip), and a planar upper contact to a melanorite. A change in texture in the UG2 can be recognised close to the middle of the layer where a semi-continuous, often pegmatitic, pyroxenite lens is frequently observed (near top of hammer shaft).

typically only a few m thick. It also displays a significant increase in the initial Sr isotope ratio close to its basal contact, suggesting addition of a fundamentally different composition of magma at this level (Hamilton 1977, Kruger & Marsh 1982).

The vertical succession and the PGE mineralization within the Merensky Reef package are much more variable than in the UG2 (Fig. 3-7), both on a small scale and a regional scale. The Merensky Reef should be regarded as that portion of the succession that contains economic mineralization, and can be seen to be lithologically variable (Fig. 3-7). The PGE are closely associated with the 2–3% sulfides (pyrrhotite, chalcopyrite and pentlandite) that are clearly interstitial to the cumulus pyroxene (or plagioclase in the case of mineralization in the rocks below the pyroxenite). Because mining of this reef began in the Rustenburg area (Fig. 3-1), where some earlier publications originated (*e.g.*, Vermaak 1976), the Rustenburg facies reef has been considered the normal or typical section. However, considerable variation exists (Wagner 1929, Viljoen 1999, Cawthorn *et al.* 2002a). In the Rustenburg facies (Rustenburg Platinum Mine) the basal chromitite (typically <1 cm) rests on an anorthosite or leuconorite layer (Fig. 3-7). It is overlain by a 30–90 cm-thick pegmatitic feldspathic pyroxenite that may contain some olivine. (The local name of “pegmatoid” is not recommended in IUGS nomenclature.) This layer has another thin chromitite at its top, above which is a feldspathic pyroxenite of normal grain size and is olivine-free. This pyroxenite sharply grades into a thin norite, overlain by anorthosite. In such a section, PGE mineralization occurs from 30 cm into the footwall to close to the upper chromitite, with distinct peaks at the two chromitite layers (Fig. 3-7).

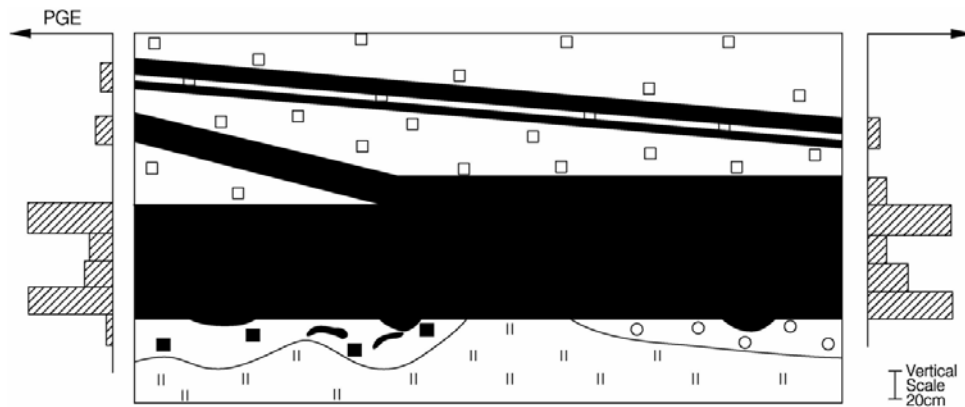


FIG. 3-4. Schematic profile through the UG2 and leader layers, and the qualitative distribution of PGE, from Karee mine (after Davey 1992)

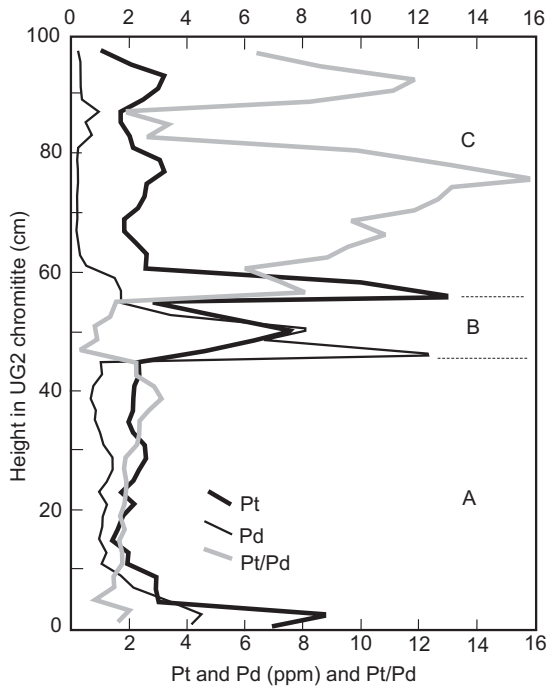


FIG. 3-5. Detailed study by Hiemstra (1985) through the UG2 Chromitite, Western Platinum Mine. A, B and C denote the three cycles comprising the entire layer.

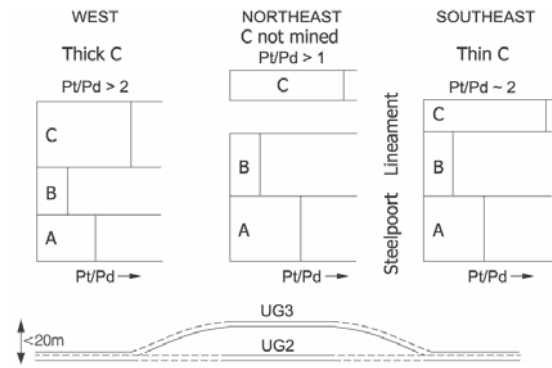


FIG. 3-6. Schematic relationships between UG2 and UG3 chromitites inferred in the eastern limb (based in part on Gain 1985), demonstrating how the Pt/Pd value is influenced by the merging of the UG3 at the top of the UG2.

Grade rapidly decreases above the upper chromitite. When traced to the west (Impala Platinum Mine), there is a change involving the disappearance of the intermediate pegmatitic layer, and the presumed merging of the two chromitite layers or elimination of the lower one (Fig. 3-7). With this geometry, the grade distribution approximately straddles the chromitite layer. To the east of Rustenburg

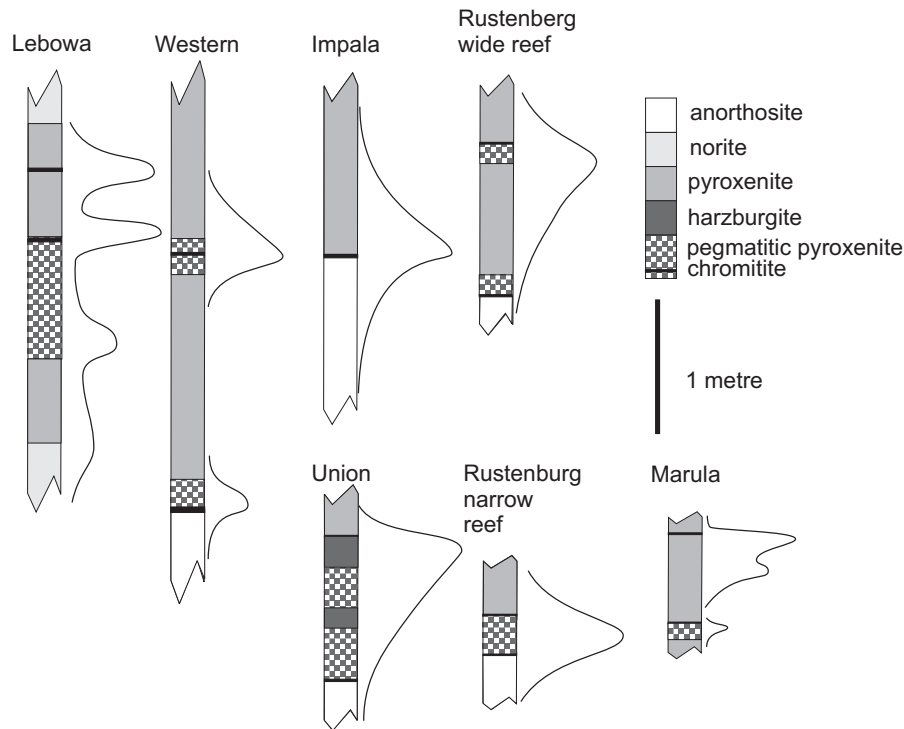


FIG. 3-7. Variation in lithology and PGE distribution in sections of the Merensky Reef around the Bushveld Complex (from various sources, see Cawthorn *et al.* 2002a).

Platinum Mine, the gap between the two chromitite layers increases. Above the basal chromitite there is a normal grain-sized feldspathic pyroxenite that becomes pegmatitic only immediately below the upper chromitite. The separation of the two chromitite layers can reach 7 m (Davey 1992) on Western and Eastern Platinum Mines (Fig. 3-7). PGE mineralization can occur around both chromitites, but the higher grade is always associated with the upper one. Further to the east, close to and beyond the Brits graben, at Crocodile River/Barplats Mine (Fig. 3-1) the chromitites and the pegmatitic pyroxenite disappear. PGE mineralization occurs in the feldspathic pyroxenite, which is up to 14 m thick, and in the footwall anorthosite (Wagner 1929), but is uneconomic. However, the UG2 Chromitite is still economically mineralized in this eastern extremity.

North of the Pilanesberg Complex in the western limb (Fig. 3-1), the normal Merensky cyclic unit and its footwall are similar to those seen on Rustenburg mine, although possibly with more olivine in the pegmatitic pyroxenite between the chromitite layers. The separation of the chromitite layers may also be variable and up to 5 m. The term “normal Merensky” distinguishes it from another facies, called “regional pothole reef” (Viljoen 1999, Viring & Cowell 1999) that is discussed below.

Until recently the only active mine in the eastern limb was the Atok/Lebowa mine (Figs. 3-1 and 3-7). The deep footwall consists of a pyroxenite overlain by a pegmatitic pyroxenite up to 1 m thick. In the overlying 2 m thick pyroxenite two thin chromitite layers are found at the bottom and less than 1 m up. Norite and anorthosite complete the Merensky cyclic unit. In this setting, the PGE mineralization occurs in and above the lower chromitite layer, and so occurs above the pegmatitic pyroxenite. Since 2002 new mines have been developed in the eastern limb that will expand detailed understanding of the reef in the eastern limb. To the south of the Steelpoort Lineament (Fig. 3-1), the Merensky Reef has similarities with the thick reef facies at Rustenburg Mine (Wagner 1929). Hence, within each limb there are considerable facies variations, but between eastern and western limbs similarities can be recognized.

On all the mines, irregularities occur in the largely planar Merensky and UG2 Reefs. The thickness of the footwall anorthosite may vary gently, producing what is called rolling reef, but more dramatic changes in the footwall also occur,

and are called potholes. The normal footwall succession may be abruptly displaced by the Merensky Unit in circular to irregularly shaped areas that may penetrate up to 30 m into the footwall, and may extend many tens of metres across (Fig. 3-8a). The angle on the edge of the pothole may range from about 30° to vertical or even undercut, and the angular discordance on the up-dip side is usually greater than on the down-dip side. Bottoms of potholes may be sub-planar to irregular. The Merensky Unit plunges into these potholes, and most layers of the unit are thickened relative to their thickness outside of the pothole, such that layering in the Bastard cyclic unit above a Merensky pothole is usually perfectly planar. For a few metres from the edge of a pothole the two chromitite layers gradually merge, and they and the pyroxenite thin. North of the Pilanesberg Complex, a greater proportion of the Merensky Reef is subject to this potholing process, and on Union and Northam Platinum Mines (Fig. 3-1) mining takes place in a “regional pothole reef”. This pothole descends over 20 m into the footwall in irregular steps (Fig. 3-8b). The angle of cross-cutting is quite steep where the lithology of the footwall is dominated by plagioclase, and tends to be sub-concordant where the footwall is pyroxene- or olivine-dominated. The southeastern limit of this pothole has not been defined, but it has an extent of at least 2 km down-dip and over 20 km along strike (Viljoen 1999, Viring & Cowell 1999).

Potholes also occur below the UG2 Chromitite and are generally similar to those on the Merensky Reef (Hahn & Owendale 1994, Lomberg *et al.* 1999). However, frequently the UG2 Chromitite and its leaders coalesce and are reduced in thickness in a pothole compared to normal reef thickness. No correlation between locations of potholes on UG2 and Merensky has been reported (Cawthorn & Barry 1992).

PGE grade information about the Merensky Reef usually derives from annual mining company reports, which give an ore grade over a mining width of typically 80 to 120 cm. For thinner reef, high grades in the true reef are obviously reduced by mining dilution, and for thicker reef the quoted value is the best cut at the normal mining width, not the total contained metal. Thus, reported figures are not perfect representations of total PGE content (Lee 1996). In the only publication in which statistical information has been quoted, Viring & Cowell (1999) report that for 291 mining width

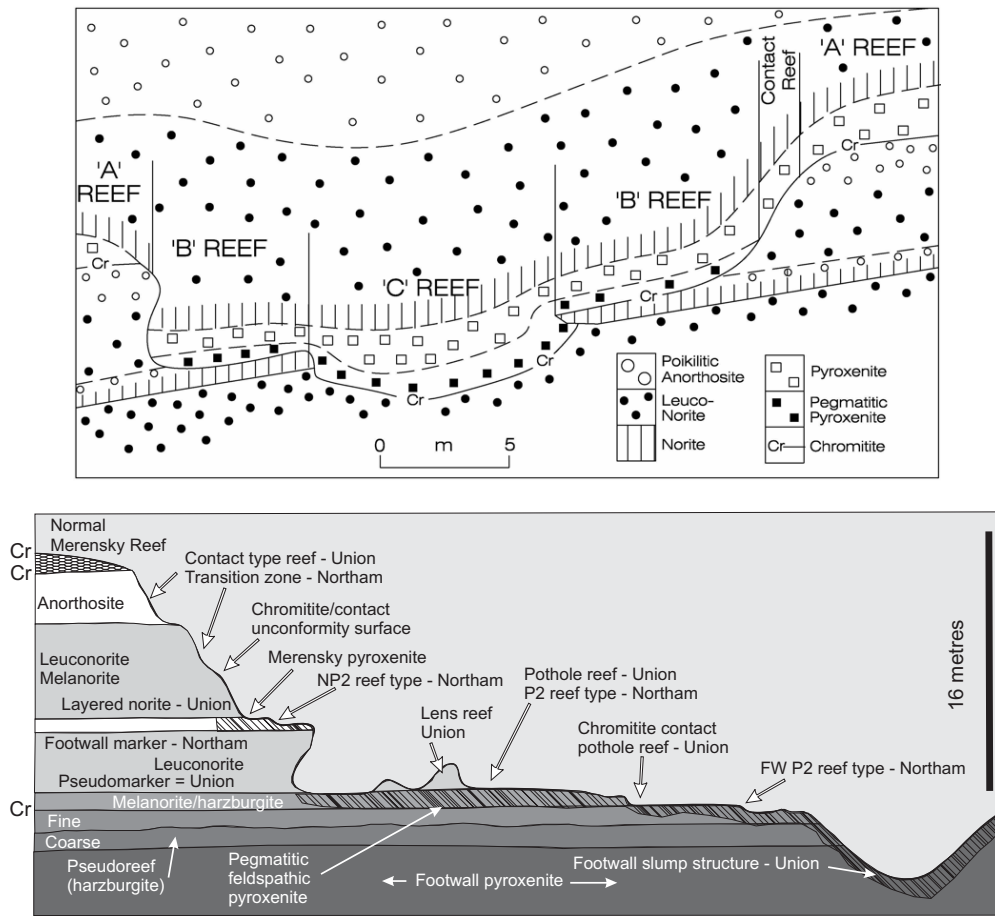
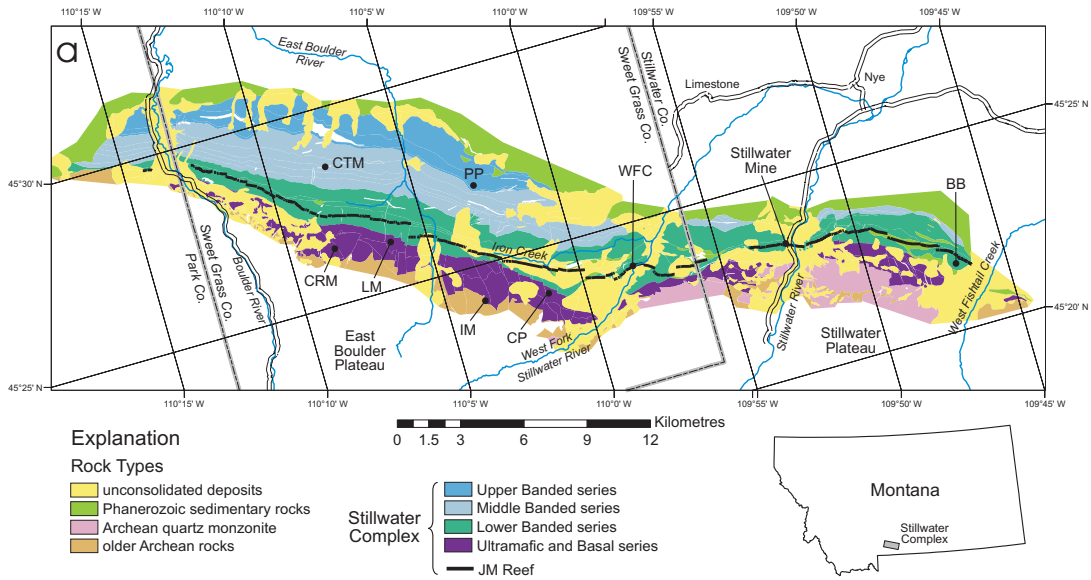


FIG. 3-8. Geometry through a pothole. A. Small pothole on Impala Platinum Mine. B. Regional pothole at Northam mine (after Viring & Cowell 1999)

sections of Merensky Reef the abundance of Pt+Pd+Rh+Au ranges from 1.29 to 21.36 g.t⁻¹, with a mean of 6.97 g.t⁻¹ and a variance of 10.97. Hence, the grades published for a very few detailed vertical sections cannot be considered representative of average ore grade. However, they do provide information on trends within different lithologies within the reef, and also on the relative proportions of the different metals. Given these provisos, the mining company quoted grades, compiled by Cawthorn *et al.* (2002b), range from 5.6 to 9.2 g.t⁻¹ in the western limb to 4.9 to 5.9 in the eastern limb. Also the relative proportions of the different PGE averaged over entire mines are extremely uniform, with a Pt/Pd value close to 2.

The distribution of the PGE vertically within the reef can be extremely variable. The simplified profiles, shown in Fig. 3-7, suggest that the highest grades occur with chromitite layers, especially of the upper layer. PGE data for a few samples of

chromitite have been published. Lee (1983) quoted grades of total PGE of 36 and 16 g.t⁻¹ in the lower and upper chromitite from Rustenburg Mine. Barnes & Maier (2002b) gave higher grades of 50 and 28 g.t⁻¹ for Impala Mine, and Cawthorn *et al.* (2002b) reported 57 g.t⁻¹ also at Impala Mine where there is a single chromitite and no pegmatitic facies. Such grades relate to extremely narrow sections of chromitite within the reef. The distribution of PGE in the footwall anorthosite or norite is variable. Lee's data (1983) showed an abrupt termination downward below the lower chromitite, whereas Barnes & Maier (2002b) and Cawthorn *et al.* (2002b) reported significant grades for 23 cm and 60 cm into the footwall in their two profiles. What is important is that mining practice in areas of thin pyroxenite almost always considers a portion of the footwall anorthosite to be ore grade. The silicate rocks between multiple chromitite layers may contain relatively high grade (6 g.t⁻¹, Lee 1983).



However, above the upper chromitite the grade rapidly decreases. Both data sets of Lee (1983) and Barnes & Maier (2002b) are taken from extremely thin reef, with grades up to 16 g.t^{-1} , but extending over less than 40 cm. The two sections by Cawthorn *et al.* (2002b) refer to thicker reef where grades of 6 g.t^{-1} extend for 80 and 110 cm. In the two studies by Lee (1983) and Barnes & Maier (2002b) an extremely good correlation exists between all the PGE and Ni, Cu and S. Sulfur content typically reaches a maximum of 3% (Lee 1996).

Total minable ore for all reefs in the Bushveld Complex to a depth of 2 km exceeds 2 billion ounces or 62 thousand tonnes of Pt + Pd, with a Pt/Pd value of 1.5 (Cawthorn 1999).

STILLWATER COMPLEX

The 2.7 Ga-old Stillwater Complex has been partially metamorphosed, and ranges from an ultramafic (olivine>orthopyroxene) lower part to an olivine- and orthopyroxene-bearing gabbroic upper part. The top has been truncated. Detailed documentations of the PGE mineralization given by Bow *et al.* (1982), Todd *et al.* (1982) and Zientek *et al.* (2002) are summarized here. The Stillwater Complex contains several stratabound sulfide-bearing intervals that show anomalous PGE enrichment. One such interval, the J-M Reef (Fig. 3-9), occurs about 400 m above the base of the Lower Banded Gabbroic Series and is currently being exploited. Within the Banded Series is a package called the Olivine-bearing Zone 1 or Troctolite-Anorthosite Subzone (Fig. 3-9b).

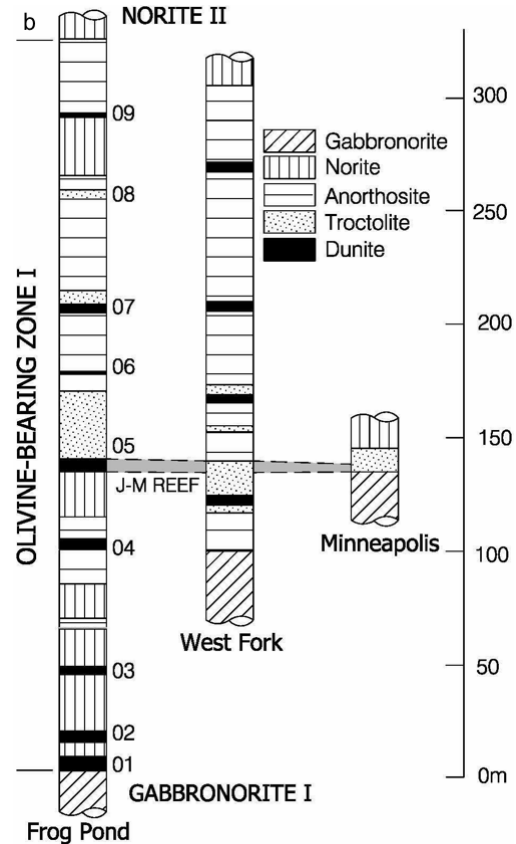


FIG. 3-9. Geology of the Stillwater Complex (from Zientek *et al.* 2005– see page 391 for full description). a. Location of the J-M Reef; b. Stratigraphic section through the interval including the J-M Reef. Numbered zones refer to olivine-bearing members within the olivine-bearing zone.

Olivine-bearing rocks in this subzone are coarse-grained troctolite and subordinate dunite, interlayered with minor anorthosite, norite and gabbro-norite, with thickness on the order of one to a few metres and are characterized by mineral inhomogeneity in the extreme, being called “mixed rock” (Fig. 8c of Campbell *et al.* 1983). Phlogopite, apatite and chromite are important accessory phases. The layering is not well developed or as regular as in the Bushveld Complex, and olivine-bearing lenses pinch out along strike. The J-M mineralized zone occurs in one of a number of olivine-bearing units. The lower olivine-bearing layers are not continuous, and so the numbering scheme for these olivine-bearing layers is difficult to implement across the entire intrusion. In one of the more complete sections in the East Boulder River area, mineralization occurs in olivine layer 5b (enumerated from the base), but there are fewer underlying olivine-bearing layers elsewhere.

The vertical location of best mineralization may vary within the olivine 5b unit and need not be confined to a single rock type; locally it can cut across silicate layering. Typical mineralized widths of the mined reef are 1.6 m, but within this width mineralization is not uniform and barren patches are common. PGE mineralization is typically associated with 0.2–5.0% disseminated sulfide mineralization (pyrrhotite, chalcopyrite, pentlandite and a number of trace phases) although in at least one locality the sulfides form small bodies of massive sulfide about 0.5 m in diameter as cores to pegmatitic silicate bodies. Locally, disseminated mineralization can extend into the underlying rocks in voluminous high-grade regions known as “ballrooms” that can be up to 30 m thick over a strike length of 15 m. Mineralization is also variable laterally on scales of 10’s–100’s m, such that an extensive drilling program is required to define mineralized from barren sections of the reef. Only about 38% of the reef horizon makes the current economic cut-off and is actually mined.

Extensive mining development by the Stillwater Mining Company has revealed a significant region in which Olivine-bearing Zone I (OB1) cuts down into the underlying rocks, locally reaching as far down as the lower parts of Norite Zone I just above the Ultramafic Series. Within this unconformable region, the thickness of OB I itself thins, such that at the deepest penetration into the underlying cumulates, there is a very rapid transition from Norite Zone I to Norite Zone II

overlying OB I. It is also observed that in the region of this unconformity, the olivine-rich layers of the Troctolite subzone change laterally into melanocratic gabbro-norite layers of Gabbro-norite Zone I.

Sulfide mineralization also occurs in the Picket Pin Pt–Pd zone (Boudreau & McCallum 1986), nearly 3 km stratigraphically higher, in the thickest and uppermost anorthosite of the Middle Banded series (Fig. 3-9). Grades are very erratic, but reach 3 g.t⁻¹. Elevated PGE concentrations are also associated with some of the chromitites of the Ultramafic Series, but values are again extremely erratic.

The J-M reef is Pd-rich, with a Pt/Pd value of 0.3, and has proven reserves of 2,778,000 tons and probable reserves of 32,864,000 tons, both containing 22 g.t⁻¹ of Pd + Pt (Stillwater Mining Company estimates from 2001–2002).

GREAT DYKE

The Great Dyke is an extremely long early Proterozoic intrusion, cutting across most of Zimbabwe and flaring upward (Wilson 1996). Despite its apparent dyke-like shape it has gently inward dipping layers of ultramafic rocks in its lower part and gabbroic rocks in the upper part. Detailed descriptions of the mineralization are reported by Prendergast and Keays (1988), Wilson *et al.* (1989, 2000) and Oberthür (2002). In the Great Dyke (Fig. 3-10a), PGE mineralization occurs close to the top of the ultramafic sequence, called the P1 pyroxenite (Fig. 3-10b). From axis to edge the thickness of this P1 pyroxenite decreases from 250 to 150 m. There is a broad, but low grade, mineralized zone 30–50 m thick near the middle of the P1, and a thinner, 2–8 m-thick zone with higher grade near the top. The uppermost portion of the P1 pyroxenite is a websterite that thins from 70 to 15 m from axis to edge. The Main Sulfide Zone, carrying the PGE, occurs at the base of this websterite. Mineralization in each of the sub-chambers is very similar, and the three mining and exploration areas report similar grades and metal distributions, about 5 g.t⁻¹ (*in situ*), and Pt/Pd value of 1.5.

Within the Main Sulfide Zone there is a clear separation of the base and precious metals, such that the basal half shows an upward increase in total PGE content, with only minor Cu and Ni enrichment, whereas in the upper half, the PGE content rapidly declines but the Cu and Ni content

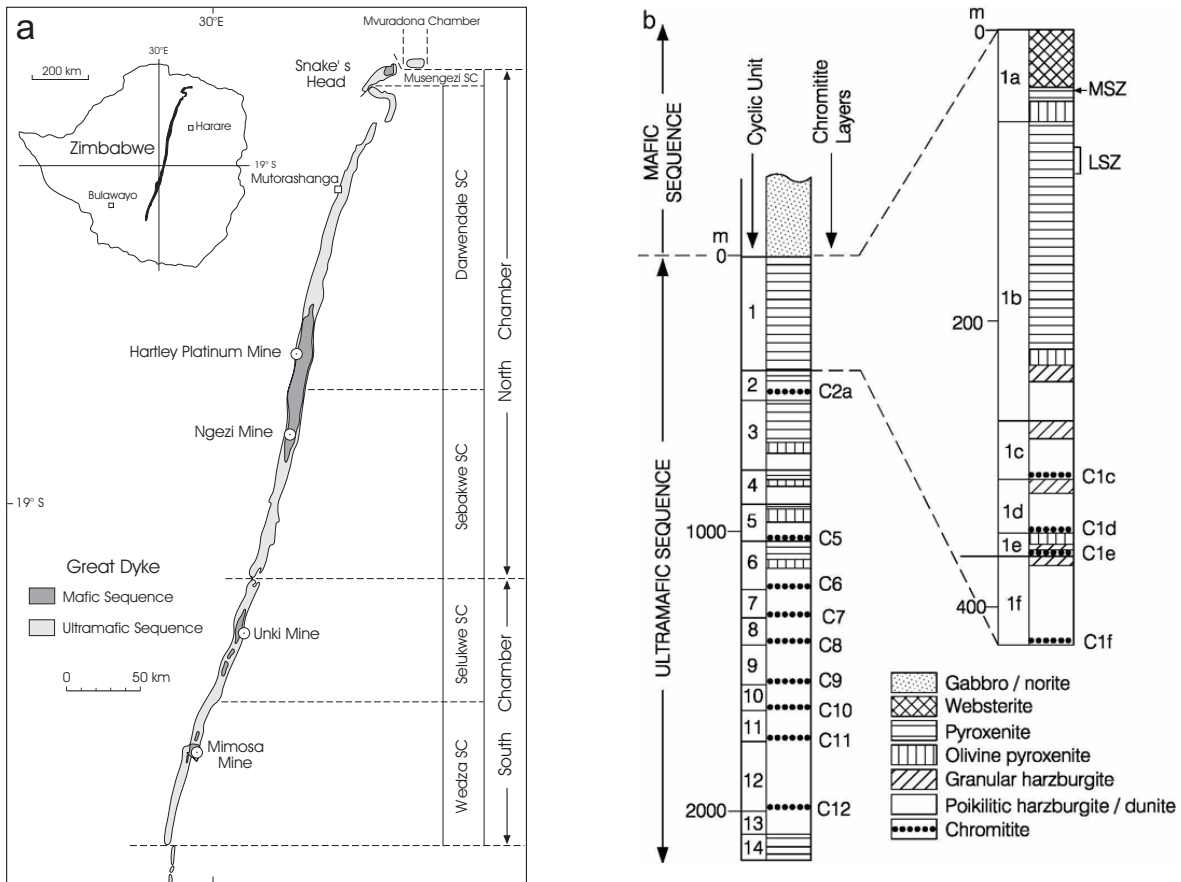


FIG. 3-10. a, Geology of the Great Dyke (from Oberthür & Melcher 2005); b, Stratigraphic section, indicating the Main Sulfide Zone (MSZ) and Lower Sulfide Zone (LSZ) (after Wilson 2001).

remain relatively high. There is an even more subtle separation of all the metals through this zone of mineralization, such that from base to top the highest concentration of the different metals occurs in the order Ir, Pd, Pt, Ni, Au, Cu (Wilson *et al.* 1989, 2000, Wilson 2001). Because highest PGE and sulfide contents do not correlate, delimiting a mining width is difficult.

MUNNI MUNNI INTRUSION

The Munni Munni intrusion is Archean in age, 9 by 25 km in preserved extent, with a shape similar to a tilted canoe (Barnes & Hoatson 1994). It has mineralization in a layer called the Ferguson Reef (Fig. 3-11), close to the boundary between an ultramafic lower half and gabbro-noritic upper portion (Barnes *et al.* 1992). The mineralized layer is a stratiform accumulation of PGE-enriched disseminated sulfides over an interval of 2–10 m within the top 20 m of the Porphyritic Websterite Zone along its entire exposed strike length, with

maximum total PGE grades up to 8 ppm over 50-cm widths, and 30 mt at 2.9 ppm Pt+Pd+Au (Barnes & Hoatson 1994). Like the Great Dyke it has vertical offsets between the highest base metal and PGE peaks.

SKAERGAARD INTRUSION

Mineralization in the 55 Ma Skaergaard Complex, Greenland, differs in one important aspect relative to those described above, in that the zone of mineralization systematically migrates laterally through a series of distinct silicate layers. A continuous zone of PGE mineralization, called the Platinova Reef (Fig. 3-12), occurs at the top of the Middle Zone in the Skaergaard Intrusion, in a package of rocks referred to as the Triple Group (Andersen *et al.* 1998). In fact, detailed mapping, drilling and assaying has indicated that there are four, not three, diffusely layered melagabbro to leucogabbros packages, each unit being 15 to 20 m thick. The lowest one is the most subtle in terms of

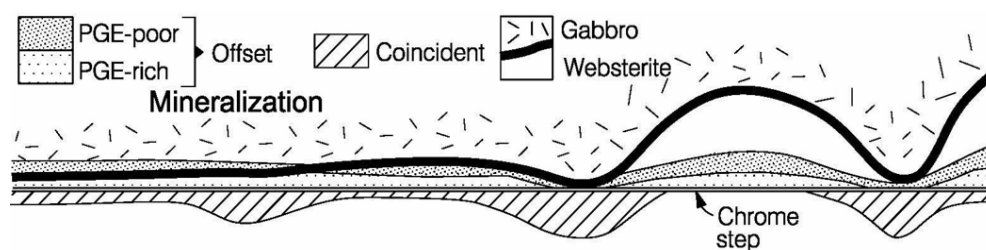


FIG. 3-11. Stratigraphic section through the mineralized layer of the Munni Munni intrusion (After Barnes & Hoatson 1994).

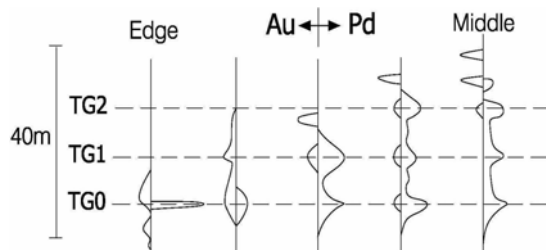


FIG. 3-12. Section through the Platinova Reef of the Skaergaard intrusion (after Anderson *et al.* 1998).

its layering, but hosts the stratigraphically lowest of the PGE reefs. The mineralization is dominated by Pd and Au, with maximum values over 1 m being about 5 g.t^{-1} . Several mineralized layers may be vertically stacked, but there are a number of complex relations. Within each unit, the mineralization is not restricted to any single lithological facies (melanocratic or leucocratic). When traced laterally towards the margin, total metal content (grade multiplied by thickness) decreases. The lateral extent of the mineralization also decreases upward through the succession, such that the outer rim of the upper mineralized zone is barren. The Pd/Au value decreases upward and the Pd/Pt value increases markedly upward and inward in each layer. The main sulfide mineral is bornite, which makes this mineralization very different from the other examples where pyrrhotite, chalcopyrite and pentlandite predominate.

CONTRASTS AND COMPARISONS

It is not possible to identify a common set of parameters unique to all PGE deposits, but some similarities appear common, although never diagnostic. Common features identified here contrast with some of those identified by Naldrett (1999) for the genesis of magmatic Ni–Cu sulfide deposits, in which PGE may be a significant byproduct.

Stratigraphic Association

Most chromitites in layered intrusions

contain a small but distinct PGE anomaly, those in the Stillwater having comparable grades to those in the Bushveld succession except the UG2 (Fig. 3-2). The uppermost chromitite layers of the Pantom Sill, Australia contain up to 6 g.t^{-1} , with a Pt/Pd value about unity (Hoatson 2000). The UG2 Chromitite is the only one that is mined. Values of $5\text{--}8 \text{ g.t}^{-1}$ of the UG2 are dwarfed by some values in the basal chromitite of the Merensky Reef where up to 50 g.t^{-1} were reported by Cawthorn *et al.* (2002b), although from an extremely thin sample.

Chromium content in magma related to these layered intrusions is about 1000 ppm and in chromitite 300,000 ppm. Hence, the processing of extremely large volumes of magma is required to produce a thick chromitite layer, analogous to the R-factor in PGE modeling (Campbell & Naldrett 1979), but insignificant PGE contents are rarely exceeded in most chromitite layers. Uniquely high Pt and high total PGE contents cannot be attributed solely to some chromite-associated process, because the Platreef has moderately high Pt without the necessary association with chromite, and the Main Sulfide Zone of the Great Dyke and the J-M Reef also have high PGE with no significant chromite present.

The Merensky and UG2 Chromitite Reefs occur in a succession of strongly layered pyroxenitic, noritic and anorthositic rocks, overlying a thick succession of ultramafic rocks (Fig. 3-1). This location prompted the development of a model that depended critically upon the density of primitive and evolved magmas (Campbell *et al.* 1983). Its validity appeared to be confirmed by the identification of the J-M Reef, again in a mixed succession of melanocratic and leucocratic rocks above an ultramafic succession. However, this geometry is not carried through into the Great Dyke and Munni Munni intrusions, where the mineralization occurs at the very top of the ultramafic successions. The Platinova Reef is even more distinct in occurring in magnetite gabbros.

Mineral Compositions

A commonality exists for the first four intrusions mentioned, in that the hanging wall succession is a gabbro-norite (with some olivine in the Stillwater Complex). Furthermore, these and other PGE-bearing bodies usually have orthopyroxene as a major constituent, and the second mineral to crystallize after olivine in the lower succession. Olivine followed by plagioclase, and olivine followed by clinopyroxene are magmatic trends that become more important close to the J-M and Ferguson Reefs respectively, whereas orthopyroxene with and without plagioclase are found through the UG2–Merensky and Main Sulfide Zone successions. Remarkably, the footwall rocks to all these deposits have orthopyroxene with mg# of 80–82 and 0.3–0.4% Cr₂O₃, and a hanging wall in which the minerals are more evolved (Fig. 3-13). Again, the Platinoval Reef is distinct in being much more evolved.

The initial Sr isotopic ratio shows a distinct break close to the Merensky Reef (Kruger & Marsh 1982), indicating addition of magma of a distinct and different lineage. No such isotopic distinctions exist for other intrusions, but the decrease in mg# and Cr content indicates addition of a more evolved (not more primitive as in the model of Naldrett & von Gruenewaldt 1989) magma in each case. Why such new magma should always be added when the earlier magma had reached the same stage of differentiation remains to be explained. A contradiction also appears in that the mineralized layers (except for the UG2) in all four intrusions occur where the low-Cr (and low-PGE?) magma is introduced, begging the question as to the source magma for the PGE.

A very different set of mineral chemical

information is offered by data on the Cl content of apatite (and other hydrous minerals). The entire lower halves of the Bushveld and Stillwater Complexes contain apatite enriched in Cl, in strong contrast to the succession overlying the mineralized layers (Boudreau, 1995). However, such chemical characteristics do not occur for the Great Dyke or Munni Munni, and there is no evidence of Cl enrichment in apatite from the Skaergaard.

Within-Reef Fractionation of the PGE

A double challenge to the mining in the Great Dyke lies in the facts that the mineralized layer lies entirely within a much thicker homogeneous pyroxenite, and that the main concentration of sulfide that might be expected to be a useful guide to PGE actually overlies the highest PGE grades. This feature has been referred to as an "offset" (Fig. 3-14), referring to the disassociation of base metals from PGE. Even within these offsets, the different PGE are slightly separated.

In the Ferguson Reef, two sulfide-bearing layers are present in the area of highest PGE grades. The lower layer has lower PGE-in-sulfide tenors but generally higher grades, and is characterised by coincidence of peak Cu, Ni, S and PGE abundances (Fig. 3-14). The upper half is variable in composition, strongly PGE-enriched at the base and depleted at the top, and characterized by systematic vertical offsets between the peak PGE and Cu abundances. The "offset" sulfides always occur immediately above the "coincident" sulfides (Barnes 1993). Coincident sulfides, and the higher overall PGE grades within the reef, are restricted to a strike extent of about 3 km centered on a dike-like feature interpreted as the feeder conduit to the websterite and overlying gabbros.

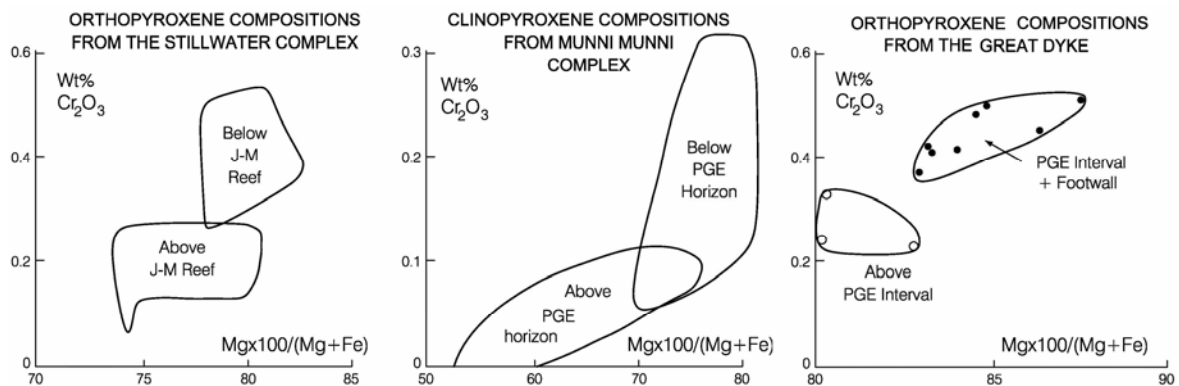


FIG. 3-13. Values for mg# and Cr contents of pyroxenes straddling major PGE-mineralized layers, J-M Reef (Barnes & Naldrett 1986), Ferguson Reef (Barnes & Hoatson 1994) and Main Sulfide Zone (Wilson 1996).

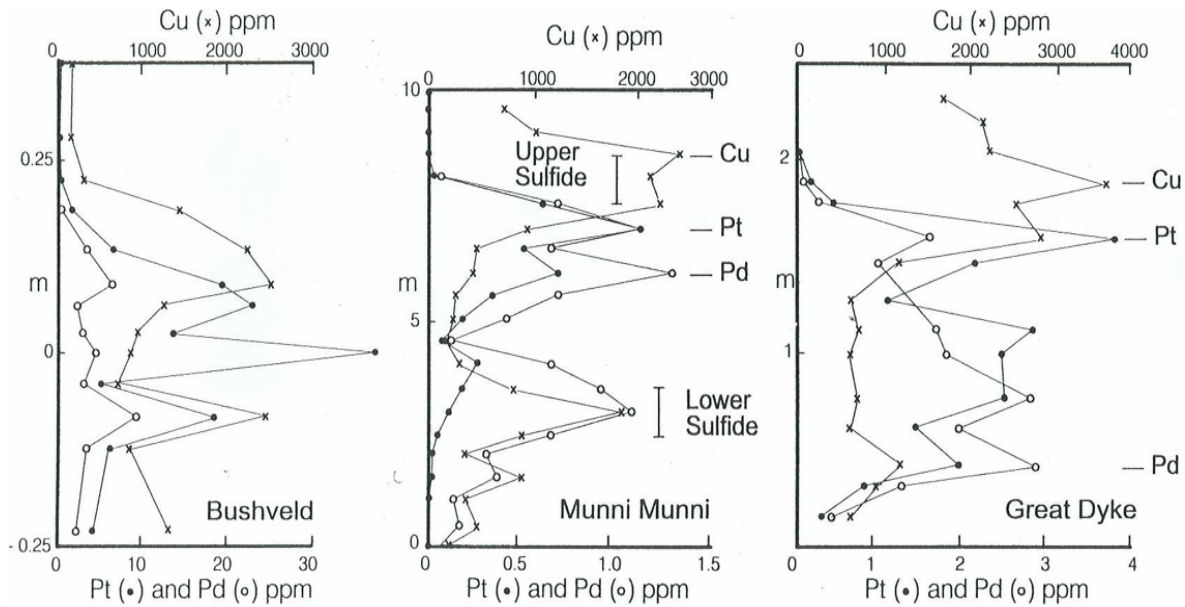


FIG. 3-14. Distribution of Pt, Pd and Cu through so-called "Offsets" in Great Dyke (Wilson *et al.* 1989) and Munni Munni (Barnes 1993) contrasted with "coincident" peaks in the Bushveld Complex (Barnes and Maier, 2002b).

The Platinova Reef displays an even greater separation of base metals and Pd, the Pt content being almost insignificant (Fig. 3-12). Upward displacement of residual sulfide over several metres was suggested by Andersen *et al.* (1998), although the high Cu/S values and presence of abundant bornite suggest that sulfur loss or hydrothermal oxidation was concomitant. An even more extreme case of offsets has been proposed by Prendergast (2000) for the Rincon del Tigre (Bolivia) where base metal and Pd peaks are separated by over 50 m vertically. The complexities for exploration as a result of this disassociation of PGE from sulfides are obvious.

In contrast to these offsets, there is no systematic vertical displacement of the PGE (and Cu) in the Merensky Reef or UG2 (Fig. 3-14). Also in the UG2 (Fig. 3-7) up to three cycles of PGE enrichment may occur in the layer, but the respective peaks for Pt and Pd (of different relative magnitudes) all occur at the same levels. Also, detailed sampling through the footwall mineralization and J-M Reef of the Stillwater appears to show two layers of mineralization, both with a good correlation between PGE, Cu and S (Fig. 9 of Zientek *et al.* 2002).

In the Merensky Reef a rather different distribution for Pt and Pd occur. Barnes & Maier (2002b) showed that PGE and base metals were closely correlated. However, variations in Pt/Pd do

occur (Fig. 3-15). High Pt/Pd values and absolute abundances occur associated with each chromitite layer, while oxide-poor, sulfide-bearing samples have a different Pt/Pd ratio and lower total PGE abundance, suggesting a derivation by two different processes (chromite association and sulfide-

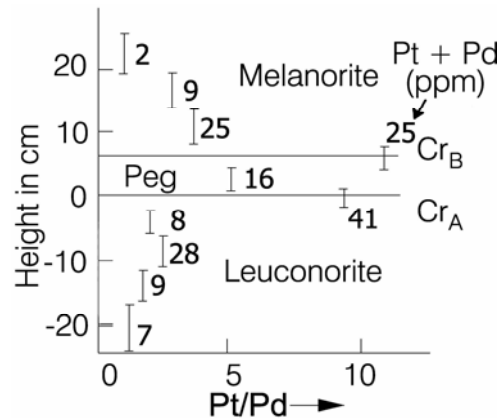


FIG. 3-15. PGE grade and Pt/Pd values through one section of the Merensky Reef from Impala Mine (from Barnes & Maier 2002a). Vertical bars indicate Pt/Pd value for sample over that vertical distance. The number beside vertical bar is absolute Pt+Pd value in ppm. High Pt/Pd values and absolute grade are associated with chromitite layers compared to the sulfide-hosted mineralization, and suggest that there are two discrete mineralizing events, one associated with chromite and one associated with sulfide.

association). The PGE associated with chromite is due to a concurrent accumulation with chromite, whereas the sulfide-associated PGE settled through a maximum of 1 m of unconsolidated crystal mush (Cawthorn 1996), without fractionating the PGE. Such restriction in post-cumulus (downward) migration results in a much more localized and more easily identifiable exploration target.

Cu/Pd values

A final comment about host rock geochemistry is warranted. Systematic sampling through long sections of the mineralized layered intrusions has indicated that there are breaks in the Cu/Pd value. Increases in this ratio close to the Merensky Reef (Fig. 3-16), Main Sulfide Zone of the Great Dyke and the Ferguson Reef at Munn Munn have been used to suggest that this parameter can be used as a marker for the level of mineralization (Barnes & Maier 2002a). There is, however, no major break above the UG2 (Fig. 3-16). It is claimed that high PGE tenors in these reefs are the result of processing of extremely large volumes of magma – the R-factor of Campbell & Naldrett (1979). In this hypothesis, such a large volume of magma is processed that the PGE content of the remaining magma is insignificantly depleted by the mineralizing event. If this were the case, then there is no apparent reason for the distinct increase in Cu/Pd value above all mineralized layers.

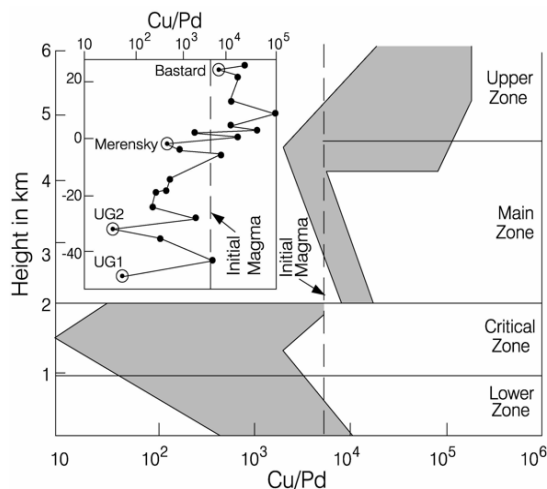


FIG. 3-16. Plot of whole-rock Cu/Pd in the Bushveld Complex (from Maier & Barnes 1999). Two scales are shown. The main diagram shows summarized data for the entire intrusion. The inset shows data from the UG1 chromitite to just above the Bastard unit. Note the increase in Cu/Pd value by an order of magnitude immediately above the Merensky Reef.

SUMMARY

Many examples of the world's major Pt and Pd economic mineralization are hosted in extremely well-defined stratiform reefs occurring towards the centre of large layered intrusions. In the Bushveld Complex (South Africa), the Great Dyke (Zimbabwe), and the Stillwater Complex (USA) are major mining activities, but other examples that are currently not economic display similar features and presumably reflect similar processes in their genesis. In most cases the PGE are associated with primary magmatic sulfides with interstitial textures to the silicate host. PGE, Cu, Ni and S are strongly correlated in the Merensky and J-M Reefs, but the base metal peaks are displaced upward in the Main Sulfide Zone of the Great Dyke and Ferguson Reef. In the first two examples, a specific sequence of layered rocks is recognizable, but the PGE mineralization is not confined to a single rock type. In the second two examples, mineralization occurs within a thicker lithologically homogeneous zone. Chromite-hosted mineralization is also an important association. In chromitite layers the PGE association is very strictly defined by the host lithology.

Common parameters that may characterize most of such occurrences, include (i) mainly late Archean-Proterozoic age, (ii) evidence of addition of a more differentiated magma, (iii) footwall successions containing orthopyroxene as a major mafic mineral, (iv) increase in Cu/Pd values above the reefs, (v) chlorine-enriched minerals in the footwall. However, exceptions occur to all of these criteria, as shown by the Skaergaard Complex.

ACKNOWLEDGEMENTS

The writer has been able to pursue his interests in the Bushveld Complex and its mineralization thanks to the generous support of Implats, Lonplats and Angloplats mining companies, and the National Research Foundation, South Africa. Reviews by Tony Naldrett, Jim Mungall and an anonymous referee are appreciated.

REFERENCES

- ALAPIETI, T.T. & LAHTINEN, J.J. (1986): Stratigraphy, petrology and platinum-group element mineralization of the early Proterozoic Penikat layered intrusion, northern Finland. *Econ. Geol.* **81**, 1126-1136.
- ALAPIETI, T.T. & LAHTINEN, J.J. (2002): Platinum-

- group element mineralization in layered intrusions of northern Finland and the Kola Peninsula, Russia. *In* The geology, geochemistry, mineralogy and beneficiation of platinum-group elements. (L.J. Cabri, ed.). *Can. Inst. Mining Metall. Petrol., Spec. Vol.* **54**, 507-546.
- ANDERSEN, J.C.O., RASMUSSEN, H., NIELSEN, T.F.D. & RONSBO, J.G. (1998): The Triple Group and the Platinova Gold and Palladium Reefs In the Skaergaard Intrusion – stratigraphic and petrographic relations. *Econ. Geol.* **93**, 488-509.
- BARNES, S.J. (1993): Partitioning of the platinum group elements and gold between silicate and sulphide magmas in the Munni Munni Complex, Western Australia. *Geochim. Cosmochim. Acta* **57**, 1277-1290.
- BARNES, S.J. & HOATSON, D.M. (1994): The Munni Munni Complex: Western Australia: stratigraphy, structure and petrogenesis. *J. Petrol.* **35**, 715-751.
- BARNES, S.J. & NALDRETT, A.J. (1986): Geochemistry of the J-M Reef of the Stillwater Complex, Minneapolis adit area. II. Silicate mineral chemistry and petrogenesis. *J. Petrol.* **27**, 791-825.
- BARNES, S.J., KEAYS, R.R. & HOATSON, D.M. (1992): Distribution of sulphides and PGE within the porphyritic websterite zone of the Munni Munni Complex, Western Australia. *Austral. J. Earth Sci.* **39**, 289-302.
- BARNES, S.-J. & FRANCIS, D. (1995): The distribution of platinum-group elements, nickel, copper and gold in the Muskox layered intrusion, Northwest Territories, Canada. *Econ. Geol.* **90**, 135-154.
- BARNES, S.-J. & MAIER, W.D. (2002a): Platinum-group element distribution in the Rustenburg Layered Suite of the Bushveld Complex, South Africa. *In* The geology, geochemistry, mineralogy and beneficiation of platinum-group elements (L.J. Cabri, ed.). *Can. Inst. Mining Metall. Petrol., Spec. Vol.* **54**, 431-458.
- BARNES, S.-J. & MAIER, W.D. (2002b): Platinum-group elements and microstructures from Impala Platinum Mines, Bushveld Complex. *J. Petrol.* **43**, 171-198.
- BOUDREAU, A.E. (1995): Some geochemical considerations for platinum-group-element exploration in layered intrusions. *Explor. Mining Geol.* **4**, 215-225.
- BOUDREAU, A.E. & MCCALLUM, I.S. (1986): Investigations of the Stillwater Complex: III. The Picket Pin Pt/Pd deposit. *Econ. Geol.* **81**, 1953-1975.
- BOW, C., WOLFRAM, D., TURNER, A., BARNES, S., EVANS, J., ZDEPSKI, M. & BOUDREAU, A. (1982): Investigations of the Howland Reef of the Stillwater Complex, Minneapolis adit area: stratigraphy, structure and mineralization. *Econ. Geol.*, **77**, 1481-1492.
- CAMPBELL, I.H. & NALDRETT, A.J. (1979): The influence of the silicate: sulfide ratios on the geochemistry of magmatic sulfides. *Econ. Geol.* **74**, 1503-1505.
- CAMPBELL, I.H., NALDRETT, A.J. & BARNES, S.J. (1983): A model for the origin of the platinum-rich sulfide horizons in the Bushveld and Stillwater Complexes. *J. Petrol.* **24**, 133-165.
- CAWTHORN, R.G. (1996): Re-evaluation of magma compositions and processes in the uppermost Critical Zone of the Bushveld Complex. *Mineral. Mag.* **60**, 131-148.
- CAWTHORN, R.G. (1999): The platinum and palladium resources of the Bushveld Complex. *S. Afr. J. Sci.* **95**, 481-489.
- CAWTHORN, R.G. & BARRY, S.D. (1992): The role of intercumulus residua in the formation of pegmatoid associated with the UG2 Chromitite, Bushveld Complex. *Austral. J. Earth Sci.* **39**, 263-276.
- CAWTHORN, R.G., MERKLE, R.K.W. & VILJOEN, M.J. (2002a): Platinum-group element deposits in the Bushveld Complex, South Africa. *In* The geology, geochemistry, mineralogy and beneficiation of platinum-group elements (L.J. Cabri, ed.). *Can. Inst. Mining Metall. Petrol., Spec. Vol.* **54**, 389-430.
- CAWTHORN, R.G., LEE, C.A., SCHOUWSTRA, R. & MELLOWSHIP, P. (2002b): Relations between PGE and PGM in the Bushveld Complex. *Can. Mineral.* **40**, 311-328.
- DAVEY, S.R. (1992): Lateral variations within the upper Critical Zone of the Bushveld Complex on the farm Rooikoppies 297 JQ, Marikana, South Africa. *S. Afr. J. Geol.* **95**, 141-149.

- EALLES, H.V. & CAWTHORN, R.G. (1996): The Bushveld Complex. *In Layered Intrusions* (R.G. Cawthorn, ed.). Elsevier, Amsterdam, 181-225.
- GAIN, S.B. (1985): The geologic setting of the platinumiferous UG2 Chromitite layer on Maandagshoek, eastern Bushveld Complex. *Econ. Geol.* **80**, 925-943.
- HAHN, U.F. & OVENDALE, B. (1994): UG2 Chromitite layer potholes at Wildebeestfontein North Mine, Impala Platinum Limited. *Proc. S. Afr. Inst. Mining Metall.* **3**, 195-200.
- HAMILTON, P.J. (1977): Sr isotope and trace element studies of the Great Dyke and Bushveld mafic phase and their relation to early Proterozoic magma genesis in southern Africa. *J. Petrol.* **18**, 24-52.
- HIEMSTRA, S.A. (1985): The distribution of some platinum-group elements in the UG2 Chromitite layer of the Bushveld Complex. *Econ. Geol.* **80**, 944-957.
- HIEMSTRA, S.A. (1986): The distribution of chalcophile and platinum-group elements in the UG2 Chromitite layer of the Bushveld Complex. *Econ. Geol.* **81**, 1080-1086.
- HOATSON, D.M. (2000): Mineralisation and economic potential of the mafic-ultramafic intrusions. *In Geology and Economic Potential of the Palaeoproterozoic Layered Mafic-Ultramafic Intrusions in the East Kimberley, Western Australia* (D.M. Hoatson & D.H. Blake, eds.). Australian Geological Survey Organisation Bulletin, Canberra, **246**, 278-311.
- ILJINA, M. & LEE, C.A. (2005): Marginal series-hosted PGE deposits. *In Exploration for Platinum-group Element Deposits* (J.E. Mungall, ed.). *Mineral. Assoc. Canada, Short Course* 35, 75-96.
- KRUGER, F.J. & MARSH, J.S. (1982): Significance of $^{87}\text{Sr}/^{86}\text{Sr}$ ratios in the Merensky Cyclic Unit of the Bushveld Complex. *Nature* **298**, 53-55.
- LEE, C.A. (1983): Trace and platinum-group element geochemistry and the development of the Merensky Reef of the Bushveld Complex. *Mineral. Deposita* **18**, 173-180.
- LEE, C.A. (1996): A review of mineralization in the Bushveld Complex and some other layered mafic intrusions. *In Layered Intrusions* (R.G. Cawthorn, ed.). Elsevier, Amsterdam, 103-146.
- LEE, C.A. & PARRY, S.J. (1988): Platinum-group element geochemistry of the Lower and Middle Group chromitites of the eastern Bushveld Complex. *Econ. Geol.* **83**, 1127-1139.
- LOMBERG, K.G., MARTIN, E.S., PATTERSON, M.A. & VENTER, J.E. (1999): The morphology of potholes in the UG2 Chromitite layer and Merensky Reef (pothole reef facies) at Union Section, Rustenburg Platinum Mines. *S. Afr. J. Geol.* **102**, 209-220.
- MAIER, W.D. & BARNES, S.-J. (1999): Platinum-group elements in silicate rocks of the Lower, Critical and Main Zones at Union Section, western Bushveld Complex. *J. Petrol.* **40**, 1647-1672.
- NALDRETT, A.J. (1999): World-class Ni-Cu-PGE deposits: key factors in their genesis. *Mineral. Deposita* **34**, 227-240.
- NALDRETT, A.J. & VON GRUENEWALDT, G. (1989): Association of platinum-group elements with chromitite in layered intrusions and ophiolite complexes. *Econ. Geol.* **84**, 180-187.
- OBERTHÜR, T. (2002): Platinum-group element mineralization of the Great Dyke, Zimbabwe. *In The geology, geochemistry, mineralogy and beneficiation of platinum-group elements* (L.J. Cabri, ed.). *Can. Inst. Mining, Metall. Petrol., Spec. Vol.* **54**, 483-506.
- OBERTHÜR, T. & MELCHER, F. (2005): PGE and PGM in the supergene environment: a case study of persistence and redistribution in the Main Sulfide Zone of The Great Dyke, Zimbabwe. *In Exploration for Platinum-group Element Deposits* (J.E. Mungall, ed.). *Mineral. Assoc. Canada, Short Course* 35, 97-111.
- PECK, D.C., SCOATES, R.F.J., THEYER, P., DESHARNIS, G., HULBERT, L.J. & HUMINICKI, M.A.E. (2002): Stratiform and contact-type PGE-Cu-Ni mineralization in the Fox River sill and the Bird River belt, Manitoba. *In The geology, geochemistry, mineralogy and beneficiation of platinum-group elements* (L.J. Cabri, ed.). *Can. Inst. Mining Metall. Petrol., Spec. Vol.* **54**, 367-388.
- PRENDERGAST, M.D. (2000): Layering and Precious Metals mineralization in the Rincon del Tigre Complex, eastern Bolivia. *Econ. Geol.* **95**, 113-130.

- PRENDERGAST, M.D. & KEAYS, R.R. (1988): Controls of platinum-group element mineralization and the origin of the PGE-rich Main Sulphide Zone in the Wedza Subchamber of the Great Dyke, Zimbabwe. *In* Magmatic sulphides – the Zimbabwe volume (M.D. Prendergast & M.J. Jones, eds.). *Inst. Mining Metall.* 43-70.
- RAEDEKE, L.D. & VIAN, R.W. (1986): A three-dimensional view of mineralization in the Stillwater J-M Reef. *Econ. Geol.* **81**, 1187-1195.
- SCOON, R.N. & TEIGLER, B. (1994): Platinum-group element mineralization in the Critical Zone of the western Bushveld Complex: I. Sulfide-poor chromitites below the UG2. *Econ. Geol.* **89**, 1094-1121.
- TODD, S.G., KEITH, D.W., LEROY, L.W., SHISSEL, D.J., MANN, E.I. & IRVINE, T.N. (1982): The J-M platinum-palladium Reef of the Stillwater Complex, Montana: I. Stratigraphy and petrology. *Econ. Geol.* **77**, 1454-1480.
- VERMAAK, C.F. (1976): The Merensky Reef – thoughts on its environment and genesis. *Econ. Geol.* **71**, 1270-1298.
- VILJOEN, M.J. (1999): The nature and origin of the Merensky Reef of the western Bushveld Complex based on geological facies and geophysical data. *S. Afr. J. Geol.* **102**, 221-239.
- VIRING, R.G. & COWELL, M.W. (1999): The Merensky Reef on Northam Platinum Limited. *S. Afr. J. Geol.* **102**, 192-208.
- VON GRUENEWALDT, G., DICKS, D., DE WET, J. & HORSCH, H. (1990): PGE mineralization in the western sector of the eastern Bushveld Complex. *Mineral. Petrol.* **42**, 71-95.
- VON GRUENEWALDT, G., HATTON, C.J., MERKLE, R.K.W. & GAIN, S.B. (1986): Platinum-group element – chromite associations in the Bushveld Complex. *Econ. Geol.* **81**, 1067-1079.
- WAGNER, P.A. (1929): *The Platinum Deposits and Mines of South Africa*. Oliver and Boyd, Edinburgh, 326 pp.
- WHITE, J.A. (1994): The Potgietersrus prospect – geology and exploration history. *Proc. S. Afr. Inst. Mining Metall.* **3**, 173-181.
- WILSON, A.H. (1996): The Great Dyke of Zimbabwe. *In* Layered Intrusions (R.G. Cawthorn, ed.). Elsevier, Amsterdam, 365-402.
- WILSON, A.H. (2001): Compositional and lithological controls on the PGE-bearing sulphide zones in the Selukwe Subchamber, Great Dyke: a combined equilibrium-Rayleigh fractionation mode. *J. Petrol.* **42**, 1845-1867.
- WILSON, A.H., MURAHWI, C.Z. & COGHILL, B.H. (2000): The geochemistry of the PGE Subzone in the Selukwe subchamber, Great Dyke: An intraformational layer model for platinum-group element enrichment in layered intrusions. *Mineral. Petrol.* **68**, 115-140.
- WILSON, A.H., NALDRETT, A.J. & TREDOUX, M. (1989): Distribution and controls of platinum-group element and base metal mineralization in the Darwendale Subchamber of the Great Dyke, Zimbabwe. *Geology* **17**, 649-652.
- ZIENTEK, M.L., COOPER, R.W., CORSON, S.R. & GERAGHTY, E.P. (2002): Platinum-group element mineralization in the Stillwater Complex, Montana. *In* The geology, geochemistry, mineralogy and beneficiation of platinum-group elements (L.J. Cabri, ed.). *Can. Inst. Mining Metall. Petrol., Spec. Vol.* **54**, 459-482.
- ZIENTEK, M.L., CORSON, S.R. & WEST, R.D. (2005): Discovery of the J-M Reef, Stillwater Complex, Montana: the role of soil and silt platinum and palladium geochemical surveys. *In* Exploration for Platinum-group Element Deposits (J.E. Mungall, ed.). *Mineral. Assoc. Canada, Short Course* 35, 391-407.

CHAPTER 4: PGE DEPOSITS IN THE MARGINAL SERIES OF LAYERED INTRUSIONS

Markku J. Iljina
Geological Survey of Finland,
PO Box 77, FI-96101 Rovaniemi, Finland
E-mail: markku.iljina@gsf.fi

Christopher A. Lee
Ridge Mining, 5 Harrowdene Office Park,
Western Service Road, Woodmead, 2191, South Africa

INTRODUCTION

Below is a summary of geological, geochemical and geophysical signatures of ore deposits which are located at the contacts of layered mafic intrusions. Examples are presented from Portimo and Koillismaa (Tornio-Näränkäväära Belt, Finland), Platreef and Sheba's Ridge (Bushveld Complex, South Africa) and East Bull Lake and River Valley (East Bull Lake Intrusive Suite, Canada). The examples included here are PGE-dominated base-metal sulfide deposits where the precious metals are the most important for the economics of the deposit.

It is hoped that listing the features of these deposits will help exploration geologists to recognize critical features when planning and conducting the various phases of exploration. The first and most critical step in all exploration is choosing area for exploration at the province or formation scale. The second step is definition of targeted deposit models. It is hoped that this paper will contribute to this stage of the exploration in particular. The exploration methods are very similar for any type of metal exploration. They include areal and regional geophysical and geochemical tools and preliminary or scout drilling. The exploration model can facilitate the choice of proper sampling or measurement intervals and various pathfinders. The exploration methods used depend on several geographic factors, some of which are listed in Table 4-1.

PORTIMO AND KOILLISMAA MARGINAL SERIES DEPOSITS

Portimo Stratigraphy and Structure

The Portimo Layered Igneous Complex (Portimo Complex) is part of the *ca.* 2450 Ma old and approximately 300 km long belt of layered intrusions which crosses Finland almost along the

Arctic Circle and also extends into Sweden and Russia (Fig. 4-1). This belt, consisting of about 10 intrusions, is known as the Tornio-Näränkäväära Belt (TNB) and it is an example of a major failed rift system. Furthermore, the TNB contains roughly one third of the *ca.* 2450 Ma layered intrusions of the Fennoscandian Shield.

The Portimo Layered Igneous Complex (Fig. 4-1) is composed of four principal structural units (modified after Iljina 1994):

- the Narkaus intrusion
- the Suhanko intrusion
- the Konttijärvi intrusion
- the Portimo Dykes

Each intrusion contains a marginal series and an overlying layered series. The marginal series of the Suhanko and Konttijärvi intrusions have a different thickness and prevailing rock types from that of the Narkaus intrusion. The Narkaus marginal series varies from about 10 to 20 metres in thickness, whereas the Suhanko and Konttijärvi marginal series is typically several tens of metres in thickness. The Narkaus marginal series is mainly composed of pyroxenite, whereas olivine cumulates generally make up the upper half of the Suhanko and Konttijärvi marginal series (Fig. 4-2). The metamorphic alteration of cumulates is pervasive, which, for example, prevents the study of the mineral chemistry.

The principal difference between the layered series overlying the marginal series of the intrusions is the presence of marked reversals in the Narkaus intrusion, as shown by the thick ultramafic olivine-rich cumulate layers, whereas crystallization in the Suhanko and Konttijärvi intrusions continued without any notable reversals (Fig. 4-2). The major reversals in the Narkaus layered series resemble those of the Penikat intrusion and enable its layered series to be divided into three megacyclic units

TABLE 4-1. GEOGRAPHIC FACTORS AND RELATED EXPLORATION METHODOLOGY

Climate	Landscape	Geochemical	Geophysical
Tropical	Deep <i>in situ</i> soil	Soil, rock, soil profile and stream sediment sampling	Magnetics/IP/EM
Temperate	Residual	As above	As above
Semi-desert	Residual with lag of heavy mineral	Sampling of magnetic lag, geochemistry of wind-winnowed material	As above
Temperate to Cold	Till; transported soils, alluvium	Till geochemistry, boulder sampling with transport directions deduced. Bio-geochemistry.	Aeromagnetic and EM mapping for possible source anomalies
Any	Dissected	Drainage heavy mineral sampling, rock geochemistry.	As above

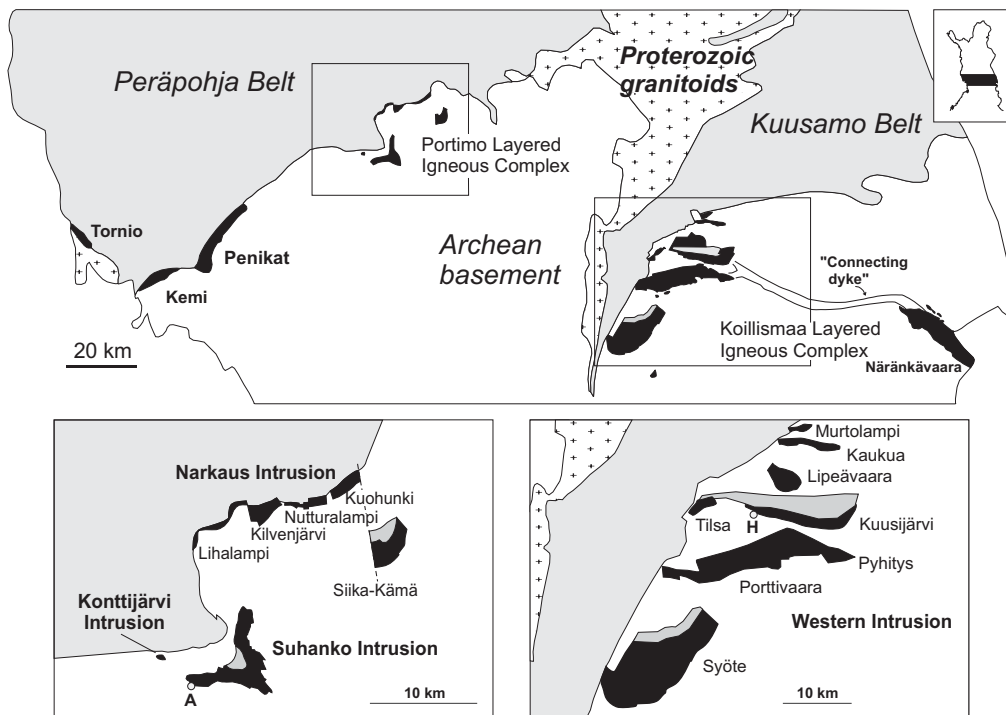


FIG. 4-1. Mafic-ultramafic layered intrusions (black) in the Tornio-Näränkäväära Belt. The white areas are mainly Archean gneisses and the grey indicates Proterozoic domains. Insets show the distribution of intrusions and intrusion blocks of the Portimo (left) and Koillismaa Layered Igneous Complexes. The location of the Ahmavaara (A) and Haukiaho (H) deposits are also indicated. The 'connecting dyke' in the Koillismaa area refers to a strong magnetic and gravimetric anomaly joining the Näränkäväära intrusion to the Pyhitys and Kuusijärvi blocks of the Western Intrusion.

(MCU, Fig. 4-2). These megacyclic units are a result of major influxes of mafic magma into the chamber. These kinds of sequential magma influxes and the significant differences between subsequent chemical compositions of incoming magmas are features of both the Portimo and Bushveld Complexes. In Portimo the MCU I and MCU II crystallized from Mg-Cr-richer magma whereas Mg-Cr-poorer magma made up MCU III and the

entire Suhanko and Konttijärvi intrusions. The Mg-Cr-richer magma type produced the Portimo Dykes in the Ahmavaara and Konttijärvi regions.

Mafic and ultramafic Portimo Dykes can be found in the basement below the Konttijärvi intrusion and in the Ahmavaara area of the Suhanko intrusion. They have also been found as fragments in the marginal series of Konttijärvi (Fig. 4-3). The dykes have not been dated and their link to the same

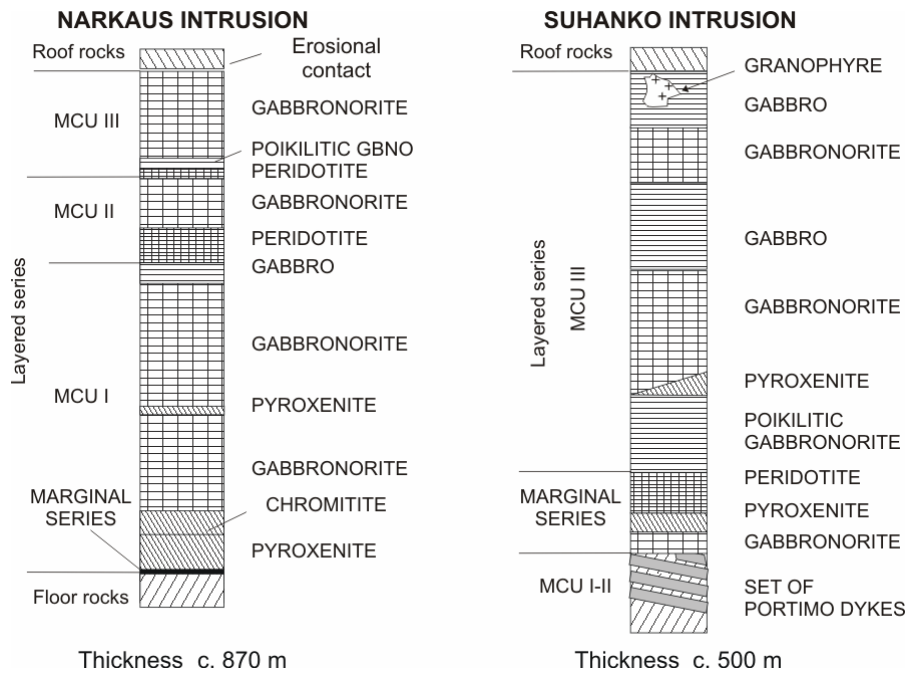


FIG. 4-2. Cumulus stratigraphies of the Narkaus and Suhanko Intrusions.



FIG. 4-3. Large blocks of Portimo Dykes in the olivine cumulate (darker) of the Konttijärvi marginal series. Photo by M. Iljina.

magmatic event as the main intrusions is based on geochemical observations. The dykes are subparallel to the basal contact of the intrusion and merge with it locally, so that a dyke can actually form the basement of the intrusion. It has also been verified that the marginal series cross-cuts the Portimo Dyke on an outcrop.

The layered series cumulus sequences of the

small Konttijärvi intrusion and the western end of the Suhanko intrusion (Ahmavaara section) resemble one another. Pyroxenite, which separates the lowermost poikilitic orthocumulate from the overlying gabbroic adcumulate, is over tens of metres thick in both sections and makes up about one fifth of the whole Konttijärvi layered series. The gabbroic rocks of the Konttijärvi marginal

series are, in fact, mostly pyroxene cumulates with variable portions of felsic material introduced by floor rock contamination. This and the thick layered series pyroxenite make the present day Konttijärvi stratigraphy largely ultramafic when cumulus terminology is applied. The lower contact of the Konttijärvi intrusion is also unique in the TNB intrusions. Below the lowermost more homogenous cumulate there is a thick Mixing Zone, which in some places is up to approx. 150 m wide (Fig. 4-4). The combined thickness of the Konttijärvi marginal and layered series is only slightly more (approx. 160 m) than this Mixing Zone.

The *Mixing Zone* is made up of a rock type termed 'hybrid gabbro' and of banded gabbro (Fig. 4-5). The 'hybrid gabbro' is characterized by grain

size variations from fine to medium and also contains an almost assimilated felsic contaminant. Further away from the intrusion the hybrid gabbro turns into the banded gabbro, which according to outcrop evidence, is recrystallized banded Archean quartz dioritic gneiss which still has a primary folded texture but gabbroic mineralogy (Fig. 4-5). Contacts between homogenous gabbro (of marginal series proper), hybrid gabbro and banded gabbro are arbitrary but the hybrid and banded gabbros are included in the basement domain in this paper. This division is due to the pattern that in many drill holes there are several sections of hybrid and banded gabbros (1–20 m in length) right next to each other, so that the two gabbro types together form a distinctive, mappable unit. This unit also contains

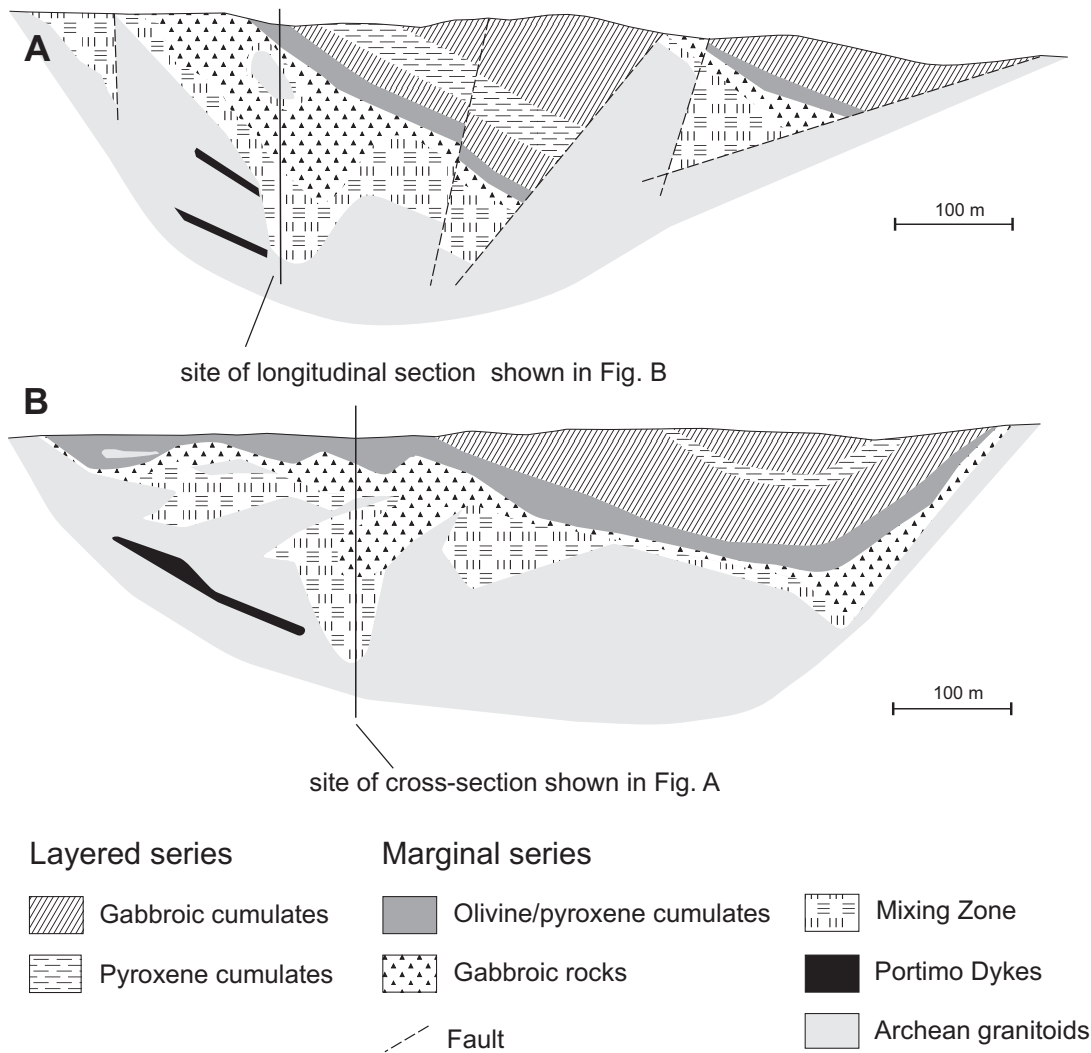


FIG. 4-4. Cross-section (A) and longitudinal section (B) of the Konttijärvi body.

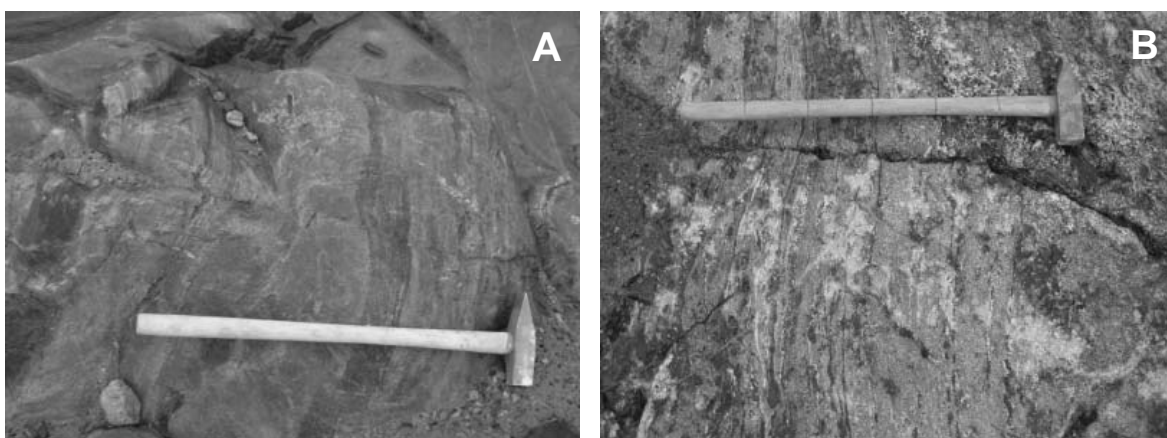


FIG. 4-5. Two outcrop photographs depicting unaltered banded Archean gneiss (A) and banded gabbro. The recrystallization into gabbro has progressed along the primary banding. Close to the right end of the hammer (B) there is an irregular area of unbanding, where banding has disappeared. Photos by Iljina.

basement gneiss blocks which are up to several tens of metres in size. The Mixing Zone 'gabbros' appear to be a result of the mechanical mixing of melted Archean gneiss and mafic magma and also the metasomatic recrystallization of the basement gneiss into mafic gneiss. The Mixing Zone seems to dip to form a depression structure, some tens of metres in diameter (Fig. 4-4) at the center of the Konttijärvi igneous body.

Diverse Portimo sulfide-PGE mineralizations

The Portimo Complex is exceptional among the layered intrusions as it hosts a variety of PGE mineralization styles (Figs. 4-6 – 4-8). The principal

mineralization types are (Iljina 1994):

- PGE-bearing Cu–Ni–Fe sulfide disseminations in the marginal series of the Suhanko and Konttijärvi intrusions (Figs. 4-6 to 4-8).
- predominantly massive pyrrhotite deposits located close to the basal contact of the Suhanko intrusion (Figs. 4-6 and 4-8).
- the Rytikangas PGE reef in the Suhanko layered series (Fig. 4-6).
- the Siika-Kämä PGE reef in the Narkaus layered series (Fig. 4-6).
- the offset Cu–PGE mineralization below the Narkaus intrusion (Fig. 4-6).

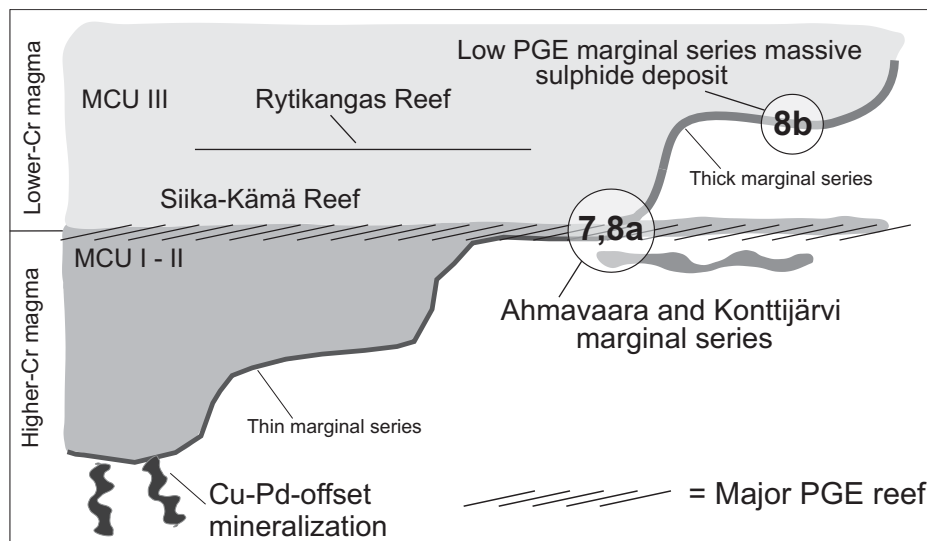


FIG. 4-6. Schematic presentation of the locations of the various PGE enrichments encountered in the Portimo Layered Igneous Complex. The numbers refer to the figures in this paper.

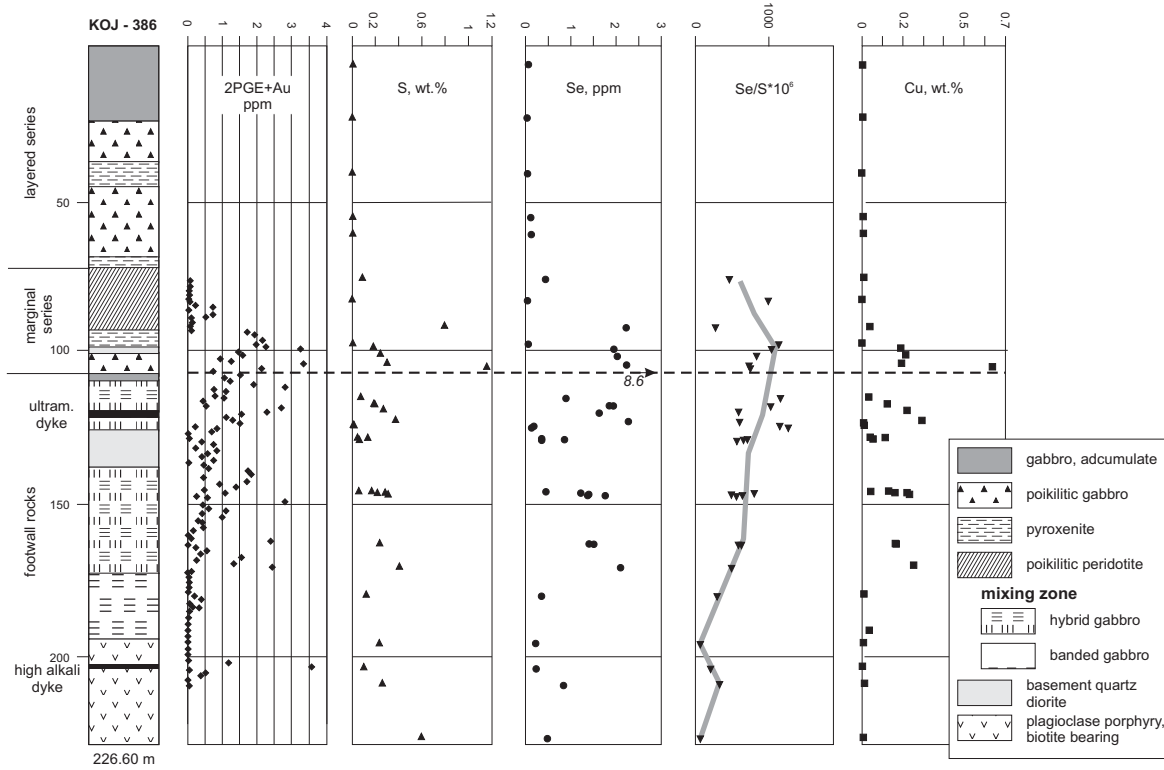


FIG. 4-7. Stratigraphic sequence of the Kontijärvi marginal series showing variations in bulk Pt+Pd+Au, S, Se, Se/S and Cu. For the structural position, see Fig. 4-6.

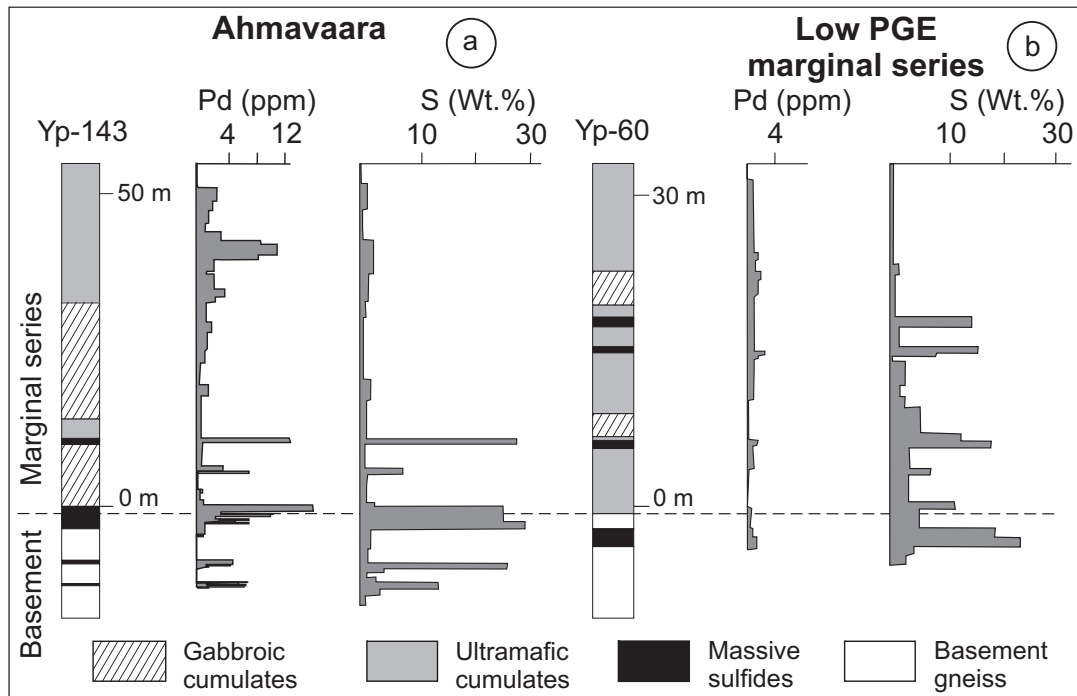


FIG. 4-8. Comparison of the Ahmavaara deposit and one low grade, disseminated and massive sulfide deposit of the Suhanko Intrusion. For the structural position, see Fig. 4-6.

The high PGE concentrations in the Konttijärvi marginal series sulfides were first discovered in a mineralogical study by Outokumpu Oy in the late 1970s (Vuorelainen *et al.* 1982). Because of these findings together with developments in cost-effective automatic analytical instrumentation the entire Portimo Complex was subjected to extensive platinum exploration. Although the pyrrhotite-dominated sulfides in the Suhanko marginal series had already been explored extensively in the 1960s, reassays of the old drill core did not reveal significant platinum contents until in 1986 a new drilling campaign hit the more highly Cu–Ni–PGE-enriched sulfides in the Ahmavaara area. Since then the exploration has produced results indicated in Table 4-2 and the Konttijärvi and Ahmavaara deposits are now considered economically viable.

Disseminated Suhanko and Konttijärvi marginal series sulfides

Disseminated PGE-bearing base metal sulfide mineralizations (Table 4-3; Figs. 4-6 – 4-8) of the contact zone, which are normally 10–30 metres in thickness, occur throughout the entire marginal series of the Suhanko and Konttijärvi intrusions. Their distribution is erratic and their occurrence typically extends from the lower peridotitic layer downwards for some 30 metres into the basement. In Konttijärvi, this mineralization sometimes extends 100 metres below the actual marginal series, hosted in rock types belonging to the Mixing Zone (Fig. 4-7). In places, the mineralization seems to have occurred along the mafic replacement bands, possibly indicating concurrent metasomatism and mineralization in the banded gabbro (Fig. 4-5).

The bulk of the platinum-group minerals (PGM) in the Portimo Complex is composed of various arsenides, bismutotellurides and arsenoantimonides, with some sulfarsenides, sulfides, stannides, selenides and bismuthides, in descending order, whereas native elements and Fe-PGE alloys are totally absent (McElduff & Iljina 1991, Iljina 1994). Of the platinum-group elements, palladium, platinum and rhodium were found to form minerals deficient in the other PGE, whereas traces of osmium, iridium and ruthenium were found to be present in minerals mainly composed of other PGE. The platinum-group minerals are associated with silicates, sulfides and oxides, the silicates being the most common environment

(Table 4-4). In base metal mineralogy, a peculiar kind of composite sulfide intergrowth (Fig. 4-9), composed of galena, pentlandite, sphalerite, pyrite and sometimes even platinum-group minerals, is common in the mineralized Konttijärvi basement gneisses. This kind of assemblage is not characteristic of fractionated mss sulfides, but suggests a paragenesis introduced by or re-equilibrated with fluids.

The PGE contents vary from only weakly anomalous values to 2 ppm in most places in the marginal series of the Suhanko intrusion but rises to >10 ppm in a number of samples from Konttijärvi and Ahmavaara (Figs. 4-6 and 4-8). Highly PGE-enriched marginal series of this kind are rare in layered intrusions; another well-known occurrence is the Platreef in the Northern Bushveld Complex, described below. In the case of the Suhanko intrusion, the PGE grade and Cu and Ni contents of the sulfide fraction seem to correlate with the presence of the Portimo Dykes underneath the intrusion.

Figure 4-7 shows a lithological log and variation of some elements in one drill core close to the depression structure mentioned earlier (Fig. 4-4). In the drill hole depicted, the precious metals appear in the lower peridotite layer and are present down to the base of the hybrid gabbro of the Mixing Zone with an additional peak at a depth of approximately 200 m. The copper correlates well with the precious metals, but the sulfur does not, indicating variations in the relative amounts of iron and copper sulfides.

Massive Suhanko marginal series sulfides

Massive sulfide deposits are characteristic of the marginal series of the Suhanko intrusion. They are in the form of dykes and obviously also plate-like bodies conformable to layering and generally vary in thickness from 20 cm to 20 m. The deposits are also found in various locations from 30 m below the basal contact of the intrusion to a position 20 m above it and range in size from less than 1 million tonnes to more than 10 million tonnes. The sulfide assemblage is composed almost exclusively of pyrrhotite, except for the Ahmavaara deposit, which also contains chalcopyrite and pentlandite. Outcrop evidence from Ahmavaara shows that massive sulfides occur exclusively as crosscutting dykes.

The PGM are approximately the same as in the disseminated sulfide mineralization. Despite the

TABLE 4-2. COMPARATIVE VALUES FOR OPERATING AND POTENTIAL PGE OPEN PIT OPERATIONS ON THE PLATREEF, N. BUSHVELD.

Project	Company	Resource Status	PGE+Au g/t	Ni %	Cu %	Mt
N. BUSHVELD						
Drenthe	Anooraq – Angloplat	Inferred	1.3 (4E)	0.16	0.1	99.4
Nonnenwerth (Aurora)	Genmin (now Pan Palladium)	Inferred? (Historical)	1.19 (3E?)	0.07	0.21	50.4
Volspruit	Pan Palladium	Inferred	1.15 (4E)	0.15	0.04	23.8
Volspruit	Pan Palladium	Inferred	1.2 (4E)	0.16	0.03	17.5
Mokopane	AIM Resources	Inferred	.55 (2E)	0.085	0.146	39 (?)
Tweespalk	Platinum Group Metals	Intersection values over 28 metres	1.09 (3E)	–	–	–
Potgietersrus Platinums	Anglo Platinum	Measured and indicated	2.34 (4E)	–	–	350.8
Potgietersrus Platinums	Anglo Platinum	Inferred	2.44 (4E)	–	–	153.6
E. BUSHVELD						
Sheba's Ridge	Ridge Mining	'Main zone' Indicated and Inferred	0.94 (3E)	0.22	0.08	370
Sheba's Ridge	Ridge Mining	'Upper zone' Indicated and Inferred	0.48 (3E)	0.12	0.03	577
PORTIMO						
Konttijärvi	Gold Fields– Arctic Platinum	JORC classified resources, 1.0 3E cut-off	2.46 (3E)	0.07	0.19	35.6
Ahmavaara	Gold Fields– Arctic Platinum	JORC classified resources, 1.0 3E cut-off	1.88(3E)	0.11	0.28	61.8
Ahmavaara east	Gold Fields– Arctic Platinum	JORC classified resources, 1.0 g/t 3E cut-off	1.54 (3E)	0.08	0.20	16.3
KOILLISMAA						
Murtolampi	Geological Survey of Finland	cut-off 0.7 g/t 3E, average of 49 1m long drill hole samples	0.99 (3E)	0.13	0.19	–
Haukiaho	Geological Survey of Finland	Intersection values over 51.5 metres	0.79 (3E)	0.22	0.36	–
RIVER VALLEY						
Dana Lake	Pacific North West Capital	Measured	2.2 (3E)	0.02	0.13	4.1

3E = Pt+Pd +Au; 4E = Pt+Pd+Rh+Au

Data here are compared with those from the Sheba's Ridge deposit (E. Bushveld) and Portimo, Koillismaa and River Valley examples. Koillismaa information taken from Iljina (2004) data CD-ROM and the other examples from published company Annual Reports and/or press releases.

PGE DEPOSITS IN THE MARGINAL SERIES OF LAYERED INTRUSIONS

TABLE 4-3. NI, CU, S, PGE AND AU CONCENTRATIONS OF SOME CONTACT-STYLE PGE DEPOSITS IN THE TORNIO-NÄRÄNKÄVAARA BELT.

		Ni (wt.%)	Cu	S	Pt (ppm)	Pd	Au
Portimo Layered Igneous Complex							
Konttijärvi	A (5)	0.056	0.239	0.323	1.3	4.07	0.24
marginal series	B	6.1	25.9	35.0	141	441	26
	D	5.4	14.4	36.7			
Ahmavaara, massive sulfides	A (3)	2.00	0.719	25.8	1.51	11.0	0.104
	B	3.0	1.1	39	2.28	16.7	0.160
	D	2.7	2.4	37	2.12	15.2	
Vaaralampi, massive sulfides	A (2)	0.284	0.143	23.3	–	0.485	0.005
	B	0.48	0.24	39.5	–	0.820	0.009
	D	0.94	0.63	37			
Koillismaa Layered Igneous Complex							
Murtolampi, marginal series	C	0.128	0.193	0.541	0.33	0.60	0.01
	D	10.6	17.0	37			
Haukiahö, marginal series	C	0.223	0.357	0.819	0.16	0.43	0.19
	D	10.1	16.1	37			

A, Average of selected type samples (n=number of samples); B, concentrations in the type samples, recalculated to 100% sulfide; C, metal concentrations in a large number of samples and D, metal concentrations in a large number of samples, recalculated to 100% sulfide. Portimo data from Iljina (1994) and Koillismaa calculated from the data CD-ROM Iljina (2004). In Murtolampi cut-off 0.7 ppm 2PGE+Au was used.

TABLE 4-4. PERCENTAGES OF PGM IN VARIOUS HOST MINERALS IN SOME PORTIMO DEPOSITS

Deposit	su	su/si	si	ox
Konttijärvi marginal series, n=54	19	8	49	27
Ahmavaara disseminated sulfides, n=42	39	32	17	12
Ahmavaara massive sulfides, n=14	50	29	21	0

su: sulfides only; su/si: sulfide/silicate margins; si: silicates only; ox: oxides; n, number of identifications. (from Iljina 1994).

massive nature of base metal sulfides, the proportion of PGM in the interstitial silicate is rather large (21%, Table 4-4).

The massive pyrrhotite deposits show relatively low PGE values with the maximum Pt + Pd normally reaching a few ppm. PGE concentrations are, however, much higher in the Ahmavaara deposit, attaining a level of 20 ppm (Figs. 4-6 and 4-8), which is similar to the disseminated Ahmavaara sulfide mineralization.

Table 4-3 shows some representative element contents and ratios for the Portimo

mineralizations. Konttijärvi and Ahmavaara are both examples of the higher PGE tenor marginal series and Vaaralampi is taken to represent the lower PGE tenor marginal series. Contrary to the fact that copper generally dominates over nickel, the Ahmavaara massive sulfide dykes are nickel-dominated. Despite this, the disseminated sulfides in Ahmavaara are copper-dominated and the PGE show low correlation with the modal amounts of sulfides (Iljina 1994). In a way, the base metal sulfide and PGE mineralizations superimpose each other.

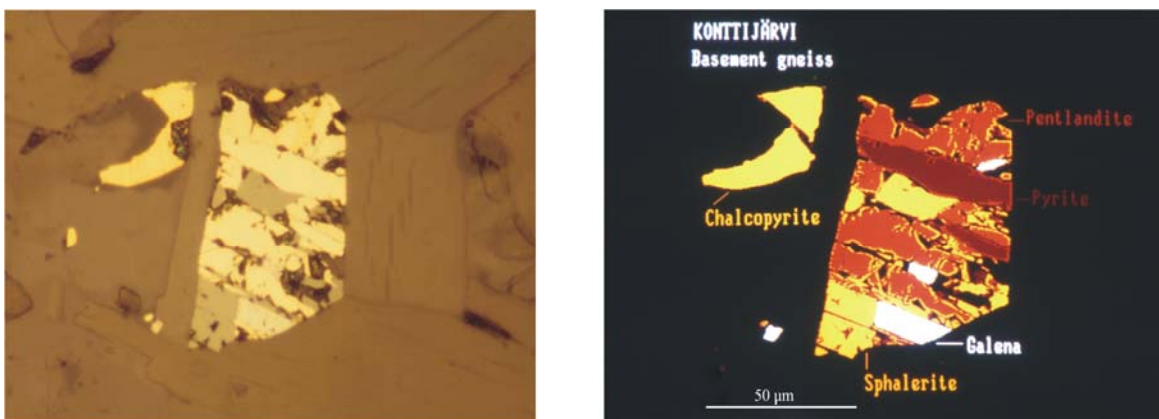


FIG. 4-9. Microscope photograph (left) and processed backscattered electron image of the same composite sulfide grain. Photo and image processing by M. Iljina.

Correlation of Portimo and Penikat Complexes

Figure 4-10 shows the stratigraphic correlation of the Portimo Complex intrusions and the nearby Penikat Intrusion. The correlation was made by taking the boundary between the two parental magmas as a reference height. An interesting observation is that in this interpretation the Sompujärvi Reef of the Penikat Intrusion, the Siika-Kämä Reef of the Narkaus Intrusion, and the high-PGE grade marginal series of the Konttijärvi and Ahmavaara plot on the same stratigraphic level (Lahtinen *et al.* 1989; Iljina 1994).

Haukiahö and Murtolampi Sulfide–PGE Deposits, Koillismaa

The Western Intrusion of the Koillismaa Layered Igneous Complex (KLIC, Fig. 4-1) is the third intrusion of the TNB where the thick border zone is encountered in addition to the Suhanko and Konttijärvi intrusions. The interaction between the felsic footwall gneisses and mafic magma is even more pronounced in the KLIC than in most places below the Konttijärvi or Suhanko Intrusions. In the Koillismaa area, the footwall rocks are pervasively recrystallized into albite–quartz rocks, sometimes up to few hundreds of metres below the basal contact of intrusion, and the marginal series is also thicker on average and attains a few hundreds metres. A full description of the KLIC stratigraphy is given by Alapieti (1982) and the structural development and mineralization are described by Iljina *et al.* (2001) and Iljina (2004).

The PGE–sulfide precipitation has taken place throughout the entire strike length (>100 km) of the marginal series. However, the northernmost

blocks, Kaukua and Murtolampi, have a higher PGE tenor, although with a slightly lower base metal content compared with the other intrusion blocks to the south of them (Iljina 2004). Fig. 4-11 shows a drilling profile through the Murtolampi marginal series, and Tables 4-3 and 4-2 gives metallogenic data on the Haukiahö and Murtolampi marginal series. Compared to Suhanko and Konttijärvi, the Murtolampi PGE concentrations are lower but the base metals are in about the same order. The Haukiahö example (Table 4-3) represents a more base-metal-enriched marginal series. Koillismaa marginal series is also unique in having a Pt/Au ratio close to one, however, this does not include Murtolampi, which has higher PGE/Au ratio and low absolute Au concentrations. The PGM and their distribution within silicates and sulfides resemble those of the Konttijärvi and Ahmavaara sulfide disseminated marginal series (Kojonen & Iljina 2001).

BUSHVELD COMPLEX Platreef, Northern Bushveld

The Platreef is probably the largest PGE resource in the world. It extends for over 100 km and ranges in thickness from 50 to 200 m. The dip is variable, around 40° to the west, and has been intersected by drilling at 1400 m below the surface. The sequence is at present the focus of intense exploration (Table 4-2). It is also where the largest one of the three PGE open pit mines in the world is located (Potgietersrus, Lac des Iles, and Ngezi) and operated by Anglo Platinum. Two pits at Potgietersrus, Sandsloot and Zwartfontein, are mined at a rate of 48 million tonnes per annum.

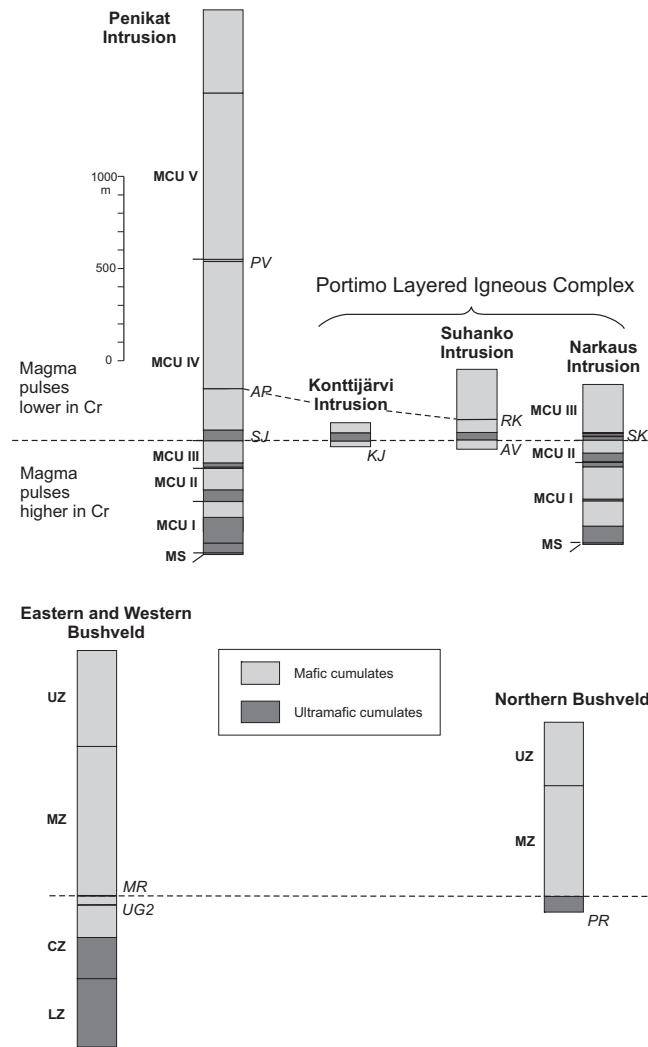


FIG. 4-10. Simplified stratigraphic columns of Penikat, Konttijärvi, Suhanko and Narkaus Intrusions (above) and Western, Eastern and Northern Bushveld Complexes. MCU, megacyclic unit. MS, marginal series. SJ, AP, PV, RK and SK, Sompujärvi, Ala-Penikka, Paasivaara, Rytikangas and Siika-Kämä PGE reefs, respectively. KJ and AV, Konttijärvi and Ahmavaara high PGE-grade marginal series mineralizations. LZ, CZ, MZ and UZ, Lower, Critical, Main and Upper Zones, respectively. UG2 and MR, UG2 and Merensky Reef PGE reefs, respectively. Modified from Lahtinen *et al.* 1989 and Sharpe 1989.

The term Platreef is an informal stratigraphic name for a PGE-sulfide deposit hosted at the margin of the Bushveld Complex, in the northern limb of the complex (Figs. 4-12 and 4-13). The name appears to have originated in the 1960s when the South African mining company Johannesburg Consolidated Investments were exploring the area. Van der Merwe (1976) proposed the use of the term Platreef in analogy with the term Platinum Horizon

used by Wagner (1929).

Sedimentary rocks of the 2.2–2.5 Ga Transvaal Sequence and Archean granites comprise the floor rocks of the Platreef. This has a transgressive contact progressively cutting older sedimentary rocks and eventually the granite from south to north. The Platreef is overlain by Main Zone gabbro and Upper Zone ferrogabbro.

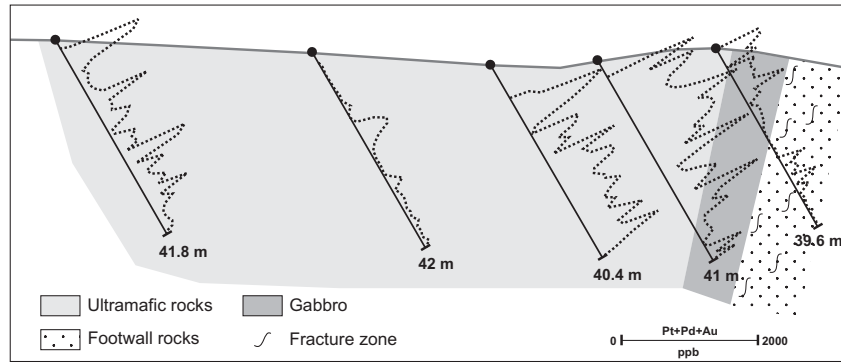


FIG. 4-11. Drill hole profile through the marginal series of the Murtolampi block, Koillismaa Layered Igneous Complex, showing the variation in Pt+Pd+Au concentration.

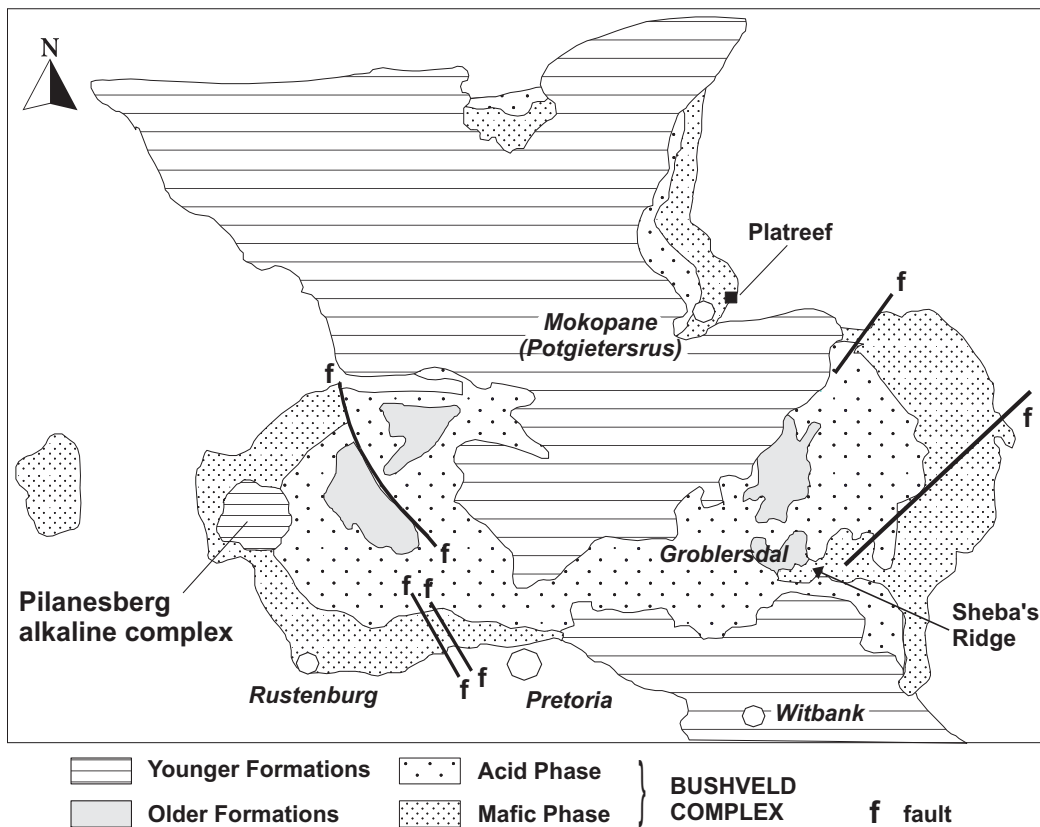


FIG. 4-12.: Schematic map of the Bushveld Complex with the Platreef and Sheba's Ridge margin-hosted sulfide-PGE deposits indicated.

The sedimentary rocks are quartzite, shale (carbonaceous in places), iron formation, and dolomite. The thermal metamorphic aureole of the Bushveld Complex was created in two stages, indicating a multiple magma intrusion (Nell 1985). The first event indicates a pressure of about 1.5 kb and temperatures up to 750°C, during which most of

the water in the sedimentary rocks was driven off, but the temperature was not high enough to cause partial melting. In the second stage, the estimated pressures were between 4 and 5 kb, and the maximum temperatures attained were 850° to 900°C. Nell (1985) attributed the first event to the intrusion of Lower Zone magma, now preserved as pyroxene-

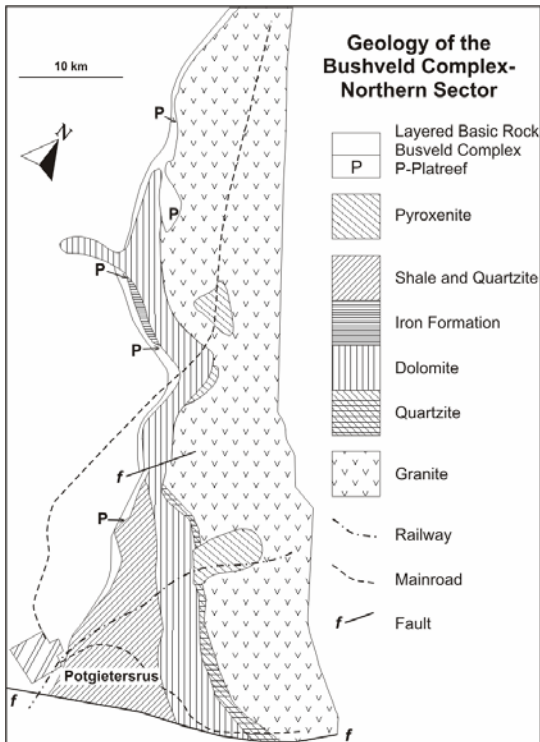


FIG. 4-13. Geological Map of the Potgietersrus limb, Northern Bushveld Complex.

and olivine-dominant satellite bodies in the floor rocks. The second event is related to the intrusion of the bulk of the Main and Upper Zones of the complex. The implicit assumption in this model is that the Platreef is related to the later event.

It is interesting to compare the structural position of the Platreef occurrence and the higher PGE-grade Konttijärvi and Ahmavaara deposits as shown in Fig. 4-10. This correlation might be an artifact and its relevance to ore genesis is tenuous and under current investigation. In the Bushveld, Penikat and Portimo Complexes, the lowermost more significant PGE reefs are located rather low in the stratigraphy and no major ultramafic cumulate sequences are found above them (Fig. 4-10). The names of the reefs are UG2 and Merensky in Bushveld, Sompujärvi in Penikat and Siika-Kämä in Portimo. In the Portimo Complex the higher PGE grade mineralization is found irrespective of the thickness of the underlying cumulate sequence and it is also where the earlier magma injections are represented only by the dykes lying under the intrusion proper (Portimo Dykes). The Konttijärvi and Ahmavaara deposits are located in this kind of structural position. When the higher levels of the

MCU III of the Portimo Complex face the country rock, the PGE, Cu and Ni contents of the marginal series mineralization drop significantly. In the case of the Northern Bushveld Complex, the Platreef sequence underlies the Main Zone and the earlier magma pulses are represented by discrete bodies in the same way as the Portimo Dykes represent MCU I and II phases below the Konttijärvi and Ahmavaara marginal series.

Platreef stratigraphy

Gain & Mostert (1982) demonstrated that the Platreef consists of a complex assemblage of norite, pyroxenite, serpentinite, and xenoliths of floor rock dolomite. The Platreef is about 250 metres thick, between the underlying floor rocks and the overlying Main Zone gabbro and norite.

An informal stratigraphic zoning to the Platreef pyroxenite was devised and has been in use since the 1980s. The sequence is subdivided into three zones (Buchanan 1988) termed, from the base up, 'A reef', 'B reef', and 'C reef'. Broadly these divisions correlate with the metal zoning in the reef, with 'B reef' being the main carrier of economic mineralization. 'A reef' is erratically mineralized and 'C reef' is usually barren. The zoning was originally defined to give datum marks for the application of geostatistical modeling and resource estimation of the deposit. The internal geochemical and mineral compositions also broadly correlate with this zoning, though it is not consistent along the strike, in particular the upper 'C zone' pyroxenite, which is in many places absent.

'A reef' is coarse-grained feldspathic pyroxenite in which pyroxene and feldspar form aggregates that give the drill core a patchy appearance which can also be seen when the rock is exposed in mining operations. Orthopyroxene is iron-rich compared to that in the overlying 'B reef'. This basal compositional reversal could constitute a stratigraphic marker in the initial phases of exploration for margin-hosted sulfide.

'B reef' is medium-grained feldspathic pyroxenite with an even texture. In proximity to metasedimentary xenoliths there is serpentinization and a coarsening of the rock. This sequence is consistently sulfide-bearing. This is the main ore zone of the Platreef.

'C reef' pyroxenite is fine- to medium-grained feldspathic pyroxenite. Pyroxene composition is similar to that in the B reef, but the whole-rock Cr is higher.

Platinum-group minerals

Kinloch (1982) observed the PGM trends in the Platreef. Vertical trends in a 200 m thickness of the Platreef show statistically significant amounts of platinum-group sulfides near the footwall contact, whereas, when present, platinum-group alloys occur towards the hanging wall contact. Pd alloyed with Sn, Sb, Bi, and Te minerals, as well as Pt–Fe alloys, occur in significant quantities in the Zwartfontein area of the Platreef. Platinum-group sulfides are the dominant minerals to the south of Zwartfontein. Armitage *et al.* (2002), however, reported the Platreef to be devoid of PGE sulfides in mineralized footwall lithologies and they found this to be also the case at the Platreef proper at the Sandsloot area. The PGM identified comprise high temperature metal (Pt–Fe, Pt–Sn) and semi-metal alloys (Pt, Pd arsenides), and a dominant assemblage of lower temperature semi-metals and alloys.

Inter-relationship of metals

The sulfide distribution is heterogeneous and rarely exceeds 5 per cent of the mode. The sulfides generally occur as droplets within the silicate grains or as irregular blebs up to 30 mm across between the silicates. The lower part of the reef is dominated by pyrite, monoclinic pyrrhotite, pentlandite and chalcopyrite, whereas in the upper Platreef the assemblage is hexagonal pyrrhotite, pentlandite, and chalcopyrite (\pm cubanite). Variation in the composition of the base metal sulfide minerals indicates a change from a sulfur rich to a sulfur poor (or metal rich) environment during the crystallization of the Platreef. There is an upward decrease in the Ni/Cu ratio and the Pt/Pd ratio. Nickel and Cu tend to be strongly correlated. Correlation of PGE and S is only moderate.

The proportions of the precious metals in the Platreef are illustrated in the pie chart (Fig. 4-14), representing 200 data points. Platinum and palladium are generally well correlated but with scatter, possibly brought on by later stage redistribution. There is also a general relationship between the base metals and Pt and Pd, but with considerable scatter (Fig. 4-15). A detailed description of Platreef metal ratios is given by Mostert (1982).

Isotope studies on the Platreef

As indicated in the studies summarized below, the Platreef has evidence of crustal contamination. It appears that this has occurred in at least two stages. The sulfide and cumulus mineral

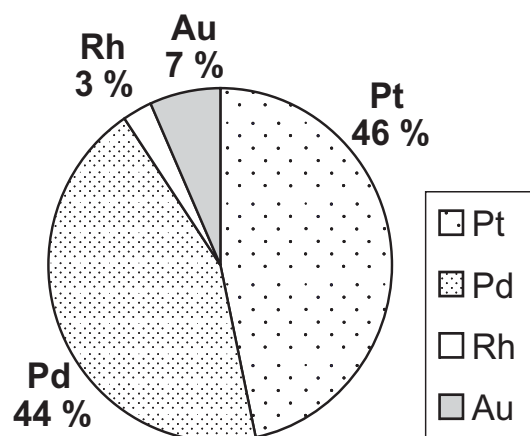


FIG. 4-14. Precious metal ratios in the Platreef (unpublished data, with acknowledgement, Anglo Platinum).

component has an overall crustal imprint, possibly due to an interaction with crust in an intermediate staging magma chamber. This is overprinted by the local interaction with floor rocks at the site of emplacement, and with the later circulation of hydrothermal fluids. This last event accounts in part for the de-coupling of sulfur and PGE, noted earlier.

Sulfur isotope data from the Platreef show a range of $\delta^{34}\text{S}$ values, from 0 to +2 up to as much as +6 to +10 close to or at the contact with dolomite xenoliths. These higher values have led to the suggestion that the sulfide liquation in the Platreef was directly associated with local contamination from floor rocks (Buchanan & Rouse 1984). More recently, $\delta^{34}\text{S}$ values of 4.8–5.6 have been reported from chalcopyrite and values of 4.5–5.3 from pyrrhotite of the Platreef, suggesting a crustal component within the sulfides (Sharman-Harris & Kinnaird 2004). That magmatic and near magmatic $\delta^{34}\text{S}$ values (0 – +2) are recorded in the Platreef where the floor rock is granite, and there appears to be little magmatic interaction with floor, suggests contamination was a local imprint, and may not be the cause of sulfide liquation.

Re–Os systematics on sulfides of the Platreef from a single bore hole yield an isochron with a Re–Os age of 2011 ± 50 Ma and an initial $^{187}\text{Os}/^{188}\text{Os}$ value of 0.226 ± 0.021 , which corresponds to the accepted age of the Bushveld Complex of ~ 2050 Ma. The initial Os ratio suggests that the source of the Os in the sulfides has a strong crustal component, possibly in an intermediate magma chamber within the crust (Ruiz *et al.* 2004).

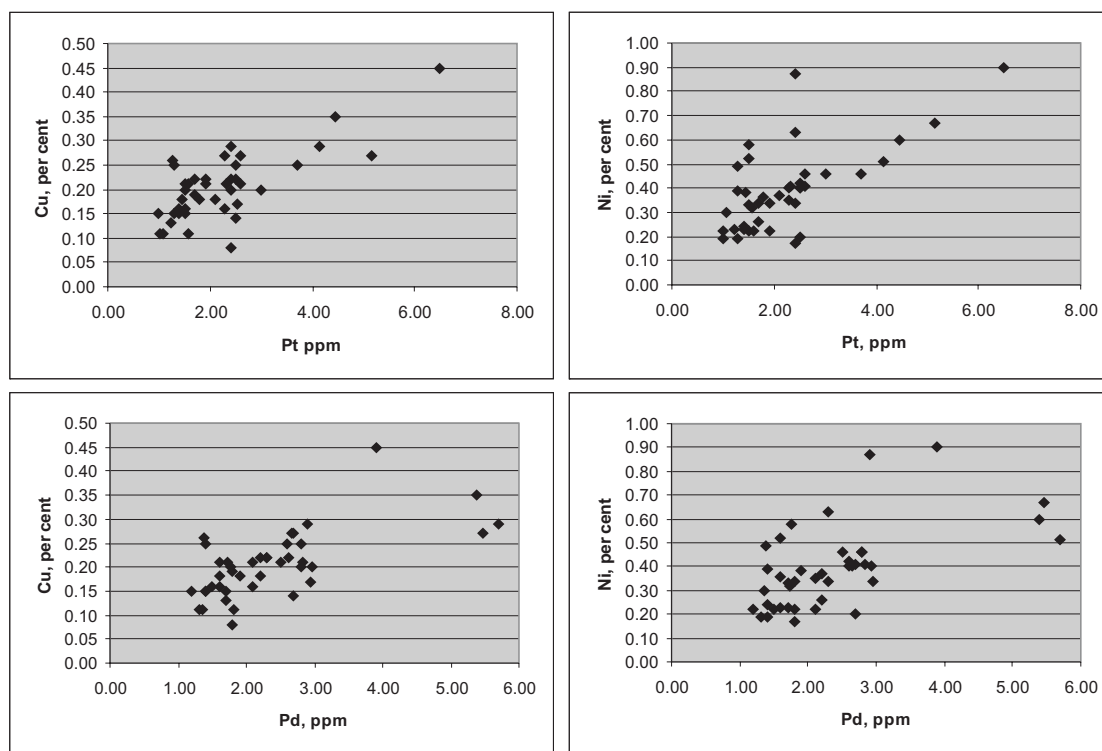


FIG. 4-15. Scatterplots of Pt, Pd against Cu, Ni (unpublished data, with acknowledgement, Anglo Platinum).

Oxygen isotope studies show that the Upper and Main Zones in the Platreef area are crystallized from a well-mixed contaminated magma, and that higher $\delta^{18}\text{O}$ values in the Platreef indicate the addition of dolomite country rocks (Harris & Chaumba 2001).

Geochemical profiles for Rb and Sr isotope ratios through the Platreef and the overlying Main Zone show differences depending on the footwall composition. Where granite is the floor rock, the initial $^{87}\text{Sr}/^{86}\text{Sr}$ ratio of the Platreef ranges from 0.7107 to 0.7226. For dolomite footwall there is a lower initial ratio of 0.7054 to 0.7147. Orthopyroxene has a much lower initial ratio than the whole-rock, indicating that this cumulus phase formed prior to contamination. It is also inferred that the separation of sulfide liquid predated the main contamination process (Cawthorn *et al.* 1985 and Barton *et al.* 1986).

Widespread reaction of Platreef inter-cumulus melt with floor rock-derived fluids and dolomite xenoliths had presented obstacles in determining the nature of “uncontaminated” Platreef. Lee *et al.* (1989) sampled a sequence from an area of Platreef inferred to be unaffected by

xenoliths or close to granite but with floor rock composed of cordierite hornfels. A lower facies of the Platreef gave whole-rock Mg number in the range 0.72–0.75, and an upper facies with an Mg range of 0.77–0.82. Whole-rock Sr isotope ratios (R_0) range from 0.7069–0.7087; the higher values correlate with higher PGE and higher Mg number in the upper facies. The role of contamination was deemed to be insignificant.

SHEBA’S RIDGE, EASTERN BUSHVELD COMPLEX

In the Western and Eastern Bushveld Complex, the cumulate rocks of the Lower and Critical Zones are isolated from the floor rocks by the marginal zone. This zone is norite in composition; pyroxene is around En_{65} , compared to the En_{80} of the overlying cumulates. In places, the texture resembles that of the ‘A reef’ of the Platreef. Despite several exploration endeavors, no margin-hosted sulfide or sulfide–PGE sequence has been identified in the Eastern or Western Bushveld Complex, except for Sheba’s Ridge, which is located in an enclave of Bushveld rocks close to the town of Groblersdal (Fig. 4-12).

The Sheba's Ridge occurrence was first explored about 25 years ago, as a result of soil geochemical surveys in the vicinity of a vein-hosted Cu occurrence. The margin-hosted sulfide deposit of Sheba's Ridge is presently being evaluated as a potential open pit Ni mine with PGE credits (Sharpe *et al.* 2002). It is a stratabound mineralized sequence and analogies with the Platreef proper have been made.

The base metal sulfide is blebby to disseminated in texture within a medium-grained feldspathic pyroxenite. The sulfide occurs as irregular blebs 1 to 5 mm in size. The major sulfides are pyrrhotite (10 to 20%), pentlandite (5 to 30%), and chalcopyrite (60 to 70%). The pentlandite also occurs as an exsolution product of pyrrhotite. Occasional small blebs of covellite were also noted. Chalcopyrite and pentlandite tend to occur as the large dominant grains, with pyrrhotite locked in pentlandite. Most of the fine-grained, interstitial sulfide is chalcopyrite. The PGM are dominantly semi-metal alloys.

The mineralization is located close to, but not at, the contact with hornfelsed metasedimentary rocks. A chilled margin is present. The Sheba's Ridge sulfide envelope is defined on grade and continuity into a lower grade sulfide zone, bounding

the contiguous sulfide 'Main Sulfide Zone' (Fig. 4-16). For a Main zone modelled thickness of 45 metres, the average whole-rock Ni is 0.22% and Cu is 0.08%. Pt+Pd+Au is on average 0.94 g.t⁻¹, and ranges up to contiguous blocks of 1-4 g.t⁻¹ (see Table 4-2) The Pt/Pd ratio is 0.5, making the sequence the most Pd-dominant in the Bushveld Complex. Preliminary S isotope results give δ³⁴S values of 1-2 for sulfide in the pyroxenite, and around 12 for sulfide in the floor rock metasedimentary rock. This appears to preclude significant floor rock contamination and sulfur addition as a control on the sulfide mineralization.

EAST BULL LAKE INTRUSIVE SUITE

Intrusions of the ca. 2480 Ma East Bull Lake Intrusive Suite (EBLIS) occur as an east-west-trending belt along the boundary (Fig. 4-17) of Archean and the Proterozoic provinces (Vaillancourt *et al.* 2002; Easton *et al.* 2004), Ontario, Canada, similar to the TNB intrusions in Fennoscandia. Common features of EBLIS and TNB also include the geotectonic location within the intracontinental rift zone, bimodal magmatism and crystallization from low-Ti, moderate to high-MgO, possibly PGE-enriched parental magmas. Intrusions of EBLIS are characteristically gabbroic,

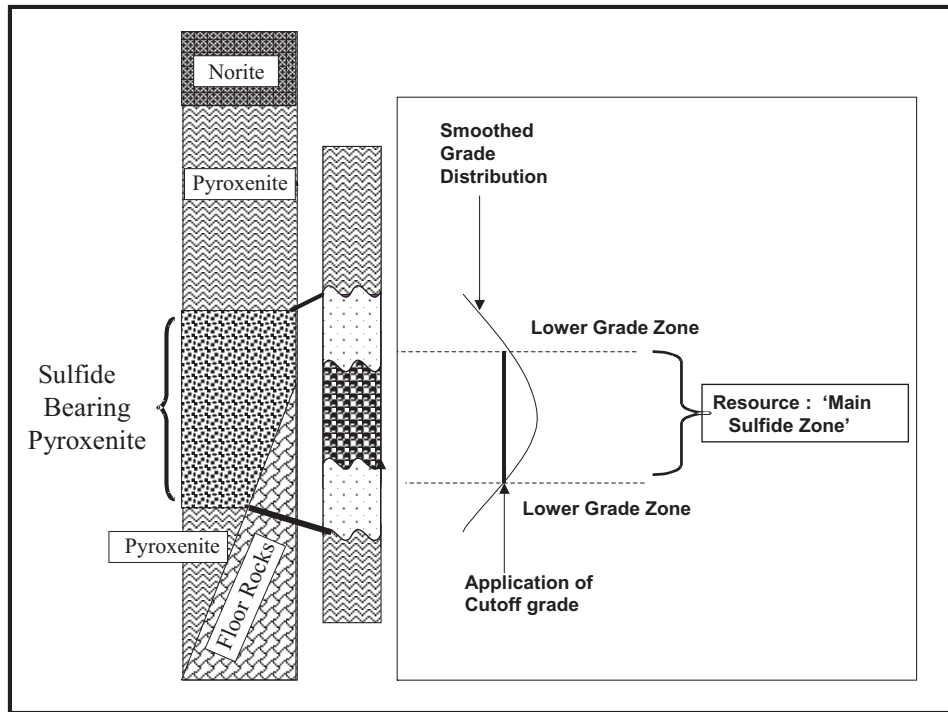


FIG. 4-16. Definition of the Sheba's Ridge Main Sulfide Zone, by the application of cut-off grade.

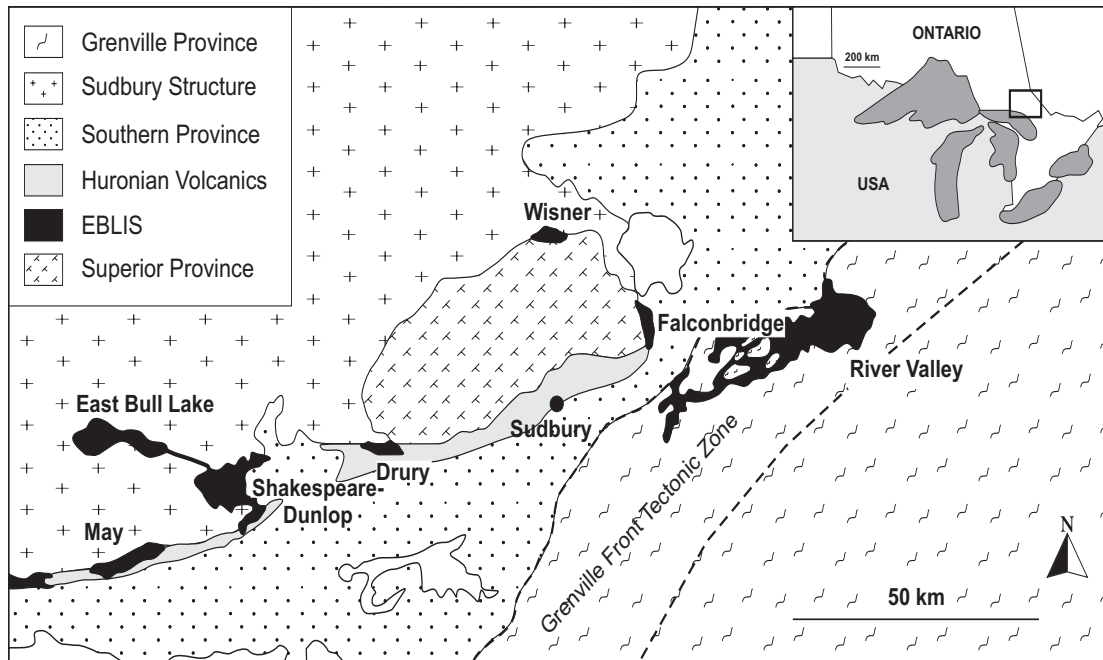


FIG. 4-17. Location of Palaeoproterozoic East Bull Lake Intrusive Suite (EBLIS) complexes. Modified after Peck *et al.* (1995) and James *et al.* (2002).

even rather leucocratic, and ultramafic portions are insignificant, in contrast to the Fennoscandian intrusions as well as the Bushveld Complex. Sulfide–PGE mineralization has been documented to have taken place in many of the EBLIS intrusions and we present two examples in this paper, namely the East Bull Lake and River Valley contact-style enrichments.

Figure 4-18 compares the igneous stratigraphy of five EBLIS intrusive bodies, and it also shows the positions of the mineralized zones. The lower portions of each intrusion are made up of a heterogeneous zone of breccias that is several tens of metres thick and other structures indicative of extensive interaction between mafic magma and the footwall gneisses (Fig. 4-19). In its lower part this so-called inclusion-bearing zone, also called marginal zone or border zone, contains higher amounts of footwall xenoliths, whereas the proportion of mafic xenoliths increases upwards as the footwall material disappears. All this suggest a vigorous intrusion event in which successive magma injections disrupted previously crystallized material from the intrusion margins and prevented the preservation of chilled margins.

The ferromagnesian silicate minerals become more magnesian upwards within the marginal series as the Fo of olivine rises from 68 to 72–76 and the

En of orthopyroxene from 44–69 to 55–69 (James *et al.* 2002), which corresponds with the pattern of Sheba's Ridge in the Bushveld Complex.

PGE–sulfide mineralization is erratically distributed within the lowermost, ca 100 m, rock units. The most favorable rock unit for the sulfide–PGE precipitation has been the inclusion-bearing or breccia zone. Fig. 4-20a demonstrates the lithological interpretation and precious metal concentrations in drill holes through the mineralized lower part of the East Bull Lake Intrusion. The Cu+Ni concentrations in the intersections shown are <0.5 wt.%, with variable Cu/Ni ratios. Fig. 4-20b gives corresponding information from the River Valley Intrusion/Dana Lake prospect, which shows a higher concentration tenor compared with East Bull Lake. The individual intersections of East Bull Lake and River Valley are comparable to many of the Konttijärvi and Ahmavaara ones, but the tonnages are much below those of the Finnish examples (Table 4-2).

James *et al.* (2002) reported that the PGM assemblage is made up of six Pd–Te(-Bi), Pd–Bi, Pd–As(-Sb) mineral species and two platinum mineral species, sperrylite (Pt–As) and platarsite (Pt–As–S). This mineralogy closely resembles that of Konttijärvi and Ahmavaara.

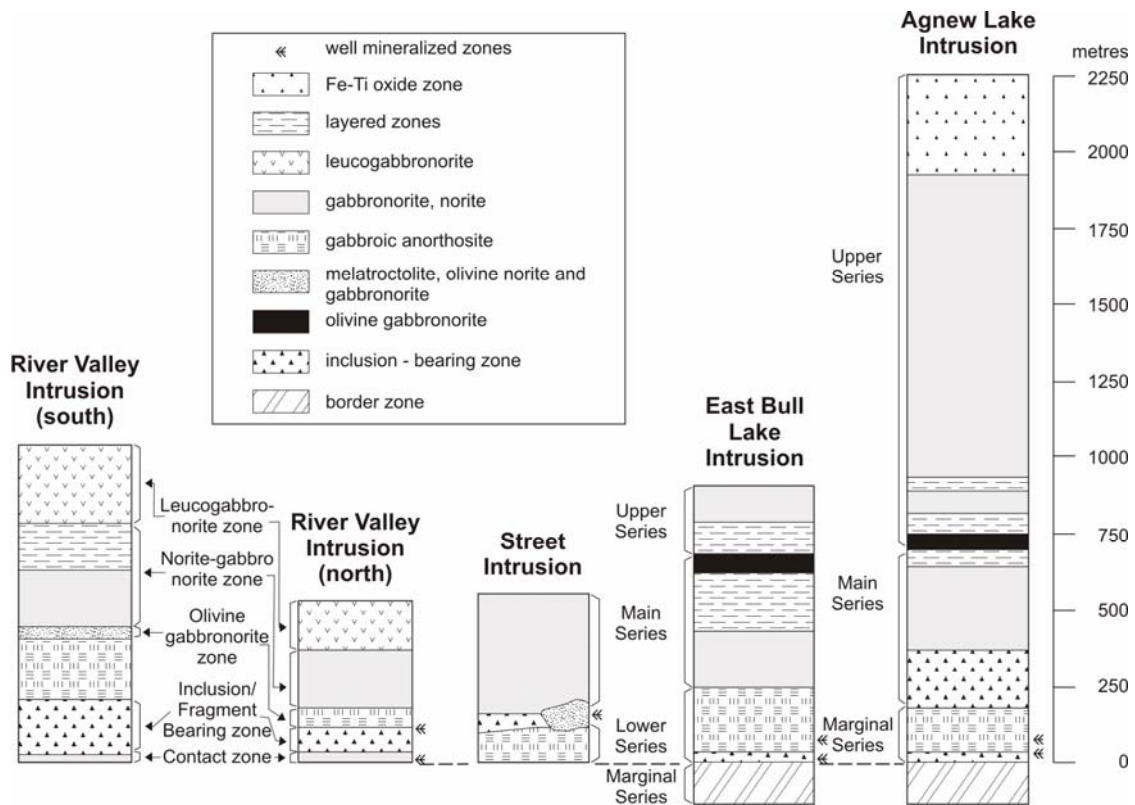


FIG. 4-18. Generalized cross-sections of some East Bull Lake Intrusive Suite intrusions. Modified after Easton *et al.* (2004).

Se/S RATIO

Selenium is a chalcophile element, which geochemically tends to follow sulfur and frequently occurs in sulfides, replacing sulfur. The estimated $(Se/S) \times 10^6$ ratios in the mantle are in the range of 230 to 350 and a typical ratio in crustal rocks is lower, and generally less than 100 in clastic sedimentary rocks. Selenium is also thought to be less soluble and mobile than sulfur, especially in oxidizing environments. The partitioning coefficient for selenium between sulfide and silicate melts is of the order of 10^3 (Peach *et al.* 1990). The Se/S ratio has also been used alongside the sulfur isotope composition as a guide when estimating the source of the sulfur in magmatic Cu–Ni–Fe deposits.

The sulfides in the PGE-rich reefs within the Bushveld and Stillwater Complexes turned out to have Se/S ratios well above the mantle range, and Paktunc *et al.* (1990) concluded that the pentlandite, chalcopyrite and pyrrhotite in the Merensky and UG2 Reefs and the Platreef tended to have higher Se/S ratios than are found in the reefs of lower grade PGE elsewhere in the Bushveld intrusion or in many other massive to disseminated sulfide

deposits low in PGE. Hattori *et al.* (2002) concluded that high Se/S ratios are characteristic features of boninitic high-MgO second stage melts; the magma type proposed for the Bushveld and Portimo Complexes, for example.



FIG. 4-19. An outcrop photograph depicting the inclusion-bearing zone, River Valley Intrusion. Photo by M. Iljina.

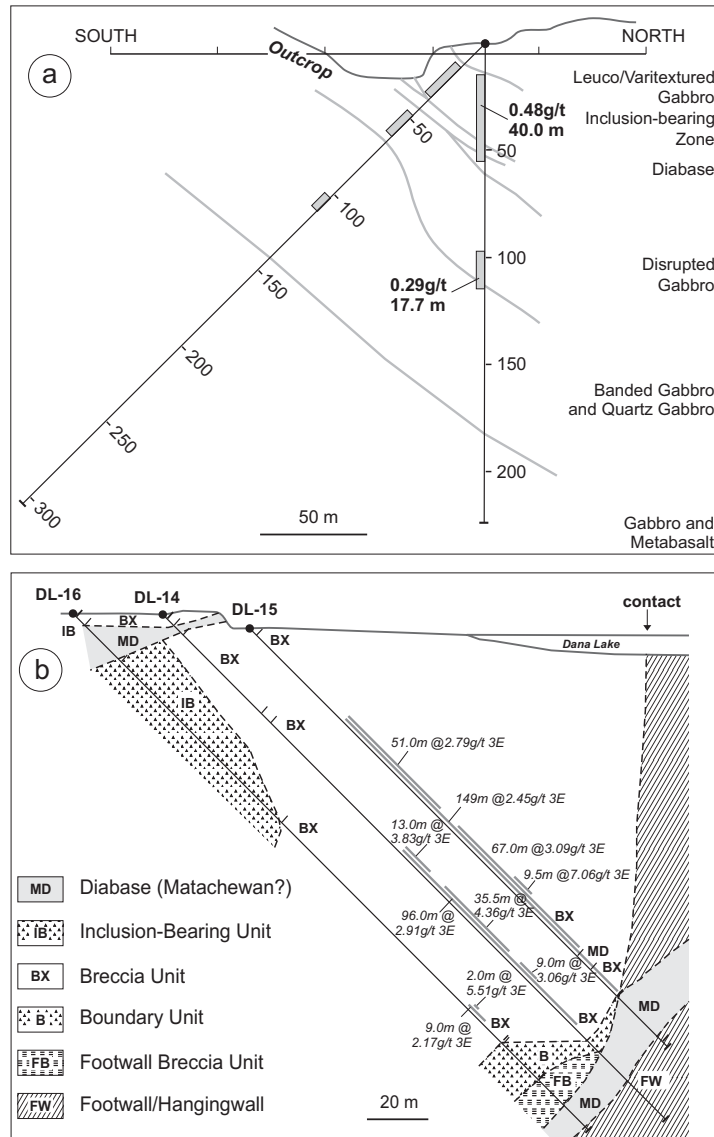


FIG. 4-20. Geology and examples of metal concentrations in the East Bull Lake Intrusion (a) and River Valley Intrusion (b). Modified after James *et al.* (2002).

Within the Portimo Complex, mineralization types with higher PGE tenor tend to have higher Se/S ratios at a given S content (Iljina 1994). Figure 4-21 depicts Se/S versus whole-rock sulfur of the various mineralization types of the Portimo Complex. It is worth mentioning that high Se/S versus S describes the likelihood of a particular mineralization type to have a higher PGE tenor, *i.e.*, the results suggest that the high Se/S *versus* S value is an indication of a higher tenor PGE and points to the higher economic potential of the mineralization encountered in the exploration. Within the Portimo

Complex, economically more viable PGE mineralization types seem to have a Se/S*10⁶ ratio 300–1,500 at low whole-rock sulfur (disseminated sulfides) content. In more massive sulfides the ratio drops to ca 200. Correspondingly mineralization types of lower economic potential have lower Se/S ratios and the ratio seems to drop more steeply with increasing sulfide content.

Figure 4-7 depicts the variation of copper, precious metals and Se/S ratio in one representative drill hole of the Konttijärvi marginal series. Whole-rock PGE seems to have a good correlation with

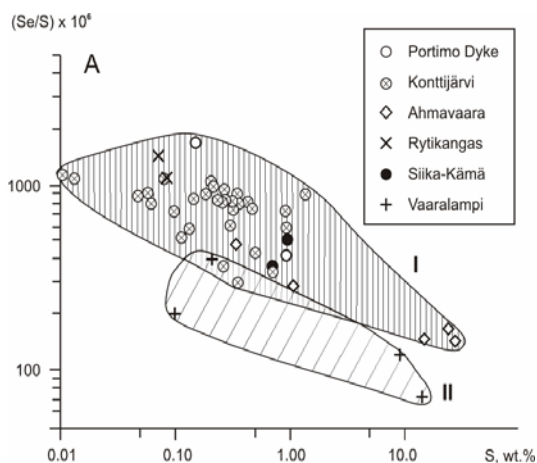


FIG. 4-21. $(\text{Se}/\text{S}) \times 10^6$ ratio versus whole-rock sulfur content in various mineralizations of the Portimo Layered Igneous Complex. The more highly PGE mineralized Portimo Dykes, Konttijärvi and Ahmavaara marginal series and Rytikangas and Siika-Kämä Reefs form a distinct group (I) having a higher Se/S ratio at a given sulfur content, thus differing from the lower PGE-grade Vaaralampi marginal series (II). Data combined from Iljina 1994 and this study (Fig. 4-7).

copper, Se and Se/S. At the depth of approximately 170 m, PGE drops and so do the elements and the ratio mentioned. The copper-deficient sulfide mineralization seems to continue further away from the intrusion. Further downhole the PGE kick associated with the high alkali dyke is accompanied by elevated Cu, Se and Se/S, but these components do not correspond to the higher S peak closer to the end of the hole.

Reported $\text{Se}/\text{S} \times 10^6$ values for East Bull Lake and River Valley are within the range of mantle-derived sulfides of 350–800 (Easton *et al.* 2004) for the former and 470–2,000 (James *et al.* 2002) for the latter. In the case of East Bull Lake the whole-rock PGE, Se and Se/S ratio have a strong positive correlation resembling the situation of the Portimo Complex.

CONCLUSIONS

The following concluding remarks can be made on the basis of the features described above.

- The marginal series hosted, 'contact-style' PGE deposits are generally zones which are tens of metres wide and have developed at the base or sides of mafic layered intrusions. They are also erratic in nature and in individual drill holes the highest PGE values can be found tens of metres

above or below the contact of the intrusion; they are also variable along the strike.

- The contact-type mineralizations are typically base metal sulfide bearing, often enriched in copper, but Ni is dominant in the case of the Platreef and Sheba's Ridge.
- The PGE concentrations are lower than in the reef-type deposits and the exploitability is based on the huge tonnages. These features lead to a broad geophysical signature and the possibility of using elements like copper, nickel and sulfur as pathfinders in geochemical exploration.
- The PGM assemblage is dominated by the low temperature assemblages of Pd–As, Pd–As–Sb, Pd–Bi–Te and Pt–As minerals, with the sulfides and Fe-alloys being rarer. This mineralogy differs from that of the UG2 and Merensky Reefs of the Bushveld Complex. However, the mineral paragenesis is metamorphic in most cases and may not necessarily correspond to the primary assemblage.

Contact-style PGE enrichments seem to be related to an areally larger igneous event, but the size of the hosting intrusion is not necessarily the unambiguous requirement. Sheba's Ridge is hosted by a pyroxenitic to melanoritic 'marginal zone', which is probably a separate intrusion phase, which predates the Lower, Critical and Main Zone phases of the Bushveld Complex. Although elsewhere in the Bushveld Complex it is unmineralized, the body has Ni–Cu–PGE-enriched sulfides at Sheba's Ridge; the genesis of the sulfide formation is unclear, but the local structures of the igneous body may have played a role in the genesis.

The key conclusion is that the host rocks of contact-style PGE deposits are characterized by extensive and prolonged interaction of mafic magma with the surrounding host rock. This results in thick marginal zones, which also show compositional reversals in modal mineralogy and mineral chemistry. The absolute PGE contents and relative PGE content over the base metals vary in the examples described of which the Platreef and Portimo stand as more highly and particularly more pervasively mineralized. The involvement of more than one magma type and/or sequential magma pulses may favor Platreef and Portimo-grade PGE-enriched base metal sulfide mineralization.

The applicability of Se/S ratios have not been widely enough tested and the results quoted here are tentative. The results, however, suggest selenium should be included in the rock geochemical exploration package and the Se/S

ratios ought to be considered when the significance of the first findings is evaluated.

ACKNOWLEDGEMENTS

The authors are grateful for the publication rights and cooperation with the companies Anglo Platinum (Platreef) and Gold Fields – Arctic Platinum (Konttijärvi and Ahmavaara). Thanks are extended to Professor Richard James from Laurentian University for arranging field excursions for the first author to the East Bull Lake and River Valley Intrusions.

REFERENCES

- ALAPIETI, T. (1982): The Koillismaa layered igneous complex, Finland: its structure, mineralogy and geochemistry, with emphasis on the distribution of chromium. *Geol. Surv. Finland, Bull.* **319**.
- ARMITAGE, P.E.B., McDONALD, I., EDWARDS, S.J. & MANBY, G.M. (2002): Platinum-group element mineralisation in the Platreef and the calc-silicate footwall at Sandsloot, Potgietersrus district, South Africa. *Trans. Instn. Min. Metall. Sect. B: Appl. Earth Sci.* **111**, B36-B45.
- BARTON, J.M. JR., CAWTHORN, G. & WHITE, J. (1986): The role of contamination in the evolution of the Platreef of the Bushveld Complex. *Econ. Geol.* **81**, 1096-1104.
- BUCHANAN, D.L. (1988): Platinum-group element exploration. *Developments in Economic Geology*, **26**, Elsevier.
- BUCHANAN, D.L. & ROUSE, J.E. (1984): The role of contamination in the precipitation of sulfides in the Platreef of the Bushveld Complex. *In Sulfide deposits in mafic and ultramafic rocks*, Institution of Mining and Metallurgy, London, 141-146.
- CAWTHORN, G., BARTON, J.M. JR. & VILJOEN, M.J. (1985): Interaction of floor rocks with the Platreef on Overysel, Potgietersrus, northern Transvaal. *Econ. Geol.* **80**, 988-1006.
- EASTON, R.M., JOBIN-BEVANS, L.S. & JAMES, R.S. (2004): Geological Guidebook to the Paleoproterozoic East Bull Lake Intrusive Suite Plutons at East Bull Lake, Agnew Lake and River Valley, Ontario. *Ontario Geological Survey, Open File Report 6135*, 84p.
- GAIN, S.B. & MOSTERT, A.B. (1982): The geological setting of the platinoid and base metal sulfide mineralisation in the Platreef of the Bushveld Complex in Drenthe, north of Potgietersrus. *Econ. Geol.* **77**, 1395-1404.
- HARRIS, C. & CHAUMBA, J.B. (2001): Crustal contamination and fluid-rock interaction during the formation of the Platreef, northern limb of the Bushveld Complex, South Africa. *J. Petrology*, **42**, 1321-1347.
- HATTORI, K.H., ARAI, S., CLARKE, D.B. (2002): Selenium, tellurium, arsenic and antimony contents of primary mantle sulfides. *Can. Mineral.* **40**, 637-650.
- ILJINA, M. (1994): The Portimo Layered Igneous Complex with emphasis on diverge sulphide and platinum-group element deposits. *Acta Univ. Ouluensis, Ser. A, Sci. Rer. Natur.* **258**.
- ILJINA, M. (2004): Tutkimustyöselostus valtausalueilla Koskiahon 1–2, Kuusi 4–23, Maaselkä 1–14, Murto 1–2 sekä Portti 1–37 Pudasjärven, Taivalkosken ja Posion kunnissa suoritetusta tutkimuksesta vuosina 1996–2002. M 06/3543/2004/1/10. Extended English abstract.
- ILJINA, M.J., KARINEN, T. & RÄSÄNEN, J. (2001): The Koillismaa Layered Complex: general geology, structural development and related sulphide and platinum-group element mineralization. *In Mineral Deposits at the Beginning of the 21st Century*. (Piestrzynski, A. et al., ed.), A.A. Balkema, Lisse, 649-652.
- JAMES, R.S., JOBIN-BEVANS, S., EASTON, R.M., WOOD, P., HROMINCHUK, J.L., KEYS, R.R. & PECK, D.C. (2002): Platinum-group element mineralization in Paleoproterozoic basin intrusions in central and northern Ontario. *In The Geology, Geochemistry, Mineralogy and Mineral Beneficiation of Platinum-Group Elements* (Cabri, L.J. ed.). *Can. Inst. Mining Metall., Special Vol.* **54**, 339-365.
- KINLOCH, E.D. (1982): Regional trends in the platinum-group mineralogy of the critical zone of the Bushveld Complex, South Africa. *Econ. Geol.* **77**, 1328-1347.
- KOJONEN, K. & ILJINA, M. (2001): Platinum-Group Minerals in the Early Proterozoic Kuusijärvi Marginal Series, Koillismaa Layered Igneous Complex, Northeastern Finland. *In Proceedings of the sixth Biennial SGA–SEG meeting* (A. Piestrzynski et al. (ed.). A.A. Balkema, Lisse, 653-656.

- LAHTINEN, J.J., ALAPIETI, T.T., HALKOAHO, T.A.A., HUHTELIN, T.A. & ILJINA, M.J. (1989): PGE mineralization in the Tornio-Näränkäväära layered intrusion belt. *In* 5th International Platinum Symposium. Guide to the Post-Symposium Field Trip, (Alapieti, T., ed.). *Geol. Surv. Finland, Guide* **29**, 43-58.
- LEE, C.A., CAWTHORN, R.W. & BARTON J.M., JR. (1989): Further Sr-isotope and trace element studies on the Platreef, Bushveld Complex. *Bull. Geol. Soc. Finland* **61**, 21.
- MCELDUFF, B. & ILJINA, M. (1991): Sulphide and PGE mineralogy of the marginal series of the Suhanko-Konttijärvi intrusion, Finland. *In* Sixth International Platinum Symposium, (Barnes, S.J., ed.), programme and extended abstracts, 37.
- MOSTERT, A.B. (1982): The mineralogy, petrology and sulphide mineralisation of the Platreef north-west of Potgietersrus, Transvaal, Republic of South Africa. *South African Geol. Survey Bull.* **72**, 48p.
- NELL, J. (1985): The Bushveld metamorphic aureole in the Potgietersrus area: evidence for a two-stage metamorphic event. *Econ. Geol.* **80**, 1129-1152.
- PAKTUNC, A., HULBERT, L. & HARRIS, D. (1990): Partitioning of the platinum-group and other trace elements in sulfides from the Bushveld Complex and Canadian occurrences of nickel-copper sulfides. *Can. Mineral.* **28**, 475-488.
- PEACH, C., MATHEZ, E. & KEAYS, R. (1990): Sulfide melt-silicate melt distribution coefficients for noble metals and other chalcophile elements as deduced from MORB: Implications for partial melting. *Geochim. Cosmochim. Acta* **54** 3379-3389.
- PECK, D.C., JAMES, R.S., CHUBB, P.T. PREVEC, S.A. & KEAYS, R.R. (1995): Geology, Metallogeny and Petrogenesis of the East Bull Lake Intrusion, Ontario. *Ontario Geological Survey, Open File Report* **5923**.
- RUIZ, J., BARRA, F., ASHWELL, L.D. & LE GRANGE, M. (2004): Re-Os systematics on sulfides of the Platreef, Bushveld Complex, South Africa. *Geoscience Africa 2004, Abstract Volume*, University of the Witwatersrand, Johannesburg, South Africa, 564.
- SHARMAN-HARRIS, E.R. & KINNAIRD, J.A. (2004): Sulfur isotope studies of the southern Platreef, Northern limb, Bushveld Igneous Complex. *Geoscience Africa 2004, Abstract Volume*, University of the Witwatersrand, Johannesburg, South Africa, 589-590.
- SHARPE, M. (1986): Bushveld Complex - Excursion guidebook. *Geocongress '86*, guide 23C, 142 p.
- SHARPE, M.R. CROUS, S.P. GAIN, S.B. CHUNNETT, G.K. & LEE, C.A. (2002): Sheba's Ridge – an unconventional setting for Platreef, UG2 and Merensky-style PGE-BMS deposits in the Bushveld Complex. *9th International Platinum Symposium*, Abstract with Program, Billings, Montana p. 407-408.
- VAILLANCOURT, C., SPROULE, R.A., MACDONALD, C.A., LESHNER, C.M. & HULBERT, L.J. (2002): Classification of mafic-ultramafic intrusions in Ontario and implications for platinum-group element mineralization. *9th International Platinum Symposium*, Abstract with Program, Billings, Montana, 457-459.
- VAN DER MERWE M.J. (1976): The layered sequence of the Potgietersrus limb of the Bushveld Complex. *Econ. Geol.* **71**, 1377-1351.
- VUORELAINEN, Y., HÄKLI, T., HÄNNINEN, E., PAPUNEN, H., REINO, J. & TÖRNROOS, R. (1982): Isomertieite and other platinum-group minerals from the Konttijärvi layered mafic intrusion, northern Finland. *Econ. Geol.* **77**, 1511-1518.
- WAGNER, P. A. (1929): *The platinum deposits and mines of South Africa*. Oliver and Boyd, Edinburgh, 326 p.

CHAPTER 5: PGE AND PGM IN THE SUPERGENE ENVIRONMENT: A CASE STUDY OF PERSISTENCE AND REDISTRIBUTION IN THE MAIN SULFIDE ZONE OF THE GREAT DYKE, ZIMBABWE

Thomas Oberthür & Frank Melcher
 Federal Institute for Geosciences and Natural Resources (BGR), Stilleweg 2,
 D-30655 Hannover, Germany.
 E-mail: thomas.oberthuer@bgr.de, f.melcher@bgr.de

INTRODUCTION

The Great Dyke of Zimbabwe constitutes the world's second largest reserve of PGE after the Bushveld Complex in neighboring South Africa. Economic concentrations of PGE are restricted to sulfide disseminations of the Main Sulfide Zone (MSZ). Currently, pristine, sulfide-bearing MSZ ores are mined underground (Mimosa mine) or from surface (Ngezi mine) and are treated following conventional metallurgical practice (grinding, milling, flotation, smelting and production of a matte, chemical refining). Near-surface oxidized MSZ ores have a large potential at an estimated resource of 400 Mt of ore (Prendergast 1988). A first attempt to mine oxidized MSZ ores was undertaken at the Old Wedza mine (close to Mimosa mine) between 1926 and 1928, and again at the Hartley mine from late 1997 to 1999. However, all these attempts to extract the PGE from this ore type proved uneconomic due to low PGE recoveries (<50%) achieved by conventional metallurgical methods. At present, oxide ores of the MSZ and also of the Merensky Reef and the Platreef of the Bushveld Complex are left *in situ*, are stockpiled or discarded as waste. However, oxidized PGE-bearing ores definitely present an important resource that will be tapped in the near future.

The present contribution reports on the study of oxidized MSZ ores taken at the mines and prospects at the Hartley, Ngezi, Unki and the Old Wedza/Mimosa mines (Fig. 5-1). Vertical profiles across the MSZ and bulk samples were investigated and changes down dip were followed. The geochemical and mineralogical studies pursue the redistribution of the PGE and PGM from the pristine, sulfide-bearing ores into the supergene environment (oxidized ores). The main aim is to locate the PGE in their mineralogical form in order to understand the mineralogical balance of the PGE in the ores and thereby facilitate the evaluation of metallurgical options for their recovery. Direct relationships between primary and secondary PGE/PGM miner-

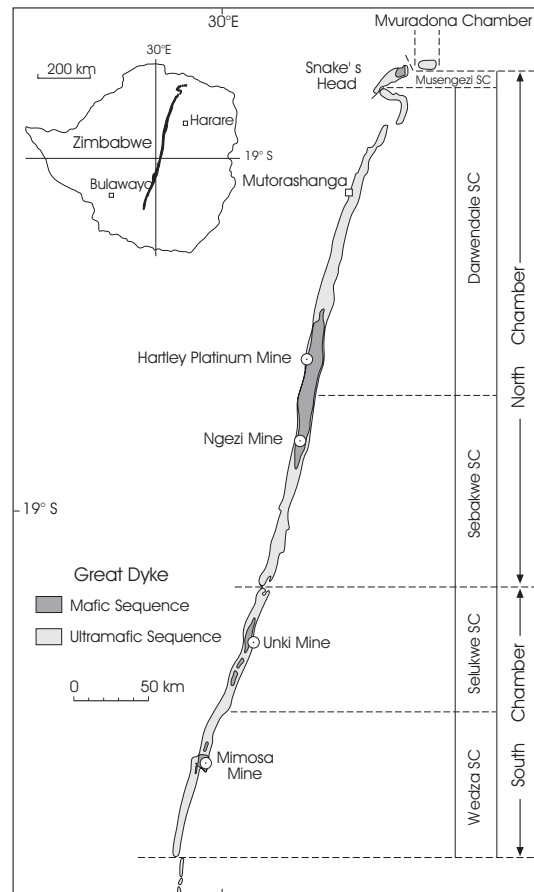


FIG. 5-1: Generalized geology of the Great Dyke and its subdivision into chambers and sub-chambers (SC) after Wilson and Prendergast (1989). Also shown are the localities of platinum mines and prospects.

alization are established.

GEOLOGICAL SETTING

The Great Dyke layered intrusion is Archean (2575.4 ± 0.7 Ma; Oberthür *et al.* 2002a) in age. It is linear in shape and trends over 550 km NNE at a maximum width of about 11 km, and cuts Archean granites and greenstone belts of the

Zimbabwe craton (Fig. 5-1). Stratigraphically, the layered series of the Great Dyke is divided into a lower Ultramafic Sequence and an upper Mafic Sequence. Economic concentrations of PGE, Ni and Cu in the form of disseminations of mainly intercumulus sulfides are found in the Main Sulfide Zone (MSZ) hosted in pyroxenites, some metres below the transition from the Ultramafic to the Mafic Sequence. The Main Sulfide Zone is generally between 1.5 and 4 m wide. Pervasive oxidation of the sulfides exceeds 30 metres below surface in the Hartley open pits. In the Ngezi mine area, the irregularly undulating border between the pervasively oxidized MSZ and ores showing incipient oxidation, *i.e.*, containing relict sulfides, lies between 15 and 25 metres below surface.

SAMPLES AND METHODS

Sampling in open pits and trenches showed that the oxidized ores comprise relatively competent rocks of light to dark brownish color which locally have some greenish or bluish staining caused by secondary Cu- and Ni-minerals. The grains of orthopyroxene making up the pyroxenites mostly show incipient alteration only, whereas the interstitial network is filled by iron hydroxides and brownish smectites. Vertical profiles and bulk samples of oxidized MSZ were taken in open pits at Hartley mine, from drill cores of the Ngezi project, and from trenches at Unki and the Old Wedza mines. Due to the fact that only small quantities of discrete PGM were encountered in polished sections of the oxidized samples, heavy mineral concentrates were prepared from a number of samples weighing between 1.1 and 1.7 kg. These were step-wise reduced in size using a RETSCH crusher at steps 8, 6, 4, 2 and 1 mm. After each step, the material <1 mm was sieved and collected. Finally, the total <1 mm material was transferred to a wash pan to concentrate the heavy mineral fraction. The concentrates were studied under a binocular microscope and grains of interest were extracted and transferred onto a SEM sample holder. The single grains and additional polished sections were studied with a SEM having an energy dispersive analytical system attached. Polished sections were made from the rock and concentrate samples. The whole rock samples were analyzed for major and trace elements by XRF, and PGE contents were determined by INAA after Ni-sulfide extraction. The polished sections were investigated by reflected light microscopy and SEM/EDS. Mineral analyses were first performed using the

Camebax, followed (since 2001) by the Cameca SX100 electron microprobe at BGR. Both the routine analytical mode (20 kV, 20 nA, *ca.* 1 μ m beam diameter and counting times 10–20 seconds on peak) and the trace element program (35 kV, 300 nA, *ca.* 5–10 μ m beam diameter and counting times 600 seconds on peak) were employed.

PRISTINE MAIN SULFIDE ZONE

Geochemistry

Geochemical profiles across the pristine, sulfide-bearing MSZ were studied extensively in the forefront of and during mining activities. Apart from minor variations of the MSZ metal profiles, all previous workers agree that the MSZ is characterized by a typical vertical pattern of base metal sulfide and PGE distribution (*e.g.*, Prendergast 1988, Prendergast and Wilson 1989, Wilson 2001, Oberthür 2002). This pattern is characterized by a distinct zonation, also called “offsets”, *i.e.*, a certain degree of decoupling, and separation of the respective element distribution patterns and peak concentrations, especially of Pd from Pt, and also of all PGE from the base metals. This has led to the subdivision of the MSZ into a lower PGE subzone and an upper BMS subzone, as proposed by Prendergast (1988, 1990), and the further subdivision of the PGE subzone into a lower (Pd>Pt) and an upper part (Pd<Pt). Wilson *et al.* (2000) showed that the MSZ is composed of a number of chemically distinct, consecutive layers which they interpreted as resulting from minor emplacements of primitive magma into the chamber causing undersaturation of sulfur.

The typical vertical distribution pattern of the base metals and sulfur (BMS = Cu, Ni, and sulfur), Pt and Pd is shown in Figure 5-2, which is a 2.70 metres wide profile across the MSZ, from the Ngezi mine (drill hole NG 36). MSZ sections from the other localities show very similar patterns. Following the onset of sulfide mineralization (sulfur contents > 0.10 wt% S) at the bottom of the profile, the metal zonation within the MSZ is characterized by a number of consecutive peaks of the PGE, the base metals and sulfur. From bottom to top, BMS contents increase continuously; the peak of Pd is reached first whereas the peak of Pt follows further up in the sequence. The main BMS peak is reached either coincident with the Pt peak or slightly displaced further up. From the BMS peak upwards, undulating values of Ni and Cu are observed whereas the PGE contents drop to low levels.

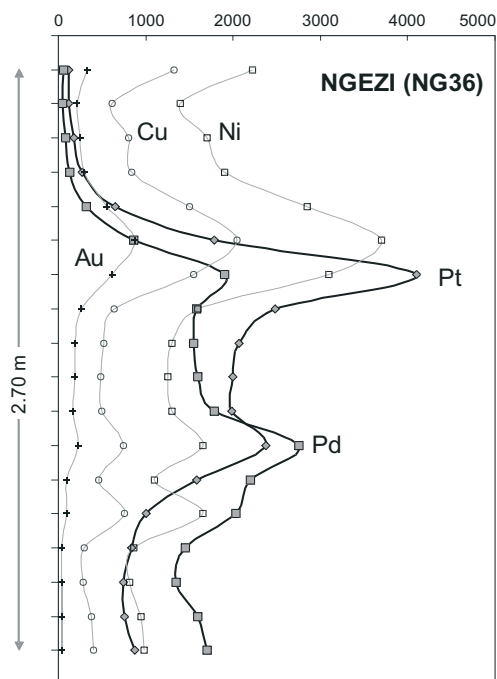


FIG. 5-2: Geochemical profile (core NG 36) of selected elements (Cu and Ni in ppm; Pt, Pd and Au in ppb) across the pristine MSZ at Ngezi Mine showing the zonation of the MSZ (“offsets”). Cu and Ni in ppm; Pt, Pd and Au in ppb.

PGM and PGE-Carriers

The pyroxenites of the MSZ contain between 0.5 and 10 vol% of sulfides, mainly pyrrhotite, pentlandite, chalcopyrite and subordinate pyrite. The sulfide grains and aggregates are up to several mm across and occur mainly interstitial to grains of cumulus orthopyroxene and minor chromite, intercumulus clinopyroxene, plagioclase, and alteration products such as calcic amphibole, anthophyllite, magnetite, serpentine, talc and chlorite. The PGM are usually included in pyrrhotite or chalcopyrite, rarely in pentlandite, or they occur at sulfide/sulfide or sulfide/silicate contacts, or within silicates. PGM intergrown with pyrite are extremely rare. Grain sizes (apparent maximum diameters) of the PGM range from < 5 to 50 μm in general, but may in exceptional cases reach up to 373 μm in longest dimension (Oberthür 2002).

The suite of PGM found in the MSZ comprises (Pt,Pd)-bismuthotellurides (*i.e.*, moncheite, maslovite, merenskyite, michenerite), sperrylite, the (Pt,Pd)-sulfides cooperite and braggite (termed cooperite/braggite in the following), and some rarer phases (Prendergast

1990, Coghill and Wilson 1993, Evans *et al.* 1994, Oberthür 2002). In his summary encompassing all mining activities along the Great Dyke, Oberthür (2002) has shown that mineral proportions by number demonstrate the predominance of (Pt,Pd)-bismuthotellurides (50.1%), followed by sperrylite (19%), cooperite/braggite (8.5%), the PGE-sulfarsenides hollingworthite, platarsite, irarsite and ruarsite (11.9%), laurite (5.0%), Pt-Fe alloy (2.4%) and some less common PGM (Table 5-1). The various PGM are heterogeneously distributed within the MSZ sequence. Larger numbers of discrete PGM are found from about 20 cm above to 60 cm

TABLE 5-1. PLATINUM-GROUP MINERALS (PGM) AND PGE-CARRIERS IN PRISTINE MSZ ORES OF THE GREAT DYKE

PGM and PGE carriers	ideal formula	relative frequency
moncheite	PtTe ₂	***
maslovite	PtBiTe	**
insizwaite	PtBi ₂	o
merenskyite	PdTe ₂	***
michenerite	PdBiTe	***
froodite	PdBi ₂	o
kotulskite	PdTe	*
sobolevskite	PdBi	o
Pd-bearing melonite	NiTe ₂	*
Pd-bearing empressite	AgTe	o
cooperite	PtS	***
braggite	(Pt,Pd)S	***
laurite	RuS ₂	*
malanite	CuPt ₂ S ₄	o
unnamed	PtSnS	*
sperrylite	PtAs ₂	***
hollingworthite	RhAsS	**
platarsite	PtAsS	*
irarsite	IrAsS	*
ruarsite	RuAsS	o
menshikovite	Pd ₃ Ni ₂ As ₃	o
atheneite	(Pd,Hg) ₃ As	o
isomertieite	Pd ₁₁ (Sb,As) ₄	o
stibiopalladinite	Pt ₅ Sb ₂	o
rustenburgite	Pt ₃ Sn	o
Pt-Fe alloy		*

Relative frequencies are: *** = very common (>10%), ** = common (3–10%), * = rare (1–3%), and o = very rare (<1%) (from Oberthür 2002).

below the Pt peak of the MSZ (Figs. 5-2 and 5-3). The (Pt,Pd)-bismuthotellurides concentrate in the area around the Pt peak of the MSZ only.

Trace PGE Contents in Sulfides

Micro-PIXE studies (Oberthür *et al.* 1997) revealed that pentlandite from the lower PGE subzone of the MSZ at Hartley, Unki and Mimosa mines have elevated contents of Pd (maximum value 2,236 ppm Pd), and Rh (max. 259 ppm Rh), and SIMS analysis showed that pyrite was a carrier of Pt (0.4–244, mean 35.5 ppm; n=37). Electron microprobe analysis using the CSIRO Trace program revealed maximum contents of 2,506 ppm Pd and 562 ppm Rh in pentlandite (Oberthür *et al.* 2003a). Within the MSZ sequence, Pd contents in pentlandite appear to attain and stay at a plateau level of *ca.* 1000–1200 ppm Pd through most of the PGE subzone of the MSZ (maximum average value = 1,379 ppm Pd). Further up in the sequence, Pd contents in pentlandite drop to values below the detection limit of the method (about 40 ppm Pd) just before reaching the Pt peak. The data obtained underline that most of the Pd is hosted by pentlandite in the lower and central parts of the PGE subzone.

Figure 5-3 summarizes the major geochemical and mineralogical variations and trends observed in the MSZ, exemplified especially by profiles from the Hartley mine. Notable are the elevated contents of Pd in pentlandite in the lower

part of the PGE subzone, the overlapping distributions of the various PGM or PGM groups within the profile, and the preferred concentration of laurite in the basal part of the PGE subzone. Gold and the tellurides of Bi, Ag, Ni and Pb mainly occur in the transition from the PGE to the BMS subzone of the MSZ. Changes in pyrrhotite compositions and the presence of pyrite in the upper part of the PGE subzone and the BMS subzone indicate increasing fS_2 up sequence.

OXIDIZED MAIN SULFIDE ZONE Geochemistry

Geochemical profiles across the oxidized MSZ resemble those of pristine MSZ sequences with respect to their general shapes and Pt grades. However, the element distributions show wider dispersions and the different peaks appear less pronounced. In the profiles of oxidized MSZ, the offsets of Pd → Pt are well discernable as exemplified by two sections from the Hartley mine open pit (profile HOP-20x; Fig. 5-4) and a drill core from Ngezi mine (profile NRC 146; Fig. 5-5). In drill core NRC 146 (Fig. 5-5) all peaks coincide in one sample, probably due to the wide sample width of 50 cm. Compared to profiles of pristine MSZ (*e.g.*, Fig. 5-2), the depletion of Pd relative to Pt is evident in Figs. 5-4 and 5-5. Indeed, relative to Pt, a variable proportion of the Pd is “missing” in the average data of the profiles of oxidized MSZ relative to those of the sulfide MSZ. Whereas

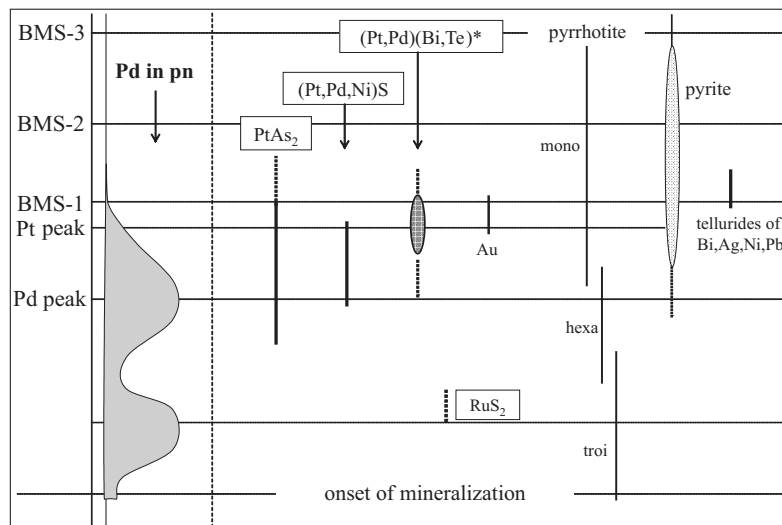


FIG. 5-3: Summary of geochemical and mineralogical data in profiles across pristine MSZ, mainly based on data from the Hartley mine. Abbreviations: BMS-1, -2, -3: Base metal sulfide peaks. Pd in pn = Pd contents in pentlandite (schematic). (Pt,Pd)(Bi,Te)* = (Pt,Pd)-bismuthotellurides (*cf.* Table 1). Pyrrhotite: troi = troilite; hexa = hexagonal; mono = monoclinic (suggested from microprobe analyses).

average Pt/Pd ratios of 1.28 (n=12) characterize pristine sulfide MSZ, pervasively oxidized MSZ ores have average Pt/Pd ratios of 2.43 (n=9). Figure 5-6 underlines this trend and corroborates the findings of *e.g.*, Wagner (1929) on the Merensky reef of the Bushveld and of Evans *et al.* (1994) on surface ores of the Great Dyke, that Pd is more mobile than Pt and is dispersed in the supergene environment. The present data from the Great Dyke demonstrate that relative to Pt, whose concentration ranges are nearly identical in pristine and oxidized MSZ ores, about 50% of the Pd is lost from the system. On the other hand, cementation zones or supergene enrichment horizons in or around the oxidized MSZ ores were neither discovered during open pit mining at Hartley mine nor in the course of extensive exploration drilling in the Ngezi project area (R. Brown, H. Wilhelmij, pers. comm.).

The obvious trend seen in Fig. 5-6 is underlined by gain/loss calculations following equations given by Gresens (1967). At measured average specific gravities of 3.23 g.cm^{-1} (pristine

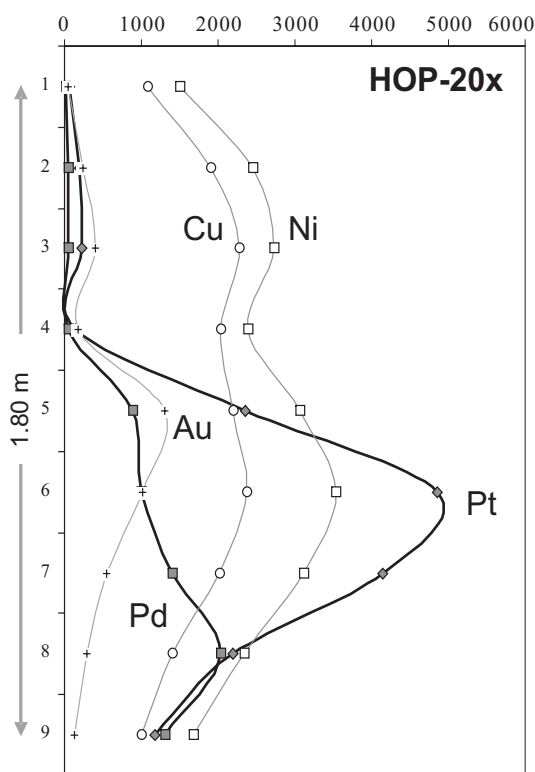


FIG. 5-4: Profile HOP-20x across oxidized MSZ at Hartley Mine (9 samples, each 20 cm wide) showing the distribution patterns of Cu and Ni (in ppm), Pt, Pd and Au (in ppb).

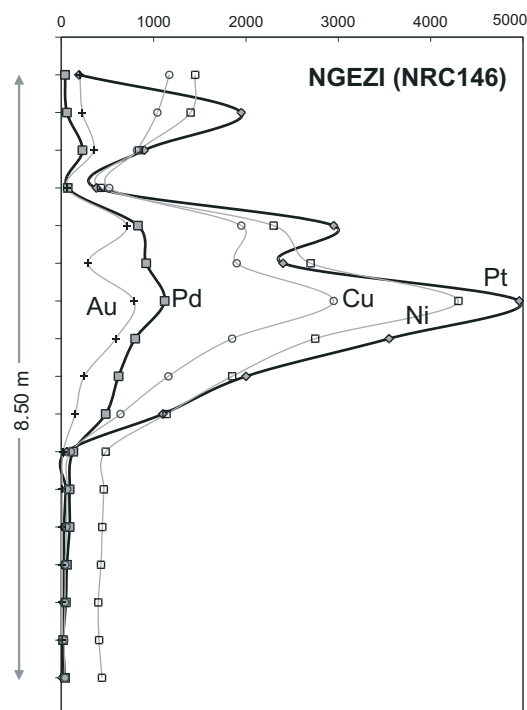


FIG. 5-5: Profile NRC 146 across oxidized MSZ at Ngezi Mine (sample widths = 50 cm each) showing the distribution patterns of Cu and Ni (in ppm), Pt, Pd and Au (in ppb).

MSZ) and 3.05 g.cm^{-1} (oxidized MSZ), and regarding Al_2O_3 (Al) as constant, the following principal gains and losses due to weathering are observed from pristine to oxidized MSZ (example from Hartley mine; Fig. 5-7).

Most major elements are relatively immobile; significant losses are observed for Na, K and S (partial destruction of opx, feldspar, phlogopite, and sulfides, respectively), combined with a large gain of LOI (formation of hydrous silicates, FeOOH). There is a conspicuous gain of Cu and Au which may point to a certain supergene enrichment of these elements in the section (HOP-20x) studied. In general, PGE contents remain relatively constant except for Pd, which shows a marked loss of 37%. The role of Os is not that clear as a large number of analyses are close to or below the detection limit of Os (5 ppb).

Downdip trends in Pt contents were studied along a line of four drillholes of the Ngezi mine. Figure 5-8 shows the drillholes and the relatively wide MSZ (8 metres) at this locality, divided into a lower PGE subzone and an upper base metal subzone. The peak values of Pt range

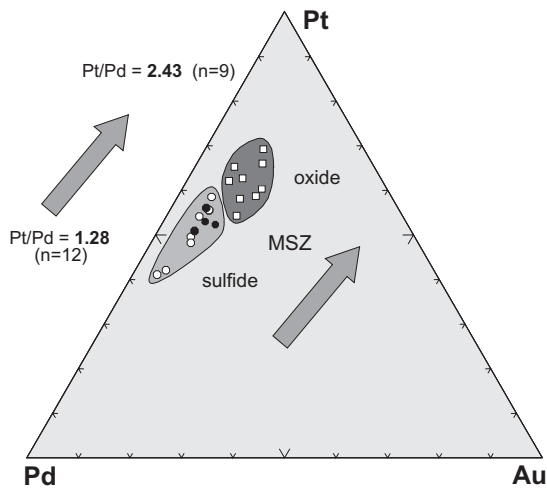


FIG. 5-6 : Triangular plot of Pt, Pd and Au contents of pristine sulfide MSZ and oxidized MSZ ores. (●) = pristine MSZ, official mine production or reserve data. (o) = averages of profiles of pristine MSZ, own data. (□) = averages of profiles of oxidized MSZ, own data.

from 2490 to 4760 ppb on 50 cm wide samples. Average values of eight samples representing the PGE subzone of the MSZ range from 1441 to 2239 ppb Pt. Obvious downdip trends of Pt grade are not discernable.

PGM and PGE-Carriers

Wagner (1929) reported sperrylite and cooperite in ores from the Old Wedza mine. Evans *et al.* (1994), Oberthür *et al.* (1999, 2000, 2002b, 2003b), Evans and Spratt (2000) and Evans (2002) studied oxidized MSZ ores and agreed that a large proportion of the primary PGE-carriers including PGM has been destroyed and that their PGE contents are now sited either in iron hydroxides, or in smectites, or occur as discrete “PGE-oxides or hydroxides”.

The oxidized samples are characterized by equidimensional cumulus orthopyroxene and subordinate intercumulus clinopyroxene and plagioclase, all of which appear relatively unaltered. The former interstitial sulfides and sulfide aggregates of the pristine MSZ are totally decomposed to iron hydroxide clots that still retain the original shape of the sulfides. An interstitial network of iron hydroxides and brownish smectites is commonly observed (Fig. 5-9). Rare relict sulfides, mainly pyrrhotite, are surrounded by rims of iron hydroxides. Although iron oxides/hydroxides may carry up to 5 wt.% Ni and Cu, respectively, they are not considered a major carrier of these elements in oxidized MSZ. Instead, according to microprobe analyses, a large proportion of the Ni and Cu is hosted in chlorites

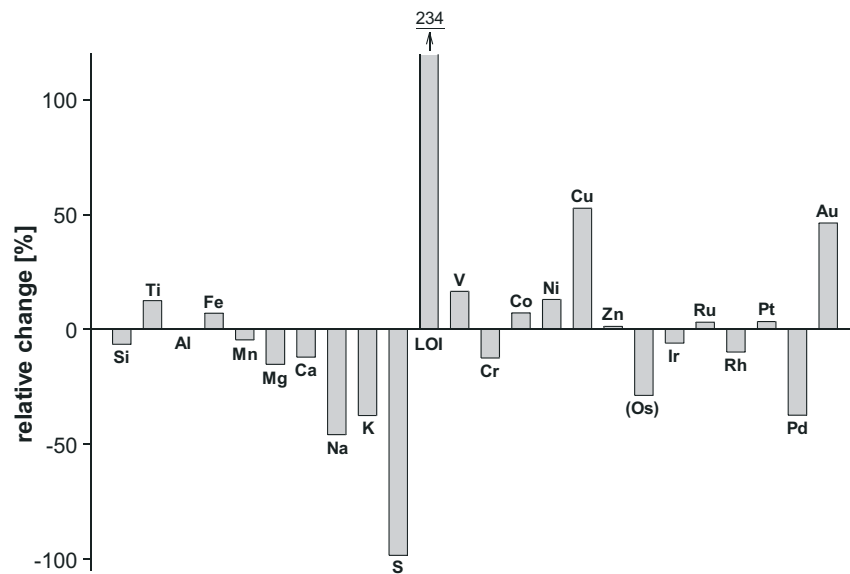


FIG. 5-7: Relative gains and losses of selected elements (Al = constant) in the oxidized MSZ compared to pristine MSZ from Hartley Mine. Oxidized MSZ sample set is from profile HOP-20x, pristine MSZ sample set comprises comparable sections of drill core CD-02 + SD-04, from Hartley Mine (Oberthür *et al.*, 2003a, b).

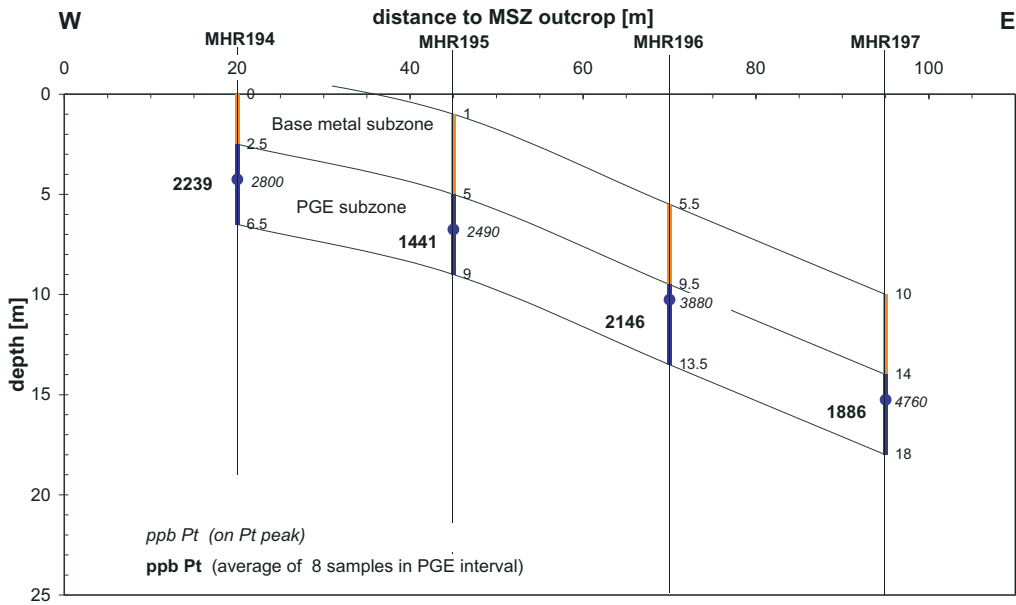


FIG. 5-8 : Depth profile of oxidized MSZ, drill line MHR 194–197, Ngezi mine. Pt contents of the samples (sample width = 0.5 m) on the Pt peak are shown in italics, and average Pt contents of the PGE subzone of the MSZ are shown in bold.

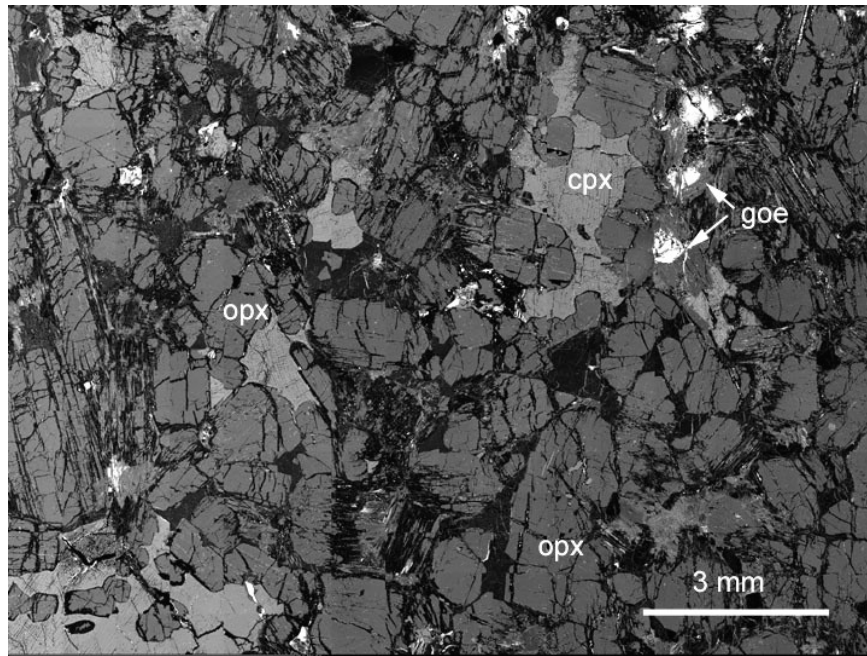


FIG. 5-9: Large area backscatter electron image of polished thin section, oxidized MSZ, surface sample from the Old Wedza mine. Note excellent preservation of cumulus orthopyroxene (opx), oikocrysts of clinopyroxene (cpx), and interstitial aggregates of goethite (goe).

and smectites. Primary sulfides are only preserved as small inclusions, usually <10 μm in size, in unaltered orthopyroxene grains. Trace concentrations of Pd (up to 1140 ppm) and Pt (up to 210

ppm) in pentlandite are very similar to what would be expected from unaltered samples in the respective stratigraphic positions within the MSZ. This indicates that a small proportion of the original

PGE content is still “in place”.

The inspection of numerous polished sections of oxide MSZ yielded an unsatisfying amount of PGM detected *in situ*. Therefore, heavy mineral concentrates were prepared and their study led to a certain quantification especially of relict PGM and to the detection of a number of other PGE carriers. In the concentrates of the samples (starting weights between 1.1 and 1.7 kg; 50 cm samples on Pt peak each) from the downdip trending drill holes shown in Fig. 5-8 (MHR 194–197), 62 distinct PGM grains were detected with grain sizes between 25 and 60 μm (Table 5-2). Obviously, (Pt,Pd)-bismuthotellurides only occur in the deepest sample (MHR 197), which shows incipient oxidation only, but are non-existent (destroyed) in the samples nearer to surface. Sperrylite and cooperite/braggite, on the other hand, are stable in the supergene environment. This is a general rule in oxidized MSZ ores, as documented by our studies at the other localities of the MSZ (see further below).

Our complementary investigations of concentrates and polished sections by SEM and microprobe analysis revealed that the PGE show a polymodal distribution in the ores of oxidized MSZ, being present in a variety of different PGM and PGE-carriers.

(1) Relict PGM, and gold

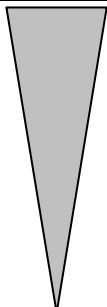
Altogether 1293 discrete PGM grains were extracted from the concentrates. Sperrylite is most common (57.2%), followed by cooperite/braggite (28.3%) and Pt-Fe alloy grains (3.1%). The ratio of

sperrylite to cooperite/braggite is nearly identical to that of the pristine MSZ, indicating that these minerals are relicts of the pristine MSZ ores. Relict (Pt,Pd)-bismuthotellurides (11.4%) were only found in a few samples (MHR 197 and Adit A) from the Ngezi mine which showed incipient alteration.

Sperrylite mostly shows idiomorphic crystal shapes (Figs. 5-10a and b). Cooperite/braggite grains, in contrast, are usually present as splinters of irregular shape with clean surfaces. In general, the sperrylite and cooperite/braggite grains show no distinct features of alteration. Rare Pt–Fe alloy grains, both compact and porous ones, were found in samples from Hartley and Ngezi. The porous grains of Pt–Fe alloy (close to Pt_3Fe) probably represent replacements of other precursor PGM of unknown chemical composition. Notably, Schneiderhöhn and Moritz (1939) showed texturally similar porous grains of “native Pt” from oxidized Merensky Reef and proposed that these grains represent relicts of sperrylite or cooperite grains. Grain sizes of the PGM (true maximum diameters) range from ca. 50–400 μm for hand-picked grains. However, in polished sections grain sizes of PGM down to 1 μm were frequently observed.

The PGM assemblage thus strongly contrasts to that of the pristine MSZ ores especially with respect to the proportion of (Pt,Pd)-bismuthotellurides (Table 5-3). The fate of the Pd hosted in interstitial pentlandite is only partly known. With the exception of a few relict grains of Pd-rich (Pt,Pd)-bismuthotellurides and some secondary Pd-bearing phases (see below), the ores

TABLE 5-2. PGM IN OXIDIZED MSZ, DRILL LINE MHR 194–197, NGEZI MINE

Sample	Depth (m)	Degree of oxidation	PtAs ₂	(Pt, Pd)S	Pt–Fe alloys	(Pt,Pd) (Bi,Te)	Σ PGM	Oxide minerals	Sulfides
MHR 194	4–4.5		1	1	–	–	2	goe, cr	None
MHR 195	6.5–7		–	–	5	–	5	goe, hm, mt, cr	None
MHR 196	10–10.5		9	–	1	1	11	goe, hm, mt, ru	Sparse relicts in silicates
MHR 197	15–15.5		4	12	–	28	44	mt, cr	po, pn, cpy, py. Incipient oxidation at rims

Number frequencies and types of PGM recovered from concentrates of oxidized MSZ, downdip trend of drill line MHR 194–197, Ngezi mine. (Pt,Pd)(Bi,Te) = (Pt,Pd)-bismuthotellurides; goe = goethite; cr = chromite; mt = magnetite; hm = hematite; ru = rutile; po = pyrrhotite; pn = pentlandite; cpy = chalcopyrite; py = pyrite.

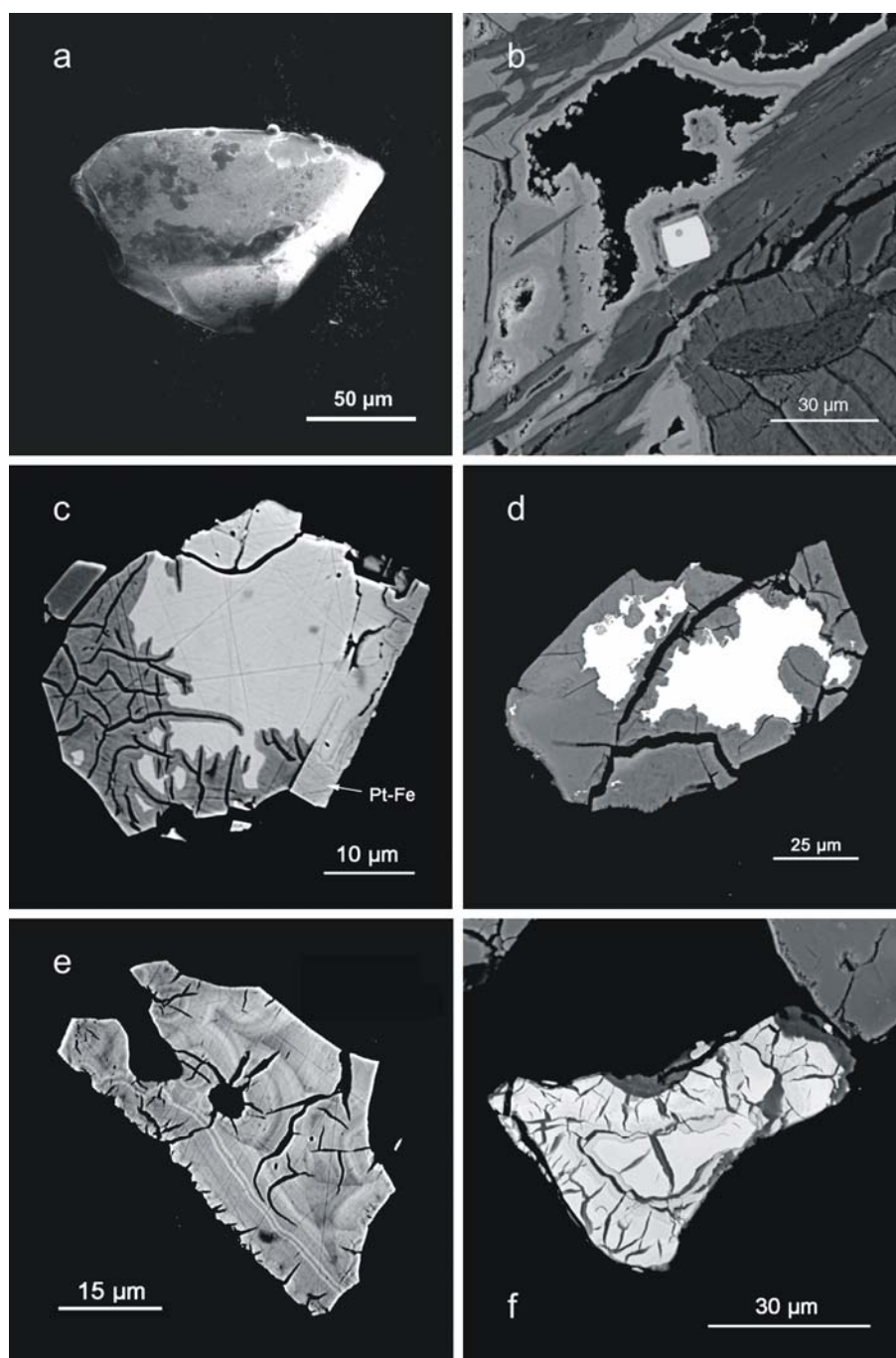


FIG. 5-10: Scanning electron microscope image (a), and backscatter electron (BSE) images (b – f) of polished sections. **a**, Idiomorphic grain of sperrylite extracted from oxidized MSZ ore, Hartley mine open pit; **b** Sperrylite grain (white) surrounded by iron-hydroxides (shades of light grey, to the left) and silicates (medium grey, right). Oxidized MSZ ore, Old Wedza mine; **c** Pt-bearing sobolevskite (light grey) being replaced by $[\text{Pd}_{49}\text{Pt}_{27}\text{Bi}_{19}]_{\Sigma 88}$ -oxides (left and bottom). Note attached grain of Pt-Fe alloy (Pt-Fe). Adit A, Ngezi mine; **d** Grain of Pd-Bi-Cu-oxide (medium grey) with relict core of michenerite (white). Hartley mine open pit; **e** Finely banded grain of PGE-oxide of slightly variable composition (see lighter and darker bands; lighter areas have between 3-5 wt.% more Pt than darker areas), on average $\sim[\text{Pt}_{67}\text{Fe}_{14}\text{Bi}_{10}]_{\Sigma 81}$, with shrinkage cracks. Adit A, Ngezi mine; **f** finely banded grain of PGE-oxide (composition $\sim[\text{Pt}_{60}\text{Pd}_3\text{Fe}_{15}\text{Cu}_8\text{Te}_5\text{Bi}_3]_{\Sigma 94}$). Adit A, Ngezi mine.

TABLE 5-3. PROPORTIONS OF DISCRETE PGM IN PRISTINE MSZ AND IN OXIDIZED MSZ ORES

locality		sulfide MSZ	oxide MSZ
PGM type ↓	(n) → [%]	801	1293
(Pt,Pd)(Bi,Te) *		50.1	11.4*
PtAs ₂		19.0	57.2
(Pt,Pd)S		8.5	28.3
Pt and Pt-Fe alloys		2.4	3.1
PGE-AsS ⁺		11.9	—
others		8.7	×

Proportions (by number of grains; in %) of discrete PGM in pristine MSZ (observed in polished sections), and in oxidized MSZ ores (extracted from concentrates). (Pt,Pd)(Bi,Te)* = (Pt,Pd)-bismuthotellurides. (* The number frequency of (Pt,Pd)-bismuthotellurides in oxide MSZ is considerably lower; 11.4 % given includes some samples showing incipient oxidation only). (Pt,Pd)S = cooperite and braggite. PGE-AsS⁺ = PGE-sulpharsenides. Proportions of (Pt,Pd)-oxides/hydroxides and other PGE-bearing phases in the oxidized MSZ cannot be estimated.

of oxidized MSZ only contain discrete grains of Pt-rich PGM.

A distinct variation in the proportions of discrete PGM grains is obvious within vertical profiles of oxidized MSZ. For example, from the samples of profile HOP-20x from Hartley mine (see Fig. 5-2), 407 PGM grains were extracted and it was observed that the ratio of sperrylite to cooperite/braggite steadily increases from bottom to top. Similar relationships were also found in profiles across the MSZ from the Ngezi and Unki mines. The varying proportions of these PGM probably reflect original features of the respective pristine MSZ sequences as described by Oberthür *et al.* (2003a) and schematically depicted in Fig. 5-3.

Gold grains from concentrates of oxidized MSZ have various shapes (filigree, hooked, platy with crystal faces) and far more resemble gold from primary deposits than rounded, detrital gold. Their sizes range from 40–300 µm, much larger than gold grains from pristine MSZ (usually < 25 µm). The size distribution combined with their shapes indicates that the gold grains are products of remobilization processes and coagulated to larger grains in the oxidized MSZ.

(2) (Pt,Pd)-oxides and/or hydroxides

The formation of mineralogically and chemically ill-defined “PGE-oxides or hydroxides” was observed around relict, disintegrating (Pt,Pd)-bismuthotellurides (Figs. 5-10c and d). These alteration phases are generally porous to various degrees and chemically inhomogeneous. Preliminary data show that they are characterized by relative losses of Bi and Te, an upgrade of Pt and/or Pd contents (*e.g.*, from *ca.* 30–35 atomic% Pt in moncheite to 60–70 atomic% Pt in the alteration rims, analyzed on an oxygen-free basis), and substantial gains in mainly Fe and Cu (up to some wt%). The presence of oxygen in these phases was confirmed by electron microprobe analysis in progress, underlining that these phases are oxides or hydroxides as also stated by Evans and Spratt (2000). In addition to the alteration rims around disintegrating (Pt,Pd)-bismuthotellurides, individual, finely banded grains of (Pt,Pd)-oxides or hydroxide phases were also detected (Figs. 5-10 e and f). Notably, these grains show prominent shrinkage cracks indicating dewatering.

(3) Secondary PGM (neoformations)

A detailed investigation of polished sections from oxidized MSZ of the Old Wedza mine (Gregor 2004) revealed the presence of a few relict PGM only, and a larger number of small PGM grains of secondary nature. The first group comprises sperrylite, up to 10 µm in size (Fig. 5-11a), moncheite enclosed by magnetite, and a grain of rustenburgite (Pt,Pd)₃Sn, 8 µm long, enclosed by orthopyroxene and accompanied by amphibole, chlorite and smectite (Fig. 5-11b). The second group comprises very small (<5 µm in size) grains of poorly defined phases (Fig. 5-11 a, c, d, e). Some of them may actually be oxides or hydroxides, others are alteration products of primary PGM, or neoformations. Compounds of Pt-S, Pd-S, Pt-Pd-As-Cu, Pd-Cu-Fe, Pt-Fe and Pt were also identified, either hosted by Fe hydroxides or by hydrous silicates, or commonly by amphibole, chlorite- or smectite-like phases. None of the PGM grains has stoichiometric composition; concentrations of sulfur and arsenic, if present, are much lower than in their presumed precursor phases. Notably, both Pt and Pd phases are present.

(4) PGE in iron- and manganese-hydroxides

Iron hydroxides forming rounded aggregates, up to 0.5 mm in size, interstitial to orthopyroxene and

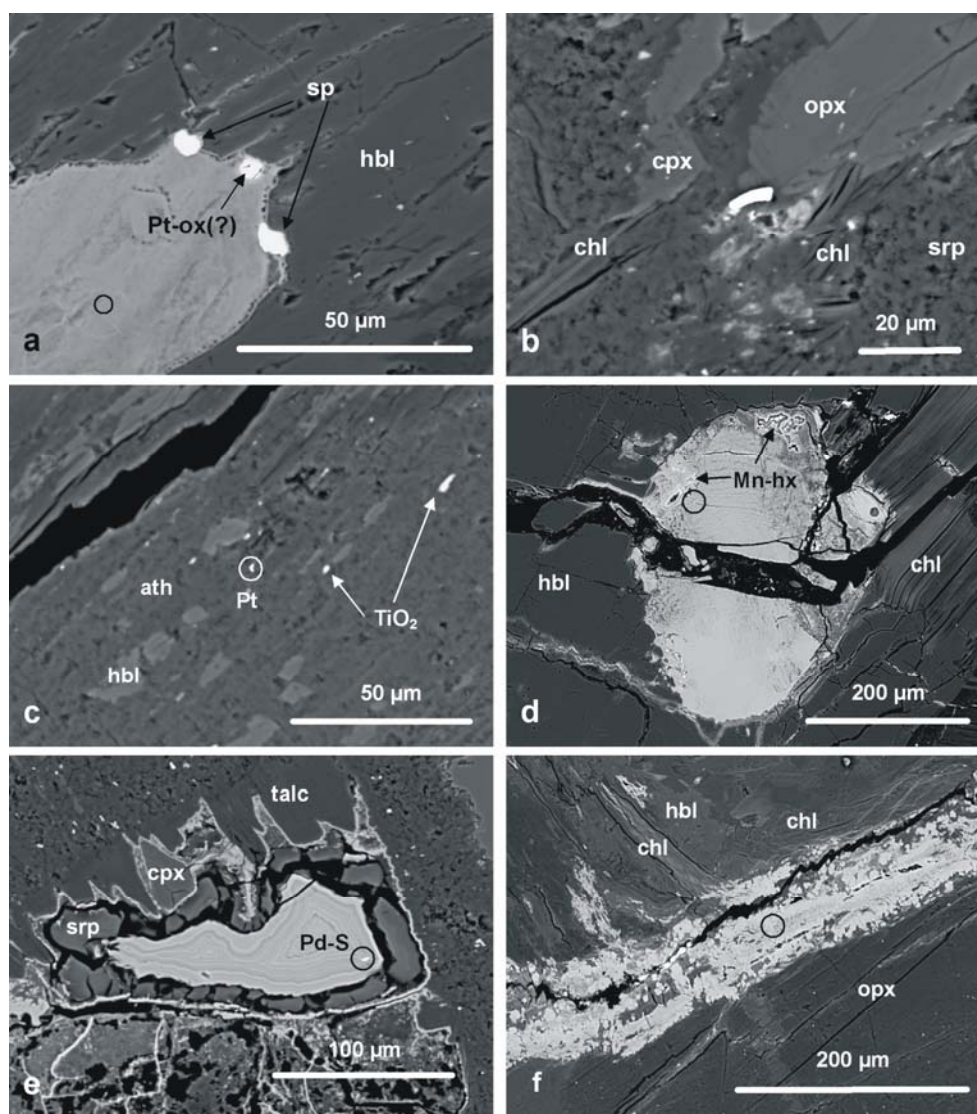


FIG. 5-11: Backscatter electron images of PGE-bearing phases in oxidized MSZ, Old Wedza Mine. **a**, two sperrylite (sp) grains and a Pt-Fe-oxygen (?) compound on the rim of an Fe-hydroxide aggregate (light grey) and tremolitic hornblende (hbl). The Fe-hydroxide has completely replaced an interstitial sulfide aggregate and carries ca. 200 ppm Pt (circle indicates position of microprobe trace analysis), 7 wt.% SiO₂ and 2 wt.% NiO. MIM-804 (section 6829). **b**, primary rustenburgite [(Pt,Pd)₃Sn; white] at margin of altered orthopyroxene (opx) intergrown with clinopyroxene (cpx). The inhomogeneous area (shades of grey) below the PGM consists of Mn-rich, Pd-bearing phyllosilicates (2–13 wt.% Pd), probably intermixed chlorite and smectite. Associated are PGE-free Ni-Cu-rich chlorite (chl), serpentine (srp) and amphibole. MIM-803 (section 6828). **c**, small grain (circle) of platinum oxide (?) in amphibole matrix (anthophyllite, ath; tremolitic hornblende, hbl) at the periphery of an altered sulfide droplet (not visible). Other bright dots are TiO₂ phases. MIM-11 (section 5320a). **d**, Fe-hydroxide aggregate enclosed by chlorite (chl) and hornblende (hbl). The Fe-hydroxide (24 wt.% SiO₂, elevated Mg, Al, Ca, V and Cu contents) has areas and veinlets of Mn-Co-hydroxide (Mn-hx) carrying 150–400 ppm Pt, and a small PGM (Pt) in a crack (circle). Coarse-grained chlorite is Ni- and Cu-rich (up to 6 and 4 wt.%, respectively). MIM-11 (section 5320a). **e**, Fe-hydroxide with colloform texture and inclusion of Pd-S compound (circle) within a matrix of Fe-rich serpentine (srp), talc, and clinopyroxene (cpx). The Fe-hydroxide carries 20 wt.% SiO₂ and elevated contents of Ca, V, Cu; trace analysis gave 30 ppm Pt and <25 ppm Pd. MIM-803 (section 6828). **f**, iron hydroxide vein at the border of altered orthopyroxene (opx) and a chlorite (chl)-amphibole (hbl) assemblage. The Fe-hydroxide contains 10 wt.% SiO₂ and up to 2.5 wt.% CuO; Pt and Pd are below 25 ppm (circle indicates position of trace analysis). Chlorite carries up to 5.5 wt.% NiO (bright areas) along with Ti and Cr. MIM-11 (section 5320a).

other silicates represent altered magmatic sulfide droplets (Fig. 5-11 a, d, e). They also occur as vein-like structures that crosscut the silicates (Fig. 5-11f). Both types of Fe hydroxides reveal characteristic layered and zoned internal textures. Fe hydroxides pseudomorphous after sulfide droplets may carry small grains of secondary PGM (mainly Pt, but also relict PGM, *e.g.*, a Pd-S compound; see Figs. 5-11 a, d, e), whereas the vein-like hydroxides are barren of PGM. Preliminary microprobe analyses reveal a distinct suite of minor and trace elements in the Fe hydroxides. Most notable are highly variable concentrations of SiO₂ (5–25 wt.%), correlating remarkably with V₂O₅ (up to 0.5 wt.%), MgO (up to 0.8 wt.%), CaO (up to 2 wt.%) and CuO (up to 2.5 wt.%). Additional significant impurities are Al₂O₃ (up to 4 wt.%), NiO (up to 3 wt.%) and Cl (up to 0.3 wt.%). On average, Fe hydroxides replacing sulfide droplets have higher concentrations of impurities than the vein-like material. The extraordinary correlation of presumably silicate-bound elements and metals corroborates that mixtures of Fe hydroxide with Si-rich material are present, probably amorphous or very fine-grained clayey substances. As determined by microprobe trace analysis, the Fe hydroxide aggregates may carry up to 230 ppm Pt and 150 ppm Pd (detection limit of the TRACE method is Pt ~ 30 ppm and Pd ~ 25 ppm). In the iron-hydroxide veinlets, however, the Pt and Pd concentrations invariably are below the detection limits.

In some cases, Fe hydroxides pseudomorphous after sulfide droplets are veined by bluish/grey Mn–Co–Ni–Cu-hydroxides (17–47 wt.% Mn, 7–18 wt.% Co, 8–13 wt.% Ni, 4–23 wt.% Cu) that have elevated concentrations (40–400 ppm) of Pt, but Pd contents are below the detection limit of 25 ppm (Fig. 5-11d).

(5) PGE in smectites and chlorites

Fine-grained weathering products in oxidized MSZ comprise serpentine, smectite and Ni–Cu-bearing chlorite-like phases (*e.g.*, Herb 2000). Smectite and chlorite carry up to several wt.% Ni and Cu. Rarely, PGE were detected in phyllosilicates. The example presented in Fig. 5-11b shows an area of intermixed Ni–Cu-rich chlorite and Pd-bearing Mn-rich smectite (?), close to primary rustenburgite. The smectite phase has areas containing up to 18 wt.% Pd and 6.5 wt.% Pt, together with high MnO (up to 20 wt.%), CuO (up to 15 wt.%), NiO (up to 9 wt.%), CaO (up to 3 wt.%) and CoO (up to 2 wt.%). The structural siting of the PGE and the phase

identities are not yet determined unequivocally. However, secondary fluorescence from the nearby rustenburgite seems unlikely to account for the PGE. Therefore, it is envisaged that phyllosilicates forming during weathering may incorporate some dissolved PGE.

DISCUSSION AND CONCLUSIONS

Figure 5-12 summarizes the basic mineralogical and geochemical trends emerging from the oxidation of the MSZ and observed in the present study. Within the ores of pristine, sulfide-bearing MSZ, the PGE are bimodally distributed. Pt mainly occurs in the form of discrete PGM grains (mainly bismuthotellurides; sulfides; arsenides), whereas approximately 80% of the Pd (and some Rh) is hosted in pentlandite.

Within the ores of oxidized MSZ, the PGE show a polymodal distribution. In the course of weathering, the PGE-sulfides and arsenides (cooperite/braggite, sperrylite), which make up about 25% of the original Pt content of the ore, remain stable in the oxidized environment. The (Pt,Pd)-bismuthotellurides disintegrate and may form chemically complex (Pt,Pd)-oxides/hydroxides.

The sulfides are destroyed during weathering, partly releasing their base metal and PGE contents, and are replaced by iron oxides or hydroxides. Up to 50% of the Pd is lost from the system, probably dispersed and transported away by acid surface waters. Some other proportions of the PGE are redistributed and are found either as secondary PGM, in PGE-“oxides/hydroxides”, in

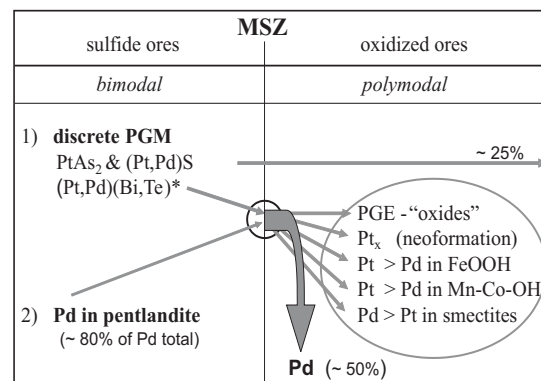


FIG. 5-12. Summary graph showing trends of preservation of PGM and redistribution of Pt and Pd from pristine to oxidized MSZ. (Pt,Pd)(Bi,Te)* = (Pt,Pd)-bismuthotellurides (*cf.* Table 1). For details see text.

iron-hydroxides, in Mn–Co-hydroxides, and in chlorites/smectites.

The processes of PGE redistribution and their mobilities in the supergene environment are much debated and cases of both dispersion and concentration have been proposed by various authors. In contributing to the discussion, it is fortunate that near-continuous underground and surface exposures of the MSZ allowed us to investigate some aspects of the fate of the PGE and PGM in the exogenic environment in detail.

Vertical profiles across oxidized MSZ showed that the general metal distribution and zonation patterns (“offset”) of the pristine MSZ are grossly preserved. During weathering, the sulfides disintegrate and parts of the PGM are destroyed. However, at similar Pt grades, up to about 50% of the Pd is lost from the system as shown by the increasing Pt/Pd ratios from pristine (average 1.28) to oxidized (average 2.43) MSZ. This finding is corroborated by mass balance calculations (see Fig. 5-7) which highlight the fact that Pd (mainly released from disintegrating sulfides) is more mobile than Pt and is partly dispersed and removed, probably in solution (ground- and/or surface waters), in the exogenic environment. Relict sperrylite and cooperite/braggite grains remain stable in the oxidized MSZ. Major changes from pristine to oxidized MSZ comprise the disintegration of the (Pt,Pd)-bismuthotellurides and sulfides, part of which are PGE-bearing, and the concomitant neo-formation of chemically and mineralogically ill-defined (Pt/Pd)-oxides or hydroxides, native Pt, and redistribution of PGE (adsorbed or lattice-bound) into iron hydroxides and smectites.

It is widely accepted that oxides or hydroxides of the PGE exist in the oxidized zone or in laterites of many deposits in the world (*e.g.*, Augé and Legendre 1994; Bowles 1986, 1995; Jedwab 1995; Hey 1999; Salpéteur *et al.* 1995). The presence of Pt and Pd in the form of PGE-oxides or hydroxides has been substantiated in ores of the MSZ by the present study and those of Evans and Spratt (2000) and Oberthür *et al.* (2003b). Furthermore, microprobe trace analysis has shown that especially Pt is also present in appreciable amounts in other PGE-bearing phases. Our ongoing work concentrates on the chemical and mineralogical characterization of these phases, and the establishment of their mineralogical balance in the ores.

METALLURGICAL IMPLICATIONS

Recovered grades of Pt and Pd from pristine MSZ ores were 86% and 90%, respectively, at Hartley mine (Rule 1998), and are slightly lower at Mimosa mine. Prendergast (1990) stated that all early attempts of processing oxidized MSZ ores resulted in Pt recoveries below 50% by either gravity concentration or flotation. Metallurgical test work performed by Zimplats on pervasively oxidized MSZ ores (from surface down to *ca.* 10–15 metres) from the Ngezi mine achieved recoveries of 15–30% only. These results indicate that probably only relict sperrylite and cooperite/braggite grains were recovered, as also suggested by the present mineralogical study. Evidently, novel methods have to be developed for the processing of oxidized MSZ ores. Prendergast (1990) and Evans (2002) have highlighted possible pyrometallurgical and hydrometallurgical methods capable of treating the ores and extracting the PGE. However, in case of bulk treatment of the ores, these methods require large-scale technical equipment or expensive chemicals, and are uneconomic at present. Bulatovic (2003) reported poor recovery of PGE from oxidized ores with conventional reagent schemes. By using various clay and gangue depressants/dispersants and PGE collectors during flotation, concentrate grades and recoveries were improved significantly. In general, however, some process of preconcentration of the PGE would be desirable to reduce ore volumes to be processed.

Our work in progress aims at a better chemical and mineralogical characterization of the PGE-carriers in the ores in order to arrive at a precise knowledge of the proportions of PGE hosted in discrete PGM, being present as (Pt/Pd)-oxides or hydroxides, or found in a dispersed form in iron oxides/hydroxides or smectites. With this knowledge at hand, suitable paths for the economic recovery of the PGE can be developed.

ACKNOWLEDGEMENTS

We thank Greg Holland, Ray Brown, Andrew Du Toit, and the managements of Anglo American Zimbabwe, BHP, Delta Gold, Cluff Resources, Zimplats, Mimosa, Ngezi and Hartley mines for their continuous assistance during our field work. Part of the field and laboratory work was competently carried out by Dipl. Ing. Lothar Gast, Sarah Gregor, Patrick Herb, Marek Locmelis, Jerzy Lodziak and Christian Wöhr. The comments

of an anonymous reviewer, Louis Cabri, and the Editor J. Mungall, considerably improved the paper and are gratefully acknowledged.

REFERENCES

- AUGÉ, T. & LEGENDRE, O. (1994): Platinum group element oxides from the Pirogues Ophiolitic Mineralization, New Caledonia: Origin and Significance. *Econ. Geol.* **89**, 1454-1468.
- BOWLES, J.F.W. (1986): The development of platinum-group minerals in laterites. *Econ. Geol.* **81**, 1278-1285.
- BOWLES, J.F.W. (1995): The development of platinum-group minerals (PGM) in laterites: mineral morphology. *Chronique de la Recherche Minière* **520**, 55-63.
- BULATOVIC, S. (2003): Evaluation of alternative reagent schemes for the flotation of platinum group minerals from various ores. *Mining and Engineering* **16**, 931-939.
- COGHILL, B.M. & WILSON, A.H. (1993): Platinum-group minerals in the Selukwe subchamber, Great Dyke, Zimbabwe: implications for PGE collection mechanisms and post-formational redistribution. *Mineral. Mag.* **57**, 613-633.
- EVANS, D.M. (2002): Potential for bulk mining of oxidized platinum-group element deposits. *Trans. Inst. Mining Metall.* **111**, B81-B86.
- EVANS, D.M. & SPRATT, J. (2000): Platinum and palladium oxides/hydroxides from the Great Dyke, Zimbabwe, and thoughts on their stability and possible extraction. In *Applied Mineralogy* (Rammelmair *et al.*, eds.). AA Balkema, Rotterdam, 289-292.
- EVANS, D.M., BUCHANAN, D.L. & HALL, G.E.M. (1994): Dispersion of platinum, palladium and gold from the Main Sulphide Zone, Great Dyke, Zimbabwe. *Trans. Inst. Mining Metall.* **103**, B57-B67.
- GREGOR, S. (2004): Evaluation of PGE mineralization in the oxidized Main Sulfide Zone at Mimosa Mine, Great Dyke, Zimbabwe. *BGR Internal File 10748/04*, 55 pp.
- GRESENS, R.L. (1967): Composition-volume relationships of metasomatism. *Chem. Geol.* **2**, 47-55.
- HERB, P. (2000): Geochemical and mineralogical studies of PGE mineralizations of the Great Dyke: The Main Sulfide Zone at Unki Mine, Shurugwi, and the Dream reef, Lalapanzi. *Internal report, BGR Archive No. 0120191*, 99 p.
- HEY, P.V. (1999): The effects of weathering on the UG2 chromitite reef of the Bushveld Complex, with special reference to the platinum-group minerals. *South African J. Geol.* **102**, 251-260.
- JEDWAB, J. (1995): Oxygenated platinum-group element and transition metal (Ti, Cr, Mn, Co, Ni) compounds in the supergene domain. *Chronique de la Recherche Minière* **520**, 47-53.
- OBERTHÜR, T. (2002): Platinum-Group element mineralization of the Great Dyke, Zimbabwe. In *The Geology, Geochemistry, Mineralogy and Mineral Beneficiation of Platinum-Group Elements* (Cabri, L.J., ed.). *Can. Inst. Mining Metall., CIM Special Volume* **54**, 483-506.
- OBERTHÜR, T., CABRI, L.J., WEISER, T., MCMAHON, G. & MÜLLER, P. (1997): Pt, Pd and other trace elements in sulfides of the Main Sulfide Zone, Great Dyke, Zimbabwe – a reconnaissance study. *Can. Mineral.* **35**, 597-609.
- OBERTHÜR, T., DAVIS, D.W., BLENKINSOP, T.G. & HÖHNDORF, A. (2002a): Precise U-Pb mineral ages, Rb-Sr and Sm-Nd systematics for the Great Dyke, Zimbabwe – constraints on late Archean events in the Zimbabwe Craton and Limpopo Belt. *Precamb. Res.* **113**, 293-305.
- OBERTHÜR, T., MELCHER, F., WEISER, T.W. & GAST, L. (2002b): Distribution of PGE and PGM in oxidized ores of the Main Sulfide Zone of the Great Dyke, Zimbabwe. In *9th International Platinum Symposium, Ext. Abstr.*, (Boudreau, A., ed.), 333-336.
- OBERTHÜR, T., WEISER, T.W. & GAST, L. (1999): Mobility of PGE and PGM in the supergene environment at Hartley Mine, Great Dyke, Zimbabwe – a case study. In *Mineral Deposits: Processes to Processing* (Stanley *et al.* eds.). AA Balkema Rotterdam, 763-766.
- OBERTHÜR, T., WEISER, T.W., GAST, L. & KOJONEN, K. (2003a): Geochemistry and mineralogy of platinum-group elements at Hartley Platinum Mine, Zimbabwe. Part 1. Primary distribution patterns in pristine ores of the Main Sulfide Zone of the Great Dyke. *Mineral. Deposita* **38**, 327-343.

- OBERTHÜR, T., WEISER, T.W., GAST, L. & KOJONEN, K. (2003b): Geochemistry and mineralogy of platinum-group elements at Hartley Platinum Mine, Zimbabwe. Part 2. Supergene redistribution in the oxidized Main Sulfide Zone of the Great Dyke, and alluvial platinum-group minerals. *Mineral. Deposita* **38**, 344-355.
- OBERTHÜR, T., WEISER, T.W., GAST, L., WITTICH, C. & KOJONEN, K. (2000): Mineralogy applied to the evaluation and processing of platinum ores of the Main Sulfide Zone, Great Dyke, Zimbabwe. *In Applied Mineralogy* (Rammelmair *et al.*, eds.). AA Balkema Rotterdam, 379-382.
- PRENDERGAST, M.D. (1988): The geology and economic potential of the PGE-rich Main Sulfide Zone of the Great Dyke, Zimbabwe. *In Geoplatinum 87* (Prichard, H.M. *et al.*, eds.). Elsevier, 281-302.
- PRENDERGAST, M.D. (1990): Platinum-group minerals and hydrosilicate 'alteration' in the Wedza-Mimosa Platinum Deposit, Great Dyke, Zimbabwe – genetic and metallurgical implications. *Trans. Inst. Mining Metall.* **99**, B 91-B105.
- PRENDERGAST, M.D. & WILSON, A.H. (1989): The Great Dyke of Zimbabwe – II: Mineralisation and mineral deposits. *In Magmatic Sulphides – the Zimbabwe Volume* (Prendergast, M.D. & Jones, M.J., eds). *Institution for Mining and Metallurgy, London*, 21-42.
- RULE, C.M. (1998): Hartley Platinum Mine – Metallurgical Processing. *In Guidebook*, 8th International Platinum Symposium, Pre-Symposium Excursion to the Great Dyke of Zimbabwe (Prendergast, M.D., compiler), 20-22.
- SALPÉTEUR, I., MARTEL-JANTIN, B. & RAKOTOMANANA, D. (1995): Pt and Pd mobility in ferralitic soils of the West Andrianema area (Madagascar). Evidence of a supergene origin of some Pt and Pd minerals. *Chronique de la Recherche Minière* **520**, 27-45.
- SCHNEIDERHÖHN, H. & MORITZ, H. (1939): Die Oxydationszone im platinführenden Sulfidpyroxenit (Merensky-Reef) des Bushvelds in Transvaal. *Zentralblatt Mineralogie Geologie Paläontologie, Abteilung A*, 1-12.
- WAGNER, P.A. (1929). *The Platinum Deposits and Mines of South Africa*. Oliver & Boyd London, 326 pp.
- WILSON, A.H. (2001): Compositional and lithological controls on the PGE-bearing sulfide zones in the Selukwe Subchamber, Great Dyke: A combined equilibrium – Rayleigh fractionation model. *J. Petrol.* **42**, 1845-1867.
- WILSON, A.H., MURAHWI, C.Z. & COGHILL, B.M. (2000): The geochemistry of the PGE subzone in the Selukwe subchamber, Great Dyke: an intraformational layer model for platinum-group element enrichment in layered intrusions. *Mineral. Petrol.* **68**, 115-140.

CHAPTER 6: PLATINUM-GROUP ELEMENT PLACERS ASSOCIATED WITH URAL-ALASKA TYPE COMPLEXES

Tolstykh, N.D.

Institute of Geology, SB RAS, pr. Ak. Koptyuga, 3, 630090, Novosibirsk, Russia

E-mail: tolst@uiggm.nsc.ru

Sidorov, E.G.

Institute of Volcanology, FEB RAS, Piipa Ave. 9, 683006, Petropavlovsk-Kamchatski, Russia

E-mail: kec@mail.iks.ru

and

Krivenko, A.P.

Institute of Geology, SB RAS, pr. Ak. Koptyuga, 3, 630090, Novosibirsk, Russia

INTRODUCTION

Since the early 19th Century (circa 1825) discovery of platinum-bearing placers in the Ural Mountains of eastern Europe, ultramafic-mafic massifs have drawn the attention of researchers as bedrock sources of these placers. It is well known that the zoned mafic-ultramafic igneous complexes of the Ural-Alaska type are the lode sources of the most significant economic platinum-group element (PGE) placer resources and reserves. In contrast, Alpine type (ophiolitic Iherzolite type) mafic-ultramafic complexes have thus far only generated modest economic concentrations of PGE in placer deposits. Understanding the geologic framework, structural and lithologic controls of mineralization, thermodynamic processes of the zoned intrusions, and the geochemical evolution the ore-forming system can result in determining the genetic type of a placer deposit and its economic potential. Much geotechnical data concerning the classification of Ural-Alaska complexes has been published. An important practical task is to determine systematic mineral associations and relationships that can be used as reliable and effective criteria for correlation of specific placers to a type of the bedrock source. Most platinum-group element minerals (PGM), with the exception of Pd-bearing minerals and alloys, are stable under supergene conditions. The PGE ratios in the placer deposits, the compositions of PGM as determined through microprobe analyses, and their paragenetic relationships are the factors that allow us to estimate the conditions of ore formation and the presumed bedrock source. Descriptions of mineral associations in scientific literature often include detailed information on the composition of PGM in a placer, and compositions of inclusions in

PGM. The same stability fields of isoferroplatinum, Os-Ir-Ru alloys, laurite, and sperrylite occur in both PGE placer deposits related to the zoned Ural-Alaska type, as well as those related to ophiolite complexes. Hence, only the use of all the complex paragenetic relationships can provide the necessary evidence that distinguishes between Ural-Alaska and ophiolite lode sources.

Our synthesis begins with the systematic study of PGE-bearing placer deposits where the lode source has clearly been identified. The second part of the chapter is a systematic study of PGE-bearing placer deposits in which the lode source is poorly understood or unknown. Generally the PGM material under study has been heavy mineral concentrated from placer gold dredges or the heavy black sands recovered from PGE placer exploratory holes. All PGM sites under investigation have been analyzed by the scanning electron microprobe (SEM). Further work where judged to be necessary included electron microprobe analysis (EMPA). The data set described in this chapter summarizes the geochemistry and mineralogy of thirteen (13) PGM placer deposits associated with Ural-Alaska type intrusions, and eleven (11) PGM placer deposits, related to ophiolite complexes. Also included in this study are 1,400 EMPA analyses and additional data from the published scientific literature.

CLASSIFICATION OF PGM PLACERS AND THEIR LODE SOURCES

PGM-bearing placer mineralogy and its economic potential are primarily defined by the nature of the presumed lode source(s). Primitive mantle was exposed to partial melting with division into two components and formation of two different

substances: basalt (tholeiitic or picritic) magma and depleted ultramafic restite. Thus fractionation of both lithophile elements (Mg, Al, Si, Fe, Ti, etc.) and ore components, including the platinum-group elements Pd, Pt, and Rh (or PPGE) concentrated in basalt magma, whereas the platinum group elements Os, Ir, and Ru (IPGE) concentrated in the depleted ultramafic restite. The basaltic magma, separated from restite, contains, in addition to Pt, Rh and Pd, some refractory elements, and experienced further fractionation in an intermediate magma chamber during intrusion. This fractionation led to the development of two series: 1) pyroxenite-dunite with a Pt-rich oxide-metal component; and 2) gabbro, with a Pd-bearing sulfide phase and minor Pt and Rh concentrations. These two evolutionary branches, being derivatives of basaltic magma, formed magmatic complexes with unequal placer-forming potential. Moderately depleted restite differs from an intensively depleted restite by an increased proportion of its remaining, low-melting point components, chalcophile elements, volatile liquid and sulfide phases.

The genesis of primary magma finally defines the geochemical specialization of platinum-group mineral (PGM) placers and their economic potential. The classification of placers, based only on the results of fractionation of the initial, primitive substance of the mantle is shown in Figure 6-1. This classification results in seven placer subtypes, which take into account mineral associations and the parent source as follows:

- 1A. Widespread Pt-Fe alloy placers, genetically related to zoned complexes of Ural-Alaska type, both in mobile belts and platforms, are similar to each other by their mineralogical characteristics. These placers are commercially viable, and are either in production now, were mined in the past, or have inferred resources.
- 1B. Placers related to the Guli massif are unique in their enrichment in osmium, and are also related to zoned complexes, associated with meimechite (Malitch *et al.* 1998).
2. Sperrylite-bearing placers, with lesser quantities of Fe-free platinum, crystallized on sperrylite, as well as Pd phases which are more stable under supergene conditions (*e.g.*, rustenburgite-atokite, paolovite, stibiopalladinite, and braggite). Sperrylite-bearing placers are derived from layered gabbroic complexes and Cu-Ni deposits with Pt-Pd mineralization.

These placers seldom have economic potential; more often, they are valuable as indicators for delineation of economically important, sulfide-hosted lode PGE mineralization.

- 3A. Os-Ir-Ru alloy placers are derived from an intensively depleted restite ultramafic series. Only Os-Ir-Ru alloys are present, and they have economic value only as by-products of gold-bearing placers.
- 3B. Os-Ir-Ru alloy placers, though dominated by Os-Ir-Ru alloys, also containing platinum-group PGE (Rh, Pt, Pd, the PPGE), as well as significant Pt-Fe alloys, and multi-component solid solutions. These placers are eroded from moderately fractionated ophiolite complexes. They do not have economic value, but can be significant by-products of placer gold production.
- 3C. Pt-Fe alloy placers of the Viluiskiy type contain Rh-rich Pt-Fe alloys and a subordinate quantity of Os-Ir-Ru alloys theoretically eroded from mafic or ultramafic massifs that are not clearly defined (Okrugin 2000). Our point of view is that the PGE minerals of these placers are derived from cumulate (banded or hybrid) mafic-ultramafic series within ophiolites. This type of PGE-bearing placer also has marginal economic value.
4. Os-Ir-Ru alloy-bearing placers derived from non-ophiolitic, Fe-rich ultramafic intrusions. This magma rises into crustal levels in the liquid state (Glazunov 1981) and forms a stratiform ultramafic intrusion with Os-Ir-Ru concentrations (Volchenko & Koroteyev 1999).

Taking into account other factors than fractionation of initial melts leads to further subdivisions and allocation of new subtypes of placers. This process can be unlimited, and also useful and scientifically possible, depending on the purpose of specific investigations. For example, within the Pt-Fe alloy placer type, the Pd-rich-platinum subtype can be present (*e.g.*, the Pustaya placer in Kamchatka), or an Ir-rich platinum subtype may be present (*e.g.*, the Inagli or Konder PGE placer deposits). The appearance of these subtypes depends on the depth of intrusion of the complexes, temperature of formation, and outcrop area of the marginal clinopyroxenite that is available for exhumation. In the generalized type 3 PGE-bearing placer above, it is possible to define a laurite subtype, which formed

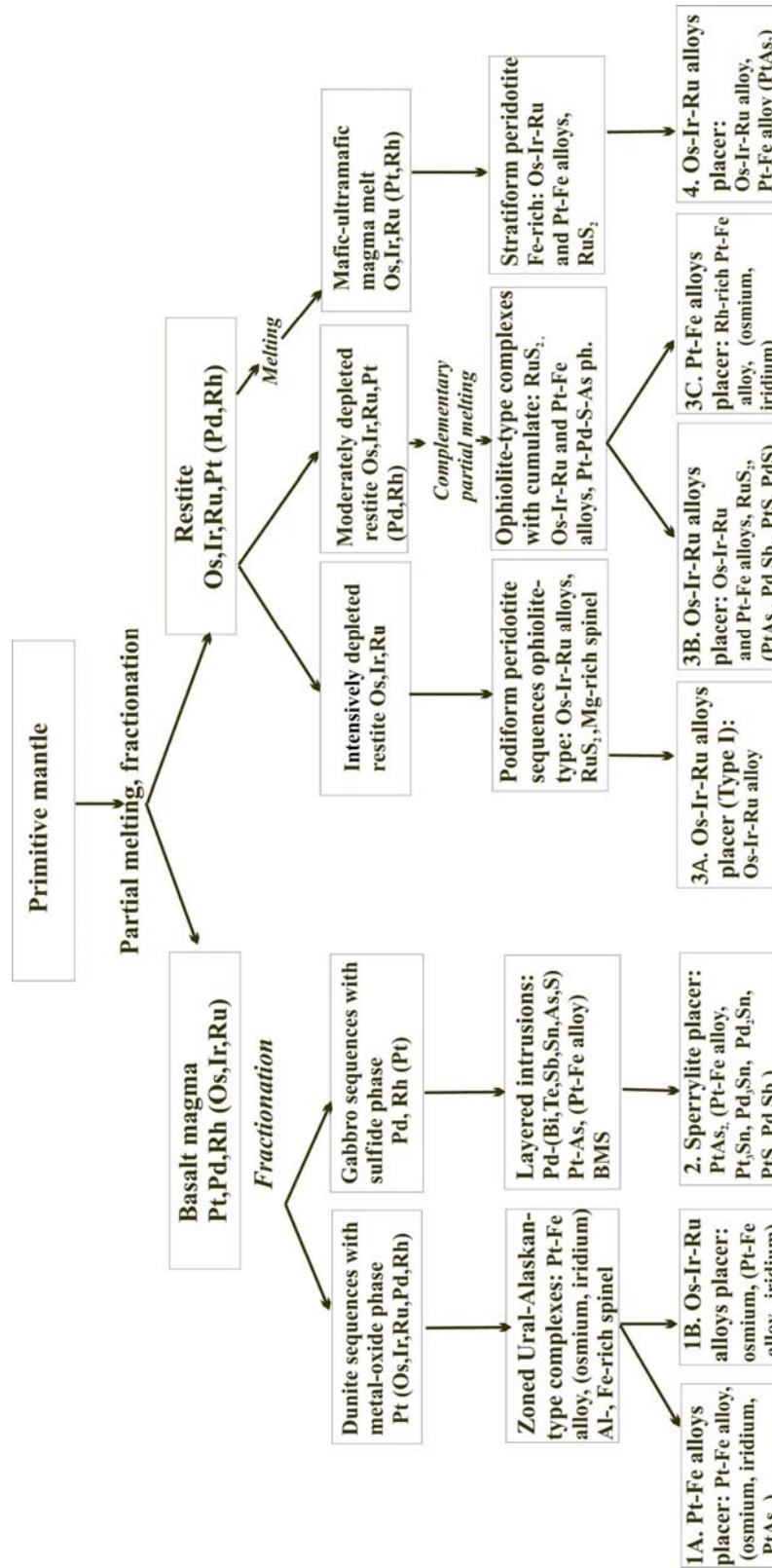


FIG. 6-1. Classification of PGM placers belonging to different types of source rock, determined by fractionation of initial magmas.

under conditions of high sulfur activity in the ore-forming system.

URAL-ALASKA TYPE COMPLEXES

Historical Geological Concepts for Ural-Alaska Type Zoned, Igneous Complexes

The history of understanding of Ural-Alaska type zoned intrusions, associated lode PGE mineralization, and their associated platinum placer deposits is described in many publications, including Ivanov (1997), Zoloev *et al.* (2001), Johan (2002), and Weiser (2002). As a result of intensive mining of placer platinum in the Ural Mountains, which reached an aggregate production total of 250 tons by 1922 (Dodin *et al.* 2000), the Ural Mountains ultramafic intrusions were intensively explored for their lode platinum endowment. The rocks comprising such intrusions were assigned an independent magmatic origin and given the name 'gabbro-pyroxene-dunite' (Levinson-Lessing 1900). In the classic papers of Vysotsky (1923, 1933) and Zavaritsky (1928), the concentric structures of the intrusions were described, consisting of a dunite core and a clinopyroxenite periphery. Later, similar massifs in southeastern Alaska have received the name of concentric-zoned complexes of Ural-Alaska type (Taylor 1967, Taylor & Noble 1969). This term appeared the most appropriate and has been accepted in the world literature. Other complexes, to which commercial platinum placers are connected, have been found and include: 1) the Tulameen complex in British Columbia (Camsell 1913, Rice 1947, Nixon *et al.* 1990), 2) the Youbdo massif in Ethiopia (Duparc & Molly 1928, Augustithis 1965, Evstigneeva *et al.* 1992), 3) the Gal'moenan and Sejnav zoned intrusions in the Olutorsky zone of Koryak folded belt (Anikeeva 1968, Kutyevev *et al.* 1988, 1991, Astrakhantsev *et al.* 1991), and 4) the Goodnews Bay and Susie Mountain zoned intrusions in southwest Alaska (Mertie 1940, 1976, Foley *et al.* 1997).

It appears that pyroxene-dunite and ophiolite associations are both located in mobile folded belts and are confined to continental-oceanic transition zones. In the Urals, Kamchatka, southeast Alaska, and in the Western Cordillera, they form paired belts, stretching for hundreds of kilometres parallel to the strike of the main folded structures (Tistl 1994, Himmelberg & Loney 1995, Volchenko *et al.* 1998, Volchenko & Koroteyev 1999, Johan 2002). At first, the identification of the massifs of Ural-Alaska type and their separation from alpine type complexes was not always a simple task because of:

1) the spatial combination of the various complex types, 2) significant structural deformation of the zoned structure of the massifs of Ural-Alaska type, and 3) the similarity of PGM mineralization in the cumulative wehrlite-clinopyroxenite-gabbro series of ophiolite sequence and Ural-Alaska complexes. Earlier workers thought that pyroxene-dunite intrusions of the Ural-Alaska type were the cumulative, basal parts of ophiolite suites. For example, the mafic-ultramafic intrusions of the Olutorsky zone of the Koryak-Kamchatka platinum-bearing belt were related to the fragments of a banded complex of an ophiolite sequence (Alexeev 1987, Velinsky 1979). The later study of the massifs of Olutorsky zone (Kutyevev *et al.* 1988, 1991, Astrakhantsev *et al.* 1991, Batanova & Astrakhantsev 1992, Batanova *et al.* 1991, Ledneva 2001) resulted in a modified view of the nature of the Korak-Kamchatka mafic-ultramafic intrusions and their classification as zoned complexes of the Ural-Alaskan type. Detailed investigations of the mafic-ultramafic complexes in the Ural folded belt, where processes of collision and accretion led to a spatial imposition of their various igneous suites (Vorobjeva *et al.* 1962, Efimov & Efimova 1967, Ivanov 1986, Ivanov & Rudashevsky 1987) also led to an understanding of the principal difference of two combined associations: 1) dunite-harzburgite (ophiolite), and 2) pyroxenite-dunite (Ural-Alaska zoned intrusion).

Geodynamic Conditions of Formation of the Ural-Alaska type complexes

Subsequent research on Ural-Alaska type zoned intrusions has shown that they can be formed in the continental mobile folded belts (the Urals), in transitional continental-oceanic zones (Alaska, Kamchatka, Cordillera), and in cratonal-platform environments (Aldan Shield). It has also been established that ophiolite-type and zoned Ural-Alaskan complexes, bearing various types of mineralization, were formed under different geodynamic conditions of the same mobile belts. Within the platinum-bearing folded belt of the Urals, intrusion of podiform ophiolite complexes with a refractory component was related to oceanic rifting, and the platinum-bearing belts of zoned massifs of the Urals (Nizhny Tagil, Kytlym) with Pt-Ir mineralization were formed in island arc conditions (Volchenko & Koroteyev 1999, Zoloev *et al.* 2001, Malakhov 1999).

Concentric-zoned massifs of the alkaline-ultramafic formations within the Aldan

shield (Konder, Inagli, Chad) were formed by introduction of mantle plumes within heterogeneous mantle blocks (Nekrasov *et al.* 1994). Despite the differing geodynamic conditions of formation of concentrically zoned intrusions of the Aldan and Ural-Alaska types, the characteristic features of platinum mineralization are identical in both types of zoned intrusions (Rozhkov *et al.* 1962, Efimov & Tavrín 1978). Detailed petrologic, structural, and mineralogical research of the Aldan Shield zoned intrusions (Razin & Smirnov, 1974, Razin 1976, Lazarenkov *et al.* 1992, Rudashevsky *et al.* 1992, Nekrasov *et al.* 1994, Gurovich *et al.* 1994, Tolstykh & Krivenko 1997, Mochalov & Khoroshilova 1998, Okrugin 2001) have identified a number of characteristic features for these massifs: 1) a zoned structure with a dunite core and clinopyroxenite rim, 2) correlation of platinum mineralization with chromite ore, 3) dependence of the extent of mineralization on the intensity of fluid-metasomatic processes, and 4) placer-forming potential of chromite-bearing dunite with accessory Pt mineralization. Hence, the basic characteristics of the concentrically zoned intrusions of the Aldan Shield share many mineralogical and petrological characteristics with the clinopyroxenite-dunite massifs of the Ural platinum bearing belt (Begizov *et al.* 1975, Garuti *et al.* 1997, 2003, Anikina *et al.* 1999, Zoloev *et al.* 2001, Chashchuhin *et al.* 2002), the Koryak-Kamchatka belt, and the Goodnews Bay (Sidorov *et al.* 2001, Ledneva 2001, Zajtsev *et al.* 2001, Landa *et al.* 2001, Tolstykh *et al.* 2001, 2002a, 2002b, 2004 Nazimova *et al.* 2003). Thus, magmatic complexes related to the Ural-Alaska type, on one hand, can be formed under different geodynamic conditions, but also possess similar attributes in the development of their ore-forming systems. On the other hand, the mafic-ultramafic intrusions generated in uniform geodynamic environments can also have different types of PGE-bearing ores.

PGE-BEARING PLACERS CONNECTED WITH URAL-ALASKA TYPE COMPLEXES
The commercial significance of the platinum placers

Pt-Fe alloy placers associated with complexes of Ural-Alaska type have been the most important type of PGE placers. In the 18th and 19th centuries, placer deposits of platinum from these deposit types were practically the only source of

this metal. In 1723, platinum was discovered in diamondiferous placers of Brazil and about 70 kg of PGE were mined each year (Vysotsky 1923). Platinum has been mined from the placers of Colombia since 1735, and during the early years, about 140 kg was produced annually. In 1992–1993 the level of platinum production reached more than 2 tons per year. Prior to 1927, platinum placer production in the USA was confined to modest by-product production of PGE (mainly Os–Ir alloys) from gold placer deposits in California, Oregon, and Alaska. From 1928 to 1983, about 21 tons of platinum (mainly isoferroplatinum) were mined from the Goodnews Bay mining district of southwest Alaska (Foley 1992, Foley *et al.* 1997). The Goodnews Bay district was the USA's primary producer of PGE until the Stillwater lode complex opened up in Montana during the 1990s.

The mining of platinum-rich placers derived from the Nizhny-Tagil dunite intrusion of the Ural Mountains began in 1885. Initially, production of PGE averaged 1–2 tons per year and later increased to up to 6 tons per year. In 1920, production ceased due to extreme political events (Vysotsky 1923), but was later resumed. By 2000 the total production of platinum mined in the Ural Mountains was estimated to be 370 t (Zoloev *et al.* 2001).

The mining of placer platinum deposits of the Konder River of northern Khabarovsk Oblast began in 1985; this PGE placer has been mined from streams that cut the Konder dunite intrusion of the Aldan Shield (Nekrasov *et al.* 1994). Initially production ranged from 3.0–4.5 tons of platinum annually, with lower levels of production in recent years. Since 1994, mining of placer platinum in the Koryak Autonomous Region of the Kamchatka Peninsula area began in streams dissecting the Gal'moenansky clinopyroxenite-dunite intrusion. By 1997, production reached 7.5 tons PGE per year. The mining of placer platinum in the Konder and Gal'moenansky areas continues today. At the end of the 20th century, Russian annual placer platinum production varied from 4.2 to 12.3 tons per year, which amounts to 20–48% of the total production of the platinum mined in Russia (Table 6-1). In the middle of the 20th century, mining of PGM from lode sulfide deposits was initiated in Russia, mainly from the great Noril'sk camp of the Taimyr Peninsula region. By 2000, total PGE output from Russia, much of it being palladium, amounted to 168 tons per year (Fig. 6-2). Though currently the

TABLE 6-1. PLATINUM PRODUCTION IN 1993–2000, TONNES.

Production	1993	1994	1995	1996	1997	1998	2000
Total production in the world	134.8	129.7	134.4	136.9	150.3	157.6	168.3
Total production in Russia	20.0	21.2	21.0	21.8	25.0	27.0	29.5
Including from the placers:							
Konder	3.7	4.0	4.16	4.5	4.4	4.3	3.5
Gal'moenan	-	0.66	1.43	4.64	7.33	7.5	4.5
Other regions	0.5	0.5	0.5	0.5	0.5	0.5	1.0
Total from placers of Russia	4.2	5.16	6.1	9.6	12.2	12.3	9.0

Source: Mineral resources 2000, Boyarko 2001, Mamaev and Van-Van-E 2000.

amount of platinum from placers is only 4–5% of the world production, it should be mentioned that this contribution remains constant.

Features of PGM Placer Deposits

Pt–Fe alloy placers are subdivided into those that are spatially directly confined to two groups: 1) Ural-Alaska type complexes, and 2) those for which the bedrock source is not known or is hypothetical but whose relationship to a Ural-Alaska type might be presumed. The first group of PGE-bearing placers include the Gal'moenan, Sejnav, Epil'chick, Itchayvayam zoned intrusions in the Koryak folded belt (Tolstykh *et al.* 2001, 2004, Nazimova *et al.* 2003), Filippa in southern Kamchatka (Sidorov *et al.* 2004), Konder, Inagli, and other related deposits in the Aldan Shield (Rudashevsky *et al.* 1992, Nekrasov *et al.* 1994, Tolstykh & Krivenko 1997, Malitch 1999, Okrugin 2001), Nizhny Tagil, Uktus, Kachkanar and Kytlym in the Ural Mountains (Zoloev *et al.* 2001, Garuti *et al.* 2002, 2003), the

Tulameen Complex in Canada (Nixon *et al.* 1990), Viravira and Alto Condato in Colombia (Cabri *et al.* 1996), Fifield in Australia (Johan *et al.* 1989, Slansky *et al.* 1991), Goodnews Bay in Alaska (Mertie 1976, Tolstykh *et al.* 2002a), Joubdo in Ethiopia (Cabri *et al.* 1981, Evstigneeva *et al.* 1992), and a zoned complex in the Alyuchin Horst of northeast Russia (Gornostayev *et al.* 1999).

The second group of PGE-bearing placers include the Durance River in France (Johan *et al.* 1990), East Madagascar (Legendre & Augé 1992, Augé & Legendre 1992), Ecuador (Weiser & Schmidt-Tomé 1993), Papua New Guinea (Johan *et al.* 2000), the Pustaya River in Kamchatka (Tolstykh *et al.* 2000) and the Koura, Kaurchak, Mrassu, Tyulenevsky Rivers, in southern Siberia (Tolstykh *et al.* 2002b). However, along with the above mentioned systems, a number of placer occurrences of PGM, for which the source is not established, or is ambiguously determined, occur. These are the PGE-bearing placers of Canada (Yukon, Alberta and Northwest Territories), Borneo in Malaysia, the southern Kalimantan placers in Indonesia, placers in the Chindwin River area in Burma (Cabri *et al.* 1996), and numerous minor PGE-bearing placer occurrences throughout Alaska (Foley *et al.* 1997). Many PGE placer occurrences are of unknown provenance either because the bedrock source is insufficiently eroded or is completely destroyed by denudation processes, or because they are at a considerable distance away from the studied placers. A variety of placer-forming processes have resulted in the formation of placer deposits of PGM of various genetic types, among which deluvial, alluvial and beach-marine are recorded. Alluvial placers are of great practical importance.

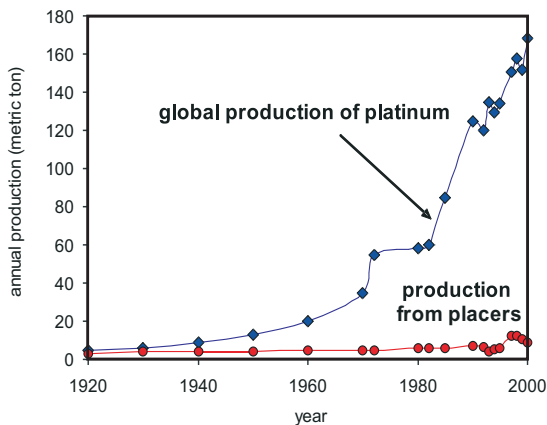


FIG. 6-2. World production of platinum from 1920 to 2000.

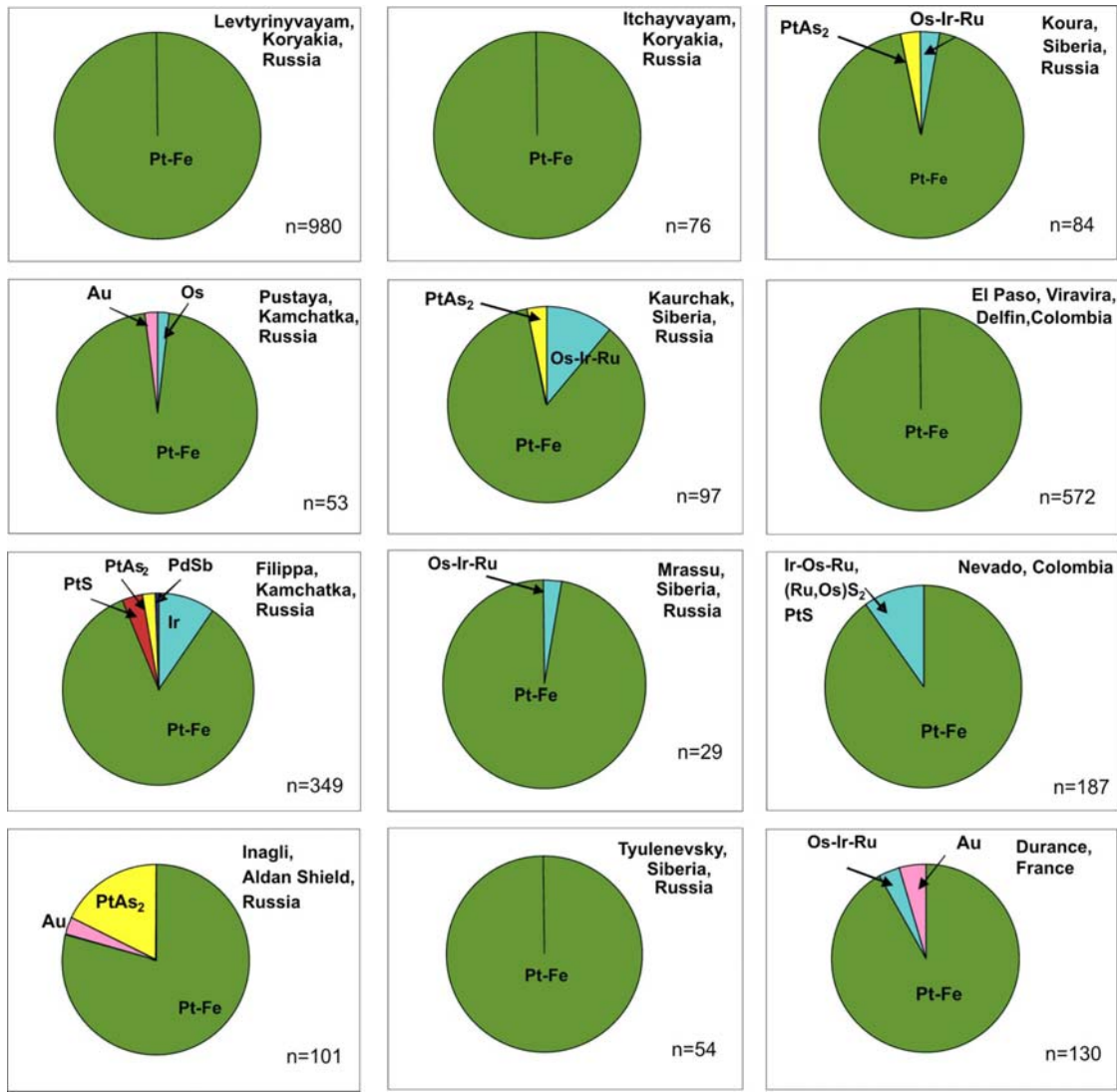


FIG. 6-3. Modal distributions of PGM in the placers derived from Ural-Alaska type complexes.

Morphology of PGM grains

PGE-bearing placers associated with zoned Ural-Alaska complexes are dominated by Pt-Fe alloys (Fig. 6-3). The proportion of Os-Ir-Ru alloys in this association is usually insignificant, but can amount to 1–10% as laurite, *e.g.*, the Nevado placer in Colombia (Cabri *et al.* 1996). Among the refractory PGE minerals, either native osmium (Kaurchak) or iridium (Filippa) can occur. The quantity of PGM related to a later paragenesis can also be present in a placer, *e.g.*, sperrylite, cooperite, stibiopalladinite, or isomertieite. The relative amounts of these minor PGE occurrences depend on the intensity of postmagmatic hydrothermal alteration of bedrock sources.

In the alluvium of river placers, the PGM consist mostly of platinum nuggets in the flaky, lamellar shape, less than 1 mm across (Fig. 6-4a), or in rounded grains (Fig. 6-4b,c) to 2 mm in size, and occasionally of irregular shape or with crystallographic surfaces. Non-rounded, hackly grains are generally uncommon and usually occur directly near the bedrock source (Fig. 6-4d). The platinum nuggets are silvery white with metallic appearance. Sometimes they are coated by hydroxides of Fe and Mn, which in reflected light of polished sections exhibit gray-brown rims. Visible inclusions in the nuggets consist of chromian spinel and clinopyroxene. Chlorite and serpentine are localized along cracks and grain edges.

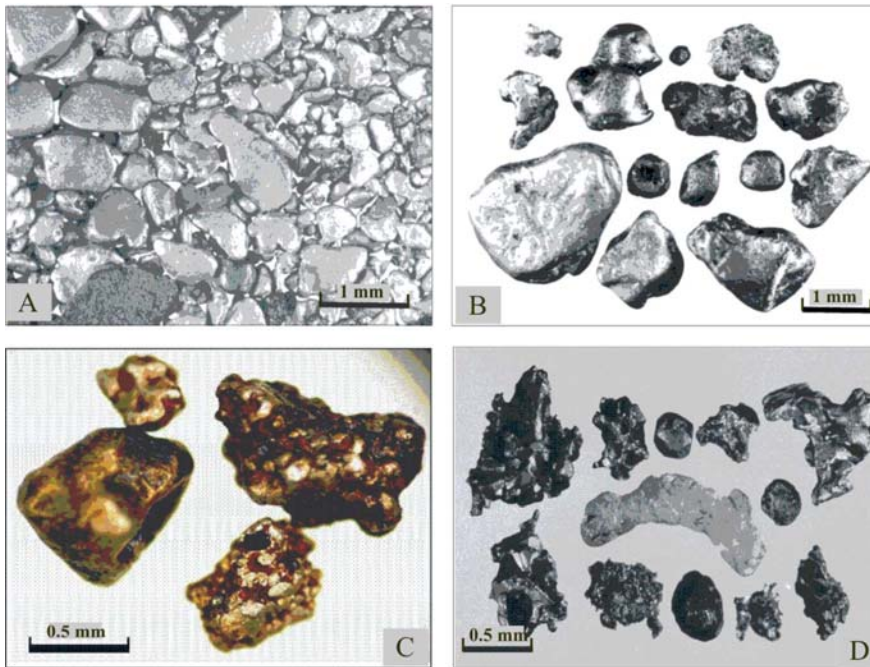


FIG. 6-4. The morphology of grains of the Pt-Fe alloy in Koura (a), Itchayvayam (b), Filippa (c) and Inagli (d) river placers.

Composition of Pt–Fe alloys in Placers

Pt–Fe alloys from placers related to Ural-Alaska type complexes have wide ranges of Fe concentrations, which can vary from native platinum with 3–5 wt.% Fe in placers of Madagascar, Ecuador, Burma and the Alyuchin Horst areas, to Fe-rich platinum, where Fe content reaches 12 wt.% (Tulameen and Goodnews Bay). The Fe content varies from 15 to 33 wt.% in various minor occurrences (Fig. 6-5). In magmatic processes, iron is always included into the structure of platinum, and variations of its concentration are defined by the $f(\text{O}_2)$, with which its concentration shows a negative correlation (Roeder & Jamieson, 1992, Nekrasov *et al.* 1994, Amossé *et al.* 2000, Johan *et al.* 1989, Johan 2002). Reduction in the temperature of crystallization of the melt with an increase in oxygen fugacity results in a reduction of Fe in Pt–Fe alloys. This indicates that the Fe-rich alloys of the Tulameen, and Nizhny Tagil massifs were formed at a lower $f(\text{O}_2)$, than the Pt–Fe alloys from the placers of Ecuador, the Aluchin Horst, and East Madagascar (Fig. 6-5). Variations in the concentration of Fe in Pt–Fe alloys frequently can be observed within a single placer. A bimodal distribution of Fe in Pt–Fe alloys on frequency diagrams as, for example, for the El Paso and Viravira placers (Cabri *et al.* 1996) sometimes occurs and can be related to the accumulation in one placer of Pt–Fe alloys from two different sources or

from different units from one massif. More often, native platinum is characteristic of source rocks of an insignificant size that formed under shallow conditions and is represented mainly by clinopyroxenite units of zoned Ural-Alaska complexes. Native platinum can also occur in placers with an unknown lode source (placers of Ecuador, the Alyuchin Horst, etc.). On the other hand, isoferroplatinum and Fe-rich platinum is usually confined to those placers derived from large and well-eroded massifs (Gal'moenan, Inagli, Konder, Nizhny Tagil). The distribution of Fe concentration in platinum, to some extent, can be used as a criterion to estimate the bedrock source of a specific PGE placer being investigated.

The study of Cu, Ni and minor element concentrations in Pt–Fe alloys from different placers indicates that Ni is relatively concentrated in Fe-rich alloys, whereas Cu concentration, on the contrary, increases in Fe-poor alloys (Fig. 6-5). Minor elements such as Pd, Rh and Cu, more often enter into native platinum than in Fe-rich platinum. These correlations as a whole correspond to the evolution of an ore-forming system in a magmatic process, when the concentration of Cu and volatile elements increases in the residual melt and may enter Pt–Fe alloys at a later stage. Secondary phases of the series tetraferroplatinum–tulameenite ($\text{PtFe} - \text{Pt}_2\text{CuFe}$), as well as native near-pure platinum, which were formed at a postmagmatic stage and

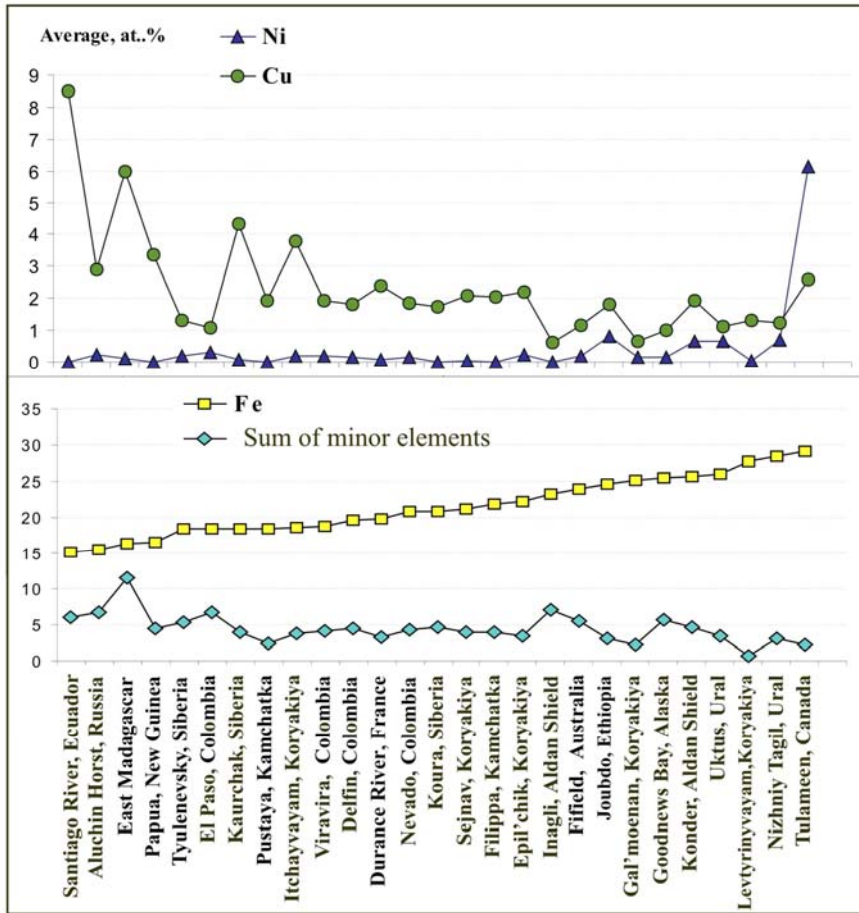


FIG. 6-5. Change of the average concentrations of Cu, Ni and minor elements in Pt-Fe alloys in various placers of the world related to Ural-Alaskan-type complexes. The placers are listed by increasing average concentration of Fe in Pt-Fe alloys; sources are published data, the references are in the text.

have another genetic path, do not enter into consideration here.

Minor elements can enter into the structure of Pt-Fe alloys, and sometimes reach high concentrations (Table 6-2). Their concentration and ratios characterize particular ore-forming systems. There are placers with high Ir-, Rh- and Pd concentrations in Pt-Fe alloys (Fig. 6-6). Ir-rich Pt-Fe alloys are characteristic of the placers from Inagli (Tolstykh & Krivenko 1997), Nizhny Tagil (Zoloev *et al.* 2001), Fifield (Johan *et al.* 1989, Slansky *et al.* 1991), Goodnews Bay (Tolstykh *et al.* 2002a), Alyuchin Horst (Gornostayev *et al.* 1999), and Gal'moenan massifs (Tolstykh *et al.* 2004). For example, the average Ir content of Pt-Fe alloys in the Inagli placers is 5.5 wt.%, but in some grains attains 16.6 wt.%. On the other hand, Pt-Fe placers with high concentrations of Pd are also known, attaining 8.44 wt.% in East Madagascar (Augé & Legendre 1992) and up to 9.52 wt.% in the Pustaya River placers of Kamchatka (Tolstykh *et al.* 2000). Elevated concentrations of Pd in Pt-Fe

alloys appear during the late stages of development of the ore-forming system and are characteristic of rocks that formed from more fractionated parts of the melt, *i.e.*, wehrlite-clinopyroxenite in the margins of zoned massifs. If Pd-rich Pt-Fe alloys are observed in an unknown placer, then their source can be clinopyroxenite, in which case the dunite may be not yet have been exposed by erosion.

In some placers, Rh prevails among minor elements in Pt-Fe alloys, reaching, for example, 2.2 wt.% Rh in the Papua New Guinea placers (Johan *et al.* 2000), 4.46 wt.% Rh in the El Paso placers in Colombia (Cabri *et al.* 1996) or 3.97 wt.% Rh in the Tyulenevsky River placers of southern Siberia. Evolution of an ore-forming system occurs according to a fractionation trend of the PGE and changes of the ratio of minor elements in Pt-Fe alloys from iridium to iridium-rhodium, then to rhodium-palladium, and, at lastly, to palladium. All known placers worldwide occupy specific positions along the general fractionation trend (Fig. 6-7), with

TABLE 6-2. SELECTED COMPOSITION OF PT-FE ALLOYS FROM PLACERS.

	Pt	Fe	Ni	Cu	Ru	Rh	Pd	Os	Ir	Total
Placers connected with Ural-Alaskan type massifs										
Levtyrnyvayam River placer (Gal'moenan massif)										
1	94.76	4.62	0.00	0.00	0.00	0.00	0.26	0.00	0.00	99.64
2	91.10	6.85	0.00	0.45	0.00	0.00	1.02	0.00	0.00	99.42
3	93.22	7.05	0.00	0.15	0.00	0.00	0.00	0.00	0.00	100.42
4	89.35	9.15	0.00	0.45	0.00	0.18	0.00	0.00	0.00	99.13
5	85.84	9.26	0.08	0.70	0.00	0.90	0.53	0.00	0.00	97.31
6	90.17	9.26	0.00	0.33	0.00	0.49	0.00	0.00	0.00	100.25
7	89.34	9.35	0.00	0.09	0.00	0.00	0.00	0.00	1.36	100.14
8	86.13	9.50	0.07	0.67	0.07	0.62	0.55	0.00	0.00	97.61
9	90.26	9.54	0.00	0.00	0.00	0.00	0.00	0.00	0.65	100.45
10	88.16	9.67	0.00	0.00	0.00	1.03	1.16	0.00	0.36	100.38
11	90.00	9.89	0.00	0.18	0.00	0.40	0.00	0.00	0.00	100.47
Ledyanoy Creek placer (Gal'moenan massif)										
28	87.86	6.23	0.07	0.32	0.08	0.57	0.06	0.24	4.99	100.42
29	88.92	6.50	0.00	0.51	0.00	0.68	0.22	0.12	2.40	99.35
30	84.22	7.19	0.00	0.16	0.09	0.78	0.08	0.11	6.58	99.21
32	87.48	7.83	0.00	0.28	0.08	0.46	0.35	0.10	3.12	99.70
33	82.77	8.05	0.06	0.17	0.05	0.86	0.11	0.35	7.11	99.53
34	88.69	8.05	0.00	0.46	0.00	0.56	0.48	0.00	1.97	100.21
37	90.52	8.30	0.00	0.32	0.00	0.47	0.26	0.00	0.23	100.10
38	88.57	8.37	0.00	0.00	0.06	0.30	0.13	0.10	2.52	100.05
39	86.22	8.54	0.07	0.29	0.08	0.89	0.51	0.00	3.68	100.28
40	88.03	8.57	0.00	0.31	0.11	0.30	0.09	0.00	0.59	98.00
41	85.50	10.51	0.35	1.48	0.00	0.10	0.00	0.08	1.75	99.77
Penisty Creek placer (Gal'moenan massif)										
42	88.89	8.24	0.00	0.18	0.07	0.35	0.00	0.48	1.42	99.63
43	88.15	9.35	0.14	0.21	0.06	0.67	0.25	0.12	0.22	99.17
44	87.23	9.59	0.14	0.33	0.07	0.99	0.39	0.07	1.09	99.90
45	86.56	9.84	0.17	0.60	0.00	0.83	0.04	0.00	0.16	98.20
46	84.07	10.10	0.08	1.06	0.08	0.81	0.72	0.00	2.85	99.77
47	85.31	11.50	0.10	0.51	0.08	0.63	0.57	0.08	1.03	99.81
48	77.30	13.71	1.40	4.83	0.00	0.00	0.00	0.09	0.79	98.12
Tapel'vayam River placer (Sejnav massif)										
49	86.90	3.30	0.00	3.80	0.10	1.10	2.60	1.70	0.40	99.90
50	88.10	4.80	0.00	2.90	0.00	0.90	1.80	1.30	0.10	99.90
51	89.40	5.80	0.10	1.60	0.00	0.80	1.10	0.60	0.10	99.50
52	87.90	6.60	0.00	2.00	0.00	1.00	0.70	0.90	0.60	99.70
53	87.30	7.10	0.10	2.40	0.10	0.80	0.50	1.10	0.30	99.70
54	88.70	7.40	0.00	1.10	0.10	0.90	0.60	0.20	0.60	99.60
55	88.20	7.80	0.10	1.00	0.00	1.20	0.90	0.40	0.20	99.80
56	86.70	8.00	0.00	1.30	0.10	1.30	1.00	0.60	0.10	99.10
57	87.80	8.40	0.00	0.70	0.00	1.30	1.20	0.10	0.10	99.60
58	86.30	9.20	0.00	1.00	0.00	0.90	0.80	0.70	0.20	99.10
Snegovaya River placer (Epil'chik massif)										
59	91.30	4.20	0.10	0.30	0.20	1.60	1.10	0.20	1.30	100.30
60	87.45	6.54	0.09	2.26	0.08	1.03	0.82	0.22	1.11	99.60
61	86.80	6.90	0.10	1.40	0.10	0.80	0.50	0.00	3.00	99.60
62	88.10	7.30	0.10	1.30	0.00	1.10	0.70	0.10	0.80	99.50
63	88.87	7.98	0.04	0.74	0.13	0.84	0.36	0.14	0.83	99.93
64	87.80	8.00	0.10	0.90	0.00	0.80	0.70	0.20	1.50	100.00
65	89.21	8.30	0.00	0.37	0.00	0.56	0.00	0.33	0.74	99.51
66	89.33	8.51	0.00	0.35	0.05	0.43	0.00	0.00	1.35	100.02
67	86.65	9.03	0.10	0.56	0.00	0.83	0.18	0.23	2.58	100.16

PGE PLACERS ASSOCIATED WITH URAL-ALASKA TYPE COMPLEXES

68	86.53	9.55	0.38	0.69	0.00	0.49	0.17	0.07	2.71	100.59
Itchayvayam River placer (Itchayvayam massif)										
69	91.45	3.61	0.15	1.91	0.04	0.84	1.46	0.29	0.54	100.30
70	91.54	4.05	0.06	1.52	0.00	1.12	0.91	0.25	0.63	100.09
71	89.05	5.24	0.06	1.51	0.07	0.35	2.85	0.39	0.55	100.06
72	89.88	5.59	0.00	1.23	0.14	1.01	0.51	0.89	0.45	99.69
73	89.29	5.68	0.05	1.79	0.00	0.65	2.39	0.23	0.25	100.33
74	88.53	6.65	0.04	1.90	0.04	0.98	1.31	0.04	0.36	99.84
75	88.91	6.89	0.12	1.49	0.04	1.01	0.25	0.45	0.86	100.03
76	88.77	7.21	0.00	1.37	0.00	1.31	0.53	0.29	0.77	100.25
77	87.80	7.52	0.04	1.16	0.00	0.99	0.46	0.23	1.75	99.96
78	88.67	8.10	0.00	0.55	0.06	0.84	1.34	0.01	0.28	99.86
79	88.82	8.12	0.12	0.91	0.04	1.12	0.58	0.06	0.49	100.25
Pustaya River placer										
80	82.68	4.65	0.00	0.85	0.14	0.74	8.82	0.70	0.72	99.30
81	82.41	4.68	0.00	0.81	0.25	1.07	9.52	0.61	0.82	100.16
82	87.85	4.80	0.00	0.81	0.16	1.04	2.14	1.10	1.05	98.95
83	88.24	4.83	0.00	0.53	0.37	1.24	1.01	1.01	1.45	98.67
84	82.89	4.90	0.00	1.05	0.00	0.69	8.01	0.57	0.00	98.10
85	88.67	5.18	0.00	0.70	0.00	0.00	4.44	0.16	0.00	99.15
86	90.04	7.92	0.00	0.99	0.00	0.53	0.78	0.06	0.00	100.32
87	88.74	8.00	0.00	0.56	0.06	0.90	0.22	0.00	1.01	99.50
88	85.69	12.91	0.00	0.06	0.00	0.00	0.00	0.00	0.00	98.66
Major River placer (Filippa massif)										
89	90.72	4.88	0.00	0.29	0.13	1.53	0.28	0.97	0.13	98.93
90	90.95	5.14	0.00	0.36	0.07	1.14	0.49	0.81	0.00	98.96
91	84.01	6.37	0.00	2.31	0.00	0.89	2.11	0.01	2.95	98.65
92	88.48	7.51	0.00	0.87	0.09	0.99	0.64	0.00	0.63	99.21
93	88.69	7.88	0.00	1.22	0.13	1.23	0.31	0.06	0.54	100.06
94	82.21	7.90	0.00	0.45	0.12	0.91	0.48	0.40	6.42	98.90
95	87.06	8.17	0.00	0.55	0.06	0.56	0.50	0.00	2.50	99.40
96	88.18	8.20	0.00	0.79	0.06	0.28	1.69	0.00	0.17	99.36
97	89.87	8.43	0.00	0.91	0.00	0.14	0.00	0.00	0.00	99.34
Salmon River placer (Red Mountain, Goodnews Bay, Alaska)										
98	73.72	7.54	0.00	0.47	0.16	2.22	0.25	1.00	13.92	99.28
99	89.80	8.08	0.00	1.15	0.05	0.45	0.00	0.00	0.00	99.53
100	85.61	8.23	0.00	0.66	0.00	0.40	1.63	0.00	2.76	99.29
101	82.99	8.99	0.08	0.63	0.09	1.32	0.36	0.13	3.93	98.52
102	86.11	9.22	0.08	0.61	0.00	0.92	0.90	0.00	0.98	98.82
103	82.52	9.25	0.09	0.32	0.07	1.52	0.21	0.00	4.51	98.49
104	87.26	9.72	0.00	0.00	0.00	0.00	1.74	0.00	0.00	98.72
105	87.52	9.75	0.27	0.34	0.00	0.00	0.32	0.00	0.00	98.20
106	84.90	10.21	0.17	0.73	0.06	1.05	0.08	0.00	1.92	99.12
Inagli River placer (Inagli massif)										
107	66.03	5.13	0.00	0.26	3.78	3.65	0.00	2.73	16.69	98.27
108	81.01	6.84	0.00	1.06	0.20	3.35	0.00	0.91	5.64	99.01
109	82.01	7.58	0.00	0.00	0.00	0.60	0.09	0.59	7.68	98.55
110	87.80	7.88	0.00	0.33	0.11	1.53	0.00	0.00	1.60	99.25
111	85.60	8.08	0.00	0.00	0.12	0.21	0.00	0.26	3.93	98.20
112	77.59	8.19	0.00	1.26	0.66	0.91	0.00	0.42	10.85	99.88
113	86.73	8.48	0.00	0.00	0.00	0.45	0.00	0.07	3.17	98.90
114	82.83	9.21	0.00	0.60	0.47	2.20	0.00	0.65	3.68	99.64
115	86.96	9.38	0.00	0.29	0.00	0.38	0.00	0.00	3.44	100.45
Koura River placer (Sengibir massif)										
116	88.73	5.69	0.00	1.50	0.33	0.00	0.00	1.12	1.00	98.37
117	86.49	6.40	0.00	1.05	0.56	0.00	0.00	2.12	1.72	98.34
118	83.84	7.18	0.00	0.25	1.02	0.00	0.00	2.70	4.69	99.68

119	90.22	7.50	0.00	0.35	0.16	0.00	0.00	0.82	0.00	99.05
120	90.09	8.19	0.06	0.16	0.15	0.00	0.62	0.00	0.65	99.92
121	88.57	8.88	0.13	0.52	0.00	0.00	0.09	0.00	0.00	98.19
122	81.28	9.45	0.00	0.55	0.47	2.67	1.08	0.82	2.09	98.41
Kaurchak River placer										
123	89.93	3.75	0.00	4.38	0.12	0.14	0.00	0.00	0.44	98.76
124	87.36	5.30	0.19	0.23	0.79	1.46	0.37	0.64	2.62	98.96
125	89.77	5.93	0.00	0.72	0.00	0.83	0.94	0.00	0.63	98.82
126	89.8	6.09	0.00	0.84	0.12	1.50	0.47	0.00	0.14	98.96
127	85.97	7.03	0.16	0.55	1.94	1.53	0.43	0.53	0.86	99.00
128	90.44	7.70	0.00	0.57	0.00	0.00	0.80	0.00	0.00	99.51
129	89.03	8.02	0.00	0.44	0.00	0.45	0.38	0.00	0.83	99.15
130	90.47	8.47	0.00	0.14	0.00	0.00	0.23	0.00	0.00	99.31
Tyulenevsky River placer										
131	89.58	5.50	0.13	0.35	0.46	1.52	0.59	0.00	1.41	99.54
132	87.30	5.73	0.20	0.28	0.44	1.51	0.51	0.67	2.93	99.57
133	88.19	6.07	0.12	0.53	0.61	1.78	0.81	0.56	0.31	98.98
134	86.72	6.44	0.00	0.53	0.47	2.02	1.19	0.00	0.69	98.06
135	86.93	8.60	0.00	0.49	1.16	1.48	0.41	0.00	0.87	99.94
Mrassu River placer										
136	86.88	5.92	0.00	3.83	0.00	0.92	0.86	0.00	0.00	98.41
137	88.26	6.96	0.00	1.50	0.00	0.75	0.73	0.00	0.00	98.20
138	89.60	7.12	0.00	0.48	0.09	0.82	0.83	0.00	0.00	98.94
139	86.55	8.83	0.00	0.30	1.01	1.33	0.30	0.00	1.13	99.45
140	89.15	9.00	0.00	0.48	0.00	0.10	0.00	0.00	0.26	98.99
Placers connected with ophiolite-type massifs										
Zolotaya River placer (Kurtucshibinsky ophiolite belt)										
141	88.32	8.80	0.00	0.41	0.00	0.42	1.19	0.00	0.28	99.42
142	89.02	9.16	0.00	0.20	0.07	0.00	0.46	0.00	0.00	98.91
143	85.09	9.27	0.00	0.40	0.00	0.28	1.09	0.00	1.38	97.51
144	85.41	9.54	0.00	0.88	0.05	1.18	1.19	0.00	0.00	98.25
145	73.34	0.00	0.00	24.19	0.00	0.11	0.00	0.09	0.00	97.73
Gar'-1.2 rivers placers (Ust'- Depsky ophiolite belt)										
146	88.73	6.55	0.00	0.51	0.04	0.68	0.27	0.07	2.68	99.53
147	86.10	7.85	0.00	0.95	0.09	1.52	0.00	0.07	3.06	99.64
148	88.86	8.94	0.00	0.49	0.06	0.10	0.62	0.08	0.00	99.15
149	82.82	9.75	0.00	0.53	0.30	2.00	0.21	0.06	3.37	99.04
Ol'khovaya River placer (Ust'- Kamchatsky ophiolite massif)										
150	92.23	4.50	0.00	0.00	0.00	0.77	0.00	1.55	0.00	99.05
151	90.89	7.99	0.00	1.05	0.00	0.00	0.51	0.00	0.00	100.44
152	88.11	8.36	0.37	0.34	0.00	0.00	0.00	0.81	2.93	100.92
153	90.42	9.60	0.00	0.00	0.00	0.00	0.08	0.01	0.00	100.11
154	82.12	10.11	1.43	0.45	0.00	2.27	0.00	0.00	3.61	100.00
Suenga River placer										
155	87.41	8.42	0.00	0.00	0.11	0.00	0.00	0.09	1.12	97.84
156	89.44	8.95	0.00	0.27	0.00	0.45	0.29	0.09	0.00	99.49
Balyksa River placer										
157	83.48	8.71	0.00	1.55	0.11	1.07	0.00	0.00	3.22	98.14
158	85.46	8.50	0.00	0.66	0.00	0.46	0.00	0.00	4.24	99.32

Compositions of PGMs were determined by a Camebax-Micro microprobe, using the RMA-92 program (analysts L.N. Pospelova and V.M. Chubarov). Acceleration voltage was 20 kV, probe current 20-30 μ A, counting time 10 seconds for each analytical line. Standards: Pt, Ir, Os, Pd, Rh, Au and Ru as metals, CuFeS₂ (for Cu, Fe, S), InAs (for As), and CuSbS₂ (for Sb). The following X-ray lines were used: L $_{\alpha}$ for Pt, Ir, Pd, Rh, Ru, As, Sb; K $_{\alpha}$ for S, Fe, Cu and M $_{\alpha}$ for Os. Line interference was corrected with the help of the data file of experimental calculated coefficients (Lavrent'ev and Usova, 1994). The data are given in compliance with mineral detection limit.

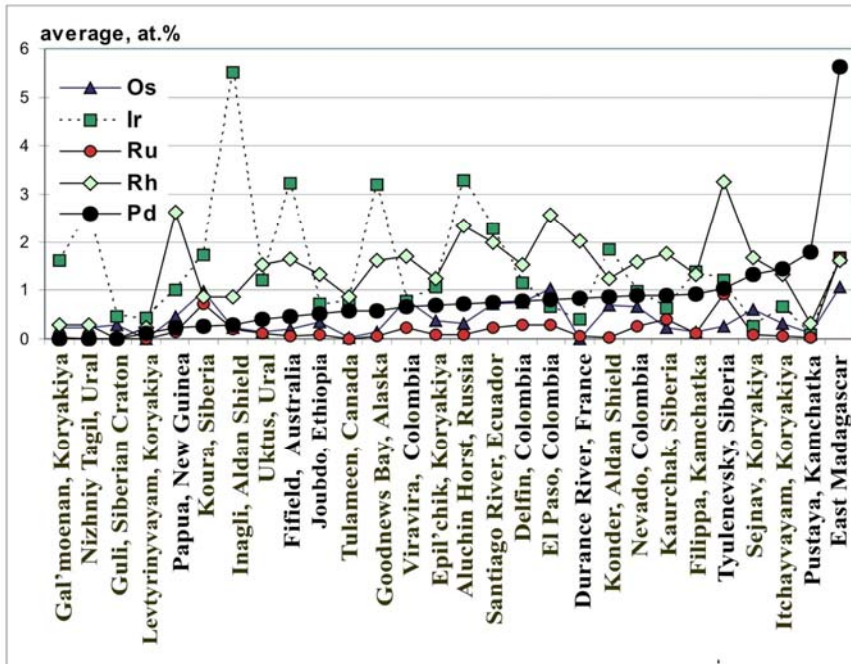


FIG. 6-6. Average values of concentrations of minor PGE in Pt-Fe alloys in various placers of the world, related to Ural-Alaskan-type complexes. The placers are listed by the increase of average concentration of Pd; published data, the references are in the text.

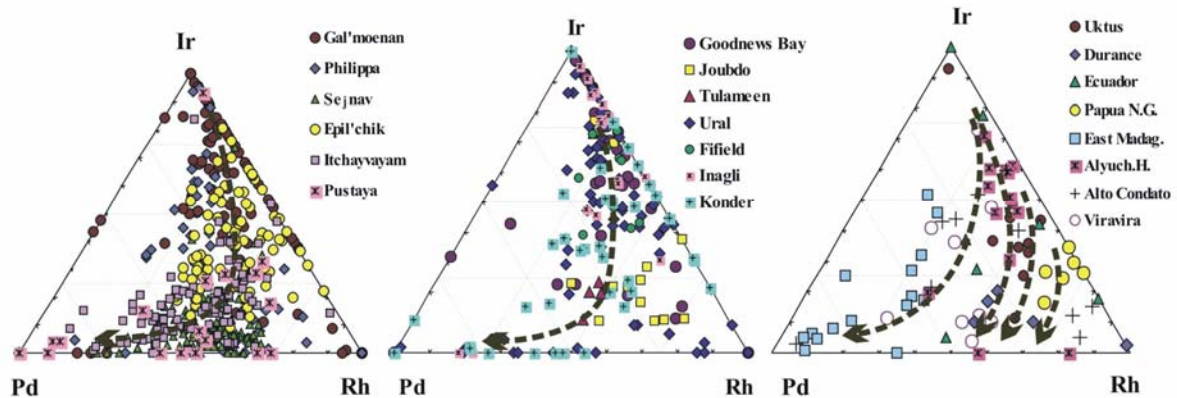


FIG. 6-7. Plots of the Pd, Ir and Rh concentrations in Pt-Fe alloys from placers (published data). The trends correspond to the evolution of the ore-forming system of Ural-Alaskan-type complexes.

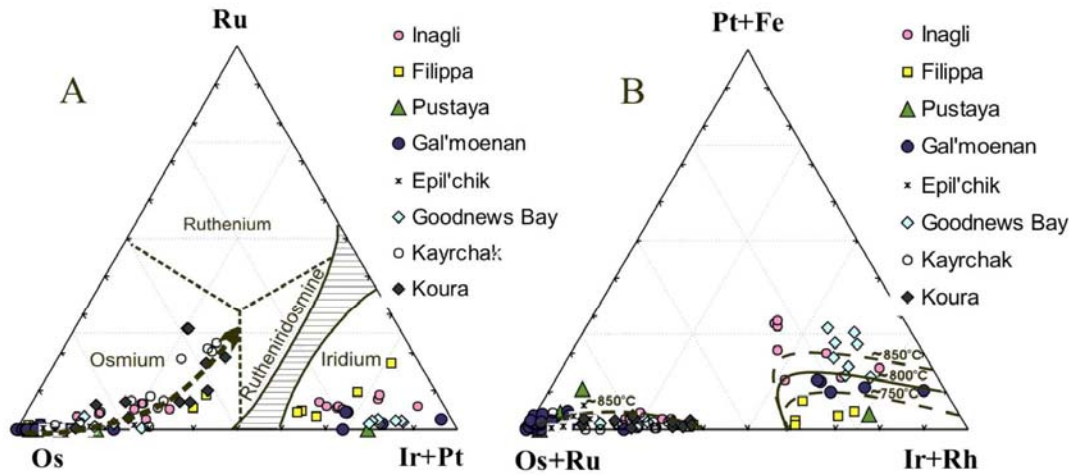
some variations due to the gradient of temperature of crystallization of the alloys.

Composition of Os–Ir–Ru alloys in placers

Os–Ir–Ru alloys in placers connected to the Ural-Alaska type are usually inclusions in Pt–Fe alloys, and infrequently they are as discrete grains in placer concentrates. Os–Ir–Ru alloys represent solid solutions of refractory elements in which Pt also is present. They are subdivided into hexagonal solid solutions in which Os and Ru are dominant and cubic alloys that are rich in Ir. These groups are divided by an immiscibility gap in the diagram

Os–Ru–(Ir+Pt) (Fig. 6-8), caused by full mutual solubility between Os and Ru, and the existence of limited solid solutions between these two elements and Ir (Harris & Cabri 1973). Using the classification of Harris & Cabri (1991) the hexagonal solid solutions are subdivided into osmium, ruthenium and rutheniridosmine. In placers of the Ural-Alaska type, as a rule, only two minerals from the Os–Ir–Ru ternary are observed: osmium and iridium. Both form independent grains or occur as inclusions in Pt–Fe alloys, but do not crystallize concurrently. In contrast, in the placers related to ophiolite, all mineral species of the system Os–Ir–

Placers of Ural-Alaskan type complexes



Placers of ophiolite-type complexes

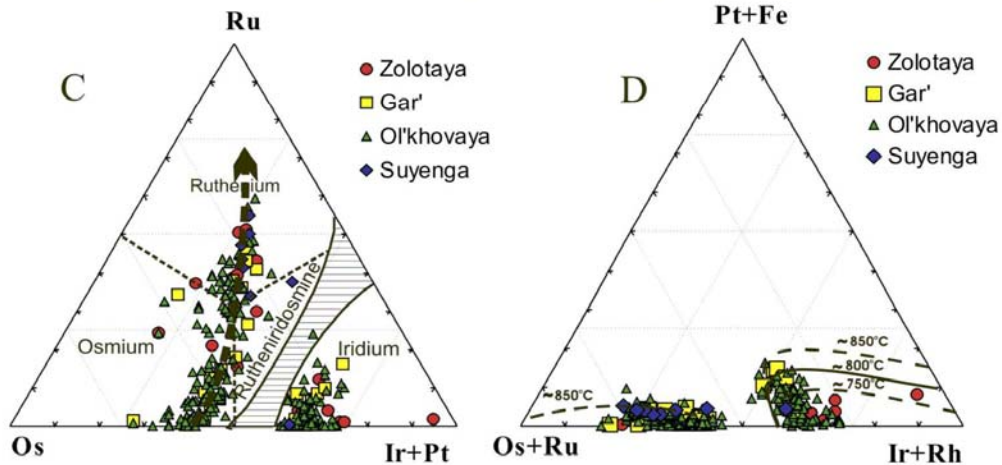


FIG. 6-8. Composition of Os-Ir-Ru alloys from placers of Ural-Alaskan (a, b) and ophiolitic (c, d) complexes.

Ru are characteristically seen in the mineral suite (Krivenko & Tolstykh 1994, Nakagawa & Ohta 1995).

Osmium from Ural-Alaska zoned intrusive complexes is characterized by low concentrations of Ru, and contains moderate amounts of Ir (Table 6-3). Plots of analyses given on the Os–Ru–(Ir+Pt) diagram are located along a trend directed away from Os (Fig. 6-8a). The composition of osmium from inclusions in Pt–Fe alloys is close to pure, and discrete crystals of osmium from the placer are enriched in Ir, as in the placers from Koura,

Kaurchak or Filippa. Native iridium from placers of the Ural-Alaskan type is also poor in Ru, but rather, it is enriched in Pt. On the diagram (Os+Ru) – (Pt+Fe) – (Ir+Rh) the analyses of iridium form a wide field (Fig. 6-8b). Iridium, which is present in isoferroplatinum-iridium decomposition structures with more than 10 wt. % Pt, in accordance with the isolines of the solvus temperature (Slansky *et al.* 1991), was formed within a range of temperatures of decomposition between 750°C and 850°C. Discrete grains of Pt-poor iridium are formed at lower temperatures (Fig. 6-8b).

PGE PLACERS ASSOCIATED WITH URAL-ALASKA TYPE COMPLEXES

TABLE 6-3. SELECTED COMPOSITION OF OS-IR-RU ALLOYS FROM PLACERS.

	Ir	Os	Ru	Pt	Rh	Cu	Fe	Total
Placers connected with Ural-Alaskan type massifs								
Levtyrnyvayam River placer (Gal'moenan massif)								
1	0.00	99.54	0.00	0.56	0.00	0.00	0.00	100.10
2	0.00	98.54	0.00	1.27	0.00	0.00	0.00	99.81
3	0.93	97.57	0.00	0.31	0.00	0.00	0.00	98.81
4	1.70	93.70	0.00	3.90	0.00	0.00	0.00	99.30
5	2.30	94.80	0.00	1.90	0.00	0.00	0.00	99.00
6	4.70	92.80	0.00	2.30	0.00	0.00	0.00	99.80
7	7.80	87.90	0.00	3.60	0.00	0.00	0.00	99.30
8	9.08	88.47	0.00	1.38	0.00	0.00	0.00	98.93
9	10.20	86.10	0.00	2.60	0.00	0.00	0.00	98.90
10	21.83	76.70	0.00	0.00	0.00	0.00	0.00	98.53
11	59.77	23.36	2.46	11.72	1.72	0.00	0.39	99.42
12	63.41	25.63	0.00	9.98	0.20	0.00	0.00	99.22
13	69.98	16.04	0.80	11.17	0.28	0.00	0.00	98.27
Tapel'vayam River placer (Seynav massif)								
14	0.70	97.30	0.00	0.00	0.40	0.00	0.00	98.50*
15	1.10	94.00	0.00	1.20	0.50	0.00	0.10	97.00*
16	1.80	97.90	0.00	0.00	0.10	0.00	0.00	99.90*
17	2.80	83.10	1.30	10.20	0.60	0.00	1.00	99.20**
18	11.50	80.40	0.90	3.20	1.00	0.20	0.20	97.60**
Snegovaya River placer (Epil'chik massif)								
19	0.27	95.53	0.00	2.30	0.00	0.00	0.00	98.10
20	5.01	92.10	0.21	0.00	0.22	0.07	0.07	97.76
21	7.87	90.79	0.14	0.00	0.33	0.19	0.13	99.72
22	9.34	83.81	0.46	3.53	0.42	0.29	0.56	98.54
Itchayvayam River placer (Itchayvayam massif)								
23	0.48	97.20	0.00	1.63	0.00	0.00	0.00	99.31
24	2.81	95.13	0.13	0.75	0.37	0.15	0.16	99.50
25	5.12	91.69	0.14	0.00	0.37	0.10	0.06	97.48
26	14.18	84.06	0.00	0.28	0.45	0.29	0.10	99.36
27	16.97	79.65	0.41	1.11	0.26	0.33	0.15	98.88
Puctaya River placer								
28	2.43	95.49	0.00	1.92	0.00	0.00	0.00	99.84
29	3.06	95.03	0.00	0.00	0.00	0.00	0.00	98.09
30	7.57	82.47	0.00	10.83	0.00	0.00	0.00	100.87
31	74.75	19.97	0.00	3.83	0.00	0.00	0.00	98.55
Major River placer (Filippa massif)								
32	0.00	98.12	0.04	1.03	0.00	0.00	0.00	99.19
33	0.00	96.87	0.51	1.20	0.42	0.00	0.00	99.00
34	1.86	93.70	0.76	2.04	0.41	0.00	0.00	98.76
35	38.87	54.83	4.93	0.48	0.09	0.00	0.25	99.51
36	59.83	33.32	2.52	1.88	0.59	0.00	0.18	98.32
37	71.68	18.49	5.40	1.86	0.44	0.00	0.60	98.57
38	77.51	6.95	9.91	2.65	0.89	0.00	0.79	98.78
Salmon River placer (Red Mountain, Goodnews Bay, Alaska)								
39	10.69	84.15	1.85	1.51	0.77	0.00	0.08	99.06
40	14.59	81.31	0.31	1.48	0.73	0.00	0.00	98.42
41	19.42	77.35	0.76	1.52	0.34	0.00	0.00	99.40
42	25.90	71.09	0.18	1.62	0.39	0.00	0.08	99.25
43	57.05	17.57	0.95	20.65	2.00	0.12	0.80	99.14
44	59.29	19.94	0.87	17.10	2.00	0.21	0.69	100.10
45	62.97	17.62	1.38	13.34	3.36	0.45	0.88	99.99
46	71.47	13.69	1.39	8.55	3.16	0.50	1.53	100.29

Inagli River placer (Inagli massif)								
47	0.00	96.40	0.00	2.20	0.00	0.00	0.00	98.60
48	1.70	93.70	0.00	3.90	0.00	0.00	0.00	99.30
49	4.70	92.80	0.00	2.30	0.00	0.00	0.00	99.80
50	7.80	87.90	0.00	3.60	0.00	0.00	0.00	99.30
51	8.79	85.16	1.89	2.79	0.39	0.00	0.00	99.02
52	10.20	86.10	0.00	2.60	0.00	0.00	0.00	98.90
53	13.69	80.30	2.26	2.56	0.38	0.08	0.00	99.27
54	19.89	72.59	3.63	3.23	0.96	0.00	0.07	100.37
55	21.19	70.87	3.66	3.31	0.91	0.00	0.00	99.94
56	29.69	64.39	2.90	2.78	0.42	0.00	0.00	100.18
57	44.02	25.85	3.36	22.64	1.67	0.35	1.81	99.70
58	54.18	19.45	3.77	19.34	1.80	0.22	1.64	100.40
Koura River placer								
79	10.03	82.39	3.63	3.03	1.28	0.00	0.00	100.36
80	17.97	74.30	3.81	2.46	0.87	0.00	0.00	99.41
81	21.63	73.51	0.93	1.94	0.35	0.08	0.00	98.44
82	24.10	74.17	1.59	0.00	0.00	0.00	0.08	99.94
84	31.45	62.15	2.36	1.89	0.95	1.00	0.00	99.80
85	34.02	61.73	4.04	0.41	0.19	0.00	0.15	100.54
86	35.88	58.29	3.86	0.36	0.18	0.00	0.16	98.73
87	40.40	47.68	10.85	0.68	0.18	0.00	0.24	100.03
Kaurchak River placer								
88	2.44	91.08	0.54	4.02	0.88	0.00	0.08	99.04
89	13.57	84.45	0.92	0.00	0.00	0.00	0.00	98.94
90	17.20	80.18	2.36	0.00	0.09	0.00	0.00	99.83
91	21.69	72.32	4.12	1.12	0.10	0.00	0.08	99.43
92	26.37	68.37	4.83	0.36	0.06	0.00	0.13	100.12
93	29.63	66.40	3.08	0.00	0.00	0.00	0.10	99.21
94	30.74	64.97	4.23	0.00	0.00	0.00	0.09	100.03
95	35.02	48.78	13.27	2.52	0.12	0.00	0.21	99.92
96	36.68	50.17	11.91	0.77	0.21	0.00	0.13	99.87
Tyulenevsky River placer								
97	27.14	68.73	0.42	1.59	0.44	0.00	0.06	98.38
Mrassu River placer								
98	91.48	4.41	1.01	0.89	0.09	0.00	1.15	99.03
Placers connected with ophiolite-type massifs								
Zolotaya River placer (Kurtuchibinsky ophiolite belt)								
99	68.11	24.72	0.57	5.00	0.40	0.13	0.43	99.36
100	90.22	4.61	1.05	2.12	0.06	0.14	1.76	99.96
103	33.27	50.33	12.53	1.87	1.96	0.08	0.14	100.18
104	37.14	42.65	17.87	1.86	0.84	0.00	0.34	100.70
105	33.20	37.13	25.86	2.11	1.50	0.09	0.20	100.09
106	35.74	30.00	29.69	3.60	2.25	0.09	0.11	101.48
107	30.00	31.64	35.75	1.97	1.40	0.00	0.11	100.87
108	29.94	29.36	36.74	3.70	1.65	0.00	0.15	101.54
Gar'-1,2 rivers placers (Ust'- Depsky ophiolite belt)								
109	61.16	35.63	0.90	1.31	0.27	0.00	0.33	99.60
111	41.20	53.72	3.11	1.05	0.23	0.00	0.29	99.60
113	54.88	19.53	9.65	11.49	2.79	0.00	0.86	99.20
114	38.94	38.66	16.44	4.36	1.06	0.00	0.43	99.89
115	23.77	54.19	21.66	0.00	0.29	0.00	0.07	99.98
116	36.13	30.80	27.35	4.03	1.44	0.00	0.30	100.05
118	27.77	31.66	32.54	5.10	3.29	0.00	0.10	100.46
Ol'khovaya River placer (Ust'- Kamchatsky ophiolite massif)								
119	60.85	26.75	5.27	4.72	0.80	0.00	1.79	100.19
122	59.29	34.00	0.00	5.56	0.00	0.00	0.90	99.75

PGE PLACERS ASSOCIATED WITH URAL-ALASKA TYPE COMPLEXES

128	43.17	53.95	2.53	0.17	0.00	0.00	0.11	99.92
131	42.60	51.17	5.96	0.00	0.00	0.00	0.16	99.89
134	41.71	46.01	10.98	1.30	0.00	0.00	0.14	100.14
136	37.96	41.47	17.14	2.56	0.00	0.00	0.13	99.27
138	33.14	41.12	21.30	2.93	0.69	0.00	0.00	99.19
139	27.78	43.03	25.55	2.55	0.66	0.00	0.00	99.56
140	26.72	38.90	29.13	3.39	1.03	0.00	0.22	99.39
141	28.33	30.24	35.15	5.38	0.64	0.00	0.35	100.09
142	28.73	25.31	42.37	2.36	1.94	0.00	0.00	100.74
143	26.71	21.36	44.13	3.64	2.83	0.00	0.00	98.67
Suenga River placer								
145	58.53	29.96	6.90	3.12	0.86	0.12	0.29	99.78
146	39.49	53.28	5.28	0.37	0.16	0.22	0.57	99.37
147	37.72	59.68	0.52	0.37	0.08	0.00	0.18	98.53
148	38.04	39.52	18.22	2.88	0.68	0.11	0.30	99.75
150	33.33	37.10	23.82	2.35	2.02	0.00	0.38	99.00
151	35.10	33.60	27.14	1.55	0.32	0.00	0.65	98.35
153	28.85	28.60	35.29	5.03	1.88	0.00	0.20	99.85
154	21.03	26.33	40.00	4.90	4.24	0.11	0.51	97.12
Balyksa River placer								
155	56.52	28.75	7.56	5.68	0.81	0.08	0.35	99.75
157	41.47	51.79	4.56	0.81	0.58	0.00	0.29	99.50
158	36.91	52.60	8.26	0.60	0.10	0.00	0.16	98.63
159	34.28	48.17	13.44	2.69	0.65	0.08	0.00	99.31
160	38.52	37.84	21.36	1.29	0.35	0.00	0.16	99.52
161	33.86	37.81	23.51	3.09	1.56	0.09	0.47	100.39

* total includes 0.1 wt.% Pd. ** - 0.2 wt.% Pd

Equilibrium Mineral Paragenesis in PGE-Bearing Placers

In spite of the fact that Os–Ir–Ru and Pt–Fe alloys are characteristic of placers of various origins (Cabri & Harris 1975), their compositions and ratios can vary strongly, depending on the degree of fractionation of the initial melt, the temperatures of their formation, and the amount of volatile components in the source. Characteristic features exist which allow us to presume a bedrock source with confidence and to identify its genetic type. These characteristics are related to the magmatic equilibrium, mineral paragenesis, a development which has been caused by the evolution of the ore-forming system of source rock. In the placers derived from the Ural-Alaska type complexes, there are two types of magmatic equilibrium paragenesis:

1. Pt–Fe Alloy-Osmium Paragenesis

This paragenesis occurs where crystals of osmium are included in a Pt–Fe matrix. In placers of the Pustaya, Koura, Itchayvayam, Sejnav and Levtyrynivayam Rivers, these can be fine-grained, 10–20 μm single inclusions (Fig. 6-9a). In the Inagli River example (Fig. 6-9b), they occur as large randomly oriented plates of the osmium

crystals, protruding from grains of isoferroplatinum. This paragenesis is early, and genetically connected with fine- and medium-grained dunite of zoned intrusions. The composition of osmium is close to pure (Table 6-3); the Pt–Fe alloy has Pt₃Fe composition or it is a little enriched in Fe and poor in minor elements (Table 6-2). It is formed in a temperature interval that evolves with Ir enrichment of osmium crystals. In some occurrences of the Ural-Alaskan type, this paragenesis is accompanied by magmatic sulfides of the laurite–erlichmanite series (Fig. 6-9b), which indicate elevated $f(\text{S}_2)$ in the bedrock source.

2. Isoferroplatinum-Iridium Paragenesis

This paragenesis is represented by iridium inclusions in Pt₃Fe alloys. Most often it is derived from the decomposition of a high temperature Pt–Fe–Ir solid solution, when fine isometric inclusions of cubic iridium or larger crystals, formed as a result of collecting crystallization, are scattered in Pt–Fe matrix (Fig. 6-9c,d). Isoferroplatinum-iridium paragenesis with similar textures has been established in the Fifield placer of Australia, the Levtyrynyvayam and Inagli localities in Russia and the Delfin deposit in Colombia (Slansky *et al.* 1991,

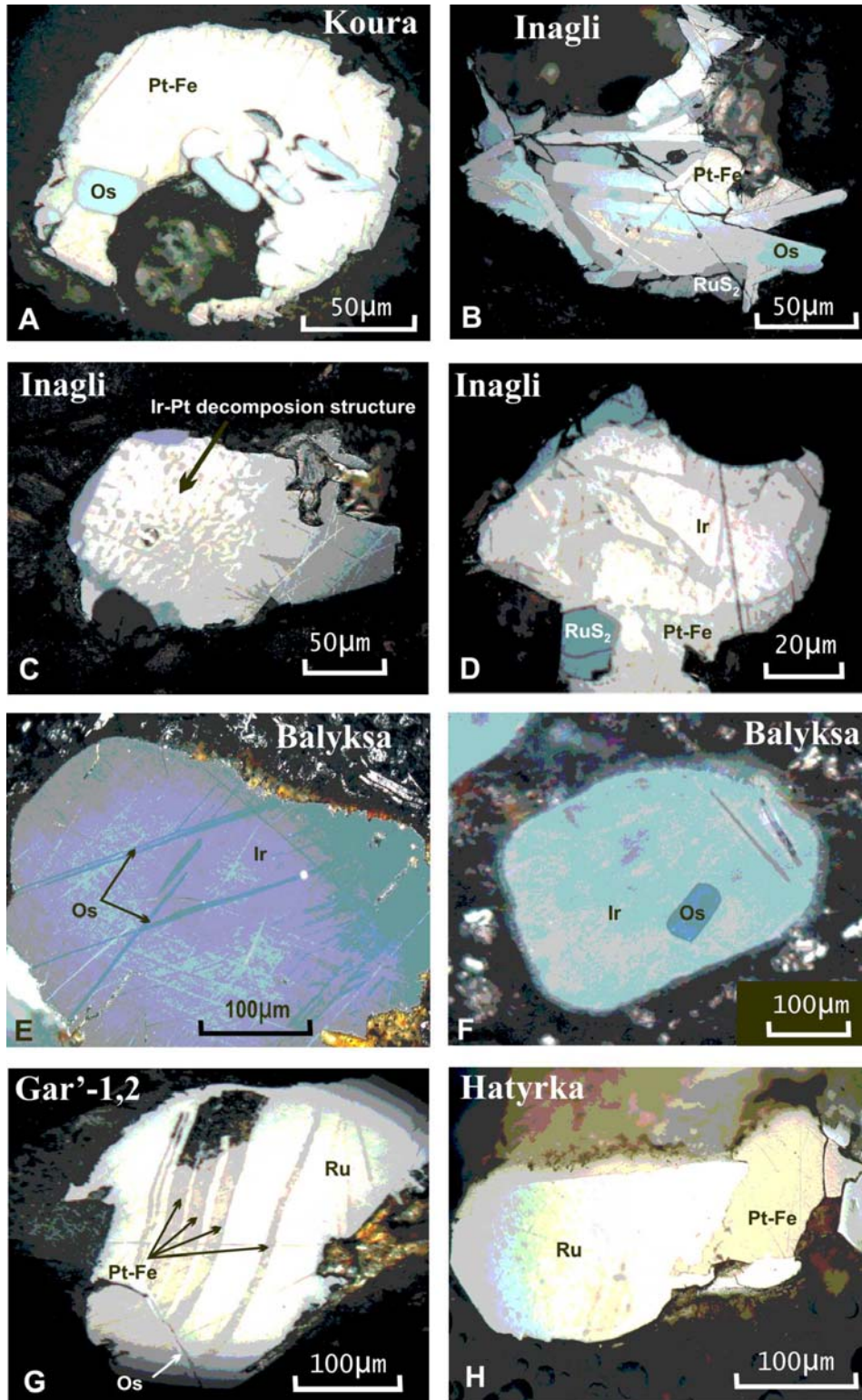


FIG. 6-9. Microphotographs of PGM showing different paragenesis from placers related to the Ural-Alaskan-type: a,b - Pt-Fe alloy-osmium; c,d - isoferroplatinum-iridium; and from placers related to ophiolite-type ultramafic rocks: e,f – osmium-iridium, g,h – isoferroplatinum-ruthenium.

TABLE 6- 4. MINERALOGICAL-GEOCHEMICAL FEATURES OF PLACERS RELATED TO URAL-ALASKAN TYPE COMPLEXES.

№	Placer names and information about the bedrock sources	The characteristics of Pt-Fe alloys	Magmatic mineral parageneses; characteristics of Os-Ir-Ru alloys	Inclusions of minerals in Pt-Fe and Os-Ir-Ru alloys	Unnamed phases; particular features of composition of minerals
1	Levtyrynyayam River placer; Ledyanoy Creek placer; Penisty Creek placer; Gal'moenan massif: dunite outcrop > 50 %; clinopyroxenite, gabbro; K; Koryak region	Pt(Fe), Pt ₃ Fe, (Pt,Fe); the replacement by Pt ₂ FeCu and PtFe; Ir- rich alloy in a bedrock source, Ir,Rh-rich alloy in Ledyanoy Creek placer, and Pd,Rh-rich in Levtyrynyayam River placer	1. Pt-Fe alloy – osmium; 2. intermediate Pt-Fe alloy – osmium – iridium, 3. isoferroplatinum – iridium Ru content in Os-Ir alloy <10 at. % Osmium-iridium trend of compositions	bowieite cooperite cuproiridsite cuprothodsite erlichmanite ferronickelplatinum genkinitite gexaferum and its analogs hollingworthite irarsite kashinite laurite malanite osarsite palladodymite platarsite sperrylite stibiopalladinite tetraferroplatinum tulameenite laurite	Mss Iss Rh ₄ S ₅ (Rh,Fe) ₃ S ₂ Rh ₃ As Rh ₂ As Pd ₂ CuSb RhSb Oxides of Os,Ir,Rh,Ru,Pt,Fe Solid solution: OsS ₂ -OsAsS; PtAsS-PtAs ₂ PtAs ₂ -PtSb ₂
2	Tapel'vayam River placer; Sejnav massif: dunite outcrop about 40 %; wehrlite, clinopyroxenite; K; Koryak region	Pt(Fe), Pt ₃ Fe, (Pt,Fe); Pd,Rh-rich alloy; Cu- 2-10 at. %; the replacement by Pt ₂ FeCu и PtFe	1. Pt-Fe alloy – osmium; Ru content in Os-Ir alloy < 1.5 at. %,	laurite	Cu-rich Pt-Fe alloy

TABLE 6-4 (CONTINUED). MINERALOGICAL-GEOCHEMICAL FEATURES OF PLACERS RELATED TO URAL-ALASKAN TYPE COMPLEXES.

N ^o	Placer names and information about the bedrock sources	The characteristics of Pt-Fe alloys	Magmatic mineral parageneses; characteristics of Os-Ir-Ru alloys	Inclusions of minerals in Pt-Fe and Os-Ir-Ru alloys	Unnamed phases; particular features of composition of minerals
3	Snegovaya River placer; Epilchik massif: dunite, clinopyroxenite, gabbro; K; Koryak region	Pt(Fe), Pt ₃ Fe, (Pt ₄ Fe); Ir,Rh-rich Pt-Fe alloy; the replacement by Pt ₂ FeCu and PtFe	1. Pt-Fe alloy – osmium; Ru content in Os-Ir alloy <1 at. % Osmium-iridium trend of compositions	cooperite	
4	Itchayayam River placer; Itchayayam massif: gabbro outcrop about 40 %; clinopyroxenite, diorite; K; Koryak region	Pt(Fe), Pt ₃ Fe, (Pt ₄ Fe); Ir,Rh-rich and Rh-Pd-rich alloy Cu- up to 5 at. %	1. Pt-Fe alloy – osmium; Ru content in Os-Ir alloy <1 at. % Osmium-iridium trend of compositions	bowieite braggite cooperite laurite <i>In sulphide ore:</i> hessite merticite II temagamite	Au ₂ PdHg Cu-rich Pt-Fe alloy The presence of sulphide ore in bedrock source
5	Prizhimny Creek placer; gabbro massif; K; Koryak region	Pt(Fe) is predominates; Pt ₃ Fe; Rh,Pd-rich alloy; Cu > 5 at. %	1. Pt-Fe alloy – osmium; Ru content in Os-Ir alloy <4 at. % Osmium-iridium trend of compositions	cooperite laurite hollingworthite	Mss (Rh,Ir,Os,Ru)AsS - RuS ₂ solid solution

TABLE 6-4 (CONTINUED). MINERALOGICAL-GEOCHEMICAL FEATURES OF PLACERS RELATED TO URAL-ALASKAN TYPE COMPLEXES.

№	Placer names and information about the bedrock sources	The characteristics of Pt-Fe alloys	Magmatic mineral parageneses; characteristics of Os-Ir-Ru alloys	Inclusions of minerals in Pt-Fe and Os-Ir-Ru alloys	Unnamed phases; particular features of composition of minerals
6	Pustaya River placer; clinopyroxenite-gabbro massifs;	Pt(Fe) is predominates;	1. Pt-Fe alloy – osmium;	braggite	Pt ₃ Cu
<i>K;</i>	Pt ₃ Fe, (Pt,Fe), PtCu;	Ru content in Os-Ir alloy is below of limit of the elements detectability;		cooperite	Mss (Fe,Rh) _{1-x} S
<i>K;</i>	Cu- rich Pt-Fe alloy;	Osmium-iridium trend of compositions		hollingworthite	Iss (Cu,Fe,Pd) ₉ S ₈
<i>K;</i>	Pd in Pt-Fe alloy up to 10 wt. %			hongshiite	Pd ₂ Te
7	Major River placer;	Pt ₃ Fe is predominates; Pt(Fe), (Pt,Fe), Pt-Fe-Cu alloy;	1. Pt-Fe alloy – osmium;	irarsite	(Pt,Pd) ₃ S ₂
Filippa massif:	dunite outcrop about 70 %; vehrlite, clinopyroxenite, hornblende	Ir, Rh-rich alloy;	Ru content in osmium < 2 at. %;	keithconite	(Pt,Pd) ₃ S
<i>K;</i>	Ir up to 10 wt.%, and Rh up to 3.5 wt. %	2. iridium grains in placer		platarsite	solid solutions:
<i>K;</i>				rhodarsenide	(Ir,Pt)AsS - PtAs ₂
<i>K;</i>				stibiopalladinite	PtAs ₂ - RhAsS
<i>K;</i>				vasilite	Pt- analog of inaglyite
<i>K;</i>				bowieite	Co-bearing malanite
<i>K;</i>				cooperite	Mss (Fe,Ni,Rh) _{1-x} S
<i>K;</i>				cuprorhodsite	Iss (Cu,Fe,Pt) ₉ S ₈
<i>K;</i>				cuprorhodsite	IrAs(Sb,S)
<i>K;</i>				genkinitite	Pt(As,Sb,S)
<i>K;</i>				hollingworthite	(Rh,Pt,Os,Fe) ₂ (S,As) ₃
<i>K;</i>				inaglyite	(Fe,Cu)(Pd,Pt) ₃ (S,Sb,As) ₃
<i>K;</i>				irarsite	As ₃

TABLE 6-4 (CONTINUED). MINERALOGICAL-GEOCHEMICAL FEATURES OF PLACERS RELATED TO URAL-ALASKAN TYPE COMPLEXES.

N ^o	Placer names and information about the bedrock sources	The characteristics of Pt-Fe alloys	Magmatic mineral parageneses; characteristics of Os-Ir-Ru alloys	Inclusions of minerals in Pt-Fe & Os-Ir-Ru alloys	Unnamed phases; particular features of composition of minerals
8	Salmon River placer Goodnews Bay, Alaska; Red Mountain massif: dunite outcrop about 90 %; wehrlite, pyroxenite, hornblendite	Pt ₃ Fe is predominates; Pt(Fe), (Pt ₃ Fe); Ir- rich Pt-Fe alloy Ir up to 6.5 wt. %; the replacement by Pt ₂ FeCu and PtFe	1. Pt-Fe alloy – osmium; 2. isoferroplatinum – iridium; Ru content in Os-Ir alloy <2 at. %;	irarsite tulameenite	solid solutions: (Ir,Pt)AsS - PtAs ₂ and OsS ₂ – (Ir,Os)AsS
9	Inagli River placer; Inagli massif: dunite outcrop about 80%; pyroxenite, ijolite syenite-porphyr, pulaskite; J; Aldan Shield	Pt ₃ Fe is predominates; Pt(Fe); Ir-rich Pt-Fe alloy; Ir up to 16,5 wt. %	Osmium-iridium trend of compositions 1. Pt-Fe alloy – osmium; 2. intermediate Pt-Fe alloy – osmium – iridium; 3. isoferroplatinum – iridium;	cooperite cuproiridsite erlichmanite	Ir-rich specialization of ore-forming system
10	Koura River placer; Sengibir massif (?); gabbro, pyroxenite; Cm ₂ ; Gornaya Shoriya, Southern Siberia	Pt(Fe) is predominates; Pt ₃ Fe; Ir,Rh rich Pt-Fe alloy	Ru content in Os-Ir alloy <5 at. %; Osmium-iridium trend of compositions; Pt-rich iridium (up to 20 at %) 1. Pt-Fe alloy – osmium; Ru content in inclusions of osmium up to 10 at. % Ru content in individual osmium grains up to 25 at. %; Osmium-iridium trend of compositions;	irarsite laurite malanite mertiteite II rustenburgite cooperite cuprorhodsite hollingworthite malanite sperryite sperryite	Mss (Cu,Fe,Pt) _{1-x} S (Ir,Pt)AsS - PtAs ₂ solid solution Sb up to 5.73 wt. % in PtAs ₂

TABLE 6-4 (CONTINUED). MINERALOGICAL-GEOCHEMICAL FEATURES OF PLACERS RELATED TO URAL-ALASKAN TYPE COMPLEXES.

Nº	Placer names and information about the bedrock sources	The characteristics of Pt-Fe alloys	Magmatic mineral parageneses; characteristics of Os-Ir-Ru alloys	Inclusions of minerals in Pt-Fe & Os-Ir-Ru alloys	Unnamed phases; particular features of composition of minerals
11	Kaurchak River placer; Azart mountain (?): gabbro; <i>Cm₂</i> ; Gornaya Shoriya, Southern Siberia	Pt(Fe) is predominates; Pt ₃ Fe; Pd,Rh-rich Pt-Fe alloy Pt-Cu-Fe alloy;	Pt-Fe and Os-Ir-Ru alloy without intergrowths; Ru content in Os-Ir-Ru alloy ap to 20 at. % Osmium-iridium trend of compositions;	cooperite cuprorhodsite sperrylite prassoite	Mss (Rh,Cu,Fe) _{1-x} S Rh -rich specialization of ore-forming system the replacement of Pt-Fe alloy by PtS, PtAs ₂ , Au-Ag
12	Tyulenevsky River placer; Azart mountain (?) Gabbro; <i>Cm₂</i> ; Gornaya Shoriya, Southern Siberia	Pt(Fe); Rh- rich Pt-Fe alloy (up to 6.5 wt. %)	1. Pt-Fe alloy – osmium; Ru content in Os-Ir alloy is below of limit of the elements detectability; Osmium-iridium trend of compositions;	Sperrylite	Rh -rich specialization of ore-forming system; Pt-Fe alloy has covered by Pt-C compounds and Au-Ag; PtAs ₂ – PtAsS solid solution
13	Mrassu River placer; Sinyaya mountain (?): gabbro; <i>Cm₂</i> ; Gornaya Shoriya, Southern	Pt(Fe) is predominates; Pt ₃ Fe; Pd,Rh- and Rh,Ir-rich Pt-Fe alloys	Pt-Fe alloy and iridium without intergrowths;	braggite cooperite cuprorhodsite hollingworthite irarsite malanite sperrylite	vasilite (?) or Pd ₄ CuS ₂ Mss (Fe,Ir,Ni) _{1-x} S

Note: Pt(Fe) - native platinum with Fe < 25 at.%; Pt₃Fe - isoferroplatinum in which Fe ~25 a t.%; (Pt,Fe) ferroan platinum with Fe >25 at.%;

Okrugin 2000, Tolstykh *et al.* 2001, Weiser 2002). This paragenesis is later than the preceding one and is generated directly associated with chromite from coarse-grained dunite, crystallized at a late magmatic stage. Thus, isoferroplatinum is enriched with Ir, and iridium is enriched with Pt. It is sometimes possible to find a transitional three-phase situation between these two: the Pt–Fe alloy–osmium–iridium paragenesis. However, the osmium–iridium paragenesis never occurs in the placers of Ural-Alaskan type.

DISCUSSION

Typomorphic Features of Placers Related to Ural-Alaska Complexes as Compared to Placers Associated with Ophiolites

The predominance of Pt–Fe alloys in placers connected to Ural-Alaska type complexes is not an exclusive attribute of this type of PGE-bearing placer. Placers related to ophiolitic ultramafic complexes also contain Pt–Fe alloys, whose quantity can reach significant volumes, especially if their source was from cumulate parts of ophiolites (Fig. 6-1, type of placers 3C.). Moreover, Pt–Fe alloys derived from ophiolites essentially do not differ in their structure and distribution of minor elements from those derived from Ural-Alaska type complexes. Pt–Fe alloys from placers of Siberia and the Russian Far East, derived from alpine-type ultramafic complexes, show similar dependencies and distributions of the component elements (Fig. 6-10). Thus, wide variations in the compositions of Pt–Fe alloys, both in the main components, and in the minor elements, allow us to assert that the composition of Pt–Fe alloys is not a typomorphic sign for the placers of Ural-Alaska type.

Compositional trends of Os–Ir–Ru alloys are important criteria for differentiating PGE-bearing placers related to Ural-Alaska type complexes from the PGE-bearing placers related to ophiolitic ultramafic complexes. In the first case Os–Ir–Ru alloys on the diagram Os – Ru – (Ir+Pt) show the osmium–iridium trend of composition. In PGE-bearing placers related to Ural-Alaska complexes, iridium is more enriched with Pt (Fig. 6-8a,b). In placers associated with ophiolite, the hexagonal alloys on similar diagrams form a ruthenium trend of compositions stretching across the compositional fields of osmium, ruthenium and rutheniridosmine (Fig. 6-8c). Iridium is more enriched with Ru in PGE-bearing placers associated with ophiolite than in placers associated with Ural-Alaska type

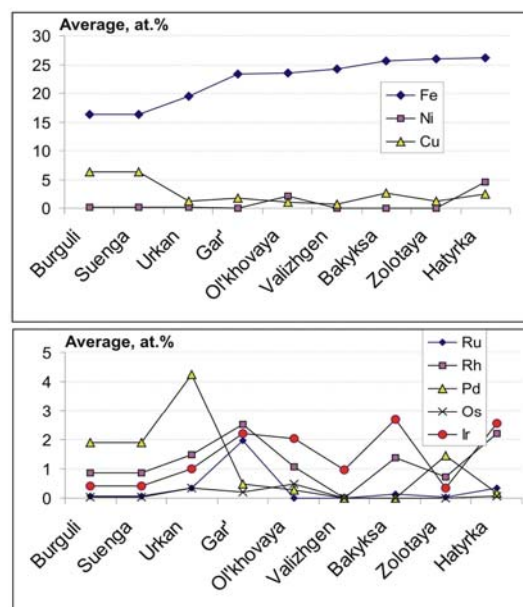


FIG. 6-10. Change of the average values of concentrations of Cu, Ni and minor PGE in Pt–Fe alloys, depending on the change of total Fe content of these alloys in placers related to ophiolite complexes.

complexes (Fig. 6-8d). The points of analyses of hexagonal and cubic alloys are close to the immiscibility gap on both sides. These distinctions are caused by a primary fractionation of the elements, hence, from having an unequal composition of metal components in the initial melt. Thus, Pt > IPGE is characteristic of zoned complexes and IPGE > Pt for ophiolitic complexes; these being important criteria for characterizing and evaluating prospecting targets.

Also the development of the mineral parageneses agrees with the evolution of an ore-forming system of bedrock sources. In complexes of Ural-Alaska type the Pt–Fe alloy – osmium paragenesis evolves, with lowering of temperature and saturation of the melt with iridium, to an isoferroplatinum–iridium paragenesis. These two types of mineral intergrowths can only be observed in placers connected with the Ural-Alaska type (Fig. 6-11a). However in contrast, the development of an early osmium–iridium paragenesis, followed by an isoferroplatinum–ruthenium paragenesis, is typical only of ophiolite (Fig. 6-11b). The osmium–iridium and isoferroplatinum–ruthenium intergrowths occur in the PGE-bearing placers related to ophiolite. The osmium–iridium paragenesis represents the inclusions of osmium in iridium or can be formed as

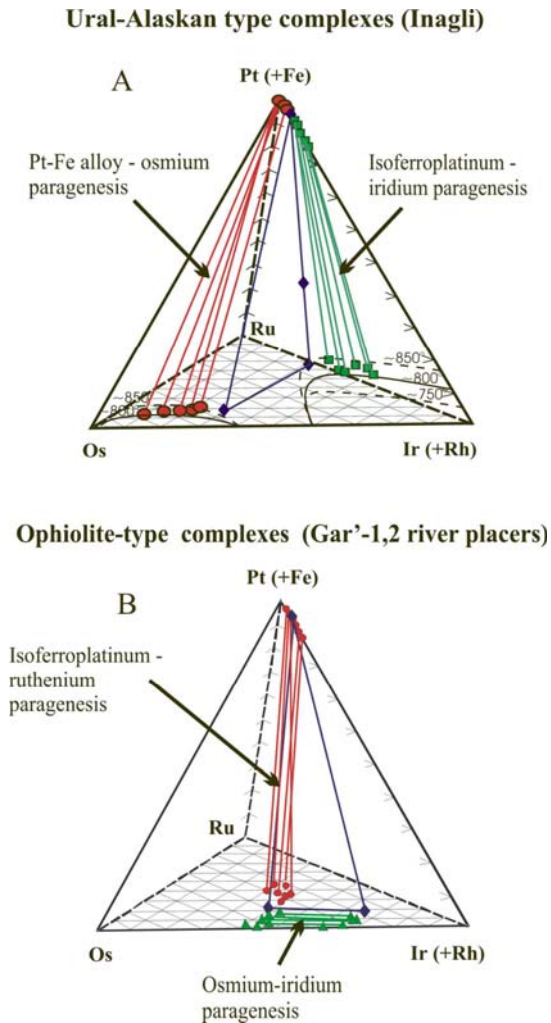


FIG. 6-11. Equilibrium magmatic paragenesis in examples of Ural-Alaskan (a) and ophiolitic (b) complexes plotted on a Pt(+Fe) - Ir(+Rh) - Os diagram.

numerous lamellae in iridium (Fig. 6-9e,f). During formation of the isoferroplatinum-ruthenium paragenesis, ruthenium (or Ru-rich osmium, or rutheniridosmine) frequently forms together with Pt-Fe alloy, and resulting crystals exhibit banded structure or oriented exsolution lamellae of ruthenium (Fig. 6-9g, *e.g.*, the Aikora River area, Papua New Guinea as described by Weiser & Bachmann 1999) or the simple intergrowths (Fig. 6-9h).

Considering the distinctive mineral paragenesis of PGE-bearing placers related to Ural-Alaska and ophiolitic complexes (Cabri *et al.* 1996, this chapter), it is possible to assume that PGE-bearing placers from the Yukon, Canada, on the islands of Borneo in Malaysia and southern

Kalimantan in Indonesia, and at Tanga and Wunbe in Burma are related to Ural-Alaska type complexes, and the Alberta placers, Canada, and Manawtha, Nawng-Pusawng, Kyain and Indawgyi Lake in Burma are related to ophiolites. We believe that the Rh-rich, Pt-Fe alloy-dominant placers of the Siberian platform are probably eroded from ophiolites (Fig. 6-1), on the basis of PGM intergrowths in equilibrium as described by Okrugin (2000).

Evolution of the Ore-Forming System of Ural-Alaska Complexes

From a silicate melt or an oxide-metal liquid that has a PGE budget dominated by Pt, osmium begins to crystallize before olivine crystallization. Os is the most refractory metal of the PGE. With a drop in temperature, olivine and the first generation of Pt-Fe alloys crystallize, forming an early Pt-Fe alloy-osmium paragenesis, characteristic of the higher-temperature fine-grained dunite. Pt-Fe alloys in this paragenesis are more Fe-rich than those formed at later stages, since they form under relatively low $f(O_2)$. Fe-rich Pt-Fe alloys (Fe = 9–10 wt.%) in intergrowths with osmium were recorded in the Gal'moenan deposit, Koryak region (Tolstykh *et al.* 2001, Nazimova *et al.* 2003), and in the Nizhny-Tagil intrusion of the Ural Mountains (Zoloev *et al.* 2001). This iron-rich Pt paragenesis is named the 'dunite subtype'. When the crystallization front deep into the magma chamber advanced, the residual melt and new portions of osmium crystals were gradually saturated with Ir. The concentration of Ru in the system is insignificant; it is mostly consumed in formation of laurite (RuS_2), being in equilibrium with Os-Ir alloys and residual melts.

The ore-forming system evolves with an increase of $f(S_2)$ and $f(O_2)$ and an increase of Ir concentration in oxide-metal liquids and in the residual melt as a whole. The associated fluid gradually changes its properties from reduction to oxidation. Chromite begins to crystallize, together with Ir-rich osmium crystals and with Mg-rich olivine. The interstices between the chromite grains are filled with the Pt-Fe alloys, mainly Pt_3Fe and high-temperature Pt-Ir-Fe solid solution, which exsolve into Ir-rich isoferroplatinum and Pt-rich iridium at temperatures lower than 845°C. In this case the 'chromite subtype' of mineralization occurs (Zoloev *et al.* 2001), which is represented by an isoferroplatinum-iridium paragenesis or occurs as decomposition products of these two phases. After

Ir depletion is finished in the system, the magmatic process of formation of PGE minerals comes to an end with the crystallization of Pt–Fe alloys, which formed directly from residual melt that is enriched with Pd, Rh and Cu. Commonly, it is native platinum with less than 25 wt.% Fe and Rh and Pd as minor elements, generated at higher $f(\text{O}_2)$ values than earlier mineral parageneses. As this residual melt is strongly enriched in volatile components, and most likely coexists with a high-temperature fluid, it is not surprising that it easily filters through permeable coarse- and medium-grained dunite, forming the late magmatic paragenesis in shallow horizons of the viscous clinopyroxenite cap (Stolyarov, 2001).

The post-magmatic stage of development of the ore-forming system depends on the nature of the volatile components rising from deeper chambers, as well as geodynamic conditions, which influence the fluid channels. Some examples may be: 1) jets of regenerative fluids causing crystallization of native metals on sulfides, *e.g.*, awaruite or Fe–Ru–Os–Ir alloys formed on laurite, 2) metamorphic serpentinizing fluids replacing magmatic Pt–Fe alloys with tetraferroplatinum, tulameenite and hongshiite, and 3) hydrothermal solutions saturated with S and As, replacing Pt–Fe alloys with cooperite and sperrylite.

CONCLUSIONS

Thus, when economic platinum placers related to Ural-Alaska type complexes are targets of exploration programs, it is necessary to take into account that the composition of Pt–Fe alloys is not a unique typomorphic sign. Rather, Pt–Fe alloy compositions only indirectly reflect the physical-chemical conditions of development of ore-forming systems. When Pt–Fe alloys dominate over Os–Ir–Ru alloys in evaluated placer fields, then one could generally assume that the PGM mineral assemblage was derived from Ural-Alaska type zoned intrusion. However, this supposition requires a more precise definition. When the compositions of hexagonal Os–Ir–Ru alloys are Ru-poor osmium and show a osmium-iridium trend on a Os–Ru–(Ir+Pt) diagram, and iridium is Pt-rich, these data will provide added confidence to the assumption that the PGE minerals were derived from Ural-Alaska type complexes. Even more reliable criteria for classifying this type of PGE-bearing placer include the presence of the following equilibrium mineral associations: 1) Pt–Fe alloy–osmium, and 2) isoferroplatinum–iridium, whose development is caused by the specific type of

parent magma and of evolution of the PGE-bearing lodes in Ural-Alaska complexes.

ACKNOWLEDGEMENTS

The authors greatly acknowledge the constructive comments by referees L.J. Cabri, and K.N. Malich. The work was partly supported by a research grant of the Science and Innovation Committee of the Government of the Russian Federation to the scientific school #1573.2003.5, and grants of the Russian Academy of Science #6.2.2 and 6.4.1.

REFERENCES

- ALEXEEV, E.S. (1987): Geodynamics of the zone of transition ocean – continent on an example of the Late Mesozoic-Cenozoic history of Koryak uplands. *Geotectonika* **4**, 102-114, (in Russian).
- AMOSSÉ, J., DABLE, P. & ALLIBERT, M. (2000): Thermochemical behaviour of Pt, Ir, Rh, and Ru vs $f\text{O}_2$ and $f\text{S}_2$ in a basaltic melt. Implications for the differentiation and precipitation of these elements. *Mineral. Petrol.* **68**, 29-62.
- ANIKEEVA, L.I. (1968): Mafic-ultramafic intrusive complex of the southern part of Koryak uplands: The authors abstracts. Leningrad: Leningrad State University, 24 p. (in Russian).
- ANIKINA, E.V., PUSHKAREV, E.V., GARUTI, G., ZACCARRINI, F. & ZEDLER, I. (1999): Chrome-platinoid mineralization in the complexes of Ural-Alaskan-type: composition and origin. Materials of the Urals summer mineralogical school – 99. Ekaterinburg 62-82, (in Russian).
- ASTRAKHANTSEV, O.V., BATANOVA, V.G. & PERFILYEV, A.S. (1991): Structure of Galmoenan dunite-clinopyroxenite-gabbro massif. *Geotectonika* **2**, 47-62, (in Russian).
- AUGÉ, T. & LEGENDRE, O. (1992): Pt–Fe nuggets from alluvial deposits in eastern Madagascar. *Can. Mineral.* **30**, 983-1004.
- AUGUSTITHIS, S.S. (1965): Mineralogical and geochemical studies of the platiniferous dunite-birbirite-pyroxenite complex of Yubdo. *Chem. Der Erde* **2**, (24), 159 p.
- BATANOVA, V.G. & ASTRAKHANTSEV, O.V. (1992): Tectonic position and genesis the zoned mafic-ultramafic plutons of the north of Olutor zone (Koryak uplands). *Geotectonika* **2**, 87-103, (in Russian).

- BATANOVA, V.T., ASTRAKHANTSEV, O.V. & SIDOROV, E.G. (1991): Dunite of Gaol'moenan ultramafic-gabbro massif (Koryak uplands). *Izv. Akad. Sci. USSR, ser. Geol.* **6** (1), 24-35, (in Russian).
- BEGIZOV, V.D., BORISENKO, L.F. & USKOV, E.D. (1975): Sulfide and natural solid solutions of platinumoids from ultramafic of Gusevogorsk massif (the Urals). *Dokl. Acad. Sci. USSR* **225** (6), 1408-1411, (in Russian).
- BOYARKO, G. (2001): The metals of PGE at 2000 year (the world review). *Precious metals. Precious stone* **4**, 110-122. (in Russian).
- CABRI, L.J. & HARRIS, D.C. (1975): Zoning in Os-Ir alloys and the relation of the geological and tectonic environment of the source rocks to the bulk Pt:Pt+Ir+Os ratio for placers. *Can. Mineral.* **13**, 266-274.
- CABRI, L. J., HARRIS, D.C. & WEISER, T.W. (1996): Mineralogy and distribution of platinum-group minerals (PGM) in placer deposits of the world. *Explor. Mining Geol.* **5** (2), 73-167.
- CABRI, L.J., CRIDDLE, A.J., LAFLAMME, J.H.G., BEARNE, GH. & HARRIS, D.C. (1981): Mineralogical study of complex Pt-Fe nuggets from Ethiopia. *Bull. Mineral.* **104**, 508-525.
- CAMSELL, C. (1913): Geology and mineral deposits of the Tulameen District, British Columbia. *Geol. Surv. Can., Mem.*, 26 p.
- CHASHCHUHIN, I.S., VOTYAKOV, S.L., PUSHKAREV, E.V., ANIKINA, E.V., MIRONOV, A.B. & UIMIN, S.G. (2002): Oxithermobarometry of the ultramafic belt of the Urals. *Geochim.* **6**, 1-18., (in Russian).
- DODIN, D.A., CHERNYSHOV, N.M. & YATSKEVICH, B.A. (2000): Platinum-metal deposits of Russia. St. Petersburg: Nauka Press, 775 p., (in Russian).
- DUPARC, L. & MOLLY, E. (1928): Les gisements platinifères du Biber (Abyssinie). *Schweiz. Mineral. Petrogr. Mitt.* **8**, 240-257.
- EFIMOV, A.A. & EFIMOVA, L.P. (1967): *Kytlym platinum bearing massif*. Moscow: Nedra Press, 340 p., (in Russian).
- EFIMOV, A.A. & TAVRIN, I.E. (1978): About genetic uniqueness of platinum-bearing dunites of the Urals and the Aldan Shield. *Dokl. Acad. Sci. USSR* **243**, 991-994, (in Russian).
- EVSTIGNEEVA, T.L., KUDRYAVTSEV, A.S. & RUDASHEVSKY, N.S. (1992): Minerals of PGE from Yubdo (Ethiopia): the new data. *Mineral. Zh.* **14** (1), 29-41, (in Russian).
- FOLEY, J.Y. (1992): Ophiolitic and other mafic-ultramafic metallogenic provinces in Alaska. Open File Report. OF – 92 – 20B.
- FOLEY, J.Y., LIGHT, T.D., NELSON, S.W. & HARRIS, R.A. (1997): Mineral occurrences associated with mafic-ultramafic and related alkaline complexes in Alaska. *Econ. Geol. Monograph* **9**, 396-449.
- GARUTI, G., FERSHTATER, G., BEA, F., MONTERO, P., PUSHKAREV, E.V. & ZACCARINI F. (1997): Platinum-group elements as petrological indicators in mafic-ultramafic complexes of the central and southern Urals: preliminary results. *Tectonophysics* **276**(1-4), 181-194.
- GARUTI, G., PUSHKAREV, E.V. & ZACCARINI, F. (2002): Composition and paragenesis of Pt alloys from chromitites of the Ural-Alaskan-type Kytlym and Uktus complexes, Northern and Central Urals, Russia. *Can. Mineral.* **39**, 353-372.
- GARUTI, G., PUSHKAREV, E.V., ZACCARINI, F., CABELLA, R. & ANIKINA, E. (2003): Chromite composition and platinum-group mineral assemblage in the Uktus Uralian-Alaskan-type complex (Central Urals, Russia). *Mineral. Deposita* **38**, 312-326.
- GLAZUNOV, O.M. (1981): *Geochemistry and ore content of gabbroids and ultramafics*. Novosibirsk: Nauka Press, 191 p., (in Russian).
- GORNOSTAYEV, S., CROCKET, J., MOCHALOV, A. & LAAJOKI, K. (1999): The platinum-group minerals of the Baimka placer deposits, Aluchin Horst, Russian Far East. *Can. Mineral.* **37**, 1117-1129.
- GUROVICH, V.G., ZEMLYANUHIN, V.N., EMEL'YANENKO, E.P., KARETNIKOV, A.S., KVASOV, A.I., LAZARENKOV, V.G., MALITCH, K.N., MOCHALOV, A.G., PRIHOD'KO, V.S. & STEPASHKO, A.A. (1994): *Geology, petrology and ore-forming potential of the Konder massif*. Moscow: Nauka Press, 176 p., (in Russian).
- HARRIS, D.C. & CABRI, L.J. (1973): The nomenclature of the natural alloys of osmium, iridium, and ruthenium based on new compositional data of alloys from worldwide occurrences. *Can. Mineral.* **12**, 104-112.
- HARRIS, D.C. & CABRI, L.J. (1991): Nomenclature

- of platinum-group-element alloys: review and revision. *Can. Mineral.* **29**, 231-237.
- HIMMELBERG, BY, G.R. & LONEY, R.A. (1995): Characteristics and petrogenesis of Alaskan-Type ultramafic-mafic intrusions, southeastern Alaska. U.S. *In* U.S. Geol. Surv. Prof. Paper **1564**, 1-43.
- IVANOV, O.K. (1986): Disseminated platinum and palladium in concentric-zoned ultramafic massifs of the Urals. *Dokl. Acad. Sci. USSR* **291**, 1226-1230, (in Russian).
- IVANOV, O.K. (1997): Concentric-zoned pyroxenite-dunite massifs of the Urals: (Mineralogy, petrology, genesis). Ekaterinburg: publishing house of Ural university, 488 p., (in Russian).
- IVANOV, O.K. & RUDASHEVSKY, N.S. (1987): Composition of olivine and chrome spinel from dunite of the platinum bearing belt of the Urals. *In* Minerals of deposits of the Urals. Sverdlovsk: The Ural branch of the Academy of sciences of the USSR, 16-35, (in Russian).
- JOHAN, Z. (2002): Alaskan-type Complexes and Their platinum-group element mineralization. *In* The Geology, Geochemistry, Mineralogy and Mineral beneficiation of platinum-group elements. L.J. Cabri (ed.). Can. Inst. Mining, Metall. Petrol. **54**, 852 p.
- JOHAN, Z., OHNENSTETTER, M., FISCHER, W. & AMOSSE J. (1990): Platinum-group minerals from the Durance River Alluvium, France. *Mineral. Petrol.* **42**, 287-306.
- JOHAN, Z., OHNENSTETTER, M., SLANSKY, E., BARRON, L.M. & SUPPEL, D. (1989): Platinum mineralization in the Alaskan-type intrusive complexes near Fifield, New South Wales, Australia Part 1. Platinum-group minerals in clinopyroxenites of the Kelvin Grove prospect, Owendale intrusion. *Mineral. Petrol.* **40**, 289-309.
- JOHAN, Z., SLANSKY, E. & KELLY, D.A. (2000): Platinum nuggets from the Kompiam area, Enda Province, Papua New Guinea: evidence for an Alaskan-type complex. *Mineral. Petrol.* **68**, 159-176.
- KRIVENKO, A.P. & TOLSTYKH, N.D. (1994): Composition of native minerals in Os-Ir-Ru system and conditions of their formation. Abstracts of VII International platinum symposium, Moscow, Russia, 1-4 August, p. 57.
- KUTYEV, F.S., SIDOROV, E.G., REZNICHENKO, V.S. & SEMENOV, V.L. (1991): The new data about platinoids in the zoned ultramafic complexes of the south of Koryak uplands. *Dokl. Acad. Sci. USSR* **317** (6), 1458-1461, (in Russian).
- KUTYEV, F.S., SIDOROV, E.G., SEMYONOV, V.L., REZNICHENKO, V.S., SIMONOVA, L.S. & ASTRAHANTSEV, O.V. (1988): Platinum bearing formation of the zoned massifs of the Olutor zone of Koryak uplands. *In* Problems of magmatism, metamorphism and mineralization of the Far East (abstracts of reports to IV Far East regional petrographic meeting). Yuzhno-Sakhalinsk, 87-88, (in Russian).
- LANDA, E.A., MARKOVSKY, B.A., SIDOROV, E.G. & SLYADNEV B.I. (2001): Features of structure and composition of dunite-clinopyroxenite massifs in the southern part of the Sredinny Ridge of Kamchatka. *In* Petrology and metallogeny of mafic-ultramafic complexes of Kamchatka. Moscow: Nauchny Mir Press, 87-105, (in Russian).
- LAVRENT'EV, YU.G. & USOVA, L.V. (1994): New version of the KARAT program for quantitative X-ray spectral microanalysis. *Zh. Analit. Chim.* **49** (5), 462-468, (in Russian).
- LAZARENKOV, V.G., MALITCH, K.N. & SAKHYANOV, L.O. (1992): Platinum metal mineralization of the zoned ultramafic and komatiitic massifs. Leningrad: Nedra, 217 p., (in Russian).
- LEDNEVA, G.V. (2001): Geochemistry, conditions and mechanism of formation of rocks from layered dunite-clinopyroxenite-gabbro series (on example of Seinav massif, Olutor zone, Koryakia). *In* Petrology and metallogeny of the mafic-ultramafic complexes of Kamchatka. Moscow: Nauchny Mir Press, 31-63, (in Russian).
- LEGENDRE, O. & AUGÉ, T. (1992): Alluvial platinum-group minerals from the Manampotsy area, East Madagascar. *Austral. J. Earth Sci.* **39**, 389-404.
- LEVINSON-LESSING, F.J. (1900): Geological description of Southern-Zaozerskaya dacha and Denezhkin Stone in the Northern Urals. Works of St-Petersburg association of scientists. Yuriev, 30, 257 p., (in Russian).

- MALAKHOV, I.A. (1999): Conditions of formation of the zoned massifs of the platinum bearing belt of the Urals and confined to them platinum mineralization. *In Materials of the Urals summer mineralogical school – 99*. Ekaterinburg, 101-112, (in Russian).
- MALITCH, K.N. (1999): *Platinum-group elements in clinopyroxenite-dunite massifs of the East Siberia (geochemistry, mineralogy, and genesis)*. St-Petersburg: St-Petersburg Cartographic Factory VSEGEI Press, 296 p., (in Russian).
- MALITCH, K.N., LOPATIN, G.G. & SIMONOV, O.N. (1998): New Russian very perspective source of osmium. *In: Large and unique deposits of rare and precious metals*, St-Petersburg, 257-270, (in Russian).
- MAMAYEV, YU.A. & VAN-VAN-E, A.P. (2000): The mining of the Far East – the present and the future. *Gorniy J.* **6**, 62-64, (in Russian).
- MERTIE, J.B. Jr. (1940): The Goodnews Bay Platinum Deposits: *U.S. Geol. Surv. Bull.* **918**, 97 p..
- MERTIE, J.B., Jr. (1976): Platinum deposits of the Goodnews Bay district, Alaska: *U.S. Geol. Surv. Prof. Paper* **938**, 42 p.
- MINERAL RESOURCES OF THE WORLD AT THE BEGINNING OF 1999 (2000): *Materials of the State Scientific Industrial Company “Airogeologia”*. Moscow:
- MOCHALOV, A.G. & KHOROSHILOVA, T.S. (1998): The Konder alluvial placer of platinum metals. *International platinum*. Athens: Theophrastus Publications, 206-220.
- NAKAGAWA, M. & OHTA, E. (1995): Preponderance of Ir–Os–Ru Alloys in Depleted Ophiolite, Hokkaido, Japan: A Window to the Mantle. *Resource Geol., Special Issue*, **18**, 49-56.
- NAZIMOVA, J.V., ZAYTSEV, V.P. & MOCHALOV, A.G. (2003): PGM of gabbro-pyroxenite-dunite of Gal'moenan massif of the southern part of Koryak uplands (Russia). *Geol. Rudn. Mestor.* **45** (6), 547-565, (in Russian).
- NEKRASOV, I.J., LENNIKOV, A.M., OKTJABRSKIY, R.A., ZALISHCHAK, B.L. & SAPIN, V.I. (1994): Petrology and platinum content of the ring alkaline-ultramafic complexes. Moscow: Nauka Press, 381 p. (in Russian).
- NIXON, G., CABRI, L.J. & LAFLAMME, J.H.G. (1990): Platinum-group-element mineralization in lode and placer deposits associated with the Tulameen Alaskan-type complex, British Columbia. *Can. Mineral.* **28**, 503-535.
- OKRUGIN, A.V. (2000): Placer platinum content of the Siberian platform. *Edited by G.N. Gamyatin*. Yakutsk: publishing house of the Siberian Branch of the Russian Academy of Science, 183 p., in Russian
- OKRUGIN, A.V. (2001): Mineral paragenesis and genesis of nuggets of Pt–Fe alloy from Inagli placer (the Siberian platform). *Geol. Rudn. Mestor.* **43** (3), 268-279, (in Russian).
- RAZIN, L.V. & SMIRNOV, V.I. (1974): Deposits of the platinum metals. *In Ore deposits of the SSSR*, 3, Moscow: Nedra Press, 96-116, (in Russian).
- RAZIN, L.V. (1976): Geologic and genetic features of forsterite dunites and their platinum-group mineralization. *Econ. Geol.* **71**, 1371-1376.
- RICE, H.M.A. (1947): Geology and mineral deposits of the Princeton map area, British Columbia. *Geol. Surv. Can., Memoirs* **243**, 136 p.
- ROEDER, P.L. & JAMIESON, H.E. (1992): Composition of chromite and co-existing Pt–Fe alloy at magmatic temperatures. *Austral. J. Earth Sci.* **39**, 419 - 426.
- ROZHKOV, I.S., KITSUL, V.I., RAZIN, L.V. & BORISHANSKAYA, S.S. (1962): Platinum of Aldan shield. Moscow: Publishing house of the Academy of sciences of the USSR, 119 p., (in Russian).
- RUDASHEVSKY, N.S., BURAKOV, B.E., MALITCH, K.N. & HAETSKIY V.V. (1992): Accessory platinum mineralization of chromite of Konder alkaline-ultramafic massif. *Mineral. Zh.* **14** (5), 12-22, (in Russian).
- SIDOROV, E.G., KOZLOV, A.P., LANDA, E.A., OSIPENKO, A.B. & MARKOVSKY, B.A. (2001): Petrogeochemical features of the rocks of Gal'moenan mafic-ultramafic massif, Koryakia. *In Petrology and metallogeny of the mafic-ultramafic complexes of Kamchatka*. Moscow: Nauchny Mir Press, 14-30, (in Russian).
- SIDOROV, E.G., TOLSTYKH, N.D., PODLIPSKY, M.YU., & PAKHOMOV, I.O. (2004): Placer PGE minerals from the Filippa clinopyroxenite-dunite massif, Kamchatka. *Russ. Geol. Geophys.* **45** (9),

- 1128-1144.
- SLANSKY, E., JOHAN, Z., OHNENSTETTER, M., BARRON, L.M. & SUPPEL, D. (1991): Platinum mineralization in the Alaskan-type intrusive complexes New Fifield, N.S.W., Australia. Part 2. Platinum-group minerals in placer deposits at Fifield. *Mineral. Petrol.* **43**, 161-180.
- STOLYAROV, S.A. (2001): Structure of Konder and Nizhny Tagil ultramafic concentric-zoned massifs and the features of platinoid mineralization (Aldan shield, the Urals). Moscow, 1-22, (in Russian).
- TAYLOR, H.P. (1967): The zoned ultramafic complexes of southeastern Alaska. *In Ultramafic and related rocks*. P.J.Wyllie (ed.). J. Wiley and Sons Inc., New York, London, Sydney, 97-121.
- TAYLOR, H.P. & NOBLE, J.A. (1969): Origin of magnetite in the zoned ultramafic complexes of southeastern Alaska. *In Magmatic Ore Deposits*. H.D.B. Wilson (ed.). *Econ. Geol. Monographs*, **4**, 209-230.
- TISTL, M. (1994): Geochemistry of platinum-group elements of the Zoned ultramafic Alto Condoto complex, Northwest Colombia. *Econ. Geol.* **89**, 158-167.
- TOLSTYKH, N.D. & KRIVENKO, A.P. (1997): Platinum-group minerals in the Inagli placer (Aldan shield). *Russ. Geol. Geophys* **38** (4), 808-817.
- TOLSTYKH, N.D., FOLEY, J.Y., SIDOROV, E.G. & LAAJOKI, K.V.O. (2002a): Composition of the platinum-group minerals in the Salmon River placer deposit, Goodnews Bay, Alaska. *Can. Mineral.* **40**, 463-471.
- TOLSTYKH, N., KRIVENKO, A., SIDOROV, E., LAAJOKI, K. & PODLIPSKY M. (2002b): Ore mineralogy of PGM placers in Siberia and the Russian Far East. *Ore Geol. Review*, **20**, p.1-25.
- TOLSTYKH, N., SIDOROV, E., LAAJOKI, K., KRIVENKO, A. & PODLIPSKIY, M. (2000): The association of platinum-group minerals in placers of the Pustaya River, Kamchatka, Russia. *Can. Mineral.* **38**, 1251-1264.
- TOLSTYKH, N.D., SIDOROV, E.G., VIDIK, S.V., KOZLOV, A.P. & VILDANOVA E.J. (2001): Mineralogical-geochemical features of PGM of the placer deposit of the Levtyrynovayam River. *In Petrology and metallogeny of the mafic-ultramafic complexes of Kamchatka*. Moscow: Nauchny Mir Press, 106-136, (in Russian).
- TOLSTYKH, N.D., SIDOROV, E.G., & KOZLOV A.P. (2004): Platinum-group minerals in lode and placer deposits associated with the Ural-Alaskan-type Gal'moenan complex, Koryak-Kamchatka platinum belt, Russia. *Can. Mineral.* **42** (2), 619-630.
- VELINSKY, V.V. (1979): Alpine-type ultramafic of the transitive zones ocean – continent. Moscow: Nauka. 264 p., (in Russian).
- VOLCHENKO, J.A. & KOROTEYEV, V.A. (1999): Fractionation of platinum metals at development of mobile systems of the Ural type and a problem of forecasting of platinum-metal deposits. *In Materials of the Ural summer mineralogical school - 99*. Ekaterinburg, 41-60, (in Russian).
- VOLCHENKO, J.A., ZOLOEV, K.K., KOROTEEV, V.A., MARDIROSJAN, A.N. & NEUSTROYEVA V.A. (1998): New and prospective types of platinum-metal mineralization of the Urals. *In Geology and metallogeny of the Urals, the collection of scientific works. Materials of the scientific-practical conference*. Book 1. Ekaterinburg, 238-254, (in Russian).
- VOROBJEVA, O.A., SAMOJLOVA, N.V. & SVESHNIKOVA, E.V. (1962): Gabbro-pyroxenite-dunite belt of Sredinniy Ural. Works of IGEN of the Academy of sciences of the USSR, 65, 319 p, (in Russian).
- VYSOTSKY, N.K. (1923): Platinum and areas of its mining, parts 2 and 3. Petrograd: Publishing house of the studies of the Academy Sciences, 345 p., (in Russian).
- VYSOTSKY, N.K. (1933): Platinum and areas of its mining. Leningrad Publishing house of the Academy of sciences of the USSR, part 5, 240 p, (in Russian).
- WEISER, T.W. (2002): Platinum-group minerals (PGM) in placer deposits. *In The Geology, Geochemistry, Mineralogy and Mineral Beneficiation of platinum-group elements*. L.J. Cabri (ed.). Can. Inst. Mining, Metall. & Petrol., Special Vol. **54**, 721-756.
- WEISER, T.W. & BACHMANN H.G. (1999): Platinum-group minerals from the Aikora River Area, Papua New Guinea. *Can. Mineral.* **37**, 1131-1145.

- WEISER, T. & SCHMIDT-THOMÉ M. (1993): Platinum-group minerals from the Santiago River, Esmeraldas province, Ecuador. *Can. Mineral.* **31**, 61-73.
- ZAJTSEV, V.P., KOLJADA, A.A. & MELKOMUKOV, V.N. (2001): Sejnav-Ga'lmoenan unit and its platinum content. *In*. Petrology and metallogeny of mafic-ultramafic complexes of Kamchatka. Moscow: Nauchn. Mir Press, 78-86, (in Russian).
- ZAVARITSKY, A.N. (1928): Bedrock deposits of platinum in the Urals. Materials on the general and applied geology, 108, 56 p., (in Russian).
- ZOLOEV, K.K., VOLCHENKO, J.A., KOROTEEV, V.A., MALAHOV, I.A., MARDIROSIAN, A.N. & HRYPOV, V.N. (2001): Platinum-metal mineralization in geological complexes of the Urals. Ekaterinburg, 198 p., (in Russian).

CHAPTER 7: DESCRIPTIVE ORE DEPOSIT MODELS: HYDROTHERMAL & SUPERGENE Pt & Pd DEPOSITS

Andy Wilde

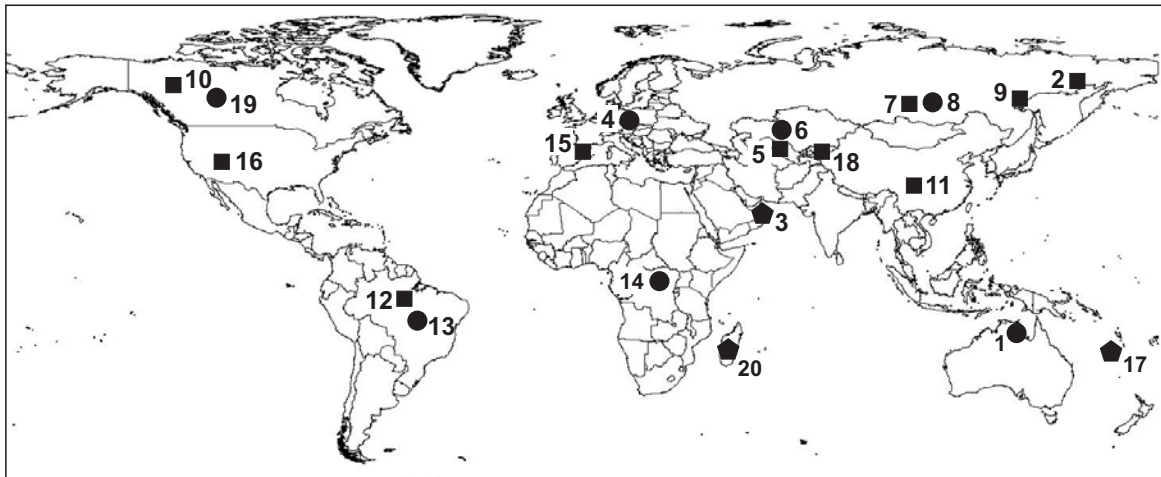
Co-Operative Research Centre in Predictive Mineral Discovery,
School of Geosciences, Monash University, Clayton, Victoria, Australia
E-mail: Andy.Wilde@sci.monash.edu.au

INTRODUCTION

Potentially economic grades and in some cases significant tonnages of Pt and Pd occur in a range of hydrothermal deposits without obvious direct or even indirect association with magmatism. A number of occurrences are also generated in the near-surface environment. In most cases Pt and Pd in these occurrences and deposits are by-products or potential by-products from the production of other metals, notably uranium, gold and base-metals (Fig. 7-1, Table 7-1). In this chapter I review some of these deposits and group them into three broad types: deposits of reduced passive margins, deposits of oxidized intra-cratonic basins and near-surface (supergene) deposits. The terms “reduced” and “oxidized” are used loosely to reflect the abundance

of carbon and sulfide *versus* hematite and sulfate minerals respectively within the sedimentary or metasedimentary host sequences. This reflects the fundamental importance of oxidation state and sulfur abundance in controlling Pt and Pd solubility (Wood 2002, Wilde *et al.* 2003, Hanley 2005).

The apparently disparate sediment-hosted orogenic Au deposits and the sediment-hosted Ni-Mo-Zn deposits are grouped together in the reduced passive margin category. In so doing, the role of the host-rock the sedimentary package is emphasized as a fundamental control on the ore-forming process. A common feature of the sequences that host these deposits is the abundance of carbon- and sulfur-rich rocks and the overall paucity of oxidized (hematite or sulfate-rich) lithologies. Irrespective of the



- Oxidized, terrestrial basin deposit
- Reduced, passive margin deposit
- ◆ Low temperature near-surface deposit

- | | |
|-------------------------------|---------------------------|
| 1 - Coronation Hill, Jabiluka | 11 - Nunitang Formation |
| 2 - Nataoka, Vetren, Pavlik | 12 - Serra Pelada |
| 3 - Liswaenites of Oman | 13 - "Jacutinga" deposits |
| 4 - Kupferschiefer | 14 - Zambian copperbelt |
| 5 - Muruntau, Amantaytau | 15 - Catalonia |
| 6 - Dzhokazgan | 16 - Boss |
| 7 - Sukhoi Log | 17 - New Caledonia |
| 8 - Udokan | 18 - Kumtor |
| 9 - Nezdansinskoye | 19 - Beaverlodge |
| 10 - Nick | 20 - Andriamina |

FIG. 7-1. Location of some hydrothermal ore deposits reported to be Pt and Pd enriched as discussed in the text.

TABLE 7-1: COMPARISON OF ELEMENT CONCENTRATIONS IN PGE-ENRICHED DEPOSITS HOSTED IN OXIDIZED INTRACRATONIC BASINS, REDUCED PASSIVE MARGINS AND NEAR-SURFACE DEPOSITS.

<i>Deposit Type</i>	<i>Deposit/Region</i>	<i>Rock type/comments</i>	<i>n</i>	<i>Pt</i>	<i>Pd</i>	<i>Au</i>
REDUCED PASSIVE MARGINS						
Orogenic Au	Sukhoi Log , Siberia	Altered carbonaceous and pyritic meta-siltstone	22	10	1.6	18056
Orogenic Au	Muruntau, Uzbekistan	Altered carbonaceous and pyritic metasiltstone (Au >10 ppb)	19	<10	<1	347
Orogenic Au	Natalka, Russia	Altered carbonaceous and pyritic meta-siltstone	20	4	4	18686
Sediment-hosted Ni-Mo	Guizhou, China	Ni-Mo-Zn Ore	8	190	240	170
Sediment-hosted Ni-Mo	Western Hunan, China	Ni-Mo-Zn Ore	1	0.3	0.33	2490
Sediment-hosted Ni-Mo	Jiangxi, China	Black shale	1	10	20	160
Sediment-hosted Ni-Mo	Nick, Canada	Representative mineralized samples	9	410	214	86
OXIDIZED INTRACRATONIC BASINS						
Sediment-hosted Cu	Kupferschiefer (Lubin-Glogow mine)	Copper Ore	25	8	7	48
Sediment-hosted Cu	Kupferschiefer (Lubin-Glogow mine)	Oxidized but copper-poor sandstones	56	145	74	460
Sediment-hosted Cu	Kupferschiefer	Thucholite	na	2-340	1-1000	1-3000
Sediment-hosted Cu	Udokan, Siberia	Copper Ore	na	30-2100	15-3250	16-3700
Sediment-hosted Cu	Katangan copper belt	Lithology not specified	56	10.29 ppm	3.72 ppm	4.68 ppm
Sediment-hosted Cu	Katangan copper belt	Lithology not specified	na	1.3 - 10.3 ppm		0.5 - 15 ppm
Unconformity-type U-Au-Pd	Jabiluka U-Au-Pd ore	Uranium ore (graphitic schist)	1	16	30.7 ppm	1163 ppm
Unconformity-type U-Au-Pd	Jabiluka U-Au-Pd ore	Uranium ore (graphitic schist)	27	na	290	2630
NEAR-SURFACE DEPOSITS						
Listwaenite	Semail Ophiolite, Oman	Carbonated serpentinite	20	446	24	5
Listwaenite	Semail Ophiolite, Oman	Silica-iron oxide rock	31	448	26	7

Comparison of element concentrations in PGE-enriched deposits in oxidized intracratonic basins, reduced passive margins and near-surface deposits as discussed in text. Units for Pt, Pd and Au are in ppb whereas the other elements are in ppm unless specified.

DESCRIPTIVE ORE DEPOSIT MODELS: HYDROTHERMAL & SUPERGENE PT & PD DEPOSITS

TABLE 7-1 (CONTINUED)

<i>As</i>	<i>Cu</i>	<i>Mo</i>	<i>Ni</i>	<i>Pb</i>	<i>U</i>	<i>V</i>	<i>Zn</i>	<i>Source/comments</i>
96	132	<3	63	18	<2	71	116	This study. Samples supplied by V.A. Buryak
319	31	36	40	3	<100	83	57	This study
13064	63	<3	31	30	<2	<100	91	This study
na	na	3.23%	3.55%	na	na	0.48%	na	Fan Delian 1983
na	na	18.28%	5.15%	na	na	0.63%	na	Fan Delian 1983
na	na	0.055%	0.01%	na	na	1.12%	na	Fan Delian 1983
3067	322	2400	5.40%	82	48.8	632	7,600	Hulbert <i>et al.</i> 1992
na	83000	na	na	na	na	na	na	Piestrzynski <i>et al.</i> 1999
na	8000	na	na	na	na	na	na	Piestrzynski <i>et al.</i> 1999
na	na	na	na	na	na	na	na	Kucha & Przybylowicz 1999
na	na	na	na	na	na	na	na	Makariev <i>et al.</i> 1999
na	na	na	na	na	na	na	na	Sources in Jedwab <i>et al.</i> 1999a. Analysis in 1905
na	na	na	na	na	na	na	na	Sources in Jedwab <i>et al.</i> 1999a. Analysis in 1906
100	3950	na	41	21100	291000	na	na	A. R. Wilde, unpub. data
na	na	na	na	na	24000	na	na	Pancontinental Mining unpub. data
4	18	na	2124	2	na	57	58	Wilde <i>et al.</i> 2002
12	14	na	1202	2	na	72	46	Wilde <i>et al.</i> 2002

processes that create permeability and drive hydrothermal fluid flow, the nature of these reduced host-rocks is likely to be reflected in the chemical composition of transient hydrothermal fluids. Conversely, unconformity-type U-Au and sediment-hosted Cu deposits occur in relatively oxidized host-rock sequences containing hematite and evaporite minerals such as halite and sulfate and relatively low volumes of reducing carbonaceous lithologies. In these environments hydrothermal fluids are likely to be more oxidized and chloride-rich. In near-surface or supergene deposits a key control is likely to be availability of highly oxidized groundwater and in this case the nature of the host sequence is less important.

DEPOSITS OF REDUCED PASSIVE MARGINS

Orogenic Au-Pt-Pd Deposits in Carbonaceous Metasedimentary Rocks

During the early 1990s, Russian researchers began to document high levels of Pt and Pd in many so-called “black-shale hosted” Au deposits (Table 7-2). By 1994, potentially economic levels of PGE (mainly Pt and Pd) had been reported at Natalka, Pavlik, Nezdansinskoye, and Vetrenskoe in the Russian Far East (Goncharov *et al.* 1995), Srednaya Padma in Karelia, Kvartsitovye Gorki, Kirli and Altynburiylkol in Kazakhstan, Kumtor in Kyrgyzstan, and Muruntau and Amantaytau in Uzbekistan among others (Ermolaev *et al.* 1992, Poluarshinov & Konstantinov 1994; Fig. 7-1). I include these deposits in the “orogenic gold deposit” classification as proposed by Groves *et al.* (1998) as confusion exists in the literature over the term “black shale” and Russian authors have used it to describe various metasedimentary rocks including carbonaceous slate, phyllite or schist. Pasava (1993) has included these deposits not only with sediment-hosted Ni-Mo-Zn but also sediment-hosted Cu in a “marine, metal-rich black shale”-hosted category. Gold-rich orogenic deposits, however, are differentiated from unconformity-type and sediment-hosted Cu deposits discussed below by location within a passive margin carbonaceous and sulfidic host-rock sequence, greenschist-facies metamorphosed and cleaved host rocks, characteristic chemical composition of the ore (usually low in Cu, Co, Ni, Mo, and Zn; see Table 7-1), association with quartz vein systems that post-date regional greenschist-facies metamorphic fabrics, and transgressive geometry. The ore is

crudely stratabound but not stratiform (Ermolaev *et al.* 1992). Thus, there is little in common between these orogenic Au-Pt-Pd deposits and the other deposits cited below.

The Sukhoi Log deposit in the Lena (or Bodaibo) goldfields (Fig. 7-2) is the deposit for which data on PGE grades and distribution are most readily available, and could be regarded as a type example of this deposit class (Distler & Yudovskaya 2005). The gold resource is believed to exceed 75 million oz at an average of 2.7 g.t^{-1} Au. According to Distler *et al.* (1996) Pt grades of about 1 g.t^{-1} are common and Pt values generally exceed Pd (see also Korobeinikov 1998). High-grade intersections of 1.45 g.t^{-1} Pt over 102.3 m and 2.42 g.t^{-1} over 40.5 m have been reported. According to Distler *et al.* (1996) Pt grades exceeding 1 g.t^{-1} extend beyond the gold ore body, but the highest grades (typically $3\text{--}5 \text{ g.t}^{-1}$) occur in the upper part of the gold ore body (Fig. 7-2). Pt is associated with elevated volumes of pyrite and traces of pyrrhotite, chalcopyrite, cubanite, gersdorffite and cobaltite among others. Inclusions of various Pt minerals have been found within pyrite and elevated PGE detected by electron microprobe in pentlandite and a range of other Fe, Ni and Co sulfides and sulfarsenides (Distler *et al.* 1996, 2004, 2005). PGE minerals identified using SEM include native platinum, Pt-Fe-Cu alloys, Pt-Fe alloys, sperrylite and cooperite (Distler *et al.* 2004). Fluid inclusion microthermometry suggests ore formation from hydrothermal fluids of 4–9.5 wt.% NaCl equivalent salinity and temperatures in the range 130 to 395°C (Distler *et al.* 2004).

The host-rocks to Sukhoi Log and similar deposits are clastic metasedimentary rocks with abundant carbonaceous matter and sulfide. Tectonic reconstructions of the host terranes suggest the metasedimentary rocks were deposited in passive margin environments, in some cases superimposed on early rift sediments (Yakubchuk 1998). At each deposit deformation has resulted in complex folding and faulting. At most of the deposits cited above, gold deposition can be related to emplacement of quartz veins that postdate major deformation (Eremin *et al.* 1994, Drew *et al.* 1996, Bortnikov *et al.* 1998, Wilde *et al.* 2001). This temporal relationship is, however, disputed at Sukhoi Log where much of the gold is believed to be related to early pyrite, rather than quartz veins (Buryak 1983, Buryak & Khmelevskaia 1997).

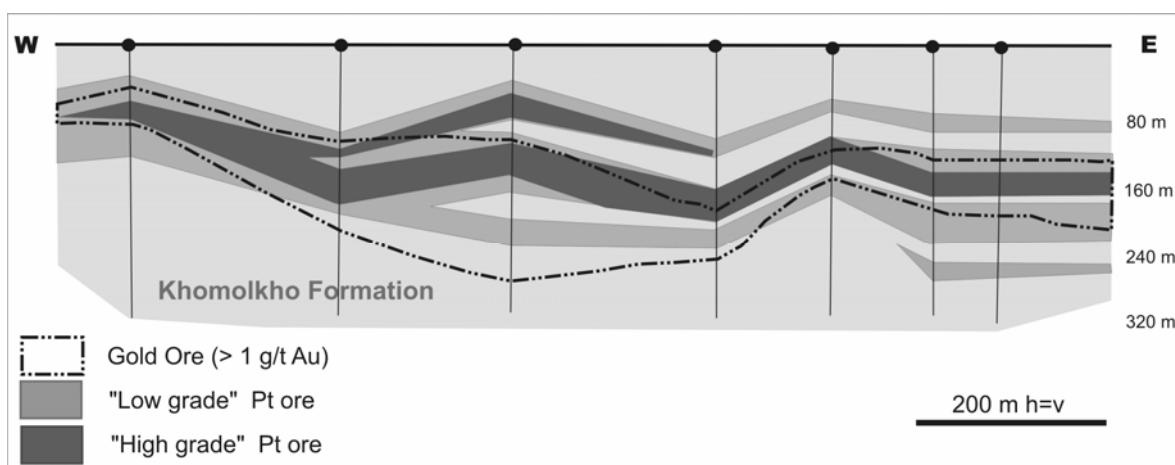


FIG. 7-2. Schematic long section of the Sukhoi Log deposit showing the spatial association of Au and Pt (Distler *et al.* 1996). Note that the source does not quote Pt grades.

Another deposit that shares some similarities with the “orogenic” deposits is Serra Pelada in Brazil. It is estimated that the resource prior to mining was 110 t of Au, 35 t of Pd and 18 t of Pt with a current resource of 3.7 Mt at 15 g.t⁻¹ Au, 4 g.t⁻¹ Pd and 1.9 g.t⁻¹ Pt (C. Grainger, in prep.). The deposit is hosted by carbonaceous greenschist-facies metasedimentary rocks, but intense weathering precludes a definitive statement as to its affinities. Grainger (in prep.) includes the deposit with the iron-oxide Cu-Au family.

In many of the papers dealing with Pt and Pd analyses in orogenic gold deposits there is little or no discussion of analytical techniques or quality control measures, such as details of standards, duplicates, blanks and so on. There is also at least one instance of a discrepancy between different analytical datasets (compare the data of Goncharov *et al.* 1995, and Korobeinekov 1998, for Nezdanskoye; Table 7-2), possibly indicating that the analytical values are in error. Wilde & Bierlein (2003) and Wilde (unpub. data) have obtained analyses of samples from Kumtor, Nataalka, Sukhoi Log and Muruntau using NiS fire assay collection and INAA or ICP-MS finish (Table 7-2). They provide little support for the presence of economic or even sub-economic PGE, except at Muruntau where maxima of 100 ppb Pt and 132 ppb Pd were found (Table 7-2). However, the number of samples is small in comparison to Russian studies.

Furthermore, in many of the cited orogenic deposits, high analytical values of Pt and Pd have yet to be supported by identification of Pt and Pd

minerals, perhaps reflecting very fine grain size and/or location in carbonaceous material. The Boss mine in Nevada (USA), for example, contains bitumen shown to contain elevated Au, Pt and Pd, in some cases as very fine crystals of potarite detectable only using TEM-EDAX (Jedwab *et al.* 1999b). Conversely, there is no correlation between bulk-rock Pt and organic carbon at Sukhoi Log (Distler *et al.* 1996, 2004, 2005).

Absence of platinoids in associated placer gold deposits could also be used to argue that there is little PGE enrichment in the source deposit. The Sukhoi Log placers have yielded more than a million ounces of Au, and although traces of cooperite have been recorded, Pt and Pd are generally conspicuous by their absence (Buryak 1983, Buryak & Khmelevskaia 1997). PGE may, however, have been dissolved in oxygenated groundwater and carried a considerable distance from source in solution (Wilde *et al.* 2003). Low-grade Pt deposits in contemporary drainages north of Sukhoi Log contain rounded grains of PGM chemically distinct from ultramafic-sourced PGM, and for which no known ultramafic source rocks are known (Wilde *et al.* 2003).

Sediment-Hosted Ni-Mo-Zn Deposits

Sediment-hosted Ni-Mo-Zn deposits are thin (< 10 cm) but apparently very extensive stratiform sulfide occurrences that contain high levels of Pt and Pd (Table 7-1). Stratiform sulfide is hosted in unmetamorphosed or weakly metamorphosed carbonaceous fine-grained sedimentary rocks

TABLE 7-2: ANALYSES OF SULFIDE CONCENTRATES AND ROCKS FROM OROGENIC AU DEPOSITS IN CARBONACEOUS METASEDIMENTARY ROCKS FROM RUSSIA AND OTHER COUNTRIES OF THE FORMER SOVIET UNION.

<i>Deposit</i>	<i>Location</i>	<i>Rock Type</i>	<i>Average/R ange</i>	<i>n</i>	<i>Pt (ppb)</i>	<i>Pd (ppb)</i>
SUKHOI LOG	Not specified	Siltstone with disseminated pyrite	Average	15	5	6
	Various drillholes	Disseminated sulfide separates	Average	829	857	227
	Not specified	Flotation sulfide conc.	Average	2	2200	na
	Not specified	Gravity sulfide conc.	Average	2	25000	na
	Supra-ore zone	Not specified	Average	12	400	20
	Ore zone	Not specified	Average	15	300	60
	Infra-ore	Not specified	Average	9	890	20
	Not specified	Sulfide concentrate	Average	11	960	340
	Not specified	Carbonaceous phyllite	Range	7	<2 - 35	<2 - 10
NATALKA	Not specified	Host-rock	Average	5	n.d	200
	Not specified	Altered host-rock	Average	20	1700	300
	Not specified	Ore	Average	32	500	600
	Not specified	Carbonaceous phyllite	Range	20	<5 - 7	<2 - 14
NEZDANINSKOYE	Ore Zone 1	Not specified	Average	2	n.d	1300
	Ore Zone 8	Not specified	Average	7	800	440
	Not specified	Quartz sulfide veins	Average	10	5290	5.7
	Not specified	Arsenopyrite separate	Average	3	5230	23.7
	Not specified	Pyrite separate from "disseminated ore"	Average	4	2860	9.3
	Not specified	Pyritic carbonaceous siltstone	Average	20	6150	7.3
MURUNTAU	Not specified	High grade gold ore	Average	na	4560	7440
	Not specified	Low grade gold ore	Average	na	1340	5700
	Not specified	Carbonaceous "shale" (Besopan Formation)	Average	10	610	300
	Not specified	Auriferous "metasomatic rocks"	Average	15	3490	5130
	Not specified	Graphitic tectonites in ore zones	Average	4	13610	8740
	High grade ore dumps	Mineralized carbonaceous meta-pelites and "metasomatites" (Au > 10 ppb)	Range	20	<0.5 - 100	<0.5 - 132
	Beyond mine area	Unmineralized carbonaceous meta-pelites (Au < 10 ppb)	Range	11	<10 - 17	<1 - 2
KUMTOR	Not specified	"Sub-stratiform"	Average	5	1060	2460
	Not specified	"Stockwork"	Average	7	1210	3010
	Not specified	Carbonaceous phyllite	Range	13	<2 - 15	<2 - 30

n = no. of samples

DESCRIPTIVE ORE DEPOSIT MODELS: HYDROTHERMAL & SUPERGENE PT & PD DEPOSITS

TABLE 7-2 (CONTINUED)

<i>Au (ppm)</i>	<i>Ag (ppm)</i>	<i>Source</i>	<i>Analytical Methods</i>
na	na	Korobeinekov 1998	Inversion voltammetric and other [unspecified] techniques
na	na	Korobeinekov 1998	Inversion voltammetric and other [unspecified] techniques
na	na	Korobeinekov 1998	Inversion voltammetric and other [unspecified] techniques
na	na	Korobeinekov 1998	Inversion voltammetric and other [unspecified] techniques
3.74	2.29	Distler <i>et al.</i> 2004	Unspecified "chemical analysis". Some samples analyzed by ICP-MS.
3.02	3.28	Distler <i>et al.</i> 2004	Unspecified "chemical analysis". Some samples analyzed by ICP-MS.
0.11	1.22	Distler <i>et al.</i> 2004	Unspecified "chemical analysis". Some samples analyzed by ICP-MS.
12.22	10.75	Distler <i>et al.</i> 2004	Unspecified "chemical analysis". Some samples analyzed by ICP-MS.
0.050 - 141	<1.0	Wilde & Bierlein 2003	NiS fire assay & ICP-MS finish. GENALYSIS laboratories
0.02	na	Goncharov <i>et al.</i> 1995	Various analytical methods with spiked standards used for calibration
0.80	na	Goncharov <i>et al.</i> 1995	Various analytical methods with spiked standards used for calibration
2.40	na	Goncharov <i>et al.</i> 1995	Various analytical methods with spiked standards used for calibration
<0.5 - 8.8	<1 - 60	Wilde & Bierlein 2003	NiS fire assay & ICP-MS finish. GENALYSIS laboratories. Samples supplied by Placer.
16.10	na	Goncharov <i>et al.</i> 1995	Various analytical methods with spiked standards used for calibration
12.30	na	Goncharov <i>et al.</i> 1995	Various analytical methods with spiked standards used for calibration
na	na	Korobeinekov 1998	Inversion voltammetric and other [unspecified] techniques
na	na	Korobeinekov 1998	Inversion voltammetric and other [unspecified] techniques
na	na	Korobeinekov 1998	Inversion voltammetric and other [unspecified] techniques
na	na	Korobeinekov 1998	Inversion voltammetric and other [unspecified] techniques
> 1.5	na	Ermolaev <i>et al.</i> 1992	Analytical methods & quality control measures not specified
1.5 - 1.0	na	Ermolaev <i>et al.</i> 1992	Analytical methods & quality control measures not specified
na	na	Ermolaev 1995	Analytical methods & quality control measures not specified
na	na	Ermolaev 1995	Analytical methods & quality control measures not specified
na	na	Ermolaev 1995	Analytical methods & quality control measures not specified
16 - 991 ppb	<0.2 - 6.4	A. R. Wilde., unpub. data	Fire-assay and ICP finish, ANALABS & CONE GEOCHEMICAL
<1 - 2 ppb	<0.2 - 36	A. R. Wilde., unpub. data	Fire-assay and ICP finish, ANALABS & CONE GEOCHEMICAL
4.26	na	Ermolaev 1995	Analytical methods & quality control measures not specified
7.14	na	Ermolaev 1995	Analytical methods & quality control measures not specified
16 - 79689 ppb	<1 - 22.6	Wilde & Bierlein 2003	NiS fire assay & ICP-MS finish. GENALYSIS laboratories. Samples supplied by Kevin Ansdell.

(Hulbert *et al.* 1992). Two main areas of occurrence are currently recognized, the Selwyn Basin of Canada and the Cambrian Nunitang Formation of southern China (Fig. 7-3). Other possible occurrences of this type are the Pd and Pt-rich “sedex” sulfide deposits of Catalonia, Spain (Canet *et al.* 2003).

The Nick deposit is hosted by Lower to Middle Devonian passive margin rocks of the Selwyn Basin close to a transition to deeper basin environments (Hulbert *et al.* 1992). This time interval incorporates major Pb-Zn deposits elsewhere in the basin. The deposit is a thin (2–7 cm) rhythmically laminated massive sulfide layer (or “vaesite horizon”) extending over 80 km² (Hulbert *et al.* 1992). While the very thinness of the sulfide layers would probably preclude an economic deposit, economic levels of Pt and Pd may be present beyond the massive sulfide layers. Sulfides include vaesite, pyrite and minor sphalerite associated with bitumen, phosphatic chert and amorphous silica. The mineralized sulfide layer occurs near the contact between siliceous shale, mudstone, phosphatic chert, and spheroidal limestone (Lower Earn Group) and older calcareous dark gray to black “fetid” meta-pelitic rocks (Road

River Group). The rocks exhibit lower greenschist-facies metamorphism and, locally, isoclinal folding. The Road River “shale” exhibits a penetrative cleavage (Hulbert *et al.* 1992). Bitumen also occurs as veins in the Road River Group which are regarded as important fluid conduits by Hulbert *et al.* (1992). Lack of hydrothermal quartz in the Nick deposit has precluded fluid inclusion study.

The Nunitang Formation contains numerous stratiform, low-grade Ni, Mo and Zn “polymetal” sulfide deposits hosted in extensive sulfide-rich carbonaceous black shale (Lott *et al.* 1999). The shale is between 10 and 100 m thick and contains 5 to 10% total organic (algal) carbon, in places grading into “stone coals” (combustible black shale). The host sequence is rich in phosphate and was deposited in a relatively high energy, shallow-water environment (Lott *et al.* 1999). Stratiform Ni-Mo-Zn ores are typically thin (<30 cm) layers of Fe, Mo, and Ni sulfides, “stone coals”, phosphorite and chert. Some occurrences have nodules and clasts of sulfide whereas others are thinly laminated. Ore minerals include jordisite (amorphous MoS₂ and carbon), pyrite, bravoite, vaesite, gersdorffite, polydymite, and millerite. Zhang *et al.* (2005) have detected no discrete PGM but report high Pt

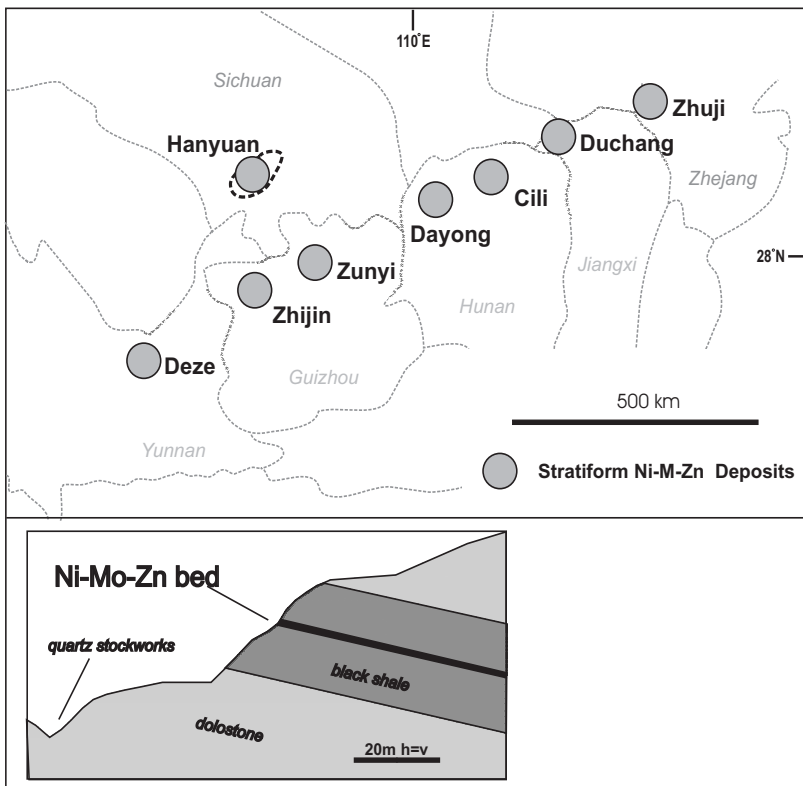


FIG. 7-3. Map showing distribution of Ni deposits in the Nunitang Formation of China. The inset shows a schematic section of one of these deposits (from Lott *et al.* 1999).

concentrations in vaesite, high Pd concentrations in a poorly characterized MoSC phase, and also found evidence for the occurrence of nanometre-scale particles of native Pt. Quartz veins within and underlying the deposits are regarded as hydrothermal conduits (Lott *et al.* 1999). Fluid inclusions in this quartz have a large range of salinity (0.1–22 wt.% NaCl equiv.) and homogenize at between 65 and 190°C.

DEPOSITS OF OXIDIZED INTRACRATONIC BASINS

Unconformity Type U-Au-Pt-Pd Deposits

Potential by-product Pt and Pd occur at the Coronation Hill unconformity Au-U deposit (Northern Territory, Australia; Fig. 7-4). The currently defined resource contains 4.85 Mt at 4.85 g.t⁻¹ Au, 0.19 g.t⁻¹ Pt, and 0.65 g.t⁻¹ Pd (Carville *et al.* 1990) but the deposit was mined originally for uranium and yielded 26,000 tonnes of ore at 2.6 k g.t⁻¹ U₃O₈ and 10.4 g.t⁻¹ Au. Anecdote has it that the recognition of PGE at Coronation Hill was due to the diligence of a chemist who noted an unusual discoloration of analytical solutions that were to be analyzed only for gold, and which he attributed to the presence of PGE. At the nearby Jabiluka deposit (Fig. 7-4) significant, but sub-economic amounts of Pd are associated with gold-rich zones (Wilde 1988). The possibility of more widespread Pd and

Pt at Jabiluka remains untested because only the relatively restricted gold-rich zones were routinely analyzed for Pd (but not Pt). Both deposits are spatially and genetically associated with the unconformity between a thin (<2 km), Middle Proterozoic, coarse clastic rift-fill sequence (Ojakangas 1986) and Lower Proterozoic greenschist to amphibolite-facies metamorphic basement rocks, locally rich in carbon and sulfide. The rift-fill is represented by the Kombolgie Formation which is dominated by coarse sandstone, commonly with hematite preserved as rims to detrital quartz grains (Wilde 1988).

Economic precious metals at Coronation Hill are controlled by near-vertical faults and the distribution of Pt and Pd is closely related to that of gold (Carville *et al.* 1990). Uranium tends to be most abundant in carbonaceous lithologies whereas Au and platinum group elements (PGE) are generally associated with feldspathic lithologies such as feldspar porphyry (Mernagh *et al.* 1994; Fig. 7-4). Pt and Pd occur as a variety of minerals, including stibiopalladinite (Pd₅Sb₂), sudburyite (PdSb), native Pd, PdSbSe, palladseite (Pd₁₇Se₁₅), porpezite (Au-Pd), (Pt,Pd)Se₂, Pt-Pd-Fe alloys, and rare native Pt (Bloom *et al.* 1992, Carville *et al.* 1990).

The Jabiluka 2 uranium deposit is hosted by Lower Proterozoic carbonaceous pelitic schist of

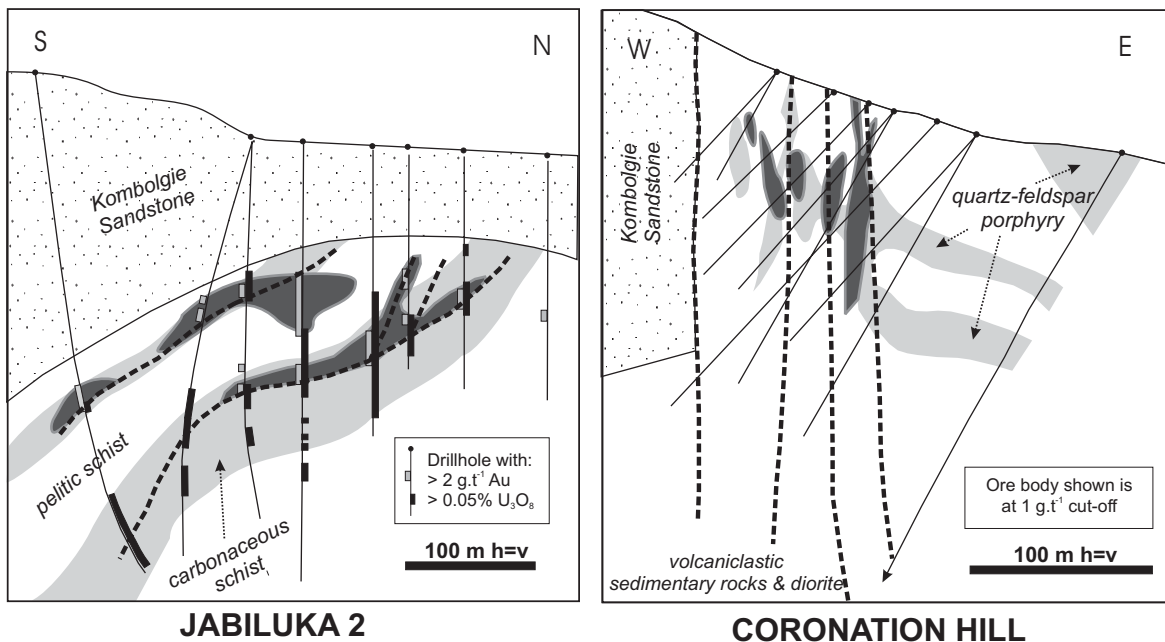


FIG. 7-4. Sections through the Jabiluka and Coronation Hill unconformity-type U-Au-PGE deposits (Wilde 1988, Carville *et al.* 1990).

the Cahill Formation, immediately beneath the unconformity with the Kombolgie Formation (Fig. 7-3). Reverse fault breccias and related foliation-parallel veining appear to have been crucial in generating permeability for hydrothermal fluids (Johnston 1984). Jabiluka differs from Coronation Hill in that high Pd concentrations (typically 0.1–1 g.t⁻¹ in gold-rich zones) are spatially coincident with high Au (up to 500 g.t⁻¹) and U grades within brecciated carbonaceous schist (Johnston 1984). Pd occurs in palladian gold (porpezite) but no discrete Pd-bearing minerals have been found (D. Gilbert, unpub. data).

Fluid inclusion studies of the Jabiluka and Coronation Hill deposits show that ore deposition was from hypersaline brines at temperatures in excess of 100°C (Wilde *et al.* 1989b, Mernagh *et al.* 1994). The alteration assemblages (with abundant hematite and low sulfide) are evidence that the brine was oxidized.

PGE enrichment was noted during the 1950's in similar deposits from the Beaverlodge deposits of Saskatchewan in Canada (Sibbald 1988) and PGE have been recovered from the Shinkolobwe deposit, in Central Africa, a deposit better known for its U and Ra yield. This deposit has some characteristics of the unconformity type but also of the sediment-hosted copper type (Jedwab *et al.* 1999a) discussed in the next section. Here, Pd, Pt and Re were extracted from “slurries” containing Pd as merenskyite (Jedwab *et al.* 1999a).

Sediment-Hosted Cu Deposits

Stratiform sandstone-hosted Cu deposits share some characteristics with unconformity-type deposits which include occurrence in an intracratonic rift environment and dominance of “oxidized” (*i.e.*, hematite and sulfate-rich) sedimentary rocks in the rift fill. High levels of Pt and Pd have been documented in the Kupferschiefer deposits of Poland (Kucha & Przybyłowicz 1999, Piestrynski & Sawłowicz 1999, Piestrynski *et al.* 2002), the Udokan and Igarka deposits of Siberia, and the Dzhezkazgan deposits of Kazakhstan (Makariev *et al.* 1999) as well as in the Central African (Zambian) copper belt (Jedwab *et al.* 1999a).

The Triassic Kupferschiefer Cu and associated Au-Pt-Pd deposits occur within a dominantly terrestrial, red bed sequence of evaporitic sedimentary rocks and bimodal volcanic rocks that unconformably overlie grey-colored

(reduced?) deformed Carboniferous clastic and Proterozoic metamorphic rocks (*e.g.*, Piestrynski & Sawłowicz 1999, Kucha & Przybyłowicz 1999, Piestrynski *et al.* 2002). Economic Cu is spatially related to carbonaceous shale, the Kupferschiefer (“copper shale”), although only 20% of Cu is actually hosted by it. Copper ore is not, however, generally enriched in Au, Pt, and Pd (Piestrynski and Sawłowicz 1999; Table 7-1). Extensive, and potentially economic Au, Pt, and Pd grades occur *below* economic Cu mineralization in the Polkowice-Sieroszowice mine (Piestrynski *et al.* 2002; Fig. 7-5) in the Zechstein sandstone and lowermost Kupferschiefer, both relatively poor in organic carbon (see Piestrynski *et al.* 2002). Average grades are 2.25 g.t⁻¹ Au, 0.14 g.t⁻¹ Pt, and 0.08 g.t⁻¹ Pd. Pt and Pd have been found as inclusions in gold and in bornite (Piestrynski *et al.* 2002).

Kucha & Przybyłowicz (1999) described another type of precious metal occurrence, apparently of limited spatial extent, associated with unusually carbon-rich rocks. The carbon is thucholite, a bitumen modified by radiation damage. Elevated concentrations of Pt and Pd (Table 7-1) are restricted to a few centimetres vertical thickness at the interface between red sandstone and carbonaceous shale. Minerals include Pd arsenides, PdBi (sobolevskite), Pd metal, and Pd arsenates.

Tonn *et al.* (1987) report hypersaline (> 23.3 wt.% NaCl equiv.) fluid inclusions in carbonate cement in sandstone from the Kupferschiefer deposits. A role for brines in the formation of the Kupferschiefer deposits is supported by the presence of syn-ore Cl-bearing illite (Michalik 1997).

The massive Udokan copper deposit of Russia occurs within a 10 km-thick lower Proterozoic metasedimentary basin (Kodar-Udokan basin) overlying Archean metamorphic basement rocks of the Siberian craton (Makariev *et al.* 1999). Stratabound copper occurs at five stratigraphic levels of varying thickness. The host rocks are basal cupriferous black shale, intermediate varicolored cupriferous sandstone and shallow-water and deltaic facies at the top. Pd grade is typically higher than that of gold and tends to be highest in the zones of bornite-chalcocite ore, higher up the stratigraphic section. High Pd grades, however, do not always coincide with Cu ore. Pt grades are highest in the 60 m-thick basal black shale. Within the black shale, Makariev *et al.* (1999) described several thin

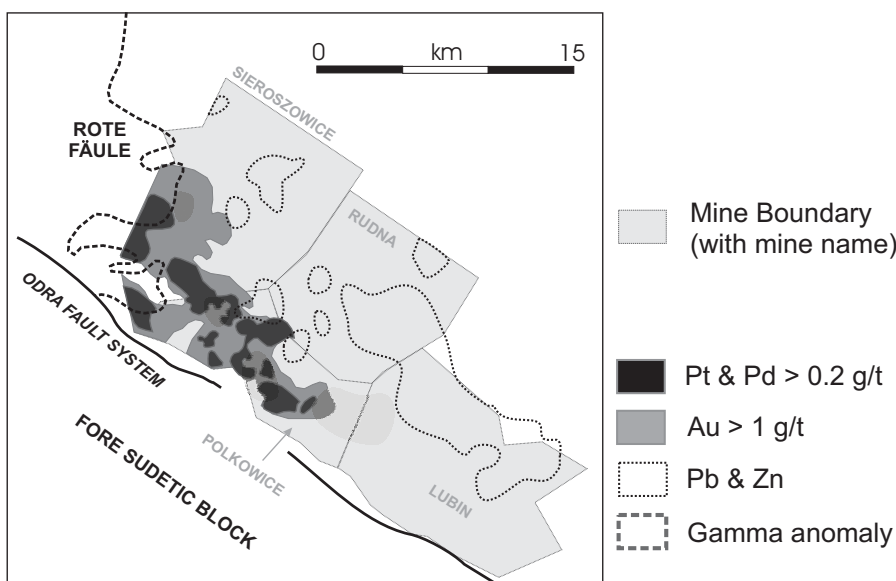


FIG. 7-5. Plan showing metal zonation in the Kupferschiefer mines of Poland (Kucha & Przybyłowicz 1999, Piestrzynski *et al.* 2002).

layers (1–3.5 m) where Pt and Pd grades exceed 1 g.t⁻¹. In addition to Pt, Pd, Au, and Ag, the black shale hosts elevated concentrations of V, Cu, Cr, Mo, Co, Ni, and Zn.

The platiniferous Dzhezkazgan deposit is hosted by Carboniferous terrestrial clastic sedimentary rocks. These are grey in the vicinity of Cu mineralization but red beyond (Gablina 1981). At the base of the terrestrial sequence is a grey “transitional” unit, containing abundant carbon and sulfide. This unit, however, hosts little Cu-PGE mineralization.

Jacutinga Au-Pd Deposits

Another type of hydrothermal Au-Pd deposit is hosted by “jacutinga” (altered iron formation) in the Proterozoic Minas Supergroup of SE Brazil (Fig. 7-1). I tentatively include this deposit type in the oxidized basin category because of the abundance of iron oxides in the host sequence and because of the inferred presence of B-rich evaporites low in the sequence (Olivo *et al.* 2001). The presence of Pd-rich gold has been known for centuries, with gold miners referring to it as black gold or “ouro preto” (*e.g.* Jebwab & Cassedanne 1998). Examples include the Cauê and Conceição mines which collectively produced 8 tonnes of gold, with the bullion grading at 6.3% and 2.8% Pd respectively (Leão de Sá & Borges 1991).

Jacutinga is a curiously speckled altered iron formation consisting of hematite, magnetite, quartz, talc, phlogopite/muscovite with minor tourmaline, phosphates and Au-Pd minerals. The latter include

palladian gold (porpezite?), arsenopalladinite (Pd₈As_{2.5}Sb_{0.5}), mertieite II (Pd₈(Sb,As)₃) palladseite (Pd₁₇Se₁₅) and various weathering products. The ore bodies consist of hematite and quartz veins oriented parallel to S₁ and S₂ foliations. Olivo *et al.* (2001) attributed the deposits to the flow of hot hydrothermal fluids (~600°C) along thrust faults juxtaposing iron formation and Archean basement rocks.

NEAR-SURFACE (SUPERGENE) DEPOSITS Listwaenite-hosted

Pt enrichment of up to 450 ppb has been found in numerous samples of hydrothermally altered harzburgite of the Semail Ophiolite of Oman associated with silicified and carbonate-altered serpentinite referred to locally as “listwaenite” (Wilde *et al.* 2002). Carbonate and silica alteration occurred along faults that developed during extension and after obduction of the Semail Ophiolite, a period of regional high heat flow reflected in intrusion of basanite and basaltic magma of continental affinity. Both alteration types are somewhat enriched in Pt. Likely hydrothermal fluids include meteoric, seawater and bittern, due to periodic emergence of the Tertiary landmass from an environment of mangrove swamp and saline coastal flats. There are few data on the temperature of Pt deposition and the composition of fluids involved, although we can surmise from the geological setting that temperatures were less than 100°C. Possible source rocks include chromite pods and sulfidic gabbro (Wilde *et al.* 2002). Parts per

million levels of Pt have also been recorded in a sample of “white serpentinite” from the Semail Ophiolite (LeBlanc *et al.* 1991) but it is not clear whether this enrichment is also a product of Tertiary hydrothermal activity. The initial oxidation state of the hydrothermal fluid (probably buffered by the atmosphere) appears to have been a crucial constraint on the Pt content of hydrothermal waters within the Semail Ophiolite (Wilde *et al.* 2002).

Lateritic Deposits

Several recent studies demonstrate that lateritization can lead to solution, transport, and concentration of Pt and Pd (Augé & Legendre 1994, Augé *et al.* 1995, Salpeteur *et al.* 1995). Up to 2 ppm (but typically 400 ppb) Pt occurs in lateritized ophiolitic pyroxenite from the Pirogues River area of New Caledonia and this enrichment has been attributed to the lateritization process (Augé & Legendre 1994, Augé *et al.* 1995; Fig. 7-6). There is no obvious source of magmatically concentrated Pt and Pd in the fresh ultramafic rocks. Chromite-rich layers elsewhere in the region contain between 2 and 10 ppm Pt as Pt-Fe alloys, but these rocks are not significantly depleted by lateritization (Augé & Legendre 1994, Augé *et al.* 1995).

Another study of Pt mobility in lateritic environment used the magmatic (granitoid-associated) deposit at Andriamena in Madagascar (Salpeteur *et al.* 1995). A variety of primary, magmatic, PGE minerals were observed including arsenides, sulfides and stibiopalladinite but only sperrylite appears to have been resistant enough to occur in the weathered zone with newly-formed Pt₃Fe and there is almost complete removal of Pd. This clear evidence of PGE mobility led Salpeteur *et al.* (1995) to ponder why the possibility of economic PGE enrichment in this environment has been neglected.

DISCUSSION

Unconventional PGE deposits in intracratonic rift settings (unconformity-type, sediment-hosted copper and perhaps Jacutinga-type deposits) are associated with gold, copper or uranium. PGE mobility is a reflection of the relative paucity of “reductant” minerals such as sulfides and carbonaceous matter within the overall stratigraphic package, and abundance of “oxidizing” minerals such as hematite and anhydrite. Initial equilibration of the ore-forming fluids with atmospheric oxygen may also be a factor (Jaireth 1988, Wilde

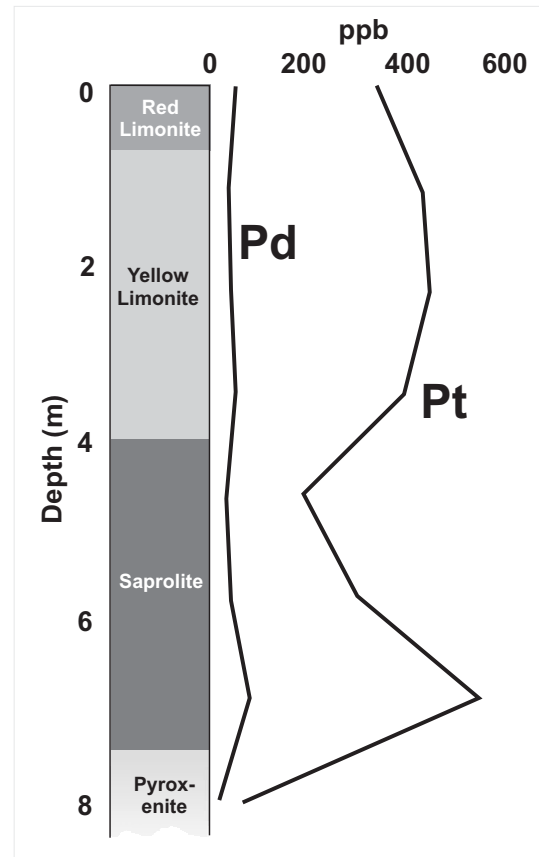


FIG. 7-6. Pt enrichment in a drill hole sample of lateritized pyroxenite from the Pirogues River area of New Caledonia (Augé *et al.* 1995).

1988, Wilde *et al.* 1989a,b). Chloride enrichment is attributed to dissolution of halite layers at depth (*e.g.*, Bechtel *et al.* 2000) or by surface evaporation (bittern brines). The hydrothermal fluids that form in these environments therefore include oxidized brines that can persist to some depth by virtue of the lack of reductant minerals (excluding those at the site of deposition) and can scavenge metals as chloride complexes.

The source of PGE (and indeed other metals) in this setting remains uncertain. Perhaps an unusually enriched source of PGE is required, but there is currently little evidence that this is the case. It could be argued that, because large volumes of fluid have moved through the ore system, even minor amounts of dissolved PGE could generate an ore deposit if extraction was reasonably efficient. This contention merits further research.

Spatial separation of Au-Pt-Pd from U at the Coronation Hill deposit, together with numerical

modeling, suggests that pH change due to reaction of brine with feldspar-rich host-rocks was a key depositional process (Mernagh *et al.* 1994). The lesson is that exploration need not be restricted to carbonaceous lithologies. At Jabiluka, however, the spatial coincidence of U, Au, and Pd suggests that reduction and hence presence of graphite, was the key depositional control (Wilde 1988, Wilde *et al.* 1989a,b). Proposed depositional mechanisms for sediment-hosted Cu deposits also include reduction by carbonaceous sediments (as in the case of the Kupferschiefer, *e.g.*, Jowett *et al.* 1987, Bechtel *et al.* 2000) and/or fluid mixing (as at Dzhezkazgan; Gablina 1981 and references therein). At Dzhezkazgan, oxidized brine in the host red-beds is thought to have mixed with relatively reduced hydrocarbon-rich fluids derived from Visean limestone (Poplavko *et al.* 1977). Indeed, Cu ore occurs in a structural trap that would have been favorable for hydrocarbon accumulation.

In contrast to intracratonic basins, the sedimentary fill of passive margins tends to be enriched in carbon and sulfide. The contained metal deposits (namely sediment-hosted Ni-Mo-Zn and later orogenic gold) reflect this fundamental control on oxygen fugacity of hydrothermal fluids. Relatively low chlorinity is another fundamental aspect of the fluids in orogenic Au deposits, and this presumably reflects absence of substantial halite bodies and the lack of evaporitic environments contemporaneous with ore deposition. The presence of abundant reduced sulfur would permit transport of Au, Pt, and Pd as bisulfide complexes. At the Muruntau Au deposit, thermochemical reduction of sulfate in anhydrite may have contributed sulfur to the hydrothermal fluids (Wilde *et al.* 2001). This scenario requires that an oxidized rift basin occurs adjacent to the deposits and that basinal fluids could be focused laterally. However, this may not be the case for many of the deposits cited above where sulfur was probably derived from the sulfidic passive margin sediments themselves. For example, proposed source rocks for the Nick deposit are pyritic and “fetid” (*i.e.*, contain H₂S gas; Hulbert *et al.* 1992).

As in intracratonic basins, the source of metals in passive margin-hosted environments remains uncertain. Ultramafic rocks are uncommon in these passive margin terranes. Some authors have argued that preservation of organic material favors syn-sedimentary concentration of metals including gold (Buryak 1983, Ermolaev *et al.* 1992, Buryak & Khmelevskaia 1997).

Two different depositional mechanisms have been proposed for sediment-hosted Ni-Mo-Zn deposits. Hulbert *et al.* (1992) speculated that ore deposition was the result of discharge of hot (and presumably reduced and sulfur-rich) basinal brines along faults into “stagnant, ooze-like, carbonaceous bottom sediments”. Lott *et al.* (1999) also envisaged formation close to the sediment-water interface at the site of “submarine hydrothermal vents in shallow water (<250 m depth)”. Boiling is interpreted as having been responsible for high fluid salinities observed in fluid inclusions.

Orogenic Au-Pt deposits evidently formed at substantial depths within the crust. Given that Au and Pt were probably carried as bisulfide complexes, cooling, dilution, pH change, and oxidation are all possible depositional processes. Exsolution of CO₂ and other gases such as H₂S as a consequence of pressure decrease during faulting is often cited as a key mechanism for gold deposition in these deposits. Such exsolution causes a drop in aqueous S content and change in pH, destabilizing gold bisulfide complexes. At Kumtor, however, there is evidence of an oxidized fluid (in equilibrium with hematite and barite) that generated carbonate by oxidation of host-rock carbon (Ivanov & Ansdell 1998). Thus, fluid mixing (oxidation) may be a key process at Kumtor.

Leaching of Pt and Pd in the near-surface environment could be extremely efficient where groundwater has an oxygen fugacity close to atmospheric and is either acidic and chloride-rich (*e.g.*, in evaporitic settings) or alkaline (pH > 10). Numerical modeling of flushing oxidized hyperalkaline groundwater through serpentinite at 35°C shows that Pt is efficiently scavenged provided that sufficient groundwater passes through the rock to convert magnetite (generated during serpentinitization) to hematite (Wilde *et al.* 2002). This modeling also shows that the PGE-enriched rocks, such as chromitite, may not be the best sources as their content of reductant minerals tends to be higher (Wilde *et al.* 2002).

Concentration of PGE in near-surface environments could occur by a number of processes. For example, a change in oxidation state at the water table may be a cause of PGE enrichment in laterite. Reduction has also been implicated to explain Pt enrichments in altered ophiolites from Oman (Wilde *et al.* 2002). Salpeteur *et al.* (1995) have suggested that PGE enrichment in laterite (and lateritic Ni deposits) needs to be further investigated.

CONCLUSIONS

This review of amagmatic Pt and Pd occurrences and deposits shows that enrichment to economic levels appears to be rather common in several deposit types. In these deposit types Pt and Pd are typically associated with economic Au, U or base-metals, and there is also evidence of local Pt enrichment as a result of near-surface modification of ophiolitic ultramafic rocks. The ability of basin-filling sedimentary rocks to control the oxidation state of any transient ore-forming solution and to supply chloride and sulfur is thought to exert a major influence on the type of deposit that forms at depth within the basin. The role, if any, for specific Pt- and Pd-enriched source rocks remains uncertain and future research should address this issue. Exploration geologists should be mindful of the possibility of by-product PGE enrichment and design their programs accordingly.

The tantalizing possibility of the common existence of economic stand-alone deposits of Pt and/or Pd, perhaps with minor or no enrichments in Au, Cu, Ni, or Mo, requires further research. Lack of suitable exploration models and unwillingness to analyze routinely for PGE, plus the possible chemical dispersion of Pt and Pd in the near-surface environment, may have conspired to hinder the discovery of mineable, unconventional, stand-alone Pt and Pd deposits. Future research needs to address the solubility of PGE with respect to that of Au, Cu, U, and other metals in the hydrothermal environment, the composition of hydrothermal solutions (requiring sophisticated analysis of fluid inclusions), fluid flow paths (3D geometry), fluid fluxes and duration, and evolution of porosity and permeability.

REFERENCES

- AUGÉ T. & LEGENDRE, O. (1994): Platinum-group element oxides from the Pirogues ophiolitic mineralization, New Caledonia: origin and significance. *Econ. Geol.* **89**, 1454-1468.
- AUGÉ T., MAURIZOT P., BRETON, J., EBERLE, J-M, GILLES C., JEZEQUEL, P., MEZIERE, J. & ROBERT, M. (1995): Magmatic and Supergene Platinum-group Minerals in the New Caledonia Ophiolite. *Chronique de la Recherches Minière* **63**, 3 – 26.
- BECHTEL A., SHIEH Y-N., ELLIOT W.C., OSZCZEPALSKI S. & HOERNES, S. (2000): Mineralogy, crystallinity and stable isotopic composition of illitic clays within the Polish Zechstein basin: Implications for the genesis of the Kupferschiefer mineralization. *Chem. Geol.* **163**, 189-205.
- BLOOM M.S., GILBERT D.J., GAMMONS C.H., WILDE A.R. (1992): Reaction Path Models for Hydrothermal Au-PGE Mineralization at Coronation Hill and similar deposits of the South Alligator mineral field, Australia. In Proceedings 7th International Symposium on Water-Rock Interaction, Kharaka Y.K., Maest A.S., (eds.). International Association of Geochemistry & Cosmochemistry **2**, p. 1569 – 1573.
- BORTNIKOV, N.S., GAMYANIN, G.N., ALPATOV, V.A., NAUMOV, V.B., NOSIK P. & MIRONOVA, O.F. (1998): Mineralogy, geochemistry, and origin of the Nezhdaninsk gold deposit (Sakha-Yakutia, Russia). *Geology of Ore Deposits* **40**, 121-138.
- BURYAK, V.A. (1983): Metamorphogenic and plutonic types of gold ores. *Dokl. Akad. Nauk SSSR* **270**, 934-937. (in Russian).
- BURYAK, V.A. & KHMELEVSKAIA, N.M. (1997): *Sukhoy Log, one of the greatest gold deposits in the world: genesis, distribution patterns, prospecting criteria*. Dalnauka, Vladivostok, 156 p. (In Russian).
- CANET, C., ALFONSO, P., MELGAREJO, J-C. & JORGE, S. (2003): PGE-bearing minerals in Silurian sedex deposits in the Poblet area, southwestern Catalonia, Spain. *Can. Mineral.* **41**, 581-595.
- CARVILLE D.P., LECKIE J.F., MOORHEAD C.F., RAYNER J.G. & DURBIN A.A. (1990): Coronation Hill gold platinum palladium deposit. In *Geology of the Mineral Deposits of Australia and Papua New Guinea*, F.E. Hughes (ed.). Aust. Inst. Mining & Metall. Monograph **14**, 759-762.
- DISTLER, V.V., MITRAFANOV, G.L., NEMEROV, V.K., KOVALENKER, V.A., MOKHOV, A.V., SEMEIKINA, L.K., YUDOVSKAYA, M.A. (1996): Modes of occurrence of platinum group elements and their origin in the Sukhoi Log Gold Deposit (Russia). *Geology of Ore Deposits* **38**, 413-428.
- DISTLER, V.V., YUDOVSKAYA, M.A., MITRAFANOV, G.L., PROKOF'EV, V.Y., LISHNEVSKII E.N. (2004): Geology, Composition and Genesis of the Sukhoi Log Noble Metals Deposit, Siberia. *Ore Geol. Rev.* **24**, 7-44.

- DISTLER, V.V. & YUDOVSKAYA, M.A. (2005): Polymetallic platinum-group element (PGE)-Au mineralization of the Sukhoi Log deposit, Russia. *In* Exploration for Platinum-group Element Deposits (J.E. Mungall, ed.). *Mineral. Assoc. Canada, Short Course* **35**, 457-485.
- DREW, L.J., BERGER, B.W. & KURBANOV, N.K. (1996): Geology and Structural Evolution of the Muruntau Gold Deposit, Kyzylkum Desert, Uzbekistan. *Ore Geol. Rev.* **11**, 175-196.
- EREMIN, R.A., VOROSHIN, S.V., SIDOROV, V.A., SHAKHTYROV, V.G., PROSTAVKO, V.A. & GASHTOLD, V.V. (1994): Geology and Genesis of the Natalka Gold Deposit, Northeast Russia. *Internat. Geol. Rev.* **36**, 1113-1138.
- ERMOLAEV, N.P. (1995): Platinum-Group Metals in Terrigenous-Carbonaceous Shales. *Geochem. Intl.* **32/2**, pp. 122-131
- ERMOLAEV, N.P., SOZINOV N.A., FILTSIYAN, Y.A., CHINENOV, V.A. & KHOROSHILOV, V.L. (1992): *New Types of Precious Metal And Rare Earth Element Ores in Carbonaceous Shales*. Nauka, Moscow. (In Russian).
- FAN DELIAN. (1983): Polyelements in the Lower Cambrian black shale series in Southern China. *In* The Significance of Trace Metals in Solving Petrogenetic Problems & Controversies, Augustithis S.S. (ed.). Theophrastus Publications, Athens, 447-474.
- GABLINA, I.F. (1981): New data on formation conditions of the Dzhezkazkan copper deposit: *Internat. Geol. Rev.* **23/11**, 1303-1311.
- GONCHAROV, V.I., VOROSHIN, S.V. & SIDOROV, V.A. (1995): Platinum group element (PGE) concentrations in and near black shale-hosted quartz-Au vein deposits of North-East Russia. *Geol. Soc. Am. Abstracts with Programs* **27/5**, 21.
- GROVES D.I., GOLDFARB R.J., GEBRE-MARIAM M., HAGEMANN S.G., ROBERT, F. (1998): Orogenic gold deposits: a proposed classification in the context of their crustal distribution and relationship to other deposit types. *Ore Geol. Rev.* **13**, 7-27.
- HULBERT, L., CARNE, R.C., GREGOIRE, D.C. & PAKTUNC, D. (1992): Sedimentary nickel, zinc and platinum group element mineralization in Devonian black shales at the Nick property, Yukon, Canada: a new deposit type. *Explor. Mining Geol.* **1**, 39-62.
- IVANOV, S. & ANSDELL, K.M. (1998): Vein paragenesis at the Kumtor gold deposit, central Tien Shan, Kyrgyzstan. *Geol. Soc. Am. Abstracts with Programs* **30**, 367.
- JAIRETH, S. (1988): Hydrothermal transport of platinum and gold in the unconformity-related uranium deposits: a preliminary thermodynamic investigation. *Bureau of Mineral Resources Record*, **1988/9**, 27 pp.
- JEDWAB, J., TARKIAN, M., CORNELISEN, B., MOELO, Y. & DEUDON, C. (1999a): Mineralogy of palladium, rhenium and gold in the Sulfidic Ores of Shinkolobwe, Katanga, Congo. *In* Mineral Deposits: Processes to Processing, Stanley *et al.* (eds.). Balkema, pp. 171-174.
- JEDWAB, J., BADAUT D., BEAUNIER, P. (1999b): Discovery of a palladium-platinum-gold-mercury bitumen in the Boss mine, Clark County, Nevada. *Econ. Geol.* **94**, 1163-1172.
- JOHNSTON, D.J. (1984): *Structural evolution of the Pine Creek inlier and mineralisation therein, Northern Territory, Australia*. PhD Thesis, Monash University, Melbourne, 335 pp.
- JOWETT, E.C., PEARCE, G.W. & RYDZEWSKI, A. (1987): A Mid Triassic age of the Kupferschiefer mineralization in Poland, based on a revised apparent polar wander path for Europe and Russia. *J. Geophys. Res.* **92**, 581-598.
- KOROBEINIKOV, A.F. (1998): Platinum Group Metals at [sic] Gold Deposits in Fold Belts of Siberia and Northeastern Kazakhstan. *Geokhimiya* **10**, 1009-1020.
- KUCHA, H. & PRZYBYLOWICZ, W. (1999): Noble metals in organic matter and clay-organic matrices, Kupferschiefer, Poland. *Econ. Geol.* **94**, p.1137-1162.
- LEÃO DE SÁ, E. & BORGES, N.R.A. (1991): Gold Mineralization in Cauê and Conceição iron ore mines, Itabira, MG: Field and mine trip to Quadrilátero Ferrífero, Minas Gerais, Brazil. Brazil Gold '91, International Symposium on the Geology of Gold, Belo Horizonte, Field Guidebook, 74-85.
- LEBLANC M., CEULENEER G., AL AZRI H., JEDWAB J. (1991): Concentration hydrothermale de palladium et platine dans les peridotites

- mantellaires du complex ophiolitique. *Comptes Rendus de l'Academie des Sciences, Serie 2, Mecanique, Physique, Chimie, Sciences de l'Univers, Sciences de la Terre* **312**, 1007-1012.
- LOTT D.A., COVENEY, R.M., MUROWCHIK, J.B., GRAUCH, R.I. (1999): Sedimentary exhalative Ni-Mo ores in South China. *Econ. Geol.* **94**, 1051-1066.
- MAKARIEV, L.B., BYLINSKAYA, L.V. AND PAVLOV, M.V. (1999): Platinum group elements in the Kodar-Udokan copper district. In *Platinum of Russia, Volume III*, Orlov, V.P. (ed.). Geoinformark, Moscow, p. 300-306.
- MERNAGH, T. P., HEINRICH, C. A., LECKIE, J. F., CARVILLE, D. P., GILBERT, D. J., VALENTA, R. K., WYBORN, L. A. I. (1994): Chemistry of low-temperature hydrothermal gold, platinum, and palladium (\pm uranium) mineralization at Coronation Hill, Northern Territory, Australia. *Econ. Geol.* **89**, 1053-1073.
- MICHALIK, M. (1997): Chlorine containing illites, copper chlorides and other chloride-bearing minerals in the Fore Sudetic copper deposit (Poland). In *Mineral Deposits*, Papunen (ed.). Balkema, 543-546.
- OJAKANGAS, R.W. (1986): Sedimentology of the basal Kombolgie Formation, Northern Territory, Australia: a Proterozoic fluvial quartzose sequence: In *Sediments Down-Under*, Abstracts. 12th International. Sedimentological Congress, 231.
- OLIVO, G.M., GAUTHIER, M., WILLIAMS-JONES, A.E. & LEVESQUE M. (2001): The Au-Pd Mineralization of the Conceição Iron Mine, Itabira District, Southern São Francisco Craton, Brazil: An Example of a Jacutinga-Type Deposit. *Econ. Geol.* **96**, 61-74.
- PASAVA., J. (1993): Anoxic sediments – an important environment for PGE: an overview. *Ore Geol. Rev.* **8**, 425-445.
- PIESTRZYNSKI, A. & SAWLOWICZ, Z. (1999): Exploration for Au and PGE in the Polish Zechstein copper deposits (Kupferschiefer). *J. Geochem. Explor.* **66**, 17-25.
- PIESTRZYNSKI, A., PIECZONKA, J. & GLUSZEK, A. (2002): Redbed-type gold mineralisation, Kupferschiefer, south-west Poland. *Mineral. Dep.* **37**, 512-528.
- POLUARSHINOV, G.P. & KONSTANTINOV, V.M. (1994): New types of platinoid mineralization. *Mineral Resources of Russia*, 20-23.
- POPLAVKO, E.M., IVANOV, V.V., SERKIES, Y.T., TARKHOV, Y.A., OREKHOV, V.S., BYDYANSKIY, D.A., MILLER, A.D., SERDOBOVA, L.I., BOL'SHAKOVA, N.A. & KOSHAROVSKAYA, G.D. (1977): Geochemical characteristics and conditions of formation of cupriferous sandstones and shales. *Geochem. Internat.* **14**, 156-171.
- SALPETEUR, I., MARTEL-JANTIN B. & RAKOTOMANANA D. (1995): Pt and Pd mobility in ferralitic soils of the West Andriamina Area (Madagascar). Evidence of a supergene origin of some Pt and Pd Minerals. *Chronique de la Recherches Minière* **520**, 27-45.
- SIBBALD, T.I.I. (1988): Nicholson Bay U-Au-PGE deposit studies. In *Summary of Investigations 1988*, Sask. Geol. Surv. **88-4**, 77-81.
- TONN, H., SCHMIDT, F., PORADA, H & HORN, E. (1987): Untersuchung von flussigkeitseinschlüssen im zechstein als beitrage zur genese des Kupferschiefers. *Fortschritte der Mineralogie, Beiheft* **65**, 184.
- WILDE, A.R. (1988): On the origin of unconformity-related uranium deposits: PhD Thesis, Monash University, Australia, 293 pp.
- WILDE, A.R., BLOOM, M.S. & WALL, V.J. (1989a): Transport and deposition of gold, uranium and platinum-group elements in unconformity-related uranium deposits. *Econ. Geol. Monograph* **6**, 637-650.
- WILDE, A.R., MERNAGH, T.P., BLOOM, M.S., HOFFMAN, C.F. (1989b): Fluid inclusion evidence on the origin of some Australian unconformity-related uranium deposits. *Econ. Geol.* **84**, 1627-1642.
- WILDE, A. R., LAYER, P., MERNAGH, T., FOSTER, J. (2001): The giant Muruntau gold deposit: geologic, geochronologic and fluid inclusion constraints on ore genesis. *Econ. Geol.* **96**, 633-644.
- WILDE, A. R., SIMPSON, L. & HANNA, S. (2002): Preliminary study of tertiary hydrothermal alteration and platinum deposition in the Oman ophiolite: *J. Virtual Explorer* **6**, 7-19
- WILDE, A.R. & BIERLEIN, F.P. (2003): Economic platinum concentrations in sediment-hosted

- orogenic gold deposits? *In* Mineral Exploration and Sustainable Development. Eliopoulos *et al.* (eds), Millpress, pp. 831-834.
- WILDE, A.R., EDWARDS, A. & YAKUBCHUK, A. (2003): Unconventional Deposits of Pt & Pd: A Review with Implications for Exploration. *SEG Newsletter*, **52**, 1-18.
- WOOD, S.A. (2002): The aqueous geochemistry of the platinum-group elements with applications to ore deposits. *In* Geology, Geochemistry, Mineralogy, Metallurgy and Beneficiation of PGE. Cabri L.J. (ed.). *Can. Inst. Mining & Metall. Spec. Paper*, **54**, 211-249.
- YAKUBCHUK, A. (1998): Should we explore black shale-hosted gold mineralization within former active or passive margins? Unpublished BHP Minerals Technical Report, 8 pp.
- ZHANG G., LI, J., XIONG, Q., & CHEN, F. (2005): Platinum-group elements in Cambrian black shale in southern China - differential enrichment of platinum and palladium. *Extended abstract, SGA 2005*.

CHAPTER 8: SUDBURY Cu(-Ni)-PGE SYSTEMS: REFINING THE CLASSIFICATION USING McCREEDY WEST MINE AND PODOLSKY PROJECT CASE STUDIES

Catharine E.G. Farrow, J.O. Everest, D.M. King, C. Jolette
FNX Mining Company Inc.
1300 Kelly Lake Road,
Sudbury, Ontario
E-mail: cegfarrow@fnxmining.com

INTRODUCTION

The Sudbury area is famous for its Ni-rich deposits and, with the Noril'sk-Talnakh region, is by far one of the two most important Ni-producing regions of the world. Platinum-group element (PGE) production from Sudbury deposits has been important since late in the 19th century. As new deposits are discovered, PGE production from the Sudbury area deposits continues to grow and it has become necessary to revise models for PGE-rich zones. For the past three decades the bulk of the PGE-rich deposits in the Sudbury camp have been exploited in the footwall, and to a lesser extent in the offsets, of the Sudbury Igneous Complex (SIC).

In this paper we do not include the Cu-PGE style of mineralization characterized by Breccia Belt or Froid-style Ni-Cu-PGE systems as defined by Farrow and Lightfoot (2002), but focus on the details of Cu-PGE mineralization in the McCreedy West Mine and the area of the Whistle offset. We expand on the existing definition of Sudbury 'Footwall' Cu-rich mineralization by describing several different types of 'Cu(-Ni)-PGE systems', and attempt to quantify the distinctions amongst them. Because of the microscopic nature of PGE mineralization, the new classification is important for the development of exploration models, understanding the application of geophysical tools (see Balch, this volume), 3-D visualization, resource modeling, mine planning and grade control.

SUDBURY AREA GEOLOGY

The most significant geological feature of the Sudbury region is the roughly oval-shaped 1.85 Ga Sudbury Igneous Complex (Krogh *et al.* 1984, Corfu & Lightfoot 1997). The tectonically modified SIC is interpreted as having been generated by either endogenic process in the crust or as a result of bolide impact, the later model having the greatest acceptance amongst the geological community

(Grieve 1991, Grieve 1994, Golightly 1994, Keays & Lightfoot 1999, Spray *et al.* 2004). It was emplaced at a major crustal boundary tectonic zone between Archean gneissic, migmatitic and granitic rocks to the north, the basal supracrustal stratigraphy of the Paleoproterozoic Huronian Supergroup to the south, and with the Whitewater Group metasedimentary rocks (Fig. 8-1). At the base of the Whitewater Group are the breccias of the Onaping Formation which are overlain by the pelitic Onwatin and turbiditic Chelmsford formations. The Archean rocks have yielded a metamorphic age of 2711 ± 7 Ma (Krogh *et al.* 1984), and the Huronian stratigraphy is cut by the Nipissing intrusive suite (2220 Ma; Corfu & Andrews 1986; Noble & Lightfoot 1992) and by early Proterozoic granitic plutons (Creighton, Murray and Skead plutons).

The Main Mass of the SIC consists of basal Mafic Norite, Felsic Norite, transitional Quartz Gabbro and Granophyre. The discontinuous, inclusion-bearing Sublayer Norite and proximal Footwall Breccia, which is interpreted to be the product of fragmentation and melting of crustal rocks during impact, are important hosts to the 'Contact style' of Ni-rich sulfide mineralization (Souch *et al.* 1969, Pattison 1979, Morrison 1984).

The country rocks surrounding the SIC are cut by radial and concentric 'offset' dykes dominantly composed of quartz diorite (QD) and locally inclusion-bearing quartz diorite (IQD). Offsets that are within Archean rocks tend to be associated with intensely brecciated and melted crustal rocks, termed metabreccia (Souch *et al.* 1969, Grant & Bite 1984, Lightfoot & Farrow 2002).

Wide zones of comminuted and frictionally melted crustal rocks, interpreted as being the result of meteorite impact, are termed Sudbury Breccia and occur in the footwall to the SIC. Sudbury

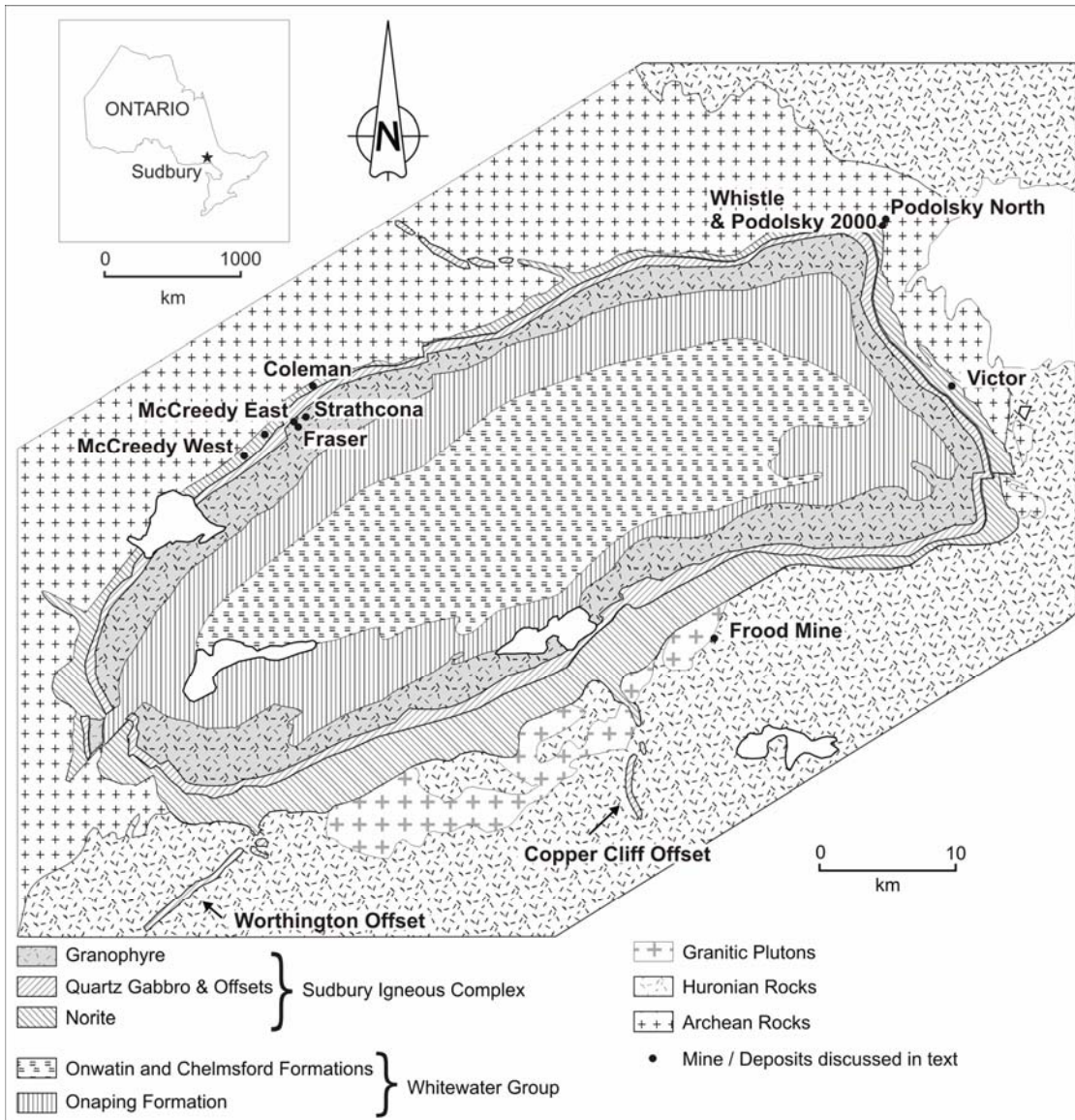


FIG. 8-1: Regional geology map of the Sudbury Igneous Complex showing the location of deposits, mines and offsets discussed in the text.

Breccia has traditionally been considered important in the preparation of the country rock for, and is an important host to, Cu–(Ni)–PGE mineralization in the footwall (Farrow 1994, Fedorowich *et al.* 1999, Hanley & Mungall 2003, in press). Zones of Sudbury Breccia, proximal to the base of the SIC, are considered to have acted as channelways for metal-bearing fluids (Farrow 1994, Jago *et al.* 1994, Hanley & Mungall 2003), and have locally preferentially developed dilational fractures that have acted as structural traps to sulfide veining (Farrow 1994, Fedorowich *et al.* 1999).

STYLES OF Ni–Cu–PGE SULFIDE DEPOSITS AT SUDBURY

The most recent compilation of Sudbury PGE-bearing deposit types was presented by Farrow & Lightfoot (2002) and references therein. A summary of these common Sudbury deposit types is provided here.

Historically contact-type Ni-rich deposits have been recognized as the most important ore type in Sudbury and were the first to be mined in the Sudbury camp (Souch *et al.* 1969). This type of deposit is commonly located at the base of the SIC

within embayment structures, and is hosted in either Sublayer Norite or Footwall Breccia (Souch *et al.* 1969, Pattison 1979, Coats & Snajdr 1984, Davis 1984, Morrison 1984, Naldrett 1984a). The sulfide assemblage is dominated by pyrrhotite and minor pentlandite, with Cu/Ni ratios of approximately 0.7 and Pt+Pd+Au contents of $<1 \text{ g.t}^{-1}$ (Naldrett 1984b, Farrow & Lightfoot 2002).

The most economically productive offset environments to date in Sudbury are radial offsets that extend into the footwall from the base of the SIC, such as the Copper Cliff and Worthington offsets. The deposits tend to be associated with discontinuities along the length of the offsets that may be the result of swells or pinches in the thickness of the dykes due to country rock lithological changes or fault-related displacements (Cochrane 1984, Mourre 2000, Farrow & Lightfoot 2002, Lightfoot & Farrow, 2002). The offset deposits are mineralogically similar to contact-type deposits, with dominant pyrrhotite and minor pentlandite + chalcopyrite. The offset-hosted sulfides typically have higher base metal tenors than sulfides in contact deposits, higher Cu/Ni ratios (1.5 to 2) and higher PGE contents (Pt+Pd+Au $>2.5 \text{ g.t}^{-1}$; Farrow & Lightfoot 2002).

South Range Breccia Belt deposits were classified as a separate deposit type by Farrow & Lightfoot (2002). These deposits, typified by the large Frood Mine system, range from pyrrhotite-rich, Ni-bearing mineralization at higher elevations in the sulfide-mineralized system through to Cu- and PGE-rich mineralization at depth. This type of mineralization is hosted in well-developed zones of Sudbury Breccia that contain pods of barren QD and are developed in Huronian supracrustal rocks. It is possible that the Breccia Belt deposits were formed through similar genetic processes to those described here for the Cu(-Ni)-PGE deposits, but further discussion on this topic is beyond the scope of this contribution.

The deposits that are the focus of this contribution have been traditionally termed 'Footwall-type' deposits, are characterized by chalcopyrite-rich, PGE-bearing sulfide assemblages, and are typically hosted within brecciated rocks in the footwall of the SIC. The best known of these deposits are along the north and east margins of the Sudbury Structure and include those at McCreey West, McCreey East, Coleman, Strathcona, Fraser and Victor mines (Abel *et al.*

1979, Coats & Snajdr 1984, Naldrett 1984a, Li *et al.* 1992, Morrison *et al.* 1994, Farrow & Watkinson 1997). Cu/Ni ratios are typically >6 , Pt+Pd+Au contents exceed 7 g.t^{-1} , and the ratio Pt/(Pt+Pd) is between 0.45 and 0.5 in most of the economically productive zones (Farrow & Lightfoot 2002). They are characterized by complex sulfide vein stockworks comprising chalcopyrite±cubanite, with minor pyrrhotite, pentlandite, millerite, bornite and magnetite, and variably developed amphibole + epidote + quartz ± chlorite ± titanite alteration selvages (Abel *et al.* 1979, Farrow & Watkinson 1992, Li *et al.* 1992, Money 1993, Jago *et al.* 1994, Everest 1999, Kormos 1999). The PGM occur as discrete, microscopic ($<150 \mu\text{m}$ in diameter) bismuthides and tellurides that are commonly located at sulfide and silicate grain boundaries. The vein systems are typically oriented sub-parallel to the base of the SIC. Existing genetic models for this deposit type include sulfide fractionation (Naldrett 1984b, Li *et al.* 1992, Li & Naldrett 1993, Jago *et al.* 1994, Ebel & Naldrett 1996) and mobilization of base and precious metals in the presence of volatiles (Farrow 1994, Farrow *et al.* 1994, Farrow & Watkinson 1996, 1997, 1999, Everest 1999, Kormos 1999, Molnar *et al.* 1997, 1999). It is likely that aspects of both models are responsible for the emplacement of Cu and PGE-rich mineralization at Sudbury (Farrow & Lightfoot 2002, Hanley & Mungall 2003, in press).

GEOLOGY OF THE Cu-(Ni)-PGE DEPOSITS AT SUDBURY

Geological Characteristics

Sudbury Cu(-Ni)-PGE systems (formerly 'Footwall-style Cu-PGE' mineralization as defined by Farrow & Lightfoot 2002) can be subdivided into three types of mineralization: 'Sharp-walled' veins, 'low-sulfide' and 'hybrid'. Both 'sharp-walled' and 'low-sulfide' mineralization occur to variable extents in all Sudbury Cu(-Ni)-PGE mineralization, but the distinction is made according to the volumetrically dominant or economically most important style of mineralization. In all three, chalcopyrite is the dominant sulfide mineral, and the platinum group minerals (PGM) occur ubiquitously as discrete minerals in either sulfide or silicate hosts, along host grain boundaries. In this paper we do not discuss the Cu-PGE mineralization of the South Range Breccia Belt.

'Sharp-Walled' Vein Systems: McCreedy West 700 Complex

The vein system used as the example for this paper is the 700 Complex of the McCreedy West Mine, formerly known as the Levack West Mine. This zone has been mined intermittently since the mid-1970s and is one of the most researched Cu(-Ni)-PGE deposits in the Sudbury area (Hoffman *et al.* 1979, Farrow 1994, Everest 1999). The 700 Complex represents an end-member 'sharp-walled' vein system, with little evidence of economic PGE-bearing disseminated sulfide in the host Sudbury Breccia. Country rocks and 'low-sulfide' disseminations in host rock are essentially considered dilution for mine production purposes. The veins are hosted within a matrix-rich Sudbury Breccia package in the footwall to the 'contact' Ni deposits of the McCreedy West Mine (Fig. 8-2). The 700 Complex vein system is physically connected to Ni-rich 'contact'-type sulfides along the base of the SIC through a Ni-Cu-PGE-enriched

vein stockwork referred to as the Middle Main zone, which was completely mined out in the 1970s. The Middle Main ore body represented the transitional environment to the contact Ni-rich mineralization and the Cu-rich sulfide vein system. It was characterized by metal-rich pods and veins of pyrrhotite with up to 20% pentlandite and up to 20% chalcopyrite hosted by Footwall Breccia. Historical grade and tonnage information for this zone are not known.

The veins tend to be chalcopyrite-dominated with minor or variable amounts of cubanite, pyrrhotite, pentlandite, millerite, bornite and magnetite (Figs. 8-3a, b). The margins of the veins mark sharp, planar surfaces across which the modal abundance of sulfide and magnetite drops from 100% to less than 5%. Major and minor mineral abundances can vary along the length of individual veins, as can base metal and precious metal ratios. Systematic changes along veins are not evident and production grades are directly linked to vein

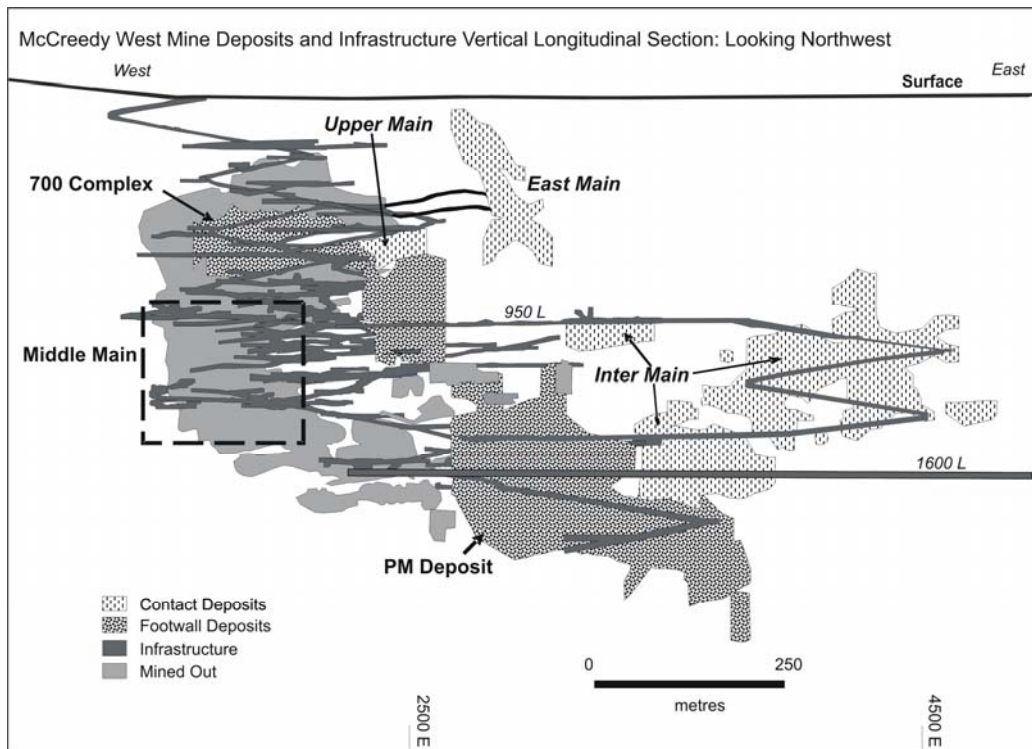


FIG. 8-2: Vertical longitudinal section showing the McCreedy West Mine deposits and infrastructure, looking northwest through the basal contact of the Sudbury Igneous Complex (SIC). The Contact Ni deposits concentrated in the basal units of the SIC (Footwall Breccia and Sublayer Norite) include the Upper Main, East Main, and Inter Main (vertical hatch fill pattern). The area of the mined out Middle Main is outlined by a box (heavy dashed line). Cu(-Ni)-PGE deposits hosted in footwall Sudbury Breccia are the 700 Complex and the PM Deposit (dotted fill pattern). Local grid unit is feet.

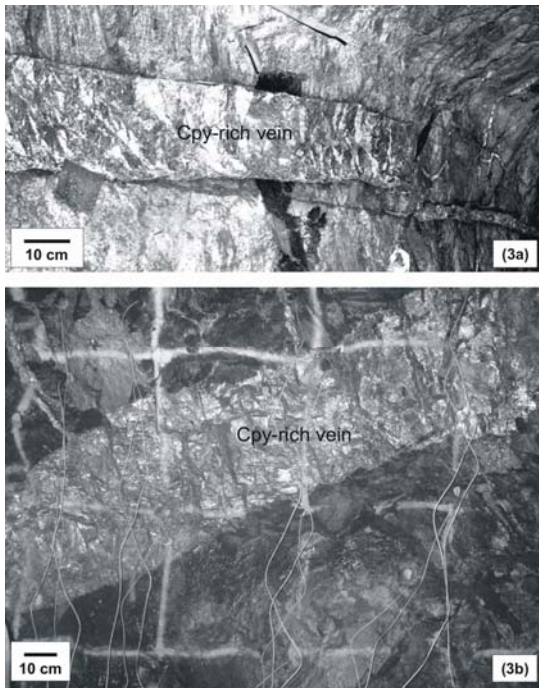


FIG. 8-3: 700 Complex ‘sharp-walled’ veins hosted by Sudbury Breccia. a) A 40 cm wide chalcopyrite-rich vein that terminates abruptly into sub-economic veining. b) A 50 cm wide chalcopyrite-rich vein in matrix-dominated Sudbury Breccia.

thickness, with massive veins consistently averaging between 10 and 20 g.t⁻¹ Pt + Pd + Au.

The platinum group mineralogy of the Cu–PGE veining of the McCreedy West 700 Complex has been described by several different investigators (Cabri & Laflamme 1976, 1984, Naldrett 1984b, Farrow 1994, Everest 1999, Farrow & Lightfoot 2002). The PGM occur as discrete minerals within the veins or along their margins and the assemblage is dominated by moncheite (PtTe₂), michenerite (PdBiTe), merenskyite (PdTe₂), kotulskite (PtTe) and froodite (PdBi₂). All typically occur as compound grains with hessite (Ag₂Te) that are rarely greater than 200 μm in diameter. Systematic variations in PGM assemblage across or along individual veins have not been documented.

‘Low-Sulfide’ Mineralization: The McCreedy West PM Deposit

The first ‘low-sulfide’ system to be developed in the Sudbury camp is the McCreedy West PM Deposit. Published resources on the PM Deposit are an indicated resource of 2.25 million tons at 1.11% Cu, 0.26% Ni, 2.12 g/ston (short ton) Pt, 2.68 g/ston Pd and 0.78 g/ston Au, and an inferred resource of 1.06

million tons at 1.11% Cu, 0.28% Ni, 2.33 g/ston Pt, 3.29 g/ston Pd and 0.78 g/ston Au (FNX Annual Report 2004). Its current dimensions are approximately 350 m east-west, 400 m down-dip with a true thickness of up to 40 m, with a dip of approximately 35°SE. The PM Deposit is hosted by the Sudbury Breccia package that contains the 700 Complex and is characterized by a similar chalcopyrite-rich sulfide assemblage, although the total sulfide content is much lower (<5 modal %). PM Deposit Cu–(Ni)–PGE mineralization is defined by a series of stacked sulfide veins (typically <30 cm thick), vein sets and stockworks that dip at approximately 40° to 50° SE. The chalcopyrite-rich stockworks commonly contain clasts of footwall gneissic rocks within the Sudbury Breccia host. However, ‘sharp-walled’ veins large enough for selective exploitation appear to contribute a small proportion of the total tonnage of the deposit. Ore grade PGE concentrations in the deposit are not limited to veins and stringers, but locally are associated with disseminated sulfides in Sudbury Breccia matrix. Only 5% of the resource is composed of massive sulfide veins greater than 30 centimetres thick. Although Cu/Ni ratios do not display systematic variations, Pt/Pd ratios decrease from >1:1 for S contents of less than 1%, to 2:3 in massive sulfide veins. This relationship is distinct in an extremely low sulfide (<0.3% S) domain on the east side of the deposit, where ore grade Pt+Pd (approximately ≥5 g.t⁻¹) concentrations occur. This domain remains open and will be subject to additional drilling.

Seven styles of mineralization occur within the PM Deposit as listed below, roughly in order of abundance. The first three represent, by far, the dominant style of ore grade mineralization by volume, whereas the balance represents local concentrations or late overprints. The PM mineralization styles are as follows:

- 1) Narrow (centimetre to decimetre-wide) veins and stringers of chalcopyrite ± millerite which may be roughly continuous for distances of up to 30 m. Such veins typically envelope large blocks in the Sudbury Breccia host. A given volume of this style of mineralization will contain between 10% and 20% sulfide over the width of a given vein set.
- 2) Stockworks of narrow (centimetre to millimeter-wide), discontinuous sulfide fracture fillings and veinlets typically occur between and with a conjugate orientation to the more continuous and locally bounding veins described above.

Individual sulfide veins commonly mantle clasts >20 cm in diameter within the Sudbury Breccia. Sulfide contents in this style of mineralization range from 2% to 15% over the mineralized intersection (Figs. 8-4a, b).

- 3) Blebs and disseminations of sulfides in the Sudbury Breccia matrix, with elevated concentrations of sulfide mineralization adjacent to clasts of country rock. Sulfide contents range between 1% and 5% in this style of mineralization (Figs. 8-4c, d).
- 4) Blebs and disseminations of sulfides + PGE which appear to have replaced the mafic mineral component in some clasts of felsic to intermediate composition.
- 5) Country rocks with extremely low sulfide domains (<1% sulfide) yet high PGE contents characterized by disseminations of chalcopyrite

and millerite (Fig. 8-4e). Locally this style of mineralization contributes significant amounts to the total metal content of an ore zone, but the low sulfide content will prohibit visual grade estimation during production.

- 6) Irregular chalcopyrite veinlets and blebs intergrown and associated with pegmatitic and granophyric veins and patches of K-feldspar and quartz. These appear to have shared the same fluid pathways and may be contemporaneous with the PGE-bearing sulfide mineralization.
- 7) Disseminated chalcopyrite and minor millerite in a patchy, discontinuous distribution within epidotized and chloritized Sudbury Breccia matrix. This style of mineralization is interpreted to be part of a late, localized re-mobilization event and contains low PGE values (<1 g.t⁻¹ Pt+Pd+Au).

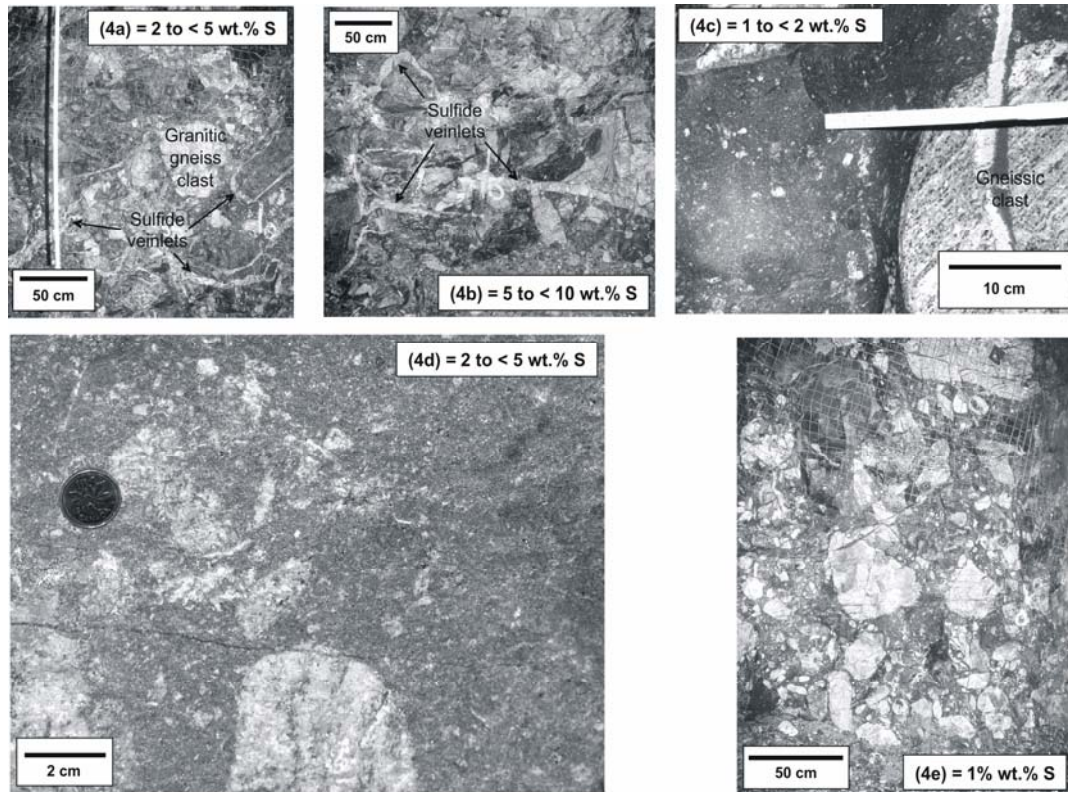


FIG. 8-4: PM Deposit mineralization styles with link to S content intervals. a) Stringers and discontinuous veinlets (chalcopyrite-rich) that locally wrap clasts in Sudbury Breccia. Representative of S ≥ 2 to < 5 wt.% interval. b) Small veins and stockwork (chalcopyrite-rich) representative of S ≥ 5 to < 10 wt.% interval. c) Sudbury Breccia matrix with disseminated sulfide and concentration of sulfide along the bottom margin of a granitic clast in the top left corner of the image. Representative of S ≥ 1 to < 2 wt.% interval. d) Sudbury Breccia matrix showing pervasive, disseminated, chalcopyrite-rich sulfide, locally with more intense concentrations of sulfide adjacent to the larger clasts. Representative of S ≥ 2 to < 5 wt.% interval. e) Sudbury Breccia with disseminated sulfide mineralization difficult to observe in underground lighting conditions. Representative of S ≤ 1 wt.% interval.

The PGM in the PM Deposit are hosted by both sulfide and silicate minerals, most commonly chalcopyrite, millerite, actinolite, epidote and quartz. The PGM assemblage is characteristic of the Levack–Strathcona embayment (Farrow & Lightfoot 2002) and consists of moncheite (PtTe₂), maslovite (PtBiTe), merenskyite (PtTe₂), sperrylite (PtAs₂) and michenerite (PdB₂Te) with rare froodite (PdB₂) and plumbopalladinite (Pd₃Pb₂). Individual PGM grains are locally >50 µm in diameter.

‘Hybrid’ Systems: Podolsky North & 2000 Zones

Details of the geology of the Whistle and Parkin offsets, located on the northeast corner of the Sudbury structure, were given by Lightfoot *et al.* (1997), and Murphy & Spray (2002). The only historical production from this part of the Sudbury structure was from the Whistle Mine, which yielded 5.7 M tons of ore grading 0.33% Cu and 0.95% Ni. Nickel-bearing sulfides were hosted by the Sublayer Norite that filled the Whistle embayment structure at the intersection of the Whistle offset with the base of the SIC. The Whistle offset extends for several kilometres northeast from the embayment (Fig. 8-5). The distal Parkin offset is further from the SIC to the northeast than the Whistle offset and may be related to it by faulting or may represent a separate offset.

Copper–PGE vein systems have been reported in offset-style deposits, typically at the margins to Ni-rich zones in both the Worthington and Copper Cliff offset dykes (Cochrane 1984, Farrow & Lightfoot 2002, Lightfoot & Farrow 2002). Historically, isolated Cu–PGE systems lacking Ni-dominant counterparts were considered rare in these environments and they remain largely unreported in the literature. However, two separate Cu–(Ni)–PGE systems occur in the Whistle offset dyke that are being evaluated for their economic potential, the North and 2000 deposits (Fig. 8-6). Neither have any known physical connection to the Ni-bearing Sublayer mineralization, but both are hosted within IQD and metabreccia entirely within the dyke. The 2000 zone is centered roughly 650 m below the Sublayer-hosted Whistle Mine mineralization at surface, but no physical connection between it and the IQD/metabreccia-hosted 2000 zone has been observed. However, the North zone is exposed at surface, approximately 800 m northeast of the Whistle open pit mineralization, and plunges to the southwest to a depth of approximately 200 m. The 2000 zone

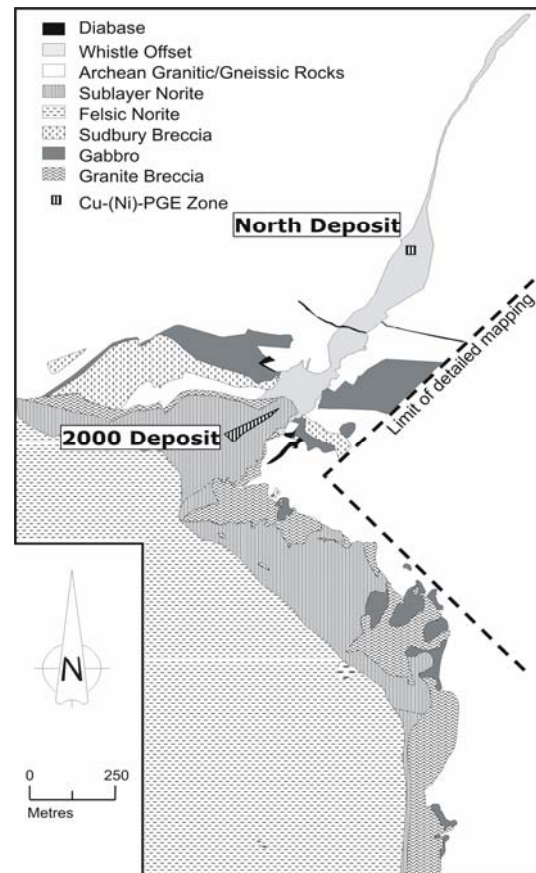


FIG. 8-5: Podolsky property geology showing the Whistle embayment and the Whistle offset trending northeast from it. The locations of the North (where it is exposed at surface) and 2000 (projected to surface) zones are shown (vertical line fill pattern). Both are hosted in Whistle offset rocks. The Sublayer-hosted Whistle open pit is now reclaimed, but it was located at surface 650 m above the 2000 zone. Resource estimates for the North and 2000 zones are not available in the public domain. Local grid unit is feet.

mineral envelope has a sub-vertical orientation, with a 200 m strike length and greater than 300 m vertical extent. Common clast types in the IQD and metabreccia of the Whistle offset include K-feldspar megacrystic/porphyroblastic granite, metagabbro, mafic and felsic gneiss, and metadiabase. Igneous-textured ‘Grey Gabbro’, most commonly recognized on the South Range of the SIC (Frood/Stobie, Creighton, Vermilion), is intimately associated with the mineralization of the 2000 deposit. Clasts of country rocks within the Whistle offset are typically sub-equant and range from less than 1 cm to tens of metres in diameter.

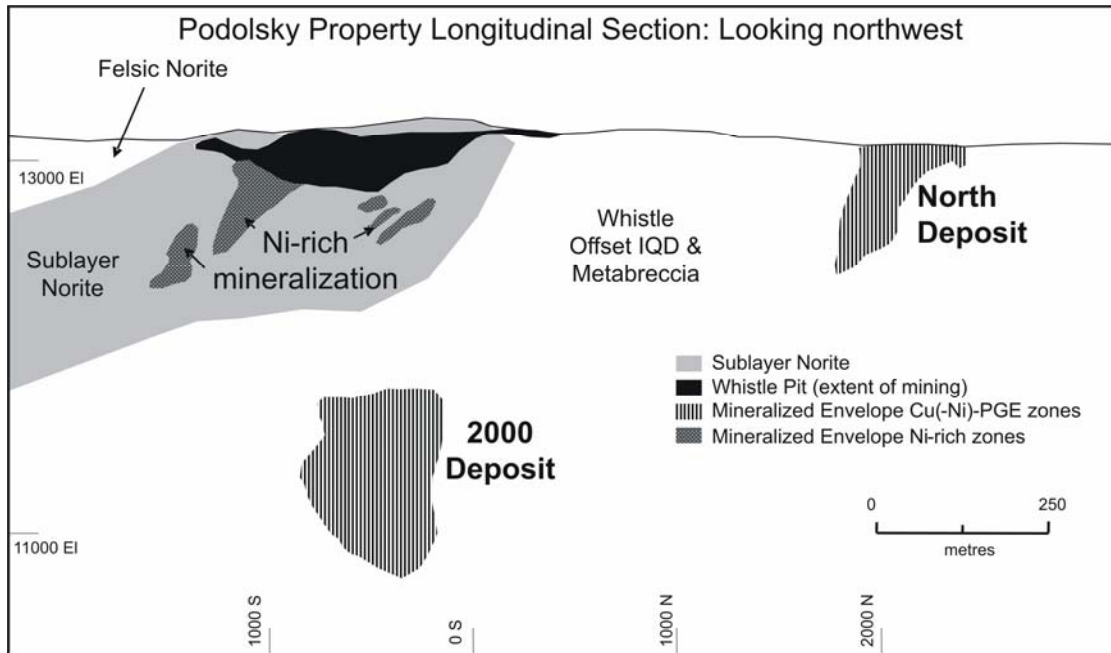


FIG. 8-6: Podolsky property longitudinal section looking northwest showing the relative locations of the original Whistle open pit and associated Ni-rich mineralization below it, and the locations of the North and 2000 zones in the plane of the Whistle offset. The Whistle offset rocks that host the North and 2000 zones are dominated by metabreccia and inclusion quartz diorite (IQD). Local grid unit is feet.

Both the North and 2000 zones are characterized by Cu–(Ni)–PGE-rich ‘sharp-walled’ veins and chalcopyrite-rich ‘breccia’ veins containing silicate inclusions (Figs. 8-7a, b), in addition to domains of poorly connected stringers and disseminated PGE-bearing sulfides. Sharp-walled massive veins appear to cross-cut the ‘breccia’ veins, stringers and disseminated sulfides (Fig. 8-7c). Timing relationships between ‘breccia’ veins, stringers and disseminated sulfides are poorly understood. The sulfide breccia veins of the North zone typically strike sub-parallel to the length of the offset, whereas discontinuous extensional jogs filled with chalcopyrite-rich sulfide are oriented oblique to the offset (roughly north–south). Three Cu–(Ni)–PGE mineralized domains are recognized in the 2000 zone. The largest and most significant is dominated by a domain of Cu–(Ni)–PGE veins and stockworks hosted by IQD and metabreccia that is connected to a smaller domain of veins and stringers within recrystallized gneissic blocks. A third domain of isolated, ‘sharp-walled’ veins hosted by a large (approximately 230 m x 275 m x 90 m), fractured grey gabbro clast occurs adjacent to the breccia-hosted mineralization (Fig. 8-8).

Sulfides with elevated PGE abundances are

locally dominated by, but not limited to, ‘sharp-walled’ veins. The ‘sharp-walled’ veins visible on surface at the North zone appear to cut both sulfide breccia veins and disseminated sulfide mineralization. Significant portions of the 2000 deposit consist of disseminated and blebby sulfide within the IQD and metabreccia. Figure 8-7c and the associated table show the relationships in core between ‘sharp-walled’, massive sulfide veins and lower sulfide stockwork sulfide veining, minor breccia sulfide veining and blebby sulfide mineralization hosted within IQD/metabreccia. Assay intervals with varying sulfide contents are illustrated, and show that Pt+Pd+Au content is not entirely dependent on sulfide content. For example, the interval A–A³ contains 24.8 wt.% Cu and 1.0 wt.% Ni with 9.3 g.t⁻¹ Pt+Pd+Au. The interval A–A² has a lower sulfide content (19.5 wt.% Cu and 0.8 wt.% Ni), but contains higher PGE content breccia sulfide veining and irregularly oriented centimetre-scale sulfide veins for a higher Pt+Pd+Au content of 10.1 g.t⁻¹.

Since both the North and 2000 zones contain elements of ‘sharp-walled’ and ‘low-sulfide’ systems and consist of similar sulfide and PGM assemblages, they are termed ‘hybrid’ Cu–PGE

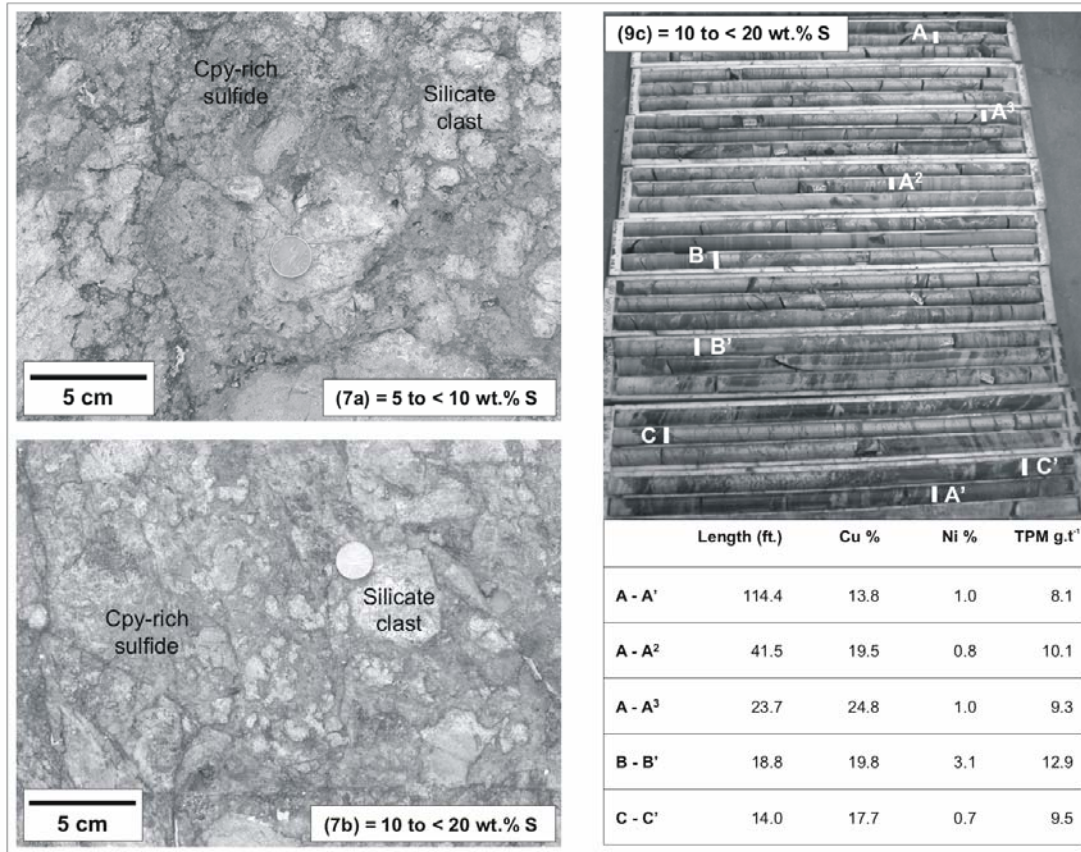


FIG. 8-7: North and 2000 zone 'hybrid'-styles of mineralization. a) Breccia sulfide mineralization at the North zone surface exposure representative of $S \geq 5$ to < 10 wt.% interval. b) Breccia sulfide mineralization at the North zone surface exposure representative of $S \geq 10$ to < 20 wt.% interval. c) Approximately 120 feet (35 m) of 2000 Deposit drill core from part of the IQD/metabreccia-hosted domain intersected in DDH FNX4130. Three zones of 'sharp-walled' veins, below the intersections marked at A, B and C, occur within breccia sulfide vein and stringer sulfide-hosting metabreccia. TPM = Pt+Pd+Au.

systems for the purpose of this discussion. Millerite is the dominant Ni-sulfide mineral, with less common pentlandite. The PGM assemblage is similar for both deposits and is similar to assemblages characteristic of deposits within the Archean footwall to the SIC (Farrow & Lightfoot 2002), and includes moncheite, maslovite, merenskyite, kotulskite, michenerite, froodite and sperrylite. These PGM are hosted by both sulfide and silicate minerals, and locally are $>75 \mu\text{m}$ in diameter.

Geochemical Characteristics

In mature exploration camps such as Sudbury, large volumes of exploration assay data may exist as the only legacy of decades of

exploration, whereas core and other geological information may have long since been discarded. Even in recent exploration programs, huge geochemical datasets of Cu and Ni assays may or may not include S, Pt, Pd and Au data. The challenge is to derive useful exploration and geological information and interpretations from these data, especially since PGE grade can only locally be visually estimated in Cu-PGE systems by sulfide content alone, due to significant variability in the PGE tenor of the sulfides. Figure 8-9a-c is an illustration of this point and shows Pt+Pd (g.t⁻¹) vs. S (wt.%) for individual assays from drill core for 17,369 samples from the PM, 700, North and 2000 zones with a wide range in PGE tenor for any given S content (the assays have not been normalized by

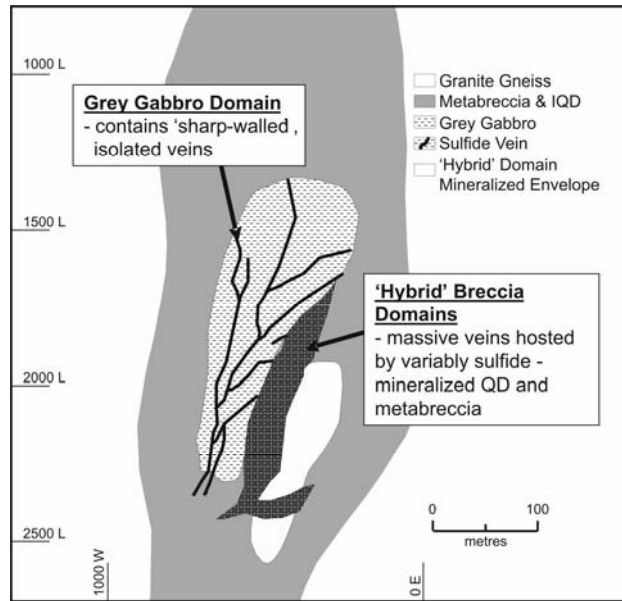


FIG. 8-8: Sectional projection of the Podolsky 2000 zone showing the distribution of the 'hybrid' breccia (IQD and metabreccia) domain, and the grey gabbro-hosted 'sharp-walled' vein mineralized domain. The veins depicted in the 'sharp-walled' domain are illustrative only as the exact orientation of the veins within the system remains unclear. Local grid unit is feet.

any type of weighting or compositing but represent raw data). These data are not fully constrained within the mineral envelope interpreted and used for block modeling purposes in each zone. The PM sample array is characterized by an overall trend to higher PGE content for given S abundance compared to the 700 Complex suite (Fig. 8-9a), with the North and 2000 zones trending between the two end-member deposit types (Fig. 8-9b). If both the 700 and PM sample suites are removed from the diagram, two separate trends can be observed for both 'hybrid' zone assay suites (Fig. 8-9c). The dominant trend represents the 'sharp-walled' veins and a second trend with higher PGE content is representative of 'low-sulfide' mineralization.

In order to understand how the grades link to geological information, the data were subdivided into intervals with different S concentrations in order to compare the metal abundances and ratios in rocks with different visible concentrations of sulfide, related textures, etc. The S intervals were designed to quantify the common distinctions between sulfide mineralization styles (*e.g.*, trace, disseminated, massive) and to link them to geochemical characteristics in the assay database (Tables 8-1 and 8-2; Figs. 8-3, 8-4 and 8-7). Assuming average Pt and Pd prices of US\$800 and US\$200 per troy ounce, respectively, ore grade can

be roughly estimated to be $>5 \text{ g.t}^{-1} \text{ Pt+Pd}$. An illustration of the Pt+Pd distribution relative to S contents for each ore zone is given in Figure 8-10. The threshold interval in each zone is considered where the number of samples in the suite with $\geq 5 \text{ g.t}^{-1} \text{ Pt+Pd}$ approaches or exceeds 50% and the average grade is $\geq 5 \text{ g.t}^{-1} \text{ Pt+Pd}$. In the case of the end-member 700 Complex 'sharp-walled' system, the only interval to attain ore grade is that with $\geq 20\% \text{ S}$ (52.17% of the samples in the suite) averaging $5.13 \text{ g.t}^{-1} \text{ Pt+Pd}$. The interpretation, and practice in the production environment, is that any rock type that is not a massive chalcopyrite-rich vein at least 20 cm wide must be considered as dilution (Figs. 8-3a, b). Conversely, the ≥ 1 to $<2 \text{ wt.}\% \text{ S}$ group in the 'low-sulfide' PM Deposit suite (Fig. 8-4c) contains 46.63% of $\geq 5 \text{ g.t}^{-1} \text{ Pt+Pd}$ samples, with an average grade of 6.09 g.t^{-1} . The implication here is that 3% modal sulfide, half of the time, will make economic grade. The significance is that recognition of almost any visible sulfide at the face in a production environment may be an indication of ore grade potential in the PM Deposit (given the high PGE tenor sulfides). This is a very different scenario than in 'sharp-walled' vein environments, where there is limited metal contribution to the ore body except for the massive sulfide veins. The 'hybrid' North Zone threshold interval is the ≥ 5 to

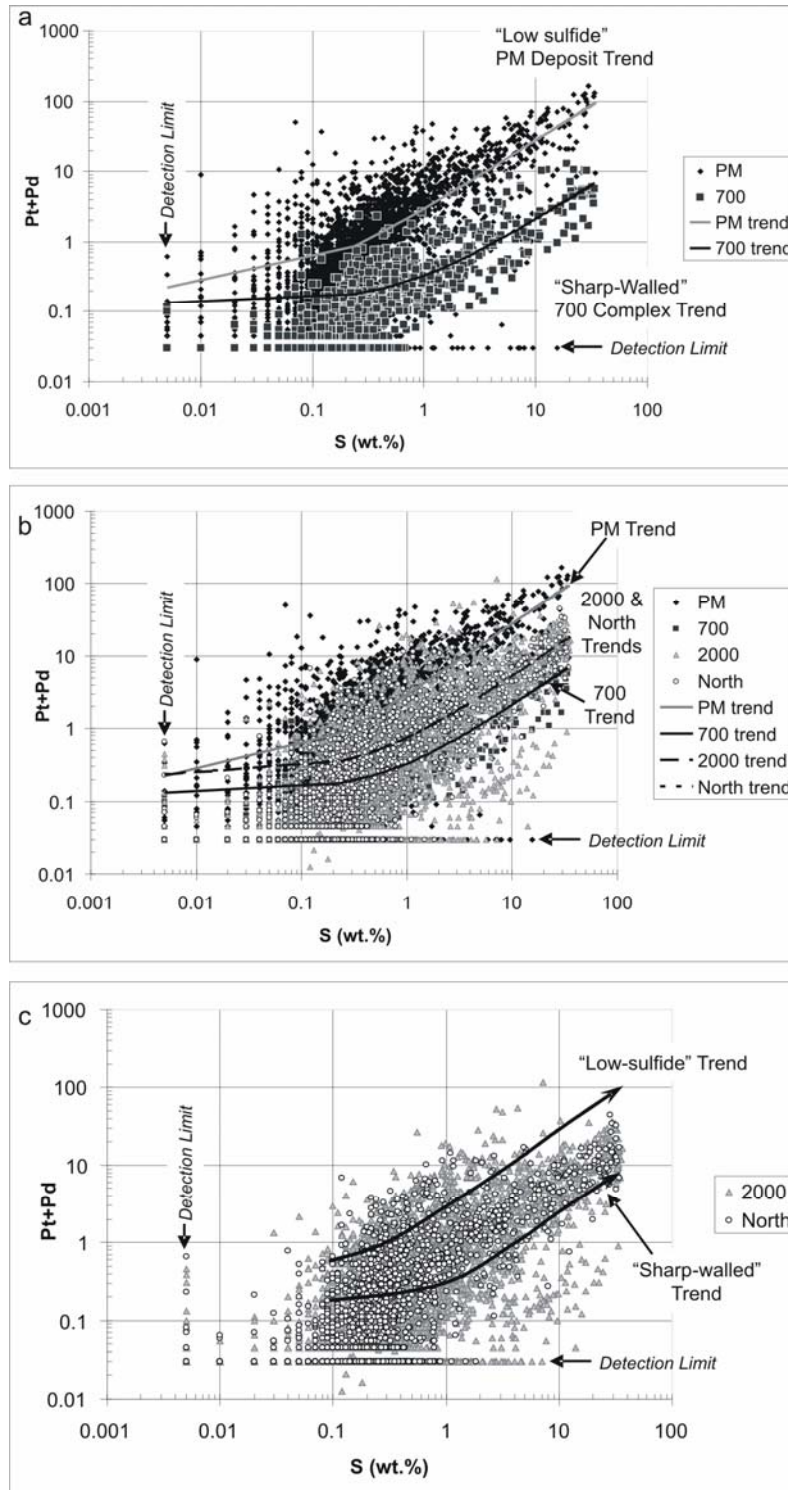


FIG. 8-9: Pt+Pd (g/t) versus S (wt.%) plots showing a) the 'low-sulfide' PM and 'sharp-walled' 700 Complex trends (both linear regression trendlines). b) The 'hybrid' North and 2000 sample distribution and linear regression trendlines with the end-member distributions. The trends for both 2000 & North zones are very similar. c) Both 'low-sulfide' and 'sharp-walled' trendlines superimposed on the North and 2000 sample distributions.

TABLE 8-1: S CONTENT INTERVALS AND ASSOCIATED COMMON SULFIDE MINERALIZATION STYLES FROM MCCREEDY WEST MINE AND PODOLSKY PROJECT

S (wt.%) Interval	Sulfide Mineralization Style	Fig #	700 Complex n=961	North Zone n=2404	2000 Zone n=7791	PM Deposit n=6213
≤1	-less than 3 modal % disseminated sulfide. -small domain in southeast extension of PM Deposit has ≥5 g/t Pt + Pd contents at these low sulfide values.	4e	0	0.57	0.48	2.04
≥1 to <2	-disseminated to blebby sulfides, locally mafic mineral replacement (by chalcocopyrite-rich sulfide) textures, discontinuous veinlets.	4c	0	5.68	8.56	46.63 (6.09)
≥2 to <5	-discontinuous, chalcopyrite-rich veinlets, stringers and stockworks, pervasive disseminations and blebs of chalcopyrite-rich sulfide.	4d, 4a	0.02	8.91	16.31	69.29
≥5 to <10	-small veins and stockworks, semi-massive and 'sulfide breccia' veins.	4b, 7a	15.38	41.67 (5.13)	28.10	76.00
≥10 to <20	-large vein stockworks, semi-massive 'sulfide breccia' veins, all chalcopyrite-dominated.	7b, 7c	17.65	72.97	55.93 (7.20)	91.43
≥20	-massive, 'sharp-walled' veins of chalcopyrite with minor pentlandite and millerite.	3a, 3b	52.17 (5.13)	95.00	90.22	100.00

S (wt.%) content intervals used in this study and associated common sulfide mineralization styles described in diamond drill logs from McCreedy West Mine and Podolsky Project are tabulated with the percentage of samples with ≥5 g/t Pt + Pd in each of the following sample suites: McCreedy West 700 Complex ('sharp-walled' vein system) and PM Deposit ('low-sulfide system'), and the Podolsky North and 2000 zones. Where the number of samples ≥5 g/t Pt+Pd approaches or exceeds 50%, and the average grade is >5 g/t Pt+Pd, the average Pt+Pd grade is shown in parentheses. 'n' is the number of samples in each suite used for this comparison study.

TABLE 8-2. S CONTENT INTERVALS AND ASSOCIATED AVERAGE PT+PD CONTENTS, AND PT/PD AND CU/Ni RATIOS.

S (wt.%) interval	Average Pt+Pd (g/t) content				Pt/Pd				Cu/Ni			
	700	PM	North	2000	700	PM	North	2000	700	PM	North	2000
≤1	0.12	0.59	0.25	0.22	1.07	0.99	1.49	1.23	9.33	4.93	10.99	9.36
≥1 to <2	0.51	6.09	1.81	1.93	0.77	0.85	1.98	1.46	12.07	10.07	14.24	14.43
≥2 to <5	1.07	10.27	2.47	3.10	0.92	0.84	1.76	1.39	18.00	18.10	13.00	22.38
≥5 to <10	1.96	20.30	5.13	4.49	1.33	0.90	1.52	1.19	27.81	24.13	24.34	33.10
≥10 to <20	3.61	36.56	7.64	7.20	0.95	0.70	1.64	1.01	44.68	86.45	92.67	66.49
≥20	5.13	73.32	13.36	13.63	0.51	0.67	1.01	1.08	54.81	89.97	167.93	147.68

Table 2: S (wt.%) content intervals and associated average Pt+Pd (g/t) contents, and Pt/Pd and Cu/Ni ratios for each of the 700 Complex, PM Deposit, and 2000 and North zone sample suite. In each of the four mineralized zones, average Pt + Pd (g/t) contents and Cu/Ni ratios increase with increased S (wt.%) contents, whereas Pt/Pd ratios decrease. However, there is variation in the rates and amounts of these changes unique to each mineralized zone.

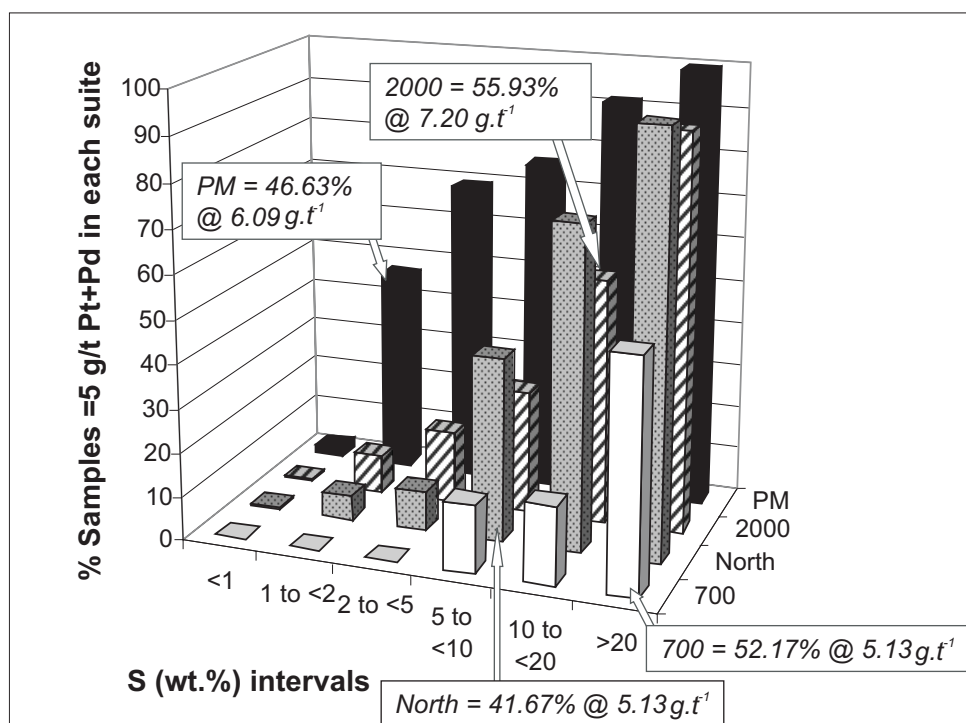


FIG. 8-10: Histogram showing S (wt.%) intervals and respective percentage distribution of samples in each with Pt + Pd ≥ 5 g/t. The percentage of samples ≥ 5 g/t Pt + Pd and average grade are provided for each threshold sulfide interval (that interval in which approximately 50% of the sample suite contains ≥ 5 g/t Pt + Pd). The threshold intervals are 1 to <2 wt.% S for the PM Deposit, 10 to <20 wt.% S for the 2000 Deposit, 5 to <10 wt.% S for the North Zone and >20 wt.% S for the 700 Complex.

<10 wt.% S group (Fig. 8-7a), with 41.67% of the samples in the suite containing ≥ 5 g.t⁻¹ Pt+Pd, with an average grade of 5.13 g.t⁻¹. The 2000 Zone, overall, requires more sulfide to attain economic PGE grades than the North Zone, with the ≥ 10 to <20 wt.% S group averaging 7.20 g.t⁻¹. It is likely that the 2000 Zone assay results are skewed to a more 'sharp-walled' vein control by the influence of the chalcopyrite-rich vein domain hosted by the grey gabbro at the top of the high grade mineral envelope.

Averages of Pt/Pd and Cu/Ni ratios for each S interval are shown in Table 8-2. Despite the limited number of elements available from such a standard assay dataset, several trends are apparent. There are differences between the two end-member environments, the 700 Complex and the PM Deposit, although both are hosted in the same Sudbury Breccia package in the McCreedy West Mine footwall. The Pt+Pd tenor is significantly higher for a given S content in the PM Deposit sample suite than that for the 700 Complex. The North and 2000 zones have similar base metal

contents and Cu/Ni ratios for each S interval, but very different Pt/Pd ratios, with the North Zone having higher Pt contents than Pd. In each of the four zones, there is a general trend to higher Pt/Pd ratios with decreasing S content (for example, 700 Complex Pt/Pd 0.51 to 1.07 for ≥ 20 wt.% S to ≤ 1 wt.% S). The economic significance of this observation is twofold. First, because of the higher current market value of Pt, high Pt could add to the economics of otherwise lower S domains in Cu(-Ni)-PGE systems. Secondly, there is no obvious relationship between Cu/Ni ratio and PGE tenor in any of the documented styles of mineralization.

DISCUSSION

Genetic Interpretation of Cu(-Ni)-PGE Systems: Towards a Unifying Hypothesis

Both evidence in underground and surface exposures and the lack of an obvious link between 'sharp-walled' veins and disseminated to blebby sulfide 'halos' surrounding them leads us to suggest that the 'sharp-walled' veins formed as a result of dilational processes in the host rocks to the PM

Deposit and North Zone. These veins appear to represent the last major magmatic sulfide event to affect the 'low sulfide' and 'hybrid' systems. Later neo-tectonic processes that have had a minor role in sulfide re-mobilization at Sudbury have not had a significant economic impact in the Cu–(Ni)–PGE mineralized zones described here (Marshall *et al.* 1999, Farrow & Lightfoot 2002).

The genetic implications of the trend to higher Pt/Pd ratios with decreasing S content are that since Pt solubility is lower than that of Pd in most modeled aqueous, halogen-bearing fluids, it is possible that Pt-bearing sulfides precipitated before the higher sulfide, lower Pt mineralization.

At temperatures above the liquidus for sulfide and silicate magmas (>850°C), magmatic sulfides were formed in contact and offset environments (Farrow & Lightfoot 2002). As the Ni-rich ore bodies evolved down-temperature, intermediate temperature volatiles (both aqueous and non-aqueous) circulated in the footwall and offset environments, driven by the heat of the SIC (Farrow & Watkinson 1996, 1999, Farrow & Lightfoot 2002). With continued cooling, the PGE and other metals were variably distributed into the

semi-permeable breccia environments, the Sudbury Breccia in the McCreehy West Mine footwall, and the metabreccia/IQD as a proxy for the Sudbury Breccia in the Whistle offset. Eventually halogen-bearing aqueous fluids established convection cells driven by the heat of the cooling SIC, thereby contributing to the re-mobilization process (*cf.* Farrow & Watkinson 1992, 1997, Li & Naldrett 1992, Farrow *et al.* 1994, Jago *et al.* 1994, Farrow & Lightfoot 2002, McCormick *et al.* 2002, Hanley & Mungall 2003, in press). At this point, a fluid flux containing PGE, Cu, Ni, S-species, Au, Te, Bi, C-species, H₂O, Cl and other halogens, Si, Mg, Fe, Ti and LREE became important to the metal transportation process (Farrow 1994, Farrow *et al.* 1994, Hanley & Mungall 2003, Mungall & Brenan 2003). 'Low-sulfide'-type PGE mineralization was deposited from this fluid as solubility was lost due to decreasing temperature and evolution of the fluid composition through fluid–rock interaction (Fig. 8-11a). A final tectonic re-adjustment and the development of dilational features resulted in the final 'freezing' of the system, possibly as a result of decompression, as the Cu–PGE-rich 'sharp-walled' veins were formed (Fig. 8-11b).

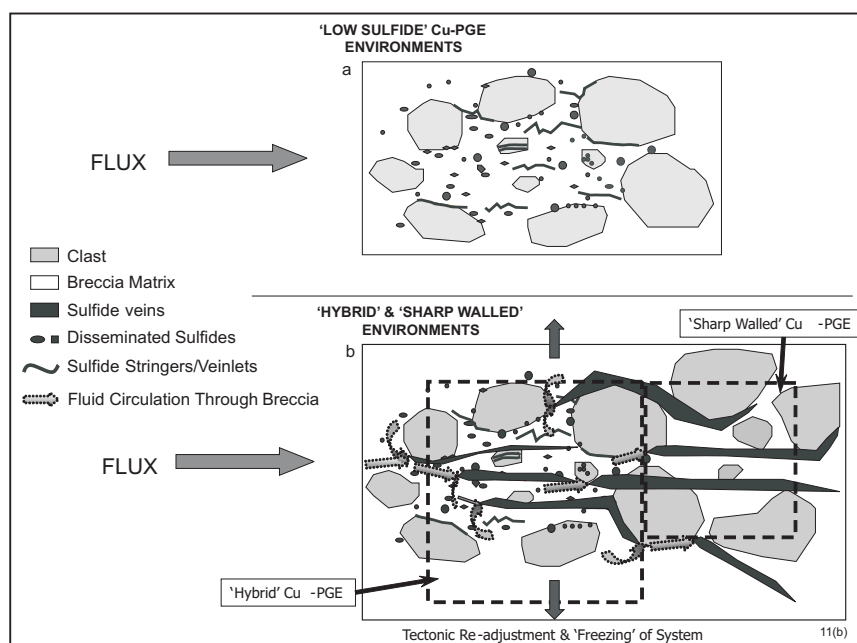


FIG. 8-11: Cartoon representation of the possible genesis of 'low-sulfide', 'sharp-walled' and 'hybrid' Cu(-Ni)-PGE systems. a) A flux of fluid through the semi-permeable Sudbury Breccia, metabreccia or IQD matrix containing PGE, Cu, Ni, S-species, Au, Te, Bi, C-species, H₂O, Cl (and other halogens), Si, Mg, Fe, Ti and LREE is trapped, resulting in the development of 'low-sulfide'-style mineralization. b) With continued tectonic re-adjustment of the post-impact crust, dilational fractures opened, resulting in the final 'freezing', or loss of solubility of the flux and the development of 'sharp-walled' or 'hybrid' systems (outlined by dashed line boxes).

CONCLUSIONS

In this paper we have attempted to subdivide Sudbury Cu(-Ni)-PGE mineralization into a more detailed classification than currently exists, and to quantify the basis for this classification using geochemical datasets. Based on composition, a quantitative distinction can be made between end-member textural variants recognized as 'sharp-walled' and 'low sulfide' PGE mineralization types at Sudbury. This has been proven to be of practical use in the further development of exploration models, advanced exploration and development of the PM, North and 2000 zones, resource modeling and mine planning. In the future it will be necessary to add additional deposit data to the comparison, as PGE tenors and trace element contents are deposit-specific and strongly influenced by the compositions of both related contact Ni zones and footwall host rocks (Farrow & Watkinson 1997).

In pyrrhotite-rich deposits, visual Ni grade estimation is commonplace as a production tool. However, visual ore/waste definition by PGE grade estimation from visible sulfide content will be locally difficult unless accurate grade modeling can be completed in advance of production in a 'low sulfide' zone. This modeling will rely heavily on the availability of an accurate link between geological domains and pre-production assaying. The broad distribution of ore-grade Pt+Pd in the PM Deposit may allow for the successful application of bulk rather than selective mining methods in this environment.

The recognition of a distinction between sharp-walled vein-type and low-sulfide-type mineralization is also important in the application of EM and IP geophysical exploration methods. Whereas EM methods have traditionally been used successfully in 'contact'-style Ni-rich deposit exploration they have variable success in Cu-PGE exploration (Balch, this volume). Further refinement of this classification of Cu(-Ni)-PGE mineralization through the development of geochemical models linked to geological mapping and logging will become increasingly important to characterize geophysical responses for exploration geologists and geophysicists.

In the long term, it will be important to attempt to quantify the contributions by end-member Cu(-Ni)-PGE ore types using detailed geological and geochemical modeling on a system-by-system basis.

ACKNOWLEDGEMENTS

The following FNX staff have had a large influence on the exploration for, definition of and geological understanding of the PM, 700, North and 2000 zones: S. Balch, S. Bernier, J. Fedorowich, J. Fee, K. Gladwin, G. Morrison, J. Muir, R. Poulin, and J. Xiong. Others who have been instrumental for their help and insights during the development of some of the ideas that have gone into this manuscript are: D. Ames (GSC), J. Hanley (University of Toronto), P. Lightfoot (INCO), J. Mungall (University of Toronto), M. Srivastava (FSS Canada), and D. Watkinson (Carleton University). Thanks are extended to FNX Mining Company Inc. senior management for permission to publish this paper.

REFERENCES

- ABEL, M.K., BUCHAN, R., COATS, C.J.A. & PENSTONE, M.E. (1979): Copper mineralization in the footwall complex, Strathcona mine, Sudbury, Ontario, *Can. Mineral.* **17**, 275-285.
- CABRI, L.J. & LAFLAMME, J.H.G. (1976): The mineralogy of the platinum-group elements from some copper-nickel deposits of the Sudbury area. *Econ. Geol.*, **71**, 1159-1195.
- CABRI, L.J. & LAFLAMME, J.H.G. (1984): Mineralogy and distribution of platinum-group elements in mill products from Sudbury. *In Proceedings, 2nd International Congress on Applied Mineralogy in the Minerals Industry* (Park, W.C., Hausen, D.M. and Hagni, R.D., eds.), AIME, 911-922.
- COATS, C.J.A. & SNAJDR, P. (1984): Ore deposits of the North Range, Onaping-Levack area, Sudbury. *In The Geology and Ore Deposits of the Sudbury Structure* (E.G. Pye, A.J. Naldrett & P.E. Giblin, eds.). *Ontario Geological Survey Special Volume 1*, 327-346.
- COCHRANE, L.B. (1984): Ore Deposits of the Copper Cliff Offset. *In The Geology and Ore Deposits of the Sudbury Structure* (E.G. Pye, A.J. Naldrett & P.E. Giblin, eds.). *Ontario Geological Survey Special Volume 1*, 347-360.
- CORFU, F. & ANDREWS, A.J. (1986): A U-Pb age for mineralized Nipissing diabase, Gowganda. *Can. J. Earth Sci.* **23**, 107-109.
- CORFU, F. & LIGHTFOOT, P.C. (1997): U-Pb geochronology of the Sublayer environment,

- Sudbury Igneous Complex, Ontario. *Econ. Geol.* **91**, 1263-1269.
- DAVIS, G.C. (1984): Little Stobie Mine: A South Range Contact Deposit. In *The Geology and Ore Deposits of the Sudbury Structure* (E.G. Pye, A.J. Naldrett & P.E. Giblin, eds.). *Ontario Geological Survey Special Volume 1*, 361-370.
- EBEL, D. & NALDRETT, A.J. (1996): Fractional crystallization of sulphide ore liquids at high temperature: *Econ. Geol.* **91**, 607-621.
- EVEREST, J.O. (1999): *The relationship of Cu-Ni-PGE veins in the Levack Gneiss Complex to contact magmatic ore at the McCreedy West Mine, Sudbury*. M.Sc. thesis, Carleton University, Ottawa, Canada, 125 p.
- FARROW, C.E.G. (1994): *Geology, alteration, and the role of fluids in Cu-Ni-PGE mineralization of the footwall rocks to the Sudbury Igneous Complex, Levack and Morgan Townships, Sudbury District, Ontario*. Ph.D. thesis, Carleton University, Ottawa, Canada, 373 p.
- FARROW, C.E.G. & WATKINSON, D.H. (1992): Alteration and the role of fluids in Ni, Cu and platinum-group element deposition, Sudbury Igneous Complex contact, Onaping-Levack area, Ontario. *Mineral. Petrol.* **46**, 67-83.
- FARROW, C.E.G. & WATKINSON, D.H. (1996): Geochemical characteristics of the Epidote Zone: its development and associated Ni-Cu-PGE remobilisation by saline fluids, Fraser mine, Sudbury, Ontario. *Explor. Mining Geol.* **5**, 17-31.
- FARROW, C.E.G. & WATKINSON, D.H. (1997): Diversity of precious-metal mineralization in footwall Cu-Ni-PGE deposits, Sudbury, Ontario: implications for hydrothermal models of formation. *Can. Mineral.* **35**, 817-839.
- FARROW, C.E.G. & WATKINSON, D.H. (1999): An evaluation of the role of fluids in Ni-Cu-PGE-bearing, mafic-ultramafic Systems. In *Dynamic processes in magmatic ore deposits and their application in mineral exploration* (Keays, R.R., Leshner, C.M., Lightfoot, P.C. & Farrow, C.E.G. (eds). Geological Association of Canada, Short Course Notes, Volume 13, 31-67.
- FARROW, C.E.G., WATKINSON, D.H. & JONES, P.C. (1994): Fluid inclusions in sulfides from North and South range Cu-Ni-PGE deposits, Sudbury Structure, Ontario. *Econ. Geol.* **89**, 647-655.
- FARROW, C.E.G. & LIGHTFOOT, P.C. (2002): Sudbury PGE Revisited: Towards an Integrated Model. In *Geology, Geochemistry, Mineralogy and Mineral Beneficiation of Platinum-Group Elements*, Cabri, L.J. (ed.). CIM Special Volume **54**, 273-297.
- FEDOROWICH, J.S., ROUSELL, D.H. & PEREDERY, W.V. (1999): Sudbury breccia distribution and orientation in an embayment environment. *Geol. Soc. Am. Spec. Paper* **339**, 305-315.
- GOLIGHTLY, J.P. (1994): The Sudbury Igneous Complex as an impact melt: evolution and ore genesis. In *Proceedings of the Sudbury-Noril'sk Symposium* (P.C. Lightfoot & A.J. Naldrett, eds.). *Ontario Geological Survey Special Volume 5*, 105-118.
- GRANT, R.W. & BITE, A. (1984): Sudbury Quartz Diorite Offset dikes. In *The Geology and Ore Deposits of the Sudbury Structure* (E.G. Pye, A.J. Naldrett & P.E. Giblin, eds.). *Ontario Geological Survey Special Volume 1*, 275-301.
- GRIEVE, R.A.F. (1991): The Sudbury structure: controversial or misunderstood? *J. Geophys. Res.* **96**, 22753-22764.
- GRIEVE, R.A.F. (1994): An Impact Model of the Sudbury Structure. In *Proceedings of the Sudbury-Noril'sk Symposium* (P.C. Lightfoot & A.J. Naldrett, eds.). *Ontario Geological Survey Special Volume 5*, p. 119-132.
- HANLEY, J.J. & MUNGALL, J.E. (2003): Chlorine enrichment and hydrous alteration of Sudbury Breccia hosting footwall Cu-Ni-PGE mineralization at the Fraser Mine, Sudbury, Ontario, Canada. *Can. Mineral.* **41**, 857-881.
- HANLEY, J.J. & MUNGALL, J.E. (in press): A study of the bulk rock halogen distribution in Sudbury Breccia at the Fraser Mine Copper Zone, Sudbury, Ontario, Canada. *Can. Mineral.*
- HOFFMAN, E.L., NALDRETT, A.J., ALCOCK, R.A. & HANCOCK, R.G.V., 1979. The noble metal content of ore in the Levack West and Little Stobie mines, Ontario. *Can. Mineral.*, **17**, 437-451.
- JAGO, B.C., MORRISON, G.G. & LITTLE, T.L. (1994): Metal zonation patterns and microtextural and micromineralogical evidence for alkali- and halogen-rich fluids in the genesis of the Victor Deep and McCreedy East footwall copper

- orebodies, Sudbury Igneous Complex. *In* Proceedings of the Sudbury-Noril'sk Symposium (P.C. Lightfoot and A.J. Naldrett, eds.). *Ontario Geological Survey Special Volume 5*, 65-75.
- KEAYS, R.R. & LIGHTFOOT, P.C. (1999): The role of meteorite impact, source rocks, protores and mafic magmas in the genesis of the Sudbury Ni-Cu-PGE Sulfide ore deposits. *In* Dynamic Processes in Magmatic Ore Deposits and their application in mineral exploration (Keays, R.R., Leshner, C.M., Lightfoot, P.C. & Farrow, C.E. eds.). *Geol. Assoc. Can., Short Course Notes 13*, 329-366.
- KORMOS, S.E. (1999): *Metal distribution within Zone 39, a Proterozoic vein-type Cu-Ni-Au-Ag-PGE deposit, Strathcona Mine, Ontario, Canada. MSc thesis, Laurentian University, Sudbury, Ontario, 163 p.*
- KROGH, T.E., DAVIS, D.W. & CORFU, F. (1984): Precise U-Pb zircon and baddeleyite ages for the Sudbury area. *In* The Geology and Ore Deposits of the Sudbury Structure (E.G. Pye, A.J. Naldrett & P.E. Giblin, eds.). *Ontario Geological Survey Special Volume 1*, 431-447.
- LI, C. & NALDRETT, A.J. (1993b): High chlorine alteration minerals and calcium-rich brines in fluid inclusions from the Strathcona Deep Copper Zone, Sudbury, Ontario. *Econ. Geol.* **88**, 1780-1796.
- LI, C., NALDRETT, A.J., COATS, C.J.A. & JOHANNSEN, P. (1992): Platinum, palladium, gold and copper-rich stringers at the Strathcona Mine, Sudbury: Their enrichment by fractionation of a sulfide liquid. *Econ. Geol.* **87**, 1584-1598.
- LIGHTFOOT, P.C. & FARROW, C.E.G. (2002): Geology, geochemistry and mineralogy of the Worthington Offset dyke: towards a genetic model for offset mineralization in the Sudbury Igneous Complex. *Econ. Geol.* **97**, 1419-1446.
- LIGHTFOOT, P.C., KEAYS, R.R., MORRISON, G.G., BITE, A. & FARRELL, K. (1997): Geologic and geochemical relationships between the Contact Sublayer, Inclusions, and the Main Mass of the Sudbury Igneous Complex: A case study of the Whistle Mine Embayment. *Econ. Geol.* **92**, 647-673.
- MCCORMICK, K.A., LESHER, C.M., McDONALD, A.M., JAMES, R.S., GIBSON, H.L. & FEDOROWICH, J.S. (2002): Geochemical variations in the Footwall Breccia and F and Cl variations in the Sublayer norite in the Strathcona Embayment, Sudbury Structure, Ontario. *Econ. Geol.* **97**, 1509-1519.
- MARSHALL, D.D., WATKINSON, D.H., FARROW, C.E.G., FOUILLAC, A.-M. & MOLNAR, F. (1999): Fluid mixing during the emplacement of the Sudbury Igneous Complex: fluid inclusion, Ar, O and H isotopic evidence. *Chem. Geol.* **154**, 1-19.
- MOLNAR, F., WATKINSON, D.H., JONES, P.C. & GATTER, I. (1997): Fluid-inclusion evidence for hydrothermal enrichment of magmatic ore at the contact zone of the 4B Ni-Cu-PGE deposit, Lindsley Mine, Sudbury, Canada. *Econ. Geol.* **92**, 674-685.
- MOLNAR, F., WATKINSON, D.H. & EVEREST, J.O., 1999. Fluid-inclusion characteristics of hydrothermal Cu-Ni-PGE veins in granitic and metavolcanic rocks at the contact of the Little Stobie deposit, Sudbury, Canada. *Chem. Geol.* **154**, 279-301.
- MONEY, D.P. (1993): Metal zoning in the Deep Copper Zone 3700 level, Strathcona Mine, Ontario. *Explor. Mining Geol.* **2**, 307-320.
- MORRISON, G.G. (1984): Morphological features of the Sudbury Structure in relation to an impact origin. *In* The Geology and Ore Deposits of the Sudbury Structure (E.G. Pye, A.J. Naldrett & P.E. Giblin, eds.). *Ontario Geological Survey Special Volume 1*, 513-522.
- MORRISON, G.G., JAGO, B.C. & WHITE, T.L. (1994): Footwall mineralization of the Sudbury Igneous Complex. *In* Proceedings of the Sudbury-Noril'sk Symposium (P.C. Lightfoot & A.J. Naldrett, eds.). *Ontario Geological Survey Special Volume 5*, 57-64.
- MOURRE, G. (2000): *Geological relationships at discontinuities in the Copper Cliff Quartz Diorite Offset: an investigation into offset dikes and their relationship to the Sudbury Igneous Complex.* Laurentian University, M.Sc. thesis. 237 p.
- MUNGALL, J.E. & BRENNAN, J.M. (2003): Experimental evidence for the chalcophile behavior of the halogens. *Can. Mineral.* **41**, 207-220.
- MURPHY, A.J. & SPRAY, J.G. (2002): Geology, mineralization and emplacement of the Whistle-Parkin offset dike, Sudbury impact structure.

- Econ. Geol.* **97**, 1369-1389.
- NALDRETT, A.J. (1984a): Ni–Cu ores of the Sudbury Igneous Complex – Introduction. *In* The Geology and Ore Deposits of the Sudbury Structure (E.G. Pye, A.J. Naldrett & P.E. Giblin, eds.). *Ontario Geological Survey Special Volume 1*, 302-307.
- NALDRETT, A.J. (1984b): Mineralogy and composition of the Sudbury ores. *In* The Geology and Ore Deposits of the Sudbury Structure (E.G. Pye, A.J. Naldrett & P.E. Giblin, eds.). *Ontario Geological Survey Special Volume 1*, 309-325.
- NOBLE, S.R., & LIGHTFOOT, P.C. (1992): U–Pb baddeleyite ages for the Kerns and Triangle Mountain intrusions, Nipissing diabase, Ontario. *Can. J. Earth Sci.* **29**, 1124-1129.
- PATTISON, E.F. (1979): The Sudbury sublayer. *Can. Mineral.* **17**, 257-274.
- SOUCH, B.E., PODOLSKY, T. & GEOLOGICAL STAFF (1969): The sulfide ores of Sudbury: their particular relationship to a distinctive inclusion-bearing species of the Nickel Irruptive. *In* Magmatic Ore Deposits, a Symposium (H.D.B. Wilson, ed.). *Econ. Geol. Monograph*, **4**, 366 p.
- SPRAY, J.G., BUTLER, H.R. & THOMPSON, L.M. (2004): Tectonic influences on the morphometry of the Sudbury impact structure: implications for terrestrial cratering and modelling. *Meteoritics & Planet. Sci.* **37**, 287-301.

CHAPTER 9: THE CONDUITS OF MAGMATIC ORE DEPOSITS

Nicholas T. Arndt
LGCA, UMR 5025 CNRS, BP 53
38400 Grenoble cedex, France
E-mail: arndt@ujf-grenoble.fr

INTRODUCTION

Through the work of Naldrett *et al.* (1992, 1995, 1996), Naldrett (1999), Brüggmann *et al.* (1993), Lightfoot *et al.* (1990), Czamanske *et al.* (1994, 1995, 2002) and Fedorenko *et al.* (1996), we know that the magmas parental to magmatic ore deposits such as the Ni-Cu-PGE deposits of Noril'sk-Talnakh, or the chromite-PGE deposits in the Bushveld Complex, form through melting deep in the mantle. Because the solubility of sulfur depends inversely on pressure (Wendlandt 1982, Keays 1995, Mavrogenes & O'Neil 1999), these magmas are strongly undersaturated in sulfur when they arrive at crustal levels. If they are to segregate an immiscible sulfide liquid, a process crucial to the formation of most base-metal and many PGE deposits, the magma must reach sulfur saturation. A common trigger is interaction between the magma and crustal wall rocks, which either changes the temperature and composition of the magma so as to decrease the sulfur solubility, or adds sulfur to the magma.

Once the sulfide liquid has formed, normally as droplets of immiscible liquid dispersed within the silicate magma, these droplets must accumulate if a commercially viable deposit is to form. In addition, if the deposit is to be rich, the tenor in ore metals must be high. This requires that the sulfide interacts with, and extracts chalcophile elements from, a large volume of magma. The extent of interaction between magma and crust depends in part on the structure and petrological make-up of the crust and in part on the physical and dynamic characteristics of the magmas themselves.

MAGMA DYNAMICS: THE PASSAGE OF MAGMA THROUGH THE CRUST

Of the physical properties that influence how magma interacts with crustal rocks, the following are the most important:

- *Density*: Magma ascends because its density is less than that of surrounding rocks. All magmas are less dense than mantle peridotite and more

magnesian varieties like komatiite and picrite are denser than lower-crustal granulites. These magmas often are trapped at the crust-mantle boundary where they differentiate into less dense and more evolved magmas (Cox 1980). The evolved magma ascends farther but becomes trapped higher in the crust at junctures where the crustal density drops. Magma chambers of various forms and dimensions result, and in these chambers, or in the conduits between them, the magma interacts with crustal rocks.

- *Viscosity*: Low-viscosity magmas flow rapidly and turbulently, if the conduit is sufficiently large. Under these conditions, the magma can thermally erode and rapidly assimilate its wall rocks (Huppert & Sparks 1985).

- *Temperature*: High temperatures enhance the extent of crustal interaction in two ways: 1) high-temperature magmas have low viscosities, which cause them to flow rapidly and in some cases turbulently, and 2) high-temperature magmas are more capable of melting or reacting with their wall rocks.

- *Magma flux*: If the magma flux is very high and if the flow regime is turbulent, thermal erosion will result in rapid assimilation of wall rocks. If the flux is high, but insufficient to cause turbulent flow, the extent of assimilation of wall rocks will be minimal because the magma spends relatively little time in contact with fusible rocks. If the flux is still lower and the magma accumulates and crystallizes slowly in large magma chambers, then there again is opportunity for massive assimilation of wall rocks.

The crustal composition and lithology are also important. Typical continental crust is made up of a lower layer of dense granulite-facies rocks, an intermediate layer of lower density granitoid and metamorphic rocks, and in many areas an upper layer of still less dense sedimentary rocks. At shallow levels, porosity increases and open fractures become abundant, and the density drops further. Ascending magma tends to become trapped and to form magma chambers at each density

discontinuity.

The upward migration of magma is also guided by the structure and state of stress of the crust. In zones of extension, steeply dipping faults provide passageways to the surface. When magma reaches horizontally bedded sedimentary strata, horizontal intrusions or sills form. Images of rifting sedimentary margins (Fig. 9-1; Planke *et al.* 2004) and maps of intrusions beneath flood basalt provinces show series of upward-stepping sills that form complexes of stacked, saucer-shaped intrusions. Near the surface, where lithostatic pressure is low and non-isotropic (far less vertical than horizontal pressure), the form and size of intrusions will depend on distance to the surface, as discussed by Planke *et al.* (2004). Magma

passing through sill complexes flows nearly horizontally for much of its passage. The complex pathway augments the period of interaction between magma and wall rocks and increases the extent of contamination.

Finally, intrusion of magma into a compressive regime should produce abundant dykes and fewer sills. Compression of magma chambers may squeeze liquids and crystal mushes to higher crustal levels, providing a mechanism for transporting upward dense mixtures of silicate magma, crystals and sulfide liquid (Czamanske *et al.* 1995, Tornos *et al.* 2001).

The nature of the interaction between magma and wall rocks should therefore change from the base to the top of the crust. At the base,

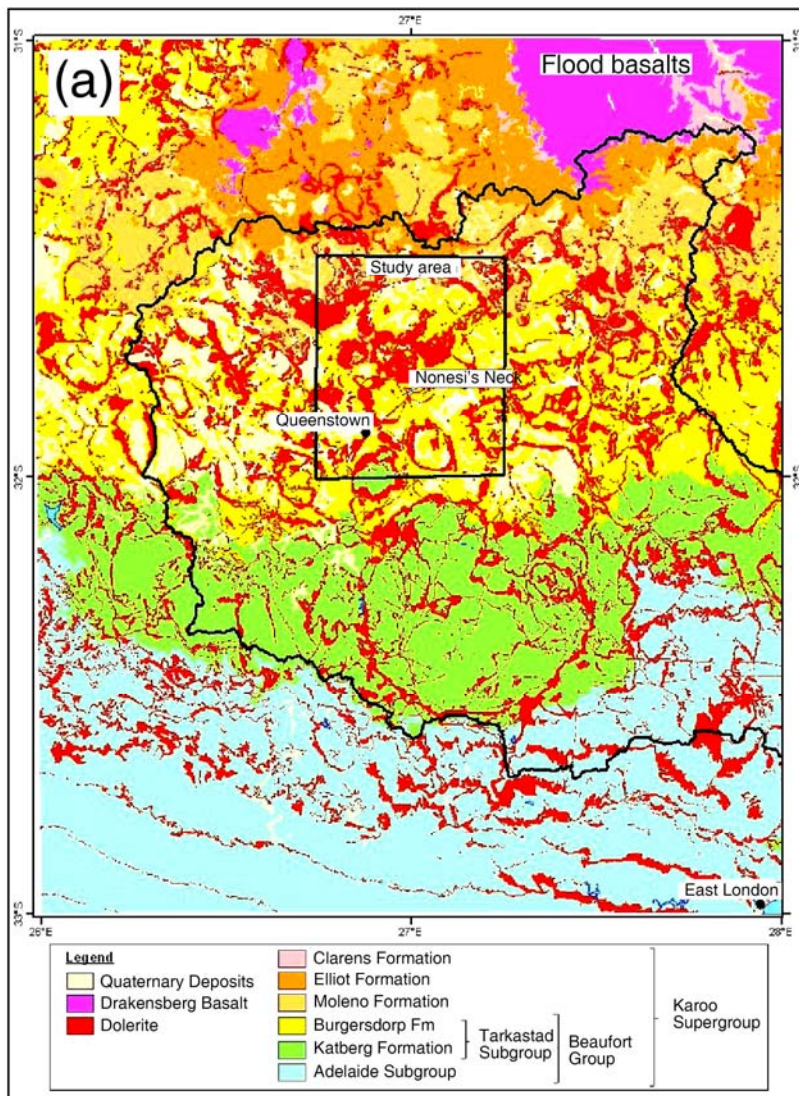


FIG. 9-1. Sill complexes in sedimentary sequences. (a) map of the Karoo flood basalts, sill complexes and underlying sedimentary basin, from Chevallier & Woodford (1990). From south to north the altitude increases and increasing shallower levels of the northward-dipping sequence are exposed. In the lowermost sediments the sill are planar; farther north they form ring-shaped bodies that are the surface expression of saucer-shaped intrusions. (For Fig 9-1b, see next page.)

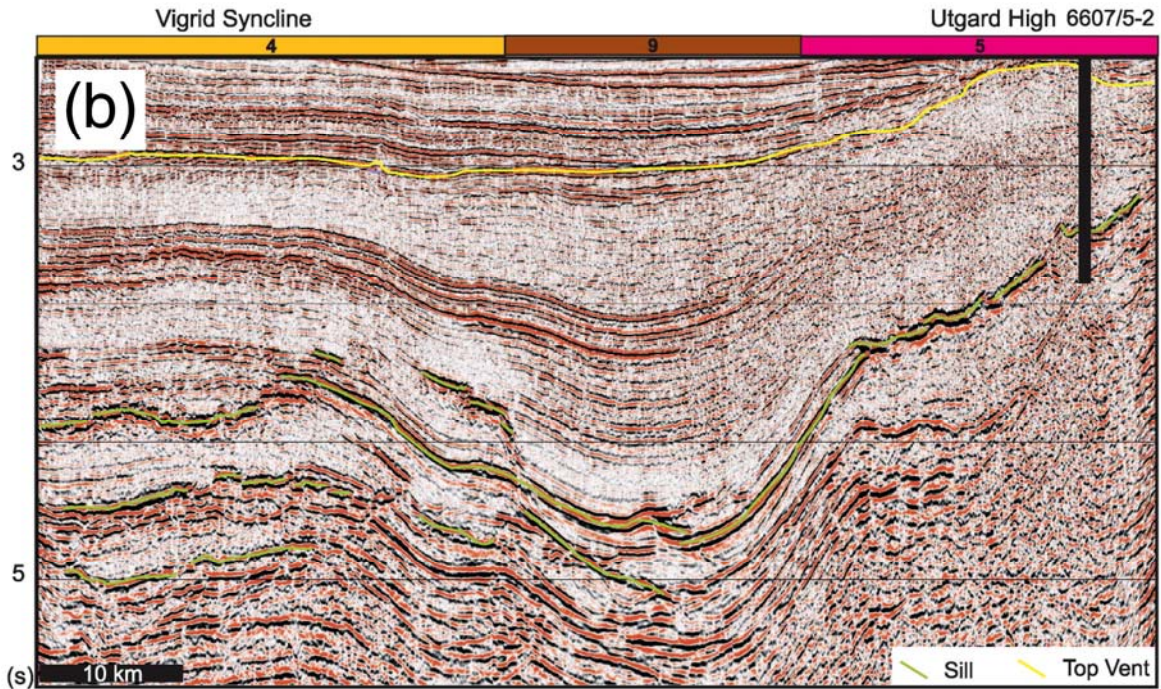


FIG. 9-1b. Interpreted seismic profile through sediments at the rifted margin offshore from Norway, from Planke *et al.* (2004). The sedimentary strata are intruded by numerous conformable, sheet or saucer-shaped intrusions probably of doleritic composition. These intrusions provide an analog for intrusions beneath many magmatic ore deposits.

both magma (primitive and undifferentiated) and crust (granulite facies) are hot and the two should interact. However, because primitive and hot magmas form deep in the mantle, they are strongly S-undersaturated when they reach the crust, and moderate contamination will not cause the separation of a sulfide liquid. Furthermore, the extent of assimilation of crustal material in the magma will be mitigated if the granulite had become depleted in low-temperature components during earlier melting events, making it refractory and difficult to melt. At mid-crustal levels temperatures of both magma and crust are lower, but the wall rocks are more fusible. Magmas in large chambers may assimilate large amounts of granitoid or metamorphic wall rocks. Finally, at shallow levels in a sedimentary sequence, temperatures of magma and wall rocks are still lower, but if the magma flows horizontally along sills within poorly consolidated, easily fusible strata, the amount of assimilation can be large. It is probably in this setting, where magma encounters S-rich rocks, that most magmatic sulfide deposits form.

NORIL'SK-TALNAKH CU-NI-PGE SULFIDE DEPOSITS

The tectonic setting and geologic environment of these deposits have been described in numerous publications (*e.g.*, Naldrett *et al.* 1992, Lightfoot *et al.* 1997, Zen'ko & Czamanske 1994a, 1994b, Czamanske *et al.* 1995, Fedorenko *et al.* 1996, Diakov *et al.* 2002, Yakubchuk & Nikishin 2004) and will only be summarized here. The Noril'sk-Talnakh region is located at the stratigraphic base of the Siberian flood volcanic province, at the rifted margin between the East Siberian craton and the West Siberian sedimentary basin (Fig. 9-2). The volcanic rocks erupted onto the Paleozoic to upper Mesozoic sedimentary rocks that fill the basin, as shown in the stratigraphic sections in Figures 9-3 and 9-4. A thick sequence of intensely deformed upper Proterozoic molasse is overlain by ~12 km of Ediacaran to Carboniferous marine to continental strata and in turn by 3–9 km of carbonates and evaporites. These are capped by the Tunguska series, 20–600 m of Carboniferous to Permian terrestrial coal-bearing sedimentary rocks that directly underlie the Permo-Triassic flood volcanic formations.

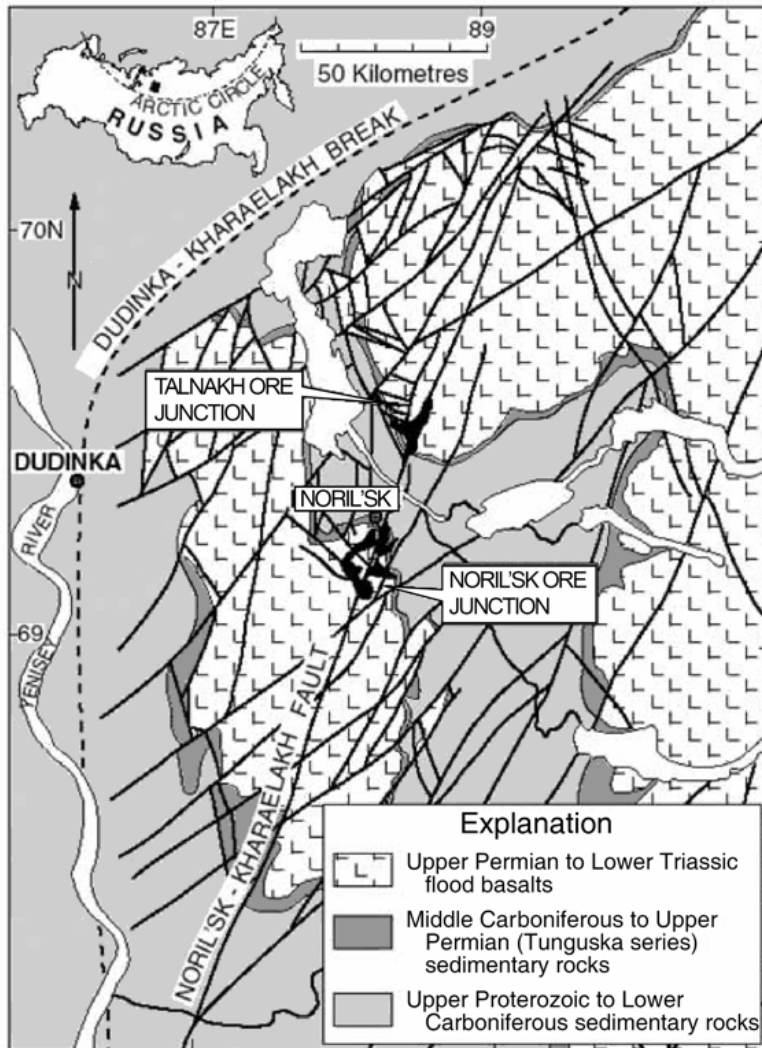


FIG. 9-2. Map of the Noril'sk-Talnakh region showing the locations of the ore deposits and the principal geological features (from Czamanske *et al.* 1994).

The petrological and geochemical characteristics of the volcanic suites are summarized in Figure 9-3 and Table 9-1, using information from Lightfoot *et al.* (1990), Czamanske *et al.* (1995), Wooden *et al.* (1993), and Fedorenko *et al.* (1996). The sequence opens with a Lower Series (or assemblage) of alkaline volcanic rocks whose compositions ranges from picrite through basalt and basanite to trachybasalt. The Middle Series comprises the tholeiitic basalts and picrites of the Tuklonsky Suite and the crust-contaminated basalts of the lower part of the Nadezhdinsky Suite. The Upper Series consists of a monotonous series of moderately contaminated, moderately evolved tholeiitic basalts. For more detailed petrological and geochemical information, see Lightfoot *et al.* (1990), Naldrett *et al.* (1992), Wooden *et al.* (1993),

Fedorenko *et al.* (1996 and references therein).

The ore deposits are located in mafic-ultramafic intrusions emplaced within a few hundred metres of the sedimentary-volcanic contact and largely confined to pronounced elliptical troughs or “volcanic-plutonic depressions”. According to Fedorenko *et al.* (1996) and Diakov *et al.* (2002), these intrusions formed during compensated downwarping of the sedimentary sequences in a shallow-water environment. The downwarping is attributed to release of magma from deeper magma chambers that underlay the depressions. Many of the ore deposits are aligned along a major NNE-trending Noril'sk-Kharaelakh Fault, which, according to most, though not all, authors (see Yakubchuk & Nikishin 2004),

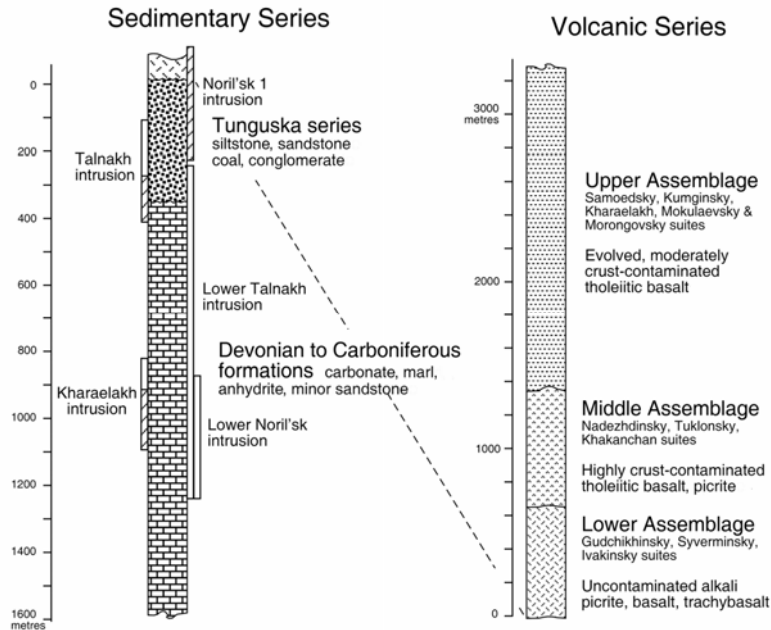


FIG. 9-3. Simplified stratigraphic columns through the sedimentary units underlying the Noril'sk flood volcanic province (left) and through the flood volcanic units themselves (right). The vertical bars on the left show positions of the main ore-bearing and weakly mineralized intrusions. More detail is shown in Zen'ko & Czamanske (1994b) and Czamanske *et al.* (1995), the sources of this diagram.

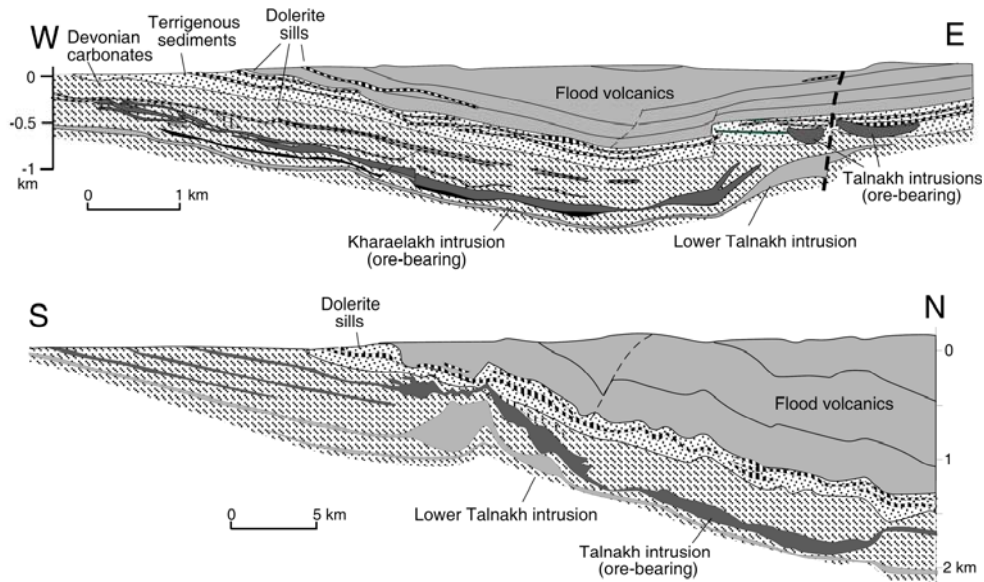


FIG. 9-4. Simplified sections through the sedimentary and volcanic units at Noril'sk-Talnakh (modified from more detailed diagrams in Zen'ko & Czamanske 1994b and Naldrett 2004). Note that the upper diagram is drawn with the vertical scale the same as the horizontal scale (unlike in the original diagram from Zen'ko and Czamanske) but that in the lower diagram, there is a ~2 times vertical exaggeration (as in the original diagram). The sections illustrate the extremely long but thin form of the ore-related intrusions and the abundant intrusions in the sedimentary and volcanic strata overlying the ore horizons.

TABLE 9-1: LITHOLOGICAL AND GEOCHEMICAL CHARACTERISTICS OF FLOOD VOLCANICS

	Suites	Rock types	Geochemical characteristics	Origin
Upper series	Samoedsky, Kumginsky, Kharaelakhsky, Mokulaevsky, upper Morongovsky (Mr2)	Tholeiitic basalt of remarkably uniform composition	Evolved moderately siliceous basalt ($\text{SiO}_2 = 48.5\text{-}50\%$; $\text{MgO} = 6.3\text{-}8.1\%$). Moderate enrichment of incompatible trace elements; negative Nb-Ta anomalies; $\epsilon_{\text{Nd}} \sim 0$.	Moderate crustal contamination of high-degree mantle melts
Middle series	lower Morongovsky (Mr1), Nadezhdinsky, Tuklonsky	Lavas and tuffs of tholeiitic basalt Basalt and picrite	Siliceous basalt ($\text{SiO}_2 = 52\text{-}55\%$; $\text{MgO} = 6.3$ to 8.1%). Moderate to strong enrichment of incompatible trace elements; large negative Nb-Ta anomalies; $\epsilon_{\text{Nd}} \sim 0$ to -11 Basalt ($\text{SiO}_2 = 49\text{-}50\%$; $\text{MgO} = 8\text{-}9\%$); picrite ($\text{SiO}_2 = 47\text{-}49\%$; $\text{MgO} = 10\text{-}17\%$). Moderate enrichment of incompatible trace elements; negative Nb-Ta anomalies; $\epsilon_{\text{Nd}} \sim -1$ to -4.5	Highly contaminated tholeiitic magma Moderately contaminated more primitive magmas
Lower series	Gudchikhinsky, Syverminsky, Ivakinsky	Lavas and tuffs of alkali picrite Lavas and tuffs of alkali trachybasalt and basalt	Basalt ($\text{SiO}_2 = 49\text{-}52\%$; $\text{MgO} = 5.5\text{-}9\%$); picrite ($\text{SiO}_2 = 46\text{-}51\%$; $\text{MgO} = 10\text{-}21\%$). Moderate enrichment of incompatible trace elements; no Nb-Ta anomalies; $\epsilon_{\text{Nd}} \sim -2$ to $+4.6$ Variable compositions ($\text{SiO}_2 = 47\text{-}55\%$; $\text{MgO} = 2.8\text{-}7.5\%$). Variable enrichment of incompatible trace elements; variable Nb-Ta anomalies; $\epsilon_{\text{Nd}} \sim 0$ to -4 .	Relatively uncontaminated moderate-degree mantle melts Relatively uncontaminated low-degree mantle melts

controlled the emplacement of the ore-forming magmas.

Numerous sills, dykes and irregular mafic and ultramafic bodies intruded the volcanic and sedimentary sequence. Estimates of their abundance in the upper part of the sedimentary pile range from 15-30% to as high as 80% (Czamanske *et al.* 1995). Diakov *et al.* (2002) stated that more than 300 intrusions have been mapped in the vicinity of the Noril'sk-Talnakh deposits. In geological maps these intrusions occur in clusters (Fig. 9-5), probably because the majority was emplaced just beneath the now-folded contact between sedimentary and volcanic sequences: most intrusions are found at places where this contact is close to the present erosion level.

The intrusions have been classified in various ways. On the basis of lithology, distribution, form and internal structure Naldrett *et al.* (1992) recognized 5 broad types; Fedorenko (1994), Fedorenko *et al.* (1996) distinguished 15 to 21 types and Diakov *et al.* (2002) identified 9 types. The situation is confused in part because these

classifications represent a somewhat arbitrary subdivision of a highly complex and variable assemblage of igneous bodies, and in part because the terminology and names applied to individual intrusions is not well established but change from paper to paper. Here I adopt a broad classification along the lines proposed in the relatively recent article by Diakov *et al.* (2002) which summarizes information in earlier papers by Naldrett *et al.* (1992), Zen'ko & Czamanske (1994a,b), Czamanske *et al.* (1995), Likhachev (1994), Kunilov (1994), Fedorenko (1994) and Fedorenko *et al.* (1996).

A threefold subdivision is based on the age of the intrusions and their association with the volcanic suites; in the subdivision, intrusions synchronous with the main phase of tholeiitic flood volcanism are distinguished from those that intruded earlier or later (Table 9-2). Pre-tholeiite intrusions such as the Ergalakh complex (also written Yergalakh(sky)) and the North Kharaelakh intrusion are linked to the alkaline volcanism that preceded the tholeiites; another group including the

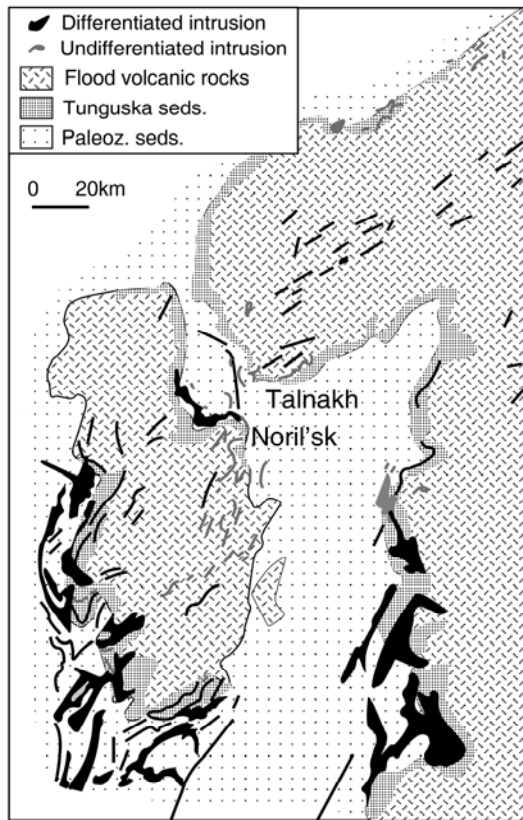


FIG. 9-5. Map of the Noril'sk region showing clusters of intrusions near the contact between the sedimentary and volcanic sequences (redrawn from Yakubchuk & Nikishin 2004).

Oganer and Daldykan mafic intrusions, as well as various more felsic bodies, were emplaced after the flood volcanism. All ore-bearing intrusions fall in the syn-tholeiite group. Three subgroups are identified: (1) differentiated mafic-ultramafic ore-bearing intrusions, referred to as the Talnakh intrusions by Naldrett *et al.* (1992) but called the Noril'sk or ore-bearing type in Czamanske *et al.* (1994), Fedorenko *et al.* (1996) and Diakov *et al.* (2002); (2) differentiated mafic-ultramafic, weakly mineralized intrusions called the Lower Talnakh type; and (3) a variety of other intrusions, some differentiated, others not, some containing disseminated mineralization, others without. The petrological and geochemical characteristics of the more important types are summarized in Table 9-2. Fedorenko *et al.* (1996) correlated the ore-bearing Noril'sk type intrusions with the Morongovsky-Mokulaevsky volcanic suites, which erupted midway through the volcanic pile. The rocks in

these intrusions share certain geochemical characteristics with the volcanic rocks. The slightly older Lower Talnakh type intrusions are correlated with, and share many geochemical features with, the volcanic rocks of the Nadezhdinsky Suite.

The intrusions are elongate and irregular in plan view and sheet-like or U- or tube-shaped in cross section (Figs. 9-4, 9-5; Zen'ko & Czamanske 1994b). In general they are conformable with the sedimentary strata – sills are far more common than dykes. Most intrusions are less than a few hundred metres thick but tens of kilometres long. The Talnakh intrusion, for example, is on average only 120 m thick but can be traced for 15–17 km (Zen'ko & Czamanske 1994b, Diakov *et al.* 2002).

The larger intrusions pinch and swell along strike, both in plan view and cross section. Many contain a thickened central portion (50 to 350 m thick and several km long), flanked by thinner (10-50 m) but more extensive (up to 15 km long) sill-like extensions or apophyses. The ore deposits are confined to basal parts of the thickened central sections. Figure 9-6 is a section through the ore-bearing Kharaelakh intrusion, based on Zen'ko & Czamanske's (1994b) diagram and description. The central portion, about 200 m thick in this intrusion, is differentiated into a lower series of olivine-rich cumulates and an upper series of gabbroic and leucogabbroic rocks. (These relatively fine- to medium-grained hypabyssal rocks are called gabbrodolerite in papers with Russian authors). The flanking apophyses, composed of relatively homogeneous gabbroic rocks, rise to higher stratigraphic levels as they pass outwards and away from the central differentiated bodies. In the volcanic sequence the intrusions are more steeply dipping.

Fedorenko *et al.* (1996), and Diakov *et al.* (2002) used a combination of geological mapping, drill-core logging and gravity, magnetic and seismic surveys to infer that the ore-bearing intrusions were the upper parts of a complex magmatic system that included several deeper staging chambers. The volcano-tectonic depressions that contain most of the ore-bearing intrusions are believed to be connected to a series of intermediate magma chambers located at upper- to mid-crustal depths at 12 to 17 km. According to Yakubchuk & Nikishin (2004), these chambers become broader and more abundant with depth and merge into a single large chamber located about 30–40 km to the north of the Noril'sk-Talnakh region. These intrusions, in turn,

TABLE 9-2: CHARACTERISTICS OF INTRUSIONS IN THE NORIL'SK-TALNAKH REGION

Example	Ore-bearing (Noril'sk type)			Lower Talnakh type
	Kharaelakh	Talnakh	Noril'sk 1	Lower Noril'sk, Lower Talnakh
Position within stratigraphy	In the sedimentary pile, top of intrusion is ~300-600 m below the volcanic contact	In the sedimentary pile, top of intrusion is ~0-500 m below the volcanic contact	Extending from the sedimentary pile into flood volcanics; top of intrusion is ~200 m below to ~200 m above the volcanic contact	Upper 50-600 m of the sedimentary pile, but normally slightly below the ore-bearing intrusions
Host rocks	Dolomite, marl, anhydrite, minor shale and sandstone	Mainly siltstone, sandstone, coals	Siltstone, sandstone, coals and alkali tuff and lava for the Noril'sk 1 intrusion	Dolomite, marl, anhydrite, minor shale and sandstone
Lithology	Picritic - differentiated with olivine-cumulate or taxitic gabbroic lower parts and gabbroic or leucogabbroic upper portions	Picritic - differentiated with olivine-cumulate or taxitic gabbroic lower parts and gabbro or leucogabbro upper portions	Picritic - differentiated with olivine-cumulate or taxitic gabbroic lower parts and gabbroic or leucogabbroic upper portions	Picritic - differentiated with olivine-cumulate lower parts and gabbroic or leucogabbroic upper portions
Size and shape	Three sheet-like branches with subparallel upper and lower contacts; thickness = 260m max, 109m av; 8 km long	Finger-like, straight; upper contact flat, lower contact convex downward; thickness ~220 m max, 120 m av; 100-1000 m wide; 14.5 km long	Finger-like, curved; upper contact concave downward; thickness = 350m max, 147m av; 20 km long	Sheetlike but with pinches and swells; ~ 1 km wide, 30-130 m thick; > 40 km long
Peripheral sills	Olivine gabbro, extending >6.5 km from main intrusion	olivine gabbro, extending 15 km from main intrusion	olivine gabbro, extending 3 km from main intrusion	>40 km

The information in this table is taken from the text and the diagrams in the following papers: Naldrett *et al.* (1992), Zen'ko & Czamanske (1994a,b), Czamanske *et al.* (1995), Likhachev (1994), Kunilov (1994), Fedorenko (1994), Fedorenko *et al.* (1996), Diakov *et al.* (2002).

may be linked to still larger chambers near the base of the crust. Diakov *et al.* (2002) used deep seismic profiles to infer the presence of a Bushveld-sized intrusive complex (~5–12 km thick and ~150 km long) just above the crust-mantle boundary, extending from immediately below the Noril'sk-Talnakh region to the SE and becoming thicker in that direction.

Models for the Formation of Noril'sk-Talnakh Deposits

Most authors accept that the intrusions that

host the Noril'sk-Talnakh deposits are fossil conduits that originally linked deeper magma chambers to the volcanic pile at the surface. According to the ore-formation model proposed by Rad'ko (1991) and developed by Naldrett and co-workers (*e.g.*, Naldrett 1999, 2004, Naldrett *et al.* 1992, 1995, 1996, 2004, Lightfoot & Hawkesworth 1997), picritic magma first assimilated granitoid wall rocks in a mid-crustal magma chamber. The contamination led to the segregation of sulfides that were transported upward in the flowing magma. The droplets of dense sulfide were deposited as the

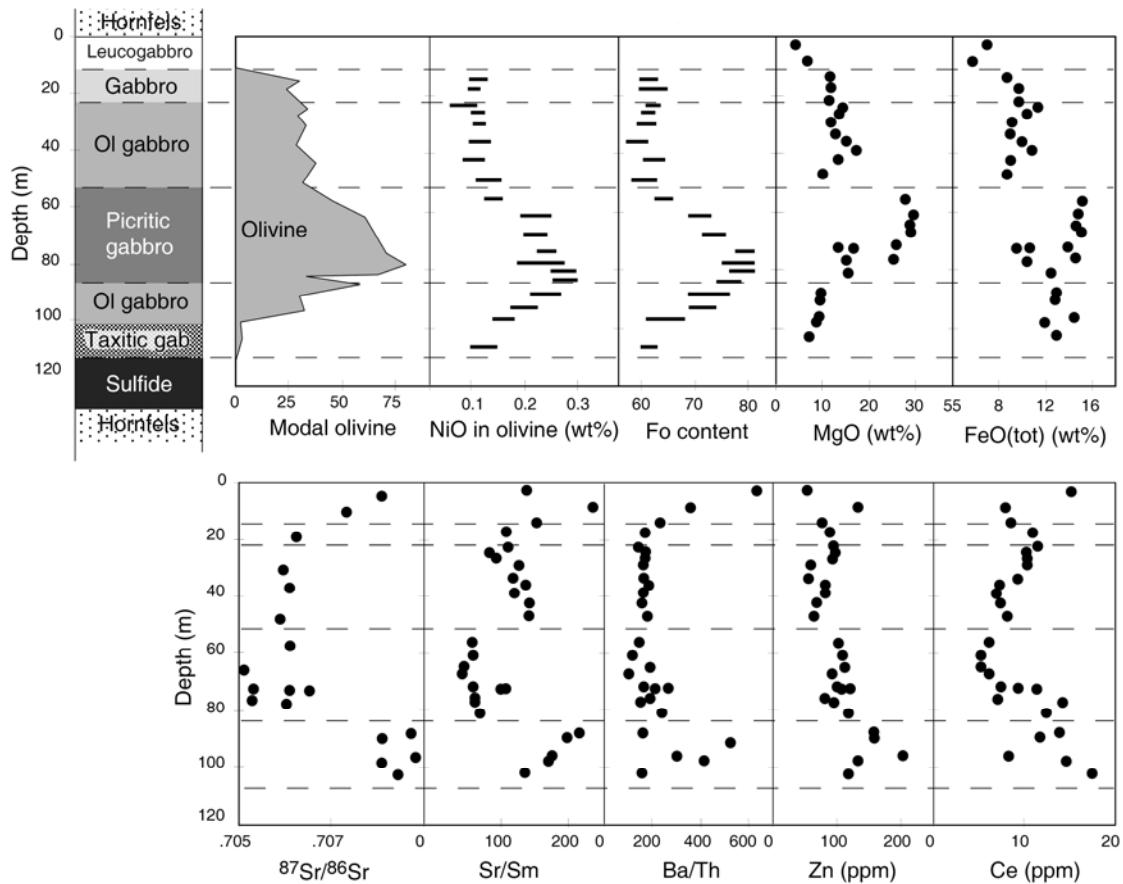


FIG. 9-6. Section through the ore-bearing Kharaelakh intrusion (drill hole KZ-1879), showing variations in rock type, olivine content and composition, and in some geochemical parameters (data from Czamanske *et al.* 1994).

upward velocity of the magma dropped when it entered a horizontal sill. More sulfide then segregated as the magma assimilated sedimentary rocks containing anhydrite (a source of sulfur) and coal (which reduced sulfate to sulfide). The accumulated sulfides interacted with magma flowing through the system, extracting Ni, Cu and PGE to produce high-grade ores. On exiting the conduits, the magmas flowed out onto the surface as flood basalts.

Some authors (*e.g.*, Czamanske *et al.* 1994, 1995, Latypov 2002) have questioned this model, arguing that the magmas that solidified in the ore-bearing intrusions were not directly related to the volcanic rocks. According to them, the intrusions were blind or formed as small-volume injections into the sedimentary sequence. Ore sulfides were injected into these intrusions either in pulses of sulfide-, phenocryst- and clast-charged magma or as sheets of sulfide magma. Arguments used to defend these interpretations depend partly on textural

relations between ore-bearing and unmineralized parts of the intrusions (see Czamanske *et al.* 1995, for example), and partly on compositional differences between intrusive and volcanic rocks.

Differences between the compositions of lavas and intrusive rocks

1. *Phase equilibria constraints.* Latypov (2002) argued that the magma that formed the intrusions had a different crystallization history from the volcanic rocks. His estimated composition of the parental magma of the intrusions is silica-undersaturated and would have crystallized olivine whereas the lavas are silica-saturated and could not have crystallized olivine (Fig. 9-7).
2. *Sulfur isotope ratios.* Ripley *et al.* (2003) showed that $\delta^{34}\text{S}$ isotope values of all lavas fall in the range -5 to $+8$ with a peak around $+2$ (Fig. 9-8). This range is very similar to that of non-mineralized intrusions but very different

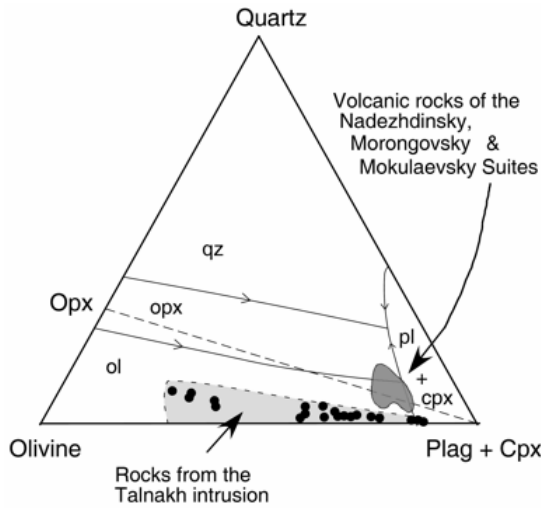


FIG. 9-7. Phase diagrams from Latypov (2002) showing that most samples from the intrusions related to ore deposits are silica-undersaturated and plot in the olivine field whereas as the volcanic rocks are silica-saturated. Latypov (2002) used these data to argue that the volcanic and intrusive rocks were not co-magmatic.

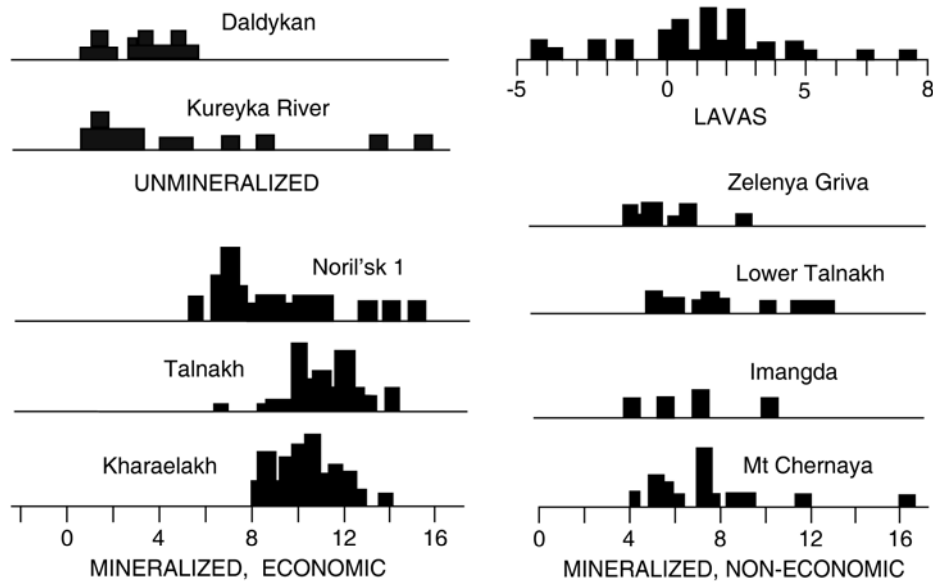


FIG. 9-8. Sulfur-isotope compositions, expressed as ν values, of various types of intrusive and volcanic rock from the Noril'sk region (from Grinenko 1985 and Ripley *et al.* 2003). The lavas show a range of $\delta^{34}\text{S}$ values centred on the mantle value of zero, like those of the unmineralized intrusions. All mineralized intrusions have higher values.

from that of the ore-bearing and weakly mineralized intrusions, which have heavy S isotopic values in the range +5 to +16. These high values, attributed to the assimilation of evaporitic sediment, constitute one of the principal arguments for the conduit model. Just why the high $\delta^{34}\text{S}$ values are missing from the lavas, if these represent magmas that passed through the ore-bearing intrusions, remains unexplained.

3. *Differences in trace-element ratios and isotopic compositions.* Figure 9-9 compares Rb/Sr ratios

and Sr and Nd isotopic compositions of intrusive and volcanic rocks. Although the fields broadly overlap, and although there is an impressive match between the compositions of Lower Talnakh-type intrusions and Nadezhdinsky basalts on one hand, and between ore-bearing intrusions and overlying basalts on the other, some differences remain. The highest Sr isotopic compositions in the intrusive rocks are absent from the lavas, and a population of lavas has a combination of low Rb/Sr, low $^{87}\text{Sr}/^{86}\text{Sr}$ and low ϵNd that is absent from the intrusive rocks.

Many of these apparent inconsistencies can be explained if we take into account the paths followed by the magmas not only *before* they reached the ore-bearing intrusions but also *after* they left the intrusions and flowed onwards towards the surface. In the literature, almost all emphasis has been placed on the magmatic plumbing below or at the level of the ore deposits, for the very good reason that this is where the ores formed. However, the compositions of the volcanic rocks will also be influenced by how the magma interacted with rocks overlying, or along strike, from the ore deposits.

Sills are far more abundant than dykes in the Noril'sk-Talnakh region. Magmas passing

through the sill complexes beneath the flood basalts flowed laterally far farther than vertically. The intrusions of the Noril'sk-Talnakh region are only a few hundreds of metres thick but tens of kilometres long, as shown in sections through the volcanic and sedimentary sequences such as Figure 9-4. This figure also shows numerous "undifferentiated intrusions of various types" (e.g., Zen'ko & Czamanske 1994b) that intruded the Tunguska series, the sequence of terrigenous sedimentary rocks that encloses or overlies the ore-bearing intrusions. At least in part, such intrusions represent a portion of the plumbing system that linked deeper intrusions with the surface. Magma flowing out of

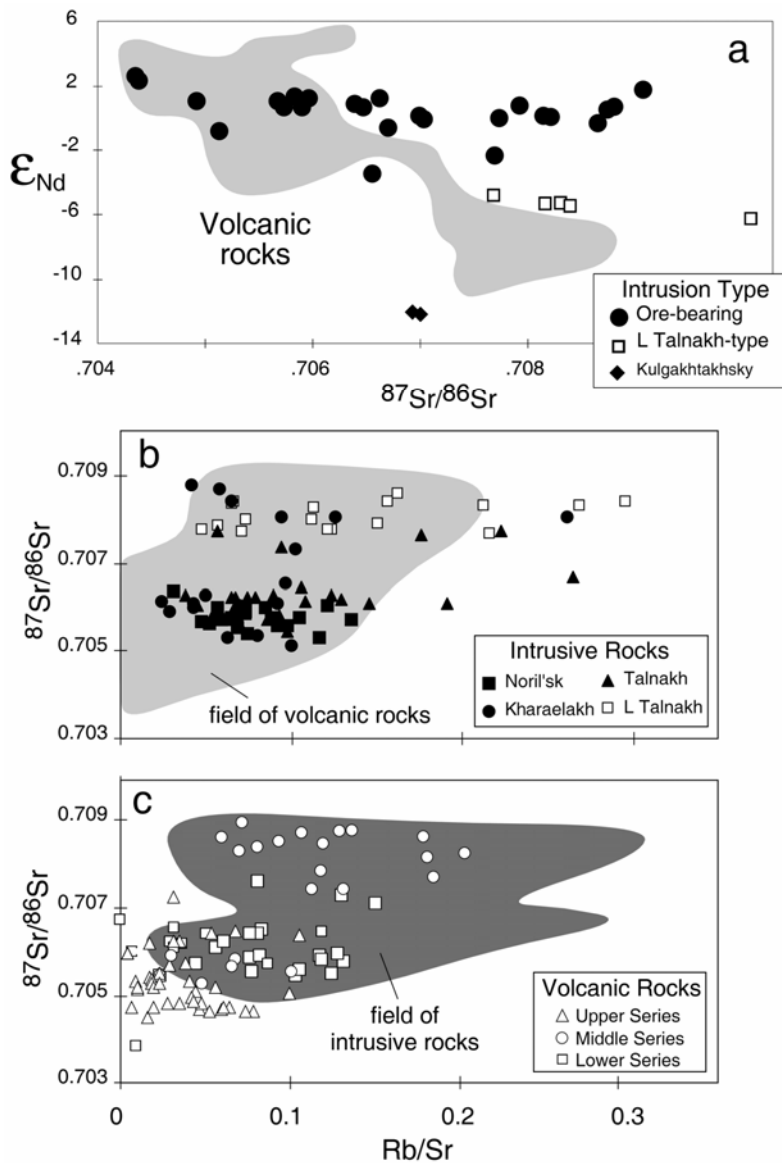


FIG. 9-9. Neodymium and strontium isotopic compositions of intrusive and volcanic rocks from the Noril'sk-Talnakh region (from Wooden *et al.* 1993 and Arndt *et al.* 2003). The fields broadly overlap, but the highest Sr isotopic compositions in the intrusive rocks (Fig. 9b) are absent from the lavas, and lavas from the upper part of the volcanic pile (Fig. 9c) have a combination of low Rb/Sr, low $^{87}Sr/^{86}Sr$ and low ϵ_{Nd} that is absent from the intrusive rocks.

the ore-bearing intrusions interacted first with the Devonian marl, evaporite and carbonate rocks deeper in the sequence, then with terrigenous sedimentary rocks of the 20–600 m thick Tunguska series, and finally with previously erupted volcanic rocks. These volcanic rocks include the entire Lower Series of alkaline volcanic rocks, a volcanic sequence whose thickness varies between 500 and 1000 m in the area of the ore deposits. The magmas passed through many kilometres of sedimentary and volcanic rocks before reaching the surface, and as they did it they would have continued to crystallize and interact with these rocks. In so doing, the composition of erupted magma became different from that of the magma that solidified in the ore-bearing intrusions. In the light of these observations we can reconsider the three points listed above.

Phase equilibria constraints

The mismatch between the compositions of rocks in the intrusions and the erupted lavas is related in part to the shallow-level processes and in part to the nature of the rocks in the intrusions themselves. As shown in Figure 9-6, the compositions of rocks in the intrusions vary widely, from the relatively evolved gabbroic and leucogabbroic rocks that form the uppermost layers in the differentiated intrusions, to the olivine-rich lower cumulates, which have highly mafic to ultramafic compositions. Czamanske *et al.* (1994, 1995) used the presence of abrupt jumps in major and trace element contents and isotope ratios at internal lithological contacts (*e.g.*, MgO, FeO and Sr/Sm at the contact between picritic gabbro and olivine gabbro in Figure 9-6, or $^{87}\text{Sr}/^{86}\text{Sr}$ at the contact between picritic gabbro and taxitic gabbro) to argue that these intrusions are not simple, internally differentiated bodies but instead were filled sequentially by a series of magma pulses. Many of the upper gabbroic rocks probably crystallized directly from gabbroic liquids and have compositions similar to these liquids. The lower olivine-rich rocks, on the other hand, formed from magmas charged with olivine phenocrysts, and their compositions are not those of silicate liquids. The compositions of these rocks, and therefore the average composition of an entire intrusion, are richer in olivine than any of the liquids that passed through the intrusion.

As seen from Figure 9-10, the main difference between the lavas and the intrusions is the presence of MgO- or olivine-enriched rocks in the intrusions. These rocks presumably are the

solidification products of phenocryst-charged, relatively viscous magmas that entered, but did not exit, the chambers. The least mafic, gabbroic and leucogabbroic, rocks in both the ore-bearing intrusions and the Lower Talnakh-type intrusions have compositions broadly comparable to those of the erupted basalts. These probably represent more mobile magmas that transited the chambers on their way to the surface, leaving in the intrusions mafic to ultramafic cumulates deposited from phenocryst-charged magmas. The difference in the extent of silica saturation that troubled Latypov (2002) is therefore due mainly to the presence of the olivine cumulates in the intrusions.

There remain, however, some types of volcanic rocks whose compositions are unmatched in the intrusions. For example, certain basalts in the Nadezhdinsky Suite are more SiO₂-rich and MgO-poor, and more Si-saturated than any analyzed sample from the intrusions (Fig. 9-10). There are two possible explanations for these differences; (1) magmas with these compositions bypassed the intrusions, or if they did pass through them, they did not solidify to form part of the layered sequence; (2) as the magmas flowed onward through the sedimentary and volcanic strata overlying the chambers, they continued to crystallize olivine and assimilate their wall rocks, processes that enhanced the differences between the compositions of the intrusive and volcanic rocks.

S isotope ratios

The systematic differences in S isotope composition between lavas and rocks in the mineralized intrusions (Fig. 9-9) might also be explained by shallow-level magma–rock interaction. Although no S isotope data are available (to my knowledge) for the sedimentary rocks of the Tunguska suite, these terrigenous sedimentary rocks should have had a wide range of compositions, including negative $\delta^{34}\text{S}$ values in pyrite-bearing sedimentary rocks. Data from Ripley *et al.* (2003) show that the alkali volcanics of the Ivakinsky, Syverminsky and Gudchikhinsky Suites have a large range of $\delta^{34}\text{S}$ values, including many negative values, and that some of the lavas have very high S contents (up to 1393 ppm). During the movement of magma within horizontal sills in the sedimentary and volcanic strata, the incorporation of sulfur from sedimentary and volcanic wall rocks may have effaced the heavy S isotopic signature of evaporite assimilation.

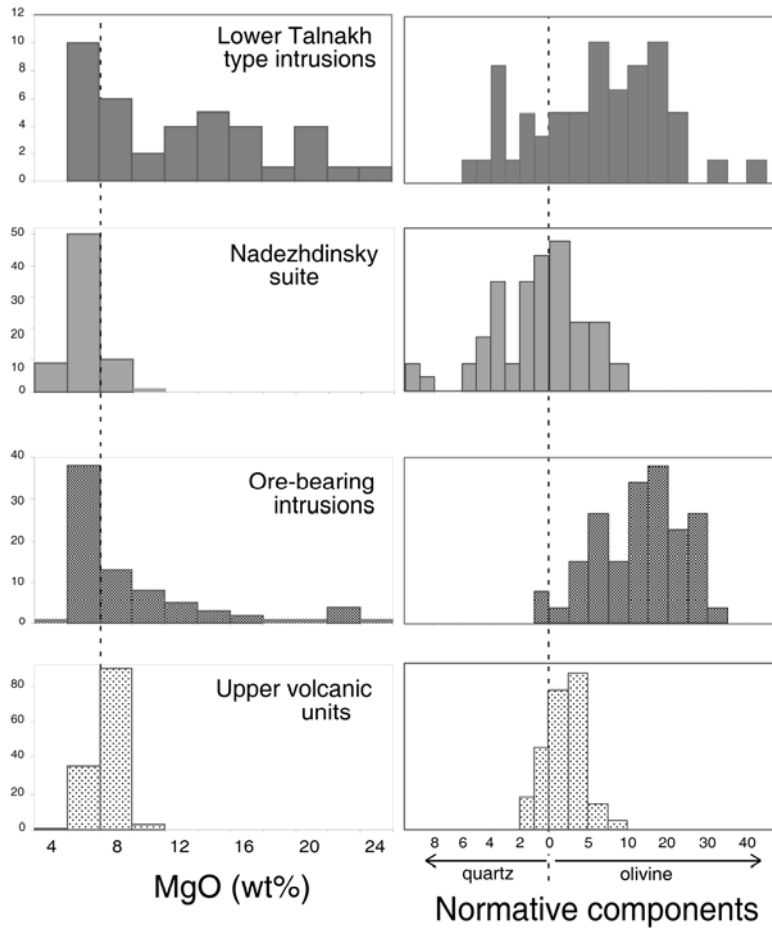


FIG. 9-10. Histograms showing the ranges of MgO and extent of silica saturation in intrusive and volcanic rocks. The intrusions have a wider range in compositions extending to more magnesian, olivine-normative compositions; these compositions are those of the olivine-enriched lower portions of the intrusions. The gabbroic and leucogabbroic upper portions of the intrusions have compositions broadly comparable to those of the volcanic rocks. The only exception is several basalts from the Nadezhdinsky suite, which are more silica-saturated than any of the intrusive rocks. (Data from Czamanske *et al.* 1994, 1995, Arndt *et al.* 2003, and unpublished data).

Differences in trace element ratios and isotopic compositions

The mismatches in Rb/Sr and radiogenic isotopes are more difficult to explain. Although compositions for Tunguska sedimentary rocks appear not to have been published, we can infer their likely characteristics. Like other Mesozoic continental sedimentary rocks, they probably had relatively high $^{87}\text{Sr}/^{86}\text{Sr}$ (about 0.715), low ϵNd (around -10) and high Rb/Sr. From published analyses, we know that most of the overlying alkali volcanic rocks are more “isotopically depleted” with lower $^{87}\text{Sr}/^{86}\text{Sr}$ (0.7045–0.7065), higher ϵNd (0 to $+5$, but with several samples around -4) and relatively low Rb/Sr. Interaction between ascending magma and sedimentary or volcanic rocks would superimpose a range of compositions that fall on the dominant array in Fig. 9-9, eliminating or diluting the high $^{87}\text{Sr}/^{86}\text{Sr}$, moderate ϵNd signature acquired through interaction with evaporitic sediments. Nonetheless, it remains unlikely that such interaction can explain the entire range of

compositions of rocks in the flood volcanic sequence. The particular combinations of low $^{87}\text{Sr}/^{86}\text{Sr}$ at a given ϵNd , and low Rb/Sr in rocks with low $^{87}\text{Sr}/^{86}\text{Sr}$ (Fig. 9-9) are not readily explained by shallow-level interaction. One possible explanation for these characteristics, which are conspicuous in lavas of the upper volcanic series, is the assimilation of lower crustal granulites. Perhaps the magmas that erupted to form the Upper Series followed a path to the surface that bypassed shallow-level magma chambers. As with the highly silica-saturated Nadezhdinsky basalts, these flood basalts apparently followed different paths from those of the magmas that fed the ore-bearing intrusions.

Magmatic Plumbing of the Noril’sk-Talnakh System

On the basis of the observations and arguments given above, the following picture of the magmatic plumbing system of the Noril’sk-Talnakh region can be developed. As illustrated in Figure

9-11, the magmas that formed the ore deposits and/or fed the flood volcanics followed a complex series of pathways as they moved from their mantle source to the surface. They transited a series of magma chambers of various sizes and forms: through some they passed rapidly, in others they stalled and crystallized and interacted with their wall rocks. Most of these magma chambers were sill-like, and, at least in the upper sedimentary series, most of the conduits between these sills were largely conformable. Magma rising through the system flowed far farther laterally than vertically.

Some magma passed rapidly through the system and interacted little with the wall rocks. This was the case for the alkali magmas (meimechite, picrite, basalt) of the Kotui River region whose high volatile contents reduced their densities and drove them quickly to the surface (Arndt *et al.* 1998, 2003). In this region, magmas of the alkali and tholeiitic series erupted synchronously, indicating that the two types of magma, which formed under very different conditions in the mantle, followed independent pathways to the surface.

In the Noril'sk-Talnakh region, the alkali magmas of the Lower Series (Fig. 9-3) erupted

rapidly with little interaction with the crust. Tholeiitic magmatism started with the picrite and basalt of the Tuklonsky suite. These magmas stalled in a mid-crustal magma chamber where they assimilated granitoid wall rocks and acquired their distinctive chemical signatures, and where they segregated sulfides. Although many authors believe that these sulfides were subsequently transported to shallower levels to form part of the ore deposits, it is equally possible that, as shown in Figure 9-11, they remained where they formed, at deep levels inaccessible to mining. Magmas escaping the mid-crustal chambers ascended to the surface, forming Lower Talnakh-type intrusions and erupting as lavas of the Nadezhdinsky Suite.

Other picritic magmas bypassed the mid-crustal chambers and arrived at the level of evaporitic sedimentary rocks with their full complement of ore metals. As they flowed through sills within the sedimentary strata, they assimilated anhydrite and segregated sulfide, as in the Naldrett-Lightfoot model. Although Naldrett (2004) suggested that assimilated coal reduced sulfate to sulfide, the ore-bearing Kharaelakh is emplaced stratigraphically below the coal-bearing Tunguska

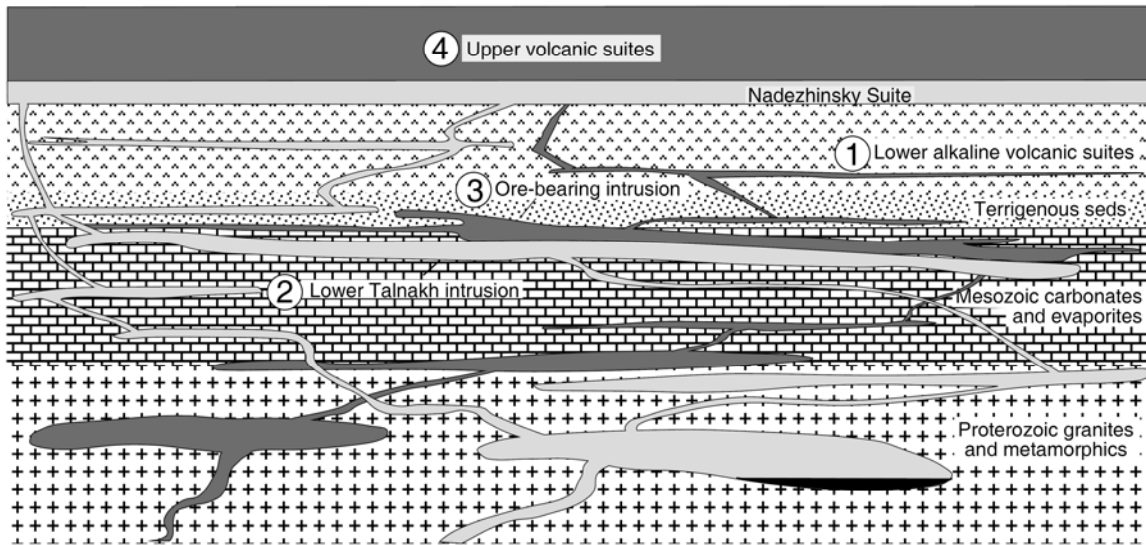


FIG. 9-11. Sketch showing the possible plumbing of the Noril'sk intrusions and volcanic rocks. The diagram illustrates a four-stage model for the formation of the magmatic sequence. (1) Eruption of the Lower Series of alkali volcanics into a sedimentary basin. (2) Lower Talnakh-type magmas first entered deep staging chambers where they interacted with granitic rocks and separated sulfide liquid. The sulfide liquid remained in the chamber while the silicate liquid rose through a complex series of sills and conduits, forming the Lower Talnakh intrusion, then interacting with sedimentary and volcanic strata before erupting as the Nadezhdinsky basalts. (3) The magmas that formed the ore deposits followed a separate pathway, arriving only slightly contaminated at the level of evaporites. They assimilated these rocks, formed the ore deposits, then continued to the surface to erupt as the lower part of the Upper Series. (4) Later magmas bypassed these chambers to erupt as the main sequence of the upper volcanic series.

series (Fig. 9-3 and Czamanske *et al.* 1995). It is more probable, therefore, that the reductant was organic matter in the Devonian carbonates (which correlate with source rocks of the giant west Siberian oil and gas fields). Following interaction with these sedimentary rocks, the evolved magma continued to the surface, crystallizing more olivine and reacting with terrigenous sedimentary rocks and previously erupted lavas, a process that effaced some of the geochemical signatures of ore formation. Subsequent magmas followed separate paths to the surface and erupted as the Upper Series of flood basalts.

ORE DEPOSITS OF THE BUSHVELD COMPLEX

The chromite, magnetite and arguably the PGE deposits of the Bushveld Complex are type examples of magmatic deposits. The overall characteristics of these deposits and their host intrusion are very different from the Noril'sk-Talnakh deposits. Descriptions of the Bushveld deposits are found in every text on economic geology and in numerous papers (*e.g.*, Campbell *et al.* 1983, Eales & Cawthorn 1996, Mathez *et al.* 1997, Wilson *et al.* 1999, Barnes & Maier 2002) and I will not repeat this information. Instead, I will

compare what we know of the magmatic plumbing of the Bushveld Complex with that inferred for the Noril'sk-Talnakh deposits.

The Bushveld Complex is much larger than the intrusions that host the Noril'sk-Talnakh deposits. As presently exposed (Fig. 9-12), it is over 200 km long, 150 km wide, and up to 9 km thick; it occupies nearly a quarter of the total thickness of the crust. The ore deposits occur as magmatic strata, albeit of unusual composition, and in terms of their overall form and origin, they constitute an integral part of the magmatic architecture of the complex. Unlike the Noril'sk-Talnakh ores, in which sulfide ores make up a disproportionately large part of the total mass of their host intrusions, the Bushveld ores represent only a minute fraction of the total mass of the complex.

Despite these differences, the processes that led to the formation of the deposits may not have been very different. The rocks of the Bushveld Complex have mineralogical and chemical compositions that are very different from those of mafic-ultramafic rocks from oceanic settings. Most of the ultramafic cumulates in the lower part of the intrusion contain orthopyroxene and not olivine as the dominant phase. Phlogopite and hydrous minerals are present in small but variable amounts

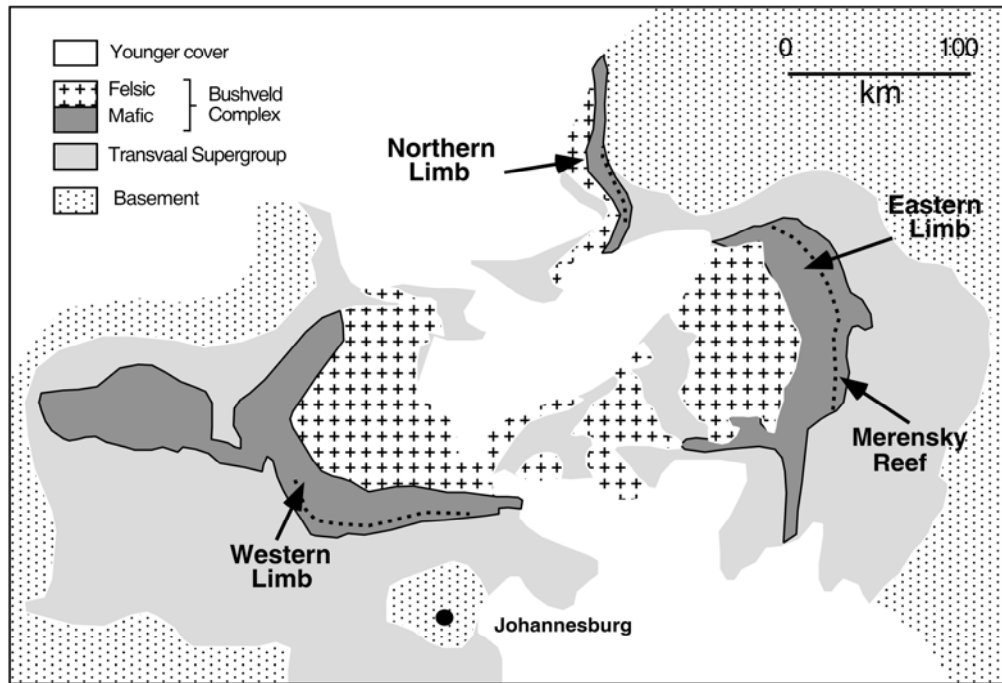


FIG. 9-12. Sketch map of the Bushveld Complex.

throughout the complex. In most samples, SiO₂ and K₂O contents are higher than in ultramafic or mafic rocks from intrusions in other settings. Trace-element patterns are distinctive: in mantle-normalized diagrams (Fig. 9-13), the more incompatible elements are strongly enriched and there are pronounced negative Nb-Ta and positive Pb anomalies (e.g., Maier *et al.* 2000). Also distinctive are the Sr-, Nd and Os isotopic compositions (Kruger 1994, Maier *et al.* 2000, McCandless & Ruiz 1991). As shown in Figure 9-12, rocks from the Bushveld complex have very low, but relatively uniform ϵ Nd values, and high but variable ⁸⁷Sr/⁸⁶Sr. Finally, the oxygen isotope ratios of Bushveld rocks are significantly higher than those of uncontaminated mantle-derived magma (Harris *et al.* 2004). These characteristics correspond to those of a “continental crustal component” which can be acquired either through the assimilation of crustal wall rocks or through partial melting of a source contaminated with crustal material.

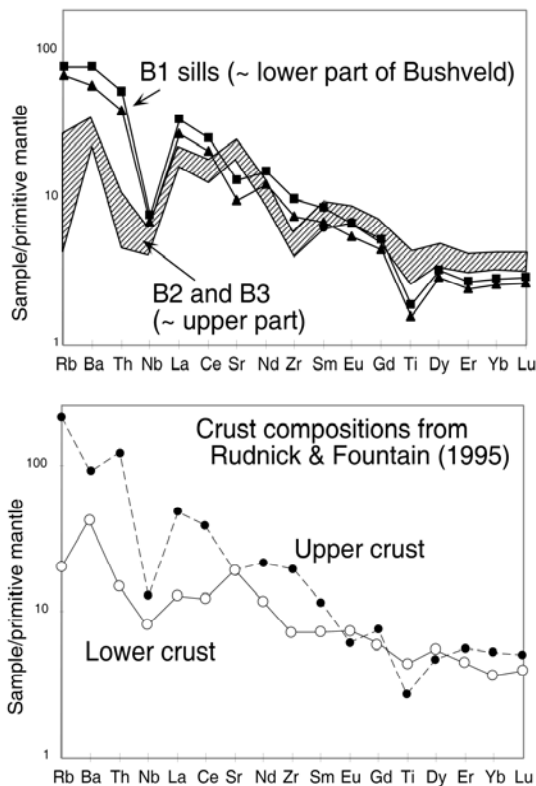


FIG. 9-13. Trace-element compositions, normalized to primitive mantle of Hofmann (1989) of the peripheral sills to the Bushveld complex.

Certain authors have suggested that the magmas parental to the Bushveld Complex were boninitic (see discussion by Barnes 1989), having been derived through partial melting of lithosphere that had been metasomatized during subduction. Figure 9-14 shows, however, that the isotopic compositions of Bushveld rocks are very different from those of boninites and are more like those of the crust-contaminated Nadezhdinsky suite from Siberia. Maier *et al.* (2000) attributed the combination of low but constant ϵ Nd values, and high but variable ⁸⁷Sr/⁸⁶Sr, to assimilation of crustal rocks. Rocks from the lower continental crust have lower Rb/Sr than rocks of the upper crust, but their Sm/Nd ratios are similar. Because the half-life of ¹⁴⁷Sm is far longer than that of ⁸⁷Rb, the Sm-Nd system evolves more slowly than the Rb-Sr system. At the time of intrusion of Bushveld lavas (2.1 Ga), continental crust of the 3.0-3.5 Ga Kaapvaal Craton, which encloses the Bushveld Complex, would have had a wide range of ⁸⁷Sr/⁸⁶Sr (low in the lower crust and high in the upper crust) and a more restricted range of ¹⁴³Nd/¹⁴⁴Nd. Many magmas in ocean basins and subduction zones form in the presence of garnet, a mineral that strongly fractionates Sm/Nd. Old reservoirs in the convecting mantle have wide ranges in both ⁸⁷Sr/⁸⁶Sr and ¹⁴³Nd/¹⁴⁴Nd, the so-called mantle array. As seen in Figure 9-14, boninites fall on this array, but rocks from the Bushveld Complex do not. Instead, they form a trend oblique to the mantle array, a trend of variable ⁸⁷Sr/⁸⁶Sr at near-constant ¹⁴³Nd/¹⁴⁴Nd that is consistent with assimilation of rocks from old continental crust.

In general, therefore, the unusual compositions of rocks in the Bushveld can be attributed to high levels of crustal contamination. To explain ϵ Nd values around -7 , Maier *et al.* (2000) proposed that the magma assimilated between 20-40% of material from the lower and upper crust, a figure confirmed by oxygen isotope data by Harris *et al.* (2004). The crustal signature persists from base to top of the complex, suggesting that the magmas became contaminated before they entered the Bushveld magma chamber. The amount of chromite in massive seams in the lower part of the complex is enormous. Eales & Cawthorn (1996) have calculated that the chromite in each seam must have been extracted from many times its mass of silicate magma. It appears that this chromite was extracted from a large volume of magma that flowed through, then out of the Bushveld Chamber.

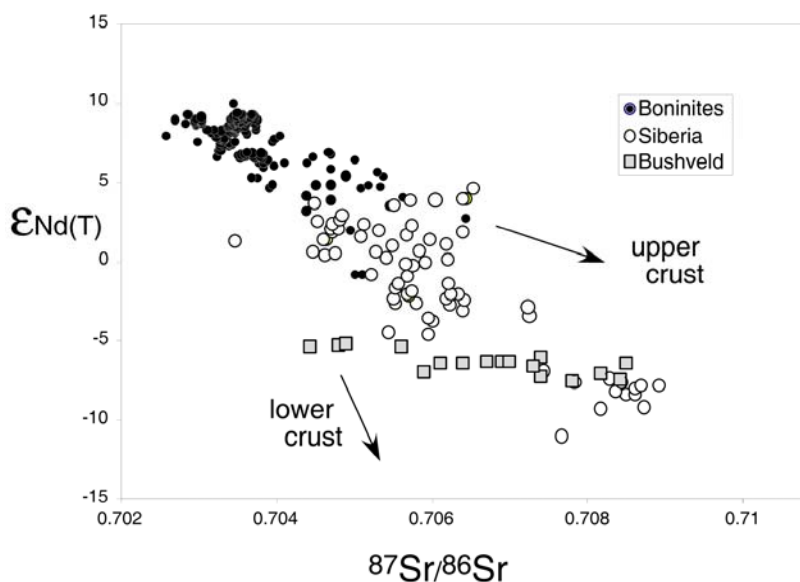


FIG. 9-14. Neodymium- and strontium-isotopic compositions of boninites (data from the GEOROC data base <http://georoc.mpch-mainz.gwdg.de/georoc/>), of Siberian flood basalts (Wooden *et al.* 1993) and rocks from the Bushveld Complex (Maier *et al.* 2000).

The picture emerges of a dynamic system comprising a lower chamber or chambers in which mantle-derived magma became contaminated with crustal rocks, and of a Bushveld intrusion that acted as a conduit between a deeper staging chamber and the surface. Although mafic volcanic rocks of Bushveld age are known in the Rooiberg Formation, their volume is small compared with that of the Bushveld Complex. Evidently most of the erupted products of the Bushveld system have been lost. Part could simply have flowed away and off the continent (like the large volumes of flood basalt off shore from the Deccan Traps in India), and part could have been removed by erosion.

The Role of Crustal Structure in Ore Formation and a New Classification of Deposits

The two examples considered above represent ore deposits that formed at different levels in the crust. The Noril'sk-Talnakh deposits are an example of mineralization that developed at very shallow levels in the crust, near the top of a sedimentary pile and just below, or at the very base, of the volcanic sequence. Other examples of this type include the Raglan deposits in northern Quebec (Leshner *et al.* 1999, Leshner & Keays 2002), and the Pechenga deposit in the Kola Peninsula of Russia (Barnes *et al.* 2001, Naldrett 2004). In all these deposits, ore formation is believed to have been triggered by the assimilation of sedimentary rock by magma flowing through shallow-level, concordant, highly elongate sills. At Bushveld and in other deposits such as Voisey's Bay, ore formation took

place at deeper levels in the crust. The assimilated material was metasedimentary or granitoid, and the magmas flowed upwards through steeply dipping conduits before erupting into magma chambers where the sulfides were deposited (Li & Naldrett 1999). The status of the Jinchuan deposit in China is uncertain: if the host intrusion is a near-vertical, discordant, trumpet-shaped body as in the models of Tang (1995) and Chai *et al.* (1992), it could be classed with Bushveld and Voisey's Bay; if it is a near-horizontal sill, as proposed by de Waal *et al.* (2004), it could be classed together with the Noril'sk deposits. Distinction between the two alternatives awaits more detailed study of contact relations between the intrusion and its wall rocks.

The subdivision into shallow- and deep-level deposits provides clues as to the manner in which magma flows through and interacts with its wall rocks. Magma ascending through a steeply dipping dyke may or may not interact with its wall rocks, depending on the width of the dyke, the flow rate and the physical and chemical characteristics of magma and wall rock. In a deep crustal setting, much of the interaction probably takes place in large, relatively static magma chambers, particularly at the top of the chamber where the rocks melt or are stoped into the magma reservoir. If this contamination leads to sulfide segregation, sulfides accumulate at the floor of the chamber. They may then be remobilized by the influx of new magma into the chamber, or unconsolidated sulfide-crystal mushes might be squeezed from the chamber during deformation. Or they may stay where they formed,

at depths inaccessible to mining.

In the near-surface setting, the controls on magma dynamics are very different. Flowage through a sill complex in the sedimentary strata beneath the volcanic pile is largely horizontal. The form and dimensions of the intrusions are strongly influenced by the heterogeneous stress regime, by horizontal planes of weakness between the sedimentary units and the elastic strength of the sedimentary rocks. These parameters change dramatically with increasing depth in the sedimentary pile as lithostatic pressure increases and becomes more homogeneous and as the rocks become more consolidated. The similar stratigraphic position of the Noril'sk-Talnakh, Raglan and Pechenga deposits – in the uppermost part of the sediment pile – probably is related to the local environment in the sedimentary pile. The process of sulfide segregation, upgrading and accumulation that gives rise to an ore deposit may well be linked to the manner in which magma flows through the sill complexes and interacts with the enclosing sedimentary rocks.

Planke *et al.* (2004) observed changes in the form and dimensions of intrusions in sedimentary strata beneath flood basalts and in volcanic rifted margins, from layer-parallel, sheet-like intrusions deep in the sequence and in unconsolidated sediments near the surface, to smaller, saucer-shaped or irregular intrusions at intermediate depths. They described how the form, size and abundance of intrusions are strongly influenced by structures and heterogeneities such as fault zones, layering and deformed strata. The rate of magma flow is linked to the thickness and continuity of the intrusions, which change with distance to the surface (Planke *et al.* 2000, 2004). In layer-parallel sills, flow will be rapid and perhaps turbulent; and turbulent flow results in thermo-mechanical erosion and enhanced assimilation of wall rocks that leads to the formation of a sulfide liquid. In thicker parts of sills, which may result from disturbed flow in regions of weaker rocks in fault zones, the flow rate decreases, resulting in sedimentation of transported sulfide (and crystals and rock fragments). Magma might erode, assimilate and segregate sulfide liquid as it flows near-horizontally through sills at moderate depths, then deposit the sulfides when it steps up to shallower stratigraphic levels or when it encounters weaker rocks in fault zones. Pulsed flow of magma through the sills could result in remobilization and re-deposition of sulfide-crystal mixtures. Such a

process provides explanations for the specific stratigraphic level of deposits such as Noril'sk-Talnakh, Raglan and Pechenga, and the spatial association between the Noril'sk-Talnakh deposits and the Noril'sk-Kharaelakh fault.

These ideas have evident application to the exploration for Noril'sk-Talnakh-type deposits. Rather than basing such exploration solely on lithology and chemistry of the magmatic rocks and on the present structure of the region (which normally is controlled by post-ore deformation), consideration should be given to the dynamics of flow in the sub-surface sedimentary environment.

CONCLUSIONS

- The magmas that formed the Noril'sk-Talnakh deposits passed through a complex plumbing system before reaching the surface. Volatile-rich, low-density alkali magmas passed rapidly to the surface, interacting little with wall rocks. Dense, volatile-poor tholeiitic picritic magmas interacted with wall rocks, and sulfides segregated because of this interaction.
- The host intrusions were broadly co-magmatic with the lava series; the conduit model is broadly correct. However, each batch of magma followed a separate path to the surface and had a different history of contamination and sulfide segregation. Shallow-level partial crystallization and wall-rock interaction influenced the compositions of erupted lavas and produced some differences between the composition of rocks in ore-bearing intrusions and those of erupted lavas. Magmas of the Lower Talnakh-type intrusions and the Nadezhdinsky suite assimilated granitic crust in a deep magma chamber. Although sulfide segregated as a result of this interaction, it is possible that this sulfide remained where it formed and does not constitute part of the ore deposits.
- Ore formation took place as magma assimilated anhydrite-rich sedimentary rocks in the near-surface sill complex in the upper levels of the sediment pile. The stratigraphic position of deposits such as Noril'sk-Talnakh, Raglan and Pechenga may be related to the dynamics of magma flow in this sub-surface sedimentary setting.
- The Bushveld Complex formed as a large, open-system magma chamber in the middle to upper crust. The compositions of magmas entering the chamber were strongly influenced by crustal contamination in deeper staging chambers. The

formation of ore deposits may be related to this deep-level contamination and not to processes within the Bushveld chamber itself.

REFERENCES

- ARNDT, N.T., CHAUVEL, C., FEDORENKO, V. & CZAMANSKE, G. (1998): Two mantle sources, two plumbing systems: tholeiitic and alkaline magmatism of the Maymecha River basin, Siberian flood volcanic province. *Contrib. Mineral. Petrol.* **133**, 297-313.
- ARNDT, N.T., CZAMANSKE, G., WALKER, R.J., CHAUVEL, C. & FEDORENKO, V. (2003): Geochemistry and origin of the intrusive hosts of the Noril'sk-Talnakh Cu-Ni-PGE sulfide deposits. *Econ. Geol.* **98**, 495-515.
- BARNES, S.J. (1989): Are Bushveld magmas boninites or contaminated komatiites? *Contrib. Mineral. Petrol.* **101**, 447-457.
- BARNES, S.-J. & MAIER, W.D. (2002): Platinum-group element distribution in the Rustenburg layered suite of the Bushveld Complex, South Africa. In *The geology, geochemistry, ogy and mineral beneficiation of platinum-group elements*, L.J. Cabri (ed.). *Can. Inst. Mining, Metall. Petroleum, Spec Vol* **54**, 431-458.
- BARNES, S.-J., MELEZHIK, V.A. & SOKOLOV, S.V. (2001): The composition and mode of formation of the Pechenga nickel deposits, Kola Peninsula, northwestern Russia. *Can. Mineral.* **39**, 447-471
- BRÜGMANN, G. E., NALDRETT, A. J., ASIF, M., LIGHTFOOT, P. C., GORBACHEV, N. S. & FEDORENKO, V. A. (1993): Siderophile and chalcophile metals as tracers of the evolution of the Siberian trap in the Noril'sk region, Russia. *Geochim. Cosmochim. Acta* **57**, 2001-2018.
- CAMPBELL, I.H., NALDRETT, A.J. & BARNES, S.-J. (1983): A model for the origin of the platinum-rich sulfide horizons in the Bushveld and Stillwater Complexes. *J. Petrol.* **24**, 133-165.
- CHAI, G. & NALDRETT, A.J. (1992): Characteristics of Ni-Cu-PGE mineralization and genesis of the Jinchuan Deposit, Northwest China. *Econ. Geol.* **87**, 1475-1495
- CHEVALLIER, L. & WOODFORD, A. (1999): Morphotectonics and mechanism of emplacement of the dolerite rings and sills of the western Karoo, S Africa. *S. Afr. J. Geol.* **102**, 43-54.
- COX, K. G. (1980): A model for continental flood vulcanism. *J. Petrol.* **21**, 629-650.
- CZAMANSKE, G. K., WOODEN, J. L., ZIENTEK, M. L., FEDORENKO, V. A., ZEN'KO, T. E., KENT, J., KING, B. S., KNIGHT, R. L. & SIEMS, D. F. (1994): Geochemical and isotopic constraints on the petrogenesis of the Noril'sk-Talnakh ore-forming system. In *Lightfoot, P. C. & Naldrett, A. J. (eds.) Proceedings of the Sudbury-Noril'sk Symposium*, Sudbury, Ontario Geological Survey, 313-342.
- CZAMANSKE, G. K., ZEN'KO, T. E., FEDORENKO, V. A., CALK, L. C., BUDAHN, J. R., BULLOCK, J. H., JR., FRIES, T. L., KING, B. S. & SIEMS, D. F. (1995): Petrography and geochemical characterization of ore-bearing intrusions of the Noril'sk type, Siberia; with discussion of their origin. *Resource Geology Special Issue* **18**, 1-48.
- DE WAAL, S.A., XU, Z., LI, N.C., MOURI, H. (2004): Emplacement of viscous mushes in the Jincuan ultramafic intrusion, western China. *Can. Mineral.* **42**, 371-392.
- DIAKOV, S., WEST, R., SCHISSEL, D., KRIVTSOV, M.L., KOCHNEV-PERVUKHOV, V. & MIGACHEV, I. (2002): Recent advances in the Noril'sk Model and its application for exploration of Ni-Cu-PGE sulfide deposits. *Soc. Econ. Geologists, Spec. Publ.* **9**, 203-226.
- EALLES, H.V. & CAWTHORN, R.G. (1996): The Bushveld Complex. In *Cawthorn, R.G. (ed.) Layered Intrusions*, Amsterdam, Elsevier, 181-230.
- FEDORENKO, V. (1994): Evolution of magmatism as reflected in the volcanic sequence of the Noril'sk region. In *Lightfoot, P. C. & Naldrett, A. J. (eds.) Proceedings of the Sudbury-Noril'sk Symposium*, Sudbury, Ontario Geological Survey, **5**, 171-183.
- FEDORENKO, V.A., LIGHTFOOT, P.C., NALDRETT, A.J., CZAMANSKE, G.K., ZEN'KO, T.E., HAWKESWORTH, C.J., WOODEN, J.L. & EBEL, D.S. (1996): Petrogenesis of the flood-basalt sequence at Noril'sk, North Central Siberia. *International Geological Review* **38**, 99-135.
- GRINENKO, L.N. (1985): Sources of sulfur of the nickeliferous and barren gabbro-dolerite intrusions of the northwest Siberian platform. *Internat. Geol. Rev.* **28**, 695-708.

- HARRIS, C., PRONOST, J.M. ASHWAL, L.D. & CAWTHORN, R.G. (2004): Oxygen and Hydrogen Isotope Stratigraphy of the Rustenburg Layered Suite, Bushveld Complex. Constraints on Crustal Contamination. *J. Petrol.* **46**, p 579-601.
- HOFMANN, A.W. (1989): Chemical differentiation of the Earth: the relationship between mantle, continental crust, and oceanic crust. *Earth Planet. Sci. Lett.* **90**, 297-314.
- HUPPERT, H.E. & SPARKS, R.S.J. (1985): Cooling and contamination of mafic and ultramafic magmas during ascent through continental crust. *Earth Planet. Sci. Lett.* **74**, 371-386.
- KEAYS, R.R. (1995): The role of komatiite and picritic magmatism and S-saturation in the formation of ore deposits. *Lithos* **34**, 1-18.
- KRUGER, F.J. (1994): The Sr-isotopic stratigraphy of the western Bushveld Complex. *S. Afr. J. Geol.* **97**, 393-398.
- KUNILOV, V.Y. (1994): Geology of the Noril'sk region: The history of the discovery, prospecting, exploration and mining of the Noril'sk deposits. In Naldrett, A. J. & Lightfoot, P. C. (eds.). Proceedings of the Sudbury-Noril'sk Symposium, Sudbury, Ontario Geological Survey Special Volume 5, 203-216.
- LATYPOV, R.M. (2002): Phase equilibria constraints on relations of ore-bearing intrusions with flood basalts in the Noril'sk region, Russia. *Contrib. Mineral. Petrol.* **143**, 438-449.
- LESHER, C.M. & KEAYS, R.R. (2002): Komatiite-Associated Ni-Cu-(PGE) Deposits: Mineralogy, Geochemistry, and Genesis. In The geology, geochemistry, mineralogy and mineral beneficiation of platinum-group elements, L.J. Cabri (ed.). Can. Inst. Mining, Metall Petroleum, Spec Vol **54**, 579-617.
- LESHER, M., GILLES, S. & RIPLEY, E.M. (1999): Ni-Cu-(PGE) Sulphides in the Raglan Block. In Komatiitic peridotite-hosted Ni-Cu-PGE deposits of Raglan Area, Cape Smith, New Quebec. Guidebook series v 2, Mineral Exploration Research Centre Laurentian University, C.M. Leshler (ed.). 177-185.
- LI, C. & NALDRETT, A.J. (1999): Geology and petrology of the Voisey's Bay intrusion: reaction of olivine with sulfide and silicate liquids. *Lithos* **47**, 1-31.
- LIGHTFOOT, P. C. & HAWKESWORTH, C. J. (1997): Flood basalts and magmatic Ni, Cu, and PGE sulfide mineralization: comparative geochemistry of the Noril'sk (Siberian Traps) and West Greenland sequences. In Large igneous provinces: continental, oceanic and planetary flood volcanism, Washington; Mahoney, J.J. & Coffin, M.F. (eds.). *American Geophysical Union Geophys. Monograph* **100**, 357-380.
- LIGHTFOOT, P.C., NALDRETT, A.J., GORBACHEV, N.S. & FEDORENKO, V.A. (1990): Geochemistry of the Siberian trap of the Noril'sk area, USSR, with implications for the relative contributions of crust and mantle to flood basalt magmatism. *Contrib. Mineral. Petrol.* **104**, 631-644.
- LIKHACHEV, A.P. (1994): Ore-bearing intrusions of the Noril'sk region. In Proceedings of the Sudbury-Noril'sk Symposium; Naldrett, A.J. & Lightfoot, P.C., (eds.). Sudbury, Ontario Geological Survey, Special Vol. **5**, 203-216.
- MAIER, W. D., ARNDT, N. T. & CURL, E. A. (2000): Progressive crustal contamination of the Bushveld Complex: evidence from Nd isotopic analyses of the cumulate rocks. *Contrib. Mineral. Petrol.* **140**, 328-343.
- MATHEZ E. A., HUNTER R. H. & KINZLER R. (1997): Petrological evolution of partially melted cumulate: the Atok section of the Bushveld Complex. *Contrib. Mineral. Petrol.* **129**, 20-34.
- MAVROGENES, J.A. & O'NEIL, H. (1999): The relative effects of pressure, temperature, and oxygen fugacity on the solubility of sulfide in mafic magmas. *Geochim. Cosmochim. Acta* **63**, 1173-1180.
- MCCANDLESS, T.E. & RUIZ, J. (1991): Osmium isotopes and crustal sources for platinum-group mineralization in the Bushveld Complex, South Africa. *Geology*, **19**, 1225-1228.
- NALDRETT, A. J. (1999): World class Ni-Cu-PGE deposits: key factors in their genesis. *Mineral. Dep.* **34**, 227-240.
- NALDRETT, A.J. (2004): *Magmatic Sulfide Deposits: Geology, Geochemistry, and Exploration*. Springer, 727 pp.
- NALDRETT, A.J., FEDORENKO, V.A., ASIF, M., SHUSHEN, L., KUNILOV, V.I., STEKHIN, A.I., LIGHTFOOT, P.C. & GORBACHEV, N.S. (1996): Controls on the composition of Ni-Cu sulfide

- deposits as illustrated by those at Noril'sk, Siberia. *Econ. Geol.* 91, 751-773.
- NALDRETT, A. J., FEDORENKO, V. A., LIGHTFOOT, P. C., KUNILOV, V. I., GORBACHEV, N. S., DOHERTY, W. & JOHAN, Z. (1995): Ni-Cu-PGE deposits of the Noril'sk region, Siberia: Their formation in conduits for flood basalt volcanism. *Trans. Inst. Mining and Metall., London* **104**, B18-B36.
- NALDRETT, A.J., LIGHTFOOT, P.C., FEDORENKO, V.A., DOHERTY, W. & GORBACHEV, N.S. (1992): Geology and geochemistry of intrusions and flood basalts of the Noril'sk region, USSR, with implications for the origin of the Ni-Cu ores. *Econ. Geol.* 87, 975-1004.
- PLANKE, S., SYMONDS, P., ALVESTAD, E. & SKOGSEID, J. (2000): Seismic volcanostratigraphy of large-volume basaltic extrusive complexes on rifted margins. *J. Geophys. Res.* **105**, 19335-19351.
- PLANKE, S., RASMUSSEN, T., REY, S. AND MYKLEBUST, R. (2004): Seismic characteristics and distribution of volcanic intrusions and hydrothermal vent complexes in the Voring and More basins. In *Petroleum Geology: North-West Europe and Global Perspectives*. Doré, A.G. & Vining, G. (eds.). *Proceedings of the 6th Petroleum Geology Conference*, Article I.D. 084, 1-12..
- RAD'KO, V.A. (1991): Model of dynamic differentiation of intrusive traps in the northwestern Siberian platform. *Soviet Geol. and Geophys.* **32(11)**, 15-20.
- RIPLEY, E.M., LIGHTFOOT, P. C., LI, C. & ELSWICK, E.R. (2003): Sulfur isotopic studies of continental flood basalts in the Noril'sk region: implications for the association between lavas and ore-bearing intrusions. *Geochim. Cosmochim. Acta* **67**, 2805-2817.
- RUDNICK, R.L. & FOUNTAIN, D.M. (1995): Nature and composition of the continental crust: a lower crustal perspective. *Rev. Geophysics* **33**, 267-309.
- TANG, Z. (1995): *Ore-forming model and geological correlation of the Jinchuan Cu-Ni-(PGE-bearing) sulfide deposit*. Beijing, Geological Publishing House, 208 pp.
- TORNOS, F., CASQUET, C., GALINDO, C., VELASCO, F. & CANALES, A. (2001): A new style of Ni-Cu mineralization related to magmatic breccia pipes in a transpressional magmatic arc, Aguablanca, Spain. *Mineral. Dep.* **36**, 700-706.
- WENDLANDT, R.F. (1982): Sulfide saturation of basalt and andesite melts at high pressures and temperatures, *Am. Mineral.* **67**, 877-885.
- WILSON A. H., LEE C. A. & BROWN R. T. (1999): Geochemistry of the Merensky Reef, Rustenburg Section, Bushveld Complex; controls on the silicate framework and distribution of trace elements. *Mineral. Dep.* **34**, 657-672.
- WOODEN, J.L., CZAMANSKE, G.K., FEDORENKO, V.A., ARNDT, N.T., CHAUVEL, C., BOUSE, R.M., KING, B.W., KNIGHT, R.J. & SIEMS, D.F. (1993): Isotopic and trace-element constraints on mantle and crustal contributions to Siberian continental flood basalts, Noril'sk area, Siberia. *Geochim. Cosmochim. Acta* **57**, 3677-3704.
- YAKUBCHUK, A. & NIKISHIN, A. (2004): Noril'sk-Talnakh Cu-Ni-PGE deposits: a review of the classic model. *Mineral. Dep.* **39**, 125-142
- ZEN'KO, T.E. & CZAMANSKE, G.K. (1994a): Tectonic controls on ore-bearing intrusions of the Talnakh ore junction: position, morphology and ore distribution. *International Geol. Rev.* **36**, 1033-1057.
- ZEN'KO, T.E. & CZAMANSKE, G.K. (1994b): Spatial and petrological aspects of the intrusions of the Noril'sk and Talnakh ore junctions. In *Proceedings of the Sudbury-Noril'sk Symposium, Sudbury*. Naldrett, A. J. & Lightfoot, P. C., (eds.). *Ontario Geological Survey, Special Volume 5*, 263-281.

CHAPTER 10: PLATINUM-GROUP ELEMENT POTENTIAL OF PORPHYRY DEPOSITS

Maria Economou-Eliopoulos,
Department of Geology, University of Athens, Athens 15784, Greece
E-mail: econom@geol.uoa.gr

INTRODUCTION

Porphyry Cu \pm Mo \pm Au deposits are major sources of these metals and are associated with alkaline and calc-alkaline rocks. Porphyry-type deposits range from porphyry Cu–Au, like Grasberg (Indonesia), Mamut (Malaysia), Santo Tomas II (Philippines), Skouries (Greece), Cadia (Australia), British Columbia (Copper Mountain, Ajax/Afton, Mount Polley, Galore Creek, Mt Milligan), Cu–Au–Mo deposits, like the giant deposit at Bingham Canyon, Utah, to porphyry Mo such as the Boss Mountain (central British Columbia). A variety of porphyry Cu, Mo, Cu–Mo and Au-rich deposits define the metallogeny of the Andean belt, extending from Ecuador, Peru, and Bolivia to Argentina and Chile, covering the early Cretaceous to Pleistocene age span (Sillitoe 1979 1997, 2000, 2004, Titley 1993, Kirkham & Sinclair 1996, Corbett & Leach 1998, Bookstrom *et al.* 1998, Brooks *et al.* 2004, Seedorff & Einaudi 2004). The Alpine-Balkan-Carpathian Dinaride belt belongs to the Alpine-Himalayan system, extending from

western Europe through Iran and the Himalaya to China and Malaysia, and is the result of convergence of the African, Arabian and Indian plates and their collision with Eurasia. Major calc-alkaline magmatism, extending over at least 25 million years (from about 90 to 65 Ma) in each segment of the metallogenic belt, is associated with certain segments only, due probably to the complex geometry of the collision interface (Heinrich & Neubauer 2002, Strashimirov *et al.* 2002). Although the Andes and Alpine-Balkan-Carpathian belts differ in terms of the subduction age span, they host some of the world's largest porphyry-type deposits and oldest mining areas (Kirkham & Sinclair 1996, Heinrich & Neubauer 2002).

Alkaline porphyry deposits represent significant gold resources owing to their large sizes. Recently, elevated levels of platinum group elements (PGE), particularly Pd and Pt, have been reported from mineralization associated with several of the alkaline porphyry deposits (Fig. 10-1) in the Cordillera of British Columbia (Copper Mountain,



FIG. 10-1. Location map of porphyry Cu \pm Mo \pm Au \pm Pd \pm Pt deposits

Galore Creek), Allard Stock, La Plana Mountains and Copper King Mine in USA, Skouries porphyry deposit, Greece, Elatsite, Bulgaria, and from Santo Tomas II in the Philippines (Werle *et al.* 1984, Mutschler *et al.* 1985, Eliopoulos & Economou-Eliopoulos 1991, Piestrzynski *et al.* 1994, Eliopoulos *et al.* 1995, Tarkian & Koopmann 1995, Tarkian & Stribny 1999, Economou-Eliopoulos & Eliopoulos 2000, Tarkian *et al.* 2003). The role of magma mixing, saturation of a sulfide melt or of a magmatic volatile phase to the base and precious metal potential of porphyry systems, and the investigation of the contribution of mantle, oceanic and continental crust to the parent magmas of porphyry Cu subvolcanic intrusions remains still uncertain (Burnham 1979, Burnham & Ohmoto 1980, McInnes & Cameron 1994, Keith *et al.* 1998, Titley 2001, Hattori & Keith 2001, Halter *et al.* 2002, Ivascanu *et al.* 2003, Halter *et al.* 2002 2005).

In this paper the characteristics of numerous porphyry Cu–Au–Pd±Pt-enriched systems are reviewed. Porphyry Mo deposits, although similar to porphyry Cu, are different in terms of their Pd and Pt contents and are not discussed in this review. Here we compile published (and some new) mineralogical and geochemical data and discuss factors controlling precious metal enrichment in the porphyry Cu systems, key characteristics of Pd–Pt-enriched porphyry deposits, which may be used in exploration, and the evaluation of Pd–Pt as an economic factor (as a by-product) for that type of deposit. Most references cited in this review are recent summary papers, which can be used as sources for more extensive research.

DISTRIBUTION OF PORPHYRY Cu DEPOSITS ALONG CONVERGENT PLATE MARGINS

Porphyry Cu deposits are spatially and genetically associated with porphyritic intrusions, emplaced at relatively high levels in the crust, which are characterized by phenocryst assemblages consisting of one or more minerals (K-feldspar, plagioclase, hornblende, quartz or biotite) in a fine-grained matrix. The majority of giant gold-rich porphyry deposits are located in the circum-Pacific region. A linear zone of volcanism at the boundary between the Pacific and adjacent Australia-India, Philippines, and Eurasian plates define the “ring of fire” (Corbett & Leach 1998, Tosdal & Richards 2001).

Many giant gold-rich porphyry deposits are generated at convergent margins during or

immediately following subduction of lithosphere, although there is a variation in the style of the tectonism in time and space. The genetic significance of the tectono-magmatic controls on large Cu±Mo±Au deposits, and the differing stress conditions in the overriding plate in arcs, which influence the style of major structures, have been emphasized by many authors. They may vary from compressional to tensional and shearing, in three dimensions: vertically (through the lithosphere), laterally (along the arc), and transversely (from forearc to back-arc) (Sillitoe 1997 2000, Müller & Groves 2000, Tosdal & Richards 2001, Richards 2003). Also, differences in oxidation state of parent magmas are reflected in the magmatic oxidation state of the ore assemblages (Mungall 2002, Sillitoe & Hedenquist 2003, Einaudi *et al.* 2003).

Fundamental changes in subduction geometry and convergence rates may result in the development of dike-like forms of many porphyry Cu deposits during periods of low differential or near isotropic horizontal stress in the arc environment. Porphyry intrusions are commonly emplaced at depths of 1–2 km. Differentiated felsic and volatile-rich intrusions may rise to higher crustal levels, whereas large batholithic bodies occur at greater depths (Corbett & Leach 1998, Tosdal & Richards 2001). The majority of these deposits are located along older fault systems. Fractures connected with tectonic and magmatic processes facilitate the intrusion of porphyry stocks or dikes near surface levels and facilitate volume expansion of the hydrothermal fluids (Lang & Titley 1998, Sillitoe 2000, Tosdal & Richards 2001, Sillitoe & Hedenquist 2003).

Dehydration of the subducting oceanic crust resulting in hydration of the overlying mantle seems to be the most favorable aspect of the arc magmatogenesis. Hydrous basaltic melts, derived by partial melting in the asthenospheric mantle wedge, intrude the overlying lithosphere, rising at the base of the crust, where they may fractionate and interact with crustal material. Furthermore, more evolved magmas (less dense) rise into the high levels of the crust, where they may undergo volatile exsolution and crystallization as porphyritic stocks. Parental magmas are considered to be moderately water-rich as indicated by the presence of hydrous minerals (amphibole, biotite), whose stability requires at least 3 wt.% H₂O in the melt. Such hydrous melts may contain metals and ligands of critical significance to the formation of Au-rich porphyry deposits (Sillitoe 2000, Tosdal & Richards

2001, Sillitoe & Hedenquist 2003). Some investigators have emphasized that uplift and crustal thickening of the continental crust has played a major role in the breakdown of hydrous minerals, as is exemplified by the central Andean Miocene porphyry deposits, formed in the shallow dip ($<30^\circ$) of the subducting plate compared to other circum-Pacific subduction zones (Isacks 1988, Allmendinger *et al.* 1990, Cahill & Isacks 1992, Kay *et al.* 1999). Mungall (2002) has suggested instead that the optimum conditions for generation of chalcophile-element-rich arc magmas involve the relatively rare process of partial melting of the subducting oceanic crust to produce adakitic or alkaline magmas.

CHARACTERISTICS OF ALKALINE INTRUSIONS

Following the definition based on total (K_2O+Na_2O) versus SiO_2 (Irvine & Baragar 1971, Jensen & Barton 2000), alkaline rock types associated with gold mineralization, range from ultramafic lamprophyres (<40 wt.% SiO_2) to fractionated, high-K rhyolite (up to 75 wt.% SiO_2), including subduction-related potassic calc-alkaline rocks and shoshonite. A subdivision of alkaline rocks, depending on the proportion of K and Na, is the shoshonitic rocks, which are potassic varieties and are considered to be particularly favorable for hosting porphyry Cu–Au deposits (Müller & Groves 2000). Less-evolved alkaline diorite, mafic syenite, and monzonite, ranging from silica-undersaturated

(quartz is absent) to silica-saturated tend to be associated with Cu (Au) base metal-rich hydrothermal systems as well (Jensen & Barton 2000). Also, alkaline-related hydrothermal systems, show distinct characteristics, including quartz-poor (or quartz-absent) style of alteration and mineralization. Quartz is variably present. It is absent from strongly silica-undersaturated deposits (Galore Creek, B.C.) but can be abundant in silica-saturated systems (Goonumbla, Australia). The degree of K enrichment in the potassic zone of alteration is variable, reaching values >10 wt.% K_2O , such as in the Galore Creek, the Allard stock and Goonumbla (Jensen & Barton 2000).

ALTERATION TYPES OF PORPHYRY INTRUSIONS

The porphyry Cu±Mo±Au deposits may develop around single intrusions or within more complex systems consisting of numerous intrusions and overlapping stages of alteration and ore deposition. Commonly they are related to multiple and multistage hypabyssal pipe-like intrusions extending at surface over widths ranging from less than 100 m to more than 1 km; their vertical extents may exceed 2 km (Tobey *et al.* 1998, Herrington *et al.* 1998, 2003, Tobey *et al.* 1998, Kroll *et al.* 2002).

Cooling of porphyry intrusions in the upper crust may be accompanied by the development of the initial alteration zone (Fig. 10-2). The subsequent alteration exhibits a zonation from K

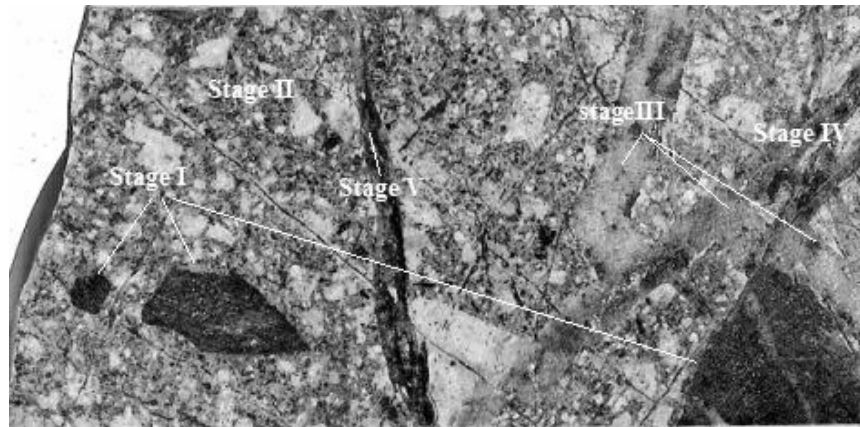


FIG. 10-2. Representative drill core sample of the Skouries Main monzonite porphyry (core width is about 4 cm), showing mineralization (disseminated and vein-type) in angular mafic fragments (stage I), pervasive (stage II), crosscutting relationships between successive quartz veins (stages III & IV) dominated by the magnetite-bornite-chalcopyrite assemblage, and a quartz-biotite vein (stage V), reflecting a range of hydrothermal evolution. The presence of mineralized mafic xenoliths within main porphyry is consistent with the multiple intrusive phases and mineralising events.

silicate (potassic) to propylitic, intermediate argillic, sericitic (phyllic) and advanced argillic as described by Meyer & Hemley (1967), Lowell & Guilbert (1970), Sillitoe (1997, 2000), Corbett & Leach (1998). Advanced argillic alteration and silicification are strongly structurally controlled by faults, including those which initially facilitated the emplacement of the multiple porphyry intrusions.

Fluid-inclusions provide evidence of genetic importance. They suggest that relatively hot (400° to 700°C) and saline to hypersaline (up to 70 wt.% NaCl_{equiv}) magmatic-hydrothermal fluids transported Cu and precious metals as chloride complexes that were precipitated during the main stage of mineralization with the K-assemblages. The cooler, more dilute and more oxidized character of meteoric water-dominated fluids may permit the outward transport of Au as bisulfide complexes (Sillitoe 1993, Lang *et al.* 1995, Jensen & Barton 2000) in hybrid fluids produced by mixing of these with the orthomagmatic fluids. Although alteration type is an important indicator of fluid composition, the ore mineral assemblages themselves reflect the nature of the ore fluids (Sillitoe & Hedenquist 2003).

MINERALIZATION OF PORPHYRY Cu SYSTEMS

Porphyry deposits constitute major sources of Cu, Cu+Mo, or Cu+Au, although many shallow-level porphyritic intrusions are devoid of, or are accompanied by, weak mineralization. The Au-rich porphyry deposits comprise a continuum of systems from Cu plus by-product Au, through Au plus by-product Cu to Au-only end members. Porphyry deposits with average gold contents ≥ 0.4 ppm Au may be defined as gold-rich, commonly deficient in Mo (Sillitoe 1979, 2000, Kesler *et al.* 2002). Gold-rich deposits are mostly linked to alkaline magmatic systems including a number of Cu(Au) and Mo(Au) in Colorado and the British Columbia Cordillera (Table 10-1) deposits, which may grade upward and/or outward into telluride-rich epithermal deposits, both characterized by high halogen (chlorine, fluorine) concentrations and by high oxygen fugacities. Epithermal parts are base-metal poor and have Au>Ag, whereas porphyry parts have significant Au and Ag>Au in a base metal-rich core.

Recently, elevated levels (over 5 ppm) of platinum group elements (PGE), particularly Pd and Pt, have been reported in high-grade bornite-chalcocopyrite and/or flotation concentrates from porphyry deposits, associated mostly with several of

the alkaline type including the Copper Mountain-Ingerbelle, Afton-Ajax, Mount Polley, Galore Creek and Mount Milligan deposits in British Columbia, Allard stock, La Plata Mountains (Colorado) (Werle *et al.* 1984, Mutschler *et al.* 1985, Mutschler & Mooney 1993, Thompson *et al.* 2001), Skouries in Greece (Eliopoulos & Economou-Eliopoulos 1991), Santo Tomas II in the Philippines (Piestrzynski *et al.* 1994, Tarkian & Koopmann 1995), Elatsite, Bulgaria and elsewhere (Eliopoulos *et al.* 1995, Tarkian *et al.* 2003, Tarkian & Stribny 1999). A review of characteristics features of some porphyry Cu–Mo–Au–Pd±Pt-enriched systems associated with alkaline magmas follows (Table 10-1, App. 10-A).

TRANSPORT OF PGE IN HYDROTHERMAL SYSTEMS

Experimental Data

The current state of knowledge of solubility of PGE has been reviewed and applied toward a better understanding of the PGE mineralization in hydrothermal systems by Wood (2002) and by Hanley (2005). The stable oxidation stages of Pt and Pd in aqueous solution under the most oxidizing conditions are Pt(II) and Pd(II). In that oxidation state strong complexes with soft (HS⁻, Cl⁻) ligands are the most common. The oxidation states of Os, Ir, Ru and Rh are more variable. Recently, Sassani & Shock (1990) have predicted that the divalent states Ru(II) and Rh(II) are likely to be their predominant oxidation state in hydrothermal solutions, which has been supported by experimental solubility measurements by Xiong & Wood (2000).

Although the lack of thermodynamic or experimental data preclude a quantitative analysis of Pt and Pd solubility in waters rich in organic material, ammonia, polysulfide, or thiosulfate (Wood 2002, Wilde *et al.* 2002), and measurements of the stability of Pd-chloride complexes at temperatures above 300°C, the Pt and Pd are quite soluble under a range of hydrothermal conditions (as chloride or hydroxyl species), in hot oxidized brines (as chlorides), and in hot, reduced, sulfur-rich waters (as bisulfide complexes). More specifically, experimental data (Gammons *et al.* 1992) indicated that at about 300°C, solubilities of Pt and Pd as chloride complexes are restricted to (a) oxidizing conditions (in the hematite stability field) over a range of pH < 6, and (b) strongly acidic conditions (pH less than ~3), under reducing conditions (pyrite

TABLE 10-1. SELECTED CHARACTERISTICS AND PRECIOUS METAL CONTENT IN FLOTATION CONCENTRATE (F.C.) AND SULFIDE CONCENTRATE (Sf.C) SAMPLES FROM PORPHYRY-CU DEPOSITS.

Deposit	Setting	Age (Ma)	Host porphyry		Alteration type	sample or average	Description	Ore tons (t x 10 ³)	concentration (ppb)				Cu wt. %	Ref.	
			type	Affinity					Pd	Pt	Au	Pd/Cu			Pt/Cu
Balkan peninsula Greece-Skouries															
(a) porphyry	C(col)	18	Monz	A	K, Prop, Q	Sk, Po.or	composite	206	76	<10	910	152	0.5	1,2,3	
						Sk, Po.or (F.C.)	composite		2400	40	22000	60	114	21	3
(b) country rocks						Sk, Po.or (F.C.)	composite		75	20	8200	13	5.6	3	
Bulgaria															
Elastite	C(col)-IA	92	Monzdi	A	K, Prop, ser	n=8	EP(Sf.C) mt-bn-cp	260	540	160	18700	3.5	26	21	4,5
Elastite						n=27	E(Sf.C), cp-py		107	31	3700	3.5	11	10	4,5
Elastite						n=3	F.C.		1130	130	16200	8.7	48	24	4,5
Medet	C(col)	92	Qmonz	A	K, Prop, ser	n=1	F.C.	244	160	8	5600	20	11	15	4,5
Assarel	C(col)	92	Qmonz	A	Prop, ser	n=1	F.C.	360	54	14	4800	3.9	2	28	4,5
Serbia															
Bor	C	78-90	Qdi	CA	K, Prop, Q	n=1	F.C.	450	40	19	1700	2.1	n.d.	4,6,7	
Majdanpek	C	78-90	Monzdi	CA	Q	n=2	F.C.	570	180	20	4600	9	7	26	4,6,7
Veliki/Krivelj	C	Late Cret.	Qdi	CA	K, Prop, Q	n=1	F.C.	1000	70	16	2250	4.4	n.d.	4,6,7	
Philippines															
Santo Tomas II	IA	1.4	Di	CA	K, Prop, Q	n=3	mt-bn-cp	330	67	10	3540	6.7	92	0.7	7,8
Santo Tomas II						n=2	cp-py		21	20	800	1.05	105	0.2	7,8

Abbreviations: Sf.C = sulfide concentrate; F.C = flotation concentrate; mt = magnetite; bn = bornite; cp = chalcopyrite; py = pyrite; C = continental margin, Col = during or following collision, IA = island arc; Monz = monzonite, Monzdi = monzodiorite, Qmonz = quartz monzonite; Di = diorite, Qdi = quartz diorite, Granod = granodiorite; Gran = granite; Syen = syenite; A = alkaline, CA = calc-alkaline, KCA = high K calc-alkaline (shoshonite), K = K silicate, Na = Na silicate, Prop = propylitic, Q = silicification, Ser = sericitic, Ca-K = calc-potassic, Na-Ca = sodic-calcic; (1) = *Tobey et al.* (1998); (2) = *Kroll et al.* (2002); (3) = *Economou-Eliopoulos & Eliopoulos* (2000); (4) = *Tarkian & Stribny* (1999); (5) = *Tarkian et al.* (2003); (6) = *Herrington et al.* (1998); (7) = *Tarkian & Koopmann* (1995); (8) = *Sillitoe* (2000); (9) = *Berzina et al.* (2005); (10) = *Lebedev & Kuzhuget* (1998); (11) = *Kovalenker et al.* (1996); (12) = *Blevin* (2002); (13) = *Lieckfold et al.* (2003); (14) = *Thompson et al.* (2001); (15) = *Mortensen et al.* (1995); (16) = *Dolbear & Company* (2003); (17) = *Mutschler et al.* (1985).

TABLE 10-1 (CONTINUED). SELECTED CHARACTERISTICS AND PRECIOUS METAL CONTENT IN FLOTATION CONCENTRATE (F.C.) AND SULFIDE CONCENTRATE (Sf.C) SAMPLES FROM PORPHYRY-CU DEPOSITS.

Deposit	Setting	Age (Ma)	Host porphyry		Alteration type	sample or average	Description	Ore concentration (ppb)				Cu wt. %	Ref.		
			type	Affinity				Pd (t x 10 ⁶)	Pt	Au	Pd/Cu				
Papua New Guinea															
Ok Tedi	C(col)	1.2	Monz	KCA	K	n=1	F.C.	768	980	24	28000	40.8	26	37	4, 8
Panguna	IA	3.4	Di,Qdi	CA	K, Prop, ser	n=1	F.C.	328	40	8	520	5	0.1	35	4, 8
Indonesia															
Grasberg	C(col)	2.8	Monzdi	KCA	K, Prop	n=1	F.C.	1952	58	15	18000	3.9	2.4	24	4
Malaysia															
Mamut	IA(Col)	5.9	Qmonz	KCA	K, Prop, ser	n=2	F.C.	1950	1400	470	15200	3	69	20	4
Russia (Siberia)															
Aksug	IA(Col)	401-404	Granod	CA	Prop, Q, ser	S-2392	Sf.C	337	920	25	1200	36.8	170	5.4	9, 10
Aksug						n=2	F.C., Cu/Mo=7-200		73	86	4900	0.8	4.9	15	9, 10
Sora	IA(Col)	388-405	Gran	KCA	K, Na	n=3	F.C., Cu/Mo=00.4-185	325	50	88	100	0.6	8.6	5.8	9, 10
Zhireken	IA(Col)	155-160	Gran	KCA	K	S-0508	F.C., Cu/Mo=0.5	100	680	300	140	2.3	252	2.7	9, 10
Ryabinovoye	IA(Col)	137-146	Syen	CA	K, Na, Ser	n=4	Sf.C		85	150		0.6			11
Mongolia															
Erdenetuin-Obo	C(col)	220-240	Granod	CA	K, Na, Ser	S-0572	Sf.C, Cu/Mo=2.5	1200	20	33	74	0.6	333	0.06	9, 10
Australia															
Cadia (Hill & East)	IA	440	Qmonz	KCA	K, Na			480			600			0.3	7, 12
Goonumbla	IA	439	Qmonz	KCA	K, Q			64			500			0.5	7, 13

See page 207 for abbreviations.

TABLE 10-1 (CONTINUED). SELECTED CHARACTERISTICS AND PRECIOUS METAL CONTENT IN FLOTATION CONCENTRATE (F.C.) AND SULFIDE CONCENTRATE (Sf.C) SAMPLES FROM PORPHYRY-CU DEPOSITS.

Deposit	Setting	Age (Ma)	Host porphyry		Alteration type	sample or average	Description	Ore tons (x 10 ⁶)	concentration (ppb)				Cu wt. %	Ref.	
			type	Affinity					Pd	Pt	Au	Pd/Cu			Pt/Cu
British Columbia Cordillera															
Galore Creek	IA(Col)	210	Syen	A	K, Ca-K	n=2	mt-py-bn-cp	159	1300	80	64000	16.2	76	17	7, 14, 15
Galore Creek						n=2	cp-py-bn		260	16	4400	10	20	13	7, 14, 15
Mt. Milligan	IA	183	Monz	A	K, Prop	MMSS-1	mt-py-cp		6300	110	18500	57	926	6.8	7, 14, 15
Mt. Polley	IA	205	Monz	A	K, K-Na, Ca-K	88-148	mt-bn-cp-py	49	320	33	23600	9.7	16	21	7, 14, 15
						88-143	cp-py-mt		83	17	6200	4.9	72	1.1	14
						88-150	cp-py		23	7	1600	3.3	12	1.1	14
Ajax	IA	195-205	Monz	A	K, K-Na, Ca-K	AE-1	cp-py	284	140	8	990	17.5	5.3	26	7, 14, 15
Afton	IA	204	Di	A	K, K-Na, Ca-K	n=60		69	130		1200		87	1.5	7, 14, 15
Cooper Mountain	IA			A		n=2	F.C.		2760	190	4800	14.5	98	28	16
Cooper Mountain						No17	Sf.C, bn-cp vein		3250	50	4200	65	81	40	16
Colorado															
Allard, La Plata	IA	70-85	Syen	A		No2	Sf.C (cp)		1920	2880	1230	0.7	107	18	16
Allard, La Plata	IA					No3	F.C.		2320	3935	1740	0.6	86	27	16
Wyoming															
Copper King Mine		Triassic		A		n=2	F.C.		2660	900	440	3	84	32	16
Copper King Mine						No6	Sf.C (cp), pegmatitic		6430	13600	190	0.5	292	22	16

See page 207 for abbreviations.

or pyrrhotite stability fields). Thus, it has been concluded that the highest Pt and Pd concentration will be attained under both oxidized and acidic conditions and that chloride is the most abundant ligand in hydrothermal solutions, forming strong complexes with Pt and Pd, and it is a potentially important ligand for aqueous transport of these metals (Wood 2002). Furthermore, it is emphasized that in the presence of significant concentrations of other metal ions, like Ca^{2+} , Mg^{2+} , Fe^{2+} , and Cu^{+} , complexation of chloride by these metals would reduce the activity of free the chloride ion, resulting in reduced solubilities of Pt and Pd minerals. On the other hand, elements like As, Bi, Sb, Se and Te form very insoluble compounds with PGE.

Hanley *et al.* (2005) have shown that hot, moderately oxidized hypersaline fluids can dissolve Pt and Au at concentrations on the order of parts per million, confirming that orthomagmatic fluids derived from arc magmas are capable of transporting and depositing significant amounts of these metals.

Field Observations

The importance of aqueous processes to PGE geochemistry and to the concentration of the PGE to economic levels has been recognized by Wagner (1929) in the Waterberg deposits (South Africa) and supported by recent investigations (see also reviews by Hanley 2005 and Wilde 2005). Based on the presence of abundant hematite, Cr (VI)-bearing minerals and Pt-oxides in those deposits, the replacement of K-feldspar by muscovite, and fluid inclusion data, McDonald *et al.* (1999) concluded that Pt and Pd were mobilized under strongly oxidizing conditions, in moderately acidic fluids (pH 4 to 5) as chloride complexes, at temperatures of 200 to 300°C.

In hydrothermally altered harzburgite of the Semail ophiolite of Oman, elevated Pt (up to 450 ppb) is associated with silicified and carbonate-altered serpentinite ("listwaenite"), which occurs along Tertiary extensional faults (Wilde *et al.* 2003). Also, the members of the irarsite-hollingworthite solid-solution series and other Os-, Ir, Ru- and Rh-bearing PGM in chromitites from some ophiolite complexes, and their association with altered chromitites may indicate either *in situ* alteration or/and re-mobilization and re-deposition of PGE during at least two stages (Tarkian & Prichard 1987). The presence of Ru-Os-Ir-Fe-oxides, with significant and variable Fe, Cr, Co, Ni and Mn contents, associated with serpentine,

chlorite, Cr-garnet, ferrian-chromite and magnetite in chromite ores, suggest that they may have been derived from *in situ* alteration of primary PGM, by desulfurization and subsequently oxidation of pre-existing sulfides of Os–Ru–Ir (Garuti & Zaccarini 1997). Also, significant concentrations of PGE (few ppm Pd and Pt) were found in magmatic breccia at the contact between the Bangur intrusion and its ultramafic host, Baula-Nuasahi Complex, India. On the basis of mineralogical and geochemical data, including oxygen, hydrogen and sulfur isotopes, it has been suggested that the precious metals in the hydrothermal fluids were derived from the magma rather than an external source (Augé & Lerouge 2004).

Platinum and palladium contents in sea-floor massive sulfides related to ophiolite complexes are very limited, but may indicate that PGE are quite soluble under a range of hydrothermal conditions. High Pt (up to 1 wt %) contents have been reported in marcasite and chalcopyrite from massive sulfides at 21°N on the East Pacific Rise (Hekinian *et al.* 1980). Sulfide deposits at 26°N on the mid-Atlantic Ridge contain significant palladium, ranging from 3 to 1000 ppb, and gold up to 8 ppb (Crocket 1990). Palladium and platinum contents in massive sulfide ores of Cyprus type from the Pindos (Kondro) ophiolite complex, Greece are lower than the detection limit of the method but contain Au up to 3.6 ppm. In contrast, significant Pt-enrichment, ranging from 160 to 1000 ppb, has been determined in an occurrence of brecciated pipeform diabase, underlying the massive ore of the complex. The mineral assemblage found in the brecciated diabase includes plagioclase (altered), clinopyroxene (altered) + chlorite + kaolinite + quartz + epidote + calcite and disseminated pyrite mineralization. Remnants of pyrrhotite within pyrite surrounded by hydroxides or magnetite are common (Economou-Eliopoulos & Eliopoulos 1998). Assuming that Au and Pt/Pd were derived from the same source area and that the transporting complexes of these metals are the same, the concentration of Au in massive sulfide ore and Pt in the underlying diabase breccia may reflect a difference of the relative solubility and the extent to which these metals are saturated in a given hydrothermal solution and the mechanism of deposition of each metal (Wood 2002). Pan & Wood (1994) pointed out that hydrothermal fluids in equilibrium with pyrite or pyrrhotite and alteration minerals such as chlorite, epidote, albite, calcite, *etc.*, would be incapable of transporting significant amounts of PGE as chloride complexes.

They suggested that a typical seafloor hydrothermal vent fluid could contain a significant amount of Pt and Pd as bisulfide complexes and that gold is transported predominantly as a bisulfide complex too. In addition, they concluded that under the conditions of their experiments, the solubility of Au as a bisulfide complex was three orders of magnitude higher than that of Pt and Pd. Thus, the elevated Pt contents in the mineralized diabase breccia of Pindos compared to massive sulfide ore seems to confirm the higher solubility of Au that remains more soluble than Pt, and therefore massive ore is accompanied by Au.

Applications to Porphyry Systems

The presence of significant Pd–Pt concentrations (over 5 ppm) in certain porphyry Cu–Au, and to a lesser extent in Cu–Mo, deposits (Mutschler *et al.* 1985, Werle *et al.* 1984, Eliopoulos & Economou-Eliopoulos 1991, Eliopoulos *et al.* 1995, Piestrzynski, *et al.* 1994, Tarkian & Koopmann 1995, Tarkian & Stribny 1999, Stribny *et al.* 2000, Tarkian *et al.* 2003, Strashimirov *et al.* 2003) is an important support to the view of the hydrothermal mass transfer. The occurrence of the main Pd-tellurides in porphyry Cu \pm Mo deposits at grain boundaries of, or exclusively as inclusions in, chalcopyrite and bornite from various porphyry deposits, indicates that Pd and Pt were deposited during the major vein stage of Cu deposition and suggest that chloride was the principal ligand for aqueous transport significant amounts of both base and precious metals in these ore-forming systems (Tompouloglou 1981, Eliopoulos & Economou-Eliopoulos 1991, Tarkian *et al.* 1991, Tarkian & Koopmann 1995, Frei 1995).

Under acid and oxidizing conditions and temperatures up to 300°C, both Pd and Pt may be transported as chloride complexes (Gammons *et al.* 1992, Wood *et al.* 1992) with these complexes becoming increasingly important for Pd at higher temperatures (Sassani & Shock 1990). Chloride transport is generally invoked for Cu and Au in the porphyry environment (*e.g.*, Sillitoe 1993) and therefore the association of Cu, Au, Pd and Pt may be explained in part by a similar transport and deposition mechanism. Pd and Pt may also be transported as bisulfide complexes, but at levels one to three orders of magnitude lower than Au under the same conditions (Wood 2002). This difference

in the efficiency of transport is similar to the relative difference in concentration between Au and Pd in the samples analysed in this study. Hanley *et al.* (2005) have suggested a dominant role for hydroxide complexes in the transport of Pt at high temperatures. Sharp reductions in Pt solubility with diminishing temperature and oxygen fugacity might cause precipitation of Pt minerals during hydrothermal fluid evolution.

PGE MINERALIZATION IN PORPHYRY SYSTEMS

Summary geological descriptions of PGE-bearing porphyry deposits worldwide is presented in Appendix 10-A. The following discussion synthesizes these observations to describe a generalized ore deposit model.

Distribution of Au in Cu-minerals, Gold and Electrum

The Skouries, Elatsite, Medet, Bor/Madjanpek, Santo Tomas II, Grasberg, Bingham, Panguna and other porphyry deposits (Fig. 10-1), contain ore associated with early potassic alteration, native gold or electrum occurs as small (5–100 μm) inclusions in chalcopyrite or along bornite margins. Native gold and electrum may also form intergrowths with Pd–Pt–Bi- and Ag-tellurides, ranging from less than 1 to tens of μm (Figs. 10-2, 10-3 & 10-4, Table 10-2, Tarkian *et al.* 1991, Tarkian & Koopmann 1995, Tarkian & Stribny 1999, Kesler *et al.* 2002, Tarkian *et al.* 2003, Strashimirov *et al.* 2003). In addition, gold inclusions in chalcopyrite of the magnetite-bornite-chalcopyrite association tend to be poorer in Ag compared to those (electrum) in the chalcopyrite-pyrite assemblages (Tarkian *et al.* 2003).

In deposits that contain abundant bornite, it is the preferred host for, or is associated with gold. For example, at the Grasberg deposit more than 60% of gold grains are associated with bornite (Rubin & Kyle 1997). In contrast, gold is associated with chalcopyrite in deposits where bornite is rare or absent, such as at the Island Copper deposit, or where bornite is found in a lesser proportion compared to chalcopyrite (Ballantyne *et al.* 1997, Kesler *et al.* 2002). Subsequent events overprinting early potassic alteration and ore commonly remobilized Cu and Au, resulting in complete destruction of bornite and deposition of a new

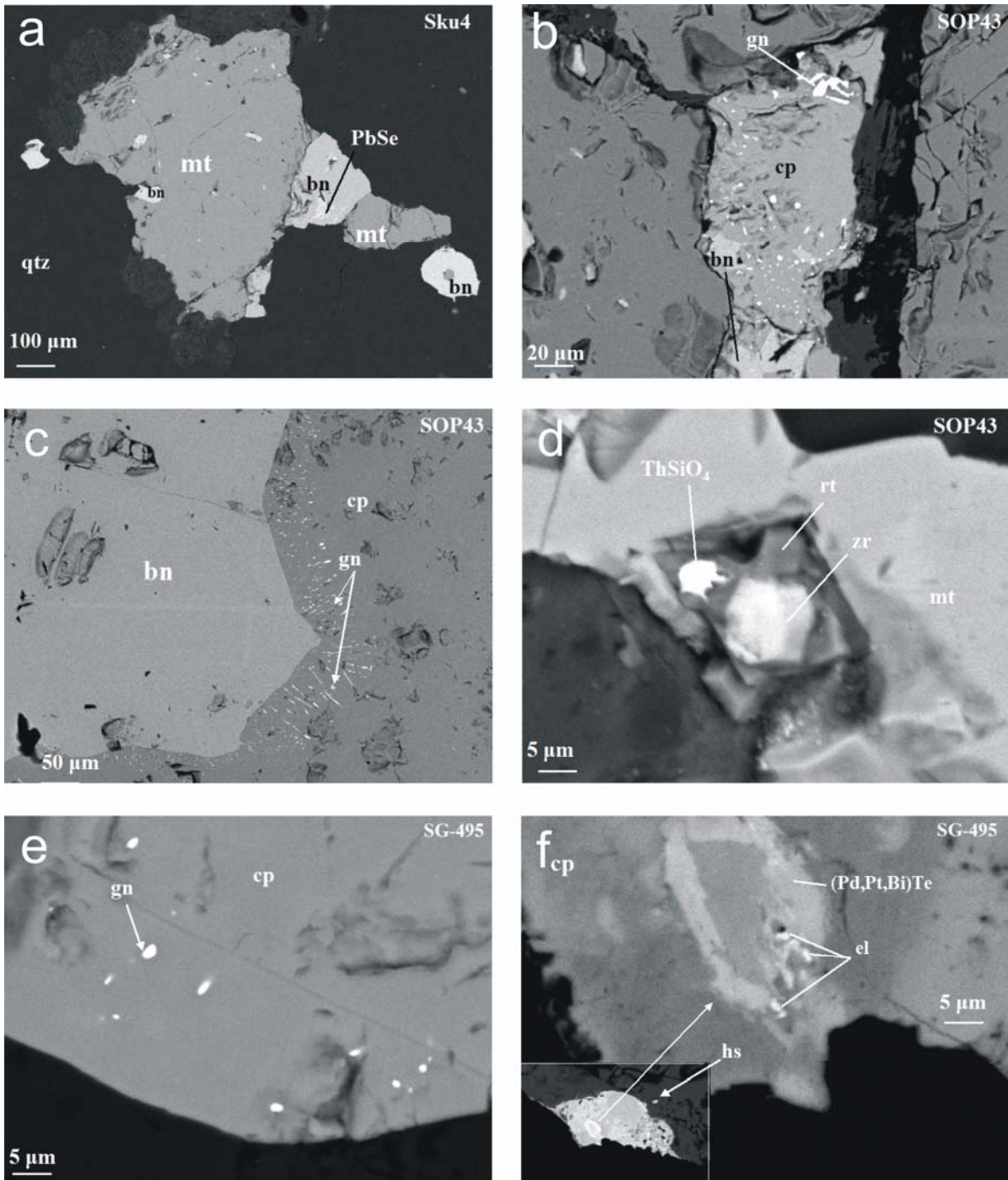


FIG. 10-3. Back-scattered electron images from various drill core samples of the Skouries porphyry deposit, showing textural relationships between base and precious metal minerals, and rare accessory minerals. **a)** clauthalite and bornite forming compound grains with magnetite; **b)** isolated grains of galena within chalcopyrite, with minor bornite; **c)** vermicular intergrowth of galena with chalcopyrite adjacent to bornite grain; **d)** association of rare accessory minerals with Ti-magnetite; **e)** rare bornite blebs hosted by chalcopyrite; **f)** intergrowth of electrum, (Pd,Pt,Bi)Te and hessite with chalcopyrite.

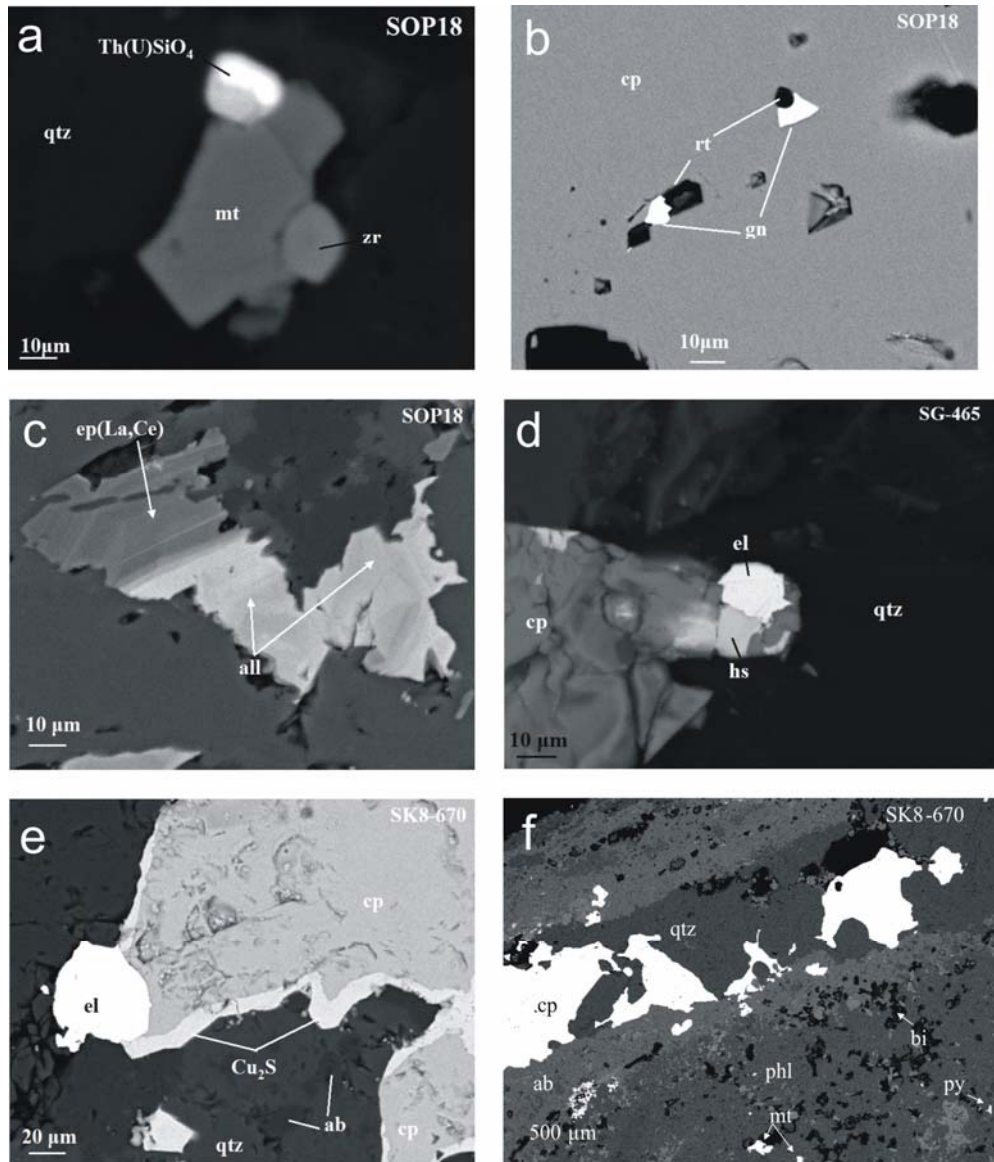


FIG.10-4. Backscattered electron images from drill core samples from Skouries porphyry deposit. **a)** Uranium-rich thorite and zircon associated with Ti-magnetite hosted by quartz; **b)** galena and rutile association hosted by chalcopyrite; **c)** REE-enriched epidote overgrown by allanite; **d)** association of hessite and electrum with chalcopyrite and quartz; **e)** electrum and chalcocite overgrowing chalcopyrite; **f)** quartz-chalcopyrite vein crosscutting biotite- and magnetite-rich potassic altered porphyry.

chalcopyrite-pyrite assemblages in which gold is associated with both minerals. In several deposits, these later gold-bearing overprints show a greater structural control than the initial mineralization (Cuddy & Kesler 1982). SIMS (ion probe) analyses of ore minerals from the gold-rich Batu Hijau, King King and Skouries porphyry copper deposits showed that bornite commonly contains about 1 ppm Au, whereas chalcopyrite contains about an order of

magnitude less. Although both supergene and hypogene chalcocite and covellite contain up to 10–24 ppm Au, typically they are not sufficiently abundant to account for a significant part of the average gold grades of bulk ore in many porphyry copper deposits. In the Skouries deposit, gold in covellite has been attributed to deposition as gold colloid particles, during the supergene enrichment (Kesler *et al.* 2002).

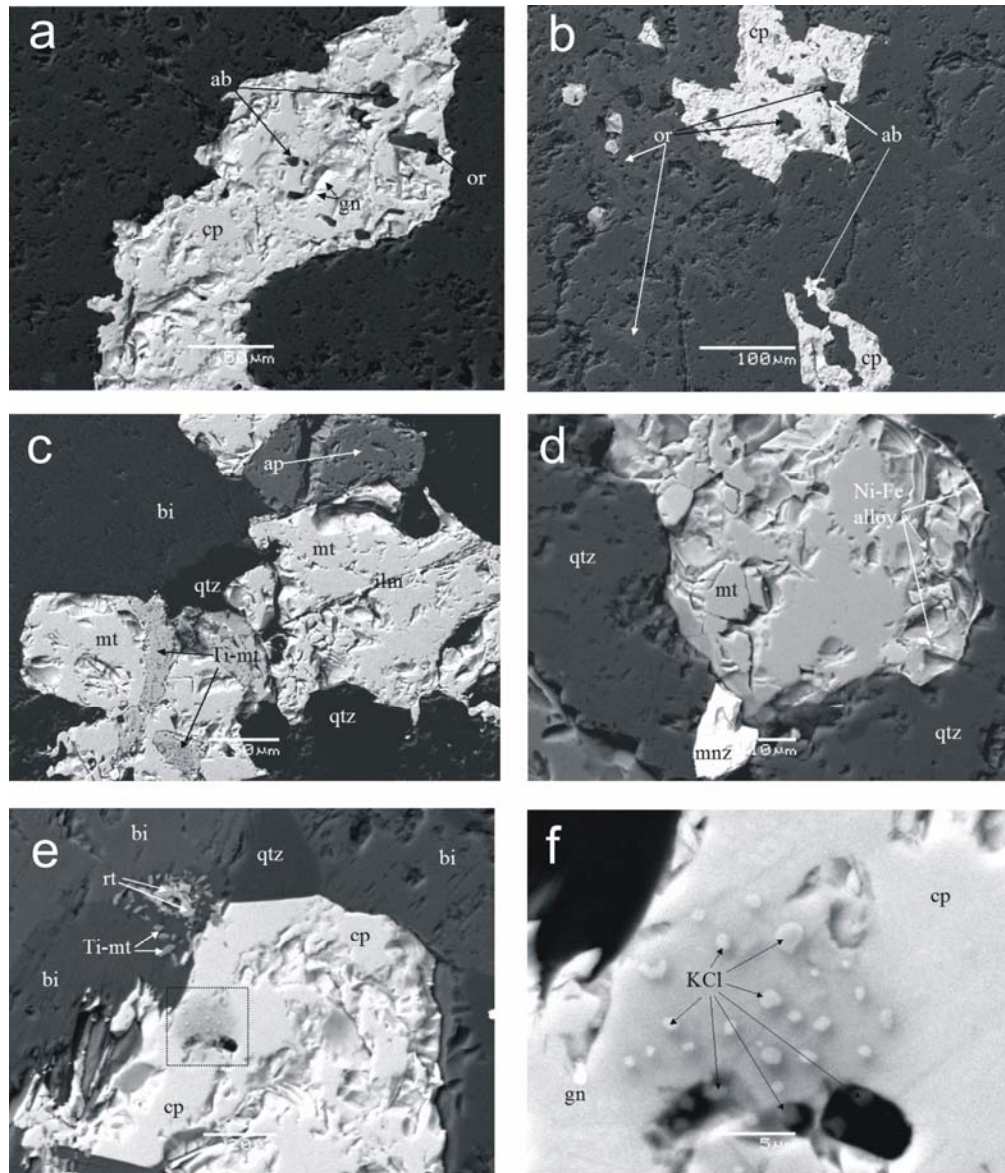


FIG.10-5. Backscattered electron images from drill core samples at Skouries porphyry deposit. **a,b**) chalcopyrite-galena intergrown with alkali feldspars; **c**) Ti-bearing magnetite-ilmenite intergrowths with apatite; **d**) association of Ni-Fe alloy with magnetite and monazite; **e, f**) sylvite crystals deposited around a decrepitated fluid inclusion hosted by chalcopyrite, associated with rutile-Ti magnetite intergrowths.

Pd-Pt-minerals

The palladium telluride, merenskyite, has been described as the main PGE mineral in porphyry Cu-Au-Pd-Pt deposits, such as Skouries, Santo Tomas II, Biga, Elatsite, Madjadanpek, Mamut (Fig. 10-1, 10-2, Tarkian *et al.* 2003). It occurs mostly as inclusions in chalcopyrite and bornite, as euhedral crystals at the margins of chalcopyrite or enclosed by electrum and hessite in chalcopyrite. Merenskyite may have only traces of

platinum or may occur as a member of the merenskyite-moncheite solid solution series, with small contents of Ni, Bi, and Ag. Intergrowths of merenskyite (PdTe_2) with kotulskite (PdTe), unnamed phases such as $(\text{Pd,Ag})_3\text{Te}_4$ and the silver telluride, hessite (Ag_2Te), are also common (Fig. 10-3, Tarkian *et al.* 1991, Piestrzynski *et al.* 1994, Tarkian & Koopmann 1995, Tarkian & Stribny 1999, Tarkian *et al.* 2003, Strashimirov *et al.* 2003).

TABLE 10-2. REPRESENTATIVE ELECTRON MICROPROBE ANALYSES OF SOME ORE MINERALS FROM THE SKOURIES AND ELATSITE DEPOSITS

Deposit	Sk	Sk	Sk	Sk	St	EL	EL	EL	EL	EL	EL	MAJ	MAJ	Sk	Sk	EL	Sk	Sk	Sk
Mineral	me	me	Pd, Bi-Tel.	me	el	el	el	el	he	sy									
Pd	27.51	26.8	16.35	14.87	29.41	28.4	26.01	15.15	17.38	27.6	28.44	n.d.	n.d.	n.d.	n.d.	n.d.	n.d.	n.d.	n.d.
Pt	0.6	1.21	14.69	8.86	3.33	0.82	3.28	16.14	13.47	1.1	0.03	n.d.	n.d.	n.d.	n.d.	n.d.	n.d.	n.d.	n.d.
Te	71.22	70.33	53.05	26.82	63.23	67.92	66.31	64.5	60.47	68.29	69.63	n.d.	n.d.	n.d.	n.d.	n.d.	n.d.	37.35	59.19
Bi	n.d.	n.d.	15.15	46.27	3.35	0.11	1.29	0.66	3.23	2.86	0.27	n.d.	n.d.	n.d.	n.d.	n.d.	n.d.	n.d.	n.d.
Au	n.d.	n.d.	n.d.	n.d.	n.d.	n.d.	n.d.	n.d.	n.d.	n.d.	n.d.	96.98	86.65	81.39	n.d.	n.d.	n.d.	24.15	n.d.
Ag	n.d.	n.d.	n.d.	1.21	n.d.	n.d.	0.55	1.03	1.57	0.02	0.01	1.96	10.42	16.34	60.21	14.81	n.d.	n.d.	n.d.
Cu	n.d.	n.d.	n.d.	n.d.	n.d.	0.97	0.5	0.57	1.89	n.d.	n.d.	0.54	0.72	3.97	0.51	0.82	n.d.	n.d.	n.d.
Ni	n.d.	n.d.	n.d.	n.d.	n.d.	n.d.	0.35	1.41	n.d.	n.d.	n.d.	n.d.							
Total	99.33	98.34	98.22	98.29	99.32	99.24	98.03	99.46	98.01	99.87	98.38	99.48	97.79	101.7	98.07	98.97	n.d.	n.d.	n.d.

Cont.

Deposit	EL	EL	MED	MED	Sk	Sk	Sk	Sk	Sk	Sk	Sk	Sk							
Mineral	lin	lin	lin	lin	sieg	sieg	sieg	sieg	sieg	Co-py	car	py	py	py	py	py	py	py	py
Fe	0.29	4	0.67	0.5	6.47	2.42	3.1	1.76	38.2	33.85	1.85	46.69	42.32	45.63	45.76	46.69	n.d.	n.d.	n.d.
Cu	18.99	19.95	13.19	14.17	11.08	1.51	0.19	0.38	0.1	0.1	15.9	n.d.	n.d.	n.d.	n.d.	n.d.	n.d.	n.d.	n.d.
Ni	1.39	7.84	8.63	11.91	24.82	33.2	39.52	41.14	5.3	0.4	3.2	1.01	2.41	0.45	1.16	1.03	n.d.	n.d.	n.d.
Co	37.95	31	35.99	33.05	18.33	21.21	14.48	15.13	2.2	12.45	37.55	n.d.	4.18	0.64	0.72	n.d.	n.d.	n.d.	n.d.
S	41.2	41.16	41.99	41.53	40.82	41.24	42.21	41.82	53.9	53.15	41.6	53.6	52.17	52.56	52.91	52.61	n.d.	n.d.	n.d.
Total	99.82	101	100.5	101.2	101.5	99.58	99.5	100.2	99.7	99.95	1001	101.3	101.1	99.28	100.6	100.3	n.d.	n.d.	n.d.

Abbreviations: me = merenskyite; el = electrum; he = hessite; sy = sylvanite; lin = linnaeite; Sieg = siegenite; py = pyrite; car = carrolite; Tel = tellurides; Sk = Skouries; St = Santo Tomas II; EL = Elatsite; MAJ = Majdanpek; MED = Medet; Data from: Tarkian *et al.* (1991); Piestrzynski *et al.* (1994); Tarkian & Stribny (1999); Tarkian *et al.* (2003); Present data (Pd-Bi-tellurides and pyrite from the Skouries deposit).

Tetrahedrite-tennantite

Tetrahedrite and tennantite are frequently associated with the magnetite-bornite-chalcopyrite assemblage of an early stage of mineralization (Tarkian *et al.* 2003). They are commonly located in those porphyry deposits which are in a spatial association with epithermal deposits, such as the Elatsite deposit associated with the Chelopech Au-Cu high-sulfidation epithermal deposit, the Assarel deposits in Bulgaria, and the Bor/Majdanpek porphyry deposits in Serbia, whereas in the Skouries deposit are rare.

Galena-clausthalite

In the Skouries porphyry deposit galena exsolution with significant selenium contents are very common in chalcopyrite, whereas in bornite they are very rare (Figs. 10-2 to 10-4). Solid solutions between galena and clausthalite are the dominant compositions, whereas end-member galena and clausthalite are rare (Tarkian *et al.* 2003). The presence of the independent selenium mineral clausthalite, in association with galena in porphyry Cu deposits, such as the Elatsite deposit, may be related with the evolution of the ore forming system (Xiong 2003).

Linnaeite-siegenite-carrollite

Carrollite with average Ni and Co contents of 2.73 and 26.22 wt.%, respectively, and Ni-Co-pyrite with Ni ranging from 0.05 to 5.3 wt.% Ni and 2.2 to 17.85 wt.% Co have been reported in the Medet porphyry deposit (Strashimirov 1982). Also, in addition to high Ni (0.5–6.7 wt.%) and Co (1.6–14.9 wt.%) in pyrite from the Elatsite deposits, members of the linnaeite-siegenite-carrollite solid-solution series have been described being replaced by chalcopyrite in the assemblages of magnetite-bornite-chalcopyrite and chalcopyrite-pyrite. Their Ni contents Ni (1.39–41.14 wt.%), and Co contents (14.48–37.95 wt.%) show a wide variation, with a preference of the Ni-poor, Co(Cu)-rich members in former assemblage (Tarkian *et al.* 2003).

SIGNIFICANT Pd AND Pt CONTENTS IN ONLY CERTAIN PORPHYRY COPPER DEPOSITS WORLDWIDE

As described in the Appendix to this article, certain porphyry Cu–Au deposits have elevated Pd–Pt contents, including Copper Mountain, Allard stock, Copper King Mt Milligan, Galore Creek, Ajax/Afton, Skouries, Elatsite, Santo Tomas II and Mamut (Table 10-1, Werle *et al.* 1984, Mutschler *et*

al. 1985, Eliopoulos & Economou-Eliopoulos 1991, Eliopoulos *et al.* 1995, Tarkian & Koopmann 1995, Tarkian & Stribny 1999), Economou-Eliopoulos & Eliopoulos 2000, Tarkian *et al.* 2003). Lower, but elevated Pd±Pt concentrations compared to those in typical porphyry deposits, have been reported in porphyry deposits such as Bor/Majdanpek, Serbia, Ok Tedi, Papua New Guinea, Grasberg, in Indonesia, Panguna, Papua New Guinea, Goonumbla/ North Parkes, and Cadia-Ridgeway, in New South Wales (Table 10-1, Jankovic 1980, Muller *et al.* 1994, Piestrzynski *et al.* 1994, Tarkian & Stribny 1999, Holliday *et al.* 2002).

Mineralization, consisting mainly of disseminated and vein-type magnetite and Cu-minerals (chalcopyrite and/or bornite), associated with central parts of the deposits exhibits the highest Pd and Pt enrichment. Although there is a variation throughout each mineralized zone the Pd/Pt and Pd/Cu ratios seem to be a characteristic feature of each porphyry Cu–Au±Mo deposit (Table 10-1) reflecting possibly the essential role of the composition of parent magmas, and in turn the genesis of alkaline arc magmas. Halter *et al.* (2002) demonstrated, by integrated microanalysis of major and trace elements in sulfide and silicate melt inclusions by laser ablation–ICP–MS, that parent magmas define the Cu/Au ratio of a related deposit, such as the Alumbraera porphyry Cu–Au deposit, Andes.

TYPICAL CHARACTERISTICS OF PORPHYRY Cu–Au–Pd±Pt DEPOSITS

The geological descriptions in Appendix A show that, in general, porphyry Cu–Au–Pd±Pt deposits are associated with alkaline rocks, in particular with alkaline porphyry systems characterized by SiO₂ <65 wt.%. Enriched mantle sources or major contributions by crustal material, are evidenced by strongly radiogenic ⁸⁷Sr/⁸⁶Sr and ²⁰⁷Pb/²⁰⁴Pb values. Parental magmas were volatile-rich, and moderately fractionated, characterized by relatively high concentrations of halogens (F, Cl), REE and Th, but commonly also showing elevated (several hundreds ppm) Cr and Ni contents (Eliopoulos *et al.* 1995, Economou-Eliopoulos & Eliopoulos 2001). Albitic (sodic) and calc-silicate (actinolite, epidote, diopside, garnet) minerals are common members of alteration assemblages in addition to biotite and K-feldspar. Copper and precious metals appear to have been transported as chloride complexes, by relatively hot (400° to 700°C) and saline to hypersaline (>70 wt.%

NaCl_{equiv}) hydrothermal fluids and were precipitated during the main stage of mineralization, as an association of bornite, chalcopyrite, pyrite and magnetite reaching up to 10 vol.% (average 6 vol.%), as veinlets and disseminations, associated with the potassic alteration type. Textural relations between Cu-minerals and the main Pd-bearing mineral, merenskyite, and Au-Ag tellurides, indicate that precious metals are closely associated with copper vein-type chalcopyrite or bornite, and are deposited during the earliest stages of alteration and mineralization in the central parts of deposits. Hydrothermal breccias are particularly abundant in large alkaline Au-Cu deposits (Jankovic 1980, Mutschler *et al.* 1985, Corbett & Leach 1998, Eliopoulos & Economou-Eliopoulos 1991, Eliopoulos *et al.* 1995, Frei 1995, Tarkian & Koopmann 1995, Sillitoe 2000, Müller & Groves 2000, Sotnikov *et al.* 2000, Tarkian *et al.* 2003, Strashimirov *et al.* 2003).

CRITICAL FACTORS FOR THE FORMATION OF PORPHYRY Cu+Au+Pd ±Pt DEPOSITS

The wide range of physicochemical conditions and the dynamic interplay between magmatic, hydrothermal and tectonic processes during the formation of porphyry Cu deposits in volcanoplutonic arcs, and the composition of alkaline parent magmas or those of large batholithic bodies underlying at greater depths the porphyry stocks may be major controls of their base/precious metal potential and characteristics. These could include such things as the hydrous and oxidized nature, and their ability to produce hydrothermal systems with ideal chemistry for transporting precious metals. In addition, alkaline magmas are inherently richer in SO₂ and CO₂ than their calc-alkaline counterparts, volatiles that have a significant influence on fluid pressures, brecciation and permeability of host rocks (Sillitoe 2000, Müller & Groves 2000, Tosdal & Richards 2001, Richards 2003).

Experimental, thermodynamic, and fluid-inclusion studies strongly suggest that Cu and precious metals in potassic alteration zones are transported as an aqueous chloride complex in high-temperature (350 to >700°C) and relatively oxidized hydrothermal brines that are produced mainly (but not always) by aqueous fluid immiscibility (Burnham & Ohmoto 1980). In contrast, given that significant quantities of Au can be transported by hot, saline, magmatic fluids under either reducing or

oxidizing conditions, whereas Cu transport is much more favored in the oxidizing environment, “reduced” porphyry Cu–Au deposits that lack primary hematite, magnetite, and sulfate minerals (anhydrite) and contain abundant hypogene pyrrhotite, are relatively Cu-poor, but Au-rich deposits (Hemley *et al.* 1992, Williams *et al.* 1995, Rowins 2000). Halter *et al.* (2002) have focussed their investigation on sulfide melt and silicate melt inclusions on the Farallon Negro volcanic complex, hosting the Alumbraera porphyry Cu–Au deposit. Most major and trace elements in silicate melt inclusions follow the differentiation trend defined by bulk rock composition, except for Cu, varying at all stages of magmatic evolution. They concluded that magmatic sulfide melts can act as intermediate metal hosts, which preconcentrate Cu and precious metals during the evolution of the magmatic system before volatile saturation, and probably participate in an important step in the genesis of porphyry-type deposits. The ore-forming hydrothermal fluid acquired its high metal content and characteristic Au/Cu ratio by bulk destabilization of magmatic sulfides with similar metal ratios.

Sources of Metals and Sulfur in Porphyry Copper Deposits

The contribution of mantle, oceanic and continental crust to the parent magmas of porphyry copper intrusions remains still uncertain (Burnham 1979, Burnham & Ohmoto 1980, McInnes & Cameron 1994, Keith *et al.* 1998, Tittley 2001, Hattori & Keith 2001). Numerous authors have suggested crustal sources for some ore metals in the southern Arizona deposits (Tittley 2001). Evidence from xenoliths, geological, mineralogical, geochemical and isotopic data indicates that the high Pd and Pt mineralization in the porphyry deposits of the British Columbia Cordillera, and the higher Pd and Pt levels in fresh and unaltered samples from the Lihir rocks compared to typical background values for crustal rocks (Taylor & McLennan 1985) are linked with the genesis of alkaline arc magmas, derived probably from an enriched mantle source (McInnes & Cameron 1994). They may reflect partial melting and incorporation into the melt of destabilized precious metal-bearing Fe–Ni–Cu-sulfides, hosted in the mantle source (Keith *et al.* 1998, Hattori & Keith 2001). The occurrence of mafic dikes, post-dating the porphyry mineralization at the Elatsite deposit (Fig. 10-6, von Quadt *et al.* 2002, Strashimirov *et al.* 2003), and relatively high Re concentrations in the molybdenite

from main stage stockwork mineralization of the Elatsite Cu–Au deposit, Bulgaria (average 1880 ppm), has been attributed to a direct involvement of mantle in an arc-subduction environment as well (Zimmerman *et al.* 2003). In addition, Xiong & Wood (2002), based on experimental data, suggested that reducing fluids containing sulfur have much less capacity for transporting Re, and environments dominated by reducing fluids are not favorable to Re deposition. However, mixing processes involving an oxidized Re-containing solution and a solution with reduced sulfur should be effective depositional mechanisms for rhenium.

Although intense hydrothermal alteration has commonly destroyed any record of possible magmatic sulfide blebs, they have been reported in submarine alkaline volcanic rocks in the Tabar-Lihir-Tanga-Feni chain and latite dikes related to the Bingham porphyry deposit (Keith *et al.* 1998, Hattori & Keith 2001, Thompson *et al.* 2001). These blebs, due probably to degassing during crystallization of high level intrusions or lavas, contain elevated Au and Pd, which may be subsequently oxidized or altered, resulting in release of the metals to the volatile phase during magmatic-hydrothermal activity. On the other hand, the oxidized nature of the alkaline arc magmas inhibits fractionation of sulfides, allowing the precious metals to remain in the magmas, and thus they were transported by magmatic-hydrothermal fluids and precipitated in the porphyry environment

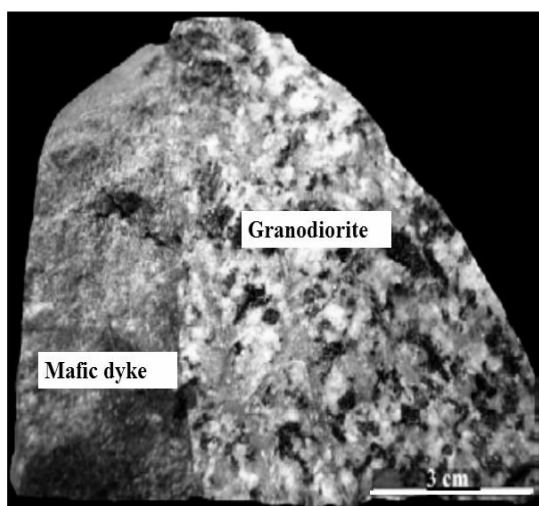


FIG.10-6. Mafic dike crosscutting granodiorite from the central part of the Elatsite porphyry deposit (after Strashimirov *et al.* 2003).

(McInnes & Cameron 1994, Thompson *et al.* 2001).

The incorporation of PGE-enriched material in the mantle source and/or within the crust at depth, prior to the final emplacement, may be evidenced by the $^{87}\text{Sr}/^{86}\text{Sr}$ and $^{207}\text{Pb}/^{204}\text{Pb}$ values (Fig. 10-7, Jankovic 1980, Frei 1995, Sillitoe 2000, Müller & Groves 2000, Sotnikov *et al.* 2000, Tosdal & Richards 2001, von Quadt *et al.* 2002) and would supply PGE to the porphyry stocks or hydrothermal systems. The contribution of crustal material and the presence of mafic/ultramafic rocks among country rocks has been suggested in the porphyry Cu systems of the Serbo-Macedonian massif (Balkan Peninsula) (Jankovic 1980, Frei 1992, Gilg 1993, Ciobanu *et al.* 2002, Heinrich & Neubauer 2002), Russia and Mongolia (Sotnikov *et al.* 2000), and the Ajax/Afton deposits, British Columbia (Ross *et al.* 1995). Also, Perugini *et al.* (2004) emphasized the spatial and temporal association of the subvolcanic stocks with lamprophyres, mafic microgranular and alkaline dikes in the Serbo-Macedonian massif, and proposed the interaction processes between mantle-derived and crustal melts. Moreover, the enrichment (hundreds ppm) in compatible elements such as Cr, Co±Ni, that occur in the Skouries, Elatsite, Medet, Assarel and Trar Asen porphyry deposits of the Balkan Peninsula (Table 10-2, 10-3, Eliopoulos *et al.* 1995), despite their otherwise more evolved geochemical signatures, may have been inherited due to magma mixing with mafic alkaline rocks. Moreover, mafic fragments with disseminated and vein-type mineralization (Fig. 10-2), Cr-bearing magnetite, Ni, Co-bearing pyrite and chalcopyrite (Tables 10-2 & 10-4), are common in particular at the peripheral parts of the Skouries main porphyry stock. Although the assimilation of amphibolites (meta-mafic rocks) and the supply of metals is not precluded, the possibility that the country rocks (amphibolites) could be a significant Cu, Pd and Pt source is inconsistent with the presence of only a narrow (< 50 m wide) halo of alteration (Frei 1995). Additional evidence for incorporation of PGE, Cr, Co, Ni-enriched material in the mantle source and/or during the upward ascent of magma within the crust, prior to the final emplacement, is the presence of linnaeite-siegenite-carrollite solid solution series and Ni-Co-pyrite in the assemblages of magnetite-bornite-chalcopyrite

PGE POTENTIAL OF PORPHYRY DEPOSITS

TABLE 10-3. PRECIOUS METAL AND ASSOCIATED TRACE ELEMENT DATA FROM THE SKOURIES PORPHYRY CU DEPOSIT.

sample	depth	ppb Pd	ppb Pt	ppb Au	Cu/Au	Pd/Pt	Pd/Cu	Au/Ag	ppm Ag	Wt.% Cu	ppm Zn	ppm Pb	ppm Cr	ppm Ni	ppm Co	ppm Mo
sku400	surface	30	<10	2210	5.9	>0.3	23	540	4.1	1.31	50	30	30	40	20	2
SOP 01	219	27	28	1170	10.8	0.96	21	509	2.3	1.29	80	64	160	140	24	2
SOP 01	326	54	43	4790	4.15	0.8	20	1842	2.6	1.99	100	80	130	300	30	2
SOP 01	328	53	42	4930	3	0.8	36	704	7	1.47	97	40	110	250	25	1
SOP 01	635	5	<10	190	3.2	>0.5	83	>95	<0.2	0.06	38	21	50	42	26	2
SOP 01	636	3	<10	50	12	>0.3	50	>950	<0.2	0.06	32	15	60	71	21	8
SOP 06	363	85	20	683	7.5	4.2	167	190	3.6	0.51	39	52	3	8	31	1
SOP 06	365	49	49	3880	3.3	1	39	<388	>10	1.27	80	60	10	210	24	2
SOP 06	525	29	22	549	12.4	0.76	42	422	1.3	0.68	110	34	260	310	62	1
SOP 06	527	6	<10	120	11.7	>0.6	43	>600	<0.2	0.14	77	32	80	224	38	4
SOP 09	252	31	33	1410	7.8	1.06	28	>7050	<0.2	1.1	73	30	8	50	35	3
SOP 18	142	42	64	3850	3.9	1.52	28	1604	2.4	1.52	75	84	4	50	22	2
SOP 18	178	16	26	532	15	1.62	20	760	0.7	0.8	67	110	6	30	30	11
SOP39	446	606	73	9600	2.6	8.3	29	806	11.9	2.53	60	29	10	8	74	3
SOP 43	200	15	<10	1520	10.3	>1.5	10	894	1.7	1.56	130	13	484	560	56	1
SOP 46	50	1	<10	70	223	>0.1	7	>350	<0.2	0.14	94	50	125	127	29	240
SOP 76	170	2	<10	590	12.03	>0.2	3	983	0.6	0.71	180	12	690	504	41	100
SG-6	30	360	31	3050	10.2	11.6	118	924	3.3	3.1	50	23	17	13	27	7
SG-6	110	28	10	850	4.6	2.8	72	1700	0.5	0.39	66	71	6	17	62	2
SG-6	465	410	26	5280	3.6	15.8	216	1650	3.2	1.89	46	31	7	7	41	1
SG-6	494	420	150	12900	2.2	2.8	53	2795	3.4	2.84	60	21	17	10	43	<1
SK8	130	20	<10	1700	7.1	>2	17	1210	1.4	1.21	53	43	8	21	48	<1
SK8	620	17	<10	1520	34.9	>1.7	3.2	585	2.6	5.3	100	26	59	70	24	<1
SK8	671	140	<10	1580	7.3	>14	120	1215	1.3	1.16	63	19	61	48	38	25

TABLE 10-4. REPRESENTATIVE ELECTRON MICROPROBE ANALYSES OF REE-MINERALS FROM THE SKOURIES DEPOSIT

Sample Minera l	SOP46 Monazite	SOP43 Thorite	SOP18 U-Thorite	SK8 U-Thorite	SK8 U-Thorite	SOP18 Epidote	SOP18 Allanite	SOP18 Allanite
SiO ₂	1.15	18.82	15.63	15.17	15.41	38.34	32.13	35.37
Al ₂ O ₃	n.d	n.d	n.d	n.d	n.d	27.18	16.18	14.11
FeO	n.d	n.d	0.57	4.26	2.64	8.32	13.91	17.41
CaO	0.76	n.d	n.d	n.d	n.d	n.d	12.38	13.59
P ₂ O ₅	30.26	n.d	n.d	n.d	n.d	22.17	n.d	n.d
La ₂ O ₃	17.21	n.d	n.d	n.d	n.d	n.d	5.11	3.89
Ce ₂ O ₃	31.57	n.d	n.d	n.d	n.d	0.85	14.53	12.54
Nd ₂ O ₃	10.45	n.d	n.d	n.d	n.d	2.16	4.74	2.18
Pr ₂ O ₃	2.76	n.d	n.d	n.d	n.d	n.d	n.d	n.d
ThO ₂	5.06	79.44	70.68	50.84	66.03	n.d	n.d	n.d
UO ₃	n.d	n.d	11.68	29.12	15.21	n.d	n.d	n.d
Total	99.22	98.26	98.56	99.39	99.29	99.02	98.98	99.09

and chalcopyrite-pyrite of the Medet and Elatsite porphyry deposits (Tables 10-2 & 10-3, Strashimirov 1982, Tarkian *et al.* 2003). Porphyry Cu–Mo±Pd±Pt deposits of Russia and Mongolia are more or less characterized by relatively large crustal contributions (Sotnikov *et al.* (2000). Although giant porphyry Cu–Mo deposits in the central Andes are characterized by a lesser degree of crustal contribution, a porphyry-skarn Cu–Au–Mo deposit at Bingham Canyon, Utah, has a strong crustal signature (Keith *et al.* 1998). The enrichment (hundreds ppm) in compatible elements,

such as Cr and Ni, that occur in the relatively more siliceous rock units of the Bingham system, may have been inherited from magma mixing with mafic alkaline magmas capable of carrying more than 3000 ppm dissolved S. Such a mixing of the silica-undersaturated component into already existing calc-alkaline, subvolcanic magma chambers could have added significantly to the overall budget of water, sulfur, and ore metals in evolving felsic magmas that eventually gave rise to the Bingham ore deposit (Waite *et al.* 1997, Hattori & Keith 2001, Maughan *et al.* 2002).

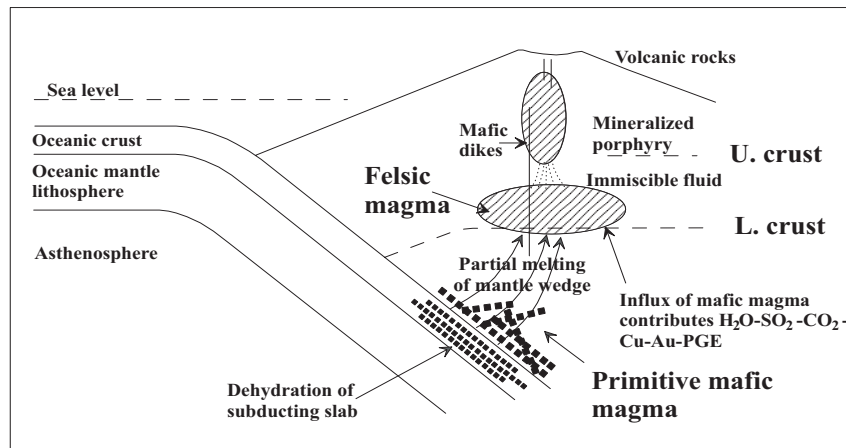


FIG.10-7. Schematic section of a subduction zone and continental arc (at convergent plate boundaries), showing the geotectonic setting for porphyry Cu mineralization. Hydrous, metal-bearing-melt extracted from the subducting slab, rising into the mantle wedge causes metasomatism. Partial melting of metasomatized mantle generates mafic melts, which at depth may contribute metal, including PGE, and sulphur, which are incorporated into the overlying felsic magma chamber (compilation from Sillitoe 2000, Richards 2003, Hattori & Keith 2001).

Evolution of Mineralized Systems

Evidence for the evolution of mineralizing fluids in porphyry systems is provided by isotope and/or fluid inclusion data. The oxygen and hydrogen isotope investigation in the Skouries deposit revealed high $\delta^{18}\text{O}$ (8 to 10 per mil) and low δD values (–95 to –70 per mil) for fluids in equilibrium with vein quartz/main stage of mineralization, and $\delta^{34}\text{S}$ values from vein and disseminated sulfides (–2.1 to +0.3 per mil) falling within the typical range of early ore-forming fluids, whereas low $\delta^{18}\text{O}$ and high δD values for fluids are linked with the pyrite-chalcopyrite mineralization (Gilg 1993, Frei 1995). Fluid inclusion studies provide evidence for two different fluid types, an early CO_2 -rich fluid of an early intermediate salinity, which locally boiled on ascent to shallower parts of the deposit and thereby formed brine and vapor-rich inclusions synchronous with the main stage of mineralization, and late low salinity fluids (Gilg 1993, Frei 1995, Kehayov *et al.* 2003).

Available analytical data (Tables 10-1 & 10-2) indicate that Pd, Pt and Au contents are relatively higher in the magnetite-bornite-chalcopyrite assemblages associated with pervasive potassic alteration found at the central parts of the deposits, than in the chalcopyrite-pyrite ores linked to the phyllic-argillic alteration type, characteristic of the upper and marginal parts of the deposits (Tarkian *et al.* 1991, 2003, Frei 1995, Economou-Eliopoulos & Eliopoulos 2000, Kouzmanov *et al.* 2001, 2003, Strashimirov *et al.* 2003). Thus, isotopic and fluid inclusion trends in porphyry Cu deposits seem to be systematic, beginning with high $\delta^{18}\text{O}$ and low δD values, and CO_2 -rich fluid/ intermediate salinity for fluids in equilibrium with vein quartz/main stage of Cu, Au, Pd, Pt mineralization to low $\delta^{18}\text{O}$ and high δD values/low salinity fluids for fluids linked with the pyrite-chalcopyrite mineralization.

Given that both Pd and Pt may be transported as chloride complexes in the porphyry environment under acid and oxidizing conditions, the association of Cu, Au, Pd and Pt in porphyry Cu deposits may be explained in part by a similar transport and deposition, with decreasing temperature to approximately 400°C (to allow the precipitation of chalcopyrite \pm bornite), an increase in pH, and a decrease in $f(\text{O}_2)$ and $a(\text{Cl}^-)$ (Gammons *et al.* 1992, Wood *et al.* 1992, Sillitoe 1993, Xiong & Wood 2000). Kesler *et al.* (2002), based on SIM (ion probe) analyses of ore minerals from numerous porphyry Cu deposits, concluded that primary gold

mineralization is overprinted by secondary enriched zones containing covellite and chalcocite with inclusions of gold and that the maximum gold endowment of porphyry copper deposits is probably fixed by the amount of gold that will go into solid solution in Cu-Fe sulfides when the deposit forms at high temperature. Gold is not commonly added later from other sources, although it can be redistributed during cooling or later events. Furthermore, the evolution of the magmatic-hydrothermal systems has been investigated on the basis of EMP, microthermometric and laser ablation–ICP–MS analyses of silicate and sulfide melt inclusions (Halter *et al.* 2002, 2005, Ivascanu *et al.* 2003).

Importance of Vapor Phase in the Transport of Ore Elements

Quartz predating the bulk of bornite precipitation in the porphyry Cu deposit of Apuseni Mountains (Romania) hosts sulfide melt inclusions and silicate melt, together with highly saline brine inclusions, providing evidence for immiscibility between magmatic liquid and hydrous salt melt as the primary source of ore metals in porphyry Cu systems (Pintea 1995). On the basis of experimental metal-solubility studies of porphyry Cu systems it has been demonstrated that Cu and Au partition into the saline aqueous brine during immiscible phase separation of oxidized high-temperature fluids (Williams *et al.* 1995). Furthermore, new micro-analytical methods, using proton-induced X-ray emission (PIXE) and laser ablation – inductively coupled plasma – mass spectrometry (LA–ICP–MS) studies of fluid inclusions from reduced porphyry Sn–W–Ag deposits and porphyry-related Au–Mo breccias indicate that Cu, and very likely Au, strongly partition into the low-density H_2S -rich vapor phase rather than the coexisting high-density chloride-rich liquid phase (Heinrich *et al.* 1999). Halter *et al.* (2002) have suggested that ore-forming hydrothermal fluids can acquire high metal content and characteristic Au/Cu ratio by bulk destabilization of magmatic sulfides with similar metal ratios. Textural relationships between successive quartz generations, microthermometry and laser ablation–ICP–MS analysis of fluid inclusions from the Elatsite, Bulgaria, deposit revealed a trend of decreasing Na, K, Cu, Ag, Bi, Sn, and Ce with decreasing temperature, while the Mo, Pb, Zn, Sr, Mn concentrations increased (Fig. 10-8), and copper in the fluids decreases from

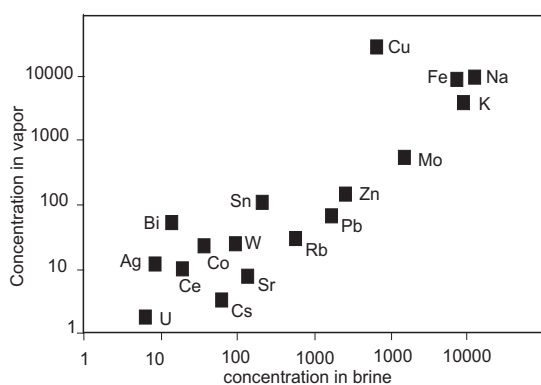


FIG.10-8: Correlation between metal contents in vapor and coexisting brine inclusions from boiling assemblages of the qtz-mt-cp-pn stage of mineralization (after Kehayov *et al.* 2003).

40000 ppm in magnetite-bornite-chalcocopyrite stage (with the precipitation of the Cu-minerals) to about 4000 ppm in the chalcocopyrite-pyrite stage, and about 1000 ppm in the quartz-pyrite stage (Kehayov *et al.* 2003).

Exploration – Key Characteristics of Cu+Au+Pd ±Pt Deposits

Elevated PGE (Pt and Pd) contents, reaching hundreds of ppb, have been recorded in both Cu(Au) and Cu–Mo–Au porphyry deposits, but the Pd and Pt contents are much higher in the former (characterized by $\text{SiO}_2 < 65 \text{ wt.}\%$), than in the latter (Table 10-1, Mutschler *et al.* 1985, Tarkian & Stirbrny 1999, Economou-Eliopoulos & Eliopoulos 2000, Sotnikov *et al.* 2000, Thompson *et al.* 2001). Moreover, many alkaline systems contain much less hydrothermal quartz compared to most subalkaline systems and quartz is even absent in some high-temperature alkaline deposits, like porphyry Cu–Au–Pd–Pt deposits of British Columbia (Jensen & Barton 2000, Thompson *et al.* 2001).

Exploration for alkaline porphyry deposits is encouraged by their large size and high grades and because they are environmentally favorable to mine, due to the low pyrite and high acid-buffering potential (Corbett & Leach 1998). The association of magnetite (>10% by volume) is a common feature of most Au-rich porphyry Cu–Au deposits; this coupled with the predominant association of PGE mineralization with the magnetite-rich potassic phase of alteration allows direct geophysical recognition of the mineralized zones (*e.g.*, the Skouries deposit, Tobey *et al.* 1998). Geophysical and geochemical signatures of these deposits are

variable, but the characteristics of the mineralization and alteration can be recognized in almost all examples, providing an effective exploration tool (Sillitoe 2000). The most productive deposits show evidence for voluminous metasomatism and multiple magmatism. Copper-gold exploration models are based on detailed structural mapping (at surface and in drill holes) and identification of alteration styles and mineralization, with the aim of identifying the optimum sites for maximum fluid permeability and mineralization (Corbett & Leach 1998). Although the alteration type is an important indicator of the fluid composition, ore mineral assemblages themselves and the bulk ore chemistry reflect the composition of the parent magma and the nature of the ore fluids, in particular the maximum precious metal endowment of porphyry copper deposits, their chemistry and capacity for transporting sufficient Au and PGE (Jensen & Barton 2000, Xiong & Wood 2000, Halter *et al.* 2002, 2005, Kesler *et al.* 2002, Sillitoe & Hedenquist 2003).

The presence of elevated concentrations of Co, Ni and Cr either in the whole ore analysis or in minerals (linnaeite-siegenite-carrollite solid solution series and Ni-Co-pyrite) in the assemblages of magnetite-bornite-chalcocopyrite and chalcocopyrite-pyrite, and the presence of Cr-bearing magnetite (Table 10-2, 10-3, Strashimirov 1982, Tarkian *et al.* 2003), may provide evidence for incorporation of PGE, Cr, Co, Ni-enriched material in the mantle source and/or during upward-rising of magma within crust prior to the final emplacement (Waite *et al.* 1997, Hattori & Keith. 2001, Maughan *et al.* 2002).

However, only certain porphyry-Cu-Au deposits are Pd-Pt-enriched, that seems to be a characteristic feature of each deposit, despite their variation throughout a deposit (Table 10-1, Halter *et al.* 2002). Apart from the capacity of a magmatic-hydrothermal system in precious metals and the possibility to form economic deposits, the association, in space and time (Cathles 1997), between porphyry and epithermal deposits may play a major role on the evolution of the whole system and the grade/size of porphyry Cu–Au–Pd–Pt deposits. Einaudi *et al.* (2003) suggested deep porphyry Cu environments as transitional into shallower porphyry-related base metal vein and replacement deposits, and near surface into epithermal Au–Ag deposits. They concluded that the majority of porphyry Cu deposits containing magnetite in association with Cu-minerals (bornite,

chalcopyrite) ± pyrite are of intermediate sulfidation state.

Many of the porphyry Cu±Mo±Au deposits in Chile, Peru, Philippines and the Balkan Peninsula are located in the same arc region as the high-sulfidation deposits. They are commonly generated in calc-alkaline andesitic to dacitic arcs, characterized by neutral or weakly extensional stress states (Werle *et al.* 1984, Sillitoe 1997, 2000, Sillitoe & Hedenquist 2003). Extension, deduced from graben control of volcanism, during intermediate to high-K calc-alkaline volcanism and formation of major high-sulfidation deposits, such as the Bor (Serbia) and Chelopech (Bulgaria) have been described too (Hedenquist *et al.* 1998, Popov *et al.* 2000, Ciobanu *et al.* 2002, Strashimirov *et al.* 2003, Sillitoe & Hedenquist 2003). The presence of fluid inclusions hosted by enargite in epithermal deposits, like Chelopech (Bulgaria) and Bor (Serbia), with moderate salinities (4 to 20 wt.% NaCl_{eq}), coupled with the common presence of sericitic roots to lithocaps in general, may suggest that the high-sulfidation ore fluids are affiliated with the sericitic stage of underlying porphyry deposits. Moreover, the Ag/Au ratios may be controlled by the metal endowment of the parent magmas rather than the chloride content of the early sulfide-precipitating fluids (Sillitoe & Hedenquist 2003).

Low-sulfidation deposits are associated with bimodal (basalt-rhyolite) volcanism and may accompany extension-related alkaline magmatism, which is capable of generating porphyry Cu deposits. For example the Porgera and Ladolam deposits, Papua New Guinea, both associated with alkaline rocks, have been interpreted as a transition stage between an early stage, low-grade porphyry gold system and that evolved into low-sulfidation epithermal conditions (Ronacher *et al.* 2000, Moyle *et al.* 1990, Carman 1994, 2003, Müller *et al.* 2002). Elevated precious metal (Au–Pt–Pd) concentrations have been interpreted as primary magmatic features suggesting a precious metal pre-enrichment of the mantle source beneath the Ladolam deposit (Taylor *et al.* 1994, Müller *et al.* 2003).

A salient feature of the Assarel and Bor porphyry deposits, which are found in close proximity (transitional) to epithermal gold deposits (Strashimirov *et al.* 2003) is their much lower Pd and Pt contents compared to those of the Elatsite porphyry Cu–Au deposit, which is found at a ~10 km distance from the Chelopech Au–Cu high-

sulfidation epithermal type deposit, and the Skouries deposit, where there is no association with epithermal deposits (Table 10-1). This seems to be consistent with the lower solubilities of Pd and Pt than Au (Wood 2002). Therefore, Pd and Pt seem to be precipitated during an earlier stage in the Elatsite deposit and hence the Chelopech area epithermal systems in general and porphyry systems with transitional features are not good targets for Pd, Pt exploration.

EVALUATION OF Pd AND Pt AS AN ECONOMIC FACTOR FOR PORPHYRY Cu–Au SYSTEMS

To assess the PGE budget of a porphyry system, it is important (a) to analyze representative ore samples, and (b) to ensure that the ore samples are not coming from zones dominated by chalcocite and covellite, as they may exhibit high Au contents and negligible Pd–Pt contents, due to preferential mobilization during subsequent epigenetic processes (Wood 2002). For example, ore samples from the Assarel deposit, Bulgaria, have gold content up to 20 ppm Au, 3 ppb Pd and < 10 ppb Pt (Eliopoulos *et al.* 1995). Therefore, although the analytical data required for the evaluation of the precious metal potential of the majority of porphyry deposit are limited, the available data are considered to be encouraging for Pd and Pt as by-products, with Au as a by- or co-product with Cu.

Relatively high Pd contents in the major vein-type mineralization of Skouries ranging between 60 and 200 ppb (average 110 ppb Pd) was documented by analysis of a composite drill hole sample (~15 kg) showing 76 ppb Pd to 5000 ppm Cu. Assuming that Pd in porphyry Cu deposits is mainly associated with chalcopyrite (measured contents are normalized to 100 % chalcopyrite), then the average Pd and Pt values (from numerous mineralized samples of the Skouries deposit) are 3000 ppb and 1230 ppb, respectively (Table 10-5, Economou-Eliopoulos & Eliopoulos. 2001).

Using 206 Mt reserves according to recent data by TVX (Tobey *et al.* 1998), and average concentrations (0.5 wt.% Cu, 75 ppb Pd and 17 ppb Pt), then the potential of the Skouries deposit is approximately 15 tons Pd and 3.5 tons Pt. Also, using reserves and average Pd and Pt contents the potential is about 13 tons Pd and 3.7 tons Pt for the Elatsite deposit, 10.5 tons Pd and 1.6 tons Pt for the Santo Tomas II, Philippines deposit, and 10.5 tons Pd for the Afton deposit, B.C.

TABLE 10-5. PALLADIUM AND PLATINUM POTENTIAL IN PORPHYRY-CU-AU-PD-PT DEPOSITS

Deposit	Ore tonnage tons x 10 ⁶	Pd grade ppm	Pt grade ppm	Pd tonnage tons	Pt tonnage tons
Skouries, Greece	206	0.076	0.017	15	3.5
Elatsite, Bulgaria	185	0.07	0.02	13	3.7
Santo Tommas, Philippines	330	0.032	0.005	10.5	1.6
Afton, B.C.	70	0.13		9	

Data from: Tarkian & Koopmann (1995), Tobey *et al.* 1998, Economou-Eliopoulos & Eliopoulos (2000), Strashimirov *et al.* (2003), Dolbear & Company (2003).

PALLADIUM AND PLATINUM RECOVERY

Significant quantities of Pd and Pt have been recovered at the final stages of copper refining in the U.S.A., although their concentration in the ores are very low (Jolly 1978). Approximately one ounce is the estimated amount of PGE that is recovered from each 35 tons of copper produced in the U.S.A. (Ageton & Ryan 1970). However, only limited data are available for roasted concentrates (Parker 1978).

Samples of milled flotation concentrates derived from large (~15 kg) composite drill-hole porphyry samples from the Skouries porphyry Cu–Au deposit were used for the extraction of Pd, Pt and Au (Kioussis 2004, Kioussis *et al.* 2005). The applied process method in this study was based on one of the methods used by the U.S. Bureau of Mines for the treatment of sulfide concentrates coming from the Stillwater deposit (Baglin 1988). This method was finally selected as it best meets the technical and environmental processing requirement of the present concentrates and its ability to minimize the environmental impacts. The recovery method includes two stages: roasting of the concentrates at 900°C for 2 h (transformation of metal sulfide to native metals), and a leaching procedure. At temperatures above 800°C the sulfides and the tellurides of palladium and platinum (merenskyite) can be oxidized and subsequently, as the roasting temperature increases, these oxides are split into native metals. Only this form of precious metals is leachable in dense aqueous solutions of hydrochloric acid plus H₂O₂ 0.03M, for 24h at 70°C. (Baglin 1988). The leaching process resulted in the recovery of 96.6% Au, 97.7% Pd and 100% Pt. Although more research is required, these results are considered to be highly encouraging and this leaching method can be environmentally friendly under certain conditions.

ACKNOWLEDGEMENTS

Many thanks are expressed to James Mungall for inviting this contribution and his patience, and to the reviewers Rob Kirkham and Thomas Pettke, for their constructive criticism and suggestions on an earlier version of the manuscript. The careful reading of this work and linguistic improvement by J. Mungall and R. Kirkham are greatly appreciated.

REFERENCES

- AGETON, R.W. & RYAN, J.P. (1970): Platinum-group metals. *In Minerals Facts and Problems. U.S. Bur. Mines Bull.* **650**, 653-669.
- ALLMENDINGER, R.W., FIGUEROA, D., SNYDER, D., BEER, J., MPODOZIS, C. & ISACKS, B.L. (1990): Foreland shortening and crustal balancing in the Andes at 30°S latitude. *Tectonics* **9**, 789-809.
- ATKINSON, W.W. JR. & EINAUDI, M.T. (1978): Skarn formation and mineralization in the contact aureole at Carr Fork, Bingham, Utah. *Econ. Geol.* **73**, 1326-1365.
- AUGÉ, T. & LEROUGE, C. (2004): Mineral chemistry and stable-isotope constraints on the magmatism, hydrothermal alteration, and related PGE-(base-metal sulphide) mineralization of the Mesoproterozoic Baula-Nuasahi Complex, India. *Mineral. Deposita* **39**, 583-607.
- BABCOCK, R.C.JR., BALLANTYNE, G.H. & PHILLIPS, C.H. (1995): Summary of the geology of the Bingham district, Utah. *In Porphyry copper deposits of the American Cordillera*, Pierce, F.W., Bolm, J.G. (eds.). Tucson, Arizona. *Geol. Soc. Digest* **20**, 316-335.
- BAGLIN, E.G. (1988): A summary of U. S. Bureau of Mines research on Stillwater complex platinum-palladium ore. Reno Research Center.

- Bureau of Mines, *U.S. Department of the Interior Reno, Nevada, U.S.A.* 17p.
- BALLANTYNE, G.H., SMITH, T.W. & REDMOND, P.B. (1997): Distribution and mineralogy of gold and silver in the Bingham Canyon porphyry copper deposit, *Utah Soc. Econ. Geol. Guidebook* **29**, 147-153.
- BAMFORD, R.W. (1972): The Mount Fubilan (Ok Tedi) porphyry copper deposit, Territory of Papua and New Guinea. *Econ. Geol.* **67**, 1019-1033.
- BERZINA, A.P. & SOTNIKOV, V.I. (1999): Magmatic centers with porphyry Cu-Mo mineralization in the Central Asian mobile belt (by the example of Siberia and Mongolia). *Russ. Geol. Geophys.* **40**, 1577-1590. – ref not used?
- BERZINA, A.P., SOTNIKOV, S., ECONOMOU-ELIOPOULOS, M. & ELIOPOULOS, D.G. (2005): Distribution of rhenium in molybdenite from porphyry Cu–Mo and Mo–Cu deposits of Russia (Siberia) and Mongolia. *Ore Geol. Reviews*, **26**, 91-113.
- BLEVIN, P.L. (2002): The petrographic and compositional character of variably K-enriched magmatic suites associated with Ordovician porphyry Cu-Au mineralisation in the Lachlan Fold Belt, Australia. *Mineral. Deposita* **37**, 87-99.
- BOOKSTROM, A.A., CARTEN, R.B., SHANNON, J.R. & SMITH, R.P. (1998): Origins of bimodal leucogranite-lamprophyre suites, Climax and Red Mountain porphyry molybdenum systems, Colorado: petrologic and strontium isotopic evidence. *Colorado School Mines Quart.* **83**, 1-22.
- BOTTOMER, L.R. & LEARY, G.M. (1995): Copper Canyon porphyry copper–gold deposit, Galore Creek area, northwestern British Columbia. In *Porphyry Deposits of the Northwestern Cordillera of North America*, Schroeter, T.G. (ed.). *Can. Inst. Mining Metall., Special Vol.* **46**, 645-649.
- BROOKS, C.K., TEGNER, C., STEIN, H. & THOMASSEN, B. (2004). Re–Os and $^{40}\text{Ar}/^{39}\text{Ar}$ ages of porphyry molybdenum deposits in the east Greenland volcanic-rifted margin *Econ. Geol.* **99**, 1215-1222.
- BURNHAM, C. (1979): Magmas and hydrothermal fluids. In *Geochemistry of Hydrothermal Ore deposits*-second edition, Barnes, H.L. (ed.). John Wiley, New York, 71-136.
- BURNHAM, C. & OHMOTO, H. (1980): Late-stage processes in felsic magmatism. *Mining Geol., Special Issue*, **8**, 1-11.
- CAHILL, T.A. & ISACKS, B.L. (1992): Seismicity and shape of the subducted Nazca plate. *J. Geophys. Research* **97**, 17,503-17,529.
- CARMAN, G.D. (1994): *Genesis of the Ladolam gold deposit, Lihir Island, Papua New Guinea*. Ph.D. thesis, Monash Univ., Melbourne, Australia, 243 p.
- CASSIDY, K.F., LANG, J.R., LUECK, B.A., MORTENSEN, J.K., RUSSELL, J.K. & THOMPSON, J.F.H. (1996): Geochemical and isotopic characteristics of Mesozoic alkalic intrusions in the Cordillera of British Columbia: Tectonic significance and implications for Cu-Au metallogeny (abs.), Geological Society of Australia, *Abstracts* No 41.
- CATHLES, L.M. (1997): Thermal aspects of ore formation. In *Geochemistry of Hydrothermal Ore deposits*. Barnes H.L. (ed.). Wiley, New York, 191-227.
- CIOBANU, C.L., COOK, N.G. & STEIN H. (2002): Regional setting and geochronology of the Late Cretaceous Banatitic Magmatic and Metallogenic Belt. *Mineral. Deposita* **37**, 541-567
- CORBERT, G.J. & LEACH, T.M. (1998): Southwest Pacific rim gold-copper systems: structural, alteration and mineralization. *SEG Spec. Pub.* **6**, 237.
- CROCKET, J.H. (1990): Noble metals in seafloor hydrothermal mineralization from the Juan de Fuca and mid-Atlantic ridges: A fractionation of gold from platinum metals in hydrothermal fluids. *Can. Mineral.* **28**, 639-648.
- CUDDY, A.S. & KESLER, S.E. (1982): Gold in the Granisle and Bell porphyry copper deposits. In *Precious Metals in the Northern Cordillera*, Levinson, A. (ed.). *Assoc. Explor. Geochem. Special Vol.* **2**, 139-155.
- DOLBEAR, B. & COMPANY, LTD. (2003): Mineral resources estimate for the Afton copper/gold. DRC Resources Corporation, Project, 28p.
- DRAGOV, P. & PETRUNOV, R. (1996): Elatsite porphyry copper-precious metals (Au and PGE)

- deposit. *Proc. of Ann. Meet. UNESCO IGCP Project 356, Sofia 1996*, 171-175.
- ECONOMOU-ELIOPOULOS M. & ELIOPOULOS, D. (1998): Selenium content in sulfide ores related to ophiolites of Greece. *J. Environ. Pathol. Oncol.*, **17**, 199-204.
- ECONOMOU-ELIOPOULOS M. & ELIOPOULOS, D.G. (2000): Palladium, platinum and gold concentrations in porphyry copper systems of Greece and their genetic significance. *Ore Geol. Rev.* **16**, 59-70.
- ECONOMOU-ELIOPOULOS M. & ELIOPOULOS, D.G. (2001): Factors controlling the Pd and Pt potential of the Skouries porphyry-Cu deposit, Chalkidiki Peninsula, N. Greece. In 6th Biennial SGA-SEG Meeting, Krakow, Mayer (ed.). Balkema, Rotterdam, 579-582.
- EINAUDI, M.T., HEDENQUIST, J.W. & INAN, E.E. (2003): Sulfidation state of fluids in active and extinct hydrothermal systems: Transitions from porphyry to epithermal environments. *SEG Special Publication* **10**, 285-313.
- ELIOPOULOS, D. G. & ECONOMOU-ELIOPOULOS, M. (1991): Platinum-group element and gold contents in the Skouries Porphyry-Copper deposit, Chalkidiki Peninsula, N. Greece. *Econ. Geol.* **86**, 740-749.
- ELIOPOULOS, D. G., ECONOMOU-ELIOPOULOS, M., STRASHIMIROV, ST., KOVACHEV, V., ZHEL'YASKOVA-PANAYOTOVA, M. (1995): Gold, platinum and palladium content in porphyry Cu deposits from Bulgaria: a study in progress. *Geol. Soc. Greece* **5**, 712-716.
- ENNS, S.G., THOMSON, J.F.H., STANLEY, C.R. & LANG, J.R. (1995): The Galore Creek porphyry copper-gold deposit, northwestern British Columbia: *Can. Inst. Mining Metall., Special volume* **46**, 630-644.
- FARAMAZYAN, A.S., KALININ, S.K. & TEREKHOVICH, S.C. (1970). Geochemistry of platinum-group elements in the ores of copper-molybdenum deposits of Armenia. *Dokl. Akad. Nauk SSSR* **190**, 220-221.
- FRASER, T.M., STANLEY, C.R., NIKIC, Z.T., PESALJ, R. & GORE, D. (1995): The Mount Polley alkaline porphyry copper-gold deposit, south-central British Columbia. *Can. Inst. Mining Metall., Special volume.* **46**, 609-622.
- FREI, R. (1992): *Isotope (Pb, Rb-Sr, S, O, C, U-Pb) geochemical investigations on Tertiary intrusives and related mineralization in the Serbo-macedonian Pb-Zn, Sb+Cu-Mo metallogenetic province, in Northern Greece*. Ph.D. Thesis, ETH Zurich, pp. 230.
- FREI, R. (1995): Evolution of mineralizing fluid in the Porphyry Copper System of the Skouries Deposit, Northern Chalkidiki (Greece): Evidence from combined Pb-Sr and stable isotope data. *Econ. Geol.* **90**, 746-762.
- GAMMONS, C.H., BLOOM, M.S. & YU, Y. (1992): Experimental investigation of the hydrothermal geochemistry of platinum and palladium: I Solubility of platinum and palladium sulphide minerals in NaCl/H₂SO₄ solutions at 300°C. *Geochim. Cosmochim. Acta* **56**, 3881-3894.
- GARUTI, G. & ZACCARINI, F. (1997): *In situ* alteration of platinum-group minerals at low temperature: evidence from serpentinized and weathered chromitites of the Vourinos Complex (Greece). *Can. Mineral.* **35**, 611-626.
- G.C.O. (GOLDEN CROSS OPERATIONS PTY. LTD) (2004): The Copper Hill porphyry gold-palladium project, New South Wales, Australia. Information Memorandum, *Report GCO No.* **202**, 15.
- GILG, H. (1993): *Geochronology (K-Ar), fluid inclusion, and stable isotope (C, H, O) studies of skarn, porphyry copper and carbonate-hosted Pb-Zn(Ag,Au) replacement deposits in the Kassandra mining district (Eastern Chalkidiki, Greece)*. Ph.D. Thesis, University of München, 153 p.
- GILMOUR, P. (1982): Grades and tonnages of porphyry copper deposits. In *Advances in geology of the porphyry copper deposits, Southwestern North America*. Part I. Titley S.R. (ed.). 7-35.
- HALTER, W.E., PETTKE, T. & HEINRICH, C.A. (2002): The origin of Cu/Au Ratios in Porphyry-Type Ore Deposits. *Science*, **296**, 1944-1846.
- HALTER, W.E., HEINRICH, C.A. & PETTKE, T. (2004): Laser ablation-ICP-MS analysis of silicate and sulfide melt inclusions in an andesitic complex II: evidence for magma mixing and magma chamber evolution. *Contrib. Mineral. Petrol.* **147**, 397-412.
- HALTER, W.E., HEINRICH, C.A. & PETTKE, T.

- (2005): Magma evolution and the formation of porphyry Cu-Au ore fluids: evidence from silicate and sulphide melt inclusions. *Mineral. Deposita* **39**, 845-863.
- HANLEY, J.J. (2005): The aqueous geochemistry of the platinum-group elements (PGE) in surficial, low-T hydrothermal and high-T magmatic-hydrothermal environments. In *Exploration for Platinum-group Element Deposits* (J.E. Mungall, ed.). *Mineral. Assoc. Canada, Short Course* **35**, 35-56.
- HANLEY, J.J., PETTKE, T., MUNGALL, J.E. & SPOONER, E.T.C (2005): Investigations of the behavior and distribution of platinum and gold in silicate melt-brine mixtures at 1.5 kbar, 600 to 800°C using synthetic fluid inclusions methods: a laser ablation-ICP-MS pilot study. *Geochim. Cosmochim. Acta*, in press.
- HATTORI, K.H. & KEITH, J.D. (2001): Contribution of mafic melt to porphyry copper mineralization: evidence from Mount Pinatubo, Philippines, and Bingham deposit, Utah. *Mineral. Deposita* **36**, 799-806.
- HEDENQUIST, J.W., ARRIBAS, A. & T.J. REYNOLDS (1998): Evolution of intrusion-centered hydrothermal systems: Far Southeast Lepanto porphyry and epithermal Cu-Au deposits, Philippines. *Econ. Geol.* **93**, 373-404.
- HEINRICH, C.A. & NEUBAUER, F. (2002): Cu-Au-Pb-Zn-Ag metallogeny of the Alpine-Balkan-Carpathian-Dinaride geodynamic province: *Mineral. Deposita* **37**, 533-540.
- HEINRICH, C.A., GUNTHER, D., AUDETAT, A., ULRICH, T., & FRISCHKNECHT, R. (1999): Metal fractionation between magmatic brine and vapor, determined by microanalysis of fluid inclusions. *Geology* **27**, 755-758.
- HEITHERSAY, P.S, O'NEILL, W.J, VAN DER HELDER, P., MOORE, C.R & HARBON, P.G. (1990): Goonumbla porphyry copper district – Endeavour 26 North, Endeavour 22 and Endeavour 27 copper-gold deposits. In *Geology of the mineral deposits of Australia and Papua New Guinea*. Hughes, F.E (ed.). *Australasian Inst. Min, Metall. Monograph*, **14**, 1385-1398.
- HEKINIAN, R., FEVRIER, M., BISCHOFF, J.L., PICOT, P. & SHANKS, W.C. (1980): Sulfide deposits from the East Pacific Rise near 21 degrees N. *Science* **207(4438)**, 1433-1444.
- HEMLEY, J.J., CYGAN, G.L., FEIN, J.B., ROBINSON, G.R., & D'ANGELO, W.M. (1992): Hydrothermal ore-forming processes in the light of studies in rock-buffered systems: I. Fe-Cu-Zn-Pb sulphide solubility relations: *Econ. Geol.* **87**, 1-22.
- HERRINGTON, R.G., FIRST, D.M. & KOZELJ, D. (2003): Copper porphyry deposits of Hungary, Serbia, Macedonia, Romania and Bulgaria. In *Europe's Major Base Metal Deposits*. Kelly, J.G. *et al.* (eds.). *Irish Assoc. Econ. Geol.* 303-321.
- HERRINGTON, R.G., JANKOVIC, S. & KOZELJ, D. (1998): The Bor and Majdanpek copper-gold deposits in the context of the Bor metallogenic zone (Serbia, Yugoslavia). In *Porphyry and hydrothermal copper and gold deposits: a global perspective*. Porter, T. (ed.). *Conf. Proc., Australian Mineral Foundation*, 169-178.
- HOLLIDAY, J.R., WILSON, A.J., BLEVIN, P.L., TEDDER, U., DUNHAM, P.D. & PFITZNER, M. (2002): Porphyry gold-copper mineralization in the Cadia district, eastern Lachlan Fold Belt, New South Wales, and its relationship to shoshonitic magmatism. *Mineral. Deposita* **37**, 100-116.
- HOUSH, T. & MCMAHON T. (2000): Ancient isotopic characteristics of Neogene potassic magmatism in Western New Guinea (Irian Jaya, Indonesia). *Lithos* **50**, 217-239
- IMAI, A. (2000): Genesis of the Mamut porphyry copper deposit, Sabah, East Malaysia. *Resource Geol.* **50** (1), 1-23.
- IRVINE, T.N. & BARAGAR, W.R.A., (1971): a guide to the chemical classification of the common volcanic rocks. *Can. J. Earth Sci.* **8**, 523-548.
- ISACKS, B.L. (1988). Uplift of the central Andean plateau and bending of the Bolivian orocline. *J. Geophys. Research*, **93**, 3211-3231.
- IVASCANU, P.M., PETTKE, T., KOUZMANOV, K., HEINRICH, C.A., PINTEA, I., ROSU, E. & UDUBASA, G. (2003): The magmatic to hydrothermal transition: Miocene Deva porphyry copper-gold deposit, South Apuseni Mts., Romania. In *Proceedings of the 7th Biennial SGA meeting, "Mineral Exploration and Sustainable Development"*. Eliopoulos *et al.* (eds.). Athens, 24-28.
- JANKOVIC, S. (1980): Ore deposit types and major copper metallogenic units in Europe. *European Copper deposits, UNESCO-IGCP Projects* 169

- and 60, **1**, 9-25
- JANKOVIC, S. (1997): The copper deposits and geotectonic setting of the Tethyan-Eurasian metallogenic belt. *Mineral. Deposita* **12**, 37-47.
- JENSEN, E.P. & BARTON, M.D. (2000): Gold deposits related to alkaline magmatism. *SEG Reviews*, **13**, 279-314.
- JOLLY, J.H. (1978): Platinum-group metals. *U.S. Bur. Mines, MCP-22*.
- KANAZIRSKI, M. (2000): Thermodynamic basis for distinguishing the acid-sulphate and adularia-sericite alteration types of rock in epithermal deposits. In *Geodynamics and ore deposits evolution of the Alpine-Balkan-Carpathian-Dinaride province. Abstr Vol ABCD-GEODE 2000 Workshop, Borovets, Bulgaria*, 34 p.
- KARAMATA, S., KNEZEVIC, V., PECSKAY, Z. & DJORDJEVIC, M. (1997): Magmatism and metallogeny of the Ridanj-Krepoljin belt (eastern Serbia) and their correlation with northern and eastern analogues. *Mineral. Deposita* **32**, 452-458.
- KAY, S.M., MPODOZIS, C. & COIRA, B. (1999). Magmatism, tectonism, and mineral deposits of the central Andes (22°–33°S). In *Geology and ore deposits of the central Andes*. Skinner, B. (ed.). *Soc. Econ. Geol. Spec. Publ.* **7**, 27-59.
- KEHAYOV, R. & BOGDANOV, K. (2002): Notes on the fluid inclusions in the Elatsite Porphyry Cu-Au-PGE deposit, Bulgaria. *Bulg. Geol. Soc. Ann. Sci. Conf., Sofia*, Nov. 21-22, Abs. 37-38.
- KEHAYOV, R. BOGDANOV, K., FANGER, L., VON QUADT, A., PETTKE, T. & HEINRICH, C. (2003): The fluid chemical evolution of the Elatsite porphyry Cu-Au-PGE deposit, Bulgaria. 7th Biennial SGA meeting “Mineral Exploration and Sustainable Development”, Athens, Greece, Abs. Eliopoulos *et al.* (eds.). 1173-1176.
- KEITH, J.D., CHRISTIANSEN, E.H., MAUGHAN, D.T. & WAITE, K.A. (1998): The role of mafic alkaline magmas in felsic porphyry-Cu and Mo systems. *Mineral. Assoc. Can. Short Course Series*, **26**, 211-243.
- KELLEY, K. & LUDINGTON, S. (2002): Cripple Creek and other alkaline-related gold deposits in the southern Rocky Mountains, USA: influence of regional tectonics. *Mineral. Deposita* **37**, 38-60.
- KESLER, S.E., CHRYSOULIS, S.L. & SIMON, G. (2002): Gold in porphyry copper deposits: its abundance and fate. *Ore Geol. Rev.* **21**, 103-124.
- KIOUSIS, G. (2004): *Sustainable development of the porphyry-Cu-Au-Pd-Pt deposit of Skouries, northern Greece*. MSc Thesis, University of Athens (in Greek with English Abstract), p. 202.
- KIOUSIS, G., ECONOMOU-ELIOPOULOS, M. & PASPALIARIS, J. (2005): Gold, palladium and platinum recovery, as by-product, from the Skouries porphyry Cu-Au deposit at Chalkidiki area, N. Greece – preliminary results. In: 8th SGA Meeting, “Mineral Deposits Research Meeting the Global Challenge” Beijing, August 18-21, 2005, Mao *et al.* (eds.). (in press).
- KIRKHAM, R.V. & SINCLAIR, W.D. (1996): Porphyry copper, gold, molybdenum, tungsten, tin, silver, In *Geology of Canadian mineral deposit types*. Eckstrand, O.R., Sinclair, W.D., and Thorpe, R.I. (eds.). *Geol. Surv. Can., Geology of Canada*, **8**, 421-446.
- KOCKEL, F., MOLLAT, H. & WALTHER, H. (1977): Erläuterung zur geologischen Karte der Chalkidiki und angrenzender gebiete. 1:100,000 Nord Griechenland, Hannover, Germany, 199p.
- KOSAKA, H. & WAKITA, K. (1978): Some geologic features of the Mamut porphyry copper deposit, Sabah, Malaysia. *Econ. Geol.* **73**, 618-627.
- KOUZMANOV, K. (2001): *Genese des concentrations et metaux de base et precieux de Radka et Elshitsa (zone de Sredna Gora, Bulgare): une approche par l'etude mineralogique, isotopique et des inclusions fluids*. Ph.D. Thesis, Univ. of Orleans, 437 p.
- KOUZMANOV, K., RAMBOZ, C., LEROUGE, C., DELOULE, E., BEAUFORT, D. & BOGDANOV, K. (2003): Stable isotopic constrains on the origin of Epithermal Cu–Au and related porphyry – copper mineralisation in the Southern Panagyurishte district, Srednogorie zone, Bulgaria. In *Mineral Exploration and Sustainable Development*, 7th Biennial SGA Meeting, 24 – 28 August, Athens, Greece, Eliopoulos *et al.* (eds.). 1181-1184.
- KOVALENKER, V.A., MYZNIKOV, I.K., KOCHETKOV, A.YA & NAUMOV, V.B. (1996): PGE-bearing gold-sulphide mineralization in the Ryabinovyi alkali massif, Central Aldan. *Geology of Ore Deposits* **38(4)**, 307-317.

- KOVALENKO, V.I. & YARMOLYUK, V.V. (1995): Endogenous rare metal ore formations and rare metal metallogeny of Mongolia: *Econ. Geol.* **90**, 520-529.
- KROLL, T., MÜLLER, D., SEIFERT, T., HERZIG, P.M. & SCHNEIDER, A. (2002): Petrology and geochemistry of the shoshonite-hosted Skouries porphyry Cu-Au deposit, Chalkidiki, Greece. *Mineral. Deposita* **37**, 137-144.
- LANG, J.R. & TITLEY, S.R. (1998): Isotopic and geochemical characteristics of Laramide magmatic systems in Arizona and their implications for the genesis of porphyry copper deposits. *Econ. Geol.* **93**, 138-170.
- LANG, J.R., LUECK, B.A., MORTENSEN, J.K., RUSSELL, J.K., STANLEY, C.R. & THOMPSON, J.F.H., (1995): Triassic-Jurassic silica-undersaturated and silica-saturated alkalic intrusions in the Cordillera of British Columbia: Implications for arc magmatism. *Geology*, **23**, 451-454.
- LEBEDEV, V.I. & KUZHUGET, K.S. (1998): Mineral potential of Tuva Republic: possibility of utilization in 1999-2001 and in future. *TuvIKORP, Kyzyl.* (in Russian), 26p.
- LICKFOLD, V., COOKE, D.R., SMITH, S.G. & ULLRICH, T.D. (2003): Endeavour Copper-Gold porphyry Deposits, North Parkes, New South Wales: Intrusive History and Fluid Evolution. *Econ. Geol.* **95**, 1607-1636.
- LIPS, A.L.W., HERRINGTON, R.J., STEIN, G., KOZELJ, D., POPOV, K. & WIJBRANS, J.R. (2004): Refining of porphyry copper formation in the Serbian and Bulgarian portions of the Cretaceous Carpatho-Balkan belt. *Econ. Geol.* **99**, 601-609.
- LOWELL, L.D. & GUILBERT, J.M., (1970): Lateral and vertical alteration mineralization zoning in porphyry ore deposits. *Econ. Geol.* **65**, 535-550.
- MAUGHAN, D.T., KEITH, J.D., CHRISTIANSEN, E.H., PULSIPHER, T., HATTORI, K. & EVANS, N.J. (2002): Contribution from mafic alkaline magmas to the Bingham Porphyry Cu-Au-Mo deposit, Utah, USA. *Mineral. Deposita* **37**, 14-37.
- MCDONALD, I., OHNENSTETTER, D., ROWE, J.P., TREDoux, M., PATTRICK, R.A.D. & VAUGHAN, D.J. (1999): Platinum precipitation in Waterberg deposit, Naboomspruit, South Africa. *S. Afr. J. Geol.* **102**, 184-191.
- MCDOWELL, F.W, MCMAHON, T.P, WARREN, P.Q & CLOOS, M. (1996): Pliocene Cu-Au-bearing igneous intrusions of the Gunung Bijih (Ertsberg) District, Irian Jaya, Indonesia; K-Ar geochronology. *J. Geol.* **104**, 327-340.
- MCINNES, B.I.A. & CAMERON, E.M. (1994): Carbonated, alkaline hybridizing melts from a sub-arc environment: Mantle wedge samples from the Tabar-Lihir-Tanga-Feni arc, Papua New Guinea, *Earth Planet. Sci. Lett.* **122**, 125-141.
- MCMILLAN, W.J. & PANTELEYEV, A. (1995): Porphyry copper deposits of the Canadian Cordillera. In: Porphyry Copper Deposits of the American Cordillera: Arizona. Pierce, F.W. & Bolm, J.G. (eds.). *Arizona Geol. Soc. Digest*, **20**, 203-218.
- MEINERT L.D., HEFTON, K.H., MAYES, D. & TASIRAN, I. (1997): Geology, zonation, and fluid evolution of the Big Gossan Cu-Au skarn deposit, Ertsberg district, Irian Jaya. *Econ. Geol.* **92**, 509-534
- MEYER, C. & HEMLEY, J.J. (1967): Wall rock alteration. In *Geochemistry of Hydrothermal Deposits*. Barnes, H.L. (ed.). New York, Holt, Rinehart and Winston, 166-235.
- MORTENSEN, J.K., GHOSH, D.K. & FERRI, F. (1995): U-Pb geochronology of intrusive rocks associated with copper-gold porphyry deposits in the Canadian Cordillera. In *Porphyry Deposits of the Northwestern Cordillera of North America*. Schroeter, T.G. (ed.). *Can. Inst. Mining Metall. Special Volume* **46**, 142-158.
- MOYLE, A.J., DOYLE, B.J., HOOGVLIET, H. & WARE, A.R. (1990): Ladolam gold deposit, Lihir Island. In *Geology and Mineral Deposits of Australia and Papua New Guinea*. Hughes, F.E. (ed.). *Australian Institute of Mining and Metallurgy, Monograph* **14 (2)**, 1793-1805.
- MÜLLER, D. & GROVES, D.I. (2000): *Potassic Igneous Rocks and Associated Gold-Copper Mineralization* (3rd ed). Springer, Berlin Heidelberg, New York, 252 p.
- MÜLLER, D., HEITHERSAY, P.S. & GROVES, D.I. (1994): The shoshonite porphyry Cu-Au association in the Goonumbla District, N.S.W., Australia. *Mineral. Petrol.* **51**, 299-321.
- MÜLLER, D., KAMINSKI, K., UHLIG, S., GRAUPNER, T. HERZIG, P.M. & HUNT S. (2002): The transition

- from porphyry to epithermal-style gold mineralization at Ladolam, Lihir Island, Papua New Guinea. *Mineral. Deposita* **37**, 61-74.
- MÜLLER, D., PETTKE, T. & HEINRICH, C.A. (2003): Characteristic features of alkaline rocks hosting the Ladolam gold deposit, Lihir Island, Papua New Guinea. *7th Biennial SGA meeting "Mineral Exploration and Sustainable Development, Athens, Greece, Abs.*, 347-350.
- MUNGALL, J.E. (2002): Roasting the mantle: slab melting and the genesis of major Au and Au-rich Cu deposits. *Geology* **30**, 915-918.
- MUTSCHLER, F.E. & MOONEY (1993): Precious metal deposits related to alkaline igneous rocks – provisional classification, grade-tonnage data, and exploration frontiers. In *Mineral Deposit Modelling*, Kirkham R.V., Sinclair W.D., Thorpe R.I. & Duke J.M. (eds.). *Geol. Assoc. Can. Special Paper* **40**, 479-520.
- MUTSCHLER, F.E., GRIFFIN, M.E., STEVENS, S.D. & SHANNON, S.S. (1985): Precious metal deposits related to alkaline rocks in the north American Cordillera – an interpretive review. *Geol. Soc. S. Afr. Trans.* **88**, 355-377.
- PAGE, R.W. & MCDUGALL, I. (1972): Ages of mineralization of gold and porphyry copper deposits in the New Guinea highlands. *Econ. Geol.* **27**, 201-121.
- PAN, P. & WOOD, S.A. (1994): Solubility of Pt and Pd sulphides and metals in aqueous bisulphide solutions. II Results at 200°C to 350°C and saturated vapour pressure. *Mineral. Deposita* **29**, 373-390.
- PARKER, J.G. (1978): Occurrence and recovery of certain minor metal in the smelting-refining of copper. *U.S. Bur. Mines, I.C.* 8778.
- PERANTONIS, G. (1982): *Genesis of porphyry copper deposits in Chalkidiki peninsula and W. Thrace, Greece*. PhD Thesis, University of Athens, 150 p.
- PERELLÓ, J., DENNIS, C. GARAMJAV, D., SANJDORJ, S., DIAKOV, S. & SCHISSEL, D. (2001): Oyu Tolgoi, Mongolia: Siluro-Devonian Porphyry Cu-Au-(Mo) and High-Sulfidation Cu Mineralization with a Cretaceous Chalcocite Blanket, *Econ. Geol.* **96**, 1407-1428.
- PERUGINI, D., POLI, G., CHRISTOFIDES, G., ELEFTHERIADIS G., KORONEOS, A. & SOLDATOS, T. (2004): Mantle-derived and crustal melts dichotomy in northern Greece: spatial, temporal and geodynamic implications. *Geol. J.* **39**, 63-80.
- PETERSEN, S., HERZIG, P.M., HANNINGTON, M.D., JONASSON, I.R. & ARRIBAS, A., (2002): Submarine gold mineralization New Lihir Island, New Ireland fore-arc, Papua Guinea. *Econ. Geol.* **97**, 1795-1813.
- PETRUNOV, R. & DRAGOV, P. (1993): PGE and gold in the Elatsite porphyry copper deposit, Bulgaria. In *Current Research in Geology Applied to Mineral Deposits*. Hach-Ali, F. *et al.* (eds.). *University of Granada, Spain*, 543-546.
- PETRUNOV, R. DRAGOV, P., IGNATOV, G., NEYKOV, H., ILIEV, T., VASILEVA N., TSATSOV, V., DJUNAKOV, S. & DONCHEVA, K. (1992): Hydrothermal PGE-mineralization in the Elatsite porphyry-copper deposit (Sredna Gora metallogenic zone, Bulgaria). *Compt. Rend. Acad. Bulg. Sci.* **45**, 37-40.
- PHILLIPS, C.H., SMITH, T.W. & HARRISON, E.D. (1997): Alteration, metal zoning, and ore controls in the Bingham Canyon porphyry copper deposit, Utah. *SEG Guidebook Series* **29**, 133-145.
- PIESTRZYNSKI, A., SCHMIDT, S. & FRANCO, H. (1994): Pd-minerals in the Santo Tomas II porphyry copper deposit, Tuba Benguet, Philippines. *Mineralogia Polonica*, **25**, 12-31.
- PINTEA, I. (1995): Fluid inclusions evidence for liquid magmatic immiscibility between hydrous salt melt and silicate melt as primary source of ore metals in porphyry copper systems from Apuseni Mountains (Romania). *Bol. de la Soc. Esp. de Min.* **18-1**, 184-185.
- POKALOV, V.T. (1997): Deposits of molybdenum. In *Ore Deposits of the USSR*. Smirnov (ed.). Transl. Pitman Publ., London, **III**, 125-179.
- POPOV, P. & KOVACHEV, V. (1996). Geology, composition and genesis of the mineralization in the Central and southern part of Elatsite-Chelopen ore field. *UNESCO-IGCP Project*, No **356**, 159-170.
- POPOV, P., PETRUNOV, R., KOVACHEV, V., STRASHIMIROV, S. & KANAZIRZKI, M. (2000): Elatsite-Chelopen ore field. In *Geology and Metallogeny of the Panagyurishte ore region. Guide to excursion A and C*. Strashimirov, S., Popov, P. (eds.). ABCD-Geode 2000 Worksh,

- Borovets, May 2000, 8-18.
- PROFFETT, J.M. (2003): Geology of the Bajo de la Alumbrera Porphyry Copper-Gold Deposit, Argentina. *Econ. Geol.* **98**, 1535-1574.
- RICHARDS, J.P. (2003): Tectono-magmatic precursors for porphyry Cu-(Mo-Au) deposit formation. *Econ. Geol.* **98**, 5-1533.
- RONACHER, E., RICHARDS, J.P. & JOHNSTON, M.D. (2000): Evidence for phase separation in high-grade ore zones at the Porgera gold deposit, Papua New Guinea. *Mineral. Dep.* **35**, 683-688.
- RONACHER, E., RICHARDS, J.P., REED, M.H., BRAY, C.J., SPOONER, T.C. & ADAMS, P.D. (2004): Characteristics and Evolution of the Hydrothermal Fluid in the North Zone High-grade Area, Porgera Gold Deposit, Papua New Guinea. *Econ. Geol.*, **99**, 843-867.
- ROSS, K.V., GODWIN, C.I., BOND, L. & DAWSON, K.M. (1995): Geology, alteration and mineralization of the Ajax East and Ajax West copper-gold alkalic porphyry deposits, southern Iron Mask Batholith, Kamloops, British Columbia. In *Porphyry Deposits of the Northwestern Cordillera of North America*. Schroeter, T.G. (ed.), *Can. Inst. Mining, Metall. Petro. Special Vol.* **46**, 565-580.
- ROWINS, S.M. (2000): Reduced porphyry copper-gold deposits: A new variation on an old theme. *Geology* **28**, 491-494.
- RUBIN, J.N. & KYLE, J.R. (1997): Precious metal distribution in porphyry, skarn and replacement-type ore deposits of the Ertsberg (Gunung Bijih) district, Irian Jaya, Indonesia. *Econ. Geol.*, **92**, 535-551.
- RUSH, P.M. & SEEGER, H.J. (1990): Ok Tedi copper-gold deposits: *Australian Institute of Mining and Metallurgy Monograph* **14**, 1747-1754.
- SASSANI, D.C. & SHOCK, E.L. (1990): Speciation and solubility of palladium in aqueous magmatic-hydrothermal solutions. *Geology* **18**, 925-928.
- SEEDORFF, E. & EINAUDI, M. (2004): Henderson Porphyry Molybdenum System, Colorado: I. Sequence and Abundance of Hydrothermal Mineral Assemblages, Flow Paths of Evolving Fluids, and Evolutionary Style. *Econ. Geol.* **99**, 3-37.
- SILLITOE, R.H. (1979): Some Thoughts on Gold-Rich Porphyry Copper Deposits. *Mineral. Deposita* **14**, 161-173.
- SILLITOE, R.H. (1993): Intrusion-related gold deposits. In *Gold Metallogeny and Exploration*. Foster, R.P. (ed.), Chapman and Hall, London, 165-209.
- SILLITOE, R.H. (1997): Characteristics and controls of the largest porphyry copper-gold and epithermal gold deposits in the circum-Pacific region. *Austr. J. Earth Sciences* **44**, 373-388.
- SILLITOE, R.H. (2000): Gold-rich porphyry deposits: Descriptive and Genetic models and their role in exploration and discovery. *SEG Reviews* **13**, 315-345.
- SILLITOE, R.H. (2004): Musing on Future Exploration Targets and Strategies in the Andes. In: *Andean Metallogeny: New Discoveries, Concepts, and Updates*, Sillitoe, R.H., Perello, J. & Vidal, C. (eds.). *SEG Special Publication* **11**, 1-14.
- SILLITOE, R.H. & HEDENQUIST, J. (2003): Linkages between volcanotectonic setting, ore-fluid compositions and epithermal precious metal deposits. *Soc. Econ. Geologists, Special Publication* **10**, 315-345.
- SKETCHLEY, D.A., REBOGLIATI, C.M. & DELONG, C. (1995): Geology, alteration and zoning patterns of the Mt. Milligan copper-gold deposits, In *Porphyry deposits of the northwestern Cordillera of North America*, Schroeter, T.G. (ed.). *Can. Inst. Mining, Metall. Petroleum Special Vol.* **46**, 650-655.
- SOTNIKOV, V.I., BERZINA, A.N., ECONOMOU-ELIOPOULOS, M. & ELIOPOULOS, D.G., (2001): Palladium, platinum and gold distribution in porphyry Cu±Mo deposits of Russia and Mongolia. *Ore Geology Reviews* **18**, 95-111.
- SOTNIKOV, V.I., PONOMARCHUK, V.A., BERZINA, A.P. & TRAVIN, A.V. (1995): Geochronological borders of magmatism of Cu-Mo porphyry Erdenetuin-Obo deposit (Mongolia). *Russian Geol. & Geophys.* **36** (3), 71-82.
- SOTNIKOV, V.I., PONOMARCHUK, V.A., BERZINA, A.N. & GIMON, V.A. (2003): The Aksug porphyry Cu-Mo deposit, Tuva, Russia: ⁴⁰Ar/³⁹Ar dating and magma constraints. In *Mineral exploration and sustainable development*,

- Eliopoulos, D.G., *et al.*, (Eds.). Millpress, Rotterdam, 391-394.
- SOTNIKOV, V.I., PONOMARCHUK, V.A., BERZINA, A.N., BERZINA, A.P., KISELEVA, V.YU. & MOROZOVA, I.P. (2000): Evolution of $^{87}\text{Sr}/^{86}\text{Sr}$ in igneous rocks of porphyry copper–molybdenum ore clusters (based on studies of accessory apatite). *Russ. Geol. & Geophys.* **41**, 1078-1088.
- STRASHIMIROV, S. (1982): *Mineral associations, conditions and development of ore-forming processes in the porphyry-copper deposit Medet*. Ph.D. Thesis. 34 p
- STRASHIMIROV, S., BOGDANOV, K., POPOV, K. & KEHANOV, R. (2003): Porphyry Systems of the Panagyurishte Ore Region. In Cretaceous Porphyry-Epithermal Systems of the Srednogoric Zone, Bulgaria. Bogdanov, K. & Strashimirov, S. (eds.). *SEG Guidebook Series* **36**.
- STRASHIMIROV, S., PETRUNOV, R. & KANAZIRSKI, M. (2002): Mineral associations and evolution of hydrothermal systems in porphyry copper deposits from the Central Srednogorie zone (Bulgaria): *Mineral. Deposita* **37**, 587-598.
- STRIBRNY, B., WELLMER, F.W., BURGATH, K.-P., OBERTHÜR, T., TARKIAN, M. & PFEIFFER, T. (2000): Unconventional PGE occurrences and PGE mineralization in the Great Dyke: Metallogenic and economic aspects. *Mineral. Deposita* **35**, 260-281.
- TARKIAN, M. & STRIBRNY, B. (1999): Platinum-group elements in porphyry copper deposits: a reconnaissance study. *Mineralogy and Petrology* **65**, 161-183.
- TARKIAN, M. & KOOPMANN, G. (1995): Platinum-group minerals in the Santo Tomas II Philex porphyry copper-gold deposit, Luzon Island, Philippines. *Mineral. Deposita* **30**, 39-47.
- TARKIAN, M. & PRICHARD, H. (1987). Irarsite-hollingworthite solid-solution series and other associated Ru-, Os-, Ir-, and Rh-bearing PGM from the Shetland ophiolite complex. *Mineral. Deposita* **22**, 178-184.
- TARKIAN, M., ELIOPOULOS, D.G. & ECONOMOU-ELIOPOULOS, M. (1991): Mineralogy of precious metals in the Skouries porphyry copper deposit, N. Greece. *Neues Jahrbuch für Mineralogie Abhand.* **12**, 529-537.
- TARKIAN, M., HUNKEN, U., TOKMAKCHIEVA, M. & BOGDANOV, K. (2003): Precious-metal distribution and fluid-inclusion petrography of the Elatsite porphyry copper deposit, Bulgaria. *Mineral. Deposita* **38**, 261-281.
- TAYLOR, S.R. & MCLENNAN, S.M. (1985): The geochemical evolution of the continental crust. *Rev. Geophys.* **33**, 241-265.
- TAYLOR, W.R., ROCK, N.M.S., GROVES, D.I., PERRING, C.S. & GOLDING, S.D. (1994): Geochemistry of Archean shoshonitic lamprophyres from the Yilgarn Block, Western Australia: Au abundance and association with gold mineralization. *Appl. Geochem.*, **9** 197-222.
- THOMPSON, J.F.H., LANG, J.R. & STANLEY, C.R. (2001): Platinum group elements in alkaline porphyry deposits, British Columbia. *Exploration and Mining in British Columbia, Mines Branch, Part B*, 57-64.
- TITLEY, S.R. (1993): Characteristics of porphyry copper occurrence in the American Southwest. In Mineral Deposit Modeling. Kirkham, R.V., Sinclair, W.D., Thorpe, R.I., Duke, J.M. (eds.). *Geol. Assoc. Can. Special Paper*, **40**, 433-464.
- TITLEY, S.R. (2001): Crustal Affinities of Metallogenesis in the American Southwest. *Econ. Geol.* **96**, 1323-1342.
- TOBEY, E., SCHNEIDER, A., ALEGRIA, A., OLCAY, L., PERANTONIS, G. & QUIROGA, J. (1998): Skouries porphyry copper-gold deposit, Chalkidiki, Greece. In Porphyry hydrothermal Cu-Au deposits: A global perspective. Porter TM (ed.). *Australian Mineral Foundation Conference Proceedings. Glenside, South Australia*, 159-168.
- TODOROV, T. & STAIKOV, M. (1985): Rhenium content in molybdenite from ore mineralization in Bulgaria. *Geologica Balcanica*, **15**, 45-58.
- TOMPOULOGLOU, C. (1981): *Les mineralisations Tertiaires, type cuivre porphyrique, du massif Serbo-Macedonien (Macedoine, La Grece) dans leur contexte magmatique (avec un traitement géostatistique pour les données due prospect d'Alexia)*. Ph.D. thesis, L'Ecole Nationale Supérieure des Mines de Paris, France, pp. 204.
- TOSDAL, R.M. & RICHARDS, J.P. (2001): Magmatic and structural controls on the development of porphyry Cu±Mo±Au deposits. *Reviews in Econ. Geol.* **14**, 157-181.
- ULRICH, T. (1999): *Genesis of the Bajo de la*

- Alumbraera porphyry Cu-Au deposit, Argentina: Geological, fluid geochemical, and isotopic implications.* Ph.D. thesis, ETH, Zürich, Switzerland, 207 p.
- VON QUADT, A., PEYTCHEVA, I., KAMENOV, B., FANGER, L., HEINRICH, C.A., & FRANK, M. (2002): The Elatsite porphyry copper deposit in the Panagyurishte ore district, Srednogie zone, Bulgaria: U-Pb zircon geochronology and isotope-geochemical investigations of magmatism and ore genesis. *Geol. Soc. London, Special Pub.* **204**, 119-135.
- WAGNER, P.A. (1929): *Platinum deposits and mines of South Africa.* C. Struik (Pty.) Ltd., Cape Town, South Africa, 338 p.
- WAITE K.A., KEITH J.D., CHRISTIANSEN E.H., TINGEY D.G., WHITNEY J.A., HOOK C.J. & HATTORI, K. (1997): Petrogenesis of the volcanic and intrusive rocks associated with the Bingham Canyon porphyry Cu-Au-Mo deposit, Utah. *Soc. Econ. Geol. Guidebook Ser.* **29**, 91-128.
- WARNAARS, F. W., SMITH, W. H., BRAY, R. E., LANIER, G. & SHAFIQUZZAH, M. (1978): Geochronology of igneous intrusions and porphyry copper mineralization at Bingham, Utah. *Econ. Geol.* **73**, 1242-1249.
- WERLE, J.I., IKRAMUDDIN, M. & MUTSCHLER, F.E. (1984): Allard stock, La Plata Mountains, Colorado – an alkaline rock hosted porphyry copper precious metal deposit. *Can. J. Earth Sci.* **21**, 630-641.
- WILDE, A.R. (2005): Hydrothermal and supergene Pt & Pd deposits. In *Exploration for Platinum-group Element Deposits* (J.E. Mungall, ed.). *Mineral. Assoc. Canada, Short Course* **35**, 145-161.
- WILDE, A.R., EDWARDS, A.C. & YAKUBCHUK, A. (2003): Unconventional deposits of Pt and Pd: a review with implications for exploration: *SEG Newsletter* **52**, 1-18.
- WILDE, A.R., SIMPSON, L. & HANNA, S. (2002): Preliminary study of Tertiary hydrothermal alteration and platinum deposition in the Oman ophiolite. *J. Virtual Explorer* **6**, in press.
- WILLIAMS, T.J., CANDELA, P.A. & PICCOLI, P.M. (1995): The partitioning of copper between silicate melts and two-phase aqueous fluids: An experimental investigation at 1 kbar, 800 °C, and 0.5 kbar, 850°C: *Contributions to Mineralogy and Petrology* **121**, 388-399.
- WILSON, A. (2003): *The genesis and exploration context of porphyry copper-gold deposits in the Cadia district, NSW.* Ph.D. thesis, Univ. of Tasmania.
- WILSON, A., COOKE, D.R. & HARPER, B.L. (2004): The Ridgeway Gold-Copper: A high-grade Alkaline Porphyry Deposit in the Lachlan Fold Belt, New South Wales, Australia. *Econ. Geol.* **98**, 1637-1666.
- WOOD, B.W. (2002): The aqueous geochemistry of the platinum-group elements with applications to ore deposits. In *Geochemistry, mineralogy, metallurgy and beneficiation of PGE Geology.* Cabri, L.J. (ed.). *Can. Inst. Mining Metall. Special Paper* **54**, 211-249.
- WOOD, S.A., MOUNTAIN, B.W. & PAN, P. (1992): The aqueous geochemistry of platinum, palladium and gold: recent experimental constraints and a re-evaluation of theoretical predictions. *Can. Mineral.* **30**, 955-982.
- XIONG, Y. (2003): Predicted equilibrium constants for solid and aqueous selenium species to 300°C: applications to selenium-rich mineral deposits. *Ore Geology Reviews* **23**, 259-276.
- XIONG, Y. & WOOD, S.A. (2000): Experimental quantification of hydrothermal solubility of platinum-group elements with special reference to porphyry copper environments. *Mineral. & Petrol.* **68**, 1-28.
- XIONG, Y. & WOOD, S. (2002): Experimental determination of the hydrothermal solubility of ReS₂ and the Re-ReO₂ buffer assemblage and transport of rhenium under supercritical conditions. *Geochem. Trans.* **3**, 1-10.
- ZACHOS, E.K. (1963): Discovery of a copper ore deposit in Chalkidiki peninsula, N. Greece. *Geol. Geophys. Res.* **8**, 1-26.
- ZIMMERMAN, A., STEIN, H., MARKEY, R., FANGER, L., HEINRICH, C. & VON QUADT, A. (2003): Re-Os ages for the Elatsite Cu-Au deposit, Srednogie zone, Bulgaria. In *Mineral Exploration and Sustainable Development.* Eliopoulos, D.G. et al. (eds.). *Proc. 7th Biennial SGA Meeting, Athens*, 1253-1256.

Appendix 10-A: A Review of Porphyry Cu±Mo±Au ±Pd±Pt Deposits

BALKAN PENINSULA

Late Mesozoic to Tertiary porphyry Cu–(Mo–Au) intrusions located within the metallogenic belt of the Alpine-Balkan-Carpathian-Dinaride orogenic system represent subduction-related magmatism following the change from east–west to north–south convergence between Africa and Eurasia. Late Cretaceous porphyry deposits, extending from Romania, through Serbia and Bulgaria to Greece are the most important, and immediately predate the subsequent continental collision and post-collision magmatism. Deposits of Majdanpek, Bor and Veliki Krivelj in Serbia; Assarel, Elatsite and Medet in Bulgaria; and Skouries, Chalkidiki Peninsula in northern Greece (Fig. 10-1), belong to the Serbo-Macedonian massif (SMM) (Kockel *et al.* 1977, Frei 1995, Ciobanu *et al.* 2002, Heinrich & Neubauer 2002, Kouzmanov *et al.* 2003).

Skouries deposit: case history discovery

Geologic framework

The Skouries porphyry Cu–Au deposit, located at the Chalkidiki Peninsula, northern Greece belongs to the SMM. The crystalline basement comprises two lithostratigraphic-tectonic units, the lower Kerdylia Formation and the upper Vertiskos Formation, separated by a NW-striking fault system. The Vertiskos Formation consists of old basement gneiss, amphibolite, schist and marble, Tertiary intrusions, ophiolites (the Therma-Volvi-Gomati). Locations of subvolcanic-porphyrific stocks and volcanic complexes related to porphyry Cu deposits (Kockel *et al.* 1977, Perantonis 1982, Frei 1992, 1995, Tobey *et al.* 1998) are mainly controlled by deep fracture systems that permitted subvolcanic intrusions to reach higher levels of the crust (Zachos 1963, Kockel *et al.* 1977, Perantonis 1982, Frei 1995). Isotope data indicate that subvolcanic-porphyrific stocks such as the Skouries, of Miocene age (18 Ma), are younger than the intrusions of the Serbo-Macedonian massif.

The Skouries deposit is related to pipe-like intrusions of subalkaline-alkaline composition, extending at surface over an area of approximately 200 m x 200 m. The defined reserves in the porphyry Cu–Au deposit of Skouries are approximately 206 Mt at 0.54 % Cu, and 0.80 ppm Au. Geological data based on recent drilling, provided by TVX Gold Inc Hellas indicated that the Skouries deposit is developed around two related porphyry centers at depths between 650 and 800 m (Tobey *et al.* 1998). At least four monzonite porphyries have been described Kroll *et al.* (2002). In decreasing age, and increasing degrees of fractionation of the parent magmas, they are: (1) pink monzonite, (2) main monzonite, (3) intra-mineral monzonite, and (4) late-stage porphyry. High-grade ore is directly associated with the main and intra-mineral monzonite phases. Late-stage monzonite dykes that are barren cut all intrusive phases. The monzonite contains phenocrysts of plagioclase, alkali feldspar and amphibole as well as apatite and titanite microphenocrysts in a fine-grained feldspar-dominated groundmass (Kroll *et al.* 2002).

Analytical methods

Platinum, palladium and gold were determined at X-ray Assay Laboratories (XRAL), Ontario, and Canada using the ICP–MS method, after preconcentration (lead fire assay technique) from large (30 g) samples. The detection limit is 10 ppb for Pt, 1 ppb for Pd and 5 ppb for Au. Copper, Ag, Pb, Zn, Cr, Ni, Co and Mo were determined at XRAL, using the ICP/MS method.

Mineral compositions were determined by electron microprobe analysis at the National University of Athens, using a Cambridge Microscan–5 instrument and a JEOL JSM–5600 scanning electron microscope, both equipped with automated energy dispersive analysis system, Link 2000 and ISIS 300 OXFORD, respectively. Accelerating voltage and beam current were kept at 20.0 kV and 0.5 nA, respectively.

Characteristic features of alteration and mineralization

The typical alteration types of the porphyry Cu intrusions described by Lowell & Guilbert (1970) are more or less present in the Skouries intrusion, due to the repeated overprinting and intense silicification, with potassic being the predominant alteration type, whereas the propylitic and surrounding phyllic alteration are limited in extent. Two mineral assemblages of mineralization, occurring as veinlets/disseminations, can be distinguished: (a) magnetite- (reaching up to 10 vol%, average 6 vol%) bornite-chalcopyrite, linked to pervasive potassic and propylitic alteration type, in the central parts of the deposit, and (b) chalcopyrite-pyrite, which dominates at the peripheral parts of the deposit. Molybdenite occurs in small amounts, commonly in late pyrite-sericite-carbonate-

bearing veinlets (Kockel *et al.* 1977, Perantonis 1982, Frei 1995, Tobey *et al.* 1998). The Skouries deposit is characterized by relatively high Pd and Pt contents (Table 10-5). Chalcopyrite, and to a lesser extent bornite, contain exsolution of galena, which commonly has significant concentrations of Se, whereas clausthalite is rare. Minor ore minerals are gold-electrum, clausthalite-galena, hessite and merenskyite-moncheite (Tarkian *et al.* 1991, Figs 10-2 to 10-4, Table 10-2). Inclusions of silicates (commonly albite and orthoclase) and crystals of sylvite (KCl) are occasionally trapped in chalcopyrite (Fig. 10-4). Sphalerite with a low iron (~3 wt.% Fe) content is rare. At the periphery of the porphyry stock pyrite occurs as thin replacive overgrowths on chalcopyrite. Also, chalcopyrite in places is surrounded by digenite suggesting relatively oxidized fluids with a high ratio of metal to reduced sulfur during the evolution of the mineralized ore forming system.

Dark green fine-grained xenoliths within mineralized porphyry are mainly composed of orthoclase, phlogopite, and lesser amounts of relict biotite, fine-grained magnetite, pyrite and chalcopyrite (Fig. 10-2 & 10-3). They may be derived from the fragmentation of mafic rocks that lie beneath the porphyries. The pervasive and vein-type mineralization in xenoliths (stage I) may be related with the hydrothermal system of an earlier porphyry stock of Skouries (Kroll *et al.* 2002). It is remarkable that magnetite is Cr-bearing, the Cr content ranging from 0.65 to 2.26 wt.% Cr₂O₃ in the matrix, to 0.29 wt.% Cr₂O₃ in magnetite of vein type, in contrast to the Cr-free magnetite of the main porphyry. Chalcopyrite and pyrite contains 0.45 to 2.4 wt.% Ni and 0.64 to 4.18 wt.% Co. Ti-magnetite, with titanium content ranging from 17.5 to 23.5 wt.%, is commonly associated with rutile, both postdating the main stage of the magnetite deposition (Fig. 10-4).

A salient feature of the Skouries porphyry is the high values of the ratios Ce/Lu (>225), relatively high Th and U contents (up to 63 ppm and 9 ppm, respectively), Ba (up to 2260 ppm) and Sr (up to 1230 ppm) contents, reflecting probably a strong fractionation of parental magmas (Eliopoulos & Economou-Eliopoulos 1991). Furthermore, the investigation using SEM/probe reveals the frequent association of magnetite and Cu-minerals (bornite and chalcopyrite) with inclusions of thorite, U-bearing thorite, hydroxyl-apatite and rare earth element (REE)-enriched silicates of the epidote-group (allanite), zircon and rutile, (Fig. 10-2 to 10-4). More specifically, Al and Ca decrease as iron and REE (La, Ce, Nd) increase outward, attaining values up to 24.4 wt.% total REE content, due probably to the substitution of Al by Fe³⁺ and Ca by La, Ce and Nd. Also, the average F content (whole rock) is 900 ppm F (Eliopoulos & Economou-Eliopoulos 1991), while mica phases contain up to 0.19 wt.% Cl and 2.48 wt.% F (Kroll *et al.* 2002). However, despite such an evolved geochemical signature of the Skouries deposit there is a Cr- and Ni-enrichment, reaching values up to 690 ppm Cr and 560 ppm Ni, and a negative relationship with the Pd, Pt contents (Table 10-5, Economou-Eliopoulos *et al.* 2001).

The discovery of palladium and its distribution in the Skouries deposit

In the course of a study of slag from prehistoric or Macedonian gold production in Greece, slag from the Skouries porphyry Cu–Au was found to contain a significant Pd content (40 ppb Pd). The subsequent analysis of representative ore samples showed a significant Pd-enrichment in mineralised samples, up to 490 ppb Pd in oxidized ore samples (Eliopoulos & Economou-Eliopoulos 1991). Subsequently, a more detailed study in the Skouries and other deposits of the Balkan Peninsula was carried out to define relationships between the Pd–Pt and vein-type Cu mineralization, various alteration types or redistribution by leaching from an early-stage. Relatively high Pd content in the major vein-type mineralization of Skouries ranging between 60 and 200 ppb (average 110 ppb Pd), was documented by analysis of a composite drill hole sample (~15 kg) showing 76 ppb Pd and 5000 ppm Cu (Economou-Eliopoulos & Eliopoulos 2000). Furthermore the analysis of mineralized material and highly mineralized portions (up to 3.4 wt.% Cu) from deeper parts of the deposit (from the potassic, propylitic alteration zone) indicated that there is a relatively high palladium, up to 610 ppb (average 130 ppb) and platinum, up to 150 ppb (average 46 ppb) contents (Table 10-5, Economou-Eliopoulos & Eliopoulos 2001).

Textural relations between base metal sulfides, PGM and Au–Ag tellurides support the association of precious metals with the Cu-minerals (bornite and chalcopyrite), indicating that the main Pd-bearing mineral merenskyite, was deposited during the major stage of Cu deposition. Thus, assuming that Pd is mainly associated with chalcopyrite in porphyry-copper deposits, calculating the measured Pd contents in chalcopyrite (measured contents are normalized to 100 percent chalcopyrite), then the Pd values in the mineralized samples from deeper parts of the Skouries deposit is 3000 ppb Pd, which is comparable to that in the chalcopyrite concentrate (2400 ppb Pd to 21 wt.%, Economou-Eliopoulos & Eliopoulos 2000), whereas the calculated Pt content is 1230 ppb.

With respect to Au, native gold or electrum occurs as small (5–100 µm) inclusions in chalcopyrite or along bornite margins; it may also form intergrowths with Pd–Pt–Bi- and Ag-tellurides, ranging from less than 1 to tens

µm (Tarkian *et al.* 1991). Where primary mineralization is overprinted by secondary covellite and chalcocite, these minerals contain inclusions of gold (Kesler *et al.* 2002). Moreover, SIMS (ion probe) analyses of ore minerals from the Skouries deposit showed that bornite contains about 1 ppm Au, whereas chalcopyrite contains about an order of magnitude less. Although both supergene and hypogene chalcocite and covellite contain 10–24 ppm Au, commonly they are not abundant enough to account for a significant part of the average gold grades of bulk ore in many porphyry copper deposits. In the Skouries deposits, gold in covellite has been attributed to deposition as gold colloid particles, during the supergene enrichment rather than from exsolution from sulfides (Kesler *et al.* 2002).

Elastsite, Medet and Assarel deposits (Bulgaria)

The Elastsite, Medet and Assarel porphyry–Cu deposits, in the central Srednogorie metallogenetic zone are related to multiphase monzonitic-monzodioritic stocks and dikes of Upper Cretaceous (92.3 ± 1.4 Ma) age. Mafic dikes post-date mineralization, and may be porphyritic, but are generally aphanitic, are present both outside of the Elastsite deposit and in the pit (von Quadt *et al.* 2002). Ages based on the $^{40}\text{Ar}/^{39}\text{Ar}$ laser probe radiometric data for hornblende and biotite from igneous rocks indicated age of emplacement around 90.8 ± 0.5 Ma for both Elastsite and Medet areas, whereas all analyses of alteration minerals (white mica) indicated younger alteration at 79.5 to 80 Ma, suggesting a time gap between the dominant intrusions and hydrothermal alteration (Lips *et al.* 2004). The porphyry rocks may have been derived from an enriched mantle source, with a contribution by crust material, as is exemplified by the $^{87}\text{Sr}/^{86}\text{Sr}$ values ranging from 0.702356 to 0.706728 and moderately radiogenic Pb (von Quadt *et al.* 2002).

Elastsite

The Elastsite porphyry Cu–Au–PGE deposit extends over an area approximately 1,300 m long and 200 to 700 m wide. The ore body has been traced to a depth of more than 550 m. Mafic dykes crosscutting granodiorite and associated with intense potassic alteration (K-feldspar, biotite and quartz), are characteristic at the central part of the deposit. The Elastsite porphyry Cu–Au deposit is found in a spatial association (~10 km distance) with the Chelopech Au–Cu high-sulfidation epithermal-type deposit, connected by east–northeast- and north–northwest-trending fault systems (Popov & Kovachev 1996, Popov *et al.* 2000). Pre-mining ore reserves of the deposit were estimated to be 185 million tonnes with 0.4 wt % Cu, 0.3 g/t Au, 0.68–1.9 g/t Ag, 0.07 g/t Pd and 0.02 g/t Pt (Strashimirov *et al.* 2002, Tarkian *et al.* 2003, Strashimirov *et al.* 2003).

The various alteration types cannot be clearly distinguished, due to the repeated overprinting and intense silicification. Four mineral assemblages can be distinguished: (a) magnetite-bornite-chalcopyrite, which is linked to pervasive potassic and propylitic alteration types, in the central parts of the deposit, crystallized from high-salinity aqueous fluids with 60–42 wt.% $\text{NaCl}_{\text{equiv}}$, (b) quartz-chalcopyrite-pyrite, (c) quartz-pyrite and (d) quartz-galena-sphalerite. The three latter assemblages are linked to phyllic-argillic alteration and characterize the upper and marginal parts of the deposit, and may have precipitated from progressively cooler and less saline fluids with 44–20 wt.% $\text{NaCl}_{\text{equiv}}$. The oxidized zone of the deposit does not exceed 50 m depth, whereas the zone of secondary sulfide enrichment is limited (less than 30 m) (Kehayov & Bogdanov 2002, Kehayov *et al.* 2003, Tarkian *et al.* 2003). The Re–Os ages (92.43 ± 0.04 to 92.03 ± 0.05 MA) of molybdenite samples, representing the main stage stockwork mineralization, suggest a minimum absolute life span of $400,000 \pm 90,000$ years in a magmatic-hydrothermal system (Zimmerman *et al.* 2003).

Precious metal contents are strongly concentrated in the magnetite (ranging from 2 to 10 vol%, reaching locally up to 30 vol%)-bornite-chalcopyrite assemblage, occurring mainly in the southern part of the ore body. Pd, Pt and Au concentrations in representative mineralized samples from the Srednogorie metallogenetic zone of Bulgaria, including the Elastsite deposit, have been published by Eliopoulos *et al.* (1995) who documented Pd and Pt contents up to 20 ppb, while Cr and Co reach values up to 100 and 116 ppm, respectively. Furthermore, precious metal contents in 35 ore samples (normalised to 1% Cu, in order to obtain comparable data) are given by Tarkian *et al.* (2003): the average contents 890 ppb Au, 40 ppb Pd and 16 ppb Pt are higher in ore samples dominated by magnetite, bornite and chalcopyrite, compared to 460 ppb Au, 14 ppb Pd and 4 ppb Pt in samples consisting mainly of chalcopyrite and pyrite. The average precious metal contents in flotation concentrates (at 23.5 wt.% Cu) are 16200 ppb Au, 1130 ppb Pd and 130 ppb Pt (Tarkian & Stribny 1999, Tarkian *et al.* 2003). Gold and Pd correlate with Te, Bi and Se, while Pt shows a strong correlation ($r = 0.93$) only with Te (Tarkian *et al.* 2003).

The mineralogical data indicate that Pd, Pt and the associated Co, Ni, Te, Se, Bi, Au, and Ag occur under the form of the following minerals: merenskyite-moncheite, carrollite, nickeliferous linnaeite, pyrrhotite, hessite, clausthalite-galena, kawazulite, naumannite, eucairite, bohdanowiczite, weissite, gold-electrum, tetrahedrite-tennantite, and unnamed phases such as $(\text{Pd}, \text{Ag})_3\text{Te}_4$ (Tables 10-2 & 10-4). Coarse-grained native gold (up to several millimetres) occurs within thin veinlets cutting the above association or under the form of individual crystals in small cavities within bornite. Minor molybdenite and sphalerite are also present (Petrunov *et al.* 1992, Petrunov & Dragov 1993, Dragov and Petrunov 1996, Tarkian *et al.* 2003, Strashimirov *et al.* 2003). The distribution of these minerals is irregular throughout the deposit, forming lenses dominated by magnetite and hematite.

Medet

The Medet porphyry deposit, discovered in 1955, the first known porphyry deposit in Bulgaria, is linked to the Assarel volcanic complex, and it is among the largest ones in Bulgaria, with defined reserves of approximately 244 Mt, grading 0.37 % Cu (Herrington *et al.* 1998). The Cu-mineralization of stockwork type is hosted by a quartz monzonite intrusion, and is associated with quartz-magnetite and K-silicates. Rutile, ilmenite, Mn-ilmenite, pseudobrookite, Co–Ni assemblages (carrollite, vaesite), Co- and Ni-bearing pyrites, reaching values up to 17.8 wt.%, and 5.3 wt.%, respectively. Cu–Sn–V-minerals (colusite and sulvanite) and micron-sized inclusions of Bi–Ag tellurides (hessite and tetradymite) within chalcopyrite have been described (Strashimirov *et al.* 2003). Molybdenite occurs mostly as polymorphic 2H and it is characterized by a high Re content (average 905 ppm) (Todorov & Staikov 1985). The quartz-pyrite association forms veins and veinlets in the middle part of the deposit, whereas the quartz-galena-sphalerite association only occurs locally at the uppermost and marginal parts of the deposit. Late hydrothermal activity was marked by precipitation of anhydrite-gypsum and calcite-zeolite (laumontite, heulandite, stilbite) in veinlets up to 2–3 cm wide that replace and crosscut the opaque minerals common in the upper marginal parts of the deposit.

Palladium, Pt and Au concentrations in representative mineralized samples from the Medet deposit indicated up to 50 ppb Pd, 26 ppb Pt and 360 ppb Au. It is remarkable that samples with the highest Cr (130 ppm) and Co (170 ppm) contents exhibit the lowest (<10 ppb) Pd and Pt contents (Eliopoulos *et al.* 1995). In addition, the reported precious metal contents in flotation concentrate (at 14.9 wt.% Cu) are 160 ppb Pd, 8 ppb Pt and 5600 ppb Au (Tarkian & Stribny 1999).

Assarel

The Assarel granodiorite porphyry deposit, with defined reserves of approximately 360 Mt, grading 0.44 % Cu (Herrington *et al.* 1998), is located in the central part of the Assarel volcano, composed predominantly of lavas of andesitic composition, and latite-andesite pyroclastic rocks. The Assarel deposit is related to two pipe-like intrusions that join at depth. The northern one crops out in an open pit. The ore mineralogy and alteration at Assarel is particularly complex compared to the other deposits. An early quartz-magnetite-hematite association, which is typical of the porphyry copper deposits in the region, occurs only in a limited part of the Assarel deposit.

The dominant alteration types are: K-silicate, propylitic and advanced argillic-acid-chlorine and acid-sulfate subtypes. Porphyritic textures in many places are overprinted by a sequence of acid-chlorine and acid-sulfate alteration-types. Transition zones between propylitic-argillic and propylitic-sericitic alteration types are well exposed. Also, a transitional sericitic-advanced argillic type of alteration defined by the assemblage as illite + quartz + pyrite + pyrophyllite (kaolinite) has been described (Kanazirski 2000).

A quartz-pyrite-chalcopyrite association is widespread in the middle and marginal parts of the deposit, whereas a quartz-galena-sphalerite association is rare and is found mainly in the uppermost part of the deposit.

Several high-sulfidation-style assemblages are also established in the uppermost levels of the deposit. These assemblages include enargite and goldfieldite (Cu–As ± Te assemblage), colusite, As-sulvanite and sulvanite (Cu–Sn–V assemblage), aikinite and wittichenite (Cu–Bi assemblage), and hessite and tetradymite (Bi–Ag–Te assemblage) found as fine mineral inclusions in chalcopyrite. This latter assemblage is related spatially to sericitic and advanced argillic alteration-type of the volcanic rocks in the uppermost parts of the deposit. It is noteworthy that this alteration type, which is developed at depth in the porphyry Cu deposit, has been overprinted by high sulfidation-style mineralisation in the upper parts of the deposit (Strashimirov *et al.* 2002, Strashimirov *et al.* 2003). Assarel is the only major deposit in the district showing much secondary chalcocite and covellite, which is of major economic importance. The zone of supergene enrichment is a band 60–70 m thick that lies

above the primary quartz-pyrite-chalcopyrite but below the oxidation zone (10–15 m). In contrast to the other deposits in the region, native gold is rare here, although near the contact between the zone of oxidation and that of the secondary enrichment exceptionally high Au contents have been reported (Strashimirov *et al.* 2003).

It is remarkable that ore samples dominated by chalcocite and covellite, with gold content up to 19.5 ppm Au contain only 3 ppb Pd and < 10 ppb Pt, and relatively high Cr, Ni and Co contents reaching values up to 110, 280 and 150 (all in ppm), respectively. In general, precious metal levels in mineralised samples from the main part of the porphyry deposit are 140 ppb Au, 10 ppb Pd and 33 ppb Pt, while Cr, Ni and Co contents are lower than 35 ppm (Eliopoulos *et al.* 1995), which may point to an epigenetic Cr, Ni and Co-enrichment, along with Au. The precious metal contents in flotation concentrates (at 27.9 wt.% Cu) are 4800 ppb Au, 54 ppb Pd and 14 ppb Pt, which are lower than those in the Medet and Elatsite porphyry deposits (Tarkian & Stribny 1999).

Bor-Majdanpek (Serbia)

The Bor porphyry Cu and high-sulfidation epithermal deposits, the gold-poor Veliki Krivelj porphyry and Majdanpek porphyry Cu and high-sulfidation epithermal deposits in Serbia, which are hosted in a volcanic-intrusive complex with calc-alkaline affinity (Jankovic 1997), are the largest deposits in Europe. The volcanic activity at the Bor region, over 80 km long and 20 km wide, is confined to the emplacement of 90–78 Ma hornblende (-biotite) andesite and dacite (Karamata *et al.* 1997, Lips *et al.* 2004). Furthermore, Lips *et al.* (2004) indicated a close link between host-rock emplacement, mineralization and alteration in the Bor area, suggesting that formation of the porphyry mineralization during an early stage of hydrothermal alteration.

Approximately 450 Mt of ore grading 0.6% Cu, 570 Mt grading 0.44% Cu, and 1000 Mt grading 0.6% Cu have estimated resources for Bor, Veliki Krivelj and Majdanpek deposits, respectively (Herrington *et al.* 1998). Approximately 1500 m of vertical section has been exploited for more than 80 years.

At Bor the mineralization is continuous from massive high-sulfidation ore near surface, to porphyry-type mineralization below. The predominant rock type in the Bor area is hornblende-biotite andesite. At Veliki Krivelj the mineralization is hosted by porphyry dike swarms and by skarns, while the Majdanpek deposit is hosted by andesite dykes (Jankovic 1997, Lips *et al.* 2004). Chalcopyrite and pyrite are major components, with lesser bornite, molybdenite, magnetite, pyrrhotite and enargite.

The Majdanpek deposit is dominated by porphyry mineralization in a mineralised zone approximately 4 km long and 300 m wide, with an increase in copper grade in zones of potassium silicate alteration. Propylitic alteration is less well developed with a grade 0.3% Cu. The uppermost part of the ore body is Au-enriched (average 1 ppm Au), whereas below 300 m grade dropped to average 0.25 ppm Au. Chalcopyrite and lesser amounts of pyrite and magnetite mainly compose mineralization. Molybdenite, pyrrhotite, bornite, galena, sphalerite, marcasite, tetrahedrite, enargite, arsenopyrite, tellurides (PdAgTe₂), selenides and native gold are also present (Jankovic 1997, Herrington *et al.* 2003). The Mo content deposit is low ranging between 30 and 80 ppm, but the Re content in molybdenite reaches values up to 2700 ppm (Herrington *et al.* 1998). The Pd and Pt contents in the Majdanpek deposit are more elevated (130–240 ppb Pd and 16–19 ppb Pt in flotation concentrates, at 22–30 wt.% Cu) compared to those in Bor (40 ppb Pd and 19 ppb Pt) and Veliki Krivelj (70 ppb Pd and 16 ppb Pt) deposits (Tarkian & Stribny 1999). Although the Pd and Pt levels in those deposits are much lower than in the Skouries deposit, Greece, in the copper production of Serbia (1988) 50 kg Pd and 3 kg as by-products along with Au and Ag have been reported (Herrington *et al.* 2003).

Santo Tomas II, Philex Philippines

The Santo Tomas II Philex porphyry Cu–Au deposit, of Miocene age (3 Ma), is located on Luzon Island in the Philippines, along the margins of a fault system. It extends at surface over an area of approximately 600m x 200 m representing approximately 800 m of vertical section. This quartz diorite porphyry with calc-alkaline affinities is spatially associated with volcanic rocks of dacite composition (Tarkian & Koopmann 1995).

The predominant wall rock alteration associated with the mineralised zone is potassic and propylitic, with a common overlapping between of these alteration types. Phyllic alteration, of limited extent, overprints earlier potassic and propylitic assemblages. Two types of mineral assemblages have been distinguished: (a) bornite-chalcopyrite-magnetite, which is concentrated in the inner part of the potassic zone (biotite and quartz), and (b) chalcopyrite-pyrite, occurring in the outer part of the potassic zone and in the propylitic zone. The central high grade copper zone (>0.3 wt.% Cu) of the deposit is surrounded by lower grade

zone (0.2–0.3 wt.% Cu). There is a positive correlation between Cu and precious metals, in particular with gold (average 1.8 ppm Au), Pd (up to 290 ppb), Pt (up to 45 Pt) and Ag (up to 100 ppb). Merenskyite occurs exclusively as inclusions in chalcopyrite and bornite. Polyphase fluid inclusions in quartz veins associated with a PGM-bearing bornite–chalcopyrite–magnetite assemblage, are characterized by high salinity 35–60 wt.% NaCl_{equiv}, and high-trapping temperature 380–520°C (Piestrzynski *et al.* 1994, Tarkian & Koopmann 1995).

Grasberg deposit, Indonesia

The Grasberg intrusive and volcanic rocks are situated in the highlands of Irian Jaya, Indonesia, and lie on the still-active collisional boundary between the north-moving Australian plate and the SW-migrating Indo-Pacific plate. This plate interaction has resulted in extensive uplift in the area to form the central ranges of Indonesia and Papua New Guinea. Numerous mineralised intrusions, dominantly calc-alkaline to alkaline, are of age ranging from Tertiary to recent, but the largest deposits are the youngest (<9 Ma), and active volcanism and mineralization continue today at several places, such as Ladolam (Meinert *et al.* 1997).

Among the world's major Cu–Au mines is the Grasberg Cu–Au deposit, of Pliocene age, discovered in 1988. The multistage Grasberg and Kali intrusions are overprinted by extensive hydrothermal alteration. The intrusions have strontium (⁸⁷Sr/⁸⁶Sr values varying from 0.70626 to 0.70707), neodymium (εNd = –13.7 to –15.3) and lead isotopic characteristics suggesting that the parental magmas have been affected by a substantial crustal component (Housh & McMahon 2000).

The Grasberg deposit is hosted within intrusive rocks, has a pipe-like form, approximately 950 m in diameter, and 2.4 by 1.7 km at surface. Extensive skarn deposits surround the porphyry deposit. Probable mineral reserves in the Grasberg deposit/ Ertsberg district are approximately 2,515 million tons with average 1.1 wt.% Cu, 1 ppm Au and 3.4 ppm Ag. Palladium and platinum in flotation concentrate (at 23.8 wt.% Cu) were 58 ppb and 15 ppb, respectively, while the gold content was 18 ppm (Tarkian & Stribrny 1999). Thus, although Pd and Pt data in concentrates is limited the comparison of the Au content between the average value (1 ppm at 1.1 wt.% Cu) and that in a flotation concentrate (18 ppm Au, at 23.8 wt.% Cu) point to much lower Pd and Pt (average) contents compared to those in the Skouries, Greece, and Elatsite, Bulgaria porphyry deposits.

The sulfide mineralization can be grouped into three main stages: (1) heavy sulfide zone, (2) Grasberg copper-gold stage, and (3) late copper mineralization (mixed copper sulfides, covellite-enargite-pyrite and pyrite-covellite-marcasite). The Grasberg copper-gold stage is a major chalcopyrite-bornite-pyrite-gold-hematite event, related to high-K calc-alkaline to shoshonitic intrusive rocks, extending to depth > 2500 m, while at the peripheral zones overprints the heavy sulfide zone (McDowell *et al.* 1996). Late copper mineralization comprises several stages and is dominantly disseminated in character. The early stages are dominated by chalcopyrite, bornite, digenite-chalcocite, covellite-nukundamite, and colusite, with the later stages containing pyrite, marcasite, covellite, and enargite and minor chalcopyrite. Late copper mineralization is essentially a high-sulfidation system, and is associated with zones of andalusite alteration, and abundant intermediate argillic alteration (McDowell *et al.* 1996).

Ok Tedi, Papua New Guinea

Ok Tedi porphyry Cu–Au deposit is associated with a younger (1.2 Ma) latite porphyry stock, of calc-alkaline affinity (Page & McDougall 1972), compared to that of the Grasberg deposit (Meinert *et al.* 1997). Mineralization, associated with the potassic alteration zone, consists mainly of chalcopyrite with subordinate bornite, chalcopyrite, covellite, pyrite, and marcasite. Molybdenite is present in lesser amounts, whereas magnetite occurs in skarns in the peripheral parts of the deposit (Bamford 1972). Pre-mining mineral reserves at Ok Tedi were approximately 275 million tons with average 0.75 wt.% Cu and 0.5 ppm Au (Gilmour 1982, Rush & Seegers 1990). Gold in the supergene zones reaches values of 3 ppm, and in the skarn mineralization 1.8 ppm. Pd and Pt in a flotation concentrate (at 37.3 wt.% Cu) were 980 ppb and 24 ppb, respectively (Tarkian & Stribrny 1999).

Ladolam deposit, Papua New Guinea

The Ladolam deposit on Lihir Island is among the world's largest, containing more than 1300 tons of Au. It has been interpreted as a transition stage between an of early-stage, low-grade porphyry gold system and that evolved into a low-sulfidation epithermal deposit (Moyle *et al.* 1990, Carman 1994, Müller *et al.* 2002). Alkaline rocks that range from trachybasalt through trachyandesite to latite, which are cut by late-stage monzodiorite

intrusions, host the Ladolam gold deposit. Their geochemical signature is typical of high-K igneous rocks transitional to shoshonite. Unaltered samples, from the Lihir rocks contain elevated noble metal abundances of up to 4 ppb Au, 13 ppb Pd, and 12 ppb Pt. These elevated precious-metal (Au–Pt–Pd) concentrations have been interpreted as primary magmatic features suggesting a precious metal pre-enrichment of the mantle source beneath the island Ladolam (McInnes & Cameron 1994, Taylor *et al.* 1994, Mungall 2002, Müller *et al.* 2003). Also, the proximity of the Ladolam epithermal gold deposit to the Conical seamount on nearby Lihir island, coupled with the similarity of the mineralogy, alteration, geochemistry and vein textures to those of some subaerial epithermal gold deposits, indicate that some features long considered to define a subaerial setting can be also formed in a submarine environment (Petersen *et al.* 2002).

Porgera deposit, Papua New Guinea

The Porgera gold deposit, located in the Pliocene fold and thrust belt that forms the highlands of Papua New Guinea, is associated with sodic-alkalic, hypabyssal intrusions of alkali basaltic composition. Reserves and resources were estimated to 113 Mt of ore at a grade of 3.5 ppm (Ronacher *et al.* 2004). The intrusions were emplaced into Cretaceous mudstone and siltstone in the latest Miocene (6 Ma). Both igneous and sedimentary rocks are mineralized. Three types of veins occur: (1) magnetite-sulfide \pm Au-carbonate veins (prestage I); (2) base-metal sulfide \pm Au-carbonate veins (stage I); and, (3) quartz-roscoelite-pyrite-gold veins and breccias (stage II), which is economically the most important. Laser $^{40}\text{Ar}/^{39}\text{Ar}$ dating of magmatic biotite (5.99 ± 0.11 Ma) dates the intrusive event and hydrothermal biotite (5.98 ± 0.13 Ma) and roscoelite (5.92 ± 0.08 Ma), date the mineralising event, indicating that the magmatic and ore-forming system at Porgera was short-lived (Ronacher *et al.* 2000).

Compilation of petrological, fluid inclusion and oxygen and hydrogen isotope data, coupled with the presence of organic-derived volatiles suggest that an ascending fluid interacted with sedimentary rocks, probably at depth prior the site of ore deposition. Furthermore, modelling the analytical data suggest that more than one process was involved in stage II mineralization, including boiling, mixing and fluid-rock reaction (Ronacher *et al.* 2004).

Mamut deposit, Malaysia

The Mamut Cu–Au deposit, east Malaysia, of upper Miocene age, belongs to the mineralised belt along a NW–SE striking tectonic zone of Sabah. It is associated with a monzonitic-granodioritic porphyry stock with calc-alkaline affinity, although approximately 40% of the mined ores were hosted in a serpentinized body. Reserves in the Mamut deposit were approximately 179 million tons with average 0.48 wt.% Cu and 0.6 ppm Au (Tarkian & Stribny 1999). Mineralization is associated with potassic-propylitic alteration zones. Chalcopyrite and lesser amounts of pyrrhotite are principal ore minerals. Biotite is common in the outer potassic alteration zone. Strong silicification is characteristic. Overlapping Pb and Zn and subsequent Sb mineralization is associated with NNE-trending fractures accompanying the phyllic and advanced argillic alteration envelope (Imai 2000). Although magnetite is locally abundant in the propylitic zones, an abundance of pyrrhotite may suggest less reducing and locally lower pH environment (Kosaka & Wakita 1978, Corbett & Leach 1998). Palladium, platinum, and gold in flotation concentrates (at 20.3 wt.% Cu) were 1400 ppb, 470 ppb and 15200 ppb, respectively (Tarkian & Stribny 1999).

Bajo de la Alumbra, Andes

The Bajo de la Alumbra deposit, one of the world's largest Cu–Au deposits, is associated with Miocene magmatism in the central Andes. Production plus remaining resources attain 780 Mt ore at 0.52% Cu and 0.67g/t Au (Sasso & Clark 1998). Detailed studies of the Alumbra deposit documented eight distinctive porphyritic intrusions, which form stocks and dike-like bodies, showing a general evolution from early silica-rich dacite toward intermediate andesite (Ulrich, 1999, Proffett 2003). Following a barren intrusion that pre-dates the porphyry stock, primary (unweathered) ore mainly consists of chalcopyrite (+/ bornite), native gold and pyrite. The highest copper-gold grades are associated with intense potassic (quartz-magnetite) alteration of two of the earliest mineralised porphyritic intrusions. Younger porphyries are less mineralized or in some cases barren (Proffett 2003). Halter *et al.* (2002, 2004, 2005) have focussed their investigation on sulfide melt inclusions on the best-exposed part of Farallon Negro volcanic complex, hosting the Alumbra porphyry Cu–Au deposit, and provide evidence for magma mixing and evolution of the magma chamber. They demonstrate an intense magma mixing (hybridization) process of a rhyodacitic magma with a crustal component, and a very mafic mantle-

derived magma resembling the composition of lamprophyre dikes. In addition, they concluded that ore metals and most of the sulfur in the ore fluid are derived from the magmatic sulfide liquid, and that Cu/Au ratios in the ore bodies are equal to that of the precursor sulfide.

Cripple Creek, Rocky Mountains, U.S.A.

The Cripple Creek deposit is one of the largest in the world (having produced nearly 700 metric tons of Au) and belongs to an important group of alkaline-related porphyry, epithermal and skarn gold deposits, occurring in a north-south belt that extends from Canada to eastern Mexico along the eastern edge of the North American Cordillera (Mutschler *et al.* 1985). Deposits in the North American Cordilleran belt, including deposits in the Black Hills, South Dakota and Galore Creek (Strike Copper), British Columbia, and Cripple Creek, to the south have produced nearly 13% of the total production in the United States and Canada (Mutschler & Mooney 1993).

Geochronological, geochemical, and isotopic data from some of these deposits suggest a genetic relationship between alkaline magmatism and gold mineralization. Gold deposits at Cripple Creek formed between 32 and 27 Ma, corresponding to the final stages of Laramide subduction-related magmatism in this region, like the giant Bingham Cu–Au deposit, Utah (Mutschler & Mooney 1993, Sillitoe 2000, Kelley & Ludington 2002). The most salient feature of these porphyry–Au deposits is the near-surface emplacement of the related porphyry intrusions, the relatively oxidized volatile-rich alkaline nature, the contribution of crustal material, and the anomalously hot, low density and thick crust (about 50 km) beneath Colorado (Kelley & Ludington 2002).

Bingham porphyry Cu–Au deposit, Utah

The Bingham Cu–Au–Mo porphyry (Fig. 10-1) is one of the largest porphyry copper deposits in the world, with combined reserves and production of more than 18 Mt of Cu (Babcock *et al.* 1995). It is spatially associated with several small monzonite and quartz monzonite stocks of Eocene age (39.8 to 37.5 Ma) emplaced in Paleozoic quartzite and limestone (Warnaars *et al.* 1978, Babcock *et al.* 1995, Ballantyne *et al.* 1997, Maughan *et al.* 2002). Some intrusions vented to the surface forming volcanic rocks, the older unit being comagmatic with the intrusive complex. Their composition has been attributed to a combination of fractional crystallization, magma mixing and assimilation (Keith *et al.* 1998). The largest porphyry–skarn Cu–Au–Mo deposit in North America, at Bingham Canyon, Utah, has a strong crustal contamination signature, although primitive alkaline lava flows are spatially and temporally associated with it. Such an association of mafic alkaline dikes with giant porphyry Cu–Mo deposits in Andes has been emphasised (Keith *et al.* 1998). Mineralization consists mainly of chalcopyrite, bornite, molybdenite and pyrite. The porphyry ore occurs mainly in monzonite, quartz monzonite porphyry, quartz latite porphyry, latite porphyry, and quartz latite porphyry breccia with large adjacent Cu skarns, vein and Manto Ag–Pb–Zn deposits, and distal disseminated Au deposits (Phillips *et al.* 1997). There is an enrichment of Pd, Pt (up to tens of ppb) and Au, which is similar to that seen in other young shoshonitic alkalic systems like those of Fiji and Lihir, Papua New Guinea. (Müller *et al.* 2003).

The relatively Pd- and Pt-rich character of the Bingham ore, and the trend of the younger Bingham intrusions to be more Cr- and Ni-rich despite their otherwise more evolved geochemical signatures is a salient feature (Atkinson & Einaudi 1978, Waite *et al.* 1997). Also, a volcanic section that is co-magmatic with ore-related porphyries is very heterogeneous containing clasts of latite and minette, flows of melanephelinite, shoshonite, and olivine latite, in addition to volumetrically dominant dacite to trachyte (Keith *et al.* 1998).

British Columbia, Cordillera

Porphyry Cu–Au deposits located in the British Columbia Cordillera are associated with alkaline, subalkaline to calc-alkaline stocks, dikes and sills, which have been emplaced into two allochthonous terranes, Quesnellia and Stikinia, North America (McMillan & Panteleyev 1995). The majority of these intrusions are late Triassic to early Jurassic in age (205–195 Ma) although some intrusions in Quesnellia are distinctly younger (~185 Ma; Mortensen *et al.* 1995). Recent U–Pb geochronology of some intrusive rocks associated with porphyry Cu–Au deposits in Cordillera, indicated that the crystallization ages obtained for porphyry-related intrusions in both alkaline and calc-alkaline composition and both Quesnellia and Stikinia units (Copper Mountain, Ajax/Afton, Mount Polley, Galore Creek, Cat Mountain and Kemess intrusions) are in the range of 210 Ma to 200 Ma, (Mortensen *et al.* 1995). Evidence from xenoliths, geological, mineralogical, geochemical, and isotopic data

indicate that this suite of intrusions belong mostly to a distinctive variety of alkaline arc magmas that were largely derived from an enriched mantle source region and that these intrusions were emplaced during collisional events (McInnes & Cameron 1994, Lang *et al.* 1995, Cassidy *et al.* 1996).

Alteration assemblages including potassic, calc-potassic and sodic/sodic-calcic characterize deposits associated with alkaline intrusions in Quesnellia and Stikinia, all show a distinct lack of associated quartz veining. Mineralization occurs in sulfide/oxide vein systems, breccias and disseminated zones, consisting mainly of Cu-minerals (chalcopyrite and/or bornite) and Au, with varying Cu/Au ratios among districts, and among and within zones in individual districts, while significant Mo is rare. The Copper Mountain and the Iron Mask Batholith have been mined extensively and significant resources exist at Galore Creek, Mt. Polley, and Mt. Milligan (Lang *et al.* 1995).

Mount Polley

The Mount Polley deposit is characterized by multiple intrusions that vary from diorite to nepheline syenite. Mineralization, consisting of chalcopyrite, bornite and magnetite, is associated with hydrothermal breccia at two main areas: The West zone, extending to a drilled depth of at least 275 m, and the central zone, approximately 200 m to 300 m width by 1100 m north-south, that is contained within an eastward dipping breccia body. Mineralization in the core of the deposit is associated with a chalcopyrite-bornite-chalcopyrite assemblage, passing out into magnetite-pyrite-chalcopyrite (Fraser *et al.* 1995). Palladium and Pt contents in sulfide concentrates from Main zone are higher (up to 320 ppb Pd and 33 ppb Pt) compared to the West zone (Thompson *et al.* 2001).

Galore Creek

Galore Creek is well known for its high Au content and close spatial relationship with high level syenitic and monzonitic intrusions. A complex succession of intrusive and hydrothermal events characterizes the Galore Creek deposits, with an intense alteration and mineralization (Lang *et al.* 1995, Bottomer & Leary 1995). The highest gold grades, exceeding 1 ppm, are associated with bornite-rich mineralization situated in the northern and southern parts of the central zone, dominated by Ca-K-silicate alteration, with a combined resource of 284 million tonnes at 0.67 wt.% Cu (Enns *et al.* 1995). Palladium and platinum contents vary among and within zones of the Galore deposit, the Pd/Cu ratio ranging between 5.7 and 53.3 in the central zone, to 120 at the Southwest zone (Thompson *et al.* 2001, Table 10-1).

Mt. Milligan

The Mt Milligan deposits are large, low grade, porphyry Cu-Au deposits hosted by monzonite stocks and adjacent volcanic rocks within the Early Mesozoic Quesnel Terrane. The measured and indicated resource for the combined deposits is 299 million tons of 0.22 wt.% Cu and 0.45 ppm Au. A biotite-rich subzone forms the core of an extensive potassic alteration zone and hosts most of the copper and gold, although numerous polymetallic veins lie within the propylitic alteration zone (Sketchley *et al.* 1995). The Au, Pd and Pt reach values up to 18500 ppb, 6310 ppb and 110 ppb, respectively, while the Pd/Cu ratio ranges from 78 to 5100 (Thompson *et al.* 2001, Table 10-1).

Ajax/Afton

The Ajax/Afton deposits, extending for over 20 km from NW to SE, and approximately 5 km width, are located at the contact between two stages of the Iron Mask intrusion, the hybrid diorite and the younger Sugarloaf diorite, which is the probable source of the Cu-Au mineralization. Along the faults system, controlling that mineralization-bearing diorite, serpentinized picrite bodies, with chromium content >2000 ppm and >900 ppm Ni, have been also distributed (Ross *et al.* 1995).

Reconnaissance data given by Thompson *et al.* (2001) indicate that, in most cases, Pd concentrations are two to three orders of magnitude lower than Au, and Pt approximately one order of magnitude lower than Pd. With the exception of occasional elevated Ru and modest Rh, most of the other PGE have low concentrations. In addition, DRC Resources Corporation estimated the mineral resources of the two deposits that comprise the Afton copper/gold project in B.C. (Dolbear & Company 2003). The assumption that the deposit delineated at Afton (1978) was a supergene-enriched porphyry Cu was the reason for the termination of mining in 1987, when at a depth of 275 m, supergene native copper, chalcocite and chalcopyrite ores were not of economic

interest. However, further drilling below the pit bottom revealed higher copper and precious metal grades at depths, and outlined a measured and indicated resource of 69 million tons characterized by the increase of Cu, Au, Ag and Pd from top 0.79 (wt.%), 0.62 (ppm), 1.96 (ppm) and 0.09 (ppm), respectively, downward to 2.76 wt.% Cu, 2.04 ppm Au, 8.02 ppm Ag, and 0.19 ppm Pd (Dolbear & Company 2003).

It has been suggested that the Pd and Pt mineralization in the above porphyry deposits is linked with the genesis of alkaline arc magmas, derived probably from an enriched mantle source. They may reflect partial melting and incorporation into the melt of destabilized precious metal-bearing sulfides, hosted in the mantle source. The oxidized nature of the alkaline arc magmas inhibits fractionation of sulfides, while the precious metals remaining in the magmas were transported by magmatic-hydrothermal fluids and were precipitated in the porphyry environment (Thompson *et al.* 2001).

Russia (Siberia)

Siberian (Russia) and Mongolian fragments of the Central Asian Fold belt comprise numerous porphyry Cu–Mo deposits (Fig. 10-1). The mineralization in the Sora (Kuznetsk Alatau), Aksug (Tuva) and Zhireken (Eastern Transbaikalia) is associated in time and space, with porphyry stocks and dikes formed during periods of a decreasing magmatic activity. There is a time gap of 20–30 Ma (Ar^{40}/Ar^{39} dating) between the porphyries and older granite intrusions (Berzina & Sotnikov 2000).

Stocks and dikes of the Cu–Mo-porphyry of quartz-diorite-granodiorite intrude a pluton of similar composition with subordinate diorite, tonalite and gabbro. $^{40}Ar/^{39}Ar$ dating indicated that porphyries are younger, of 404–401 Ma age than other intrusions of 497–462 Ma age (Sotnikov *et al.* 2003). The chemical compositions of the porphyries are similar to that of the host granitoid plutons. The Aksug porphyries belong to the calc-alkaline series and of an andesitic parental magma. They are characterized by low Rb, Cs, Th, Ta, and REE contents, high K/Rb ratios, and low F/Cl in magmatic fluids. In addition, the deposit is dominated by a mantle source component, with initial ($^{87}Sr/^{86}Sr$) varying from 0.70458 to 0.70496 (Sotnikov *et al.* 2000). The stockwork mineralization, consisting mainly of pyrite, chalcopyrite, molybdenite, and minor enargite, galena, and sphalerite, occurs in quartz-sericite altered rocks. At a lower level, the rocks are rich in anhydrite, and, to a lesser extent, in barite and celestite (Berzina & Sotnikov 2000).

Sora Mo–Cu porphyry deposit

The porphyry stock is characterized by potassic alteration (biotite, K-feldspar) and strong albitization with limited sericitization and silicification. The Sora deposit is characterized by Mo mineralization, consisting of molybdenite accompanied by pyrite and chalcopyrite. Small amounts of sphalerite, galena, and tetrahedrite are also present. The Mo ranges between 0.04 and 0.10 wt.% and Cu from 0.02 to 0.20 wt.%. Early stage of mineralization, including chalcopyrite and molybdenite disseminations, is related with quartz-biotite-K-feldspar altered rocks. The breccia ore consists of intensely K-feldspathized and albitized angular fragments of hosting rocks, cemented by quartz-fluorite matrix, containing molybdenite, pyrite, and chalcopyrite. Quartz-fluorite-galena-sphalerite veinlets, hosted in sericitized and pyritized rocks are the final products of the ore-bearing process.

Zhireken Mo–Cu porphyry deposit

The Late Jurassic age Zhireken porphyry molybdenum–copper deposit is located in Eastern Transbaikalia. Host rocks comprise a calc-alkaline suite of normal to elevated alkalinity dominated by granodiorite, syenite and granite. The Zhireken subvolcanic stocks are of K-calc-alkaline affinity, mainly diorite, syenite, and subalkaline granite porphyries. Geologic and isotopic data suggest that these high REE porphyries were related to the beginning of rifting during late Jurassic–Cretaceous time. Among the other deposits discussed, the Zhireken subvolcanic stocks exhibit high Rb, Cs, Li, and Th contents and low K/Rb ratios. Halogen-containing minerals are characterized by elevated F contents, although F/Cl ratios are generally lower than those of the Sora deposit (Sotnikov *et al.* 2000, Berzina *et al.* 2005). The most salient feature of the Zhireken deposits is elevated initial ($^{87}Sr/^{86}Sr$) values of 0.70510–0.70642, indicating a significant crustal contribution to the parent magma of these porphyries. Hydrothermal alteration consists of well-developed potassic (K-feldspar) and argillic assemblages, with ore mineral associations including molybdenite accompanied by pyrite, chalcopyrite and traces sphalerite, rutile, tetrahedrite.

The Pd and Pt contents of both chalcopyrite and molybdenite in flotation concentrates in the above porphyry Cu ± Mo of Russia are relatively low, varying from 9 to 83 ppb Pd and from <10 to 110 ppb Pt. The

highest values recorded are 920 ppb Pd in sulfide concentrates from the Aksug deposit, and 680 ppb Pd and 300 ppb Pt in sulfide concentrate from breccia of the Zhireken deposit (Table 10-1). The available analytical data indicated a positive trend between Pd and Pt in both sulfide and molybdenite concentrates (Sotnikov *et al.* 2000).

Mongolia

Several porphyry copper systems are known in Mongolia, among which the Erdenetuin and Oyu Tolgoi deposits attain the status of significant deposits (Perelló *et al.* 2001 and references therein).

Erdenetuin-Obo, northern Mongolia

The Triassic Erdenetuin-Obo Cu–Mo deposit (approximately 1,700 million Mt at 0.54% Cu, 0.016% Mo, 0.01 ppm Au) (Sotnikov *et al.* 2000, Perelló *et al.* 2001) is located in the Selenga-Vitim belt of northern Mongolia. Granite and andesite are the most volumetrically important rock types, with minor quartz diorite and granodiorite. Isotope data suggest that the host granitoid rocks formed synchronously with early volcanism at a continental margin, whereas the ore-bearing porphyries are coeval with bimodal rift-related volcanism (Sotnikov *et al.* 1995). The porphyry-generating magmas at Erdenetuin-Obo deposit had initial strontium isotope signatures ($^{87}\text{Sr}/^{86}\text{Sr}$) of 0.70406–0.70424, which suggest a mantle source. High Sr and Ba and moderate HFSE and REE contents characterize these porphyries (Berzina & Sotnikov 2000). Ore minerals occur as disseminations and veinlets in a NW-trending zone of sericitized and silicified rocks.

Mineralization is most closely related to diorite and granodiorite porphyries with minor copper associated with the granite porphyries. The ore zone is 2.8 km long and 0.3 to 1.3 km wide, hosted by the porphyry stock and extends into the neighboring granite up to 300–500 m, and a depth of 900–1000 m. Mineralization consists of chalcopyrite with pyrite, molybdenite and traces sphalerite, tetrahedrite, and hydrothermal rutile. Dominant hydrothermal alteration consists of silicification and sericitization of host rock silicates. Potassic and chloritic alteration is minor (Sotnikov *et al.* 2000). The Pd and Pt contents are relatively low (a few tens of ppb) are comparable to those in the above porphyry Cu \pm Mo deposits of Russia (Table 10-1, Sotnikov *et al.* 2000).

Oyu Tolgoi, southern Mongolia

The Oyu Tolgoi porphyry Cu–Au–(Mo) deposit of Silurian-Devonian age was discovered in 1996 in the Gobi Desert of southern Mongolia, and is associated with bimodal basalt-peralkaline magmatism (Kovalenko & Yarmolyuk 1995). The deposit consists of three main mineralized zones (North, Central, and South Oyu), with an areal extension of approximately 2.5 x 1.5 km, and is interpreted to constitute at least two separate porphyry copper centers (Perelló *et al.* 2001). Central Oyu consists of a multiple-phase hydrothermal breccia crosscutting an altered fine-grained feldspar porphyry containing porphyry-type alteration and mineralization. At South Oyu, a feldspar-hornblende porphyry of monzonitic composition intrudes a sequence of fine-grained andesite and basaltic andesite. The bulk of the Cu–Au–Mo mineralization occurs in an early magnetite-rich, pyrite-poor zone dominated by quartz, chalcopyrite, bornite and trace molybdenite. Magnetite averages 7 to 10 vol %, and copper and gold grades vary sympathetically. At central Oyu, copper mineralization is present in a supergene chalcocite blanket that formed at the expense of a pyrite-rich, hypogene chalcocite-covellite-tennantite sulfide suite that accompanied the advanced argillic alteration event (Perelló *et al.* 2001).

In general, although the information on the PGE content in Cu–Mo ores is limited, it seems likely that both chalcopyrite and molybdenite concentrates exhibit an enrichment in Pd and Pt, and sometimes lower values of the Pd/Pt ratios compared to those of Porphyry Cu–Au deposits (Table 10-1). In addition, the average (n = 4) Pd and Pt contents in sulfide concentrates from the Ryabinovoye alkaline Cu–Mo porphyry, Central Aldan, Russia, were 85 ppb and 150 ppb, respectively (Kovalenker *et al.* 1996). The Cu–Mo deposits in Armenia are considered to be similar in age and genesis to those in the Andes and western Cordillera of North America (Pokalov 1977). Highly mineralised samples contain 10–80 ppb Pd, and up to 18 ppb Pt. Molybdenum concentrates contain 5–220 ppb Pd and 12–390 ppb Pt, and copper concentrates contain from 9 to 160 ppb Pd and up to 20 ppb Pt (Faramazyan *et al.* 1970).

Cadia–Goonumbla–Copper Hill, Australia

Mineralised igneous complexes of Ordovician age from New South Wales range in composition from quartz-rich medium-K dacite (Copper Hill), to quartz-poor, high-K to ‘shoshonitic’ monzodioritic to monzonitic

complexes (Goonumbla & Cadia) (Blevin 2002, Holliday *et al.* 2002). The Cadia district lies within shoshonitic volcanic rocks of a Late Ordovician Volcanic Belt in the eastern Lachlan Fold Belt of New South Wales. Mineralization occurs in four principal porphyry deposits (Cadia Hill, Cadia Ridgeway, Cadia East/Cadia Far East and Cadia Quarry) showing a close spatial association with shoshonitic monzodiorite to quartz monzonite dykes and stocks of the Cadia Intrusive Complex. Gold-copper mineralization is hosted by these intrusions and also by the enclosing volcanic wall rocks. Hydrothermal alteration associated with mineralization is potassic, which is overprinted by selectively pervasive propylitic and silica-albite assemblages. Petrological studies and major and trace element analysis of unaltered samples from the Cadia porphyry complex are characterized by high K₂O contents (up to 6.5 wt.%) and molecular K/Na ratios consistently >1, confirming the alkalic and shoshonitic nature of the complex. A similar association occurs at the economic Goonumbla (North Parkes) porphyry gold-copper deposits in the eastern LFB, whereas sub-economic gold-copper mineralization at Copper Hill is associated with calc-alkaline quartz diorite and dacitic intrusions (Heithersay *et al.* 1990, Holliday *et al.* 2002, Blevin 2002). At Copper Hill, a porphyritic quartz-diorite, diorite-tonalite complex intrudes an andesite protolith and locally limestone. Geological, geochemical and recent geophysical data for Copper Hill suggest that the main mineralization zone occurs at the western part, over an area approximately 200 m wide and 1000 m long. Due to intense faulting of the area, it has been suggested that the mineralised block is an uplifted deeper portion of the porphyry system (GCO 2004).

The Cadia porphyry gold-copper district is the largest hydrothermal, intrusion-related gold deposit in eastern Australia. The measured resources at Cadia Hill are 260 Mt at 0.17 wt.% Cu and 0.73 ppm Au; inferred resources at East Cadia are 220 Mt at 0.37 wt.% Cu and 0.43 ppm Au. The dominance of magnetite (quartz-magnetite veins or stockwork, adjacent to monzodiorite-monzonite intrusions, at Cadia Hill and East Cadia, is distinctly different from the Ridgeway deposits which contain abundant chalcopyrite, bornite and visible gold (Blevin 2002, GCO 2004). Cadia Hill, Cadia East, and Cadia Far East are relatively large, low-grade porphyry deposits dominated by spaced, sheeted quartz vein systems. Ridgeway (78 Mt 2.0 g/t Au and 0.67 % Cu) and a deep zone in Cadia Far East are smaller but higher grade porphyry deposits characterized by Au and Cu-rich cores with intense sheeted, layered quartz-magnetite-bornite(-chalcopyrite) veins grading outward into chalcopyrite dominated assemblages. Big Cadia and Little Cadia are peripheral Au–Cu–Fe skarns. Cadia Quarry between Cadia Hill and Ridgeway contains transitional features between magmatic and hydrothermal conditions (Wilson 2003, Wilson *et al.* 2004).

Four economic porphyry Cu–Au deposits occur within the Goonumbla volcanic complex. Together these deposits have a combined ore reserve of approximately 64 million metric tons (Mt) at 1.1 wt.% Cu and 0.5 g/t Au (Lickfold *et al.* 2003). There are many similarities to the Skouries deposit, Greece, in terms of (a) both systems are characterized by small finger-like and dike systems monzonite intrusions on which individual deposits are centred. These intrusions have been interpreted to have formed as late-stage differentiates of andesitic parental magmas with shoshonitic compositions, (b) these porphyry intrusions host bornite-chalcopyrite dominated stockwork mineralization, and (c) the hypogene mineralization in both systems includes high-grade zones containing > 0.7 wt.% Cu and > 0.7 ppm Au (Kroll *et al.* 2002).

The Copper Hill deposit is much smaller and subject to on going exploration efforts. To date exploration revealed a zone of mineralization, 300 m long, 50 m wide and up to 200 m deep, consisting of magnetite, chalcopyrite, pyrite, gold, and merenskyite. Grades are similar to that at the Cadia Gold Mine: 0.5 to 1.0 wt.% Cu, 0.5 to 1.5 ppm Au, while Pd reaches values up to 900 ppb (Blevin *et al.* 2002, Holliday *et al.* 2002, GCO 2004).

CHAPTER 11: PLATINUM GROUP ELEMENTS EXPLORATION: ECONOMIC CONSIDERATIONS AND GEOLOGICAL CRITERIA

Tony Green
Falconbridge Limited, Suite 800, Queen's Quay Terminal,
207 Queen's Quay West, Toronto, Ontario, M5J 1A7, Canada
E-mail: tony.green@toronto.norfalc.com

and

Dave Peck
Anglo American Exploration (Canada) Ltd.,
800 – 700 West Pender Street, Vancouver, BC V6C 1G8 Canada
E-mail: dpeck@angloamerican.ca

INTRODUCTION

This chapter provides a series of guidelines for the successful implementation of a PGE exploration program. The principal aim of this contribution is to highlight the many excellent opportunities that exist for growth within the PGE exploration and mining sector. The comments presented are written by and couched for explorationists although, in keeping with the overall theme of this book, they attempt to identify areas of opportunity for researchers to make meaningful contributions. The chapter opens with a review of the key economic drivers for PGE markets, which provide a fundamental constraint on exploration investment and decision making. This is followed by a critical discussion of key geological targeting criteria used in selecting quality PGE prospects. Improved understanding of the fundamental behavior of the PGE in different geological environments, as discussed elsewhere in this book, should aid in identifying new deposit styles that could fundamentally alter PGE markets.

Much of our current knowledge of PGE distribution in the crust comes from detailed investigations of a few world-class deposits, particularly the Bushveld Igneous Complex, the Great Dyke, the Stillwater Complex and the Noril'sk-Talnakh ore junction. Accordingly, the current PGE supply situation continues to be dominated by traditional deposit types and mining districts. Pd supply continues to derive largely as a by-product from Ni-Cu sulfide mining at the Noril'sk-Talnakh and Sudbury camps. Global Pt supply continues to be sourced principally from reef-type, Pt-rich deposits in the Bushveld Igneous Complex. Sustained growth in PGE markets will

only arise if global supply diversity is achieved. To this end, PGE explorers and researchers are encouraged to divert a significant proportion of available resources into new geological environments while maintaining a reduced but important focus on the "known". This should lead to the development of new exploration paradigms and, hopefully, to the discovery of "unconventional" but viable new PGE deposits.

PGE DEMAND

The total value of global Pt and Pd production (approximately US\$ 6 billion in 2003) has, in recent years, begun to rival the total value of the global nickel market (approximately US\$10 billion in 2003). However, PGE are commonly perceived as being a less attractive investment option than nickel. This perception largely stems from the boom and bust trend of PGE prices. Price forecasting for PGE, especially for Pd, has been extremely difficult in recent years. Understanding the intrinsic volatility of PGE supply and demand remains a critical part of the business of knowing when and where to explore for PGE.

Over the past 35 years, major price spikes for the PGE have occurred in 1980 (both Pd and Pt), 1987-90 (Pt), 1999-02 (Pd) and 2003-04 (Pt) (see Fig. 11-1). Dating back to the 1950s, Pt has traded at a significant premium to Pd and this trend is likely to continue for the next several years. Over the past few years, the principal drivers of demand for Pd and Pt remain largely unchanged, despite ever increasing numbers of end uses and the promise of future, significant market penetration of fuel cell technology. In 2003, 48.9% of Pt demand was assigned to auto catalysts, and 37.4% to

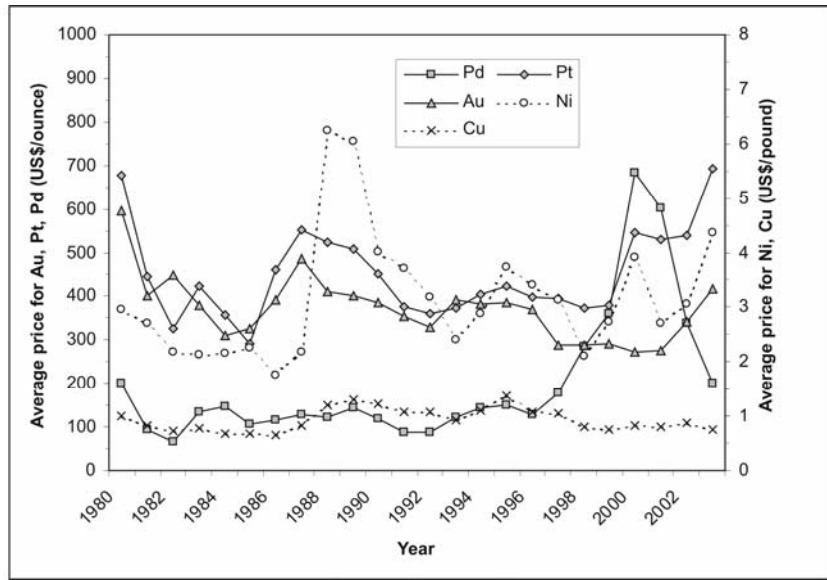


FIG 11-1. Average annual LME price for Pd, Pt, Au, Ni and Cu for the period 1980– 2003.

jeweler. Similarly, 65.8% of Pd demand in 2003 was attributable to auto catalysts with another 17.0% assigned to electronic applications (all consumption figures are from Platinum 2004–Annual Review, Johnson Matthey, London). The narrow range of critical applications, where PGE play a strategic role, has led to price hedging, stockpiling and direct purchase of supply by end users. It has also prompted mass substitution of one PGE for another, as in the case of auto catalysts (Pd↔Pt), or of a less efficient base or precious metal for the PGE, as in the case of dental amalgams and capacitors.

The overall demand for platinum metals has grown enormously in the last hundred years (Fig. 11-2). According to TIAx (2003), “World platinum production has grown at a rate of 3.5 tonnes per year since 1960 to keep pace with increases in auto catalyst and jewelry demand. In anticipation of the introduction of catalytic converters in the 1970s in the United States and the 1980s in Europe, South African mines expanded production to meet demand. In the 1980s and 1990s, South African mines continued to increase production to meet increasing demand for platinum jewelry from Japan and China. Over the past several years, demand

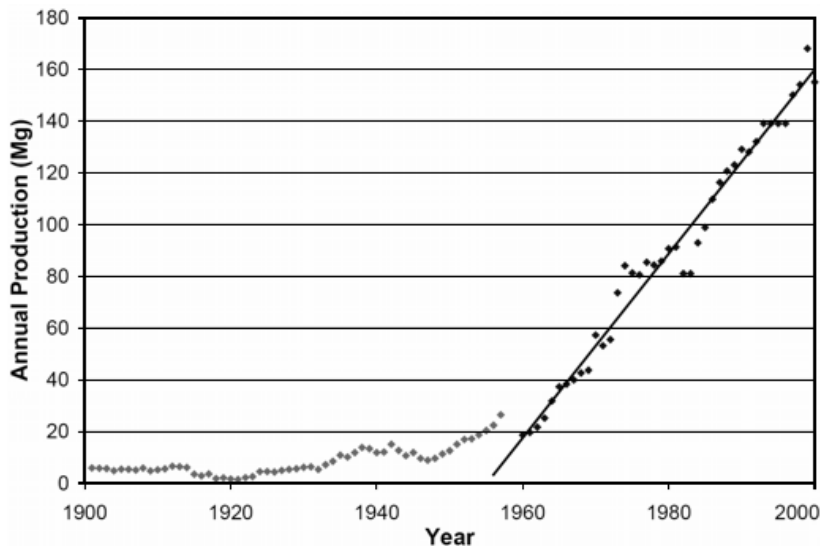


FIG. 11-2. World platinum production (1900-2000) from Tiax (2003). Data sources: 1901-1957: Die Metallischen Rohstoffe Heinrich Quiring, p 98-99; 1963-1983: Mineral Facts and Problems, US Bureau of Mines; 1986-2000: Mineral Yearbook, US Geological Survey.

demand has outpaced supply, but the industry has been aggressively expanding production to meet jewelry and auto catalyst demand.” After detailed analysis they concluded that “The two scenarios identify that following the successful commercialization of fuel cell vehicles, total platinum demand will grow at a rate three to six times the levels seen between 1960 and 2000.”

PGE SUPPLY, RESOURCES AND EXPLORATION PROGRESS

Significant price escalations for both Pd and Pt tend to relate to actual or perceived supply shortfall or interruptions. For Pd, price hikes typically reflect supply perturbations from the Noril’sk-Talnakh mining district. Johnson Matthey reports that in 2003 Russia accounted for 45.7% of the total world supply of Pd. A similar situation exists for Pt – in 2003, 74.8% of global Pt supply originated in South Africa and most of this from the Bushveld Igneous Complex. The vast majority of the world’s known PGM resources lie in the Bushveld, Noril’sk and Great Dyke as clearly shown in Table 11-1. This table uses some of the data from Naldrett (2004) but has updated other numbers as available. Several small exploration properties have been included where resource estimates have been published. These serve to emphasize the huge imbalance between the size of the currently producing deposits and all the others (Fig. 11-3). Relatively recent improvements in

technology both in mining practices and metallurgical performance have permitted access to more of the chromite-hosted resources of the Bushveld, beginning with those of the UG-2, which are the most important in the world.

Some other comments can be drawn from the table and graph of resources. First, even with its huge tonnages, the entire Sudbury Camp is not a huge resource of PGE. This is reflected in the production, which has never exceeded 500,000 ounces in a single year (equivalent today to less than 5% of world production). Second, Duluth reports as a voluminous resource but this is far from being economic. Third, apart from the big three of Noril’sk, Bushveld and the Great Dyke, the rest of the world is far less important. Fourth, after Stillwater, the exploration properties plus the producing Lac des Iles are another order of magnitude smaller. Finally, the best unconventional deposits for which a resource is established do not make the 1 million ounce lower limit for the table. The only possible exception is Sukhoi Log, for which a reliable platinum resource number is not available.

For the past 30 years this lack of diversity in supply has had both positive and negative impacts on exploration spending and, ultimately, exploration success. In periods of balanced supply and demand or of oversupply, Pd and Pt exploration spending tends to experience sustained low investment rates. During the past two major price escalations for Pd

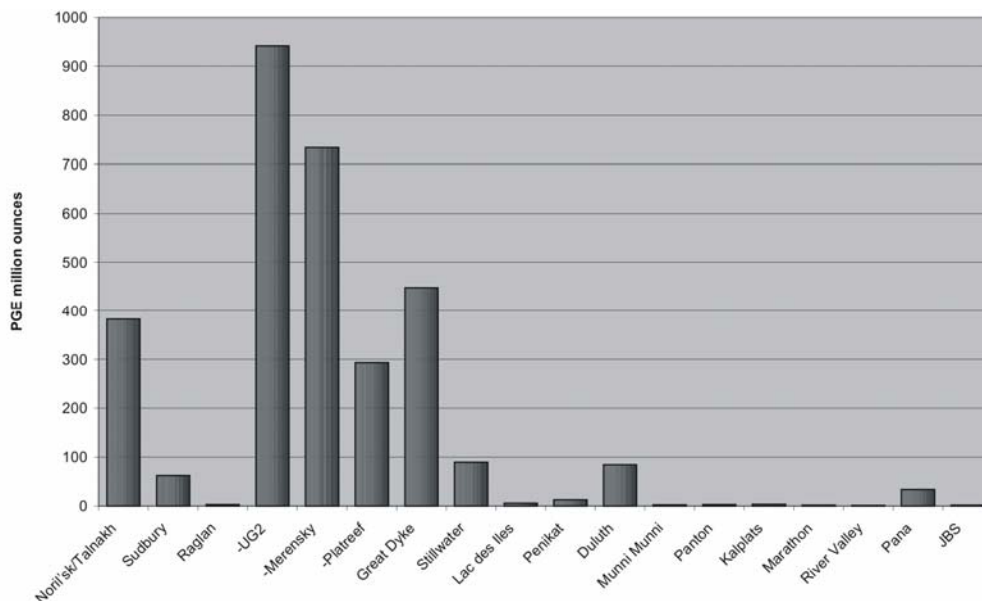


FIG. 11-3. Histogram of the major world PGE deposit resources. Data from Table 11-1.

TABLE 11-1. ESTIMATED RESOURCES CONTAINED IN THE WORLD'S MAIN PGM DEPOSITS.

Deposit/ Camp	Location	Resource 10 ⁶ t	Pt g.t ⁻¹	Pd g.t ⁻¹	PGE g.t ⁻¹	Ni% %	Cu %	Contained Pt t	Contained Pd t	Contained PGE t 3	Contained PGE 10 ⁶ oz	Reference
Nickel Producers												
Noril'sk/ Talnakh	Russia	2125	1.1	4.5	5.6	0.85	1.61	2393	9507	11900	383	MMC Noril'sk, 2004 ¹
Sudbury	Canada	1648	0.46	0.58	1.17	1.2	1.08	763	961	1933	62	Naldrett, 2004
Raglan	Canada	24.7	0.82	2.27	3.76	2.72	0.7	20	56	93	3	Naldrett, 2004
PGE Producers												
Bushveld total -UG2	South Africa	13514	2.63	1.9	4.53	0.13	0.06	35492	25738	61230	1969	Cawthorn, 1999 for PGE Naldrett, 2004 for Ni Cu
-Merensky		6251	2.58	2.11	4.69	0.04	0.02	16121	13169	29290	942	
-Platreef		4988	2.97	1.60	4.57	0.15	0.06	14833	7987	22820	734	PGE = Pt + Pd only
Great Dyke	Zimbabwe	2275	1.99	2.01	4.00	0.41	0.20	4538	4582	9120	293	
Stillwater	USA	2574	2.77	2.13	5.42	0.21	0.14	7130	5483	13946	448	Naldrett, 2004
Lac des Iles	Canada	154.5	3.90	14.07	17.97	0.24	0.14	604	2174	2778	89.3	SMC AR2004 ⁴
		63.8	0.23	2.54	2.95	0.09	0.06	15	162	188	6.0	North American Palladium press release 3/29/04
PGE Properties												
Penikat	Finland	156.7	0.46	1.83	2.42	0.09	0.20				12.6	Goldfields website ²
Duluth	USA	4000	0.15	0.49	0.66	0.20	0.60	585	1959	2621	84	Naldrett, 2004
Munni Munni	W. Australia	24			2.9					70	2.2	Helix website
Panton	W. Australia	14.3	2.2	2.4	5.2	0.3	0.08	31	34	74	2.4	Platinum Australia website
Kalplats	South Africa	75.2			1.42					107	3.4	
Marathon	Canada	31.5	0.35	1.40	1.87		0.39	11	44	59	1.9	Marathon PGE PR 3/30/05
River Valley	Canada	25.4	0.34	0.98	1.38	0.02	0.10	8	25	35	1.1	PFN website
Pana	Russia										33.4	Interfax 2001 ⁵
JBS	China	33			1.48	0.15	0.14			49	1.6	Jinshan Gold website

¹ Now that the nickel and copper resources of the Noril'sk and Talnakh deposits have been made public by MMC Noril'sk, it can be seen that the resource tonnage numbers estimated by Naldrett, 2004 are low by 100% and have therefore not been used, although his contained metal numbers are close to the estimates published. Resources mined to date are estimated by Foster (2005) and raise the pre-mining resources to 2367 Mt @ 1.03%Ni, 1.88%Cu. However, the official PGM resources are still secret. Quoted here is the total estimate only of remaining PGM resources from Levine and Wilbur (2003) divided into Pt and Pd using the camp ratio. ² Goldfields website reports a final resource total of 168.3 Mt but the detailed grades could not be located. ³ In some cases includes Au where "2E" or "3E" are reported. ⁴ Numbers for Stillwater are current resources – about 10 Mt of similar grade have been mined to date. Other PGE typically run 1.7 g.t⁻¹ Rh, 0.53 g.t⁻¹ Ir, 0.89 g.t⁻¹ Ru and are not included in resource estimates. ⁵ Mitrofanov *et al.* (2005) provided detailed grades for individual deposits within the Pana Intrusion.

(1980, 1999), Au and Cu markets were in decline, causing some mining and exploration companies to “try their hand” at PGE exploration. This “flavor of the month” approach has led to expenditures on many ill-advised PGE plays. Negative results from most of these ventures have in turn painted a bleak picture of return on exploration investment for the PGE. Diversified miners, gold and nickel producers have all tried PGE exploration on an erratic basis with limited success. Junior mining companies have been very active during the high price portions of the cycles. However, it is the world’s major PGE suppliers such as MMC Noril’sk Nickel, Anglo American Platinum, Impala Platinum and Lonmin that maintain long term exploration strategies for the PGE. None of the world’s PGE explorers maintain a truly global network of regional offices. Part of this strategy has seen major investments outside of South Africa from the major Bushveld producers, while the majority of effort by junior companies has actually been focused on portions of the Bushveld that have come available for participation in the last decade. Despite all this, spending on PGM exploration appears to be increasing significantly. Figures are only available for the last few years from the Metals Economics Group in Halifax. They report exploration spending by most companies worldwide. Their data estimate spending on PGM to have been US\$67.7 in 2001, \$104.3 in 2002, \$131.3 in 2003 and \$154.7 in 2004.

The cyclical nature of global exploration investment into PGE continues to stifle exploration success. Arguably, there has not been a significant grassroots PGE discovery since the J-M reef was discovered in 1973 by the Johns-Manville company in the Stillwater Complex in Montana (Zientek *et al.* 2002). The best discoveries such as Luanga in Brazil, Stella (Kalplats) in South Africa, Pana Tundra in Russia and Penikat in Finland have all yet to reach commercial development. It is somewhat surprising that the discovery track record for Pd and Pt deposits over the past 30 years has been so poor. In a historical context, it is difficult to determine the exact split of exploration investment in terms of deposit types. The biggest expenditures during this period have continued to be directed toward reef-type PGE deposits in layered mafic and ultramafic complexes (low S-type) and PGE-enriched base metal sulfide deposits (high S-type) in mafic and ultramafic intrusions. Very little systematic exploration of sediment-hosted PGE mineralization (*e.g.*, Sukhoi Log deposit, Eastern Russia; Serra Pelada, Brazil; Kupferschiefer copper district, Poland and

Germany; Nick, Yukon Territory, Canada) and structurally-controlled hydrothermal PGE mineralization (*e.g.*, Coronation Hill, Northern Territory, Australia; New Rambler deposits, Wyoming, U.S.A.; Messina deposit, R.S.A.) has been conducted, despite clear evidence that these environments can, locally, develop ore-grade PGE mineralization (for more information refer to Wilde, 2005).

The unique chemical and physical properties of the PGE, reviewed elsewhere in this volume, include superior catalytic properties (particularly with respect to hydrocarbons and nitrous oxides), chemical inertness, resistance to oxidation, stable and desirable thermal and electrical conductivity, and propensity to bond with enormous numbers of hydrogen atoms. These unusual properties provide for a range of end uses. The world is already being primed for the “hydrogen economy” which could permanently alter the fundamentals of Pt markets given the current, strategic role of Pt as a catalyst in many fuel cell devices. The unique properties of the PGE also lead to a significant diversity in the styles and environments for mineralization, the full range of which has only started to come to light. Based on these trends, we predict that PGE markets will continue to offer significant medium and long-term opportunities for economic success through more effective grassroots exploration in a wider range of geological environments.

ECONOMIC CONSIDERATIONS FOR EXPLORATION

Exploration uses a blend of the theoretical and the empirical. Genetic models are always under review, while observed criteria should not change. PGM deposits of economic significance are very rare, making it difficult to validate which criteria are important. Exploration strategies will be simplified into two key themes: 1) exploration for conventional deposits, known to host economic mineralization; 2) exploration for unconventional deposits. Magmatic deposits have long dominated the PGE exploration landscape. These can be effectively subdivided into low-S (reefs, contact-related deposits) and high-S (by-product PGE contained in nickel sulfide deposits) types. PGE mining companies have maintained an exploration focus on the former type. By-product PGE production has become increasingly important in the economics of nickel sulfide mines. Over the past 30 years, the global production trend for PGE has mimicked that of gold which has seen increasing by-product production from giant base

metal mines (Cu-Au porphyry and IOCG deposits). Given these facts, establishing an effective exploration strategy primarily begins with a decision to pursue opportunities related to deposit types where PGE are the principal pay metals or an important but secondary product.

The deposit descriptions presented in this book describe a wide range of mineralization processes and styles including magmatic, low- to high-temperature hydrothermal and alluvial/sedimentary. Although deposits relating to each of these process classification schemes may, in the future, fall into the realm of conventional deposits, currently only the magmatic types consistently attract exploration investment. Deposits must be of sufficient size and grade to be able to produce at an economic rate. Certain deposit types such as irregular and flat-lying narrow reefs in the Bushveld would be very difficult to mine in a country having higher labor costs. PGE reefs are very narrow and irregular, problematic to mine economically underground. Reef mining requires strict grade control (*e.g.*, Stillwater). Reef grades can be very high: \geq tens of g.t^{-1} PGE, while large tonnage, breccia-type deposits may be attractive open pit targets but tend to carry lower average grades (*e.g.*, $<3 \text{ g.t}^{-1}$ Pd+Pt) that are commonly sub-economic. Sulfide-silicate deposits are processed with well-established methods optimized for PGE recovery. The extraction of PGE from chromite deposits (sulfide-oxide) is not so well optimized, and thus may downgrade this target type. A startling observation is the incredibly small number of PGE Deposit Mining Camps known globally. Two alone – Bushveld and Noril'sk – account for the vast majority of all historical production. A key problem of the high-S type is that they really represent nickel sulfide deposits with widely varying amounts of accessory PGE. Most do not have sufficient PGE to be considered a PGE deposit, *e.g.*, Voisey's Bay.

PGE DEPOSIT CLASSIFICATION

Economically important deposits can be classified as:

- 1) **High S magmatic deposits**, *e.g.*, Noril'sk-Talnakh, footwall deposits at Sudbury. Notably only Noril'sk-Talnakh is of sufficient grade and output to be a significant contributor to global PGE production.
- 2) **Low S magmatic deposits**, *e.g.*, Bushveld, Great Dyke, Stillwater, Lac des Iles.
- 3) **Placer Deposits**, *e.g.*, Kondyor, Urals

Locally high concentrations of PGE, though not currently known to be important economically, have been documented in many diverse geological settings. In some instances, PGE are recovered as part of mining and processing, *e.g.*, in the Kupferschiefer (Wilde, 2005) and Phalabora.

A more detailed classification of deposits is advanced:

1. Low S layered intrusion-hosted.
 - a Stratabound sulfide-bearing layers, *e.g.*, Bushveld, Stillwater, Great Dyke.
 - b Contact (non-stratabound sulfide-bearing), *e.g.*, Platreef, River Valley, Lac des Iles.
 - c Stratabound chromitite layers, *e.g.*, UG2 at Bushveld (also stratabound magnetitite layers such as Haran reef at West Musgrave and the Stella intrusion, RSA).
 - d Hydrothermal remobilization, *e.g.*, Rambler.
2. High S magmatic nickel sulfide deposits, *e.g.*, Noril'sk, Raglan.
3. Placers, *e.g.*, Urals, Colombia.
4. Unconventional deposits.
 - a Ophiolites, *e.g.*, Shetlands (Unst), Troodos, Ray-Iz, Kempirsay, Acoje.
 - b Alaskan type intrusions, *e.g.*, Fifield, Urals, Wellgreen, Tulameen, Duke Island.
 - c Porphyry Au-Cu, *e.g.*, Mamut, Skouries
 - d Sedimentary copper-gold deposits (black shale-hosted) *e.g.*, Kupferschiefer, Sukhoi Log.
 - e U-Au-PGE deposits (unconformity related), *e.g.*, Rottenstone, Alligator River, Nicholson Bay, Shinkolobwe.
 - f Laterite, *e.g.*, Weld Range, Fifield, Syerston, Yubdo, Freetown, Gilgarnia Rocks.
 - g Mine tailings, *e.g.*, Kambalda, Sudbury, Noril'sk.

In this paper, exploration guides will be discussed for the conventional high and low S deposits and for the unconventional sedimentary-hosted deposits. Placer deposits are well covered by papers in the Cabri Issue of the Canadian Mineralogist (Mungall *et al.* 2002).

MAGMATIC DEPOSITS – GENERAL CHARACTERISTICS

Age

Table 11-2 provides radiometric age determinations for the host rocks to most of the world's major, magmatic PGE deposits. These do not necessarily represent the age of the

TABLE 11-2. AGES OF HOST ROCKS TO SELECTED MAGMATIC PGE DEPOSITS

Deposit(s) Name	Host Body	Location	Styles	Age Ma	References
Platreef	Bushveld Igneous Complex	RSA	Contact-Type	2060	Walraven <i>et al.</i> (1990)
Merensky	Bushveld Igneous Complex	RSA	Reef - sulfide	2060	Walraven <i>et al.</i> (1990)
UG2	Bushveld Igneous Complex	RSA	Reef - chromitite	2060	Walraven <i>et al.</i> (1990)
JM	Stillwater Igneous Complex	USA	Reef - sulfide	2705	Premo <i>et al.</i> (1990)
Main Sulfide Zone	Great Dyke	Zimbabwe	Reef - sulfide	2570	Oberthür <i>et al.</i> (2002)
Sub-Layer, Offset Dykes and Footwall Veins	Sudbury Igneous Complex	Canada	Magmatic Ni-Cu sulfide, PGE by-product	1850	Krogh <i>et al.</i> (1984)
Noril'sk-Talnakh Massive, Disseminated and Cu-rich Ores	Noril'sk-Talnakh Intrusive Suite	Russia	Magmatic Ni-Cu sulfide, PGE by-product	252	Dalrymple <i>et al.</i> (1995)
Roby Zone	Lac des Iles Complex	Canada	Breccia, Reef – chlorite (?)	2689	Watkinson <i>et al.</i> (2002)
Munni Munni	Munni Munni Complex	Australia	Reef - sulfide	2925	Hoatson & Keays (1989)
Katinniq	Raglan Horizon	Canada	Magmatic Ni-Cu sulfide, PGE by-product	1917	Parrish (1989)
Konttjarvi	Portimo Complex	Finland	Contact-Type	2440	Alapieti & Lahtinen (2002)
SJ Reef; PV and AP Reefs	Penikat Intrusion	Finland	Reef – chlorite, Reef – sulfide,	2440	Alapieti & Lahtinen (2002)
Platinova	Skaergaard Intrusion	Greenland	Reef - sulfide	56	Hirschmann <i>et al.</i> (1997)
Dana Lake	River Valley Intrusion	Canada	Contact-Type	2470	Heaman (1997)
Top Reef	Panton Sill	Western Australia	Reef - chromitite	1856	Hoatson (2000)
Dunka Road, Babbit	Duluth Complex	USA	Contact-Type	1107	Paces & Miller (1993)
Contact Mineralization, Lower Chromitite	Muskox Intrusion	Canada	Contact-Type, Reef - chromitite	1270	LeCheminant & Heaman (1989)
Marathon; Skipper Lake	Coldwell Complex	Canada	Contact-Type; Reef - magnetite	1108	Heaman & Machado (1992)
Stella	Stella Intrusion	RSA	Reef - magnetite	3033	Maier <i>et al.</i> (2003)
Lower Layered Unit	Pana Tundra	Russia	Reef - sulfide	2490	Alapieti & Lahtinen (2002)

mineralization *e.g.*, in the case of magmatic deposits modified or enhanced by younger hydrothermal or metamorphic processes. As indicated by the tabulated ages, the development of appropriate source regions, transport media and traps has occurred periodically throughout earth's history. However, many of the giant PGE deposits (*e.g.*, Bushveld, Noril'sk-Talnakh) are related to rapidly developed large igneous provinces that may have originated from plume-related magmatism. Regardless of the veracity of the plume model,

these major but relatively short-lived magmatic events constitute priority search areas for magmatic PGE deposits. Some of these large igneous provinces retained their PGE until reaching appropriate trap sites in crustal reservoirs or lava flows; here we have an ideal situation for identifying clusters of PGE deposits. These same large igneous provinces also provide ideal locations for developing hydrothermal PGE deposits, particularly along the major plumbing faults that provided the pathway for the mantle-derived melts

through the crust. There are insufficient data on sediment-hosted PGE mineralization to determine if host-rock deposition ages or fluid ingress ages are important for PGE exploration, but some age information is given below.

Size and shape

Table 11-3 documents the size and shape of the world's premier magmatic PGE deposits. Economically interesting PGE deposits are known to occur in narrow chonolith-shaped or regular sill-like intrusions (chonoliths are flattened tubes) as in the Noril'sk 1 intrusion in Russia, in plug-like breccia bodies such as the Lac des Iles complex in Canada and the Aguablanca deposit in Spain, in medium-sized layered complexes such as the Stillwater, Munni Munni and Penikat Intrusions, and in giant lopoliths or batholiths such as the Muskox intrusion, Great Dyke and Bushveld Igneous Complex. Table 11-4 documents the size of the best-known magmatic PGE deposits in terms of their tonnage and grade. In general, the largest deposits are associated with the largest magmatic provinces but are not always contained within the largest bodies in that province. Figure 11-4 shows the relative areas of many mineralized layered intrusions, while Figure 11-5 shows the positions of the reefs within them, as well as the overall thickness of the major sub-units. In general, the known giant high-S magmatic deposits appear to occur primarily in relatively small and confined bodies whereas the known giant low-S deposits tend to occupy major layered intrusions. While there are few giant layered complexes left to be discovered,

at least at explorable depths, there is certainly significant scope for discovering new, relatively small high-S type bodies. A corollary to this is the fact that high-S deposit types tend to be easier to explore once the host body is delineated, because they have more definitive geochemical and geophysical footprints.

Empirical evidence suggests that the more irregular the primary form of the host body, the greater the potential for development of appropriate physical and chemical traps and, therefore, significant PGE deposits. This is illustrated by the common association of high S magmatic deposits, including massive Ni-Cu deposits and disseminated, contact-type Cu-Ni-PGE deposits, with structural embayments along the base and sides of the host body, e.g., Kareлах intrusion of the Talnakh ore junction (Naldrett *et al.* 1992), Voisey's Bay intrusion (Naldrett *et al.* 1996), Sudbury sub-layer deposits (Farrow & Lightfoot 2002). Likewise, low-S stratiform reef-type deposits appear to be more common in sills having a thicker medial keel, e.g., Great Dyke and Bushveld complexes, Muskox Intrusion (Wilson 1996, Eales & Cawthorn 1996, Irvine 1970). Irregular intrusion form may also be a function of higher magma-fluxes which is also an important ingredient in prospectivity.

Irregular form variation in both intrusive and extrusive environments should increase the variability of both intensive (density, viscosity, bulk composition, fO_2 , fS_2 , fH_2O , fCO_2) and extensive (temperature, pressure) variables in a magmatic system, promoting chemical and physical heterogeneity and greater opportunities for

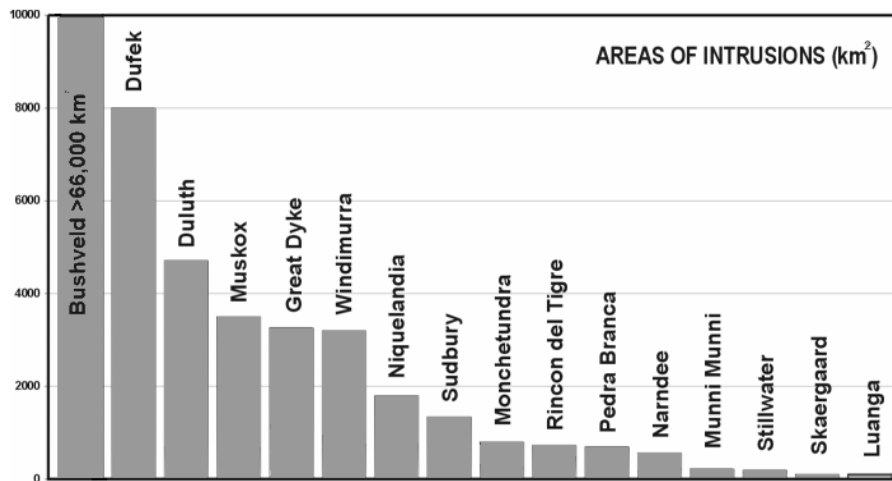


FIG. 11-4. Known areas in square kilometres of large layered intrusions, most of which contain interesting levels of PGE mineralization.

TABLE 11-3. DIMENSIONS, MORPHOLOGY AND GEOLOGICAL SETTING OF HOST ROCKS TO MAJOR MAGMATIC PGE DEPOSITS.

Deposit(s) Name	Host Body	Dimensions (plan, km)	Maximum Thickness (m)	Form	Geological Setting
Platreef	Bushveld Igneous Complex	350 x 250	5250m in northern limb	Batholith	Ensialic Rift
Merensky Reef	Bushveld Igneous Complex	350 x 250	7000	Batholith	Ensialic Rift
UG2 Reef	Bushveld Igneous Complex	350 x 250	7000	Batholith	Ensialic Rift
JM Reef	Stillwater Igneous Complex	42 x 10	5500	Batholith	Ensialic Rift
Main Sulfide Zone	Great Dyke	550 x 11	3500	Interconnected Lopoliths	Ensialic Rift
Contact Sub-Layer, Offset Dykes and Footwall Deposits	Sudbury Igneous Complex	60 x 30	>2500	Lopolith/Batholith	Meteorite Impact at Craton Margin
Noril'sk-Talnakh Massive, Disseminated and Cu-rich Ores	Noril'sk-Talnakh Intrusive Suite	Variable, generally <20 x 5	500	Chonolith/Irregular Sills	Continental Flood Basalt Province
Roby Zone	Lac des Iles Complex	8 x 4	>1000	Breccia Complex	Archean Ring Complex
Munni Munni	Munni Munni Complex	25 x 10	4900	Lopolith	Archean Greenstone Belt
Katinniq, Zone 2-3, Boundary, Donaldson, Cross Lake etc.	Raglan Formation, Chukotat Group	3 x 1	900	Stacked Sills and/or Channelized Flows	Craton Margin Rift
Suhanko-Kontijjarvi	Portimo Complex	10 x 5	<1000	Irregular Sills	Craton Margin Rift
SJ and AP reefs	Penikat Intrusion	23 x 3.5	3500	Irregular Sills	Craton Margin Rift
Platinova	Skaergaard Intrusion	11 x 6	3500	Lopolith	Continental Flood Basalt Province
Dana Lake	River Valley Intrusion	40 x 15	900	Lopolith	Craton Margin Rift
Top Reef	Panton Sill	11 x 3	1600	Major Sill	Craton Margin Rift
Dunka Road, Babbit	Duluth Complex	200 x 50	<1500	Stacked Lopoliths	Continental Flood Basalt Province
Contact Mineralization, Lower Chromitite	Muskox Intrusion	120 x 12	>2500	Elongated Funnel-Shaped Complex	Continental Flood Basalt Province
Marathon; Skipper Lake; Geordie Lake	Coldwell Alkaline Complex	30 x 20	<2500	Lopolith	Continental Flood Basalt Province
Stella	Stella Intrusion	12 x 5	>1000	Sill	Archean greenstone belt
Lower Layered Unit, Pana Tundra	Pansky Tundra Intrusion, Russia	80 x 6	3000	Major Sill	Craton Margin Rift

TABLE 11-4. TOP-RATED MAGMATIC DEPOSITS (BY SIZE AND GRADE).

High Sulfur (Ni-rich)	Low Sulfur (PGM-rich)
1 Noril'sk	1 Bushveld
2 Sudbury	2 Stillwater
3 Jinchuan	3 Great Dyke
4 Voisey's Bay	4 Penikat
5 Thompson	5 Lac des Iles
6 Mt. Keith	6 Munni Munni
7 Pechenga	7 Luanga
8 Perseverance	8 Skaergaard
9 Kambalda	9 Portimo
10 Uitkomst	10 Stella
11 Raglan	11 Panton
12 Selebi-Phikwe	12 Pansky Tundra
13 Kabanga	13 Marathon

<ul style="list-style-type: none"> hosted in largely ultramafic rocks either feeders or flows <1 km thick, irregular to intrusions active, sulfide-rich systems 	<ul style="list-style-type: none"> hosted by ultramafic-mafic intrusion >2 km thick passive, low-sulfur systems some have Fe-rich sulfide in marginal rocks at base
--	---

mineralizing processes to occur. Major structures providing the conduits for magma ingress into the crust can also act as focal points for elevated heat flow, fluid transport and flow gradients. Complex breccia dykes and breccia bodies in mafic intrusions may develop along these conduits in response to the upward channeling of magmatic vapors or vapor-rich silicate melt from crystallizing, deeper-seated magma. Irregularities along the margins and floors of intrusive bodies can also alter fluid flow regimes within the magma chamber, causing preferential deposition of suspended particles such as immiscible sulfide liquid, silicate and oxide crystals and lithic fragments. Clearly, both theoretical and empirical data suggest that the identification of irregular form variations in both intrusive and extrusive environments is an effective means of prioritizing drill targets and maximizing opportunities for discovering large deposits. Form surface mapping on the scale of most PGE deposits is best accomplished using a combination of geological surface mapping, 3D magnetic models and any available deep drilling information. Keep in mind that many apparent primary form variations in these environments are the result of post-mineralization structural modification such as interference folding.

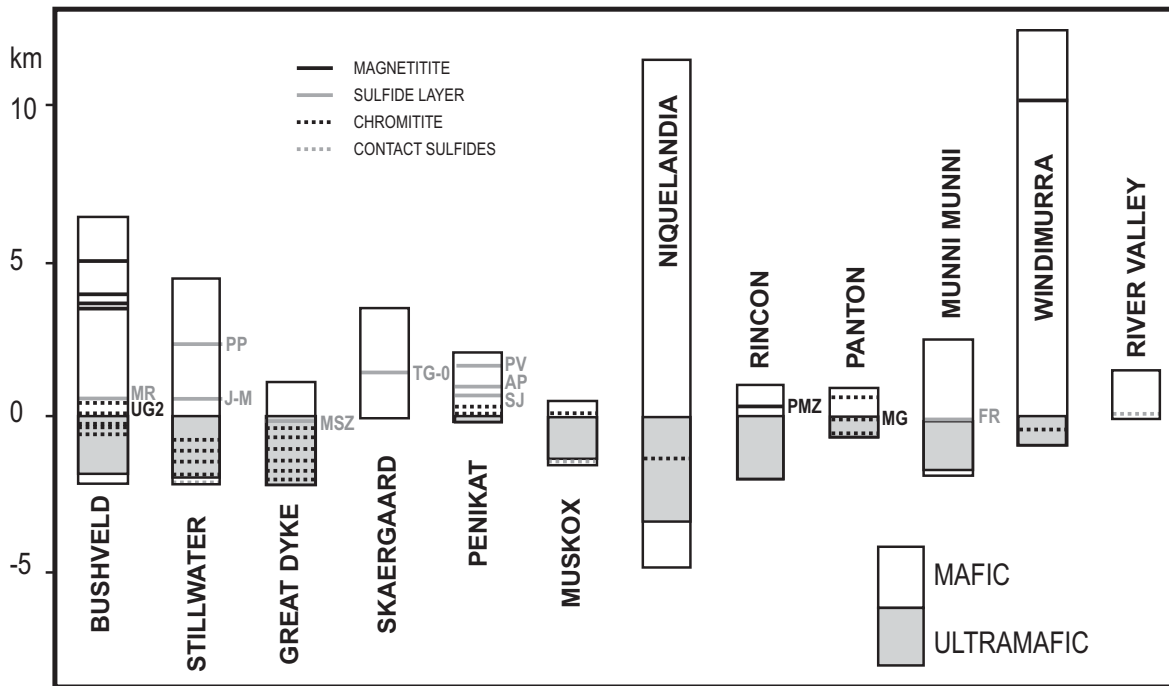


FIG. 11-5. Intrusion Hosted PGE Models showing the relative sizes of ultramafic and mafic zones, and the position of reefs and contact sulfides.

Setting

Major low-S deposits occur in singular mega-intrusions into ensialic rifts or stable crust, while major and high-S deposits occur in smaller, picritic and komatiitic sills (irregular) in flood basalt provinces and in low-Ti and high-Al tholeiites emplaced into competent sialic crust in Archean belts. No major PGE deposits have been found in island arc settings, yet this is the type location for boninite (including SHMB – siliceous high-Mg basalt) – the favored primary melt composition for the Bushveld and Stillwater reef deposits (Barnes 1989).

While the known major magmatic PGE deposits have a restricted setting, smaller but important PGE resources and producing deposits occur in a diverse range of geological environments.

These include continental and oceanic flood basalt and large igneous provinces, craton margin and ensialic rift basins, failed and mature ocean island basalt provinces, island and continental arcs, ophiolite and orogenic peridotite terranes (MORB-type and supra-subduction zone-type, Alaskan-type intrusions) and Archean greenstone belts (Crocket 2002). The key processes leading to magmatic PGE deposits could clearly operate in almost any tectonic environment given certain preferred ambient conditions including high heat flow, appropriate structural elements, high initial PGE concentrations in the source rock/magma and appropriate flow regime and chemical transfer processes. Certain settings may have advantages in consideration of individual factors governing localization of PGE, but things tend to level out when all potentially important controls are taken into account. Large igneous provinces are clearly preferred sites for PGE exploration for the simple fact that they develop enormous volumes of prospective intrusive and extrusive bodies of appropriate composition and form.

Methods used to identify favorable tectonic settings represent a critical part of the selection process. They include finite element models of potential magma conduits and advanced regional structural analysis using remote sensing data, mapping, magnetic and gravity data and, increasingly, seismic data. As with most metal deposits, structure is perhaps the most critical element in determining the location of PGE deposits.

LOW S MAGMATIC DEPOSITS**Overview**

The majority of known low-S-type magmatic deposits are associated with intrusions having Archean or Paleoproterozoic ages (Table 11-2). This is an empirical observation and is likely a reflection of the diversity of magmatic environments that have been exposed through deformation and erosion of Precambrian terranes, in contrast to Phanerozoic belts. Mineralized layered intrusions were typically emplaced in a stable cratonic setting. They tend to be more than 200 Ma younger than their country rock (Lac des Iles intrusion nearly coeval with host granitoid plutons).

The Bushveld and Stillwater Complexes are emplaced in extensional regions of stable continental shields (Table 11-3). The Great Dyke and Penikat Complexes intruded in aborted rift zones. In general these mineralized intrusions lie in proximity to major structures (*e.g.*, seismic modeling in Bushveld and relation of intrusion to T-M Lineament is well established).

According to Ohnenstetter (1996) most important PGE camps such as Bushveld, Stillwater, Great Dyke and Penikat are associated with orthopyroxene complexes. In these low S-type deposits, olivine crystallization is followed by crystallization of orthopyroxene. The resultant sequence of lithologies comprises dunite, orthopyroxenite, and/or harzburgite. This is typically overlain by cumulates of orthopyroxenite and/or websterite (opx → cpx) or gabbro (plag → opx → cpx). The orthopyroxene complexes dominate during the period 2900-2450 Ma. During the late Proterozoic (~1200-1100) the Muskox, Duluth and Coldwell Complexes were formed and all of these bodies relate to clinopyroxene-dominant systems in which the paragenetic sequence is *olivine* → *cpx* → *opx/plag*. In these cases, the ultramafic sequence comprises dunite, wehrlite, and clinopyroxenite. This is overlain by cumulates of pyroxenite or gabbro.

General Geology**Stratabound Reefs**

The Bushveld has 7 km of igneous stratigraphy divided into 4 cumulate zones: Lower zone of olivine-bronzite-chromite; Critical zone of plagioclase-pyroxene, with local olivine & chromite; Main zone of plagioclase-pyroxene; Upper zone of plagioclase-pyroxene-Fe-Ti oxide (+

apatite + Fe-rich olivine + hornblende). Economic PGE are found in the Merensky Reef and UG-2 chromitite, located within the lower 500 m of the Critical zone (Cawthorn *et al.* 2002). Within the Bushveld, PGE mineralization is also found in:

- Pothole Reef – where Merensky Reef plunges into depressions where the footwall stratigraphy has been removed; roughly equivalent to “ballrooms” in the Stillwater Complex, which are sections of expanded reef
- Dunite Pipes – transgressive bodies of postcumulus Fe-rich ultramafic pegmatite, comprising hortonolite, clinopyroxene, ilmenite, and Ti-magnetite; very high Pt contents; equivalents recently and tentatively identified in the Stillwater Complex (Zientek *et al.* 2002).

Stillwater’s stratigraphy is divided into 3 cumulate zones: Basal Contact zone of pyroxene-plagioclase with inclusions of hornfelsed wall rock and local low grade Ni-Cu, Ultramafic zone of olivine-bronzite-chromite, Banded zone of plagioclase-pyroxene-olivine (+chromite). More fractionated cumulates are likely present under Phanerozoic cover. Economic PGE are found in the J-M Reef located 500 m above the base of the Banded zone. Low-grade PGE are found in the G-Chromite layer located 500 m below the top of the Ultramafic zone and in the Picket Pin deposit, which occurs as transgressive and semiconformable zones in the anorthositic upper sections of the Banded zone (Zientek *et al.* 2002).

Non-Stratabound and Contact Types

The Platereef, South Africa, occurs where Bushveld Complex mafic rocks have intruded through older sedimentary sequences and come to rest on the Archean granitic basement. It is hosted by a complex sequence of medium- to coarse-grained pyroxenite, melanorite and norite, in places pegmatoidal and serpentized, containing numerous xenoliths of metasedimentary rocks (Cawthorn *et al.* 2002).

Lac des Iles, Ontario, Canada, shows textural evidence for mingling of two distinct magmas after formation of cumulus stratigraphy under supersolidus conditions. The hosts are:

1. moderately- to well-layered ultramafic zone olivine-pyroxene cumulates,
2. gabbro zone plagioclase-pyroxene cumulates,
3. mafic pegmatites,
4. intrusion breccia zones, and
5. hornblendite.

Mineralization

Stratabound Reefs

PGE tend to occur in, and associated with, sulfides, regardless of whether PGE occur in sulfide or chromitite reef; however, the highest PGE concentrations can be found in chromitites. Sulfides occur as fine-grained, disseminated to blebby, interstitial pyrrhotite, chalcopyrite and pentlandite, and minor PGE sulfides. Sulfide percentages are typically <5% in stratabound reef deposits. The predominant PGE are Pt, Pd and Rh, but PGE also occur as arsenides/antimonides, tellurides/selenides/bismuthides, and alloys (Cawthorn *et al.* 2002 and other papers in that volume).

At both the Bushveld and Stillwater, base-metal sulfides and associated PGE are not restricted to the Merensky or J-M Reefs themselves, but are also disseminated into footwall and hanging-wall lithologies. The PGE occur here as sulfides, alloys, arsenides, tellurides, and minor solid solution in pentlandite (Cawthorn *et al.* 2002, Zientek *et al.* 2002).

Non-Stratabound and Contact Types

In the Platereef, sulfide and associated PGE are heterogeneously distributed and constitute <5% of the rock. The sulfides are found as blebs and disseminations along the floor, as uneconomic disseminations in unaltered igneous rocks, as enrichments in the reaction aureoles of dolomite xenoliths and as relatively high concentrations in serpentized zones. Rare massive sulfide concentrations, tens of centimetres to 2 metres thick, are found close to the basal contact and in brecciated contact rocks.

At Lac des Iles, up to 5% disseminated magmatic sulfide blebs in coarse to pegmatitic gabbros are found. The PGE-sulfides occur with pyrrhotite, pentlandite, chalcopyrite and pyrite (pyrite, millerite and violarite in sheared and altered rocks), also as tellurides, arsenides, and solid solution within pentlandite.

Exploration Models

Stratabound Reefs

The commonalities, which tend to be exploration guides, are:

- The host intrusion is emplaced into a stable cratonic setting.
- Stratabound reefs occur at clearly defined horizons in the igneous stratigraphy over tens or hundreds of kilometres.

- Stratabound reefs are found at or near the base of cyclic units that are tens or hundreds of metres thick, marked by the reappearance of high temperature cumulus phases dominant in the early crystallization history of host intrusions (*e.g.*, olivine and chromite in Stillwater, bronzite and chromite (locally olivine) in Bushveld).
- Stratabound reefs occur a few hundred metres above the first appearance of cumulus plagioclase in host intrusions.
- Mineralization takes the form of interstitial, apparently magmatic, Fe-Ni-Cu sulfides with exceptionally high PGE tenors.
- PGE are commonly associated with chromitite at the bases of cyclic units.
- Pegmatoidal or coarse-grained textures are common within or immediately below mineralized units, along with hydrous minerals such as biotite and apatite, unusually high concentrations of Cl and Fe in hydrous silicates and in places graphite.

The differences include:

Merensky Reef:

- corresponds to lithological layer that is stratiform & stratabound
- mainly a pegmatoidal bronzite layer with thin chromitite layers at its base and top
- “pothole” mineralization

UG-2 Chromitite:

corresponds to lithological layer that is stratiform & stratabound

- mainly chromitite with minor pyroxenite layers
- “reef” mineralization

J-M Reef:

- stratigraphic interval, locally discordant, defined by presence of PGE-bearing sulfides
- package including peridotite, troctolite & anorthosite, only minor amounts of cumulus chromite
- “ballroom” mineralization.

Other locations of mineralization are found as listed below and illustrated along with a wider number of PGE-bearing intrusions in Figure 11-5.

1. Mixing of resident with primitive magma before plagioclase has appeared on the liquidus (before sulfide saturation) may produce sulfide- and therefore PGE-poor chromitites (*e.g.*, Bushveld

LG-6).

2. Fractional crystallization may result in a PGE-rich sulfide layer not associated with the base of a cyclic unit (*e.g.*, Great Dyke MSZ, Munni Munni)
3. Mixing of resident with primitive magma after plagioclase is crystallizing may result in sulfide- and PGE-rich chromitites or PGE-rich sulfide layers (*e.g.*, Bushveld UG-2 & Merensky Reef, Stillwater J-M Reef).
4. Marginal contamination or metasomatism of an intrusion may result in PGE-enriched disseminated sulfide zones (*e.g.*, Bushveld Platreef, Iljina & Lee 2005, and Lac des Iles, Lavigne *et al.* 2005).

Exploration Methods

Search for large lopoliths emplaced into competent basement. Identify feeder zones, breccia units and sulfides. Determine general PGE tenors by surface grid sampling. Use trenching then drilling to determine grade variation across and along strike. Remember that reefs and contact-type deposits can occur together (*e.g.*, Bushveld Platreef and Merensky Reef, Penikat suite, Finland). IP surveys provide an effective means of mapping out large concentrations of disseminated sulfides. AEM surveys can provide important information on form variation by documenting inflections in conductive footwall and hanging-wall strata. Magnetic surveys provide the cheapest and most testable potential field data. They can be used to delineate small (ground surveys) or large (airborne surveys) embayments, for lithomagnetic mapping in poorly exposed terranes, for structural analysis and for direct detection of mineralization (*e.g.*, magnetite-related reefs).

For stratabound reefs, identification of the ultramafic to mafic transition within the series permits exploration to be concentrated within the gabbroic stratigraphy (or at or just below the first appearance of cumulus plagioclase for Great Dyke-, Munni-Munni-type model). Any sulfide- or chromite-bearing unit should be sampled. If it is sulfide, not necessarily a large percentage (*e.g.*, Merensky Reef \leq 2-3%) can be significant. If chromite, typically a persistent (but thin) chromitite layer could be PGE-bearing. To a lesser extent a magnetite segregation may be interesting, such as at Stella in South Africa (Maier *et al.* 2003). Use of lithochemical profiles is highly effective in narrowing the search area by identifying profound changes in chalcophile metal ratios above and

below a reef (*e.g.*, Hoatson & Keays 1989). Typically, ratios of the PGE against other base metals (Pd:Cu) or incompatible elements (Pd:Zr) builds up below a reef and declines dramatically immediately above the reef. Such geochemical techniques are more fully discussed by Maier & Barnes (2005).

For non-stratabound and contact types, sample every gabbroic breccia based on the association of PGE mineralization with magmatic breccia at Lac des Iles and East Bull Lake. At the River Valley deposit, the distinction between matrix and fragments is usually macroscopically unclear (James *et al.* 2002), thus all rock types in the target zone should be sampled. Mineralization is related to sulfides, but not a large modal percentage; the proportion of sulfides is not always a good indication of PGE values. Accordingly, every sulfide-bearing rock should be sampled.

HIGH S MAGMATIC DEPOSITS

Overview

An important aspect of this deposit type is that the metal ratios vary widely for Ni, Cu, Co and PGE. Deposits can be found that are Ni-Cu-Co rich and PGE poor while others are much richer in PGE. The PGE content varies from insignificantly low (*i.e.*, $<0.5 \text{ g.t}^{-1}$) through to greater than 10 g.t^{-1} in examples such as some Talnakh ores. Up to the present, only the Noril'sk-type ores represent a type that can provide an economically important contribution to global PGE production. Therefore, this section will focus on that type. It should be pointed out however that some of the Cu-rich vein deposits in both Noril'sk-Talnakh district and in the Sudbury camp could be economically mined for their PGE alone – many feature average grades in excess of 15 g.t^{-1} .

Setting of the Noril'sk-Talnakh Deposits

The deposits of the Noril'sk region are associated with a period of Permo-Triassic (250 Ma) continental flood basalt volcanism, which occurred in northwestern Siberia immediately following the continental collision that gave rise to the Ural mountain chain. The ore bodies have developed within thin, elongate sills (commonly called chonoliths) measuring several km to ~20 km in length, a few km in width and less than a few hundred metres (typically $<200 \text{ m}$) in maximum thickness. The sills intruded argillites, evaporites and coal measures, sit adjacent to a major, trans-crustal fault (Kharayelakh fault) and immediately

below the central part of the 3.5 km thick volcanic basin (Naldrett 2002).

Studies of the up to 3.5 km thick basaltic lavas within the basin have shown that a 500 m-thick sequence within the package has lost 75% of its Cu and Ni and more than 90% of its PGE (Naldrett *et al.* 1992). Overlying basalts show a gradual recovery in their chalcophile element concentrations to reach “normal” undepleted values about 500 m above the top of the highly depleted zone. There is a correlation between the degree of chalcophile depletion of the basalts and their contamination by continental crust (Lightfoot *et al.* 1994). The ore-bearing Noril'sk type intrusions have been correlated with those basalts above the depleted zone that have chalcophile element contents that have returned to undepleted levels (Naldrett 2002).

General Geology – Noril'sk-Talnakh Deposits

Occurring at the northwest corner of Siberian platform with the Khatanga trough to the north and the Yenesei trough to the west, mineralization is spatially related to several major faults - Noril'sk-Kharayelakh, Imangda, and North Kharayelakh. There are three cycles of marine transgression and regression; deposition of dolomite, limestone and argillite of marine origin overlain by calcareous and dolomitic marl, dolomite and sulfate-rich evaporite in each. The Devonian- and Lower Carboniferous-age evaporites of the last cycle were succeeded after structural deformation by the terrestrial, coal-bearing, Tungusskaya series.

This was followed by eruption of late Permian and early Triassic flood basalt and tuff known as the Siberian Trap, at about 250 Ma. Cu-Ni sulfide deposits are associated with a group of comagmatic ultramafic-mafic intrusions. The internal structure of the mineralized intrusions is divisible into two distinctive zones, a relatively restricted thicker body and peripheral sills. The thicker part is vertically divisible into a lower olivine-rich gabbro-dolerite marginal zone, overlain by a plagioclase- and sulfide-rich taxitic (vari-textured) gabbro-dolerite zone. This is overlain by picritic gabbro-dolerite (~50 modal percent olivine), which, with decrease in the amount of olivine, grades up into olivine gabbro-dolerite, olivine-bearing gabbro-dolerite, gabbro-dolerite and the upper contact phases of taxitic gabbro-dolerite including leucogabbro. The peripheral sills consist of uniform gabbro-dolerite, with or without olivine. Lenses of picritic gabbro-dolerite occur towards the base.

Mineralization

The deposits of Noril'sk can be divided into three main types:

1. Massive sulfide: the most important type mined so far in the Talnakh region. It ranges from 10's of cm to 50 m in thickness and always occurs directly beneath the main intrusive body. It is not gradational upwards into disseminated ore – there is almost always an intervening selvage of chilled olivine gabbro with relatively little disseminated sulfide, and frequently a few metres of unmineralized country rock, separating the two ore types. Field relations do not support the massive ore as having settled *in situ* from the overlying intrusions.
2. Disseminated sulfide: concentrated towards the base of each intrusion within picritic- and lower taxitic-gabbro-dolerite. Typically coarse-grained and blebby with distinctive chalcopyrite caps locally developed.
3. Copper Ore: this type either encloses massive ore in the sedimentary rocks or occupies breccia zones, which can be both cross-cutting and overlying the intrusions.

Exploration Model

The Noril'sk-type (mineralized) intrusions are unusual in a number of ways, compared with most other known intrusions. They contain, or are associated with, a very high proportion of sulfide (2-10% of the total mass). These sulfides contain a high concentration of PGE (requiring >200 times more magma than that represented by the mass of the intrusions). The mineralized intrusions are surrounded by an intense metamorphic and metasomatic aureole. In many cases this extends farther into the country rocks than the thickness of the intrusions themselves, in some cases 400 m. The sulfur isotopic composition of the sulfides is very heavy for mantle-derived sulfur, ranging from +8 to +12 $\delta^{34}\text{S}$. The mineralized intrusions contain zones of taxitic olivine gabbro. The mineralized intrusions have acted as feeder conduits to the 5000-10,000 km³ of volcanic magma represented by the overlying Nadezhdinsky to Morongovsky lava formations. These data support a model for continuous flow of magma through the mineralized intrusions.

The flow of a large amount of magma through the mineralized intrusions explains the very extensive contact metamorphism. Models require deep granodiorite contamination to be linked to S saturation, implying significant sulfide removal

(~25%) at depth (Lightfoot & Hawkesworth 1997). However, much of the contamination occurred and the sulfides segregated close to the stratigraphic level of the chonolith during the differentiation and chalcophile element depletion that is reflected in part of the overlying sequence of lava flows. It is likely that the magma was progressively eroding the walls of its chamber at this time, ingesting Devonian evaporite and C-bearing Tungussskaya formation, and reducing the evaporite to produce sulfide. Field textures in the mine support this concept. An interruption in the input of magma into the high-level chamber allowed magma there to cool and line the walls of the chamber. This insulated them from further erosion when new magma entered the chamber to differentiate and form the next lavas; sulfide segregation therefore ceased, and chalcophile metals started to increase in concentration (within the sulfides). As more magma flowed through the system, the sulfides trapped there interacted with it and became progressively upgraded in chalcophile metals.

Exploration Methods

A number of mining companies have explored for Noril'sk type deposits, since their size and grade are incredibly attractive. The key attributes of the Noril'sk deposits are recognized as their tectonic setting at a major rifting centre at a continental margin, amidst a large igneous province. They are hosted in relatively small irregular chonoliths just below a thick sequence of related lavas. A distinctive signature of Ni, Cu and PGE depletion and crustal contamination is seen in a thick section of the overlying lavas. The sulfides are very chalcophile metal-rich and are much more abundant than can be accounted for by simple settling from the associated intrusion.

Focusing on areas of the world with partly eroded large igneous provinces, several areas have been noted that display a number of the key exploration criteria for this deposit type. The West Greenland flood basalts of Disco Island have one significant nickel sulfide showing in the Igdlukunguaq dyke and several layers of Ni-depleted basalt (Lightfoot *et al.* 1997). Hulbert *et al.* (2003) noted Victoria Island in the Canadian Arctic. Potentially significant Ni-Cu-PGE mineralization has been reported by junior mining companies in the Panxi Rift in southern China. The Baimazhai Ni mine (about 100 kt Ni metal) has been producing since the mid 1960s; it is associated with feeders to the Emeishan flood basalts which

are broadly coeval with the Siberian Traps. The Karoo flood basalts of southern Africa have related intrusions such as Insizwa, which hosts a number of Ni showings (Lightfoot *et al.* 1984). The Mid-Continent Rift System of North America has been recognized to have Ni depleted basalts and is known to have related intrusions that host Ni-Cu-PGE mineralization, such as the Crystal Lake Gabbro and much more recently the Eagle Deposit in the Yellow Dog peridotite (Rio Tinto website 2004).

BLACK SHALE-HOSTED PGE DEPOSITS

Classification

Black shale PGE-bearing mineral deposits can be divided into four types:

- Mo-Ni-Zn-PGE (South China type) *e.g.*, Zunyi, China; Nick, Canada; Olockitsky Trough, Russia; Mecca Quarry, USA
- Mo-U-V-(Au)-PGE (Karelian / Onezhsky type) *e.g.*, Srednyaya Padma, Karelia
- Au-PGE (Middle Asian / Sukhoi Log type) *e.g.*, Sukhoi Log, Russia; Natalka, Russia, possibly Serra Pelada, Brazil (Fig. 11-6) – carbonaceous siltstone type
- Cu-PGE (Baltic / Zechstein Polish type) *e.g.*, Kupferschiefer, Poland.

They occur at continental shelves and slopes of passive continental margins, at the passive continental margins of epicontinental troughs, within spreading marginal-continental basins and within protoplatform troughs over granite-greenstone basements. They are located in anoxic basins within clastic sedimentary (flysch) sequences containing black shale and in continental platform sedimentary sequences and possibly successor basins. Known deposits are found near the basal contact of major formations. They are generally associated with orogenic belts. Strongly anomalous shale overlying the North American craton may indicate that some potential exists over stable cratonic areas. Table 11-5 describes pertinent geological features for each of the deposit types. Figure 11-6 provides a geological section for one of these deposits (Serra Pelada, Brazil).

Underlying regional unconformities and major basin faults are possible controls on mineralization. For example, Chinese deposits occur discontinuously in a 1600 km long arcuate belt possibly controlled by basement fractures. Hydrothermal activity may be related to episodes of

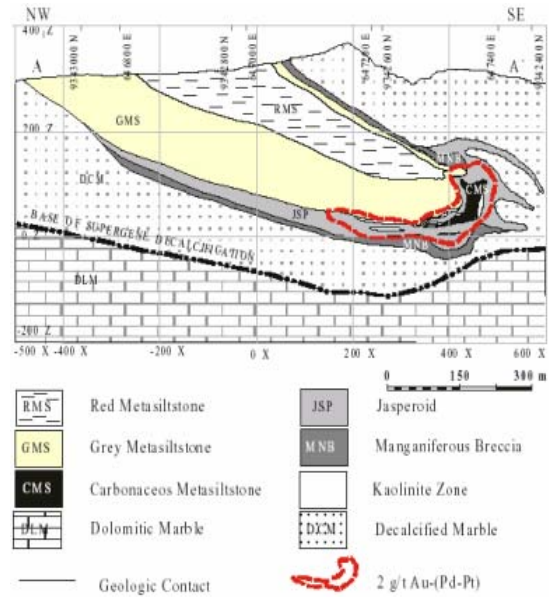


FIG. 11-6. Serra Pelada-Serra Leste, an example of a sediment-Hosted Au-PGE in the Carajas Region of Brazil, showing the variety of host rocks (Bucco-Tallarico *et al.* (2000).

thermal subsidence following periods of extension and deep rifting. Presently known localities are of Proterozoic, Early Cambrian and Devonian ages.

General Geology

The direct host rock is black shale. It is found in thin beds (0-15 cm thick, locally up to 30 cm) covering areas up to at least 100 ha and found as clusters and zones extending for tens of kilometres. Thin layers of sulfides in black shale sub-basins occur with associated phosphatic chert and carbonates. Semi-massive to massive sulfides are found as nodules, spheroids, framboids, and streaks or segregations in a fine-grained matrix of sulfides, organic matter, and nodular phosphorite or phosphatic carbonaceous chert.

Mineralization

Mineralization can be rhythmically laminated and often has thin discontinuous laminae. It can have an intraclastic texture with brecciated clasts and spheroids of pyrite, organic matter and phosphorite. It contains gold, and typically a range of elements including REE, Ni, Co and W; minor Cu, Cr, V, Mo and Pb. Table 11-6 shows typical features of mineralization for several examples.

TABLE 11-5. PALEOSTRUCTURAL AND FACIES SETTINGS OF SELECTED PGE-BEARING BLACK SHALE FORMATIONS

PGE mineralization type	Stratigraphy	Mineralized formation and its thickness	Geology of mineralized formation	Paleosetting	Paleofacies	Deposit – metallogenic province	THICKNESS OF ORE HORIZON
Mo-U-V-PGE	Laterally: shungite-bearing carbonate-terrigenous, black shale-picrite-diabase	Shungite-bearing carbonate-terrigenous; > 1000 m	Flyschoid interlayering of carbonaceous metasilstone, metamudstone, limestone; basic tuffs; dolomites, shungite-bearing metasilstone	Marine shallow water with individual separated basins	Trough depressions with stagnant water regime	Srednyaya Padma, Onezhskaya Trough, Southern Karelian	Metres
Mo-Ni-Zn-PGE	Laterally: clay-silt-conglomerate; clay-siliceous-carbonate with terrigenous tuffs; carbonaceous terrigenous-carbonate	Carbonaceous clay-silt-sand (black shale); 10s of m	Carbonaceous clay, silt-sand-clay and sand-gritstone rocks; carbonaceous-clay-carbonate shale; sideritic and siliceous concretions	Marginal sea	Local shallow- and deep-water facies zones	Dayang, Zunyi, South China	Centimetres to tens of centimetres
Au-PGE	Vertically: flyschoid terrigenous-carbonate flyschoid; olistostromal; limnal molasse	Terrigenous-carbonate flyschoid and olistostromal; 1000-1500 m	Unsorted rocks without layering; fine gravel and sandy fragments within sand-clay and clay cement; concretions of ferruginous carbonates, pyrite, rare siliceous breccia	Continental lagoon and shallow water deltaic	Stagnant depressions with turbiditic sedimentary rocks and terrigenous olistostromes	Sukhoi Log, Pribaikalia, Russia	Metres to tens of metres
Cu-PGE	Vertically: volcanic; terrigenous –clay; terrigenous-carbonate-shale-evaporitic flyschoid	Terrigenous-carbonate-shale-evaporitic cyclothem; <200-500 m	Sandstone through organic-rich to carbonate-rich shale with clay-carbonate-terrigenous qtz-fpr	Shallow water shelf	Local shallow stagnant water regimes	Zechstein Basin, Poland-Germany	Tens of cm to metres

Exploration Models

Requirements for the formation of an economic hydrothermal PGE deposit are:

- 1) solubility of PGE (predominantly as chloride or bisulfide complexes);
- 2) availability of source of PGE;
- 3) fluid flux through system (flow rate and time);
- 4) efficiency of depositional mechanism.

PGE as Bisulfide Complexes

In these conditions, PGE can have significant to moderate solubilities (Wood 2002). Optimal conditions are mildly acidic to alkaline, moderately to strongly reduced, high total fluid flux and require efficient depositional mechanism. Examples are black shale-hosted Ni-Mo deposits, seafloor massive sulfides and serpentinite.

PGE as Chloride Complexes

In these conditions, PGE can have very high solubilities ($\gg 1 \text{ mg.kg}^{-1}$, Wood 2002). The optimal conditions are strongly oxidized and acidic.

An economic deposit could be formed with smaller fluid flux and less efficient depositional mechanism (relative to bisulfide complex conditions). Examples include porphyry Cu-Au deposits, unconformity U-Au deposits, sediment-hosted stratiform Cu deposits and Jacutinga-type (iron formation) Au-Cu deposits. These are essentially "sedex"-type deposits, developed in restricted basins with anoxic conditions. Syngenetic deposition can occur from seafloor springs with

deposition of metals on or just beneath the seafloor (siliceous venting tubes and chert beds in underlying stratigraphy). They are closely associated with carbon-bearing metasedimentary rocks. The temperatures of ore formation of black shale-hosted deposits have been reported to be in the range 90-140°C (Nick) through to greater than 300°C (Sukhoi Log).

The basic model for black shale-hosted PGE deposits involves migrating hot basinal brines that extract metals associated with organic material in sediments. The brines have $\leq 30 \text{ wt\% equiv. NaCl}$ and are localized by faults that act as conduits and discharged the saline fluids towards the surface. The common well-laminated nature of the mineralization suggests that there were periodic influxes of fluid. The introduction of this nutrient-rich fluid into ooze-like, carbonaceous bottom sediments stimulated biogenic activity and led to sulfate reduction and sulfide precipitation. Sulfides are strongly depleted in ^{34}S , suggesting that they were generated by bacterial reduction of sulfate in the restricted reservoir of pore fluids in bottom sediments.

A secondary model (*e.g.*, Sukhoi Log), which to date is more important economically, involves stratabound, mesothermal, epigenetic hydrothermal mineralization. It differs from the common model above in that PGE distribution is apparently not dependent on the presence of an obvious redox boundary; deposition mechanisms, however, are unclear. The Serra Pelada Au-PGE the exact size being uncertain because it was mined

TABLE 11-6. FEATURES OF SOME SHALE-HOSTED PGE DEPOSITS.

Deposit	Type	Typical Grades		Thickness	Model	Features
		Pt	Pd			
Zunyi, South China	Mo-Ni-Zn-PGE	0.21	0.26	2-30 cm	Syn-diagenetic	7 mineral deposits along 2000 km belt
Srednyaya Padma, Onezhky Trough, Russia	Mo-U-V-PGE	0.6-0.8	0.3-0.4	30-45 m	Infiltration-epigenetic	mineralized zone 2 by 0.6 km
Sukhoi Log, Russia	Au-PGE	1.32	0.57	100 m (50-250 m)	Metamorphic-hydrothermal-metasomatic	365 Mt Au deposit
Zechstein Copper, Poland	Cu-PGE	0.2	0.1	30 cm	Polygenic-unconformity	Local mm-scale high-grade PGE

by artisanal miners (estimate 35 Mt @ 15 g.t⁻¹ Au, 7 g.t⁻¹ PGE). Groves (2004) and others have proposed it is formed by high-salinity, acid, oxidizing fluids. Once again, a careful geological study of the rock and alteration types should assist in identifying whether suitable conditions occurred for transport and deposition of PGE mineralization.

Exploration Methods

Host environments are stagnant-water lagoon-marine settings with dominant (carbonate-) terrigenous carbonaceous facies, formed in continental sea basins and continental riftogene troughs. They require an environment where a suitably enriched source (ultramafic rock, black shale, pre-existing magmatic deposit) was available and transport as chloride complexes would have been favored (oxidizing and acidic conditions – solutions in equilibrium with hematite and/or clay assemblages). Conditions for high-temperature fluids and high fluid salinity are important. Efficient depositional mechanisms such as reduction (*e.g.*, sediment-hosted stratiform Cu or unconformity-type U deposits), pH increase, introduction of As, Bi, Sb, Se, Te, or cooling are needed. Elevated ore metal values are observed in shale throughout a targeted basin, as well as in derived stream sediments. For example, in China average regional values for host shale grade 350 ppm Mo, 150 ppm Ni, several wt% P₂O₅, and 5–22% organic matter (some metals will correlate with organics). EM surveys can detect pyrite horizons. Fine-grained sulfides and other PGE-bearing compounds may pose recovery problems and the currently known occurrences of thin, laterally extensive sedimentary horizons are difficult to exploit. The large tonnage potential at potentially high grades of PGE represent an attractive target if the morphology of the deposit can be improved. For example, in China the black shale formation extends discontinuously over 1600 km; Nick sub-basin constitutes an area of over 80 km².

Examples

- Zunyi Mo Mine in China produces ~1000 tonnes/yr averaging 4% Mo and contains up to 4% Ni, 2% Zn, 0.7 g.t⁻¹ Au, 50 g.t⁻¹ Ag, 0.3 g.t⁻¹ Pt, 0.4 g.t⁻¹ Pd, and 30 g.t⁻¹ Ir (Fan 1983).
- The average grade of Nick mineralization is 5.3% Ni, 0.73% Zn, and 776 ppb PGE+Au (Hulbert 1992).

- Kupferschiefer Cu mines produce 150 kg of Pt and Pd per year; grades vary from 2–340 g.t⁻¹ Pt, 1–3000 g.t⁻¹ Au, and 2–1000 g.t⁻¹ Pd; however, concentrations of PGE and Au are restricted to a redox interface between black shale and red sandstone only a few centimetres thick (Kucha 1982).
- Sukhoi Log has reported grades of 0.91–1.17 g.t⁻¹ Pt; higher grade intersections of 1.45 g.t⁻¹ Pt over 102.3 m and 2.42 g.t⁻¹ over 40.5 m have been recorded; gold resource is believed to exceed 75 million oz at an average 2.7 g.t⁻¹ Au and ΣPGE grades of the same order. According to Distler & Yudovskaya (2005) the PGE contents of Sukhoi Log have been questioned by various workers but detailed work has confirmed they are present in significant amounts.

DISCUSSION: EXPLORATION STRATEGIES FOR PGE

Getting Started

Where will we focus? This is the single most difficult decision for a PGE exploration company to make. Putting yourself in the right place to be “lucky” is still an accepted part of a successful metal exploration strategy. The fundamental question facing PGE explorers remains “where am I most likely to find economic deposits?” Clearly, history shows us that most base metal discoveries in recent years have been made along strike from known deposits. This brownfields approach to risk reduction has very limited applicability to PGE because of the limited number of world-class deposits in existence and the difficulties of accessing land in the brownfields environment. We believe that most of the future, significant PGE discoveries are likely to come from greenfields exploration and the testing of innovative deposit and process models. For conventional magmatic PGE deposits, a simple decision tree such as that shown in Figure 11-7 can provide a useful starting point for area selection.

Source-Transport-Trap Theory

As we have outlined, the fundamental ore concentration processes for PGE are, in general terms, the same as those for other precious metals and base metals. These key process parameters can be captured in a simple “source-transport-trap” theory widely used in the petroleum industry but more and increasingly for base metal exploration. The economic potential of a PGE resource is most

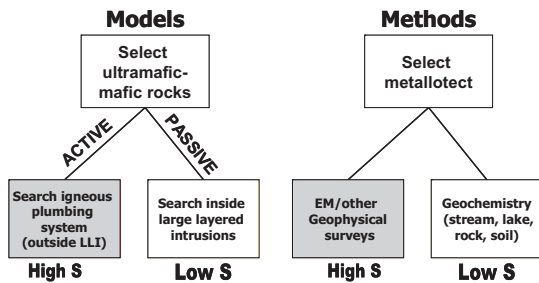


FIG. 11-7. Models and Methods showing contrast between the High S Nickel and Low S PGE deposit types and its influence on exploration drivers.

critically affected by its amenability to processing and the total tonnage/size of the resource, as opposed to just its grade. As with any metal mining proposition, forward looking economic models are required to guide the selection of target areas and develop an effective exploration strategy. For PGE, the extreme price volatility remains an inescapable drawback to successful long-term exploration planning. To balance this, successful explorers will use very conservative long-term price forecasts and will seek deposits with low up-front capital and sustaining capital cost requirements and a polymetallic character. To this end, bulk tonnage PGE deposits with base and/or other precious metal credits are highly desirable. The search for a “PGE porphyry” deposit continues. Examples of PGE-rich deposits having the potential to develop porphyry Cu-Au-type cost and value profiles include the enormous intrusion-hosted disseminated deposits of the Duluth Complex (Miller *et al.* 2002). These deposits are somewhat transitional into contact-type PGE deposits such as those developed in the 2.45 Ga mafic-ultramafic intrusions in central Finland (*e.g.*, Kontijaarvi deposit; Alapieti & Lahtinen, 2002) and north-eastern Ontario (East Bull Lake suite; James *et al.* 2002). During the most recent PGE price spike, several companies began to explore the potential for large tonnage, lower grade PGE mineralization in less conventional settings, including alkaline porphyry Cu-Au deposits (*e.g.*, Coryell pluton, British Columbia, Canada, Hulbert 2003), black shale (Wilde 2005) and Archean high-MgO felsic intrusions (Entwine Lake deposit, Ontario, Canada, Arnold *et al.* 2002). Metallurgists continue to strive for advances in hydrometallurgical processing technology for low grade Ni-Cu-PGE mineralization in deposits such as Duluth (Miller *et al.* 2002). Bulk mining of large, lower grade

deposits appears destined to become a major source for the PGE at some point in the future.

Source

Empirical evidence suggests that preferred source areas may exist for PGE deposits, whether dealing with magmatic deposits, sedimentary deposits or hydrothermal deposits. Figure 11-8 provides a simple diagrammatic representation of perceived fertile sources and magma compositions that can be used in area selection for various magmatic PGE deposit types.

Evidence indicates that the parental magmas of many large layered complexes include one of a distinctive MgO, SiO₂ and PGE-rich composition having contaminated komatiitic or boninitic affinities. These are melts apparently having chemical compositions suggesting derivation from strongly refractory harzburgitic mantle known to be present in sub-lithospheric mantle. The preferential occurrence of PGE deposits in orthopyroxene complexes highlights the potential of boninite (Hamlyn & Keays 1986, Prichard *et al.* 1996) or Archean siliceous high magnesium basalts (SHMB) (Keays 1995, Sun *et al.* 1991); primitive parental magma (determined from chilled margins) that may have been S-undersaturated and PGE-enriched prior to emplacement (Fig. 11-8). Hamlyn *et al.* (1985) and Hamlyn & Keays (1986) stressed the role of depleted mantle, residual after the extraction of MORB, in boninite genesis (*i.e.*, second-stage melts) and PGE mineralization. During extraction of MORB magma from primitive mantle, the system is S-saturated, so immiscible sulfide globules formed remain in the depleted mantle residual after MORB extraction, retaining PGE. Bockrath *et al.* (2004) have recently challenged this notion by proposing that sulfides could be physically entrained in the uprising magma, but Mungall (2005) has refuted this proposition. In consequence of the original model, depleted mantle has lower S contents than primitive mantle, but the sulfides in depleted mantle have very high PGE/S values.

Hatton & Sharpe (1989) put forward the process for the creation of a boninitic source as one of metasomatism of depleted mantle by a melt derived from subducted sediment. This would result in an alkaline residual melt, possibly giving rise to the contemporaneous Phalabora carbonatite complex (remobilized magmatic Cu (-PGE) deposit). Isotopic results suggest that globally from 2000 Ma, penecontemporaneous with the 2050 Ma

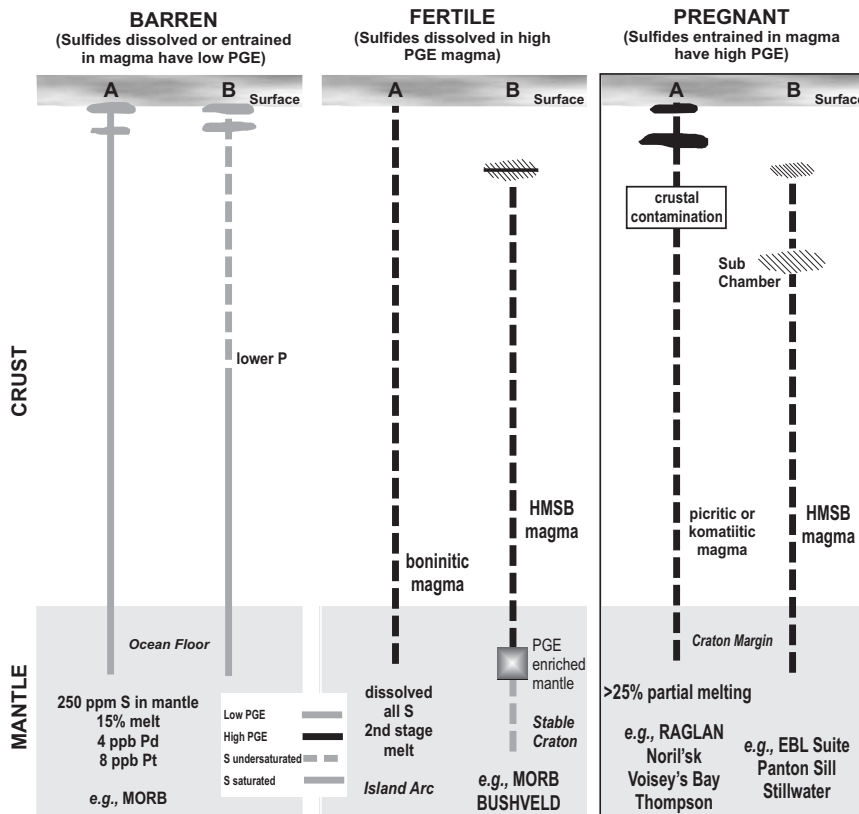


FIG. 11-8. Cartoon showing the role of magmas and sulfur saturation in ore formation. This approach is intended to assist area selection based on tectonic setting for PGE exploration (cartoon developed by Keays 2004).

Bushveld Complex, large quantities of continental material were recycled back into the mantle, probably by the subduction of sediments.

MORB-type magma will likely not give rise to a PGE-mineralized intrusion. The source of MORB-type magma is closer to the surface compared to a continental tholeiite source and MORB has already segregated sulfide. Crystallizing a magma drives it to S-saturation; however, as a deeply sourced (under high P) magma rises to surface, it is capable of dissolving more S, thus can reach surface while never reaching sulfide-saturation (as it is crystallizing, Mg# is decreasing, relative Fe increasing). Therefore, nearly saturated deep-source magma (continental tholeiite) can be appreciably undersaturated at surface, while a shallow-sourced magma (MORB) has a much smaller degree of undersaturation (sulfide undersaturation key to PGE mineralization process). However, if continental tholeiite magma stopped for any period during ascent, it would saturate and drop sulfides, and thus PGE, along the way.

Mineralization does not appear to be due to a mantle source enriched in PGE (Sun *et al.* 1989). PGE mineralization is related to the sulfide-undersaturated character of the parent magma and to

the magma chamber mixing processes including crustal contamination.

The so-called “second-stage melt” hypothesis (e.g., Hamlyn & Keays 1986) has general applications for selecting geological environments capable of hosting economic magmatic PGE deposits. However, because we do not possess an accurate 3D map of metal contents through the Earth’s mantle, the use of this concept is restricted to direct detection of chalcophile metal-enriched melts that may or may not have originated from enriched mantle sources. Hoatson & Keays. (1989) provided a series of simple metal ratio plots that allow the recognition of these PGE-enriched melts. Although simplistic, a test of fertile *versus* non-fertile melts using certain metal ratios to determine PGE content and S-saturation level is a useful first step in the evaluation of economic potential (Fig. 11-8). All things being equal, PGE-rich melts stand a higher probability of forming economic PGE mineralization than non-fertile melts such as MORB or calc-alkaline basalt. The reader is referred to the paper on “Magmatic Geochemistry of the Platinum-Group Elements” by Mungall (2005) for a more detailed and insightful review of the relationship of PGE to magma types.

In the case of hydrothermal PGE, one could argue that, based on empirical evidence, most hydrothermal PGE deposits are spatially associated with mafic and ultramafic igneous rocks. (This feature could, of course, simply reflect the fact that it is only in these environments that anyone has bothered to look for hydrothermal PGE deposits!) On a theoretical basis, mafic and ultramafic igneous rocks tend to have higher background PGE contents than other crustal rocks and provided their PGE are accessible to hydrothermal fluids (*e.g.*, there is no physiochemical reason why their PGE are less amenable to dissolution in hydrothermal fluids than in other crustal rocks) they should constitute a preferred source rock for developing PGE-rich hydrothermal fluids. Unfortunately, it has been our experience that many interesting hydrothermal PGE occurrences remain poorly documented or undocumented.

In contrast to the magmatic and hydrothermal cases discussed above, the importance of source rock PGE tenor could be much diminished in the case of sedimentary-type PGE mineralization. In the latter case, the PGE appear to be collected and deposited by pervasive basinal fluid circulation cells that remain active for long periods of time (millions of years) and which scavenge chalcophile metals from significant volumes of crust.

The evolution of mantle plume theory over the past decade (*e.g.*, Condie 2001) has already begun to influence the selection of greenfields nickel projects and will likely begin to dominate targeting for greenfields magmatic PGE properties. According to the general elements of plume theory, thermal perturbations arising from the core-mantle boundary or within the mantle itself produce plumes of superheated silicate melt that can ascend into and through the crust to produce geographically restricted but volumetrically large igneous provinces. However, recognition of plume-related magmatism in itself is not an effective means of screening fertile and non-fertile mantle sources because the thermal events believed to cause plumes are not likely to be particularly discriminating in terms of mantle source geochemistry. A positive aspect of “plume chasing” for PGE exploration is the potential to explore a diverse spectrum of host rock and mineralization styles within the target large igneous province.

Transport

This is the least understood aspect of PGE

exploration theory. In the magmatic environment, we do not possess the experimental data to support rigorous modeling of metal transport processes through the nearly infinite range of P-T-X conditions that can occur from the point of metal extraction in the mantle to the point of deposition in the crust. Accordingly, major breakthroughs in PGE exploration theory are likely to arise from new experimental work and refined thermodynamic models for the PGE over a wide range of P-T-X. Based on current experimental and empirical observations, it is believed that the principal agents for transporting PGE in magmas are various chloride, sulfide, semi-metal and hydroxide complexes (*e.g.*, Wood 2002, Makovicky 2002). However, having knowledge of this information has not provided much benefit to explorers. It is still difficult if not impossible to convincingly demonstrate how PGE travel from the mantle to the crustal repositories and then how they are concentrated during transport. Even in the best-documented PGE deposits such as the Merensky Reef and the UG2 Reef, there remains no consensus amongst industry and academic researchers concerning the principal transport mechanisms for the PGE from source to the site of deposition. By drawing together thermodynamic data from other disciplines such as medicine, engineering and organic and inorganic chemistry, we stand a much better chance of identifying the critical processes and agents involved in PGE transport across the entire spectrum of P-T-X conditions that we wish to consider. Improvement of our understanding of metal transport processes is a key to breaking the barrier of established mindsets and patterns (unsuccessful) related to current PGE exploration practices.

Trap

The site of ore formation is clearly the easiest of the three parameters in the source-transport-trap theory to constrain. PGE explorers and researchers alike have reached a general consensus that PGE can be trapped by mechanical means (gravitational settling of sulfides, particulate flow), local perturbations in P, T and X (decompression exsolution, solubility changes related to temperature decay or bulk composition of the solute), chemical processes (*e.g.*, redox reactions at constant T-P-X) and phase transition in the transporting media (boiling, for instance). Whereas magmatic traps such as stratiform reef environments and basal accumulation sites (embayments) have received a

significant amount of attention in the past, structural traps (magmatic or hydrothermal) and chemical traps (organic-rich sediments, carbonates, acidic and basic rock types) remain largely unexplored, even in environments having high background PGE contents. It would seem logical that major structures and fluid migration corridors that intersect the Bushveld Complex would be excellent places to explore for hydrothermal PGE, as would major shear zones cutting thick sequences of PGE-rich sills or flow sequences. Gold explorers should have no difficulty applying Au transport-trap theory to PGE exploration – it is clear from both empirical and experimental observations that in many “typical” mesothermal and epithermal deposits, Au, Pt and Pd are transported and deposited by similar processes. We also know that PGE are concentrated in a wide range of sedimentary environments including red-bed copper, Sedex Cu-Zn, unconformity-related U, carbonaceous shale and coal, and placer Au and heavy mineral deposits, yet the search for sediment-hosted PGE has barely begun.

Recommended Strategies

A pragmatic approach to PGE exploration is offered for consideration for explorationists and mining companies. This strategy is based on the following key tenets:

- 1) New deposit styles will be identified in the near future and the first companies to recognize this fact will be in the best position to capitalize on this trend;
 - 2) PGE mining from deposits in which PGE are the principal ore metals, with the exception of the mines in the Bushveld Complex, continues to deliver less than desired returns on investments because of severe price volatility;
 - 3) A healthy PGE mining company will have other assets to supplement the PGE mining operations. A serious evaluation of metal market trends over the past 30 years (Fig. 11-1) leads us to the inevitable conclusion that a diversified commodity portfolio is required to counter-balance PGE price volatility. “Related” commodities such as Au, Ni, Cu, Cr, Ti-V-Fe and even diamonds tend to occur in similar geological environments and/or draw upon similar exploration technologies and models. As an example, a healthy Ni-Cu mining portfolio would undeniably be well-served by inclusion of one or more PGE-rich deposits or stand-alone PGE operations. In many cases the economics of Ni sulfide mines are linked to the value of the by-product Pd and Pt recovered. Companies maintaining expertise in exploration and processing of Ni-Cu sulfide ores are favorably positioned to extend their reach into PGE-dominant magmatic deposits. It is somewhat surprising, therefore, that few of these companies have aggressively pursued expansion into the PGE business. Again, this fact likely reflects the perception that PGE markets will remain small (despite the fact that the total value of PGE produced in 2002 was only marginally less than the total value of global nickel production), are inherently unstable and are effectively closed to competition, being dominated by a handful of large operations.
- 4) Companies with exploration and processing expertise in mesothermal gold, Sedex-type Cu-Au, epithermal Au and porphyry Cu-Au-Mo may already hold a significant, relevant database that could be applied to exploration for hydrothermal, porphyry-style and sediment-hosted PGE deposits. In the past, it has not been common practice for gold and Cu-Au explorers to analyze for PGE although we have noted that this unfortunate situation is changing for the better with the advent of low-cost, multi-element analytical packages for base and precious metals.

A simple and sustainable long-term strategy for PGE should involve the following elements:

- 1) Maintain consistent funding over a multi-year timeframe through cash flow from other revenue streams. Most logically, companies that mine by-product PGE from Ni-Cu sulfide deposits or chromite deposits, or which hold title to PGE prospects in bodies that are currently mined for other metals are best positioned to persist in PGE exploration.
- 2) Develop strong ties to the major players in the new “hydrogen economy” as well as existing, principal end-use industries. Guaranteed pricing and direct sale of PGE to end users will increasingly become the norm if supply tightens and prices remain above historic levels.
- 3) Access the many, relevant public domain databases for PGE occurrences and deposits and their host rocks and develop an in-house global PGE database to support exploration decision-making.
- 4) Liaise with leading experts active in the fields of PGE chemistry, metallurgy and thermodynamics to develop new exploration models that can be

tested against existing global PGE occurrence data, then taken to the field.

- 5) At all costs, avoid purely model-driven exploration. Remain open-minded and observation-driven. Exploration for reef-type deposits may have set the PGE exploration industry back many years – it is a sobering fact that even the highest grade and largest reef-type PGE deposits remain marginal mining propositions in most western nations. While it is relatively easy to find a subeconomic classical reef, new clearly economic ones are extremely rare.
- 6) Acquire a diverse portfolio of high-quality PGE properties in periods of depressed metal prices and advance projects using a flexible but systematic ranking metric and/or decision tree.
- 7) Apply appropriate techniques to exploration – in most cases, effective mapping, prospecting and structural analysis will provide the most valuable early-stage data for PGE prospects yet companies that have traditionally explored for magmatic Ni-Cu-PGE deposits tend to be geophysically-driven. After making a discovery exploration geophysics will come into play with more value (Balch 2005) – many PGE deposits do not have a significant electromagnetic response due to the low sulfide content. Related to sedimentary and hydrothermal sulfides, magmatic breccias and contact-related magmatic deposits commonly have a clear chargeability response. Regional geochemical surveys and high-resolution magnetic surveys will typically provide critical new information concerning regional prospectivity. Geochemical methods can provide a low-cost regional and property-scale screening tool. Owing to their many unique chemical properties, PGE are concentrated in a wide variety of surficial media including organic soil, B-horizon soil, till, stream sediments and various plants species (*e.g.*, black spruce). However, we maintain that systematic geological documentation still provides the most valuable data for a given PGE prospect.
- 8) In areas of cover, PGE exploration becomes much more difficult, relying upon the indirect tools for geological interpretation such as regional magnetics or gravity, coupled with those geochemical approaches such as media sampling described above. Access to bedrock samples via trenching or drilling becomes much more expensive. Even fences of diamond drill

holes still only permit imperfect interpretation and evaluation.

SUMMARY

We believe that by maintaining a focused, long-term strategy and by drawing on relevant expertise from other disciplines and sub-disciplines, a large number of new and viable PGE deposit types will be discovered. Current PGE mining companies obviously have a significant advantage in implementing innovative new exploration strategies for PGE but it remains to be seen if they will affect these strategies. While recent price booms have led to many new discoveries of PGE mineralization in magmatic settings, this is hardly surprising given the propensity of mafic and ultramafic silicate melts to achieve S-saturation and/or volatile saturation as a normal consequence of cooling and crystallization. The channeling of hard won exploration investment into bodies having local and inconsequential PGE enrichment is a classic example of exploration without focus. The big wins for PGE explorers are unlikely to arise from this approach. New geological environments for PGE deposits will hopefully be identified in the near future. Breakthroughs on the exploration side will almost certainly be supported by new experimental data and exploration concepts as well improved integration of relevant information from the fields of chemistry, mineralogy and thermodynamics. We adhere to the belief that there is much, if not more, to be gained by considering “unconventional” deposits and settings for PGE than by pursuing “traditional” target styles.

ACKNOWLEDGEMENTS

This paper is based on work a few years ago, by a team at Falconbridge Limited including Katherine Smuk and Rob Foy, who prepared some of the information and diagrams presented here. Thanks go as well to Reid Keays for valuable discussions. However, the opinions expressed in this paper are the authors’ and do not represent any official positions of their employers.

REFERENCES

- ALAPIETI, T.T. & LAHTINEN, J.J. (2002): Platinum-Group Element Mineralization in Layered Intrusions of Northern Finland and the Kola Peninsula, Russia, in Cabri, L.J., ed., *The geology, geochemistry, mineralogy and mineral*

- beneficiation of platinum-group elements: *CIM Special Volume* **54**, p. 507-546.
- ARNOLD, J.P., JAMES, R.S. & BEAKHOUSE, G. (2002): Geology, petrology and PGE-Ni mineralization of the Neoproterozoic Entwine Lake intrusion, an intermediate to mafic igneous intrusion. 9th International Platinum Symposium, Extended Abstracts with Program, 21-25 July, Billings, Montana.
- BALCH, S. (2005): The geophysical signatures of platinum-group element deposits. In *Exploration for Platinum-group Element Deposits* (J.E. Mungall, ed.). *Mineral. Assoc. Canada, Short Course* **35**, 275-285.
- BARNES, S.J. (1989): Are Bushveld U-type parent magmas boninites or contaminated komatiites? *Contrib Mineral. Petrol.* **101**, 447-457.
- BOCKRATH, C., BALLHAUS, C. & HOLZEID, A. (2004): Fractionation of the platinum-group elements during mantle melting. *Science* **305**, 1951-1953.
- BUCCO-TALLARICO, F.H., COIMBRA, C.R. & CRAVO-COSTA, C.H. (2000): The Serra Leste sediment-hosted Au-(Pd-Pt) mineralization, Carajás Province. *Revista Brasileira de Geociências* **30**, 226-229.
- CAWTHORN, R.G. (1999): The platinum and palladium resources of the Bushveld Complex. *S. Afr. J. Sci.* **95**, p. 481-489.
- CAWTHORN, R.G., MERKLE, R.K.W. & VILJOEN, M.J. (2002): Platinum-group element deposits in the Bushveld Complex, South Africa. In: *The Geology, geochemistry, mineralogy and mineral beneficiation of platinum-group elements*. *Can. Inst. Mining Metall., Special Vol.* **54**, 389-430.
- CONDIE, K.C. (2001): Mantle plumes and their record in earth history. Cambridge University Press, Cambridge, U.K., 306 p.
- CROCKET, J.H. (2002): Platinum-group element geochemistry of mafic and ultramafic rocks. In: L. J. Cabri (editor). *The geology, geochemistry, mineralogy and mineral beneficiation of platinum-group elements*. *Can. Inst. Mining Metall., Special Vol.* **54**, 177-210.
- DALRYMPLE, B.G., CZAMANSKA, G.K., FEDORENKO, V.A., SIMONOV, M.A., LANPHERE, M.A. & LIKHACHEV, A.P. (1995): A reconnaissance $^{40}\text{Ar}/^{39}\text{Ar}$ geochronological study of ore-bearing and related rocks, Siberian Russia. *Geochim. Cosmochim. Acta* **59**, 2071-2083.
- DISTLER, V.V. & YUDOVSKAYA, M.A. (2005): Polymetallic platinum-group element (PGE)-Au mineralization of the Sukhoi Log Deposit, Russia. In *Exploration for Platinum-group Element Deposits* (J.E. Mungall, ed.). *Mineral. Assoc. Canada, Short Course* **35**, 457-485.
- EALLES, H.V. & CAWTHORN, R.G. (1996): The Bushveld Complex. In: *Layered Intrusion*. R.G. Cawthorn (editor). Elsevier Science BV, 181-230.
- FAN, D. (1983): Polyelements in the Lower Cambrian black shale series in Southern China. In: S. S. Augustithis (editor). *The Significance of Trace Metals in Solving Petrogenetic Problems and Controversies*. Theophrastus Publications, Athens, 447-474.
- FARROW, C.E.G. & LIGHTFOOT, P.C. (2002): Sudbury PGE revisited: Toward an integrated model. In: *The Geology, geochemistry, mineralogy and mineral beneficiation of platinum-group elements*. *Can. Inst. Mining Metall., Special Vol.* **54**, 273-298.
- FOSTER, J.G. (2005). Active magmatic Cu-Ni-(+/-PGE) Sulfide systems with reference to Pechenga and Noril'sk-Talnakh, Russia. CIM Annual Meeting, April 2005, Toronto
- GROVES, D.I. (2004): Unconventional PGE Deposits with Emphasis on Serra Pelada, Brazil. PGE Workshop, SEG 2004, Perth, October 2, 2004.
- HAMLIN, P.R. & KEAYS, R.R. (1986): Sulfur Saturation and Second-Stage Melts: Application to the Bushveld Platinum Metal Deposits: *Econ. Geol.* **81**, 1431-1445.
- HAMLIN, P.R., KEAYS, R.R., CAMERON, W.E., CRAWFORD, A.J., & WALDRON, H.M. (1985): Precious metals in magnesian low-Ti lavas: implications for metallogenesis and sulfur saturation in primary magmas: *Geochim. Cosmochim. Acta* **49**, 1797-1811.
- HATTON, C.J., & SHARPE, M.R. (1989): Significance and origin of boninite-like rocks associated with the Bushveld Complex. In: A.J. Crawford, A. J. (editor). *Boninites*. Unwin Hyman, 174-207.
- HEAMAN, L.M. (1997): Global mafic magmatism at

- 2.45 Ga: Remnants of an ancient large igneous province? *Geology* **25**, 299-302.
- HEAMAN, L.M. & MACHADO, N. (1992): Timing and origin of Mid-continent rift alkaline magmatism, North America: Evidence from the Coldwell Complex. *Contrib Mineral. Petrol.* **110**, 289-303.
- HIRSCHMANN, M.M., RENNE, P.R. & MCBIRNEY, A.R. (1997): $^{40}\text{Ar}/^{39}\text{Ar}$ dating of the Skaergaard Intrusion. *Earth Planet. Sci. Lett.* **146**, 645-658.
- HOATSON, D.M. (2000): Geological setting, petrography and geochemistry of the mafic-ultramafic intrusions. In: *Geology and Economic Potential of the Palaeoproterozoic layered mafic-ultramafic intrusions in the East Kimberley, Western Australia*. D.M. Hoatson & D. H. Blake (editors). Australian Geological Survey Organisation Bulletin 246, Canberra, 250-264.
- HOATSON, D.M. & KEAYS, R.R. (1989): Formation of platiniferous sulfide horizons by crystal fractionation and magma mixing in the Munni Munni layered intrusion, West Pilbara Block, Western Australia. *Econ. Geol.* **84**, 1775-1804.
- HULBERT, L.J., GREGORIE, D.C., PAKTUNC, A.D., CARNE, R.C. (1992): Sedimentary nickel, zinc and platinum group element mineralization in Devonian black shales at the Nick property, Yukon, Canada: a new deposit type. *Explor. Mining Geol.* **1**, 39-62.
- HULBERT, L.J. (2003): Magmatic platinum group element environments in Canada: Present and future exploration targets. Geological Association of Canada, Howard Street Robinson Lecture, 2002. Geol. Surv. Canada, *Misc. Publication* **2** (CD-ROM).
- ILJINA M.J. & LEE C.A. (2005): Marginal series-hosted PGE deposits. In *Exploration for Platinum-group Element Deposits* (J.E. Mungall, ed.). *Mineral. Assoc. Canada, Short Course* **35**, 75-96.
- INTERFAX MINING AND METALS REPORT (2001): Murmansk prepares to develop major PGM occurrences. **10** #5, p 30.
- IRVINE, T.N. (1970): Crystallization sequences in the Muskox Intrusion and other layered intrusions. *Geol. Soc. S. Afr., Special Publ.* **1**, 441-476.
- JAMES, R.S., JOBIN-BEVANS, S.J., EASTON, R.S., WOOD, P., HROMINCHUK, J.L., KEAYS, R.R. & PECK, D.C. (2002): Platinum-Group Element Mineralization in Paleoproterozoic Basic Intrusions in Central and Northeastern Ontario, Canada. In: L.J. Cabri (editor). *The geology, geochemistry, mineralogy and mineral beneficiation of platinum-group elements*. *Can. Inst. Mining Metall., Special Vol.* **54**, 507-546.
- KEAYS, R.R. (1995): The role of komatiitic and picritic magmatism and S-saturation in the formation of ore deposits. *Lithos* **34**, 1-18.
- KEAYS, R.R. (2004): Conventional Models for PGE Deposits Workshop 3, Platinum deposits and models: conventional and unconventional. SEG Meeting 2004, Perth.
- KROGH, T.E., DAVIS, D.W. & CORFU, F. (1984): Precise U-Pb zircon and baddeleyite ages for the Sudbury area. In *The Geology and Ore Deposits of the Sudbury Structure*, E.G. Pye, A.J. Naldrett & P.E. Giblin (editors). *Ontario Geological Survey, Special Volume* **1**, 431-46.
- KUCHA, H. (1982): Platinum-Group Metals in the Zechstein Copper Deposits, Poland: *Econ. Geol.* **77**, 1578-1591.
- LAVIGNE, M.J., MICHAUD, M.J. & RICKARD J. (2005): Discovery and geology of the Lac Des Iles palladium deposits. In *Exploration for Platinum-group Element Deposits* (J.E. Mungall, ed.). *Mineral. Assoc. Canada, Short Course* **35**, 369-390.
- LECHEMINANT, A.N. & HEAMAN, L.M. (1989): Mackenzie igneous events, Canada: Middle Proterozoic hotspot magmatism associated with ocean spreading. *Earth Planet. Sci. Lett.* **96**, 38-48.
- LEVINE, R. & WILBURN, D. (2003): Russian PGM – Resources for 100+ years. Paper presented at the Platinum-Group Metals Seminar 2002, *US Geol. Surv. Open File Report* 03-059.
- LIGHTFOOT, P.C., NALDRETT, A.J., GORBACHEV, N.S., FEDERENKO, V.A., HAWKESWORTH, C.J., & DOHERTY, W. (1994): Chemostratigraphy of Siberian Trap Lavas, Noril'sk District, Russia: Implication and source of flood basalt magmas and their associated Ni-Cu mineralization. *Proceedings of the Sudbury-Noril'sk Symposium, Ontario Geological Survey Special Publication* **5**, 283-312.

- LIGHTFOOT, P.C., HAWKESWORTH, C.J., OLSHEFSKY, K., GREEN, T., DOHERTY, W., & KEAYS, R.R. (1997): Geochemistry of Tertiary tholeiites and picrites from Qeqertarsuaq (Disko Island) and Nuussuaq, West Greenland with implications for the mineral potential of comagmatic intrusions. *Contrib Mineral. Petrol.* **128**, 139-163.
- LIGHTFOOT, P.C., NALDRETT, A.J., & HAWKESWORTH, C.J. (1984): The Geology and Geochemistry of the Waterfall Gorge Section of the Insizwa Complex with Particular Reference to the Origin of the Nickel Sulfide Deposits, *Econ. Geol.* **79**, p.1857-1879.
- LIGHTFOOT, P.C. & HAWKESWORTH, C.J. (1997): Flood basalt and magmatic Ni, Cu and PGE sulfide mineralization: Comparative geochemistry of the Noril'sk (Siberian Traps) and West Greenland sequences. In: Large Igneous Provinces: Continental, Oceanic and Planetary flood basalt volcanism. J. Mahoney & M. Coffin (editors). *American Geophysical Union, Geophysical Monograph* **100**, 357-380.
- MAIER, W.D. & BARNES, S.-J. (2005): Application of Litho-geochemistry to Exploration for PGE Deposits. In Exploration for Platinum-group Element Deposits (J.E. Mungall, ed.). *Mineral. Assoc. Canada, Short Course* **35**, 309-341.
- MAIER, W.D., BARNES, S.-J., GARTZ, V. & ANDREWS, G. (2003): Pt-Pd reefs in magnetities of the Stella layered intrusion, South Africa: A world of new exploration opportunities for platinum group elements. *Geology* **31**, 885-888.
- MAKOVICKY, E. (2002): Ternary and Quaternary Phase Systems with PGE. In: L.J. Cabri, L.J. (editor). The geology, geochemistry, mineralogy and mineral beneficiation of platinum-group elements. *Can. Inst. Mining Metall., Special Vol.* **54**, 131-176.
- MILLER, J.D., GREEN, J.C., SEVERSON, M.J., CHANDLER, V.W., HAUCK, S.E. & PETERSON, D.M. (2002): Geology and mineral potential of the Duluth Complex and related rocks of northeastern Minnesota. Minnesota Geological Survey, Saint Paul, Minnesota, 207 p.
- MITROFANOV, F.P., KORCHAGIN, A.U. DUDKIN, K.O. & RUNDKVIST, T.V. (2005): Fedorov-Pana layered mafic intrusion, (Kola Peninsula, Russia): approaches, methods, and criteria for prospecting PGEs. In Exploration for Platinum-group Element Deposits (J.E. Mungall, ed.). *Mineral. Assoc. Canada, Short Course* **35**, 343-358.
- MUNGALL, J.E. (2005): Magmatic geochemistry of the platinum-group elements. In Exploration for Platinum-group Element Deposits (J.E. Mungall, ed.). *Mineral. Assoc. Canada, Short Course* **35**, 1-34.
- MUNGALL, J.E., MEURER, W.P. & MARTIN, R.F. (EDS.) (2002): *Platinum-group Elements: Petrology, Geochemistry, Mineralogy.* *Can. Mineral.* **42**, 241-694.
- NALDRETT, A.J. (2002): Requirements for forming giant Ni-Cu sulfide deposits. In: D. Cooke, D & J. Pongraz (editors). Giant Ore Deposits, CODES Special Publication **4**, 195-204.
- NALDRETT, A.J. (2004): *Magmatic Sulfide Deposits: Geology, Geochemistry and Exploration.* Springer Verlag 728 p.
- NALDRETT, A.J., KEATS, H., SPARKES, K. & MOORE, R. (1996): Geology of the Voisey's Bay Ni-Cu-Co deposit, Labrador, Canada. *Explor. Mining Geol.* **5**, 169-179.
- NALDRETT, A.J., LIGHTFOOT, P.C., FEDORENKO, V.A., DOHERTY, W. & GORBACHEV, N.S. (1992): Geology and geochemistry of intrusions and flood basalt of the Noril'sk region, U.S.S.R., with implications for the origin of Ni-Cu ores. *Econ. Geol.* **87**, 975-1004.
- OBERTHUR, T., DAVIS, D.W., BLENKINSOP, T.G. & HOHNDRF, A. (2002): Precise U-Pb mineral ages, Rb-Sr and Sm-Nd systematics for the Great Dyke, Zimbabwe: Constraints on late Archean events in the Zimbabwe Craton and Limpopo Belt. *Precamb. Res.* **113**, 293-305.
- OHNSTETTER, M. (1996): Diversity of PGE deposits in basic-ultrabasic intrusives – single model of formation. In: D. DemaiFFE (editor). Petrology and Geochemistry of magmatic suites of rocks in the continental and oceanic crusts, Université Libre de Bruxelles, Royal Museum for Central Africa (Tervuren), 337-354.
- PACES, J.B. & MILLER, J.D. (1993): Precise u-Pb ages of the Duluth Complex and related mafic intrusions, northeastern Minnesota: new insights for physical, petrogenetic, paleomagnetic and tectono-magmatic processes associated with 1.1

- Ga Mid-continent rifting. *J. Geophys. Res.* **98**, 997-1014.
- PARRISH, R.R. (1989): U-Pb geochronology of the Cape Smith Belt and Sugluk block, northern Quebec. *Geoscience Canada* **16**, 126-130.
- PREMO, W.R., HELZ, R.T., ZIENTEK, M.L. & LANGSTON, R.B. (1990): U-Pb and Sm-Nd ages for the Stillwater Complex and its associated dikes and sills, Beartooth Mountains, Montana: Identification of the parent magma. *Geology* **18**, 1065-1068.
- PRICHARD, H.M., LORD, R.A., & NEARY, C.R. (1996): A model to explain the occurrence of platinum- and palladium-rich ophiolite complexes: *J. Geol. Soc. Lond.* **153**, 323-328.
- SUN, S.-S., NESBITT, R.W., & MCCULLOCH, M.T. (1989): Geochemistry and petrogenesis of Archean and early Proterozoic siliceous high-magnesian basalts. In: A.J. Crawford (editor). *Boninites*. Unwin Hyman, 148-173.
- SUN, S.-S., WALLACE, D.A., HOATSON, D.M., GLIKSON, A.Y., & KEAYS, R.R. (1991): Use of geochemistry as a guide to platinum element group potential of mafic-ultramafic rocks: examples from the west Pilbara Block and Halls Creek Mobile Zone, Western Australia. *Precamb. Res.* **50**, 1-35.
- TIAX LLC (2003): Platinum Availability and Economics for PEMFC Commercialization. Report to US Department of Energy.
- WALRAVEN, F., ARMSTRONG, R.A. & KRUGER, F.J. (1990): A chronostratigraphic framework for the north-central Kaapvaal craton, The Bushveld Complex and the Vredefort Structure. *Tectonophysics* **171**, 23-48.
- WATKINSON, D.H., LAVIGNE, M.J. & FOX, P.E. (2002): Magmatic-hydrothermal Cu- and Pd-rich deposits in gabbroic rocks from North America. In: The Geology, geochemistry, mineralogy and mineral beneficiation of platinum-group elements. *Can. Inst. Mining Metall., Special Vol.* **54**, 299-319.
- WILDE, A. (2005): Descriptive ore deposit models: Hydrothermal and supergene Pt & Pd deposits. In *Exploration for Platinum-group Element Deposits* (J.E. Mungall, ed.). *Mineral. Assoc. Canada, Short Course* 35, 145-161.
- WILSON, A.H. (1996): The Great Dyke of Zimbabwe. In: Layered Intrusion. R.G. Cawthorn (editor). Elsevier Science BV, 365-402.
- WOOD, S.A. (2002): The Aqueous Geochemistry of the Platinum-Group Elements with Applications to Ore Deposits. In: L.J. Cabri (editor). The geology, geochemistry, mineralogy and mineral beneficiation of platinum-group elements. *Can. Inst. Mining Metall., Special Vol.* **54**, 211-250.
- ZIENTEK, M.L., COOPER, R.W., CORSON, S.R., GERAGHTY, E.P. (2002): Platinum-Group Element Mineralization in the Stillwater Complex, Montana. In: L.J. Cabri (editor). The geology, geochemistry, mineralogy and mineral beneficiation of platinum-group elements. *Can. Inst. Mining Metall., Special Vol.* **54**, 177-210.

CHAPTER 12: THE GEOPHYSICAL SIGNATURES OF PLATINUM-GROUP ELEMENT DEPOSITS

Stephen J. Balch
Aeroquest Limited, 845 Main Street East, Unit 4,
Milton, Ontario L3T 3Z3, Canada
E-mail: sbalch@aeroquestsurveys.com

INTRODUCTION

From a geophysical point of view there are two main settings for platinum group elements (PGE) – the high sulfide setting such as Sudbury or Noril'sk and the low sulfide setting such as Bushveld or Stillwater. High sulfide ores represent easier geophysical targets because pyrrhotite is usually the dominant mineral, it is highly conductive, and it is often contained within a highly resistive host rock, providing an excellent contrast. Within the high sulfide environments, economic concentrations of PGE can also be found distal to the main sulfide body within disseminations of low percent sulfide, which will complicate the use of geophysics in these environments.

PGE occur in relatively low concentrations. The Stillwater Complex, for example, contains some of the world's richest concentrations of PGE but averages less than 20 g.t⁻¹ for its mineable reserves. In these settings there may be only 2–5% sulfide present and carrying PGE in economic concentrations. For most geophysical methods there will not be a sufficient contrast in the physical properties of the sulfide mineralization relative to the host rock to produce a measurable response. In such cases, it is necessary to detect some other mineral, such as magnetite, and hope to establish an association with the host rock or some structure that may have served as a pathway for concentrating the PGE.

GEOPHYSICAL METHODS

Geophysical techniques are sensitive to the physical properties of minerals, their host rocks, and the structures within. Selecting the best technique depends on defining the physical property that is most anomalous for the mineralization and least anomalous for the host rock and setting. This contrast defines the anomalous geophysical response.

The most common physical properties exploited by geophysicists are density (gravity),

susceptibility (magnetics), polarization (induced polarization), conductivity (electrical or electromagnetics), and acoustic (seismic).

The gravity method is based on the force of attraction between the Earth and some object within it. Measurements of the acceleration due to gravity are made with a gravimeter in units of milligals (mGal) named in honor of Galileo Galilei. One mGal is equivalent to 10^{-5} m.s^{-2} . The Earth's gravitational acceleration is approximately 980,000 mGal while a typical orebody may produce a response of only 4 mGal. Today's gravimeters have a sensitivity approaching 0.01–0.001 mGal.

Gravity anomalies result from variations in density. The amplitude and extent of a gravity anomaly is therefore dependent on the density contrast, the volume of material, and the distance to the target. Massive sulfide deposits located close to surface produce very strong gravity anomalies as do large mafic intrusive bodies surrounded by granite. Variations in overburden thickness have a great effect on gravity measurements because the density contrast between rock and overburden is high, and overburden is at surface. For these reasons, the gravity method is used more for lithologic mapping rather than for detecting mineral deposits directly.

The introduction of differential GPS to gravity surveys has made the method more practical as elevation must be measured to within a few centimetres. Since about 1999, gravimeters and gravity gradiometers have been adapted to airborne platforms. These systems are now approaching the practical sensitivities achieved with traditional ground surveys, but with much greater production levels and at a lower relative cost. Sensitivities average 0.3 mGal over a distance of 500 m for gravimeters and 2–5 E over 500 m for gradiometers. The unit E is an Eotvos named after physicist Roland Eötvös, where 1 E is equivalent to $10^{-4} \text{ mGal.m}^{-1}$. A vertical displacement of 1 m is equivalent to a change in gravity of 0.3 mGal or 3000 E, which is why accurate elevation

measurements are needed when correcting gravity data for changes in survey height.

The magnetic method is based on measurements of the Earth's total magnetic field measured in nanoteslas (nT) using a magnetometer. Magnetite is the predominant mineral although hematite and pyrrhotite can also be magnetic. High sulfide PGE deposits can be magnetic, but more often it is the host rock that is being mapped by the magnetometer. The magnetic method, therefore, is also seen primarily as a geologic mapping tool. In some cases, subtle magnetic features may offer clues as to the pathways for PGE mineralization, particularly if the PGE are associated with oxides such as magnetite.

High resolution magnetometers are of the optically pumped type. The sensor consists of a glass cell containing cesium, potassium, or rubidium gas, as these elements have only a single electron in their outermost shell. The electron has a magnetic moment and will interact with an external magnetic field, such as the Earth's static field. The gas is optically pumped by a light source of a specific frequency, which is used to pump the electron into a higher orbital. A radio frequency is then applied to the gas to knock the electron back down to its previous orbital. The frequency required to accomplish this is proportional to the external magnetic field. By counting this frequency, an accurate measurement of the magnetic field is acquired.

Optically pumped magnetometers measure the total magnetic field rather than a vector component. Additional processing of the total magnetic field reveals subtle features that may be related to structures such as faults, dikes, or compositional changes within an intrusion. The first and second vertical derivatives are commonly used to detect such features and to enhance visualization of the edges of lithologic units having different magnetite content. The analytic signal, derived from the three orthogonal gradients of the total magnetic field, is independent of the direction of induced or remanent magnetization and produces peaks directly over structures such as faults, dikes and contacts.

The induced polarization (IP) method is based on the polarization of metal-bearing minerals when a direct current is applied to the ground. Readings are based on a ratio of the measured to applied voltage, measured in millivolts per volt ($\text{mV}\cdot\text{V}^{-1}$). The measurement is usually integrated over a known time period and is known as chargeability ($\text{mV}\cdot\text{s}\cdot\text{V}^{-1}$). In low sulfide PGE, IP is

an effective tool for mapping the disseminated sulfide and estimating host rock resistivity. IP surveys are based on an array of electrodes placed in the ground, with two electrodes used to pass a current into the Earth, and two electrodes used to measure the resulting voltage. These measurements are carried out along a series of profiles, normally at right angles to the strike direction of the target. Depth of penetration is proportional to electrode spacing and the amount of sulfide present is proportional to chargeability. By varying the electrode spacing and measuring the voltage decay, disseminated sulfide mineralization can be mapped to depths of a few hundred metres.

The electromagnetic (EM) methods transmit a primary EM field into the ground that interacts with sub-surface conductors to generate a secondary EM field, which is detected at the receiver coil. EM transmitters consist of a closed loop of wire, and most EM receivers are also induction coils consisting of several loops of wire. Measurements can be made in boreholes, at surface, or from airborne platforms. In high sulfide PGE environments, EM methods can directly detect the associated sulfide minerals. Because the conductivity of sulfide is very high compared to the host rock, and given the excellent correlation between percent sulfide and economic mineral concentrations for most high sulfide deposits, EM methods have been the most successfully applied geophysical techniques for PGE exploration.

EM systems are equally sensitive to the conductivity and thickness of a conductor with the product of these values defined as conductance, measured in siemens (S). The normal range of operating frequencies for an EM transmitter is 1–1,000 Hz. Low frequencies penetrate deeper and are more easily transmitted through conductive overburden while higher frequencies produce stronger responses, especially for weakly conductive targets. In low sulfide areas, therefore, higher transmitting frequencies would have a greater chance of outlining mineralization. In high sulfide areas the lower frequency systems can better discriminate between 3 m of 10% sulfide, say, and 15 m of 60% sulfide.

Electromagnetic reflection (*e.g.*, radar imaging) is based on a resistivity contrast between the mineralization and host rock. Radar is different than the conventional EM methods in that the transmitting waves are very short (1 cm to 1 m) and are easily attenuated by even small amounts of conductive sulfide. Radar measurements made

between boreholes (*i.e.*, cross-hole) have been effective at mapping low sulfide environments over distances of several hundred metres.

The seismic method is based on measurements of acoustic velocity measured in kilometres per second (km.s^{-1}). These methods have been successfully applied to map the lithologic units containing PGE mineralization within the Bushveld, for example, and work best when the geology is layered and flat-lying or gently dipping.

Selection of a particular geophysical method depends upon on the geologic setting as well as the defining physical property of the associated mineralization. In many cases, a combination of methods is required to define the mineral outline, a process that requires an understanding of the geological environment and often considerable patience as experience is gained through trial and error. The most common geophysical methods are summarized by physical property in Table 12-1.

NI-CU SULFIDE DEPOSITS

For the world-class nickel (Ni) and copper (Cu) sulfide deposits such as Sudbury and Noril'sk, PGE are a by-product. The PGE at Noril'sk represent a large portion of the value of the mined metals (Naldrett, 1992), while at Voisey's Bay no significant PGE credits are expected. The common component to these deposits is the high concentrations of sulfide minerals, essentially pyrrhotite, with which the PGE are associated.

Geophysical exploration within the Sudbury Igneous Complex (SIC) has focused almost entirely on Ni and Cu. The contact of the SIC contains a significant amount of pyrrhotite with

pentlandite and chalcopyrite. Watts (1997) and King *et al.* (1994) described the geophysical methods that have been developed to identify the highest concentrations of sulfide, usually found in the Sublayer within traps known as embayments and terraces as described by Morrison (1984). The pioneering work of Inco Limited and Falconbridge Limited within this environment has been directed toward identifying massive sulfide accumulations where deposits have such a high conductance they pose a problem for the traditional time domain EM methods. The strategy has relied on an assumed direct relationship between the total amount of sulfide present and economic concentrations of Ni and Cu.

The PGE at Sudbury are not always associated within the highest concentrations of sulfide, however, and often occur hundreds of metres away from the Ni-Cu mineralization and within the footwall rocks. PGE are also found in higher concentrations within the offset dikes compared to the SIC contact.

The SIC is well defined on a regional scale by the total magnetic field (TMF) shown in Figure 12-1. The quartz gabbro unit within the SIC is particularly magnetic due to abundant magnetite. The surrounding country rock, which includes gneiss and granite, is variably magnetic, but never to the same extent as the quartz gabbro. Several diabase dikes that intersect the SIC are also evident in the TMF. On the southern margin of the SIC, the TMF has a much higher amplitude, resulting from the steep dip of the South Range relative to the North Range. While the TMF anomaly outlines the SIC, it does not always outline the known mineral deposits, particularly the offset deposits that occur

TABLE 12-1. GEOPHYSICAL METHODS REQUIRE A PHYSICAL PROPERTY CONTRAST FOR A GIVEN SETTING.

Property	Method	Setting
Density	Gravity	Ultramafic rocks, gabbro, norite, troctolite
Susceptibility	Magnetics	Magnetic pyrrhotite, magnetic host rock such as serpentinized ultramafic rocks, mafic intrusive rocks, dikes, faults and fractures
Polarization	Induced Polarization	Disseminated sulfide
Conductivity	Electrical/electromagnetic	Pyrrhotite, chalcopyrite
Acoustic velocity	Seismic	Sub-horizontal, layered geology

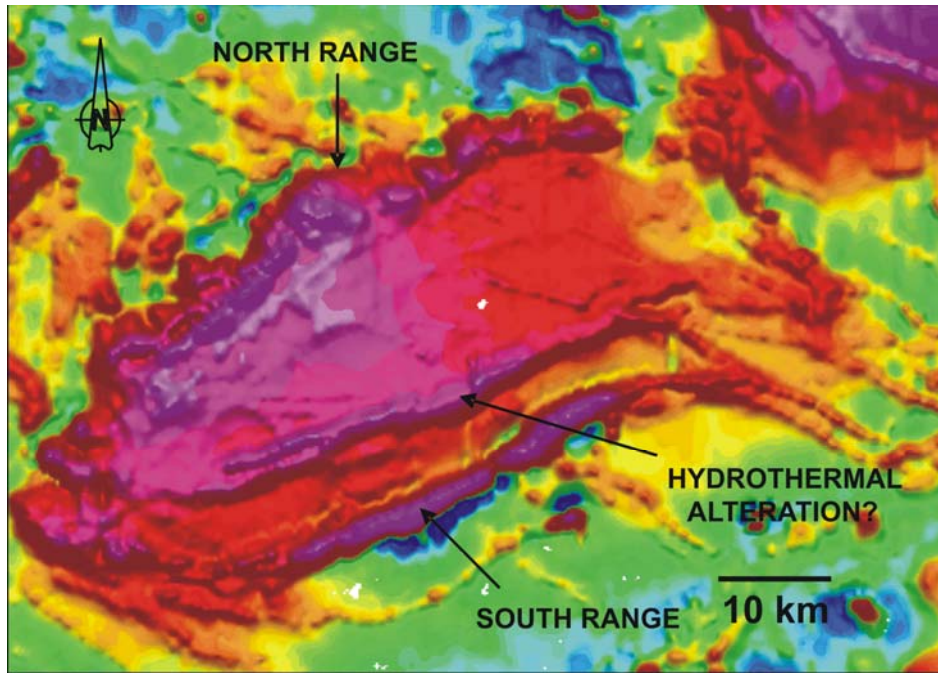


FIG. 12-1. The Sudbury Basin is outlined by this image of the total magnetic field, generated from regional government surveys. The South Range is oriented sub-vertical and produces a higher amplitude response. The western portion of the Basin is higher in amplitude than the eastern portion, the reason for which is unknown. A major magnetic linear feature extends across the center of the Basin, possibly caused by hydrothermal alteration.

within nonmagnetic quartz diorite (QD). In many cases where higher resolution magnetic field measurements have been acquired there is a good relationship between mineralization and magnetic response as long as pyrrhotite is present in significant concentrations.

Recent work by FNX Mining Company Inc. (FNX) within the Norman Offset has shown that very high PGE values are common within massive chalcopyrite veins. Surface sampling during a 2002 program, for example, encountered 15.8% Cu, 0.5% Ni, and 10.3 g.t^{-1} TPM over 18.4 ft (FNX press release, 2002). An airborne magnetic and EM survey conducted over the mineralization, known as the North Zone, showed the zone to be highly conductive but nonmagnetic (Fig. 12-2).

Further work by FNX Mining in the footwall of the McCreedy West mine intersected significant PGE mineralization known as the PM Zone. Intervals such as 1.4% Cu, 0.2% Ni, and 12.4 g.t^{-1} TPM over 30 ft were encountered within Sudbury Breccia containing only minor amounts of sulfide. Borehole magnetic and EM surveys did not outline the mineralization. A subsequent borehole IP survey detected the PM Zone but not in a diagnostic way. Non-economic sulfide at the

contact and zones of pyrite mineralization within the footwall rocks also responded strongly to the IP survey. Exploration for low-sulfide PGE-rich zones like the PM Zone is mainly geologically driven because the PGE do not appear to have a diagnostic physical property contrast.

In 2003 Wallbridge Mining Company Limited discovered the Broken Hammer Zone during a surface prospecting program. A subsequent airborne magnetic and EM survey led to the discovery of higher grade PGE mineralization toward the eastern margin of the zone (Wallbridge press release, 2004). Where PGE occur within or adjacent to chalcopyrite veins, airborne EM is proving to be an effective tool. As seen by the responses in Figures 12-3 & 12-4, the PGE zones are moderately conductive, having conductance values of 0.01–0.1 S, while the Cu-rich veins are more conductive (10–50 S) and the Ni–Cu-rich sulfide is very conductive (over 100 S).

Stevens *et al.* (2002) described the use of a cross-hole radio imaging tool to map low concentrations of sulfide near the SIC contact and within the footwall of the SIC within the Sudbury Basin. The method holds promise for areas of footwall mineralization where the sulfide is not

THE GEOPHYSICAL SIGNATURES OF PGE DEPOSITS

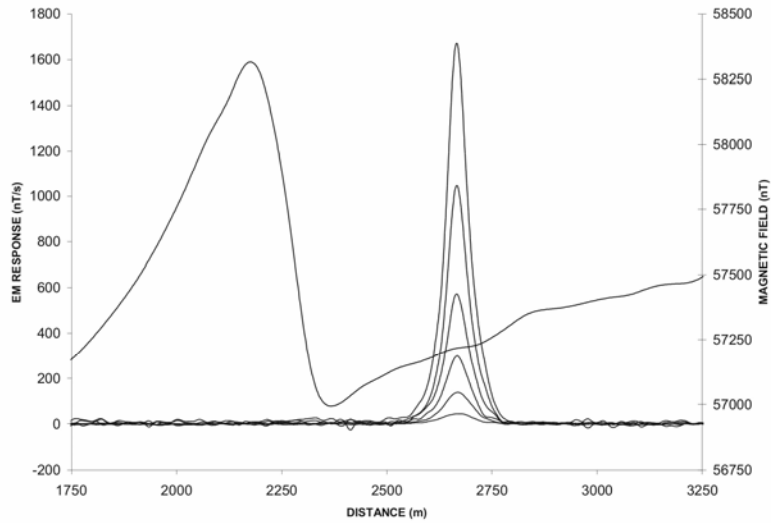


FIG. 12-2. An AeroTEM airborne EM and magnetic survey over the North Zone shows the Cu-rich mineralization to be very conductive (30 S) but non-magnetic.

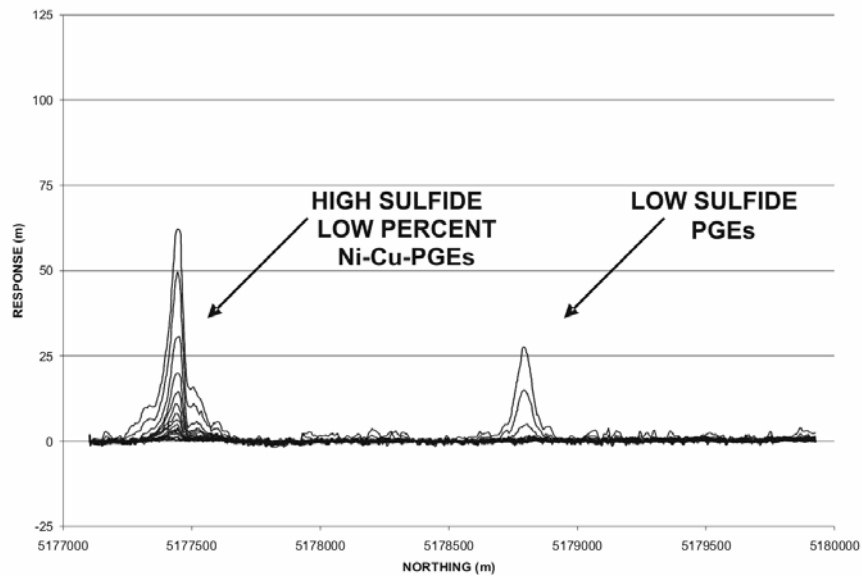


FIG. 12-3. An AeroTEM survey identifies low-grade nickel sulfide at the contact to the south and high PGE concentrations (Broken Hammer) in low sulfide to the north.

interconnected and does not respond to traditional EM methods. Subsequent radio-imaging surveys by FNX within the Levack footwall on the North Range produced images of PGE-rich mineralization that helped establish connections between widely spaced mineral intercepts defined from drillcore assays (Fig. 12-5).

The Noril'sk orebodies occur within a series of flood basalts that is now partially covered by sedimentary rocks. Recent advances in the exploration model for Noril'sk are summarized by Diakov *et al.* (2002). Ore-controlling structures such as volcanic-plutonic depressions are detected by regional magnetic and gravity surveys. The

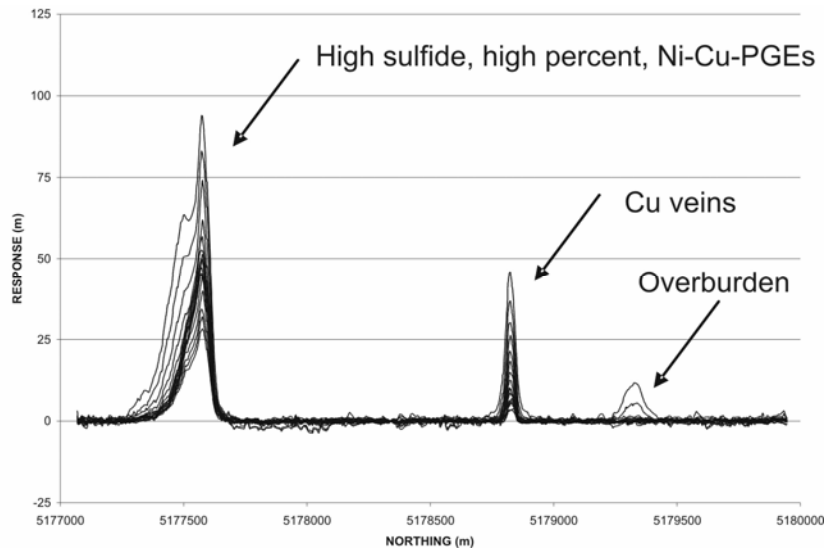


FIG 12-4. The AeroTEM survey identifies the higher grade nickel mineralization at the contact to the south, the high grade Cu-rich veins within Broken Hammer to the north, and weakly conductive overburden further to the north.

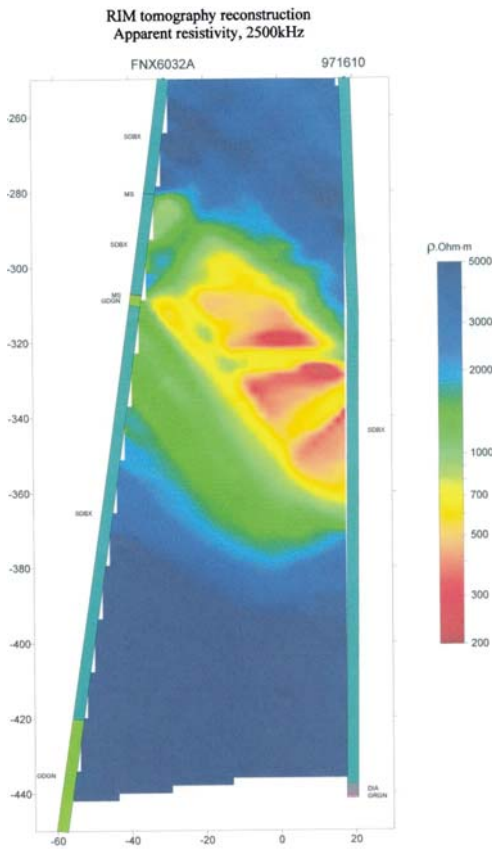


Fig. 12-5. Radio imaging tomogram from the footwall at Levack, courtesy FNX Mining Company.

strong correlation between PGE distribution and Cu and Ni grades supports the targeting of pyrrhotite sulfide within the mineralized intrusions, with massive sulfides containing the highest Ni–Cu–PGE grades.

Geophysical exploration at Noril’sk is complicated by the presence of overlying sedimentary and volcanic rocks, which can be conductive. The relatively deep nature of the deposits and the overlying conductive sedimentary rocks makes direct detection of pyrrhotite using EM methods problematic. As a result, much of the geophysics applied at Noril’sk has been magnetic, gravity and seismic.

Diakov *et al.* (2002) divided the exploration model for Noril’sk into regional scale (1:1,000,000) and mineral district scale (1:50,000). On a regional scale the magnetic method is excellent at outlining the magnetic flood basalts by their unique “etched” texture. Smoother texture magnetic highs represent magnetic sources buried below sedimentary rocks, some of which are known to be mafic intrusions. Long, linear, and narrow magnetic anomalies can represent faults, which may correspond to ancient structures that are thought to be the source of the Ni–Cu–PGE mineralization. Regional magnetic, seismic and gravity surveys have helped to define the geology better, much of which is covered by overlying sedimentary rocks.

On a mineral district scale, exploration has been heavily dependent upon drilling. Of the 300 known intrusions, only 30 have been found to be

mineralized. Borehole EM methods can be effective within the mineralized intrusions for locating the thicker massive sulfide zones.

A review of Noril'sk shows the importance of understanding the geologic setting of PGE mineralization and designing a geophysical program that is specifically tailored to that environment. At Noril'sk the massive sulfide cannot be detected directly from surface or airborne surveys. Within flood basalts elsewhere in the world, the setting is likely to be dramatically different and yet equally challenging.

Ultramafic Flows

The Ni-Cu-PGE deposits of Raglan and Kambalda, two typical examples of ultramafic flows, occur as small lenses of high-grade mineralization, often at the base of a flow. At Raglan the mineralized lenses rarely exceed 0.8 million tonnes making them relatively small targets for geophysical prospecting. The geologic setting at Raglan is very complex owing to the folding and thrust faulting of the conductive sedimentary and volcanic units. Resolution is the important factor in identifying short strike length Ni-Cu-PGE mineralization from within the large formational conductors.

At Kambalda the presence of conductive overburden reduces the effectiveness of surface and airborne EM methods that are normally the primary

tools for PGE exploration within a high sulfide environment. The Australians have put considerable effort into modifying existing EM systems to penetrate conductive cover and energize the highly conductive Ni-Cu-PGE mineralization.

Osmond *et al.* (2002) summarized the geophysical exploration strategy at Raglan. High resolution ground magnetic surveys outline the highly magnetic, serpentinized ultramafic units. Airborne and ground EM methods are selected on their ability to detect very high conductance targets within a conductive environment. For example, lower base frequencies and smaller transmitter loop footprints are common. The use of SQUID sensors in moving loop EM surveys has improved the detection of deeper targets beyond 100 m depth. The recent introduction of helicopter-borne time-domain EM (HTEM) systems has shown great promise in these complex geological environments. Figures 12-6 and 12-7 show the EM responses over the Expo Ungava and Expo North Deposits, owned by Canadian Royalties Inc. (2003) Earlier exploration in this area led to the delineation of a large low grade resource through a stratigraphic drilling program. More recent exploration, including the high resolution HTEM survey, led to the discovery of higher grade mineralization at both margins of the ultramafic sill. Drilling into the Expo North Zone, for example, encountered 2.60% Ni, 2.88% Cu and 7.45 g/t PGE over 10.0 m.

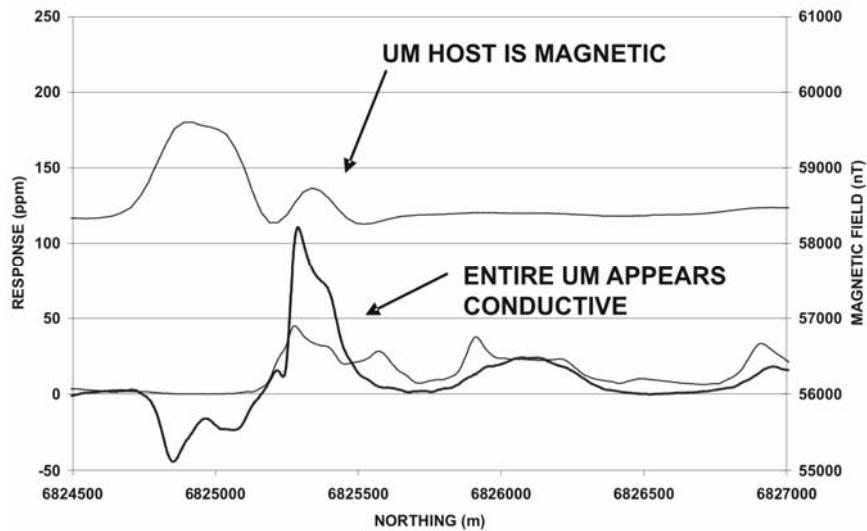


FIG. 12-6. HEM survey over Expo and Expo North, two Ni-Cu-PGE zones under exploration by owner Canadian Royalties Inc. The HEM profiles do not identify the mineralization as being more strongly concentrated along the margins of the ultramafic (UM) sill.

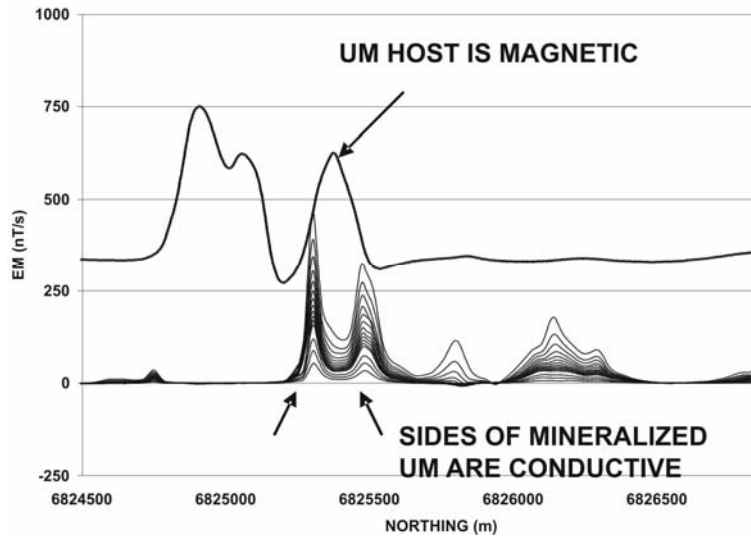


FIG. 12-7. AeroTEM survey over the Expo and Expo North Zones. The sides of the ultramafic (UM) sill are conductive while the center of the sill is not.

Emerson *et al.* (2001) discussed the conductivities of komatiitic nickel ores at Kambalda. They report conductance ranges for net-textured ores of $50\text{--}7000\text{ S.m}^{-1}$ and 135 kS.m^{-1} for massive ores. The extremely high conductance of Ni–Cu–PGE mineralization poses a problem for many EM methods, which have peak sensitivities in the range of $10\text{--}100\text{ S}$. Two metres of net-textured sulfide at Kambalda, for example, can have a conductance of $15,000\text{ S}$.

Wolfgram and Golden (2001) provided an analysis with examples of exploration for Ni sulfides over various known Australian deposits. By using lower base frequencies and having wider transmitter pulses, penetration through conductive overburden improves, making detection of discrete bedrock conductors more likely.

Large Layered Intrusions

The mafic-ultramafic portion of the Bushveld intrusion in South Africa is the largest known layered intrusion and hosts the world's largest reserves of PGE. Chromite-rich seams within the Bushveld Complex vary in thickness from a few centimetres to a few metres but extend for distances of more than 200 kilometres.

Geophysical prospecting for PGE within the Bushveld has not been widely reported, likely because a few large companies control most of the areas of favorable geology. Junior explorers have reported success with high resolution magnetometer surveys at outlining layered structures. Companies

such as Goldfields have performed a number of IP surveys. Anglo American Platinum has conducted high resolution seismic reflection surveys to aid in mine planning, particularly to define structures such as faults (Fig. 12-8). The gentle dip and layered nature of the Bushveld Complex is well-suited to seismic reflection.

The Stillwater Complex, containing the highest grades of mined PGE in the world, is a layered mafic to ultramafic complex located in the Beartooth Mountains of Montana. Mineral reserves are confined mainly to the J-M reef, which has a strike length of some 44 kilometres. Low to moderate grade Ni–Cu mineralization is common near the basal portion of the Complex. The ultramafic unit can contain high grade PGE in chromite-rich layers while the productive J-M reef is located further up stratigraphy within the Banded Series.

A high resolution magnetic and EM survey outlines the Basal Series and the Ultramafic Series. Several EM anomalies within the Basal Series suggest the presence of significant Ni–Cu sulfides. The total magnetic field shows a number of distinct linear patterns that reflect layers within the Banded Series. Analysis of the layered patterns in the HEM data has led to the identification of a volatile-enriched zone (VEZ) that has the potential to host significant PGE. The VEZ occurs at the top of the Ultramafic Series and contains graphite, disseminated sulfide and magnetite (Aurora Metals Limited news release, 2004).

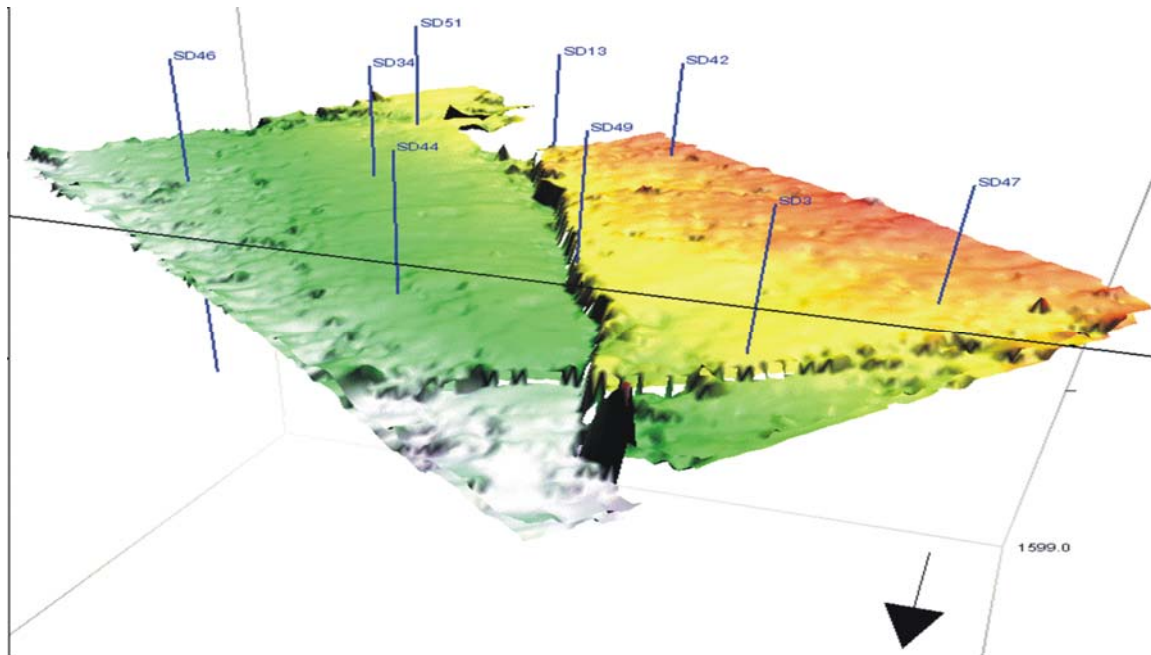


FIG. 12-8. The use of seismic reflection has helped define structural features that displace the mineralized horizon of the Bushveld Complex. Above, the method has identified a 100 m offset within a fault that was not evident in the drilling, and that will aid in mine planning.

Magmatic Intrusions

Economic concentrations of PGE can sometimes occur within magmatic intrusions, such as at Lac des Iles. The mineralization at Lac des Iles is contained within very low concentrations of sulfide, typically 2–10% pyrite where PGE concentration does not closely correlate with the amount of pyrite present. Geologically the area has been subjected to intense brecciation with much mixing of the magma. There is also considerable alteration within the ore zone (*e.g.*, serpentine and talc).

Hodges (2002) summarized the geophysical setting of Lac des Iles. The high grade mineralization occurs within a gabbro breccia adjacent to a magnetite-rich gabbro unit, and proximal to a series of iron formations containing massive magnetite. Because of its complex geologic setting, direct detection of the ore zone is not thought to be possible. The ore is situated in a magnetic low, within an area of high resistivity, which has moderate chargeability (up to 12 mV-s.V⁻¹). None of the geophysical methods on their own, magnetics, EM, or IP produce an anomalous response that outlines the mineralization.

Hodges demonstrated, however, that certain products computed from the helicopter EM

(HEM) and magnetic data can be useful in extracting useful information on a deposit scale. While the intrusions are visible in the total magnetic field (TMF) image (Fig. 12-9), the 2nd vertical derivative of the TMF reveals complex layering patterns within the Lac des Iles Gabbro that do not appear in the nearby Tib Gabbro, suggesting that the former gabbro was subject to significantly more complex magmatic processes. The calculated magnetic susceptibility map, derived from the low frequency HEM data appears to map the near-surface expressions of the ultramafic units better when compared to the TMF alone.

DISCUSSION

In resistive environments, such as the Sudbury Basin, geophysical methods are able directly to detect PGE-rich mineralization, primarily on the basis of magnetic and EM measurements. Where differentiation of the sulfide occurs, as is the case in the footwall, the ability of these methods to outline mineralization is diminished, due to the lower concentrations of pyrrhotite. The EM methods are able to identify high-grade Cu-veins that can carry PGE and that have been found to occur several hundred metres into the footwall. These veins can also have a halo of lower percent

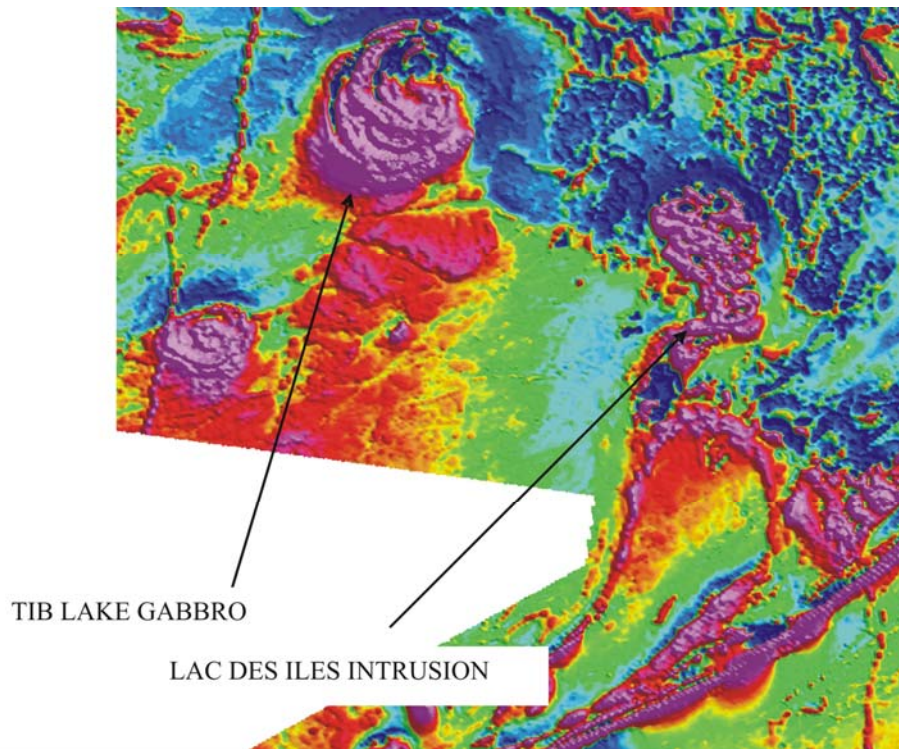


FIG. 12-9. The above image of the total magnetic field over the mineralized Lac des Iles Intrusion and the non-mineralized Tib Lake Gabbro was acquired from a high resolution HEM survey.

sulfide containing PGE in economic concentrations. EM methods that are capable of detecting low conductance targets have been proven effective in these environments as have been IP surveys. Both EM and IP are complementary in this setting with the EM survey outlining the higher sulfide concentrations and IP outlining the overall mineralized system. The combination of the two methods also reduces the chances of false IP anomalies caused by pyrite.

In more complex environments, such as Raglan, the geologic setting and the size of the targets become critical in detecting PGE-rich Ni-Cu sulfide. The high grade lenses are small and require high resolution surveys. Airborne magnetic and EM surveys offer fast and systematic coverage, while detailed ground surveys can be directed toward deeper targets.

In very complex environments, such as Noril'sk, the geologic setting takes on even greater importance. Direct detection of PGE-rich sulfide may not be possible, but by integrating different geophysical methods, host rocks can be identified, such as ultramafic and mafic intrusions, as well as the structures that may have originated or at least

concentrated the mineralization. Once inside the favorable geology, borehole EM methods are effective at focusing exploration toward the highest concentrations of sulfide, and assuming that sulfide correlates with PGE-grade, toward the highest concentrations of PGE.

The large layered intrusions are perhaps the most difficult geophysical target. The Bushveld UG2 and Merensky reefs, for example, are relatively thin units (0.5–1.5 m) and have a sub-horizontal orientation. At depth, these units have no measurable physical property contrast, other than acoustic velocity. Because high resolution seismic surveys are too expensive for typical exploration budgets they are limited to extending the resources of producing mines.

As the amount of sulfide present within PGE-rich mineralization is reduced, so too is the physical property contrast. In cases where the host rock or ore is associated with magnetite, the magnetic method then becomes the primary tool of exploration. Successful application of geophysics to PGE exploration is ultimately limited by the correlation of the associated mineral (whether sulfide or magnetite), and by the complexity of the

geologic setting. It is the knowledge of how geophysical data sets fit into a given exploration setting that is of strategic value to an exploration group, not merely the use of a specific technology.

ACKNOWLEDGEMENTS

The author gratefully acknowledges the following companies for permission to show and/or discuss geophysical results from their respective properties: FNX Mining Company Inc, Inco Limited, Canadian Royalties Inc, Wallbridge Mining Company Inc and Anglo American Platinum. Magnetic data for the Sudbury Basin and the Lac des Iles Intrusion is available from the Ontario Government.

REFERENCES

- AURORA METALS (BIV) LIMITED (2004): Stillwater Complex, Montana, U.S.A. – Platinum Group Metals and Nickel-Copper-Cobalt Minerals.
- CANADIAN ROYALTIES INC. (2003): High Grade Assays from New Expo Northeast Discovery and Mesamax Deposit, CNNMathews press release,, January 14, 2004.
- DIAKOV, S., WEST, R., SCHISSEL, D., KRIVTSOV, A., KOCHNEV-PERVOUKHOV, K. & MIGACHEV, I. (2002): Recent advances in the Noril'sk model and its application for exploration of Ni–Cu–PGE deposits. *Soc. Econ. Geol., Special Publ.* **9**, 203-226.
- EMERSON, D.W., WILLIAMS, P.K. & LUITJENS, S. (2001): The Conductivities of Komatiitic Nickel Ores at Kambalda W.A., Preview, April, p. 22-25.
- FNX MINING COMPANY LIMITED (2004): Summary of Norman Property (norman2004.pdf), www.fnxmining.com.
- HODGES, G. (2002): Application of geophysics for Lac des Iles type palladium/platinum (PGE) deposits. Ore Deposits Workshop, SEG International Exposition and 72nd Annual Meeting, Salt Lake City, Utah.
- KING, A., FULLAGAR, P.K. & LAMONTAGNE, Y. (1994): Borehole geophysics in exploration development and production. 4th Annual Can. Inst. Min. Metall, Field Conference, Sudbury, Ontario, September 1994.
- MORRISON, G.G. (1984): Morphological structures of the Sudbury Basin in relation to an impact origin. *In The Geology and Ore Deposits of the Sudbury Structure, Ont. Geol. Surv. Special Vol.* **1**, 513-520.
- NALDRETT, A.J. (1992): A model for the Ni–Cu–PGE ores of the Noril'sk region and its application to other areas of flood basalt. *Econ. Geol.* **87**, 1945-1962.
- OSMOND, R.T., WATTS, A.H., RAVENHURST, W.R., FOLEY, C.P. & LESLIE, K.E. (2002): Finding nickel from the B-field at Raglan – ‘To B or not dB’. Technical Program, Expanded Abstracts, SEG International Exposition and 72nd Annual Meeting, Salt Lake City, Utah, **1**, 404-407.
- STEVENS K., WATTS, A.H. & REDKO, G. (2002): In-mine applications of the radio-wave method in the Sudbury Igneous Complex, SEG International Exposition and 72nd Annual Meeting, Salt Lake City, Utah.
- WATTS, A.H. (1997): Exploring for Nickel in the 90's, or ‘Till Depth us do Part’, Proceedings of Exploration '97: Fourth Decennial Internat. Conf. on Mineral Expl. A.G. Gubins (ed.), 1003-1014.
- WALLBRIDGE MINING COMPANY LIMITED (2004): Wallbridge uncovers PGE-rich massive sulphide at Broken Hammer, CNW press release, June 10, 2004.
- WOLFGRAM, P. & GOLDEN, H. (2001): Airborne EM Applied to Sulfide Nickel – Examples and Analysis. *Explor. Geophys.* **32**, 136-140.

CHAPTER 13: PLATINUM GROUP ELEMENTS IN GEOCHEMICAL EXPLORATION

Eion M. Cameron
Eion Cameron Geochemical Inc., 865 Spruce Ridge Road,
Carp, Ontario, Canada, K0A 1L0
E-mail: eioncam@attglobal.net

and

Keiko H. Hattori
Department of Earth Sciences, University of Ottawa,
Ottawa, Ontario, Canada, K1N 6N5

INTRODUCTION

There are six platinum group elements (PGE): ruthenium (Ru), rhodium (Rh), palladium (Pd), osmium (Os), iridium (Ir) and platinum (Pt). The first three, the light PGE, have densities of $\sim 12 \text{ g.cm}^{-3}$, whereas the others, with densities of $\sim 22 \text{ g.cm}^{-3}$, are the heavy PGE. Osmium, Ir and Ru are refractory, with high fusion points, and tend to show compatible behavior in magmatic systems. The others, Rh, Pt and Pd, have lower fusion temperatures, and tend to show incompatible behavior in magmatic systems. In nature PGE exist as metal alloys and form compounds with S, As, Sb, Bi, Te, Sn and Hg.

Magmatic PGE deposits may be classified into several types based on a variety of criteria, but they are grouped into two in this review; sulfide-poor and sulfide-rich (Table 13-1). Important examples of sulfide-poor mineralization are at Bushveld, South Africa, and Stillwater, Montana. The second type contains sulfides, from which Ni, Cu and Co are extracted, in addition to PGE. Important deposits of this type are Noril'sk-Talnakh, Russia; Sudbury, Ontario; and Kambalda, Western Australia. Placer deposits were initially the principal source of PGE, but are of lesser importance today, and mainly produce Pt.

For geochemical exploration, the oxidation during weathering of the sulfide-rich deposits may enhance the dispersion of elements in the surface environment and the presence of Ni, Cu and Co supplement the PGE as potential indicator elements. Furthermore, sulfide-bearing ores can present a large mass with distinct physical characteristics, which are amenable to geophysical exploration.

Exploration for PGE is influenced by supply and demand for the different metals (Table 13-2). As of 2004, there is a supply deficit for Pt, with

additional metal provided from pre-existing stocks. Over the years 1994–2003 the total deficit for Pt was 71 t (Kendall 2004), which has served to increase its price; this reached \$950 per oz in April 2004. In contrast, there has been a supply surplus for Pd and Rh and declining prices. As of 2004, these factors have provided an incentive to search for Pt-rich PGE deposits. There are some industrial uses for Ir and Ru, but less than for Pt and Pd, and this is reflected in the low average prices of \$93 for Ir and \$35 for Ru in 2003.

Geochemical exploration is dependent on the availability of analytical methods that are rapid, low cost, sensitive and precise. Given the low crustal abundance of the PGE, methods must provide good precision to the part per billion levels. The development of methods has focussed on Pt and Pd, because they are the most abundant and economically significant elements of this group. Other PGE are rarely analyzed in routine surveys and data for them are scarce. PGE other than Pt and Pd are discussed only peripherally in this paper.

This paper deals with the dispersion of PGE in the surface environment and how this may be used in exploration. Another approach to exploration, litho-geochemistry, has also been used in the search for PGE and is discussed in another chapter in this volume (Maier & Barnes 2005).

BEHAVIOR OF PGE IN WEATHERING ENVIRONMENTS

In most weathering environments, there is a separation of Pt from Pd, a feature that is critical to the design of a geochemical exploration program sampling surficial materials. Platinum in minerals of magmatic origin dissolves in surface waters less

TABLE 13-1. ABUNDANCES OF PGE, AU, NI, CU AND S IN PRINCIPAL TYPES OF PGE DEPOSIT AND IN PRIMITIVE MANTLE.

Locality	Os ppb	Ir ppb	Ru ppb	Rh ppb	Pt ppb	Pd ppb	Au ppb	Ni %	Cu %	S %
Primitive Mantle ¹										
	3.4	3.2	5.0	0.9	7.1	3.9	1.0	0.196	0.03	0.03
Sulfide-Poor Mineralization										
UG2 ²	98	123	629	363	2558	1850	174	0.146	0.173	0.45
Merensky ³	63	74	430	240	3640	1530	310	0.170	0.090	0.42
Great Dyke ⁴	75	110	360	38	128	1560	21	0.141	-	0.02
Stillwater ⁵					1370	890	170	0.34	0.46	1.6
Lac des Iles ⁶	1.4	0.95	3.9	2.4	542	4740	470	0.16	0.16	0.6
Sulfide-Rich Mineralization Normalized to 100% sulfide										
Sudbury ⁷	5	8	9	19	590	511	79	3.6	2.8	
Talnakh ⁸	280	200	200	520	2350	9980	260	4.74	3.57	31.3
Lennon Shoot ⁹	357	197	365	212	1673	1899	7215	49.6	12.4	36.6
Suhanko ¹⁰	20	50	44	357	1506	11030	100	2.0	0.72	25.8
Pechenga ¹¹	64	45	112	55	359	386	12	8.9	1.94	37.4
Placer Weighted mean of cumulative production 1936 to 1972										
Goodnews Bay ¹²	Os %	Ir %	Ru %	Rh%	Pt %	Pd %	Au %			
	2.2	11.3	0.2	1.3	82.2	0.4	2.4			

¹McDonough and Sun (1995) ²UG2, Northern Limb, Bushveld Complex, von Gruenewaldt *et al.* (1989); ³Merensky, Western Limb, Bushveld Complex, Steele *et al.* (1975); ⁴Great Dyke, Zimbabwe, Sample SH2-402, Oberthür (2002); ⁵Picket Pin, west side of Contact Mountain, Stillwater Complex, Williams (1981); ⁶Average of 51 samples south Roby Zone, Lac des Iles, except for Os, Ir and Ru, average of 12, Hinchey *et al.* (2005); ⁷Weighted average of Sudbury ores, Naldrett *et al.* (1984) ⁸Talnakh massive pyrrhotite, Noril'sk, Russia, Distler (1994); ⁹Lennon Shoot, Kambalda, Australia, Cowden *et al.* (1986). ¹⁰Ahmavaara massive sulfide deposit, Suhanko, Finland, Alapieti & Lahtinen (2002); ¹¹Pechenga, Kola, Russia, Barnes *et al.* (2001); ¹²Goodnews Bay, Alaska, Mertie (1976).

readily than Pd and thus tends to be retained in clastic particles. At the Freetown Layered Complex, Sierra Leone, Bowles *et al.* (1994) reported an average Pt/Pd ratio of 1.4 for mineralized rocks, which increased to 6.0 for lateritic soils and ferricrete and to 74 for stream sediments. This separation is most obviously shown by the composition of placer deposits (Weiser 2002). More than 90% of PGM in placers are alloys of Pt-Fe and Os-Ir-Ru-Pt, the grains of which range in size from tens of μm to a few mm, although rare nuggets range up to several kg in weight. PGM in placers are of high-temperature origin derived from the erosion and weathering of mafic and ultramafic rocks (Weiser 2002). Osmium and sulfur isotope ratios of PGM in placers derived from Alpine- and Alaskan-type mafic-ultramafic intrusions are similar

to those found in the parent rocks and are homogeneous within grains, negating a supergene origin (Hattori 2002, Hattori *et al.* 2004). In 2003, the two principal placer mines of the world, Kondyor and Koryak, Russia, produced 6800 kg of Pt, but no Pd (Kendall 2004). For the Kondyor deposit, Doan and Bond (1994) estimated a grade of $1.6 \text{ g}\cdot\text{m}^{-3}$ with 84.4% Pt, 2.1% Ir, 0.6% Rh and 0.4% Pd. Cumulative production of the Goodnews Bay placer, Alaska, over 36 years comprised 82% Pt to only 0.4% Pd (Table 13-1).

In addition to Sierra Leone, lateritic weathering elsewhere in Africa has been shown to cause the separation of Pt from Pd, the Pt retained in soils and stream sediments mainly as alloys and Pd dispersed in solution. For the Main Sulphide Zone (MSZ), Great Dyke, Zimbabwe, Evans *et al.*

TABLE 13-2. SUPPLY, DEMAND AND AVERAGE PRICE IN US\$ FOR PT, PD AND RH IN 2003. FROM KENDALL (2004).

SUPPLY			
	Pt, kg	Pd, kg	Rh, kg
South Africa	145,257	71,851	16,952
Russia	32,659	91,757	4,355
North America	9,176	29,238	622
Others	9,998	7,776	467
Total Supply	194,090	200,622	22,395
DEMAND			
Auto Catalyst, Gross	99,222	107,621	20,684
Auto Catalyst, Recovery	(20,062)	(12,753)	(3,826)
Chemical	9,642	7,776	1,151
Dental	-	22,551	-
Electrical	10,575	27,838	187
Jewellery	75,894	7,776	-
Other	37,170	10,575	2,457
Total Demand	202,799	163,608	19,502
Average Price oz 2003	\$692	\$201	\$530

(1994) found that Pt sulfides and Pt–Pd–Bi tellurides predominate in fresh rock, whereas in weathered rock Pt–Fe alloys are the principal phases. There are two types of alloy, a type that appears to be of igneous origin approximates to isoferroplatinum, whereas alloys that may have formed during weathering contain significant amounts of Cu, Pd, Bi, Te, and S. The authors showed a progressive depletion of Pd relative to Pt (and Au) from weathered rock to soils to stream sediments, similar to that reported by Bowles *et al.* (1994).

In another study of the Great Dyke, Zimbabwe, Oberthür (2002) traced the relative abundance of PGM from pristine MSZ through weathered MSZ to river sediments (Fig. 13-1). There is progressive loss of Pd-bearing phases and a relative increase in Pt–Fe alloys and sperrylite. Average Pt/Pd values increase from 1.3 in the pristine MSZ to 2.4 in the weathered MSZ. Grains of Pt–Fe alloy recovered from the weathered MSZ comprise both compact and porous types. Oberthür (2002) suggested that the latter are possibly replacements of precursor PGM. In the heavy mineral concentrate (HMC) of river sediments there is partial replacement of sperrylite by Pt alloy. Most Pt–Fe grains in the HMC are compact and

chemically homogeneous, suggesting igneous origin. At the Hartley Pt mine, Oberthür *et al.* (2003) found that the Pt/Pd ratio of 1.3 for the MSZ increased to 2.0 to 2.4 in oxidized MSZ and to >10 in nearby fluvial sediments. In Madagascar soils, Salpeteur *et al.* (1995) also observed the replacement of Pt, Fe (Pd, Ni) sulfide by an alloy similar in composition to isoferroplatinum.

Although laterite environments in Africa show a strong separation of Pd from Pt, this is less marked or is absent in the laterite terrains of Australia. Examples are given in a later section showing that Pt and Pd are retained in the residual soils over mineralization and may even be enriched relative to the parent mineralized rocks. In most cases there is an increase in the Pt/Pd ratios in the weathered material but less than the African examples noted above. Laterites in Western Australia were first developed in a wet, warm to tropical climate from Cretaceous to mid-Miocene time, followed by drier climate to the present (Butt *et al.* 2001). The reason for this divergent behavior of Pt and Pd between different laterite environments is not known, although Hattori and Cameron (2004) have suggested that overall little precipitation during the development of lateritic soil likely led to little leaching of Pd in Australia.

The separation of Pd from Pt during weathering also applies to colder climates. During weathering of the PGE-enriched Cu sulfide ore at the New Rambler Mine, Wyoming, Pd has been largely removed from the oxide zone, whereas Pt

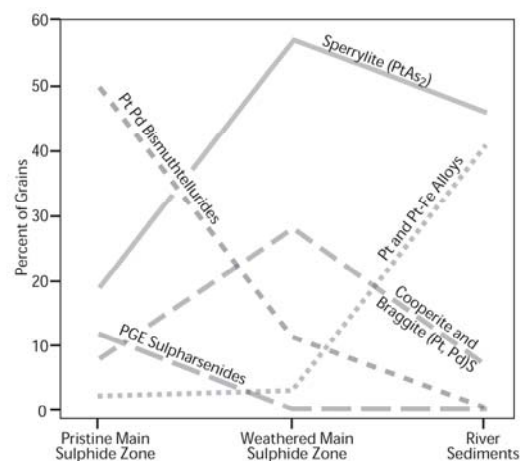


FIG. 13-1. Proportions of PGM in pristine Main Sulphide Zone, weathered Main Sulphide Zone and in river sediments, Great Dyke, Zimbabwe (Data from Oberthür 2002).

and Rh have been enriched (McCallum *et al.* 1976). In ophiolite terrain in the Shetland Islands, Scotland, Gunn (1989) noted that Pt was consistently enriched relative to Pd in stream sediment HMC, compared to bedrock. Over the same Shetland ophiolite complex, Prichard and Lord (1994) found that the Pd/Pt ratio decreases upwards in soil profiles from the mineralized bedrock interface to the surface. In soils over PGE mineralization at Ferguson Lake, NWT, Canada, Coker *et al.* (1991) found Pt more abundant in coarse fractions and HMC, whereas Pd was most abundant in fine fractions, which they attributed to clastic dispersion for Pt and hydromorphic dispersion for Pd. In soils derived from tills at the Stillwater Complex, Montana, Fuchs and Rose (1974) showed that Pt and Pd are depleted in the A-horizon relative to the B- and C-horizons and the Pd/Pt ratios are lower in the A than in the C, indicating leaching of Pd relative to Pt. Near the Lac des Iles mine, Ontario, there is loss of both Pt and Pd during conversion of C-horizon soils to B-horizon soils, but the loss of Pd is greater (Searcy 2001; Hattori and Cameron 2004).

In addition to Pt-bearing alloys, sperrylite (PtAs₂) is also found in streams in PGE-mineralized areas, including humid tropical zones, such as Madagascar (Salpeteur and Jezequel 1992). McCallum *et al.* (1976) found a greater frequency of grains of sperrylite in the oxide zone than in the underlying PGE-bearing Cu sulfide body of the New Rambler mine in Wyoming. Mountain and Wood (1988) found this mineral to be stable at the pH and *f*O₂ of typical surface waters.

MOBILITY OF PGE IN SURFACE ENVIRONMENTS

In this section emphasis is given to the dissolution of Pd in surface environments given the importance of this element in tracing PGE mineralization by hydromorphic dispersion.

In natural aqueous solutions the usual oxidation states are Pt(II) and Pd(II). Concentrations of hydrated, uncomplexed ions, Pt²⁺ and Pd²⁺, are very small in equilibrium with the metals. Significant solubility requires ligands that can form stable complexes. Pt²⁺ and Pd²⁺ ions are soft and tend to form stable complexes with soft ligands, such as HS⁻ and CN⁻, but harder ligands such as OH⁻ and carboxylic acids are also significant (Wood 2002). In saline waters, such as groundwaters in arid environments, both elements can

dissolve as chloride complexes, with the solubility of Pt favored over Pd (Williams 2001). In zones of oxidizing sulfides, thio complexes can form, but only provided that the pH is neutral to alkaline, which requires carbonate to buffer acid formed by sulfide oxidation. Most weathering regimes are not suitable for dissolution by these ligands. Near the Lac des Iles, Pd deposit, Ontario, Hattori and Cameron (2004) found that Pd migrates in solution from mineralization. Surface waters in this typical Canadian Shield environment are clear and dilute, reflecting high precipitation and low evaporation in a cool climate. Hattori and Cameron reviewed the stability constants for various Pd(II) complexes. Complexes with chloride and sulfur are unlikely to be important because most water samples contain <1 ppm Cl and <1 ppm S. The amount of PdCl⁺ is slightly less than that of Pd²⁺ considering the stability constant for complexes. Complexing with sulfate is unlikely because of low concentration of SO₄²⁻ in surface waters. This leaves hydroxide complexes as the most important inorganic species. Although there are considerable variations in the estimates of stability constants of hydroxides, the data suggest that the predominant speciation of Pd(II) in dilute surface waters is Pd(OH)₂⁰, negatively charged Pd(OH)₃⁻, or possibly Pd(OH)₄²⁻. A stability diagram after Wood and Vlassopoulos (1990) showing Pd(OH)₂⁰ as the stable phase in surface waters over a wide range of pH is shown in Figure 13-2. In contrast to the negative or neutral charge of the predominant hydroxide species of Pd(II), Azaroual *et al.* (2001) found that for waters with pH <9, and in the absence of other strong ligands, Pt(OH)⁺, was the principal species.

Most metals, such as Cu, Ni, Zn, dissolve as simple cations in dilute surface waters. These tend to be adsorbed and fixed by negatively charged iron oxyhydroxides as are found in B-horizon soils and as coatings on grains in stream sediments. Given that Pd is transported as neutral or negatively charged complexes, it will not be fixed by iron oxyhydroxides and will not tend to accumulate in B-horizon soils (Hattori and Cameron 2004).

Wood (1990), Wood *et al.* (1994) and Bowles *et al.* (1995) have shown that Pt and Pd can dissolve in solutions containing fulvic, humic and other organic acids. For Pd, in addition to hydroxy complexes, there are soluble organic complexes with humic acid, fulvic acid, amino acid, acetate and oxalate (Li & Byrne 1990, Wood 2002).

g sub-samples were taken for analysis. To an even greater extent than other types of geochemical survey, the collection of replicate stream sediment samples is required, from which sampling and analytical precision are estimated (see discussion on quality control in a later section). Composite samples will also improve reproducibility, taking sediment at several locations along, *e.g.*, a 10 or 25 m length of stream.

Glacial Till and Derived Soils

Cook and Fletcher (1993, 1994) carried out comprehensive studies of the distribution of Pt in soils of the Tulameen Alaskan-type ultramafic-mafic complex, southern British Columbia. The principal PGM in the rocks are alloys, Pt_2Fe_2 and Pt_3Fe , and tulameenite (Pt_2FeCu). Platinum has been produced from nearby placers. The area was glaciated and rocks have a thin cover of till on which immature soils have developed. Figure 13-3

shows Pt analyses for a soil profile in till over mineralized dunite. The results could suggest that Pt has been removed from the A- and B-horizons during their development from C-horizon parent material. However, Cook and Fletcher found that the soils comprising this profile are of mixed origins. The A- and B-horizons are composed of exotic, non-ultramafic material and it is only in the C-horizon that material from the underlying mineralized dunite was incorporated. In the C-horizon, the highest contents of Pt are in the coarsest fraction, -10 to +40 mesh, indicative of a local source. The highest concentration of Pt occurs in the magnetic heavy minerals, which contains chromite as well as magnetite. In other samples of dunitic till the differences between the Pt contents of the different size fractions are not as pronounced. Elsewhere in the area, where colluvial soils were derived from mineralized rock, the upper, colluvial soil horizons can have a higher content of Pt. This study shows the difficulty in interpreting data for PGE in soils where there are multiple sources for till and where high relief has caused colluvial movement of soil. For routine exploration Cook and Fletcher recommend separation and analysis of the magnetic HMC of C-horizon soils.

Coker *et al.* (1991) examined PGE distributions in soils at Ferguson Lake, Northwest Territories, Canada, and at Rottenstone, Saskatchewan. At Ferguson Lake PGE-bearing Cu-Ni sulfides are present in hornblendite. There is a thin till cover and spectacular gossans over the sulfide mineralization. The area is within the zone of continuous permafrost. Grab samples of gossanous rock contained up to 590 ppb Pt and 2500 ppb Pd. An earlier study of gossanous soils by DiLabio (1988) showed that Pd was present in the finer size fractions, whereas Pt was erratically distributed due to the nugget effect. Similar results were obtained by Coker *et al.* (1991) who found that Pt was most abundant in the HMC and coarser soil fractions, suggesting clastic dispersion, whereas Pd was most abundant in the fine fractions, suggesting hydromorphic dispersion. High contents of Pt were found in the gossanous soils, up to 1000 ppb Pt in the -180 and -63 μm soil fractions and close to 10 ppm Pt in the HMC. For Pd, several thousand ppb were found in the HMC and in all but the coarsest size fraction of soil, 2 to 6 mm. Despite these high values near source, the down-ice dispersion of anomalous values is limited to 100 to 200 m. This dispersion pattern was determined from bulk analysis of the -63 μm fraction, since it proved

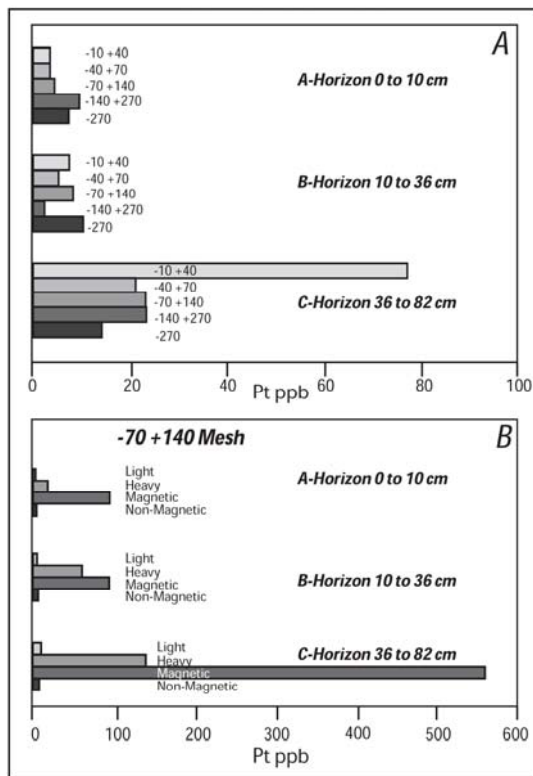


FIG. 13-3. Distribution of Pt in a profile of till soil at Tulameen complex, British Columbia. A shows distribution in different ASTM size fractions; B shows distribution in light, heavy, magnetic heavy and non-magnetic heavy components of -70 +40 mesh sieved soil. Modified from Cook and Fletcher (1994).

too difficult to extract sufficient HMC from non-gossanous tills.

The Rottenstone deposit is a small Ni–Cu deposit, but was a rich producer of PGE with 4.8 ppm Pt and 3.9 ppm Pd. On bedrock ridges there is a thin cover of till and in lower areas till interfingers with glaciofluvial and glaciolacustrine sediments. Anomalous concentrations of Pt, to 4500 ppb, along with up to 435 ppb Au were found in the HMC from tills and anomalous values for Pt extend to the limit of the survey, 1 km down-ice from the mineralization. This indicates clastic dispersion of Pt-rich grains by glacial action. The results for sieved fractions of the tills and soils were disappointing, the highest values for Pd being 6 to 31 ppb in samples from which the HMC gave results in the range 350 to 4500 ppb Pt.

The two studies by Coker and colleagues show that where there has been significant down-ice dispersion of mineralized material, as at Rottenstone, Pt in the HMC is an effective exploration tool. Where dispersion has been poor, as at Ferguson Lake, HMC are limited in amount and geochemical anomalies of any type only occur close to the mineralized body.

Based on Hydromorphic Dispersion

Organic Trapping of Pd along Drainage Courses
Palladium can be dispersed in solution along drainages as neutral or negatively charged hydroxide species or as organic complexes. These forms are not precipitated by negatively charged Fe oxyhydroxide colloids and coatings as are trace metal cations, but may be precipitated in organic traps. At the Tulameen complex, British Columbia, Cook and Fletcher (1993) found that the upper humic layer of soil mostly contained less Pt than the associated C-horizon. In seepage areas and downslope from Pt mineralization the humus gave higher Pt values. This suggests the hydromorphic transportation of Pt and fixing by organic material.

Hattori and Cameron (2004) focussed on organic trapping of Pd at the Baker Zone, an undeveloped body of PGE mineralization east of the main ore zone of the Lac des Isles Pd mine, Ontario. The Baker Zone lies on the slope above a small lake, Shorty Lake. Searcy (2001) collected C- and B-horizon soils over and peripheral to the Baker Zone. These were analyzed for Pt and Pd by fire assay–ICP–AES. The C-horizon soils represent

minimally weathered rock fragments, which have been dispersed as till down-ice to the southwest of the mineralization. Soil-forming processes involved in the conversion of C-horizon to B-horizon soils have caused a decrease in both Pt and Pd (Fig. 13-4).

Hattori and Cameron (2004) collected black peaty humic material underlying moss in swamps that border the lake on all sides (Fig. 13-5). Water in the swamps is from runoff from the higher ground surrounding the lake and from the lake itself, particularly at the southern end, where the water drains out through a boulder field covered by humus and moss. Analyses of the humus for Pd and Pt were by fire assay–ICP–MS. Palladium is greatly enriched in the swamp humus, compared to the C- and B-horizon soils, whereas Pt is depleted (Fig. 13-4). Plots of Pd and Pt (Fig. 13-5) show that high Pd values in the swamp humus are mainly at the base of the slope beneath the Baker Zone and in the area south of the lake that is saturated by lake water. Lake sediments collected at locations LS1 and LS2 (Fig. 13-5) were taken from two depths: 0 to 15 cm and 20 to 50 cm. The shallow samples contain 10 ppb Pd and 2 ppb Pt (LS1) and 14 ppb Pd and 2 ppb Pt (LS2), and the deeper samples 15 ppb Pd and 2 ppb Pt (LS2) and 10 ppb Pd and 1.4 ppb Pt, (LS2). For Pd these values are well above the regional median for lake sediments of 4.8 ppb, whereas the Pt values are similar to the regional median of 1.6 ppb Pt. The data from both the swamp humus samples and the lake sediments are consistent with precipitation of dissolved Pd derived from the upslope mineralization. The Pd contents of the shallow and deep lake sediments are similar, indicating a long-term flux of Pd into the lake. As described later, the bark of spruce trees growing along the edge of the lake is strongly anomalous in Pd.

Fortescue *et al.* (1987) collected 23 humus samples along a traverse of 200 m length over the main (Roby) ore zone at the Lac des Isles deposit and found a single high Pd value (330 ppb) directly above the mineralization, which was undeveloped at the time. This type of humus, “forest humus” is derived from the decomposition of leaf litter, rather than the moss that is the parent of the swamp humus. Significantly, they found high Pd values from three humus samples overlying barren granite, but downslope from the mineralization.

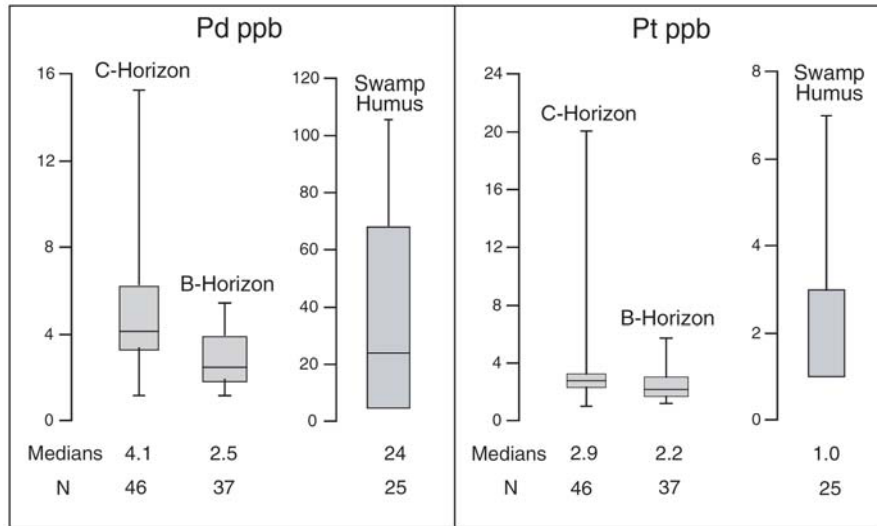


FIG. 13-4. For the Baker Zone - Shorty Lake area, box-whisker plots of B- and C-horizon soils from Searcy (2001) and swamp humus. From Hattori and Cameron (2004).

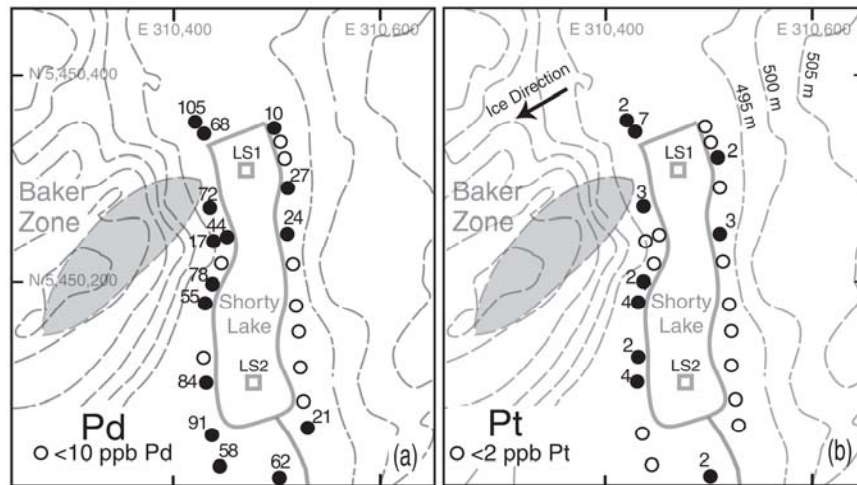


FIG. 13-5. Map of the Baker Zone and Shorty Lake showing the distribution of Pd and Pt in samples of "swamp humus" taken around the edge of the lake. Also shown are the lake sediment sampling sites LS1 and LS2. From Hattori and Cameron (2004).

Biogeochemistry

The practical application of biogeochemistry to PGE exploration was previously hindered by their low abundance. It was necessary to collect a large sample of vegetation to provide 10 g of ash for analysis (Dunn 1992). Hall *et al.* (1990) developed a method using a HF-aqua regia decomposition, followed by co-precipitation of noble metals on Te, then analysis by ICP-MS. This provides 1 to 2 ppb detection limits for Au, Pt and Pb on 1 g of ash, which requires the collection of *ca.* 50 g of dry twigs.

In an earlier section we described results obtained by Coker *et al.* (1991) on soils from Ferguson Lake, Northwest Territories. Biogeochemical studies were also carried out, collecting leaf and twig samples from dwarf birch and Labrador tea. Both species are common throughout the area and can bio-accumulate Pt and Pd (Table 13-3), with higher concentrations in the birch and in the twigs of both species. Anomalous values in these plants were found directly over the gossans and for a limited distance of a few hundred metres down-ice, corresponding to anomalies

PLATINUM GROUP ELEMENTS IN GEOCHEMICAL EXPLORATION

TABLE 13-3. CONCENTRATION OF PT AND PD IN ASH OF DWARF BIRCH AND LABRADOR TEA, FERGUSON LAKE AREA, NORTHWEST TERRITORIES.

	Pt ppb in ash			Pd ppb in ash		
	Min	Med	Max	Min	Med	Max
Dwarf Birch						
Leaf, gossan (24)	2.6	188	226	30.8	471	509
Twig, gossan (26)	4.3	1011	1350	52.9	1980	3071
Leaf, background (10)	2.1	2.7	3.8	2.3	7.6	11.2
Twig, background (10)	0.4	2.8	4.1	4.3	10.9	14.8
Labrador Tea						
Leaf, gossan (22)	6.1	45.2	52.4	99.0	1001	1688
Twig, gossan (24)	4.9	47.1	59.0	68.4	1949	2322
Leaf, background (10)	2.4	4.2	7.0	11.0	17.2	21.7
Twig, background (10)	0.9	3.5	9.1	4.1	19.4	28.7

Min = minimum, Med = median, Max = maximum, numbers in brackets = number of samples. From Coker *et al.* (1991).

identified by analysis in the $-63 \mu\text{m}$ fraction of the till. Rencz and Hall (1992) carried out further studies at Ferguson Lake, again using Labrador tea and dwarf birch. There were strong anomalies for Pt, Pd and Rh over the gossans, with Pd showing the greatest contrast in dwarf birch, a maximum of 4000 ppb over the gossans to background of 8.5 ppb. But anomaly dispersion down-ice was limited.

Following up on earlier work by Dunn (1986), Coker *et al.* (1991) carried out biogeochemical studies at the Rottenstone mine, Saskatchewan. A variety of vegetation was sampled and analyzed during an orientation survey (Table 13-4). The results show considerable variation between different types of plant tissues, with black spruce twigs and outer bark containing the most Pt and Pd. This prompted the selection of spruce twigs for a survey of the area. There is moderate to strong Pt and Pd enrichment for less than 200 m down-ice and weak enrichment in Pd farther away, but less than the 1 km dispersion for Pt in HMC. The authors noted that Pd is detectable in only some of the soils, is absent in the tills and HMC, yet is enriched in the spruce twigs. Their inference is that dissolved Pd is adsorbed to only a slight degree in the soil, but is being taken up by plant roots.

If dissolved Pd is dispersed away from mineralization, then analysis of vegetation may identify its distal presence. At the Shorty Lake

TABLE 13-4. CONCENTRATION OF PT AND PD IN ASH OF A VARIETY OF VEGETATION, FROM CLOSE TO THE OLD MINE SITE AT ROTTENSTONE LAKE, SASKATCHEWAN.

Sample Medium	Pt ppb in ash	Pd ppb in ash	Ash %
Black spruce twigs	800	1443	2.2
Black spruce outer bark	1187	1662	3.8
Black spruce inner bark	126	212	3.4
Black spruce needles	83	244	4.0
Black spruce trunk wood	89	70	0.4
Birch twigs	125	306	1.0
Birch leaves	87	326	4.0
Birch trunk wood	10	45	0.5
Alder twigs	62	170	1.1
Alder leaves	35	158	4.4
Willow twigs	16	74	1.4
Labrador tea twigs	166	368	2.0
Labrador tea leaves	279	499	3.9
Marsh grass	18	30	6.5
Background levels	<5	<2	

From Coker *et al.* (1991).

sampling site (Fig. 13-5) we have collected and analyzed bark from mature black spruce growing at the edge of the lake. For ash from samples of 8 trees the range and average concentration was 16 to 708 and 307 ppb Pd and 18 to 129 and 45 ppb Pt (Hattori and Cameron, unpublished results). This data from organic lake sediments, swamp humus and vegetation at Shorty Lake provide a consistent picture of the fixing of Pd dispersed in solution from mineralization by organic material.

Dunn (1992) provided a comprehensive review of biogeochemical methods for Au, Pt and Pd, including surveys for Pt and Pd over the Duluth Complex, Minnesota, the Stillwater Complex, Montana and the Tulameen Complex, British Columbia.

Palladium and Platinum in Waters

As might be expected from low crustal abundances, the amounts of these elements in surface waters are low, in the $\text{ng}\cdot\text{L}^{-1}$ = parts per trillion range (ppt). Most analytical methods require a concentration stage, for example by evaporation or adsorption on activated carbon or resin, prior to measurement by ICP-MS. This increases the time and cost of the analyses, lessening the practical application of the methods. Because of the low concentration in waters, isobaric interference from other constituents in the waters is a serious issue. For example, ^{40}Ar , ^{65}Cu and $^{88}\text{Sr}^{16}\text{OH}$ are isobaric with ^{105}Pd . Evaporation alone does not resolve the issue, since the interfering species increase in concentration along with Pd and Pt. Thus separation of the PGE from interfering elements by adsorption on activated carbon (Hall and Pelchat 1993), Te-co-precipitation (Cook *et al.* 1992), or the use of ion exchange resins (Hattori and Cameron, unpublished work) have been used.

A further problem is the adsorption of Pd, Pt and Au onto the walls of the sample container (Chao *et al.* 1968, Samiullah 1985). Coker *et al.* (1991) reported that ~80% of metals is lost from dilute natural water samples within 20 days. Metals lost cannot be fully recovered from the walls by leaching with $\text{Br}_2\text{-HCl}$, which is effective in recovering Au (Hall *et al.* 1996). Cook *et al.* (1992) showed that only 12% Pd but 62% Pt was recovered when 50 ppt of each metal was kept in distilled water for 7–10 days and only an additional 10% Pd was recovered by extracting the container walls with 10% HCl and 5% HNO_3 . The best recoveries of 75% Pd and 69% Pt were obtained when the metals were kept in a 20% HCl + HNO_3 solution.

Coker *et al.* (1991), who used activated charcoal for preconcentration of Pt and Pd, reported 2.8 ppt Pt and 2.0 ppt Pd in waters adjacent to gossanous zones at Ferguson Lake, Northwest Territories, but background levels of 0.2 ppt were measured just a few metres away. The Pt and Pd were separated using activated charcoal. A similar method was used by Cook *et al.* (1993) for water samples from the Tulameen Complex, British Columbia. Stream waters averaged 0.81 ppt Pt; water from seepage zones, 1.05 ppt Pt; and water from plateau bogs on dunitic till 2.45 ppt Pt. Hattori and Cameron (submitted) found up to 18 ppt Pd and 1 ppt Pt in waters draining from the Baker Zone of the Lac des Iles Pd mine. Background values in the area are ~1 ppt Pd and ~0.1 ppt Pt. Evaporation plus ion exchange resins were used to concentrate and separate the PGE.

Wood and Vlassopoulos (1990) and Cook *et al.* (1992) reported much higher values from Lac Sheen and Lac Long, Quebec, near PGE-bearing Ni sulfide mineralization. For filtered Lac Sheen waters the 1990 study reported an average of 158 ppt Pd and filtered Lac Long waters averaged 262 ppt Pd. For Pt, most lake waters were below the detection limit of 25 ppt. Analysis was by ICP-MS, preceded by evaporation of 1 L of water to 25 mL. There was no separation of PGE from the other dissolved constituents. Cook *et al.* (1992) evaporated 2 L samples and then separated the PGE and Au from the other constituents by a Te co-precipitation. They found that Pt contents in the Lac Sheen waters were generally below the detection limit of 10 ppt, but ranged up to 147 ppt in filtered waters. There were greater concentrations of Pd, but the results were inconsistent for different sampling periods, an average of 23 ppt in June, 26 ppt in August and 107 ppt in November. Possible analytical problems are suggested by higher values for filtered samples than unfiltered samples.

Based on both Clastic and Hydromorphic Dispersion

Lake Sediments

Lake sediments are used as sample media for exploration mainly in the glaciated Canadian and Fennoscandian Shield areas, where there is a high density of small lakes. Lake sediments consist of clastic particles from till and bedrock, precipitated Fe-, Al- and Mn-oxyhydroxides, and organic material. The concentrations of Pt, Pd and Au in lake sediments around a PGE-bearing Ni sulfide prospect at Lac Sheen, Quebec, were examined by

Wood and Vlassopoulos (1990) and Cook *et al.* (1992). This was combined with related studies of waters, soils and rocks. Values up to 38 ppb Pd and 122 ppb Pt were found in the lake sediments.

A reconnaissance survey of lake sediments over a large area west of Lake Nipigon, Ontario, in the Canadian Shield, was conducted by Dyer and Russell (2002) (Fig. 13-6). The eastern portion of their survey area is mainly overlain by Proterozoic Nipigon diabase sills that are emplaced during the Mid-Continental Rift and are known to contain exceptionally high concentrations of Pt and Pd as basaltic rocks, over 10 and 15 ppb, respectively (Cameron and Hattori 2003). Mafic intrusions associated with these dykes, such as the Duluth and Coldwell complexes, host significant PGE mineralization. The western part of the area is mainly Archean and includes the Lac des Iles Pd mine in an Archean mafic-ultramafic complex (Fig. 13-6). A total of 2258 centre lake sediment samples were collected and analyzed for a wide range of elements, including Pt and Pd by fire assay-ICP-MS. The median contents of the 2258 samples are 1.6 ppb Pt and 4.8 ppb Pd.

Cameron and Hattori (2003) examined the Pd lake sediment anomalies in a portion of the Dyer and Russell survey area that includes the Lac des Iles mine (Figs. 13-6 and 13-7). There are strong Pd anomalies throughout this area (Fig. 13-7A), but for

most of the anomalies there is no known PGE mineralization in the vicinity. Moreover, the Pd anomaly associated with the Lac des Iles Pd deposit is not among the strongest. To explain this contradiction, data for ten elements most closely associated with PGE mineralization were treated by factor analysis. The three most important factors are shown in Table 13-5 and the scores for Factors 1 and 2 are plotted in Figure 13-7B and Figure 13-7C. Factor 1, comprising, Co, Cr, Ni, Pt and Pd, is interpreted to represent the dispersion of predominantly clastic material of mafic/ultramafic origin. The clastic material was initially dispersed as till by the ice sheet moving south-westwards, then washed into lakes to form sediment. The strongest Factor 1 anomaly lies directly down-ice from the Lac des Iles deposit. Another strong anomaly is near Dog Lake. Bedrock around Dog Lake is largely concealed beneath Quaternary cover and has been mapped as granitic. However, there are aeromagnetic anomalies and drilling has intersected pyroxenite, sheared serpentinite and minor sulfide with anomalous values for PGE.

Factor 2 is interpreted as hydromorphic dispersion and precipitation of Pd, S and As. This factor shows a close spatial correlation with glaciofluvial deposits, notably eskers that contain abundant boulders of Nipigon diabase and reddish sedimentary rocks of the Proterozoic Sibley Group,

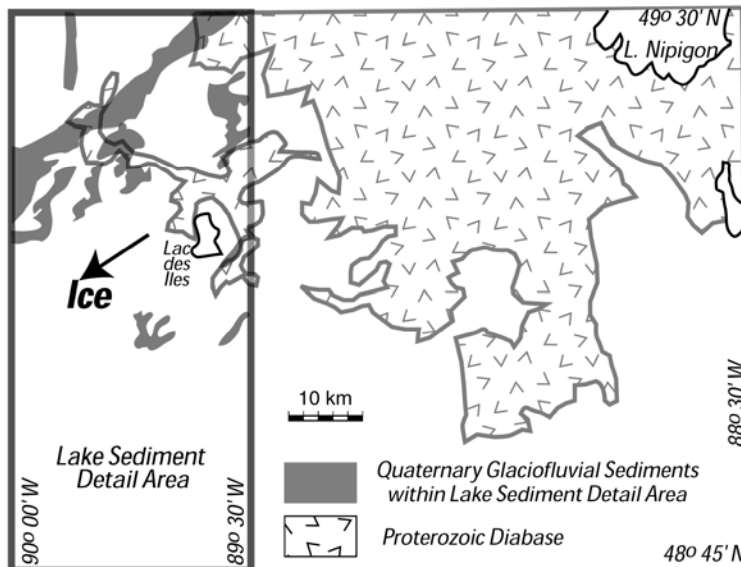


FIG. 13-6. Lake sediment survey area of Dyer and Russell (2002) lying east of 90°W. The detail area between 89°30' and 90°00' is described in text and shown in Figure 13-7.

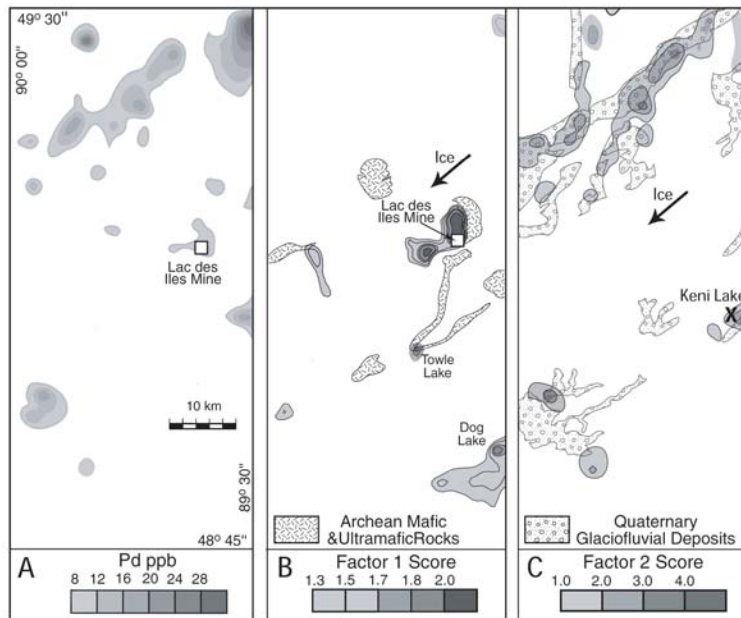


FIG. 13-7. Maps of the lake sediment survey area between 89° 30' and 90° 00'. A: Contours of Pd in lake sediments. B: Contours of scores for Factor 1 and the distribution of mafic and ultramafic rocks; C: Contours of scores for Factor 2 and the distribution of Quaternary glaciofluvial deposits, from Mollard (1979a, 1979b). Arrows indicate predominant ice direction.

TABLE 13-5. FACTOR ANALYSIS OF 675 LAKE SEDIMENT SAMPLES FOR THE TEN ELEMENTS MOST CLOSELY ASSOCIATED WITH PGE MINERALIZATION.

Element	Factor 1	Factor 2	Factor 3
Co	0.87	0.06	0.08
Cr	0.87	-0.03	0.21
Ni	0.82	0.09	0.33
Pt	0.78	0.21	0.25
Pd	0.51	0.64	0.36
S	-0.27	0.83	0.22
As	0.36	0.82	-0.22
Cu	0.23	0.33	0.86
Ag	0.15	-0.08	0.85
Au	0.38	0.04	0.50

Shown is the Varimax rotated matrix for the 3 principal component factors with eigenvalues great than 1. Data logarithmically transformed prior to analysis. Shown in bold are loadings of 0.50 or greater, which represent 25 % or more of the total variance of the element.

which outcrop east and up-ice from the area shown in Figure 13-7. Many of the boulders are thoroughly weathered and disintegrated. Two of the least weathered boulders of Nipigon diabase were analyzed; they contain 15 and 20 ppb Pd and 12 and 12 ppb Pt, substantially higher than mantle peridotite. The Sibley Group contains abundant sulfate minerals of evaporitic origin and veins with high As. Thus the source of Pd is interpreted to be boulders and finer fragments of weathered Nipigon diabase, whereas As and S come from boulders and fragments of the Sibley Group. Groundwaters leach these elements from the disintegrating boulders in the permeable eskers. The Factor 2 Pd anomalies can be classed as “false anomalies” that derive from the ready mobility of Pd in the surface environment and a source of PGE within a highly permeable aquifer. Factor 3 anomalies, which directly overlie outcrops of Nipissing diabase, were not investigated.

**Based on Residual Accumulations
Laterite Soils and Gossans**

In parts of Australia, lateritic soils may extend to 100 m depth, presenting a formidable challenge to exploration. Western Australia’s first Ni deposit at Kambalda was discovered by identifying gossanous outcrops containing 1% Ni and 0.3% Cu. Repeating

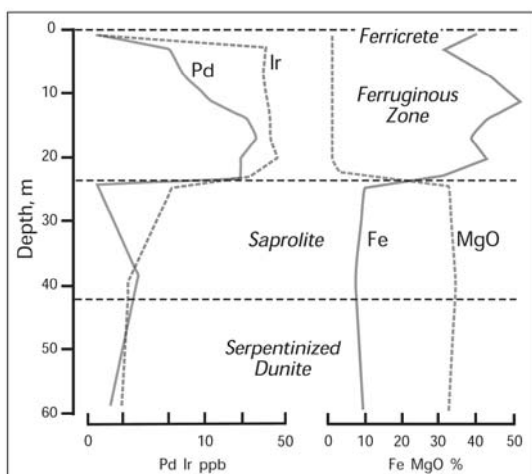


FIG. 13-8. Distribution of Ir, Pd, Fe and MgO in a lateritic profile over serpentized dunite, Gilgarna Rocks, Western Australia. Modified from Travis *et al.* (1976).

this success proved difficult because other gossans of similar appearance and Ni and Cu contents were found to overlie barren sulfides. Travis *et al.* (1976) discovered that Pd and Ir present in Ni-Cu sulfide bodies were retained in the upper ferruginous zone of the laterite (Pt was not measured). A profile (Fig. 13-8) shows the distribution of Pd and Ir and the major constituents Fe and MgO through the laterite profile. Pd is more abundant than Ir in the primary sulfides of the area, but the Pd/Ir ratio is decreased in the ferruginous laterite implying that Ir is less easily lost during lateritization.

A later study by Moeskops (1977) showed the depletion of Pt and Pd in gossans, with median

contents for both Pt and Pd of 1500 ppb, compared to median values for the Ni sulfide ores of 4500 ppb Pt and 7000 ppb Pd. Nevertheless, the contents of Pt and Pd in the gossans formed from PGE-rich rocks are distinctively different from barren gossans, the latter with values below the detection limits of 200 ppb. Taufen and Marchetto (1989) calculated the enrichment/depletion of elements in the gossan overlying Ni mineralization in Minas Gerais, Brazil; -84% for Cu, -70% for Co, -37% for Cu, -33% for Pd, -22% for Pt, -9% for Ru, +35% for Ir, and +37% for Rh.

Other studies in Western Australia have confirmed that PGE reach maximum values in the ferruginous zone at the top of the laterite profile. For soils developed on peridotite of the Ora Banda sill, Western Australia, Gray *et al.* (1996) showed maximum amounts of PGE in this ferruginous zone, rich in goethite and hematite (Fig 13-9). The enrichment factors of three to five times for PGE are comparable to those for insoluble Cr and Zr, indicating that the enrichment is due to the volume reduction of the rocks during the weathering and that the PGE were retained in the horizon during the weathering.

Near to Ora Banda is a similar PGE-mineralized ultramafic prospect, Mt. Carnage, on which laterites are developed. Butt *et al.* (2001) provided data on all of the PGE that enables comparisons to be made between the upper ferruginous zone and the underlying saprolite (Table 13-6). The results show that Pt is most enriched in the ferruginous zone relative to the saprolite.

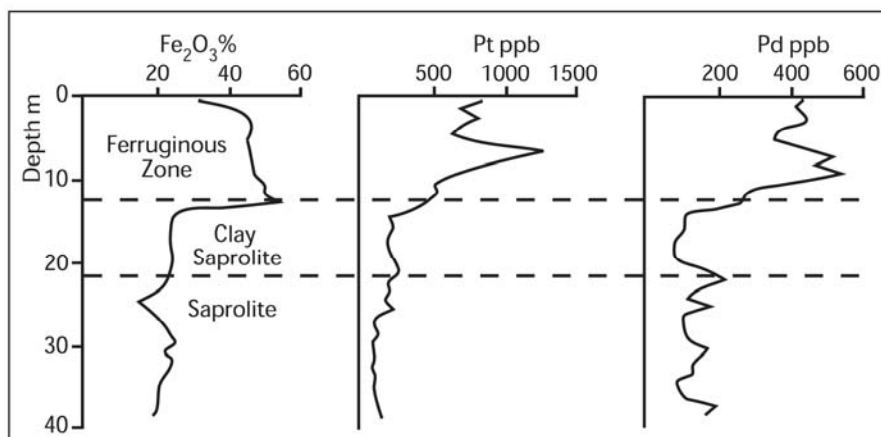


FIG. 13-9. Distribution of Fe, Pt and Pd in a lateritic profile over the Ora Banda ultramafic sill, Western Australia. Modified from Gray *et al.* (1996).

TABLE 13-6. ABUNDANCES OF ALL PGE IN THE UPPER FERRUGINOUS ZONE AND THE UNDERLYING SAPROLITE OF LATERITE OVERLYING MINERALIZED ULTRAMAFIC ROCKS, MT. CARNAGE, WESTERN AUSTRALIA.

Depth m	Pt ppb	Pd ppb	Ru ppb	Rh ppb	Os ppb	Ir ppb
Ferruginous Layer						
1	820	480	18	43	<2	12
3	780	450	22	54	<2	16
5	66	400	16	40	<2	12
7	1300	460	24	60	<2	<2
9	880	500	18	47	<2	16
11	490	440	14	33	<2	10
Average Ferruginous	723	455	19	46	1	11
Saprolite						
15	175	112	8	13	<2	6
19	195	88	8	12	8	4
23	180	215	16	26	<2	4
27	86	96	14	10	<2	4
31	94	160	14	16	8	4
35	96	94	14	12	<2	<2
39	140	170	12	10	8	4
Average Saprolite	138	134	12	14	4	4
Average Ferr./ Average Sap.	5.2	3.4	1.5	3.3	0.25	2.8

Data from Butt *et al.* (2001). Note that for some samples the Os and Ir abundances are at or below the detection limits of 2 ppb. For these samples a value of 1 ppb has been used to compute averages.

An alternative to laterite soil sampling was investigated at Ora Banda (Butt *et al.* 2001). This is to sample the surface lag, which is a cover of gravel derived from the underlying duricrust and laterite. Wind and water have removed the finer fraction. At Ora Banda the Pt and Pd contents of the lag clearly indicate the enrichment of these elements in the laterite overlying the mineralized pyroxenite.

An enrichment of Pt and Pd, along with Ni, Cu and Cr, is found in ferruginous saprolite at the top of a 80 m thick regolith over an ultramafic-hosted Ni sulfide deposit at Mt. Keith, Western Australia (Brand & Butt 2001). In this case the enriched saprolite is covered by 40 m of exotic sediment containing minimal PGE. Lateral dispersion of the PGE in this environment is limited, contrasting with the widespread dispersion of Au. Data for Pt, Pd, Cu and Ni in the profile below the exotic cover is given in Table 13-7. Relative to the sulfide-bearing primary zone, the

ferruginous zone is enriched in all elements and particularly within a manganiferous sub-zone at the base of the ferruginous zone. The ratios indicate that Pt and Ni are enriched to approximately the same extent and there is minor loss of Pd and Cu.

These examples from Western Australia and Brazil show that Pt and Pd are mostly retained or even enriched in the upper ferruginous zones of lateritic soils and gossans and can effectively serve to identify underlying PGE-bearing mineralization. In some cases, *e.g.*, Mount Keith and Kambalda, Ni and Cu are also retained, but in other cases, Ora Banda and Minas Gerais, one or both of Ni and Cu are depleted in the ferruginous zone. Iridium and Rh may be retained or enriched to a greater extent than Pt and Pd.

The Western Australia examples represent old, mature laterite terrain. Elsewhere, different results have been obtained. In Madagascar, Salpeteur *et al.* (1995) describe an earlier stage in

TABLE 13-7. DISTRIBUTION OF MEAN CONCENTRATIONS OF PT, PD, CU AND NI IN A LATERITIC WEATHERING PROFILE OVER MINERALIZED ULTRAMAFIC ROCK, MOUNT KEITH, WESTERN AUSTRALIA.

Zone	# Samples	Pt, ppb	Pd, ppb	Cu, ppm	Ni, ppm	Pd/Pt
Ferruginous	5	70	115	995	4760	1.6
Manganiferous	2	125	295	1505	21595	2.4
Quartz-Dolomite	12	40	95	690	14420	2.4
Dolomite	3	14	37	260	8275	2.6
Supergene	6	27	63	360	6020	2.3
Primary	5	19	47	295	4495	2.5

The profile is covered by transported overburden. From Butt (1986).

the development of ferralitic soils on hydrothermally altered pyroxenite that is weakly mineralized with Cu, Ni and PGE (Fig. 13-10). As in Australia there is an upward enrichment in Fe, the Fe_2O_3 content increasing from 10 to 35% and increases in Al_2O_3 (11 to 18%) and Cr (0.3 to 1.5%). But there are upward depletions in Pt (210 to 30 ppb) and Pd (130 to 35 ppb) and in MgO (13 to 5%), Cu (1200 to 200 ppm), and Ni (4000 to 800 ppm). This is a hilly region and erosion and colluvial transport has caused the formation of complicated profiles, including truncated ferralitic profiles and Pt- and Pd-enriched colluvium on top of residual soils. Although the environment is very different, the analogy to the complex soil profiles developed in the hilly Tulameen district of British Columbia should be noted. Maurizon *et al.* (1995) examined laterite-saprolite profiles up to 40 m thick in ophiolite terrain in New Caledonia. Maximum values tend to occur in yellow laterite, near the base of the profile and PGE are depleted near the surface. As noted in earlier sections, Pt-alloys may be present in lateritic soils (Salpeteur *et al.* 1995; Bowles 1995) and thus present an opportunity for collection and analysis in the HMC.

Use of Other Indicator Elements for PGE-Bearing Mineralization

Platinum-group minerals commonly contain Te, As, Sb, and Bi, but their concentrations are not necessarily significantly elevated in the bulk rocks, as shown in the Lac des Iles area (Hattori & Cameron 2004). Their precise analysis is not easy, which lessens their suitability as pathfinder elements.

PGE occur in association with a variety of base elements, most notably Ni, Co and Cu even in Lac des Iles-type sulfide-poor ore (Pettigrew and Hattori 2002, Hinchey *et al.* 2005). Therefore, the concentrations and distributions of base metals may assist in exploration for PGE deposits. However, base metal anomalies need to be carefully evaluated for PGE exploration. First, their mobility and fixing in the surface environment is different from Pd and Pt. Thus base metal anomalies may be spatially separated from those of Pd and Pt, which can either be an advantage or a disadvantage. Second, not all base metal sulfides are associated with significant PGE. It is not uncommon to have a PGE-rich zone with less sulfides. A good example is the newly discovered Suhanko deposit in Finland, that

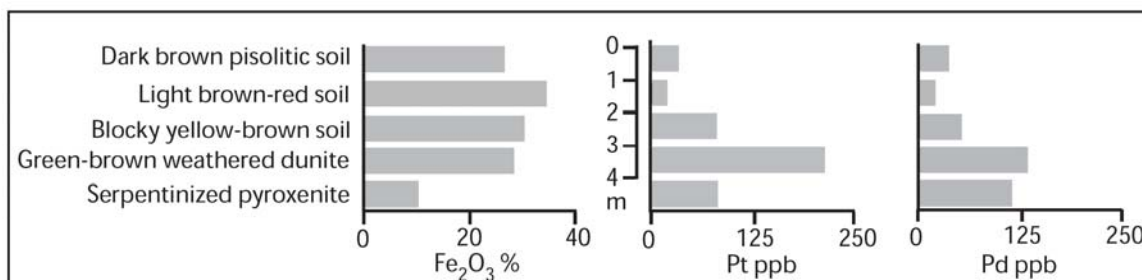


FIG. 13-10. Vertical distribution of Fe_2O_3 in lateritic soils overlying PGE-mineralized pyroxenite, Madagascar. Modified from Salpeteur *et al.* (1995).

contains massive sulfides on the margin of the complex, and a high PGE zone in the middle section of the intrusion.

ANALYTICAL CONSIDERATIONS AND QUALITY CONTROL

By far the most common method of analyzing solid samples for Pt and Pd is lead collection fire assay, followed by dissolution of the bead and analysis of the solution by ICP-MS. This provides detection limits for Pt of 0.1 ppb and 0.5 ppb for Pd. In addition, Au is determined to 1 ppb. Lead collection fire assay provides total dissolution of the sample, including alloys and PGE inclusions in chromite, which are not dissolved by aqua regia. Large samples are fluxed, typically 30 to 50 g in weight; this reduces the nugget effect to which PGE are prone. An important advantage of fire assay is that it removes elements which can cause isobaric interference during ICP-MS analysis. PGE occur in such low concentrations that several elements can potentially cause interference. For example, Sr present in carbonates and in gypsum is readily dissolved by acids and by some selective leaches. During analysis, $^{88}\text{Sr}^{16}\text{OH}$, which has mass 105, may be formed in the plasma. High peak at mass 105 is erroneously interpreted as high concentrations of Pd because ^{105}Pd is most commonly used to measure the concentration of Pd. An alternative to fire assay is aqua regia-ICP-MS. Detection limits are higher and variable because of interferences. However, aqua regia analyses are often considered a routine part of geochemical exploration programs because they provide data on up to 50 elements.

Selective leaches are widely used in geochemical exploration (Hall 1998). Leaching may enhance the signal to noise ratio, which is particularly important when trying to detect low concentrations of metals. The use of selective leaches has been proven to be effective in exploration of buried base metal deposits (Cameron *et al.* 2004). Enzyme Leach and MMI are proprietary leaches, Enzyme Leach providing analyses for Pt and Pd, with detection limits of 1 ppb; MMI providing analyses for Pd to a detection limit of 0.1 ppb. Non-proprietary leaches include ammonium acetate, that dissolves carbonate-bound elements, and hydroxylamine hydrochloride, which dissolves Mn and Fe oxides.

The most intensive study of selective extraction of Pt and Pd was on samples of lateritic

soils over the Ora Banda and Mt. Carnegie prospects, Western Australia by Gray (2001). The results should be considered specific to this environment, since the form that Pt and Pd take elsewhere may be different. Scanning electron microprobe examination plus physical and chemical extractions show that Pt and Pd are mostly present in the $<2\ \mu\text{m}$ fraction (Gray *et al.* 1996). Neither Pt nor Pd are extracted by reagents that dissolve exchangeable metals, carbonates, Mn oxides or poorly crystalline Fe oxides, indicating that they are not present in these phases. Most of the Pt and 25–50% of the Pd were dissolved by citrate-dithionite reagent, which dissolves Fe oxides, including goethite and hematite. Palladium shows an affinity for Al-rich Fe oxides and aqua regia was required to extract the largest fraction of this element (Gray *et al.* 1996).

The swamp humus sampled around Shorty Lake (Figure 13-5) near Lac des Iles is black and reduced. Hattori and Cameron (2004) experimented with a number of selective leaches to extract the Pd (Fig. 13-11). Cyanide leach removed the most Pd, but less than fire assay. Enzyme and TerraSol leaches removed only very small amounts of Pd from the humus. These data indicate that Pd is strongly bound. More than reduction of Pd may have been involved in its precipitation, with the formation of compounds resistant to dissolution, including organic complexes. Further experiments are required. Gregoire (1985) found that an

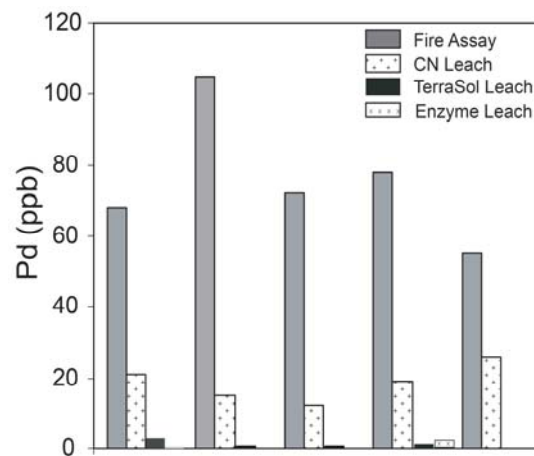


FIG. 13-11. Experiments on extracting Pd from five samples of swamp humus from around Shorty Lake using CN leach (NaCN-NaOH) TerraSol™ and Enzyme Leach™ in comparison to analysis by fire assay - ICP-MS. From Hattori and Cameron (2004).

oxidizing agent, sodium hypochlorite, was effective in extracting Au from organic-rich samples.

Quality control on sampling and analytical precision is particularly important for surveys involving PGE, given the potential for the “nugget effect” and the low detection limits required for analysis. A recommended procedure is that a field duplicate should be collected at 10% of the sampling sites. This involves collection of a second sample several metres away from the first. Once the samples are prepared for analysis, *e.g.*, by sieving, one of the field duplicate pairs is split into two to provide an analytical duplicate. The Relative Standard Deviation (RSD) may then be calculated for the field duplicates and for the analytical duplicates:

$$s^2 = (\Sigma(x_{i1}-x_{i2})^2)/2N$$

$$RSD = 100.s/Xd$$

where the squares of the differences between the duplicate pairs are summed, then divided by 2N, N being the number of pairs, to produce the variance estimate s^2 . The RSD, which is equivalent to the Coefficient of Variation, and is expressed as a percentage, is then calculated, where Xd is the mean of all duplicates. Standards of known composition should be included when sample batches are submitted for analysis. A number of these are available (Hoffman and Dunn 2002).

CONCLUSIONS

In Western Australia there has been extensive sampling of residual soils and gossans and their analysis for PGE in the search for PGE-bearing Ni–Cu deposits below thick lateritic cover. PGE are retained in the upper, ferruginous layer of these soils, even where Ni and Cu have been lost during weathering. The laterites were developed over a long period of time on a land surface of low relief. In some cases there has been subsequent erosion and truncation of the profiles, or the PGE-enriched ferruginous layer may be covered by transported overburden (Butt 1992), features that add complication to survey applications. Nevertheless, the large literature on soil PGE geochemistry in this region attests to the value of the method.

In other regions of the world, both tropical and temperate, there has been a marked separation of Pd from Pt in the surface environment. Platinum remains as PGM in detrital fragments, mainly Pt-rich alloys and sperrylite, which mostly formed at

high temperatures (Hattori *et al.* 2004). Palladium, by contrast, enters solution when its primary minerals are weathered. Except for environments with abundant chloride- and sulfur-bearing ligands, Pd(II) dissolves as neutral or negatively charged hydroxide complexes or as metal–organic complexes. Unlike positively charged base metal cations, Pd(II) hydroxide and organic complexes are not fixed by the negatively charged Fe oxyhydroxide coatings of B-horizon soils and stream sediments. Instead, Pd is fixed by organic matter, such as is present in swamps, in basins along streams, in lake sediments, in vegetation, and in the humus of soils.

The differing behaviors of Pt and Pd in the surface environment affect strategies applied to geochemical exploration. At the reconnaissance stage of exploration Pt may be sought in the HMC of stream sediments; separation of this concentrate achieves a magnification in the abundance of Pt relative to the bulk sample and an improvement in anomaly/background contrast. Where streams are poorly developed, as in the Canadian and Fennoscandian shields, sampling and analysis for Pd in organic lake sediments and humus from swamps provides a distal indicator of PGE mineralization. For the follow-up of anomalies obtained during the reconnaissance stage, sampling can focus on Pt within the HMC of tills and C-horizon soils or the Pd that accumulates in the humic layers of soil or vegetation growing on the soil. The recent development of methods that measure Pd and Pt directly in waters add a further option for more detailed levels of exploration.

ACKNOWLEDGEMENTS

For our work at Lac des Iles and nearby areas we received generous funding from Ontario Mineral Exploration Technologies program. We thank Maurice Lavigne of North American Palladium and Neil Pettigrew and Karen Rees of Avalon Ventures Ltd. for their cooperation, Monika Wilk-Aleman for laboratory assistance. We thank Richard Dyer and Eric Hoffman for their editorial reviews.

REFERENCES

- ALAPIETI, T.T. & LAHTINEN, J.J. (2002): Platinum-group element mineralization in layered intrusions of northern Finland and the Kola Peninsula, Russia. In *The Geology, Geochemistry, Mineralogy and Mineral*

- Beneficiation of Platinum-Group Elements (L.J. Cabri, ed.) *Can. Inst. Min. Metall. Spec. Vol.* **54**, 507-546.
- AZAROUAL, M., ROMAND, B., FREYSSINET, P. & DISNAR, J.-R. (2001): Solubility of platinum in aqueous solutions at 25°C and pHs 4 to 10 under oxidizing conditions. *Geochim. Cosmochim. Acta* **65**, 4453-4466.
- BARNES, S.-J., MELEZHIK, V.A. & SOKOLOV, S.V. (2001): The composition and mode of formation of the Pechenga nickel deposits, Kola Peninsula, north-western Russia. *Can. Mineral.*, **39** 447-471.
- BOWLES, J.F.W. (1995): The development of platinum-group minerals (PGM) in laterites: Mineral morphology. *Chron. Recherché Minière*, **520** 55-63.
- BOWLES, J.F.W., GIZE, A.P. & COWDEN, A. (1994): The mobility of the platinum group elements in the soils of the Freetown Peninsula, Sierra Leone. *Can. Mineral.*, **32** 957-967.
- BOWLES, J.F.W., GIZE, A.P., VAUGHAN, D.J. & NORRIS, S.J. (1995): Organic controls on platinum-group element (PGE) solubility in soils: initial data. *Chron. Recherché Minière* **520**, 65-73.
- BRAND, N.W. & BUTT, C.R.M. (2001): Weathering, element distribution and geochemical dispersion at Mt. Keith, Western Australia: implications for nickel sulfide exploration. *Geochem. Explor. Envir. Anal.* **1**, 391-407.
- BUTT, C.R.M. (1986): Platinum-group elements in weathered ultramafic rocks at Mt. Keith. Report MG 3R, CSIRO, Australia, Division of Minerals and Geochemistry, Perth, 17 p.
- BUTT, C.R.M. (1992): Semiarid and arid terrains. In *Regolith Exploration Geochemistry in Tropical and Subtropical Terrains* (C.R.M. Butt & H. Zeegers eds.) Handbook of Exploration Geochemistry, Vol. **4**, Elsevier, Amsterdam, pp. 295-392.
- BUTT, C.R.M., ROBERTSON, I.D.M., SCHORIN, K.H. & CHURCHWARD, H.M. (2001): Geochemical dispersion of platinum group elements in lateritic regolith, Ora Banda sill. In *Geochemical Exploration for Platinum Group Elements in Weathered Terrain*. CRC LEME Open File Report **85**, Vol. IIA, 80 pp.
- CAMERON, E.M. & HATTORI, K.H. (2003): Mobility of palladium in the surface environment: data from a regional lake sediment survey in north-western Ontario. *Geochem. Explor. Envir. Anal.* **3**, 299-311.
- CAMERON, E.M., HAMILTON, S.M., LEYBOURNE, M.I., HALL, G.E.M. & MCCLENAGHAN, M.B. (1994): Finding deeply buried deposits using geochemistry. *Geochem. Explor. Envir. Anal.* **4**, 7-32
- CAWTHORN, R.G. (2001): A stream sediment geochemical re-investigation of the discovery of the platiniferous Merensky Reef, Bushveld Complex. *J. Geochem. Explor.* **72**, 59-69.
- CHAO, T.T., JENNE, E.A. & HEPPTING, L.M. (1968): Prevention of adsorption of trace amounts of gold by containers. US Geol. Surv. Prof. Paper **625-C**, 17 pp.
- COKER, W.A., DUNN, C.E., HALL, G.E.M., RENCZ, A.N., DiLABIO, R.N.W., SPIRITO, W.A. AND CAMPBELL, J.A. (1991): The behavior of platinum group elements in the surficial environment at Ferguson Lake, N.W.T., Rottenstone Lake, Sask. and Sudbury, Ont., Canada. *J. Geochem. Explor.* **40**, 163-192.
- COOK, S.J. & FLETCHER, W.K. (1993): Distribution and behavior of platinum in soils, sediments and waters of the Tulameen ultramafic complex, southern British Columbia, Canada. *J. Geochem. Explor.* **46**, 279-308.
- COOK, S.J. & FLETCHER, W.K. (1994): Platinum distribution in soil profiles of the Tulameen ultramafic complex, southern British Columbia. *J. Geochem. Explor.*, **51**, 161-191.
- COOK, N.J., WOOD, S.A. & ZHANG, Y. (1992): Transport and fixation of Au, Pt and Pd around the Lac Sheen Cu-Ni-PGE occurrence in Quebec, Canada. *J. Geochem. Explor.* **46**, 187-228.
- COWDEN, A., DONALDSON, M.J., NALDRETT, A.J. & CAMPBELL, I.H. (1986): Platinum-group elements and gold in the komatiite-hosted Fe-Ni-Cu sulfide deposits at Kambalda, Western Australia. *Econ. Geol.* **81**, 1226-1235.
- DiLABIO, R.N.W. (1988): Residence sites of gold, PGE and rare lithophile elements in till. In *Prospecting in Areas of Glaciated Terrain – 1988*.

- (D.R. MacDonald & K.A. Mills eds.) *Can. Inst. of Min. and Metall.*, 121-140.
- DISTLER, V.V. (1994): Platinum mineralization of the Noril'sk deposits. *In* Proceedings of the Sudbury–Noril'sk Symposium. (P.C. Lightfoot & A.J. Naldrett eds.) *Ont. Geol. Surv. Spec. Vol. 5*, 243-260.
- DOAN, D.B. & BOND, A.R. (1994): Russia's platinum group metals: A current survey. *Inter. Geol. Rev.*, **36** 92-100.
- DUNN, C.E. (1986): Biogeochemistry as an aid to exploration for gold, platinum and palladium in the northern forests of Saskatchewan, Canada. *J. Geochem. Explor.* **25**, 21-40.
- DUNN, C.E. (1992): Biogeochemical Exploration for Deposits of the Noble Metals, *In* Noble Metals and Biological Systems (Brooks, R.R., ed.) CRC Press, Boca Raton, CRC Press, 47-89.
- DYER, R.D. & RUSSELL, D.F. (2002): Lac des Iles–Black Sturgeon River Area Lake Sediment Survey: Operation Treasure Hunt: *Ont. Geol. Surv. Open File Report 6096*, 134 pp.
- EVANS, D.M., BUCHANAN, D.L., & HALL, G.E.M. (1994): Dispersion of platinum, palladium and gold from the Main sulfide zone, Great Dyke, Zimbabwe. *Trans. Inst. Min. Metall.* **103**, B57-B67.
- FORTESCUE, J.A.C., STAHL, H., & WEBB, J.R. (1987): Humus geochemistry in the Lac des Iles area, District of Thunder Bay: *Ont. Geol. Surv., Geochemical Series Map 80,800*.
- FUCHS, W.A., & ROSE, A.W. (1974): The geochemical behavior of platinum and palladium in the weathering cycle in the Stillwater complex, Montana. *Econ. Geol.* **69**, 332-346.
- GRAY, D.J. (2001): The selective extraction of platinum and palladium from soils and regolith materials from Mt. Carnegie and Ora Banda. *In* Geochemical Exploration for Platinum Group Elements in Weathered Terrain. CRC LEME Open File Report **85**, Volume III, pp. 1-49.
- GRAY, D.J., SCHORIN, K.H. & BUTT, C.R.M. (1996): Mineral associations of platinum and palladium in lateritic regolith, Ora Banda sill, Western Australia. *J. Geochem. Explor.* **57**, 245-255.
- GREGOIRE, D.C. (1985): Selective extraction of organically bound gold in soils, lake sediments and stream sediments. *J. Geochem. Explor.* **23**, 299-313.
- GUNN, A.G. (1989): Drainage and overburden geochemistry in exploration for platinum-group element mineralization in the Unst ophiolite, Shetland, U.K. *J. Geochem. Explor.* **31** 209-236.
- HALL, G.E.M. (1998): Analytical perspectives on trace element species of interest in exploration. *J. Geochem. Explor.* **61**, 1-20.
- HALL, G.E.M. & PELCHAT, J.C. (1993): Determination of palladium and platinum in fresh waters by inductively coupled plasma mass spectrometry and activated charcoal preconcentration. *Journal of Analytical Atomic Spectrometry*, **8**, 1059-1065.
- HALL, G.E.M., PELCHAT, J-C. & DUNN, C.E. (1990): The determination of Au, Pd and Pt in ashed vegetation by ICP–mass spectrometry and graphite furnace atomic absorption spectrometry. *J. Geochem. Explor.* **37**, 1-23.
- HALL, G.E.M., VAIVE, J.E. & BALLANTYNE, S.B. (1996): Field and laboratory procedures for determining gold in natural waters: relative merits of preconcentration with activated charcoal. *J. Geochem. Explor.* **26**, 191-202.
- HATTORI, K. (2002): A review of rhenium–osmium isotope geochemistry of platinum-group minerals and platinum mineralization. *In* The Geology, Geochemistry, Mineralogy and Mineral Beneficiation of Platinum-Group Elements (L.J. Cabri, ed.). *Can. Inst. Min. Metall. Spec. Vol. 54*, 251-271.
- HATTORI, K. & CAMERON, E.M. (2004): Utilizing the high mobility of palladium in exploration for platinum group element mineralization: Evidence from the Lac des Iles and Legris Lake area, north-western Ontario. *Econ. Geol.* **99**, 157-171.
- HATTORI, K.H. AND CAMERON, E.M. (submitted): Palladium and platinum concentrations of fresh, surface waters in the Lac des Iles area, northern Ontario, Canada. *Geochem. Explor. Envir. Anal.*
- HATTORI, K.H., CABRI, L.J., JOHANSON, B. & ZIENTEK, M.L. (2004): Origin of placer laurite from Borneo: Se and As contents, and S isotopic compositions. *Mineral. Mag.* **68**, 353-368.

- HINCHEY, J.G., HATTORI, K.H., LAVIGNE, M. (2005): Geology, Petrology, and Controls on PGE mineralization of the Southern Roby and Twilight Zones, Lac des Iles mine, Canada. *Econ. Geol.* **100**, 43-61.
- HOFFMAN, E.L. & DUNN, B. (2002): Sample preparation and bulk analytical methods for PGE. *In The Geology, Geochemistry, Mineralogy and Mineral Beneficiation of Platinum-Group Elements* (L.J. Cabri ed.). *Can. Inst. Min. Metall. Spec. Vol.* **54**, 1-11.
- KENDALL, T. (2004): *Platinum 2004*. Johnson Matthey, London, 60 pp.
- LI, J-H. & BYRNE, R.H. (1990): Amino acid complexation of palladium in seawater: *Environ. Sci. and Tech.* **24**, 1038-1041.
- MAURIZON, P., BRETON, J., EBERLE, J.-M., GILLES, C., JEZEQUEL, P., MEZIERE, J. & ROBERT, M. (1995): Magmatic and supergene platinum-group minerals in the New Caledonia ophiolite. *Chron. Recherche Minière* **520**, 3-26.
- MCCALLUM, M.E., LOUCKS, R.R., CARLSON, R.R., COOLEY, E.F. & DOERGE, T.A. (1976): Platinum metals associated with hydrothermal copper ores at the New Rambler Mine, Medicine Bow Mountains, Wyoming. *Econ. Geol.* **71**, 1429-1450.
- MCDONOUGH, W.F. & SUN, S.-S. (1995): Composition of the Earth. *Chem. Geol.* **120**, 223-253.
- MERTIE, J.B. JR. (1976): Platinum Deposits of the Goodnews Bay District, Alaska. *US Geol. Surv. Prof. Paper* **938**, 42 pp.
- MILLOT, R., GAILLARDET, J., DUPRÉ, B., ALLÈGRE, C.J. (2003): Northern latitude chemical weathering rates: clues from the Mackenzie River Basin, Canada: *Geochim. Cosmochim. Acta.* **67**, 1305-1329.
- MOESKOPS, P.G. (1977): Yilgarn nickel gossan geochemistry – a review, with new data. *J. Geochem. Explor.* **8**, 247-258.
- MOLLARD, D.G. (1979a): Northern Ontario Engineering Geology Terrain Study, Data Base Map, Heaven Lake. *Ont. Geol. Surv.*, Map **5051**. Scale 1:100,000.
- MOLLARD, D.G. (1979b): Northern Ontario Engineering Geology Terrain Study, Data Base Map, Kaministikwia. *Ont. Geol. Surv.*, Map **5045**. Scale 1:100,000.
- MOUNTAIN, B.W., & WOOD, S.A. (1988): Solubility and transport of platinum-group elements in hydrothermal solutions: Thermodynamic and physical chemical constraints, *In Geo-Platinum 87* (H.M. Prichard, P.J. Potts, J.F.W. Bowles & S.J. Cribb eds.). Elsevier Applied Science, Amsterdam, pp. 57-82.
- NALDRETT, A.J. (1984): Mineralogy and composition of the Sudbury ores. *In The Geology and Ore deposits of the Sudbury Structure*. (E.G. Pye, A.J. Naldrett & P.E. Giblin eds.) *Ont. Geol. Surv. Spec. Vol.* **1**. 309-325.
- OBERTHÜR, T. (2002): Platinum-group element mineralization of the Great Dyke, Zimbabwe. *In The Geology, Geochemistry, Mineralogy and Mineral Beneficiation of Platinum-Group Elements* (L.J. Cabri ed.). *Can. Inst. Min. Metall. Spec. Vol.* **54**, 483-506.
- OBERTHÜR, T., WEISER, T.W. & GAST, L. (2003): Geochemistry and mineralogy of platinum-group elements in the Hartley Platinum Mine, Zimbabwe. *Mineral. Deposita* **38**, 344-355.
- PETTIGREW, N.T. & HATTORI, K.H. (2002): Palladium-copper-rich PGE mineralization in the Legris Lake mafic ultramafic complex, western Superior Province of Canada. *Trans. Inst. Mining Metall.* **111**, Series B, B46-B57.
- PRICHARD, H.M. & LORD, R.A. (1994): Evidence for differential mobility of platinum-group elements in the secondary environment in Shetland ophiolite complex. *Trans. Inst. Min. and Metall.* **103**, B79-86.
- RENCZ, A.N. & HALL, G.E.M. (1992): Platinum group elements and Au in arctic vegetation growing on gossans, Keewatin District, Canada. *J. Geochem. Explor.* **43**, 265-279.
- SALPETEUR, I. & JEZEQUEL, J. (1992): Platinum and palladium stream sediment geochemistry downstream from PGE-bearing ultramafics, West Andriamena area, Madagascar. *J. Geochem. Explor.* **43**, 43-65.
- SALPETEUR, I., MARTEL-JANTIN, B. & RAKOTOMANANA, D. (1995): Pt and Pd mobility in ferralitic soils of the West Andriamena area (Madagascar). Evidence of a supergene origin of

- some Pt and Pd minerals. *Chron. Recherche Minière* **520**, 27-45.
- SAMIULLAH, Y. (1985): Adsorption of platinum, gold and silver by filter paper and borosilicate glass and its relevance to biogeochemical studies. *J. Geochem. Explor.* **23**, 193-202.
- SEARCY, C.A. (2001): Preliminary Data Results of Drift Exploration for Platinum Group Elements, Northwestern Ontario: *Ont. Geol. Surv., Open File Report* **6054**, 271 pp.
- STEELE, T.W., LEVIN, J. & COPELOWITZ, I. (1975): Preparation and certification of a reference sample of precious metal ore. *South African National Inst. Metall., Report* 1696-1975, 4 pp.
- TAUFEN, P.M. & MARCHETTO, C.M.L. (1989): Tropical weathering control of Ni, Cu, Co and PGE distributions at the O'Toole Ni-Cu sulfide deposit, Minas Gerais, Brazil. *J. Geochem. Explor.* **32**, 185-197.
- TRAVIS, G.A., KEAYS, R.R., & DAVISON, R.M. (1976): Palladium and iridium in the evaluation of nickel gossans in Western Australia: *Econ. Geol.* **71**, 1229-1243.
- VON GRUENEWALDT, G., HULBERT, L.J. & NALDRETT, A.J. (1989): Contrasting platinum-group element concentration patterns in cumulates of the Bushveld Complex. *Mineralium Deposita*, **24**, 219-229.
- WEISER, T.W. (2002): Platinum-group minerals (PGM) in placer deposits: *In* The Geology, Geochemistry, Mineralogy and Mineral Beneficiation of Platinum-Group Elements (L.J. Cabri, ed.). *CIM Spec. Vol.* **54**, 721-756.
- WILLIAMS, J. (1981): *Picket Pin – Contact Mountain Pt-Pd Prospect*, The Anaconda Copper Company, Stillwater Project, Nye.
- WILLIAMS, P.A. (2001): Chemical behavior of the platinum group elements during weathering. *In* Geochemical Exploration for Platinum Group Elements in Weathered Terrain. CRC LEME Open File Report 85, Volume I, 8-29.
- WOOD, S.A. (2002): The aqueous geochemistry of the platinum-group elements with applications to ore deposits *In* The Geology, Geochemistry, Mineralogy and Mineral Beneficiation of Platinum-Group Elements (L.J. Cabri, ed.). *Can. Inst. Min. Metall. Spec. Vol.* **54**, 211-249.
- WOOD, S.A. & VLASSOPOULOS, D. (1990): The dispersion of Pt, Pd and Au in surficial media about two PGE-Cu-Ni prospects in Quebec. *Can. Mineral.* **28**, 649-663.
- WOOD, S.A., TAIT, C.T., VLASSOPOULOS, D. & JANECKY, D.R. (1994): Solubility and spectroscopic studies of the interaction of palladium with simple carboxylic acids and fulvic acid at low temperature: *Geochim. Cosmochim. Acta.* **58**, 625-637.

CHAPTER 14: APPLICATION OF LITHOGEOCHEMISTRY TO EXPLORATION FOR PGE DEPOSITS

W.D. Maier

Centre for Research on Magmatic Ore Deposits (CERMOD),
Dept. of Geology, University of Pretoria, Pretoria, South Africa, *or*
Sciences de la Terre, Université du Québec, Chicoutimi, G7H 2B1, Canada
E-mail: wdmaier@scientia.up.ac.za

and

Sarah-Jane Barnes

Sciences de la Terre, Université du Québec,
Chicoutimi, G7H 2B1, Canada

INTRODUCTION

The last 10–15 years have seen an increase in exploration for, and research on, platinum-group element (PGE) deposits. New types of magmatic and non-magmatic deposits have been identified on all continents. For example, important concentrations of PGE occur: together with Au and base metals in sedimentary rocks such as black shales (Pasava 1993, Hulbert *et al.* 1992); within veins hosted by deformed Fe formations (Jacupinga-type deposits, Olivo *et al.* 1995); and in altered clastic sedimentary rocks (Serra Pelada, Brazil, Moroni *et al.* 2001). Magmatic PGE deposits and occurrences are now known to occur in large (Bushveld, *e.g.*, Barnes & Maier 2002a, Cawthorn *et al.* 2002) and small intrusions (Panton, Australia, Hoatson & Blake 2000) as well as in relatively old (Stella, South Africa, Maier *et al.* 2003a) and, although much less commonly, in young intrusions (Jinbaoschan, China, Zhou *et al.* 2002, Skaergaard, Greenland, Andersen *et al.* 1998). They also occur in a variety of igneous rock types, including tholeiitic (Skaergaard, Noril'sk) and alkaline intrusions (Mordor, Australia, Stephen J. Barnes *et al.* 2004a), and intrusions within greenstone belts that are probably associated with komatiite magmatism (Mochila, Venezuela, Viljoen & Viljoen 2004). Examples of Ni–Cu sulfide-bearing gabbroic-pyroxenitic intrusions that contain significant amounts of PGE have also been found to be associated with calc-alkaline magmas (Riwaka, New Zealand, Smits *et al.* 2004, and possibly Aguablanca, Spain, Ortega *et al.* 2004). Furthermore, within the intrusions PGE reefs may occur in peridotite (Mochila, Kapalagulu, Tanzania), pyroxenite (Main Sulphide Zone of the Great Dyke,

Prendergast & Keays 1989, Volspruit zone of the Bushveld, Hulbert & von Gruenewaldt 1982), chromitites (many examples throughout the world), gabbroic rocks (Skaergaard), anorthosite (Penikat, Finland, Alapieti & Lahtinen 2002, Monchegorsk, Russia, Grokhovskaya *et al.* 2000), and magnetitite (Stella). Some PGE-mineralized rocks show strong evidence for contamination of the magma with crust (Platreef, Bushveld, Buchanan *et al.* 1981), but other examples seemingly formed without significant magma contamination (Main Sulphide Zone of the Great Dyke, PGE reefs in the Panton intrusion).

Since PGE deposits may be found in a variety of lithologies that may be derived from different sources, major element and compatible lithophile trace element concentrations of the rocks are of limited use to constrain PGE potential. For example, Merensky-type reefs are found in pyroxenites with relatively high Mg# (>0.8) and Cr contents (>1000 ppm), but Stella-type reefs are found in gabbroic rocks or magnetitites with low Mg# and Cr contents (< 100 ppm). Massive sulfides with PGE as by-products are associated with komatiites (*e.g.*, western Australia), komatiitic basalts (*e.g.*, Raglan, Pechenga, Kabanga), and basalts (Noril'sk), *i.e.*, rocks that show a wide range in MgO, Cr and other compatible elements. However, compatible elements (*e.g.*, Ni, Mg, Cr) have been used to define prospective volcanological environments such as komatiite lava channels as opposed to lava lakes and sheet flows (Stephen J. Barnes *et al.* 2004b, and references therein).

Other lithogeochemical indicators that are widely used to constrain the Ni–Cu–PGE sulfide

potential of mafic-ultramafic intrusions and lava flows include the following:

- (i) the degree of chalcophile metal depletion of the rocks; pronounced metal depletion may indicate that the magmas from which an intrusion or a lava flow formed reached sulfide saturation prior to emplacement. If extraction of the sulfide melt occurred at a relatively shallow depth or if the sulfide melt was entrained by the magma to a shallow depth an ore deposit could have formed.
- (ii) crustal contamination of the rocks; this is commonly the trigger for sulfide saturation and may indicate the possible presence of an ore deposit.

In the following, we discuss these techniques for the two main types of magmatic sulfide deposits that are normally distinguished (Naldrett 1981), *i.e.*,

- (i) sulfide-poor stratiform reefs in layered intrusions where the PGE are the main product, and (ii) massive or semi-massive concentrations of sulfides in relatively small, but dynamic magmatic bodies (magma conduits or lava channels) where Ni and Cu are the main products.

LITHOGEOCHEMICAL INDICATORS USED IN THE EXPLORATION FOR PGE REEF-TYPE DEPOSITS

Introduction

The understanding of the origin of PGE reefs in layered intrusions remains incomplete. The reefs occur at variable stratigraphic levels in intrusions of variable size and magmatic lineage (Naldrett 2004; Maier 2005). Thus, a single ore forming process is not applicable, but the following factors are probably important in the formation of all the important reefs.

- (i) A prerequisite for all magmatic Ni–Cu–PGE ores is that metal-rich mantle-derived magmas can ascend to upper crustal levels. PGE have extremely high D values with regard to sulfide melt (10^3 – 10^4 , see references in the reviews by Barnes & Maier 1999 and Mungall, 2005) and thus the magmas become PGE-depleted as soon as even small amounts of sulfide are extracted. As a result, saturation in sulfide prior to emplacement of the magma in the upper crust is undesirable, and it has been suggested that magmas giving rise to PGE mineralized intrusions were strongly sulfur-undersaturated during ascent and emplacement (Hoatson & Keays 1989, Keays 1995).

- (ii) Concentration of the PGE to form reefs probably occurred in response to saturation in, and segregation of, an immiscible sulfide melt. The sulfide-poor nature of some of the reefs, notably many chromitites, has been attributed to late-magmatic sulfur loss (Naldrett & Lehmann 1988). The position of a reef within an intrusion largely depends on the timing of sulfide saturation. If sulfide saturation occurs early, the reef forms in peridotite, pyroxenite, magnesian gabbro, or chromitite. If sulfide saturation occurs late, the reef may be situated in magnetite gabbro or magnetite.
- (iii) The trigger for sulfide saturation remains controversial. Contamination of the magma with crust, magma mixing, differentiation, interaction with deuteritic fluids, or a combination thereof, may all be important (see introductory chapters of this volume).

PGE-reefs are relatively easy to overlook because most of them are lithologically similar to other non-mineralized parts of the intrusions. For example, the reefs are commonly very S-poor. Many chromitite- and magnetite-hosted reefs such as those in the Bushveld and Stella intrusions contain no visible sulfides. Furthermore, the reefs are relatively thin compared to their host intrusions. The UG2 and Merensky reefs of the Bushveld Complex are each *ca.* 1 m wide, but are situated in a 7–9 km thick intrusion (Eales & Cawthorn 1996). In view of the cryptic nature of many reefs, lithogeochemical tools are potentially very useful in exploration and thus they are widely applied.

Evaluation of chalcophile metal depletion

Methods applied to whole rocks

Of specific interest in the exploration for PGE reefs is the question whether an intrusion has crystallized from a magma that was fertile in terms of PGE or, instead, had experienced sulfide segregation prior to emplacement. Segregating sulfides would extract the highly chalcophile PGE and negatively influence the PGE potential of the intrusion. Next, within the prospective intrusions it has to be determined whether, and at what stratigraphic position, a reef occurs. Ratios of elements showing different affinities for sulfide melt (*i.e.*, having different values of $D_{\text{sulfide melt/silicate melt}}$) have proven to be particularly useful in answering these questions (*e.g.*, Se/PGE, Hoatson & Keays 1989; Cu/Pd, Barnes *et al.* 1993). For example, if Cu/Pd ratios are higher than primitive mantle levels

throughout an intrusion, it is likely that sulfide and PGE extraction occurred at depth or that the PGE were retained in the mantle source during partial melting. Either way, the potential of the intrusion to host PGE deposits is low. If Cu/Pd ratios are at mantle level throughout an intrusion sulfide saturation was probably never reached during ascent and emplacement, and the presence of a reef is equally unlikely. In contrast, if Cu/Pd ratios in an intrusion show a range of values below and above primitive mantle a reef may have formed. In this case, the stratigraphic level of the intrusion where the most important change in the ratios occurs must be investigated in detail.

In theory, ratios of other trace elements with variably chalcophile characteristics, such as Pd/Zr could be used in a similar way as Cu/Pd. However, one of the main advantages of using Cu/Pd is that both Cu and Pd are routinely analyzed during most exploration programs.

Cu/Zr ratios have been applied extensively in massive sulfide deposits (to be discussed later). However, because Cu is less chalcophile than Pd (D values for Cu are *ca.* 500–1000, Barnes & Maier 1999) Cu/Zr ratios are less sensitive to sulfide melt segregation than Cu/Pd ratios, and small sulfide segregation events such as those forming PGE reefs may not be detected by this method (Fig. 14-1).

Examples of the application of Cu/Pd ratios are given in Figure 14-2, including the Mundi Mundi Complex of Australia (Barnes *et al.* 1993), the Bushveld Complex (Maier *et al.* 1996), the Sonju Lake intrusion of Minnesota (Miller *et al.* 2002), the Pantou intrusion of Western Australia (Hoatson & Blake 2000), and the Stella intrusion of South Africa (Maier *et al.* 2003a). In all these cases, the presence of reef-type PGE mineralization is delineated by sharp increases in Cu/Pd. This is thought to be the result of preferential extraction of the highly chalcophile Pd from the magma by the segregating sulfide melt.

Of note is the Cu/Pd profile through the Sonju Lake intrusion. Cu/Pd is significantly higher than primitive mantle throughout most of the rocks, including those below the “reef”. This suggests that the magma was already relatively PGE poor prior to emplacement, perhaps due to a small sulfide segregation event at depth or due to retention of PGE in the mantle source. This may be the reason for the relatively low grade of the “reef” (< 1 ppm over several m).

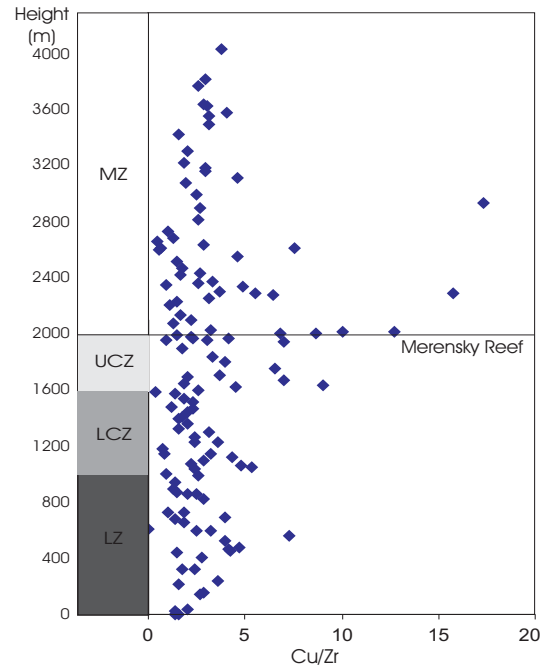


FIG. 14-1: Cu/Zr ratios in the layered sequence of the western Bushveld Complex, Union Section (data from Teigler 1990; Mitchell 1986). LZ=Lower Zone, LCZ = Lower Critical Zone, UCZ = Upper Critical Zone, MZ = Main Zone.

Methods applied to minerals

The application of mineral compositional data in the exploration for PGE reefs remains limited. This is partly because there are no specific indicator minerals associated with the reefs. Pyrrhotite, pentlandite, chalcopyrite and pyrite are all common sulfide minerals in PGE reefs, and a wide range of PGM has been observed, depending partly on the nature and magnitude of post-magmatic processes (Kinloch & Peyerl 1990). Of potential use could be IPGE concentrations in oxides if it can be confirmed that these elements partition into the oxides with high enough D values (>1000) to be detected by microanalytical techniques (see the contrasting results of Righter *et al.* 2004 and Sattari *et al.* 2002).

An example where mineral chemistry is used in exploration is chromitite-hosted PGE reefs in the Bushveld. The UG2 chromitite is the world's most important PGE deposit. It forms the uppermost of thirteen major chromitite layers in the complex. The chromitites show a broadly progressive increase in PGE contents with height (Teigler 1990a) from <100 ppb in the basal LG chromitites to *ca.* 6 ppm over a width of *ca.* 1 m in the UG2. The problem is

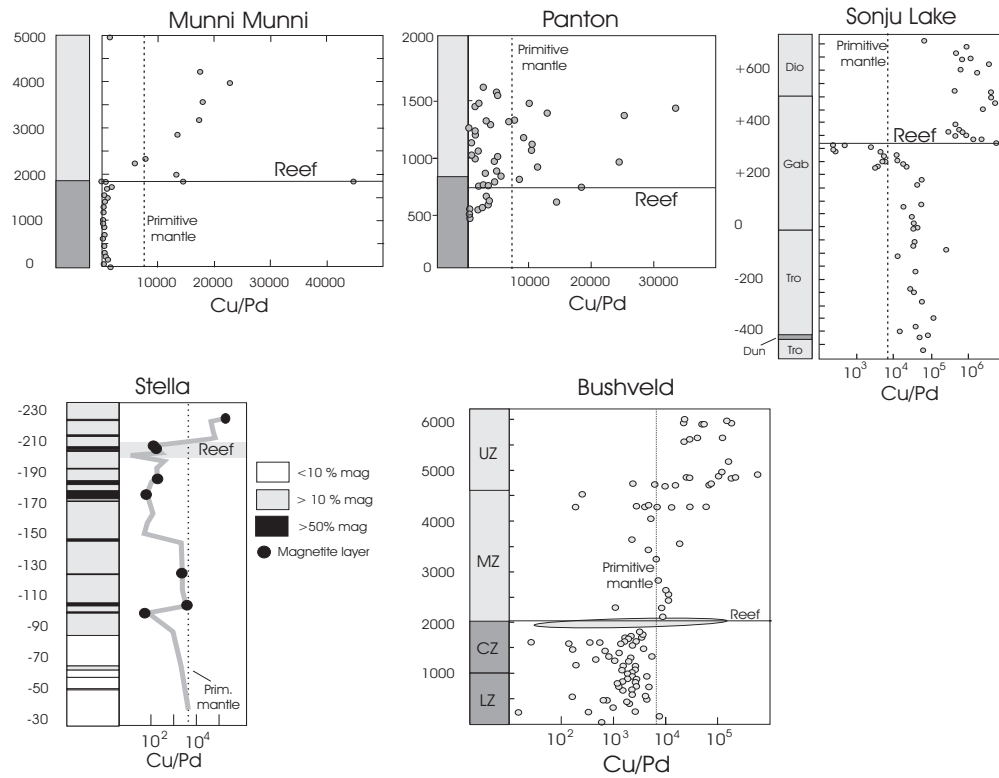


FIG. 14-2: Cu/Pd ratios in the Munni Munni, Panton, Sonju Lake, Stella and Bushveld intrusions. The position of the reefs is delineated by sharp increases in Cu/Pd. Figure from Maier (2005), modified after Barnes *et al.* (1993), Maier *et al.* (1996), Hoatson & Blake (2000), Miller *et al.* (2002), Maier *et al.* (2003a), and Sarah-Jane Barnes *et al.* (2004c). Height is in metres. In the Munni Munni, Panton, Sonju Lake and Bushveld intrusions ultramafic rocks are dark gray and mafic rocks are light grey. In the Stella intrusion, different shades of grey indicate different magnetite contents. Primitive mantle value is from Barnes and Maier (1999).

that in most chromitites there are no visible sulfides, *i.e.*, the PGE grade of a chromitite cannot be estimated in the field or using petrography. Moreover, the UG2 chromitite is hosted by similar rocks as the underlying UG1, MG3, and MG4 (*i.e.*, by layered pyroxenite–norite–anorthosite). Therefore, identification of the UG2 without extensive drilling and establishment of stratigraphic relationships can be difficult. However, the Bushveld chromitites display a broadly progressive decrease in Cr/Fe ratio with height, due to depletion of Cr in the magma in response to the fractionation of chromite. As a result, chromites of individual layers have characteristic Cr/Fe ratios (de Waal 1975, Eales & Cawthorn 1996). Microprobe analysis of chromite can thus help to determine whether a chromitite layer intersected in exploration represents the UG2 or another seam of lesser PGE potential.

Chromites in the Great Dyke and the Stillwater Complex show broadly analogous

compositional variation as those in the Bushveld Complex, with an initial increase in Cr/Fe ratios from the base upwards, followed by a progressive decrease in Cr/Fe with height through the bulk of the sequence (German & Schmidt 1999 in Oberthür 2002, Jackson 1963). This could suggest that chromite compositions in layered intrusions in general show a systematic pattern of Fe enrichment with height that could be used in exploration.

A widely applied tool in the exploration for massive sulfide ores is the Ni content of olivine. This is because Ni is both a chalcophile ($D_{\text{sulfide melt-basalt}}$ ca. 300–500, Barnes and Maier 1999) and a lithophile element ($D_{\text{olivine-basalt}}$ ca. 2–15, Li *et al.* 2001b), and thus Ni contents are potentially sensitive to detect sulfide segregation events and at the same time Ni occurs at high enough levels in silicate minerals to be analyzed reliably by microanalytical methods such as the electron microprobe. The basic idea is that segregating sulfide melt extracts Ni from the magma and thus

olivine that subsequently crystallizes from the Ni-depleted magma should equally be Ni depleted, relative to olivine with similar Mg# that crystallized from S-undersaturated magmas. The method has not been applied yet to reef-type deposits, mainly because most PGE reefs are not hosted by olivine-bearing rocks (exception: Kapalagulu). Further, it is possible that the relatively small amounts of sulfides segregating to form the reefs (essentially representing high R factor conditions, Campbell & Naldrett 1979) may not deplete the Ni content of the magma significantly enough to be detected in the composition of the olivine.

Pyroxene is a much more common phase associated with reef-type deposits and it also incorporates Ni in its structure ($D_{\text{opx/basalt}} = 1-3$, Beattie *et al.* 1991, $D_{\text{cpx/basalt}} = 2$, Steele & Lindstrom 1981). Thus, Ni contents of pyroxenes are potentially useful indicators to delineate the presence of a reef. A detailed trace element study on orthopyroxene separates across the Merensky Reef has been conducted by Kruger & Marsh (1985), but they did not find systematic compositional variation across the reef.

Contamination of magma with crust

The sulfur solubility of basaltic magma increases with falling pressure (Wendlandt 1982, Mavrogenes & O'Neill 1999) and thus primary mantle-derived basic-ultrabasic magmas, no matter whether they were saturated or undersaturated in sulfide melt in the mantle, should be initially undersaturated in sulfide melt during emplacement in the crust. This is, for example, observed in the Bushveld Complex where the parental magmas are believed to contain *ca.* 900 ppm S (Davies & Tredoux 1985) whereas the S solubility of the magma has been estimated to be 1850 ppm (Li *et al.* 2001a). To reach sulfide saturation, the magma either has to differentiate (Li *et al.* 2001a estimated that *ca.* 20% fractionation of olivine+orthopyroxene+spinel is required), and/or it has to be contaminated with crust, and/or magmas of different composition (including S content) have to mix with each other (Li & Ripley 2005). The relative importance of the three processes with regard to reef formation remains controversial.

Contamination of the magma to trigger sulfide saturation may involve the following:

- (i) Addition of external sulfur (by means of devolatilization, partial melting, or bulk assimilation of sulfur-bearing country rocks, Ripley 1999, Leshner & Campbell 1993, Baker *et*

al. 2001). The paucity of sulfides throughout virtually all of the PGE-mineralized intrusions (see review by Maier 2005, and references therein) is probably no coincidence and may indicate that the magmas were strongly undersaturated in sulfide melt upon emplacement and that assimilation of external S played a minor, if any, role in ore formation. PGE reefs located along the base of intrusions (*e.g.*, the Platreef) contain slightly higher sulfide contents (but mostly <5%) and there is evidence that contamination, including assimilation of external S, played a more important role, as indicated by heavy S isotopic signatures, enrichment in incompatible trace elements, crustal isotopic signatures and an abundance of xenoliths (Cawthorn *et al.* 1985, Barton *et al.* 1986).

- (ii) Assimilation of siliceous partial melts of the country rocks, thereby lowering the sulfide solubility of the magma (Irvine 1975, Li & Naldrett 1993).

Both types of contamination should be reflected in the presence of a crustal component in the rocks associated with the reefs. The identification of an enhanced crustal component within an intrusion could thus be of significance in exploration for reef-type deposits.

Lithophile incompatible trace elements

Many layered intrusions that host PGE deposits (Bushveld, Stillwater, Great Dyke) have highly fractionated incompatible trace element patterns and negative Nb-Ta-Ti anomalies, often particularly so in the ultramafic rocks (Bushveld: Maier *et al.* 2000; Stillwater: Lambert & Simmons 1987; Kapalagulu: present paper) (Fig. 14-3; see also Fig. 14-18). This indicates the presence of a significant crustal component, but debate continues whether the crustal component is the result of contamination of the magma during ascent through the crust (Maier *et al.* 2000) or whether it represents the melting of an enriched sub-continental lithospheric mantle (SCLM) source (Harmer & von Gruenewaldt 1991). Those authors that prefer a SCLM source for the Bushveld Complex point out that Bushveld magmas have a crustal signature similar to many other Kaapvaal flood-type basaltic magmas that erupted over a period of *ca.* 3 Ga through a variety of crustal rocks. Assimilation of crust during ascent of these magmas should presumably have resulted in a more variable trace

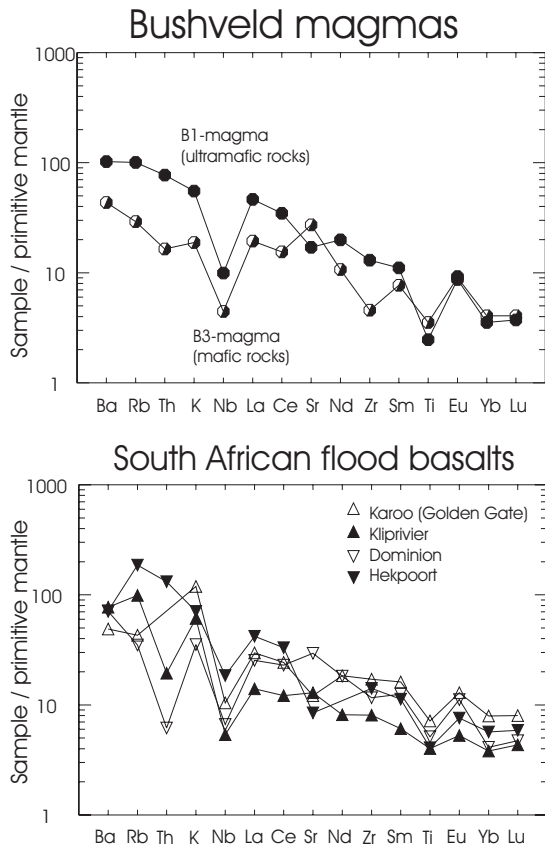


FIG. 14-3: Primitive mantle normalized incompatible trace elements concentration patterns in B1 and B3 parental magmas of the Bushveld Complex, and in various flood-type basalts from southern Africa. Note the distinct crustal signature as expressed by relative enrichment in highly incompatible trace elements, and negative Nb and Ti anomalies. Normalization factors are from Thompson *et al.* (1983). Figure has been modified after Maier *et al.* (2000). Data from Marsh *et al.* (1989, 1997), Crow & Condie (1999) and Maier *et al.* (2000).

element signature, although this remains to be modeled quantitatively. On the other hand, oxygen isotope data (Harris *et al.* 2004) appear to demand at least some crustal assimilation of the Bushveld magmas during ascent (Arndt 2005).

One of the problems in explaining the formation of PGE reefs in the Bushveld Complex and elsewhere by a model of crustal contamination during ascent and emplacement is that in the relatively well-studied reefs, *e.g.*, the Merensky Reef, there is no correlation between sulfide content and crustal component (Barnes and Maier 2002b). The Merensky Reef has similar La/Ta, La/Hf, and REE patterns as the Mg basaltic parental magma to

the Complex and many of the cumulates of the Lower and Critical Zones (Potts *et al.* 1992), and there is little change in incompatible trace element ratios across the reef (Barnes and Maier 2002b). Further, individual layers in the Bushveld Complex are compositionally homogenous across 100s of km of strike (Lee & Butcher 1990, Harris *et al.* 2004). These combined data suggest that any contamination during ascent must have occurred in a staging chamber at depth rather than the Bushveld chamber itself (Maier *et al.* 2000).

Some PGE-mineralized intrusions contain a very minor crustal component as indicated by their trace element signature, notably the Stella intrusion of South Africa (Fig. 14-4), where high-grade PGE reefs occur in magnetites and magnetite gabbros (Maier *et al.* 2003a). The lack of contamination of the Stella magma probably explains why early saturation in sulfide melt and metal depletion did not occur, thereby allowing the buildup of chalcophile elements necessary to form a reef in the differentiated portion of the intrusion.

Strontium and neodymium isotopes

The most extensive database on the concentrations of radiogenic isotopes in layered intrusions exists for the Rb/Sr system. The Bushveld Complex has been characterized in particular detail (*e.g.*, Sharpe 1985, Teigler 1990b, Eales *et al.* 1990, Kruger 1994), and Nd data have recently been added by Maier *et al.* (2000). These studies have shown that (i) all Bushveld cumulates have a distinct crustal Sr (Sr_i 0.7045–0.709) and Nd (ϵ_{Nd} –5 to –7.5) isotopic signature and (ii) there is a marked increase in Sr and Nd isotopic crustal component across a *ca.* 500 m interval in the Upper Critical Zone hosting the MG and UG chromitites as well as the Merensky Reef and several other sulfide-enriched layers including the Pseudoreefs, the Boulder Bed and the Bastard Reef (Fig. 14-5). This could be interpreted as strong evidence for a genetic link between crustal contamination and reef formation. However, the increase in Sr_i is progressive throughout most of the Upper Critical Zone and a direct correlation between the concentration of PGE or sulfides and crustal signature is not evident. Indeed, at several localities, Sr and Nd isotope data from the Merensky, as well as the Pseudo and Bastard, reefs indicate reversals towards less crustal signatures, which may be interpreted to reflect replenishment of the chamber with relatively less contaminated magma (*e.g.*, Eales *et al.* 1990, Lee & Butcher 1990). Thus, the Sr and Nd isotopic evidence for

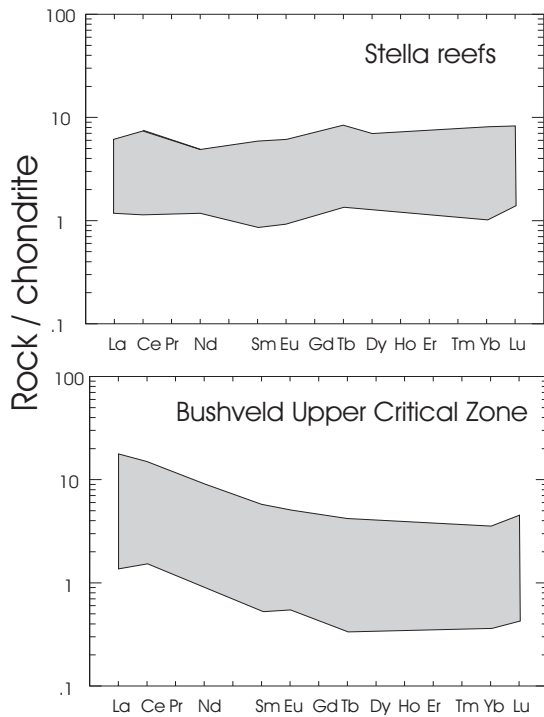


FIG. 14-4: Chondrite-normalized REE patterns in mineralized portions of the Stella and Bushveld Complex (data from Maier and Barnes 1998, Maier *et al.* 2003b). Normalization factors are from Nakamura (1974).

formation of the Merensky Reef sulfides in response to crustal contamination is inconclusive, at best. In contrast, Kruger *et al.* (2002) have recently shown elevated Sr_i in the matrix silicates to the UG and MG chromitites and interpreted this to support a model whereby the chromitites formed as a result of enhanced crustal contamination of the magma in the Bushveld chamber.

The most comprehensive Sr and Nd isotope study of the Great Dyke is that of Oberthür *et al.* (2002). These authors found a moderate to low crustal component in the Complex ($\epsilon Nd +2$ to 0; Sr_i 0.701 to 0.7045). The isotopic variation between samples was interpreted to be the result of contamination in the crust rather than the result of melting of an enriched lithospheric mantle. Notably, the Main Sulphide Zone has ϵNd 0 to 0.5 and Sr_i 0.7012 suggesting only a limited role for contamination in ore formation.

Sr isotopic ratios in the Stillwater Complex show considerable variation (ϵSr 8 to 24) and are interpreted to have been influenced by post-crystallization processes (Stewart & de Paolo 1987). Nd isotopic signatures are normally considered to

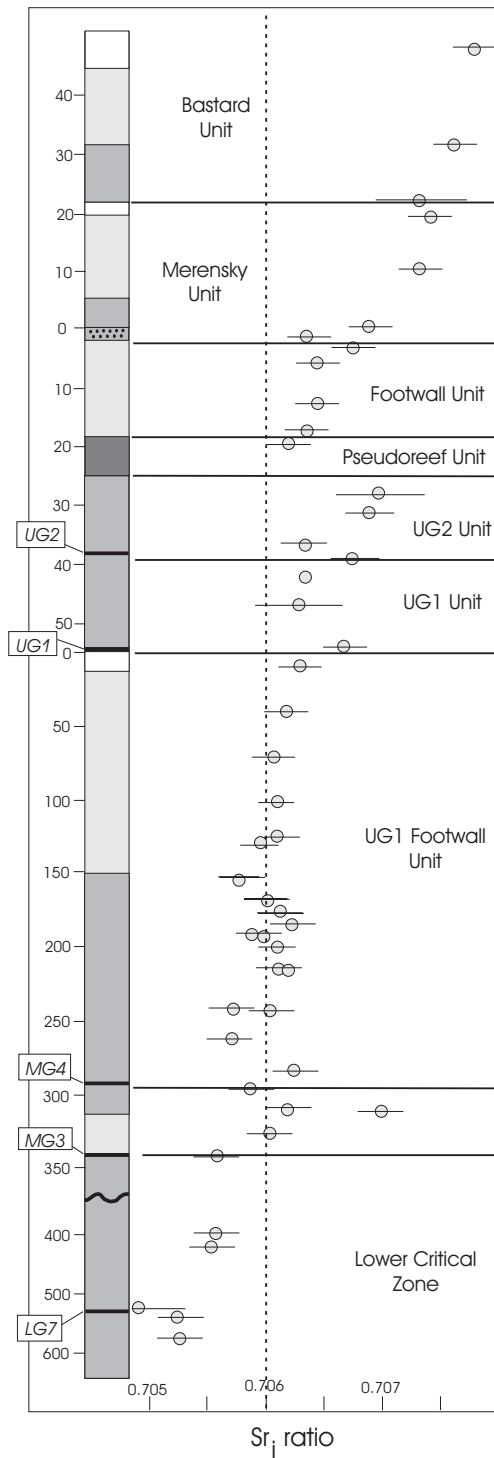


FIG. 14-5: Initial Sr isotopic stratigraphy in the Upper Critical Zone of the Bushveld Complex (figure modified after Eales *et al.* 1990). Note the progressive increase in crustal component, and the reversals towards less radiogenic ratios in the Pseudoreef and at the base of the Merensky and Bastard units.

be less readily affected by alteration. Excluding the basal samples, the Stillwater cumulates show ϵNd -1.9 to $+1.9$, providing little evidence for significant crustal contamination.

Osmium isotopes

Re/Os isotope data are available for many of the important PGE-mineralized layered intrusions, including the Bushveld Complex ($^{187/188}\text{Os}_i$ 0.11–0.18; McCandless & Ruiz 1991, Schönberg *et al.* 1999), the Stillwater Complex ($^{187/186}\text{Os}_i$ 0.8–1.4, γOs 0–35; Marcantonio *et al.* 1993; Lambert *et al.* 1994), the Great Dyke ($^{187/188}\text{Os}_i$ *ca.* 0.11–0.113, Schönberg *et al.* 2003), and the Munni Munni intrusion (γOs -120 to $+110$, Lambert *et al.* 1998a). The consensus from these studies is that most of the intrusions contain a small to moderate crustal component (between 0 and *ca.* 30%), but the derivation of this component (*e.g.*, upper crust, SCLM, or an enriched plume) remains uncertain. For example, Schönberg *et al.* (2003) rejected a possible involvement of the SCLM in the formation of the Great Dyke magma because the Zimbabwean SCLM has been shown to be Re-depleted and unradiogenic (Nägler *et al.* 1997). The Archean basement gneisses hosting the intrusion are also relatively unradiogenic and Os-poor and thus are unlikely contaminants. Furthermore, the different sub-chambers of the Great Dyke are isotopically homogenous (Mukasa *et al.* 1998), arguing against localized contamination. These considerations led Schönberg *et al.* (2003) to suggest that an enriched primitive upper mantle (PUM) source contributed to the radiogenic signature of the Great Dyke magmas.

Assimilation of crust during ascent could explain the crustal Os isotopic signature of the Bushveld Complex better than that of the Great Dyke. The Archean basement rocks associated with the Bushveld Complex are relatively unradiogenic and Os-poor (Schönberg *et al.* 2003), but the shale of the Transvaal Supergroup could be a suitable contaminant. The latter model is, however, in disagreement with the work of several authors (*e.g.*, Lee & Butcher 1990, Harmer & von Gruenewaldt 1991, Harris & Chaumba 2001, McCandless *et al.* 1999, Gomwe 2001) who found that the Bushveld and its satellite intrusions have a very homogenous crustal isotopic signature, suggesting that the Bushveld magma attained its crustal signature prior to emplacement, either in a staging chamber or in the SCLM mantle source.

The crustal Os isotopic component in the Stillwater Complex was interpreted to represent an SCLM component by Lambert *et al.* (1994), whereas Marcantonio *et al.* (1993) favored a model of Re mobilization by hydrothermal fluids. The latter process also controlled Os isotopic variation in the Munni Munni PGE reef (Lambert *et al.* 1998a).

A correlation between crustal component and the PGE reefs is again not clearly evident in any of the PGE mineralized intrusions. The Merensky Reef of the Bushveld contains higher γOs than the underlying and overlying rocks, but it also contains ehrlichmanites with mantle-like Os isotopic signature (Hart & Kinloch 1989), suggesting to some that the reef formed due to replenishment with mantle-like magma (Schönberg *et al.* 1999). The Os isotopic signature of the Great Dyke chromitites shows no variation with height, irrespective of their PGE contents (Schönberg *et al.* 2003). The J-M reef and the B chromitite of the Stillwater Complex are somewhat more radiogenic (γOs 20–35) than many of the underlying ultramafic rocks, but most of the other chromitites of the Complex have a mantle signature (γOs 1–9, Lambert *et al.* 1994, Horan *et al.* 2001).

Lead isotopes

The use of lead isotopic data as an indicator for crustal contamination in layered intrusions, and thus potentially for the presence of a reef, is complicated by the fact that crustal rocks are extremely inhomogeneous in terms of Pb isotopic composition. Thus, there is considerable uncertainty regarding average lead isotope compositions of most crustal rocks (Harmer *et al.* 1995).

One of the most detailed lead isotopic studies of a layered intrusion was conducted by Harmer *et al.* (1995) on the Bushveld Complex (Fig. 14-6). These authors reported initial lead isotope compositions mostly more radiogenic than expected for a mantle-derived magma, indicating the presence of a crustal component. The compositional variation with height broadly matches that defined by the Sr isotopes (Sharpe 1985, Kruger 1994). Thus, the μ_2 values progressively increase from the bottom of the intrusion to the base of the Main Zone. The Merensky Reef shows extreme variation in μ_2 , suggesting interaction with hydrothermal fluids. Modification of the initial lead isotopic composition of the Bushveld cumulates by fluids, albeit of late magmatic nature, has also been suggested by Mathez & Waight (2003).

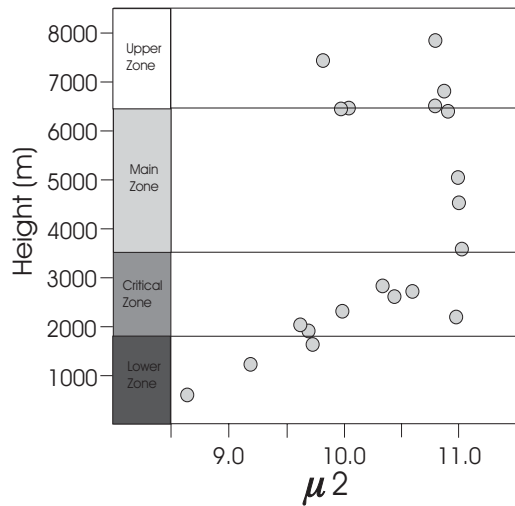


FIG. 14-6: Lead isotopic stratigraphy of the Bushveld Complex (figure modified after Harmer *et al.* 1995).

Lead isotope data are also available for the Great Dyke (Mukasa *et al.* 1998), suggesting 5–25% crustal contamination of the magma, in broad agreement with other isotopic data, *e.g.*, Re/Os and Sm/Nd (Oberthür *et al.* 2002). No detailed information is available to evaluate whether there are distinct changes associated with the Main Sulphide Zone or other PGE mineralized horizons of the Complex.

Lead isotope data on plagioclase and sulfides from the J-M reef of the Stillwater Complex have been provided by McCallum *et al.* (1992). The authors found that the bulk of the lead is derived from the mantle at *ca.* 2.7 Ga, with some additional radiogenic lead from a younger hydrothermal source also being present.

Sulfur isotopes

A recent overview of the systematics of S isotopes and their application in Ni–Cu–PGE exploration was given by Ripley (1999). Whereas most workers accept that many massive Ni–Cu sulfide deposits formed in response to addition of external sulfur to the silicate magma, addition of external sulfur is less obvious in PGE reef-type deposits which contain relatively small amounts of sulfides. Two sources of sulfur can be distinguished (Ripley 1999): sulfur within pristine mantle and sulfur within seawater which may give rise to sedimentary sulfates and, via bacterial reduction of the sulfate, sedimentary sulfides. The mantle derived sulfur has $\delta^{34}\text{S}$ values of around 0‰, whereas the sedimentary sulfur may have a wide range of $\delta^{34}\text{S}$ values. Thus,

if a sulfide-bearing igneous rock has $\delta^{34}\text{S}$ around zero it is likely, albeit not certain, that the rocks contain no external S. This would have to be regarded as a negative exploration indicator. If the rocks have $\delta^{34}\text{S}$ distinct from zero, then assimilation of external sulfur is indicated. A complication is that in rocks older than *ca.* 2.8–2.9 Ga the $\delta^{34}\text{S}$ values of sedimentary rocks do not deviate much from mantle values, possibly because bacterial sulfate reduction was less important (Strauss 2002; Fig. 14-7). Thus, in many Archean rocks the presence of external sulfur cannot be detected by sulfur isotopes.

There are still relatively few published sulfur isotopic data available on reef-type deposits. The data from the Merensky reef ($\delta^{34}\text{S}$ –0.6‰, Liebenberg 1968) indicate a mantle-like signature. The Main Sulphide Zone of the Great Dyke has $\delta^{34}\text{S}$

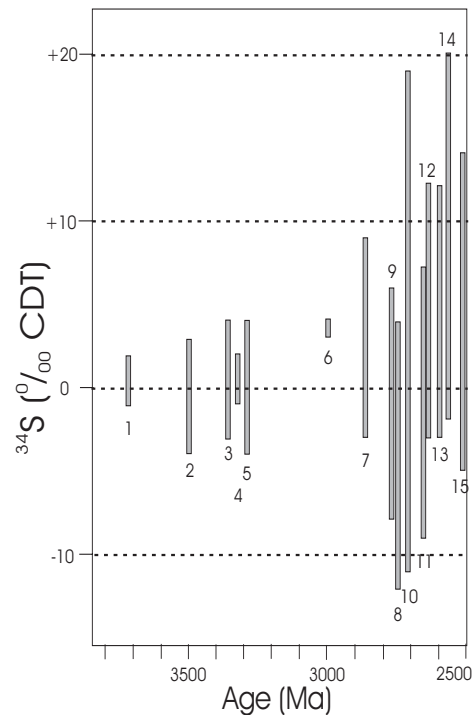


FIG. 14-7: Sulfur isotopic composition of Archean sedimentary sulfides (Fig. modified after Strauss 2002). 1: Isua metasedimentary rocks, 2: Warrawoona Supergroup, 3: Onverwacht and Fig Tree Group, 4: Swaziland Supergroup, 5: Sebakwian Group, 6: Mozaan Group, 7: Witwatersrand Supergroup, 8: Keewatin Group, 9: Uchi Greenstone Belt, 10: Late Archean BIF, 11: Yilgarn and Ventersdorp, 12: Jeerinah Formation/Lewin shale, Marra Mamba IF, 13: Deer Lake Complex, 14: Wittenoom dolomite/Carawine dolomite, 15: Hamersley Group.

+0.1 to +1‰ (C. Li, pers. comm.) possibly also indicating a mantle signature, although it has to be borne in mind that at the time of intrusion of the Great Dyke (2.57 Ga) any crustal sulfur would probably show little deviation from mantle values.

The lack of crustal sulfur in the two intrusions may partly be related to the nature of the granite-gneiss and/or quartzite host rocks. More reactive and potentially sulfur-rich pelitic and carbonaceous host rocks are essentially confined to the relatively small northern lobe of the Bushveld Complex. It cannot be a coincidence that this is the only portion of the complex hosting disseminated basal sulfides, within a 50–400 m zone referred to as the Platreef characterized by highly enriched and variable incompatible trace element contents, radiogenic Sr, Nd, Os isotopes and heavy S isotopes (e.g., $^{187/188}\text{Os}$; 0.226, Ruiz *et al.* 2004, $\delta^{34}\text{S}$ up to +10, Barton *et al.* 1986, Buchanan *et al.* 1981, Manyeruke & Maier 2005). This indicates an important role for assimilation of the country rocks in the genesis of this type of ore.

Most other PGE-mineralized intrusions elsewhere are also relatively sulfide-poor possibly suggesting that assimilation of significant external sulfur did not occur in most of the intrusions, and that addition of external sulfur may, indeed, be detrimental to the formation of PGE deposits. However, there are still too few S-isotopic data available to confirm this.

Oxygen isotopes

As oxygen is a major constituent of all important rock forming minerals, variations in oxygen isotope ratios can be applied to detect contamination in a large variety of rocks, some of which may not be readily amenable to other isotopic or incompatible trace element studies, e.g., chromitites. Further, of all the isotope systems, the oxygen system shows one of the most significant differences in isotopic ratios between mantle-derived primitive igneous rocks ($\delta^{18}\text{O}$ generally +5 to +8‰, with MORB having $+5.7 \pm 0.3\%$, Ripley 1999) and the crust ($\delta^{18}\text{O}$ mostly $>8\%$). Therefore, it is somewhat surprising that there are still relatively few oxygen isotope data available for mineralized intrusions and the reef intervals.

A summary of the oxygen isotope data on layered intrusions then available has been given by Ripley (1999). Most of the intrusions have $\delta^{18}\text{O}$ values of around +6‰. The Bushveld and the Great Dyke have somewhat higher values indicating a

larger crustal component. Detailed oxygen isotopic data for the Bushveld Complex were provided by Schiffries & Rye (1989) and Harris *et al.* (2004). The rocks have $\delta^{18}\text{O}$ 6.8–7‰, significantly higher than expected for mantle-derived magmas and indicating 20–40% crustal component in the magma. The data of Harris *et al.* (2004) further indicate relatively little O isotopic variation along strike or with stratigraphic height, suggesting that crust was assimilated in a staging chamber in the lower to middle crust, in broad agreement with the interpretations based on Re/Os (McCandless *et al.* 1999) and Nd isotopic studies (Maier *et al.* 2000). The basal Platreef has higher $\delta^{18}\text{O}$ values (Harris & Chaumba 2001), analogous to many other intrusions (e.g., Duluth, Ripley & Al-Jassar 1987) where the earliest intrusive phases also tend to be the most contaminated.

Oxygen isotopes represent a potentially powerful tool to determine the origin of the Bushveld chromitites and their associated PGE mineralization. Kruger *et al.* (2002) proposed that the layers formed in response to crustal contamination within the Bushveld chamber, whereas Eales (2000) suggested that chromite precipitation commenced at depth followed by entrainment of the crystals and precipitation in the Bushveld chamber.

Oxygen isotope data from the Main Sulphide Zone of the Great Dyke have recently been provided by Li *et al.* (2005). Pyroxenes have $\delta^{18}\text{O}$ 5.7–6.7‰, indicating little contamination.

Oxygen isotopes in the Stillwater Complex were determined by Dunn (1986). The rocks have values of $\delta^{18}\text{O}$ 4.8–8‰ with no apparent variation in the interval hosting the J-M reef. The $\delta^{18}\text{O}$ value for the Stillwater magma was calculated as ca. 5.9, suggesting little contamination of the magma with crust. Minor variation in $\delta^{18}\text{O}$ within individual zones was explained by circulation of late magmatic hydrous fluids.

The O isotope system is relatively susceptible to alteration, with hydrothermally altered rocks showing a wide ratio of $\delta^{18}\text{O}$ from –10 to +15‰ (Ripley 1999). Thus altered rocks have to be filtered out carefully when interpreting oxygen isotope data. High-T alteration can be difficult to detect (e.g., Skaergaard: Taylor & Forrester 1979), but may be characterized by widely spread anomalous $\delta^{18}\text{O}$ as opposed to a more local signature possibly to be expected in the case of crustal contamination (Ripley 1999).

LITHOGEOCHEMICAL INDICATORS USED IN THE EXPLORATION FOR MASSIVE NI-CU SULFIDE DEPOSITS

Introduction

Massive Ni-Cu-(PGE) sulfide ores may be hosted by different lithologies than PGE reefs and they occur in different geological settings. It is thus appropriate to review briefly the main ore-forming processes applicable to massive Ni-Cu-(PGE) ores before discussing the various lithogeochemical tools used in exploration:

- (i) As in the case of the PGE deposits, a prerequisite for the formation of magmatic Ni-Cu ores is that the mantle-derived magmas ascending to upper crustal levels are metal-rich. D values of Ni and Cu with regard to sulfide melt are at least an order of magnitude lower than those of the PGE, and thus the formation of Ni-Cu ores is not impeded if the silicate magma equilibrates with small amounts of sulfide melt prior to emplacement in the upper crust.
- (ii) Whereas magmatic PGE ores can be found in both primitive and differentiated rocks (peridotite to Fe-rich gabbro, chromitite to magnetitite), magmatic Ni ores are confined to relatively primitive rocks (peridotite, pyroxenite, Mg-rich gabbro and norite). This is because Ni partitions into olivine ($D_{\text{olivine-silicate magma}} = \text{ca. } 2-15$, Li *et al.* 2001b). If sulfide saturation is delayed until the magma is relatively differentiated and Ni-poor, the ores will be Ni-poor.
- (iii) Because the price of Ni and Cu is much lower than that of the PGE, large quantities of Ni-Cu sulfides are required to render a deposit mineable. Empirical evidence has shown that this almost always requires addition of external sulfur to the magma, in contrast to most PGE reefs, where addition of external sulfur is probably not required. Thus, Ni-Cu-(PGE) sulfide ores are often (but not always, *e.g.*, Selebi-Phikwe, Gordon 1973) hosted by sulfidic country rocks and many of the largest deposits are found in very sulfide-rich igneous systems (*e.g.*, Pechenga, Kabanga, Noril'sk). The PGE are diluted by the large quantity of sulfides and thus PGE contents of the sulfides are generally much lower (1-20 ppm) than in reef-type deposits (100s of ppm).
- (iv) Once large quantities of sulfide melt have segregated, the sulfides need to be entrained by the flowing magma so that they can interact with

a large volume of magma and become enriched in metals. Sulfide entrainment requires relatively high flow velocities of the magmas, which favors magma conduits and lava channels relative to large intrusions (Naldrett 1997).

- (v) The sulfides need to precipitate and accumulate to form mineable concentrations. Favorable environments are flow-dynamic traps such as widened sections of magma feeder conduits (Noril'sk, Voisey's Bay) or lava channels (Kambalda). Large magma chambers are characterized by less dynamic flow-dynamic conditions and thus, while they may contain large quantities of sulfides (*e.g.*, Duluth, Platreef) the sulfides are usually not concentrated enough to form ores (Maier *et al.* 2001).

Evaluation of chalcophile metal depletion

Methods applied to whole rocks

As in the case of the PGE reef-type deposits, one of the most diagnostic tools to identify an enhanced massive sulfide potential of an igneous system (an intrusion or a lava flow field) is the presence of distinct metal depletion. This is exemplified by the Siberian Traps, one of the largest flood basalt provinces on Earth, that hosts the world's largest Ni-Cu ore deposit. In brief, the model for ore genesis involves (i) ascent of primitive, metal-rich, mantle derived magma into the upper crust, (ii) pervasive heating of the crust by the large quantities of magma, (iii) assimilation of crust including sulfur-bearing lithologies (*e.g.*, evaporite) by some of the magma flows triggering segregation of an immiscible sulfide melt, (iv) entrainment of some of the sulfide melt by the magma and precipitation of sulfide in some of the feeder conduits (Naldrett 2004, and references therein).

Cu/Pd ratios show considerable variation between the individual lava flows, but are mostly significantly above mantle levels (Brügmann *et al.* 1993) (Fig. 14-8). This has been interpreted as a result of extraction of sulfide melt from the lavas in the upper crust. A possible application in exploration is that flood basalt provinces that show variable, but high Cu/Pd above mantle levels have the highest potential for massive sulfide ores in their feeder intrusions.

Cu/Zr data for the Siberian Traps (and the West Greenland flood basalts) have been compiled by Lightfoot & Hawkesworth (1999). Significant metal depletion is again evident in some of the

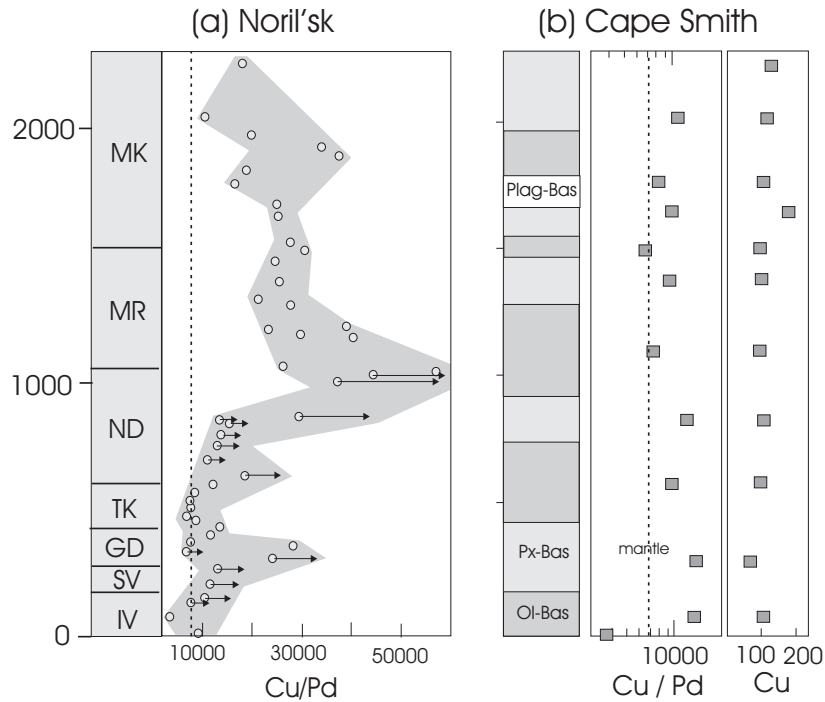


FIG. 14-8: (a) Cu/Pd ratios in the Siberian Traps. Note that most units have Cu/Pd ratios above primitive mantle. Arrows indicate that for the respective samples Pd was below the analytical detection limit and that Cu/Pd values represent minimum values. Figure modified after Maier *et al.* (1998), who used data from Brüggmann *et al.* (1993) and Lightfoot *et al.* (1994). IV=Ivakinsky unit, SV= Syverminsky unit, GD=Gudchikhinsky unit, TK=Tuklonsky unit, ND =Nadezhdinsky unit, MR=Morongovsky unit, MK =Mokulaevsky unit, KH=Kharaelakhsky unit, KM=Kuminsky unit, SM=Samoedsky unit. (b) Cu/Pd in the Chukotat lavas of the Cape Smith fold belt, northern Quebec, and the Raglan Ni sulfide deposit at the base of the sequence (data from Barnes & Picard 1993). Note that most of the basalts are depleted in Pd relative to Cu in primitive mantle. Primitive mantle value is from Barnes & Maier (1999).

units, notably the Ivakinsky (IV), Syverminsky (SV) and Nadezhdinsky (ND) units (Fig. 14-9). The West Greenland lavas also contain flows with low Cu/Zr (Fig. 14-10, as well as fractionated incompatible trace element ratios and crustal Sr and Nd isotopic ratios, see below), indicating to the explorationist an enhanced potential for hidden ore bodies at depth.

Andersen *et al.* (2002) compiled data for flood basalts in the North Atlantic Igneous Province and found that several of the basaltic sequences show evidence for metal depletion, notably in east and west Greenland as well as the British Volcanic Province. As in the cases discussed above, this has to be considered a positive exploration indicator for sulfide ores in feeder conduits.

The Karoo lavas of Lesotho show relatively uniform Cu/Zr ratios around unity (Marsh *et al.* 1997, Maier *et al.* 2003b) (Fig. 14-11b) whereas Cu/Pd ratios are consistently higher than mantle (Fig. 11b). This could suggest that these magmas

equilibrated with small amounts of sulfide melt prior to emplacement into the upper crust. As an alternative, Maier *et al.* (2003b) proposed that small amounts of PGE-enriched sulfides were retained in the mantle source during partial melting. If this model is correct then feeder conduits associated with the Lesotho basalts would have a relatively low potential to host sulfides, but this does not exclude the presence of sulfide ores in other areas of the Karoo igneous province.

Rocks within the Voisey's Bay intrusive system show considerable variability in Cu/Zr (Li & Naldrett 1999). Many of the sulfur-poor samples from the feeder conduit have Cu/Zr ratios below unity indicating crystallization from metal-depleted magmas (Fig. 14-12). Other rocks from the conduit are undepleted in metals, suggesting that these rocks crystallized from undepleted surges of magma that flushed some of the earlier metal-depleted magmas out of the conduit. The variation in Cu/Zr is believed to be the result of the segregation of the

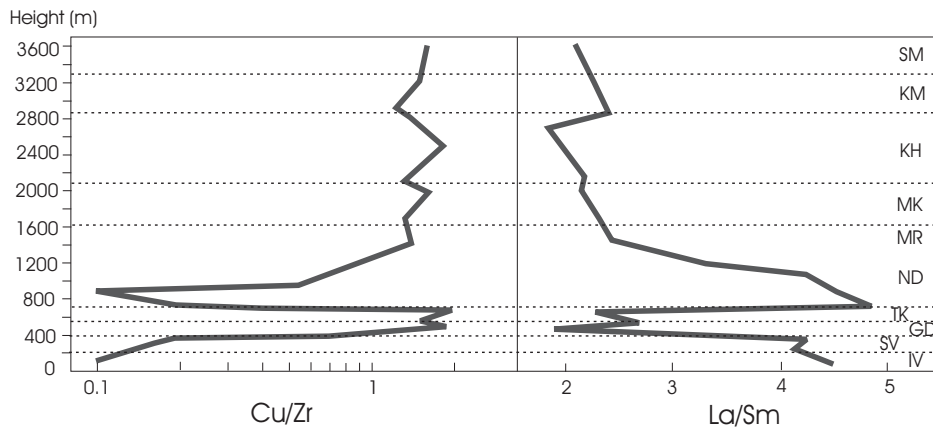


FIG. 14-9: Cu/Zr and La/Sm in the Siberian Traps. Figure modified after Lightfoot & Hawkesworth (1999).

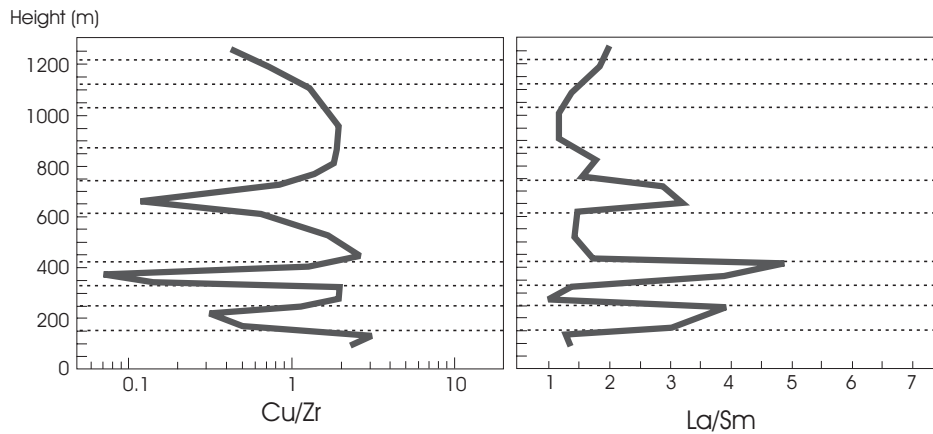


FIG. 14-10: Cu/Zr and La/Sm in West Greenland basalts (Qeqertarsuaq). Figure modified after Lightfoot & Hawkesworth (1999).

ore-forming sulfides. Notably, the sulfides are relatively PGE-poor (<1 ppm PGE in 100% sulfides, Naldrett *et al.* 2001) indicating that the magmas equilibrated with sulfides prior to emplacement. This illustrates that PGE depletion in mantle-derived magmas does not limit their Ni potential, a point that is equally evident in the PGE-poor Pechenga and Selebi-Phikwe ores (Barnes *et al.* 2001, unpublished data of Maier).

Patterns of metal depletion in komatiite lava flows are often difficult to interpret. Most komatiites were probably sulfur-undersaturated during eruption (Leshner & Groves 1986, Stephen J. Barnes *et al.* 2004c). Sulfide saturation may be reached in specific environments of high substrate erosion, notably lava channels, whereas adjacent associated sheet flows and lava lakes could remain sulfur-undersaturated and show very little PGE depletion. Thus, the apparent absence of metal

depletion in a komatiite flow field does not necessarily imply that there are no Ni deposits. Moreover, komatiites have a particularly low viscosity and high flow velocity and thus any signature of metal depletion in the residual magmas to the ores is commonly diluted by successive surges of undepleted magma. In some cases, the ores are overlain by cumulates that are undepleted in terms of metals (*e.g.*, Western Australian komatiites, Stephen J. Barnes *et al.* 2004b). Together with the relatively small size of the prospective lava channel environments compared to the size of the flow fields these characteristics make the localization of Ni sulfide ores in komatiites particularly challenging.

The Raglan deposits of northern Quebec are an example of a picrite-related Ni-sulfide deposit. The ores are located within flow channels that are overlain by 3–4 km of picritic lavas of the Chukotat

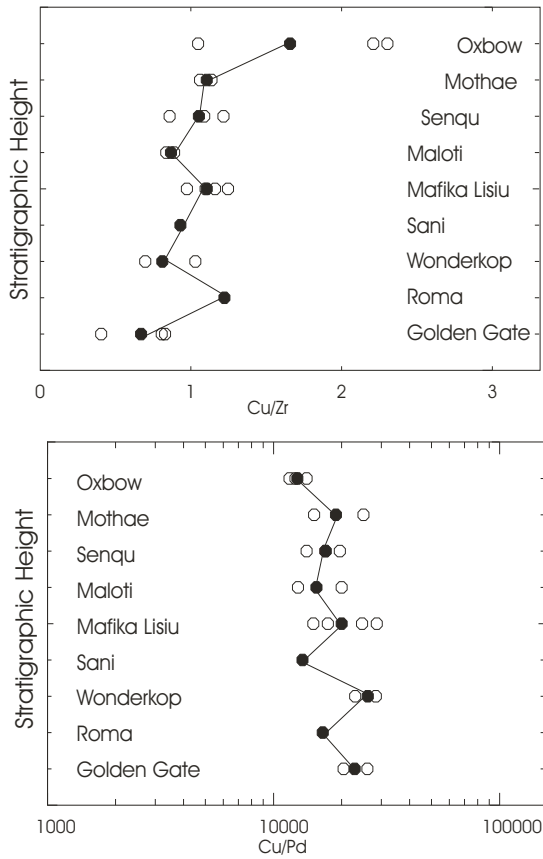


FIG. 14-11: Cu/Zr and Cu/Pd in the Karoo flood basalts in Lesotho and the eastern Cape Province of South Africa. Figure from Maier *et al.* (2003b).

Group (MgO 16.5%, Francis *et al.* 1981, Barnes & Picard 1993). Cu/Pd ratios in the Chukotat lavas show considerable variation, from primitive mantle values to strongly Pd-depleted (Fig. 14-8b). This signature of variable metal depletion is interpreted to be the result of upper crustal sulfide segregation giving rise to the ores (Barnes & Picard 1993). Of note is the fact that Cu/Zr ratios of the Chukotat basalts do not show a signature of depletion (values are mostly 1–2). This is possibly due to the much smaller size of the ore bodies relative to those at Noril'sk.

Nickel can be used in an analogous manner to Cu in tracing metal depletion of magma if one corrects for the fact that Ni also partitions into olivine, pyroxene and oxides. The Ni content of a fractionating magma that remains undersaturated with regard to sulfide melt can be readily computed using software programs such as MELTS (Ghiorso & Sack 1995). Naldrett (1989) produced curves of Ni vs. MgO contents in komatiites for variable

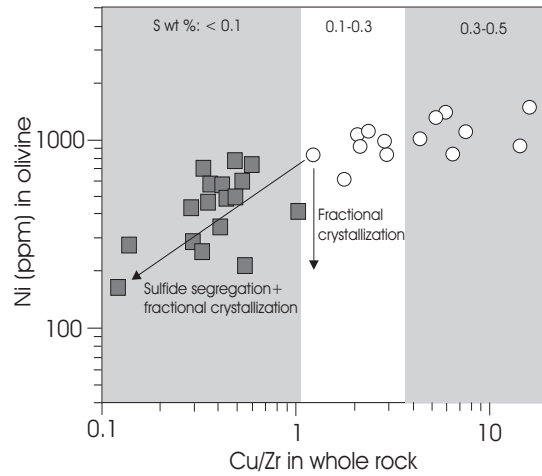


FIG. 14-12: Ni in olivine vs. Cu/Zr in the Voisey's Bay intrusion. Sulfide-poor rocks of the feeder olivine gabbro, olivine gabbro, and leucotroctolite units have Cu/Zr below unity, which is interpreted to be the result of sulfide segregation from the magmas. In contrast, rocks from the normal troctolite and varied-textured troctolite units have Cu/Zr >1 indicating cumulus sulfides. Figure from Li & Naldrett (1999).

degrees of sulfide extraction. He showed that barren komatiites plot on fractionation curves equivalent to sulfur-undersaturated magmas whereas mineralized komatiites from different localities plot on curves indicating variable degrees of sulfide extraction (Fig. 14-13). The implication is that Ni contents of komatiites can potentially be used to predict the presence of ores. However, the extensive, more recent data of Stephen J. Barnes *et al.* (2004b) from Western Australian Ni deposits including Kambalda, Black Swan, Forestania and Lake Johnston show little Ni depletion in the komatiites hosting the ores. The authors therefore suggested that small high-grade ore shoots that form at high R-factors cannot be detected using Ni/MgO ratios of the rocks as the segregating sulfides do not deplete Ni sufficiently. In contrast, komatiites at Perseverance and Mt Keith which host large low R-factor ore bodies do show marked patterns of Ni depletion in the rocks overlying the ores.

Methods applied to minerals: Ni contents of olivine and pyroxenes

Significant sulfide extraction at a low R-factor from a magma should also be reflected in relatively low Ni contents of subsequently crystallized olivine (and perhaps pyroxene and oxides). In an ideal scenario Ni content of olivine within an intrusion or a lava sequence shows considerable variation,

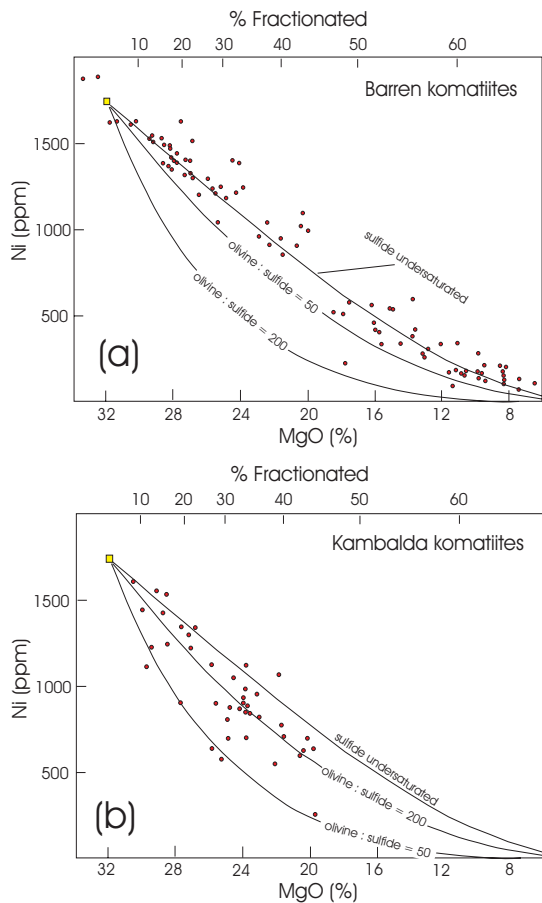


FIG. 14-13: Ni vs. MgO in komatiites that have a starting composition of 32 % MgO and fractionate olivine and sulfide in varying proportions (solid lines). (a) barren komatiites from Canada, Australia, Zimbabwe and Finland, and (b) spinifex-textured peridotites from Kambalda. Figure modified after Naldrett (1989).

i.e., one would expect to find Ni-depleted and undepleted rocks. In contrast, if all the rocks from an igneous system are depleted in Ni, then it is likely that sulfide segregation occurred prior to emplacement, at an inaccessible depth. If none of the olivine in an igneous system is Ni-depleted several possibilities arise. (i) The magmas were undersaturated in sulfide melt and the presence of sulfide ore bodies is unlikely. (ii) Sulfides could have segregated at a high R-factor possibly forming small high-grade ore bodies. (iii) The magmas from which sulfides segregated could have been displaced by undepleted magma surges.

Detailed studies of olivine compositions have recently been conducted at Noril'sk by Li *et al.* (2003) and Arndt *et al.* (2003). Both studies

concluded that individual intrusions crystallized from several surges of compositionally unrelated magma, and that in the ore-bearing intrusions there is little evidence for Ni depletion of the olivine. As an explanation, it was proposed that the magma from which the sulfides segregated was flushed out of the magma conduits by later surges of metal-undepleted magma. In contrast, the unmineralized intrusions are generally characterized by relatively Ni-depleted olivine.

Lightfoot *et al.* (1984) observed a pattern of variably, but in places distinct, Ni depletion in olivine of the Insizwa and Tabankulu lobes of the Mount Ayliff Complex, South Africa (Fig. 14-14a), which has been interpreted as a feeder chamber to the Karoo flood basalts. As the Mount Ayliff Complex does not contain any significant sulfide ores Lightfoot *et al.* (1984) went on to propose that important quantities of sulfides segregated from the magmas at depth, prior to emplacement of the Mount Ayliff Complex.

Li & Naldrett (1999) demonstrated that at Voisey's Bay rock units that show depletion in Cu/Zr also contain olivine that is Ni-depleted. Li *et al.* also analyzed olivine at other conduit-hosted sulfide deposits, notably Jinchuan and Uitkomst (Li *et al.* 2004, Li *et al.* 2002).

The Uitkomst Complex of South Africa is an example where Ni contents of olivine are indiscriminate with regard to the presence of sulfide ores. The tube-like intrusion has been interpreted as a conduit to the Bushveld Complex (Gauert *et al.* 1995). Massive sulfides are situated in the immediate floor rocks of the intrusion and disseminated sulfides are located in peridotites and pyroxenites in the basal portion of the intrusion. The sulfide-mineralized rocks are overlain by several 100 m of unmineralized harzburgite and gabbro-norite. Olivine within the sulfide-mineralized rocks has relatively lower Ni (1300–1900 ppm) and Fo (85–89) contents than that within the overlying unmineralized harzburgite (2000–3300 ppm Ni at Fo 88–90), but none of the olivine from the intrusion is plotting outside the field of layered intrusions of Simkin & Smith (1970). Analysis of the rocks would not have given any indication of the potential for massive and disseminated sulfides, analogous to some other highly dynamic systems elsewhere, *e.g.*, komatiite lava channels.

Ni contents of olivine have also been studied in the Kunene Complex of Namibia–Angola (Fig. 14-15 (Maier *et al.* 2005). This represents one of the largest anorthosite-troctolite massifs on Earth

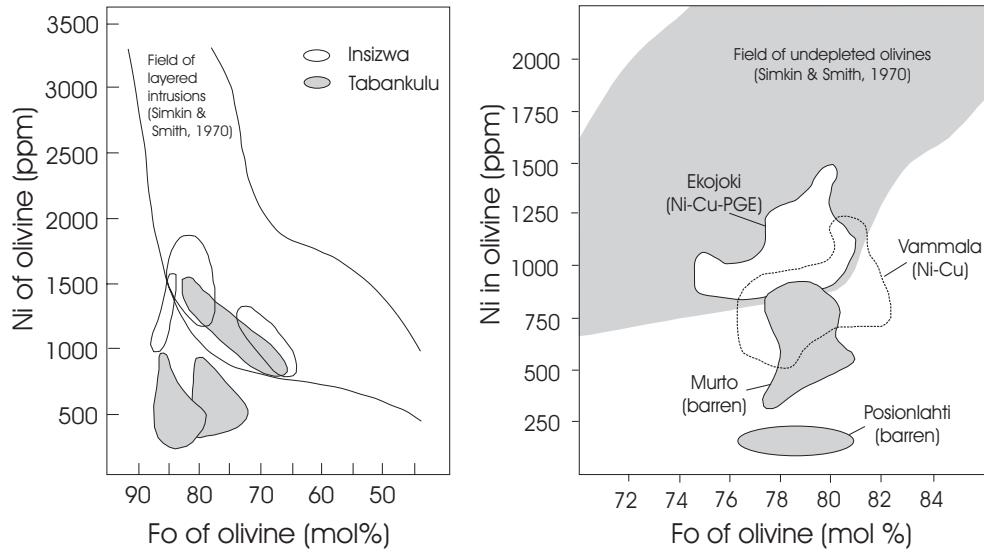


FIG. 14-14: Ni plotted vs. Fo in (a) the Insizwa and Tabankulu lobes of the Mount Ayliff Complex of South Africa (figure modified after Lightfoot *et al.* 1984), and (b) the Vammala Ni belt of western Finland (figure modified after Peltonen 1995). Note that in both cases the rocks are characterized by pronounced patterns of Ni depletion. At Insizwa, a small Ni-Cu sulfide deposit occurs. In the Vammala belt several small ore deposits occur. At Tabankulu no sulfides have been located.

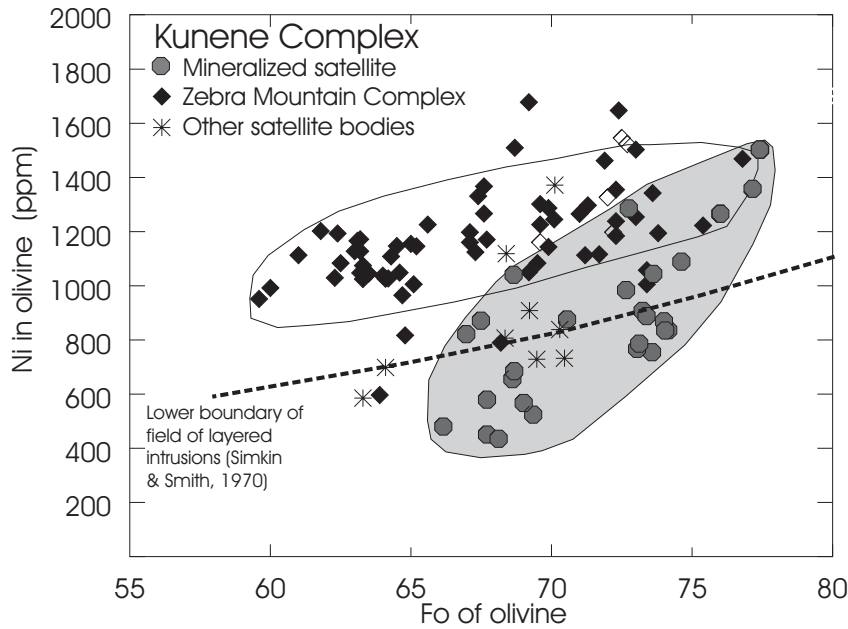


FIG. 14-15: Ni vs. Fo in olivine from the Kunene Complex, Namibia (Maier *et al.* 2005). Note that main anorthosite (Zebra Mountain lobe) has undepleted olivine, but sulfide mineralized satellite intrusion shows variably depleted olivine.

(Ashwal & Twist 1994) and has seen considerable exploration interest for Ni following the discovery of the Voisey's Bay deposit. Ni-rich disseminated sulfides (<5%) have been located in a relatively small troctolitic satellite intrusion, but the main anorthosite-troctolite mass in Namibia (the Zebra

Mountain Complex) appears to be unmineralized. This pattern is closely reflected in the composition of olivine, in that the main anorthosite-troctolite has undepleted olivine, whereas the mineralized satellite intrusions contain both depleted and undepleted olivine.

Sulfide mineralized intrusions at Kabanga, Tanzania, provide another useful case study with regard to the application of olivine compositions in exploration (Fig. 14-16). Magmatic sulfides at Kabanga are hosted by tubular and sill-like intrusions, tens to hundreds of metres in width that were emplaced into sulfidic pelite and schist. Two of the intrusions host important Ni ores (Kabanga North and Kabanga Main) whereas several others host low-grade massive and disseminated sulfides. The olivine from all intrusions is mostly depleted in Ni but shows considerable compositional variation. Those intrusions hosting metal-poor sulfides contain extremely Ni-depleted olivine whereas those intrusions hosting high-grade ores contain olivine with highly variable Ni contents.

The Vammala Ni belt of Finland contains intrusions that share certain morphological and compositional features with the Kabanga deposits (Peltonen 1995), notably the occurrence of metal rich sulfides at the base of synorogenic dyke- and pod-like intrusions. Sulfide segregation is thought to have occurred due to significant assimilation of external S, and the intrusions are characterized by variable to extreme levels of Ni depletion in olivine (Fig. 14-14b).

Compatible Elements as Indicators for Prospective Volcanological Environments

As has been pointed out earlier, compatible elements are relatively poor indicators for the sulfide potential of an intrusion or a lava flow. However, the concentrations of these elements can be used to distinguish primitive rocks that have potential to host Ni-sulfide ores from relatively more differentiated rocks in which any sulfides that may occur are likely to be Ni-poor. For example, it is unlikely to find a Ni deposit in a rock with Mg# less than *ca.* 0.65 and containing cumulus magnetite as well as abundant quartz, albite or K-feldspar.

Compatible elements have also been used to provide vectors for prospective volcanological settings, notably sulfide-mineralized lava channels within compound komatiite flow fields (Brand 1999, Stephen J. Barnes *et al.* 2004b). Primitive magmas within lava channels that are the main target for sulfide ores show relatively higher Fo and Ni contents and lower Cr contents than differentiated chromite-rich sheet flows and lava lakes that tend to be barren. However, there is little compositional difference between mineralized and unmineralized lava channels.

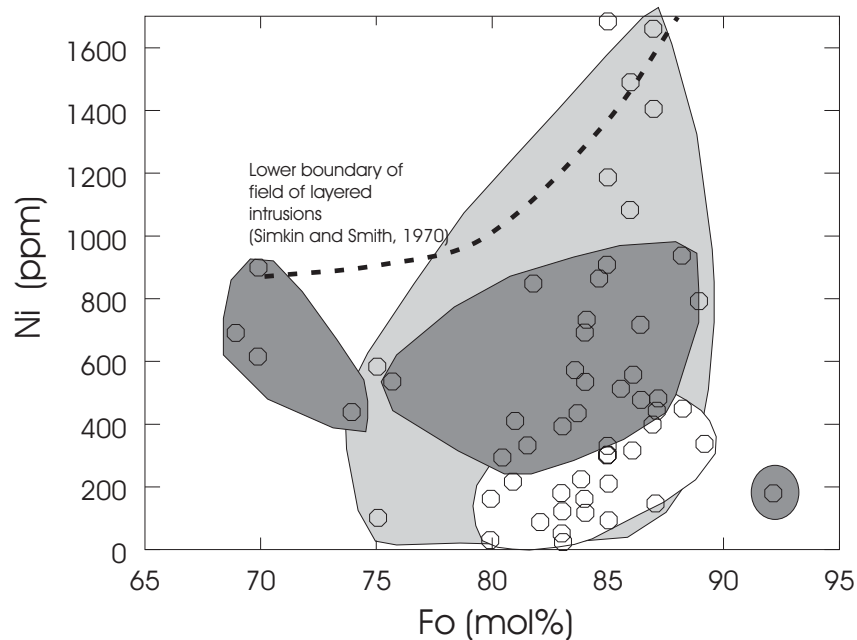


FIG. 14-16: Ni vs. Fo for olivine in the Kabanga intrusions. Dark gray fields mark intrusions containing high grade sulfides (Kabanga North and Kabanga Main). Medium gray field marks intrusions with medium grade sulfides. White field marks intrusions with low-grade sulfides; Maier *et al.* (2004).

Contamination of magma with crust

The sulfur solubility of basaltic magmas increases with falling pressure (Mavrogenes & O'Neill 1999, Wendlandt 1982) and thus primary mantle-derived magmas tend to be S-undersaturated during emplacement, no matter whether they were S-saturated or undersaturated in the mantle. Sulfur saturation may eventually be reached during differentiation (sulfur is not incorporated into the fractionating silicates and oxides) and crystallization of Fe-rich minerals (sulfur is bonded to Fe^{2+} in the magma and thus fractionation of Fe-rich minerals, notably olivine, pyroxenes, chromite and magnetite causes a decrease in sulfur solubility that may lead to sulfur saturation, Haughton *et al.* 1974, Shima & Naldrett 1975, Li *et al.* 2001a), but this may happen at a stage when the Ni in the magma is already depleted. In order to achieve early saturation in sulfide, addition of external sulfur is normally required, by means of devolatilization, partial melting, or bulk assimilation of sulfidic country rocks (Ripley 1999, Leshner & Campbell 1993, Baker *et al.* 2001). These processes should result in a crustal component in the rocks that can potentially be used as an exploration guideline. However, complications abound. The crustal component may be flushed out of dynamic igneous systems (*e.g.*, komatiite lava channels, Stephen J. Barnes *et al.* 2004b) and thus the absence of a crustal signature from an igneous rock does not necessarily exclude the possibility of a sulfide deposit. Equally, the presence of a crustal component does not necessarily indicate the presence of a deposit:

- (i) The amount of contamination may have been insufficient to trigger S saturation, particularly if the magmas were highly sulfur-undersaturated such as proposed for many second-stage mantle melts (Hoatson & Keays 1989).
- (ii) The necessary concentration mechanism may have been lacking, particularly in large intrusions such as the Bushveld Complex. Here, abundant (PGE-rich) disseminated sulfides occur along the base of the complex in the Platreef, but massive sulfides that could be mined for Ni and Cu as main products are absent.
- (iii) The crustal signature may be derived from the lithospheric mantle source as proposed in the case of siliceous high-magnesian basalts (SHMB, Hoatson & Keays 1989) and

continental flood basalts (Erlank 1984, Harmer & von Gruenewaldt 1991), a possibility that is difficult to evaluate using trace element studies alone, but complimentary oxygen isotope studies offer potential for further insight (Baker *et al.* 2000).

- (iv) The crustal signature may be the result of alteration as in many komatiites (Arndt & Jenner 1986). For example, Stephen J. Barnes *et al.* (2004b) documented addition of elements such as LREE and Zr.

In the following discussion a number of examples will be presented where the presence of a crustal component is correlated with the presence of ores and where the identification of the crustal component could have been used to predict the presence of the ores.

Lithophile-incompatible trace elements

A well-defined positive correlation between the presence of a crustal component and sulfide ores is observed in the Siberian Traps from which the Noril'sk Ni-Cu-(PGE) deposits are thought to have formed. The lavas show elevated contents of incompatible trace elements, fractionated incompatible trace element patterns and negative Nb-Ti anomalies (*e.g.*, Wooden *et al.* 1993, and Fig. 14-17). Some, but not all, of the feeder intrusions are mineralized. Individual magma flows are believed to have ascended through different crustal lithologies assimilating various amounts and types of crust and thus external S. This has not only

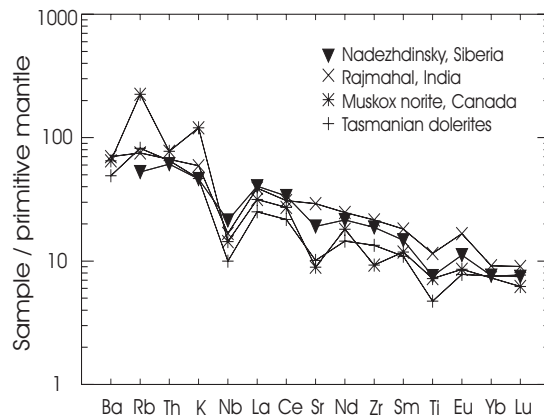


FIG. 14-17: Primitive mantle normalized trace element patterns for a number of continental flood-type basalts. Normalization factors are from Thompson *et al.* (1983). Figure has been modified after Maier *et al.* (2000) who used data of Hergt *et al.* (1989), Lightfoot *et al.* (1990), Francis (1994) and Kent *et al.* (1997).

resulted in variable degrees of mineralization in the intrusions, but also in different amounts of crustal component in the intrusions and the lava flows (Lightfoot & Hawkesworth 1999). One of the lava units with the highest crustal component (and the strongest metal depletion) is the Nadeshdinsky suite, as expressed by elevated La/Sm (Fig. 14-9) and Th/La (Wooden *et al.* 1993; Lightfoot & Hawkesworth 1999). This has caused some authors to propose that the bulk of the ores at Noril'sk precipitated from the Nadeshdinsky unit (Lightfoot *et al.* 1994), but others have expressed diverging opinions (Czamanske *et al.* 1994, Arndt *et al.* 2003, Ripley *et al.* 2003, see below). Whatever the case, the Noril'sk example illustrates that lithophile element analysis of the basalts would have indicated to the explorationist that: (i) there is evidence for an enhanced crustal component; and (ii) some of the lavas have reached sulfide saturation. This reasoning was used by Lightfoot & Hawkesworth (1999) to highlight the prospectivity of flood basalts in West Greenland, where individual lava flows also show distinct variation in incompatible trace element ratios and thus crustal component (Fig. 14-10).

An example of the potential complications in using the presence of a crustal component in a flood basaltic sequence to indicate enhanced sulfide potential of associated feeder intrusions is the Karoo flood basalts of southern Africa. The Karoo (and many other southern African) flood-type basalts have a distinct crustal trace element signature (Fig. 14-3), but only a small sulfide deposit is known to occur (at Waterfall Gorge, Insizwa lobe of the Mount Ayliff Complex, Lightfoot *et al.* 1984). It has long been debated whether the crustal signature of the Karoo lavas reflects the assimilation of crust during ascent or melting of a metasomatized lithospheric mantle source (Marsh & Eales 1984, Harmer & von Gruenewaldt 1991, Maier *et al.* 2000, 2003b). The latter model is potentially supported by the relative uniformity in trace element signature amongst the southern African flood type lavas that erupted over some 3 Ga and through a variety of crustal lithologies (Marsh *et al.* 1989). The model would also be in agreement with the apparent scarcity of sulfide deposits in the Karoo igneous province although the absence of an external S source could also play a role. On the other hand, many flood basalts show heavy oxygen isotopic signatures (*e.g.*, Baker *et al.* 2000) which indicates that at least some

crustal contamination must have occurred during ascent.

A useful example illustrating the complexity of Ni ore-forming processes is provided by a comparison between the Voisey's Bay and Pants Lake intrusions (Li *et al.* 2001c, Kerr 2003). In both cases, troctolitic-gabbroic magmas have assimilated S-bearing gneissic country rocks resulting in a crustal signature of the magmas, and triggering sulfide segregation. At Voisey's Bay the sulfides were subsequently entrained by the magma and concentrated in magma conduits. At Pants Lake the sulfides segregated in a closed magma chamber and thus could not be upgraded or concentrated. Thus, while lithophile trace element signatures can direct the explorationist to prospective igneous systems, the location of the ores is ultimately controlled by a number of additional factors.

In other cases, notably the Kabanga-Musongati belt of intrusions of Tanzania–Burundi, incompatible trace element studies are more discriminative regarding the magmatic sulfide ore potential of an intrusion. The belt contains Ni targets represented by mostly relatively small, but very sulfide-rich intrusions (Kabanga) and PGE targets represented by larger sulfide-poor layered intrusions (Kapalagulu). The sulfide-rich intrusions have a higher crustal component than the sulfide-poor intrusions (Fig. 14-18), as expressed by more fractionated trace element patterns and higher concentrations of immobile incompatible trace elements. This is presumably due to more significant assimilation of crust. Within the Kabanga group of intrusions, the ones richest in Ni (Kabanga North and Main) have the highest crustal component (Fig. 14-19). Data from poorly known or newly discovered intrusions can be compared to the Kabanga-Kapalagulu intrusions to determine if they are PGE targets or Ni targets. For example, the available data from the Musongati intrusion in Burundi (Bandyera 1997) indicate a relatively small crustal component in the ultramafic rocks, suggesting that this body is a PGE target rather than a Ni target.

A similar exercise can be attempted in the co-magmatic Uikomst and Bushveld complexes (Fig. 14-20). Ultramafic rocks of the sulfide- and xenolith-rich Uikomst Complex have relatively high La/Yb and Ce/Lu ratios compared to the bulk of the sulfide-poor Bushveld ultramafic rocks (most of the high ratios in the Bushveld come from the relatively contaminated basal rocks of the intrusion).

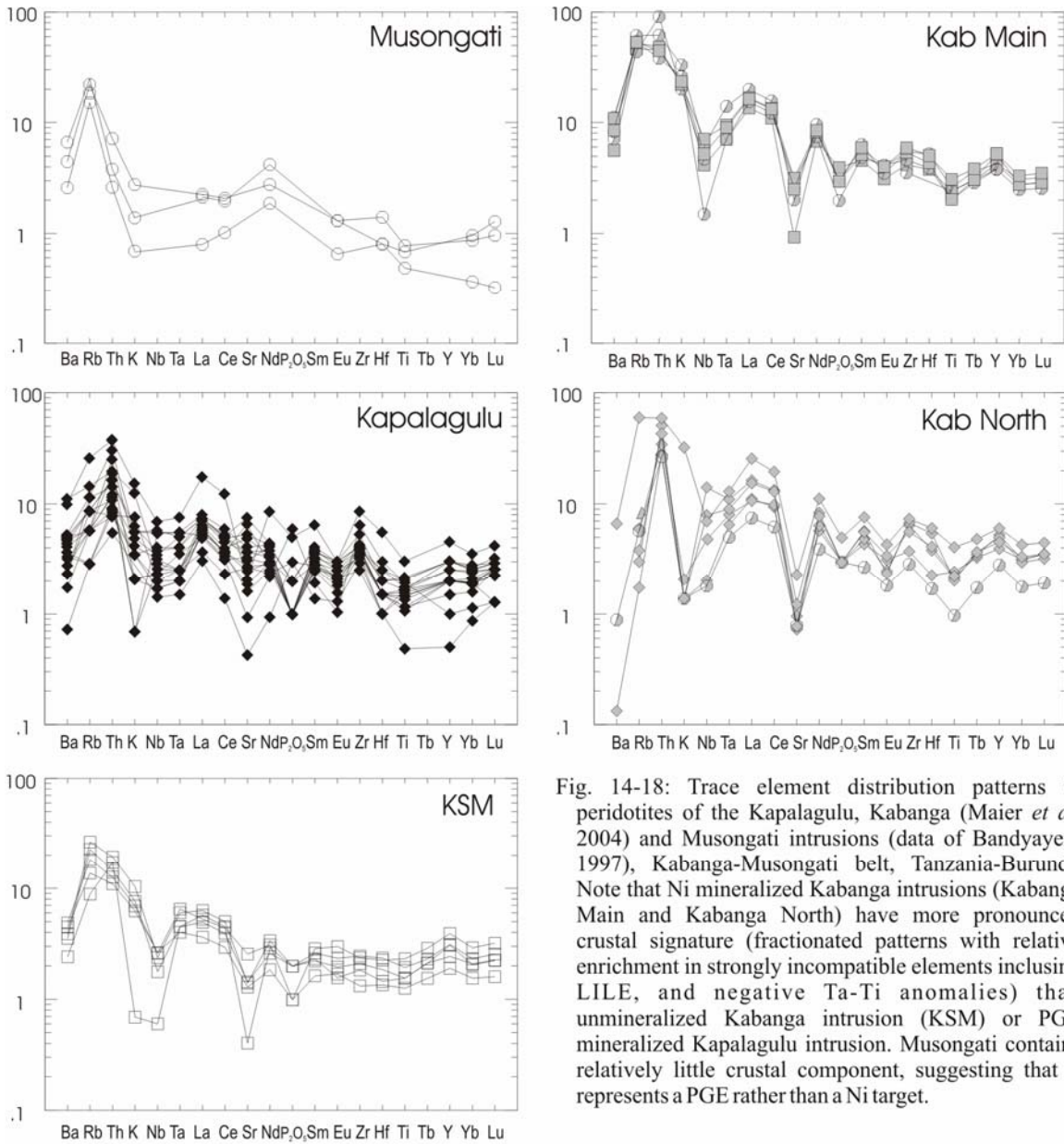


Fig. 14-18: Trace element distribution patterns in peridotites of the Kapalagulu, Kabanga (Maier *et al.* 2004) and Musongati intrusions (data of Bandyayera 1997), Kabanga-Musongati belt, Tanzania-Burundi. Note that Ni mineralized Kabanga intrusions (Kabanga Main and Kabanga North) have more pronounced crustal signature (fractionated patterns with relative enrichment in strongly incompatible elements including LILE, and negative Ta-Ti anomalies) than unmineralized Kabanga intrusion (KSM) or PGE mineralized Kapalagulu intrusion. Musongati contains relatively little crustal component, suggesting that it represents a PGE rather than a Ni target.

Strontium and neodymium isotopes

The application of isotopic studies in massive sulfide exploration, and some of the complications arising, may be illustrated by means of the well-studied Ni-Cu-PGE sulfide ores at Noril'sk-Talnakh that are thought to have precipitated from the Siberian Trap flood basalts. Amongst the individual flows building the lava sequence, the Nadeshdinsky unit is characterized by a combination of particularly fractionated and enriched incompatible trace element signatures, pronounced metal depletion, and a marked

radiogenic initial Sr isotopic ratio (Wooden *et al.* 1993; Czamanske *et al.* 1994, Lightfoot & Hawkesworth 1999) (Fig. 14-21). These features have been interpreted by some authors to reflect enhanced contamination of the Nadeshdinsky lavas triggering saturation in sulfide melt (Lightfoot *et al.* 1994) and precipitation of the sulfide melt to form the ore deposits. As there are some discrepancies between the composition of the mineralized intrusions and the Nadeshdinsky lava flow (Czamanske *et al.* 1994, Ripley *et al.* 2003), it was proposed that the sulfide magmas may have

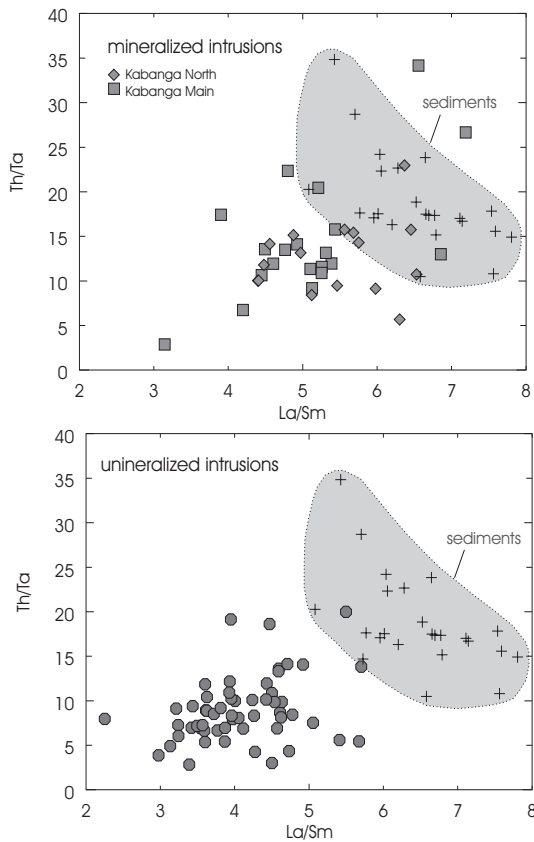


FIG. 14-19: Trace element ratios in the Ni sulfide mineralized Kabanga North and Main intrusions and in intrusions containing Ni-poor sulfides in the Kabanga area (Maier *et al.* 2004).

intruded at a relatively late stage along the base of the intrusions (Likhachev 1994; Lightfoot *et al.* 1994). Other authors feel that the ores in the mineralized Noril'sk intrusions precipitated from the MR and MK magmas that have a much less pronounced crustal isotopic signature, whereas the poorly mineralized lower Talnakh intrusions crystallized from the ND magmas (Naldrett *et al.* 1995). The message for the explorationist is that the precise locality of ores in the system cannot be determined by relying on isotopic (or trace element) studies alone, but that such studies can confirm the presence of a crustal signature in the larger system which is an indicator for enhanced prospectivity.

An analogous correlation between enrichment in incompatible trace elements and crustal Sr (and Nd) isotopes to that observed in the Siberian traps was also observed in the west Greenland basalts (Lightfoot & Hawkesworth 1999), causing speculation about hidden ore bodies.

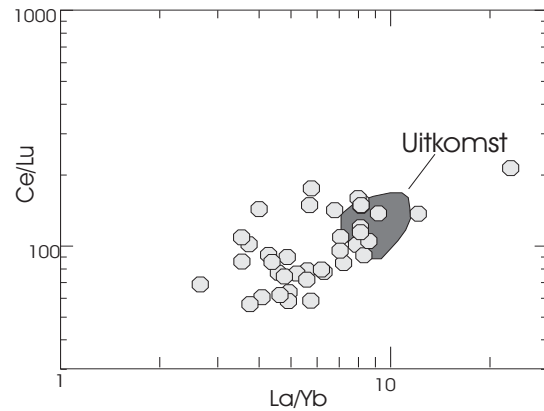


FIG. 14-20: Comparison of REE ratios in ultramafic rocks of sulfide-poor Bushveld Complex and sulfide-rich Uitkomst Complex (data from Maier and Barnes 1998, and Gomwe 2003). Note that bulk of Bushveld rocks has lower crustal component than Uitkomst rocks.

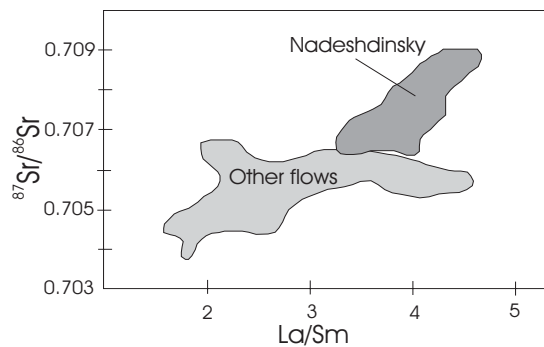


FIG. 14-21: Initial Sr isotope ratios plotted vs La/Sm in the Siberian Traps. Figure modified after Lightfoot & Hawkesworth (1999). See text for explanation.

The Karoo basalts also show considerable variation in their Sr isotopic signature (Marsh *et al.* 1997), with elevated Sr_i values being particularly characteristic for some of the basal flows (*e.g.*, Golden Gate and Roma units, Marsh *et al.* 1997). However, contrary to the preferred model at Noril'sk, many workers studying the Karoo magmas favor a lithospheric mantle derivation of the crustal signature (*e.g.*, Marsh & Eales 1984), which would be a less positive indicator for sulfide potential than contamination during ascent. On the other hand, a positive correlation between crustal Sr_i isotopic ratios and the presence of Ni-Cu sulfides is observed in the basal ultramafic cumulates of the Insizwa intrusion (at Waterfall Gorge) that is interpreted to represent a staging chamber to the flood basalts (Maier *et al.* 2002).

Radiogenic isotope data on the Kabanga-Kapalagulu intrusions are not yet available, but data from the presumably related intrusions in Burundi (Deblond & Tack 1999, Duchesne *et al.* 2004) indicate a high and variable crustal component ($\epsilon\text{Nd} +9$ to -8 , Sr_i 0.701–0.713). Duchesne *et al.* (2004) and Evans *et al.* (1999) felt that the isotopic (and trace element) data from the intrusions indicate derivation of the magmas from an enriched lithospheric mantle source. However, the variability of the trace element data (Figs. 14-18, 14-19), the abundance of country rock xenoliths, and the heavy S isotopic signatures of the rocks (discussed below) all indicate that contamination during emplacement must have happened as well.

Osmium isotopes

Lambert *et al.* (1998b) summarized the Re–Os isotopic information then available from a number of magmatic sulfide deposits. One of the main conclusions of their review was that the Os isotopic signature of sulfide ores is strongly dependent on the R-factor during sulfide segregation. For example, the Noril'sk-Talnakh ores have relatively unradiogenic Os isotopic ratios (γOs 0 to +13, Walker *et al.* 1994), which has been interpreted to be the result of modification of the isotopic composition during entrainment of the sulfides by successive batches of fertile magmas, essentially constituting a high R-factor environment. Komatiite-hosted ores from western Australia (Kambalda, Perseverance, Mt Keith) typically also have near chondritic Os isotopic ratios, but in these cases an interpretation whereby the sulfides equilibrated with successive surges of metal-undepleted magmas is inappropriate because other data (notably metal ratios) indicate relatively low R factors for the ores. Thus, the Os isotope data of the komatiites suggest low degrees of crustal contamination to some authors (Lambert *et al.* 1998b).

Pechenga sulfides show a much higher crustal component (γOs +50 to +250, Walker *et al.* 1997), indicating up to *ca.* 10% *in situ* crustal contamination. On the other hand, the Nd isotopic study of Hanski *et al.* (1990) showed mantle-like values ($\epsilon\text{Nd} +1.4$) in the ferropicrites, suggesting that the elevated Os isotopic signature could at least partially be the result of alteration.

Basal sulfides in the Duluth and Stillwater Complexes have radiogenic Os ratios suggesting contamination with old crust (Ripley *et al.* 1998, Lambert *et al.* 1994). This interpretation is in accord

with the presence of xenoliths in the rocks (Zientek *et al.* 2002, Ripley & Al-Jassar 1987).

Sulfide ores at Voisey's Bay have high γOs (1040 ± 20 , Lambert *et al.* 1999) suggesting an important component of crustal Os and supporting a model of sulfide supersaturation in response to between 2–16% upper crustal contamination. Equilibration of the sulfides with fluids during metamorphism may have led to some modification of the Os isotopic data (Lambert *et al.* 2000).

Sulfur isotopes

Sulfur isotopic studies have shown that many large Ni–Cu sulfide deposits formed by addition of external sulfur to the magma (Fig. 14-22, Ripley 1999 and references therein; *e.g.*, Noril'sk, Pechenga, Kabanga, Kambalda, Duluth, Voisey's Bay). In some cases there is excellent agreement between the grade of mineralization and the amount of crustal sulfur present in the rocks (Noril'sk, Grinenko 1985). At Kabanga, the magmatic and sedimentary sulfides have virtually identical signatures (Fig. 14-23) suggesting a relatively local derivation of the S. Kabanga sulfides have the heaviest S isotopes of any large magmatic sulfide deposit, indicating an unusually large contribution of external S to the ores. This model is supported by extreme degrees of metal depletion in some of the intrusions (*e.g.*, Fig. 14-16).

The relative importance of addition of external sulfur in ore genesis has remained more controversial at Pechenga. Some of the ores have a crustal S isotopic signature ($\delta^{34}\text{S}$ up to +10) but in other deposits the sulfur is mantle-like. Melezhik *et al.* (1998) showed that the $\delta^{34}\text{S}$ of the sedimentary rocks hosting the deposits evolves from near zero at the synsedimentary stage to strongly positive values at the late stage of diagenesis. According to Melezhik *et al.* (1998), those deposits that have crustal signatures formed during emplacement of magma into consolidated sediments, whereas those deposits with mantle-like signatures formed during eruption of lavas onto poorly consolidated sediments.

The exploration implication of the available S isotope data is that if an intrusion or a lava flow contains crustal sulfur there is enhanced potential for the presence of a deposit, but if the sulfides have a mantle-like S isotopic signature the presence of sulfide ores cannot be ruled out. This is particularly so in rocks older than *ca.* 2.8 Ga, including many early Archean komatiites or Archean magma

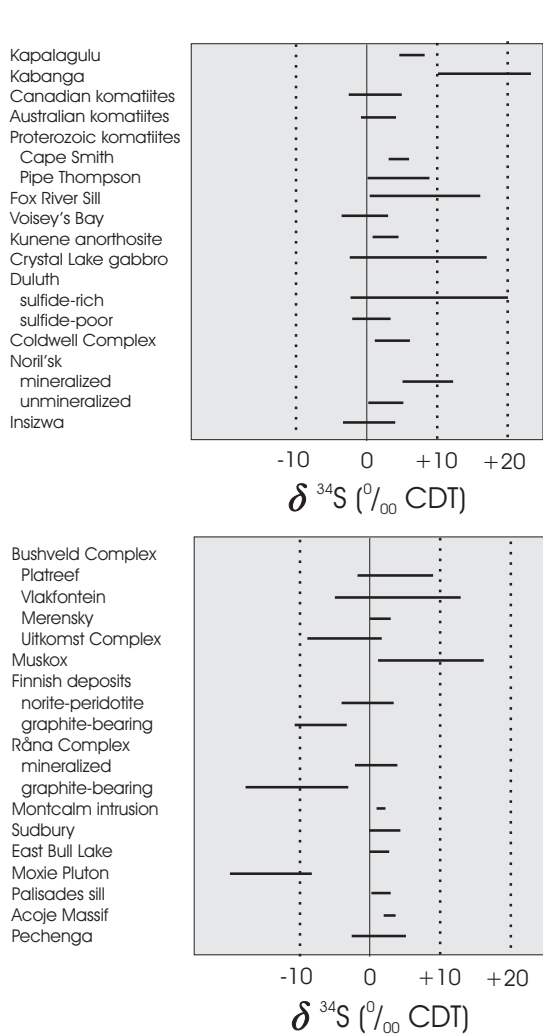


FIG. 14-22: Range of $\delta^{34}\text{S}$ values from various magmatic sulfide deposits. Figure modified after Ripley (1999). Data for Kabanga, Kapalagulu and Kunene are from Maier (unpublished).

conduit-type deposits (probably Phoenix and Selkirk, Botswana, Johnson 1986).

Oxygen isotopes

The available oxygen isotope data on massive magmatic Ni–Cu–(PGE) sulfide deposits has been reviewed by Ripley (1999). These data provide support for crustal contamination of magmas at, e.g., Noril'sk, Voisey's Bay, and Duluth, and for a model whereby assimilation of siliceous (sulfide-poor) crustal rocks can trigger saturation in sulfide melt in the magmas. On the other hand, many other continental flood basalts, and their basal flows in particular (Deccan, Peng *et al.* 1994; Grande

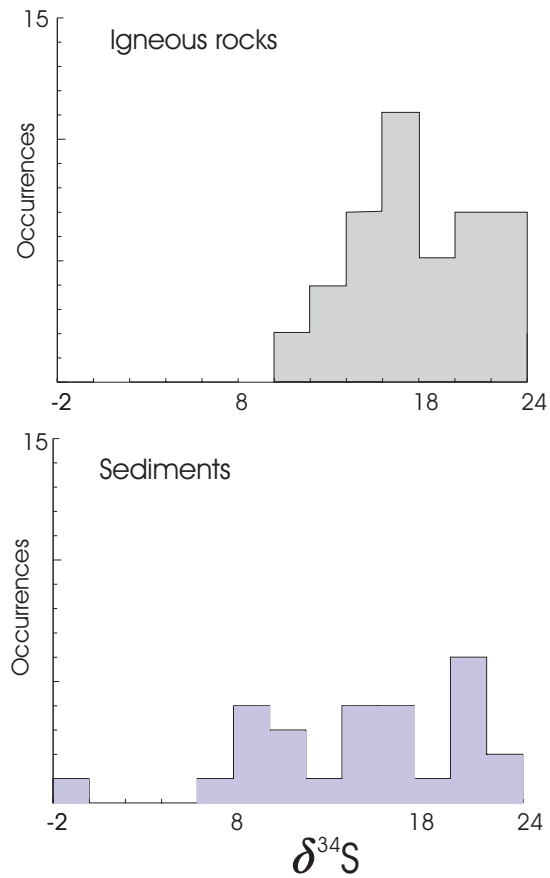


FIG. 14-23: $\delta^{34}\text{S}$ in intrusions and sedimentary rocks at Kabanga, Tanzania (Maier *et al.* 2004).

Ronde, Nelson 1983) have a crustal oxygen isotopic signature (e.g., Baker *et al.* 2000) but do not appear to host magmatic sulfide ores. Thus, the oxygen isotopic signatures of the lavas are not discriminative with regard to magmatic sulfide potential.

At Voisey's Bay values of $\delta^{18}\text{O}$ up to +11 have been identified in basal gabbroic zones containing xenoliths. However, other troctolitic rocks within the Voisey's Bay intrusions have a signature similar to the mantle and other troctolitic intrusions in the Nain Province, e.g., Kiglapait. Thus, the oxygen isotopic signature of the rocks is not discriminative with regard to the presence of contaminated or mineralized rocks at depth. As with other indicators of crustal contamination, oxygen isotopes are susceptible to dilution in dynamic systems where late, uncontaminated magma batches may flush out earlier contaminated magma batches from which ores have segregated, particularly if fast cooling prevented sub-solidus equilibration. For

example, Ripley & Al-Jassar (1987) showed that xenolith-rich rocks at Duluth may show no crustal signature. Thus, the absence of a crustal oxygen isotopic signature in a dynamic igneous system does not necessarily rule out the presence of ores.

A distinct crustal component has been determined in many massif-type anorthosites, *e.g.*, Marcy ($\delta^{18}\text{O} +9.5$, Morrison & Valley 1988). Taylor (1968) proposed a range of values between 5.8 and 7.6 for massive-type anorthosites. This would seem to suggest an enhanced potential of massif-type anorthosites to host magmatic Ni sulfide ores. On the other hand, the magmas giving rise to anorthosite-troctolite massifs are thought to be relatively cold and contain a large amount of plagioclase phenocrysts. In many cases, the magmas are thought to have ascended as crystal mushes (Ashwal 1993). We would argue that such magmas have relatively limited potential to assimilate crustal material and, if sulfides segregate, to allow concentration of the sulfides through the viscous silicate crystal mush.

SUMMARY

PGE deposits can be found at various stratigraphic levels in intrusions of various size and different magmatic lineage. The formation of the reefs depends largely on the timing of sulfide saturation. In many cases, contamination of the magma with country rocks may not be important. In some types of PGE reefs (*e.g.*, Stella-type reefs) contamination may even be a negative factor. Therefore, lithophile-incompatible trace element contents and isotopic signatures are of limited use in determining whether an intrusion hosts a reef or in locating a PGE reef in an intrusion, but such data help to constrain the petrogenesis of an intrusion and thus may aid in understanding the broader geological context and in formulating an exploration strategy for a region. The potential of an intrusion to host PGE reefs can be best determined using metal ratios, *e.g.*, Cu/Pd. If Cu/Pd is above primitive mantle levels throughout an intrusion, the magma probably reached sulfide saturation prior to emplacement and the reef potential is low. If the rocks have mantle ratios throughout an intrusion, sulfide saturation was not reached and the reef potential is equally low. In the ideal case, Cu/Pd shows variation through an intrusion, with a significant change indicating the position of the reef.

Massive Ni–Cu–(PGE) sulfide deposits are hosted by rocks that crystallized from relatively primitive magmas. Due to the partitioning of Ni into

early forming silicates, differentiated rocks have low potential to host Ni deposits, but they may be enriched in Cu sulfides. Lithogeochemical studies are extremely useful in identifying the primitive target rocks. Crustal contamination and addition of external S appears to be essential in the formation of many of the ore deposits. A crustal signature of the rocks may be expressed by enriched and fractionated incompatible trace elements, negative normalized Nb–Ta–Ti anomalies, relatively high initial $^{87/86}\text{Sr}$, $^{143/144}\text{Nd}$, and $^{188/187}\text{Os}$, low initial $^{143/144}\text{Nd}$, and heavy S and O isotopes. Factors unrelated to magma composition are also important in ore formation, notably the presence of dynamic magmatic systems such as magma conduits and lava channels. It is important to remember that in such systems the magmas residual to the ores may be flushed out of the system by primitive metal-rich and uncontaminated magmas. In such cases, a crustal component or metal depletion in the magma may be diluted, but there are few examples where it is entirely absent.

ACKNOWLEDGEMENTS

Financial support for some of the research presented in this review has been provided by CERMOD (Centre for Research on Magmatic Ore Deposits, University of Pretoria) to WDM, and NSERC (Natural Sciences and Engineering Research Council, Canada) to SJB. Financial and/or logistic support was additionally provided by several mining companies, including Falconbridge Ventures of Africa, Anglo American base metals division, Barrick Gold, Impala Platinum Mines, Anglo Platinum, Avmin, Harmony Gold, and Southern Era Resources. Nick Arndt and John Mavrogenes are thanked for their constructive reviews.

REFERENCES

- ALAPIETI, T.T. & LAHTINEN, J.J. (2002): Platinum-group element mineralization in layered intrusions of northern Finland and the Kola Peninsula, Russia. in Cabri L.J. (ed) *The geology, geochemistry, mineralogy and mineral beneficiation of platinum-group elements*, *Can. Inst. Min. Metall. Spec. Vol.* **54**, 507-546.
- ANDERSEN, J.C.Ø., RASMUSSEN, H., NIELSEN, T.F.D. & RONSBO, J.G. (1998): The Triple Group and the Platinova Au and Pd reefs in the Skaergaard Intrusion: stratigraphic and petrographic relations. *Econ. Geol.* **93**, 485-509.

- ANDERSEN, J.C.O., POWER, M.R. & MOMME, P. (2002): Platinum-Group elements in the Paleogene North Atlantic igneous province. In *The geology, geochemistry, mineralogy and mineral beneficiation of platinum-group elements*. Cabri L.J. (ed.). *Can. Inst. Min. Metall. Spec. Vol. 54*, 637-667.
- ARNDT, N.T. & JENNER, G.A. (1986): Crustally contaminated komatiites and basalts from Kambalda, Western Australia. *Chem. Geol.* **56**, 229-255.
- ARNDT, N.T., CZAMANSKE, G.K., WALKER, R.J., CHAUVEL, C. & FEDORENKO, V.A. (2003): Geochemistry and origin of the intrusive hosts of the Noril'sk-Talnakh Cu-Ni-PGE sulfide deposits. *Econ. Geol.* **98**, 495-515.
- ASHWAL, L.D. (1993): Anorthosites. Heidelberg, Springer, 442 pp.
- ASHWAL, L.D. & TWIST, D. (1994): The Kunene complex, Angola/Namibia: a composite massif-type anorthosite complex. *Geol. Mag.* **131**, 579-591.
- BAKER, J.A., MACPHERSON, C.G., MENZIES, M.A., THIRLWALL, M.F., AL-KADASI, M. & MATTEY, D.P. (2000): Resolving crustal and mantle contributions to continental flood volcanism, Yemen; constraints from mineral oxygen isotope data. *J. Petrol.* **41**, 1805-1820.
- BAKER, D.R., BARNES, S.-J., SIMON, G. & BERNIER, F. (2001): Fluid transport of sulfur and metals between sulfide melt and basaltic melt. *Can. Mineral.* **39**, 537-546.
- BANDYAYERA, D. (1997): *Formation des Laterites Nickelifères et Mode de Distribution des Elements du Groupe du Platine dans les Profils Lateritiques du Complexe de Musongati, Burundi*. PhD thesis, Université du Québec à Chicoutimi, 440 p.
- BARNES, SARAH-JANE & MAIER, W.D. (1999): The fractionation of Ni, Cu and the noble metals in silicate and sulphide liquids. In *Dynamic processes in magmatic ore deposits and their application to mineral exploration*. Keays, R.R., Leshner, C.M., Lightfoot, P.C. & Farrow, C.E.G., (eds.). *Geol. Assoc. Can., Short Course Notes*, **13**, 69-106.
- BARNES, SARAH-JANE & MAIER, W.D. (2002a): Platinum-group element distributions in the Rustenburg Layered Suite of the Bushveld Complex, South Africa. In *The geology, geochemistry, mineralogy and mineral beneficiation of platinum-group elements*. Cabri L.J. (ed.). *Can. Inst. Min. Metall. Spec. Vol. 54*, 431-458.
- BARNES, SARAH-JANE & MAIER, W.D. (2002b): Platinum-group elements and microstructures of normal Merensky Reef from Impala Platinum Mines, Bushveld Complex. *J. Petrol.* **43**, 103-128.
- BARNES, SARAH-JANE & PICARD, C.P. (1993): The behaviour of PGE during partial melting, crystal fractionation, and sulfide segregation: an example from the Cape Smith Fold Belt, northern Quebec. *Geochim. Cosmochim. Acta* **57**, 79-87.
- BARNES, SARAH-JANE COUTURE, J.-F., SAWYER, E.W. & BOUCHAIB, C. (1993): Nickel-copper occurrences in the Belleterre-Angliers belt of the Pontiac Subprovince and the use of Cu-Pd ratios in interpreting platinum-group element distributions. *Econ. Geol.* **88**, 1402-1419.
- BARNES, SARAH-JANE MAIER, W.D. & ASHWAL, L. (2004): PGE distribution in the Main Zone and Upper Zone of the Bushveld Complex. South Africa. *Chem. Geol.* **208**, 293-317
- BARNES, STEVEN J., SMITH, T., ANDERSON, J. & KAVANAGH, M. (2004a): PGE mineralization related to cyclic layering in the Mordor Complex, Northern Territory: an unusual association of PGE-enriched magmatic sulfides with cumulates from an ultrapotassic hydrous magma. *Abstr., 17th Austr. Geol. Conv., Hobart*, p. 51.
- BARNES, STEVEN J., HILL R.E.T., PERRING, C.S. & DOWLING S.E. (2004b): Lithogeochemical exploration for komatiite-associated Ni-sulfide deposits: strategies and limitations. *Mineral. & Petrol.* **82**, 259-293.
- BARTON, J.M., CAWTHORN, R.G. & WHITE, J.A. (1986): The role of contamination in the evolution of the Platreef of the Bushveld Complex. *Econ. Geol.* **81**, 1096-1108.
- BEATTIE, P., FORD, C. & RUSSELL, D. (1991): Partition coefficients for olivine-melt and orthopyroxene-melt systems. *Contrib. Mineral. Petrol.* **109**, 212-224.
- BRAND, N.W. (1999): Element ratios in nickel sulfide exploration: vectoring towards ore

- environments. *J. Geochem. Explor.* **67**, 145-165.
- BRÜGMANN, G.E., NALDRETT, A.J., ASIF, M., LIGHTFOOT, P.C., GORBACHEV, N.S. & FEDORENKO, V.A. (1993): Siderophile and chalcophile metals as tracers of the evolution of the Siberian Trap in the Noril'sk region, Russia. *Geochim. Cosmochim. Acta* **57**, 2001-2018.
- BUCHANAN, D.L., NOLAN, J., SUDDABY, P., ROUSE, J.E., VILJOEN, M.J. & DAVENPORT, J.W.J. (1981): The genesis of sulfide mineralization in a portion of the Potgietersrus limb of the Bushveld Complex. *Econ. Geol.* **76**, 568-579.
- CAMPBELL, I.H. & NALDRETT, A.J. (1979): The influence of silicate:sulfide ratios on the geochemistry of magmatic sulfides. *Econ. Geol.* **74**, 1503-1505.
- CAWTHORN, R.G., BARTON, J.M., JR. & VILJOEN, M.J., (1985): Interaction of floor rocks with the Platreef on Overysel, Potgietersrus, northern Transvaal. *Econ. Geol.* **80**, 988-1006.
- CAWTHORN, R.G., MERKLE, R.K.W. & VILJOEN, M.J., (2002): Platinum-group element deposits in the Bushveld Complex, South Africa. In *The geology, geochemistry, mineralogy and mineral beneficiation of platinum-group elements*. Cabri L.J. (ed.). *Can. Inst. Min. Metall. Spec. Vol.* **54**, 389-429.
- CROW, C. & CONDIE, K.C. (1990): Geochemistry and origin of early Proterozoic volcanic rocks from the Transvaal and Soutpansberg successions, South Africa. *Precamb. Res.* **47**, 17-26
- CZAMANSKE, G.K., WOODEN, J.L., ZIENTEK, M.L., FEDORENKO, V.A., ZEN'KO, T.E., KENT, J., KING, B-S.W., KNIGHT, R.J. & SIEMS, D.F. (1994): Geochemical and isotopic constraints on the petrogenesis of the Noril'sk-Talnakh ore forming system. In *Proceedings of the Sudbury-Noril'sk symposium*. Lightfoot, P.C. & Naldrett, A.J. (eds.). *Ontario Geol. Surv., Sec Vol* **5**, 313-341.
- DAVIES, G. & TREDOUX, M. (1985): The platinum-group element and gold contents of the marginal rocks and sills of the Bushveld Complex. *Econ. Geol.* **80**, 838-848.
- DEBLOND, A. & TACK, L. (1999): Main characteristics and review of mineral resources of the Kabanga-Musongati mafic-ultramafic alignment in Burundi. *J. Afr. Earth Sci.* **29**, 313-328.
- DE WAAL, S.A. (1975): The mineralogy, chemistry, and certain aspects of reactivity of chromite from the Bushveld igneous Complex. *Nat Inst Metallurgy, Jhb, S Africa, Report No* **1709**, 80 p.
- DUCHESNE, J.C., LIEGEOIS, J.P., DEBLOND, A. & TACK, L. (2004): Petrogenesis of the Kabanga-Musongati layered mafic-ultramafic intrusions in Burundi (Kibaran Belt): geochemical, Sr-Nd isotopic constraints and Cr-Ni behaviour. *J. Afr. Earth Sci.* **39**, 133-145.
- DUNN, T. (1986): An investigation of the oxygen isotope geochemistry of the Stillwater Complex. *J. Petrol.* **27**, 987-997.
- EALLES, H.V. (2000): Implications of the chromium budget of the Western limb of the Bushveld Complex. *S. Afr. J. Geol.* **103**, 141-150.
- EALLES, H.V. & CAWTHORN, R.G. (1996): The Bushveld Complex In *Layered intrusions*. Cawthorn, R.G. (ed.). Elsevier, Amsterdam, 181-229.
- EALLES, H.V., DE KLERK, W.J., BUTCHER, A.R. & KRUGER, F.J. (1990): The cyclic unit beneath the UG1 chromitite (UG1FW unit) at RPM Union Section Platinum Mine – Rosetta stone of the Bushveld Upper Critical Zone? *Mineral. Mag.* **54**, 23-43.
- ERLANK, A.J. (1984): Petrogenesis of the volcanic rocks of the Karoo Province. *Geol Soc S Afr, Johannesburg, Spec. Pub.* **13**.
- EVANS, D.M., BYEMELWA, L. & GILLIGAN, J. (1999): Variability of magmatic sulphide compositions at the Kabanga nickel prospect, Tanzania. *J. Afr. Earth Sci.* **29**, 329-351.
- FRANCIS, D. (1994): Chemical interaction between picritic magmas and upper crust along the margins of the Muskox intrusion, Northwest Territories. *Geol. Soc. Can., Paper* **92-12**.
- FRANCIS, D.M., HYNES, A.J., LUDDEN, J. & BEDARD, J. (1981): Crystal fractionation and partial melting in the petrogenesis of a Proterozoic high-MgO volcanic suite, Ungava, Quebec. *Contrib. Mineral. Petrol.* **78**, 27-36.
- GAUERT, C.D.K., DE WAAL, S.A. & WALLMACH, T. (1995): Geology of the ultrabasic to basic Uitkomst Complex, eastern Transvaal, South Africa: an overview. *J. Afr. Earth Sci.* **21**, 553-570.

- GHIORSO, M.S. & SACK, R.O. (1995): Chemical mass transfer in magmatic processes: IV. A revised and internally consistent thermodynamic model for the interpretation and extrapolation of liquid–solid equilibria in magmatic systems at elevated temperatures and pressures. *Contrib. Mineral. Petrol.* **119**, 197-212.
- GOMWE, T. (2002): *A Geochemical Profile through the Uitkomst Complex on the Farm Slaaihoek, with Special Reference to the Platinum-group Elements and Sm–Nd Isotopes*. MSc thesis, University of Pretoria, 107 p.
- GORDON P.S.L. (1973): The Selebi-Pikwe nickel-copper deposits, Botswana. In Symposium on Granites, Gneisses and Related Rocks. Lister L.A. (ed.). *Spec Pub Geol Soc S Afr.* **3**, 167-187.
- GRINENKO, L.N. (1985): Sources of sulfur of the nickeliferous and barren gabbro-dolerite intrusions of the northwest Siberian platform. *Int. Geol. Rev.* **27**, 695-708.
- GROKHOVSKAYA, T.L., BAKAEV, G.F., SHELEPINA, E.P., LAPINA, M.I., LAPUTINA, I.P. & MURAVITSKAYA, G.N. (2000): PGE mineralization in the Vuruchuaivench gabbro-norite Massif, Monchegorsk Pluton (Kola Peninsula, Russia). *Geol. of Ore Deposits* **42**, 133-146.
- HANSKI, E.J., HUUMA, H., SMOLKIN, V.F. & VAASJOKI, M. (1990): The age of the ferropicritic volcanics and comagmatic Ni-bearing intrusions at Pechenga, Kola peninsula, USSR. *Bull. Geol. Soc., Finland*, **62**, 123-133.
- HARMER, R.E. & VON GRUENEWALDT, G. (1991): A review of magmatism associated with the Transvaal Basin – implications for its tectonic setting. *S. Afr. J. Geol.* **94**, 104-122.
- HARMER, R.E., AURET, J.M. & EGLINGTON, B.M. (1995): Lead isotope variations within the Bushveld complex, South Africa: a reconnaissance study. *J. Afr. Earth Sci.* **21**, 595-606.
- HARRIS, C. & CHAUMBA, J.B. (2001): Crustal contamination and fluid-rock interaction during the formation of the Platreef, northern limb of the Bushveld Complex, South Africa. *J. Petrol.* **42**, 1321-1347.
- HARRIS, C., PRONOST, J.J.M., ASHWAL, L.D. & CAWTHORN, R.G. (2004): Oxygen and hydrogen isotope stratigraphy of the Rustenburg Layered Suite, Bushveld Complex: constraints on crustal contamination and evidence for the influx of magma. *J. Petrol.* (in press).
- HART, S.R. & KINLOCH, E.D. (1989): Osmium isotope systematics I Witwatersrand and Bushveld ore deposits. *Econ. Geol.* **84**, 1651-1655.
- HAUGHTON, D.R., ROEDER, P.L. & SKINNER, B.J. (1974): The solubility of sulfur in mafic magmas. *Econ. Geol.* **69**, 451-462.
- HERGT, J.M., CHAPPELL, B.W., MCCULLOCH, M.T., MCDUGALL, I. & CHIVAS, A.R. (1989) Geochemical and isotopic constraints on the origin of the Jurassic dolerites of Tasmania. *J. Petrol.* **39**, 841-883.
- HOATSON, D.M. & BLAKE, D.H. (2000): Geology and economic potential of the Palaeoproterozoic layered mafic-ultramafic intrusions in the East Kimberley, Western Australia. *Australian Geological Survey Organization, Bulletin* **246**, 469 p
- HOATSON, D.M. & KEAYS, R.R. (1989): Formation of platiniferous sulfide horizons by crystal fractionation and magma mixing in the Munni Munni layered intrusion, west Pilbara block, Western Australia. *Econ. Geol.* **84**, 1775-1804.
- HORAN, M.F., MORGAN, J.W., WALKER, R.J. & COOPER, R.W. (2001): Re–Os isotopic constraints on magma mixing in the peridotite zone of the Stillwater Complex, Montana. *Cont. Min. Petrol.* **141**, 446-457.
- HULBERT, L.J. & VON GRUENEWALDT, G. (1982): Nickel, copper, and platinum mineralization in the Lower Zone of the Bushveld Complex, south of Potgietersrus. *Econ. Geol.* **77**, 1296-1306.
- HULBERT L.J., GREGOIRE, C.D. & PAKTUNC, D. (1992): Sedimentary nickel, zinc, and platinum-group-element mineralization in Devonian black shales at the Nick property, Yukon, Canada: A new deposit type. *Expl. Min. Geol.* **1**, 39-62.
- IRVINE, T.N. (1975): Crystallization sequences in the Muskox intrusion and other layered intrusions – II. Origin of chromitite layers and similar deposits of other magmatic ores. *Geochim. Cosmochim. Acta* **39**, 991-1020.
- JACKSON, E.D. (1963): Stratigraphic and lateral variation of chromite composition in the Stillwater Complex. *Min. Soc. Am., Spec. Paper* **1**, 46-54.

- JOHNSON, R.S. (1986): The Phoenix and Selkirk nickel–copper sulphide ore deposits, Tati Greenstone Belt, eastern Botswana. *In* Mineral Deposits of Southern Africa. Anhaeusser C.R. & Maske, S. (eds.). *Geol. Soc. S. Afr.*, 243-248.
- KEAYS, R.R. (1995): The role of komatiitic and picritic magmatism and S-saturation in the formation of ore deposits. *Lithos* **34**, p. 1-18.
- Kent, W., Saunders, A.D., Kempton, P.D. & Ghose, N.C. (1997): Rajmahal basalts, eastern India: Mantle sources and melt distribution at a volcanic rifted margin. *In* Large Igneous Provinces, Mahoney J.J. & Coffin M.F. (eds.). *Amer. Geophys. Union Geophys. Monogr.* **100**, 145-182.
- KERR A. (2003): Nickeliferous gabbroic intrusions of the Pants Lake area, Labrador, Canada: implications for the development of magmatic sulfides in mafic systems. *Amer. J. Sci.* **303**, 221-258.
- KINLOCH, E.D. & PEYERL, W. (1990): Platinum group minerals in various rock types of the Merensky Reef: genetic implications. *Econ. Geol.* **85**, 537-555.
- KRUGER, F.J. (1994): The Sr-isotopic stratigraphy of the western Bushveld Complex. *S. Afr. J. Geol.* **97**, 393-398.
- KRUGER, F.J. & MARSH, J.S. (1985): The mineralogy, petrology and origin of the Merensky Cyclic Unit in the western Bushveld Complex. *Econ. Geol.* **80**, 958-974.
- KRUGER, F.J., KINNAIRD, J.A., NEX, P.A.M. & CAWTHORN, R.G. (2002): Chromite is the key to PGE. 9th Int. Plat. Symp., Abstracts & Program, Billings, Montana.
- LAMBERT, D.D. & SIMMONS, E.C. (1987): Magma evolution in the Stillwater Complex, Montana: I Rare earth element evidence for the formation of the ultramafic series. *American J. Sci.* **287**, 1-32.
- LAMBERT, D.D., WALKER, R.J., MORGAN, J.W., SHIREY, S.B., CARLSON, R.W., ZIENTEK, M.L., LIPIN, B.R., KOSKI, M.S. & COOPER, R.L. (1994): Re–Os and Sm–Nd isotope geochemistry of the Stillwater Complex, Montana: Implications for the petrogenesis of the J-M reef. *J. Petrol.* **35**, 1717-1753.
- LAMBERT D.D., FOSTER, J.G., FRICK, L.R., HOATSON, D.M. & PURVIS, A.C. (1998a): Application of the Re–Os isotopic system to the study of Precambrian magmatic sulfide deposits of Western Australia. *Austr. J. Earth Sci.* **45**, 265-284.
- LAMBERT, D.D., FOSTER, J.G., FRICK, L.R., RIPLEY, E.M. & ZIENTEK, M.L. (1998b): Geodynamics of magmatic Cu–Ni–PGE sulfide deposits: new insights from the Re–Os isotope system. *Econ. Geol.* **93**, 121-136.
- LAMBERT, D.D., FOSTER, J.G., FRICK, L.R., LI, C. & NALDRETT, A.J. (1999): Re–Os isotopic systematics of the Voisey’s Bay Ni–Cu–Co magmatic ore system, Labrador, Canada. *Lithos* **47**, 69-88.
- LAMBERT, D.D., FRICK, L.R., FOSTER, J.G., LI, C. & NALDRETT, A.J. (2000): Re–Os isotopic systematics of the Voisey’s Bay Ni–Cu–Co magmatic sulfide system, Canada. II. Implications for parental magma chemistry, ore genesis, and metal redistribution. *Econ. Geol.* **95**, 867-888.
- LEE, C.A. & BUTCHER, A.R. (1990): Cyclicality in the Sr isotope stratigraphy through the Merensky and Bastard Reefs, Atok Section, eastern Bushveld Complex. *Econ. Geol.* **85**, 877-883.
- LESHER, C.M. & CAMPBELL, I.H. (1993): Geochemical and fluid-dynamic modelling of compositional variations in Archean komatiite-hosted nickel sulfide ores in Western Australia. *Econ. Geol.* **88**, 804-816.
- LESHER C.M. & GROVES, D.I. (1986): Controls on the formation of komatiite-associated nickel-copper sulfide deposits. *In* Geology and Metallogeny of copper deposits. Friedrich G.H., Genkin A., Naldrett A.J., Ridge J.D., Sillitoe R.H., Vokes F.M. (eds.). *Proc. 27th Int Geol Cong*, Springer, Berlin, 43-62.
- LI, C. & NALDRETT, A.J. (1993): Sulfide capacity of magma: a quantitative model and its application to the formation of the sulfide ores at Sudbury. *Econ. Geol.* **88**, 1253-1260.
- LI, C. & NALDRETT A.J. (1999): Geology and petrology of the Voisey’s Bay intrusion: reaction of olivine with sulfide and silicate liquids. *Lithos* **47**, 1-31.
- LI, C., MAIER, W.D. & DE WAAL, S.A. (2001a): The role of magma mixing in the genesis of PGE mineralization in the Bushveld Complex: thermodynamic calculations and new

- interpretations. *Econ. Geol.* **96**, 653-659.
- LI, C., MAIER, W.D. & DE WAAL, S.A. (2001b) : Magmatic Ni–Cu vs PGE deposits: contrasting genetic controls and exploration implication. *S. Afr. J. Geol.* **104**, 309-318.
- LI, C., NALDRETT, A.J. & RIPLEY, E.M. (2001c): Critical factors for the formation of a Ni–Cu deposit in an evolved magmatic system: lessons from a comparison of the Pants Lake and Voisey's Bay sulfide occurrences in Labrador, Canada. *Min. Deposita* **36**, 85-92.
- LI, C., RIPLEY, E.M., MAIER, W.D. & GOMWE, T.E. (2002): Olivine and sulfur isotopic compositions of the Uitkomst sulfide-bearing intrusion, South Africa: evidence for sulfur contamination and multiple magma emplacements. *Chem. Geol.* **188**, p. 149-159.
- LI, C., RIPLEY, E.M. & NALDRETT, A.J. (2003): Compositional variations of olivine and sulfur isotopes in the Noril'sk and Talnakh intrusions, Siberia: Implications for ore-forming processes in dynamic magma conduits. *Econ. Geol.* **98**, 69-86.
- LI, C., XU, Z.H., DE WAAL, S.A., RIPLEY, E.M. & MAIER W.D. (2004): Magmatic and metamorphic controls on the compositions of olivine from the Jinchuan Ni–Cu sulfide deposit, western China, with implications for ore genesis. *Mineral. Deposita* **39**, 159-172.
- LI, C. & RIPLEY, E.M. (2005): Empirical equations to predict the sulfur content of mafic magmas at sulfide saturation and applications to magmatic sulfide deposits. *Min. Deposita*, in press.
- LI, C., RIPLEY, E.M., OBERTHÜR, T., THAKURTA, J. & SHAFER, P. (2005): Mineralogic and Stable Isotopic Constraints on the Formation of the Main Sulfide Zone of the Great Dyke, Zimbabwe, submitted.
- LIEBENBERG, L. (1968): *The sulfides in the layered sequence of the Bushveld igneous complex*. DSc thesis, University of Pretoria, 260 p.
- LIGHTFOOT, P.C. & HAWKESWORTH, C.J. (1997): Flood basalts and magmatic Ni, Cu and PGE sulfide mineralization: comparative geochemistry of the Noril'sk (Siberian Traps) and West Greenland sequences. In Large Igneous Provinces. Mahoney J.J., Coffin M.F. (eds.). *Geophys Monogr* **100**, Amer. Geophys. Union, 357-380.
- LIGHTFOOT, P.C., NALDRETT, A.J. & HAWKESWORTH, C.J. (1984): The geology and geochemistry of the Waterfall Gorge Section of the Insizwa Complex with particular reference to the origin of the nickel sulfide deposits. *Econ. Geol.* **79**, 1857-1879.
- LIGHTFOOT, P.C., NALDRETT, A.J., GORBACHEV, N.S., DOHERTY, W. & FEDORENKO, V.A. (1990) Geochemistry of the Siberian Trap of the Noril'sk area, USSR, with implications for the relative contributions of crust and mantle to flood basalt magmatism. *Contrib. Mineral. Petrol.* **104**, 631-644
- LIGHTFOOT, P.C., NALDRETT, A.J., GORBACHEV, N.S., FEDORENKO, V.A., HAWKESWORTH, C.J., HERGT, J. & DOHERTY, W. (1994): Chemostratigraphy of Siberian Trap lavas, Noril'sk district, Russia: Implications for the source of flood basalt magmas and their associated Ni–Cu mineralization. In Proceedings of the Sudbury-Noril'sk symposium. Lightfoot, P.C., Naldrett, A.J. (eds.). *Ontario Geol Surv., Sec Vol 5*, 283-312.
- LIKHACHEV, A.P. (1994): Ore-bearing intrusions of the Noril'sk region. In Proceedings of the Sudbury-Noril'sk symposium. Lightfoot, P.C., Naldrett, A.J. (eds.). *Ontario Geol Surv., Sec Vol 5*, 185-201.
- MAIER, W.D. (2005): Platinum-group element (PGE) deposits and occurrences: mineralization styles, genetic concepts, and exploration criteria. *J. Afr. Earth Sci.* in press.
- MAIER, W.D. & BARNES, S.-J. (1998): Concentrations of rare earth elements in silicate rocks of the Lower, Critical and Main Zones of the Bushveld Complex. *Chem. Geol.* **150**, 85-103.
- MAIER, W.D. & BARNES, S.-J. (1999): Platinum-group elements in silicate rocks of the lower, critical, and main zones at Union Section, western Bushveld Complex. *J. Petrol.* **40**, 1647-1671.
- MAIER, W.D., ARNDT, N.T. & CURL, E.A. (2000): Progressive crustal contamination of the Bushveld Complex: evidence from Nd isotopic analyses of the cumulate rocks. *Cont. Mineral. Petrol.* **140**, 316-327.
- MAIER, W.D., BARNES, S.-J. & DE WAAL, S.A. (1998): Exploration for magmatic Ni–Cu–PGE sulphide deposits: a review of recent advances in

- the use of geochemical tools, and their application to some South African ores: *S. Afr. J. Geol.* **101**, p. 165-182.
- MAIER, W.D., BARNES, S.-J. & MARSH, J.S. (2003b): The concentrations of the noble metals in southern African flood-type basalts and MORB: implications for petrogenesis and sulfide exploration. *Cont. Mineral. Petrol.* **146**, 44-61.
- MAIER, W.D., BARNES, S.-J., DE KLERK, W.J., TEIGLER, B. & MITCHELL, A.A. (1996): Cu/Pd and Cu/Pt of silicate rocks in the Bushveld Complex: implications for platinum-group element exploration. *Econ. Geol.* **91**, 1151-1158.
- MAIER, W.D., BARNES, S.-J., GARTZ, V. & ANDREWS, G. (2003a): Pt-Pd reefs in magnetitites of the Stella layered intrusion, South Africa: a world of new exploration opportunities for platinum-group elements. *Geology* **31**, 885-888.
- MAIER, W.D., LI, C., DE WAAL, S.A. (2001): Why are there no major Ni-Cu sulfide deposits in large layered mafic-ultramafic intrusions? *Can. Mineral.* **39**, 547-556.
- MAIER, W.D., LIVESEY, T.J., BARNES, S.-J., RIPLEY, E. & LI, C. (2004): The Kabanga Ni sulfide deposits, Tanzania: geology and geochemistry. *Geoscience Africa 2004, Abstract Volume*, University of the Witwatersrand, Johannesburg, 400-401.
- MAIER, W.D., MARSH, J.S., BARNES, S.-J. & DODD, D.C. (2002): The distribution of platinum-group elements in the Insizwa lobe, Mount Ayliff Complex, South Africa: implications for Ni-Cu-PGE sulfide exploration in the Karoo Igneous Province. *Econ. Geol.* **97**, 1293-1306.
- MAIER, W.D., TEIGLER, B. & MILLER, R. (2005): The Kunene anorthosite complex and its satellite intrusions. In *Geology of Namibia*. R. Miller, (ed.). Handbook Geol. Survey of Namibia.
- MANYERUKE, T.D. & MAIER, W.D. (2005): The petrography and geochemistry of the Platreef on the farm Townlands, near Potgietersrus, northern Bushveld Complex. *S. Afr. J. Geol.* (in press).
- MARCANTONIO, F., ZINDLER, A., REISBERG, L. & MATHEZ, E.A. (1993). Re-Os systematics in chromitites from the Stillwater Complex. *Geochim. Cosmochim. Acta* **57**, 4029-4037.
- MARSH, J.S. & EALES, H.V. (1984): The chemistry and petrogenesis of igneous rocks of the Karoo Central area, southern Africa. In *Petrogenesis of the volcanic rocks of the Karoo Province*. Erlank, A.J. (ed.). *Geol. Soc. S. Afr., Johannesburg, Spec Pub* **13**, 27-67.
- MARSH, J.S., BOWEN, M.P., ROGERS, N.W. & BOWEN, T.B. (1989): Volcanic rocks of the Witwatersrand Triad, South Africa, I: Petrogenesis of mafic and felsic rocks of the Dominion Group. *Precamb. Res.* **44**, 39-65.
- MARSH, J.S., HOOPER, P.R., REHACEK, J., DUNCAN, R.A. & DUNCAN, A.R. (1997): Stratigraphy and age of Karoo basalts of Lesotho and implications for correlations within the Karoo igneous province. In *Large Igneous Provinces*. Mahoney J.J., Coffin M.F. (eds.). *Geophys Monogr* **100**, *Amer. Geophys. Union*, 247-272.
- MATHEZ E.A. & WAIGHT, T.E. (2003): Lead isotope disequilibrium between sulfide and plagioclase in the Bushveld Complex and the chemical evolution of large layered intrusions. *Geochim. Cosmochim. Acta* **67**, 1875-1888.
- MAVROGENES, J.A. & O'NEILL, H.St.C. (1999): The relative effects of pressure, temperature and oxygen fugacity on the solubility of sulfide melts in mafic magmas. *Geochim. Cosmochim. Acta* **63**, 1173-1180.
- MCCANDLESS, T.E. & RUIZ, J. (1991): Osmium isotopes and crustal sources for platinum-group mineralization in the Bushveld Complex, South Africa. *Geology*, **19**, 1224-1228.
- MCCALLUM, I.S., THURBER, M.W., BOSCH, D. & NELSON, B.K. (1992): Lead isotopic compositions of plagioclases and sulfides in the Stillwater Complex: evidence for isotopic disequilibrium and remobilization. *Lunar Planet Sci*, **XXIII**, 867-868.
- MCCANDLESS, T.E., RUIZ, J., ADAIR, B.I. & FREYDIER, C. (1999): Re-Os and Pd/Ru variations in chromitites from the Critical Zone, Bushveld Complex, South Africa. *Geochim. Cosmochim. Acta* **63**, 911-923.
- MELEZHNIK, V.A., GRINENKO L.N. & FALICK, A.E. (1998): Ma year sulfide concretions from the "Productive" formation of the Pechenga Greenstone Belt, NW Russia: genetic history based on morphological and isotopic evidence. *Chem. Geol.* **148**, 61-94.
- MILLER, J.D., GREEN, J.C., SEVERSON, M.J.,

- CHANDLER, V.W., HAUCK, S.A., PETERSON, D.M. & WAHL, T.E. (2002): Geology and mineral potential of the Duluth Complex and related rocks of northeastern Minnesota. *Minnesota Geological Survey Report of Investigations* **58**, 207 p.
- MITCHELL, A.A. (1986): *The petrology, mineralogy and geochemistry of the main Zone of the Bushveld Complex at Rustenburg Platinum Mines, Union Section*. PhD thesis, Rhodes University, Grahamstown, South Africa, 104 p.
- MORONI, M., GIRARDI, V.A.V. & FERRARIO, A. (2001): The Serra Pelada Au–PGE deposit, Serra dos Carajas (Para State, Brazil): geological and geochemical indications for a composite mineralising process. *Mineral. Deposita* **36**, 768-785.
- MORRISON, J. & VALLEY, J.W. (1988): Contamination of the Marcy anorthosite Massif, Adirondack Mountains, NY: Petrologic and isotopic evidence. *Cont. Min. Petrol.* **98**, 97-108.
- MUNGALL, J.E. (2005): Magmatic geochemistry of the platinum-group elements. In *Exploration for Platinum-group Element Deposits* (J.E. Mungall, ed.). *Mineral. Assoc. Canada, Short Course* **35**, 1-34.
- MUKASA, S.B., WILSON, A.H. & CARLSON, R.W. (1998): A multi-element geochronological study of the Great Dyke, Zimbabwe: significance of the robust and reset ages. *Earth Planet. Sci. Lett.* **164**, 353-369.
- NÄGLER, T.F., KRAMERS, J.D., KAMBER, B.S., FREI, R. & PRENDERGAST, M.D.A. (1997): Growth of subcontinental lithospheric mantle beneath Zimbabwe started at or before 3.8 Ga: Re–Os study on chromites. *Geology* **25**, 983-986.
- NALDRETT, A.J. (1981): Platinum-group element deposits. In *Platinum-group elements: Mineralogy, Geology, Recovery*. Cabri, L.J. (ed.). *Can. Inst. Min. Metall. Spec. Vol.* **23**, 197-232.
- NALDRETT, A.J. (1989): Magmatic sulphide deposits. Oxford Monographs on *Geology and Geophysics* **14**, 186 p.
- NALDRETT, A.J. (1997): Key factors in the genesis of Noril'sk, Sudbury, Jinchuan, Voisey's Bay and other world-class Ni–Cu–PGE deposits: implications for exploration. *Austr. J. Earth Sci.* **44**, 283-315.
- NALDRETT, A.J. (2004): Magmatic sulfide deposits. Springer Verlag, Berlin-Heidelberg, 727 pp.
- NALDRETT, A.J. & LEHMANN, J. (1988): Spinel non-stoichiometry as the explanation for Ni-, Cu-, and PGE-enriched sulphides in chromitites. In *Geo-Platinum 87*. Pritchard H.M., Potts P.J., Bowles J.F.W. & Cribb S.J. (eds.). London, Elsevier Applied Science, pp 113-143.
- NALDRETT, A.J., FEDORENKO, V.A., LIGHTFOOT, P.C., GORBACHEV, N.S., DOHERTY, W., ASIF, M., LIN, S. & JOHAN, Z. (1995): A model for the formation of the Ni–Cu–PGE deposits of the Noril'sk region, Siberia: Their formation in conduits for flood basalt volcanism. *Trans. Inst. Min. Metall.* **104**, B18-B36.
- NALDRETT A.J., ASIF, M., KRSTIC, S. & LI, C. (2001): The composition of mineralization at the Voisey's Bay Ni–Cu sulfide deposit, with special reference to platinum-group elements. *Econ. Geol.* **95**, 845-865.
- NELSON, D.O. (1983): Implications of oxygen isotope data and trace element modeling for large-scale mixing model for the Columbia River basalt. *Geology* **11**, 248-251.
- OBERTHÜR, T. (2002): Platinum-group element mineralization of the Great Dyke, Zimbabwe. In *The geology, geochemistry, mineralogy and mineral beneficiation of platinum-group elements*. Cabri L.J. (ed.). *Can. Inst. Min. Metall. Spec. Vol.* **54**, 483-506.
- OBERTHÜR, T., DAVIS, D.W., BLENKINSOP, T.G. & HOEHNDORF, A. (2002): Precise U–Pb mineral ages, Rb–Sr and Sm–Nd systematics for the Great Dyke, Zimbabwe – constraints on late Archean events in the Zimbabwe craton and Limpopo belt. *Precamb. Res.* **13**, 293-305.
- OLIVO, G.R., GAUTHIER, M., BARDOUX, M., DE SA, E.L., FONSECA, J.T.F., & SANTANA, F.C. (1995): Palladium-bearing gold deposit hosted by Proterozoic Lake Superior-type iron formation at the Caua iron mine, Itabira district, southern Sao Francisco craton, Brazil: geologic and structural controls. *Econ. Geol.* **90**, 118-134.
- ORTEGA, L., LUNAR, R., GARCIA-PALOMERO, F., MORENO, T., MARTIN-ESTEVEZ, J.R., PRICHARD, H.M. & FISHER, P. (2004): The Aguablanca Ni–Cu–PGE deposit, southwestern Iberia: magmatic ore-forming processes and retrograde evolution. *Can. Mineral.* **42**, 325-350.

- PASAVA, J. (1993): Anoxic sediments – an important environment for PGE; An overview. *Ore Geology Reviews* **8**, 425-445.
- PELTONEN, P. (1995): Magma–country rock interaction and the genesis of Ni–Cu deposits in the Vammala Nickel Belt, SW Finland. *Min. Petrol.* **52**, 1-24.
- PENG, Z.X., MAHONEY, J., HOOPER, P., HARRIS, C. & BEANE, J. (1994): A role for lower continental crust in flood basalt genesis? Isotopic and incompatible element study of the lower six formations of the western Deccan Traps: *Geochim. Cosmochim. Acta* **58**, 267-288.
- POTTS, P.J., TINDLE, A.G. & WEBB, P.C. (1992): Geochemical reference material compositions. Latherronwheel, Caithness, UK: Whittles Publishing, CRC Press, UK.
- PRENDERGAST, M. & KEAYS, R.R. (1989): Controls of platinum-group element mineralization and the origin of the PGE-rich Main Sulfide Zone of the Great Dyke, Zimbabwe: Implications for the genesis of, and the exploration for stratiform PGE mineralization in layered intrusions. *In* Magmatic sulfides – the Zimbabwe volume. Prendergast, M.D. & Jones, M.J. (eds.). Inst. Mining Metall., London, 43-69.
- PRENDERGAST, M., BENNETT, M. & HENICKE, G. (1998): Platinum exploration in the Rincon del Tigre Complex, eastern Bolivia. *Trans. Inst. Min. Metall.* **107**, B39-47.
- RIGHTER, K., CAMPBELL, A.J., HUMAYUN, M. & HERVIG, R.L. (2004): Partitioning of Ru, Rh, Pd, Re, Ir, and Au between Cr-bearing spinel, olivine, pyroxene and silicate melts. *Geochim. Cosmochim. Acta* **68**, 867-880.
- RIPLEY, E.M. (1999): Systematics of sulphur and oxygen isotopes in mafic igneous rocks and related Cu–Ni–PGE mineralization. *In* Dynamic processes in magmatic ore deposits and their application to mineral exploration. Keays, R.R., Leshner, C.M., Lightfoot, P.C., Farrow, C.E.G. (eds.). *Geol. Assoc. Can., Short Course Notes*, **13**, 133-158.
- RIPLEY, E.M. & AL-JASAAR, T.J. (1987): Sulfur and oxygen isotopic studies of melt–country rock interaction, Babbitt Cu–Ni deposit – Duluth Complex, Minnesota. *Econ. Geol.* **82**, 87-107.
- RIPLEY, E.M., LAMBERT, D.D. & FRICK-LOUISE, R. (1998): Re–Os, Sm–Nd and Pb isotopic constraints on mantle and crustal contributions to magmatic sulfide mineralization in the Duluth Complex. *Geochim. Cosmochim. Acta* **62**, 3349-3365.
- RIPLEY, E.M., LIGHTFOOT, P.C., LI, C. & ELSWICK, E.R. (2003): Sulfur isotope studies of continental flood basalts in the Noril'sk region: implications for the association between lavas and ore-bearing intrusions. *Geochim. Cosmochim. Acta* **67**, 2805-2817.
- RUIZ, J., BARRA, F., ASHWAL, L.D. & LE GRANGE, M. (2004): Re–Os systematics on sulfides from the Platreef, Bushveld Complex, South Africa. *Abstr., Geoscience Africa, Wits University, Johannesburg*, p. 564.
- SATTARI, P., BRENNAN, J.M., HORN, I. & MCDONOUGH, W.F. (2002): Experimental constraints on the sulfide- and chromite-silicate melt partitioning behavior of rhenium and platinum-group elements. *Econ. Geol.* **97**, 385-398.
- SCHIFFRIES, C.M. & RYE, D.M. (1989): Stable isotope systematics of the Bushveld Complex: I. Constraints of magmatic processes in layered intrusions. *Amer. J. Sci.* **289**, 841-873.
- SCHÖNBERG, R., KRUGER, F.J., NAEGLER, T.F., MEISEL, T. & KRAMERS, J.D. (1999): PGE enrichment in chromitite layers and the Merensky Reef of the western Bushveld Complex; a Re–Os and Rb–Sr isotope study. *Earth Planet. Sci. Lett.* **172**, 49-64.
- SCHÖNBERG, R., NAEGLER, T.F., GNOS, E., KRAMERS, J.D. & KAMBER, B.S. (2003): The source of the Great Dyke, Zimbabwe, and its tectonic significance: evidence from Re–Os isotopes. *J. Geol.* **111**, 565-578.
- SHARPE, M.R. (1985): Strontium isotope evidence for preserved density stratification in the Main Zone of the Bushveld Complex. *Nature* **316**, 119-126.
- SHIMA, H. & NALDRETT, A.J. (1975): Solubility of sulfur in an ultramafic melt and the relevance of the system Fe–S–O. *Econ. Geol.* **70**, 960-967.
- SIMKIN, T. & SMITH, J.V. (1970): Minor element variation in olivine. *J. Geol.* **78**, 304-325.
- SMITS, R., BERESFORD, S. & SCHAEFER, B. (2004): Emplacement of a dyke-hosted NiS deposit,

- Nelson, New Zealand. *Abstr., 17th Austr. Geol. Conv., Hobart, Tasmania*, p. 122.
- STEELE, I.M. & LINDSTROM, D.J. (1981): Ni partitioning between diopside and silicate melt: A redetermination by ion microprobe and recognition of an experimental complication. *Geochim. Cosmochim. Acta* **45**, 2177-2183.
- STEWART, B.M. & DE PAOLO, D.J. (1987): Sr isotopic stratigraphy of the Stillwater Complex, Montana: Evidence for multiple magma injection. *EOS: Trans. Amer. Geophys. Union* **68**, 429.
- STRAUSS, H. (2002): The isotopic composition of Precambrian sulfides – seawater chemistry and biological evolution. In Precambrian sedimentary environments: a modern approach to ancient depositional systems. Altermann, W., & Corcoran, P.L. (eds.). *Spec. Publ. Int. Ass. Sed.*, **33**, 67-105.
- TAYLOR, H.P. (1968): The oxygen isotope geochemistry of igneous rocks. *Cont. Min. Petrol.* **19**, 1-21.
- TAYLOR, H.P. & FORRESTER, R.W. (1979): An oxygen and hydrogen isotope study of the Skaergaard intrusion and its country rocks: a description of a 55 my old fossil hydrothermal system. *J. Petrol.* **20**, 355-419.
- TEIGLER, B. (1990a): Platinum-group element distribution in the Lower and Middle Group chromitites in the Western Bushveld Complex. *Mineral. Petrol.* **42**, 165-179.
- TEIGLER, B. (1990b): *Mineralogy, petrology and geochemistry of the lower and lower Critical Zones, northwestern Bushveld Complex*. Ph.D. thesis, Rhodes University, Grahamstown, South Africa.
- THOMPSON, R.N., MORRISON, M.A., DICKIN, A.P. & HENDRY, G.L. (1983): Continental flood basalts...arachnids rule OK? In Continental flood basalts and mantle xenoliths. Hawkesworth C.J. & Norry M.J. (eds.). Nantwich, Shiva, 158-189.
- VILJOEN, R.P. & VILJOEN, M.J. (2004): PGE mineralization in lower ultramafic assemblages of layered complexes with special reference to Mochila – Venezuela. *Abstr., Geoscience Africa 2004, Johannesburg*, 678-679.
- WALKER, R.J., MORGAN, J.W., HORAN, M.F., CZAMANSKE, G.K., KROGSTAD, E.J., FEDORENKO, V.A. & KUNILOV, V.E. (1994): Re–Os isotopic evidence for an enriched-mantle source for the Noril'sk-type ore-bearing intrusions, Siberia. *Geochim. Cosmochim. Acta* **58**, 4179-4197.
- WALKER, R.J., MORGAN, J.W., HANSKI, E.J. & SMOLKIN, V.F. (1997): Re–Os systematics of Early Proterozoic ferropicrites, Pechenga Complex, northwestern Russia: evidence for ancient ¹⁸⁷Os-enriched plumes. *Geochim. Cosmochim. Acta* **61**, 3145-3160.
- WENDLANDT, R.F. (1982): Sulfur saturation of basalt and andesite melts at high pressures and temperatures. *Amer. Mineral.* **67**, 877-885.
- WOODEN, J.L., CZAMANSKE, G.K., FEDORENKO, V.A., ARNDT, N.T., CHAUVEL, C., BOUSE, R.M., KING, B.S.W., KNIGHT, R.J. & SIEMS, D.F. (1993): Isotopic and trace element characterization of the Siberian continental flood basalts of the Noril'sk area. *Geochim. Cosmochim. Acta* **57**, 3677-3704.
- ZHOU, M.-F., YANG, Z.-X., SONG, X.-Y., KEAYS, R.R. & LESHER, C.M. (2002): Magmatic Ni–Cu–(PGE) sulphide deposits in China. In The geology, geochemistry, mineralogy and mineral beneficiation of platinum-group elements. Cabri L.J. (ed.). *Can. Inst. Min. Metall., Spec. Vol.* **54**, 619-636.
- ZIENTEK, M.L., COOPER, R.W., CORSON, S.R. & GERAGHTY, E.P. (2002): Platinum-group element mineralization in the Stillwater Complex, Montana. In The geology, geochemistry, mineralogy and mineral beneficiation of platinum-group elements. Cabri L.J. (ed.). *Can. Inst. Min. Metall., Spec. Vol.* **54**, 459-481.

**CHAPTER 15: FEDOROV-PANA LAYERED MAFIC INTRUSION (KOLA PENINSULA, RUSSIA):
APPROACHES, METHODS, AND CRITERIA FOR PROSPECTING PGEs**

Felix P. Mitrofanov, Alexey U. Korchagin, Kirill O. Dudkin, Tat'yana V. Rundkvist
Geological Institute KSC RAS, JSC "Pana",
14 Fersman St., Apatity, 184200, Russia
E-mail: felix@geoksc.apatity.ru

**FEDOROV-PANA INTRUSION: GEOLOGY
AND PGE-MINERALIZATION**

History of PGE prospecting

Layered mafic-ultramafic intrusions in the Baltic Shield (Fig. 15-1) can be divided into two belts: the Southern (or Feno-Karelian) belt and the Northern (or Kola) belt. Layered intrusions in the two belts are confined to the boundaries of Early Proterozoic rifts, which were filled with volcano-sedimentary rocks, and the Archean basement. Intrusions of this type intruded over a long period of

time from 2505 to 2400 Ma. These intrusions are characterized by a uniform mineralogical-geochemical signature suggesting a common mantle source enriched in lithophile elements (with $\epsilon_{Nd}(T)$ from -1.2 to -1.1 , I_{Sr} ratio of $0.702-0.703$) (Mitrofanov & Bayanova, 1999). The Fennoscandian layered mafic intrusions contain great reserves of Cr, Cu-Ni, and PGE-bearing ores.

The Fedorov-Pana intrusion belongs to the Northern belt. U-Pb ages in the intrusion include: gabbro-norite (2501 ± 1.7 , 2491 ± 1.5 Ma), gabbro-

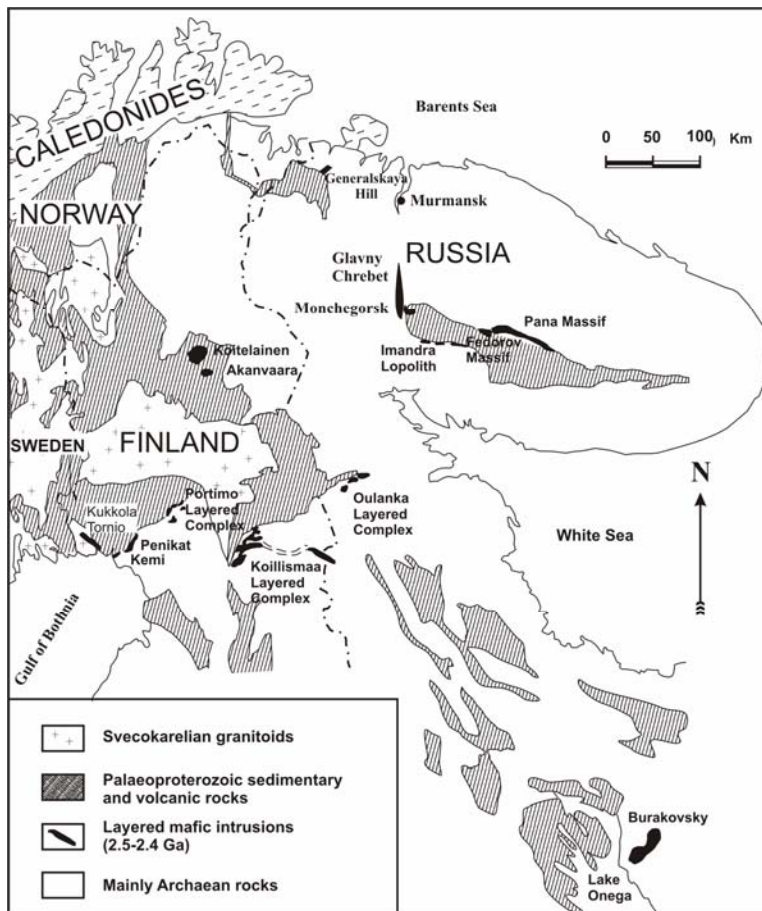


FIG. 15-1. Generalized geological map of the northeastern part of the Baltic Shield and the location of Early Proterozoic mafic layered intrusions.

pegmatite (2470±9 Ma), and anorthosite (2447±12 Ma). All analytical techniques followed the methods of Krogh (1973), and analyses were performed using a mixed ^{208}Pb – ^{235}U isotope spike (Bayanova, 2004). There are two known types of PGE-bearing mineralization in the Fedorov-Pana intrusion: a basal deposit of low sulfide Cu–Ni ores with PGE in the Fedorov Massif, and low sulfide PGE-bearing reefs in the western and eastern parts of the Pana Massif.

Since the 1930's the Fedorov-Pana intrusion was explored for Cu–Ni sulfide ores. The most recent and extensive investigation was completed in the Fedorov Massif between 1986–1989 by the Pechenga Expedition, but only subeconomic mineralization was located.

The first significant PGE grades were found by D.V. Shifrin in 1939 in the Fedorov Massif. Since 1986 the Geological Institute of Kola Science Center, Russian Academy of Science (KSC RAS) has undertaken PGE investigation in the Fedorov-Pana intrusion. By 1990, high PGE content was found in samples taken from different parts of the intrusion by V.S. Dokuchayeva, M.F. Radchenko and N.N. Veselovski under the direction of F. Mitrofanov. In 1990–1992, as a result of systematic geological surveys, the Northern PGE-Reef in the West-Pana Massif was identified and traced for 11 km (Korchagin *et al.* 1994). Since this discovery, systematic geological and geophysical surveys, sampling and diamond drilling have been routinely employed in research.

In 1992 the Geological Institute KSC RAS founded the JSC “Pana”, which received a license for prospecting, exploring and mining in the Fedorov-Pana intrusion. From 1993 to 1998 the JSC “Pana” and BHP Minerals, utilizing the work of the earlier researchers, undertook prospecting and exploration for PGE mineralization in the Fedorov Massif (Schissel *et al.* 2002). As a result, a large PGE resource of significant thickness of the Platreef, or Lac Des Iles style was identified. During this period, high PGE grades of the Southern PGE reef were identified in the Upper Layered Horizon of the West Pana Massif.

In 1997–1998 BHP Minerals initiated exploration for Cu–Ni mineralization with elevated PGE grades (“sweet spot”) in order to develop the Fedorov PGE deposit. The Fedorov and West Pana Massifs were explored by a combined airborne (magnetic and EM) and ground (magnetic, EM and

IP) geophysical survey and diamond drilling.

In 2001 exploration of the Fedorov Massif was renewed by Barrick Gold Corporation and JSC “Pana”. The PGE grades and reserves were estimated and proven, and detailed exploration is on-going. Simultaneously, the Northern Reef was re-estimated and proven, and the Southern Reef was traced along the whole West Pana Massif.

In 1995 the JSC “Pana” studied the East Pana Massif, which had previously been considered as non-prospective. In 2000, a PGE occurrence was identified in the Churozero area. In 2001, an airborne geophysical survey was completed over the East Pana Massif. Since 2002 the JSC “Pana” has been working in collaboration with the Kola Geological-Mining Company and the Puma Company (a subsidiary of Bema Gold). The East Pana Massif has been shown to be PGE-bearing, and its exploration is ongoing.

General Description

The Fedorov Pansky intrusion occurs at the northern contact between volcano-sedimentary rocks of the Early Proterozoic Imandra-Varzuga paleorift and the Archean basement. At the present-day erosion surface, the Fedorov-Pana intrusion extends for over 80 km and has a width up to 6–7 km. It is a NW-trending sheet-like body, which is split up by a set of transverse faults into three large blocks: the Fedorov, West Pana and East Pana Blocks or Massifs (Fig. 15-2). The Fedorov Massif, the westernmost part of the intrusion, is composed of mafic and ultramafic rocks and is separated from the West Pana Massif by a wide fault zone. The West Pana Massif is the thickest, best exposed and most studied part of the intrusion. It comprises the Upper Layered Horizon (ULH) and Lower Layered Horizon (LLH), and is mostly composed of gabbro. The East Pana Massif forms the eastern flank of the intrusion. It is laterally heterogeneous, and is characterized by mostly gabbro, gabbro and mafic pegmatite rock varieties. Recently, a layered horizon (LH) has been identified at the base of the East Pana Massif. Combined modeling from gravity and seismic reflection data show that the Fedorov-Pana intrusion is a SW-dipping plate-shaped body extending down to a depth of 4–5 km.

The rocks of the Fedorov-Pana intrusion are variably metamorphosed. The metamorphic grade reaches amphibolite facies at the lower contact zone

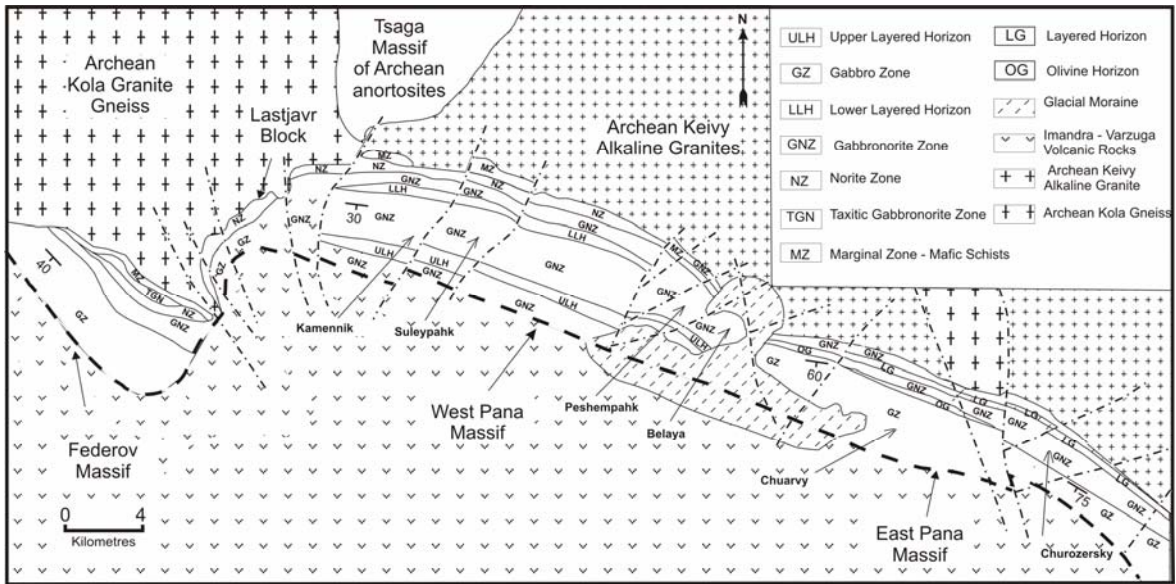


FIG. 15-2. General geological map of the Fedorov-Pana layered intrusion.

in a 100 m thick plagioclase-amphibole schist. Near the intersecting faults, the rocks of the massif are amphibolitized and epidotized.

Fedorov Massif

The Fedorov massif is a lopolith-shaped body. The base of the massif is composed of a spotted-textured “taxitic” gabbrorite (pbaC; here and below letters correspond to the symbols proposed by Streckeisen 1973). This is overlain by a 200 m thick unit of meso- to melanocratic fine-grained norite (pbCa) and orthopyroxenite (bCp) with plagioclase <10%. The lower part of the zone contains lens-like layers of breccia, with pyroxenite clasts (bCp) in a matrix of gabbrorite (pbCa).

The majority of the Fedorov Massif is composed of a thick gabbrorite (pbaC) layer overlain by gabbro (pCa, paC). The gabbro unit is composed of coarse-grained mesogabbro with rare thin layers of leucogabbro to anorthosite (pC).

At the base of the Fedorov Massif, where sulfide is widely disseminated (2–5 vol.%), but distributed irregularly, several horizons of low sulfide PGE-bearing mineralization are present. The abundance of sulfides increases in pegmatitic or taxitic rocks. The sulfide-enriched intervals vary in thickness from 10–20 to 100 m. Sampling and assaying has revealed a zone, subdivided into the upper and lower ore bodies, with the total PGE content of more than 1 g.t⁻¹. Sulfide abundances are greater at the base of each of these ore bodies.

Schissel *et al.* (2002) described the PGE mineralization in the Fedorov Massif and discussed its genesis.

The largest and thickest upper ore body has a strike length of 3.5 km and varies in thickness from 8.4 to 86.7 m. The body is conformable to igneous layering, but is cut by NW-trending faults into three parts. The ore body has been traced down to a depth of 200–300 m. Using a Σ PGE+Au cutoff grade of 1 g.t⁻¹, the mean thickness of the Upper ore deposit is 35.9 m. The average grade is Ni = 0.08%, Cu = 0.14%, and PGE+Au = 1.84 g.t⁻¹, with a Pd/Pt = 4.33 and Ni/Cu = 0.57.

Figure 15-3 shows the cross section of the upper ore body through borehole P-106. The mineralization is associated with a zone of taxitic gabbrorite. The 80 m thick ore body plunges steeply south-west to a depth of 100–150 m, but the dip shallows at depth.

Figure 15-4 shows the downhole distribution of Ni, Cu, Pt, Pd, Rh and Au in the upper ore body. The highest sulfide content and PGE abundance is associated with leucocratic gabbroic rocks in the middle part of the section.

The lower ore body is a sinuous body 6 to 42 m thick, located in the eastern part of the Fedorov Massif. It is separated from the Upper body by a 10–20 m thick barren mostly gabbrorite layer, and plunges southwards at a dip of 20–25° in its central part, steepening to a dip of 40–45° on the flanks. The abundance of sulfide is 1.5–2

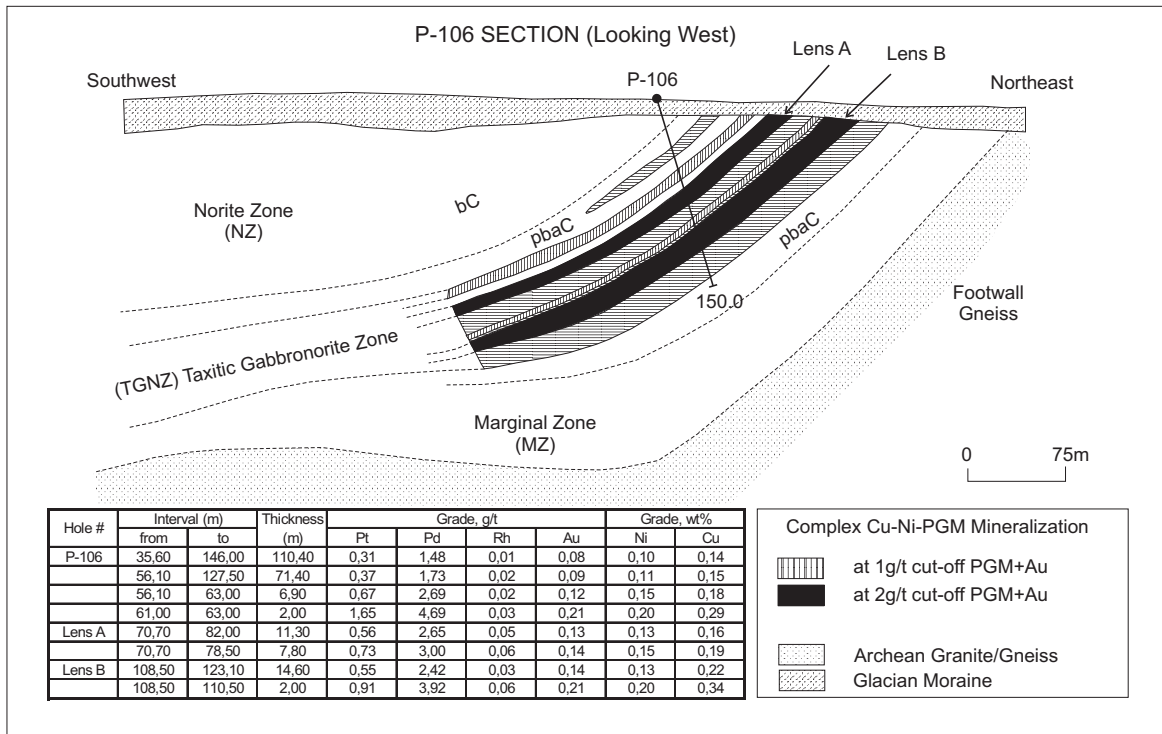


FIG. 15-3. Fedorov Massif. Northeast-to-Southwest cross-section of the Upper ore body through drill hole P-106, looking West. Mineralized intervals and Pt, Pd, Rh, Au, Cu and Ni average grades shown at 2-m sampling intervals (after Schissel et al., 2002).

times higher than that in the upper body. In fact, small lenses of massive sulfide are also present. Using a Σ PGE+Au cutoff grade of 2 g.t^{-1} , the lower ore body consists of six lenses varying from 1.8 to 5.6 m in thickness. The average grade is Ni = 0.16%, Cu = 0.23%, and PGE+Au = 3.28 g.t^{-1} , with a Pd/Pt = 4.71 and Ni/Cu = 0.70 (Schissel et al., 2002).

There are 42 PGM phases recognized in the mineralization of the Fedorov Massif. The most common Pd and Pt PGM include bismuthotellurides (merenskyite, moncheite, kotulskite, michenerite), arsenides (sperryite), and sulfides (braggite) (Balabonin et al., 1998a, 1998b).

West Pana Massif

The West Pana Massif is the thickest (ca. 4 km) part of the intrusion, which extends for more than 25 km along strike. It is a sheet-like body, with a well-developed layering striking south-west and dipping at an angle of 30–35°. The West Pana Massif is subdivided into a thin (50–100 m) norite (bpC, bCp) basal layer overlain by a thick gabbronorite zone, which is composed of 70% medium- and fine-grained mesocratic gabbronorite

(pabC, pbaC). The gabbronorite zone in the West Pana Massif is split by the Lower Layered Horizon (LLH) and the Upper Layered Horizon (ULH). These horizons are composed of fine alternations of melanocratic to leucocratic rocks, including gabbronorite (pabC, pCab), norite (bpC), leucocratic gabbro (pCa), anorthosite (pC) and pyroxenite (bCp). Low sulfide PGE mineralization is associated with these layered horizons. The main gabbronorite zone contains numerous small bodies of fine-grained magnetite gabbro that are located in two stratigraphic levels. Magnetite gabbro generated from the most fractionated liquid was found to be PGE-free (Latypov & Chistyakova 2000). In the upper part of the West Pana chamber, above the ULH, there is a layer of alternating olivine rocks – olivine gabbronorite (paboC, pboCa), troctolite (pCo) and anorthosite (pC, pCa).

Latypov and Chistyakova (2000) showed that the West Pana Massif consists of two coeval intrusive phases: the first covers the lower part of the chamber from the base till the ULH; the second includes the ULH and the overlying rock layer with olivine species.

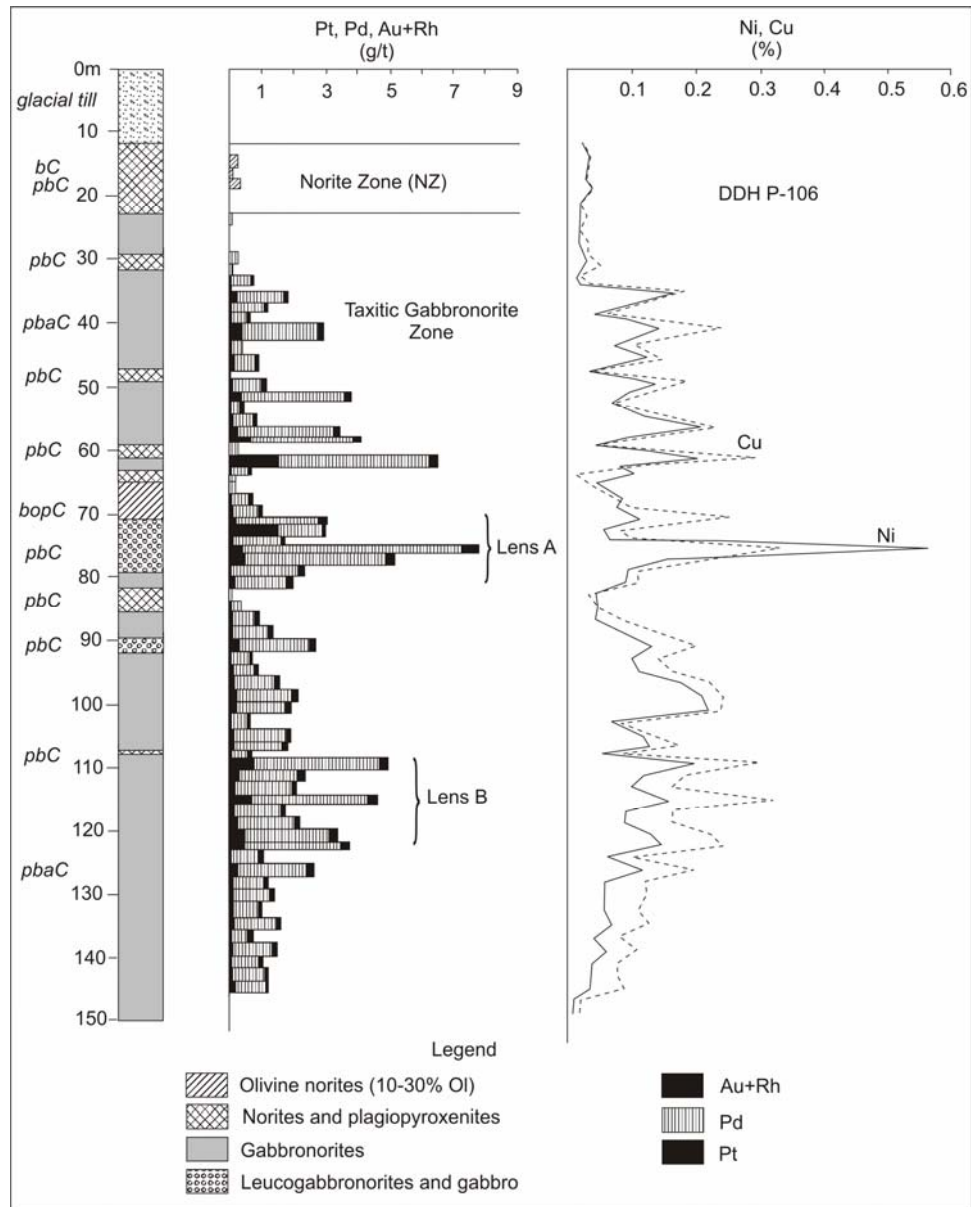


FIG. 15-4 Geological distribution and Pt, Pd, Rh, Au, Ni and Cu grades across the upper mineralized section in the Federov vertical section, core hole P-106 (after Schissel *et al.*, 2002).

Northern PGE-bearing Reef

The Northern PGE-bearing Reef in the Lower Layered Horizon is a sulfide-enriched zone, which is continuous along strike for over 16 km and is concordant with the rock layering. Ore bodies and lenses are concentrated mainly in the central part of the LLH. Occasionally, PGE-bearing sulfide mineralization is found in monotonous leucogabbro layers. The thickness of the reef varies from 1 to 15 m.

The structure of the LLH and the position of the Northern PGE-bearing Reef are shown on Figure 15-5. Ni, Cu, PGE and Au are irregularly distributed in the ore body (Figure 15-6). The Northern PGE-bearing Reef is composed of the Main and Upper ore bodies and several ore lenses.

The Main Ore Body, which is intersected by 54 boreholes for 9700 m along the strike, holds 80% of the estimated reserves of the Northern PGE-bearing Reef. Using a Σ PGE+Au cutoff grade of 1

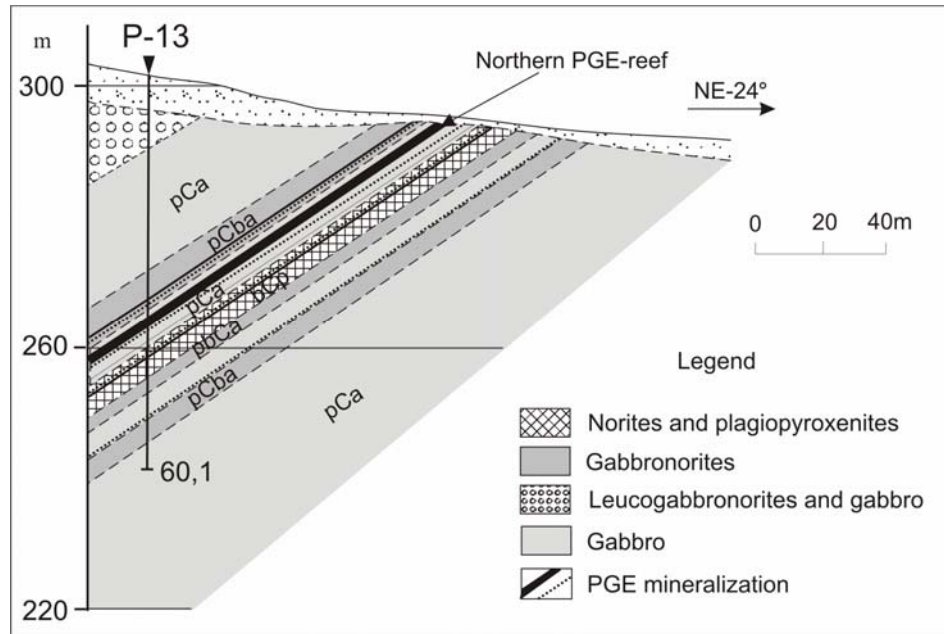


FIG. 15-5. Northeast-to-southwest cross-section of the Lower Layered Horizon in the West Pana Massif, through drill hole P-13, looking west.

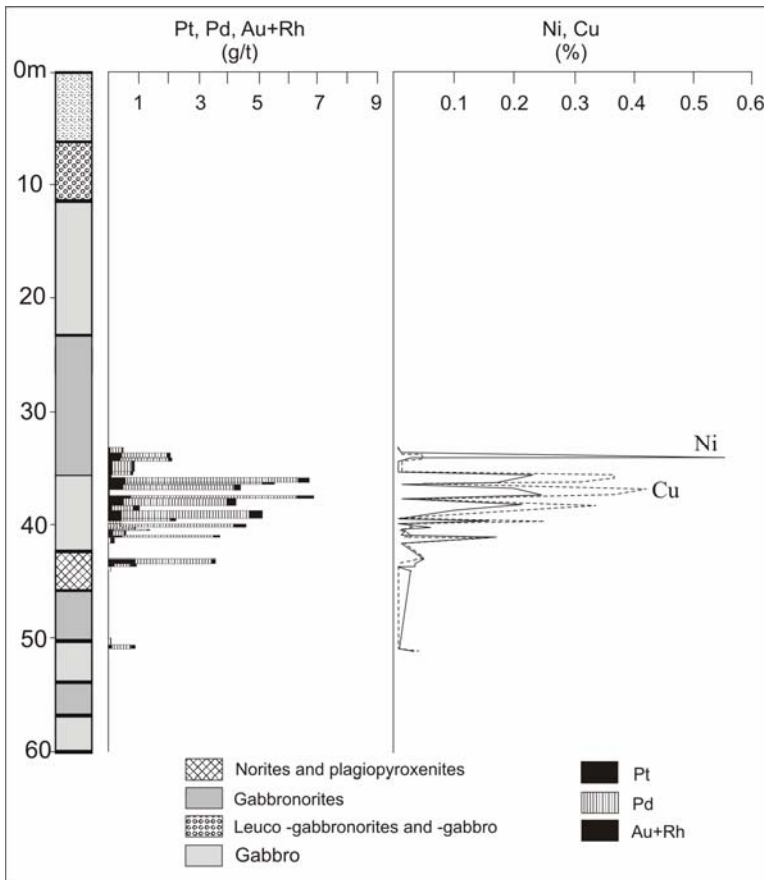


FIG. 15-6. Distribution geology and Pt, Pd, Au+Rh, Ni and Cu grades across the Lower Layered Horizon in the West Pana Massif, core hole P-13.

g.t^{-1} , the average thickness of the Main Ore Body varies from 1.1 to 2.1 m. The average grade is: Ni = 0.12–0.16%, Cu = 0.16–0.19%, and PGE+Au = 3.09–4.23 g.t^{-1} , with a Pd/Pt = 8.28 and Ni/Cu = 0.90. Though assays may grade up to 21 g.t^{-1} PGE+Au, base metal and PGE grades are generally uniform throughout the Main Ore Body.

PGE-bearing mineralization is characterized by low sulfide disseminated pentlandite-chalcopyrite-pyrrhotite with an average sulfide content of 0.5–2 vol.%. The most common and abundant PGM are Pd and Pt bismuthotellurides and arsenides, including kotulskite, merenskyite, moncheite, and braggite. The grain size of PGM ranges from 1 μm to 300 μm , with an average diameter of 9 μm . Coarser PGM grains (>10 μm) usually are located: 1) at the borders of coarse-grained sulfides and 2) in an “aureole” of fine-grained sulfides around coarse-grained ones. Finer PGM grains (<10 μm) are disseminated in silicates close to sulfide accumulations.

Within the Northern Reef, above and below the Main Ore Body, other low sulfide PGE-bearing lens-like bodies of various thickness and length are present.

Southern PGE-bearing Reef

The sulfide and PGE-bearing ore zones in the Upper Layered Horizon are combined into the Southern PGE-bearing Reef.

The PGE-bearing mineralization is confined to anorthosite bodies in the gabbro zone, and is traceable along strike in outcrop by sulfide-bearing boulders and boreholes. The zone dips south at an angle of 30°. The true thickness of the mineralized rocks varies from 0.6 to 3.3 m with a PGE+Au grade varies from 1.3 to 41.5 g.t^{-1} . The average Ni and Cu grades are 0.11% and 0.20% respectively. The average Pd/Pt ratio is 10.15 and Ni/Cu ratio = 0.7. Based on eluvial boulders tracing the ore-bearing zone, the PGE+Au content is 24–26 g.t^{-1} . The zone has been intersected to a depth of 60–100 m by boreholes, and exploration is ongoing.

Sulfide-hosted PGE-bearing mineralization is also found in the olivine rocks above the Upper Layered Horizon up-section. This type of mineralization is poorly studied.

East Pana Massif

The East Pana Massif extends for over 40 km and is up to 3.5 km in thickness. Igneous layering dips to the south-west at an angle of 50–

75°. The lower part of the East Pana Massif is composed mostly of the Gabbro Zone, overlain by a thick Gabbro Zone.

The base of the Gabbro Zone is composed of a horizon of inequigranular gabbro (gabC) with several lens-like bodies of gabbro-pegmatite, which range in length from several to tens of metres, as well as of pyroxenite and norite. Above it, within homogeneous gabbro, there is a layered horizon (LH). The LH is composed in a lower part of leucocratic and mesocratic gabbro (pCa), and an upper part of finely alternating gabbro (pabC, pCab, paCb), gabbro (paC), norite (bpC), leucogabbro (pCa), and anorthosite (pC). Above the LH, within homogeneous gabbro again, there are layers of olivine-bearing cumulates (paboC, pboCa). In the transition zone from the gabbro to the gabbro unit, there are lenses of gabbro with inverted pigeonite.

Gabbro (pCa, paC) makes up most of the section (up to 2400 m), and is represented mainly by leuco- and mesocratic, coarse- and medium-grained amphibolitized varieties. Olivine gabbro (paoC), gabbro (pabC) and pigeonite gabbro layers are also present.

PGE-mineralization

Prospecting work has shown that PGE mineralization occurs in at least three stratigraphic levels in the lower (gabbro) part of the East Pana Massif. The first level is confined to the Layered Horizon, where PGE mineralization is associated with heterogeneous horizons, mottled gabbro lenses and occurs at the contacts of different layers. Higher in the stratigraphy the second PGE-bearing horizon is present near the lower boundary of the olivine gabbro layer. The third and uppermost PGE-bearing horizon is confined to layers of alternating gabbro and gabbro within the transition zone from the gabbro to gabbro unit. The thickness of each of the PGE-bearing layers is 1–3 m. They can be traced by PGE-enriched boulders and intersecting boreholes for 100–1000 m along strike.

Figure 15-7 gives a schematic geological cross-section through the lower part of the Churozero area. The high grade PGE mineralization has a lens-like shape and is associated with anorthositic and leucocratic gabbroic rocks (Fig. 15-8). The PGE mineralization is represented by sulfide-poor (1–2% sulfide) disseminated

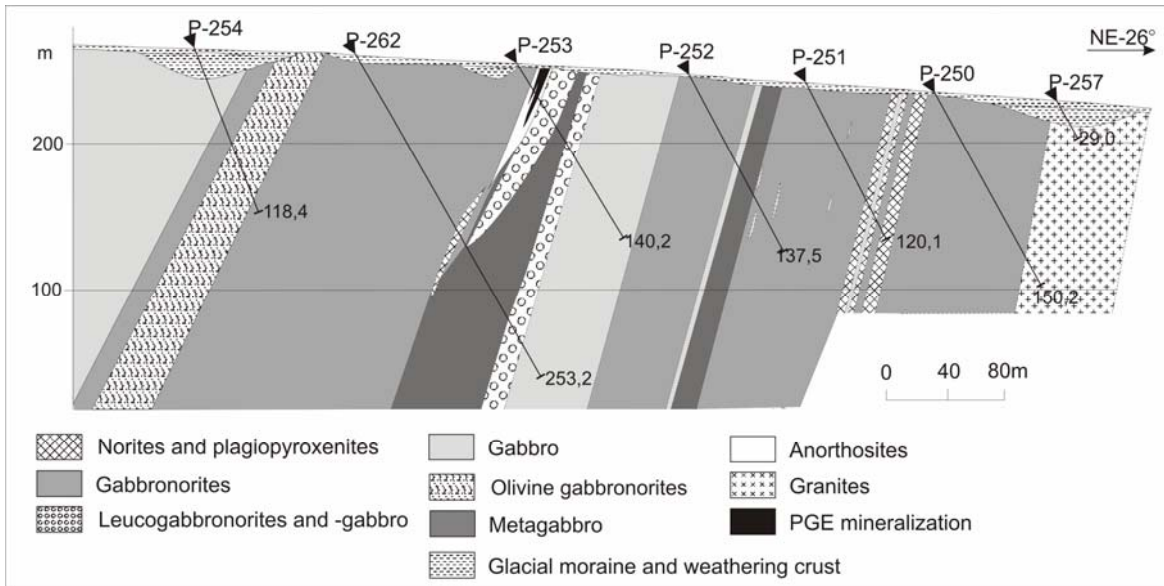


FIG. 15-7. North-to-South crosssection of the Northern part of the East Pana Massif through drillholes P-254, P-262, P-253, P-252, P-250, P-257, looking West

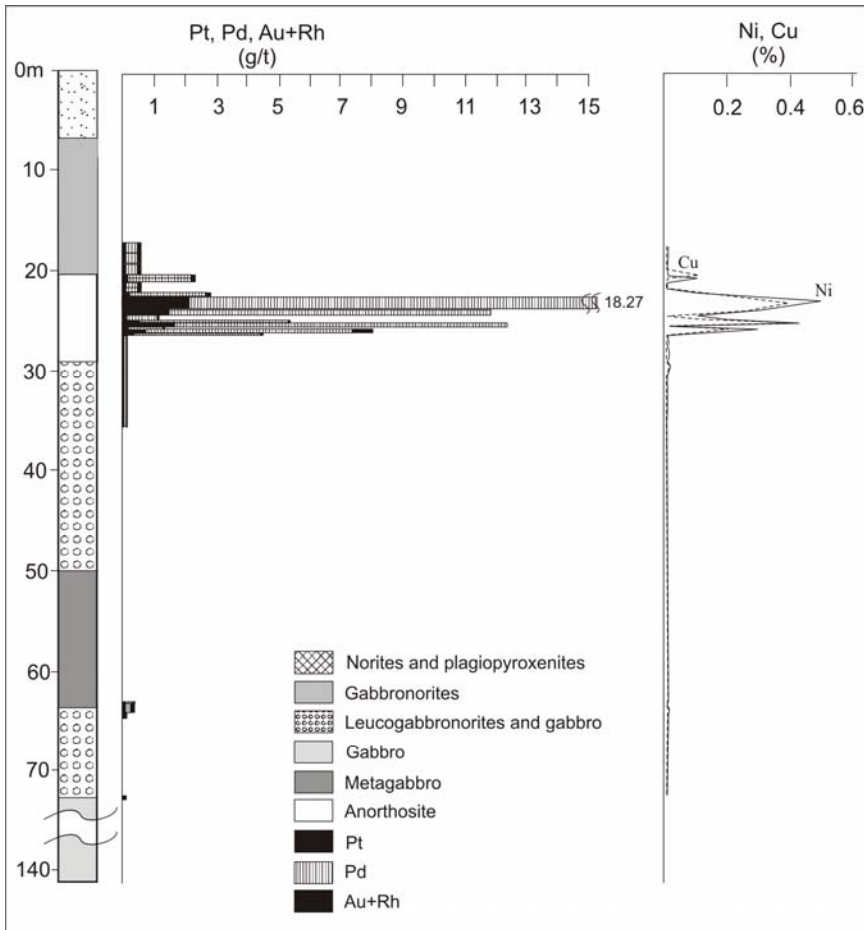


FIG. 15-8. Distribution geology and Pt, Pd, Au+Rh, Ni and Cu grades across the layered horizon of the East Pana Massif, core hole P-253.

pentlandite-chalcopyrite-pyrrhotite. Occasionally sulfide increases up to 5–10% with up to 5mm sulfide blebs. Large sulfide blebs and veinlets occur only locally. Semi-massive and massive ores are absent.

The PGE+Au content in the East Pana Massif varies from 2.03 to 10.7 g.t⁻¹. The average Ni and Cu grade are 0.08–0.25% and 0.08–0.39% respectively. Pd/Pt ratio ranges from 1.2 to 8.2, and Ni/Cu ratios range from 0.23 to 1.4.

At present, 16 PGM have been identified in the East Pana mineralization. The most common Pd and Pt minerals are bismuthotellurides and arsenides. Kotulskite, merenskyite, moncheite, sperrylite are the most common PGM (Subbotin *et al.*, 2000).

PROSPECTING FOR PGE IN THE FEDOROV-PANA LAYERED INTRUSION OF THE KOLA PENINSULA: APPROACH AND EXPERIENCE

Prospecting Methodology

Up until the 1980's PGE analyses had not been completed on rocks from the Baltic Shield, excluding the Pechenga Cu–Ni ore, from which only negligible amounts of PGE were recovered as a by-product.

In the earliest stages from 1986, specialists of the Geological Institute KCS RAS under the direction of Felix Mitrofanov examined all geological reports on the mafic-ultramafic massifs of the Kola Peninsula with the aim of identifying layered intrusions with anorthosite rocks and PGE-bearing associations similar to those known in the Stillwater Complex (USA). Such prospective rock types were identified in the Fedorov-Pana mafic intrusion. Assaying of a series of grab samples from the intrusion assayed up to 5–6 g.t⁻¹ PGE+Au.

Since 1990, systematic prospecting for PGE was completed in three stages on the Fedorov-Pana intrusion. The first stage involved geological prospecting with PGE assays of chip samples. The second stage included detailed geological study of the stratigraphy of the intrusion, and prospecting for PGE-bearing horizons within a 1 km wide and 6 km long zone across the stratigraphy. Topographic grids at 400 x 20 m or 200 x 20 m were employed in the second stage. The third stage involved tracing of promising PGE horizons along strike length within a <1 km wide zone on 200 x 20 m or 100 x 20 m grids. The second and third stages employed a range of techniques including detailed geological

mapping, chip and channel sampling, assaying of outcrops and boulders for PGE, ground and airborne geophysical survey (mostly magnetic and electrical), geochemical surveys, trenching and diamond drilling. The fourth stage, involving delineation of the PGE target by detailed diamond drilling at a spacing of 100 x 50 m and 50 x 50 m, took place only after the third stage successfully identified a promising prospect.

As a result of a fifteen-year program including the drilling of tens of shallow boreholes and analyzing thousands of samples, ore reserves were indicated (category C according to the Russian nomenclature) in the Fedorov Massif and inferred ore reserves (category P₂ according to the Russian nomenclature) of the whole Fedorov-Pana intrusion were defined. Specific technical aspects used for the geological study of layered intrusions and for PGE prospecting are discussed below.

Geological Mapping and Prospecting Using Eluvial Boulders

The topographic expression of the Fedorov-Pana intrusion is a chain of low hills. The outcrop is poor, typically less than 2%. The lowest parts of the intrusion, especially in the Fedorov Massif and East Pana Massif, are not exposed. This makes traditional geological mapping by outcrop impossible. Instead a program of mapping and prospecting eluvial boulders, commonly employed by many geologists on the Baltic Shield, was successfully employed in the Fedorov-Pana intrusion. In fact, in 1990–1992 a drilling program carried out on the Northern PGE-Reef of the West Pana Massif showed that most mineralized eluvial boulders were transported less than 5–10 m. Since that discovery, detailed geological mapping and assaying of boulders with even trace amounts of sulfide has become the main PGE-prospecting method in the intrusion. In most cases, diamond drilling supported the geological cross sections determined by boulder mapping. Continuity is a major feature of the PGE mineralization. In the continuous Northern PGE-Reef, 92% of 65 boreholes that were drilled based on mineralized boulder mapping intersected mineralization at a predicted depth. In the East Pana Massif *ca.* 75% of 63 boreholes that were drilled based on mineralized boulder mapping were successful. In the Southern PGE-Reef of the West Pana Massif only 25% of 23 boreholes successfully intersected PGE mineralization, although a promising horizon with

leucocratic lenses was intersected in all cases. The last example shows the discontinuity of the Southern PGE-Reef, but still indicates to the value of boulder mapping, and allows for some tracing of discontinuous mineralization.

Mistakes are rare when boulder mapping is employed but typically occur where large eluvial boulders have been moved by glaciers. For example, a group of massive (up to 10 m) gabbro-norite boulders north of the Fedorov Massif were found to be of underlying Archean gneiss and banded iron formation. The strong magnetic anomaly of the iron formation also contributed to this error. Nevertheless, boulder mapping remains the most efficient technique for studying PGE-bearing intrusions in the Kola Peninsula.

Magnetic Survey

The Fedorov-Pana intrusion occurs as a positive magnetic high (thousands of nanoteslas, Fig. 15-9). The remanence component of the rock magnetization, caused by aligned fine magnetite grains in plagioclase, predominates throughout the intrusion (Q~20–30) and exhibits a shallow dip (~30°) (Dudkin & Rundkvist 2002). Magnetic survey, both airborne and on ground, was the most commonly used geophysical method. With this method the different stratigraphic units identified by mapping and prospecting of eluvial boulders and studied by drilling could be traced, which allowed for efficient mapping of the intrusion.

Faults were identified by magnetic lows, which result from fine magnetite disintegration during epidotization of plagioclase. Igneous

layering is also clearly visible in the magnetic field. Rocks with variable magnetic responses often have no other petrological differences than the presence or absence of fine magnetite inclusions in plagioclase. This allowed tracing of stratigraphic units even in monotonous units (Fig. 15-9). Furthermore, a magnetite gabbro (likely related to the most fractionated liquid) and other highly magnetic units were also useful as stratigraphic references (Fig. 15-10).

Correlation of magnetic field with PGE-mineralization is of special interest. Usually, fine alternations of petrologically different rocks (*e.g.*, leucocratic and melanocratic rocks) host PGE reef mineralization. This layering manifests itself as a differentiated magnetic field (Fig. 15-11), but this can be nearly invisible in intensive magnetic fields. It is often possible to trace a PGE reef along a continuous magnetic horizon. In most cases, PGE reefs correlate with the footwall of a continuous non-magnetic level. This can probably be accounted for by magnetite disintegration during the crystallization of fluid-saturated leucogabbro. This is observed in 75% of the cases in the Pana Massifs, and is typified by the Northern PGE-Reef (Fig. 15-12). The remainder of the cases (25% of cases) is observed near fault zones and near magnetite gabbro lenses that disturb the magnetic layering pattern, though sometimes (*ca.* 10% of cases) the cause is unknown. In the Churozero block, for example, the PGE Reef was traced by drilling through overburden after the target was delineated by a continuous magnetic field for 1.5 km along strike.

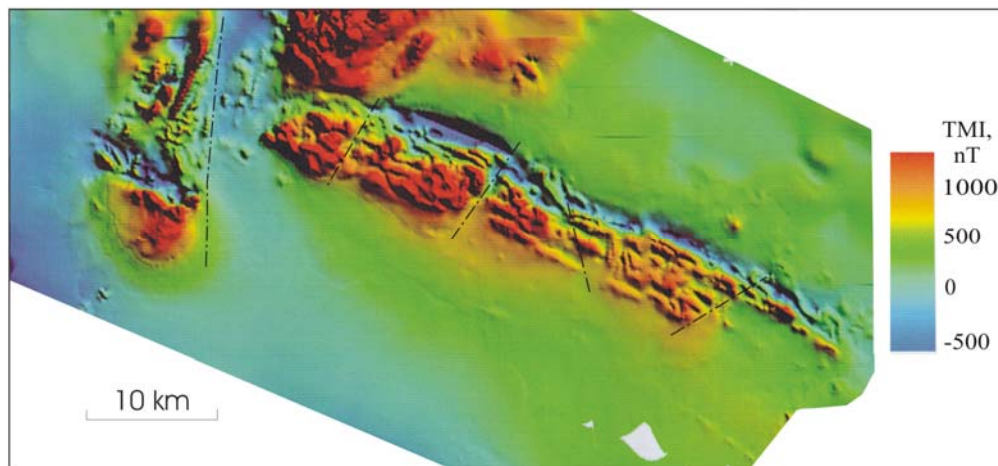


FIG. 15-9. Aeromagnetic map over the Fedorov-Pana intrusion. Data were hand-digitized and regridded by BHP Minerals from the contoured data provided by Russian Geological Survey (L.M.Lyubavin, 1978). The most significant faults are shown by dash-dotted lines.

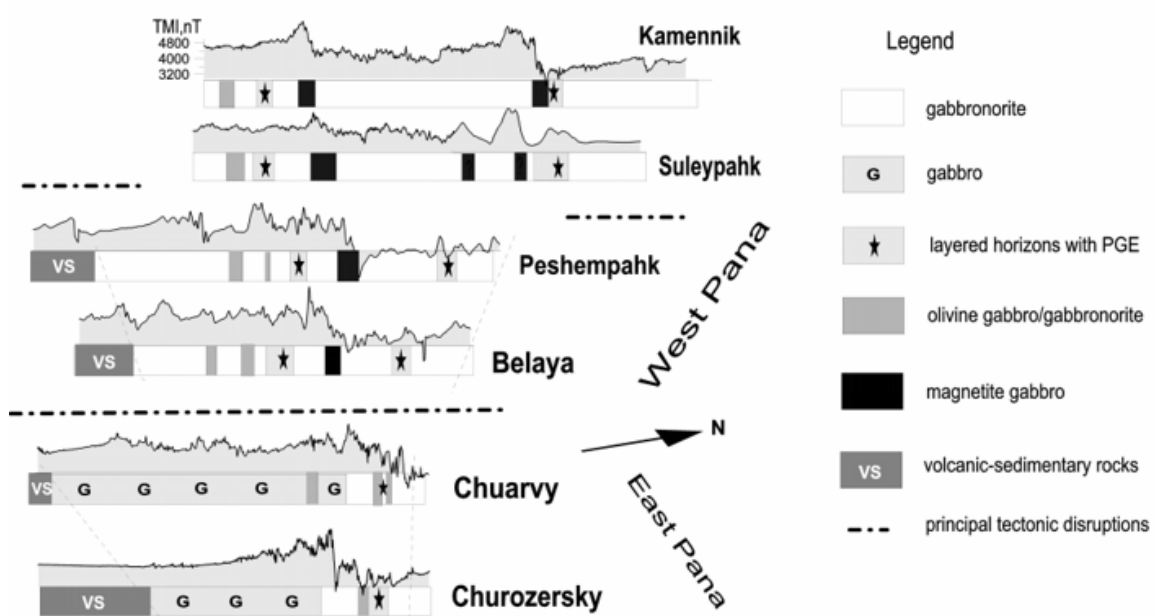


FIG. 15-10. Schematic correlation of magnetic cross-sections through the West and East Pana Massifs (looking west). The southernmost level of magnetite gabbro (the West Pana) and highly-magnetic transition zone from gabbronorite to gabbro (East Pana) can be considered as the magnetic stratigraphic reference.

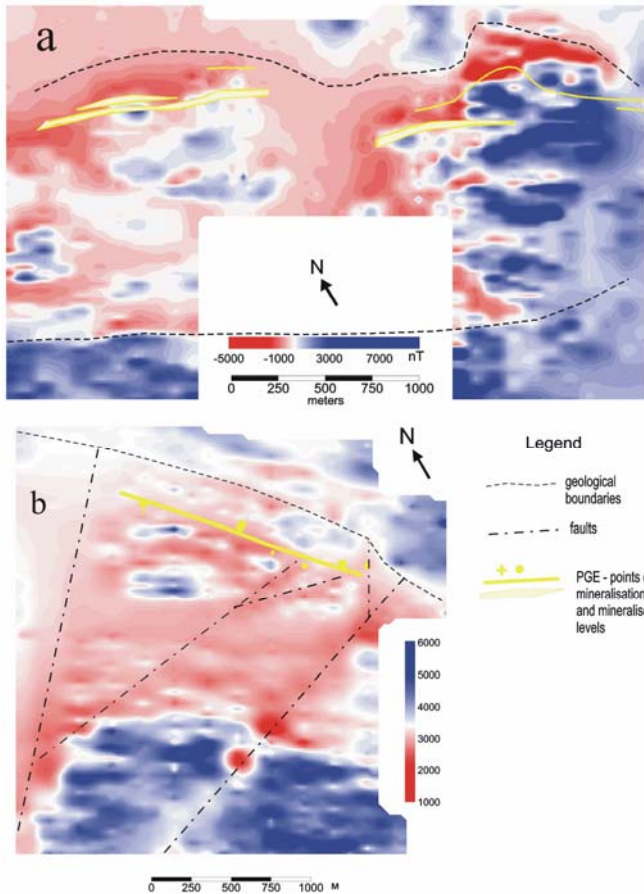


FIG. 15-11. Magnetic field over the northern part of the Fedorov Massif (a) and Northern Peshempakh area, West Pana Massif (b): PGE mineralization is confined to the northern (lower) parts of magnetic differentiated blocks.

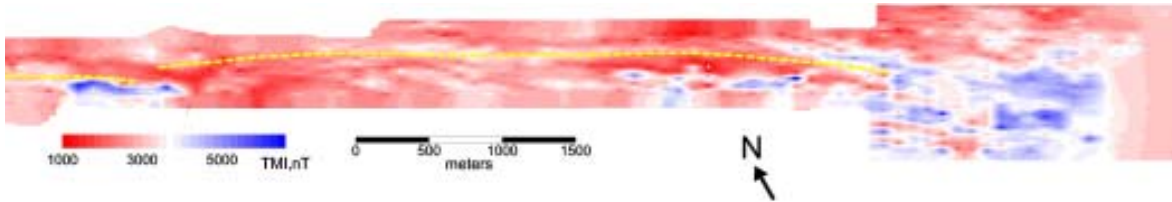


FIG. 15-12. Northern PGE-Reef (Lower Layered Horizon of the West Pana Massif) in the magnetic field. The PGE-Reef (white dashed line) follows along the northern (lower) part of non-magnetic horizon.

Electrical IP Survey

The induced polarization method is the only useful geophysical technique for identification of disseminated sulfide mineralization, but it is difficult to apply for low-sulfide PGE-mineralization. IP efficiency, in our experience, strongly depends on the details of the technique and geological conditions.

The principal issues in the technique include time regime, array, system sensitivity and interpretation software. We chose a technique designed by JSC Tellur StP as the best among 5 tested (Table 15-1).

Correlation of high IP and high resistivity is a signature of low-sulfide PGE-mineralization for all observed cases. Mineralization styles are different in terms of IP efficiency.

For the Platreef-style PGE-mineralization of the Fedorov Massif (sulfide content up to 3% and thickness of 10–100 m), ore bodies predicted by the Tellur IP-technique in 1996 have been proved by drilling in 85% of the cases with the depth error no more than $\pm 15\%$ (in 13 drill-holes) (see Fig. 15-13).

The PGE-reefs of the West and East Pana Massifs (with a sulfide content of 0.5–2% and thickness of 0.1–2 m) are distinguished by IP slightly above the sensitivity limit. Interpretations based on the geoelectrical section are supported by drilling in 50–70% of cases, and prediction of promising PGE-rich zones were proved in 20–40% of cases (1997–2001, the East Pana Massif, in 30 drill-holes). As a result, a new (upper) PGE-reef was identified in 2000 by IP and proven in 2002 by geological survey in the Churozero area.

IP efficiency is reasonably successful for the identification of thick PGE-mineralized zones but is still poor for detection of thin PGE-reefs. Correlation with other techniques is important. However, continued development of the IP technique ensures continued use of the method over completely covered areas.

Inductive EM Survey

The inductive EM techniques (both airborne and ground) were used in 1997–2001 to assist in locating massive conductive sulfides. In 1997 20

TABLE 15-1. IP TECHNIQUES TESTED IN THE FEDOROV-PANA INTRUSION FOR IDENTIFICATION OF DISSEMINATED SULFIDE MINERALIZATION

<i>Measurement system and surveyor</i>	<i>Domain</i>	<i>Time regime</i>	<i>Geometrical array</i>	<i>Interpretation system</i>
INFAS, Russian Geological Survey, 1989-1990, 1999-2000	frequency f=9,76 Hz	16 millisec*	gradient	manual from graphs, forward modeling
RSVP, S-03 Russian Geological Survey, 1993-1994	time, pulse 1 sec	1-20 millisec	A100B20M20N	manual from graphs
Newmont, Scintrex, BHP Minerals, 1995	time, pulse 1-3 sec	0.1-1 sec	dipole-dipole, n=6, spacing up to 120 m	manual from pseudosections, inverse modeling
TLR-IP, JSC Tellur StP, 1995-2002	time, pulse 1-3 sec	0.1-2 sec	gradient, point sounding	forward modeling
Strob, JSC CKE, 2002	time, pulse 1-3 sec	0.1-1 sec	pole-dipole, spacing up to 50 m	manual from graphs, forward modeling

* the equivalent time is estimated as $t = (2\pi f)^{-1}$

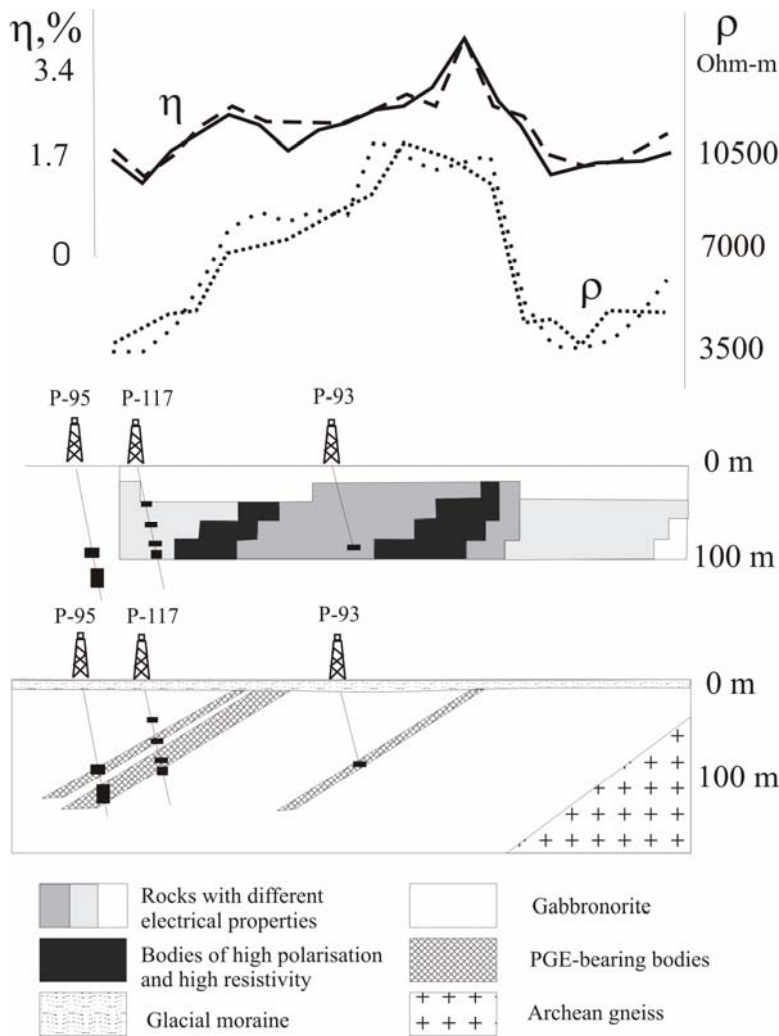


FIG. 15-13. Results of the IP-survey (a), a forward geoelectrical model (b) and results of drilling (c) on Fedorov Massif, 1995, drillholes P-93, P-95, P-117. PGE-intersections in the drillholes are shown on both cross-sections in black.

conductors were identified by a DIGHEM-airborne survey, which were later studied by ground surveys and drilling. Two of these conductors are vein and massive sulfide occurrences with high PGE content in the Fedorov Massif, three represent sulfide mineralization with low PGE concentrations, three are remobilized sulfide-magnetite mineralization along the tectonized northern contact of the West Pana Massif, 10 are faults, and 2 are lake clay deposits. Thus, conductive PGE bearing mineralization is almost absent in the Fedorov-Pana intrusion. The EM technique is efficient for mapping of tectonic zones. It is noteworthy that airborne EM is more efficient for mapping both high magnetic susceptibility and low remanence magnetite gabbros rather than the magnetic survey, which measures a mixture of inductive and remanent magnetization.

Geochemical Survey

Geochemical surveys are widely used in PGE exploration, as high PGE concentrations can be present in a vast secondary aureole (Ministry of Geological Research USSR 1983). In our program, a number of geochemical techniques were tested. Traditional soil geochemistry with acid digestion followed by inductively coupled plasma – mass spectrometry (ICP-MS) analysis revealed a distinctive Pt and Pd anomaly over the known PGE-mineralization (the Fedorov Massif). Similarly, a distinctive Pt and Pd anomaly is obtained when the layer is tested directly on top of the bedrock. This technique has been systematically employed since 2002. The bottom parts of the moraines were sampled employing the mini-drill devices used in eluvial boulder mapping (see above). The average sampling depth was 1.5–5 m and the samples were assayed for Pd, Pt using OES and for Ag, As, Pb,

Zn, Sb, Bi, Mo, W, Cu, Co, Ni, Mn, Cr, Sn, P, Ti, Sc, and V by estimating spectrum analysis. The resultant Pt+Pd anomalies correspond to the PGE-reef in 50–70% of cases (Churozero area in 6 drill-holes). An example of geochemical anomalies corresponding to PGE-rich units intersected by drilling is shown on Figure 15-14.

Drilling

Drilling is the most important (and expensive) part of exploration. By the second and third stages of prospecting, a series of shallow diamond drill holes (up to 100–200 m) were used to trace PGE-mineralization along dip and strike. The drill-holes were positioned based on ground surveys. Specifically (1) 60–65% of the drill-holes were positioned based on eluvial boulder mapping and sampling, outcrops with PGE-mineralization, and ground magnetic survey results, (2) up to 15% of drill-holes were positioned on IP targets, (3) up to 5% of drill-holes were positioned based on geochemical anomalies, (4) up to 15% of drill-holes were positioned by tracing PGE-reefs along strike based on magnetic data, and (5) 5% of drill-holes were positioned as short drill-hole profile fences to study geological cross-sections of the PGE-bearing horizons (east part of the West Pana and East Pana Massif, 1997–2003). The core samples with sulfides were assayed by atomic absorption (AA) following acid digestion.

The efficiency of ground survey methods may be estimated by the drilling results. In

summary (1) up to 90% of all successful PGE-mineralization diamond drill-hole intersections were selected based on a combination of geological (including mapping and assaying of eluvial boulders) and magnetic surveys, (2) up to 8% of successful intersections were selected based on IP-survey, (3) up to 2% of successful intersections were selected based on geochemical survey (e.g., East Pana Massif, 1997–2003). It should be noted that the number of geological and magnetic surveys completed is much greater than that of electrical and geochemical surveys.

Key criteria for PGE-localization within the Fedorov-Pana intrusion

The low sulfide content is a major feature of the PGE-mineralization in the Fedorov-Pana intrusion, since it is unlikely to be found completely without sulfides. Newly established criteria for identification of PGE-mineralized levels in the intrusion are as follows:

1. Alternation of thin layers of petrologically different rocks (e.g., leuco- and mesocratic gabbro, anorthosite, norite, pyroxenite) is a classic signature of PGE-reefs. Sulfides in monotonous units (up to 10–15 levels through the whole intrusion) contain, as a rule, no more than 1 ppm of total PGE. The layered horizons (LLH, ULH, LH of the East Pana Massif) host the main PGE-mineralization. Not every level with alternating rock layers is mineralized, but all layers have significant PGE anomalies.

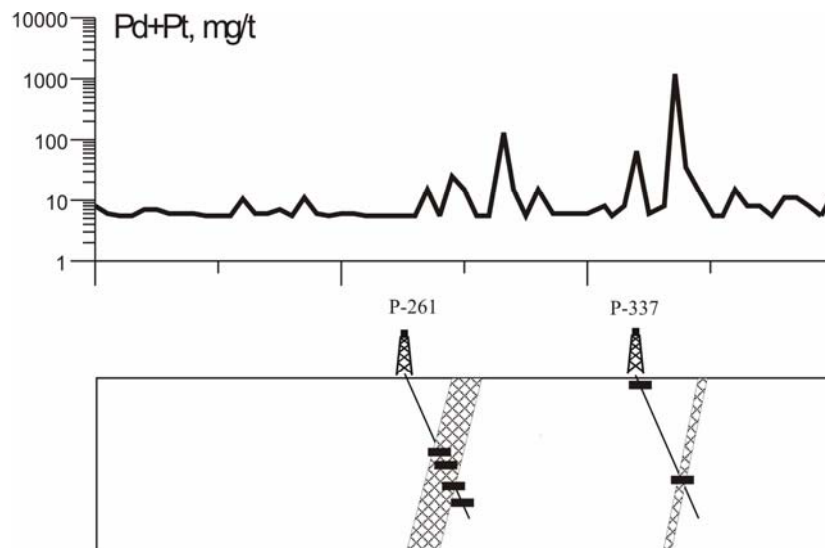


FIG. 15-14. Results of the top-of-bedrock geochemical survey and drill proving, East Pana Massif, Churozersky area. Legend for the geological cross-section see on Fig. 15-13.

Furthermore, an absence of PGE anomalies in certain outcrops or boulders of a layered horizon is often caused by nugget effect, *e.g.*, the Southern Reef.

2. All PGE-reefs in the Fedorov-Pana intrusion are associated with lens-like bodies of leucocratic rock species (leucogabbro, anorthosite, “mottled gabbro”) that represent another classic signature of PGE-reefs. In most cases they occur as a series of lens-like bodies, so that the absence of leucogabbro in a certain drill-hole section does not indicate its complete absence in the horizon. In fact, leucogabbro can commonly be observed in a more detailed study. Leucogabbro is an excellent sign for field geologists because its light color is easily visible on black gabbro boulders.
3. Taxitic and coarse-grained rocks are typical of those parts of layered horizons that are enriched in PGE. Sometimes, as in the East Pana Massif, the PGE-mineralization is associated with pegmatitic rocks. However, it should be noted that this criterion is reliable only in combination with the first two criteria.

Unfortunately, a litho-geochemical feature of the PGE-enriched horizons in the geological section has not been recognized, possibly as a result of insufficient data. The geophysical signatures of PGE-mineralization are described above, but these signatures only work when combined with geological criteria.

Criteria for the identification of PGE-bearing layered intrusions in the Kola platinum belt

While the Fedorov-Pana intrusion is the most prospective, it is not the only PGE target in the Kola Peninsula. The Kola Platinum Belt (Mitrofanov *et al.* 2002) also includes the Monchegorsk, Monchetundra, Imandra, and Generalskaya Mt. intrusions, as well as other small and probably still unknown PGE-bearing intrusions. The Kola Platinum Belt is similar to the Fenno-Karelian Platinum Belt. In summary, some of the most important features of PGE-bearing intrusions on the Baltic Shield include:

1. Regional setting: All the known PGE-bearing intrusions are situated at the contact of the Proterozoic paleorift, filled with volcanic-sedimentary rocks, and Archean basement.
2. Composition: The PGE-targets are mafic-ultramafic layered intrusions with a predominant mafic component.
3. Age: The PGE-bearing intrusions are in the

range of 2500–2400 Ma. The intrusions of the Northern Kola Belt (2500–2450 Ma) are 50 Ma older than those of the Southern Fenno-Karelian Belt (2450–2400 Ma). This suggests most likely asynchronous evolution of two different Early Proterozoic mantle plumes.

4. Geochemical features: The known PGE-bearing intrusions have similar Nd and Sr isotopic signatures ($\epsilon_{Nd}(T) = -1.2$ to -2.3 , $I_{Sr} = 0.702-0.703$) which reflects an enriched mantle reservoir which resembles the EMI source in the $\epsilon_{Nd}(T) - I_{Sr}$ diagram.

All attempts to find PGE in intrusions that do not fit at least one of the above criteria have failed in the Kola Peninsula. For example, the Ondozersky and Fomkin Ruchey mafic intrusions have similar geochemical composition and regional settings to the PGE-bearing intrusions, but differ in age (2050 Ma) and in isotopic signature ($\epsilon_{Nd}(T) = +2$ to $+4$), and do not contain PGE-mineralization. It should be also noted that the known Pechenga Cu–Ni basic layered intrusions differ from the PGE-bearing intrusions of the Kola region in age (1980 Ma) and positive $\epsilon_{Nd}(T)$ values. Thus, the criteria stated above can be used for quick identification of new PGE targets in the Kola Peninsula and Baltic Shield.

CONCLUSIONS

The Kola and Fenno-Karelian PGE provinces are well-known mineralized belts that are currently undergoing extensive exploration for PGE by numerous mining companies. The main research on the Kola Peninsula is undertaken by the Geological Institute KSC RAS and JSC “Pana”, who apply world-class regional selection criteria, exploration approaches and methods.

ACKNOWLEDGEMENTS

The authors are grateful to L. Kostenko and A. Telezhkin for the digital image processing, and to A. Rybnikova for contributing to the translation. Reviews and editing by two anonymous reviewers and the editor are sincerely appreciated.

REFERENCES

- BALABONIN N.L., MITROFANOV F.P., SUBBOTIN V.V., KORCHAGIN A.U., VOITEKHOVSKY YU.L., VOLOSHINA Z.M., PAKHOMOVSKY YA.A. & PETROV V.P. (1998a): Platinum Group Minerals – indicators of the evolution of the ore-concentrating processes. *In* Great and Unique

- Deposits of Rare and Noble Metals, St. Petersburg, 271-281 (in Russian).
- BALABONIN N.L., SUBBOTIN V.V., SKIBA V.I., VOITEKHOVSKY YU.L., SAVCHENKO E.E. & PAKHOMOVSKY YA.A. (1998b): Forms and balance of noble metals in the ores of the Fedorovo-Pansky intrusion. *Ore Dressing* **6**, 24-30 (in Russian).
- BAYANOVA T.B. (2004): The age of reference geological complexes of the Kola region and duration of magmatism. Nauka, St. Petersburg, 174 p (in Russian).
- DUDKIN K.O. & RUNDKVIST T.V. (2002): Brown plagioclases as a source of magnetic anomalies on the Pana intrusion. *Russ. Geophys. J.*, **27-28**, p. 25-34 (in Russian).
- KORCHAGIN A.U., BAKUSHKIN E.M., VINOGRADOV L.A., KARPOV S.M. & MEDNIKOV A.I. (1994): Geology and PGE-mineralisation of low marginal zone of Pansky Massif. *In Geology and Genesis of PGE-deposits*. Nauka, St. Petersburg, p.100-106 (in Russian).
- LATYPOV R.M. & CHISTYAKOVA S.YU. (2000): *Mechanism of differentiation of the West Pansky Tundra layered intrusion*. Apatity: Kola Science Center, RAN, 350 p. (in Russian).
- KROGH, T.E. (1973): A low-contamination method for hydrothermal dissolution of zircon and extraction of U and Pb for isotopic age determinations. *Geochim. Cosmochim. Acta* **37**, 485-494.
- MINISTRY OF GEOLOGICAL RESEARCH USSR (1983): *Instruction on Geochemical Methods of Ore Deposit Exploration*, Moscow, 191 p. (In Russian).
- MITROFANOV F.P. & BAYANOVA T.B. (1999): Duration and timing of ore-bearing Paleoproterozoic intrusions of Kola province. *In Mineral Deposits: Processes to Processing*. Stanley *et al.* (eds.). Balkema, Rotterdam. p. 1275-1278.
- MITROFANOV F.P., KORCHAGIN A.U., BALABONIN N.L., GONCHAROV YU.V., KARPOV S.M., SUBBOTIN V.V. & PRIPACHKIN P.V. (2002): Major research results for PGE mineralization of the layered mafic-ultramafic intrusion of the Fedorovo-Pansky Tundra. *In Russian Arctic: geological evolution, mineralogy, geoecology*. St. Petersburg, 572-579 (in Russian).
- STRECKEISEN A. (1973): Plutonic rocks: classification and nomenclature recommended by IUGS Subcommittee on the Systematics of Igneous Rocks. *Geotimes* **18**, 26-30.
- SUBBOTIN V.V., KORCHAGIN A.U., BALABONIN N.L., SAVCHENKO E.E., KARPOV S.M. & KULAKOV A.N. (2000): Mineral composition of the new PGE-bearing ore manifestations in the eastern part of the Pansky Tundra massif. *Bulletin of MSTU* **2**, 225-234 (in Russian).
- SCHISSEL D., TSVETKOV A.A., MITROFANOV F.P., KORCHAGIN A.U., 2002. Basal Platinum-Group Element Mineralization in the Fedorov Pansky Layered Mafic Intrusion, Kola Peninsula, Russia. *Econ. Geol.* **97**, 1657-1677.

CHAPTER 16: THE DISCOVERY AND CHARACTERIZATION OF THE NICKEL RIM SOUTH DEPOSIT, SUDBURY, ONTARIO

S.A. McLean, P.Geo., K.H. Straub, P.Geo., K.M Stevens, P.Geo.
Sudbury Exploration, Falconbridge Limited
P.O. Box 40, Falconbridge, ON, P0M 1S0, Canada
E-mail: smclean@sudbury.falconbridge.com

INTRODUCTION

The Sudbury Igneous Complex (SIC) has been a focus of exploration, mine development and production of Ni–Cu–PGE ores for more than a century. Falconbridge Limited has been producing ore from SIC deposits since 1929. During the decade preceding 2000, exploration activities in the SIC were commonly undertaken to depths exceeding 2000 m. Exploration targeted large, 10–20 Mt contact deposits. During this campaign, nearly 30 Mt of new resources were discovered, however, to date these have mostly been too deep to be of immediate economic interest to Falconbridge.

On November 13, 2001, a high-grade mineral deposit was discovered approximately 3 km north of the Sudbury Airport on the East Range of the Sudbury Basin on Falconbridge's 100%-owned Nickel Rim property. This discovery is significant in that it is located at a relatively moderate depth of 1,100–1,700 m below surface. An important factor in the discovery was a re-tooling of the exploration strategy that demonstrated that small to medium-sized, higher grade deposits were economic above 1,500 m depth. The new strategy rejuvenated exploration and initiated a re-evaluation of exploration opportunities around the basin. The combination of favorable geology, known mineralization and geophysical indications enhanced targeting leading to the Nickel Rim South deposit discovery, containing an inferred resource of 13.4 Mt grading 1.8 % Ni, 3.3 % Cu, 1.8 g.t⁻¹ Pt, 2.0 g.t⁻¹ Pd, 0.8 g.t⁻¹ Au and 14.8 g.t⁻¹ Ag within three distinct zones.

General Geology

The most conspicuous and economically significant feature of the Sudbury area geology is the Sudbury Basin, a 60 x 25 km broadly elliptical scar caused by a catastrophic Mid-Proterozoic meteorite impact (Fig. 16-1). The Sudbury Structure is located at the juncture of three distinct geological

provinces, the southern margin of the Archean Superior Province, the northern margin of the Proterozoic Southern Province and the northern margin of the late Proterozoic Grenville Province.

The Sudbury Structure suite of rocks can be divided into three broad groups consisting of 1) footwall rocks, 2) the Sudbury igneous complex (SIC) and 3) the post-impact fall-back breccias and basin-filling sedimentary rocks. The SIC includes a differentiated suite of basal norite cumulates and an upper, residual, granophyre unit, commonly referred to as the Main Mass. Transition Zone rocks consist of a thin zone of magnetite-bearing, quartz gabbro that separates the lower norite from the upper granophyre. Sudbury Sublayer represents a heterogeneous gabbroic to noritic rock containing a wide variety of inclusions occurring locally at the base of the SIC norite sequence and is intimately associated with contact-style mineralization. The Main Mass of the SIC exhibits cryptic mineral and chemical variations typical of fractional crystallization in layered intrusions (Naldrett & Hewins 1984), (Fig. 16-2). The footwall consists of a variety of rock types that are typically brecciated close to the SIC. Late Granite Breccia is an igneous to metamorphic-textured unit that typically occurs locally immediately below the Sudbury Sublayer at the contact between SIC and footwall rocks.

Current research supports the idea that the SIC formed as the result of a catastrophic meteorite impact (Dietz 1964, Guy-Bray *et al.* 1966, French 1966, 1967, 1968, Grieve *et al.* 1991), which has been dated at 1850 Ma (Krogh *et al.* 1984). The meteorite excavated a large crater, causing brecciation and shock metamorphism of the country rocks. Impact melt pooled to form a melt sheet that filled the crater and differentiated to form the SIC Main Mass. Fall-back breccias and basin sedimentary rocks covered the complex resulting in the formation of the Whitewater Group rocks.

Sudbury mineralization formed during the

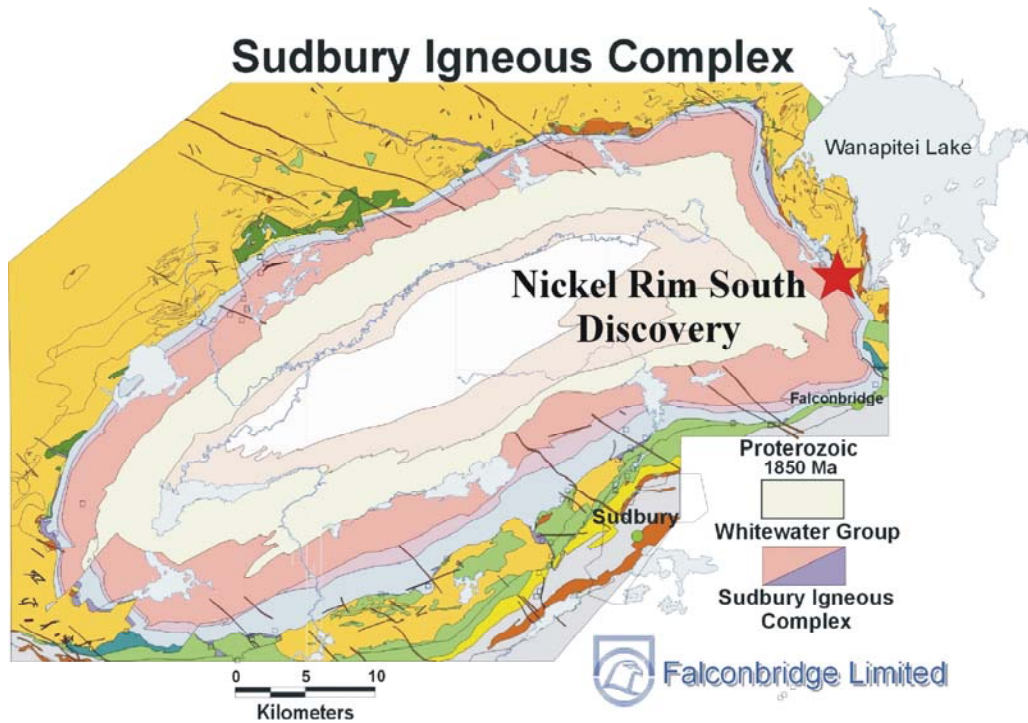


Fig. 16-1. Sudbury Igneous Complex geology and location of the Nickel Rim South discovery.

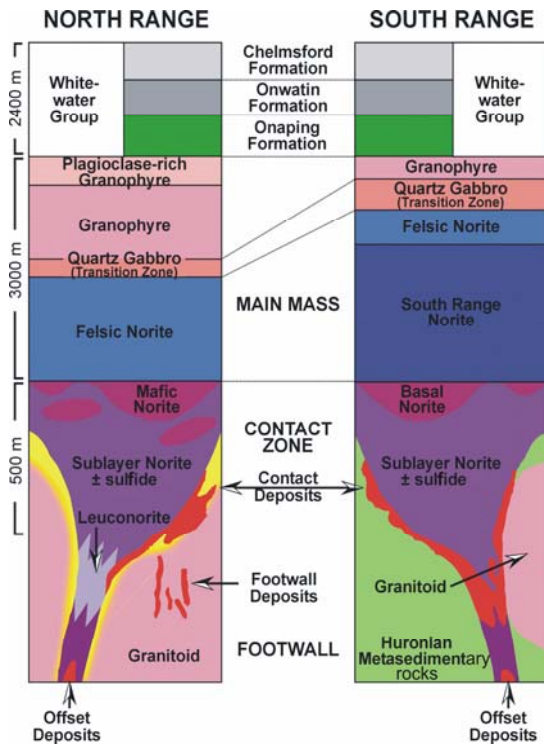


FIG. 16-2. Stratigraphy of the Sudbury Structure (after Lightfoot *et al.* 1997).

cooling of the melt sheet, as immiscible Ni-Cu-PGE-enriched sulfide liquid precipitated out of the liquid and collected at the base of the complex as contact-type deposits. The sulfides along the contact have historically been interpreted to have collected in local depressions and terraces along the footwall (Pattison 1979, Morrison 1984).

After deposition, the sulfide further fractionated to sulfide melt rich in Cu, Ni, and PGE concurrently with remobilization of the sulfide into the country rock along pseudotachylite breccia zones (locally known as Sudbury Breccia) resulting in the formation of the typically high grade Sudbury Footwall deposits.

Discovery

As a result of intense exploration activity for nearly a decade preceding the discovery of Nickel Rim South, much of the large-tonnage contact-style ore potential of the Sudbury contact environment had been evaluated above depths of 2000 m on Falconbridge property. In 2001, however, economic modeling using contemporary cost estimates demonstrated that smaller, >3 Mt contact deposits could be economically viable between 500 m and 1,500 m depth and even smaller deposits, >500,000 t could be economically extracted above

500 m depth. Furthermore, using these target size criteria, it was estimated that approximately 120 km² of contact on Falconbridge property remained untested for such deposits above 1500 m.

Historically, footwall deposits had not been systematically explored for by Falconbridge. At the start of 2001 it was estimated that 74.5 km³ of footwall host rock occurred on Falconbridge property within 500 m of the SIC contact and above 1,500 m. Additional economic modeling further demonstrated that a footwall deposit with typical footwall grades and of minimum 750,000 t could be economically exploitable between 500 m and 1500 m depth and that the minimum size requirement was about 500,000 t above 500 m. Given these parameters, it was estimated that only about 10% of the prospective portion of the footwall volume had been tested and approximately 67 km³ of footwall remained untested.

As a result of the analysis of economic opportunity for small to medium-sized deposits, in 2001 Falconbridge initiated a new exploration strategy for the Sudbury area. The plan included an aggressive search for small to medium-sized deposits above 1,500 m within the contact and footwall environments. This approach was an evolution from traditional company exploration strategy that had concentrated on targets that had potential for large (>10 Mt) orebodies in the contact environment.

Prior to the discovery, exploration on the Ni

Rim property consisted of regional geophysical surveys including airborne electro-magnetic (EM), magnetic surveys and ground-based audio-magnetotelluric (AMT) surveys, (Fig. 16-3). In addition, minor mapping and reconnaissance diamond drilling together with borehole EM surveys were also carried out. As part of the renewed exploration effort a re-compilation of all existing data was directed towards the construction of a basin-wide 3D model that would provide enhanced querying and visualization of the data and afford a platform by which to start a systematic review of the Falconbridge Sudbury Basin properties.

Early in the technical review process, the Ni Rim Property, located on the southern part of the East Range of the SIC, was identified as being prospective for the newly defined exploration target. Notably, the area hosted interesting geology including an anomalous occurrence of Sublayer and Late Granite Breccia in the contact environment as well as a significant abundance of Sudbury Breccia in the Footwall. Elevated and anomalous Ni–Cu–PGE mineralization had been reported from various historic exploration boreholes within in the area and two past producers had operated in the vicinity (Inco's MacLennan Mine and the McVittie-Graham Mine also known as the Ontario Nickel Mine and the East Rim or Nickel Rim Mine). Other significant examples of mineralization in the area

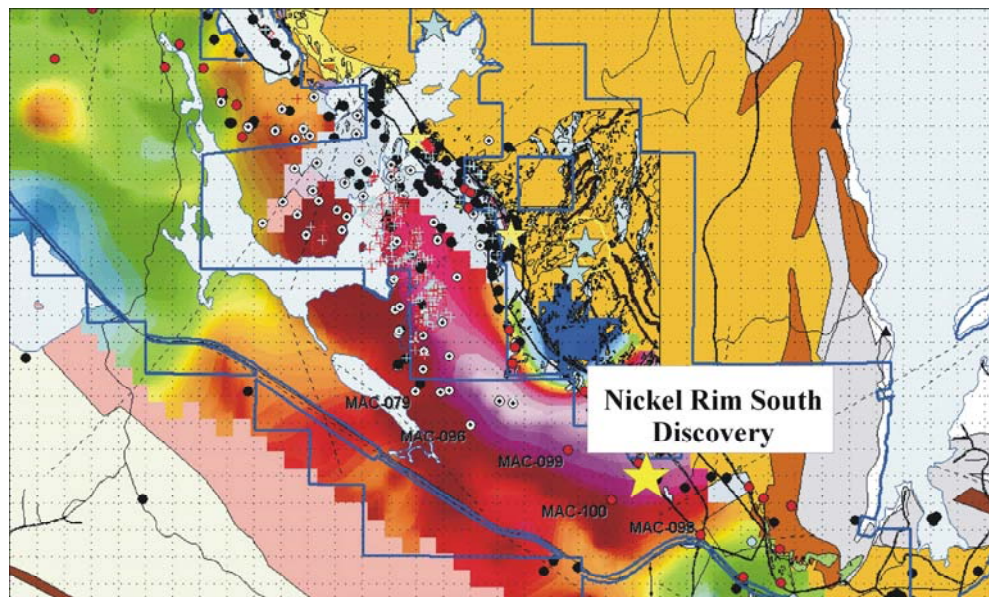


FIG. 16-3. Contoured 100 Hz AMT phase map East Range, SIC.

include Inco's Victor Main and Victor Depth deposits and Falconbridge's Ni Rim Depth deposit, both situated north of the property.

Of significance in targeting the discovery of Nickel Rim South, were the results of work carried out in the area by Falconbridge Exploration between 1992 and 1996. The Nickel Rim Depth deposit was discovered in 1992 by drilling the down-plunge extension of Inco's Victor Depth deposit. During this period the deposit was drilled from surface to establish an inferred resource of 1.6 Mt grading 1.58% Ni, 10.13% Cu, 4.18 g.t⁻¹ Pt, 3.5 g.t⁻¹ Pd and 2.51 g.t⁻¹ Au. Although this deposit was determined to be too deep for effective economic exploitation, exploration in the area continued in 1995 and 1996 with a series of exploratory "scout" holes established at approximately 500 m step outs along the strike direction to the south of Nickel Rim Depth in order to test stratigraphy and establish geophysical platforms for borehole electromagnetic surveying (BHEM).

As part of the step-out drill program, drill hole Mac-100, located approximately 2.1 km south of Ni Rim Depth, was put down to a depth of 1,852.5 m. The hole intersected weak mineralization at the contact (1.89% Ni, 0.71% Cu, 0.21 g.t⁻¹ Pt, 0.17 g.t⁻¹ Pd and 0.24 g.t⁻¹ Au over 0.10 m; 1,443.0m to 1443.1m). More important, however, was the intersection of a 30 cm interval containing a 15 cm (true thickness), irregular massive chalcopyrite vein located 28.17 m below the contact. This interval returned 0.26% Ni, 20.3% Cu, 0.99 g.t⁻¹ Pt, 0.08 g.t⁻¹ Pd, and 0.28 g.t⁻¹ Au over 0.3 m between 1,561.2m and 1,561.5m. Follow-up BHEM surveying identified a conductive response; however the target was not followed up.

In 2001, the reconnaissance borehole platforms established in 1995 and 1996 were optimized by the use of modern borehole electromagnetic profiling. The 3 component, low frequency (3.8 Hz) UTEM IV system (Lamontagne Geophysics) was used to increase the effective sampling radius of the drill holes, in an effort to detect far-field sulfide-bearing sources and to define highly conductive sulfide sources better. The survey identified two significant, non-decaying anomalies, interpreted to lie up-dip from minor mineralized contact and footwall zones intersected in Mac-100. A wedge (Mac-100A) was subsequently set in the hole on October 21, 2001, and significant mineralization was initially cored on November 13 (Fig. 16-4).

The discovery intersections were reported as follows:

Contact Zone: 5.30 m (1,440.75 m to 1,445.05 m) grading 2.86% Ni, 1.91% Cu, 0.84 g.t⁻¹ Pt, 0.67 g.t⁻¹ Pd and 0.24 g.t⁻¹ Au

Footwall Zone; 88.85 m (1,575.90 m to 1,664.75 m) grading 1.76% Ni, 6.45% Cu, 5.2 g.t⁻¹ Pt, 6.53 g.t⁻¹ Pd and 3.67 g.t⁻¹ Au

Including: 10.85m (1,652.15m to 1,663.0m) grading 2.17% Ni, 12.76% Cu, 15.00 g.t⁻¹ Pt, 21.16 g.t⁻¹ Pd and 13.64 g.t⁻¹ Au.

Nickel Rim South Deposits

Subsequent exploration has permitted the delineation of three principal mineralized zones that comprise the Nickel Rim South deposit; the Main Contact Zone (HW), a second, smaller Contact Zone (HW2) and the Footwall Zone (FW) (Table 16-1). The initial discovery and characterization focus was the high-grade footwall mineralization. More recently, the scope of exploration and delineation has been expanded to include the characterization of the main contact mineralization. Notably, however, there has been little work completed to date on the HW2 zone.

Contact mineralization

Contact mineralization at Nickel Rim South occurs along the basal SIC contact and is hosted in mafic

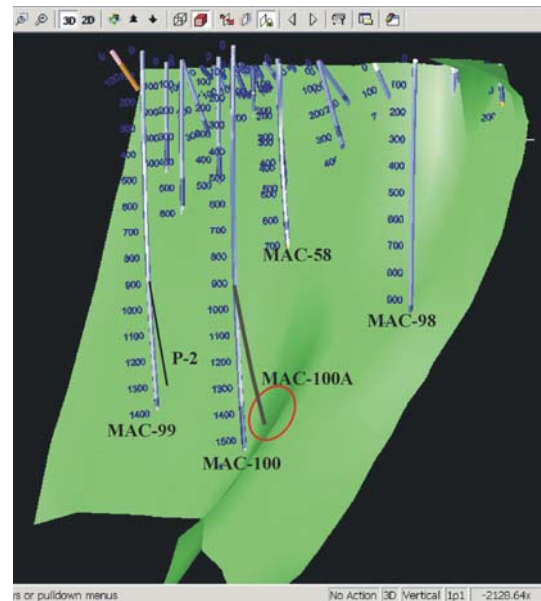


FIG. 16-4. 3D SIC contact surface, Mac-100 pilot hole and BHEM anomaly targeted with Mac-100A. Nickel RIM South Discovery hole.

TABLE 16-1. RESOURCE ESTIMATE, DEC 31, 2004

Category	Tonnes	% Ni	% Cu	% Co	% S	Au g.t ⁻¹	Pt g.t ⁻¹	Pd g.t ⁻¹	Ag g.t ⁻¹
Inferred HW2	300,000	2.4	0.3	0.06	14.3	0.0	0.1	0.1	2.1
Inferred HW	6,700,000	1.9	1.2	0.05	11.1	0.1	0.6	0.5	6.1
Inferred FW	6,400,000	1.7	5.7	0.02	8.1	1.5	3.1	3.7	24.5
Total	13,400,000	1.8	3.3	0.04	9.7	0.8	1.8	2.0	14.8

norite, Sudbury Sublayer and late granite breccia. Mineralization within the basal portion of the mafic norite is typically finely disseminated mm-sized sulfide blebs and increases in abundance within lower SLN and LGBX units where it forms semi-massive and massive sulfide zones (Fig. 16-5). The core area of sulfide mineralization is typified by heavily disseminated and inclusion-bearing semi-massive to massive sulfide.

The contact mineralization consists dominantly of pyrrhotite with minor pentlandite, magnetite and chalcopyrite. Sulfide content varies from less than 1% sulfide minerals in the upper disseminated intervals to >65% in the semi-massive sulfide and massive sulfide sections near the contact (Fig. 16-6a). The semi-massive to massive mineralization is comprised of 40–75 % pyrrhotite

with 5–10% pentlandite and 3–7% chalcopyrite. Sulfide textures vary from fine disseminations to coarse blebby disseminations, stringers and veins through to semi-massive and massive inclusion-bearing sulfide zones.

The core area of HW zone has been intersected and characterized over an area approximately 590 m in plunge length by 360 m in strike length and ranges from 5 m to 105 m in thickness. The zone generally tracks the SIC footwall contact along its base with the thickest intersections corresponding with topographic lows or depressions in the footwall contact (Fig. 16-5). The upper contact of the mineralization tends to be less well defined and gradational compared to the lower contact. Inclusion-rich zones locally affect the grade and thickness of the mineralization.

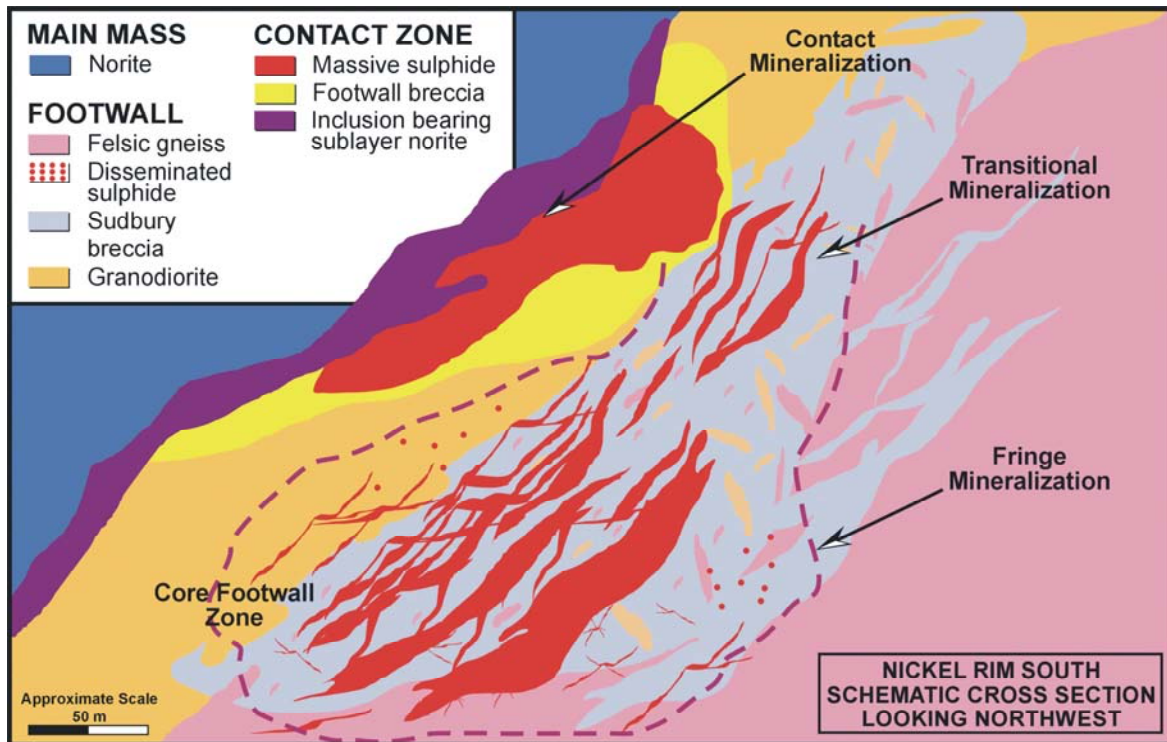


FIG. 16-5: Schematic cross section of the Nickel Rim South Deposit.

Transitional mineralization

Contact-like mineralization within the immediate footwall is referred to as Transitional mineralization and occurs up to a distance of 40 m below the main igneous contact. This style of mineralization is characterized by a network of massive sulfide veins (from 0.25–3.00 m in core length) surrounded by a halo of subordinate minor stringer and disseminated sulfide (Fig. 16-6b). Mineralization closely resembles contact-style mineralization in bulk mineralogy, containing high pyrrhotite content (greater than 50–60 %) with lesser chalcopyrite (20–30 %) and pentlandite (10–20 %) and minor magnetite. The veins exhibit compositional banding of pyrrhotite, chalcopyrite and pentlandite. Banding in most instances is sub-parallel to vein margins. Chalcopyrite forms aggregates and lozenges of sulfide interstitial to pyrrhotite resulting in interconnected bands or chains. Pentlandite occurs as aggregates of euhedral to subhedral grains also aligned sub-parallel to vein banding. Vein margins are marked by sub-centimetre- to centimetre-wide alteration haloes dominated by millimetre-sized chlorite rinds with lesser actinolite and epidote. This silicate assemblage is often present as euhedral crystals intergrown along the vein margin with sulfides.

Footwall mineralization

The style of the Nickel Rim South Footwall mineralization closely resembles other Sudbury footwall deposits, such as Strathcona Deep Copper (Fraser Deep Copper Zones 36, 37, 38 and 39), McCreedy East and McCreedy West in the North Range and Lindsley 4B in the South Range (Naldrett & Kullerud 1967, Morrison *et al.* 1994a, Binney *et al.* 1994). Mineralization is intimately associated with a zone of intensely brecciated footwall rocks (Sudbury Breccia). This brecciation appears to be lithologically-controlled along a transition from fine- to medium-grained massive equigranular granodioritic gneiss (immediately adjacent to the SIC) outwards to a coarse grained felsic to intermediate strongly foliated gneiss.

Sudbury Breccia and other footwall lithologies exhibit subtle textural and color changes with increasing proximity to mineralization (*cf.* Morrison 1994b, Hanley & Mungall 2003). The Sudbury Breccia matrix color in particular varies from black to light greenish-grey with increasing proximity to mineralization. This color variation is accompanied by a coarsening of the breccia matrix

from fine-grained and aphanitic to a biotite-porphyroblastic texture (3–10% mm-scale porphyroblasts) containing fine-grained acicular amphibole and euhedral epidote and chlorite. In addition, 3–10% wispy to stringer-style anatectic granitic melt zones occur within the breccia matrix and other footwall lithologies proximal to mineralization.

Footwall mineralization predominantly occurs as massive sulfide veins, smaller subordinate stringers, and disseminations. The sulfide assemblage is dominantly chalcopyrite (CuFeS_2) with lesser amounts of pentlandite ($(\text{Ni,Fe})_9\text{S}_8$), cubanite (CuFe_2S_3), pyrrhotite (Fe_{1-x}S), millerite (NiS), bornite (Cu_5FeS_4), magnetite, and several significant precious metal-bearing minerals in trace quantities (Figs. 16-6c and 16-6d). Mineralogical zonation outwards from the SIC contact is well-developed and comprises three distinct end-members. High iron and sulfur minerals (such as pyrrhotite and cubanite) are found proximal to the contact. Copper-nickel sulfides such as chalcopyrite and pentlandite form the core of the Footwall Zone. Sulfur and iron-poor sulfides (such as bornite and millerite) occur near the outer margins of the zone. The latter form a broad halo surrounding the core area of the deposit that is referred to as Fringe mineralization. In addition to these three end-member mineralization types, zones of 1% to 5% disseminated mineralization that are characterized by very low sulfide content and high PGE content (high PGE, low sulfide zone) have been recognized locally within the periphery of, spatially beneath, and removed from, the core Footwall Zone.

The core zone of footwall mineralization typically occurs 65–90 m below the SIC contact. This zone is composed of a network of massive sulfide veins, ranging from 0.25–26 m in core length typically enclosed by a halo of subordinate stringers and disseminated sulfide (Figs. 16-6c and 16-6d).

The massive veins are composed of greater than 65–70% massive chalcopyrite with large 0.5 to 5.0 cm-sized blocky euhedral pentlandite, accompanied by minor cubanite, pyrrhotite, millerite and magnetite (Fig. 16-6d). Magnetite forms euhedral to subhedral skeletal grains and grain aggregates distributed throughout the veins whereas cubanite tends to form large acicular blades up to 1 cm in length. Mineralization in the core Footwall zone locally is weakly banded parallel or

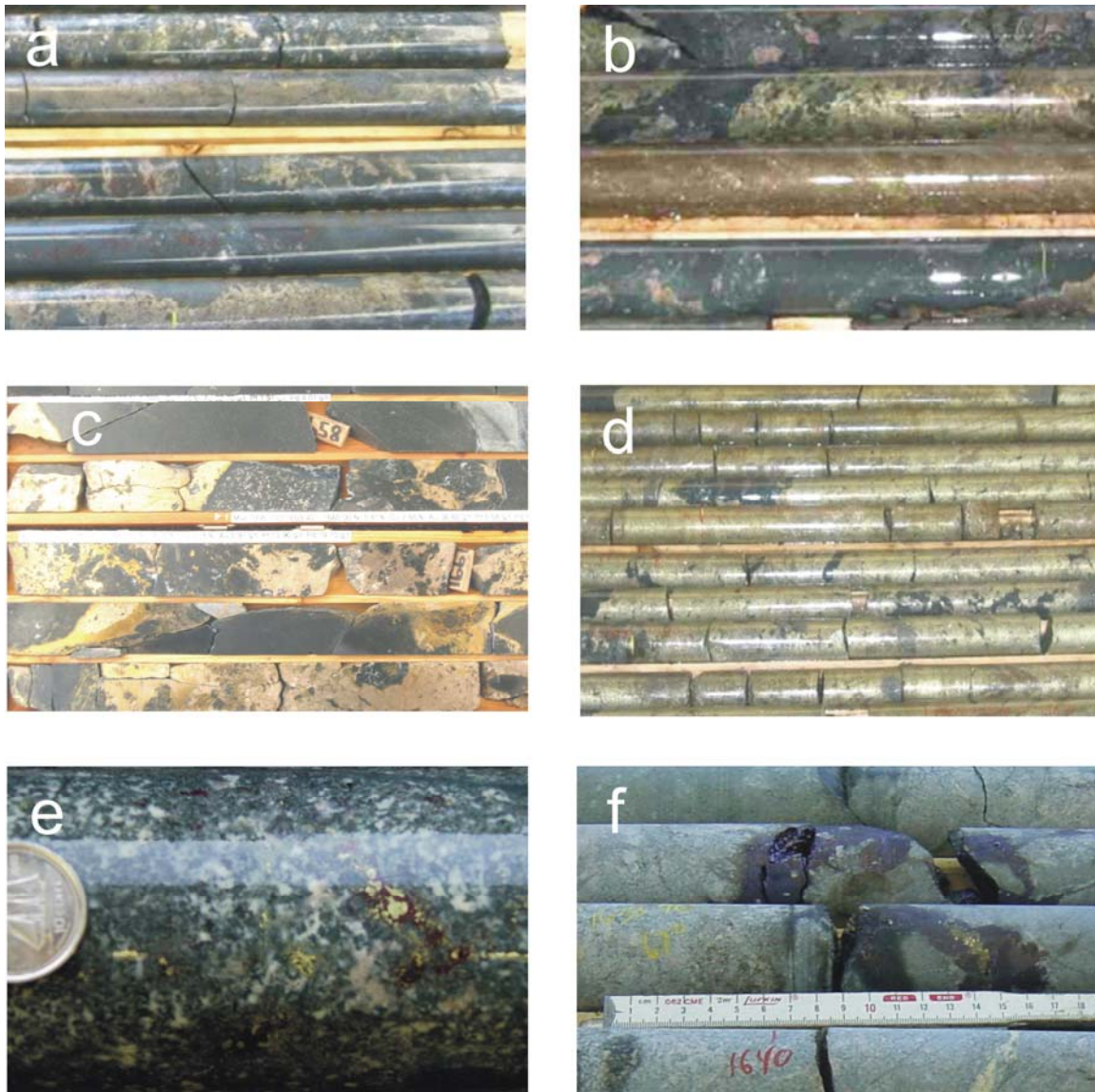


FIG. 16-6. **a**, massive inclusion-bearing contact mineralization hosted in SLN/LGBX; drill hole Mac-103D; **b**, transitional footwall pyrrhotite-pentlandite-chalcopyrite mineralization hosted in Sudbury Breccia and granitic gneiss from drill hole Mac-123A; **c**, dm to m scale chalcopyrite-pentlandite veins hosted in Sudbury breccia and granodioritic gneiss from the discovery hole Mac-100B; **d**, multi-metre scale chalcopyrite-pentlandite-pyrrhotite veins hosted in Sudbury breccia from Mac-116B; **e**, bornite-chalcopyrite low-S mineralization hosted in Sudbury Breccia from Mac-100B; **f**, Sudbury Breccia hosted bornite-millerite fringe mineralization from Mac-124C.

sub-parallel to the vein contacts typified by chains of coarse pentlandite defining the compositional banding.

The margins of the veins are typically marked by centimetre-wide alteration haloes of chlorite-actinolite and epidote. As in the Transitional Zone, this silicate assemblage is often intergrown with sulfides and exhibits well-preserved euhedral textures. However, vein margins

in the core Footwall zone appear to contain a slightly higher abundance of actinolite and epidote than vein margins in the transitional environment. Fringe-style footwall mineralization occurs peripheral to the Core zone veins but also forms a broader zone of mineralization that envelops the whole Core Footwall zone. This style of mineralization is characterized by stockwork stringer and disseminated sulfides varying in

thickness from 0.25–1.75 m in core length, (Figs. 16-6e and 16-6f). Sulfide mineralization in this zone is dominantly chalcopyrite, millerite, bornite and pentlandite. Bornite tends to occur as fine interstitial disseminated grains within the footwall rocks, (Fig. 16-6e), and as interconnected stringers and veinlets, (Fig. 16-6f). Veins commonly contain elevated contents of quartz and carbonate that form intergrown silicate-carbonate-sulfide veinlets and stringers.

Alteration surrounding vein and stringer margins in the Fringe zone is more intense and pervasive than those surrounding veins in the Core and Transitional footwall zones. Alteration haloes

are typically centimetre- to decimetre-thick zones with well-developed chlorite-epidote alteration. Chlorite and epidote in this zone tend to be much finer grained and less acicular in habit than in other mineralized areas.

The low sulfide, PGE-rich sub-group of the Fringe-style of mineralization occurs 20–60 m stratigraphically below the Core footwall zone. Mineralization is chiefly disseminated to stringer chalcopyrite, millerite and bornite (commonly less than 2%). Associated alteration minerals (chlorite, epidote, and actinolite) are pervasive. These zones are up to several metres in core length and are interpreted to be discontinuous in nature.

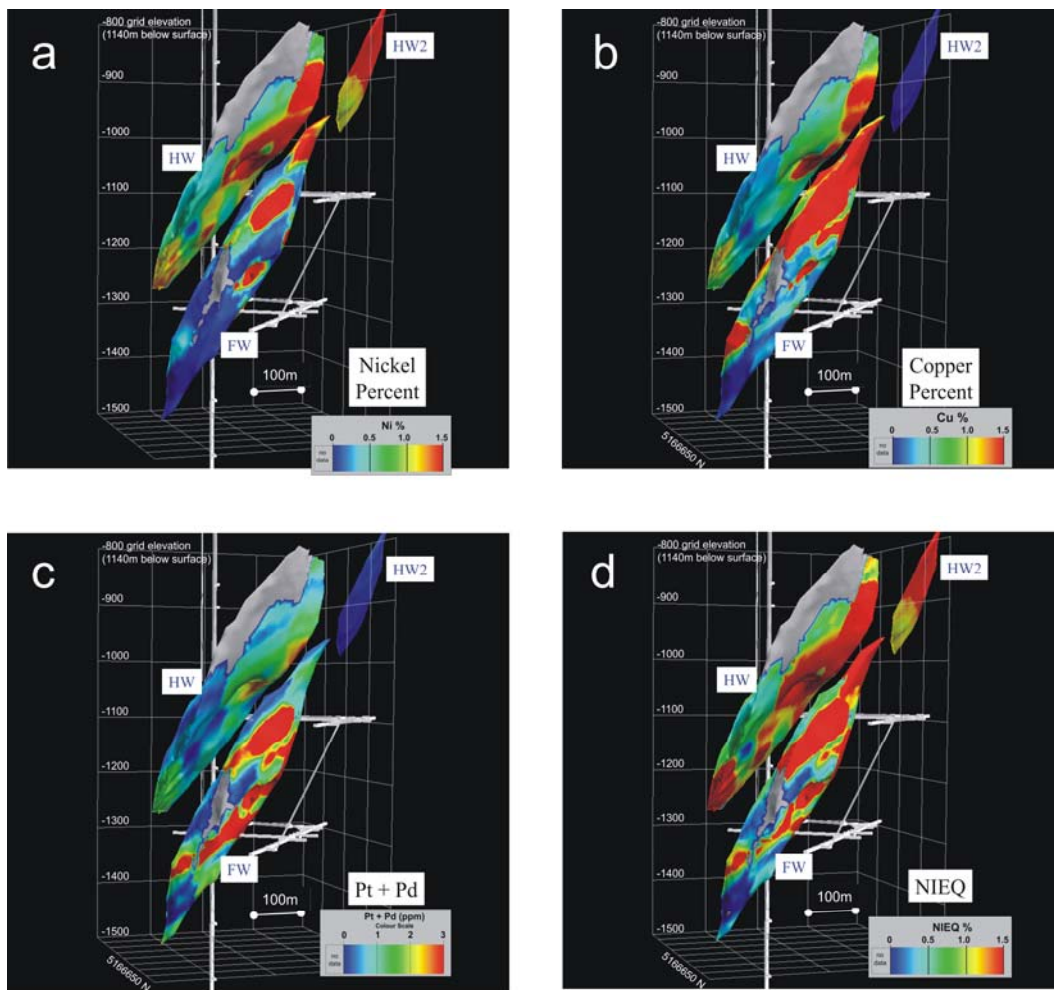


FIG. 16-7. **a**, 3D representation of Ni Rim South mineralized zones contoured with Ni content; **b**, 3D representation of Nickel Rim South mineralized zones contoured with Cu content; **c**, 3D representation of Ni Rim South mineralized zones contoured with Pt+Pd content; **d**, 3D representation of Ni Rim South mineralized zones contoured with NIEq content; Ni = \$3.35/lb, Cu = \$0.90/lb, Co = \$5.00/lb, Pt = \$450/oz, Pd = \$300/oz, Au = \$300/oz, Ag = \$5.25/oz (US\$).

Metal Zonation and Distribution

Metal zonation occurs throughout the deposit and defines a broad fractionation sequence from high Fe–Ni contact mineralization through to high Cu–Ni–PGE footwall mineralization. Overall, the sequence exhibits a characteristic increase in metal tenor with depth and increasing distance away from the SIC contact. The highest grades of copper, nickel, platinum and palladium occur in the lowermost portion of the core zone (Figure 16-7). These high-grade zones also coincide with the thickest intersections of Footwall mineralization.

Metal zonation can be directly associated with fractionation of the sulfide with lower grades occurring near to and at the SIC contact within the Contact zone. Ni and Cu grades increase within the Transitional and upper portions of the Footwall zone (Figs. 16-7a and 16-7b). PGE grades show dramatic upgrading from the Contact, through Transitional zones and attain exceptionally high values within the core of the Footwall zone (Fig. 16-7c). Nickel equivalent distribution can be calculated using typical pay metals such as Ni, Cu, PGE, Au, Ag and Co to depict the distribution of value (Fig. 16-7d). Mineralogically the higher grades of nickel and copper can be attributed directly to the changing sulfide mineral assemblage through this fractionated suite. Lower base metal contents typify areas dominated by high Fe–S mineralogy (pyrrhotite, pentlandite, chalcopyrite and cubanite), with higher base metal abundances corresponding to low Fe–S mineralogy (chalcopyrite, pentlandite, millerite and bornite).

SUMMARY

Surface exploration has been ongoing since the initial discovery in 2001. A systematic phased approach to exploration has met with success over the past 3 years. The deposit provides an excellent example of a fully fractionated SIC sulfide system including Fe–Ni rich Contact, Ni–Cu Transitional and a very high grade Cu–Ni–PGE Footwall zones of mineralization. On March 11, 2004 the Falconbridge Limited Board of directors approved an underground exploration program that will see the development of a 1,785 m main shaft, a 1675 m ventilation shaft, 10.4 km of lateral development and 104 km of definition drilling.

ACKNOWLEDGEMENTS

The authors would like to thank the members of the Sudbury Exploration and Mines Geology Departments of Falconbridge Limited for numerous

insightful discussions surrounding the geology of the Nickel Rim South deposit, from which much of the information has been drawn. In particular Bruce Churchill and Dave Richardson are thanked for their work on resource calculations and computer modeling of the data. In addition the Mineral Processing and Metallurgical Technology group for mineralogical and microprobe data on the footwall zone samples, particularly P. Whittaker and L. Kormos are also thanked.

REFERENCES

- BINNEY, W.P., POULIN, R.Y., SWEENEY, J.M. & HALLIDAY, S.H. (1994): The Lindsley Ni–Cu–PGE deposit and its geological setting. In Proceedings of the Sudbury-Norilsk Symposium (P.C. Lightfoot & A.J. Naldrett, eds.). *Ont. Geol. Surv. Spec. Vol. 5*, 91-103.
- DIETZ, R.S. (1964): Sudbury Structure as an astrobleme. *J. Geol.* **72**, 412-434.
- FRENCH, B.M. (1966): Shock metamorphism of natural materials. *Science* **153**, 903.
- FRENCH, B.M. (1967): Sudbury Structure, Ontario—some petrographic evidence for origin by meteorite impact. *Science* **156**, 1094.
- FRENCH, B.M., (1968): Deformation lamellae in quartz. *Science* **160**, 905.
- GRIEVE, R.A.F., STOFFLER, D. & DEUTSCH, A. (1991): The Sudbury structure: controversial or misunderstood? *J. Geophys. Res.* **96**, 22,753-22,764
- GUY-BRAY, J. & GEOLOGICAL STAFF (1966): Shatter cones at Sudbury, *J. Geol.* **74**, 243-245.
- HANLEY, J.J. & MUNGALL, J.E. (2003): Chlorine enrichment and hydrous alteration of Sudbury Breccia hosting footwall Cu–Ni–PGE mineralization at the Fraser Mine, Sudbury, Ontario, Canada. *Can. Mineral.* **41**, 857-881.
- KROGH, T.E., DAVIS, D.W. & CORFU, F. (1984): Precise U–Pb zircon and baddeleyite ages for the Sudbury area. In The Geology and Ore Deposits of the Sudbury Structure, (E.G. Pye, A.J. Naldrett & P.E. Giblin, eds.), *Ont. Geol. Surv. Spec. Vol. 1*, 431-446.
- LIGHTFOOT, P.C., KEAYS, R.R., MORRISON, G.G., BITE, A. & FARRELL, K.P. (1997). Geologic and geochemical relationships between the contact sublayer, inclusions, and the main mass of the

- Sudbury Igneous Complex: a case study of the Whistle mine embayment. *Econ. Geol.* **92**, 647-673.
- MORRISON, G.G. (1984): Morphological features of the Sudbury Structure in relation to an impact origin. *In* The Geology and Ore Deposits of the Sudbury Structure, (E.G. Pye, A.J. Naldrett & P.E. Giblin, eds.). *Ont. Geol. Surv. Spec. Vol. 1*, 513-520.
- MORRISON, G.G., JAGO, B.C. & WHITE, T.L. (1994a): Footwall mineralization of the Sudbury Igneous Complex. *In* Proceedings of the Sudbury-Norilsk Symposium (P.C. Lightfoot & A.J. Naldrett, eds.). *Ont. Geol. Surv. Spec. Vol. 5*, 57-64.
- MORRISON, G.G., JAGO, B.C. & WHITE, T.L. (1994b): Metal zonation patterns and micro-textural and micromineralogical evidence for alkali- and halogen-rich fluids in the genesis of the Victor Deep and McCreedy East footwall copper orebodies, Sudbury Igneous Complex. *In* Proceedings of the Sudbury-Norilsk Symposium (P.C. Lightfoot & A.J. Naldrett, eds.). *Ont. Geol. Surv. Spec. Vol. 5*, 65-75.
- NALDRETT, A.J. & KULLERUD, G. (1967): A study of the Strathcona Mine and its bearing on the origin of the nickel-copper ores of the Sudbury district. *J. Petrol.* **8**, 453-531.
- NALDRETT, A.J. & HEWINS, R.H. (1984). The Main Mass of the Sudbury Igneous Complex. *In* The Geology and Ore Deposits of the Sudbury Structure, (E.G. Pye, A.J. Naldrett & P.E. Giblin, eds.). *Ont. Geol. Surv. Spec. Vol. 1*, 235-251.
- PATTISON, E.F. (1979): The Sudbury Sublayer: its characteristics and relationships with the Main Mass of the Sudbury Irruptive. *Can. Mineral.* **17**, 257-274.

CHAPTER 17: DISCOVERY AND GEOLOGY OF THE LAC DES ILES PALLADIUM DEPOSITS

M.J.Lavigne,
Galantas Gold Corporation, Omagh Minerals Ltd,
56 Botera Road Upper, Cavanacaw, Omagh, Co.Tyrone, U.K., BT78 5LH
E-mail: m.lavigne@btinternet.com

M.J.Michaud,
China Diamond Corporation, 1724 Hyde Park Road, London, Ontario, N6H 5L7, Canada

and

J. Rickard,
North American Palladium, 710 Norah Cres. Thunder Bay, Ontario, P7C 4T8

EXPLORATION AND DEVELOPMENT HISTORY

Prior to 1963, few were familiar with the Lac des Iles area despite its being only 100 km north of the present city of Thunder Bay, which is on the northwestern shore of Lake Superior (Fig. 17-1). The area was difficult to access due to a lack of roads; it had not yet been subjected to logging. In addition, the area straddles the height of land and therefore lacks navigable waterways. The difficulty of access is highlighted by the fact that neither the Geological Survey of Canada, nor the Ontario

Department of Mines had mapped the area in sufficient detail to discover the Lac des Iles Intrusive Complex (LDI-IC). A few prospectors however, were familiar with the area. An Ontario Department of Mines report (Pye 1968) documented the earliest activity, "Following the discovery, by an aeromagnetic survey in 1958 of a large magnetically anomalous area at Lac des Iles, F.H. Jowsey Limited acquired two groups of 80 claims covering a large part of the north end of the lake (Lac des Iles)". Subsequent to both an airborne and ground electromagnetic and magnetometer

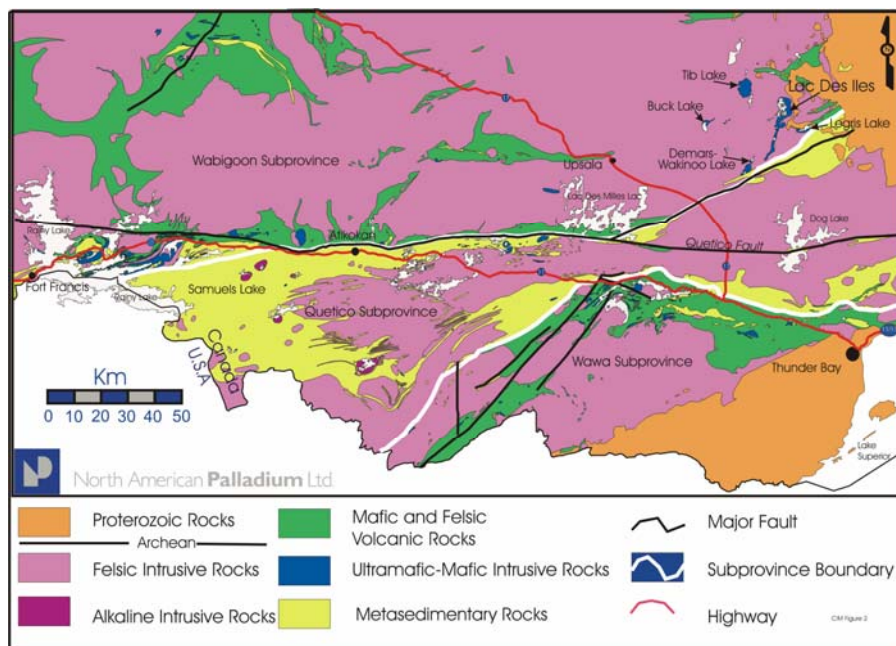


FIG. 17-1 Location of Lac des Iles, Lake Superior Region, North America.

Mineralogical Association of Canada Short Course 35, Oulu, Finland, p. 369-390

surveys, five diamond drill holes were bored to test four zones.

"The drillholes did not intersect anything of importance and indicated that, in general the anomalies were caused by magnetite in peridotite layers associated with pyroxenite." The individual responsible for managing these activities was Fred Jowsey, better known for his involvement with the discovery of uranium at Elliot Lake.

Subsequent to the abandonment of the exploration program at Lac des Iles, Fred Jowsey remained optimistic about the area's potential. In subsequent years he made several attempts to grubstake a prospecting party, specifically a party that included Walter Baker of Kirkland Lake. Walter did not make himself available until 1963 as he was preoccupied prospecting in Hemlo, where he discovered gold west of the now famous Williams claims. Walter was later recognized for his contribution to the eventual discovery of the Hemlo Gold camp by the Prospectors and Developers Association of Canada who awarded him the Prospector of the Year award in 1987. Shortly after breakup in May, 1963, a prospecting party composed of Walter Baker, his son Clement, George Moore and geologist Bruce Arnott flew to Lac des Iles and set up camp on an island at the south end of Lac des Iles.

The prospecting party went to Lac des Iles with a new tool in hand. In 1963 the Geological Survey of Canada and the Ontario Department of Mines released aeromagnetic maps covering the Lac des Iles area (GSC-ODM 1962) as part of its

ongoing nation-wide airborne magnetic survey. Magnetic highs became prospecting priorities, the first being a prominent magnetic high south of the lake, within sight of their camp, illustrated in Figure 17-2 (results of 2004 aeromagnetic survey). Success was immediate. They discovered coarse-grained disseminated chalcopyrite and iron sulfides minerals. Samples were sent to Swastika Laboratories on the next supply flight, to be assayed for base metals only. A note to the assayer from Walter Baker asked him to "keep an eye on the bead" as he suspected PGE may have been present. In 1963 assaying for PGE was difficult and expensive. Walter's intuition was correct; the samples sent contained appreciable amounts of Pd, Pt, Au, Cu and Ni. Within weeks, the property was optioned to Gunnex Limited. The prospectors discovered 8 mineralized areas, and claims were staked and recorded on Walter Baker's prospecting license.

Gunnex documented the mineralized areas and cored 12 drill holes. The best result, 302 feet (90 m) assaying 4.89 g.t^{-1} Pd, was from hole #5. Figure 17-3 shows the location of most of the mineralized zones that were discovered by Gunnex drilling. For reference, the Roby Phase 2 pit, circa 1999 and the distribution of pyroxenite are shown. The magnetic high that attracted the prospectors is created by magnetite-rich gabbro-norite, including numerous lenses of semi-massive magnetite. The magnetite-bearing rocks are devoid of mineralization, and their palladium tenor is usually at background levels. In contrast, the mineralized

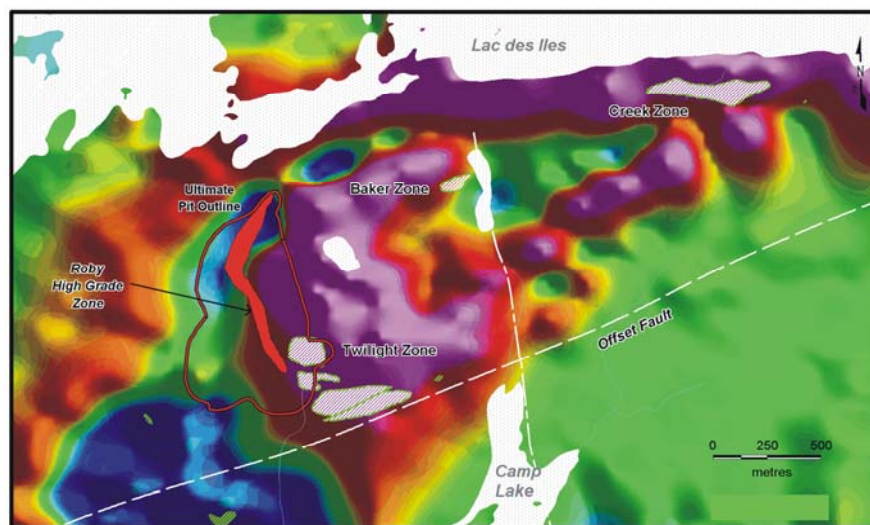


FIG. 17-2 Lac des Iles magnetic map, based on 2004 detailed airborne survey.

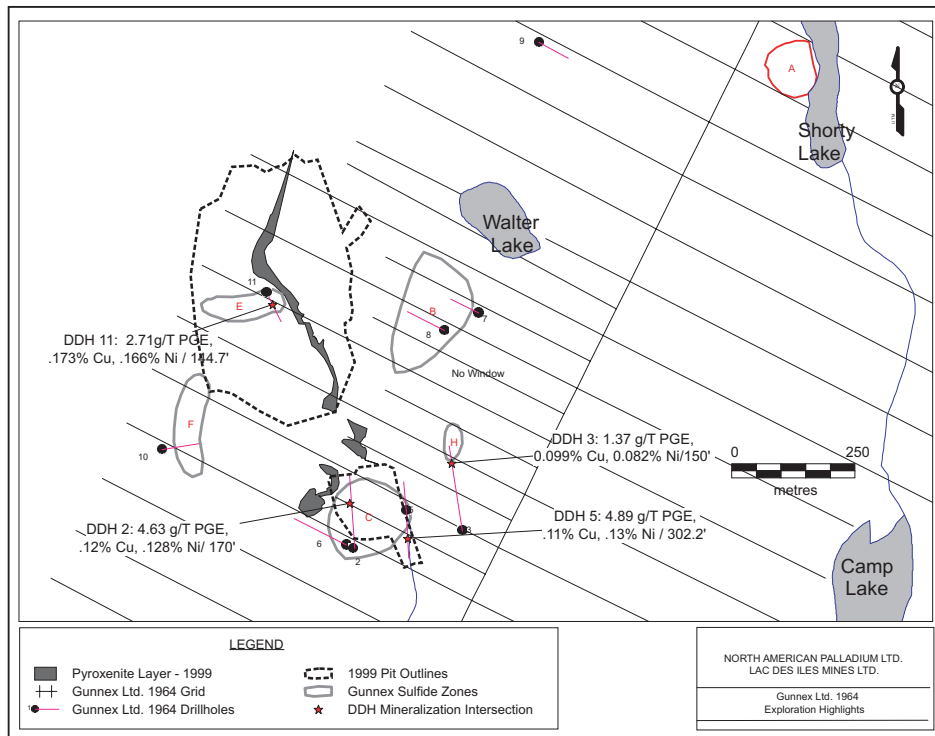


FIG. 17-3 Discovery map *ca.* 1963 with Gunnex drilling, superimposed on Phase 2; Roby Pit and pyroxenite *ca.* 1998.

rocks have low magnetic susceptibility. Subsequent detailed magnetic surveys, superimposed on the outline of the currently known Pd mineralization, clearly separate the barren magnetic rocks from the mineralization of the Roby and Baker Zones (Fig. 17-2). The exceptions to this are a narrow zone of the most intensely altered pyroxenite where talc and magnetite occur in addition to other alteration minerals and are associated with high-grade mineralization, and the Twilight Zone. The Twilight Zone is distinguished from the Roby Zone by the dominance of gabbro, and relatively weak silicate alteration, and the near absence of vari-textured gabbro.

The discovery of palladium at Lac des Iles prompted the Ontario Department of Mines to initiate regional-scale mapping (Pye & Fenwick 1965, Pye 1968) and attracted the interest of a large mining company, Anaconda American Brass Limited, who optioned the property. Anaconda conducted an exhaustive examination of the area over 3 years, mapped the LDI-IC and conducted geophysical surveys. This was followed by drilling 13 more core holes, mostly on the existing mineralization, with similar results. Anaconda drilled geophysical targets as well, which was

unsuccessful at discovering additional mineralization. Palladium at this time was worth approximately \$35 per ounce, and the mineralization, despite its volume potential, was deemed uneconomic. Anaconda dropped the option and the property became dormant.

In 1973, Gunnex held and administered Walter Baker's prospecting license. This common practice provided assurances to mining companies that mining claims held under an individual prospector's license weren't cancelled if a prospector failed to renew his/her license. While Walter was out prospecting in northern Canada, the anniversary date of his license passed without renewal, and all the mining claims attached to it were cancelled. This went unnoticed until Thunder Bay prospector Knut Kuhner asked a clerk at the mining recorder's office for the Lac des Milles Lacs claim map. The clerk gave him the Lac des Iles map by mistake. Kuhner noticed a block of cancelled claims and recognized the property. Kuhner found financial backers, organized a grubstake and flew to Lac des Iles to re-stake the claims. It subsequently took a year to find a company interested in the property as palladium prices were still low. In 1974, the property was optioned to Boston Bay Mines

Limited, a company controlled by Patrick Sheridan. Yet another grid was established and more geophysical surveys conducted. The individual with the on-site responsibility was Phillippe Roby. The discovery of high-grade mineralization is attributed to him, and he was responsible for orienting two key holes in this campaign. Holes # P014 and # P015 were oriented to intersect newly discovered mineralization in highly altered pyroxenite east of the Gunnex E-Zone (Fig. 17-4). Hole # P015 returned $8.37 \text{ g.t}^{-1} \text{ Pd}$, $0.247\% \text{ Cu}$ and $0.245\% \text{ Ni}$ over 180 feet (55 m). This drilling led to the realization that a lenticular zone of higher-grade mineralization occurred on the margin of a broader zone of lower grades. Subsequent systematic follow-up drilling defined an ore body named the Roby Zone.

The discovery of both higher base and precious metal values in a coherent ore body attracted Texasgulf Inc., discoverers of the Kidd Creek Mine in Timmins. Texasgulf optioned the property in 1975, accelerated the resource definition drilling program, re-examined the entire LDI-IC, examined many other intrusions in the area, and

conducted more geophysical surveys. As the result of a negative scoping study on production in 1976, the option was abandoned. The property then lay dormant until 1985.

Palladium in 1976 was valued at less than \$100 per ounce, a consequence of oversupply created by incidental palladium production as by-product of copper-nickel mining at Noril'sk, (as much as 3 million ounces a year), and Sudbury and from the Bushveld platinum mines. It was the "energy crisis" and the development of alternate energy sources such as PGE-based fuel cells in the 1980's that led the speculative market to drive palladium prices to \$150 per ounce. On this basis, Patrick Sheridan was able to finance renewed activity at Lac des Iles. Madeleine Mines Ltd. acquired 50% ownership of the leased claims from The Sheridan Platinum Group in 1986 and continued to delineate the Roby Zone. Madeleine Mines also built a 2400 ton per day plant which was in operation for 3 months in 1990. In 1991, Kaiser Francis Oil Company Limited gained control of Madeleine Mines Ltd., which changed its name to North American Palladium Ltd in 1993. A

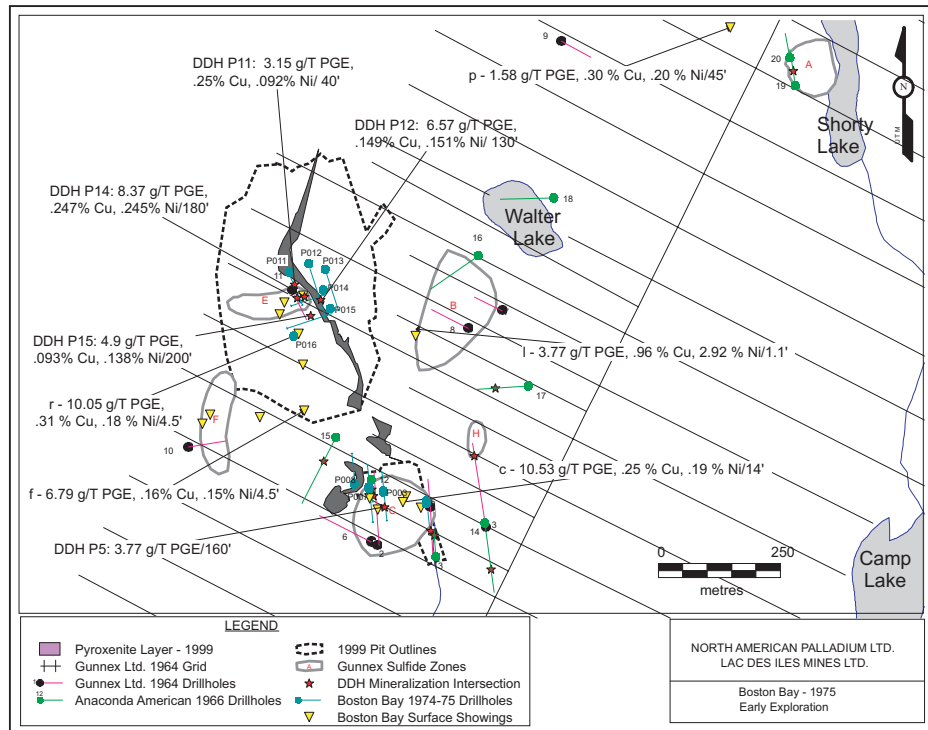


FIG. 17-4. Diamond drill holes traces (circa 1964–66 and 1974) and mineralized areas as mapped in 1963, are shown relative to the position of a current pit and a pyroxenite unit as mapped in 1992 and 1998.

significant investment in infrastructure from 1991 onwards led to the start of continuous production in December 1993.

The mine struggled with profitability, and in 1997, the potential residual profit in the existing open pit operation was less than the existing debt. Fortunately, rising palladium prices in 1998 (now driven by increased use of palladium in catalytic converters) led to a scoping study which examined the potential profitability of mining the more voluminous low-grade ore. The result of the scoping study was positive, contingent on the delineation of additional ore. This precipitated a drilling campaign in 1999 that doubled the total amount of drilling done to date to 100,000 metres. The result of the drilling, in combination with the lowering of mining cut-off grades led to increasing proven and probable reserves from 1.3 to 5 million ounces of palladium and a positive feasibility study on establishing a 15,000 tpd operation. Concurrent with increasing reserves at the Roby Zone, the entire Lac des Îles complex, and all other significant intrusions in the area were subjected to another round of exploration. Continued step-out drilling on the Roby Zone further expanded the resources. The discovery of the fault-offset high-grade zone at depth was made possible by geological interpretation based on core logging. Subsequent to 114,000 m of drilling in 2000, the total resource grew to 11.3 million ounces of Pd.

The key elements that were the basis of strategy development for the 1998–2004 exploration campaign are:

- 1) the Roby Zone is composed of variable-grade, irregularly distributed, vertical breccia pipes surrounded by lower-grade vari-textured gabbros (as opposed to being layer-controlled);
- 2) with few exceptions, all rock types in the LDI-IC can be “ore or waste” regardless of sulfide content (ore control by simple rock types is not possible);
- 3) the mineralization commonly contains disseminated sulfide, but some significant mineralization is almost devoid of sulfide or any other visual markers;
- 4) although the mineralization is usually associated with variable alteration of silicates, some areas of altered silicates are unmineralized;
- 5) the Roby Zone has a surface area greater than 1 km²;
- 6) the intrusion had been thoroughly mapped and prospected on two occasions, and variably

explored on at least three other occasions;

- 7) a variety of geophysical surveys, both ground and airborne had been conducted;
- 8) more than 50% of the target area has less than 1 m of overburden;
- 9) palladium values are elevated throughout the LDI-IC (mean >30 ppb Pd), but is less than 7 ppb Pd in barren intrusions .

The existence of PGE-rich rock without appreciable sulfide was seen as an exploration opportunity, as none of the previous programs were designed to discover such an ore type. To this end, the entire LDI-IC was sampled systematically at spacings ranging from 5 to 20 ft (1.5 to 6 m) along overburden trenches whose density was commensurate with the discovery potential. Outcrop was sampled at the highest possible and practical density. More than 20,000 samples were collected, and areas with anomalous PGE values were followed up with further trenching and sampling (Fig. 17-5). This exploration technique was considered cost-effective (approximately \$12,000 CAD per linear trench km) and provided two-dimensional information (as opposed to one-dimensional drill core). Where significant mineralization was discovered, extensive overburden removal was conducted (Fig. 17-6). This was also done in areas of previously known mineralization with the objective of better defining the nature and the boundaries of the mineralized zones as it allowed assays to be superimposed on lithology. These large, washed bedrock exposures were especially valuable in demonstrating the chaotic nature of the rocks associated with mineralization. The knowledge gained from examination of large bedrock surfaces was transferred to core logging which then led to realistic three dimensional geological models. In areas covered with greater thicknesses of overburden or lakes, induced polarization (IP) electro-magnetic surveys were conducted. Concurrent magnetic surveys helped to screen out IP anomalies created by disseminated magnetite. Areas with known and well-exposed mineralization were also surveyed. Previously, IP had seen limited application and its effectiveness was unknown. Anomalies were investigated by trenching and sampling.

Detailed sampling and assaying of newly created bedrock exposures led to many new discoveries. The most significant discovery was the Twilight Zone, separated from the Roby Zone by

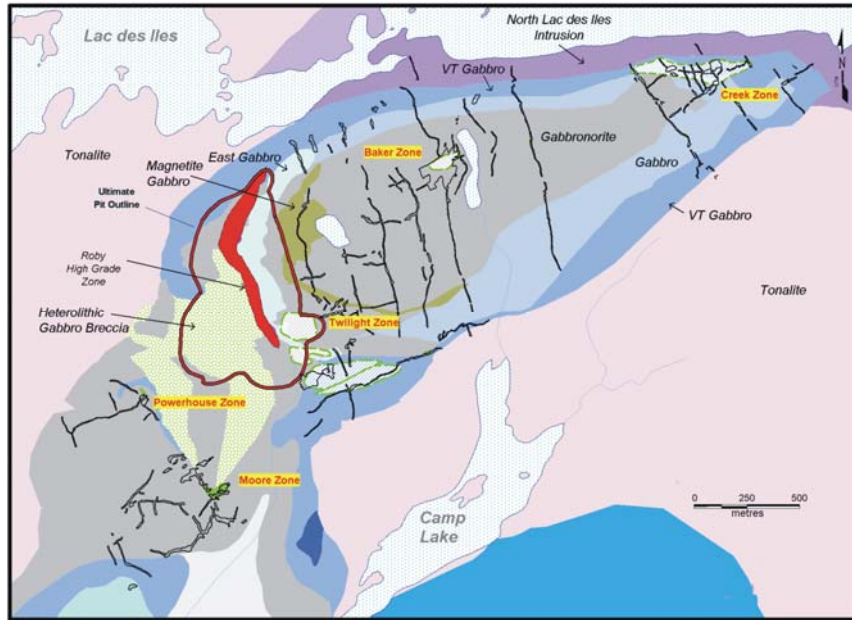


FIG. 17-5. 2000 North American Palladium Ltd trench location map.



FIG. 17-6 1999 overburden removal at Twilight Zone (picture)

the barren East Gabbro. Isolated, low-grade Pd assays had been known since 1963, and although subsequent diamond drilling did intersect mineralization, it was not deemed significant enough to be followed up by definition drilling. Trench sampling uncovered significant amounts of higher grade palladium mineralization. Mineralized zones were subsequently expanded in two dimensions by extensive overburden removal and in the third dimension by diamond drilling. Similarly,

trenching and sampling of the Baker Zone demonstrated that a significant volume of mineralized rock existed. This was subsequently augmented by diamond drilling. Numerous discoveries were made throughout the complex, all of which were evaluated on surface for volume and grade, thus avoiding costly diamond drilling. Included in this were a dozen targets generated by IP. Most of the high-chargeability anomalies were generated by zones of silicate alteration, where

pyroxenes and olivine were converted to hydrous silicates such as actinolite, talc, and serpentine. In some cases, minor amounts of magnetite also created anomalies.

The superposition of IP results on detailed surface sampling maps of the Baker Zone showed weak chargeability anomalies over the sulfide-rich zone, surrounded by numerous, stronger anomalies that were not demonstrably associated with mineralization (Fig. 17-7). A Titan 24 magneto-telluric (MT) survey also produced similar results. The limiting factor in utilizing techniques that measure chargeability and resistivity is that anomalies are manifestations of the most voluminous minerals. The presence of chargeable and variably resistive silicates and the production of numerous anomalies that are not associated with mineralization distract attention away from more legitimate targets. Despite this understanding, some anomalies under deep cover were tested by drilling, with negative results.

The use of indirect geochemical surveys (sampling of media other than bedrock) was also investigated, but only to a limited extent by the private sector. The Ontario Geological Survey (Dyer & Russel 2002, Searcy 2001) and university-based researchers (Cameron & Hattori 2003, Hattori & Cameron 2004) have examined Pd distribution and mobility in the surficial environment. The

preponderance of situations that create false anomalies, combined with palladium's high mobility in the surficial environment, prevents the use of soil and lake sediment sampling as an effective exploration technique. Trial surveys, conducted by North American Palladium Ltd., involving bark sampling were carried out along linear bedrock trenches that traversed mineralized and unmineralized rock. Poor correlation existed between bedrock and bark assays. In fact, the highest assay came from an area of barren rock, whereas trees close to and downslope from the Baker Zone returned much lower assays. Airborne, Pd-bearing dust created by the mining operation may have masked any real anomalies. Hattori and Cameron (2004) did find anomalous Pd in humus downslope from the Baker Zone. Interpretation of these results must take into account factors such as overburden source and groundwater flow.

In summary, Pd mineralization was discovered by traditional prospecting techniques. Magnetic surveys will discover mafic intrusions, and cursory traversing, sampling and assaying will discriminate between pregnant and barren intrusions. Systematic bedrock sampling is the most pragmatic discovery tool, as the targets are large. This deposit type is not well-disposed to being discovered by geophysical and geochemical surveys.

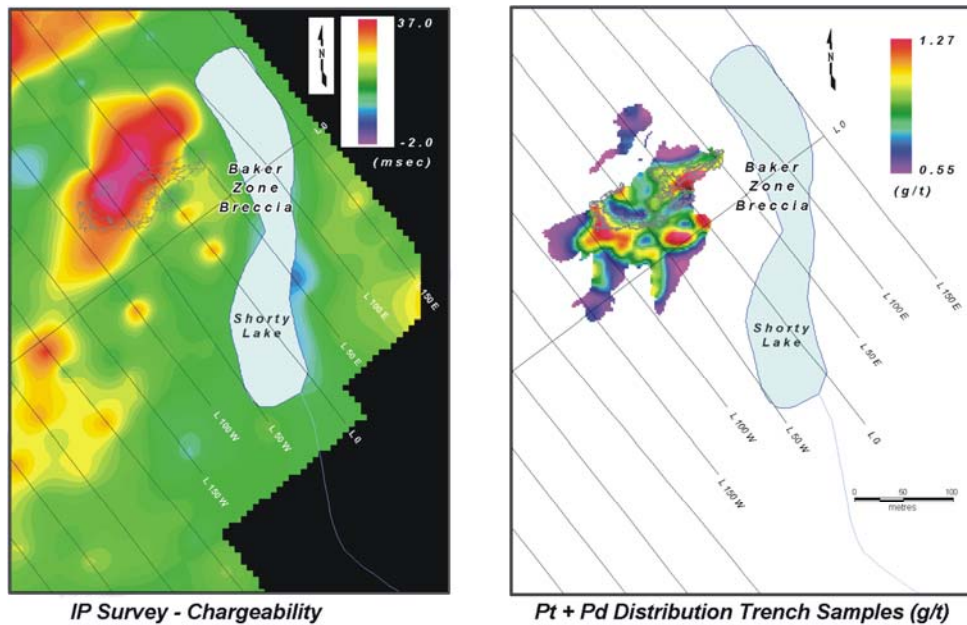


FIG. 17-7 Baker Zone IP-EM on Pd grade contour.

REGIONAL GEOLOGY

The Neoproterozoic Lac des Iles Intrusive Complex (LDI-IC) lies within the Eastern Marmion terrane of the Wabigoon Subprovince, immediately north of the Wabigoon-Quetico Subprovince boundary, along which mafic and ultramafic intrusions are common, extending 300 km from Rainy Lake to Lake Nipigon (Fig. 17-1). The Marmion terrane was defined by Tomlinson *et al.* (in press) as the south-central Wabigoon Subprovince and contains juvenile 3.0 Ga crust (Marmion batholith) and minor younger Mesoproterozoic and Neoproterozoic volcanic and plutonic rocks which dominantly yield 3.0 to 2.8 Ga Nd model ages. The LDI-IC is the largest of a series of mafic to ultramafic intrusions defining a circular pattern in the LDI area that is approximately 30 km in diameter (Fig. 17-1). The LDI-IC had previously

been sub-divided into three distinct chambers, the ultramafic North LDI-IC, the Mine Block Intrusion, and the Camp Lake Intrusion to the south (Fig. 17-8). The LDI suite consists of the Taman, Demars Lake, Buck Lake, Dog River, Tib Lake, North LDI and the Mine Block intrusions. Whereas several other mafic intrusions nearby were formerly considered part of the LDI suite, recent mapping, age dating and lithogeochemistry by the Ontario Geological Survey, (Hart *et al.* 2000a,b, Hart *et al.* 2001a,b, Stone 2002) and subsequent age dating, lithogeochemistry and compilation (Stone *et al.* 2003) has led to significant new realizations. The new mapping has defined the monzodioritic Shelby Lake batholith of the sanukitoid suite directly south of the LDI-IC. Early gabbroic phases occur locally at the rim of the Shelby Lake batholith, at localities such as Wakino Lake, Camp Lake and Legris

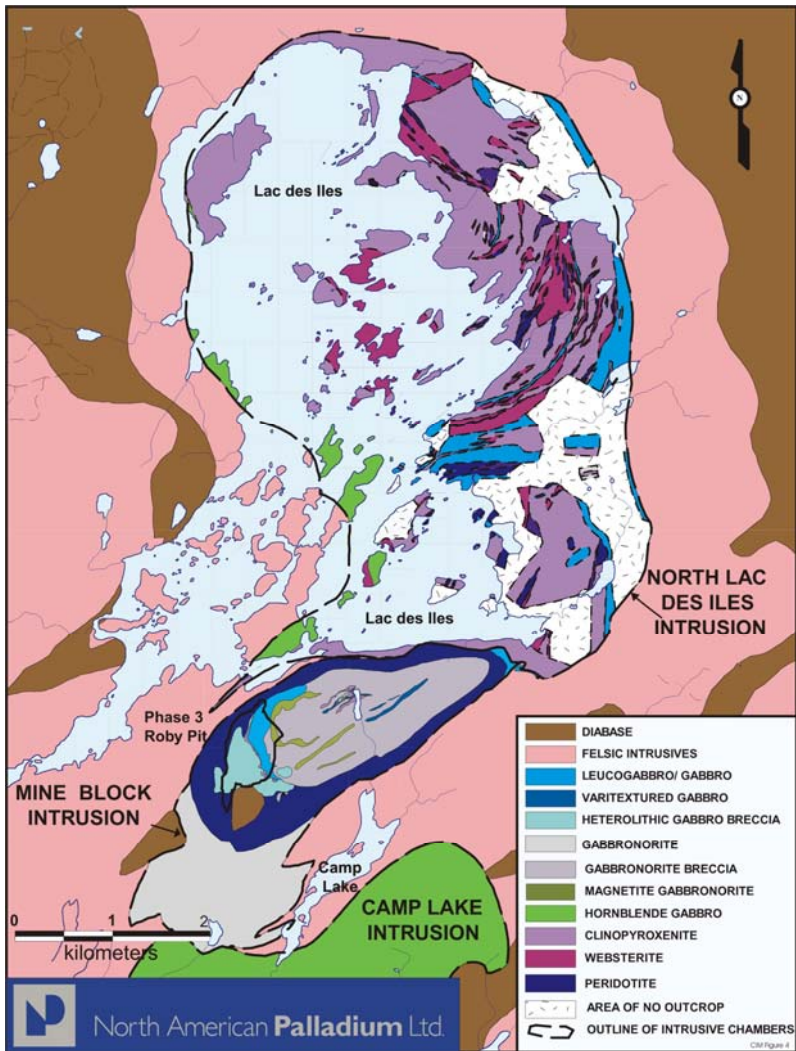


FIG. 17-8 Geology of the Lac des Iles Intrusive Complex. (Mine Block Intrusion and Camp Lake Intrusion modified after Sutcliffe & Sweeney 1986, Macdonald & Lawson 1987. North Lac des Iles Intrusion mapped B. Nelson, M. MacIsaac, A. MacTavish and J. Rickard for North American Palladium Ltd, 1999–2001).

Lake, all of which host PGE mineralization. Although these gabbroic bodies were previously thought to belong to the LDI suite, it now appears more likely that they are the early phases of the Shelby Lake batholith. The Shelby Lake batholith is dated at 2690 ± 0.9 Ma (Kamo 2004) which is similar to an age date of 2689.0 ± 1 for gabbro pegmatite from the Roby Zone in Mine Block intrusions of the LDI suite (Davis 2003).

Stone (2003) mapped regional-scale mylonitic zones associated with major intrusions of the LDI suite, the largest of which is the Shelby Lake fault, which extends 75 km southwest from the Mine Block Intrusion to the boundary of the Quetico Subprovince at Lac des Mille Lacs. Other mylonitic zones are spatially associated with the Buck Lake and Tib Lake Intrusions. The mafic intrusions themselves are not strained, although repeated magmatic injection and brecciation observed at the Buck Lake Intrusion can be attributed to episodic magmatic activity along a crustal-scale fault.

Geology of the Lac des Îles Intrusive Complex (LDI-IC)

The following description of the geology and its interpretation is based on observations made during the course of an intense exploration program that lasted six years. This was the third significant exploration program conducted at Lac des Îles by well funded companies at the direction of qualified geologists. Most of the observations made by the first two programs have been lost and the following is an attempt to bring into the public domain some observations and thoughts of geologists who are too busy (at earning a living trying to find mines) to write papers. The observations were made during detailed mapping and assaying of several thousand square metres of outcrop generated by extensive overburden removal, the examination and assaying of 200,000 metres of core, for the sole purpose of discovering mineralization. The interpretation of these observations was conducted for the purpose of developing a pragmatic exploration model. As such, this was not an academic study and this paper does not compare the observations with previous work, or similarities elsewhere. The most significant distinction between the data gathering of this exploration program and a typical academic study is the scale and coverage. The entire LDI-IC was mapped with the aid of overburden removal, and sampled excessively (>20,000 samples), and the mineralized zones were almost completely stripped

of overburden, and mapped and sampled in detail. They were also defined in the third dimension by drilling. A companion study (Rickard *et al.*, in prep.) was the first mineralogical study to examine the entire deposit comprehensively and systematically. This study was driven by the needs of the metallurgist. In addition to mineralogy, this paper will also bring into the public domain an analysis of the mine-planning assay database which revealed deposit-wide geochemical trends that shed much light on the genesis of the deposit. The results of the most recent academic study were published by Hinchey *et al.* (2005).

In addition to geological mapping conducted by various mining companies, mapping and petrographic analysis of the LDI-IC has been undertaken by university-based geologists and government geological surveys including Pye (1968), Guanera (1967), Linhardt & Bues (1987), Michaud (1998), Sutcliffe (1986), Sutcliffe & Sweeny (1985, 1986), Sweeny (1989) and Watkinson & Dunning (1979).

The LDI-IC has two chambers, each a distinct lithological domain (Fig. 17-8). Ultramafic intrusions are centered on Lac des Îles (North Lac des Îles Intrusion, NLDI-I). Chaotic gabbroic intrusions occur immediately south of Lac des Îles (Mine Block Intrusion, MBI). These two intrusions are partially separated from each other by tonalite septa. The presence of widespread breccia and the rarity of rhythmic layering suggest a dynamic intrusive environment with disruptive magmatic pulses.

The North Lac des Îles Intrusion (NLDI-I) is ultramafic in composition with a minor mafic component. On the basis of mapping by North American Palladium (Lavigne and Michaud, 2001) the NLDI-I can be subdivided into four domains based on lithological variations and structure. The four domains are:

- 1) massive to broadly layered, east-trending clinopyroxenite, with lesser websterite and minor olivine-bearing units underlying the extreme north-northwestern portion of the NLDI-I;
- 2) massive to locally well-layered, north-trending clinopyroxenite, websterite, thin olivine-rich units and underlying gabbro in the northeastern portion of the NLDI-I;
- 3) east-trending, massive gabbro, gabbronorite, vari-textured gabbro/gabbronorite, and heterolithic gabbro/gabbronorite breccia, interfingering with massive clinopyroxenite and

- minor websterite and olivine-bearing units in the south-central portion of the NLDI-I;
- 4) clinopyroxenite with less-abundant, olivine-bearing units, websterite and gabbro, underlying the southern portion of the NLDI-IC, whose geological contacts and geophysical trends define a circular structure.

In all four domains, outcrop-scale rhythmic layering is uncommon and weak. Detailed mapping has revealed that proportions of orthopyroxene, clinopyroxene and olivine vary considerably, randomly and gradually, thus rendering the extrapolation of geological units from outcrop to outcrop difficult. The most common style of mineralization in the NLDI-I consists of zones up to 10 m in thickness of disseminated chalcopyrite, containing up to 1.0 g.t⁻¹ Pd + Pt.

The Mine Block Intrusion (MBI) is texturally and compositionally complex (Fig. 17-9). Its composition ranges from anorthosite to clinopyroxenite, leuco-gabbronorite to melanonorite

and includes magnetite-rich gabbronorite. Textures include equigranular, fine- to coarse-grained, porphyritic, and pegmatitic, vari-textured units and heterolithic gabbro breccia. These last three textural types are the most common hosts to PGE mineralization, including the Roby Zone.

The MBI consists of two lithologically distinct domains. The oval-shaped domain immediately south of Lac des Iles is lithologically complex and contains widespread PGE mineralization, whereas the domain further to the south is dominated by massive, medium-grained, PGE-barren gabbronorite. Systematic surface sampling of the massive gabbronorite has demonstrated its PGE content to be anomalously low, as no samples exceeded the analytical detection limit of 30 ppb. Extensive stripping has revealed that the interior of the oval-shaped domain south of Lac des Iles has an abundance of monolithic and heterolithic breccia with an average composition of gabbronorite. Within this area,

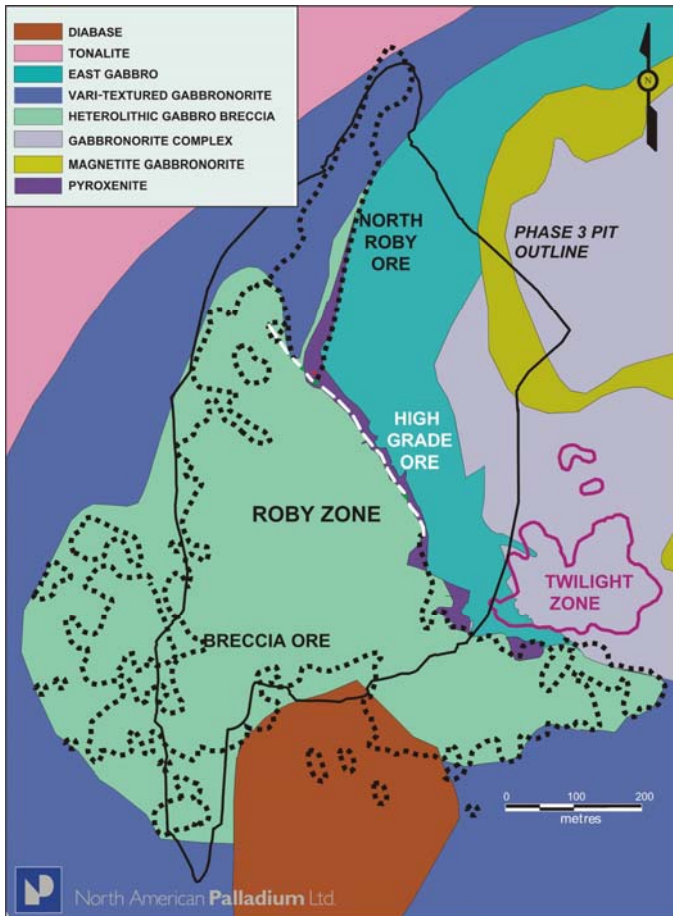


FIG. 17-9 Simplified geology of the Roby and Twilight zones (LDI-IC). (Modified after Sutcliffe & Sweeney 1986; Macdonald & Lawson 1987, Michaud 1998).

individual lithological units are not laterally extensive but rather chaotically distributed. The most laterally continuous unit is a massive, medium-grained gabbro, referred to as the East Gabbro. It is adjacent to a vari-textured gabbro “rim” to the west and more equigranular gabbro to the east. The vari-textured rim is host to the Roby Zone palladium deposit where heterolithic gabbro breccia is common, occurring as pipes and pods, and large blocks (~60 m) of varying composition.

Geology of the Roby Zone

The Roby Zone is a bulk-mineable deposit with a minimum north to south length of 950 m and a width of 815 m (including the Twilight Zone). Its dimensions are much greater if mineralized rock that is below the mining cutoff grade of $0.7 \text{ g.t}^{-1} \text{ Pd}$ is included. The southern boundary to the mineralization as seen on Figure 17-9 extends to include the Powerhouse and Moore zones adjacent to the massive barren gabbro, while its western boundary is basement tonalite, and its eastern boundary is the East Gabbro. A tail of mineralization extends northwards within the rim of vari-textured gabbro pinched in between the East Gabbro and basement tonalite. Similarly, mineralization extends eastward from the southeastern corner within the rim of vari-textured gabbro. The Roby Zone has been intersected to a depth of 1000 m by core drilling. For mining purposes, the Roby Zone comprises three distinct ore types (Fig. 17-9): High Grade Ore (7.6% of volume), North Roby Ore (5.3% of volume) and Breccia Ore (87.1% of volume), all of which contain multiple styles of mineralization.

The volumetrically most significant host to mineralization is vari-textured gabbro and heterolithic gabbro breccia. With the exception of the East Gabbro, every equigranular rock type within the MBI has a vari-textured counterpart. As a result, the term “vari-textured gabbro” covers a broad range of both textures and composition. It varies from leucocratic to ultramafic (pyroxenitic), fine-grained with medium-grained patches and “veinlets”, medium-grained with coarse-grained and pegmatitic patches and “veinlets”, and coarse-grained with pegmatitic patches and “veinlets” (Figs. 17-10a and b). The coarser patches and “veins” have nearly identical mineralogy (plagioclase + clinopyroxene + orthopyroxene) to the equigranular host. The terms “vein” and “veinlets” are used to describe thin planar features,

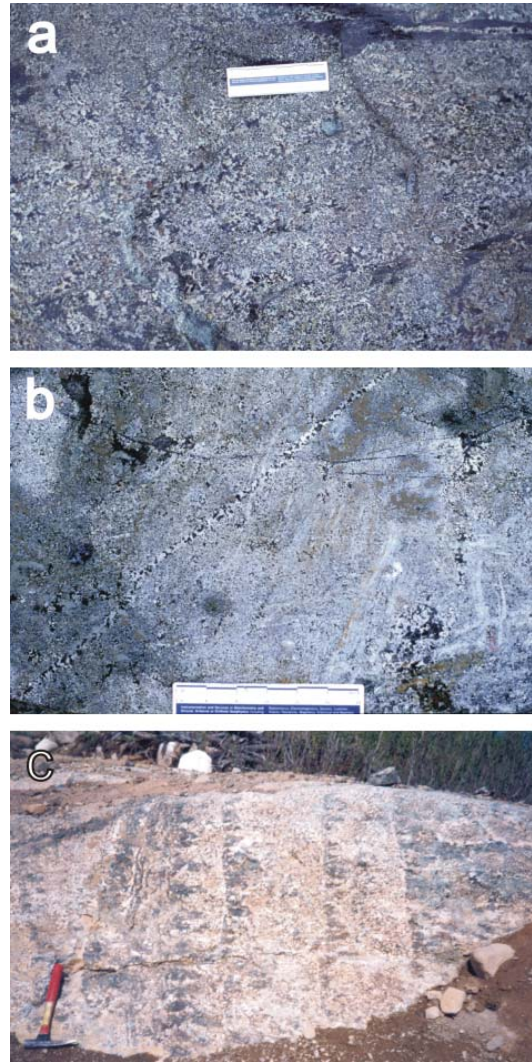


FIG. 17-10. a, vari-textured gabbro consisting of coarse-grained patches in medium-grain equigranular matrix each with similar mineralogy; b, vari-textured gabbro consisting of coarse-grained patches and veins hosted by fine-grained gabbro with similar mineralogy; c, comb layering.

and the use of these terms in this case does not imply an introduction of material. In this case, the transition from “wallrock” to veins is simply a change of grain size without any disruption of interlocking minerals.

Randomly oriented, pegmatitic gabbro pods up to several metres in diameter occur throughout the Roby Zone. The pegmatitic pods occur as layer-like bodies, apparently crosscutting dikes, cusped lenses interleaved with gabbro, and sub-spherical pods commonly with quartz + tourmaline-bearing cores (Fig. 17-10c). The gabbroic pegmatites may

owe their origin to the same fluids thought to be responsible for the development of vari-textured gabbros in the MBI. As seen on Figure 17-8, vari-textured gabbro defines an ovoid rim on the MBI, which is coincidentally the principal host to Pd occurrences and deposits, including the Roby Zone.

High-Grade Ore

High-Grade Ore is mostly hosted by and adjacent to a planar unit of pyroxenite and melanogabbro 15 to 25 m thick. It is located in the east-central portion of the Roby Zone, bounded by the PGE-barren East Gabbro hanging wall (Fig. 17-11) and Breccia Ore footwall to the west. The High-Grade Ore deposit is planar, trends at 341° and dips nearly vertical to a depth of 250 m, and subsequently dips less steeply at greater depth, to the east. It is confined along strike to a 400 m length of the pyroxenite; the on-strike extensions of the pyroxenite are barren to low-grade. Across strike, only the western side of the pyroxenite is ore, with much of the higher grades occurring within the adjacent wallrock. The composition of the wallrock along the western contact of the pyroxenite varies along strike and with depth, and it includes most rock types present in the MBI.

High-Grade Ore is composed almost entirely of secondary silicates, including amphibole and chlorite. The restriction of well-developed, planar fabric to the most altered portions of the pyroxenite, and its lack of lateral continuity is consistent with the fabric being the product of volume loss during compression, as opposed to simple shear. (Figs. 17-12a, b and c). The host pyroxenite is a compositionally uniform, medium- to coarse-grained unit of primarily cumulus and intercumulus clinopyroxene. The cumulus clinopyroxene grains form a mesocumulate texture or, more rarely, an adcumulate texture. Cumulus plagioclase and orthopyroxene account for only approximately 5 volume percent. Although clinopyroxene displays isomodal layering, very subtle grain size-graded layering has been observed. Coarser crystals, up to 1.5 cm, occur along the western side of the unit creating a vari-textured zone, whereas equigranular, medium-grained clinopyroxenes occur along the eastern side. Thus, the western side of the pyroxenite, that which has a higher Pd tenor and is closest to the Breccia Ore, is vari-textured. The equigranular, eastern portion of the pyroxenite, furthest removed from Breccia Ore, is lower-grade. In addition, the pyroxenes in the western half are strongly altered and a minor amount of relict,

unaltered clinopyroxene, orthopyroxene and feldspar is preserved. These relict grains of clinopyroxene have been completely pseudomorphed by actinolite and hornblende and are commonly granulated and brecciated.

Sulfide mineralization within the pyroxenite consists of 0.25% to 3.0% fine-grained, disseminated sulfides with local net-textured patches containing up to 10% sulfide minerals. The dominant sulfide minerals are pyrrhotite,

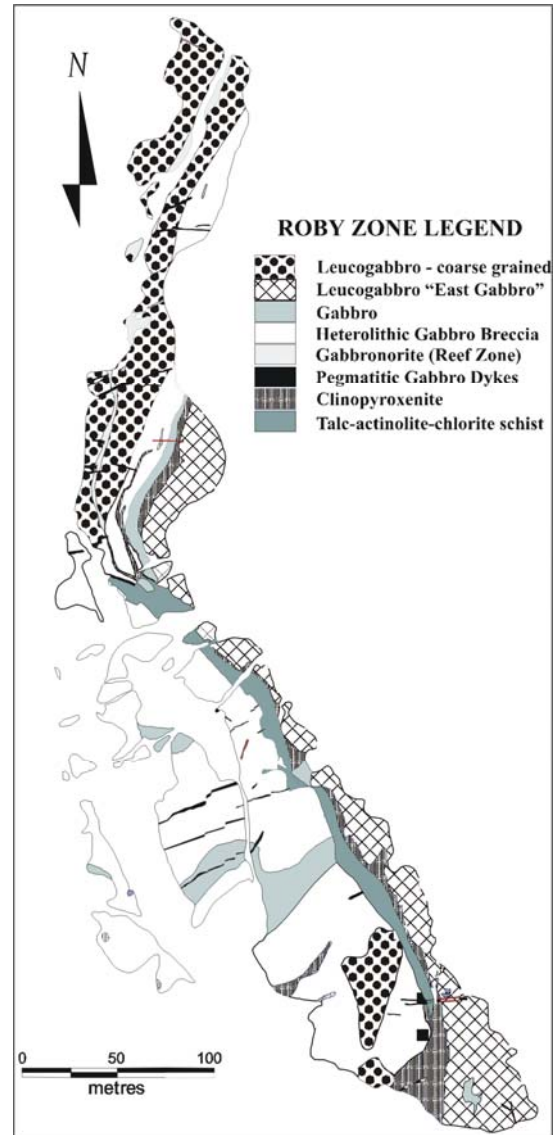


FIG. 17-11 Geology of the north-central portion of the Roby Zone, mapped by Michaud (1998).

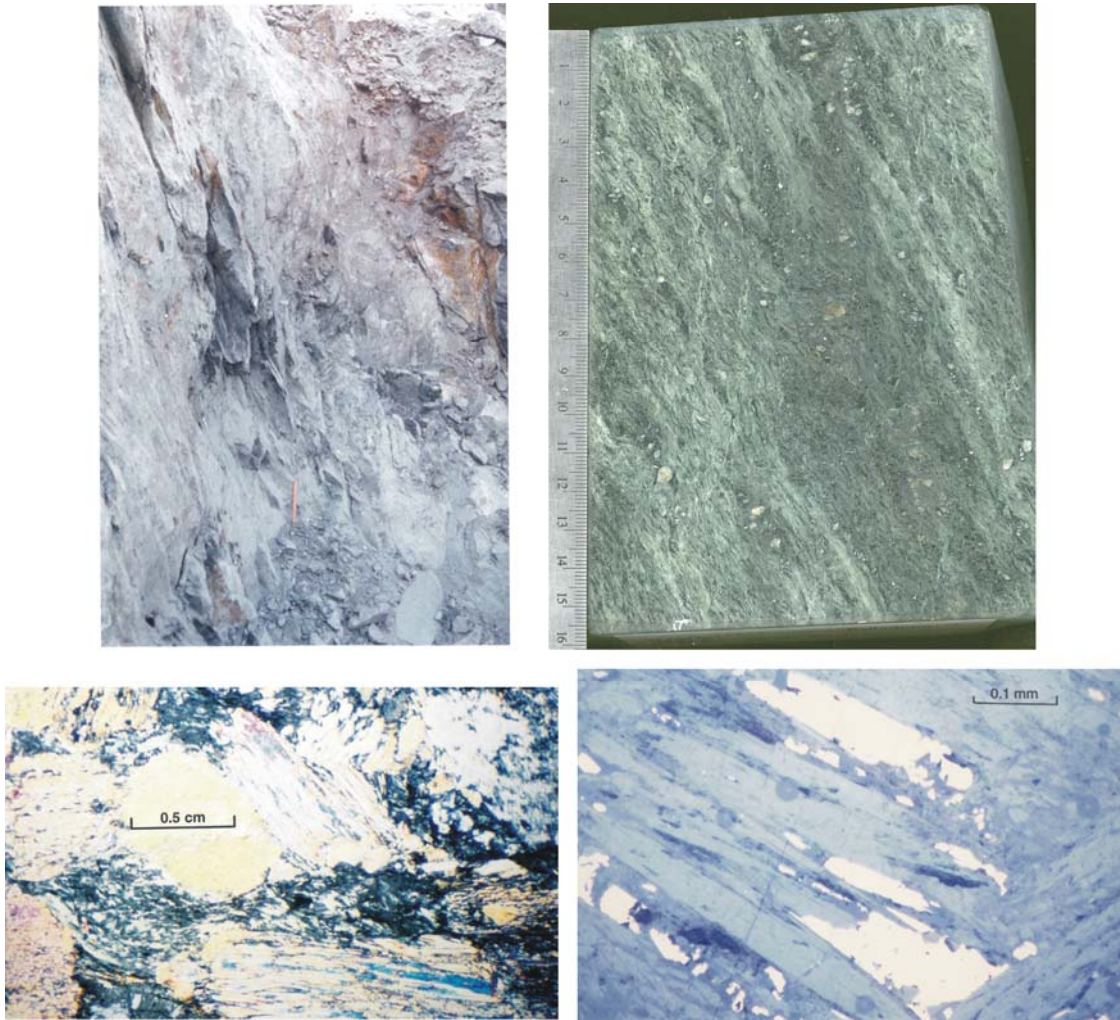


FIG. 17-12. a, High Grade Ore in the Roby Pit showing fissile nature of rocks, photograph taken facing south; b, hand specimen of High Grade Ore ($22 \text{ g.t}^{-1} \text{ Pd}$), low sulfide, and foliated; c, photomicrograph of High Grade Ore showing pseudomorphing actinolite alteration of clinopyroxene grains and development of chlorite [crossed polars]; d, photomicrograph of sulfides (light colored) as fine inclusions within secondary silicates and paralleling the long axes of actinolite grains [polished section].

chalcopyrite, pyrite and pentlandite. Palladium and platinum mineralization within the High-Grade Ore consists predominantly of fine-grained PGE-bearing sulfide minerals; these are predominantly braggite (Pt,Pd,NiS) and the telluride minerals merenskyite ($\text{Pd,Pt}(\text{Te,Bi})_2$) and kotulskite $\text{Pd}(\text{Te,Bi})$ (Sweeny 1989), which occur interstitial to cumulus grains or as inclusions within secondary silicates (Fig. 17-12d).

Higher PGE grades (mean: $7.89 \text{ g.t}^{-1} \text{ Pd}$, maximum: $55.95 \text{ g.t}^{-1} \text{ Pd}$) occur in those portions of the pyroxenite that are altered to an assemblage of amphibole (anthophyllite – actinolite – hornblende) – talc – chlorite. The PGE tenor is not proportional

to the sulfide content and samples free of visible sulfide commonly contain more than $10 \text{ g.t}^{-1} \text{ Pd}$. The sulfide-poor sample of Figure 17-12c contains $22 \text{ g.t}^{-1} \text{ Pd}$. This is reflected by a poor correlation between base metal and precious metal contents. The high-grade mineralization is located primarily within the western, highly altered portion of the pyroxenite, as much of the pyroxenite in between the barren East Gabbro and High Grade Ore is low-grade. Within the pyroxenite, the intensity of silicate alteration decreases eastward towards the East Gabbro contact, as does the Pd tenor. In addition, a 6 m selvage of alteration on the western border of the East Gabbro, along the pyroxenite

contact, is coincidental with anomalously high Pd tenor when compared to East Gabbro further from the contact. This tenor/alteration relationship is graphically demonstrated by plotting the average grades for the entire deposit against distances from the pyroxenite contacts (Fig. 17-13). Pd grades increase within the breccia ore towards the pyroxenite contact, with a dramatic increase in the western portion of the pyroxenite and a gradual decrease to the east, into East Gabbro. The higher-

grade “High Grade Ore” is not restricted to the pyroxenite but commonly straddles its western contact. At depths exceeding 250 m, the volume of high-grade ore outside the pyroxenite is greater than within; high-grade ore may attain a thickness of 50 m within some sections (Fig. 17-14). Occasionally drilling fails to intersect the pyroxenite as expected. However, typical Pd grades are still present in other host rocks such as breccia and vari-textured gabbro.

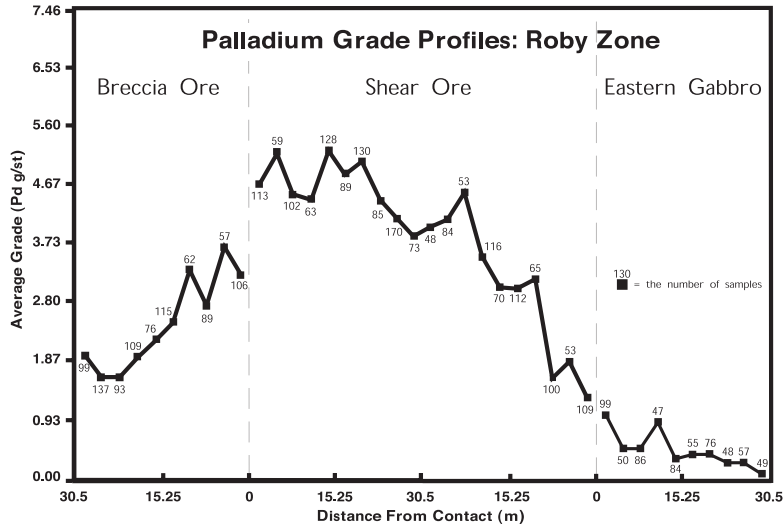


FIG. 17-13. Roby Zone palladium grade profile (based on averaging all assay data equidistant from contact).

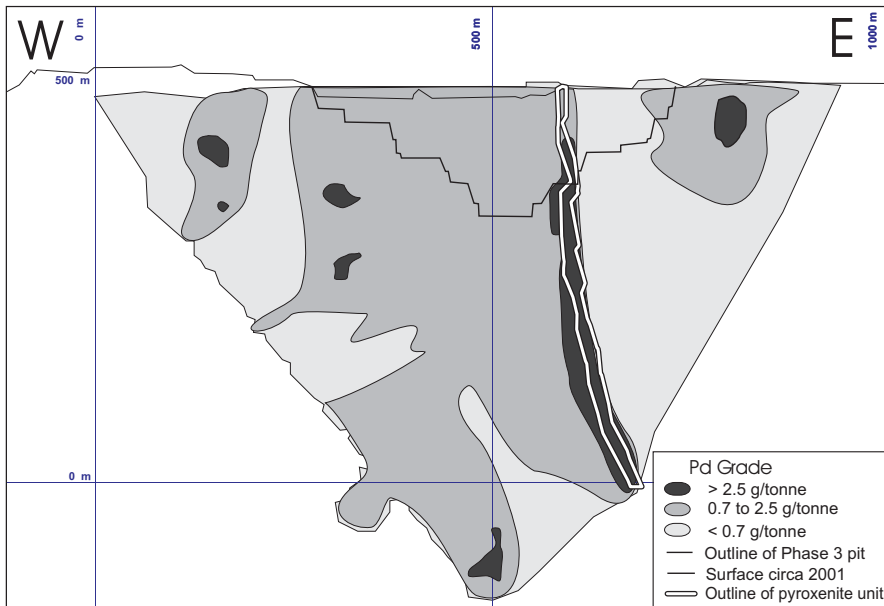


FIG. 17-14. Cross-section of contoured Pd grade block model, Roby and Twilight Zones (see Fig. 17-15 for plan view of section location).

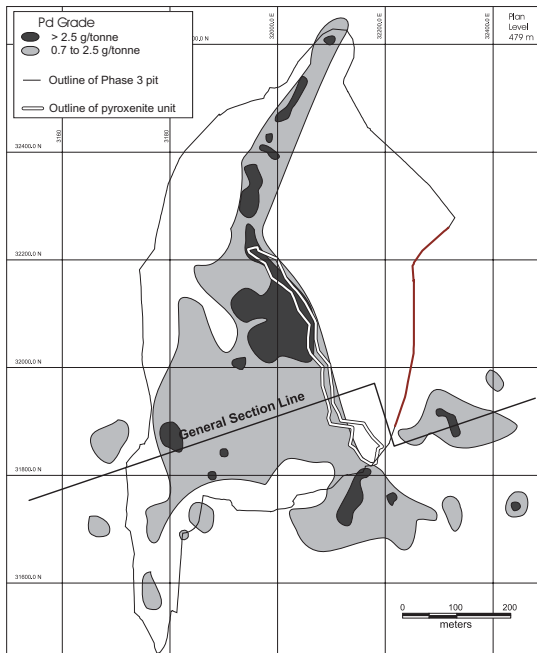


FIG. 17-15 Plan of contoured Pd grade block model, Roby and Twilight Zones

As seen on plan view of the contoured grade model (Fig. 17-15), the higher grade segment of the High Grade Ore is juxtaposed with the higher grades found in the adjacent Breccia Ore. The PGE tenor of the pyroxenite declines dramatically to the south and it also declines coincidentally in the adjacent Breccia Ore. The juxtaposition of the highest grade Breccia Ore, with the highest grade High Grade Ore is consistent with the interpretation that the pyroxenite was mineralized during the event that created the Breccia Ore and that the pyroxenite, backed by the thick and rigid East Gabbro, acted as a barrier to the mineralizing fluid. The fact that a vari-textured equivalent to the East Gabbro does not exist suggests that it was the first lithologic unit to fully crystallize and was thus rendered impervious to the fluids fluxing through the crystal mush (resulting in vari-textured rocks) that dominated the rest of the chamber.

North Roby Ore

North Roby Ore is a tabular zone that is 20 to 40 m thick and 200 m long. The zone strikes at 020° , with the footwall dipping variably to the east at 45° to 60° , with a somewhat steeper hanging wall. It is hosted by a wide variety of lithologic units and at surface is dominated by coarse-grained leucogabbro containing irregular masses of vari-

textured gabbro and medium- to coarse-grained gabbro and clinopyroxenite.

The contacts between gabbro and clinopyroxenite and the encompassing coarse-grained leucogabbro are very sharp, lack mineral zonation and often have a “dimpled texture” (Fig. 17-16a and b), indicating that several of the adjacent layers may have co-existed as a semi-solid, crystal mush. However, intrusive pulses occasionally resulted in brittle deformation of the adjacent rocks (Fig. 17-16c). Silicate alteration is moderate to weak near the mineralization, however, the most widespread and intense zone of alteration occurred in the footwall.

Sulfide mineralization occurs primarily within gabbro and clinopyroxenite. Total sulfide mineral volumes range from trace amounts to 4%, and are typically less than 0.25%. The dominant sulfides are pyrrhotite, pentlandite, chalcopyrite and pyrite. Net-textured sulfides are common in gabbro and clinopyroxenite and occur locally within the gabbroic matrix of the heterolithic gabbro (Fig. 17-17a, b).

PGE mineralization of the North Roby Zone occurs primarily within gabbro and clinopyroxenite, and consists mainly of braggite and vyskoskite ((Pd,Ni)S). These are considered to be high-temperature minerals that form early in the formation of many magmatic deposits (Cabri & Laflamme 1979) and their presence was interpreted by Sweeny (1989), to be indicative of a magmatic origin. The distribution of PGE is erratic, with a mean of 1.7 g.t^{-1} Pd and a maximum assay value of 39.7 g.t^{-1} Pd within the gabbro, generally decreasing to the northeast. A central core of higher grade rock is bounded by a broad halo of lower grade material, itself containing tabular zones of moderate grade. Although the PGE mineralization is typically associated with sulfides, it is often difficult to visually distinguish the sulfide-poor ore from the barren wallrock.

Breccia Ore

Southwest of the High-Grade Ore, the central mass of the Breccia Ore is contained within a mineralized complex that measures 550 m north-south by 350 m wide. An arm of this mineralization has been traced for an additional 250 m to the southeast. Rock composition ranges from clinopyroxenite to anorthosite to norite. Textures include equigranular, fine- to coarse-grained, porphyritic, pegmatitic, vari-textured and

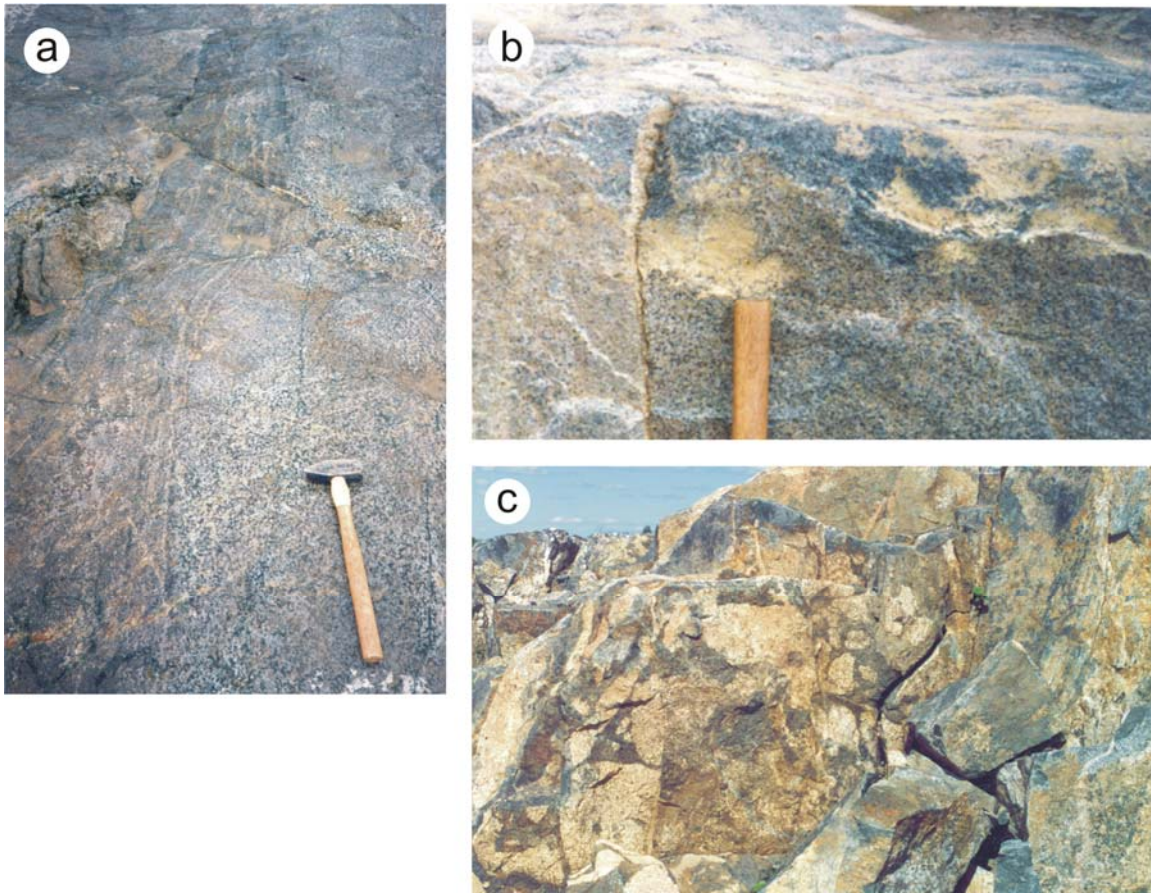


Figure 17-16. a, Modal layering within gabbronite defined by varying proportions of feldspar and clinopyroxene/orthopyroxene grains. The long axis of the hammer is oriented approximately north-south, with the head of the hammer towards the north; b, clinopyroxenite-East Gabbro dimpled contact; c, clinopyroxenite in the central portion of the Roby Zone containing numerous angular fragments of leucogabbro (East Gabbro).

heterolithic gabbroic breccia, of which the latter three textures are host to the PGE mineralization. The eastern boundary to the central portion of the Breccia Ore is well-defined by the sub-vertical contact with the pyroxenite that is host to the High-Grade Ore. The other boundaries are more gradational and typically the variability in composition and texture decreases to the west and south.

Heterolithic gabbro breccia is composed of numerous, irregularly shaped, angular, rounded and sub-rounded fragments ranging from several centimetres to several metres in size that are representative of most of the lithologic units in the complex, as well as a few exotic clasts, within a gabbroic to melanogabbroic matrix (Fig. 18a, b and c). This breccia commonly consists of sub-angular fragments crowded together with very little matrix and grades locally to a matrix-supported breccia

consisting of 10% sub-rounded fragments interpreted as digested xenoliths and 90% matrix. The superposition of detailed sampling on mapping at the southern end of the Roby Zone has shown that higher grades are returned in the matrix-supported breccias, which also are interpreted to record the greatest degree of digestion of clasts, based on their rounded shapes. Sampling of matrix and clast in the southern portion produced average assays of $8 \text{ g.t}^{-1} \text{ Pd}$ and $0.8 \text{ g.t}^{-1} \text{ Pd}$, respectively. The various fragments often have convoluted edges, with numerous tongues or lobes that protrude into the adjacent matrix, suggesting that the fragments and the encompassing magma co-existed in a liquid or crystal mush state. The gabbroic composition of the matrix in many locations is interpreted as a compositional change due to digestion of less mafic xenoliths.

All rock types within the Breccia Ore also

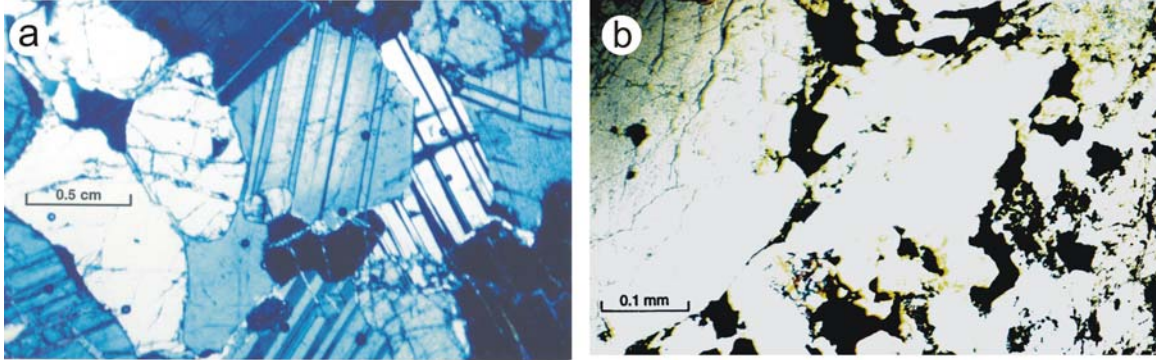


Figure 17-17. a, photomicrograph of gabbronorite showing unaltered cumulate texture consisting of subhedral to euhedral orthopyroxene grains and albite twinning of plagioclase feldspar grains. [crossed polars]; b, photomicrograph of gabbronorite containing net-textured sulfides (opaque). [plane-polarized light].

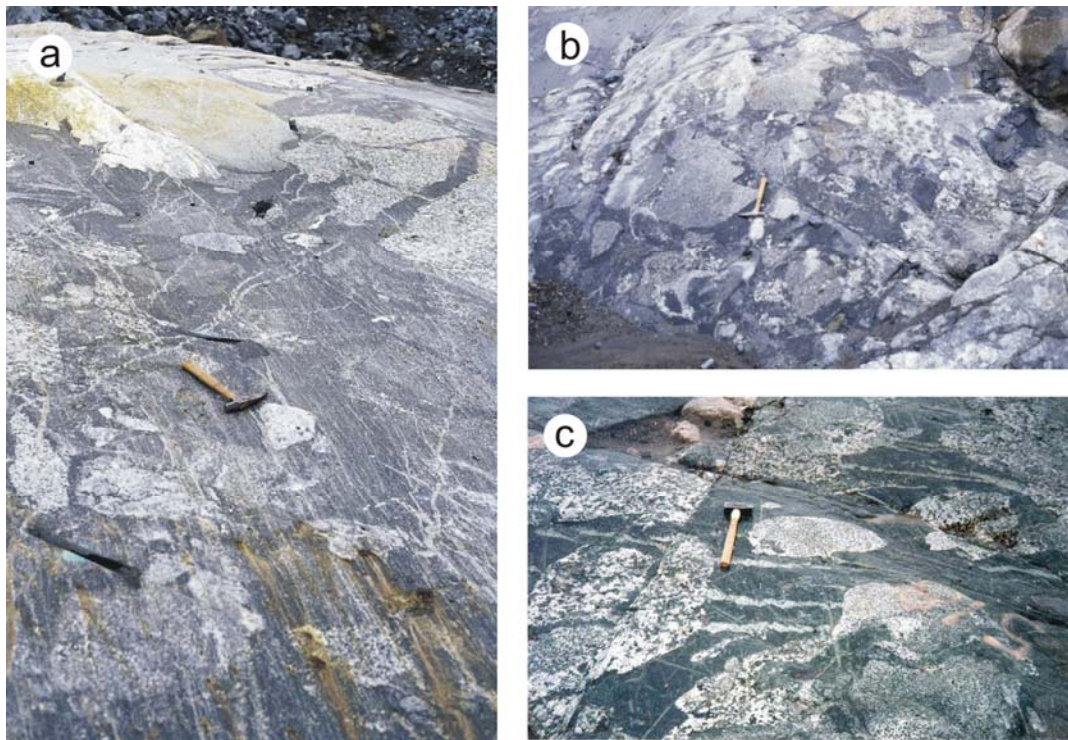


FIG. 17-18. a, Photograph looking west across contact from matrix rich, high grade heterolithic melanogabbro breccia towards matrix poor, low grade heterolithic gabbro breccia located near northwestern corner of the South Roby Pit, as seen on Figure 17-15; b, low-grade heterolithic gabbro breccia from South Roby Zone; c, high-grade heterolithic gabbro breccia from the north-central Roby Zone.

occur as irregularly shaped domains with maximum dimensions of 60 m with chaotic distribution and brecciation at a larger scale. A large block of equigranular leucogabbro has a rim of vari-textured leucogabbro. The transition from equigranular protolith to vari-textured rim is interpreted as the incomplete impregnation of the deuteric fluid into

the more massive unit. The mineralogy remains the same, indicating that the fluid was a catalyst for crystal growth only.

Alteration within the Breccia Ore consists of moderate to strong, pervasive uralitization of clinopyroxene, producing actinolite pseudomorphs. Plagioclase has undergone saussuritization, forming

patches of zoisite and epidote within the center of the grain and along the grain boundaries. Orthopyroxene has been altered to talc, anthophyllite and serpentine. More intensive alteration typically occurs as isolated patches, suggesting that deuteric fluids have modified the original magmatic textures and compositions.

Sulfide mineralization within the Breccia Ore consists of up to 5% intergrown chalcopyrite, pentlandite, pyrrhotite and pyrite. Sulfides occur as fine-grained, disseminated grains throughout, and as irregularly shaped blebs up to 1.0 cm in diameter, interstitial to clinopyroxene and plagioclase grains (Figs. 19a and b). Sulfides also occur as inclusions and thin streaks parallel to the long axis of the secondary silicate pseudomorphs, suggesting that the sulfides may have been remobilized during alteration or were introduced during the alteration of pyroxene to actinolite.

PGE mineralization within the Breccia Ore is associated with heterolithic gabbro breccia and accompanying vari-textured gabbro. Although gabbro-noritic and pyroxenitic fragments (some in

the 10's of metres) can be of ore grade, the matrix to the breccia typically contains the bulk of the PGE mineralization. The mean grade of the Breccia Ore is 1.2 g.t^{-1} Pd, with a maximum of 36 g.t^{-1} Pd. The southern and western boundaries of the Breccia Ore are defined by a gradual decrease in PGE content. As defined by the 0.7 g.t^{-1} Pd assay cutoff, the western boundary is sub-vertical and the southern boundary dips steeply to the north, whereas the southeastern extension of the Breccia Ore remains open.

The platinum group minerals within the Breccia Ore consist of predominantly kotulskite, merenskyite, braggite and vysotskite, and are associated with fine-grained, disseminated and irregularly shaped blebs of pyrrhotite, pyrite, pentlandite and chalcopyrite (Sweeny 1989).

Although certain patterns of mineralization distribution have been documented, extensive sampling of outcrop and drill core has shown that every rock type in the Roby Zone, regardless of sulfide content, can either be ore or waste. This observation is not unexpected since the Roby Zone was created by an evolving process with successive superimposition of related, but distinct processes, as explored in the discussion.

Geology of the Twilight Zone

The Twilight Zone, most recently studied by Dionne-Foster (2001) (Fig. 17-9), is a small pod of gabbro-noritic breccia found on the eastern side of the Roby Pit. It is separated from the Roby Zone on its western boundary by the 50–70m thick East Gabbro and separated from the southeastern extension of the Roby Zone by a 100 m thick barren, post-mineralization gabbro dike. The breccia is characterized by large, sub-rounded, noritic clasts set within a matrix of melanogabbro-norite. Unlike the Roby Zone, these rocks are almost devoid of vari-textured/pegmatitic textures. The alteration is variable and in some places intense, but for the most part the rocks are weakly altered to fresh. Orthopyroxene is most commonly fresh, but may be altered along grain boundaries or completely pseudomorphed by amphibole and talc. Plagioclase is more resistant to alteration and is typically only weakly altered.

Macroscopically, the mineralization appears primary, dominated by large sulfide blebs. However, the Pegs are associated with both the primary sulfides and secondary silicate minerals such as amphibole, chlorite, and to a lesser extent talc. Palladian tellurides (kotulskite, merenskyite)



FIG. 17-19. Samples of net textured sulfide in gabbroic (above) and sulfide (below) pods in the pegmatitic gabbro.

and arsenides (stillwaterite, isomertieite) are the most abundant PGM, with a lesser amount of vysotskite. Many of the PGM are found as discrete grains completely enclosed by silicates, but they are still in close proximity to the sulfides. These rocks contain 0.25–0.5 vol.% pyrrhotite and chalcopyrite.

A unique feature of Twilight Zone, as compared to the Roby zone, is the strong correlation of the precious metals with the base metals and sulfur. This geochemical evidence, together with microscopic observations and the near absence of vari-textured/pegmatitic textures and silicate alteration, suggests that only minor remobilization of the PGM has occurred in the Twilight Zone breccias.

Baker Zone

The Baker zone is a lower grade deposit situated approximately 1 km east of the Roby Zone Pit. The zone consists mostly of equigranular norite/gabbronorite that has been intruded by heterolithic melanogabbro breccia, melanogabbro, and a small amount of vari-textured gabbro. The breccia zone strikes east-northeast and dips at approximately 50 to 90 degrees to the south-southeast. Both surface mapping and diamond drill core intersections show that the vari-textured gabbro is often at the margins of the breccia zone. Sub-vertical pyroxenitic dikes and more shallowly dipping late mafic dikes cross-cut the other units in the outcrop.

Mineralized rock is continuously distributed throughout the heterolithic melanogabbro breccia and melanogabbro units, but is distributed sporadically throughout the surrounding norite and gabbronorite. The highest grading unit is a small exposure of leucogabbro breccia that is characterized by gabbro and melanogabbro clasts set within a matrix of leucogabbro. The melanogabbro breccia predominantly contains clasts of vari-textured gabbro and equigranular norite and gabbronorite derived from the surrounding rocks, with smaller amounts of various other gabbroic rocks. Both the matrix and some of the clasts host sulfide and PGM mineralization. Precious metal grades in all of the mineralized units show a strong correlation with the base metal content. PGM identified within these rocks are merenskyite and kotulskite. Some narrow, massive sulfide stringers cross-cut the norite/gabbronorite and melanogabbro.

This zone, which exhibits sub-horizontal igneous layering, has been affected by two deformational events. The first is manifested as a

north-trending foliation, produced by a minor shearing event that occurred after the intrusion of the breccias and melanogabbro. The second event is manifested as northeast-trending, tightly spaced shear fractures with significant sinistral offsets, which has resulted in sinistral transposition of the mineralized zones into an east-trending orientation from an original north-trending orientation.

DISCUSSION

Several new observations were made possible as a result of creating, mapping and thoroughly assaying large exposures of the mineralization and country rock throughout the LDI-IC and examining the entire Roby Zone through logging and assaying of core. Key observations that support the proposed processes are:

- 1) Gabbro breccia is high grade ore (matrix has the highest metal content), vari-textured gabbro is medium to low grade, and equigranular gabbro is low grade to barren.
- 2) The above pattern is overprinted with the common, but not universal association of high grade and silicate alteration.
- 3) Breccia and vari-textured gabbro and Pd mineralization have a close spatial association
- 4) The mineralogy of “veins” is commonly identical to “wallrock”.
- 5) Within the Roby Zone, there is poor correlation between sulfide content and grade whereas in the neighboring weakly altered Twilight Zone, correlation is good.
- 6) There is a spatial relationship between “vari-textured gabbro” and silicate alteration. This is largely based on the near absence of both in the Twilight Zone, and their near universality in the Roby Zone.
- 7) Breccia fragments are round and lack reaction rims.
- 8) Grade is correlated with grain size and alteration in the High-Grade zone.
- 9) The Roby Zone contains multiple styles of PGE mineralization.

PGE are associated with Cu–Ni-sulfide in the matrix of magmatic breccia and in vari-textured to pegmatitic “gabbro” (which together represent the Breccia Zone) and in the pyroxenite unit that is part of the High-Grade Zone. PGE also occur with sulfide-poor, vari-textured to pegmatitic gabbro that is found throughout the Roby Zone (and is the dominant style in the North Roby Zone) and occur with sulfide-poor mineralization associated with

strong silicate alteration found throughout the Roby Zone (exemplified by the portions of the High-Grade Zone).

The implication of these observations is that the Roby Zone is the product of multiple stages of intrusion, alteration and mineralization. It is envisioned that the mineralization sequence was initiated by the energetic injection of sulfide- and PGE-enriched magma into a partially crystallized chamber, creating intrusive breccia. This energetic intrusion is a result of an abundance of dissolved volatiles. These volatiles resolved from the magma and fluxed through the crystal mush, acting as a catalyst, accelerating crystallization in its path, creating vari-textured “gabbro”, and pegmatite. These volatile plumes would differentially transport and deposit metals, resulting in a broad range of PGE and base metal ratios, including sulfide-poor mineralization. The intergrowth of pyroxenes with this mineralization implies high temperatures of formation and the evacuation of water and other volatiles. In this scenario, the already crystallized and rigid, sub-vertical sheet of East Gabbro acted as a barrier to the volatiles emanating from the breccia to its west, resulting in greater localized accumulation of PGE, creating the High-Grade Zone. The unconfined volatiles fluxing towards the north created the North Roby Zone and eventually dispersed. The widespread association of PGE with lower temperature silicate alteration is interpreted to represent continued fluxing, or a lagging volatile plume fluxing through the crystal mush at progressively lower temperatures. At the Twilight Zone, the positive correlation between base and precious metals and the virtual absence of both vari-textured gabbro and lower temperature alteration both support the contention that the high-temperature fluid thought to be responsible for generating the vari-textured gabbros also worked to mobilize metals and overprinted the magmatic metal ratio signature at lower temperatures. Mineralization associated with low-temperature silicates is the result of continued circulation and cooling of its high-temperature precursor that created vari-textured gabbro. The PGE and base metals at Lac des Iles were carried in an energetic magma and were subsequently remobilized by its deuteric fluids.

This model can be used to evaluate exploration targets. The great volume of breccia, geological chaos, evidence of fluids, and anomalous metal content are features that can be observed by reconnaissance. An examination of bedrock at LDI

gives one the impression of a very dynamic system. It is unlikely this type of system would be present at a significant scale in a massive or layered intrusion, especially one with less than 7 ppb Pd content. Early recognition of potential based on the above features is key to evaluating intrusions. Chaos dictates that subsequent more detailed activities be unconstrained by preconceived geological control, and that they are applied broadly and evenly, sampling and survey spacing dictated by expected dimensions. Direct exploration, *i.e.*, sampling bedrock is the most efficient method as indirect methods, such as sampling overburden and conducting geophysical surveys, amount to being distracting activities that produce false anomalies.

ACKNOWLEDGEMENTS

A better understanding of this deposit is the result of many who dug, washed, sampled and documented geological relationships on the extensive bedrock exposures and 200,000 metres of drill core created during the recent exploration program. In addition to the authors this includes exploration team members Scott Burgess, Mike MacIsaac, Al McTavish and Brian Nelson. Interpretation was made possible by those who compiled the database and generated two and three-dimensional images, a fraction of which is included herewith. Key to these efforts are Douglas Kim, mine geologist, Paul Nielsen, Karen Kettles and Gerry Katchen.

REFERENCES

- CABRI, L.J. & LAFLAMME, J.H.G. (1979): Mineralogy of samples from the Lac des Iles area, Ontario. *Can. Inst. Mining Metall. Report 79-27*, 20.
- CAMERON, E.M. & HATTORI, K.H. (2003): Mobility of palladium in the surface environment: data from a regional lake sediment survey in northwestern Ontario. *Geochemistry* **3**, 299-311.
- DAVIS, D.W. (2003): U-Pb geochronology of rocks from the Lac des Iles area, northwest Ontario; Ontario Geological Survey, internal report, June 12, 2003.
- DIONNE-FOSTER, C. 2001 *Étude minérigraphique et pétrologique de la zone Twilight, Complexe du Lac des Îles, Ontario*. B.Sc. thesis, Université du Québec à Chicoutimi.
- DYER, R.D. & RUSSELL, D.F. (2002): Lac des Iles-

- Black Sturgeon River area lake sediment survey; Operation Treasure Hunt. Ont. Geol. Surv. Open File Report **6096**, 134
- GEOLOGICAL SURVEY OF CANADA – ONTARIO DEPARTMENT OF MINES (1962): Lac Des Iles, Map 2099, Aeromagnetic Series, scale 1:50 000.
- GUARNERA, B.J. (1967): *Geology of the McKernan Lake phase of the Lac des Iles Intrusive, Thunder Bay District, Ontario*. M.Sc. thesis, Michigan Technical University, Houghton, Michigan.
- HART, T.R., MACDONALD, C.A.K. & LEPINE, D. 2001a. Precambrian geology, Lac des Iles greenstone belt. Ontario Geological Survey, Preliminary Map P.3435, scale 1:20 000.
- HART, T.R., MACDONALD, C.A.K. & LEPINE, D. 2001b. Precambrian geology, Heaven Lake greenstone belt. Ontario Geological Survey, Preliminary Map P.3434, scale 1:20 000.
- HART, T.R., MEYER, P., MARTIN, L.A. & ZUREVINSKI, S.M. 2000a. Precambrian geology, Garden Lake greenstone belt (west half). Ontario Geological Survey, Preliminary Map P.3422, scale 1:20 000.
- HART, T.R., MEYER, P., MARTIN, L.A. & ZUREVINSKI, S.M. 2000a. 2000b. Precambrian geology, Garden Lake greenstone belt (eastern half). Ontario Geological Survey, Preliminary Map P.3423, scale 1:20 000.
- HATTORI, K.H. & CAMERON, E.M. (2004): Using the high mobility of palladium in surface media in exploration for platinum group elements: evidence from the Lac des Iles region, Northwestern Ontario. *Econ. Geol.* **99**, 157-171.
- HINCHEY, J.G., HATTORI, K.H. & LAVIGNE, M.J. (2005): Geology, Petrology, and Controls on PGE Mineralization of the Southern Roby and Twilight Zones, Lac des Iles Mine, Canada.
- KAMO, S. (2004): U–Pb geochronological investigations of rocks from the Lac des Iles area, northwestern Ontario, the Michipicoten Greenstone belt, Wawa, and the Tomiko Terrane, Mattawa, Ontario. Ontario Geological Survey, internal report, July 2004.
- LAVIGNE, M.J. & MICHAUD, M.J. (2001): Geology of North American Palladium Ltd.'s Ruby zone deposit, Lac des Iles. *Explor. Mining Geol.* **10**, 1-17.
- LINHARDT, E. & BUES, C.C. (1987): Geology of the northern Lac des Iles Complex, District of Thunder Bay. In Summary of Field Work and Other Activities, Ontario Geological Survey Miscellaneous Paper **137**, 281-285.
- MACDONALD, A.J. & LAWSON, G.E. (1987): Lac des Iles (Pd–Pt–Au) deposit: geology of the mineralized zone, contact phenomena and mafic/ultramafic dikes within the gabbroic complex. In Summary of Field Work and Other Activities 1987 by the Ontario Geological Survey, Miscellaneous Paper 137, 256-264.
- MICHAUD, M.J. (1998): *The Geology, Petrology, Geochemistry and Platinum Group Element–Gold–Copper–Nickel Ore Assemblage of the Roby Zone, Lac des Iles Mafic-Ultramafic Complex, Northwestern Ontario*. M.Sc. Thesis. Lakehead University, Ontario.
- PYE, E.G. (1968): Geology of the Lac des Iles Area, District of Thunder Bay. Ontario Dept. Mines, Geological Report **64**, 47 p.
- PYE, E.G. & FENWICK, K.G. (1965): Atikokan–Lakehead Sheet. Ontario Dept. Mines, Map **2065**, scale 1:253 440.
- STONE, D. (2002): Geology of the Upsala area, south-central Wabigoon Subprovince. In Summary of Field Work and Other Activities 2002, Ontario Geological Survey, Open File Report **6100**, 14-1 – 14-12.
- STONE, D., LAVIGNE, M. J., SCHNIEDERS B., SCOTT J. & WAGNER D. (2003): Regional Geology of the Lac des Iles area. In Summary of Field Work and Other Activities 2003, Ontario Geological Survey, Open File Report **6100**, 14-1 – 14-12.
- SUTCLIFFE, R.H. (1986): Regional geology of the Lac des Iles area, District of Thunder Bay. In Summary of Field Work and Other Activities 1986. Ontario Geological Survey Miscellaneous Paper 132, 70-75.
- SUTCLIFFE, R.H. & SWEENEY, J.M. (1985): Geology of the Lac des Iles Complex, District of thunder Bay. In Summary of Field Work and Other Activities 1985. Ontario Geological Survey Miscellaneous Paper **126**, 47-53.
- SUTCLIFFE, R.H. & SWEENEY, J.M. (1986): Precambrian Geology of the Lac des Iles Complex, District of Thunder Bay, Ontario. Ontario Geological Survey, Map 3047,

- Geological Series – Preliminary map, scale 1:15840.
- SWEENEY, J.M. (1989): *The geochemistry and origin of platinum group element mineralization of the hybrid zone, Lac des Iles Complex, Northwestern Ontario*. M.Sc. Thesis, University of Western Ontario, London, Ontario, 185p.
- TOMLINSON, K.Y., STOTT, G.M., PERCIVAL, J.A. & STONE, D. (in press) Basement terrane correlations and crustal recycling in the western Superior Province: Nd isotopic character of granitoid and felsic volcanic rocks in the Wabigoon Subprovince, N. Ontario, Canada. Submitted to Precambrian Research.
- WATKINSON, D.H. & DUNNING, G.R. (1979): Geology and platinum-group mineralization, Lac des Iles complex, northwestern Ontario. *Can. Mineral.* **17**, 453-462.

CHAPTER 18: GEOCHEMICAL SURVEYS OF SOIL AND TALUS FINES AND THE DISCOVERY OF THE J-M REEF, STILLWATER COMPLEX, MONTANA

Michael L. Zientek
U.S. Geological Survey, 904 W. Riverside Ave.,
Spokane, Washington 99201, U.S.A.
E-mail: mzentek@usgs.gov

Sam R. Corson
East Boulder Mine, Stillwater Mining Company,
Big Timber, Montana 59011, U.S.A.

and

Richard D. West
Department of Geology, Eastern Washington University,
Cheney, Washington 99004, U.S.A

INTRODUCTION

The Stillwater Complex is a layered ultramafic to mafic intrusion that is exposed in the Beartooth Mountains in south-central Montana. It was intruded and crystallized in the Late Archean (2,705±4 Ma; U–Pb zircon, Premo *et al.* 1990). The complex was intruded by younger Archean quartz monzonite plutons, Proterozoic mafic dikes, and Tertiary felsic and intermediate composition sills and has been affected by several episodes of deformation. The original size and shape of the complex are not known inasmuch as only a portion of the complex is exposed in a fault-bounded block along the northern margin of the Beartooth uplift. About 5,500 m of layered rocks are preserved between the intrusive lower contact of the complex and the pre-Middle Cambrian unconformity that truncates the top of the complex. Layering features can be traced for 42 km along strike, limited only by exposures (Fig. 18-1). Glacial deposits, colluvium, talus, and alluvium are the most common surficial materials in the Stillwater area.

In 1974, a stratiform layer of magmatic disseminated PGE-enriched interstitial sulfide mineralization, the J-M Reef, was found in the Stillwater Complex. Geologic mapping, soil and talus fines geochemistry surveys, magnetometer surveys, induced polarization (I.P.) surveys, very low-frequency electromagnetic surveys (VLF EM), trenching, diamond drilling, and underground exploration were used to delineate this PGE reef-type deposit. Geochemical analysis of soil and talus fines identified anomalies that encouraged

continued geologic mapping that ultimately led to the discovery of the reef in outcrop in the cliffs along the West Fork of the Stillwater River. This paper summarizes the original results of the soil and talus fines geochemical surveys and provides new interpretations of these data.

Surficial Geology of the Study Area

The Beartooth Mountains are a rugged mountain range that extends for about 120 km in a northwesterly direction in south-central Montana and north-western Wyoming (Simons & Ambrustmacher 1976). Except along its southwestern flank, the mountains are clearly defined topographically, rising steeply 1,200 to 1,500 m from adjacent terrain. The Stillwater Complex occurs along the northern margin of the Beartooth Mountains in an area dominated by high plateaus (the East Boulder and Stillwater Plateaus) separated by widely spaced deep and steep-walled canyons (the Boulder River, West Fork of the Stillwater River, and Stillwater River canyons) (Fig. 18-1). Tributary drainages from these major canyons often head in ice- or snow-filled cirques.

Mountain ridges that make up the East Boulder and Stillwater Plateaus can be underlain by bare rock, or are largely mantled by felsenmeer (angular blocks of frost-riven rock), talus, or colluvium. The high plateaus commonly are snowcapped for most of the year; permafrost occurs in scattered locations and solifluction has created patterned ground in some alpine areas (Woods *et al.* 1999). However, in the Pleistocene, these plateau

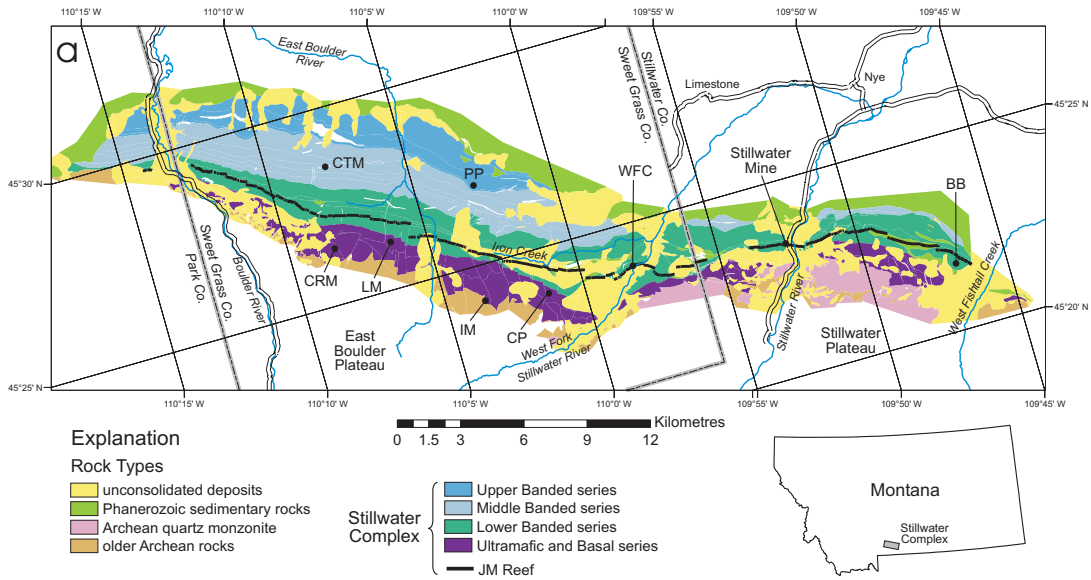


FIG. 18-1. Simplified geologic map of the Stillwater Complex and surrounding rocks showing the location of selected geographic features near the Stillwater Complex, Montana: CTM – Contact Mountain, CRM – Chrome Mountain, LM – Lost Mountain, PP – Picket Pin Mountain, IM – Iron Mountain, CP – Chrome Peak, WFC – West Fork Cliffs, and BB – Black Butte. Geologic map modified from Segerstrom & Carlson (1982). See page 509 for a color version.

surfaces were in part covered by icecaps that drained into valley glaciers that occupied the major canyons (Ten Brink 1972, Pierce 1979). Glacial till covers the south end of the East Boulder Plateau at an elevation of 2,860 to 2,750 m (Simons & Ambrustmacher 1976, Segerstrom & Carlson 1982). However, most of the clasts in glacial deposits that overlie the Stillwater Complex appear to be locally derived.

The main canyons that cut the Stillwater Complex were occupied by valley glaciers during the Pleistocene. At least three major glaciations have been recorded in the Stillwater drainage (Ten Brink 1972) and deposits from two glaciations have been described from the Boulder River drainage (Drain 1985). Bare rock may be exposed on steep glaciated canyon walls along the major tributaries that cut the Stillwater Complex. Lateral moraines mantling the west wall of the canyon along the Stillwater River contain cobbles and boulders of gneissic material that crop out far to the south of the Stillwater Complex. Large deposits of glacial material are found down-slope of large hanging valleys that open into the large canyons. Large landslides, consisting of glacial debris, talus, and large, semi-coherent blocks of bedrock, occur on the steep canyon sides of the major drainages, especially in the Stillwater River canyon (Page 1977). Talus cones are quite extensively developed

on all steeper slopes in the Stillwater area.

In general, deeply weathered rocks are rarely found in the Stillwater Complex area. Relatively unweathered sulfide minerals can be found in near-surface rock samples. Only the sulfide-rich rocks found stratigraphically near the base of the Stillwater Complex may be deeply weathered.

Soils have developed on rocks of the Stillwater Complex as well as on overlying glacial deposits (Fuchs & Rose 1974). The extent of soil development in the area is variable given the extreme range of geologic, topographic, and climatic conditions. The soils in the study area are largely inceptisols and are typically very gravelly to stony (USDA 1999, Woods *et al.* 1999). Inceptisols are soils that have altered horizons, but still retain some weatherable minerals (USDA 1999); however, soil horizons are minimally developed (McDaniel, undated). These soils often develop on fairly steep slopes, young geomorphic surfaces, and on resistant parent materials (McDaniel, undated).

Igneous Stratigraphy of the Stillwater Complex

This paper focuses on the J-M Reef, a stratiform layer of disseminated PGE-enriched interstitial sulfide mineralization that is associated with a rock unit in the Stillwater Complex (Todd *et al.* 1982, Bow *et al.* 1982, Barnes & Naldrett 1985, Raedeke & Vian 1986, Zientek *et al.* 2002, see also

Cawthorn 2005). The average grade of the reef is 0.55 ounces/ton (opt) palladium and platinum with a palladium- to platinum ratio of 3.4 to 1 (Zientek *et al.* 2002). The J-M Reef sulfide mineralization has been traced for 42 km along strike and at least 1 km down-dip. Sulfide- and PGE-mineralized rock typically extends over a 1 to 3 m thick stratigraphic interval, although mineralization is locally absent or may be more than 12 m thick. Sulfide minerals make up 0.5 to 3 volume percent of the mineralized interval. A brief description of the rock unit that hosts the J-M Reef, the Lower Banded series, is provided here; readers are referred to Jackson (1961), Page (1979), McCallum *et al.* (1980), Segerstrom & Carlson (1982), Zientek (1983), Raedeke & McCallum (1984), and Zientek *et al.* (1985) for descriptions of the other units.

The igneous rocks of the Stillwater Complex are prominently layered on scales ranging from mineral laminae to thick mappable layers that are laterally continuous over many kilometres. The layers were nearly horizontal when they originally formed; subsequent tectonic deformation has tilted these layers northward. As a result, the map pattern reveals a cross section through this layered intrusion (Fig. 18-1).

The layered igneous rocks are divided into a hierarchy of mappable stratigraphic units based on mineral proportions and rock-type sequences (Fig. 18-2). Five series, which are subdivided into zones, have been recognized (Zientek *et al.* 1985). The five series divisions are Basal, Ultramafic, Lower Banded, Middle Banded, and Upper Banded. The Lower, Middle, and Upper Banded series are distinguished from the Ultramafic series by the presence of cumulus plagioclase. The presence (or absence) and proportion of cumulus orthopyroxene, augite, and olivine, as well as changes in apparent crystallization order, are the basis for subdivision of the Lower, Middle, and Upper Banded series (McCallum *et al.* 1980, Segerstrom & Carlson 1982, Todd *et al.* 1982). The stratigraphic nomenclature for the Lower, Middle, and Upper Banded series used in this paper is based on the work by McCallum *et al.* (1980).

The Lower Banded series comprises those rocks between the top of the Ultramafic series and the base of the Anorthosite I zone of the Middle Banded series (Fig. 18-2). McCallum *et al.* (1980) divided these rocks into six zones. The lowest is the Norite I zone, approximately 270 m thick, which largely consists of plagioclase-bronzite cumulate.

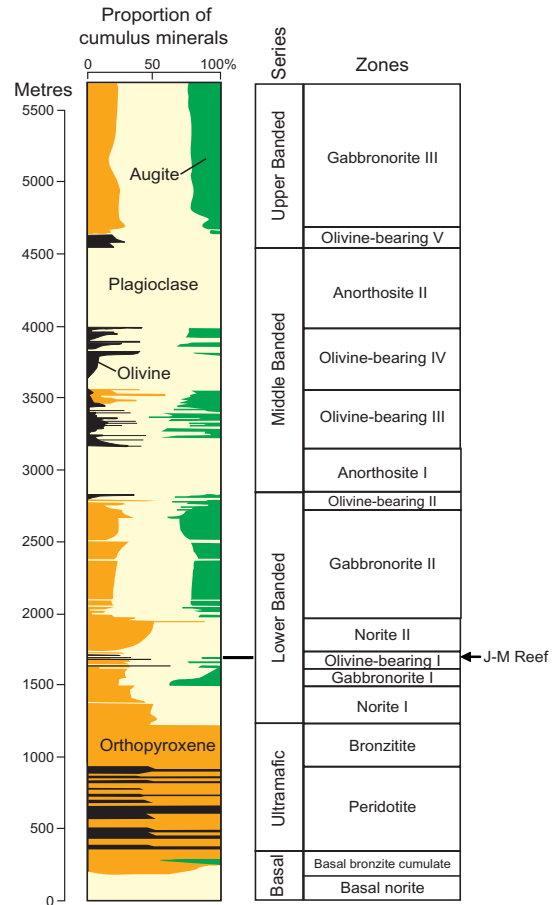


FIG. 18-2. Chart illustrating the stratigraphic nomenclature used for the Stillwater Complex, the stratigraphic location of the J-M Reef, and the distribution and proportion of cumulus minerals in the East Boulder Plateau section of the Stillwater Complex. Cumulus mineralogy from McCallum *et al.* (1980) and Raedeke & McCallum (1984). Nomenclature from McCallum *et al.* (1980) and Zientek *et al.* (1985).

The Gabbronorite I zone, approximately 130 m thick, overlies the Norite I zone and consists of cyclically layered rocks that are made up of cumulus plagioclase, orthopyroxene, and augite. The Olivine-bearing I zone, in which olivine reappears as a cumulus mineral, overlies the Gabbronorite I zone. Troctolites and anorthosites are characteristic rock types of the Olivine-bearing I zone. This unit is approximately 100 m thick. PGE mineralization referred to as the J-M Reef is associated with rocks in the Olivine-bearing I zone (Todd *et al.* 1982). A monotonous sequence of plagioclase-bronzite cumulates, approximately

240 m thick, is called the Norite II zone and overlies the Olivine-bearing I zone. The Gabbronorite II zone overlies the Norite II zone. In the western part of the complex, the Gabbronorite II zone is approximately 790 m thick and consists of plagioclase–bronzite–augite cumulates that are separated from the base of the Anorthosite I zone by a 50 m thick sequence of olivine-bearing rocks (Olivine-bearing II zone). In the eastern part of the complex, rocks correlative with the Gabbronorite II zone include plagioclase–bronzite–augite cumulates with many sequences of olivine-bearing rocks (Peterson *et al.* 1995).

Discovery of the J-M Reef

Howland *et al.* (1936) recognized the potential for finding reef-type PGE mineralization in the Stillwater Complex. Sulfide-bearing samples they collected were analyzed for PGE by INCO; in one of the samples from layered gabbro of the Banded series, they reported the presence of sperrylite and a mineral they called stibiopalladinite. They compared this part of the complex to the Merensky Reef of the Bushveld Complex. Thirty-seven years later (1973), the J-M Reef was discovered by Johns-Manville exploration geologists (Conn 1979). The first mine on the J-M Reef, the Stillwater mine near Nye, Montana, started in commercial production in 1986 and produces platinum and palladium as well as gold, silver, rhodium, copper, nickel, and cobalt. The East Boulder mine that accesses the J-M Reef at the western end of the complex started production in 2002.

A variety of exploration methods were used in the discovery and delineation of the J-M Reef – geologic mapping, soil and talus fines geochemistry surveys, magnetometer surveys, induced polarization (I.P.) surveys, very low frequency electromagnetic surveys (VLF EM), trenching, diamond drilling, and underground exploration. One of the principal reasons for the success of the exploration program was the development in 1968 of practical, sensitive and relatively inexpensive techniques for the analysis of platinum and palladium in soils and rocks by Bondar & Clegg Company, Ltd. of Ottawa. The method combined fire assay and atomic absorption and was modified from techniques developed by the U.S. Geological Survey. This breakthrough made it possible to conduct an extensive geochemical sampling program of soil and talus fines samples, and rock samples from trenches and drill core.

Reconnaissance talus fines and soil geochemical surveys resulted in the identification of numerous anomalies related to sources in the Lower Banded series. These regional anomalies were in general followed up with more detailed soil sampling, time-domain I.P. and magnetometer surveys and geologic mapping that ultimately led to the discovery of the J-M Reef. The following summary of the discovery of the J-M Reef is largely derived from Conn (1979) and Mann *et al.* (1985).

In 1961, H. K. Conn of the Johns-Manville Corporation attended the Commonwealth Mining Congress in South Africa and visited the Rustenburg platinum mines on one of his tours. Based on his knowledge of the complex and the work of Howland *et al.* (1936), he thought there might be a zone similar to the Merensky Reef in the Stillwater Complex. In 1967, E. L. Mann, S.G. Ellingwood, and Johns-Manville staff geologists carried out a limited reconnaissance program in which they collected rock samples from previously described disseminated sulfide zones in the Lower, Middle, and Upper Banded series and initiated a modest soil geochemistry program. This program led to the discovery, in 1968, of PGE mineralization associated with an unusual and discontinuous chromite-rich margin of a younger granitic intrusion in the Banded series at Picket Pin Mountain (Fuchs & Rose 1974, Czamanske *et al.* 1991). In 1969, soil geochemical surveys, together with I.P. and magnetometer surveys, focused attention on the area north of upper Iron Creek, where numerous small copper–nickel–chromium–platinum–palladium anomalies were identified. During 1970, trenching and limited diamond drilling revealed that these anomalies resulted from glacially transported mineralized boulders. During 1971, A.W. Rose of the Pennsylvania State University traced the mineralized glacial float to its source, some 900 m northeast of Iron Mountain North. This sulfide-bearing outcrop became known as the Janet 50 zone. Extensive mapping, sampling, trenching and drilling in the area, and on other identified targets in 1971 and 1972, revealed sulfide-rich zones in graphite-rich pegmatoidal bronzitite within the Lower Banded series. Trenching of superimposed magnetic, I.P. and geochemical anomalies led to the discovery of the Camp zone immediately to the west of the Janet 50 occurrence. Diamond drilling was continued into December of 1973. By March 1974, analyses of drill core had confirmed ore grade platinum–palladium mineralization in the Camp zone, a segment of the J-M Reef. PGE-rich outcrops

of the J-M Reef were discovered along the West Fork of the Stillwater River in the summer of 1974. The reef was first found on the southeast side of the West Fork in June or July; on August 22, 1974, the reef was discovered in glaciated cliffs northwest of the river. This discovery allowed exploration geologists to fully appreciate the stratigraphic context of the mineralized layer. After mapping, trenching and drilling demonstrated the stratiform character and lateral continuity of this mineralization, claim staking was accelerated; by the summer of 1976, the Johns-Manville Corporation held claims over all but approximately 2.4 km of the entire 42 km strike length of the J-M Reef.

Soil and Talus Fines Sampling Program

Geochemical analysis of soil and talus fines samples for platinum and palladium was one of the exploration methods used to discover and delineate the J-M Reef of the Stillwater Complex. Soils and talus fines have proven to be equally effective in defining platinum and palladium anomalies over the apex of the J-M Reef. B-horizon soils were sampled where available, with the C-horizon serving as a second choice. For soil samples, about two heaping handfuls of material were collected. For talus samples, the finest material available in a 7.6 m radius around the site was taken.

Over 10,900 samples of soil and talus fines were collected and analyzed for platinum and palladium (Fig. 18-3). Most of these samples were collected along lines perpendicular to the strike of igneous layering in the complex. The spacing between samples along these lines was approximately 30 m. The spacing between lines varies from 30 m to about 240 m. Samples were also collected on contour traverses through the upper part of the Stillwater Complex east and west of the Boulder River and the West Fork of the Stillwater River and along roads and ridge lines in the eastern third of the complex. Sample spacing along contour traverses ranged from 30 to 60 m. For this study, a spatial database of sample locations and geochemistry was constructed from 1:4800 scale paper maps provided by Stillwater PGM Resources in the early 1990s.

Palladium was below detection limit for fourteen percent of the locations (1,498); almost half of the sites (5,415) had platinum analyses

below detection limit. For most of these samples, the detection limit for palladium was 2 ppb; however, detection limits as high as 10 ppb were reported for 275 of the sites. The detection limit for most platinum analyses was below 20 ppb; however 336 of the 5,415 censored samples (those with values below detection limit) had detection limits that ranged from <25 to <150 ppb. As expected, the data for both platinum and palladium are both characterized by positive, skewed distributions. The median of uncensored values (values above detection limit) for palladium and platinum are 8 ppb and 20 ppb, respectively. Maximum values for palladium and platinum are 6.4 ppm and 5.76 ppm, respectively.

The geochemical data for these samples are presented using 3 different schemes based on: A) anomalous samples determined by Johns-Manville geologists at the time the survey was completed, B) population statistics, and C) interpolated surfaces.

Johns-Manville anomalous samples

By 1976, geologists with Johns-Manville had largely completed their sampling program and classified the samples into 4 groups based on their geochemistry:

- Negative samples had less than 50 ppb platinum + palladium (where platinum \leq palladium) or less than 80 ppb platinum + palladium (where platinum $>$ palladium).
- Weakly anomalous samples had 50 to 100 ppb platinum + palladium (where platinum \leq palladium) or 80 to 200 ppb platinum + palladium (where platinum $>$ palladium).
- Moderately anomalous samples had 100 to 200 ppb platinum + palladium (where platinum \leq palladium)
- Highly anomalous samples had over 200 ppb platinum + palladium (with any ratio).

Population statistics

Cumulative frequency diagrams for both platinum and palladium show the analyses are multimodal (Figs. 18-4, 18-5). More than 95 percent of the samples belong to a population consisting of unmineralized material with less than 30 to 40 ppb palladium and less than 40 to 50 ppb platinum. The remaining approximately 460 samples appear to be made up of two populations (Fig. 18-5). The range

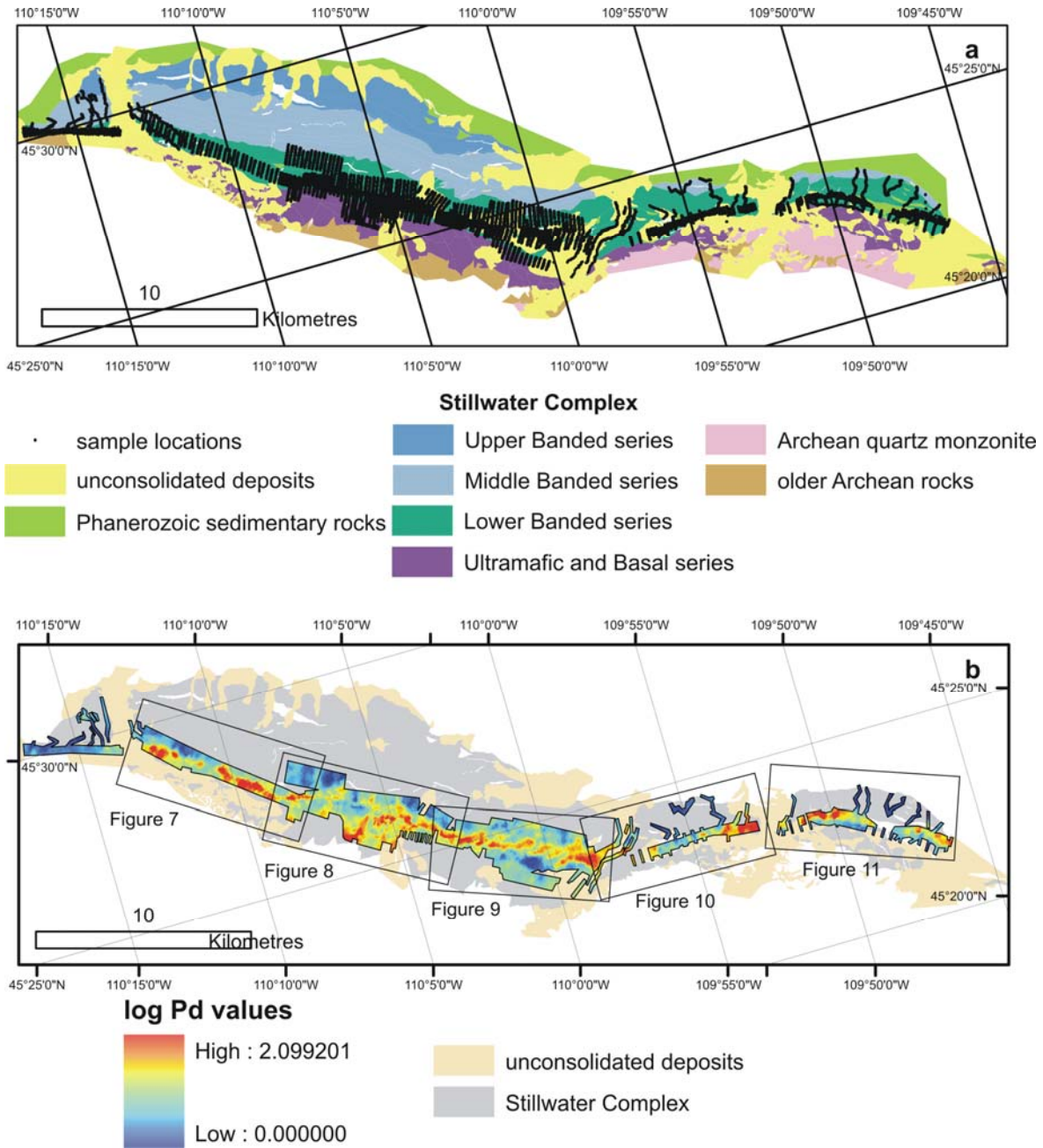


FIG. 18-3. Maps showing the distribution and results of soil and talus fines geochemistry surveys in relation to the geology of the Stillwater Complex. **a**, location of talus and soil samples on map showing series level subdivisions of the Stillwater Complex. **b**, Surface of log palladium values generated from sample data shown relative to the Stillwater Complex and unconsolidated deposits. Inset show the locations of Figs. 18-7 through 18-11.

of values for the largest population in the remaining 5 percent varies from about 40 ppb to 200 ppb palladium and about 50 to about 200 ppb platinum. About 50 samples make up the third population and consist of material with more than 200 ppb platinum or palladium. On a log-transformed bivariate plot of

platinum *versus* palladium, this third group forms a positive linear trend that extends from the diffuse cloud of samples that contain less than 200 ppb platinum or palladium (Fig. 18-6). The ratio of

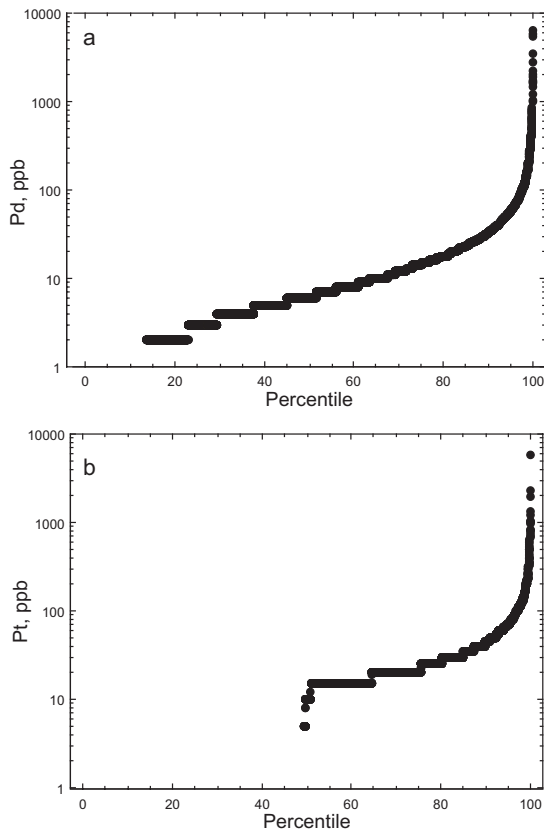


FIG. 18-4. Cumulative frequency plots for palladium and platinum soil and talus fines geochemical samples. Only values above detection limit are shown.

palladium-to-platinum in this trend of highly mineralized samples is about 3:1, the same as typical samples from the J-M Reef.

Interpolated surfaces

Surfaces were calculated to represent the soil and talus fines geochemical data. Before the surface was created, censored values were replaced by a value of half the reported detection limit and the logarithms of the platinum and palladium values were calculated. Several methods to interpolate a surface from point data were investigated (inverse distance weighted, normalized spline, tension spline, and kriging). Surfaces illustrated in this paper were generated using the ordinary kriging method with a spherical semivariogram model. A variable search radius and 12 points were used. The surfaces were generated with the spatial analyst extension in ESRI ArcGIS 8.3.

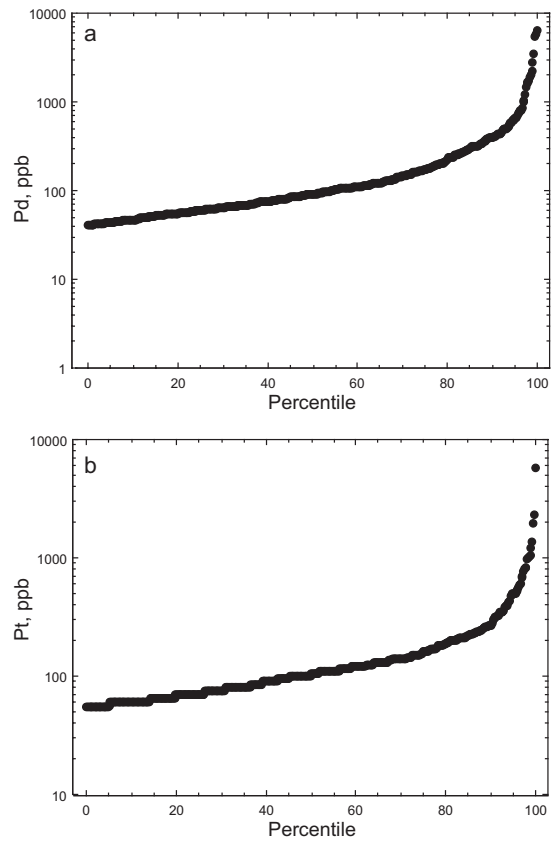


FIG. 18-5. Cumulative frequency plots for palladium and platinum soil and talus fines geochemical samples. Only values above that have palladium greater than 40 ppb and platinum greater than 50 ppb are shown.

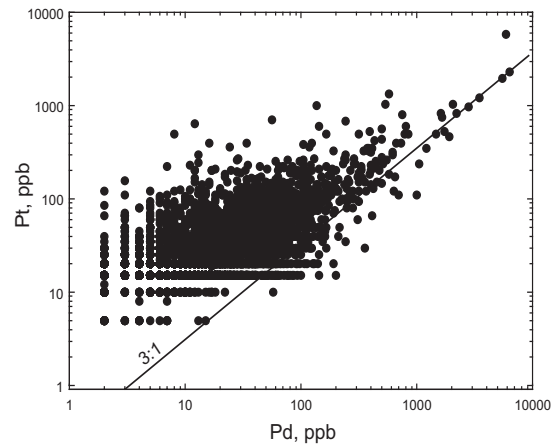


FIG. 18-6. Bivariate scattergram for palladium and platinum soil and talus fines geochemical samples. Only values above detection limit are shown.

Platinum and Palladium Soil and Talus Fines Geochemistry in Relation to the Outcrop Trace of the J-M Reef

The highest density of sample lines are found in the central part of the complex extending from slightly below the contact of the Ultramafic series and the Lower Banded series to slightly above the contact between the Lower Banded series and the Upper Banded series. Sample lines in the eastern and western part of the complex are more widely spaced and focus on a narrower range of the igneous stratigraphy surrounding the J-M Reef.

The results of the geochemical survey are illustrated in 5 maps. The distribution of weakly, moderately, and highly anomalous samples relative to the mapped and drill-delineated trace of the J-M Reef is shown in figures 18-7a, 18-8a, 18-9a, 18-10a, and 18-11a. The locations of anomalous samples were determined by Johns-Manville geologists and were digitized from 1:12,000-scale paper maps. The three sample groups based on population statistics of the entire dataset are shown relative to the mapped and drill delineated trace of the J-M Reef in figures 18-7b, 18-8b, 18-9b, 18-10b, and 18-11b. The interpolated surfaces of the logarithmic values of palladium in soil and talus fines are illustrated as shaded relief maps in figures 18-7c, 18-8c, 18-9c, 18-10c, and 18-11c.

East side of Boulder River Canyon

Figure 18-7 illustrates the soil and talus fines geochemical data for the east side of the Boulder River canyon. The J-M Reef occurs on steep terrain in the Graham Creek and Blakely Creek drainages. Surficial deposits in this area are dominated by colluvium and talus. Sample lines focus on the stratigraphic interval that contains the J-M Reef. Anomalies are coincident with the trace of the reef or are displaced downslope.

East Boulder Plateau and headwaters of East Boulder River

Figure 18-8 illustrates the soil and talus fines geochemical data for the headwaters of the East Boulder River on the East Boulder Plateau. The J-M Reef occurs in an area of subdued terrain dissected by numerous drainages that make up the headwaters of the East Boulder River. The offset in the trace of the reef in the center of the illustration is caused by displacement along the Fishscale fault. Glacial deposits, talus, and colluvium commonly make up most surface exposures; outcrop is sparse. Sample

lines vary in spacing and cover the entire stratigraphic interval from the Ultramafic series to the Middle Banded series. Geochemical anomalies associated with the J-M Reef are either coincident with the trace of the reef or are offset downslope. Some of the anomalies south (and stratigraphically downsection) from the J-M Reef are mineralized pegmatoids that occur in rocks below the J-M Reef at the Coors 602 locality. Trenching, drilling, and mapping in the Coors 602 area have located several orthopyroxene-rich pegmatoids in the Lower Banded series below the J-M Reef and a dike-like body of orthopyroxenite that cuts the Lower Banded series (McIlveen 1996). The bedrock source of the anomaly south and east of Lost Mountain (LM) has not been determined. The rectangular grid of samples in the upper left portion of the illustration covers the Gabbronorite II zone of the Lower Banded series.

Iron Creek drainage and cliffs along the West Fork of the Stillwater River

Figure 18-9 illustrates soil and talus fines geochemical data for the Iron Creek drainage and the cliffs along the West Fork of the Stillwater River. Sample lines vary in spacing and cover the entire stratigraphic interval from the Ultramafic series to the Middle Banded series. Immediately north of Iron Mountain (IM), the discovery locality for the J-M Reef (the Camp zone) is exposed. Immediately to the east of the Camp zone, anomalies south and stratigraphically downsection from the reef are associated with mineralized graphite-bearing pegmatoids in ultramafic rocks of the Janet 50 occurrence. The Janet 50 occurrence in the upper part of the Bronzite zone extends over an area of 30 by 50 m and consists of a pegmatoidal orthopyroxenite with disseminated sulfide minerals and local concentrations of graphite (Volborth & Housley 1984). From the Janet 50 occurrence to longitude 110°W, the J-M Reef occurs in the southern part of the Iron Creek drainage; east of 110°W, the reef is offset to the south and crops out in glaciated cliffs along the West Fork of the Stillwater River. The Iron Creek drainage is almost entirely covered by glacial deposits; Cambrian limestone locally crops out in the watershed and unconformably overlies the Stillwater Complex. Despite the lack of exposure in the Iron Creek drainage, a pronounced palladium anomaly extends downslope from the trace of the reef. The palladium-platinum zone in the West Fork

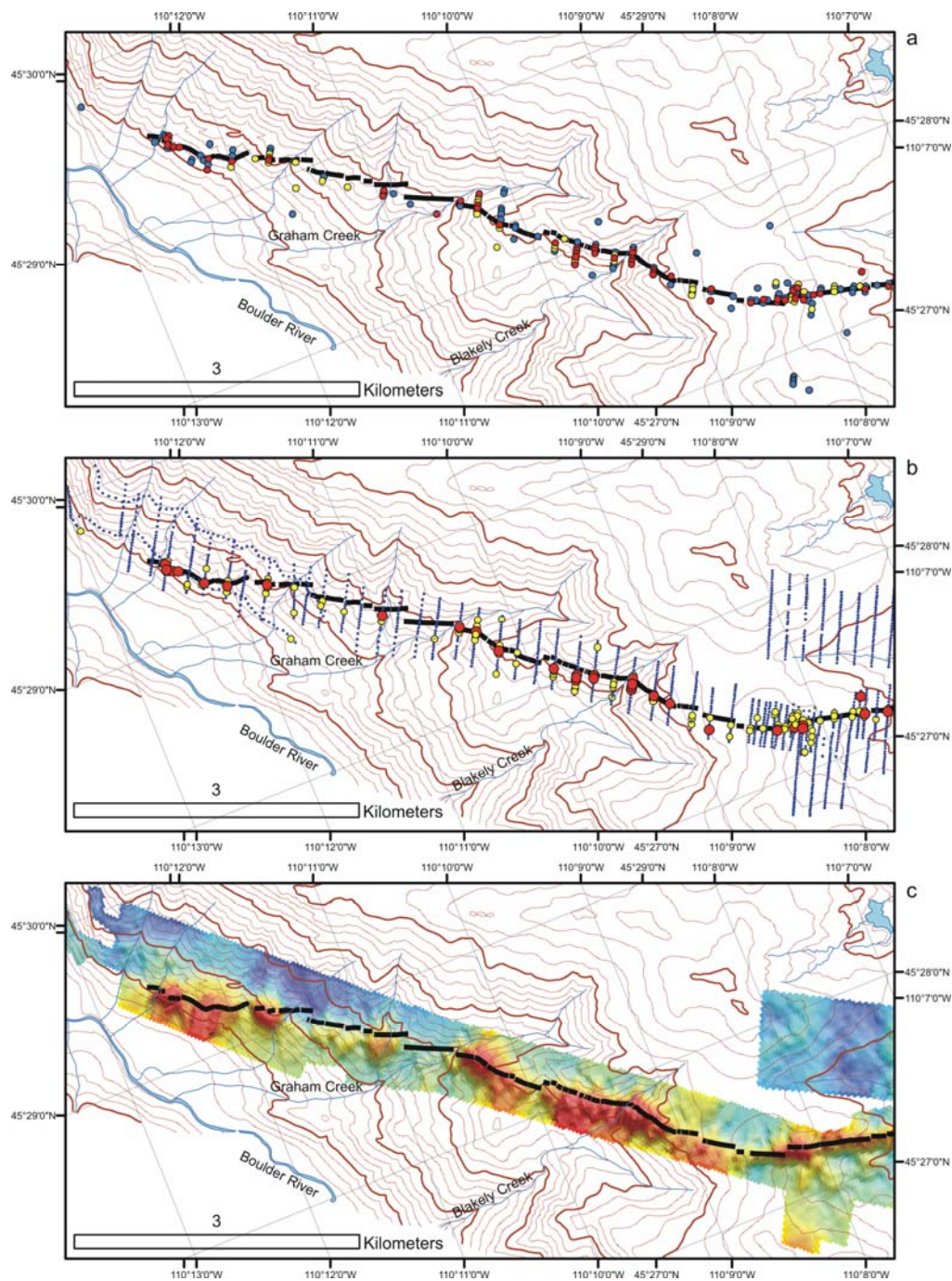


FIG. 18-7. Maps illustrating the results of geochemistry surveys of palladium and platinum in soil and talus fines on the east side of the Boulder River Canyon. Heavy black line is the surface trace of the J-M Reef as defined by surface sampling, mapping, and drilling. Topographic contours are shown in grey; contour interval is 50 m. **a**, Samples identified as anomalous for palladium and platinum by Stillwater PGM Resources in 1976: white – weakly anomalous; grey – moderately anomalous; black – highly anomalous. **b**, Samples classified into 3 populations based on palladium geochemistry. small spots: <40 ppb palladium; grey circles: 40 to 200 ppb palladium; large black spots: greater than 200 ppb palladium. **c**, Representation of the surface interpolated from log palladium values calculated from survey data. Interpolation method is described in the text. Color ramp utilizes a 2 standard deviation stretch; see Fig. 18-3 for explanation of values.

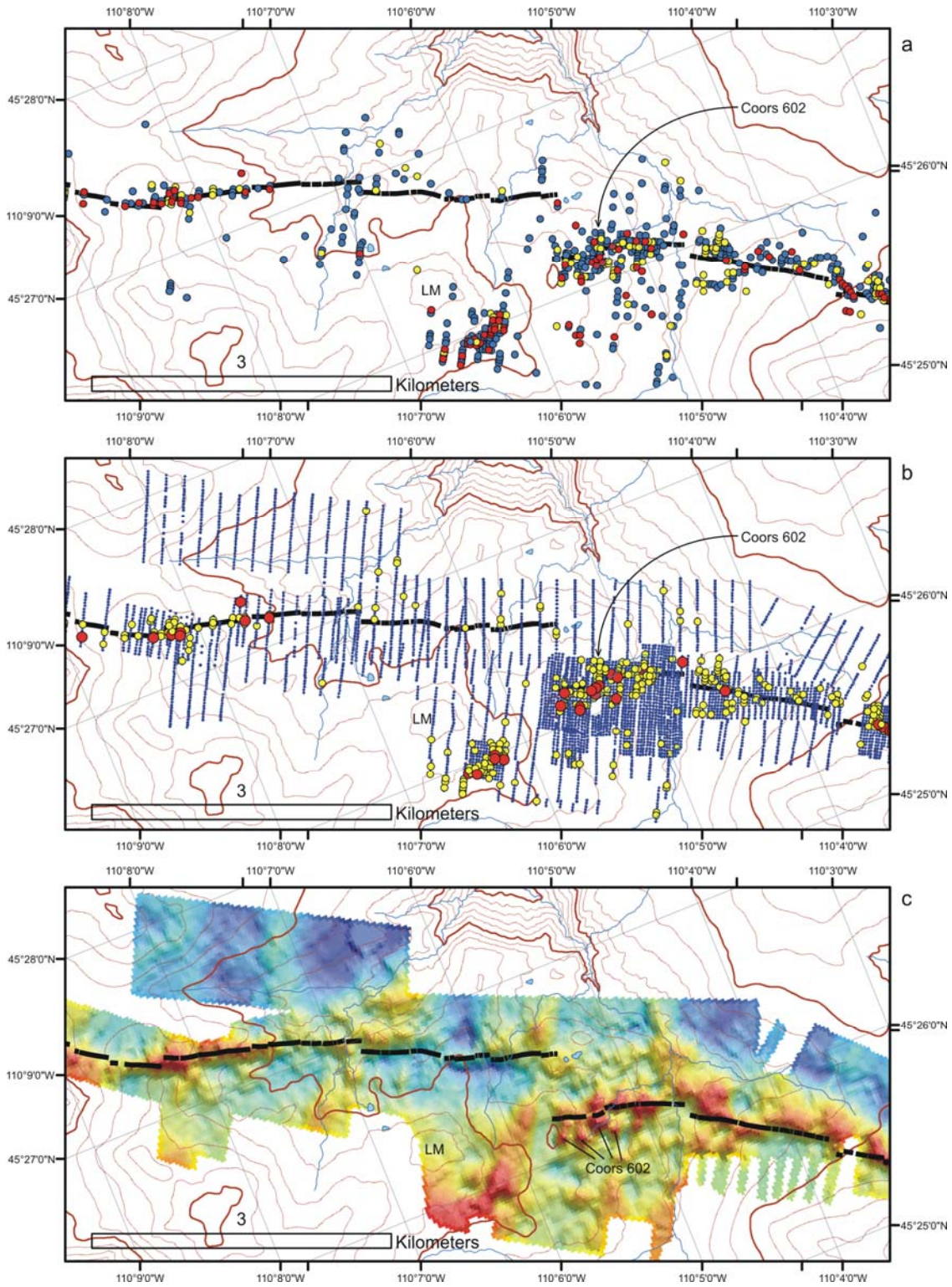


FIG. 18-8. Maps illustrating the results of geochemistry surveys of palladium and platinum in soil and talus fines for the headwaters of the East Boulder River on the East Boulder Plateau. Explanation of symbols is given in the caption for Fig. 18-7. LM is Lost Mountain.

GEOCHEMICAL SURVEYS AND DISCOVERY OF THE J-M REEF, STILLWATER COMPLEX, MONTANA

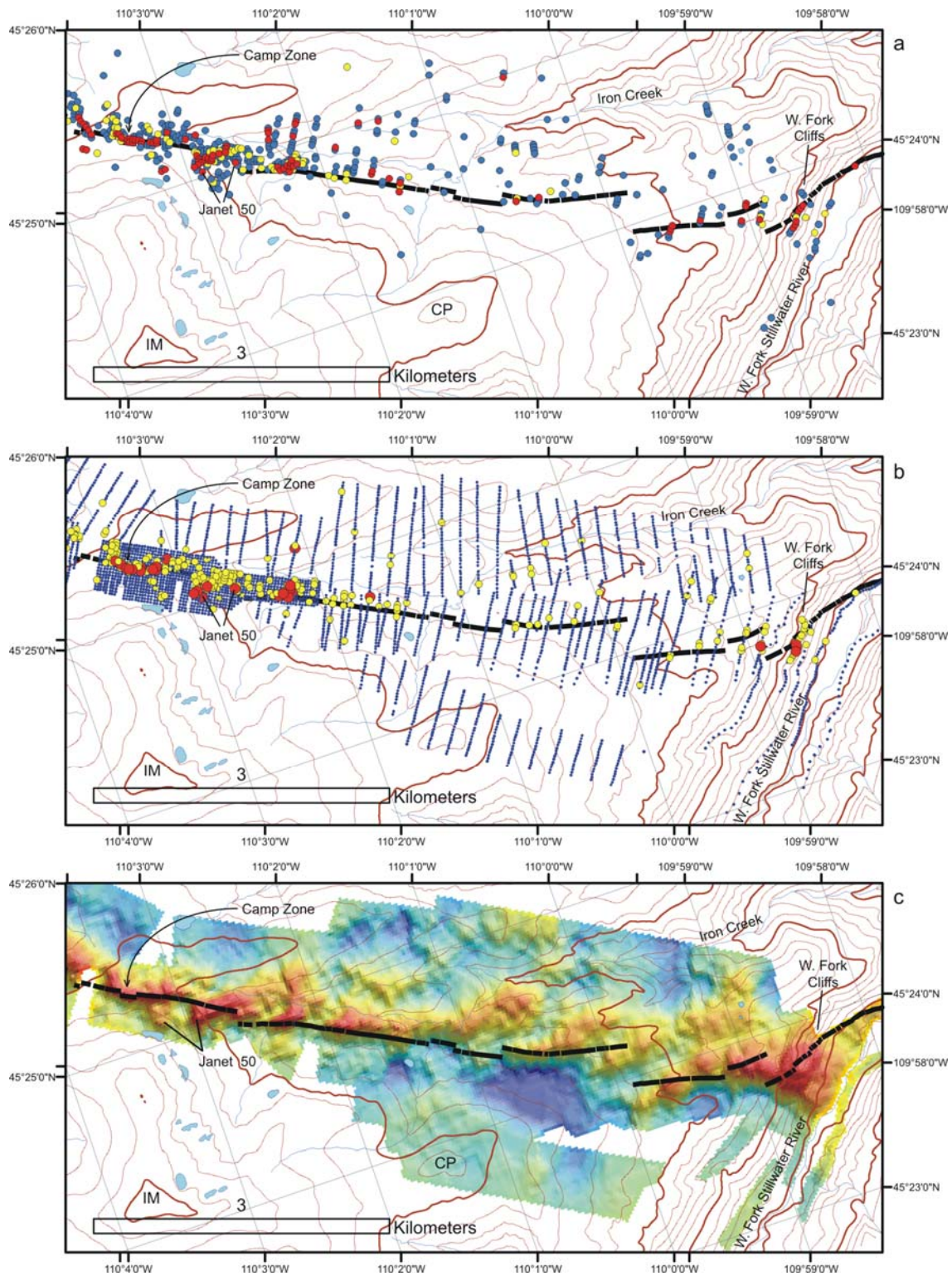


FIG. 18-9. Maps illustrating the results of geochemistry surveys of palladium and platinum in soil and talus fines for the Iron Creek drainage and the cliffs along the West Fork of the Stillwater River. Explanation of symbols is given in the caption for Fig. 7. CP is Crescent Peak; IM is Iron Mountain.

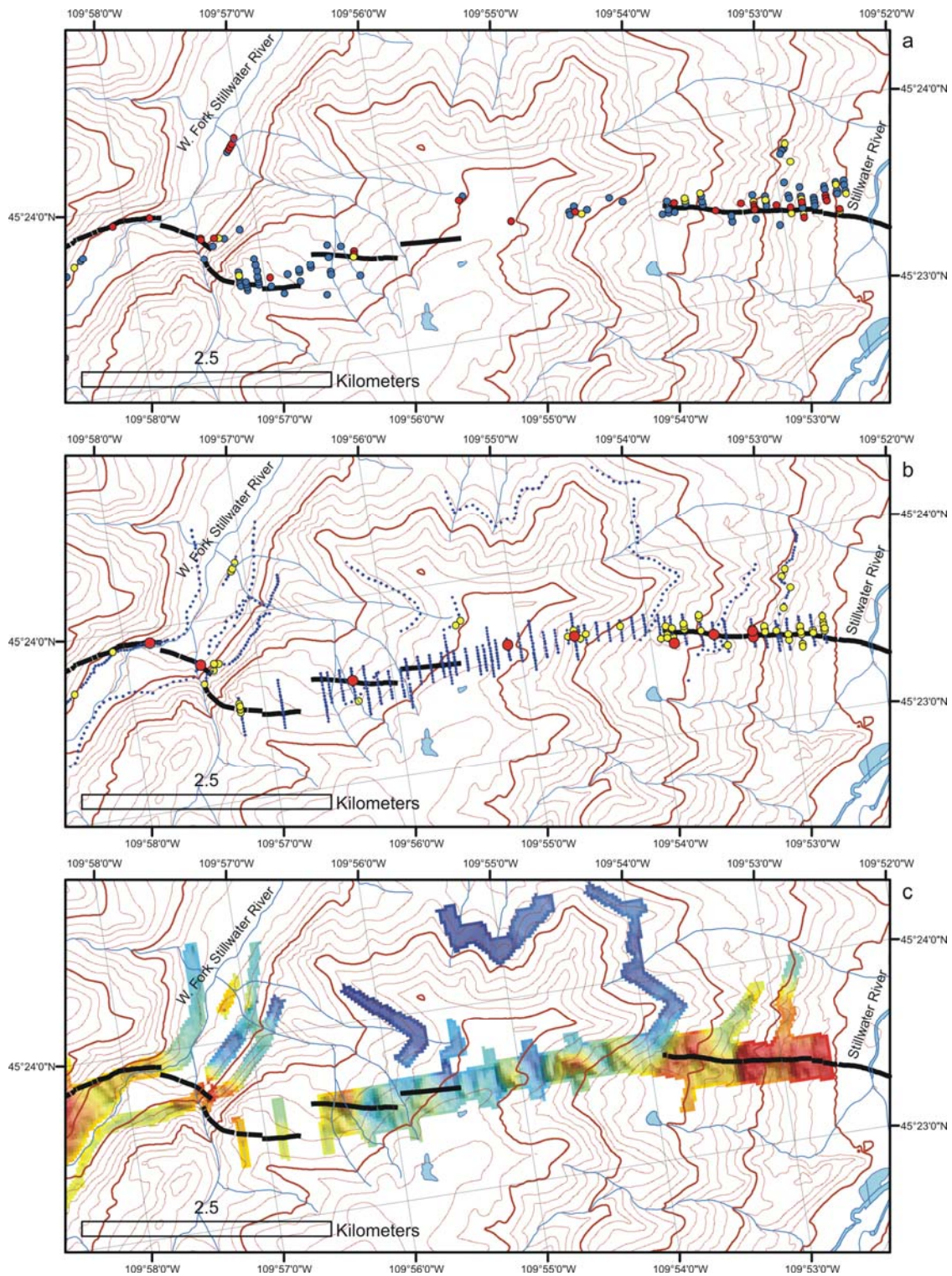


FIG. 18-10. Maps illustrating the results of geochemistry surveys of palladium and platinum in soil and talus fines for the area between the West Fork of the Stillwater River and the Stillwater River. Explanation of symbols is given in the caption for Fig. 18-7.

GEOCHEMICAL SURVEYS AND DISCOVERY OF THE J-M REEF, STILLWATER COMPLEX, MONTANA

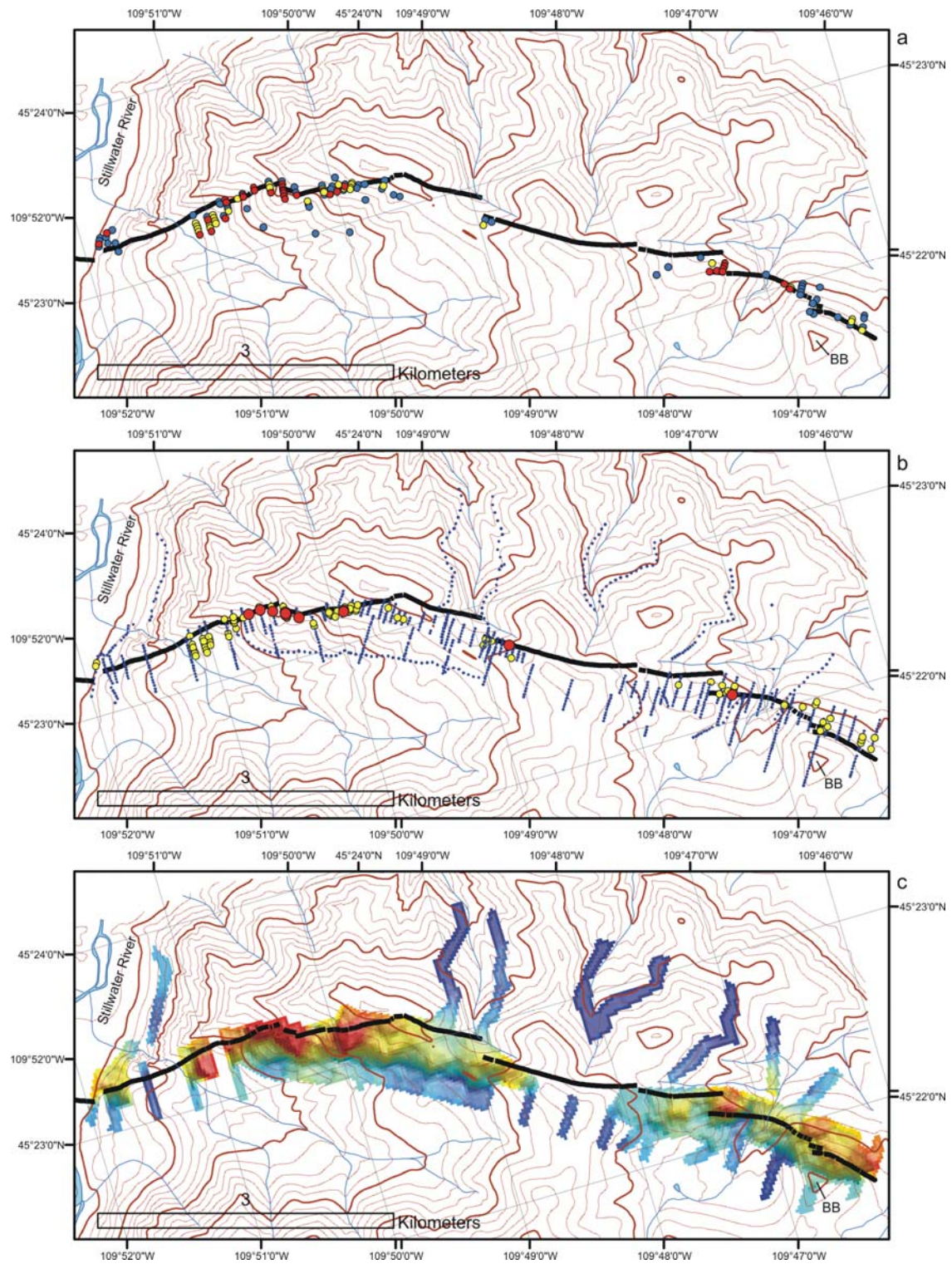


FIG. 18-11. Maps illustrating the results of geochemistry surveys of palladium and platinum in soil and talus fines for the area between the Stillwater River and Black Butte. Explanation of symbols is given in the caption for Fig. 7. BB is Black Butte.

valley was first traced in spring 1974 along three contour traverses at approximately 8,000 ft (2,438 m), 7,400 ft (2,255 m), and 6,600 ft (2011 m) elevations (Mann *et al.* 1985). The upper line defined a broad platinum–palladium anomaly on strike with the Camp zone. The middle and lower lines had wider anomalies, displaced in turn further to the north. Detailed prospecting of the anomalous area resulted in the discovery of the reef in the West Fork cliffs in August 1974. Sample lines extending southeast from Crescent Peak (CP) follow the contact between the Ultramafic series and the Lower Banded series.

West Fork Stillwater River to Stillwater River

Figure 18-10 illustrates soil and talus fines geochemical data for the area between the West Fork of the Stillwater River and the Stillwater River. Regularly spaced sample lines focus on the narrow stratigraphic interval that contains the J-M Reef. Contour traverses extend sampling to the cover the exposures of the Lower and Middle Banded series. Anomalies are coincident with the reef in the near the Stillwater River and the West Fork of the Stillwater River. The reef is poorly exposed at higher elevations and is not characterized by consistent anomalies. With the exception of the easternmost sections, the contour traverses are not anomalous with the exception of the easternmost sections which follow a road that was cut through the J-M Reef; anomalous values there may reflect contamination from the road building process.

Stillwater River to Black Butte

Figure 18-11 illustrates soil and talus fines geochemical data for the area between the Stillwater River and Black Butte (BB). Regularly spaced sample lines focus on the narrow stratigraphic interval that contains the J-M Reef but were extended at wide intervals to include the contact between the Ultramafic series and the Lower Banded series. No samples were collected where the reef is concealed by younger deposits of limestone. Contour traverses extend sampling to the cover the exposures of the Lower and Middle Banded series. Anomalies are coincident with the reef and are displaced slightly down slope.

DISCUSSION AND SUMMARY

In the late 1960s and the early 1970s, soil and talus fines geochemistry proved to be an effective exploration method that contributed to the

discovery of the J-M Reef. The results of the soil and talus fine survey document the geochemical expression of a high-grade reef-type deposit in an area characterized by young geomorphic surfaces, gentle to steep slopes, ecological settings that range from alpine to temperate forests, and soils that are dominantly inceptisols. The results of the survey document both the values of platinum and palladium that can be expected under these conditions and the extent of dispersion in transported surficial deposits. Studies by Fuchs & Rose (1974) suggested limited mobility of platinum and palladium in the soils developed in the Stillwater area. This is consistent with our observation that the patterns of soil anomalies defined by palladium and platinum were similar at the scale of this study. Anomalies are generally coincident with the surface trace of the reef but may be displaced downslope or downstream.

Based on the stratigraphic position of the Merensky Reef in the Bushveld Complex, rocks slightly above the contact with the Ultramafic series were a logical place to focus exploration activity in the late 1960s and early 1970s. Geologic mapping had previously located the position of this contact throughout the complex (Jones *et al.* 1960, Page & Nokleberg 1974). A road constructed in the 1950s to evaluate the iron formation that occurs below the basal contact of the Stillwater Complex provided access to a large area in the central part of the complex in which the favorable stratigraphy was exposed and open for exploration. Accordingly, the area extending from the East Boulder plateau to the West Fork of the Stillwater River was the initial focus of exploration activity. This area has the highest density of sample lines that extend over a wide stratigraphic interval (Figs. 18-8 and 18-9). Unfortunately, this part of the complex is also characterized by relatively subdued terrain, widespread surficial deposits of unconsolidated material (largely glacial deposits), and limited outcrop. Thin deposits of Cambrian sedimentary rocks that overlie the Stillwater Complex are also present.

The anomalous samples identified by Johns-Manville in this area (Figs. 18-8a and 18-9a) are widely dispersed and only locally define the trace of the J-M Reef. These surveys also discovered anomalies that correspond to mineralized pegmatoids that occur stratigraphically below the J-M Reef (Volborth & Housley 1984, McIlveen 1996) and mineralized boulders in glacial deposits (Fuchs & Rose 1974). Even though the soil

and talus fine samples could not completely delineate the reef in this area mantled by transported surficial deposits, the anomalous values provided the encouragement needed to continue exploration until the reef was discovered in outcrop in the cliffs along the West Fork of the Stillwater River in 1974. From that time forward, igneous stratigraphy became the primary method used to locate and trace the J-M Reef (Todd *et al.* 1982). The likely location of the J-M Reef could be estimated using the distance from contact between the Ultramafic series and the Lower Banded series or from several prominent anorthosite marker layers that occur near the base the Gabbronorite II zone. Soil geochemical surveys were then used to help validate the results of geologic mapping and sampling, the surveys strictly focused on the stratigraphic interval that contained the reef (Figs. 18-7, 18-10, and 18-11).

Modeling the geochemical data as a surface provides more information about the location of the J-M Reef, the dispersion of material away from it, and identifies subtle anomalies that may be related to other features. Grouping the geochemical data into three or four classes and displaying the data as points (Figs. 18-7a to 18-11a and 18-7b to 18-11b) simplifies the analysis of the data and emphasizes the location of anomalous samples. However, this approach obscures any fine structure present in the data. The surface created using kriging methods indicates there is more structure in the data that would help interpret the results of the geochemical surveys. For example, the surfaces for the Iron Creek area (Fig. 18-9c) clearly illustrate the northeast-trending trains of material dispersed down slope from the J-M Reef. Subtle north-south trending anomalies in the headwaters of East Boulder River (Fig. 18-8c) do not appear to be related to the reef but are spatially associated with faults mapped by Segerstrom & Carlson (1982). The surfaces have to be used with caution; edge effects can create open anomalies where none are present. The actual location of the sample must be used in interpreting anomalies in the surface to make sure they are not related to an edge of the surface.

In addition to contributing to the discovery of the J-M Reef, these surveys provide additional insight into the mineral resource potential of this part of the Stillwater Complex. The contact between ultramafic and mafic cumulates is mineralized in the Great Dyke in Zimbabwe (Wilson & Tredoux 1990), the Munni Munni intrusion in Australia (Barnes *et al.* 1990), and the Weld Range intrusion

in Australia (Parks 1998); no mineralization is indicated by the soils surveys that cover the equivalent stratigraphic position at Stillwater (the contact between the Ultramafic series and the Lower Banded series). In addition, the sampling suggests that no significant mineralization is present in the stratigraphic interval that extends from the J-M Reef to the lower contact of the Middle Banded series.

ACKNOWLEDGEMENTS

We would thank the management of Stillwater PGM Resources for providing access to the data and to Stillwater Mining Company for permission to publish this information. Tom Mooney and Michael Carver, Eastern Washington University, and Jeremy C. Larsen, Information Systems Support, Inc., assisted with data compilation. Art Bookstrom, Steve Ludington, Jim Miller, and an anonymous reviewer provided constructive reviews of the manuscript.

REFERENCES

- BARNES, S.J. & NALDRETT, A.J. (1985) Geochemistry of the J-M (Howland) Reef of the Stillwater Complex, Minneapolis adit area. I. Sulfide chemistry and sulfide-olivine equilibrium. *Econ. Geol.* **80**, 627-645.
- BARNES, S.J., MCINTYRE, J.R., NISBET, B.W. & WILLIAMS, C.R. (1990) Platinum group element mineralisation in the Munni Munni Complex, Western Australia. *Mineral. Petrol.* **42**, 141-164.
- BOW, C.S., WOLFGRAM, D., TURNER, A., BARNES, S., EVANS, J., ZDEPSKI, M. & BOUDREAU, A. (1982) Investigations of the Howland reef of the Stillwater Complex, Minneapolis Adit area: Stratigraphy, structure, and mineralization. *Econ. Geol.* **77**, 1481-1492.
- CAWTHORN, R.G. (2005): Stratiform platinum-group element deposits in layered intrusions. In *Exploration for Platinum-group Element Deposits* (J.E. Mungall, ed.). *Mineral. Assoc. Canada, Short Course 35*, xx-xx.
- CONN, H. K. (1979) The Johns-Manville platinum-palladium prospect, Stillwater Complex, Montana, U.S.A.. *Can. Mineral.* **17**, 463-468.
- CZAMANSKE, G.K., ZIENTEK, M.L. & MANNING, C.E. (1991) Low-K granophyres of the Stillwater Complex, Montana. *Am. Mineral.* **76**, 1646-1661.

- DRAIN, V.K. (1985) Glaciation in the Boulder River area, south central Montana. *Geol. Soc. Am. Abstr. with Prog.* **17**, 216.
- FUCHS, W.A. & ROSE, A.W. (1974) The geochemical behavior of platinum and palladium in the weathering cycle in the Stillwater Complex, Montana. *Econ. Geol.* **69**, 332-346.
- HOWLAND, A.L., PEOPLES, J.W. & SAMPSON, E. (1936) The Stillwater Igneous Complex and associated occurrences of nickel and platinum metals. *Montana Bureau of Mines and Geology Miscellaneous Contribution* **7**, 15 p.
- JACKSON, E.D. (1961) Primary textures and mineral associations in the Ultramafic zone of the Stillwater Complex, Montana. *U.S. Geol. Surv. Prof. Paper* **358**, 106 p.
- JONES, W.R., PEOPLES, J.W. & HOWLAND, A.L. (1960) Igneous and tectonic structures of the Stillwater Complex, Montana. *U.S. Geol. Surv. Bul.* **1071-H**, 281-340.
- MANN, E.L. (BOB), LIPIN, B.R., PAGE, N.J., FOOSE, M.P. & LOFERSKI, P.J. (1985) Guide to the Stillwater Complex exposed in the West Fork area. In *The Stillwater Complex, Montana: Geology and guide*, Czamanske, G.K. & Zientek, M.L. (eds.). *Montana Bureau of Mines and Geology Special Publ.* **92**, 231-246.
- MCCALLUM, I.S., RAEDEKE, L.D. & MATHEZ, E.A. (1980) Investigations of the Stillwater Complex: Part I. Stratigraphy and structure of the Banded zone. *Am. J. Sci.* **280-A**, 59-87.
- MCDANIEL, P. (undated) The twelve soil orders – inceptisols. ONLINE. Available at <http://soils.ag.uidaho.edu/soilorders/inceptisols.htm> [accessed March 16, 2005].
- MCILVEEN, C.L. (1996) *An anomalous platinum-group element occurrence below the JM Reef, Stillwater Complex, Montana*. University of Montana, M.S. thesis, Missoula, Montana, 74 p.
- PAGE, N.J. (1977) Stillwater Complex, Montana: Rock succession, metamorphism and structure of the complex and adjacent rocks. *U.S. Geol. Surv. Prof. Paper* **999**, 79 p.
- PAGE, N.J. (1979) Stillwater Complex, Montana – structure, mineralogy, and petrology of the Basal zone with emphasis on the occurrence of sulfides. *U.S. Geol. Surv. Prof. Paper* **1038**, 69 p.
- PAGE, N.J. & NOKLEBERG, W.J. (1974) Geologic map of the Stillwater Complex, Montana. *U.S. Geol. Surv. Misc. Inv. Series Map* **I-797**, scale 1:12,000, 5 sheets.
- PARKS, J. (1998) Weld Range platinum group element deposit. In *Geology of Australian and Papua New Guinean mineral deposits*. Berkman, D.A. & Mackenzie, D.H. (eds.). *The Australasian Inst. Mining & Metall.*, Melbourne, 279-286.
- PETERSON, J.A., ZIENTEK, M.L. & COOPER, R.W. (1995) Stratigraphic columns for traverses through the Lower and Middle Banded series, Stillwater Complex, Stillwater County, Montana. *U.S. Geol. Surv. Misc. Field Studies Map* **MF-2274**, 2 sheets.
- PIERCE, K.L. (1979) History and dynamics of glaciation in the northern Yellowstone National Park area. *U.S. Geol. Surv. Prof. Paper* **729-F**, 90 p.
- PREMO, W.R., HELZ, R.T., ZIENTEK, M.L. & LANGSTON, R.B. (1990) U–Pb and Sm–Nd ages for the Stillwater Complex and its associated sills and dikes, Beartooth Mountains, Montana: Identification of a parent magma? *Geology* **18**, 1065-1068.
- RAEDEKE, L.D. & MCCALLUM, I.S. (1984) Investigations in the Stillwater Complex: Part II. Petrology and petrogenesis of the Ultramafic series. *J. Petrol.* **25**, 395-420.
- RAEDEKE, L.D. & VIAN, R.W. (1986) A three-dimensional view of mineralization in the Stillwater J-M Reef. *Econ. Geol.* **81**, 1187-1195.
- SEGERSTROM, KENNETH & CARLSON, R.R. (1982) Geologic map of the Banded Upper zone of the Stillwater Complex and adjacent rocks, Stillwater, Sweet Grass, and Park Counties, Montana. *U.S. Geol. Surv. Misc. Inv. Series Map* **I-1383**, scale 1:24,000, 2 sheets.
- SIMONS, F.S. & AMBRUSTMACHER, T.J. (1976) High-level plateaus of the southeastern Beartooth Mountains, Montana and Wyoming – remnants of an exhumed sub-Cambrian marine plain. *J. Res. of the U.S. Geol. Surv.* **4**, 387-396.
- TEN BRINK, N.W. (1972) Glacial geology of the Stillwater drainage and Beartooth Mountains near Nye, Montana. *Geol. Soc. Am. Abstr. with Programs* **4**, 415.

- TODD, S.G., KEITH, D.W., LEROY, L.W., SHISSEL, D.J., MANN, E.L. & IRVINE, T.N. (1982) The J-M platinum–palladium Reef of the Stillwater Complex, Montana: I. Stratigraphy and petrology. *Econ. Geol.* **77**, 1454-1480
- USDA (1999) Percent of land area in inceptisols. U.S. Dept. of Agriculture, NCRS Map ID m4032. www.nrcs.usda.gov/technical/land/meta/m4032.html [accessed March 16, 2005].
- VOLBORTH, A. & HOUSLEY, R.M. (1984) A preliminary description of complex graphite, sulphide, arsenide, and platinum group element mineralization in a pegmatoid pyroxenite of the Stillwater Complex, Montana, U.S.A.. *Tschermaks Mineral. Petrogr. Mitt.* **33**, 213-230.
- WILSON, A.H. & TREDOUX, M. (1990) Lateral and vertical distribution of platinum-group elements and petrogenetic controls on the sulfide mineralization in the P1 pyroxenite layer of the Darwendale Subchamber of the Great Dyke, Zimbabwe. *Econ. Geol.* **85**, 556-584.
- WOODS, A.J., OMERNIK, J.M., NESSER, J.A., SHELDEN, J. & AZEVEDO, S.H. (1999) Ecoregions of Montana (color poster with map, descriptive text, summary tables, and photographs). *U.S. Geol. Surv.*, Reston, Virginia (map scale 1:1,500,000).
- ZIENTEK, M.L. (1983) *Petrogenesis of the Basal zone of the Stillwater Complex, Montana*. Stanford University, Ph.D. dissertation, Stanford, California, 246 p.
- ZIENTEK, M.L., COOPER, R.W., CORSON, S.R. & GERAGHTY, E.P. (2002) Platinum-group element mineralization in the Stillwater Complex, Montana, in Cabri, L.J., The geology, geochemistry, mineralogy, and mineral beneficiation of platinum-group elements. *Can. Inst. Mining, Metall. & Petrol. Special Vol.* **54**, 459-481.
- ZIENTEK, M.L., CZAMANSKE, G.K. & IRVINE, T.N. (1985) Stratigraphy and nomenclature for the Stillwater Complex. In The Stillwater Complex, Montana: Geology and guide. Czamanske, G.K. & Zientek, M.L. (eds.). *Montana Bureau of Mines and Geology Special Publication* **92**, 21-32.

CHAPTER 19: EXPLORATION AND MINING OF THE MAIN SULPHIDE ZONE OF THE GREAT DYKE, ZIMBABWE – CASE STUDY OF THE HARTLEY PLATINUM MINE

Allan H. Wilson
School of Geological Sciences, University of KwaZulu-Natal
Durban 4041, South Africa
E-mail: wilsona@ukzn.ac.za

and

Raylan T. Brown
School of Geological Sciences, University of KwaZulu-Natal
Durban 4041, South Africa
present address: Anglo Platinum, 55 Marshall Street, Johannesburg 2001, South Africa

INTRODUCTION

The Great Dyke of Zimbabwe is the second largest world resource of platinum and the platinum group elements (PGE) after the Bushveld Complex in South Africa. The main zone of platinum mineralization in the Great Dyke is a laterally continuous horizon in all subchambers called the Main Sulphide Zone (MSZ). Extensive, but sporadic exploration of the MSZ has been carried out over nearly 80 years and although several mining operations have been initiated these have either closed, or remain on a relatively small-scale, especially when compared to the platinum-mining operations on the Bushveld Complex. The reasons for this are complex and involve issues such as the different nature of the ore body compared to the Merensky Reef of the Bushveld Complex, relatively lower ore grades, perceived difficulties in the underground recognition of the ore body and structural problems, as well as political pressures and uncertainties.

The Hartley Platinum Mine commenced operation in 1994 after several phases of diamond drilling, trial mining operations and exhaustive exploration, carried out by a number of mining companies spanning a period of more than 20 years. In spite of this huge amount of collective information the mine operated for only five years. The quality of data and exploration methodologies also significantly improved over the period of exploration and many of the earlier data were of limited value due to poor precision and high detection limits using the analytical methods at the time. Inadequate sampling practices and insufficient knowledge of the geological controls on the mineralization also hampered the earlier

exploration. The final phase of exploration (1990–1994) carried out prior to the opening of Hartley Platinum Mine used newly established methods of PGE analysis, rigorously investigated the use of the drill core, and established a systematic evaluation of the entire mining property.

The purpose of this paper is to re-evaluate the drilling data from the final exploration phase in a way that illustrates the subtle characteristics of the mineralized zone. In addition, the mining practices will be described, how and why they were developed, and how they improved over the life of the mine. Some of the difficulties of the mining operation that relate specifically to mining ore bodies of this type are described, as well as some of the practices that operated on the mine in relation to reef recognition and grade control.

This is not in any way aimed at explaining why the mining operation failed as that relates to many issues other than those presented here. Attention will also be drawn to similarities and differences between the MSZ and the Merensky Reef, and where practices relating to mining of the latter may have severe limitations in the Great Dyke. For regional, historical, cultural and geological reasons the perceptions and practices relating to the exploration, evaluation and exploitation of the MSZ seem, over the years, to have been closely tied with those relating to the Merensky Reef.

EXPLORATION HISTORY

Platinum was discovered in the Great Dyke two years after the initial discovery of the metal in the Merensky Reef in 1925, in a similar plagioclase pyroxenite. The first attempt at extracting platinum

minerals was by the Grainger brothers in 1926 in the Wedza Subchamber (Fig. 19-1) using primitive and inadequate techniques. The attempt was unsuccessful and there was little further activity in this regard for the next 30 years. With the subsequent realization of the regional strategic importance of platinum, extensive exploration was carried out in the Great Dyke during the late 1960s and 1970s in all areas where the host pyroxenite was known to occur.

An extensive drilling program was carried out in the southernmost Wedza Subchamber by Union Carbide, which resulted in Wedza No. 1 and 2 trial mining shafts being developed in 1969–1970. At the same time Union Carbide carried out exploration in the Darwendale Subchamber. The Darwendale Subchamber is the largest subchamber, and potentially the largest single platinum resource in the Great Dyke. The Subchamber is the northern part of what was previously called the Hartley Complex (Worst 1958) after the colonial name of the nearby town of Hartley, now Chegutu. Encouraging results were obtained from the Selous area in the Darwendale Subchamber and the mining equipment from Wedza was relocated to this new prospect. Diamond drilling continued and an incline

shaft was developed at Selous from 1970 to 1973. Difficulties with the ground conditions in these near-surface operations created uncertainty about the long-term prospects of the mining area and the mining infrastructure was relocated back to the Wedza Subchamber in 1974, and the Mimosa trial mine was established. Mimosa Mine closed in 1978 but reopened in 1989 (Prendergast, pers. comm.) and continues to this day. It remains a viable mining operation and is currently the world's lowest cost platinum producer (Prendergast, pers. comm.).

Union Carbide also carried out limited exploration in other subchambers of the Great Dyke, including the most northerly Musengezi Subchamber where limited diamond drilling was carried out. In the early to mid-1980's Rio Tinto and Anglo American Corporation also carried out exploration on the Great Dyke. Rio Tinto mainly explored the area close to the western portion of the abutment of the two largest subchambers (Darwendale and Sebakwe) at the Zinca Project, while Anglo American explored the mid areas of the Great Dyke in the Sebakwe and Selukwe Subchambers (the latter at Unki trial mining operation), and part of the Wedza Subchamber (Fig. 19-1). The Unki area of the Selukwe Subchamber is at present held by Anglo Platinum (devolved from Anglo American Corporation) and is the site of the current development of a major underground mine.

The relatively weak market forces in the mid- to late-1980s saw little concerted effort to bring further platinum mining on the Great Dyke to fruition. Exploration commenced in the far-northern Musengezi Subchamber (at Snake's Head) in 1989 by Cluff Minerals, but structural complexities and the remoteness and ruggedness of the area terminated activities in 1991. In the mid-1990s the Metals Mining Agency of Japan carried out exploration in the Snake's Head area of the Musengezi Subchamber.

In the late 1980s and early 1990s further exploration was carried out in the vicinity of the previous Selous trial mine in the Darwendale Subchamber and in an area immediately south of it at Mhondoro (Fig. 19-1) by Delta Gold NL. A joint venture was established between Delta Gold NL and BHP to undertake further exploration and diamond drilling. In August 1994 construction of Hartley Platinum Mine commenced. This paper summarises and interprets the BHP exploration data for the Darwendale Subchamber from the geological mining perspective and the development

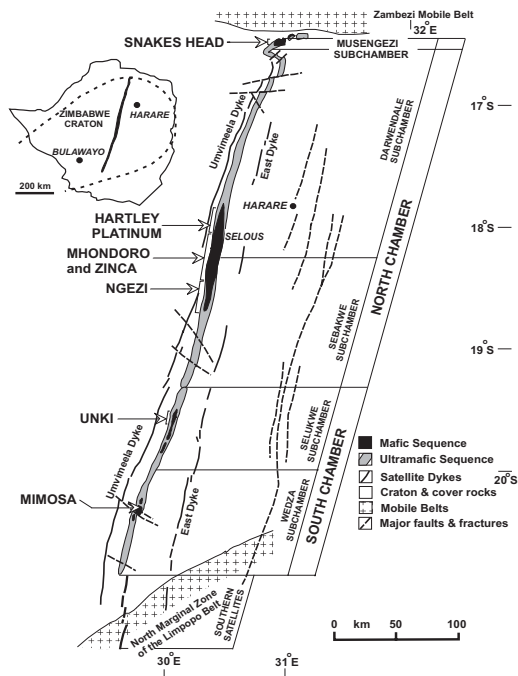


FIG. 19-1. Generalized geological map of the Great Dyke showing the magma chambers and subchambers, and principal mining and exploration areas.

of the mining operation. Hartley Platinum Mine closed in May 1999 due largely to economic reasons and a change of focus by BHP. Current open pit operations mine the MSZ at Ngezi (Fig. 19-1) in a joint venture between Zimplats and Impala Platinum Mines.

GEOLOGICAL SETTING, STRUCTURE AND STRATIGRAPHY

The Great Dyke is a linear NNE-trending intrusion of mafic and ultramafic rocks that transects the Archean rocks of the Zimbabwe Craton (Fig. 19-1). It is bounded by the Zambezi metamorphic belt in the north, and the Limpopo belt to the south, and is 550 km in length and 4 km to 11 km wide (Worst 1960). Satellite dykes are located parallel to the intrusion and are associated with the craton-wide fracture pattern that is postulated to be the main structural control for the emplacement of the Great Dyke (Wilson 1996, Wilson 1987). Precise U–Pb age determinations on zircon (SHRIMP) and rutile indicated an emplacement age of 2579 ± 7 Ma (Armstrong & Wilson 2000, Mukasa *et al.* 1998). A Sm–Nd age of 2586 ± 16 Ma was obtained using both mineral separates and whole rocks (Mukasa *et al.* 1998). Two U–Pb ages were presented by Armstrong & Wilson (2000) giving 2579 ± 3 Ma and 2574 ± 7 Ma. Further SHRIMP U–Pb studies (Wingate 2000) yielded emplacement ages of 2581 ± 11 Ma for zircons and 2574 ± 2 Ma for baddeleyite. These ages contrast with the previously accepted and precise Rb–Sr age of 2455 ± 16 Ma (Hamilton 1977). The most recent U–Pb age determinations (Oberthür *et al.* 2002) give a Great Dyke emplacement age of 2575.4 ± 0.7 Ma.

Two main magma chambers (the North and South Chambers) make up the Great Dyke (Fig. 19-1) and these in turn comprise a series of subchambers recognised on the basis of structure, style of layering and continuity of layers (Podmore & Wilson 1987, Prendergast 1987, Wilson & Prendergast 1989). The North Chamber is subdivided into the Musengezi, Darwendale and Sebakwe Subchambers, and the South Chamber comprises the Selukwe Subchamber and the Wedza Subchamber.

The broad stratigraphic subdivision is an upper Mafic Sequence (gabbro and norite), overlying the well-layered Ultramafic Sequence (dunite, harzburgite and pyroxenite) (Fig. 19-2) (Wilson & Wilson 1981). In the Darwendale

Subchamber that hosts the Hartley Platinum Mine deposit, the Mafic and Ultramafic Sequences are 1200 m and 3000 m thick respectively. The Great Dyke subchambers are similar in structure and are synclinal in shape and have essentially the same lithological sequence. The synclinal nature of the structure results in similar patterns of the layering being exposed approximately symmetrically about the longitudinal axis. The plunge of the layering is to the centers of the subchambers, resulting in the characteristic ‘boat-like’ structures observed for the field distributions of rock types (Worst 1960).

The dominant internal feature of the geology of the Great Dyke is the differentiated layering that is present in all subchambers. Hartley Platinum Mine is located close to the east-dipping west margin of the Darwendale Subchamber and the detailed sequence, as it applies to the Hartley Platinum area (Fig. 19-2), indicates a down-dip facies variation relating to thickness, composition, and types of rock units (Wilson 1996, Wilson & Prendergast 1989). In the area of the Hartley Platinum Mine the dip is 18° to the east. The geological control related to this facies variation is one of the most crucial factors impacting on the exploitation of this ore body. The MSZ is contained within the uppermost differentiated unit of the Ultramafic Sequence in a plagioclase pyroxenite known as the P1 pyroxenite (Fig. 19-2) and is remarkably similar in the broadest terms for all areas of the Great Dyke where it occurs. By virtue of its westerly location within the P1 pyroxenite, Hartley Platinum Mine contains some of the highest PGE grades observed in the Great Dyke (Wilson *et al.* 1989). The PGE grades obtained from exploration sampling supported the present position of Hartley Platinum Mine as a feasible mining proposition.

The Host Rocks to the MSZ and the Enclosing Rock Types

In a broad lithological sense the MSZ is a medium-grained plagioclase orthopyroxenite comprising cumulus granular orthopyroxene (65–99 vol.%) in an interlocking crystal network with interstitial clinopyroxene and plagioclase (combined 1–30 vol.%) and minor amounts of phlogopite, K-feldspar, micrographic intergrowths of quartz with either albite or K-feldspar, spinel, rutile, apatite and zircon (combined <0.5–5 vol.%) (Prendergast & Keays 1989, Wilson 1996, Wilson 2001, Wilson & Prendergast 1989). Plagioclase in the orthopyrox-

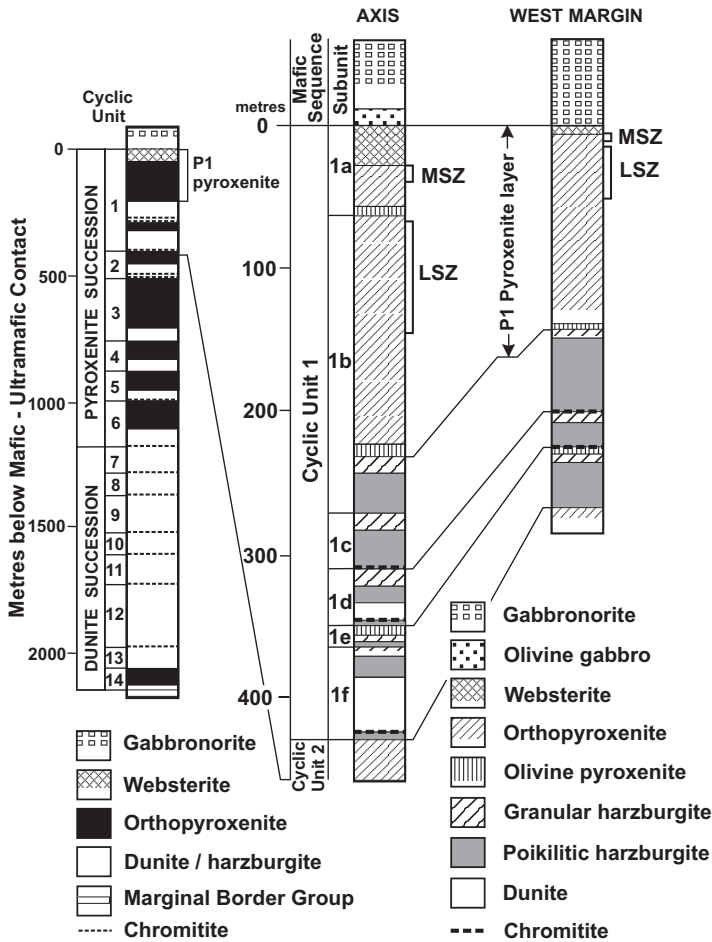


FIG. 19-2. Stratigraphy of the Darwendale Subchamber showing major subdivisions, cyclic units and details of the P1 pyroxenite, host to the PGE mineralized zones. Lateral changes from axis to margin in the vicinity of Hartley Platinum Mine are indicated. Positions of the Main Sulphide Zone (MSZ) and Lower Sulphide Zone (LSZ) are indicated.

enite commonly forms large zoned oikocrysts enclosing orthopyroxene and clinopyroxene crystals, whereas clinopyroxene tends to form either irregular or well-formed megacrysts (Wilson 1992). The pyroxenite grades from almost pure adcumulates in the axis of the Darwendale Subchamber to orthocumulates on the margins. This is a critical feature of the Great Dyke which is best represented in the wide Darwendale Subchamber and is related to the higher rates of crystallization closer to the wall as a result of high heat loss compared with the roof of the intrusion (Prendergast 1991, Wilson & Prendergast 1989).

In the area of the Hartley Platinum Mine in the Darwendale Subchamber, the axial facies is marked by distinct grain-size changes occurring in well-defined layers, which also show changes in mineral fabrics and compositions (Wilson 1992, Wilson & Tredoux 1990). Several narrow layers of olivine-bearing orthopyroxenite (not present in the

smaller subchambers) are developed in the axial facies and die out towards the margins. The orthopyroxenite is overlain by a websterite containing both cumulus clinopyroxene and orthopyroxene. Plagioclase remains interstitial to the pyroxenes and increases in abundance (5–25%) upwards in the succession and on approaching the base of the gabbronorite. The boundary between the orthopyroxenite and websterite is generally well defined, but in the exposed axis of the Darwendale Subchamber the transition occurs by way of series of alternating layers (10–30 cm thick) of fine-grained orthopyroxenite and coarser-grained websterite (Fig. 19-3a). The websterite layers contain sulfide mineralization but the fine-grained orthopyroxenite layers do not. The gabbronorite overlying the websterite is commonly strongly layered (Fig. 19-3b) in the axis of the Darwendale Subchamber and also contains large oikocrysts of olivine (Fig. 19-3b) which produce characteristic

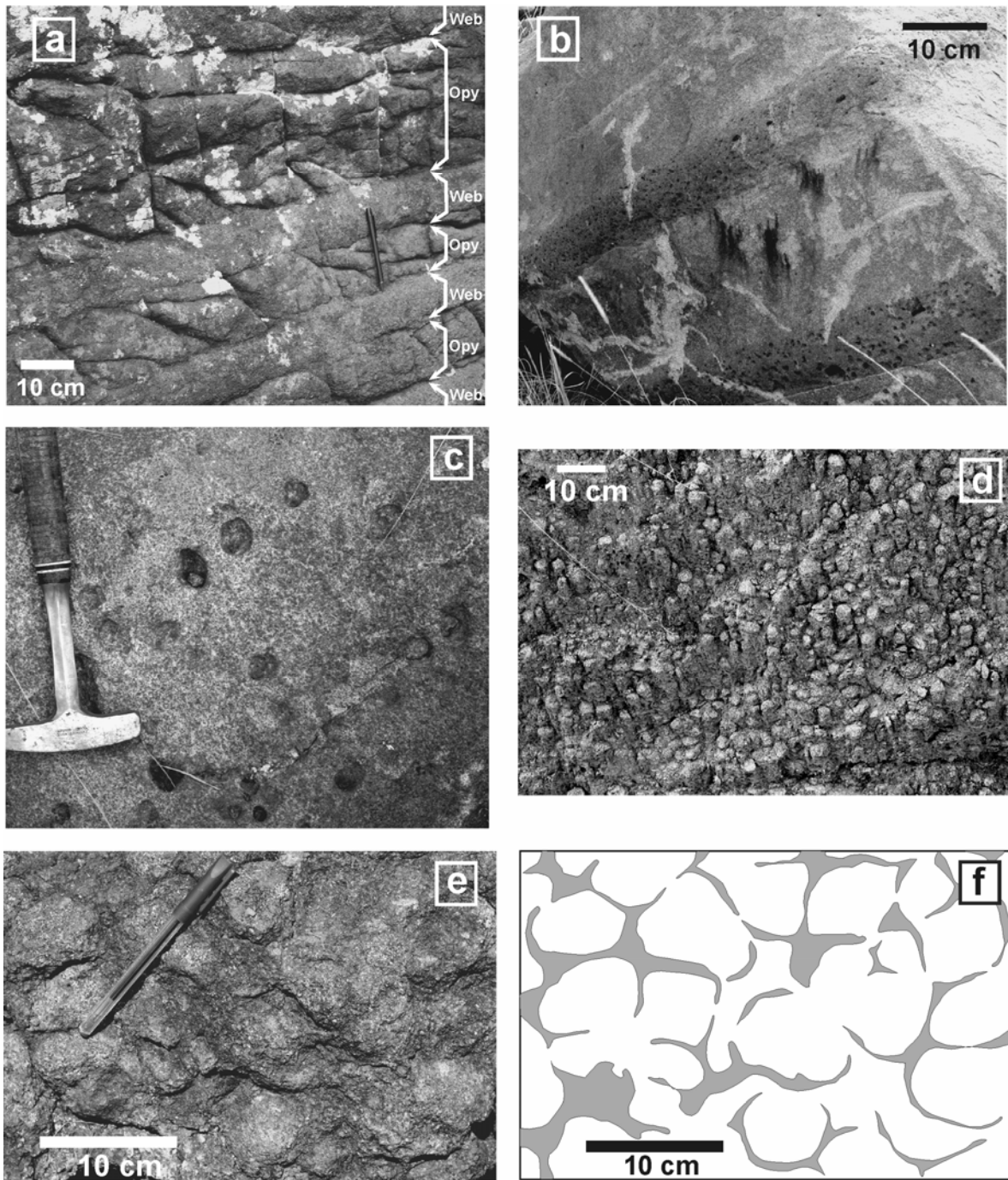


FIG. 19-3. Rock types observed in the vicinity of Hartley Platinum Mine. **(a)** Alternating layering of websterite and orthopyroxenite in the axis of Darwendale Subchamber. **(b)** Olivine gabbro layering in gabbro in the axis of the Subchamber. **(c)** Oikocrystic olivine gabbro in the axis of the Subchamber. **(d)** Thick development of nodular pyroxenite on the east margin of the Subchamber. **(e)** Well-developed nodular orthopyroxenite in the vicinity of Hartley Platinum Mine on the east side of the Subchamber. The light colored oikocrysts of plagioclase are visible. **(f)** The same view as image 'e'. The highlighted zones trace red and green staining from the weathering of sulfide interstitial to the plagioclase oikocrysts.

negative weathering features (Fig. 19-3c). The layered websterite and gabbronorites, and the olivine gabbro die out progressively towards the margins of the Subchamber where these rock types change respectively to a uniform narrow websterite layer and gabbronorite devoid of olivine.

The websterite layer becomes progressively thinner from 35–40 m in the axis to less than 5 m at the margins (Fig. 19-2). In a similar fashion the orthopyroxenite layer thins from 210 m to 120 m. The nature of the orthopyroxenite changes from a sparsely plagioclase-bearing pyroxenite in the axial environment of the Darwendale Subchamber to a true plagioclase pyroxenite at the margins, as well as changing in thickness. These characteristics further emphasize the strong lateral controls in the magma chamber.

Distribution of Sulfide in the MSZ

The amount of sulfide in the MSZ is variable and in some occurrences can be as high as 10%, but it is usually about 2.5% by volume. The dominant sulfides are (in order of decreasing abundance) pyrrhotite, pentlandite, chalcopyrite and pyrite. There is a general tendency in the MSZ for a vertical mineralogical zonation with the Fe–Ni sulfides appearing lower in the sequence and Cu sulfides higher up (Coghill & Wilson 1993, Oberthür *et al.* 1997). The same zonation is seen on a within-sample scale. Pentlandite and pyrrhotite are commonly intergrown, or pyrrhotite forms the core of the sulfide association and these sulfides are mantled by chalcopyrite. Chalcopyrite also has a tendency to be distributed as veinlets between and within silicate mineral crystals.

Where the abundance of sulfide is low (<0.1% by volume) it occurs as small ragged grains usually located at, or close to, grain boundaries of the silicate minerals. As the abundance increases, concentrations of interconnected sulfide develop, eventually forming locally developed net-textured sulfide. The sulfide is also interstitial to the orthopyroxene and tends to concentrate on the boundaries of the plagioclase oikocrysts resulting in characteristic weathering that highlights the heterogeneous distribution of sulfide (Wilson 1992). The association of the resistant plagioclase oikocrysts (3–8 cm in diameter) and the sulfide produces a unique weathering feature, which characterizes this nodular pyroxenite in outcrop (Fig. 19-3d & e). The plagioclase pyroxenite nodules are commonly surrounded by red and green

staining from the oxidation of the sulfides (Fig. 19-3f).

This local distribution of sulfide in the mineralized nodular pyroxenite has important implications for the evaluation of drill core sampling and reproducibility of assay data. Much of the 1970s drilling used BQ core (38 mm diameter) for which the standard practice was to use half or even quarter core, 10–15 cm in length, for assays. The reported poor reproducibility of the assays may at least in part be attributed to the inhomogeneous distribution of sulfide controlled by the primary silicate textures. The BHP data is based on 55 mm diameter NQ core which was assayed in half core samples 15 cm in length.

PGE and Base Metal Mineralization in the MSZ

The MSZ contains the PGE (Pt, Pd, Rh, Ru, Ir and Os), Au and Ag, and the base metals Co, Cu and Ni as a stratabound zone 1 m–3 m thick, located entirely within plagioclase pyroxenite, and close to or overlapping the boundary between the plagioclase pyroxenite and the overlying plagioclase websterite layer (Fig. 19-2). The PGE are associated with sulfide and are mainly concentrated in the lower part of the MSZ, called the PGE-Subzone (PSZ); an upper part enriched in base metals is called the Base Metal Subzone (BMSZ). This gives rise to the broad subdivisions within the MSZ (Fig. 19-4) based on the distinct zones of metal enrichment. For the entire mineralized zone, Cu and Ni distributions show a strong correlation with sulfide content for all samples analyzed (Fig. 19-5a) and is similar to that observed in other areas of the Great Dyke (Wilson *et al.* 2000). The separation of the various PGE peaks (Fig. 19-4), their different distributions in the vertical profile, lack of direct correspondence between PGE and sulfide distributions, and the absence of distinct markers in the plagioclase pyroxenite (such as the narrow chromitites in the Merensky reef and the distinct footwall), pose challenges for the successful mining of the MSZ.

The MSZ in the exploration and mining sense is the metal-rich interval that is economic, and in this study is defined as that interval represented by a contiguous set of samples each of which has ≥ 2 ppm for Pt, Pd, Rh and Au combined (total gravimetric prill analysis for total PGE plus Au, and expressed hereafter as 4T PGE).

Relative dependence of S and Cu in the MSZ forms a less well defined relationship (Fig.

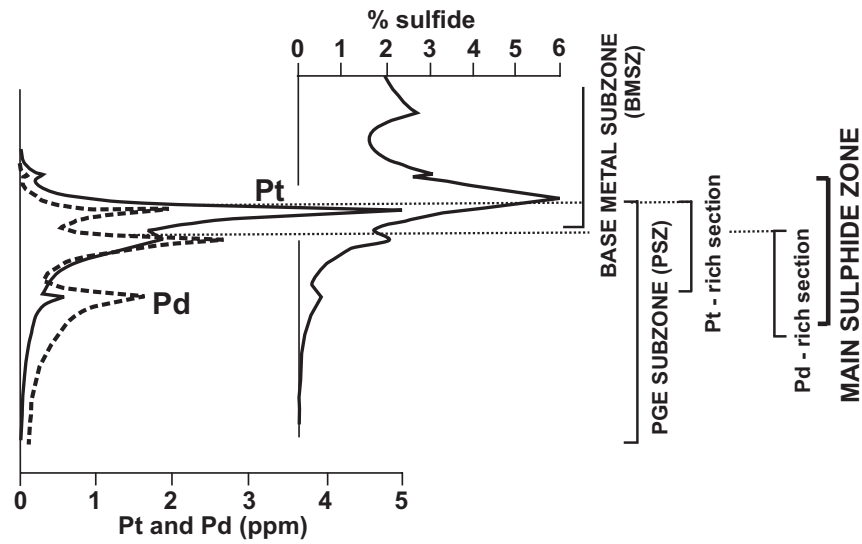


FIG. 19-4. Generalized pattern of the distributions of Pt, Pd and sulfide in the Main Sulphide Zone (MSZ), together with subdivisions of the ore zone into the PGE-Subzone (PSZ) and base metal subzone (BMSZ) and the sections of Pt and Pd enrichment.

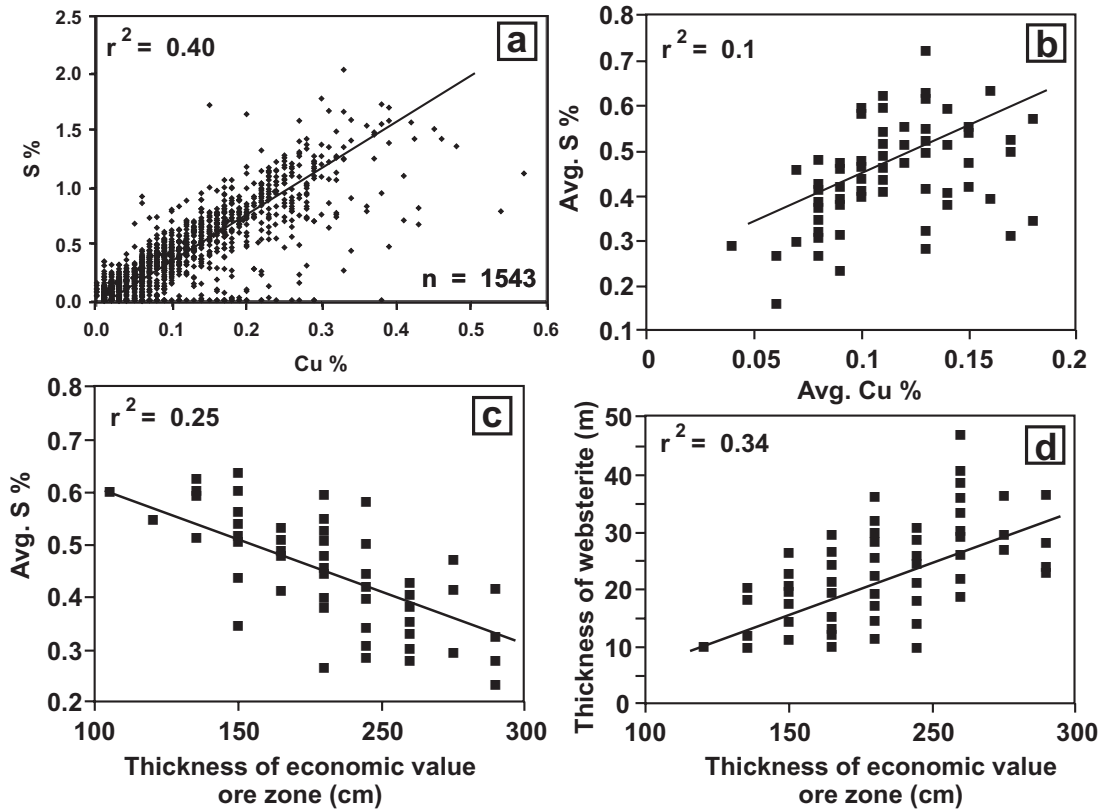


FIG. 19-5. Mutual dependencies for several parameters related to the MSZ. (a) Data derived from all drill core data show the dependence between average wt.% Cu and wt.% S. (b) Dependence between wt.% Cu and wt.% S for the economic zone of the MSZ defined by the cut-off sample values of ≥ 2 ppm total PGE plus Au for each drill core. (c) Dependence of sulfide content (expressed in terms of wt.% S) for the economic ore zone defined as samples with ≥ 2 ppm total PGE plus Au. (d) Relationship between thickness of websterite and width of the economic ore zone.

19-5b), compared with the entire mineralized zone indicating that some decoupling has taken place between Cu and sulfide, where sulfide is abundant. However, there is also a clear dependence between the average S content for all drill core intersections and the thickness of the MSZ (Fig. 19-5c) with thicker reef having lower average sulfide contents. A further relationship is the correspondence of the thickness of the MSZ and the overlying websterite layer (Fig. 19-5d).

A second zone of sulfide-associated platinum mineralization occurs stratigraphically below the MSZ and is called the Lower Sulphide Zone (LSZ). The LSZ is generally thicker (10–60 m depending in locality) than the MSZ but is considerably lower grade and remains relatively poorly characterised. At present it is not economic, but it is an important potential PGE resource.

Platinum Group Mineralogy of the MSZ

Platinum group minerals (PGM) are generally very fine grained and occur as minute inclusions (on average about 20 μm) within sulfides (Johan *et al.* 1989) in the size range of <5 μm to 50 μm . Occasionally larger grains up to 250 μm in diameter are observed (Oberthür *et al.* 1998). The PGM species are dominated by Bi and Te bearing minerals with the order of crystallization of the PGM assemblage (Johan *et al.* 1989) being michenerite [PdBiTe], merenskyite [(Pd,Pt)(Te,Bi)₂], moncheite [(Pt,Pd)(Te,Bi)₂], melonite [(Ni,Pd,Pt)(Te,Bi)₂], hessite [Ag₂Te], volynskite [AgBiTe₂], rucklidgeite [(Pd,Ag)Bi₂Te₄], altaite [PdTe], sperrylite [PtAs₂], hollingworthite [RhAsS], gesdorffite [(Ni,Co)AsS], and electrum [Au,Ag]. The order in which the minerals appear in the succession indicates that Pd precedes Pt (in keeping with the PGE profiles) whereas Pb and Ag are concentrated above the PGM peak. Arsenides appear late in the succession and the final stages are characterized by Se-bearing minerals (Johan *et al.* 1989). Other PGM reported from the Hartley deposit include cooperite, braggite, vysotskite [(Pt,Pd,Ni)S], laurite [RuS₂], and irarsite [IrAsS] (Oberthür *et al.* 1998). Detailed textural studies of the PGM were carried out on the Unki (Coghill & Wilson 1993) and Mimosa deposits (Prendergast 1990) and they are similar to those reported for the Hartley deposit.

Sulfide minerals in the MSZ of the Hartley deposit contain significant amounts of PGE (Johan *et al.* 1989) with pentlandite and chalcopyrite

containing up to 0.15 wt.% Pt and 0.2 wt.% Pd respectively. Ion-probe studies (Oberthür *et al.* 1997, Oberthür *et al.* 1998) show the presence of significant concentrations of PGE in sulfides. Similar results have been found for the Mimosa deposit (Weiser *et al.* 1998) with Pd in pentlandite exhibiting a systematic decrease upwards from the base of the PGE-Subzone.

Nature of the MSZ at Hartley Platinum Mine

The MSZ in the area of the Hartley Platinum Mine was investigated using high quality data arising from the final phase of the diamond-drilling program as well as that from underground sampling. This provides a basis for understanding exploration approaches in the Great Dyke, and other intrusions of this type. The positions of the drill holes, as well as of selected holes used in more detailed treatment are shown in Fig. 19-6. These drill holes represent both the initial grid-based drilling and the later infill drilling by BHP. An important aspect illustrated in this diagram is the distribution of the drilling array in relation to the geometry of the Darwendale Subchamber. The southerly plunge of the Subchamber results in the exposure of the MSZ being located progressively closer to the margins of the Great Dyke towards the south. Hartley Platinum is located in that part of the Subchamber where it becomes physically narrower to the north and therefore parallel axial trend lines (Fig. 19-6) intersect the margin. The combination of the facies changes in relation to the relative margin-axis position, as well as the change in the shape of the Subchamber are factors that need to be considered in an exploration model. The data therefore potentially provide information on the down-dip variation as well as controls that may result from the shape and cross-sectional area of the Subchamber.

The subchambers in the South Chamber of the Great Dyke which also contain the MSZ (Wedza and Selukwe Subchambers) have considerably smaller volumes than the Darwendale Subchamber, and the lithologies overlying the MSZ are also more deeply eroded (Wilson 1996, Wilson & Prendergast 2001). The result is that in these areas the only preserved occurrences of the MSZ are in the axial environments, but at the same time the relatively small volumes of these Subchambers has imposed textural and lithological characteristics similar to the marginal facies observed in the Darwendale Subchamber (Prendergast 1991, Wilson *et al.* 2000).

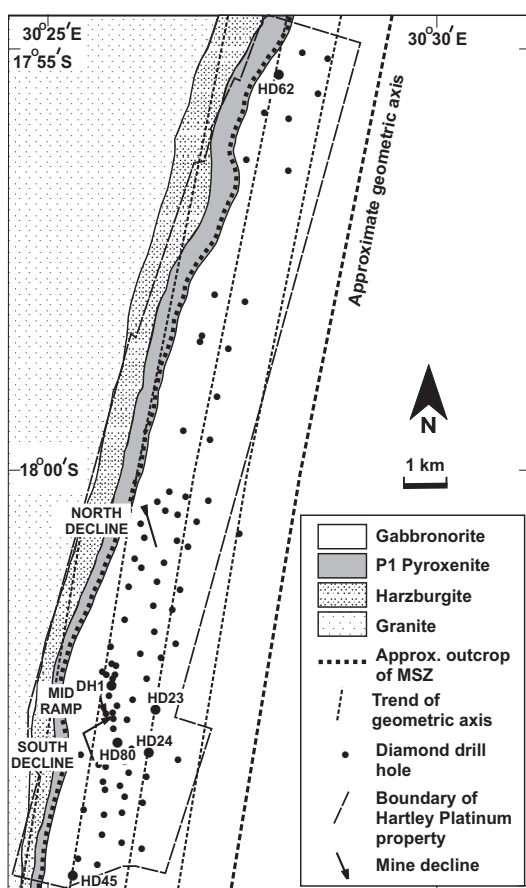


FIG. 19-6. The Hartley Platinum Mine property on the west margin of the Darwendale Subchamber, and the location of drill holes. Labelled drill holes are those used in more detailed analysis. Declines to the underground operations are marked. Also shown is the axis of the Subchamber and the trend lines to the axis. The approximate position of the MSZ is marked.

PGE Distribution in the Ore Zone

Stratigraphic PGE distributions in a single borehole

One drill core (DH-1) was selected for detailed geochemical and petrological study and was analyzed over a wider vertical interval, above and below the MSZ, and at higher precision than that carried out for the exploration drilling program. It is used as a type section to compare the entire data base comprising 80 drill core intersections and over 1500 samples analyzed. The PGE distribution pattern in the MSZ is generally similar throughout the Great Dyke. Specific data points are labelled (Fig. 19-7a) to highlight domains in the profile for Pd. The concentrations of all PGE rise gently from the footwall (Fig. 19-7b) and after reaching peak

values, decrease rapidly in the hanging wall. The fall-off of Pt is particularly sharp. The Pt and Pd peaks are displaced, and both elements have quite different profiles. Au tends to follow Pt but falls away far more gently in the hanging wall with appreciable values coinciding with the base metal peaks (Fig. 19-7c). In this section the Ni, Cu and S peaks coincide with the Pt peak, but this is somewhat unusual compared to the most common situation where base metals peak at least one sample width above Pt. Minor peaks for Au coincide with base metal peaks in the MSZ.

The different metal distributions therefore give rise to highly contrasting patterns for the ratios of PGE and for PGE/S ratios. Controls on PGE ratios in layered intrusions are not fully understood but may reflect distinct compositions in the primary magmas that gave rise to the deposit (Naldrett 1989). Values for Pt/Pd (Fig. 19-7d) remain essentially constant in the PGE-Subzone (PSZ), rise rapidly to coincide with the Pt peak and then drop off gently through the hanging wall by way of a series of peaks. The ratio of Pt/Au (Fig. 19-7d) also remains relatively constant in the lower PSZ and peaks at a level below the Pd peak position and then falls off sharply in the upper PSZ. The ratio of Au/S (Fig. 19-7e) peaks at a position roughly coincident with the maximum of Pt, whereas Pd Pt/S and Pd/S (Fig. 19-7f) both reach maxima below the Pd peak position.

The consistency of these distributions over wide areas is important in defining the nature of the ore zone as well as having implications for the origin of the MSZ. The positions of PGE peak values do not always coincide with those of sulfide and base metals and therefore may indicate a series of mineralizing events rather than a continuous process relating to the onset of sulfide precipitation, or to transport of the PGE by upward migrating fluids (Boudreau & McCallum 1992).

Inter-element Variations for the Data Set

Interdependency between the PGE, Au and base metals for the entire data set was ascertained on the basis of two-element variation diagrams. While such variation diagrams may encompass all the elements analyzed, two examples are given: Pd vs. Pt and Pd vs. Au (Fig. 19-8). These are shown respectively as individual data points in Figs. 19-8a and 19-8c, and with fields of point densities delineated in Figs. 19-8b and 8d. Superimposed on the fields are the specific data points for the drill

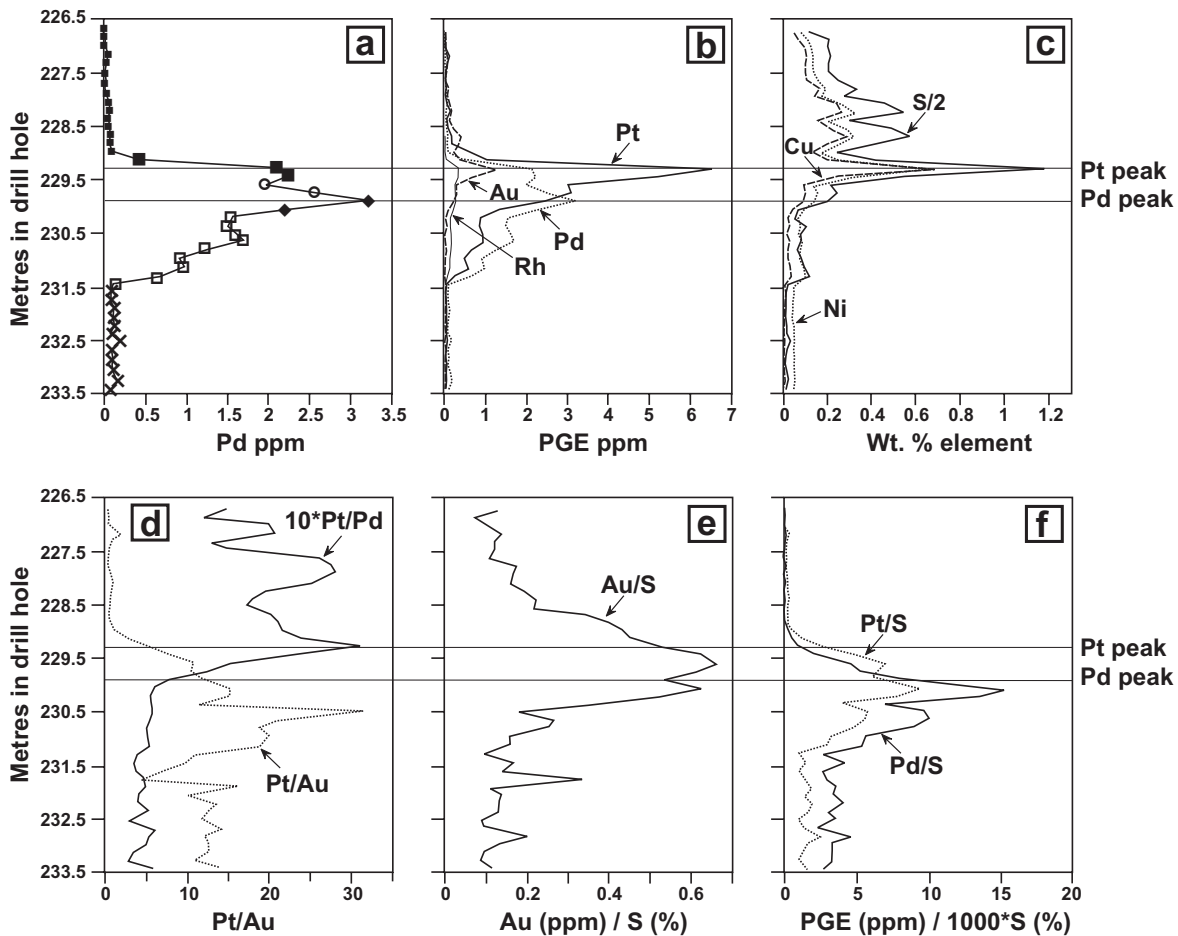


FIG. 19-7. Distribution of PGE, S and base metals, and element ratios in drill core DH-1. (a) Variation of Pd through the mineralized zone as well as the hanging wall and footwall. Different symbols delineate specific intervals in the metal distributions used in subsequent illustrations. (b) Distribution of Pt, Pd, Rh and Au in ppm. (c) Distribution of Cu, Ni and S. (d) Variation of the ratios Pt/Pd and Pt/Au. (e) Variation of Au/S. (f) Variations of Pt/S and Pd/S.

core DH-1 studied in detail using the same symbols as in Fig. 19-7a. At least six domains are clearly recognizable when all elements are considered, and these are related to the detailed stratigraphic section shown in core DH-1 (Fig. 19-7). Data distributions for the different domains have generally linear arrays but also commonly show sharp changes in slopes.

Considering the area represented, and the lateral change of MSZ thickness from ~1 m at the margin to ~3 m at the axis (Fig. 19-2), the distributions are remarkably consistent. This contrasts with the much more variable Merensky reef of the Bushveld Complex which, although having more clearly defined lithologies and metal variations, cannot be extrapolated in detail from one section to the next (Wilson & Chunnnett, in press). This suggests the operation of a highly regular

process in the Great Dyke extending over wide areas. Such regular patterns and distributions are unlikely to have resulted from fluid migration controls on the mineralization (Boudreau & Meurer 1999). They are equally unlikely to have been the result of a progressive separation of metals by the continuous scavenging of PGE by magmatic sulfide (Prendergast & Wilson 1989) as a single mineralizing event. It is most likely that the PGE were concentrated in sulfide during a sequence of distinct mineralizing events relating to changes in the magmatic system.

Regional Controls on PGE distribution in the MSZ

It has previously been reported (Wilson 1992, Wilson & Prendergast 2001, Wilson & Tredoux 1990) that the thickness of the MSZ changes

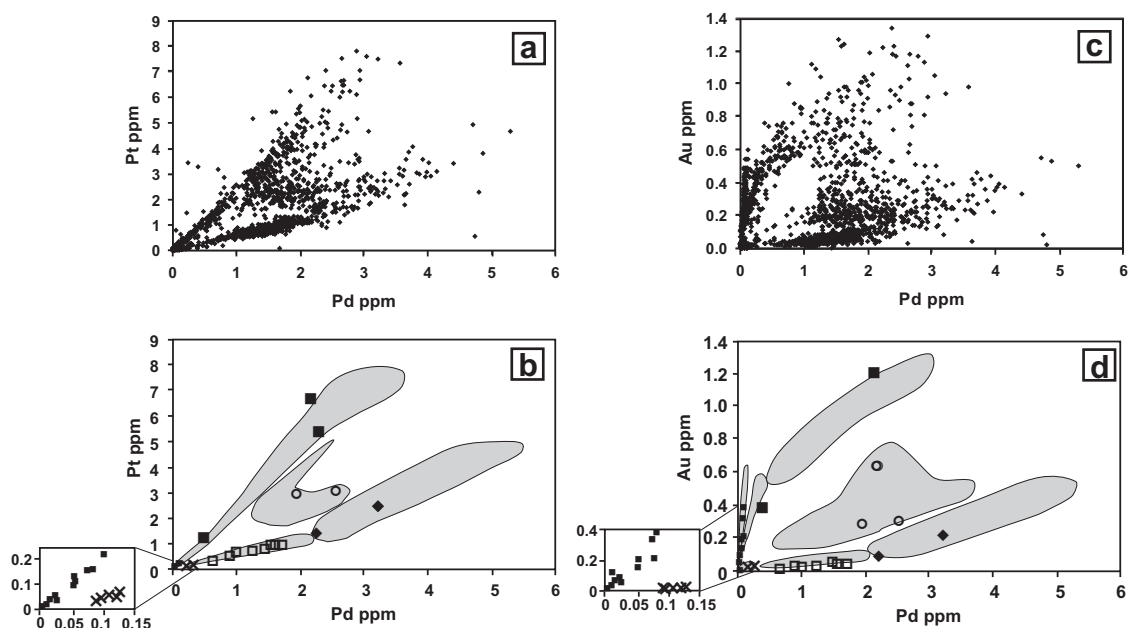


FIG. 19-8. Interdependence of Pt, Pd and Au for all samples. Composition fields are reconciled against the detailed section of DH-1 in Fig. 5. (a) Pt vs. Pd for all samples. (b) Highlighted areas for the main data concentrations for Pt vs. Pd with specific points related to parts of the ore zone stratigraphy from DH-1 in Fig. 19-7a. (c) Variations for Au vs. Pd for all samples. (d) Highlighted areas of data concentration together with specific symbols from DH-1. The insets to (b) and (c) show details for the low-level concentrations.

laterally in the Great Dyke, becoming thicker in the axial zone compared to the margins. This variation was further investigated in the present study as related to the economic value zone defined for that interval in which all samples have ≥ 2 ppm 4T PGE. The variation of sulfide content relative to thickness of the economic value zone has already been considered (Fig. 19-5c). Variations of average PGE values for the MSZ relative to thickness of the economic value zone are shown in Fig. 19-9. Pt (Fig. 19-9a), Au (Fig. 19-9b) and Rh (Fig. 19-9c) exhibit well defined relationships whereas Pd (Fig. 19-9d) has a poor dependence on thickness of the economic value zone because a significant proportion of Pd occurs in the lower part of the PGE-subzone, which was excluded by the 2 ppm 4T PGE cut-off. Ni (Fig. 19-9e) has a relatively high degree of dependence on thickness of the economic value zone whereas that for Cu (Fig. 19-9f) is low. This is the result of Cu being concentrated higher in the MSZ compared with Ni, and therefore not being completely represented in the economic value zone. The average 4T PGE value ≥ 2 ppm (Fig. 19-9g) has a relatively high level of dependence because of the dominance of Pt in this metal budget. Metal ratios, such as Pt/Pd (Fig. 19-9h), exhibit no

observable dependence on MSZ thickness.

While a clear dependence of the average concentrations of the metals with the thickness of the economic value zone is demonstrated, there is considerable scatter of the data which arises from restricting the data only to the economic value zone. This in itself indicates the variability of the ore zone which arises because of the marked lateral changes.

Cumulative PGE Contents

Cumulative metal contents through the mineralized zone (from the base upwards) are represented by curves that indicate the different zones of concentrations of the metals in the sequence. These curves level off at a position above which there are no further effective concentrations of the elements of interest. The cumulative metal contents can be expressed as a percentage for each individual element. Similarly, the positions of every sample can be expressed on a relative % basis through the zone. The uppermost sample in the zone of interest is at 100%. For the detailed section of DH-1 (Fig. 19-10) the positions of the curves indicate the relative stages where the PGE are enriched in the economic value zone. The sequence of enrichment from the base upwards is Pd–Pt–4T–Au–Cu. The Pd

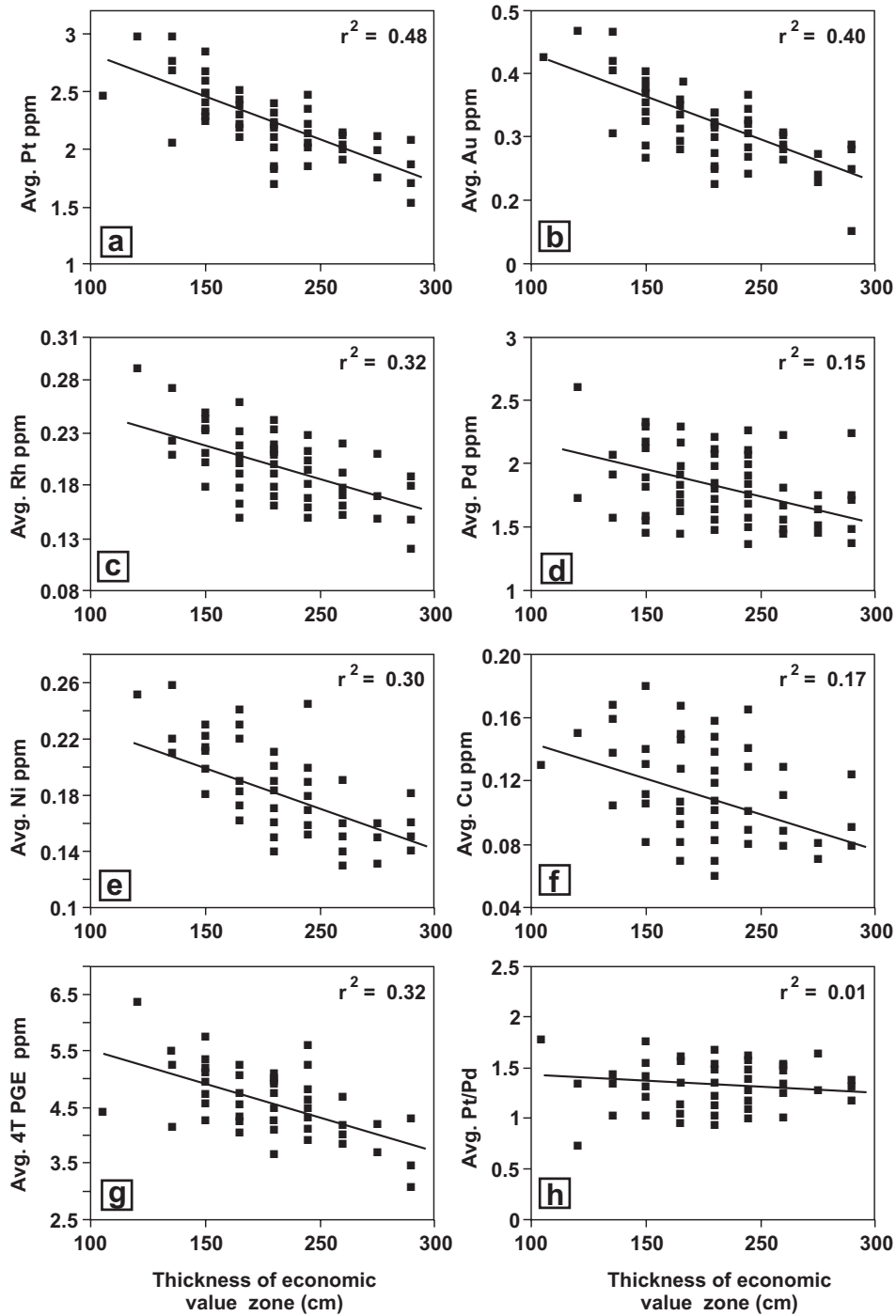


FIG. 19-9. Variation of average PGE and Au concentrations for each drill hole intersection related to the width of the MSZ economic value zone as defined by the cut-off value of 4T PGE ≥ 2 ppm. r^2 is the correlation coefficient. (a) Variation of Pt has a strong dependence because of its complete incorporation in the ore zone interval. (b) Variation of Au. (c) Variation of Rh. (d) Variation of Pd exhibiting relatively poor dependence because of its incomplete incorporation in the ore zone interval as a result of part of the Pd budget remaining in the footwall below the cut-off limit. (e) Variation of Ni. (f) Variation of Cu exhibiting relatively poor dependence because part of the base metals budget remains in the hanging wall below the 4T PGE ≥ 2 ppm cut-off limit. (g) Variation of total PGE and Au within the cut-off limits as 4T PGE ppm. (h) Variation of Pt/Pd which shows little dependence on width of the ore zone.

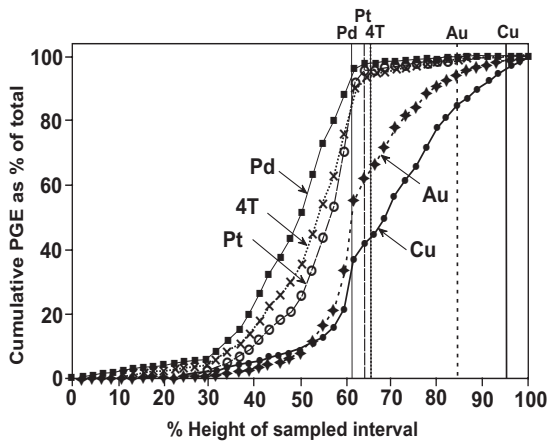


FIG. 19-10. Cumulative metal contents from the base of the sampling interval upwards for drill core DH-1 represented as a percentage of the total of each metal. The metal enrichment is progressive in the order of Pd, Pt, 4T PGE, Au and Cu. The 4T PGE are the combined metals Pt, Pd, Rh and Au.

budget is effectively accounted for at the 62% mark (measured from the lowest sample position), Pt at 64%, 4T at 66%, Au at 84% and Cu at 97%. Slight irregularities in the curves for Au and Cu reflect the stratigraphically higher sulfide peaks.

A similar exercise can be carried out for the cumulative metal content (expressed in ppm) and limiting the thickness of the zone to the footwall and hanging-wall 4T PGE cut-off levels of 2 ppm. Six examples are shown representing the different reef types, with distributions shown for 4T and Pt PGE (Fig. 19-11a and b). Cores with thicker economic value zones (thick reef types) are HD-23 and HD-24 and those representing sections with thin economic value zones (thin reef types) are DH-1 and HD-45. Cores HD-80 and HD-62 are intermediate to these two types. The thick reef types have higher cumulative metal contents as well as showing a more even build-up upwards from the

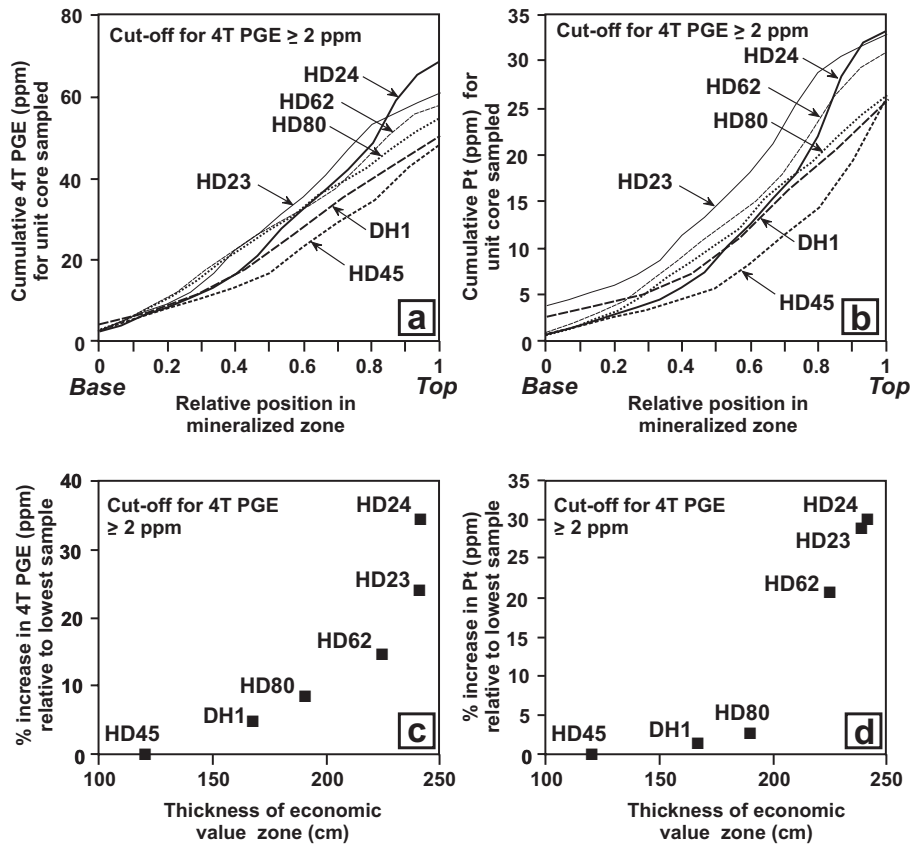


FIG. 19-11. Cumulative metal curves for six drill core intersections reflecting the range from narrow to thick reef type as defined by the cut-off values 4T PGE \geq 2 ppm. The thicker reef types are HD-23 and HD-24 and thinner reef types are DH-1 and HD-45. Intermediate reef types are HD-62 and HD-80 (a) Cumulative curves for 4T PGE metals. (b) Cumulative curves for Pt. (c) Plot of percentage increase in 4T PGE metal values relative to HD-45 in relation to width of the ore zone. (d) Plot of percentage increase in Pt values relative to HD-45 in relation to width of the ore zone.

footwall. Core HD-24 has a relatively slow build-up at the base. The relationship of metal contents to thickness of the economic value zone is best illustrated by plotting the percentage difference for each section relative to that of the lowest metal content for the set of examples given (HD-45). The relative metal enrichment of the other sections can therefore be compared within the cut-off thickness of the ore zone (Fig. 11c and d). A systematic variation is observed with a relative maximum enrichment of over 30% for both Pt and 4T PGE for the thick reef types. Thus in spite of the lower grades and lower average per-sample metal concentrations, the thicker reef types have a higher relative total metal content.

MINING GEOLOGY AT HARTLEY PLATINUM MINE

Hartley Platinum Mine was the first large-scale attempt at mining the MSZ. The mining method developed as a direct result of the exploration and therefore brief consideration is relevant in this context. The mine consists of three decline shaft systems (Fig. 19-12) that penetrate the western margin of the gabbronorite of the Mafic Sequence, the underlying plagioclase websterite, and plagioclase orthopyroxenite of the P1 pyroxenite. Access to the mine is by way of a twin decline system developed at -11° , with one carrying the conveyor belt and chairlift systems, and the other serving as a trackless vehicle and material roadway. The declines access footwall strike haulages developed at approximately 15 m vertically below the MSZ, and at an inter-level spacing of 58 m (giving a stope back of about 180 m). Crosscuts were developed normal to the

haulages at 108 m spacing in the downdip direction, and these intersect the MSZ from which point in-stope raises (updip) and winzes (downdip) were developed. Advance strike gullies (ASGs) were then developed from the raises and winzes at 12° updip of strike at an apparent dip of $+3.6^\circ$, and at a center-to-center ASG spacing of 30.5 m. The ASGs were developed as the access ends to the 25 m long breast panel mining stopes, established on the updip side of the ASGs (Fig. 19-12).

Hartley Platinum Mine operated a scattered breast stoping layout, where ASGs and panels were mined from a raise-winze connection in one direction only, with panels finally terminating against a 6 m wide dip-rib pillar left against the adjacent raise-winze connection. The one-way breast configuration was adopted primarily for rock mechanics reasons.

Grade Control

Although the MSZ falls into the category of a magmatic stratabound ore deposit it is not clearly delineated by distinct marker horizons or lithological changes. The entire mining environment is a relatively uniform (from the mining perspective) plagioclase pyroxenite, from well beneath the footwall to a few metres above the MSZ, and there are no lithological distinctions to assist with location of the economic value zone (Fig. 19-13). At the same time the relative changes in metal concentrations are significant, particularly at the transition from the PGE-Subzone to the Base Metal Subzone (Fig. 19-4). Therefore the potential for dilution with non- or poor-mineralized rock is high.

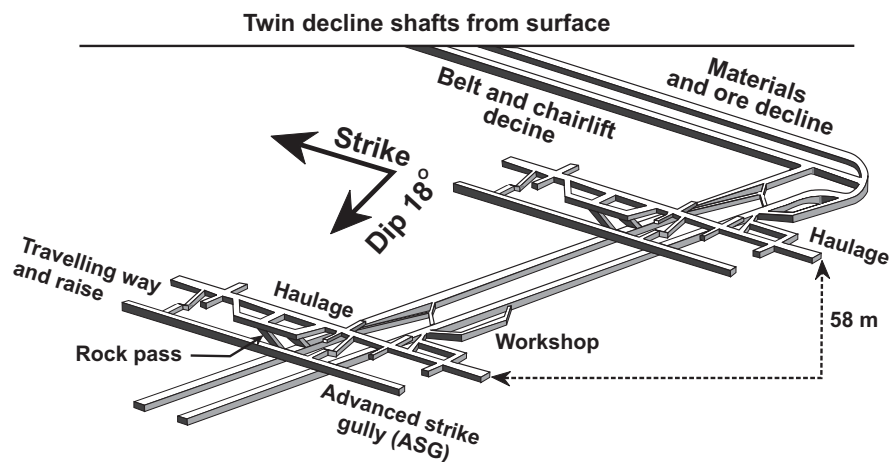


FIG. 19-12. Decline and footwall haulage layout of Hartley Platinum Mine.

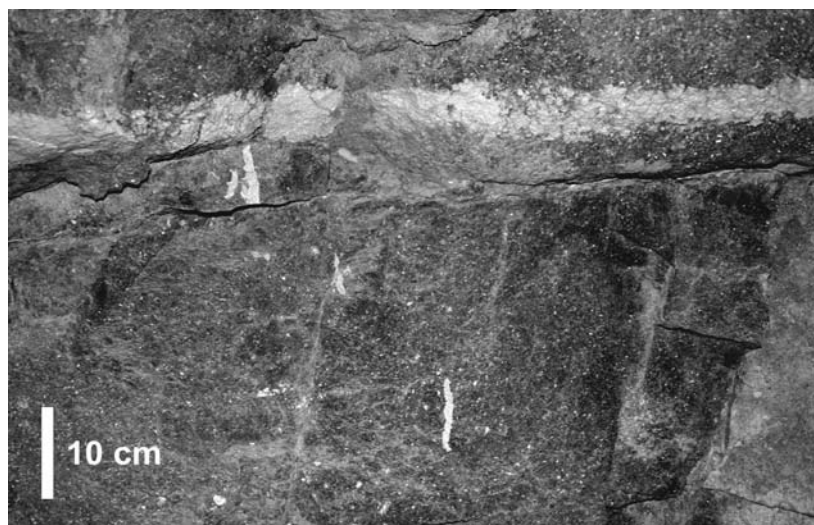


FIG. 19-13. Typical view of the mining face in the MSZ with the painted line marking the base of the Base Metal Subzone (BMSZ) and used as the datum for all sampling.

This is further complicated by the sequential enrichment of metals upwards from the base of the economic value zone as described previously, with the order being Pd, Pt + Rh and then Au. Base metals are concentrated above Au.

In an ore body where the economic zone is commonly of variable visibility underground (in relation to sulfide development) it is essential to have a well-designed and effective grade control system. The visibility is dependent on the small-scale distribution of sulfide, low levels of alteration, and the proximity of joints and secondary structures. It also depends on the extent to which the rock face has been cleaned. Central to the issue of recognition of the economic zone is the relation of sulfide to the PGE distribution. It has been emphasised in the previous section that the peak PGE concentrations occur at, or close to, the zone of maximum sulfide development but *most* of the metal content is contained *below* this zone. Except at the very base, the BMSZ is effectively devoid of PGE (Fig. 19-4). The crucial issue of grade control in the MSZ is the distribution of the value metals (PGE) in relation to the only visible marker, that being the sulfide.

In practice, the highest stoping grades at Hartley Platinum were achieved by mining a 90 cm stope width at an optimum cut of 30 cm above the stratigraphically lowest appearance of abundant visible sulfide at the base of the BMSZ and 60 cm below this datum, thereby incorporating the highest values in the PGE-Subzone. This datum, the only

stratigraphic control within the value zone at the base of the BMSZ, was represented by a yellow line painted on the panel faces (Fig. 19-13). It was identified visually and checked geochemically by quick turnaround (24 hr) chip samples (see below). Due to the tonnage build-up an average stope width of 105 cm was selected to incorporate respectively 30 cm above, and 75 cm below the base of the BMSZ. The relatively low, and progressively depleting hanging wall PGE grades required careful control on the stope hanging wall, as any overbreak or falls of ground would have negatively impacted on stope grade because of the dilution factor of non-mineralized rock. The most effective grade control was to set a standard hanging wall cut of 30 cm above the base of BMSZ, and any optimum cut changes were taken up by altering the less critical footwall cut.

Marking the BMSZ

Due to the difficulty in MSZ reef identification, all raise, winze, ASG and panel faces were cleaned with powerful water jets prior to drilling and blasting cycles after which the base of the BMSZ was painted with a yellow line (Fig. 19-13). The procedure required careful identification of the distribution of the sulfide on the mining face. This served as the zero reference, or stratigraphic datum, from which mining markings and panel measurements were made. The base of the BMSZ was seldom visible along the entire length of any end, particularly in panels, but

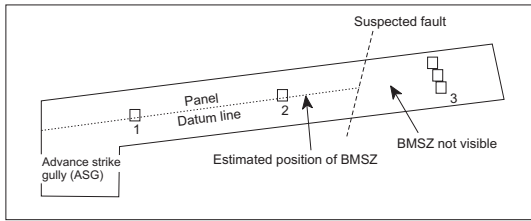


FIG. 19-14. Example of the chip sampling strategy as applied to a panel at Hartley Platinum Mine. Samples 1 and 2 were taken routinely above the base of BMSZ where sulfide was most visible to check on reef position. Sample suite labelled 3 represents the strategy in areas of poor sulfide visibility. From the combination of PGE and base metal values it was possible to ascertain 'off-reef' situations and whether the face was located in the hanging wall or footwall.

extrapolation was usually possible between areas of clearer recognition. Once this exercise had been completed blast hole marking and drilling could proceed.

Chip sampling

Where the base of the BMSZ was visible, sampling took the form of hand-specimen-sized samples chipped off the face before each drill and blast cycle at a position directly above the yellow BMSZ line, over a 0 cm–15 cm interval. The samples were treated on a priority 24 hour turnaround basis and were analyzed for 4T PGE, Ni and Cu. In addition, three samples were taken in each panel, at the top, middle and bottom. In raises (and pre-developed ASGs) a single sample was similarly taken immediately above the BMSZ at the center of the excavation (Fig. 19-14). The samples served as immediate checks to confirm the 'on-reef' status of each panel and in-stope development end. If any sample did not indicate 'on-reef', the combination of PGE, Ni and Cu grades made it possible to identify whether that sample was located on the hanging wall or footwall to the MSZ. For example a sample with < 0.5 ppm 4T PGE with high Ni and Cu grades would indicate hanging wall in the BMSZ, and a sample with both low Ni and Cu grades and low PGE, would represent footwall, i.e. below the base of the BMSZ.

Where peak sulfide (corresponding to the base of the BMSZ) was not visible, either along an entire panel, or portion thereof, appropriate positions along the panel were selected and three chip samples in a vertical arrangement were taken across the suspected locality of the BMSZ (Fig. 19-14). These samples were extremely important in

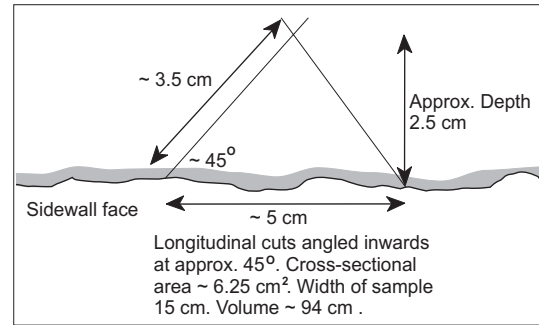


FIG. 19-15. Section view of the V-cut channel sampling method.

the grade control process in that, due to the remarkably consistent PGE and displaced Cu and Ni profiles, they could be located to within 15 cm of the base of the BMSZ. This technique was also commonly used to evaluate displacement of the MSZ due to minor faulting.

Channel sampling

Underground channel sampling consisted of sections of continuous samples cut normal to layering from the sidewalls of raises, winzes and ASGs, and were primarily used for continuous on-mine evaluation. Such sampling was routinely carried out in all these ends at either 5 m or 10 m spacing depending on reef visibility and structural complications. Channels were cut using the V-cut method (Fig. 19-15) and consisted of four 15 cm wide samples above the BMSZ reference line, and eight 15 cm wide samples below (Fig. 19-16). Each channel received a unique borehole-type number, with the samples further identified using a sequential 'Z' grade control reference number system.

The sample containing the highest sulfide at the base of the BMSZ was always numbered Z16 (reference sample), with samples above it identified in decreasing order, (i.e. Z15, Z14 etc), and in increasing order from the base of the BMSZ down (i.e. Z17, Z18 etc) (Fig. 19-16). This provided additional stratigraphic control on the sampling and associated grade control exercises. Samples were analyzed for Pt, Pd, Rh, Au, Ni, Cu and S, and from the grade control reference numbers the relative stratigraphic position of each was readily apparent. In cases where the Z16 reference sample had apparently been incorrectly positioned this was easily corrected by referring to the S analysis, which geochemically indicated the base of the BMSZ. As well as for routine evaluation purposes,

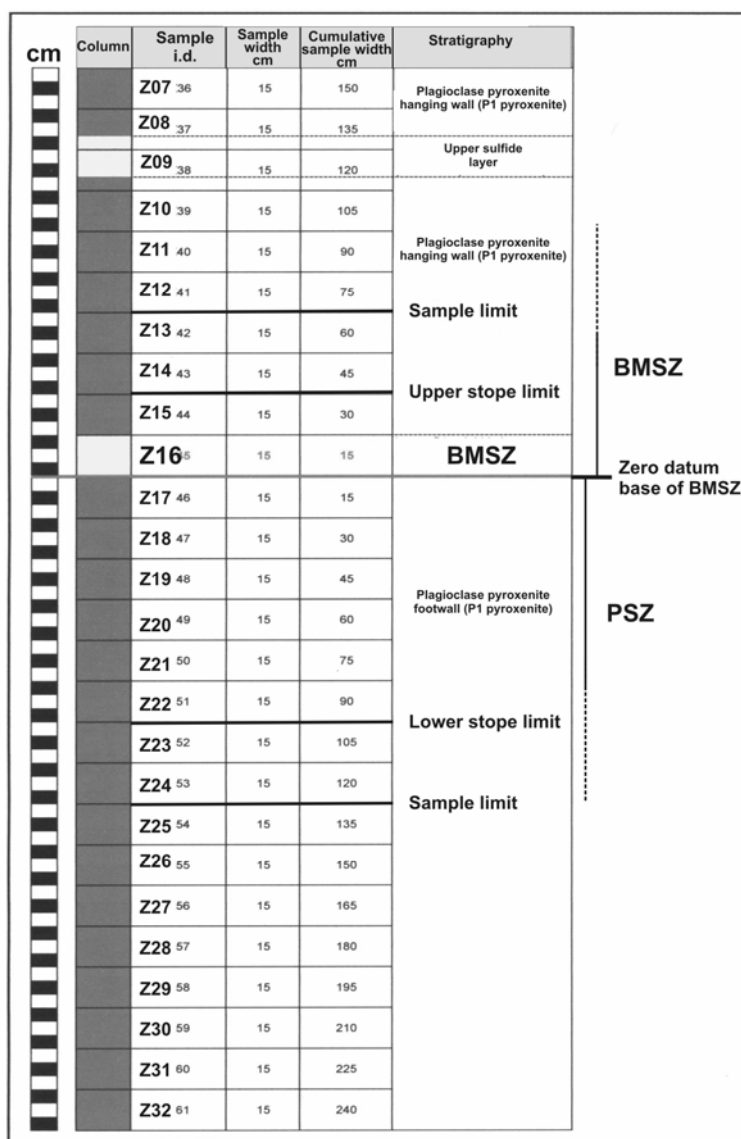


FIG. 19-16. Standardized evaluation sampling through the MSZ succession as related to underground channel samples for grade control. Also shown is the position of optimum mining cut (upper and lower stope limits) in relation to the base of the BMSZ datum line. Routinely, the sampling limit was two samples both above and below the ideal stope limits.

channel samples were also sometimes used to identify the BMSZ in conditions of poor sulfide visibility. An average PGE, Ni and Cu grade profile for Hartley Platinum Mine, as established from many thousands of routine channel samples was used as a comparative standard (Fig. 19-17).

Grade History

The grade history of the mine (Fig. 19-18) reflects both mining conditions and controls over the period from May 1995 to April 1999. Initially, production was erratic while tonnages were increased with the lowest grade being less than 2 ppm in September 1995, but a steady increase from this point reflected the increasingly stringent grade

control practices as detailed above. These measures involved closer scrutiny at individual areas of the mine, which due to their PGE distribution patterns required slightly different optimum cuts. It also involved a general reduction in optimum cut stope width to an average of 105 cm. After January 1997 the grades remained above 4 ppm. However, clear trends are observed over the period March 1997 to March 1998 as result of dilution of easily mineable ore with low grade material from areas of poor ground which incorporated a high proportion of waste. Non-ideal ground was mined to maintain the required tonnage. Prior to the mine closure a steady drop-off grade reflected increasing amounts of poor material being processed.

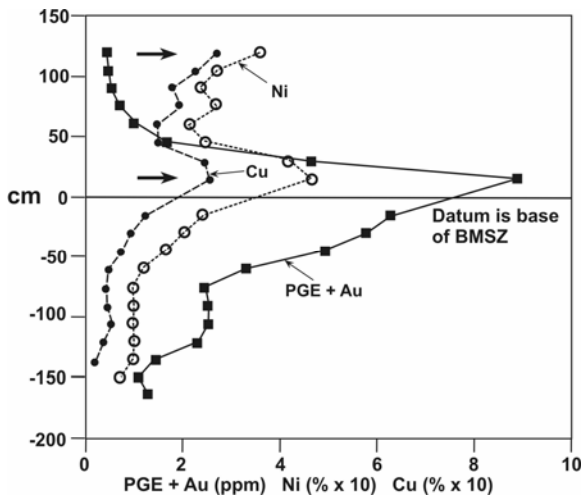


FIG. 19-17. Average of total PGE, Cu and Ni profiles from extensive underground sampling at Hartley Platinum Mine over the period 1996 to 1999 and representing several thousands of samples. The horizontal line represents the BMSZ datum from which all sampling, measuring and mining activities were measured. The bold arrows indicate the peak concentrations of sulfide with the lower zone being part of the MSZ ore zone and the upper zone being almost barren in PGE.

INTEGRATION OF EXPLORATION DATA, MINE EVALUATION AND GRADE CONTROL

A comprehensive and internally consistent data set of PGE, base metal and S concentrations arising from the exploration program on the MSZ in the Darwendale Subchamber of the Great Dyke has been used to illustrate the complex dependence of the mineralization on geological controls. The nature of the lithologies, the vertical metal distributions and systematic lateral variations as detailed by the geochemistry and cryptic layering in the MSZ, and the variation between axis and margin, bear directly on the exploration, evaluation and grade control. Compared with the Merensky reef, the MSZ is a relatively low grade PGE deposit in which the economic value zone is more difficult to delineate. In spite of this, the lateral continuity of the MSZ, the persistence of the mineralization, and high Pt/Pd ratios (compared with the Bushveld Complex), make this a world class deposit. Successful exploration, evaluation and mining practice require a thorough understanding of the geological controls, particularly as these relate to the lateral and vertical distributions of the mineralization. The potential for dilution with non-

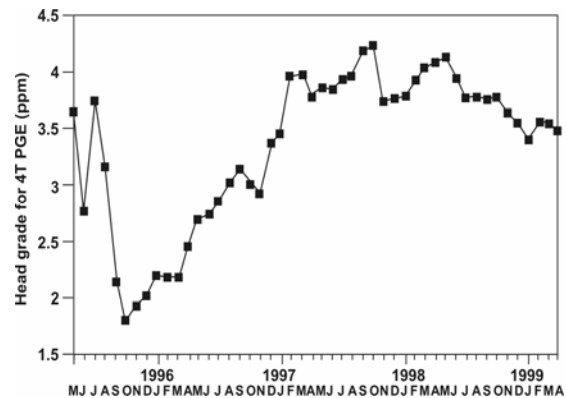


FIG. 19-18. Monthly PGE head-grade history for Hartley Platinum Mine from May 1995 to April 1999. The variation reflects both the history of achieving targeted tonnages together with the affects of dilution arising from the incorporation of poorly mineralized ore and emphasises the importance of stringent grade control on daily mining operations on the MSZ.

or poorly-mineralized rock is high. This is further complicated by the sequential enrichment of metals upwards from the base of the value zone with the order being Pd, Pt + Rh and then Au. Base metals are concentrated above Au. In the exploration and mining context the MSZ economic value zone is defined as the interval limited by sample cut-off grades of 4T PGE \geq 2ppm for the combined elements Pt, Pd, Rh and Au. Base metals Cu and Ni were included in the total metal budget. This zone varies from 1–3 m in thickness.

The average metal content is related to the thickness of the ore zone and shows a marked tendency to decrease in thicker ore zones down-dip (towards the Great Dyke axis) in the mine. However, as illustrated by cumulative metal calculations the total metal content also significantly increases in thicker ore zones. As the thickness of the ore zone increases towards the axis this also indicates that the feasibility of mining operations will improve at greater depths because of higher total metal content, wide stopes and the likelihood of fresher and more competent rock. However, this has to be viewed in the light of increased mining costs in deeper underground operations. The balance between grade and total metal content indicates that there are some zones of the MSZ, particularly in the axial regions, which are likely to be uneconomic. It also highlights the potential for open pit and near-surface underground operations in the axis of the Great Dyke where the MSZ is exposed on surface.

The case study presented here indicates that effective grade control is essential for successful mining of the MSZ and highly effective practices relating to borehole and underground sampling are required to monitor constantly the mining development.

SUMMARY AND CONCLUDING COMMENTS

The data used in this paper are an important body of information which highlight the cryptic layering and lateral variations in a world class platinum deposit that is a classic example of a specific type of PGE deposit. Although the MSZ falls into the category of a magmatic stratabound ore deposit it is not clearly delineated by distinct marker horizons or lithological changes. Marked changes in metal and sulfide concentrations, particularly at the transition from the PGE-Subzone to the Base Metal Subzone, are an important feature of this deposit and therefore a thorough academic and practical understanding of the ore body is essential for its successful exploitation and mining. The aim of this study was to provide a case study to illustrate the links between sound geological investigations, incorporating the latest academic research, and the practical aspects of exploration and mining.

The data were used to assess the mining feasibility of the MSZ in the exploration program, which subsequently resulted in the establishment of Hartley Platinum Mine. The data and the unique record of operations on the mine allow a retrospective view of the integration of exploration data and mining development as well as the implementation of rigorous grade controls on the basis of the geological understanding. For prospective future mines on the MSZ it is important that such procedures, arising directly from the exploration data, be established at the evaluation stage.

The distribution of the PGE mineralization in the MSZ has a distinct and predictable vertical pattern and also varies down-dip in relation to grade, total metal content, sulfide association and thickness of the ore zone. The axial and marginal environments in the Great Dyke, particularly as observed in the Darwendale Subchamber, provide the extreme facies-types for these variables. These characteristics are also likely to vary along strike in response to changing shape and volume of the magma chamber, but are less well documented and difficult to quantify. Each magma chamber, and

therefore each occurrence of the MSZ will therefore possess its own distinct characteristics within the general framework described. Rigorous implementation of grade control, crucial to successful mining of the MSZ, requires a thorough understanding of the geological controls of each occurrence and proposed mine sampling practices.

The origin of the mineralization in the MSZ is still not completely understood and is not the focus of this paper. The most widely accepted model to date is the progressive scavenging of PGE by base metal sulfides (Naldrett & Wilson 1989, Prendergast & Wilson 1989, Wilson & Prendergast 2001) with possibly minor redistribution by late stage processes (Wilson *et al.* 2000). Theoretical modelling using a range of silicate-liquid partition coefficients cannot satisfactorily duplicate the observed patterns (Wilson 2001), a similar conclusion reached for modelling of metal profiles in the Munni Munni Complex, Australia (Barnes 1993). The remarkably consistent pattern obtained for the MSZ and predictable lateral changes are also unlikely to support fluid migration as the dominant transport mechanism (Boudreau & Meurer 1999). Strong theoretical and practical considerations (Mungall 2002) support the orthomagmatic sulfide collection model for deposits of this type. More recently, a combined magmatic and fluid equilibration process has been postulated (Li *et al.* 2004). It is suggested in this work by an as yet untested model, that the patterns were established by a series of distinct mineralizing magmatic events. As more high quality data become available constraints on possible models will also improve.

ACKNOWLEDGEMENTS

AHW and RTB acknowledge BHP for the use of the drill core and mining data. Cuthbert Mujuru is acknowledged for assistance in sampling the detailed drill core DH-1. RTB acknowledges the support of many colleagues while in the position of Chief Geologist at Hartley Platinum Mine. The National Science Foundation of South Africa, through the THRIP initiative is thanked for financial support as part of a regional program to study PGE in layered intrusions. The paper was greatly improved by constructive comments from Martin Prendergast, Jim Mungall and an anonymous reviewer.

REFERENCES

- ARMSTRONG, R. & WILSON, A.H. (2000): A SHRIMP U–Pb study of zircons from the layered sequence of the Great Dyke, Zimbabwe, and a granitoid anatectic dyke. *Earth Planet. Sci. Lett.* **180**, 1-12.
- BARNES, S.J. (1993): Partitioning of the platinum group elements and gold between silicate and sulphide magmas in the Munni Munni Complex, Western Australia. *Geochim. Cosmochim. Acta.* **57**, 1277-1290.
- BOUDREAU, A.E. & MCCALLUM, I.S. (1992): Concentration of platinum-group elements by magmatic fluids in layered intrusions. *Econ. Geol.* **87**, 1830-1848.
- BOUDREAU, A.E. & MEURER, W.P. (1999): Chromatographic separation of the platinum-group elements, gold, base metals and sulfur during degassing of a compacting and solidifying igneous crystal pile. *Contrib. Mineral. Petrol.* **134**, 174-185.
- COGHILL, B.M. & WILSON, A.H. (1993): Platinum group minerals in the Selukwe Subchamber, Great Dyke, Zimbabwe: implications for PGE collection mechanisms and post-formational redistribution. *Mineral. Mag.* **57**, 613-633.
- HAMILTON, J. (1977): Strontium isotope and trace element studies on the Great Dyke and Bushveld mafic phase and their relation to early Proterozoic magma genesis in southern Africa. *J. Petrol.* **18**, 24-52.
- JOHAN, Z., OHNESTETTER, D. & NALDRETT, A.J. (1989): Platinum-group minerals and associated oxides and base metal sulphides of the Main Sulphide Zone, Great Dyke, Zimbabwe. *Bull. Geol. Soc. Finland.* **61**, 53-54.
- LI, C., OBERTHÜR, T., RIPLEY, E. & JOYESHISHI, T. (2004): The roles of sulfide liquid segregation and vapor refining in PGE distribution in the Main Sulphide Zone of the Great Dyke, Zimbabwe: mineralogic and stable isotopic constraints. *32nd International Geological Congress.* 472.
- MUKASA, S.B., WILSON, A.H. & CARLSON, R.W. (1998): A multielement geochronological study of the Great Dyke, Zimbabwe: significance of the reset and robust ages. *Earth Planet. Sci. Lett.* **164**, 353-369.
- MUNGALL, J.E. (2002): Kinetic controls on the partitioning of trace elements between silicate and sulfide liquids. *J. Petrol.* **43**, 749-768.
- NALDRETT, A.J. (1989): *Magmatic Sulfide Deposits*. Oxford University Press. New York.
- NALDRETT, A.J. & WILSON, A.H. (1989): Distribution and controls of platinum group-element mineralization in Cyclic Unit 1 of the Great Dyke, Zimbabwe. *Bull. Geol. Soc. Finland.* **61**, 3.
- OBERTHÜR, T., CABRI, L.J., WEISER, T.W., MCMAHON, G. & MULLER, P. (1997): Pt, Pd and other trace elements in sulfides of the Main Sulphide Zone, Great Dyke, Zimbabwe: a reconnaissance study. *Can. Mineral.* **35**, 597-609.
- OBERTHÜR, T., DAVIS, D.W., BLENKINSOP, T.G. & HOHNDÖRF, A. (2002): Precise U–Pb mineral ages, Rb–Sr and Sm–Nd sytematics for the Great Dyke, Zimbabwe – constraints on late Archean events in the Zimbabwe craton and Limpopo belt. *Precamb. Res.* **113**, 293-305.
- OBERTHÜR, T., WEISER, T.W., LODZIAK, J. & CABRI, L.J. (1998): New observations on the distribution of platinum group elements (PGE) and minerals (PGM) in the MSZ at Hartley Mine, Great Dyke, Zimbabwe. *8th Internat. Platinum Symp.* 293-296.
- PODMORE, F. & WILSON, A.H. (1987): A reappraisal of the structure, geology and emplacement of the Great Dyke, Zimbabwe. In *Mafic Dyke Swarms* (H.C. Halls & W.F. Fahrig, eds.). *Geol. Assoc. Can Special Paper* **34**, 433-444.
- PRENDERGAST, M.D. (1987): The chromite ore field of the Great Dyke, Zimbabwe. In *Evolution of Chromite Ore Fields* (C.W. Stowe, ed.). Van Nostrand Reinhold, New York, 89-108.
- PRENDERGAST, M.D. (1990): Platinum-group minerals and hydrosilicate 'alteration' in Wedza – Mimosa Platinum Deposit, Great Dyke, Zimbabwe. *Trans. Inst. Mining Metall. (Sect. B: Appl. Earth Sci.)* **99**, 91-105.
- PRENDERGAST, M.D. (1991): The Wedza-Mimosa platinum deposit, Great Dyke, Zimbabwe: layering and stratiform PGE mineralization in a narrow mafic magma chamber. *Geol. Mag.* **128**, 235-249.

- PRENDERGAST, M.D. & KEAYS, R.R. (1989): Controls of platinum-group element mineralization and the origin of the PGE-rich Main Sulphide Zone in the Wedza Subchamber of the Great Dyke, Zimbabwe: implications for the genesis of, and exploration for, stratiform PGE mineralization in layered intrusions. *In* Magmatic Sulphides – the Zimbabwe Volume (M.D. Prendergast, M.D. & M.J. Jones, eds.). Inst. Mining Metall., London. 43-69.
- PRENDERGAST, M.D. & WILSON, A.H. (1989): The Great Dyke of Zimbabwe II: Mineralization and mineral deposits. *In* Magmatic Sulphides – The Zimbabwe Volume (M.D. Prendergast & M.J. Jones, eds.). Inst. Mining Metall., London, 21-42.
- WEISER, T.W., OBERTHÜR, T., KOJONEN, K.K., AND JOHANSON, B. (1998): Distribution of trace PGE in pentlandite and of PGM in the Main Sulphide Zone (MSZ) at Mimosa Mine, Great Dyke, Zimbabwe. *8th Internat. Platinum Symp.* 443-445.
- WILSON, A.H. (1992): The geology of the Great Dyke, Zimbabwe: Crystallization, layering, and cumulate formation in the P1 Pyroxenite of cyclic unit 1 of the Darwendale Subchamber. *J. Petrol.* **33**, 611-663.
- WILSON, A.H. (1996): The Great Dyke of Zimbabwe. *In* Layered Intrusions (R.G. Cawthorn, ed.). Elsevier Science B.V., Amsterdam, 365-402.
- WILSON, A.H. (2001): Compositional and lithological controls on the PGE-bearing sulphide zones in the Selukwe Subchamber, Great Dyke: a combined equilibrium – Rayleigh fractionation model. *J. Petrol.* **42**, 1845-1867.
- WILSON, A.H., MURAHWI, C.Z. & COGHILL, B.M. (2000): The geochemistry of the PGE Subzone in the Selukwe Subchamber, Great Dyke: an intraformational layer model for Platinum Group Element enrichment in layered intrusions. *Mineral. & Petrol.* **68**, 115-140.
- WILSON, A.H., NALDRETT, A.J. & TREDoux, M. (1989): Distribution and controls of platinum-group element and base metal mineralization in the Darwendale Subchamber of the Great Dyke, Zimbabwe. *Geology* **17**, 649-652.
- WILSON, A.H. & PRENDERGAST, M. (1989): The Great Dyke of Zimbabwe I: Tectonic setting, stratigraphy, petrology, structure, emplacement and crystallization. *In* Magmatic Sulphides – the Zimbabwe Volume (M.D. Prendergast & M.J. Jones, eds.). Inst. Mining Metall., London. (1-20).
- WILSON, A.H. & PRENDERGAST, M.D. (2001): Platinum-group element mineralization in the Great Dyke, Zimbabwe, and its relationship to magma evolution and magma chamber genesis. *S. Afr. J. Geol.* **104**, 319-342.
- WILSON, A.H. & TREDoux, M. (1990): Lateral and vertical variation of the platinum-group elements, and petrogenetic controls on the sulphide mineralization in the P1 Pyroxenite Layer of the Darwendale Subchamber of the Great Dyke, Zimbabwe. *Econ. Geol.* **85**, 556-584.
- WILSON, A.H. & WILSON, J.F. (1981): The Great Dyke. *In* Precambrian of the Southern Hemisphere (D.R. Hunter, ed.). Elsevier, Amsterdam, 572-578.
- WILSON, J.F. (1987): The tectonic setting of the Great Dyke of Zimbabwe and the Mashonaland Igneous Event. *14th Colloquium of African Geology, CIFEG Occasional Publication.* **12**, 140-141.
- WINGATE, M.T.D. (2000): Ion-microprobe U–Pb zircon and baddeleyite ages for the Great Dyke and its satellite dykes, Zimbabwe. *S. Afr. J. Geol.* **103**, 74-80.
- WORST, B.G. (1958): The differentiation and structure of the Great Dyke of Southern Rhodesia. *Trans. Geol. Soc. S. Afr.* **61**, 283-354.
- WORST, B.G. (1960): The Great Dyke of Southern Rhodesia. *Southern Rhodesia Geol. Surv. Bulletin.* **47**, pp. 234.

CHAPTER 20: THE PLATINOVA REEF OF THE SKAERGAARD INTRUSION

T.F.D. Nielsen, Geological Survey of Denmark and Greenland,
1350 Copenhagen K, Denmark
E-mail: tfn@geus.dk

J.C.Ø. Andersen, Camborne School of Mines, University of Exeter in Cornwall,
Penryn, Cornwall, TR10 9EZ, UK
E-mail: J.C.Andersen@exeter.ac.uk

and

C.K. Brooks, Geological Institute, University of Copenhagen,
1350 Copenhagen K, Denmark
E-mail: kentb@hotmail.com

INTRODUCTION

During the 1980's, Paleogene gabbro intrusions in East Greenland became the targets of platinum group element (PGE) and gold (Au) exploration by Platinova Resources Ltd. This interest was fuelled by an increasing demand for PGE in auto catalysts. At the same time, new petrogenetic models for PGE deposits were developed leading to a better understanding of their geochemical fractionation in mafic intrusions (*cf.* Boudreau *et al.* 1986, Naldrett *et al.* 1987). The subsequent focus of interest was voluminous intrusions with documented episodes of magma replenishment. Such intrusions were assumed potentially to have undergone mineralization analogous to the world-class PGE deposits in the Bushveld and Stillwater complexes. On East Greenland, the primary target was the 49.4 ± 0.2 to 47.3 ± 0.3 Ma old (Nevle *et al.* 1994, Tegner *et al.* 1998, respectively) and 400 km² Kap Edvard Holm complex (Bernstein *et al.* 1992). During reconnaissance trips in 1986 and 1987, Platinova Resources Ltd. located zones with elevated concentrations of PGE and Au in most Paleogene East Greenland gabbro intrusions (*e.g.*, Arnason 1995, Nielsen 2002). Of these, the Platinova reef in the 70 km² Skaergaard intrusion remains the only major, possibly economic, deposit located to date (Andersen *et al.* 1998).

During the earliest stages of the reconnaissance, the Skaergaard intrusion was considered to be an academic curiosity rather than the potential host of a major PGE and Au deposit. Both its small size and well-documented closed-system fractionation were in direct conflict with the favored models for PGE concentration.

Nevertheless, small PGE and Au anomalies were unexpectedly found in layered gabbros, stream sediment samples, and sulfide blebs in the marginal gabbros. Assays revealed concentrations up to 0.4 g.t⁻¹ PGE and Au, concentrations high enough to warrant further exploration. The source of the PGE and Au anomalies in stream sediment samples was suggested to be the Triple Group, a section of the layered gabbros characterized by three massive leucogabbro layers. The reasons were: (1) the Triple Group succession exhibits first signs of S-saturation in the magma (Turner 1986); (2) the succession displays significant changes in the crystallization, most notably expressed by the erratic re-appearance of cumulus olivine (Maaløe 1987). A follow-up survey by classic chip line exploration and pack sack drilling located a stratabound zone anomalously rich in PGE (mainly Pd) and Au. This zone, in subsequent studies known as the Platinova reef, is at present the subject of a major exploration program by Skaergaard Minerals Corporation (a company fully owned by Galahad Gold PLC).

The Platinova reef (Andersen *et al.* 1998) is a low grade PGE and Au deposit hosted by ilmenite-rich ferrogabbro. It contains in the order of 50 million oz. Pd, Au and Pt (Galahad Gold PLC 2004a). The sulfide content is very low (*ca.* 0.05 vol. %) and in contrast to the classic stratabound PGE deposits (such as the Merensky and J-M reefs), the Platinova reef cannot readily be identified by texture or mineral assemblages in the field. However, since the reef is perfectly concordant with the magmatic layering, once located, it can be traced by a trained eye along strike in outcrop as well as in drill cores. The structure and mineralogy of the Platinova reef suggests the mineralization to

be a primary high-T, syn-magmatic process. The Platinova reef shows similarities to PGE deposits in the Sonju Lake (Miller 1999) and Rincón del Tigre (Prendergast 2000) complexes. These deposits have been referred to jointly as “Skaergaard-type” PGE reefs (Prendergast 2000, Miller & Andersen 2002).

REGIONAL MAGMATIC AND GEOCHEMICAL CONTEXT

The Skaergaard intrusion is exposed on the east shore of the deep Kangerlussuaq Fjord, at 68°N in East Greenland. It was emplaced around 55.65 ± 0.3 Ma ($^{40}\text{Ar}/^{39}\text{Ar}$ on amphibole, Hirschmann *et al.* 1997) ago into the Paleogene North Atlantic volcanic rifted margin above the proto-Icelandic hot spot (Fig. 20-1). The host rocks of the intrusion are Precambrian basement, Mesozoic to Paleogene sedimentary rocks and a >6 km thick succession of Paleogene flood basalts

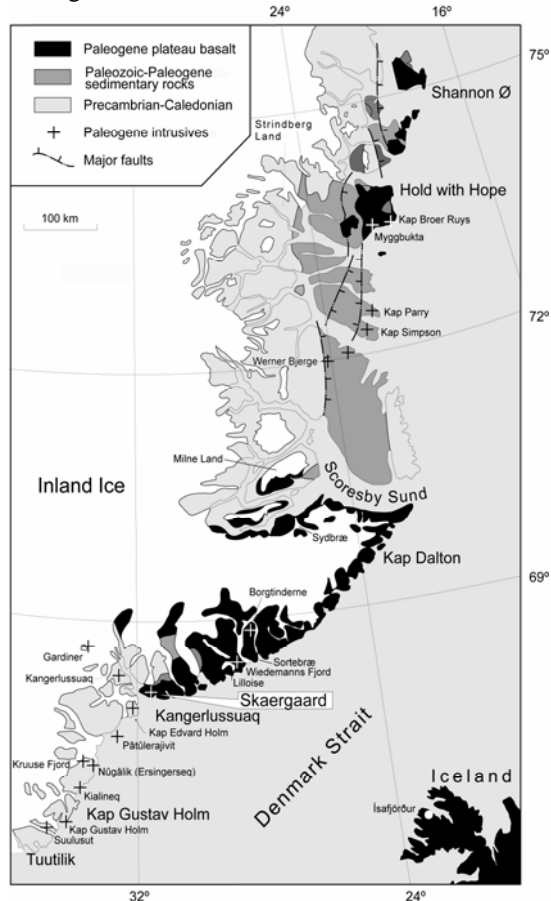


FIG. 20-1. Geological map of East Greenland showing the extent of the Paleogene plateau basalts and locations of the major intrusive complexes.

(Pedersen *et al.* 1997). The intrusion was emplaced after the formation of the lower 3 km plateau basalts, as suggested from the age of the intrusion (Hirschmann *et al.* 1997), the ages of the plateau basalts and the pressure estimated for the crystallization of the gabbros.

Precambrian Basement and Mesozoic to Paleogene Sedimentary Rocks

The Precambrian basement, composed of banded and agmatitic gneiss with folded supracrustal successions, gives metamorphic ages of *ca.* 2.6 Ga (Leeman *et al.* 1976). The Archean precursors are more than 3.0 Ga old (Leeman *et al.* 1976). The oldest sedimentary rocks found in the area are of Early Cretaceous age (Higgins & Soper 1981, Nielsen *et al.* 1981). They were deposited near the margin of a large basin, which can be followed to the European side of the North Atlantic. The youngest Paleogene sedimentary rocks are shallow water deposits, including bitumen-rich shale and fluvial, coarse sedimentary rocks that in some areas contain significant volcanoclastic components (Larsen *et al.* 1999b, 2001). The sedimentary record suggests a continued history of basin formation due to crustal attenuation followed by a rapid uplift of the basin floor at the onset of the voluminous Paleogene volcanism.

Paleogene Volcanic Rocks

In the Skaergaard region, the volcanic succession (Table 20-1) can be simplified to include a succession of early rift volcanic rocks (the Lower Basalts), pre-breakup and syn-breakup plateau basalts (*cf.* Larsen *et al.* 1989, 1998, 1999a). The early rift volcanic rocks show a large petrographic and geochemical variation from Ti-rich, plume-derived, tholeiitic picrite to evolved and crustally contaminated tholeiitic basalt (Nielsen *et al.* 1981, Brooks & Nielsen 1982, Fram & Lesher 1997, Hansen & Nielsen 1999). The wide chemical spectrum is seen as the result of a heterogeneous plume source, magmatic differentiation processes in the feeder systems, and interaction with the old East Greenland continental crust (Table 20-2).

The pre-rift plateau basalts, 2–3 km thick (Table 20-1), include the Milne Land and the Geikie Plateau Formations (Larsen *et al.* 1989). They show a more restricted chemical variation than the Lower Basalts and are dominated by Fe- and Ti-rich tholeiitic lavas, with a sub-population of low-Ti, high Mg/(Mg+Fe) basalts approaching MORB-type

TABLE 20-1. SUMMARY OF THE GEOLOGICAL DEVELOPMENT IN THE KANGERLUSSUAQ AREA, EAST GREENLAND

Time	Main event	Sedimentary and Volcanic Rocks		Plutonism
13 Ma	Youngest volcanic rocks	Vindtop Fm.		
until <i>ca.</i> 40 Ma				Gabbro, monzonite syenite, and ultramafic alkaline intrusions. Alkaline dyke swarms.
<i>Ca</i> 53 Ma	Cessation of plateau basalt volcanism. Initiated seafloor spreading	Syn-rift plateau basalts: Skrænterne and Rømer Fjord Formations.	Fe-Ti tholeiites, evolved plume-type basalts, 2–3 km in thickness	Tholeiitic and alkaline dyke swarms.
<i>ca.</i> 55 Ma	Rifting. Collapse of continental margin. Shield building			Skaergaard intrusion; gabbro macrodykes. Tholeiitic dyke swarms
<i>ca.</i> 57 Ma	Initiation of plateau basalt volcanism. Shield building	Pre-rift plateau basalts: Geikie Plateau and Milne Land Formations	Fe-Ti tholeiites and depleted high Mg basalts, 2–3 km in thickness	Tholeiitic dyke swarms
<i>ca.</i> 61 Ma	Initiation of volcanism. Continental rift-zone volcanism	Lower Basalts: Vandfaldsdalen and Mikis Formations.	incl. plume-type high-Mg basalts (picrite) 2–3 km in thickness.	Tholeiitic dyke swarms
> 61 Ma	Continental crustal extension and basin formation	Kangerlussuaq Group sedimentary rocks	Mesozoic to Paleocene sedimentary rocks	

composition (Table 20-2). The latter were, on the basis of geochemistry, suggested to have formed at a developing oceanic rift-type thin crust environment to the east of the present-day coast of East Greenland (Tegner *et al.* 1998). In this paper, a tectonic rather than a geochemical definition of the rifting is preferred. As the physical rifting process is related to the coast-parallel flexure along the east coast of Greenland, this lower succession of the plateau basalts refers to a pre-rifting scenario. The collapse of the continental margin is suggested to be pene-contemporaneous with the upper Geikie Plateau Formation and the emplacement of the Skaergaard intrusion (Nielsen 2004). The 2–3 km thick, syn-rift, plateau basalts (Table 20-1) include the Rømer Fjord Formation and the Skrænterne Formation (Larsen *et al.* 1989). They are again Fe- and Ti-rich tholeiites (Table 20-2), but additionally include a sub-group of very Ti-rich evolved basalts (Tegner *et al.* 1998). Additional information on the volcanic succession can be found in Larsen *et al.* (1989), Hansen & Nielsen (1999) and Andreasen *et al.* (2004).

Platinum-group element data for the onshore volcanic rocks were published by Nielsen & Brooks (1995) and Momme *et al.* (2002) and in drilled offshore volcanic rocks by Philipp *et al.* (2001). The

general consensus is that, apart from contaminated strata in the Lower Basalts and equivalent offshore successions, the plateau basalts were all sulfur-undersaturated and retained high PGE concentrations. Exceptions are some of the most evolved, Fe- and Ti-rich lavas (Momme *et al.* 2002). The distribution of PGE in the volcanic rocks was discussed in detail by Andersen *et al.* (2002) (Fig. 20-2). Similar to the West Greenland flood basalts (Lightfoot *et al.* 1997), there is at present no evidence for extensive PGE-depleted volcanic successions indicative of large PGE-rich Cu–(Ni) sulfide deposits similar to those at Noril'sk, Siberia.

THE SKAERGAARD INTRUSION

Access

The Skaergaard intrusion (Fig. 20-3) is located directly on the East Greenland shoreline at 68°10', 31°40'W (Fig. 20-1). The intrusion can be reached by ice-strengthened ships from July to October. The crossing time from Ísafjörður (Fig. 20-1) in NW Iceland is 18–24 hours. A gravel airstrip (500–700 m) for STOL aircraft is located in Sødalen, approximately 10 km east of the intrusion. The flight time from Ísafjörður is approximately 1:45h at 150 knots. With two huts, the Sødalen

TABLE 20-2. EXAMPLES OF COMPOSITIONS OF PALEOGENE EAST GREENLAND VOLCANIC ROCKS.

rock type	Lower Basalts			Pre-rift plateau basalts			Syn-rift plateau basalts				
	Picrite	Olivine basalt	Ol-cpx basalt	basalt	Olivine basalt	low-Ti tholeiite	medium-Ti tholeiite	high-Ti tholeiite	low-Ti tholeiite	mediumTi tholeiite	high-Ti tholeiite
Sample no.	361026	20332	20351	40626	404217*	404232*	436027*	436068*	83893*	435536*	83877*
SiO ₂	45.41	47.06	48.08	48.94	47.8	47.3	49.2	47.2	49.1	48.0	46.1
TiO ₂	1.83	2.12	2.68	2.89	1.11	0.90	2.51	4.24	1.61	3.29	4.88
Al ₂ O ₃	9.00	10.72	7.94	12.94	7.9	13.9	14.2	14.2	13.7	14.0	13.4
Fe ₂ O ₃	1.60	9.57	4.18	4.26	1.71	1.44	1.53	1.76	1.85	1.77	1.98
FeO	9.80	5.64	8.90	6.98	11.4	9.61	10.2	11.7	12.4	11.8	13.2
MnO	0.19	0.16	0.16	0.16	0.19	0.18	0.18	0.19	0.25	0.20	0.24
MgO	17.73	11.80	11.01	7.08	23.6	14.0	8.26	6.17	6.97	6.84	6.47
CaO	8.19	9.44	10.77	10.19	5.77	11.2	11.4	10.5	11.7	10.9	10.5
Na ₂ O	1.41	2.00	1.48	2.70	0.34	1.37	2.17	2.76	2.24	2.44	2.22
K ₂ O	0.15	0.38	0.38	0.67	0.04	0.03	0.18	0.69	0.12	0.50	0.52
P ₂ O ₅	0.19	0.31	0.27	0.24	0.11	0.07	0.23	0.48	0.16	0.30	0.55
LOI	2.65	3.09	3.20	2.48	n.r.	n.r.	n.r.	n.r.	n.r.	n.r.	n.r.
Sum	98.16	100.31	99.05	99.53	n.r.	n.r.	n.r.	n.r.	n.r.	n.r.	n.r.
Ni, ppm	803	735	387	144	913	436	179	98	63	109	93
Cr, ppm	954	1396	1057	313	2022	950	434	206	81	190	155
V, ppm	275	283	360	374	n.r.	n.r.	n.r.	n.r.	n.r.	n.r.	n.r.
Cu, ppm	138	104	82	176	57	118	142	239	246	245	453
Pt, ppb	8	7	6	8	7.34	9.25	5.27	5.76	2.54	3.80	5.33
Pd, ppb	5	4	5	7	4.78	10.4	5.87	13.2	23.8	13.3	16.3
Au, ppb	17	2	5	4	6.2	7.9	9.5	9.7	6.0	9.2	10.8

Notes: * Data from Momme *et al.* (2002); n.r. = not reported

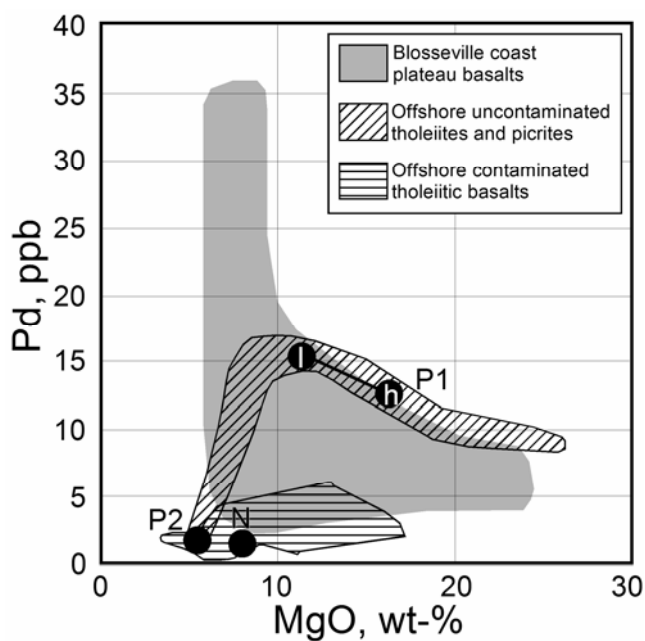


FIG. 20-2. Distribution of the platinum-group elements in East Greenland basalts. Data from Philipp *et al.* (2001) and Momme *et al.* (2002). P1 (picrite and high-PGE plume source; h – high degree of melting, l – low degree of melting), P2 (low PGE plume source), and N (N-MORB) represent the different end-member primary mantle melts suggested by Andersen *et al.* (2002).

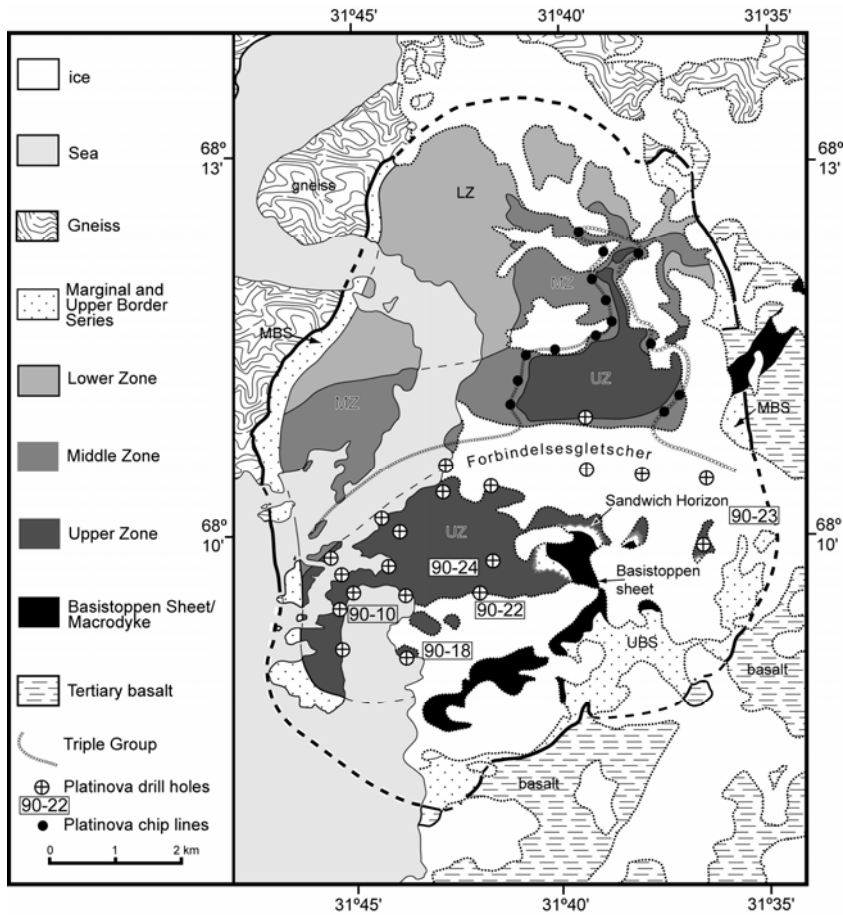


FIG. 20-3. Geological map of the Skaergaard intrusion (modified after Wager & Brown 1968 and McBirney 1989b). The map shows the location of the major chip line profiles from the 1988 and drill cores from the 1989–1990 exploration program.

gravel strip has for more than two decades been the operational base for both exploration and research activities in the Kangerlussuaq region. The nearest permanent settlements along the East Greenland coast are found in Ittoqqortoormiit (Scoresby Sund) some 500 km to the northeast and Tasillaq (Ammassalik) some 400 km to the southwest.

Geological Introduction

The Skaergaard intrusion is a classic layered gabbro intrusion with excellent exposures and well-developed magmatic layering (Wager & Deer 1939, Wager & Brown 1968). It is a foremost natural laboratory for the study of crystal fractionation processes in basaltic magmas. The literature on the intrusion is significant and includes >600 references (cf. Andersen & Brooks 2004). Recent descriptions and reviews were presented by Irvine *et al.* (1998) and McBirney (1996).

Skaergaard is oval-shaped, 11 km N–S and

7–8 km E–W and with a surface area of *ca.* 70 km². The total exposed stratigraphic height is close to 3500 m. About half of the margin is exposed and in many areas chilled. Post-Skaergaard flexuring of the continental margin has rotated the intrusion to the south revealing what appears to be an almost complete and continuous cross section of the stratigraphy. Gabbro close to the base of the intrusion is exposed to the north and an uneroded remnant of the roof to the south.

Shape of the Intrusion

The shape of the intrusion has been one of the most significant unknown factors for evaluations of the Skaergaard liquid line of decent by mass balance (Fig. 20-4). The fact that most of the contacts are steep led Wager & Deer (1939) to interpret the intrusion as an inclined, funnel-shaped, magma chamber with a total stratigraphic height of some 15–20 km (Fig. 20-4a). This implied the

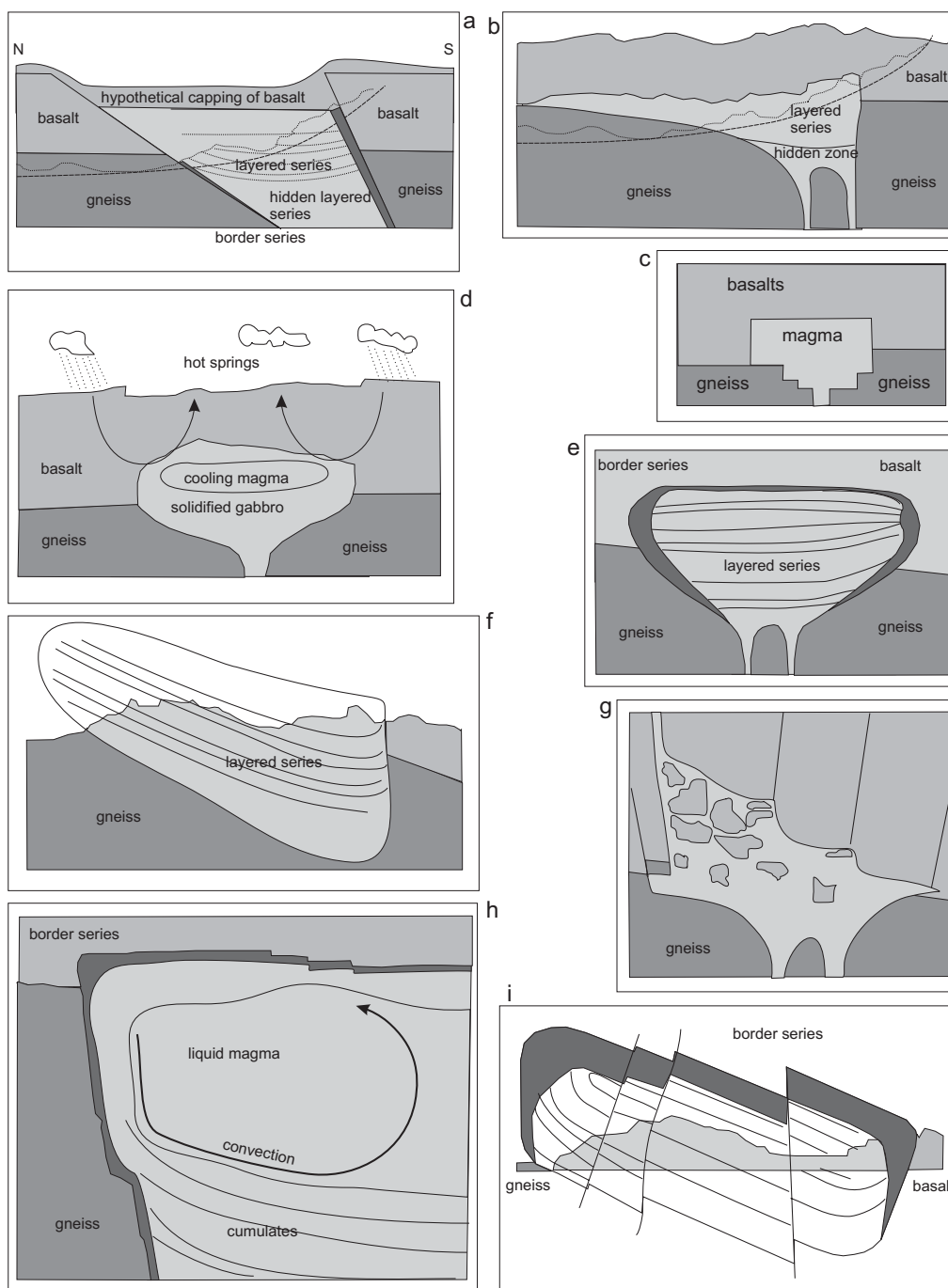


FIG. 20-4. Models for the inferred shape of the Skaergaard intrusion through time. **a**, shape proposed on the basis of dipping contacts by Wager & Deer (1939); **b**, Revised shape proposed by McBirney (1975) taking into account the gravimetric measurements by Blank & Gettings (1973); **c**, Shape used for the modeling of hydrothermal alteration by Norton & Taylor (1979); **d**, Model presented by McBirney (1984); **e**, Shape presented by Naslund (1984); **f**, Sill-like shape adapted by Irvine (1987); **g**, Shape adapted by Stewart & DePaolo (1990). The large vertical extent of the magma chamber was inferred (on the basis of Nd-isotopic variations) to accommodate an extensive cap of granophyric material derived by partial melting of the basement; **h**, Inferred dynamics of the Skaergaard magma during crystallization in relationship to the stump-like shape and steep margins of the magma chamber (Irvine et al. 1998); **i**, Fault-controlled box-shape reconstructed from outcrop relations and drill-core intercepts by Nielsen (2004).

existence of a large, unexposed “Hidden Zone” that subsequently had a great influence on their calculations of the liquid line of descent. Gravimetric studies by Blank and Gettings (1973, see also McBirney 1975, Norton & Taylor 1979, and Norton *et al.* 1984) did not support this, and instead they suggested the intrusion to be a *ca.* 4 km thick, inflated sill with two, deep, funnel-shaped, feeder channels (Fig. 20-4b to 20-4e). Based on field observations Irvine (1987) suggested a more stumpy sill-like body (Fig. 20-4f). Stewart & DePaolo (1990) suggested that the magma was overlain by an extensive volume of granophyric magma (Fig. 20-4g). Irvine (1992) and Irvine *et al.* (1998) emphasized that at least some contacts were fault controlled following directions parallel to the regional dyke swarms and coastal flexure, and inferred that the internal structure and magma dynamics are tightly controlled by the magma chamber geometry (Fig. 20-4h). Nielsen (2004, Fig. 20-4i) suggested on the basis of fault-controlled contacts and contact orientations that the intrusion occupies a box-like magma chamber, 11 x 7.5 x 3.8

km in size and with a total volume close to 300 km³.

Zone and sub-zones

The gabbros of the intrusion are subdivided into three main series (*e.g.*, Figs 20-4a, 20-4h and 20-4i). The Upper Border Series (UBS) is gabbro formed under the roof of the intrusion, the Marginal Border Series (MBS) formed on the walls and the Layered Series (LS) accumulated up from the base of the intrusion (Wager & Deer 1939, Wager & Brown 1968, Irvine *et al.* 1998). The LS and UBS meet in the so-called Sandwich Horizon (SH). The volume of UBS and MBS is regarded by most to be small compared to the volume of LS and all fractionation models for the intrusion are based on the systematic chemical evolution in LS. The unexposed gabbros of the intrusion are referred to as the Hidden Zone (HZ).

Phase layering in LS allows the subdivision into zones and subzones (Fig. 20-5). The exposed gabbros are initially divided into: (1) the olivine-

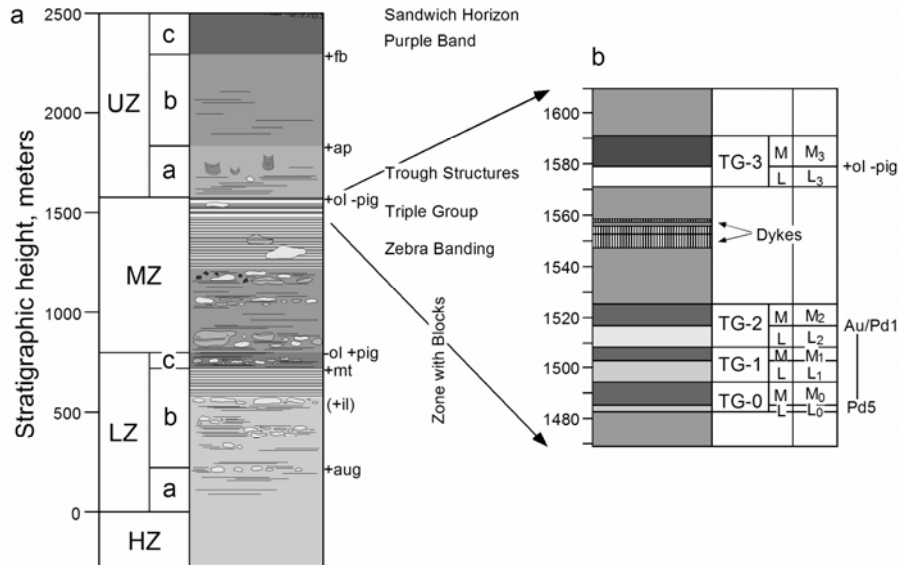


FIG. 20-5. **a)** Stratigraphic evolution of the Skaergaard Layered Series. Stratigraphic heights follow Wager & Brown (1968). HZ = Hidden zone; LZ = Lower zone with subzones a, b, and c; MZ = Middle zone; UZ = Upper zone with subzones a, b, and c. Mineralogical changes are indicated as follows: aug = augite; il = ilmenite; mt = titanomagnetite; ol = olivine; pig = pigeonite (now inverted); ap = apatite; fb = ferrobustamite. The appearance and disappearance of cumulus phases are marked with + and – respectively. Distinctive lithological units are outlined next to the column. The Triple Group and the Platinova reef occur in the uppermost 100 m of the MZ. **b)** Stratigraphic evolution of the Triple Group near the center of the intrusion (drill hole 24) showing the systematic repetition of leuco-, meso-, and melanocratic layers. TG-0 to TG-3 denote individual Triple Group units from Andersen *et al.* (1998) with subscript L and M signifying their leucocratic and melanocratic members; L0 – M3 are notations used by the exploration and mining companies, and have been used throughout this text. The figure is modified after Andersen *et al.* (1998).

bearing Lower Zone, (2) the olivine-free Middle Zone (MZ) and (3) the olivine-bearing (Fe-rich olivine) Upper Zone (UZ). LZ is again subdivided into LZa, LZb and LZc on the basis of changes in the cumulus paragenesis shown in Fig. 20-5. UZ is likewise subdivided into UZa, UZb and UZc. Equivalent zones and subzones are mapped out also in UBS and MBS (*cf.* Irvine *et al.* 1998).

The upper 100 m of MZ host the Triple Group. The name refers to a succession of characteristic leucogabbro layers (L1–L3) hosted in brownish-orange to dark weathering meso- and melanogabbro. The top of L3 identifies the reappearance of cumulus olivine and therefore the boundary between the MZ and UZ. The Triple Group hosts the Platinova reef and is easily identified from afar (Fig. 20-6).

Internal Structure

Several of the cross sections in Fig. 20-4 show a trough-like internal structure of LS, but it is only after information from exploration drill cores has become available that the trough structure has been quantified. Nielsen (2004) took the consequence of the correlation between zones and subzones in LS, MBS and UBS and suggested the internal structure to be of onion-type (Fig. 20-7). The structure is seen as the result of contemporaneous cooling, crystallization, and crystal accumulation at the floor, on the walls and under the roof of the intrusion. From the drill cores,

it is apparent that the contact between MZ and UZ (Fig. 20-7) shows a basin shape similar to a flat bowl, 7 km from E–W and 700 m deep in the center of the intrusion. The known Au–PGE mineralization is concordant with this basin shape and located between 40 and 110 m below the MZ/UZ boundary.

Line of Liquid Descent

Wager (1960) and later Wager & Brown (1968) computed the line of liquid descent on the basis of the chilled margin composition and the estimated volumes and compositions of the cumulate units. The tholeiitic melt develops to very Fe-rich compositions (>20 wt.%, so-called “Fenner” trend) with a small terminal proportion of granophyre. The origin of the “Fenner” trend has been debated for decades (*e.g.*, Hunter & Sparks 1987, Brooks & Nielsen 1990, McBirney & Naslund 1990, Morse 1990, Tegner 1997). Despite all of the detailed field, petrographic, and geochemical studies on the Skaergaard intrusion, the fractionation processes are not yet fully understood. The calculated composition of the parental liquid (Nielsen 2004), and average compositions of zones and subzones in LS (McBirney 1989a) are shown in Table 20-3.

EXPLORATION HISTORY

The early studies of gold and PGE in the Skaergaard intrusion were entirely academic aimed at describing the behavior of these elements during

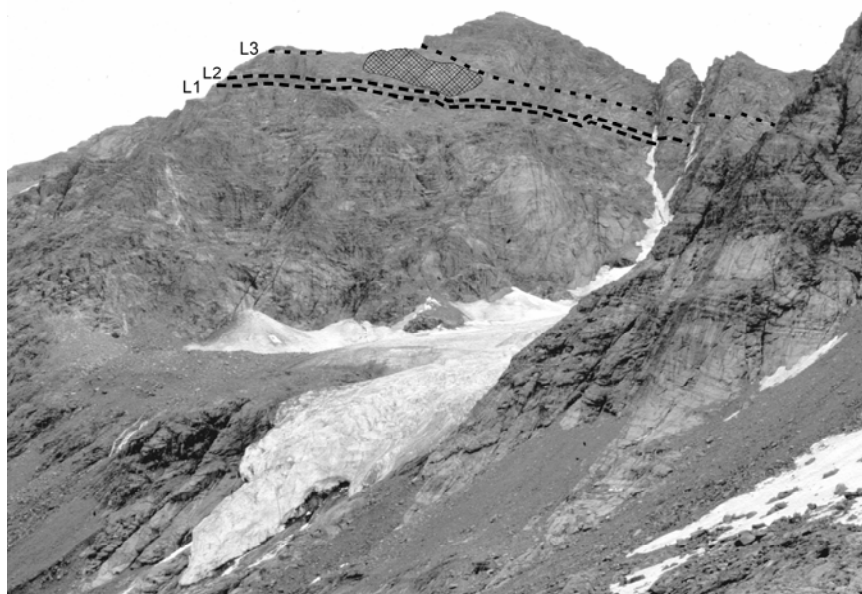


FIG. 20-6. The Triple Group exposed in the western cliff face of Wagers Top. L1, L2, and L3 are highlighted. Note that a block (cross hatched) has been embedded in the mesogabbro between L2 and L3. The height of the cliff (from the glacier) is approximately 700 m.

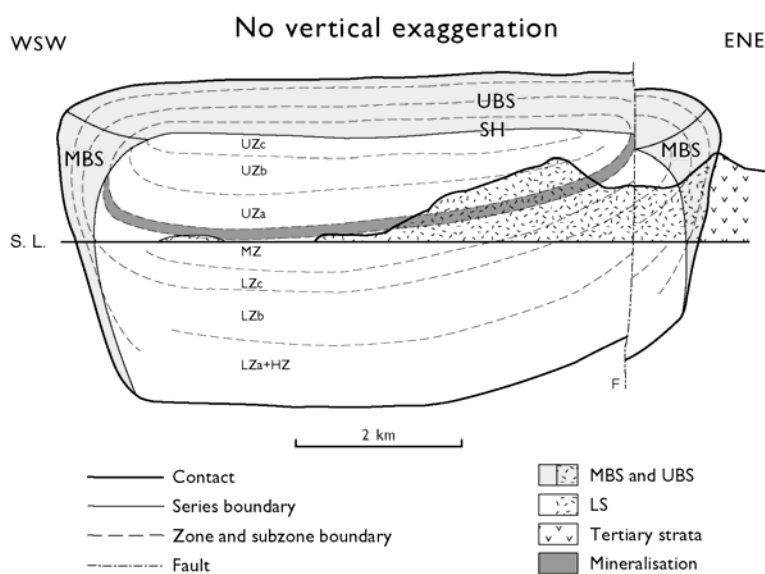


FIG. 20-7. Cross section of the Skaergaard intrusion showing its internal structure. Note the semi-concentric cumulate "shells" formed during progressive inward crystallization towards the compositional center of the intrusion (the Sandwich Horizon, SH). The difference in thickness of the LS and UBS cumulates signifies the preferential crystal accumulation on the magma chamber floor. The LS unit boundaries display topography of around 700 m between the margins and center of the intrusion. This is believed to represent largely the original shape of the magma-cumulate interface (Andersen 1996). Modified from Nielsen (2004).

TABLE 20-3: PARENTAL MELT AND AVERAGE COMPOSITIONS FROM THE SKAERGAARD INTRUSION

	SK-TFDN	LZ*	MZ*	UZ*	Melanogranophyre
SiO ₂	47.91	47.60	42.79	42.88	62.18
TiO ₂	3.09	2.00	7.79	4.7	1.07
Al ₂ O ₃	13.8	14.64	11.53	10.15	12.41
FeO	15.43	12.84	20	14.84	12.37
MnO	0.24	0.19	0.26	0.39	0.2
MgO	6.13	9.48	6.24	4.16	0.63
CaO	10.16	10.60	9.87	9.08	4.65
Na ₂ O	2.57	2.32	2.23	2.55	4.19
K ₂ O	0.4	0.24	0.21	0.32	1.99
P ₂ O ₅	0.28	0.10	0.08	0.95	0.31
Sum	100	100	100	100	100
Ni, ppm	80	183	57	20	8
Cr, ppm	89	119	29	16	9
Cu, ppm	265	111	375	860	93
Pt, ppb	8	7	22	6	n.d.
Pd, ppb	27	17	115	8	n.d.
Au, ppb	11	6	29	7	n.d.

* Weighted averages using mass proportions from Nielsen (2004) and average compositions in McBirney (1989). Pt, Pd and Au data (T.F.D. Nielsen, unpublished) based on mass balance model in Nielsen (2004) and systematic assays. n.d. = not determined

the fractionation of a tholeiitic magma. This also applies to the investigation of sulfides by Turner (1986). It is probably fair to state that few researchers imagined that the relatively small Skaergaard intrusion could host a major PGE and Au deposit.

Pre-exploration Geochemical and Mineralogical Studies

The earliest investigations (Vincent & Smales 1956, Crocket *et al.* 1958, and Vincent & Crocket 1960) showed only small and uneconomic concentrations of Au and Pd. Vincent & Smales (1956) reported 17 ppb Pd and 7 ppb Au in the Skaergaard chilled margin. Vincent & Crocket (1960) reported Au concentrations of 2–9 ppb throughout the Layered Series. The data gave no indications for mineralization at any stratigraphic level, although rocks carrying sulfides had elevated concentrations of 11–73 ppb. The distribution of sulfur (Wager *et al.* 1958) and sulfides (Wager *et al.* 1957) also gave no indication for any major mineralization. Turner (1986) in contrast, provided evidence to suggest that S-saturation was reached at the level of the Triple Group, and that the intrusion therefore potentially could host sulfide-related mineralization.

Discovery Stage (1986–1988)

The earliest exploration was conducted by Nordisk Mineselskab in 1969–70. Reconnaissance visits did not support continued exploration (Vohryzka & Vohryzka 1971). In 1986 a Platino

Resources Ltd./Teck Corporation Joint Venture conducted an exploration program in the Kangerlussuaq area (Waters 1987). The main target was the Kap Edvard Holm complex approximately 40 km south of Skaergaard (for references see Nielsen 2002). During this campaign 16 stream sediment samples and 118 whole rocks were sampled throughout the Skaergaard intrusion.

A systematic increase in the concentration of Pd from <10 to 40–70 ppb was observed in the gabbros with liquidus magnetite in LZc and zones and subzones above (Fig. 20-5). Single grab samples from the margins of the intrusion showed significant enrichments in Pd or Au (up to 400 ppb). One stream sediment sample draining the UZ of the intrusion showed 110 ppb Au (Waters 1987). It was argued that the source of the precious metals could be hosted in the Triple Group of the intrusion. The arguments for the search in the Triple Group were:

- 1 the occurrence of massive plagioclase-rich layers (the leucogabbro layers L1, L2 and L3) of the Triple Group (C. K. Brooks),
- 2 the unexpected presence of olivine phenocrysts in the Triple Group gabbros (S. Maaløe) and
- 3 the presence of immiscible sulfide droplets in Triple Group gabbros which suggests S-saturation in the magma at the time when the Triple Group formed (H. R. Naslund).

All of these features suggest changes in the crystallization parameters in the Triple Group succession, changes that could also have resulted in the deposition of Au and PGE.

Teck left the joint venture by the end of 1986 and in 1987 Platinova Resources Ltd. set out to identify the source of the anomalous Au and Pd. The Triple Group section was sampled in 10 traverses. The anomalous Au and Pd-bearing succession was found to be located in the lower L1 leucogabbro layer of the Triple Group and in a melanogabbro layer (M0) below L1 (Goodwin & Turner 1988). In the follow-up program in 1988 by a Platinova Resources Ltd./Corona Corporation joint venture the Triple Group was systematically chipped throughout the intrusion. The results from 36 chip lines, 22 packsack drill holes (up to 6 m deep) and four saw-cut profiles showed the presence of a continuous Au and Pd-rich zone from ca. 20 m below and up into L1 (Turner & Mosher 1989).

Early Exploration Stage (1989–1991)

By the end of 1988 the target zone was delineated and a drill operation was planned for

1989 by Platinova Resources Ltd./Corona Corporation joint venture. In the course of 2 months ca. 3000 m was cored (size: BQ) from holes 9 to 445 m deep (DDH 89-1 to 89-9B, Turner 1990). One hole was wedged twice. Magnetic susceptibility was measured at drill sites, but due to the many close-spaced anomalies not found to be useful during exploration. Cores were airlifted to the operation base in Sødalen, approximately 10 km to the east, where they were logged. The target interval was divided into 1m sections, split, crushed and sent for Pt, Pd and Au assays.

The anomalous zone was shown to continue underground in the south-central part of the intrusion and to include a lower PGE (Pd2) zone and an upper gold zone (Au–Pd1). Concentrations vary, but the recorded maximum grades were 5.5 g.t⁻¹ PGE (Pt/Pd=0.1) per m in Pd2 and 3.3 g.t⁻¹ Au per m and 8 g.t⁻¹ per 0.2 m in Au–Pd1 (Turner & Mosher 1989).

The results led the joint venture to drill 18 additional holes (BQ, DDH 90-10 to 90-27) from April to October 1990. The holes were up to 1100 m deep and a total of ca. 13,600 m of gabbro was cored. Watts, Griffis & McOuat Ltd. managed the operation and compiled the results (Watts, Griffis & McOuat 1991). As in 1989, the cores were airlifted to the operational base in Sødalen, logged, sectioned, split, crushed and sent for assaying on a weekly basis. Assay results were also received on a weekly basis to help guide the exploration. In a follow-up assay program, parts of the mineralized intervals were divided into 20 cm, and later in ca. 5 cm, sections for verification of the results of the first pass. The 1990 campaign confirmed the continuity of the mineralized section in the Triple Group. In Pd2 maximum PGE grades of 3 g.t⁻¹ over 3 m and in Au–Pd1 maximum Au grades of 2.8 g.t⁻¹ over 2 m and 14.3 g.t⁻¹ over 20 cm were recorded.

Preliminary resource estimates

Platinova Resources Ltd. and partners were entirely focused on the gold potential of the deposit. It was believed that it consisted of a continuous PGE-bearing gold horizon (Au–Pd1) and a lower gold-poor palladium horizon (Pd2) located at a variable depth of 20–40 m below the gold horizon. Palladium was at the time of no major interest and no resource estimates were made for the Pd2-horizon. Watts, Griffis & McOuat (1991) and Teck Corporation (1991) presented resource estimates for the Au–Pd1 horizon (Table 20-4).

THE PLATINOVA REEF OF THE SKAERGAARD INTRUSION

TABLE 20-4. RESOURCE ESTIMATES FOR THE AU-PD1 LEVEL

Au cut-off	Mio. tons	grade			contained metal		
		g Au.t ⁻¹	g Pd.t ⁻¹	g Pt.t ⁻¹	tons Au	tons Pd	tons Pt
Platinova Resources Ltd.							
global	91.036	1.827	0.388	0.066	166.303	35.562	6.041
> 2.0 g/t	38.396	2.383	0.451	0.103	91.513	17.321	3.963
> 2.2 g/t	25.526	2.503	0.524	0.136	63.883	13.364	3.484
> 2.5 g/t	14.212	2.577	0.352	0.038	36.620	4.996	0.543
Teck Corporation							
> 1.0 g/t	68,926	1.986	0.448	0.047	130.68	30.88	3.24
> 1.4 g/t	50,684	2.274	0.477	0.050	115.26	24.18	2.53
> 1.9 g/t	37,981	2.386	0.485	0.048	90.62	18.42	1.82
> 2.1 g/t	27,653	2.478	0.525	0.051	68.52	14.52	1.41

POST-EXPLORATION STUDIES (1991–2004)

Although a major and continuous Au and Pd deposit had been identified, the concentrations were seen as sub-economic, particularly in light of the falling gold prices. Platinova A/S as well as the Geological Survey of Greenland (now the Geological Survey of Denmark and Greenland, GEUS) continued investigations on the available material in an attempt to increase the potential value of the identified deposit. The deposit also attracted academia, surprised by the evidence for major PGE and Au mineralization in this quite small, well investigated intrusion.

Structure of the Platinova Reef

Bird *et al.* (1991) described the Platinova reef to consist of: (1) an upper gold-bearing horizon (Au) that partially overlaps with a palladium-rich horizon which together were referred to as Au–Pd1; (2) a gold-bearing palladium horizon 10 m below Au–Pd1 and (3) a lower Pd-horizon (Pd2) at a variable depth of 20 to 40 m below Au–Pd1. This description was based on the initial data obtained from chip lines in 1987–1988 and cores drilled in 1989.

Nielsen (2001) recompiled all the drill core data and developed a new model for the structure of the mineralization. The model, with a preliminary outline published by Andersen *et al.* (1998), shows the Platinova reef to comprise 8 continuous Pd-rich levels (from base to top: Pd5, Pd4b, Pd4a, Pd3b, Pd3a, Pd2b, Pd2a and Pd1, see Fig. 20-8 and Table 20-5). All of these levels can be correlated between widely spaced drill cores and chip lines over an area >23 km² (Nielsen 2001). The five main levels (Pd5, Pd4a, Pd3a, Pd2a and Pd1) with an internal

stratigraphic separation of *ca.* 10 m define a 40 m thick reef structure (Andersen *et al.* 1998, Nielsen 2001). The lower Pd5-level is found at the exact same stratigraphic position in all drill cores. It is located *ca.* 21 m below the center of L1 of the Triple Group in the lower part of a 2 m thick leucogabbro layer referred to as L0 and in the melano- and mesogabbro immediately below L0.

The concordance and lateral continuity of the Platinova reef suggests that it originally spanned the entire LS. It is believed that Pd5 was originally present throughout the upper MZ of the intrusion, although in many northern parts of the intrusion it has been lost to erosion (Fig. 20-3). From Pd4 up through Pd1 the concentration of Pd >0.5 g.t⁻¹ becomes more and more restricted to the central part of the intrusion (Fig. 20-9 and 20-10). The five Pd-levels can be followed wherever the Triple Group is preserved and maintain constant stratigraphic separation in the concordant, bowl-shaped reef (Nielsen 2001).

If the Platinova reef is defined as the sections of the Pd-levels with >0.5 g.t⁻¹ precious metals, its entire structure is similar to a stack of flat bowls with decreasing diameter upwards (Fig. 20-9). The lowermost bowl (Pd5) would be app. 7 x 10 km wide and 700 m deep. Pd5 is up to 5 m thick (at 1 g.t⁻¹ cut-off). The uppermost Pd-level (Pd1) is suggested to be *ca.* 3 km in diameter and 2–3 m thick (Fig. 20-9). The restricted number of intersects over the significant area covered by the Platinova reef do not allow at present a more detailed 3D model for the Pd-structure.

Gold is not concentrated in a specific stratigraphic level. In all cores the gold is concentrated in the uppermost, well-defined, Pd-

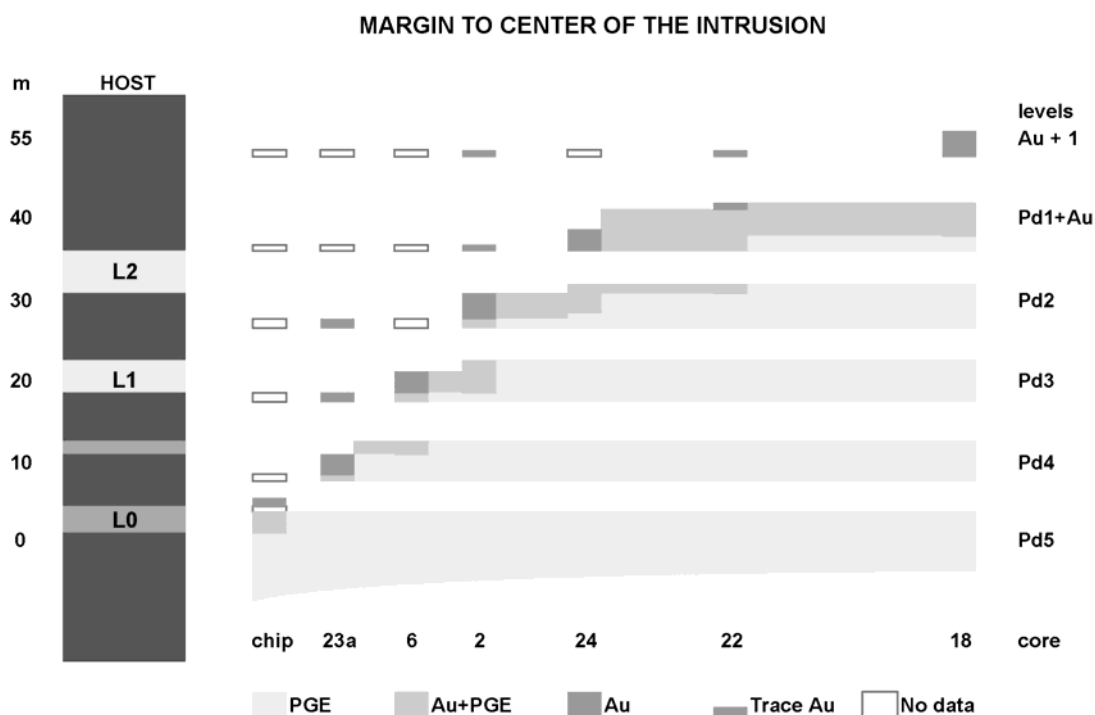


FIG. 20-8. Lithological cross section of the Triple Group and the Platinova reef displaying the changes in the reef from the northern margin towards the south center of the intrusion.

level or in a level above. The Pd-levels are concordant and continuous and the so-called “Au-horizon” is accordingly discontinuous. There is not at present evidence for continuity of the Au-horizon. Instead, Au appears to be concentrated in the rims of the individual Pd-bowls. The fundamental difference between the interpretation of the stratigraphy of the Pd and Au levels between Bird *et al.* (1991) and Nielsen (2001) is illustrated in Fig. 20-10.

Four additional levels with strongly decreasing concentrations of gold (Au+1 to Au+4) are identified in the 60 m section above Pd1 (see Table 20-5). These gold levels are identified in several drill cores and the “Au+1” level shows an increase in “grade times width” value toward the south-central part of the intrusion (Bird *et al.* 1991) which has not yet been drilled.

Stratigraphic Control

No direct correlation is apparent between the lithology of the host rocks and the PGE or Au concentration. Pd-levels are hosted in leuco-, meso- as well as melanogabbro. The mineralization can not be identified with the naked eye or a hand lens in cores or grab samples. It takes a trained eye to identify the leucogabbro layers in the cores. The petrographic and chemical stratigraphy shows,

however, a remarkable conformity. Whatever process caused the concentration of PGE and Au in the well-defined mineralization levels, it seems to have been linked to the formation of the primary magmatic layering in the gabbro.

A main emphasis of the scientific studies has been the development of methods that would allow for precise identification of the mineralized section(s) within narrow limits and the correlation along strike between cores. Density profiles combined with chemical analysis and assays allow a very detailed inter-hole correlation of the Pd-levels and the magmatic layering. The Pd-levels are, within the limits of the analytical data, perfectly concordant with the magmatic layering in the host gabbros (Andersen *et al.* 1998, Nielsen 2001). The stratigraphic column in Fig. 20-8 gives the position of the leucogabbro layers in the Triple Group and the position and approximate thickness of the Pd-levels.

Mineralogy of the Platinova reef

Sulfides, magnetite and ilmenite.

In all investigations the main sulfides of the Platinova reef are bornite, chalcocite and digenite with minor chalcopyrite and idaite. Rare sulfides include pentlandite, cobaltian pentlandite, sphalerite

TABLE 20-5: CHARACTERIZATION OF CONFORMABLE MINERALIZATION LEVELS AND THE PGE AND AU MINERALOGY REPORTED TO DATE.

metres above peak in Pd5	Pd/Au level	east margin	west margin	Toward center of mineralization →	central	south center
		core DDH-23A	Core DDH-14	Bird et al (1991), Turner (1991) and core DDH 89-08	core DDH 89-02	core DDH-18
c. 105	Au+4	no data	no data	no data	no data	Low Au atokite, vasilite, vysotskite, (Ag,Au)- alloys
c. 90	Au+3	no data	no data	no data	no data	low Au, no mineralogical data
c. 70	Au+2	no data	no data	no data	no data	low Au, no mineralogical data
c. 56	Au+1	no data	no data	no data	no data	Top of mineralization Au Pb-imagreite, Pd- melonite, (Au,Cu)- alloys
40.9	Au/Pd1	low Au, no mineral- ogical data	low Au, no mineral- ogical data	no data	no data	Pd+Au keithconnite, native copper, SK**, vysotskite, zvyagintsevite, (Pd,Au,Cu)-alloy
32	Pd2a	low Au, no mineralogical data	no data dike cut-out	Low Au+Pd, no mineralogical data	Top of mineralization Au+Pd, no mineralogical data	Pd arsenopalladinite, atokite, guanglinite, kotulskite, (Au,Cu)- alloys

Dominant PGE and Au minerals and phases in bold. Dominant element in alloys in bold. Dominant precious metal in assays and bulk rock comments in italics. Table continues on next page.)

TABLE 20-5 (CONTINUED)

metres above peak in Pd5	Pd/Au level	east margin	west margin	Toward center of mineralization →	central	south center
28.1	Pd2b	core DDH-23A <i>low Au, no mineralogical data</i>	core DDH-14 <i>no data, dike cut- out</i>	Bird et al (1991), Turner (1991) and core DDH 89-08 <i>Low Au+Pd, no mineralogical data</i>	core DDH-24 Pd SK**, (Pd,Cu,Sn)- alloy, (Pd,Ag)-alloy	core DDH-18 Pd keithomite, kotulskite, SK**, vasilite, (Pd,Cu,Sn)- alloys
19.5	Pd3a	<i>low Pd+Au, no mineralogical data</i>	<i>no data, dike cut- out</i>	Top of mineralization <i>Au+Pd, no mineralogical data</i> (Au,Cu)-alloys***	Pd limited data SK**	Pd limited data atokite, native silver, kotulskite, SK**, vysotskite, zvyagintsevite, (Pt,Pd,Fe,Cu)-alloys
16	Pd3b	<i>low Au+Pd, no mineralogical data</i>	<i>no data, dike cut- out</i>	Pd+Au, no mineralogical data	Pd, no mineralogical data	Pd, no mineralogical data
9.2	Pd4a	Top of mineralization <i>Au+Pd, limited mineralogical data</i> kotulskite	Top of mineralization <i>Au+Pd, no mineralogical data</i>	Pd, no mineralogical data	Pd, no mineralogical data	Pd, no mineralogical data
4.9	Pd4b	Pd, no mineralogical data	Pd, no mineralogical data	Pd, no mineralogical data	Pd, no mineralogical data	Pd no mineralogical data

Dominant PGE and Au minerals and phases in bold. Dominant element in alloys in bold. Dominant precious metal in assays and bulk rock comments in italics. (Table continues on next page.)

TABLE 20-5 (CONTINUED)

metres above peak in Pd5	Pd/Au level	east margin	west margin	Toward center of mineralization →	central	south center
0	Pd5	core DDH-23A	core DDH-14	Bird et al (1991), Turner (1991) and core DDH 89-08 <i>Pd, no mineralogical data</i>	core DDH-24 <i>Pd, no mineralogical data</i>	core DDH-18
		arsenopalladinite* atokite* bogdanovite* guanglinite* isomertiteite* keithconnite* kotskite* native palladium* native silver* palladoarsenide* polybasite* SK* sperryite* stephanite* tetraauricupride* vasilite* vysotskite* zvyagintsevite* (Au,Ag)-alloys* (Au,Pd,Cu)-alloys* (Au,Pd,Cu,Ag)-alloys* (Pt,Pd,Au,Cu,Fe)-alloys*	arseno-palladinite braggite guanglinite isomertiteite keithconnite Pt-SK** sperryite zvyagintsevite arseno-palladinite		atokite bogdanovite* hongshiite* keithconnite* SK** tetraferroplatinum* unn. PdAuCu2* unn. Pd3Cu* unn. (Pt,Pd)Cu3* vasilite* zvyagintsevite* (Pd,Cu,Sn)-alloy*	atokite* bogdanovite* braggite* guanglinite* isomertiteite* keithconnite* SK** tetraauricupride* unn. PdAuCu2* unn. Pd3Cu* unn. (Pt,Pd,Cu)3* vasilite* vysotskite* zvyagintsevite* (Ag,Au)-alloy* (Pd,Cu,Sn)-alloy* (Pt,Fe,Cu,Pd)-alloys*

Data sources: Bird *et al.* (1991), Turner (1991), Andersen *et al.* (1998), Nielsen *et al.* (2003a-e) and H.Rasmussen (unpublished). All mineralogical data from cores DDH 90-14, 90-18, 90-23A and 90-24 from Pd4b to Au+4 levels by H. Rasmussen (unpublished, but partially included in Nielsen *et al.* 2003a-e). Dominant PGE and Au minerals and phases in bold. Dominant element in alloys in bold. Dominant precious metal in assays and bulk rock comments in italics.

* Minerals identified in detailed investigations (Nielsen *et al.* 2003a-e).

** New mineral (Pd,Cu): Accepted by IMA as Skaergaardite (Rudashevsky *et al.* 2004).

*** Data from the top Au level in Pd3 at Puku section (Bird *et al.*, 1991 and Turner, 1991).

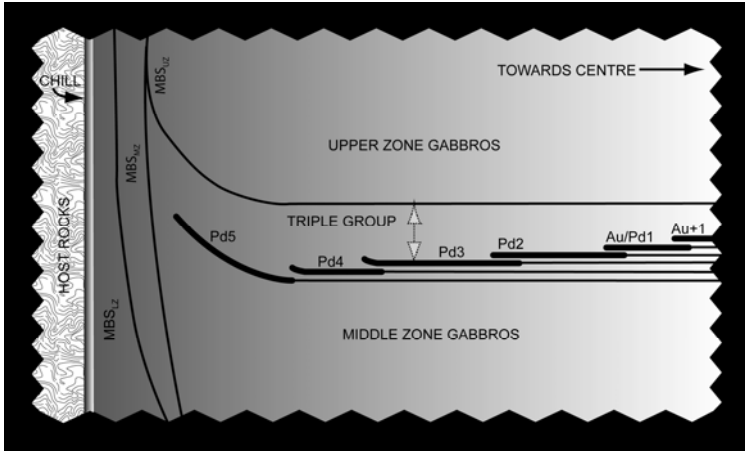


FIG. 20-9. Schematic outline of the structure of the stratiform Pd-levels of the Platinova reef (not to scale). Thick lines mark intervals where individual levels are dominated by Au, and thin lines where the levels are dominated by Pd. In contrast to the continuous (and concordant) stratiform Pd-levels, the “Au-horizon” represents the discontinuous (and discordant) combination of intervals where the Pd-levels are dominated by Au.

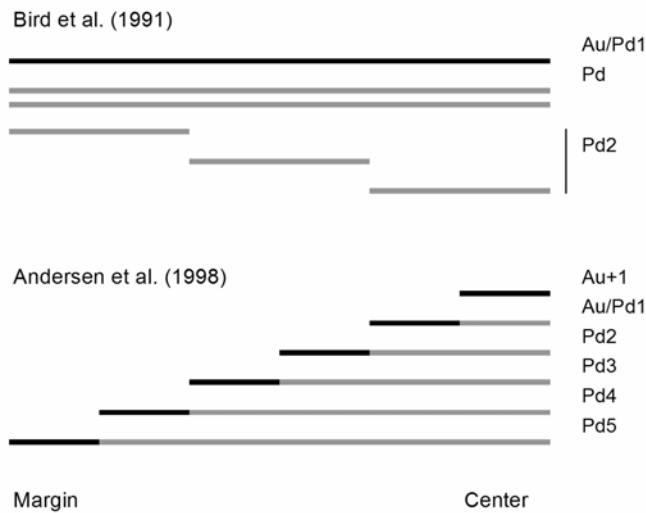


FIG. 20-10. Evolution in the perceived structure of the Platinova reef from the earliest interpretations (Bird *et al.* 1991) to the current model.

and covellite. Pure iron sulfides (pyrrhotite and pyrite) appear to be completely absent; instead the sulfides commonly include crystals of Ti-poor magnetite. Andersen *et al.* (1998) and Nielsen *et al.* (2003a–e) give detailed descriptions.

The Cu-dominated sulfides are found in crystallized melt inclusions in liquidus magnetite and ilmenite (Fig. 20-11a–b), in rims of silicate minerals, and as interstitial masses spatially related to matrix magnetite and ilmenite. The inclusions mostly form negative crystals, suggesting that the sulfide melt droplets were melts during the crystallization of their host Fe–Ti-oxides. Some sulfide droplets contain equilibrium magnetite (Nielsen *et al.* 2003a–e). Bornite, digenite and chalcocite form >90% of the sulfide paragenesis in the main Pd5-level. The primary textures and the

bornite–chalcocite paragenesis suggest a partial preservation of high temperature textures and sulfide paragenesis.

PGE and Au phases

PGE and Au minerals are found: (1) as euhedral and anhedral crystals in sulfide droplets (Fig. 20-11c–d), (2) as free grains in the rims of silicates phases and the matrix (Bird *et al.* 1991, Andersen *et al.* 1998) and (3) in intergrowth with sulfide blebs in the matrix (Bird *et al.* 1991, Andersen *et al.* 1998). In some cases precious metal phases can be seen to drop out of sulfide blebs. This suggests that the precious metal phases were liquidus phases that originally crystallized in the sulfide droplets. Precious metal grains enclosed in the rims of silicate phases could originally have been liquidus

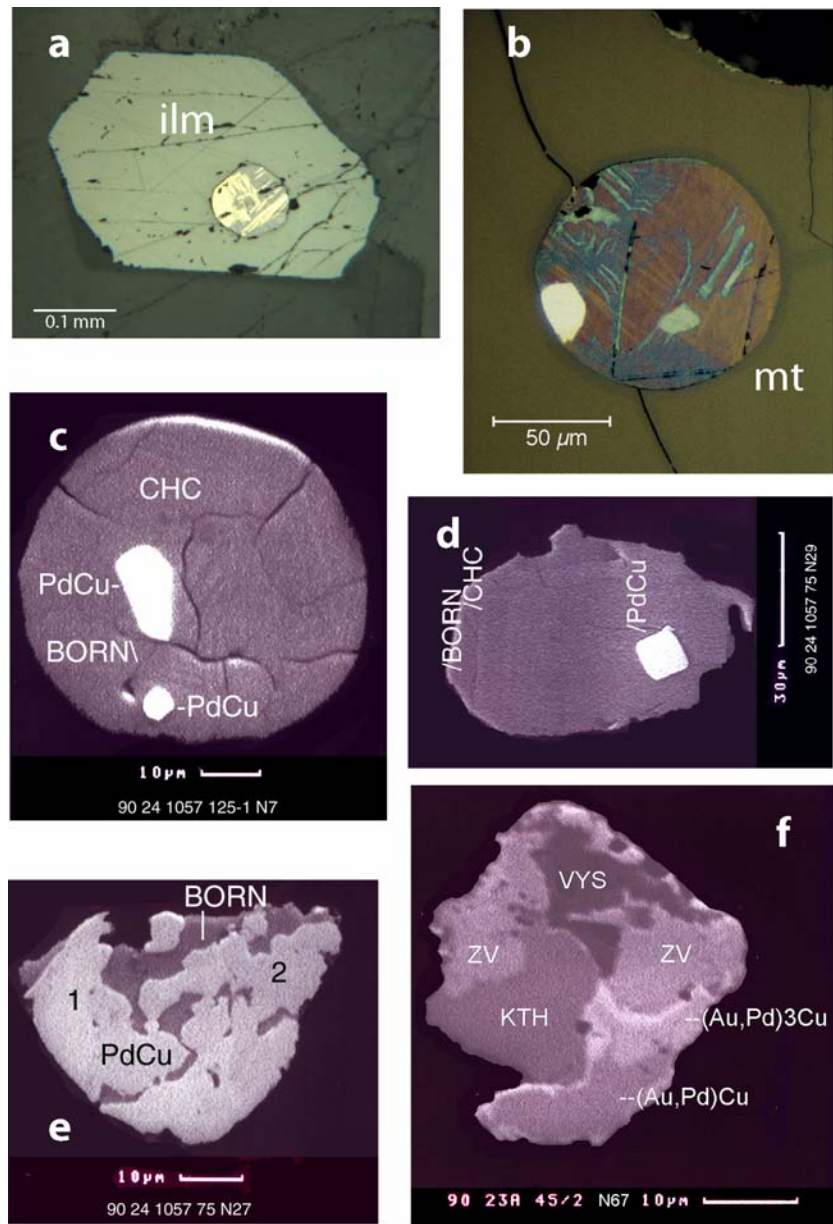


FIG. 20-11. Petrographic relations of sulfide and Au-Pd minerals. (a) Globular sulfide grain of intergrown bornite and chalcocite enclosed in cumulus ilmenite (ilm) crystal. (b) Globular composite sulfide droplet (lamellar intergrowth of bornite and chalcocite) including a grain of skaergaardite in titanomagnetite (mt) crystal. (c) Composite sulfide grain with two inclusions of skaergaardite. (d) Sulfide grain (bornite and chalcocite intergrowth) with euhedral crystal of skaergaardite (PdCu). (e) Intricate intergrowth (or exsolution) texture between skaergaardite and bornite. (f) Intricate intergrowth of different noble metal minerals (VYS = vysotskite, KTH = keithconnite, ZV = zvyagintsevite) showing the complex mineralogical relations of the Platinova reef near the Eastern margin of the intrusion.

phases dropped out of sulfide droplets.

The PGE and Au minerals reported by Bird *et al.* (1991), Turner (1991), Andersen *et al.* (1998), unpublished data by H. Rasmussen, and Nielsen *et al.* (2003a–e) are summarized in Table 20-5. Andersen *et al.* (1998) and unpublished data from

H. Rasmussen (GEUS) suggest a systematic variation in the PGE and Au mineral paragenesis (Table 20-5). Detailed analysis of five samples from the Pd5 level by Nielsen *et al.* (2003a–e) recorded 35 different PGE and Au minerals and phases. The parageneses are characteristically poor in sulfur.

The mineralogical data (Table 20-5) are insufficient for a detailed description of the stratigraphic and lateral variation in the mineralogy of the Platinova reef. It is however observed that:

1. The main part of the Platinova reef, except for the marginal cores (DDH 90-14 and 90-23A), seems dominated by the new mineral skaergaardite (PdCu) and vysotskite.
2. Platinum minerals are not common, due to the low concentration of Pt. They appear in the relatively Pt- and Au-rich, upper parts of individual Pd-levels and include sperrylite (PtAs₂) and a suite of Pt-alloys.
3. The marginal parts of the intrusion are dominated by zvyagintsevite (Pd₃Pb).
4. Pd-arsenides, arsenopalladinite (Pd₈As₃) and guanglinite (Pd₃As) are common in skaergaardite- and zvyagintsevite-dominated parageneses.
5. The gold-rich Pd levels are dominated by tetraauricupride (AuCu), Au-alloy with minor Cu (*e.g.*, Bird *et al.* 1991), and tellurides including the Pd-bearing tellurides imgreite (NiTe) and melonite (NiTe₂) and the Pd-tellurides kotulskite (PdTe) and keithconnite (Pd₃Te).
5. Ag minerals are rare, but include stephanite (Ag₅SbS₄), native silver, and polybasite (Ag₁₆Sb₂S₁₁).
6. Many other phases and minerals have been observed including a suite of (PGE,Au,Fe,Cu, *etc.*)-alloys and vasilite (Pd₃Sn).

Skaergaardite, as described by Rudashevsky *et al.* (2004), appears to be the totally dominating PGE mineral in Pd5 in all of the central part of the intrusion. The preserved parts of the Pd5 level contains >285 million tons of ore (Nielsen 2001), and the entire level before erosion probably amounted to some 450 million tons. With 2 g.t⁻¹ Pd the Pd5 level potentially contains >1,000 tons of skaergaardite composed of *ca.* 60 wt.% Pd, 35 wt.% Cu and minor Pt, Zn, Sn, Au, *etc.* Despite the extensive erosion, a search for placers has so far not yielded positive results.

The apparently primary textures suggest skaergaardite to be a liquidus phase in the sulfide droplets. Karup-Møller & Makovicky (1999) investigated the Cu–Pd–S system and found that a PdCu phase was on liquidus in equilibrium with digenite and a Pd–Cu–S melt at temperatures up to at least 900°C (Fig. 20-12). It is tempting to interpret the bornite-chalcocite sulfide melt inclusions with euhedral skaergaardite (Fig. 20-11c)

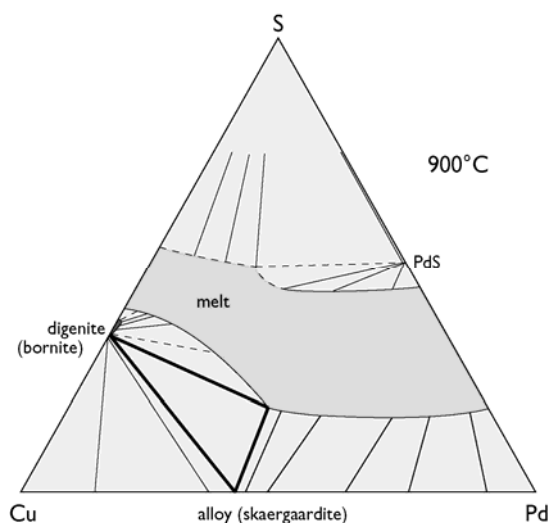


FIG. 20-12. Phase relations of the Cu–Pd–S system at 900°C (Karup-Møller & Makovicky 1999). The bold lines indicate the stability of skaergaardite and digenite in equilibrium with sulfide liquid.

and the coexisting immiscible PdCu structures (Fig. 20-11e) as the natural equivalent to the experimental system: Skaergaardite as the original liquidus PdCu phase, the bornite-chalcocite paragenesis as the Fe-bearing equivalent to digenite in the Cu–Pd–S system, and the amoeboid PdCu-bornite intergrowths as the equivalent to the Pd–Cu–S liquid in the system.

Metallurgic investigations

Platinova Resources Ltd. conducted metallurgical tests on the gold-rich horizon. Initially, the only interesting commodity was gold. As gold prices declined the focus was also directed toward ilmenite, which as a by-product could increase the contained value of the gold horizon. Palladium has since the late 1990's been considered a major contributor to the contained value of the Platinova reef.

Lakefield Research (1988) studied on behalf of Pegasus Gold three 1 kg composites with a maximum grade of 1.2 g.t⁻¹ gold. The preliminary flotation tests indicated excellent response, short flotation times, and recoveries of gold up to 87%. Cyanidation tests on 500 g samples of the composites gave recoveries up to 95%. In a similar investigation (Lakefield Research 1989) recoveries of 84.6% could be obtained by flotation. By selective leaching the same composites gave recoveries for gold up to 95%.

In 1995 Platinova A/S investigated the

possibilities for the production of a marketable grade ilmenite concentrate from a copper/gold flotation tailing. A 150 kg bulk sample with 6.47 wt.% TiO₂, 1.35 g.t⁻¹ gold and 0.12 wt.% Cu was used for the test. The results reported by Lakefield Research (1996), indicate that a marketable ilmenite concentrate with 49.7 wt.% TiO₂ can be produced. The recovery of TiO₂ was 68.2%, with two-thirds of the remaining TiO₂ in titaniferrous magnetite.

RE-JUVENATED EXPLORATION (2000–2004)

The investigations of the potential of the Skaergaard mineralization came to a halt in the 1990's. Gryphon Metals Corporation (Vancouver, Canada) acquired the concession in the beginning of 2000. The results and activities are at date (2004) confidential. In 2002 Shambhala Gold Corporation and Gryphon Metals Corporation formed the company Skaergaard Minerals Corporation (SMC), which from the end of 2003 is wholly owned by Galahad Gold PLC.

Skaergaard Minerals Corporation (SMC) initiated renewed exploration in 2003, including detailed saw-cut and bulk sampling as well as drilling. A major exploration campaign is planned for 2004 and 2005. The basis for the new interest is the multi-element approach and the improved knowledge on the structure of the mineralization originally proposed by GEUS. SMC sees the mineralization as an ilmenite, V, Ga, Au, Pd, Pt and Cu deposit. The Platinova reef is by Galahad Gold PLC (2004b) suggested to contain:

- 1) 1.87 billion tonnes of ore (global tonnage),
- 2) 38.8 million ounces precious metal Au-equivalents including 10.8 million oz. Au, 34.8 million oz. Pd and 3 million oz. Pt.
- 3) precious metal host rocks with 23 \$US per tonnes of recoverable Cu, Ti, V and Ga.

TOWARD A MODEL FOR THE SKAERGAARD-TYPE MINERALIZATION

Current models for the formation of PGE reefs include: (1) S-saturation of the magma and accumulation of immiscible, PGE and Au-bearing sulfide in response, *e.g.*, to magma replenishment (“downers process”, *e.g.*, Naldrett *et al.* 1990) and (2) chromatographic separation and deposition of PGM by migrating melt/fluid (“uppers process”, *e.g.*, Boudreau & McCallum 1992). As described below, neither of these models appear to account fully for the systematics and structure of the

Platinova reef. The complex structure of the Platinova reef is likely to have formed under the influence of several processes, possibly involving both the “downers” and the “uppers” categories.

Turner (1986) documented changes in the S-content and the Cu–S ratio in the upper part of the Middle Zone, which she interpreted to represent silicate-sulfide liquid immiscibility. Andersen *et al.* (1998) documented that the Pd and Au concentrations in the Lower and Middle Zones (below the Platinova reef) are as expected from the amount of interstitial trapped liquid, whereas rocks from the Upper Zone (above the reef) appear to have been almost completely drained of Pd and Au. This indicates that the metals were collected from the residual magma body consistent with a “downer” model of silicate-sulfide liquid immiscibility and sulfide accumulation. The strong textural association of Pd and Au minerals with sulfides and the preserved drop-like shapes of sulfide blebs support such a model (Nielsen *et al.* 2003a–e). However, no evidence for magma replenishment has been found, indicating that the liquid immiscibility was reached entirely during closed system fractional crystallization.

Although the general progression from Pd to Au to Cu upwards through the Platinova reef can be explained by fractional segregation of sulfide liquid (as proposed for the Great Dyke, Wilson & Tredoux 1990, and the Munni Munni complex, Barnes 1993), a straightforward “downer” model cannot explain the intricate structure and mineralogical systematics of the Platinova reef. In particular, the repetitive nature of the mineralization and the outward zoning from Pd to Au (to Cu) within the individual strata (the Pd-levels) are difficult to explain in the light of a simple, single stage silicate-sulfide liquid immiscibility process. It could, in contrast, be suggested that each Pd-level in part exemplifies the concentration and separation of PGE and Au in migrating liquids within the confines of stratigraphic units in the layered gabbros. It is possible that the leucocratic layers of the Triple Group, which approach accumulate textures, could act as semi-impermeable barriers for interstitial liquids. This could lead to the ponding and subsequent outward migration of filter-pressed interstitial liquid immediately below the leucocratic layers. Fractional crystallization of the sulfide liquid (Ballhaus *et al.* 2001) or chromatographic separation (*cf.* Boudreau & Meurer 1999) during interstitial liquid migration could potentially be

responsible for the lateral variation within the individual strata. A detailed understanding of the origin of the macrorhythmic layering in the Triple Group appears to be a prerequisite for the development of a rigorous and detailed mineralization model. Such a model is not presently at hand.

It is a further enigma that the observed immiscible sulfide droplets are Cu-rich and Fe-poor. This is contradictory to experimental data which suggest that immiscible sulfide liquids in Fe-rich basaltic magmas should be Fe-rich and crystallize monosulfide solid solution. The Platinova reef sulfides contain no Fe-sulfides but have abundant magnetite. Cu-rich sulfide melt inclusions occur in cumulus Fe–Ti oxides as well as in interstitial oxides. Matrix sulfide blebs in the Pd5-level are commonly found in intergrowths with patches rich in Fe–Ti-oxides (Nielsen *et al.* 2003a–e). The absence of pyrrhotite could be explained by desulfurization, but this contradicts the preserved droplet and negative crystal shapes of the sulfide melt inclusions. In contrast, the Cu-rich melts appear to be trapped in Fe–Ti-oxide cumulus grains as Cu-rich, Fe-poor sulfide melts. It is possible that with extremely high concentrations of Cu and low S, that such Cu-rich, Fe-poor sulfides can form – perhaps governed by the Cu rather than the S solubility in the silicate magma. Sulfides dominated by primary magmatic bornite were observed in experimental studies on basalts doped with Cu by Ripley *et al.* (2002).

LESSONS LEARNED FROM THE PLATINOVA REEF

The foremost lesson to be learned from the Platinova reef is there is much to be learned about the behavior of PGE and Au in layered intrusions. The Skaergaard gabbros only contain traces of sulfide, stream sediment and grab samples gave only little indication, and field observations did not suggest the existence a major PGE reef structure. Commonly accepted models would not have predicted the existence of the Platinova reef.

The second lesson is that the reef would never have been found without significant luck and perseverance. It is was a stroke of luck that the first indications of PGE and Au mineralization were observed, and it was defiance of common views and perseverance using classic exploration tools that led to the discovery of the Platinova reef.

With the current knowledge it is clear that a whole group of PGE deposits may have been overlooked in evolved mafic intrusions (*cf.* Miller & Andersen 2002). From a genetic point of view, the formation of Skaergaard-type mineralizations appears to require evolved, Fe-rich basaltic magmas with low S, perhaps of plume origin. In such magmas PGE concentrations may be high and S-saturation will occur late in the crystallization history (Momme *et al.* 2002). This may be a prerequisite for the formation of economic Skaergaard-type mineralizations.

The detailed structure and genesis of the individual levels of PGE enrichment may reflect local conditions. It is accordingly difficult to give general suggestions for an exploration strategy for Skaergaard-type mineralizations. The best suggestion seems to be a targeted exploration of differentiated intrusions formed from S-unsaturated parental magmas in hot spot settings. A systematic exploration program should involve a detailed testing of geochemical indicators of silicate–sulfide liquid immiscibility (S, Cu, Ni, Co) followed by targeted assaying for Au and PGE.

The discovery of the Platinova reef is not the first time a “Monte Carlo approach” involving luck, perseverance and detailed sampling has yielded interesting results. Commonly though, such an approach led only to the testing of the mythological boulders with exceptional concentrations (one was found on Kap Edvard Holm, another on the Carlingford complex, Republic of Ireland) rather than the discovery of economic mineral deposits. Although random testing cannot be recommended as a general approach, the Platinova reef demonstrates that on occasions it can lead to unexpected and interesting discoveries.

ACKNOWLEDGEMENTS

This contribution is published with the permission of the Geological Survey of Denmark and Greenland. The authors wish to acknowledge the continued support by Platinova A/S, Skaergaard Minerals Corporation, and the Danish Lithosphere Centre. Long-term cooperation and discussions with Dennis Bird, Robert Gannicott, Neil Irvine, William Mosher, Patricia Turner, and Richard Naslund are greatly appreciated. The authors are also grateful for constructive reviews by Markku Iljina, James Mungall, and Christian Tegner.

REFERENCES

- ANDERSEN, J.C.Ø. (1996): *The Skaergaard intrusion and the Platinova gold and palladium deposit, Kangerlussuaq area, East Greenland*. Ph.D. thesis, Copenhagen University, 230 p.
- ANDERSEN, J.C.Ø. & BROOKS, C.K. (2004): The (virtual) Skaergaard intrusion. www.skaergaard.org.
- ANDERSEN, J.C.Ø., POWER, M.R. & MOMME, P. (2002): Platinum-group elements in the Paleogene North Atlantic Igneous Province. In *The Geology, Geochemistry, Mineralogy, and Mineral Beneficiation of Platinum-group Elements*. Cabri, L.J. (ed.). Can. Inst. Mining, Metall., & Petrol. *CIM Special Volume* **54**, 637-667.
- ANDERSEN, J.C.Ø., RASMUSSEN, H., NIELSEN, T.F.D. & RØNSBO, J.G. (1998): The Triple Group and the Platinova gold and palladium reefs in the Skaergaard intrusion: Stratigraphic and petrographic relations. *Econ. Geol.* **93**, 488-509.
- ANDREASEN, R., PEATE, D.W. & BROOKS, C.K. (2004): Magma plumbing systems in large igneous provinces: Inferences from cyclical variations in Paleogene East Greenland basalts. *Contrib. Mineral. Petrol.* **147**, 438-452.
- ARNASON, J.G. (1995): *Gold and platinum-group element mineralization in Tertiary mafic intrusions of East Greenland*. Ph.D. dissertation, Stanford University, California, 197 p.
- BALLHAUS, C., TREDOUX, M. & SPATH, A. (2001): Phase relations in the Fe–Ni–Cu–PGE–S system at magmatic temperature and application to massive sulphide ores of the Sudbury Igneous Complex: *J. Petrol.* **42**, 1911-1926.
- BARNES, S.J. (1993): Partitioning of the platinum group elements and gold between silicate and sulphide magmas in the Munni Munni complex, Western Australia. *Geochim. Cosmochim. Acta*, **57**, 1277-1290.
- BERNSTEIN, S., ROSING, M.T., BROOKS, C.K. & BIRD, D.K. (1992): An ocean-ridge type magma chamber at a passive volcanic, continental margin: the Kap Edvard Holm layered gabbro complex, East Greenland. *Geol. Mag.* **129**, 437-456.
- BIRD, D.K., BROOKS, C.K., GANNICOTT, R.A. & TURNER, P.A. (1991): A gold-bearing horizon in the Skaergaard Intrusion, East Greenland. *Econ. Geol.* **86**, p. 1083-1092.
- BLANK, H.R. & GETTINGS, M.E. (1973): Subsurface form and extent of the Skaergaard Intrusion, East Greenland. *EOS, Trans. Am. Geophys. Union* **54**, p. 507.
- BOUDREAU, A.E. & MCCALLUM, I.S. (1992): Concentration of platinum-group elements by magmatic fluids in layered intrusions. *Econ. Geol.* **87**, 1830-1848.
- BOUDREAU, A.E. & MEURER, W.P. (1999): Chromatographic separation of the platinum-group elements, gold, base metals and sulfur during degassing of a compacting and solidifying igneous crystal pile: *Contrib. Mineral. Petrol.* **134**, 174-185.
- BOUDREAU, A.E., MATHEZ, E.H. & MCCALLUM, I.S. (1986): Halogen geochemistry of the Stillwater and Bushveld Complexes: Evidence for transport of the platinum-group elements by Cl-rich fluids. *J. Petrol.* **27**, 967-986.
- BROOKS, C.K. & NIELSEN, T.F.D. (1982): The Phanerozoic development of the Kangerdlugssuaq area, East Greenland. *Meddelelser om Grønland, Geoscience* **9**, 1-30.
- BROOKS, C.K. & NIELSEN, T.F.D. (1990): The differentiation of the Skaergaard Intrusion. A discussion of Hunter & Sparks (Contrib Mineral Petrol 95: 451-461). *Contrib Mineral. Petrol.* **104**, 235-247.
- CROCKET, J.H., VINCENT, E.A. & WAGER, L.R. (1958): The distribution of gold in some basic and ultrabasic igneous rocks and minerals. *Geochim. Cosmochim. Acta* **14**, 153.
- FRAM, M.S. & LESHER, C.E. (1997): Generation and polybaric differentiation of East Greenland Early Tertiary flood basalts. *J. Petrol.* **38**, 231-275.
- GALAHAD GOLD PLC (2004a): Galahad Gold PLC investor presentation. www.galahadgold.com/ggp/ir/presentations/invpresmay04/pdf.pdf, accessed May 2004.
- GALAHAD GOLD PLC (2004b): Galahad Gold PLC website. www.galahadgold.com/, accessed May 2004.
- GOODWIN, J.A. & TURNER, P.A. (1988): East Greenland Kangerdlugssuaq Concession, Summary report of 1987 program, 43 pp.

- Exploration report (in archive of the geological Survey of Denmark and Greenland, GRF no. 20844).
- HANSEN, H. & NIELSEN, T.F.D. (1999): Crustal contamination in Paleogene East Greenland flood basalts: plumbing system evolution during continental rifting. *Chem. Geol.* **157**, 89-118.
- HIGGINS, A.C. & SOPER, N.J. (1981): Cretaceous–Palaeogene sub-basaltic and intrabasaltic sediments of the Kangerdlugssuaq area, Central East Greenland. *Geol. Mag.* **118**, 337-448.
- HIRSCHMANN, M.M., RENNE, P.R. & MCBIRNEY, A.R. (1997): $^{40}\text{Ar}/^{39}\text{Ar}$ dating of the Skaergaard intrusion. *Earth Planet. Sci. Lett.* **146**, 645-658.
- HUNTER, R.H. & SPARKS, R.S.J. (1987): The Differentiation of the Skaergaard Intrusion. *Contrib. Mineral. Petrol.* **95**, 451-461.
- IRVINE, T.N. (1987): Layering and related structures in the Duke Island and Skaergaard Intrusions: Similarities, differences and origins. In *Origins of Igneous Layering*, Parsons, I. (ed.). NATO ASI Series C, Dordrecht, Reidel, **196**, 185-245.
- IRVINE, T.N. (1992): Emplacement of the Skaergaard intrusion. *Carn. Inst. Wash. Year Bk* **91**, 91-96.
- IRVINE, T.N., ANDERSEN, J.C.Ø. & BROOKS, C.K. (1998): Included blocks (and blocks within blocks) in the Skaergaard Intrusion: Geological Relations and the Origins of Rhythmic Modally Graded Layers. *Geol. Soc. Am. Bull.* **110**, 1398-1447.
- KARUP-MØLLER, S. & MAKOVICKY, E. (1999): The phase system Cu–Pd–S at 900 degrees, 725 degrees, 550 degrees, and 400 degrees C. *Neues Jb. Mineral.–Monatshefte* **1999**, 551-567.
- LAKEFIELD RESEARCH LTD. (1988): An investigation of the recovery of gold from Skaergaard – Greenland project samples submitted by Platinova Resources INC. Progress report 1 (project report No. L.R. 3633), 41 pp. Internal report (in archive of the Geological Survey of Denmark and Greenland, GRF. no. 20920).
- LAKEFIELD RESEARCH LTD. (1989): An investigation of the recovery of gold from Skaergaard – Greenland project samples submitted by Platinova Resources Ltd. Progress report no. 2 (per Lavana/Royex) 29 pp. Internal report (in archive of the Geological Survey of Denmark and Greenland, GRF. no. 20918).
- LAKEFIELD RESEARCH LTD. (1996): An investigation of the recovery of ilmenite from a copper/gold flotation tailings submitted by Platinova A/S, Progress report No. 1, Technical report 1995 Skærgaard project licence 08/92. 26 pp. Internal report (in archive of the Geological Survey of Denmark and Greenland, GRF. no. 21439).
- LARSEN, L.M., FITTON, J.G. & FRAM, M.S. (1998): Volcanic rocks of the Southeast Greenland Margin in comparison with other parts of the North Atlantic Tertiary Igneous Province. *Proceedings of the Ocean Drilling Program, Scientific Results* **152**, 315-330.
- LARSEN, L.M., FITTON, J.G. & SAUNDERS, A.D. (1999a): Composition of the volcanic rocks from the Southeast Greenland Margin, Leg 163: Major and trace element geochemistry. *Proceedings of the Ocean Drilling Program, Scientific Results* **163**, 63-75.
- LARSEN, L.M., WATT, W.S. & WATT, M. (1989): Geology and petrology of the Lower Tertiary plateau basalts of the Scoresby Sund region, East Greenland. *Bull. Grønlands Geologiske Undersøgelse (Geol. Surv. Greenland Bull.)* **157**, 164.
- LARSEN, M., BJERAGER, M., NEDKVITNE, T., OLAUSSEN, S. & PREUSS, T. (2001): Pre-basaltic sediments (Aptian–Paleocene) of the Kangerlussuaq Basin, southern East Greenland. *Geol. Surv. Greenland Bull.* **189**, 99-106.
- LARSEN, M., HAMBERG, L., OLAUSSEN, S., NØRGAARD-PEDERSEN, N. & STEMMERIK, L. (1999b): Basin evolution in southern East Greenland: An outcrop analog for Cretaceous–Paleogene basins on the North Atlantic volcanic margins. *AAPG Bull.* **83**, 1236-1261.
- LEEMAN, W.P., DASCH, E.J. & KAYS, M.A. (1976): $^{207}\text{Pb}/^{206}\text{Pb}$ whole-rock age of gneisses from the Kangerdlugssuaq area, eastern Greenland. *Nature* **263**, 469-471.
- LIGHTFOOT, P.C., HAWKESWORTH, C.J., OLSHEFSKY, K., GREEN, T., DOHERTY, W. & KEAYS, R.R. (1997): Geochemistry of Tertiary tholeiites and picrites from Qeqertarsuaq (Disko Island) and Nuussuaq, West Greenland with implications for the mineral potential of

- comagmatic intrusions. *Contrib. Mineral. Petrol.* **128**, 139-163.
- MAALØE, S. (1987): Rhythmic layering of the Skaergaard intrusion. In *Origins of Igneous Layering*, Parsons, I. (ed.). NATO ASI Series C, Dordrecht, Reidel, **196**, 247-262.
- MCBIRNEY, A.R. (1975): Differentiation of the Skaergaard Intrusion. *Nature* **253**, 691-694.
- MCBIRNEY, A.R. (1984): *Igneous Petrology*. San Francisco, Freeman, Cooper and Co., 509 p.
- MCBIRNEY, A.R. (1989a): The Skaergaard Layered Series: I. Structure and Average Composition. *J. Petrol.* **30**, 363-397.
- MCBIRNEY, A.R. (1989b): Geological Map of the Skaergaard Intrusion, East Greenland, 1:20,000: University of Oregon.
- MCBIRNEY, A.R. (1996): The Skaergaard Intrusion. In *Layered Intrusions*, Cawthorn, R.G., (ed.). Amsterdam, Elsevier, 147-180.
- MCBIRNEY, A.R. & NASLUND, H.R. (1990): The differentiation of the Skaergaard Intrusion. A discussion of Hunter & Sparks (Contrib Mineral Petrol 95: 451-461). *Contrib. Mineral. Petrol.* **104**, 235-247.
- MILLER, J.D., JR. (1999): Geochemical evaluation of platinum group element (PGE) mineralization in the Sonju Lake intrusion, Finland, Minnesota. *Minn. Geol. Surv. Inform. Circ.* **44**, 32 p.
- MILLER, J.D., JR. & ANDERSEN, J.C.Ø. (2002): Attributes of Skaergaard-type PGE reefs. In 9th International Platinum Symposium, Boudreau, A.E. (ed.). Abstracts, 305-308.
- MOMME, P., TEGNER, C., BROOKS, C.K. & KEAYS, R.R. (2002): The behavior of platinum-group elements in basalts from the East Greenland rifted margin. *Contrib. Mineral. Petrol.* **143**, 133-153.
- MORSE, S.A. (1990): The differentiation of the Skaergaard Intrusion. A discussion of Hunter & Sparks (Contrib Mineral Petrol 95: 451-461). *Contrib. Mineral. Petrol.* **104**, 235-247.
- NALDRETT, A.J., CAMERON, G., VON GRUENEWALDT, G. & SHARPE, M.R. (1987): The formation of stratiform PGE deposits in layered intrusions. In *Origins of Igneous Layering*, Parsons, I. (ed.). NATO ASI Series C, Dordrecht, Reidel, **196**, 313-397.
- NALDRETT, A.J., BRÜGMANN, G.E. & WILSON, A.H. (1990): Models for the Concentration of PGE in Layered Intrusions. *Can. Mineral.* **28**, 389-408.
- NASLUND, H.R. (1984): Petrology of the Upper Border Series of the Skaergaard Intrusion, East Greenland. *J. Petrol.* **25**, 185-212.
- NEVLE, R.J., BRANDRISS, M.E., BIRD, D.K., MCWILLIAMS, M.O. & O'NEILL, J.R. (1994): Tertiary plutons monitor climate change in East Greenland. *Geology* **22**, 775-778.
- NIELSEN, T.F.D. (2001): The palladium potential of the Skaergaard intrusion, South-East Greenland: Danmarks og Grønlands Geologiske Undersøgelse Rapport, 2001/23, 39 p.
- NIELSEN, T.F.D. (2002): Palaeogene intrusions and magnetic complexes in East Greenland 66 to 75 N.: Danmarks og Grønlands Geologiske Undersøgelse Rapport, 2002/113, 249 p.
- NIELSEN, T.F.D. (2004): The shape and volume of the Skaergaard intrusion, Greenland: Implications for mass balance and bulk composition. *J. Petrol.* **45**, 507-530.
- NIELSEN, T.F.D., SOPER, N.J., BROOKS, C.K., FALLER, A.M., HIGGINS, A.C. & MATTHEWS, D.W. (1981): The pre-basaltic sediments and the Lower basalts at Kangerdlugssuaq, East Greenland: their stratigraphy, lithology, palaeomagnetism and petrology. *Meddelelser om Grønland, Geoscience* **6**, 28 pp.
- NIELSEN, T.F.D. & BROOKS, C.K. (1995): Precious metals in magmas of East Greenland: Factors important to the mineralization in the Skaergaard intrusion. *Econ. Geol.* **90**, 1911-1917.
- NIELSEN, T.F.D., RASMUSSEN, H., RUDASHEVSKY, N.S., KRETZER, YU.L. & RUDASHEVSKY, V.N. (2003a): PGE and sulfide phases of the precious metal mineralisation of the Skaergaard intrusion. Part 1: Sample 90-23A, 807: Danmarks og Grønlands Geologiske Undersøgelse Rapport, 2003/47, 20 p.
- NIELSEN, T.F.D., RASMUSSEN, H., RUDASHEVSKY, N.S., KRETZER, YU.L. & RUDASHEVSKY, V.N. (2003b): PGE and sulphide phases of the precious metal mineralisation of the Skaergaard intrusion: Part 2: Sample 90-24, 1057. Danmarks og Grønlands Geologiske Undersøgelse Rapport, 2003/48, 20 p.

- NIELSEN, T.F.D., RASMUSSEN, H., RUDASHEVSKY, N.S., KRETZER, YU.L. & RUDASHEVSKY, V.N. (2003c): PGE and sulphide phases of the precious metal mineralisation of the Skaergaard intrusion. Part 3: Sample 90-18, 1010. Danmarks og Grønlands Geologiske Undersøgelse Rapport, **2003/52**, 25 p.
- NIELSEN, T.F.D., RASMUSSEN, H., RUDASHEVSKY, N.S., KRETZER, YU.L. & RUDASHEVSKY, V.N. (2003d): PGE and sulphide phases of the precious metal mineralisation of the Skaergaard intrusion: Part 3: Sample 90-23A, 806. Danmarks og Grønlands Geologiske Undersøgelse Rapport, **2003/53**, 18 p.
- NIELSEN, T.F.D., RASMUSSEN, H., RUDASHEVSKY, N.S., KRETZER, YU.L. & RUDASHEVSKY, V.N. (2003e): PGE and sulphide phases of the precious metal mineralisation of the Skaergaard intrusion: Part 3: Sample 90-23A, 808. Danmarks og Grønlands Geologiske Undersøgelse Rapport, **2003/54**, 16 p.
- NORTON, D. & TAYLOR, H.P., JR. (1979): Quantitative simulation of the hydrothermal systems of crystallizing magmas on the basis of transport theory and oxygen isotope data; an analysis of the Skaergaard intrusion. *J. Petrol* **20**, 421-486.
- NORTON, D., TAYLOR, H.P., JR. & BIRD, D.K. (1984): The geometry and high temperature brittle deformation of the Skaergaard intrusion. *J. Geophys. Res.* **89**, 10178-10192.
- PEDERSEN, A.K., WATT, M., WATT, W.S. & LARSEN, L.M. (1997): Structure and stratigraphy of the Early Tertiary basalts of the Blossville Kyst, East Greenland. *J. Geol. Soc. Lond.* **154**, 565-570.
- PHILIPP, H., ECKHARDT, J.-D. & PUCHELT, H. (2001): Platinum-Group Elements (PGE) in Basalts of the Seaward-Dipping Reflector Sequence, SE Greenland Coast. *J. Petrol.* **42**, 407-432.
- PRENDERGAST, M.D. (2000): Layering and Precious Metals Mineralization in the Rincón del Tigre Complex, Eastern Bolivia. *Econ. Geol.* **95**, 113-130.
- RIPLEY, E.M., BROPHY, J.G. & LI, C.S. (2002): Copper solubility in a basaltic melt and sulfide liquid/silicate melt partition coefficients of Cu and Fe. *Geochim. Cosmochim. Acta* **66**, 2791-2800.
- RUDASHEVSKY, N.S., McDONALD, A.M., CABRI, L.J., NIELSEN, T.F.D., STANLEY, C.J., KRETZER, Y.L. & RUDASHEVSKY, V.N. (2004): Skaergaardite, PdCu, a new platinum-group intermetallic mineral from the Skaergaard intrusion, Greenland. *Mineral. Mag.* **68**, 615-632.
- STEWART, B.W. & DEPAOLO, D.J. (1990): Isotopic studies of processes in mafic magma chambers: II. The Skaergaard Intrusion, East Greenland. *Contrib. Mineral. Petrol.* **104**, 125-141.
- TECK CORPORATION (1991): Tonnage beregning for Skaergaarden. 6 pp. Exploration report. (in archive of the Geological Survey of Denmark and Greenland, GRF. no. 21026).
- TEGNER, C. (1997): Iron in plagioclase as a monitor of the differentiation of the Skaergaard Intrusion. *Contrib. Mineral. Petrol.* **128**, 45-51.
- TEGNER, C., LESHER, C.E., LARSEN, L.M. & WATT, W.S. (1998): Evidence from rare-earth-element record of mantle melting for cooling of the Tertiary Iceland plume. *Nature* **395**, 591-594
- TURNER, P.A. (1986): *The sulfide mineralogy and the behavior of S and certain trace elements in the Skaergaard intrusion, East Greenland*. MS thesis, Dartmouth College, Hanover, New Hampshire, 79 p.
- TURNER, P.A. (1990): Report of the 1989 field season, Skaergaard concession. 47 pp. (in archive of Danmarks og Grønlands Geologiske Undersøgelse, GRF. no. 20843).
- TURNER, P.A. (1991): Preliminary petrographic characterization of the Platinova reef. In 1990 Skaergaard project, Platinova/Corona concession, East Greenland. Exploration report, 55 pp. and appendixes Watts, Griffis & McOuat (ed.) (in archive of the Geological Survey of Denmark and Greenland, GRF no. 20848), Appendix VII, vol 2B, 12 pp.
- TURNER, P.A. & MOSHER, G.W. (1989): Report of the 1988 field season, Skærgaard concession and East Greenland prospecting license, 71 pp. Company report. Toronto: Platinova Resources Ltd. (in archive of Danmarks og Grønlands Geologiske Undersøgelse, GRF. no. 20845).
- VINCENT, E.A. & CROCKET, J.H. (1960): Studies in the geochemistry of gold – I: The distribution of gold in rocks and minerals of the Skaergaard intrusion, East Greenland. *Geochim. Cosmochim.*

- Acta* **18**, 130-142.
- VINCENT, E.A. & SMALES, A.A. (1956): The determination of palladium and gold in igneous rocks by radioactivation analysis. *Geochim. Cosmochim. Acta* **9**, 154-160.
- VOHRYZKA, K. & VOHRYZKA, E. (1971): Bericht über die Prospektion im Jahr 1970 im Gebiet des Kangerdlugssuakfjordes, Ostgrönland, 68° n1 Breite. Nordisk mineselskab report, 47 pp. (in archives of the Geological Survey of Denmark and Greenland, GFR no. 20906).
- WAGER, L.R. (1960): The major element variation of the Layered Series of the Skaergaard Intrusion and a Re-estimation of the Average Composition of the Hidden Layered Series and of the Successive Residual Magmas. *J. Petrol.* **1**, 364-398.
- WAGER, L.R. & BROWN, G.M. (1968): *Layered Igneous Rocks*. Edinburgh and London, Oliver and Boyd, 588 p.
- WAGER, L.R. & DEER, W.A. (1939): Geological Investigations in East Greenland, Part III. The Petrology of the Skaergaard Intrusion, Kangerdlugssuaq, East Greenland. *Meddelelser om Grønland* **105**, 1-352.
- WAGER, L.R., VINCENT, E.A. & SMALES, A.A. (1957): Sulfides in the Skaergaard intrusion, East Greenland. *Econ. Geol.* **52**, 855-903.
- WAGER, L.R., VINCENT, E.A. & SMALES, A.A. (1958): The behaviour of sulphur during fractionation of basic magma. *Geochim. Cosmochim. Acta* **14**, 165-166.
- WATERS, B.C. (1987): Geological report, Platinova Resources Ltd. Kangerdlugssuaq concession, East Greenland. Platinova Resources Ltd report, 43 pp. (in archives of the Geological Survey of Denmark and Greenland, GRF no. 20838).
- WATTS, GRIFFIS & MCOUAT (1991): 1990 Skaergaard project, Platinova/Corona concession, East Greenland. Exploration report, 55 pp. and appendixes (in archive of the Geological Survey of Denmark and Greenland, GRF no. 20848).
- WILSON, A.H. & TREDOUX, M. (1990): Lateral and Vertical Distribution of Platinum-Group Elements and Petrogenetic Controls on the Sulfide Mineralization in the P1 Pyroxenite Layer of the Darwendale Subchamber of the Great Dyke, Zimbabwe. *Econ. Geol.* **85**, 556-584.

CHAPTER 21: POLYMETALLIC PLATINUM-GROUP ELEMENT (PGE)-Au MINERALIZATION OF THE SUKHOI LOG DEPOSIT, RUSSIA

Vadim V. Distler, Marina A. Yudovskaya

Institute of the Geology of Ore Deposits, Petrography, Mineralogy, and Geochemistry

Russian Academy of Science, Staromonetny Per., 35, Moscow, 119017, Russia

E-mail: maiya@igem.ru

INTRODUCTION

Some unconventional styles of platinum mineralization (*i.e.*, not related to classical layered igneous complexes) have recently received much attention as possible future sources of PGE. However, the distribution and mineralogy of PGE in metalliferous black shale has not been thoroughly studied to date. The basic characteristics of PGE mineralogy have not yet been determined for some large occurrences of black shale-hosted PGE mineralization with elevated Pt contents (*e.g.*, Nick deposit, Canada (Coveney *et al.* 1992), Muruntau deposit, Uzbekistan (Ermolaev *et al.* 1999), Hunan/Guizhou Province deposits, China (Coveney & Nansheng C. 1991)). In other occurrences, PGE mineral assemblages are known to be locally developed within a single thin layer (*e.g.*, thucolite in the Kupferschiefer-type deposits, Poland (Kucha 1982, Piestrzynski & Sawlowicz 1999) or as rich, isolated patches (Padma, in Karelia, Russia) (Savitsky *et al.* 1998). Compared to such occurrences, the giant hydrothermal Sukhoi Log deposit is unique in having relatively low, but uniformly distributed PGE concentrations which have been verified mineralogically throughout the whole ore body.

In this review paper, we concentrate on some problems of discovery and identification of platinum mineralization in black shale hosted-ore, because the occurrence of this mineralization significantly affects the assessment of such deposits. The general geochemistry and mineralogy of ores are also presented to support the proposed genetic model.

HISTORY OF EXPLORATION

The Sukhoi Log deposit is situated in the Irkutsk Region of Russia (Eastern Siberia) about 120 km north of Bodaibo (Fig. 21-1). The deposit occurs within the Lena gold-bearing district, a major gold placer region which has produced more than 1500 tonnes of gold since 1846. The Lena



FIG. 21-1. Location map of the Sukhoi Log deposit.

Province comprises placers of many diverse genetic types, including modern stream deposits and highly productive Lower Pleistocene age, buried glaciofluvial and alluvial placers (Vysotskii 1933). Quartz-vein gold mineralization is also widespread in the province. It has been suggested that the gold placers were formed by disintegration of mineralization of this kind. Weak mechanical wearing of gold particles indicated proximate sources, and their fineness was close to that of gold in the vein-type deposits. Such placers were also found near the future Sukhoi Log deposit. A prospect with lode quartz-vein gold mineralization has been known since 1886 in the Nygri River basin (Buryak & Khmelevskaya 1997). Prospecting, sampling and assessment of these quartz veins in 1886, 1932–1933 and 1952–1961 confirmed very heterogeneous gold distribution in the veins, resulting in their rejection as potential mineable sources of gold. Rare, very high-grade Au veins from a few decimetres to 1–2 m thick contained up to several tens of ppm of Au as scarce patches and nuggets and some were developed during exploration. Shallow pits and trenches within this prospect were developed to sample outcropping quartz-sulfide veins, but failed to reveal significant Au concentrations. The first relatively deep diamond drill holes were drilled in the area only in

1961 and discovered quartz–Au-sulfide vein-disseminated mineralization at depths of 20–40 m. Low Au concentrations (~3 ppm) and inhomogeneous lateral and vertical distribution of Au grades hampered attempts at ore reserve estimation. Most ore zones were later explored by core drilling on regular grid spacings of 50 by 50 m for B category (measured reserves) and 50 by 100 m for C1 category (indicated reserves) to the depth of 300–400 m. Eighteen years after the onset of exploration work, Sukhoi Log was evaluated as a giant gold ore deposit with reserves of >1100 t recoverable Au. Given the laterally extensive and shallow depth of the ore bodies, open pit mining was proposed for the deposit.

Since the 1970s the Sukhoi Log deposit has been explored and evaluated as a typical single commodity Au deposit. An economically favorable feature of the deposit that was determined by mineralogical studies is that gold generally occurs in the native form, although closely associated with sulfide minerals. Single grains of a platinum sulfide (cooperite) were identified in the same studies in the ore mineral assemblage (Mitrofanov *et al.* 1994). However, bulk platinum contents were not determined quantitatively in that study. Later studies of platinum potential of the Sukhoi Log deposit demonstrated that PGE are present as separate platinum-group minerals (PGM) (Distler *et al.* 1996). The discovery of Pt mineralization in Au ores of the Sukhoi Log deposit and the determination of modes of Pt occurrence (Mitrofanov *et al.* 1994, Distler *et al.* 1996, Distler *et al.* 2003, Distler *et al.* 2004) began a new stage in the study of the deposit. Sukhoi Log can now be considered as a large polymetallic deposit with Au as the main ore component and Pt as an important by-product. A final mineral processing scheme for Pt and Au recovery has not been developed yet. Whereas the Au–Pt association at Sukhoi Log has been referred to recently as an 'unconventional' PGE deposit (*e.g.*, Wilde *et al.* 2003), we prefer to refer to this deposit as an example of a new class of polymetallic Au–Pt deposit. For example, many types of gold deposits are known where Au is a single valuable component, and PGE are absent in ores (*e.g.*, porphyry Au, Archean quartz–carbonate vein-hosted gold, *etc.*). In contrast, ores of classical platinum deposits (Cu–Ni sulfide or chromite-associated, *etc.*) are poor in Au. Although it seems reasonable at present to consider this extraordinary deposit as 'unconventional', we might expect that

these deposits will eventually be considered *conventional* sources of noble metals in future with further development of research and exploration techniques.

In 1992–1996, Australian company Star Mining NL, Australia by contract with Lenzoloto drilled several boreholes to verify gold resources and confirmed them completely by new sampling.

A competition for a license to develop the Sukhoi Log deposit was expected to be announced in 2004, but at the beginning of 2005 Sukhoi Log was described by Russia's Natural Resources Minister Yuri Trutnev as a strategically important deposit and therefore it falls under the conditions described in the new law "On subsoil use" which prohibits foreigners from taking part in auctions for major strategic deposits. Large Russian mining companies (including Noril'sk Nickel, Polymetall and IG Alrosa) showed their preliminary interest. Some foreign firms have expressed interest in this particular deposit of Russia's mineral riches, including the world's number three gold company Barrick Gold Corporation of Toronto and Britain's Highland Gold Mining. In the absence of competition from foreign companies Russia's mining and metals giant Noril'sk Nickel is considered to be the main contender for Sukhoi Log.

Data presented here were obtained from diamond drill core materials obtained during exploration work in 1992–1994 and 1994–1996, and from sampling of old adits.

REGIONAL GEOLOGICAL SETTING

The Sukhoi Log deposit (translated as the "Dry Gulch") is located within the regional Bodaibo synclinorium regional structure; a Lower–Middle Riphean depression in the Proterozoic-age structures of the Baikal-Patom region, which forms a part of the Baikalian Barguzin-Vitim fold system on the southern margin of the Siberian plateau. The marginal belt of mafic and ultramafic rocks in the southern Siberian Platform is an important component in the structure of the studied territory (Alakshin & Pismennyi 1988) (Fig. 21-2). The Bodaibo synclinorium can be considered as one of the flysch terranes of the Baikal-Patom region (Bulgatov & Gordienko 1999). The Sukhoi Log deposit occurs in an overturned anticline that falls within the larger high order Marakan-Tunguska

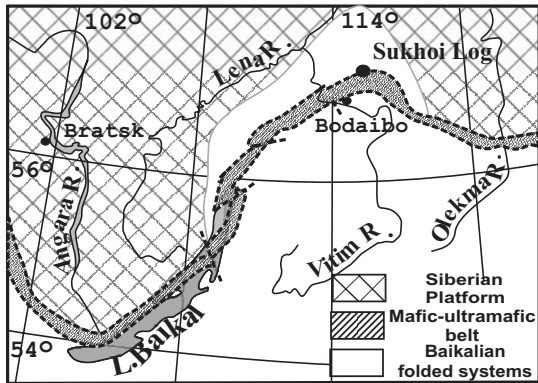


FIG. 21-2. The mafic-ultramafic marginal belt along the southern boundary of the Siberian craton. (Distler *et al.* 2004).

Middle–Late Riphean and Vendian age (Fig. 21-3), that lie unconformably on a complexly deformed basement of Archean-Proterozoic sedimentary syncline. The Bodaibo synclinorium is composed of terrigenous and carbonate-terrigenous rocks of sequences (Kazakevich *et al.* 1971, Ivanov *et al.* 1995).

The Lower Riphean stratigraphy (thickness ~4 km) consists of conglomeratic sandstone, conglomerate and shale, overlain by intercalated sandstone, conglomerate and ferruginous quartzite with volcanogenic andesite, basalt and derived tuff. The formation of the volcano-terrigenous complex is related to the initial stages of rifting. The Middle Riphean section comprises about 2500 m of shale, bedded sandstone and conglomeratic sandstone

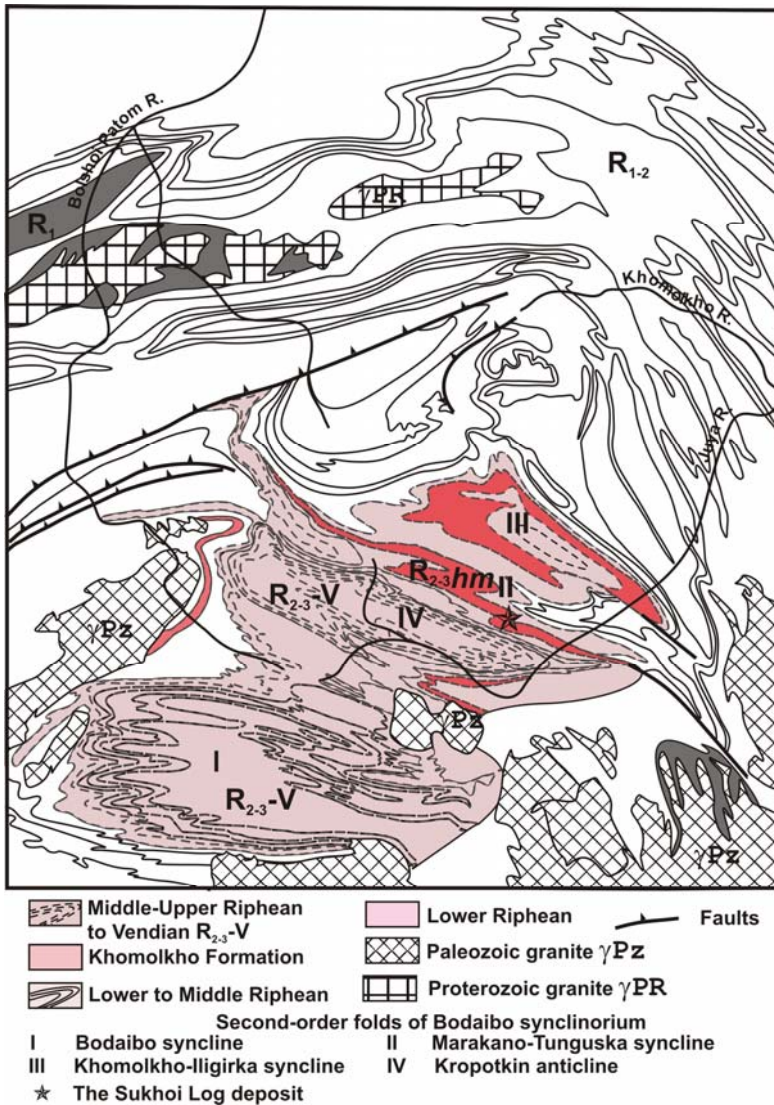


FIG. 21-3. Simplified geological map of the Bodaibo synclinorium showing the distribution of the Khomolkho Formation among Riphean-Vendian sequences. Map is based on data from Kazakevich *et al.* 1971, Ivanov *et al.* 1995, Mitrofanov *et al.* 1994.

alternating with carbonaceous sandstone and shale. The Middle–Late Riphean sequence is about 1500 m thick and includes the ore-hosting flysch sequences of the Khomolkho Formation. Riphean age is roughly equivalent to the Neoproterozoic Cryogenian period with absolute age of 630–850 Ma according to Gradstein *et al.* (2004). Khomolkho carbonaceous shale is variably enriched in organic carbon and diagenetic sulfides. The Imnyakh Formation, composed of a flysch-like intercalation of carbonaceous shale and colored limestone, conformably overlies the Khomolkho Formation. Its thickness varies from 160 to 400 m. The Vendian sequence is over 2500 m thick, and is composed of rhythmically interbedded sandstone, shale, carbonaceous shale and limestone.

Terrigenous and carbonaceous layers, enriched in organic carbon, are common in Riphean–Vendian sequences of the region. The maximum accumulations of organic carbon are found in the Middle–Late Riphean pelitic strata. Similar sedimentary rocks occur in neighboring regions, developed within the limits of the same Riphean rift system. For example, the Late Riphean black shale in the adjacent Olokit fold zone hosts the giant Kholodninskoe SEDEX base metal deposit.

The internal architecture of the Bodaibo synclinorium is established by the alternation of gently plunging isoclinal synclines and anticlines of latitudinal strike. Northwest-striking thrust faults commonly occur, concordant to bedding.

All sedimentary rocks in the Bodaibo synclinorium are metamorphosed. Metamorphic grades increase from greenschist facies in the central part to epidote-amphibolite and amphibolite facies on the periphery of the synclinorium. Such metamorphic zoning is related to occurrences of granite intrusions.

Igneous rocks are practically absent in the central part of the Bodaibo synclinorium. The Konstantinovsk granite stock (about 1.5 km²) occurs 6 km southwest of the deposit. The much larger Dzhegdakar massif composed of biotite granite is located in 35 km east from Sukhoi Log.

Deposit-scale geologic setting

The deposit is located on the axial portion of a third-order overturned anticline developed on the northern flank of the larger second order Marakan-Tunguska syncline. Mineralization is controlled by an axial part of the fold (Figs. 21-4, 21-5). The axial plane plunges at 30–40° to the west or northwest. Bed dips from 15 to 30° on the gentler northern flank and from 30 to 50° on the overturned southern flank. The axial plane of the fold coincides with a fault which appears as a zone of both ductile deformation and cataclasis. The thickness of the Khomolkho shale is significantly reduced in the core of the fold in comparison to its flanks. The anticline is complicated by numerous minor folds of different scale down to puckering associated with

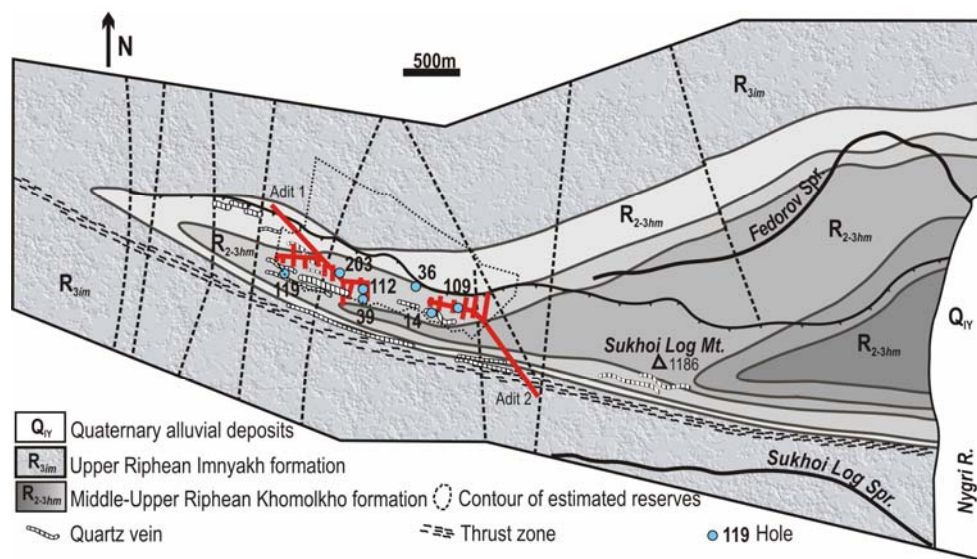


FIG. 21-4. Geological map of the Sukhoi Log deposit with location of the drill holes and adits mentioned in the text (adapted after exploration data, 1975, 1996).

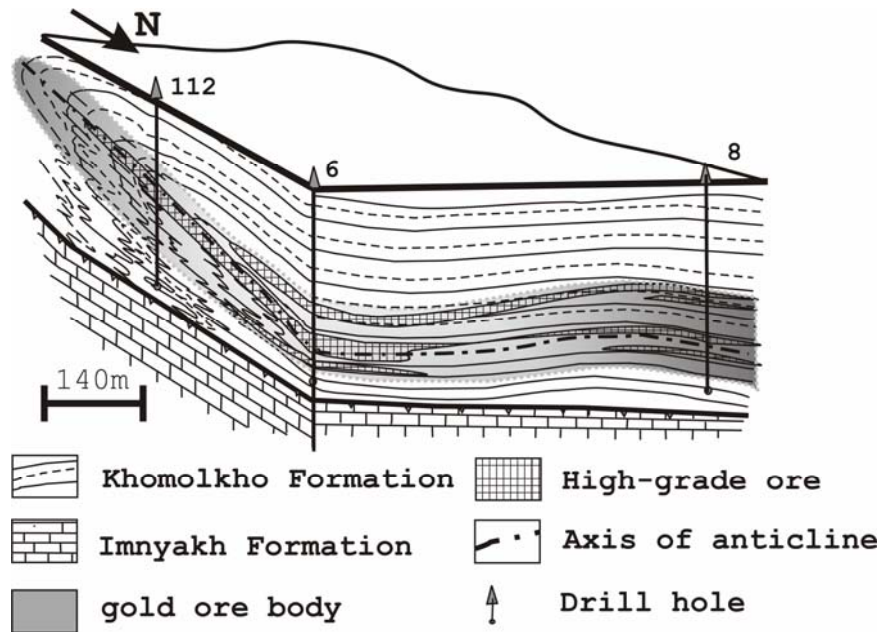


FIG. 21-5. Block-diagram illustrating geological structure and gold ore distribution of the Sukhoi Log deposit (Distler *et al.* 2004).

fractures, axial cleavage and microthrusts. Structures of plastic flow are selectively developed in the fine-grained rock types whereas rigid sandstones and quartz-sulfide aggregates have deformed by boudinage.

The ore zone is stratabound, and is composed of intervals of veining and disseminated mineralization of variable thickness. Disseminated pyrite and carbonate minerals are confined to the margins of an axial plane fracture cleavage that commonly cuts the bedding in the hinges of minor folds.

Types of ore

Three main zones are observed in the deposit: the “supra-ore” upper zone, the central zone and the “infra-ore” lower zone. The boundaries of these ore zones have been established purely on the basis of drill core sampling and assay. The central ore zone is localized in the axial portion of the anticline, in a rock volume rich in quartz-sulfide disseminations and veins. Veins commonly have a complex morphology concordant with the foliation and shearing of the host rocks. Quartz-sulfide veinlets are not extensive; lenses and aggregates of irregular form are also abundant. The thickness of the ore zone varies from 10–15 m on the flanks to 140 m in the central part. Auriferous

intervals (with grades more than $2 \text{ g.t}^{-1} \text{ Au}$) occur sporadically above and below the ore zone envelope. The current outline of the ore zone is determined in terms of exploratory requirements, and actual reserves appear to be higher when taking into account hypothetical resources at depth. In the central ore zone, there is a correlation between ore grade and volumetric abundance of quartz-sulfide and sulfide mineralization, however similar quartz-sulfide mineralization developed widely within the upper and lower ore zones contains much less gold. The ore zone as traced by prospecting drill holes extends 3000 m along strike and from 1100 to 1500 m down-dip.

A series of late, thick (up to 2 m) quartz veins, relatively depleted in gold, strike northeast and generally dip steeply at 50 to 70°. They form a vein stockwork in the upper part of deposit where it outcrops on the surface. These veins were the first type of lode mineralization discovered in the region and were mined in the nineteenth century. A separate, gently sloping family of Au-poor quartz veins are observed at the deeper levels of the deposit (greater than 200 m from surface). Insignificant gold concentrations are developed in the outer contacts of these veins.

Recrystallized granoblastic textures in sulfides and boudinage of quartz-sulfide aggregates

within folded shale in the axial part of the anticline are the evidence of ore dynamometamorphism related to folding. Ore mineralization confined to gentle limbs of the anticline is not metamorphosed dynamically.

The basic morphological types of gold mineralization are documented in Figure 21-6:

1. Stratified interlayers and lenses of diagenetic fine- and medium-grained pyrite;
2. Stratified impregnations of rounded ovoid pyrite;
3. Cleavable and foliated impregnations of fine-grained pyrite and pyrrhotite;
4. Large zoned metacrystals of pyrite with or without quartz margins;
5. Granoblastic pyrite aggregates;
6. Quartz-sulfide stockwork veinlets up to 2 to 4 cm in thickness.

Some of the above morphological types of mineralization (*e.g.*, types 1 to 4) occur outside the deposit, but in such occurrences they are usually barren or contain only low-grade mineralization.

Ore composition

The host Khomolkho shale has been regionally metamorphosed to greenschist facies and is dominated by 30 to 35 vol.% quartz and 35 to 50 vol.% sericite, with a carbonate content from 5 to 30 vol.%. Minor minerals are rutile, magnetite, tourmaline, zircon, monazite and albite. The carbonaceous-terrigenous sediments enriched in organic matter were transformed into quartz-sericite shale containing rare Na-bearing muscovite, Fe-poor chlorite and epidote. Porphyroblastic disseminations of Fe–Mg carbonates are abundant both in the mineralized rocks and in the unaltered rocks. Fine-grained matrix carbonates are mainly ankeritic in composition. Larger porphyroblasts and carbonates from the quartz-sulfide veinlets are mainly magnesian siderite; ankerite is less often found as porphyroblasts.

The mineralized black shale is depleted in SiO₂ compared to the unaltered host shale. Content of SiO₂ decreases from 62 wt.% outside the deposit to 57 wt.% in the ore zone with increasing MgO, CaO and FeO (Table 21-1) (Buryak & Khmelevskaya 1997), reflecting addition of sulfides and carbonates to the ore zone. Unfortunately, these analyses do not provide sulfur and organic carbon abundances. According to our data, content of sulfidic sulfur can reach 25 wt.% in sulfide ore.

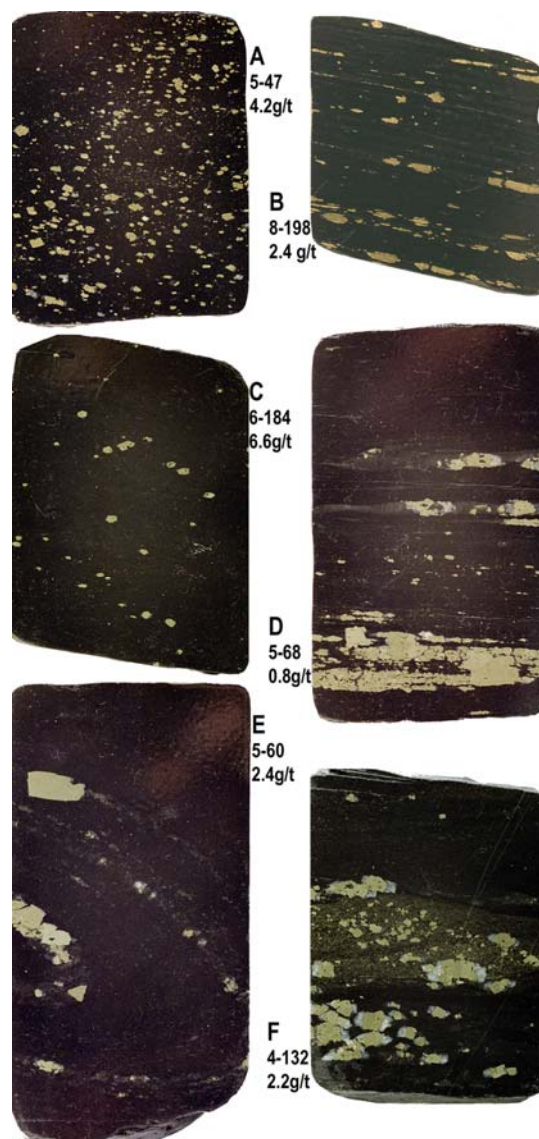


FIG. 21-6. Typical structures of platinum-gold ore of the Sukhoi Log deposit. Polished core sections (diameter of core is 6 cm) (partially from Distler *et al.* 2004). Notes include number of hole, depth (m) and Au grade (g.t¹). **A** – impregnation of Au-bearing ovoid pyrite without quartz; **B** – cleavage-oriented pyrite impregnation without quartz; **C** – rare dissemination of Au-bearing ovoid pyrite; **D** – cleavable oriented disseminated pyrite Au-free; **E** – curve of small fold with stratified pyrite-quartz-carbonate dissemination; **F** – fine-grained and coarse-grained pyrite mineralization. Figure continues on next page.

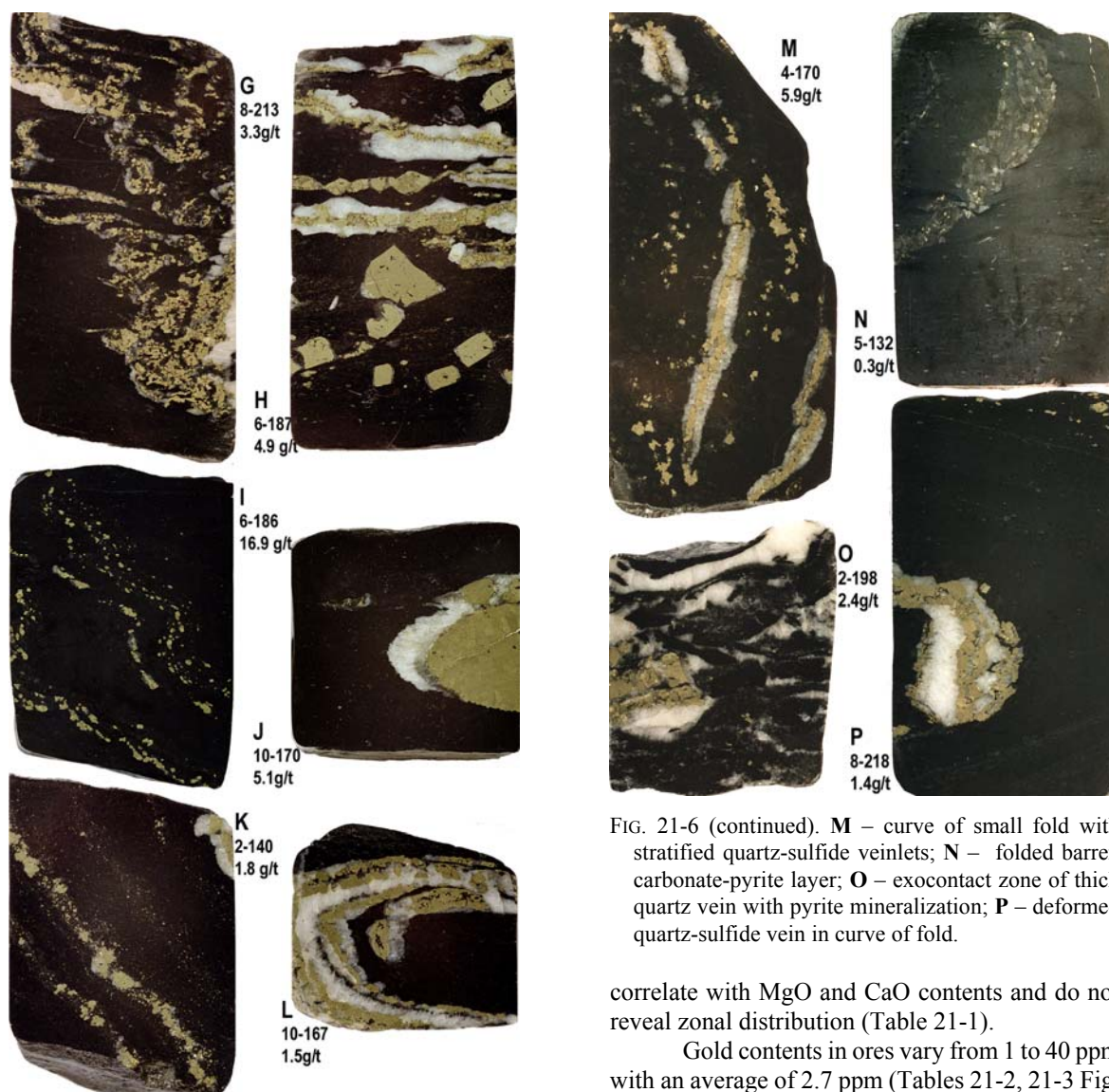


FIG. 21-6 (continued). **G, I, K, L** - complexly folded quartz-pyrite veinlets in the axial part of the Sukhoi Log anticline; **H** - quartz-pyrite veinlets and porphyroblastic pyrite from the central part of ore body; **J** - separate lenticular metagranoblastic quartz-pyrite aggregate.

However, the local heavy enrichment of pyrite and Fe–Mg carbonates in separate intervals does not increase Fe, Mg and Mn abundances much in the ore zone relative to their abundances in initial shale. Comparison of total composition of altered and unaltered black shale indicates insignificant metasomatic input to ore zone, but rather local redistribution. Altered and unaltered rocks have similar abundances of organic carbon which do not

FIG. 21-6 (continued). **M** – curve of small fold with stratified quartz-sulfide veinlets; **N** – folded barren carbonate-pyrite layer; **O** – exocontact zone of thick quartz vein with pyrite mineralization; **P** – deformed quartz-sulfide vein in curve of fold.

correlate with MgO and CaO contents and do not reveal zonal distribution (Table 21-1).

Gold contents in ores vary from 1 to 40 ppm with an average of 2.7 ppm (Tables 21-2, 21-3 Fig. 21-7). Silver contents are about 3 ppm reaching rarely 10 ppm. Contents of Pb (up to 65 ppm), Zn (up to 138 ppm) and Cu (up to 122 ppm) are similar to those in the black shale (respectively 25, 140 and 87 ppm) or slightly higher (Tables 21-2, 21-3). Also, As (up to 110 ppm), Cr (up to 170 ppm), Ni, Ti, Zr are enriched relative to their average abundances in black shale sequences. Contents of V and P in ores and unaltered black shale are lower (Yudovich & Ketris 1994).

Age of mineralization

Dating of ore deposition in the case of the Sukhoi Log deposit has proven difficult because it requires not only accurate dates for mineralization but also clarification of the entire geological history

TABLE 21-1. CHEMICAL COMPOSITION (WT.%) OF KHOMOLKHO BLACK SHALE (BURYAK & KHEMELEVSKAYA 1997)

	1	2	3	4
SiO ₂	57.20	59.70	62.97	62.50
TiO ₂	1.08	1.03	1.09	1.15
Al ₂ O ₃	16.46	16.32	17.38	17.60
Fe ₂ O ₃	1.85	1.81	2.62	6.20
FeO	4.67	5.61	4.03	
MnO	0.11	0.14	0.06	0.05
MgO	3.13	3.75	2.69	2.22
CaO	1.3	1.76	0.42	0.40
Na ₂ O	1.82	1.90	1.79	1.83
K ₂ O	2.90	2.57	3.12	3.13
l.c.	7.91		3.77	4.80
P ₂ O ₅	0.12			0.12
S	(1.45)			
C org	1 - 5			
SO ₃	0.07			
n	90	15	15	80
Sum	98.62	94.59	99.94	100.00

Note: 1 – mineralized ore zone; 2 – upper zone; 3 – lower zone; 4 – unaltered shale outside of the deposit. Blank – not analyzed; l.c. – the loss of combustion.

of the host rocks and adjacent intrusions. All available data on radiogenic isotope dating of regional metamorphism, granite formation and mineralization events are given below.

Rundqvist *et al.* (1992) published zircon ages (Pb–Pb thermionic method) from the Konstantinovsk massif ranging from 500 to 300 Ma. Titanite from the same body was dated at 354 Ma by U–Pb methods, and biotite yielded a K–Ar age of 298±7 Ma age. U–Pb dating of zircon (650–530 Ma) and titanite (290±20 Ma) from the Konstantinovsk granite by Neimark *et al.* (1993) are not in complete agreement with the data of Rundqvist *et al.* (1992). Such differences may be interpreted as the result of analysis of inherited zircons from more ancient crust.

Geochronological Pb–Pb studies of placer gold and lode gold (data on native gold separates) from Sukhoi Log ore have shown an age range from 450 to 175 Ma (Rundqvist *et al.* 1992). More recent Rb–Sr dating of hydrothermal minerals and whole rocks (Laverov *et al.* 2000b) revealed two different age estimations for the ore zones: Rb–Sr isotopic data for quartz and carbonate from ore veins gave an age of 316±16 Ma with (⁸⁷Sr/⁸⁶Sr) = 0.7168±0.0007, which we interpret to represent the most probable age of the mineralization. A Rb–Sr age of 439±16

Ma measured on the bulk-mineralized Khomolkho shale sample probably reflects incomplete overprinting of older regional metamorphic ages by hydrothermal processes, whereas Rb–Sr data (516±22 Ma) for a sample of unaltered Khomolkho shale provides the age of greenschist metamorphism in the Bodaibo synclinorium.

Synthesis of isotopic data indicates a significant gap between the age of sedimentation (Middle–Late Riphean 650–850 Ma), regional metamorphism, and the ore-forming process.

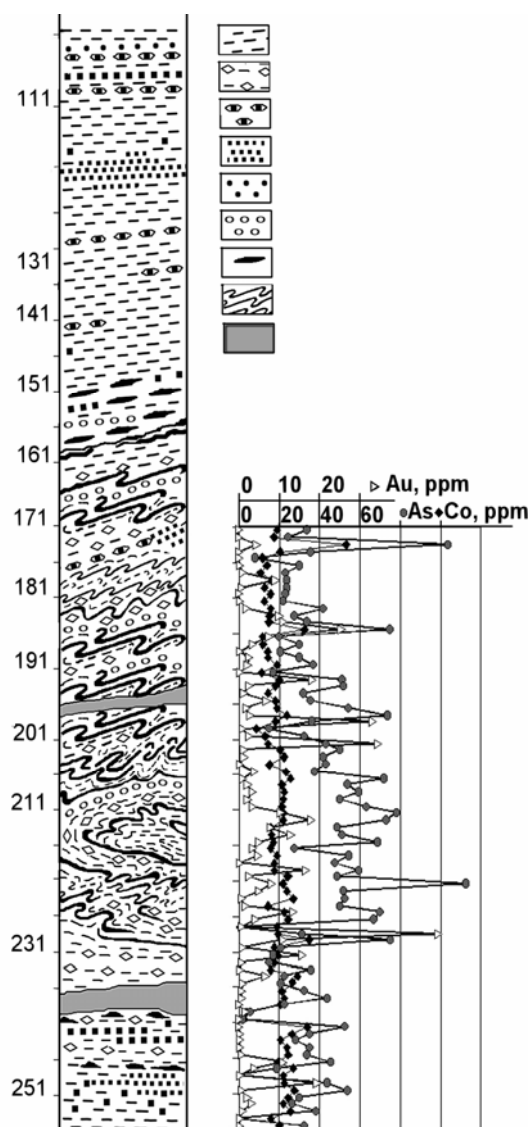


FIG. 21-7. Cross sections through ore body of the deposit on drill core 6 illustrating the main morphological types of quartz-sulfide mineralization and Au, As and Co distribution (Distler *et al.* 2004).

TABLE 21-2. CONCENTRATION OF ORE ELEMENTS IN REPRESENTATIVE BULK-ROCK SAMPLES FROM DRILL CORE 6 BY INAA ANALYSIS (PPM) (SEE ALSO FIG. 21-7)

N	Sample	H, m	Sc	Cr	Co	As	Se	Rb	Sr	Ag	Sb	Cs	Ba	Hf	Ta	Au	Th	U
1.	6-5936	173	17.9	99	53.0	103.8		103			3.7	3.9		4.2	0.69	2.866	6.9	0.8
2.	6-5952	189	19.8	112	14.2	29.8		118		3.4	0.8	4.3	459	4.1	0.64	1.577	4.9	1.0
3.	6-5955	192	20.0	104	20.0	51.2		119		3.2	1.1	4.4	287	3.5	0.55	12.060	7.2	0.7
4.	6-5962	199	8.0	97	8.5	15.1		50		2.4	1.5	1.8	170	1.5	0.26	0.654	2.5	0.4
5.	6-5963	199.9	19.7	119	12.9	32.4		123			0.6	5.3	282	3.2	0.55	1.686	5.9	0.9
6.	6-5964	200.8	22.5	108	14.7	43.4		154			5.0	4.2	752	4.1	0.63	22.820	6.2	1.2
7.	6-5975	211.8	22.6	123	22.1	73.2		117		3.6	0.9	5.8	512	4.0	0.70	11.880	5.7	1.4
8.	6-5983	219.8	20.3	113	24.1	49.1		130		4.0	1.1	4.6	400	4.3	0.73	1.757	6.9	1.0
9.	6-5984	221	15.9	90	21.8	112.8	7.2	123	663	2.4	4.5	3.7	243	3.1	0.60	5.510	5.8	2.0
10.	6-5985	222.2	19.0	123	23.7	51.6		160		3.9	4.7	4.4	409	4.2	0.64	3.321	6.7	1.4
11.	6-5991	228.2	21.7	127	19.6	31.2		131		9.3	-	4.9	495	4.9	0.82	32.820	7.5	-
12.	6-6017	254.4	17.3	126	19.8	32.7		88		2.2	0.6	3.7	249	4.4	0.64	0.107	6.2	1.0

blank – not detected

TABLE 21-3. CONCENTRATION OF ORE ELEMENTS (PPM) AND SOME OXIDES (WT.%) IN BULK-ROCK SAMPLES FROM DRILL CORE 10 (ORE ZONE) BY RFA.

Him	K ₂ O	CaO	TiO ₂	MnO	Fe ₂ O ₃	P ₂ O ₅	S	Cr	Sc	V	Co	Ni	Cu	Zn	Rb	Sr
120	2.76	0.62	0.97	0.099	7.94	0.091	0.33	103	19	138	16	45	56	138	105	135
142	3.2	0.57	1.11	0.099	7.85	0.108	0.12	109	18	138	20	40	30	132	128	153
170	3.29	0.59	0.75	0.053	6.66	0.07	1.12	81	15	179	18	47	55	77	121	120
180	2.79	0.55	0.81	0.065	10.07	0.097	1.81	114	17	145	27	72	122	89	104	108
193	3.51	0.47	0.93	0.066	7.66	0.071	0.78	97	15	152	17	47	54	110	138	114
197	3.35	0.32	0.99	0.066	7.72	0.09	0.39	106	21	150	14	46	57	131	132	112
200	3.36	0.79	1.04	0.082	6.76	0.079	0.6	110	17	141	11	36	34	91	130	122
207	2.74	0.79	0.97	0.1	7.43	0.098	0.2	101	17	126	13	40	38	101	107	144

H, m	Y	Zr	Nb	Ba	Pb	As	Th	U	Cl	Ga	Au
120	31	218	13	466	29	65	18	3.1	69	23	1
142	35	240	14	512	8	33	10.2	2	59	28	3.4
170	25	159	9	488	65	94	11.6	4.7	70	21	5.1
180	30	173	11	418	55	128	6.1	5.5	81	22	8
193	30	190	14	507	31	79	9.1	2	62	22	2.2
197	32	209	15	540	17	43	8.7	2.6	69	26	0.6
200	34	212	13	539	23	32	10.9	1.5	70	23	2.7
207	28	210	13	414	16	0	11.3	2.9	78	20	0.6

However, the data are generally consistent with an epigenetic origin for the ore deposit, related to the passage of younger metamorphic fluids possibly at the time of emplacement of granitoid rocks of the Konstantinovsk suite.

Carbonaceous matter in the ore-hosting black shale

Carbonaceous matter has been considered to be a key factor controlling metal accumulation for

black shale-hosted deposits (Varshal *et al.* 1994, Razvozhzaeva *et al.* 2002). Because Sukhoi Log is hosted by black shale sequences rich in carbonaceous material that have been metamorphosed to the greenschist facies, we characterized the composition of the carbonaceous matter using a variety of methods. By the term carbonaceous matter, we are referring to a multiphase mixture of carbon compounds irrespective of origin, and excluding carbonate. In

summary, a soluble component (mainly bitumen), an insoluble carbonaceous substance (kerogen), and a gas phase were identified in the metamorphosed organic matter of the black shale.

The concentration of organic carbon in the unaltered Khomolkho black shale can reach 5 wt.%, although it typically ranges from 1 to 2 wt.%. The average concentration of organic carbon in the altered host rocks of the Sukhoi Log deposit is about 0.5 wt.% ranging from 0.15 to 1.1 wt.%, whereas total carbon content averages about 2.3 wt.% (Table 21-4, 21-5), so the amount of carbonate-bound carbon is locally elevated in concentration at least two to four times higher than the amount of organic carbon. A significant amount of nitrogen (from 0.08 to 0.19 wt.%) also occurs in the black shale of the Sukhoi Log deposit. Sulfur contents range up to 25 wt.% and correlate with the intensity of mineralization, *i.e.*, the amount of quartz-sulfide dissemination. No correlation is obvious between organic carbon content and ore grade.

The gas phase released from the crushing of shale is composed of non-hydrocarbon (CO_2 , N_2 , H_2) and light hydrocarbon (CH_4 and C_2H_6) components with total volatile phases content up to 10 mol.kg^{-1} .

Soluble organic matter (bituminoids) is of greatest interest as possible concentrators of noble metals compounds as it has been shown that the PGE and Au will form strong complexes with organic ligands under certain conditions (Varshal *et al.* 1994, Wood 2002). The total soluble organic content in samples from the central ore, upper and lower zones of the deposit is 9 ppm, 10 ppm and 8 ppm, respectively. Such low concentrations are common in highly metamorphosed sedimentary rocks. Phase composition of the soluble organic matter was analysed with "Hewlett Packard" and "Varian" chromatograph – mass spectrometers after sample crushing and hot extraction in chloroform. Analyses of the chloroform extract revealed the following organic compounds:

- (a) *in the central ore zone*—non-branched saturated hydrocarbons (C_{15} , C_{17} , C_{19-21} , C_{23} , C_{24} , C_{36}), ethyl esters of carboxylic acids (C_{14} , C_{18}), phthalates; high molecular-weight compounds ($\text{C}_{12}\text{H}_{17}$, C_5H_{44} , $\text{C}_{21}\text{H}_{44}$, $\text{C}_8\text{H}_{34}\text{O}_8$), and amides;
- (b) *in the upper zone*—non-branched saturated hydrocarbons (C_{14-19} , C_{21-25} , $\text{C}_{24}\text{H}_{50}$, branched saturated hydrocarbons (tetramethyl C_{15}), ethyl esters of carboxylic acids (C_{16} , C_{18}); phthalates;
- (c) *in the lower zone*—nonbranched saturated

hydrocarbons (C_{15} , C_{17-20} , C_{23} , C_{24} , C_{26}), branched saturated hydrocarbons (dimethyl C_{13} , tetramethyl C_{17} , carboxylic acids (C_9 , C_{16}), ethyl esters of carboxylic acids (C_{11} , C_{14} , C_{18}), phthalates, high-molecular compounds ($\text{C}_5\text{H}_4\text{NS}$, $\text{C}_{12}\text{H}_{17}\text{ON}$, $\text{C}_{21}\text{H}_{44}$, $\text{C}_{18}\text{H}_{34}\text{O}_4$), and amides. All samples contain molecular sulfur S_8 and S_6 with concentrations of $\sim 1 \times 10^{-4} \text{ g.L}^{-1}$. The less variable composition of soluble organic matter in the ore zone is related to intense hydrothermal alteration in this zone as high-temperature metasomatic alteration and metamorphic processes led to the removal of volatile components and the simplification of composition.

The insoluble carbonaceous matter is present as a dispersed phase disseminated in host shale, and also forms fibrous segregations in association with fibrous sericite. Some finely dispersed carbonaceous matter is included inside metamorphogenic porphyroblasts of carbonates, quartz, pyrite and other metasomatic minerals.

Ashless concentrates of the insoluble organic carbon contain 95.22 wt.% carbon and 1.44 wt.% hydrogen; the sum of nitrogen, sulfur and oxygen is 3.36 wt.%.

Inspection of the insoluble carbon-bearing matter by TEM (microdiffraction data) shows the existence of two structural types of carbonaceous matter. The more abundant type is structurally amorphous, represented by aggregates of ultra-fine oval (600–1000Å) nanoparticles and films (Fig. 21-8). Aggregates of graphite microcrystals occur also. Crystals of graphite in the form of fine flakes reach 600 Å in size, though zones of monocrystal diffraction as shown on the dark-field images of 100 and 101 reflections are about 200Å in size. These crystals form ring diffraction patterns with three basic reflections only. Thus the 100 reflection is distinct, and the following 101 reflection is not detected (Fig. 21-6d), observations which can be explained by corrugation of graphite crystals along {001} plane of its crystal lattices. Twirled spherical particles of graphite less than 1 micron in size rarely occur also (Fig. 21-8).

Thus, the organic matter is greatly dominated by kerogen – graphite-like matter that does not contain functional groups and originates during the greenschist-facies metamorphism of sedimentary organic matter. Less than 0.01 wt.% of soluble organic matter is possibly relict of primary organic matter that survived alteration.

TABLE 21-4. AVERAGE VALUES OF C, H, N AND S CONTENTS (WT%) AND ISOTOPIC COMPOSITION (‰) OF BLACK SHALE FROM ORE, UPPER AND LOWER ZONES OF THE SUKHOI LOG DEPOSIT

hole	Interval, m	n	zone	$\delta^{18}\text{O}_{\text{carb}}$	$\delta^{13}\text{C}_{\text{carb}}$	$\delta^{13}\text{C}_{\text{tot}}$	$\delta^{13}\text{C}_{\text{org}}$	C _{total}	C _{org}	C _{carb} *	H	N	S
36	90-124	3	upper	26.4	-6.4	n.a	-15.9	2.60	n.a		0.25	0.09	0.41
	178-200	2	ore	17.3	-9.3	n.a	-6.7	2.02	n.a.		0.25	0.13	6.60
	233-291	4	lower	27.5	-6.4	n.a	-15.2	1.92	n.a		0.35	0.12	5.17
112	14-84	6	upper	21.4	-15.3	-10.3	-26.6	2.54	0.61	1.93	0.22	0.15	n.a.
	102-160	6	ore	24.5	-12.8	-12.7	-22.5	2.41	0.42	1.99	0.24	0.18	n.a.
	184-236	4	lower	23.0	-11.3	-13.6	-30.3	1.98	0.49	1.5	0.3	0.17	n.a.
Average		25		23.4	-10.3	-12.2	-19.5	2.25	0.51	1.81	0.27	0.14	4.1

*- Carbonate C content = total C content – organic C content; n – the number of analyses; n.a. – not analyzed.

Carbonaceous matter and noble metals

The known propensity for complexation or sorption of noble metals with organic carbon has led numerous researchers to establish genetic links between these components (Ermolaev *et al.* 1999, Gize 1999, Pašava 1993, Coveney *et al.* 1992). Identification of metal-organic compounds in ores by direct analytical methods is always difficult due to low PGE contents close to routine detection limits. Therefore, the most widespread approach involves the use of bitumen extracts mentioned

above and carbon-rich concentrates (rather than the original bulk rocks) for analysis.

The different procedures of organic matter hot extraction with different solvents (chloroform, spirit, spirit-benzene and benzene) allow the determination some metal-organic compounds using gas chromatography with atom-emission detector (GC–AED method). The volatile metal-organic compounds of mercury, arsenic, and silicon were found in chloroform and spirit-benzene extracts of the bitumen from the bulk ore samples (Distler *et al.* 1996). Gold contents in spirit-benzene extract are slightly higher than in chloroform with range of from 0.21 to 3.49 g.t⁻¹. Thus the prevalence of carbon-bonded compounds in the total metal balance is estimated to be insignificant, when the content of total soluble carbonaceous matter (0.003–0.010 wt.%) is considered.

TABLE 21-5. AVERAGE C, H, N AND S CONTENTS OF BLACK SHALE FROM ORE, UPPER AND LOWER ZONES OF THE SUKHOI LOG DEPOSIT BY CHEMICAL CHNS ANALYSIS (WT.%).

Hole	zone	n	H, m	S	C	H	N
119	upper	2	15-26	0.1	2.53	0.21	0.17
	ore	3	35-57	0.25	2.54	0.33	0.19
	lower	6	64-105	0.13	1.97	0.28	0.17
36	upper	4	101-161	2.07	2.42	0.26	0.10
	ore	4	178-221	6.05	2.10	0.27	0.14
	lower	5	234-292	4.27	1.89	0.35	0.12
109	lower	13	185-254	1.53	1.78	0.23	0.12
112	upper	7	38-85	5.98	2.29	0.20	0.10
	ore	10	99-127	7.04	1.88	0.23	0.13
39	upper	3	20-45	0.21	1.73	0.19	0.10
	ore	3	119-136	1.18	2.76	0.27	0.14
	lower	2	198-213	0.54	1.63	0.36	0.11
203	upper	2	81-83	0	3.61	0.23	0.11
	ore	8	98-173	16.15	2.44	0.24	0.12

n – the number of analyses
organic matter that survived alteration.

On the basis of the above consideration, if any significant binding of noble metals to carbonaceous matter occurred, it should be detectable in the insoluble fraction. To obtain the insoluble fraction, flotation of the fine-grained carbonaceous portions of the rocks was carried out in pure water with subsequent decantation of floating product. Neither gold nor platinum were identified in the insoluble flotation products of the Sukhoi Log ores. This preliminary result indicates that neither metal-organic compounds nor particles sorbed in organic matter can be the sources of elevated PGE abundance.

Data in support of this preliminary find were obtained from a selection of samples of insoluble carbonaceous matter obtained by serial acid digestion, leading to concentration of an acid-resistant residue (see below: *Carbon-rich concentrates*).

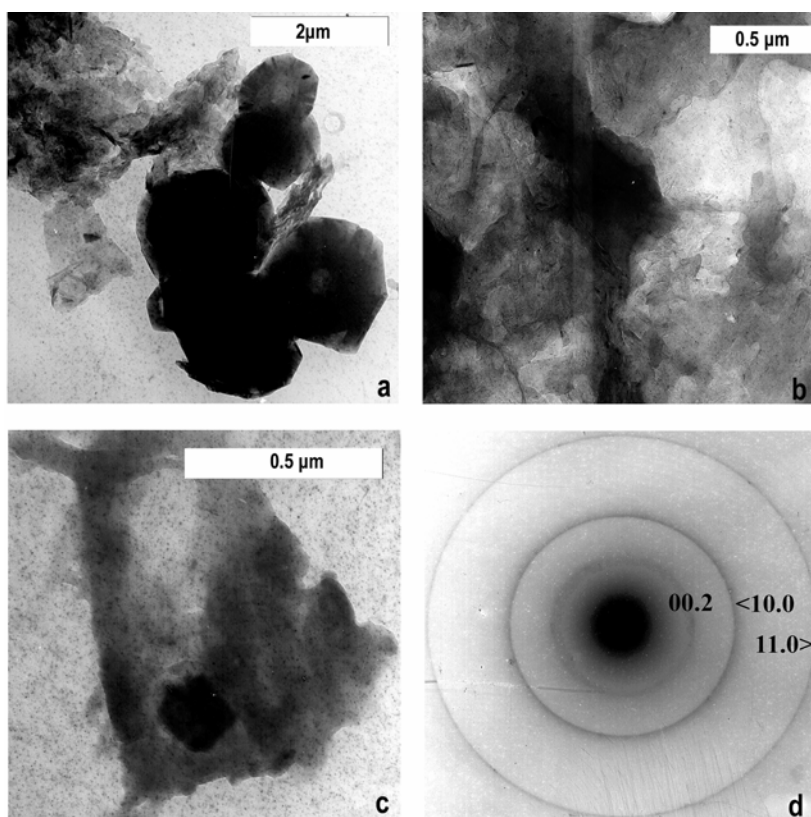


FIG. 21-8. TEM images of two structural types of carbonaceous matter in Sukhoi Log ore. a – rounded particles of graphite; b, c- amorphous aggregates of fine particles, black particle – carbonate; d – microdiffraction pattern of graphite particle.

Mineralogy of the ores

Ore minerals form only 3 to 5 vol.% of the samples but include approximately 90 ore mineral species and varieties, including native metals, metal alloys, and sulfides (Table 21-6) (Vikulova *et al.* 1977, Distler *et al.* 2003). In contrast to many other gold deposits, including black shale-hosted deposits, Fe–Ni–S and Ni–Co–Fe–As–S minerals are almost as abundant as pyrite in the mineralized rocks of the Sukhoi Log deposit.

Native gold

Native gold is the main economic species of the deposit. It occurs mostly as small grains within quartz and pyrite (Fig. 21-9), although its intergrowths with pyrrhotite, galena, gersdorffite and other Ni–Co minerals are common. Free gold (in association with tellurides and Ag sulfosalts) is also found as fracture fillings in pyrite and quartz grains, but gold veinlets are absent in host rocks.

Gold particles are mostly xenomorphic (Figs. 21-9, 21-10), appearing as irregularly shaped clots and aggregates (Fig. 21-9h) with numerous prints of neighbor minerals (quartz, pyrite, tourmaline) (Figs. 21-10c, d). The largest

aggregates occur in interstitial spaces. Locally named “black gold” (gold grains surrounded by fine platelets of graphite or graphite-like organic matter, Fig. 21-9d) occur as well. In heavy mineral fractions and concentrates, the “black-gold” appears as black, rounded particles. Idiomorphic crystals of native gold are extremely rare; dendrite-like aggregates are found only in rare cases where apparently local re-precipitation of gold has occurred. (*e.g.*, intergrowths of native copper and gold; Fig. 21-10a, b).

Ultrafine-grained gold (fractions of a micron in size) are rare; the most abundant grain size observed is in the range of 5–10 μm. Native gold of the Sukhoi Log deposit normally has fineness as high as up to 900, but ranges from 850 to 997 (Table 21-7).

Minerals of the Fe–Ni–S system

Pyrite, the most abundant mineral of this system, usually occurs as coarse-grained crystals or as segregations in quartz-sulfide veinlets. Medium- and fine-grained aggregates are common within thin layers in gangue or wall-rock matrix. Pyrite usually

TABLE 21-6. ORE MINERALS OF THE SUKHOI LOG DEPOSIT (DISTLER *ET AL.* 1996)

<i>Class</i>	<i>Mineral</i>	<i>Formula</i>	<i>Class</i>	<i>Mineral</i>	<i>Formula</i>	
<i>Native metals</i>	Gold	Au	<i>Arsenides and sulphoarsenides</i>	Sperrylite	PtAs ₂	
	Platinum	Pt		Niccolite	NiAs	
	Silver	Ag		Maucherite	Ni ₉ As ₁₁	
	Iron	Fe		Rammelsbergite	NiAs ₂	
	Tin	Sn		Smaltite	CoAs ₃₋₂	
	Lead	Pb		Safflorite	CoAs ₂	
	Copper	Cu		Skutterudite	(Co, Ni)As ₃	
	Titanium	Ti		Gersdorffite	NiAsS	
	Tungsten	W		Cobaltite	CoAsS	
	Chromium	Cr		Arsenopyrite	FeAsS	
	Indium	In		Enargite	Cu ₃ AsS ₄	
<i>Metal solid solutions and intermetallic compounds</i>	Gold-Silver	(Au,Ag)	<i>Tellurides and sulfotellurides</i>	Altaite	PbTe	
	Gold-Silver-Copper-Mercury	(Au,Ag,Cu,Hg)		Calaverite	AuTe ₂	
	Silver amalgam	Hg ₃ Ag		Hessite	Ag ₂ Te	
	Platinum-Copper-Iron	Pt ₁₋₂ (Cu,Fe)		Petzite	Ag ₃ AuTe ₂	
	Platinum-Iron	Pt ₃ Fe-PtFe		Cervelleite	Ag ₄ TeS	
	Nickel-Tin	(Ni, Sn)		Stutzite	Ag ₇ Te ₄	
	Nickel-Antimony	(Ni, Sb)		Krennerite	Au ₄ AgTe ₁₀	
	Lead-Tin	(Pb, Sn)		Joseite	BiTeS	
	Antimony-Tin	(Sb, Sn)		<i>Selenides</i>	Umangite	Cu ₃ Se
	Lead-Antimony-Tin	(Pb, Sn, Sb)			Klockmannite	CuSe
	Copper-Zinc	(Cu, Zn)	Berzelianite		Cu ₂ Se	
	Tellur-Bismuth	(Bi, Te)	<i>Antimonides and sulfosalts</i>		Dyscrazite	Ag ₃ Sb
	Ag and Pb tellurobismuthide	(Ag, Pb) (TeBi)		Galenobismuthite	PbBi ₂ S ₄	
	Pd and Ag tellurobismuthide	(Pd, Ag) (TeBi)		Corynite	NiAsSbS	
		Tetrahedrite		Cu ₁₂ Sb ₄ S ₁₃		
<i>Sulfides</i>	Pyrite	FeS ₂	<i>Cylindrite</i>	Cylindrite	Pb ₃ Sn ₄ Sb ₂ S ₄	
	Cooperite	PtS		<i>Oxides, phosphates and tungstates</i>	Rutile	TiO ₂
	Pyrrhotite	Fe _{1-x} S			Baddeleyite	ZrO ₂
	Pentlandite	(Fe, Ni) ₉ S ₈			Magnetite	Fe ₃ O ₄
	Cubanite	CuFe ₂ S ₃	Scheelite		CaWO ₄	
	Chalcopyrite	CuFeS ₂	Wolframite		(Fe, Mn)WO ₄	
	Millerite	NiS	Monazite		(La,Ce,Nd)PO ₄	
	Mineral NiFe ₂ S ₄	NiFe ₂ S ₄	Xenotime		YPO ₄	
	Mineral Ni ₃ FeS ₄	Ni ₃ FeS ₄	<i>Halides</i>		Iodyrite	AgI
	Heazlewoodite	Ni ₃ S ₂			Mineral Pb,Bi)Cl ₂	
	Violarite	FeNi ₂ S ₄			Mineral PtTiCl ₄	
	Sphalerite	ZnS				
	Galena	PbS				
	Molybdenite	MoS ₂				
	Greenockite	CdS				
	Acanthite	Ag ₂ S				
	Rheniite	ReS ₂				

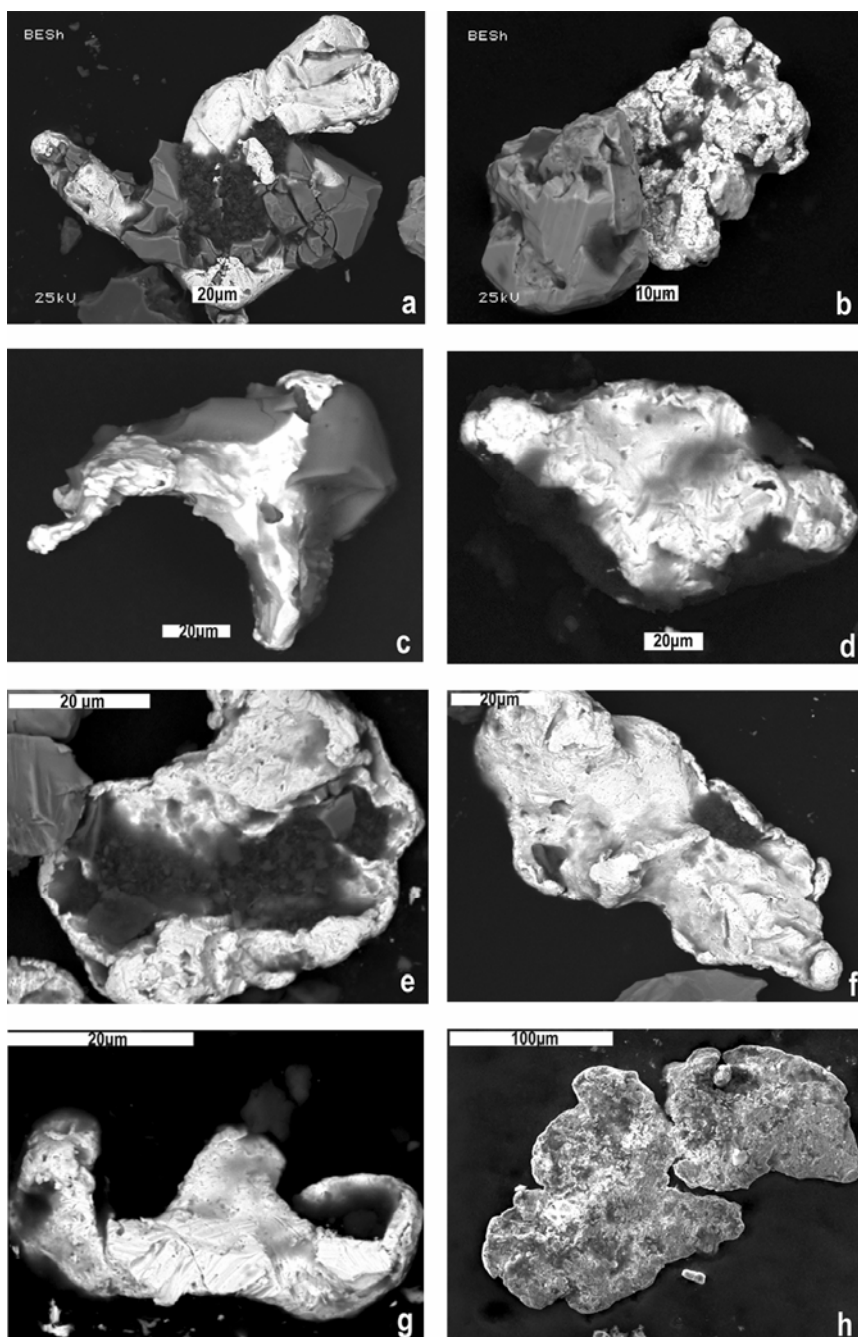


FIG. 21-9. Native gold from heavy mineral concentrates. SEM. a, b, c – intergrowths of xenomorphic gold with euhedral pyrite; d, e – xenomorphic gold surrounded by carbonaceous matter; f, g – morphology of xenomorphic aggregates with prints of associated minerals; h – lamp-like aggregates of native gold.

includes disseminated grains of the earlier Ni-bearing pyrite, pyrrhotite, pentlandite, chalcopyrite and cubanite in association with numerous gangue minerals. The chemical compositions of pyrite and other sulfides are given in Table 21-8. Early Ni-rich pyrites, containing more than 0.8 wt.% Ni, occur in the centers of large porphyroblasts. Most of the pyrite grains analyzed contain 0.01 to 1.0 wt.% of As but one grain contains 2.9 wt.% As.

Pyrrhotite is much less abundant than pyrite in the ores, but occurs in grains as large as 0.5 mm in most samples. Two main varieties of pyrrhotite are distinguished; one occurs earlier than pyrite, and the other is coeval with or later than pyrite. The earlier pyrrhotite grains contain laminar, flame-shaped and rounded or anhedral inclusions of pentlandite. Later intergrowths of pyrrhotite with native gold, chalcopyrite, galena and sphalerite are

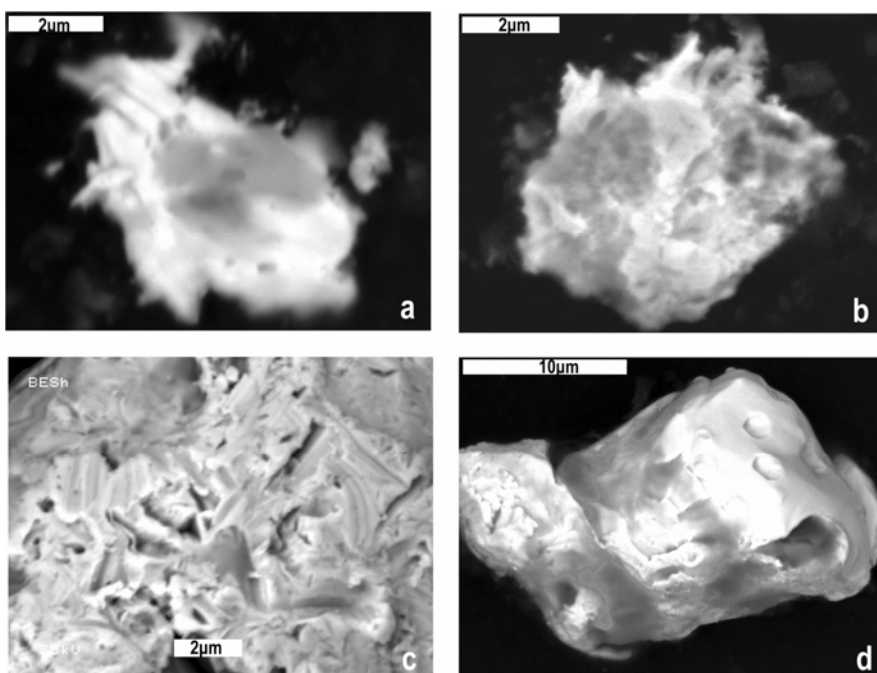


FIG. 21-10. Detailed morphology of the surface of gold. SEM. a,b – intergrowth of native copper with tubular and dendrite-like gold crystals; c,d – numerous prints of associated minerals on the gold surface.

TABLE 21-7. REPRESENTATIVE ELECTRON MICROPROBE ANALYSES OF NATIVE GOLD (WT.%)

N	Au	Ag	Cu	Σ	N	Au	Ag	Cu	Σ
1.	75.57	24.51		100.08	13.	89.5	9.7		99.2
2.	78.35	18.55		96.9	14.	89.6	10.1		99.7
3.	81.31	17.83		99.14	15.	89.75	9.61	0.03	99.39
4.	83.49	16.05		99.54	16.	90.1	9		99.1
5.	84.02	16.58	0.06	100.66	17.	90.3	9		99.3
6.	85.3	15.07	0.09	100.46	18.	91.27	8.36	0.05	99.68
7.	86.2	13.3		99.5	19.	92	7.8		99.8
8.	87.25	10.88	0.11	98.24	20.	92.1	7.3		99.4
9.	87.6	12		99.6	21.	93.8	6		99.8
10.	88.08	11.34	0.05	99.47	22.	99.2	0.5		99.7
11.	88.6	11.3		99.9	23.	99.6	0.3		99.9
12.	89.2	10.6		99.8	24.	99.7			99.7

Note: blank – below detection limits.

common. The composition of pyrrhotite (Table 21-8) ranges from Fe-rich hexagonal pyrrhotite to S-rich monoclinic pyrrhotite.

Pentlandite usually occurs as small inclusions in pyrrhotite but also as separate grains coexisting with millerite and heazlewoodite. The ΣMe/S are close to the stoichiometric ratio. Low As and Sb contents occur in some pentlandite grains, but no Co or Cu was detected.

Millerite with up to 3.5 wt.% Fe forms intergrowths with pyrite and other minerals, including native gold. Violarite is close to

pentlandite in chemical composition, differing by its higher sulfur content. The violarite is found as fine idiomorphic and anhedral grains but may be pseudomorphs after pentlandite.

Minerals of the Ni-Co-Fe-As-S system

Co, Ni and Fe sulfarsenides are represented by nearly pure arsenopyrite and gersdorffite; phases of variable composition from Fe-rich gersdorffite up to Fe-Ni-rich cobaltite are observed (Table 21-8). Arsenopyrite is the least abundant of the sulfarsenides, occurring as fine idiomorphic

TABLE 21-8. REPRESENTATIVE CHEMICAL COMPOSITION OF Fe–Ni–S AND Ni–Co–Fe–As–S MINERALS OF THE SUKHOI LOG DEPOSIT BY ELECTRON MICROPROBE ANALYSIS (WT.%) (PARTIALLY FROM DISTLER *ET AL.* 2004).

N	sample	Mineral	Ni	Fe	S	As	Co	Sb	Cu	Σ
1	1/2	Ars		34.5	19.6	45.2				99.3
2	45/4	Cb	2.4	6.8	20.8	43	26.6			99.6
3	45/4	Cb	9.4	9.5	19.5	44.5	16.5			99.4
4	45/4	Cb	13.3	11.4	19.7	44.8	10.2			99.4
5	45/4	Gf	13.6	12.2	19.3	44.3	9.8			99.2
6	45/4	Gf	14.9	11.9	19.6	45.8	7.6			99.8
7	1/2	Gf	23.12	13.47	20.35	43.04	0.95	0.01	0.02	100.96
8	45/4	Gf	30.6	1.7	19.7	46	1.2			99.2
9	45/4	Gf	34.5	1	18.8	45.4				99.7
10	112-084	Mil	59.89	2.92	36.31				0.08	99.2
11	109-73	Mil	63.81	2.16	34.2	0.06		0.02		100.25
12	2/6	Mil	65.94	0.51	34.15	0.08	0.06			100.74
13	45/4	Pn	30	36.3	33.5					99.8
14	45/4	Pn	33	33.2	33.1					99.5
15	112-150	Pn	35.64	31.51	32.39			0.03		99.57
16	112-150	Pn	39.85	26.26	33.25					99.36
17	112-150	Pn	44.79	21.09	33.97	0.01				99.86
18	1/5	Pn	48.32	13.71	36.29	0.01	0.01			98.34
19	1/3	Po	0.59	60.76	38.34				0.01	99.7
20	45/4	Po		61.2	38					99.2
21	45/4	Po	0.2	62.3	37.2					99.7
22	1/5	Py		44.33	53.72	0.56	1.19			99.82
23	1/9	Py	0.38	47.46	51.3					99.14
24	1/9	Py	1.04	46.47	52.86	0.05	0.03		0.04	100.49
25	1/2	Viol	32.87	23.54	43.32	0.05		0.04		99.82
26	1/4	Viol	36.3	21.03	43.19					100.52
27	1/5	Viol	40.16	16.97	43.34	0.03		0.03		100.53

Note: 1/2, 1/4, 1/5, 1/9, 45/4 – ore zone, the adit; 112, 109 – the numbers of the drill holes and the depth from the surface. Py – pyrite, Po-pyrrhotite, Pn – pentlandite, Mil – millerite, Viol – violarite, Ars – arsenopyrite, Cb – cobaltite, Gf – gersdorffite; blank – not detected.

crystals, usually hosted in pyrrhotite, and are free of Ni and Co.

Gersdorffite commonly occurs as anhedral inclusions in pyrite or as individual euhedral grains and aggregates in gangue minerals. Arsenopyrite, sphalerite, native gold and platinum are found intergrown with gersdorffite. Iron-poor (0.76 to 3.65 wt.% of Fe) and iron-rich (11.8 to 13.93 wt.% of Fe) compositional varieties of gersdorffite are distinguished. Elevated Co contents are typical of iron-rich gersdorffite.

Fe-rich gersdorffite and Fe–Ni-rich cobaltite are observed as inclusions in pyrite and in intergrowths with pyrrhotite and pentlandite and form an isomorphous series, in which Ni and Co content varies and Fe contents are fairly stable (20 to 40 at.% Fe).

Minor and rare minerals

Minor ore constituents include galena, tetrahedrite and sphalerite. Numerous rare selenides, tellurides and sulfosalts generally occur as inclusions in pyrite and galena crystals, fracture fillings or intergrowths with native gold.

Galena occurs as intergrowths with chalcopyrite, pyrite, native gold and native silver and it can contain up to 0.55 wt.% Ag, up to 1.36 wt.% Bi, up to 0.17 wt.% Te. Tetrahedrite occurs as intergrowths with chalcopyrite, galena, pyrite, millerite and native gold. Sphalerite is associated with pyrite, pyrrhotite, galena, and native gold and forms two main varieties: one with iron content lower than 0.8 wt.%, and the other with iron contents ranging from 4.2 to 5.1 wt.%. The cadmium concentrations in sphalerite are uniform

(0.2 to 0.4 wt.%) regardless of their iron contents. Greenockite (CdS) was found in ultraheavy concentrates that are enriched in PGE contents and contains 73.0 wt.% Cd, 2.6 wt.% Zn and 23.4 wt.% S. Molybdenite and rheniite (ReS₂), occurring as idiomorphic crystals (Fig. 21-11c), were found in the carbon-rich concentrates.

Native metals and alloys

Ores were found to contain native platinum, indium, iron, chromium, tantalum, tungsten, titanium, lead, tin and copper besides native gold and silver. The native metals occur as anhedral grains a few microns to a few tens of microns in size, which are similar in habit to the platinum-group minerals (PGM). Native chromium is located in interstices in the rock-forming silicates, where an undetermined Cl-bearing phase also occurs.

Native indium was first identified at the deposit in the carbonaceous concentrates. The mineral, 5 micron in size, was found in intergrowths with pyrite (Fig. 21-11f). Native gold, platinum, tantalum and chromium, besides indium, were found in these concentrates.

Intergrowths of native metals include native tin and lead, which form aggregates where tin droplets are included in a lead matrix, or *vice versa*. Ni-Sn metallic solid solutions were also found in intergrowths with these aggregates that may result from exsolution.

Many native metals form intergrowths with each other or form aggregates with exsolution textures and are probably coeval. Grains of native metals and metallic alloys are also found as inclusions in minerals within the gold-bearing assemblages. For example, Ni-Sn inclusions occur in native gold.

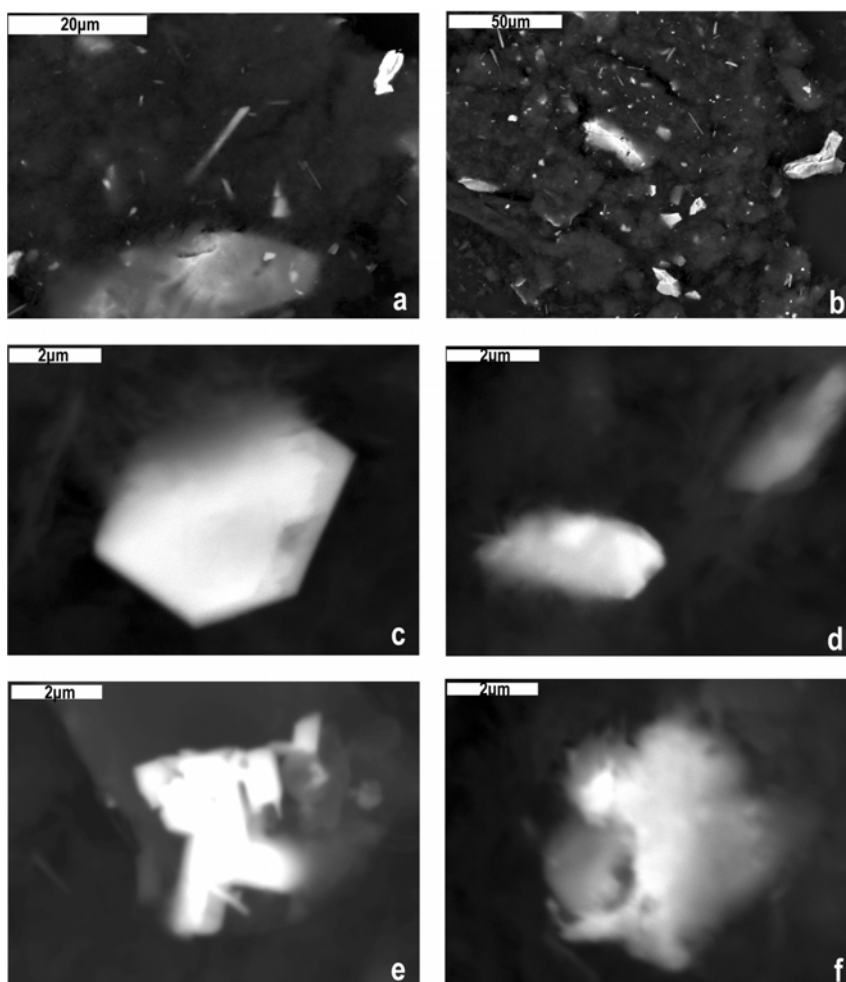


FIG. 21-11. BSE images of carbon-rich concentrate and separate minerals in it. a, b – common view with graphite-like matter as background and minor pyrite (light-grey), rutile (needles) and rare platinum (bright-white); c – crystal of molybdenite; d – crystal of rheniite; e – plates of PtTlCl₄; f – intergrowth of pyrite with native indium (partially from Distler *et al.* 2004).

PLATINUM MINERALIZATION

Analytical procedures

Accurate and reproducible analyses of the PGE poses a great challenge for samples of unconventional ore types. Uncertainty in PGE measurements is caused by several principal factors, all of whose individual and combined effects are difficult to assess. Below are a few of the factors that introduce uncertainties into analyses of the Sukhoi Log ores:

1. PGE and gold in the ores commonly form discrete mineral phases. Heterogeneity of their distribution results in the so-called “nugget” effect. The mass of representative samples analyzed depends on the type of analysis being done; determinations with larger samples generate more reproducible results, generally. Thorough mixing of sample fractions during sample preparation is also necessary to eliminate the “nugget” effect.
2. The ores contains both soluble and insoluble organic matter. It is impossible to exclude the interaction between PGE and organic matter, possibly leading to the formation of volatile compounds in any analytical method, which could be lost during analysis. The sorptive capacity of carbonaceous matter can also be a source of inaccuracy during dissolution and digestion of samples. The insoluble residue is excluded from the analysis together with noble metals sorbed on carbonaceous matter. The presence of carbonaceous substance also affects the oxidation state of the solutions.

In light of these complicating factors, we determined PGE concentrations in large samples making extensive comparison with results obtained by different methods and in different laboratories. A number of analytical schemes were tested at first to select satisfactory methods and representative amounts of samples required for precise measurements.

In addition to traditional methods of noble metal analysis, some unconventional methods of analysis were also tested. Each sample was analyzed by two or three independent methods to evaluate average noble metal content and characterize the distribution of platinum mineralization in the ores. The following methods (from a series of different laboratories) were used: (i) chemical-spectral method with preconcentration on polystyrene and coal collectors; (ii) chromatography with preconcentration on thiourea and organic sorbent; (iii) kinetic method; (iv)

atomic absorption spectrometry; (v) instrumental neutron activation analysis with fire assay preconcentration; (vi) extraction-atomic absorption spectrometry; (vii) voltampermetric method; (viii) XRF (X-ray fluorescence spectrometry) and (ix) ICP-MS (inductively coupled – plasma mass spectrometry). The most valid and reproducible results were obtained by chemical analysis of 2–5 g of sample with acid decomposition, subsequent concentration on organic sorbent, and final determination by either chromatographic/kinetic analysis or by ICP-MS. Despite high dispersion in the data, detectable concentrations were identified by all methods above. Detection limits for the chromatographic method were (in ppm): Pt – 0.02, Pd – 0.01, Rh – 0.001, Ir – 0.002; and for the ICP-MS analyses (in ppm): Pt – 0.005, Pd – 0.005, Rh – 0.0005, Ru – 0.0002, Ir – 0.0005. Os and Ir determination was carried out by a combined diffusively atomic emission method, which involves autoclave digestion, preconcentration (*e.g.*, as OsO₄) in diffusion cells and finally, ICP-MS or kinetic determination. This method allows accurate detection of Os over a concentration range from 1 to 1000 ppb.

Unfortunately, it was impossible to use fire assay analysis, one of the best methods of gold determination, because reliable PGE determination in highly oxidized and highly reduced materials is hampered by severe analytical problems (Kucha 1982, Juvonen *et al.* 2000). Inadequacy of the neutron activation method is connected to the formation of isotope ¹⁹⁹Au from gold-bearing materials since platinum content is measured on the same isotope by INAA. Irreproducibility of the voltampermetric method is explained by influence of minor and trace elements in polymetallic ore.

Direct determination of the mode of occurrence of PGE

The most reliable evidence for the presence of PGE in ores is identification of their mineral phases and other phases using X-ray microanalysis, X-ray photoelectronic spectroscopy, Auger-spectroscopy and electron microscopy study. PGE solid solutions in sulfide, sulfoarsenides and arsenides are common in magmatic platinum deposits (Distler *et al.* 1999, Cabri *et al.* 1985). We initially assumed that high PGE contents in the Sukhoi Log deposit were related to their admixtures in ore sulfides. More than 1000 grains of various minerals (pyrite, pyrrhotite, pentlandite and sulfoarsenides) were studied. Platinum is absent at

the routine detection limit of microanalysis, but Pd contents up to 0.12 wt.% were established in separate grains of cobaltite. To obtain sufficient numbers of grains for analyses, special ultra-heavy and carbon-rich concentrates were prepared from the ores.

Ultra heavy concentrates

The scheme of the separation of ultraheavy concentrates is shown in Fig. 21-12. Sandy fractions of crushed rocks were divided into several size fractions (from 0.25 to 0.09, from 0.09 to 0.06 and less than 0.06 mm). Each size fraction was split in heavy liquids followed by cleaning of heavy fractions in bromoform to obtain light fractions. In general, by this method, sulfide concentrates dominated by pyrite, pyrrhotite, and chalcopyrite and ultraheavy concentrates with a varied mineralogy were obtained. Possible loss of the PGE was controlled by chemical determination of PGE contents at selected stages of the concentration process. The output concentrates were analyzed for mineral compositions using a scanning electron microscope with an EDS Link-10000 microanalyzer. Ultraheavy concentrates were

separated from samples previously determined to have contents of PGE of 1 to 7 ppm. The highest PGE contents occur in the finest and densest fraction separates. One sample from an ultraheavy (PGE) concentrate (size fraction less than 0.06 mm) contains 9.9 wt.% of the total, whole-rock PGE. The weights of fractions (Fig. 21-12) were: 2 – 0.127 mg, 3 – 0.024 mg, 4 – 19.5 mg, 5 – 0.5 mg, 6 – 0.0076 mg.

Carbon-rich concentrates

Carbon-rich concentrates from the Sukhoi Log were originally selected for study of the relations between the PGE and organic matter. These two may be chemically or physically associated with one another by 1) the formation of PGE-volatile compounds (such as carbonyls and carbonyl-chlorides of platinum metals) and 2) the sorption of metals by solid organic matter. In the first case, elevated PGE concentration would be associated with soluble fraction of organic matter, in second case – with insoluble graphite-like matter which comprises more than 98 wt.% of total reduced carbon in the rocks.

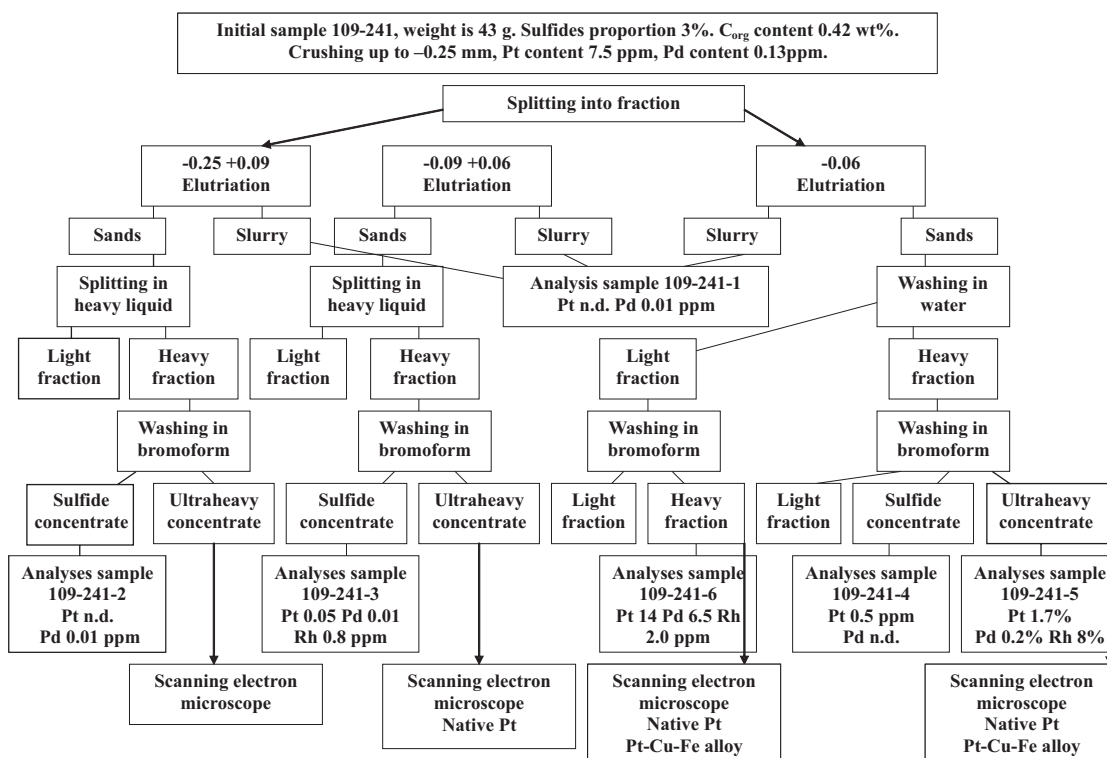


FIG. 21-12. Technological scheme for analyzing gold ore samples from the Sukhoi Log deposit (Distler *et al.* 2004).

The concentrates were obtained by the following multistage procedure: decantation in water with natural flotation of finely-dispersed phases, dissolution in HCl to remove carbonates and some aluminosilicates, dissolution in HF to remove the other silicates and quartz, and dissolution in HNO₃ to remove sulfides. It should be noted that the first and lightest fraction of the natural flotation process mainly consisted of sericite and graphite-like matter without any traces of platinum metals, as discussed previously. But the residual “insoluble carbonaceous matter” contained between 53 and 92 wt.% carbon and was heavily enriched in Pt (300–1000 ppm). For comparison, the initial bulk samples contained 0.6–0.9 wt. % C_{org} and <0.03 ppm Pt, demonstrating the effectiveness in the carbon-rich concentration method.

The concentrates are composed of acid-resistant minerals including native platinum, gold, rutile, monazite, molybdenite, rhenium sulfide (Fig. 21-11c, d), as well as relict grains of some ore minerals (pyrite, Ni–Co sulfoarsenides), native indium and tantalum (Fig. 21-11 a, b). The elevated contents of trace elements in the carbon-rich concentrates (ppb: Ni 25–1200, Co 2–200, V 30–300, Cr 80–150, Mo 20–100, Pb 20–60, Cu 30–1000, Zn 20–600, Zr 300–1500, Nb 10–80, Ti 8000–10000, REE 20–300) reflect various mineralogical compositions. The presence of relict grains of some ore minerals explains the elevated concentrations of some metals in the concentrations related to Ni–Co sulfoarsenides mainly. PGE accumulation in these types of concentrates may be due to the presence of their acid-resistant mineral phases (native platinum, for example) and does not necessarily indicate that the PGE were extracted from metal-organic compounds.

General features of PGE mineralization

The distribution of platinum metals in ores of the deposit was determined by analysis of more than 400 samples from different vertical sections of the gold-bearing zone and the overlying and underlying host rocks. The zone of PGE enrichment has a complex morphology and is localized in the upper portion of the aureole of the gold ores and in the superjacent rocks, which do not contain economic gold contents. Hence, the maximum of PGE mineralization are somewhat offset relative to the maximum Au content in the vertical direction.

Platinum contents higher than 0.1 ppm are limited to the hydrothermal-metasomatic halo and

the zone of sulfide mineralization (Table 21-9). Such concentrations were determined in all rock types of supra-ore, ore, and infra-ore zones. Platinum concentrations higher than 1 ppm occur in the part of the supra-ore zone adjacent to the mineralized zone as well as within the ore itself, with the highest concentrations (up to 3 to 5 ppm) found in the upper part of the gold ore. Elevated platinum concentrations are irregularly distributed in the infra-ore zone. Thus, the significant platinum concentrations mainly lie outside of the zone of highest gold contents as reflected in the absence of correlation between Pt and Au values. No significant correlation exists between Pt and organic carbon content or between Au and organic carbon content (Fig. 21-13).

TABLE 21-9. CONCENTRATION OF PT, PD, AU AND AG (PPM) IN BULK SAMPLES, SULFIDE AND ULTRA-HEAVY CONCENTRATES (PARTIALLY FROM DISTLER *ET AL.* 2004)

zone	hole	depth, m	Pt	Pd	Au	Ag		
Upper	36	101	0.18	0.02		4.51		
		125	1.6	0.02		1		
		161	0.05	0.03	0.62	3.52		
Ore		189	0.55	0.03	8.5	6.53		
		200	0.2	0.005	4.8	2.33		
		221	0.05	0.01	0.26	2.49		
Lower		244	0.04	0.02	0.22	1.88		
		274	0.02	0.06		0.55		
		109	241	7.5	0.03	0.042	n.d.	
		109	241 UHC	17000	2000	n.d.	n.d.	
		ore	6	103*	0.26	0.35	0.31	1.8
				104*	8.30	0.33	0.83	11.0
120.3*	0.02			0.13	21.00	6.8		
130.7*	0.16			0.37	0.57	3.9		
153*	0.01			0.26	1.40	10.0		
	165*	0.06	0.52	1.30	24.0			
	173*	0.02	0.14	1.20	10.0			
	197.3*	1.50	0.26	91.00	19.0			
	221*	0.26	0.22	13.00	19.0			
	242*	0.00	0.42	3.30	11.0			

Notes: data of chemical analysis; * - sulfide concentrates by ICP-MS; n.d. – not determined; blank – not detected; UHC – ultra-heavy concentrate.

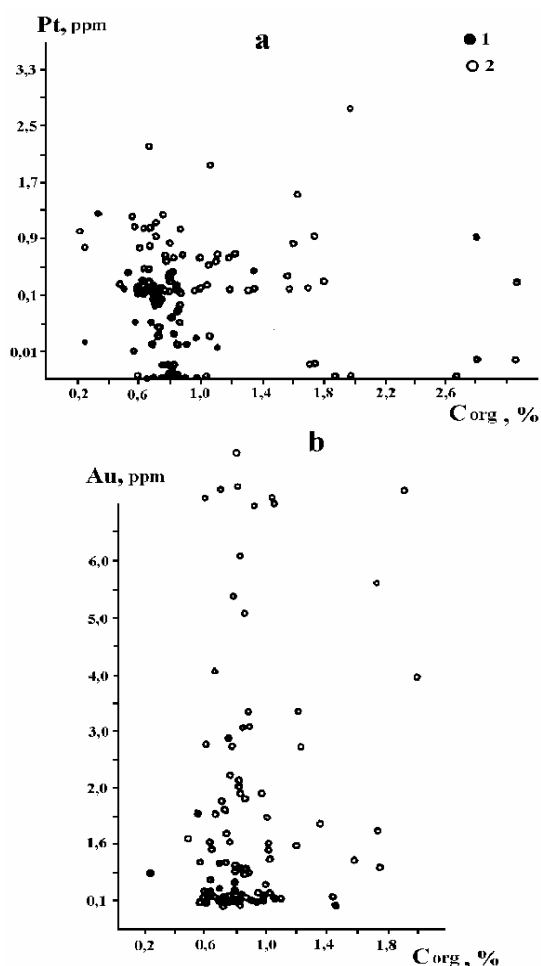


FIG. 21-13. Correlation of organic carbon contents with Pt (a) and Au (b) concentrations (Distler *et al.* 2004). 1 - supra-ore zone; 2 - ore zone.

Other PGE show a similar distribution pattern. The concentrations of palladium, however, are one order of magnitude lower than that of platinum, whereas the other PGE were detected only in some cases. The highest contents of Rh (up to 0.8 ppm) correspond to the highest platinum concentrations.

PGE mineralogy

Scanning electron microscopy showed that ultraheavy fractions generally contain PGE minerals as separate grains and more rarely as intergrowths with ore-forming sulfides. Native platinum, Pt-Fe-Cu alloys with variable composition, Pt-Fe alloys, sperrylite and cooperite were found in the ultraheavy concentrates. Platinum-group minerals most frequently occur as inclusions in sulfides and

sulfoarsenides. However, PGM were also found as inclusions in gangue minerals.

Native platinum occurs as individual grains up to 10 μm in size (Fig. 21-14) and in intergrowths with pyrite, which commonly have anhedral or dendritic shapes.

Hundreds of tiny native platinum crystals were observed in the carbon-rich concentrate using a scanning electron microscope. Among them the crystals 0.5–2 μm in size are dominant, while 5–10 μm grains also exist (Fig. 21-15). The largest grains reach 50 μm and are represented by thin band-like elongated particles (Fig. 21-15c). Aggregates of platy crystals, each < 1 μm thick, were also found (Fig. 21-15 g, h). The native Pt crystals are composed of almost pure Pt (98–99 wt.%) with a small admixture of Cu and Fe (about 1 wt.%).

Pt-Fe-Cu solid solutions dominate the PGE mineral grains analyzed (Table 21-10). They occur as separate grains about 5 to 10 μm in size and as inclusions and intergrowths with pyrite, cobaltite, carbonate and quartz (Fig. 21-15d). Varieties with atomic ratio Pt: (Cu+Fe) from 1.4:1 to 2:1 were distinguished. A phase with composition close to Pt (Cu, Fe) was found and a phase with (Cu+Fe) > Pt corresponding to $\text{Pt}_{0.85}$ (Cu, Fe)_{1.0} was analyzed. Thus, a series of disordered (and possibly continuous) solid solutions Pt_2 (Cu, Fe) - Pt (CuFe) with dominantly Cu occurs in the mineralized zone. Pt-Fe solid solutions have the same morphological features as Pt-Fe-Cu alloys and occur in the same mineral associations. There is no evidence for extensive miscibility between (Pt, Cu) and (Pt, Fe) for which significant Cu content are usually absent. The atomic ratios Fe:Pt show that most of the analyzed grains are Pt_3Fe and PtFe compounds.

Sperrylite is confined to the supra-ore zone associated with low-grade quartz-sulfide veinlets and occurs as idiomorphic crystals about 10 μm in size (Fig. 21-14g). The mineral composition is nearly stoichiometric but contains up to 0.33 wt. % Ag and up to 1.1 wt. % Au. A sample consisting of aggregates of pyrite metacrystals with quartz margins from the supra-ore zone yielded a sulfide concentrate containing 8.3 ppm Pt. An ultraheavy concentrate from this sulfide fraction contained idiomorphic crystals of cooperite up to 7 μm in size (Fig. 21-14h). This sample of low-grade ore, containing 1 ppm Au, is characterized by elevated contents of Ag (11 ppm) and Ni (799 ppm) with Ni/Co=7.

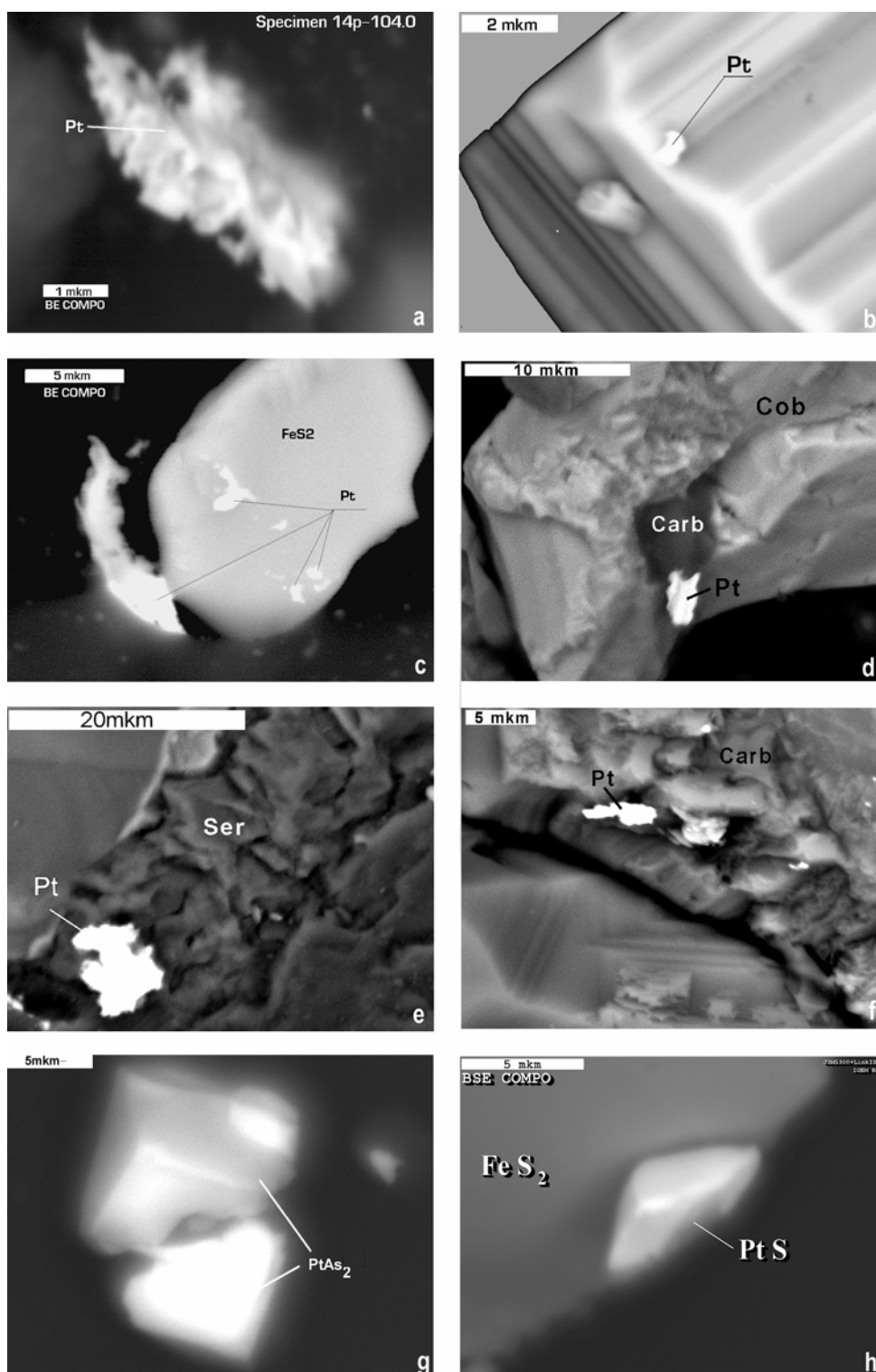


FIG. 21-14. Platinum minerals in ores of the Sukhoi Log deposit. SEM. (Distler *et al.* 2004). a – a skeletal crystal of native platinum; b – intergrowth of native platinum with pyrite; c – grain of native platinum in pyrite; d – intergrowth of native platinum with Fe-Mg carbonate (Carb) in cobaltite (Cob); e – inclusions of native platinum in sericite (Ser); f – inclusion of native platinum in Fe-Mg carbonate (Carb); g – crystals of sperrylite (PtAs₂); h – crystal of cooperite (PtS) with pyrite.

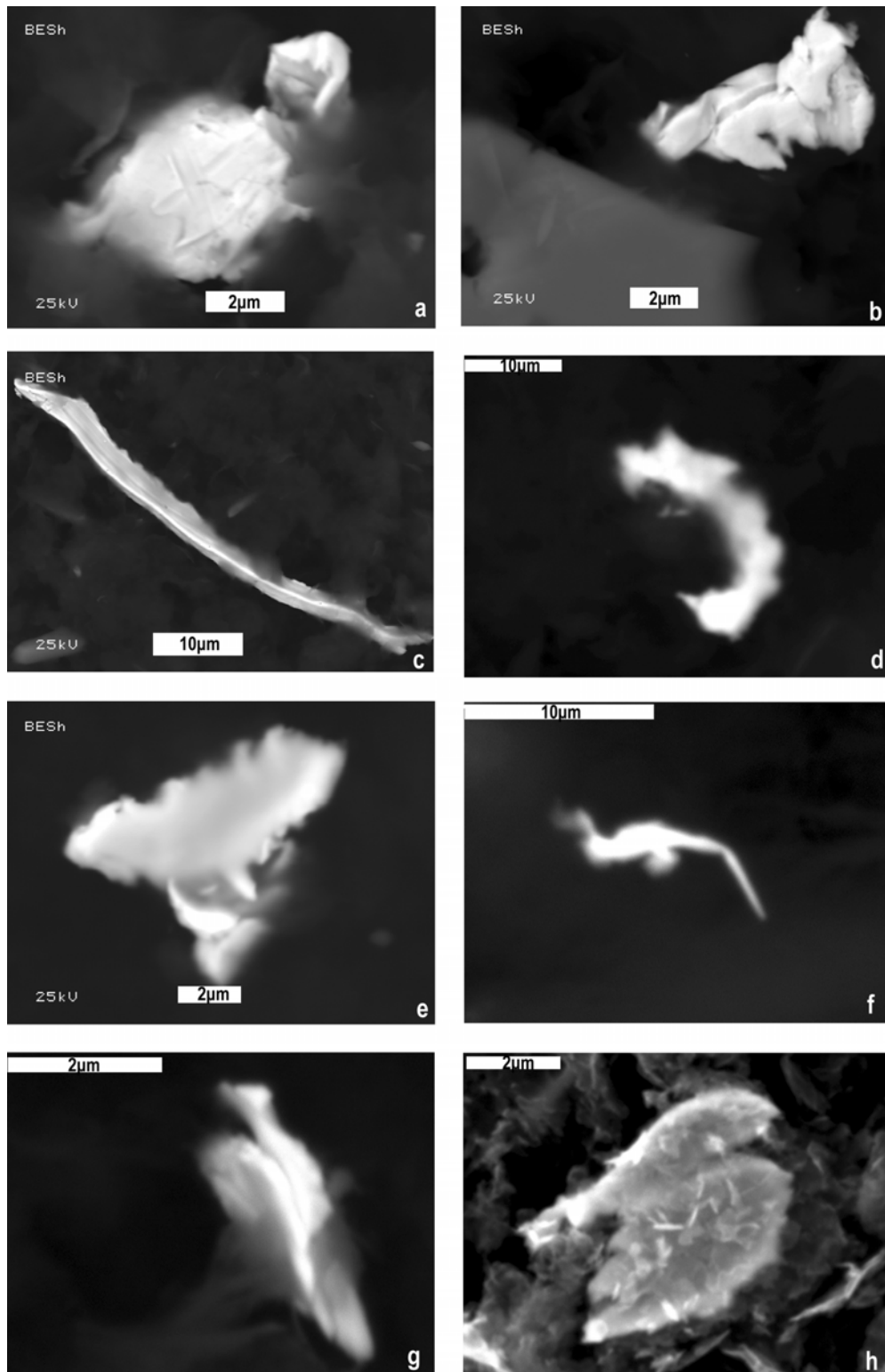


FIG. 21-15. Morphology of native platinum particle in carbon-rich concentrates of the Sukhoi Log deposit. SEM. (Distler *et al.* 2004). The background is carbonaceous matter, light-grey – pyrite.

TABLE 21-10. CHEMICAL COMPOSITION (WT.%) OF PLATINUM MINERALS FROM THE SUKHOI LOG DEPOSIT BY EDA (DISTLER *ET AL.* 2004)

Mineral	Pt	Cu	Fe	Ag	Au	As	S	Σ
Native platinum	97.44	1.12						98.56
Pt-Cu-Fe alloy	84.12	11.31	4.35					99.78
	82.55	12.84	4.7					100.09
	80.65	16.21	2.5					99.36
	79.13	14.96	2.60					96.69
	77.76	21.06	1.90					100.72
	77.13	18.38						95.51
	71.54	26.20	0.8					98.54
Pt-Fe alloy	73.65		15.60					99.25
	89.27		8.82					98.09
Sperrylite	52.91	1.27	0.19			45.26		99.63
	55.44	0.82		0.33	0.93	42.15		99.67
	53.32			0.05	1.11	44.79		99.27
Cooperite	86.4						13.7	100.1

Note: blank – not detected.

We have identified a single grain of a previously unknown mineral composed of Pt, Tl and Cl. It is too small to be analyzed quantitatively (Fig. 21-11e), but the ratio of peak intensities in its X-ray spectrum suggests a stoichiometry of PtTlCl₄.

Palladium is not incorporated in native platinum or gold but forms intermetallic compounds including a palladium silver tellurobismuthide, close to kotulskite–merenskyite, that occurs as intergrowths with galena and sphalerite. Minerals containing rhodium and other rare PGE also can be found in some parts of the deposit. This is shown by high Rh concentrations of up to 8 wt.% in an ultraheavy fraction of sample 109-241 (Table 21-9).

Some important results on mineral and concentrate studies

1. Light separates of mineralized shale do not contain elevated PGE concentration, so sorption of PGE with carbonaceous matter is negligible.
2. No platinum metal-organic compounds were established in the soluble fraction of organic matter and the amount of this soluble fraction is insignificant.
3. The elevated PGE concentrations are related to both heavy fine mineral separates and acid-resistant carbon-rich separates.
4. Sulfides are not enriched in PGE according to obtained data.
5. The main mode of PGE occurrence in Sukhoi Log ores is as discrete minerals, dominated by native platinum and Pt–Fe–Cu alloys.

Geochemical characteristics of mineralization REE fractionation

The geochemically anomalous contents of various metals are a characteristic feature of Sukhoi Log ore. At least two geochemical assemblages can be distinguished, comprising metallogenic elements that usually do not occur together: the Ni–Co–Cr–Pt–Pd assemblage is typical of mafic and ultramafic rocks whereas the Sn–W–REE–Mo assemblage typifies granitoid rocks. A part of these elements can concentrate during the processes of sedimentation and diagenesis. For example, the elevated background levels of REE observed in black shale are caused by their sorption both by organic matter and clay minerals. Black shale of the Sukhoi Log deposit shows similar REE distribution patterns in the ore and near-ore zones with an enrichment in LREE and its range is close to the NASC standard (Taylor & McLennan, 1985). The metamorphic redistribution of REE is connected to recrystallization and new growth of REE phosphate porphyroblasts. It should be noted that monazite and xenotime are common minor phases both in metamorphosed black shale and in Au–PGE-bearing hydrothermal assemblages. Hydrothermal minerals (carbonates, quartz) are enriched in HREE compared to host rocks (Distler *et al.* 2004) and hydrothermal monazite is enriched in Nd and HREE compared to monazite of sedimentary associations. An essential correlation between total REE and Pt contents in ore confirms that REEs were mobile in hydrothermal solutions crystallizing PGE minerals.

Stable isotopes

Carbon appears in ore as metamorphosed organic matter and as a component of Mg–Fe carbonates. In terms of paragenetic analysis and organic carbon depletion in mineralized zone we suggest hydrothermal oxidation of organic carbon to form carbonate minerals. Bulk carbon-isotopic compositions of Sukhoi Log black shale and carbonate have a wide spread (from –3.4 up to –28.6 ‰, PDB) and differ from marine carbonates (Faure, 1986), whereas the average composition of unaltered organic matter ($\delta^{13}\text{C}_{\text{org}} = -22\text{‰}$ PDB) is close to the isotopic composition of typical Precambrian sedimentary organic matter. A difference between average means of $\delta^{13}\text{C}_{\text{org}}$ and $\delta^{13}\text{C}_{\text{carb}}$ points to extensive isotopic exchange in mineralized zones close to equilibrium. The $\delta^{13}\text{C}_{\text{carb}}$ of hydrothermal fluid calculated from its equilibrium with vein siderite ($\delta^{13}\text{C}_{\text{carb}} - 1.1\text{‰}$) at a temperature of 200°C is estimated as –3.8‰, similar to the estimate of –2.5‰ derived from consideration of the equilibration of CO₂ and graphite ($\delta^{13}\text{C}_{\text{org}} - 24.9\text{‰}$) at the same temperature.

These data indicate that metamorphic graphitization of organic matter and recrystallization of carbonate are followed by homogenization of carbon isotope composition of wall rocks. On the other hand, the distinct isotopic features of the hydrothermal source of carbon are clearly evident.

Thermochemical characteristics of ore-forming fluids

Evolution of crystallization conditions and fluid regime was determined by thermometric and cryometric study of 1012 individual fluid inclusions in quartz and carbonate (Laverov *et al.*, 2000a). Microthermometric studies were carried out on a THMSG–600 Linkam stage, the salinity was obtained from the ice melting temperature, and corrected on the basis of measurement of the volumetric proportions of CO₂ and H₂O phases. Concentration of methane was estimated on the basis of volumetric proportions and methane's density connected with its partial pressure which in turn determines methane's clathrate melting temperature. Element concentrations in aqueous extracts from ore-bearing quartz were analyzed using a VG-Plasma Quad 2 inductively coupled plasma – mass spectrometer (ICP–MS). The procedure was described in detail by Distler *et al.* (2004).

Variations of the main parameters of Au–Pt mineralization in the Sukhoi Log deposit were estimated as follows: $T = 385\text{--}130^\circ\text{C}$, $P = 2450\text{--}170$ bar, salt concentration 9.5–3.7 wt.% NaCl equiv., CO₂ content 7.6–1.8 mol.kg⁻¹ of solution, CH₄ content 1.1–0.3 mol/kg of solution, density of aqueous solution 1.09–0.65 g.cm⁻³, $(P_{\text{H}_2\text{O}} + P_{\text{gas}})/P_{\text{H}_2\text{O}}$ 70.6–1.0 (Table 21-11). Magnesium, potassium and sodium chlorides are the dominant dissolved salts judging from the eutectic

TABLE 21-11. THE BASIC PARAMETERS OF MINERALIZATION AND ORE-FORMING FLUID (EVIDENCE FROM FLUID INCLUSIONS) (DISTLER *ET AL.* 2004)

Type of mineralization	Mineral, type of inclusion	Temperature, °C (number of inclusions)	Pressure, bar	$P_{\text{total}}/P_{\text{H}_2\text{O}}$	C salts, wt.% NaCl equiv	C_{CO_2}	C_{CH_4}	CO ₂ /CH ₄	Composition of vapor phase
Quartz-sulfide veinlets	Quartz (^{3,4})	385-185 (334)	2290-200	70.6-2.9	8.6-5.3				N ₂
	Quartz (^{1,2})	350-210 (184)	2370-190	54.0-1.03	8.1-5.6	7.6-1.8	1.1-0.3	1.1-1.9	CO ₂ , CH ₄ , N ₂
	Quartz (⁵)	335-130 (147)			9.5-3.7				CO ₂
	Carbonate (^{1,2})	340-280 (24)	1780-1560	13.3-13.2	6.7-5.0	6.7-5.3	1.0-0.7	8.0-6.0	CO ₂ , CH ₄ , N ₂
	Carbonate	205-185 (24)			6.3-5.5				
Quartz veins	Quartz (^{1,2})	385-275 (214)	2450-130	22.3-1.6	7.6-5.8	7.0-2.1	1.0-0.5	8.6-2.1	CO ₂ , CH ₄ , N ₂
	Quartz (⁵)	210-185 (42)			7.6-5.4				

Note: Types of inclusions (see text): 1 - gas-saturated N₂-CH₄-CO₂ inclusions; 2 – vapor N₂-CH₄-CO₂ inclusions; 3 - vapor-liquid inclusions; 4 - vapor inclusions with dense nitrogen; 5 - vapor-liquid inclusions of diluted solution.

temperatures of -25 to -34°C . The ore-forming solutions also contain N_2 , CO_2 , CH_4 , Ca; also Au, Ag, Pb, Zn, Sb, Be, B, Mn, V, Cr, Ni, Li, Sr, Ba, Mo, W, Sc, Ga and La are detected.

The fluid inclusions were divided into five compositional types. Type 1 – vapor-rich, consisting of an aqueous solution and a dense N_2 – CH_4 – CO_2 vapor phase; Type 2 – vapor-rich containing a dense N_2 – CH_4 – CO_2 vapor mixture, syngenetic with type 1; Type 3 – two-phase vapor-rich inclusions containing aqueous fluid often with N_2 in the vapor phase; Type 4 – vapor-rich inclusions filled with dense N_2 and syngenetic to type 3; Type 5 – two-phase inclusions of homogeneously trapped, low salinity fluid (Distler *et al.* 2004).

Genetic model

The origin of gold-sulfide-quartz mineralization in the black shale sequences of the Bodaibo synclinorium is now disputable. The traditional point of view (Kazakevich *et al.* 1971) considers an endogenous source of fluids as the main factor of the gold endowment after folding. According to another hypothesis (Buryak & Khmelevskaya 1997) gold-sulfide mineralization was mainly formed during sedimentation followed by redistribution and concentration of disseminated ores at diagenesis and metamorphism.

In the following section we present a brief summary of a genetic model for the Sukhoi Log deposit, based on regional structures, age relationships, and the geochemistry of the ore. A more detailed discussion of this model was published by Distler *et al.* (2004).

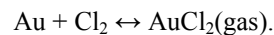
Several features of the regional geology are significant. First, the Bodaibo synclinorium appears as an internal trough superimposed on the Proterozoic fold structures of the Baikal-Patom Highland (Fig. 21-2). A marginal mafic-ultramafic magmatic belt 50 to 70 km wide can be traced over more than 2000 km along the southern margin of the Archean Siberian platform, and probably continues at depth beneath the Bodaibo synclinorium (Alakshin & Pismennyi 1988). Within the synclinorium there are no igneous rocks except the Konstantinovsk granite stock, however a major regional gravity low might represent a deep-seated granitic pluton directly underlying the Sukhoi Log deposit (Lishnevskii & Distler 2004).

We consider crustal granitoid magmatism to be the main heat source for mineralizing processes at Sukhoi Log. This is somewhat

supported by similar Paleozoic ages of magmatism and ore formation. Extensive fluid flows related to Paleozoic granitoid rocks and deep-seated granitization of ancient rocks led to large-scale redistribution of components within the Bodaibo synclinorium with mobilization of ore components from all underlying rocks including ancient ultramafites. The black shale sequences occur over the whole carbonate-terrigenous section of the synclinorium. However, the Sukhoi Log deposit remains the only giant gold-sulfide deposit to have been discovered in the region and we suggest that deep-seated hidden granitic pluton under the Sukhoi Log anticline played the leading role in ore localization.

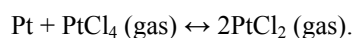
The carbonaceous material of the Khomolkho Formation either accumulated no ore components, or they were removed during metamorphic graphitization; thus, lithologic factors did not prevail during the ore formation. Calcareous black shale probably served as a favorable geochemical medium, and oxidation and redistribution of organic carbon buffered reactions of wall-rock metasomatism. Gold accumulation was controlled by an anticlinal structure in the frontal part of a thrust zone originated in the Late Paleozoic. The simple zonal structure with respect to a fold axis is related to infiltration zoning, where the richest mineralization is confined to the sheet-shaped central zone. Ore distribution within this zone is controlled by lower order folds and faults. As a conclusion, the Sukhoi Log mineralization is hydrothermal and metasomatic.

Long-term circulation of vast volumes of hydrothermal solutions enriched in gold and other ore elements resulted in significant ore accumulation. According to experimental data and natural observations, such hydrothermal solutions could not be rich in PGE (Wood 2002). So, the PGE–Au mineralization is assumed to form from supercritical low-density fluid by gas-transport reactions. These gaseous fluids saturated with chlorides and CO_2 are capable of transporting various chemical compounds as it was showed at experimental and industrial crystal growth (Givargizov 1977, Schafer 1961). For example, one of the best-studied reactions is the gold transport in a chlorine atmosphere, which results at 700°C in precipitation of euhedral crystals:



The disproportionation reactions also present a kind of gas-transport reactions, where an element with

variable valence can be transported as a gas compound with a lower oxidation state of this element:



The temperature of gas transport is commonly lower than the crystallization temperature of the same compound from melt and the only significant temperature gradient between the zone of initial reaction and zone of precipitation is important.

Some evidence of an early high-temperature process can be observed in assemblages of PGE minerals, native metals, and some sulfides in the Sukhoi Log. The gas-transport mechanism can satisfactorily explain the formation of native metals in the earlier stage. Thus, the high-temperature assemblages were preserved in an outer zone, which was least altered by the later processes. Organic matter appears to support the gold and PGE reduction from chloride complexes and simultaneously was altered at a superimposed high-temperature process.

Searching criteria for the Sukhoi Log-type ore mineralization

The Sukhoi Log has many comparable structural and mineralogical features to other giant orogenic deposits. The following exploration criteria for large and super-large deposits of this type were formulated for the Bodaibo synclinorium and are based on general geologic and structural features of the territory and composition of host black shale sequences.

1. Quartz-vein ore mineralization does not form individual large deposits. Large gold reserves in the region are related only with gold-sulfide-type mineralization. However, the shallow quartz-vein (with Au) mineralization is indicative of deeper seated gold-sulfide ore bodies.
2. The main ore-controlling structures are third-order anticlines with the most promising zones at bends of axial surfaces, flexures, hanging thrust zones, and low-angle cleavage zones.
3. Favorable host rocks are fine-grained shale with elevated diagenetic sulfidization, which were metamorphosed under greenschist-facies conditions beyond the contact aureoles of granitoid intrusions.
4. Negative gravity anomalies, which indicate the occurrence of buried granitoid bodies at depths of about 2–3 km.
5. Geochemical anomalies of base metals (Cu, Pb,

Zn) are more informative than the anomalies of iron-group elements (Ni, Co, Cr). The latter often associate with a nonproductive diagenetic sulfide assemblage.

ACKNOWLEDGEMENTS

The research was realized through funding from Russian Academy of Sciences, Russian Foundation of Basic Research (grants 98-05-64775, 00-05-64378, 04-05-64946), Ministry of Natural Resources, Ministry of Industry and Science of Russia as well as the Lenzoloto Company. The authors particularly thank J.E. Mungall, J. Hanley and anonymous reviewer for their constructive comments that resulted in significant improvement of the manuscript.

REFERENCES

- ALAKSHIN, A.M. & PISMENNYI, B.M. (1988): About earth crust structure in the jointed zone between Sibir platform and surrounded folded belts. *Geol. Geof.* **11**, 24-31 (in Russ.).
- BULGATOV, A. N. & GORDIENKO, I. V. (1999): Terrains of the Baikal Mountain Range and the Location of Gold Deposits. *Geol. Ore Deposits* **41**, 204-213 (in Russ.).
- BURYAK, V.A. & KHMELEVSKAYA, N.M. (1997): *Sukhoi Log – one of the giant gold deposits in the world*. Dalnauka, Vladivostok (in Russ.).
- CABRI, L.J., CAMPBELL, J.L., LAFLOMME, J.H.G., LEIGH, R.G., MAXWELL, J.A. & SCOTT, J.D. (1985): Proton-microprobe analysis of trace elements in sulfides from massive sulfide deposits. *Can. Mineral.* **23**: 133-148.
- COVENEY, R.M., & NANSHENG, C. (1991): Ni–Mo–PGE–Au-rich ores in Chinese black shales and speculations on possible analogues in the United States. *Mineral. Dep.* **26**, 83-88.
- COVENEY, R.M., JR., MUROWCHICK, J.B., GRAUCH, R.I., GLASCOCK, M.D. & DENISON, J.R. (1992): Gold and platinum in shales with evidence against extraterrestrial sources of metals. *Chem. Geol.* **99**: 101-114.
- DISTLER, V. V., MITROFANOV, G. L., NEMEROV, V. K., KOVALENKER, V. A., MOKHOV, A. V., SEMEYKINA, L. K. & YUDOVSKAYA, M. A. (1996): Mode of occurrences of platinum group metals and their origin in the Sukhoi Log gold deposit (Russia). *Geol. Ore Deposits* **38**, 467-484

- (in Russ.).
- DISTLER, V.V., SLUZHENIKIN, S.F., CABRI, L.J., KRIVOLUTSKAYA, N.A., TUROVTSEV, D.M., GOLOVANOVA, T.A., MOKHOV, A.V., KNAUF, V.V. & OLESHKEVICH, O.I. (1999): Platinum ores of the Noril'sk Layered intrusions: magmatic and fluid concentration of noble metals. *Geol. Ore Deposits* **41**, 214-237 (in Russ.).
- DISTLER, V.V., YUDOVSKAYA, M.A., RAZVOZJAEVA, E.A., MOKHOV, A.V., TRUBKIN, N.V., MITROFANOV, G.L. & NEMEROV, V. K. (2003): New data on platinum mineralization of gold ore of the Sukhoi Log deposit (Lena gold bearing district, Russia). *Dokl. Earth Sciences* **393**, 524-527.
- DISTLER, V.V., YUDOVSKAYA, M.A., MITROFANOV, G.L., PROKOF'EV, V.YU. & LISHNEVSKII, E.N. (2004): Geology, composition, and genesis of the Sukhoi Log noble metals deposit, Russia. *Ore Geol. Rev.* **24/1-2**, 7-44.
- ERMOLAEV, N.P., SOZINOV, N.A., KOTINA, R.P., PASHKOVA, E.A. & GORYACHKIN, Y.I. (1999): *The mechanism of noble metal concentration in the terrigenous -carbonaceous rocks*. Nauchny Mir, Moscow (in Russ.).
- FAURE G. (1986): *Principles of Isotope Geology*. 2d ed. John Wiley & Sons.
- GIVARGIZOV, E.I. (1977): *Growth of Crystal Whiskers and Lamellas from Vapor*. Nauka, Moscow (in Russ.).
- GIZE A.P. (1999): A special issue on organic matter and ore deposits: Interactions, applications, and case studies (Introduction). *Econ. Geol.* **94**, 963-966.
- GRADSTEIN, F.M., OGG, J.G., SMITH, A.G., BLEEKER, W. & LOURENS L. (2004): A new geologic time scale with special reference to Precambrian and Neogene. *Episodes* **27**, 83-100.
- IVANOV, A.I., LIFSHITS, V.I., PEREVALO, V.O., STRAKHOVA, T.M., YABLONOVSKY, B.V., GRAIZER, M.I., ILINSKAYA, K.G. & GOLOVENOK V.K. (1995): *Precambrian of the Patom Highland*. Nedra, Moscow (in Russ.).
- JUVONEN, M.-R., LAKOMAA, T.M. & KALLIO E.I. (2000): The nickel sulfide fire assay procedure for different types of rocks in the determination of gold and the platinum group elements by inductively coupled plasma-mass spectrometry. *Abs. 31st International Geological Congress*. Rio de Janeiro, Brasil.
- KAZAKEVICH, Y.P., SHER, S.D., ZHADNOVA, T.P., STOROZHENKO, A.A., KONDRATENKO, A.K., NIKOLAIEVA, L.A. & AMINEV V.B. (1971): *Lensky gold-bearing region*. v.1-2. Nedra, Moscow (in Russ.).
- KUCHA, H. (1982): Platinum Group metals in the Zechstein copper deposits, Poland. *Econ. Geol.* **77**, 1578-1591.
- LAVEROV, N. P., PROKOF'EV, V. YU., DISTLER, V. V., YUDOVSKAYA, M. A., SPIRIDONOV, A. M., Grebenshchikova, V. I. & Matel N. L. (2000a): New data on conditions of ore deposition and composition of ore-forming fluids in the Sukhoi Log gold-platinum deposit. *Dokl. Earth Sciences*, **371**, 357-361.
- LAVEROV, N.P., CHERNYSHOV, I.V., DISTLER, V.V., BAIROVA, E.D., GOLZMAN, YU.V., GOLUBEV, V.N., CHUGAEV, A.V. & YUDOVSKAYA, M.A. (2000b): Geochronology and possible sources of ore matter of the Sukhoi Log deposit: results of isotope study. *In Isotope dating of geological processes: new methods and results*. Geos, Moscow (211-214 in Russ.).
- LISHNEVSKII, E.N. & DISTLER, V.V. (2004): Deep-seated structure of earth's crust in the region of gold-platinum Sukhoi Log deposit by geologic-geophysic data (Eastern Siberia, Russia). *Geol. Ore Deposits* **46**:88-104.
- MITROFANOV, G.L., NEMEROV, V.K., KOROBENIKOV, N.K. & SEMEIKINA, L.K. (1994): Platinum-bearing potential of Precambrian carbonaceous sequences of the Baikal-Patom Highland. *In Platina Rossii*. Geoinformmark, Moscow. (150-154 in Russ.).
- PAŠAVA, J. (1993): Anoxic sediments – an important environment for PGE; An overview. *Ore Geol. Rev.* **8**, 425-445.
- PIESTRZYNSKI, A. & SAWLOWICZ Z. (1999): Exploration for Au and PGE in the Polish Zechstein copper deposits (Kupferschiefer). *J. Geoch. Explor.* **66**, 17-25.
- RAZVOZJAEVA, E. A., PROKOF'EV, V. YU., SPIRIDONOV, A. M., MARTIKHAEV, D. KH. & PROKOPCHUK, S. I. (2002). Precious metals and carbonaceous substance in ores of the Sukhoi Log deposit (Eastern Siberia, Russia). *Geol. Ore*

- Deposits* **44**, 2: 103-111(in Russ.).
- RUNDQIST, I.K., BOBROV, V.A., SMIRNOVA, T.N., CMIRNOV, M.Y., DANILOVA, M.Y. & ASCHEULOV, A.A. (1992): The stages of the Bodaibo gold region development. *Geol. Ore Deposits* **34**, 3-15 (in Russ.).
- SAVITSKY, A.V., PETROV, YU.V. & SHUSTOV B.N. (1998): Types and structural position of PGE-bearing ores in the rift-related black shales formations of Karelia. *In* International Platinum (N.P.Laverov & V.V.Distler, eds). Theophrastus publications. 194-198.
- SCHAFFER, H. (1961): *Chemische Transportreaktionen*. Verlag Chemie GmbH, Weinheim.
- TAYLOR, H.P. & MCLENNAN, S.M. (1985): *The continental crust: Its composition and evolution*. Blackwell, Oxford.
- VARSHAL, G.M., VELYUKHANOVA, T.K., KOSHCHEEVA, I.Y., BARANOVA, N.N. & KOSERENKO S.V. (1994): Concentration of noble metals by carbonaceous matter. *Geokhimiya* **6**, 814-823 (in Russ.).
- VIKULOVA, P.P., SEROVA, N.L. & NOVIKOVA, A.N. (1977): The combination of methods to study pyrite from the gold deposit in the Eastern Siberia. *In* New methods of analysis. Vostsibniigims, Irkutsk (46-54 in Russ.).
- VYSOTSKII, N.K. (1933): *Platinum and the regions of its mining*. Izdatelstvo Akademii nauk SSSR, Leningrad (in Russ.).
- WILDE, A., EDWARDS, A. & YAKUBCHUK, A. (2003): Unconventional deposits of Pt and Pd: a review with implications for exploration. *SEG Newsletter*, **52**: 10-18.
- WOOD, S.A. (2002): The aqueous geochemistry of the platinum group elements with applications to ore deposits. *In* The geology, geochemistry, mineralogy and mineral beneficiation of PGE. CIM, Motreal.
- YUDOVICH, YA.E. & KETRIS, M.P. (1994): *The admixture elements in black shales*. Nauka, Ekaterinburg (in Russ.).

CHAPTER 22: Ni–Cu–Cr–PGE MINERALIZATION TYPES: DISTRIBUTION AND CLASSIFICATION

O. R. Eckstrand
115 James Cummings Avenue
Ottawa, ON K2H 9B9, Canada
Email: reckstrand@sympatico.ca

INTRODUCTION

Platinum-group elements (PGEs) are recovered from a wide range of mineral deposit types worldwide and are generally associated with Ni and/or Cu. Most PGE deposits have a primarily magmatic origin, and occur in magmatic rocks of mafic-ultramafic composition. Others may be broadly classified as sedimentary, hydrothermal, or laterite. Sedimentary deposits are either sulfidic deposits hosted by black shale which contain recoverable PGE, or placer deposits derived from mafic-ultramafic magmatic sources. Hydrothermal Ni–Cu–PGE deposits include a variety of depositional environments in which transported metals have been deposited in vein-like or replacement mode. Some hydrothermal deposits show a clear relationship to a mafic/ultramafic parent body, but in others the relationship is not obvious. Ni–Co laterite deposits occur in the deeply weathered profiles developed on olivine-rich peridotites, in tropical or semi-tropical humid climates, and some of these deposits contain minor amounts of PGEs.

The associated table and accompanying explanations present a tentative classification of Ni–Cu–PGE deposits and indicate in which of these the PGE are the principal economic commodities or contribute significantly to the economic viability of the deposits. See also the expanded table and poster on the CD accompanying this volume.

A MAGMATIC DEPOSITS

Magmatic deposits of Ni, Cu and PGE metals occur in mafic and/or ultramafic magmatic bodies, and result from magmatic processes of crystallization, differentiation, and concentration. The Ni, Cu and PGE in these deposits are associated with widely ranging amounts of sulfides which typically include pyrrhotite, pentlandite and chalcopyrite. At the magmatic stage the sulfide existed as a separate immiscible liquid in the form of disseminated droplets which became concen-

trated to varying degrees within the silicate magma. In the resulting ores, Ni, Cu, Pt and Pd are the main economic commodities at current metal prices, and Au, Rh and Co are common by-products.

Magmatic Ni–Cu–PGE deposits tend to fall into one of two groups. Sulfide-rich deposits are Ni and Cu rich and contain only by-product amounts of PGE. These Ni–Cu deposits appear to owe much of their abundant sulfur content to contamination by sulfide-bearing crustal wallrocks.

In the second group, sulfide-poor deposits, the PGE content generally has greater economic value than the Ni and Cu content, and this group is known as PGE deposits. The low sulfur content appears to be a primary magmatic constituent, not due to crustal contamination.

A1 Basal Sulfide Concentrations

These magmatic Ni–Cu deposits consist of sulfide-rich concentrations that occur in the basal portions of the associated mafic/ultramafic bodies. The basal position of these deposits resulted during flow of the hosting silicate magma by settling of the immiscible liquid sulfide due to its greater relative density. Significant portions of the deposits commonly comprise greater than 25% sulfide. The economic value of these deposits is dominated by Ni and to a lesser but variable degree by Cu. Pt and Pd are generally by-products, but their value in some cases approaches that of the base metals.

A1a Sills/chonoliths

These basal Ni–Cu sulfide concentrations occur in mafic/ultramafic sill-like or irregular intrusions, and commonly occupy depressions or embayments in the basal portion of those magmatic bodies. Some of these deposits consist in significant part of massive sulfide. Examples include Noril'sk, Voisey's Bay.

A1b Impact melt

Ni–Cu–PGE sulfide ores in the Sudbury Igneous Complex are the unique examples of this type of

magmatic sulfide deposit. They occur at the base and in the footwall of the mafic melt sheet and in related radiating and concentric dykes ("offsets"), all of which resulted from a meteorite impact.

A1c Komatiites

Basal Ni–Cu–PGE sulfide concentrations of this type occur in extrusive komatiitic flow units generally as matrix and/or massive sulfides. These sulfides commonly occupy depressions at the bases of the flow units, and mainly in the lowermost flow units of the komatiitic flow sequence. As well there may be internal conformable lenses of disseminated sulfide (see A3, Internal zones of sulfide dissemination). The most prominent examples include deposits in the Kambalda camp.

A2 Reefs

PGE Reefs are Ni–Cu–PGE deposits that occur as sparsely disseminated sulfide concentrations, generally less than 5% and which form relatively thin pseudo-conformable, laterally continuous zones within mafic/ultramafic layered intrusions. The low abundance of sulfide probably reflects the original low S content of the magma, which barely achieved saturation. Pyrrhotite, pentlandite and chalcopyrite make up most of the sulfides. Pt and Pd predominate over Cu and Ni in economic value.

A2a Sulfide Reefs

These deposits occur as relatively thin pseudo-conformable zones of sparsely disseminated sulfides in silicate layers of the hosting mafic/ultramafic layered intrusions. Two types of sulfide reef are recognized, the "unzoned sulfide reef" and "zoned sulfide reef".

The "unzoned sulfide reef" is characterized by coextensive concentrations of Pt, Pd, Cu and Ni, all within the one reef unit. Sulfide saturation is believed to have been achieved through magma mixing. Both the Merensky Reef of the Bushveld Complex and the J-M Reef of the Stillwater Complex are of this type, and are situated somewhat above the ultramafic lower zone in both layered intrusions.

The "zoned sulfide reef" is composite, and comprises overlapping or even separate reef-like concentrations of the several metal constituents. The stratigraphically lowermost metal concentration is Pt, either coinciding with or followed upward by Pd, and subsequently Au, all accompanied by very low sulfide abundance. Immediately above these

concentrations, a significant increase in Cu and S forms a separate reef containing a few percent of mainly Cu sulfide. Sulfide saturation probably occurred through progressive fractional crystallization. In some intrusions, these zoned cycles are repeated. Examples include the Great Dyke, Skaergaard and Munni Munni.

A2b Chromitite Reefs

Chromitite reefs comprise near-massive chromite layers in mafic/ultramafic layered intrusions, and are a major source of chromite. As well, some chromitite reefs contain PGE that are associated with very sparsely disseminated sulfides. Economic chromitite reefs of both types are found mainly in the ultramafic, lower portions of layered intrusions, and are believed to originate through magma mixing. The most important chromitite example of a chromite source is the Kemi intrusion in Finland, and that of a PGE source is the UG-2 chromitite in the Bushveld Complex.

A2c Magnetitite Reefs

Conformable zones containing PGE are found in magnetitite layers that occur in the more evolved upper parts of mafic/ultramafic layered intrusions and, like the other reef-type deposits, are associated with sparsely disseminated sulfides. Sulfide saturation likely occurred through progressive fractional crystallization. An example is the Panzihua magnetitite in China.

A3 Internal Zones of Sulfide Dissemination

These magmatic Ni–Cu–PGE deposits comprise zones of disseminated sulfides, usually lens-shaped and conformable, within mafic/ultramafic bodies which may be either intrusive units or volcanic flows. The proportion of Ni–Cu sulfides relative to pyrrhotite, and the Cu/Ni ratio are both generally greater than in the basal sulfide type of Ni–Cu–PGE deposits. At least some of these deposits owe part of their sulfur to contamination from sulfidic wallrocks. Examples include many of the Noril'sk deposits which are hosted in gabbro-norite sills, and Mt. Keith which is an ultramafic sill.

A4 Magmatic Breccia

Broad zones of PGE mineralization occur in mafic magmatic breccias, and are associated with sparsely disseminated Ni–Cu sulfides in both matrix and clasts. These mineralized magmatic breccias are found in basal or near basal stratiform units of mafic

layered intrusions (Platreef, River Valley), or in certain facies of stock-like mafic intrusions (Lac des Iles).

A5 Stock-like Intrusions

Some stock-like mafic/ultramafic intrusions contain Ni–Cu sulfide-rich lenses and bands. Examples are Lynn Lake, Manitoba and Akarem, Egypt. Some zoned Alaskan intrusions contain PGE associated with sparsely disseminated sulfides.

A6 Sulfides in Ophiolites

Minor amounts of sulfides, generally disseminated, form small zones in both harzburgitic and gabbroic units of ophiolite suites. The Ni–Cu–Fe sulfides have associated PGE.

A7 Tectonically Remobilized Sulfides

Tectonically remobilized sulfides represent intensely deformed originally magmatic Ni–Cu sulfide rich deposits. These ores have been deformed in a ductile fashion (folded, thinned, thickened, dispersed), and their relation with the original magmatic hosts has been obscured. Examples include the Thompson deposits in Manitoba and the Selebi-Phikwe deposits in Botswana.

A8 Podiform Chromite

Podiform chromite deposits consist of pod-like, rod-like, or irregularly shaped massive chromitite bodies. Some of these chromite deposits contain trace amounts of sulfide and associated PGE. They are found principally within dunitic portions of ophiolite complexes. Examples are found in Philippines and New Caledonia.

A9 Chromite-arsenide

Magmatic-textured Ni arsenides and associated PGE occur in chromitite bands in upper mantle lherzolitic intrusions in areas of the western Mediterranean (Ronda, Spain and Beni Bousera, Morocco).

B SEDIMENTARY DEPOSITS

Sedimentary deposits of Ni, Cu and PGE are of two distinct types; placer concentrations, and sulfidic black shales.

B1 Placer deposits

Placer deposits of Pt result primarily from the mechanical weathering of ultramafic rocks and deposition of the clastic Pt-bearing grains either in residual detritus or in down-drainage alluvial

gravels. The most common sources are zoned Alaskan type of mafic/ultramafic intrusions. Examples include placer Pt deposits in the Urals and northwestern Colombia.

B2 Black Shale

Some black shales contain marine sedimentary exhalative sulfides that carry Ni and traces of PGE along with other metals in thin sulfidic strata rich in organic matter. An example is the Zunyi mine in the Niutitang Formation in southern China.

C HYDROTHERMAL DEPOSITS

Hydrothermal Ni–Cu–PGE deposits include a variety of depositional environments in which transported metals have been deposited in vein-like or replacement mode. Some deposits show a clear relationship to a mafic/ultramafic parent body, but in others the relationship is not obvious.

C1 Polymetallic Veins

Polymetallic veins containing PGE typically include other metals in quartz-carbonate gangue, in some cases spatially associated with a likely mafic/ultramafic source rock. Examples include the Boss Mine, Nicholson Bay and Waterberg.

C2 Hydrothermally Remobilized Sulfide

These Ni–Cu–PGE deposits generally comprise irregular vein-like masses, stringers and disseminations in deformed host rocks that commonly include the likely parent mafic/ultramafic bodies. The New Rambler deposit is an example. Many of the magmatic deposits show some development of hydrothermally remobilized Ni–Cu–PGE mineralization.

C3 Unconformity U–Au–PGE

Some “unconformity uranium” deposits also contain PGE and Au in zones below the unconformably overlying basinal sandstone. This mineralization and accompanying alteration apparently resulted from downward migration of oxidized acidic basin brines into neutralizing footwall rocks. The prime example is the Coronation Hill deposit.

C4 Clastic sediment-hosted

Thick sequences of clastic sedimentary rocks contain widely dispersed sulfide- and quartz-vein-associated Au–Pd–Pt mineralization accompanied by broad alteration. Examples include Serra Pelada,

Muruntau and Sukhoi Log.

C5 Iron formation

Au–Pd mineralization is associated with quartz and hematite veins and their alteration halos in hematite-rich sheared Lake Superior type iron formation in the Itabira district, Brazil.

C6 Cu Porphyry

Some Cu porphyry deposits of the alkalic type and mainly of island arc affinity contain appreciable Pd associated with high Au contents. Examples include Ingerbelle and the Robinson district.

C7 Kupferschiefer

The Kupferschiefer deposits of Poland have associated Pt–Pd–Ag–Au mineralization that lies distinctly below the Cu zone, and essentially at the transgressive redox front. The metals were transported by oxidizing waters in sandstone, and deposited on contact with the overlying black shale.

D LATERITE

Ni–Co laterite deposits occur in the deeply weathered profiles developed on olivine-rich peridotites, in tropical or semi-tropical humid climates. Ni may be concentrated in limonite or oxide in the upper part of the laterite profile, in nontronite or clay minerals in the intermediate part of the profile, or as garnierite or hydrous Mg–Ni silicate in the saprolitic or lowest part of the laterite profile. The latter type has the highest Ni grades, and results from the most humid climates. Examples include the ophiolite-based deposits in New Caledonia, Indonesia and Cuba. Some PGE content is known in a few cases.

NI-CU-CR-PGE MINERALIZATION TYPES

TABLE 22-1. CLASSIFICATION OF DEPOSIT TYPES

CLAN	DEPOSIT TYPE	MAIN ECONOMIC METALS	SUPPLY SIGNIFICANCE (Ni-Cu-Cr-PGE)	EXAMPLES (Camps, Deposits)		
A MAGMATIC	A1 Basal sulfide concentration	A1a Sill/Chonolith	Ni, Cu, Co, PGE, Au	Major producer of Ni, Cu; No.1 source of Pd (Noril'sk)	Noril'sk, Voisey's Bay	
		A1b Impact melt	Ni, Cu, Co, PGE, Au	Major producer of Ni, Cu; significant for PGE, Co	Sudbury	
		A1c Komatiite	Ni, Cu, Co, PGE, Au	Significant Ni producers, by-product Cu, Co, PGE, Au	Kambalda, Ungava, Pechenga	
		A2 Reef*	A2a Sulfide reef	PGE, Au, Ni, Cu	No.1 source of Pt (Pd), by-product Au, Ni, Cu (Merensky)	Merensky Reef, J-M Reef, Great Dyke
			A2b Chromitite reef	PGE, Cr, Au, Ni, Cu	Major producer of PGE, Cr	UG-2 (Pt, Pd), Kemi (Cr)
			A2c Magnetitite reef	V, PGE	Little or none	Panzihua, Stella
		A3 Internal zone of sulfide dissemination	Ni, Cu, Co, PGE, Au	Major Ni-Cu-PGE producer (Noril'sk)	Noril'sk, Mt. Keith, Duluth Complex	
		A4 Magmatic breccia	PGE, Ni, Cu	Significant PGE producers	Platreef, Lac des Iles	
		A5 Sulfides in stock-like intrusion	Ni, Cu, Co, PGE	Significant Ni-Cu-PGE producer	Lynn Lake, Kotalahti, Giant Mascot, Nizhni Tagil	
		A6 Sulfides in ophiolite	Ni, Cu, PGE	Minor production	Acoje, Faeoy	
		A7 Sulfide, tectonically remobilized	Ni, Cu	Significant Ni producer, by-product Cu, PGE (Thompson)	Thompson, Selebi-Phikwe, Ferguson Lake	
	A8 Podiform chromitite	Cr	Major source of Cr	Philippines, New Caledonia		
	A9 Chromite arsenide	Ni, PGE	None	Ronda, Beni-Bousera		
B SEDIMENTARY	Placer	PGE, Au	Major past source of Pt, current producers	Ural Mtns, Colombia Goodnews Bay		

CLAN	DEPOSIT TYPE	MAIN ECONOMIC METALS	SUPPLY SIGNIFICANCE (Ni-Cu-Cr-PGE)	EXAMPLES (Camps, Deposits)
C HYDRO- THERMAL	C1 Polymetallic veins	PGE (Ni, Zn, Co, Ag, Bi)	Minor production (Waterberg)	Boss mine, Nicholson Bay Waterberg
	C2 Hydrothermally remobilized	Ni, Cu, PGE	Minor production	New Rambler (Wyoming)
	C3 Unconformity U-Au-PGE	U, Au, PGE	No PGE production reported to date	Coronation Hill (Australia)
	C4 Clastic sediment-hosted	Au, PGE	Au: Pd is a common byproduct	Serra Pelada, Muruntau, Udokan
	C5 Iron formation	Au, Pd	Minor production	Cauê, Conceição mines (Brazil)
	C6 Cu-Porphyry	Cu, Pd	Minor byproduct Pd	Ingerbell. Robinson district (Nevada)
	C7 Kupferschiefer	Cu, Ag, Pb, Zn, Au, PGE	Minor Au, PGE production	Lubin (Poland)
D LATERITE	Laterite	Ni, Co	Major ; largest reserves of Ni in the world	Yubdo (Ethiopia)

Bold-face font indicates classes, camps and deposits in which PGE production contributes significantly to their economic viability.

NI-CU-CR-PGE MINERALIZATION TYPES

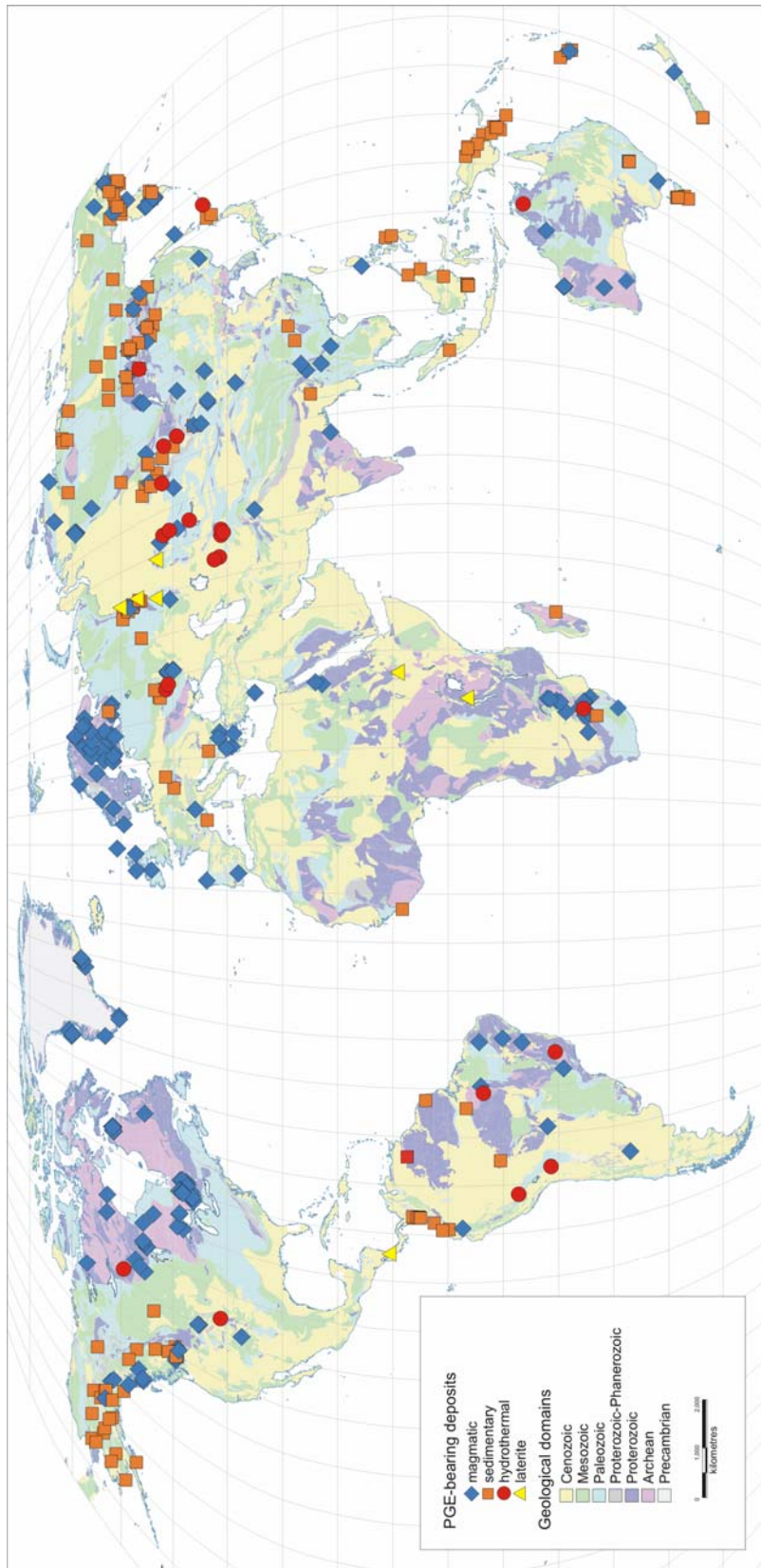


FIG. 22-1. World distribution of deposit types.

INDEX

- Afton deposit 24, 203, 209, 223, **243**
- Agnew intrusion 92
- Aguablanca deposit 254, 309
- Ahmavaara deposit **76**, 82, 288
- Ajax deposits 203, 209, **243**
- Aldan shield **116**, 134, 245
- alkaline magma **5**, **21**, 86, 184, 192,
203-246, 255, 266, 309, 433
- Allard stock deposit 204, 209
- Alligator River deposit 252
- alloy solubility 8, 12
- Alpine-type complex **113**, 136, 288
- Alto Condato placer 118
- Altynburiylkol 148
- Alumbrera deposit 203, **241**
- Alyuchin Horst intrusion 118, 120
- Amantaytau 148
- Apuseni Mt deposit 221
- aqueous PGE solubility 8, 20, **35-56**,
145, 158, 176, **206-211**, 264, **268-291**
- arc magma 4, 6, **20-24**, **203-246**
- Assarel deposit 203, 207, **238**
- assimilation **7**, **13-17**, **181-198**,
218, 242, **309-331**
- Atok/Lebowa mine 62
- Baimazhai deposit 261
- Baker zone 293, 371, **387**
- Bastard unit 59, 62, 70, 314
- Biga deposit 203, 214
- Bingham Canyon deposit 203, **242**
- biogeochemistry 38, 76, **294**
- bisulfide complexes 38, **42-51**, 157, 206, 211, 264
- black shale-hosted 146, **148-155**, 252,
262-265, 309, **457-485**, 489
- boninite **4**, **22-26**, **196**, 257, 266
- Bor deposit 203, 207, **239**
- Boss Mountain deposit 203
- Broken Hammer zone 278
- Bushveld complex 7, 22, 50, **57-73**, **75-96**, 97,
195-198, 249, 255, 282, 288, 291, **309-341**, 488,
- C isotopes 481
- Cadia deposit 203, 208, **246**
- calcalkaline magma 203, 217, 240
- carbonaceous rocks **146-157**,
262-269, 318, **460-482**
- chalcophile element depletion 14, 23
- Chelopech deposit 216, 223, **237**
- chloride complexes **35-56**, 148, 156,
206-211, 216, 221, **264**, 268-290, 475, 483
- chonolith **254**, 260, 487
- Cl in apatite 46, 68, 259
- Coldwell complex 253, 297, 331
- Coleman mine 165
- conduit **7**, 17, 24, 68, **181-201**,
256, 310, 319, 323, 327
- contact (basal) type deposits 75, **75-96**, 253
- contact (Sudbury sublayer) deposits **163-180**,
359-368
- contamination **22-25**, 78, 88, **181-198**,
242, 259, 267, **309-331**, 432, 487
- Copper King deposit 204, 209
- Copper Mountain deposit 203, **241**
- Coronation Hill deposit 145, **153**, 489, 492
- Cripple Creek deposit 203, **242**
- Crocodile River/Barplats mine 62
- Crystal Lake deposit 262, 331
- Cu/Pd ratio **14**, 70, **310**, 320
- Cu/Zr ratio 311, 320
- deuteric fluid 20, 46, 310, 385
- differential GPS 275
- Drenthe deposit 82
- Duluth complex 249, 266, 296, 318, 331, 491
- dunite pipes 46, 50, 258
- Durance River placer 118
- Dzhezkazgan 154
- Eagle deposit 262
- East Boulder mine 64, 391, 394
- East Bull Lake deposit 75, **90**, 260, 266, 331
- Eastern Platinum mine 62
- Elatsite deposit 203, 207, 215, **237**
- electromagnetic (EM) survey 76, 259, 265, 270,
276-284, 354, 362, 369, 391, 394
- epithermal deposits 24, 203-245, 269
- Erdenetuin-Obo deposit 208, **245**
- Expo Ungava deposit 15, 281
- Fedorov-Pana complex **343-358**
- Ferguson Lake deposit **290**
- Ferguson reef **66**, 68, 70, 290-296, 491
- Fifield placer 118, 121, 129, 252
- Fox River intrusion 57, 331
- Fraser-Strathcona mine 52, 165, 364
- Freetown Layered complex 252, 288
- Frood mine 163, 165
- Gal'moenan intrusion **116**, 122, 137
- Galore Creek deposit 203, 209, **243**
- Giant Mascot deposit 22, 491
- Goodnews Bay placer 116, 120, 288, 491
- Goonumbla deposit 205, 208, 244
- grade control 163, 252, **422-427**
- Grasberg deposit 203, 208, **240**
- gravity survey 187, 257, 270, **275**, 344, 482

Great Dyke	17, 25, 65, 97 , 288,	Lower Talnakh intrusions	16, 57, 187, 198, 329
Guli massif	114	low-sulfide deposits (Sudbury)	163-180, 359-368
Haran reef	252	Luanga deposit	251, 256
Hartley mine	66, 97 , 106, 289, 409-429	MacLennan mine	361
heavy mineral concentrates	76, 98, 104, 113, 269, 289, 468, 470	Madjanpek deposit	211
humus chemistry	38, 293 , 303, 375	magmatic unconformity	25, 63, 65
Hunan/Guizhou Province deposits	146, 457	magnetic survey	76, 187, 257, 259, 270, 276-284 , 344, 352-355, 361, 369, 394, 440
hydrogen isotope	48, 221, 241	magnetotelluric survey	361, 375
hydrothermal fluids	20, 24, 35-56 , 69, 88, 119, 138, 145-161, 203-246 , 251, 253-264, 268, 278, 301, 316, 436, 457-485	Main Sulfide zone (Great Dyke)	57, 65 , 70, 97-111 , 253, 289, 409-429
Igarka	154	Mamut deposit	203, 208, 214, 241
Inagli placer	114, 123, 128, 134	mantle plume	5, 20-24 , 253, 268 , 316, 357, 432
induced polarization (IP) survey	76, 259, 275-277 , 354-356, 373, 391, 394	Marathon deposit	250, 253, 255
iron formation-hosted deposits	45, 155, 264, 490	McCreeley East mine	364
iron oxide Cu-Au deposits	149	McCreeley West mine	163-180 , 364, 278
Jabiluka deposit	145, 153	McVittie-Graham mine	361
Jacutinga deposit	155 , 309	Mecca Quarry deposit	262
Jinbaoschan intrusion	309	Medet deposit	203, 207, 238
Jinchuan deposit	197, 256, 323	meimechite	114, 194
J-M reef	17, 25, 47, 64	Merensky reef	17, 25, 45, 57-73 , 87, 101, 250, 255, 258, 284, 288, 291, 311-317, 394, 409, 488
Joubdo placer	118	Messina deposit	251
Kabanga deposit	256, 325,	Mimosa mine	66, 97, 109, 410
Kalplats deposit	250	Minas Gerais	299
Kambalda deposits	17, 256, 281 , 298, 319, 488	Mochila deposit	309
Kapalagulu deposit	309, 319, 328	Mokopane deposit	82, 86
Katinniq deposit	253, 255	Monchegorsk intrusion	309, 357
Kharaelakh intrusion	187	monosulfide solid solution (mss)	2, 9, 17-21 , 81, 131-135, 209
Kirli deposit	148	Montcalm deposit	22, 331
Koillismaa complex	75, 84	MORB	3-6 , 13, 20, 257, 266, 318, 432
komatiite	4-6 , 15, 22 , 181, 257, 266, 282, 309, 321-326 , 330, 488	Mordor intrusion	309
Konder (Kondyor) River placer	117 , 252, 288	Mt Carnagen deposit	299
Konttijaarvi deposit	75 , 85, 255, 266	Mt Keith deposit	256, 300, 322, 330, 488
Koryak belt	116, 288	Mt Milligan deposit	203, 209, 243
Kumtor	148	Mt Polley deposit	203, 209, 243
Kupferschiefer deposit	45, 145, 154 , 251, 262, 457, 490	Munni Munni intrusion	17, 25, 66 , 70, 250, 255, 311, 405, 449, 488
Kvartsitovye Gorki deposit	148	Muruntau deposit	145, 150, 457, 489
Lac Des Iles complex	17, 41, 84, 249, 258, 283, 287-302, 369-390 , 489	Muskox intrusion	57, 253, 257, 326, 331
Lac Long	296	Narkaus intrusion	57, 75 , 85
Lac Sheen	296	Natalka deposit	145, 150, 262
Ladolam deposit	223, 239, 241	Nd-isotope	190-193, 314-318, 329 , 436
laterite/lateritic	38, 157, 252, 289, 298-303 , 487, 490	New Caledonia	145, 156, 301, 490
Lena gold district	457	New Rambler deposit	39, 251, 289, 489
Lennon Shoot	288	Nezdaninskoye deposit	145, 150
Levack	166, 279	Ngezi mine	66, 97-109, 410
Lindsley mine	18, 364	Nicholson Bay deposit	252, 489
listwaenite-hosted	146, 155, 210	Nick deposit	145, 152 , 251, 265, 265, 457
		Nickel Rim deposit	359-368
		Nizhny Tagil massif	116-120 , 491
		Nonnenwerth deposit	82

Norilsk-Talnakh deposits 7, 16, 23, 57, 117,
 181-198, 247-274, 277, 281, 319,
 323, 330, 372, 487
 Norman deposit 278
 offset reef 25, **68, 98**, 476
 Ok Tedi deposit 203, 208, **240**
 ophiolite (Alpine type complexes) 8, **113-143**,
 146, 155, 210, 252, 257, 290, 301, 489
 Ora Banda intrusion 299
 organic complexes 38, **51-56**, 241, 268, **290**,
 302, 466
 orogenic gold deposits **145-150**, 157, **457-485**
 Os isotopes 196, **316, 330**
 oxygen fugacity 8, **11**, 24, 29, **35**, 50, 55, 120,
 157, 211
 oxygen isotope 89, 196, 314, **318, 331**
 Oyu Tolgoi deposit 203, **245**
 Padma deposit 148, 262, 457
 Pana Tundra deposit 251-253
 Panguna deposit 203, 208
 panning **291**
 Panton sill 67, 250, 255, 309, 312
 partition coefficients **1-34**, 92, 221, 311, 319,
 322, 427
 Pavlik deposit 145, 148
 Pb isotopes 240, **316-318**
 Pechenga deposit 17, 288,
 Penikat intrusion 57, 70, 75, 84, 250-259
 PGE demand **247-249**, 287, **289**, 431
 PGE price 172, **247-249**, 265, 269, 287,
 289, 319, 371, 441, 448, 487
 PGE supply 1, **247-249**, 269, 287, **289**, 372, **491**
 Phalabora deposit 252, 266
 Picket Pin zone 50, 65, 258, 288, 394
 picrite **4-6**, 13, **22-24**, 114, **181-198**, 243,
 257, 260, 321, 330, 432, 434
 placers 24, **113-143**, 149, 252, 269, 288,
 448, 457, 489
 Platinova reef 66-69, 253-255, **431-455**
 Platreef deposit 57, 67, 82, **84-89**, 97, 250,
 253, 255, 258, 309, 313, 331, 354, 488, 491
 PM deposit **166-168**, 174
 Podolsky deposit **163-180**
 Polkovice-Sierszowice mine 154
 porphyry deposits 24, 38, 44, **203-245**,
 252, 266, 490
 Portimo complex **75-94**, 253, 255, 256
 Potgietersus Platinums deposit 58, 82
 pothole reef 46, **62**, 258
 Raglan deposit 17, 197, 250, 253, 255,
 281, 309, 320
 reef deposits 25, 47, **57-73**, **75-96**, 97, **252-260**,
 284, **310-318**, **343-358**, **391-407**, **409-429**,
 431-455, 488, 491
 River Valley deposit 75, **82-95**, 250, 253, 255, 488
 Riwaka deposit 309
 Roby zone 17, 253, 255, 288, 293, **369-390**
 rolling reef **62**
 Rottenstone deposit 252, 292, 295
 Rustenburg mine 58, **60**, 394
 Rytikangas reef 79, **85**, 94
 S isotopes 88, 90, 189, 192, 210,
 217, 261, 288, **317-318**, **330**
 Santo Tomas II deposit 203, 215, **239**
 Se/S ratio 80, **92-94**
 secondary PGM 97, **104-108**
 seismic survey 183, 187, 257, **277**, 282-284, 344
 seiving 98, **291**
 Selebi-Phikwe deposit 256, 319, 489
 selective leach **302**, 448
 Selous mine **410**
 Serra Pelada deposit 145, 149, 251, **262**, 309, 489
 sharp-walled vein deposits **163-180**, **359-368**
 Sheba's Ridge deposit 75, 82, **89**, 94
 Shetlands ophiolite 252, 290
 Shinkolobwe deposit 154, 252
 Siika-Kama reef 76, **79**, 94
 Skaergaard intrusion 17, 25, **66**, 253, 255,
 309, **431-455**, 488
 Skouries deposit 203, 207, 224, **235**, 252
 soil geochemistry 38, 76, 90, 266, **287-307**,
 355, 375, 391-407
 Sonju Lake intrusion 311, 432
 Sora deposit 203, 208, **244**
 Srednaya Padma deposit 148, 262, 264
 Sr-isotope 28, 60, 68, 89, 190, 197, 245,
 314-318, 328, 357, 464
 St Stephens deposit 22
 Stella intrusion 253, 255, 259, **309**, 315, 491
 Stillwater Complex 7, 22, 25, 45, **64**, 92, 224,
 250-255, 275, 282, 288, 296, 313-330,
 391-407, 488
 Stillwater mine 64, 394
 stream sediment 265, 270, **291**, 404, 431, 440, 457
 Sudbury igneous complex (SIC) 18, 39, 49,
 163-180, 250, 253, 255, 277,
 278, 288, **359-368**, 487
 Suhanko intrusion **75-96**, 255, 288, 301
 Sukhoi Log deposit **145-150**, 249, **262-265**,
 457-485, 489
 sulfide fractionation **18**, 367
 sulfide liquation (immiscibility) 10, **12-20**, 46,
 88, 89, 181, 256, 266, 310, 319, 360,
 440, 449, 487

sulfur solubility	12-21 , 313, 326, 450	252, 489
supergene alteration	38, 97-111 , 112, 145-148 , 213, 237-246, 288, 301	148
Susie Mountain intrusion	116	165, 362
Talnakh intrusion	16, 187	118
Tib Lake intrusion	284, 376	Voisey's Bay deposit 17, 197, 252, 256, 273, 319-331, 487
Tulameen complex	116, 120, 252, 292-301	Volspruit deposit 82, 309
Tweespalk deposit	82	weathering 97-111 , 155, 287-303 , 392, 413, 489, 490
Udokan deposit	145, 154, 492	Wedza mine 97-107, 410
UG2 (UG-2) reef	25, 57-59 , 67, 85, 92, 250, 253, 255, 284, 288, 310-315 , 488	Western Platinum mine 61
Uitkomst deposit	25, 323, 329	Whistle mine 169
unconformity U-Au deposits	45, 146, 153 , 252, 264, 489	Youbdo massif 116
Unki mine	66, 97-109 , 410, 416	Zhireken deposit 203, 208, 244
Ural-Alaskan type complexes	7, 24, 113-143 ,	Zunyi deposit 152, 263-265, 489